Studies Towards the Synthesis of Nitrogen Containing Heterocycles Using Au(I) Catalysis and the Photochemical Synthesis of Cyclopropanes

Ali Mansour Jamal Eddine

A thesis submitted to the University of Ottawa in partial fulfillment of the requirements for the Doctorate in Philosophy degree in Chemistry

Department of Chemistry and Biomolecular Sciences
Faculty of Science
University of Ottawa

© Ali Mansour Jamal Eddine, Ottawa, Canada, 2024

TABLE OF CONTENTS

ABSTRACT ..... **VI**
ACKNOWLEDGEMENTS ..... **IX**
STATEMENT OF CONTRIBUTION ..... **XI**
PUBLICATION AND PRESENTATIONS OF WORK IN THIS THESIS ..... **XIII**
LIST OF FIGURES ..... **XIV**
LIST OF SCHEMES ..... **XV**
LIST OF TABLES ..... **XXII**
LIST OF ABBREVIATIONS ..... **XXIV**
PART I. Strategic Utilization of Au(I) catalysis for the Synthesis of Polycyclic Indole and Nitrogen Containing Heterocycles **1**
CHAPTER 1. Introduction to Homogeneous Gold Catalysis **2**
1.1 A golden revolution 3
1.2 Gold catalysis in the activation of carbon π-systems 3
1.2.1 Relativistic effect and binding mode of gold-alkyne complexes 3
1.2.2 Counterion and ligand effects 5
1.2.3 General reactivity modes in Au(I) catalysis 8
1.2.4 Addition of *C*-, *O*-, and *N*-nucleophiles to alkynes 9
1.2.5 Miscellaneous reactions 15
1.3 Gold catalysis in total synthesis 19
1.4 Conclusion 22
CHAPTER 2. Au(I) Catalysis in the α-C-H Functionalization of Tertiary Amines **23**
2.1 Introduction 24
2.1.1 Csp^3-H functionalization 24
2.1.2 Au(I) catalyzed redox-neutral hydrogen atom transfer 25
2.1.2.1 Dialkyl ether and benzyl ether hydride donors 27
2.1.2.2 Tertiary amine hydride donors 30
2.2 Au(I) catalyzed formal nitrene transfer reactions 34
2.2.1 Azirines 35
2.2.2 Isoxazoles and related derivatives 36
2.2.3 *N*-pyridinium and sulfilimine ylides 37
2.2.4 Azides 38

2.3 Objective of the project 41
2.4 Substrate synthesis and intrinsic hydride donor reactivity studies 43
2.4.1 Preliminary experiments and challenges with reactivity 43
2.4.2 Rational incorporation of a malonate blocking group 49
2.5 Optimization of the catalytic system 52
2.5.1 Ligand and catalyst optimization 53
2.5.2 Solvent optimization 55
2.5.3 Additive optimization 57
2.5.4 Catalyst loading optimization 60
2.6 Evaluating the effect of the malonate blocking group 61
2.7 Methodology for the α-Csp^3-H functionalization of tertiary amines 65
2.7.1 Successful scope examples 65
2.7.2 Limitations and failed examples 70
2.7.3 Unexpected results when using acyclic hydride donor substrates 72
2.8 Product derivatization 75
2.8.1 Derivatization of the malonate blocking group 75
2.8.2 Oxidative derivatization of the indole skeleton 77
2.9 Mechanistic studies 81
2.9.1 Isolation of reaction intermediates 81
2.9.2 Deuterium labelling experiments 82
2.9.3 DFT studies and calculations 84
2.10 Conclusion 86
CHAPTER 3. Total Synthesis of (±)-Brevianamide A 88
3.1 Introduction 89
3.1.1 Fungal derived prenylated indole alkaloids 89
3.1.2 The brevianamides 91
3.2 Studies toward the biosynthetic origins of (+)-brevianamides A and B 94
3.3 Previous syntheses of brevianamide A 99
3.3.1 Lawrence's total synthesis of (+)- and (–)-brevianamide A 101
3.3.2 Smith's total synthesis of (±)-brevianamide A 102
3.4 Objective of the project 104
3.5 Initial retrosynthetic analysis 107
3.6 Forward synthesis (first-generation) 109

3.6.1 Model study on a truncated Au(I) catalysis precursor 109
3.6.2 Efforts toward the synthesis of free amide Au(I) catalysis precursor 109
3.6.3 Completion of the synthesis (first-generation) 114
3.6.4 Manipulation of the protecting group for the Au(I) catalysis precursor 115
3.7 Revised retrosynthetic analysis 118
3.8 Efforts towards the synthesis of a propargylated enamide substrate 119
3.8.1 α-hydroxy acid route 119
3.8.2 Meldrum's acid route 122
3.8.3. Propargyl glycine route 124
3.9 Completion of the synthesis (second-generation) 128
3.10 Conclusion 135
PART II. Synthesis of Cyclopropane Building Blocks *via* the Photochemical Extrusion of Sulfur Dioxide (SO_2) 137
CHAPTER 4. Photochemical Ring Contraction of Thietane-1,1-dioxide Derivatives ... 138
4.1 Introduction 139
4.1.1 Importance and properties of the cyclopropane ring 139
4.1.2 Methods for the synthesis of the cyclopropyl motif 140
4.1.2.1 Formal [2+1] cycloaddition strategies 141
4.1.2.2 Nucleophilic displacement strategies 145
4.1.2.3 Ring contraction strategies 147
4.1.3 Fundamentals of photochemistry 149
4.1.4 Radical chemistry of sulfone derivatives 152
4.2 Objective of the project 154
4.3 Precedent, initial results, and reaction optimization 155
4.4 Issues with substrate access and evaluation 160
4.4.1 Enamine/sulfonyl chloride [2+2] strategy 160
4.4.2 Ketene acetal/sulfonyl chloride [2+2] strategy 163
4.5 Synthesis and evaluation of 2-bromothiete-1,1-dioxide as a platform for diversity 169
4.6 Methodology for the photochemical ring contraction of thietane-1,1-dioxides 175
4.6.1 Successful scope examples thus far 176
4.6.2 Limitations and failed examples 177
4.7 Outlook and future directions 180
CHAPTER 5. Conclusion 182
CHAPTER 6. Supporting Information 186

6.1 General information 187
6.2 Supporting information for Chapter 2 188
6.2.1 Experimental procedures 188
6.2.2 ^{1}H- and ^{13}C-NMR spectra 250
6.2.3 DFT studies and calculations 364
6.3 Supporting information for Chapter 3 364
6.3.1 Experimental procedures 364
6.3.2 ^{1}H- and ^{13}C-NMR spectra 379
6.4 Supporting information for Chapter 4 389
6.4.1 Experimental procedures 389
6.4.2 ^{1}H- and ^{13}C-NMR Spectra 422
REFERENCES 477

ABSTRACT

The work presented in this thesis will be split into two parts. Part I of this thesis focuses on the utilization of gold(I) catalysis towards heterocyclic and total synthesis. Gold(I) catalysis is strategically applied in developing a new synthesis of tetracyclic indole products in addition to the total synthesis of the complex alkaloid natural product brevianamide A. Part II of this thesis shifts gears from gold(I) catalysis and focuses on the photochemical synthesis of cyclopropane building blocks. This strategy relies on the ring contraction of α-arylated thietane-1,1-dioxide substrates (four-membered cyclic sulfones) that extrude sulfur dioxide (SO_2) upon irradiation with ultraviolet light.

In Chapter 1, a general and non-comprehensive introduction to homogeneous gold(I) catalysis is discussed. This chapter is meant to help prime the reader in understanding the concepts of reactivity that are referenced in both Chapters 1 and 2. Brief sections on relativistic effects, catalyst structures, general reactivity modes, and applications are provided.

In Chapter 2, the exploration of a unique and novel approach towards the rare Au(I) catalyzed α-Csp^3-H functionalization of tertiary amine substrates was investigated. Direct C-H bond functionalization for the formation of new C-C or C-X bonds is an incredibly useful and straightforward strategy. Our approach to this challenge relied on combining and leveraging the unique reactivity of highly electrophilic α-imino gold carbene intermediates with redox-neutral hydrogen atom transfer from tertiary amine motifs. To the best of our knowledge, no such reports of these intermediates have been used in tandem with the Csp^3-H functionalization of tertiary amines despite having been used in numerous other transformations with many different nucleophiles. At the outset, we were cognizant of the favorable coordination ability of Lewis basic tertiary amines with Lewis acidic cationic Au(I) complexes. This interaction would likely prevent catalysis from taking place, not only from an alkyne activation standpoint but also from the perspective of hydride transfer. A work around to this problem was rationally designed and implemented in the form of a malonate blocking group. The malonate was incorporated into the substrate structure and was key to the success of the reaction through the exertion of steric, electronic, and conformational effects. Importantly, these effects seemed to be operating in

synergy rather than in competition with one another. After thorough optimization, we also demonstrated that this reaction is broadly applicable, tolerates different functional groups, and affords us valuable tetrahydro-γ-carboline products that can be selectively oxidized and functionalized to result in biologically and synthetically relevant structural motifs.

In Chapter 3, the total synthesis of racemic brevianamide A using gold(I) catalysis as a key step was investigated. Brevianamide A is a prototypical dioxopiperazine natural product that was isolated in 1969 by Birch and Wright from the fungus *Penicillium brevicompactum*. In addition to its bicyclo[2.2.2]diazaoctane substructure, brevianamide A possesses a characteristic pseudoindoxyl motif and two adjacent quaternary centers. These features make this natural product a challenging synthetic target, especially when it comes to generating structural complexity efficiently. Previous syntheses of brevianamide A installed the key structural features of the natural product (mentioned above) in a less than ideal manner. Based on these considerations, a new synthetic approach towards brevianamide A that would shortcut and improve access to the natural product was designed and executed. Key to our synthesis is the strategic use of a gold(I) catalyzed cascade process that quickly assembles the characteristic pseudoindoxyl motif, reverse prenyl group, and two quaternary centers in a single step. This is achieved using the readily available prenyl alcohol in conjunction with gold(I) catalysis to introduce the reverse prenyl unit at *C*2 of the natural product. Thanks to the increase in structural complexity that can be achieved with gold catalysis, we were able to develop two complementary and concise routes to racemic brevianamide A from readily available amino acid building blocks. Moreover, the conditions necessary to affect the formation of the natural products bicyclo[2.2.2]diazaoctane core proved to be highly compatible with gold catalysis, allowing for the development of a one-pot process and further streamlining our new approach towards this natural product. As a result, we have published the shortest and highest yielding synthesis of brevianamide A to date.

In Chapter 4, the photochemical ring contraction and synthesis of α-arylated thietane-1,1-dioxide substrates were investigated towards accessing cyclopropane building blocks. The cyclopropane motif is very sought after in medicinal chemistry as a privileged structural motif and is also present in various natural products, agrochemicals, and fragrances. Common methods to access cyclopropanes have traditionally relied on either cycloaddition or nucleophilic

displacement strategies and while successful, these approaches can be limited in terms of their scope and ability to access substrates in a modular manner. Furthermore, scalability and reaction efficiency are a common issue owing to the use of highly reactive intermediates and/or reagents. With these issues in mind, we have developed an uncommon photochemical ring contraction strategy that uses thietane-1,1-dioxide precursors containing an aryl ring chromophore. Light is a cheap and renewable energy source, offering the potential to circumvent issues of reactivity and selectivity of the more traditional cyclopropanation methods. Optimization of photochemical conditions allowing access to the cyclopropane scaffolds was therefore developed and studied. While initially promising, substrate synthesis utilizing reported enamine and/or ketene acetal [2+2] cycloadditions with sulfonyl chlorides proved to be unsatisfactory for the introduction of modularity and diversity. To alleviate this issue, an investigation into the use of the unsaturated thiete-1,1-dioxide derivatives was performed and enabled access to several thietane-1,1-dioxide derivatives. Subsequently, a scope of the ring contraction process was extended to include the synthesis of a diverse set of cyclopropane building blocks, particularly cyclopropylamine structures that are valuable in medicinal chemistry. Additionally, a brief overview of the future directions for the project is also discussed.

ACKNOWLEDGEMENTS

I would like to first thank my supervisor, Professor Fabien Gagosz, for allowing me the opportunity to join his research group and for providing such a welcoming lab environment that was filled with enthusiastic colleagues. Thank you for all your help and guidance over the years. You were always encouraging me to do my best and were always available for advice and help when things were not working out in the lab. I will always appreciate your intense passion for organic chemistry that was often contagious and helped spur me to continue to tackle difficult problems in the lab. I would also like to thank the members of my thesis advisory committee, Professors Louis Barriault and André Beauchemin, in addition to all the support and administrative staff within the uOttawa Department of Chemistry and Biomolecular Sciences.

Thank you to all Gagosz group members (past and present) for all the knowledge and laughs shared throughout my time in the group. David, it was so great to be able to work on the azide/H-transfer project with you. You were an awesome partner to do chemistry with and your immense well of knowledge, techniques, and advice was something I missed greatly after you left for the "real world". The lab became very different without you, but I am very thankful for everything you taught me. Dom, while we did not work on any projects together, I could always count on you for help in the lab. You always had such great ideas and advice. I will miss our daily chats near our fume hoods where we shared a bunch of good laughs. Karim, your enthusiasm for chemistry can only be matched by your love for tea. I always enjoyed our conversations about chemistry but more importantly about food (even though you think tacos and shawarma are basically the same). Congrats again on becoming Dr. Karim Muratov! Alice, you were always a huge source of positivity and encouragement when things were rough in the lab (despite my constant complaining). We shared a lot of good laughs, and I will always remember coffee runs at FSS. Thanks for being a great friend. Jessica, it's been great to work with you on the cyclopropane project. Your enthusiasm in the lab was always appreciated and I am confident in your ability to continue doing research. Elyssa, Elisabeth, Dante, Liam, Martin, Thomas, Noah, Miguel, and past members: Unteni, Daniel, Supreeta, Tamba, Loïc, Stéphane, Samuel, and Mila: I wish you all the best of luck in your future endeavors! I am grateful to have worked alongside such bright and young scientists.

Thank you to all past and present members of the Barriault group for being so welcoming, allowing me to borrow as many chemicals as I wanted, and tolerating my forgetfulness in bringing them back. I always looked forward to group meetings together where we could all discuss chemistry and share ideas. A big shout out to Chad for being an amazing friend and for all our discussions about chemistry and life. I will always appreciate your advice, and I hope you complete that total synthesis! I know you can do it. A special thank you also goes out to members of the Pratt and Beauchemin labs for their help and support with chemicals and in the use of equipment. Thank you to Dr. Zijun Wu, Eda, and Mel for helping me in the booking and use of the photoreactor in addition to letting us use dry solvents! Thank you to Alshimaa, Bhavana, Maxime, and Sherif for always helping me find any chemicals I needed.

I want to also thank my family and friends for their unconditional love and support in my career but also in life. Mom, you raised two young (and troublesome) teenage boys on your own and you did so with courage and strength. Despite everything, you always encouraged me to be the best I can be and supported my decision to study chemistry. I am who I am today because of you. To my little brother, I am proud of the man you have become, and it gives me immense joy to see all you have accomplished. Thank you for always lending your ear when I needed it and for grounding me in a way that I could not do so for myself. To my friends, thank you all for your continued support and everlasting friendship. You are all the craziest and best of friends that I could ask for. I am so happy to have you all in my life.

Most importantly, I want to thank my wife, Monida. You have sacrificed so much to help and support me through graduate school. Research is unforgiving and can often be devastating when things are not going well. Thanks to you, I had the courage to continue moving forward and face my challenges head on. You never let me quit and gave me the strength and motivation to push through. Even when I did not believe in myself or in my own capabilities, you were there every step of the way and gave me courage. You have been nothing but patient, understanding, and supportive throughout this whole journey and for that I will be forever grateful. I of course cannot forget a special mention to our two cats: Kaiya and Suki. They have been such a joy in our lives and have made my Ph.D. experience all the better.

STATEMENT OF CONTRIBUTION

The projects and experiments discussed in this thesis were performed both individually (Chapter 3) and in collaboration with past and present members of the Gagosz group (Chapter 2 and Chapter 4). Contributions within schemes or tables that are not my own will be indicated with "+" or "++" symbols.

In Chapter 2, myself, and Dr. David Fabian León Rayo (DFLR; previous postdoctoral fellow) were equal contributors to the project. Both of us were involved in the work discussed in **Sections 2.4–2.7**, including substrate synthesis, evaluation, and optimization of the model reaction. Specific examples for either mine or Davids's contributions will be indicated in schemes, tables, and the main text. pK_a estimation was computed by Professor Fabien Gagosz. The portion of **Section 2.7.2** that describes experiments related to substrates which were unsuccessful or less efficient were done by me. The subsequent schemes describing experiments with substrates possessing a malonate group outside of the linker and substrates which are acylic were primarily done by David. I was involved in the synthesis of substrate **2.175** (not shown in **Scheme 2.30**) but did not perform the gold catalysis. For the section of product derivatization (**Section 2.8**), all experiments pertaining to the functionalization of the malonate group (**Section 2.8.1**) were performed by David. All other experiments pertaining to the oxidative functionalization of indole products (**Section 2.8.2**) were performed by me. Experiments and reactions done in **Sections 2.9.1–2.9.2** were performed by both David and I with specific examples for each of our contribution being referenced in the schemes, tables, and main text. DFT calculations discussed in **Section 2.9.3** were performed entirely by Professor Fabien Gagosz.

In Chapter 4, work towards a photochemical synthesis of cyclopropanes from cyclic sulfone derivatives was made possible through collaboration with Jessica Parent (JP; Honour's/summer student) and Loïc Rochez (LR; summer exchange student). Their contributions (in addition to my own) will be accredited throughout the schemes, tables, and main text where necessary. The initial hit involving the synthesis of the cyclopropane **4.73** (**Section 4.3**) was done by me. The subsequent optimization of the photochemical reaction was done by Jessica. The examples in **Section 4.4.1** were done primarily by me and Jessica with some contribution by Loïc.

In **Section 4.4.2**, the synthesis of the diethylketal cyclopropane **4.84** was done by me, while the attempted derivatization of **4.84** by reductive amination was done by Loïc. All other attempts at derivatization of thietane-1,1-dioxide **4.83** by acidic deprotection and reductive amination were performed by me. The rest of the section concerning photoredox or cross-coupling functionalization of α-halo thietane-1,1-dioxides was done by myself. The majority of **Section 4.5** was done by me with Jessica joining on during optimization of the Suzuki-coupling for heteroaromatic boronic acids (**Section 4.5, Table 4.1**) where she is a primary contributor. For the scope of the reaction (**Section 4.6.1**), most of the examples listed were done by me with some examples done by Jessica which will be indicated in **Table 4.2**. In **Section 4.6.2**, all the examples shown in **Table 4.3** and **Scheme 4.30** were done by me, with the examples shown in **Scheme 4.31** done by Jessica.

PUBLICATION AND PRESENTATIONS OF WORK IN THIS THESIS

Publications (⁺Co-first authors ie: contributed equally, *corresponding author):

Mansour, A.; Gagosz, F.* Expedited Total Synthesis of (±)-Brevianamide A *via* the Strategic Use of Gold(I) Catalysis. *Org. Lett.* **2022**, *24*, 7200–7204. **[Featured in Org. Chem. Highlights]**

León Rayo, D. F.⁺; **Mansour, A.⁺**, Wu, W.; Bhawal, B. N; Gagosz, F.* Steric, Electronic and Conformational Synergistic Effects in the Gold(I)-catalyzed α-C-H Bond Functionalization of Tertiary Amines. *Angew. Chem. Int. Ed.* **2022**, *e202212893*. **[Selected as a hot paper]**

Presentations (presenting author is shown in bold):

Mansour, A.; León Rayo, D. F.; Wu, W.; Bhawal, B. N; Gagosz, F. Strategic use of gold(I)-catalysis for the concise synthesis of polycyclic indole motifs. *Symposium for Synthetic and Bioorganic Chemistry (QOMSBOC)*, poster presentation. Montréal, QC. October 2023.

Mansour, A.; León Rayo, D. F.; Wu, W.; Bhawal, B. N; Gagosz, F. Strategic use of gold(I)-catalysis for the concise synthesis of polycyclic indole motifs. *International Society of Heterocyclic Chemistry Congress (ISHCC)*, poster presentation. Santa Barbara, CA, USA. August 2022.

Mansour, A.; Gagosz, F. Efforts towards the concise total synthesis of (±)-brevianamide A. *Quebec-Ontario Mini-Symposium for Synthetic and Bioorganic Chemistry (QOMSBOC)*, virtual oral presentation. Hamilton, ON. October 2021.

Mansour, A.; León Rayo, D. F.; Gagosz, F. A gold-mediated nitrene-transfer/hydride shift cascade for the synthesis of polycyclic indoles. *Chemistry and Biochemistry Graduate Research Conference (CBGRC)*, virtual oral presentation, Montréal, QC. November 2020.

LIST OF FIGURES

Figure 1. (A) Schematic representation of the relativistic contraction and expansion of the gold 6s and 5d orbitals and (B) overview of the DCD model for gold-alkyne complexes……5

Figure 1.1. Examples of some generally common Au(I) and Au(III) catalyst structures and ligands/counteranions……..6

Figure 1.2. (A) Counterion and ligand trends in Au(I) catalysis and (B) formation of catalytically active and stable Au(I) catalysts from LAuCl complexes and silver salts……..7

Figure 2. (A) Classical hydride donors and (B) orbital diagram for heteroatom assisted hydrogen atom migration……...26

Figure 2.1. Structures for various types of nitrene-transfer reagents……...35

Figure 3. Key structural features of the bicyclo[2.2.2]diazaoctane family of alkaloids…...89

Figure 3.1. Representative examples and biological activity of prominent members within both monooxo- and dioxopiperazine sub-families…….90

Figure 3.2. Structures of brevianamides A–F……...91

Figure 4. Physical properties of the cyclopropane ring……...139

Figure 4.1. Examples of compounds which feature the cyclopropane ring……...140

Figure 4.2. Representative structures of free or metal-stabilized carbenes……142

Figure 4.3. Simplified Jablonski diagram illustrating the formation of a molecules excited state from its ground state……150

LIST OF SCHEMES

Scheme 1. General mechanistic summary for the Au(I) catalyzed functionalization of alkynes which are (A) non-polarized and (B) specially activated……9

Scheme 1.1. General mechanism for the Au(I) catalyzed 1,6-enyne cycloisomerization……..10

Scheme 1.2. Examples of 1,6-enyne cycloisomerization reactions under homogeneous Au(I) catalysis……..11

Scheme 1.3. Addition of *C*-based nucleophiles using homogeneous Au(I) catalysis……....12

Scheme 1.4. Examples for the addition of *O*-nucleophiles to Au(I) activated alkynes……..13

Scheme 1.5. Examples of Au(I) catalyzed hydroamination reactions of alkynes……..14

Scheme 1.6. (A) General mechanism for the Au(I) catalyzed rearrangement of propargylic acetates and (B) one pot synthesis of β-CF_3-enones……..16

Scheme 1.7. (A) Formation of α-oxo gold carbenes and (B) examples using *N*-oxides as oxidants……..17

Scheme 1.8. Generation and reactions of Au(I)-vinylidene intermediates……18

Scheme 1.9. Tandem Au(I) catalyzed furan formation/furan-allene [4+3] cycloaddition cascade for the core synthesis of the reported structures of curcusones I and J……..20

Scheme 1.10. Au(I) catalyzed 1,6-enyne cycloisomerization for rapid access to the angular diquinane core of ventricosene……...21

Scheme 1.11. Intramolecular hydroamidation/enamide cyclization cascade as a key step towards the total synthesis of (–)-rhazinicine and (–)-rhazinilam……....22

Scheme 2. Classical functional group interconversion as compared to more direct C-H functionalization pathway……..24

Scheme 2.1. General representation of (A) "inner sphere" and (B) "outer sphere" mechanisms for transition metal catalyzed C-H functionalization reactions……...25

Scheme 2.2. C-H functionalization using Au(I) catalysis by means of redox-neutral [1,n]-H transfer strategies……...26

Scheme 2.3. Hydroalkylation of alkynyl ethers *via* a Au(I) catalyzed [1,5]-H transfer/cyclization cascade……...27

Scheme 2.4. Synthesis of allene building blocks by Gagosz and co-workers using a Au(I) catalyzed [1,5]-H transfer/fragmentation cascade……....28

Scheme 2.5. Tandem Au(I) catalyzed cycloisomerization triggered by a [1.6]-H transfer…....29
Scheme 2.6. Total synthesis of (+)-archangiumide using Au(I) catalyzed hydride transfer as a key step……..30
Scheme 2.7. Au(I) catalyzed reactions of tertiary amine derivatives…….31
Scheme 2.8. Cascade processes for the Au(I) catalyzed C-H functionalization of tertiary amines……....32
Scheme 2.9. Cascade hydroamination/[1.5]-H transfer for the enantioselective synthesis of cyclic aminals……..…33
Scheme 2.10. General mechanism for Au(I) catalyzed formal nitrene transfer onto activated alkynes……...34
Scheme 2.11. Intramolecular synthesis of highly functionalized pyridines from 2*H*-azirines as masked alkenyl nitrenes…….36
Scheme 2.12. Intermolecular synthesis of (A) tetrasubstituted pyrroles and (B) acyl indoles using isoxazoles and benzisoxazoles as nucleophilic nitrenoid precursors……...37
Scheme 2.13. Utilization of *N*-pyridinium and sulfilimine ylides for heterocyclic synthesis…..38
Scheme 2.14. Azides as nitrene-transfer agents in Au(I) catalysis with [1,2]-H migration onto α-imino gold carbenes……...…39
Scheme 2.15. Azides as nitrene-transfer agents in Au(I) catalysis with trapping of α-imino gold carbenes……..40
Scheme 2.16. Cascade reactions of α-imino gold carbenes generated from azides as nitrene-transfer reagents…….41
Scheme 2.17. A new approach towards the Au(I) catalyzed C-H functionalization of tertiary amines……42
Scheme 2.18. Potential challenges associated with the Au(I) catalyzed C-H functionalization of tertiary amines……43
Scheme 2.19. Three step synthesis of initial *homo*-propargyl piperidine and dibenzylamine substrates **2.83** and **2.84**. $^{+}$Result by DFLR……...44
Scheme 2.20. Synthesis of tosyl, carbamate, and phenyl protected substrates **2.94**–**2.96**. $^{+}$Result by DFLR……46
Scheme 2.21. Examples of benzannulation reactions in the synthesis of medium-sized rings…48

Scheme 2.22. Previous application of a malonate blocking group by our lab in Au(I) catalyzed hydroarylation reactions……49
Scheme 2.23. (A) Synergistic conformational, electronic, and steric effect by the malonate blocking group. (B) Using the malonate as a versatile synthetic handle for product derivatization……..50
Scheme 2.24. Synthesis of model substrate **2.103** containing a dimethyl malonate group in the linker……..51
Scheme 2.25. Ligands used for the Au(I) catalyzed reaction of model substrate **2.103**……..55
Scheme 2.26. Synthesis of substrates **2.111**, **2.112**, and **2.113**. $^{+}$Results by DFLR…….62
Scheme 2.27. Computed and predicted *p*K_a values for the conjugate acid of substrates **2.83**, **2.103**, and **2.111**–**2.113**……..65
Scheme 2.28. Different routes used to access substrates **2.114**–**2.139** in a modular manner…..66
Scheme 2.29. Unsuccessful hydride donor substrates……..71
Scheme 2.30. Unsuccessful substrates with the malonate group not on the two-carbon linker. $^{+}$Results by DFLR……..72
Scheme 2.31. Unexpected formation of a new rearranged product **2.183** from dibenzyl and dibutyl substrates **2.178** and **2.179**. $^{+}$Results by DFLR…….74
Scheme 2.32. Preliminary mechanism explaining the formation of rearranged product **2.183** from indole **2.180** in the presence of Au(I) and acid…….75
Scheme 2.33. Common pathways for the oxidation of indole scaffolds……..77
Scheme 2.34. Possible mechanism explaining the formation of **2.192**……79
Scheme 2.35. Summary of indole product derivatization post C-H functionalization. $^{+}$Result by DFLR…….81
Scheme 2.36. Successful isolation, characterization, and conversion of aminal **2.196** into indole product **2.161** supporting its role as a reactive intermediate. $^{+}$Results by DFLR..82
Scheme 2.37. Synthesis of partially and fully deuterated substrates d_7-**2.200** and d_{14}-**2.200**…..83
Scheme 2.38. Deuterium labelling experiments……...84
Scheme 2.39. Computational analysis of the free energy reaction profile……...85
Scheme 2.40. Proposed mechanism for the Au(I) catalyzed α-C-H functionalization of tertiary amines……86
Scheme 3. Birch and Russell's photolysis studies on (+)-brevianamide A…….92

Scheme 3.1. (A) (+)-brevianamides A and B are co-isolated in ~10:1 *d.r.* from *P. brevicompactum* and (B) semi-synthesis of unnatural (–)-brevianamide B from natural (+)-brevianamide A……...93
Scheme 3.2. (A) Birch's early labelling/incorporation studies and (B) Sammes and Porters proposed *hetero*-IMDA reaction……94
Scheme 3.3. Williams and co-workers' first-generation biosynthetic proposal…….96
Scheme 3.4. Williams and co-workers' second-generation biosynthetic proposal……97
Scheme 3.5. Attempts by Williams and co-workers to rearrange hydroxy-indolenine **3.12** *via* late-stage semi-Pinacol to access pseudoindoxyl intermediates……98
Scheme 3.6. Williams, Sherman, and Li's revised and most recent biosynthetic proposal…...99
Scheme 3.7. Failed end-game strategy for oxidative access to brevianamide A……..100
Scheme 3.8. Lawrence's 2020 biomimetic total synthesis of (+)/(**–**)-brevianamides A and B……...102
Scheme 3.9. Smith's 2021 total synthesis of (±)-brevianamide A……...104
Scheme 3.10. Limitations associated with previous syntheses of brevianamide A by the groups of Lawrence and Smith……105
Scheme 3.11. Previous work from the Gagosz lab on the synthesis of 2,2-disubstituted pseudoindoxyl products using Au(I)-catalysis…….106
Scheme 3.12. Our groups approach towards an expedited synthesis of racemic brevianamide A using Au(I) catalysis……107
Scheme 3.13. Initial retrosynthetic analysis of (±)-brevianamide A……..108
Scheme 3.14. Model study towards testing our proposed Au(I) catalyzed cascade process…..109
Scheme 3.15. One step enamide synthesis from imine acylation as compared to other methods……...….110
Scheme 3.16. Synthesis and attempted acylation reactions of imine **3.21**…….111
Scheme 3.17. Synthesis of PMB-protected diketopiperazine **3.58**…….112
Scheme 3.18. Synthesis of Au(I) catalysis precursor **3.41**…….114
Scheme 3.19. First-generation synthesis of (±)-brevianamide A……...115
Scheme 3.20. Synthesis of PMB- and *o*-NB-protected arylazide substrates **3.61** and **3.63** respectively……..116

Scheme 3.21. (A) Formation of protected pseudoindoxyl products **3.64** and **3.65** using Au(I) catalysis and (B) unsuccessful attempts at protecting group removal……117
Scheme 3.22. Revised retrosynthetic analysis of (±)-brevianamide A……...119
Scheme 3.23. Initial test reactions……..120
Scheme 3.24. Synthesis of acetonides **3.79** and **3.81**……121
Scheme 3.25. Unsuccessful attempts at manipulating Meldrum's acid derivatives in the formation of enamide products……123
Scheme 3.26. Efforts towards the synthesis of protected propargyl glycine derivatives **3.92–3.94**……...125
Scheme 3.27. Synthesis of acetate protected diketopiperazine **3.104** as the precursor to our key Au(I) catalyzed transformation……129
Scheme 3.28. One-pot synthesis of (±)-brevianamide A starting from acetate protected diketopiperazine **3.104**……131
Scheme 3.29. One-pot synthesis of (±)-brevianamide A starting from linear arylazide precursor **3.103**……135
Scheme 3.30. Overview of the total synthesis of (±)-**3** from (A) acetyl protected diketopiperazine **3.104** and (B) linear arylazide intermediate **3.103**……...136
Scheme 4. Current strategies towards the synthesis of cyclopropanes……..141
Scheme 4.1. General mechanism for the Simmons-Smith cyclopropanation……..142
Scheme 4.2. Representative asymmetric Simmons-Smith cyclopropanation reactions……...143
Scheme 4.3. General catalytic cycle for the transition-metal catalyzed cyclopropanation of alkenes *via* the decomposition of diazo compounds……144
Scheme 4.4. Representative examples of transition-metal catalyzed cyclopropanation reactions *via* metal-stabilized carbenes……...145
Scheme 4.5. (A) MIRC and (B) carbanion strategies towards the synthesis of cyclopropane rings……..146
Scheme 4.6. Representative examples of cyclopropane synthesis employing nucleophilic displacement strategies……147
Scheme 4.7. Cyclopropane synthesis through the ring contraction of pyrazoline derivatives.148
Scheme 4.8. Cyclopropane synthesis through the ring contraction of cyclobutyl derivatives.149
Scheme 4.9. Direct *vs* indirect photoexcitation of organic molecules……..152

Scheme 4.10. Some examples of desulfonylative radical reaction modes……152
Scheme 4.11. General mechanism for radical desulfonylation……..153
Scheme 4.12. Examples of radical processes involving extrusion of the sulfonyl group for the formation of new C-C bonds……154
Scheme 4.13. Utilizing cyclic sulfones under photochemical conditions to affect a ring contraction strategy *via* SO_2 extrusion……155
Scheme 4.14. (A) Scope of the photolysis of thietane-1,1-dioxides and γ-sultines towards cyclopropanes by Durst and Smith and (B) the proposed mechanism……156
Scheme 4.15. (A) General access to cyclopropylamines and (B) synthesis and evaluation of a model substrate under photochemical conditions……158
Scheme 4.16. Synthesis of different 2-aryl-3-aminothietane-1,1-dioxides by the enamine/sulfonyl chloride [2+2] strategy……161
Scheme 4.17. Issues with varying the enamine component in the [2+2] cycloaddition towards thietane-1,1-dioxides. $^{+}$Results by JP. $^{++}$Results by LR……...162
Scheme 4.18. Issues with varying the sulfonyl chloride component in the [2+2] cycloaddition towards thietane-1,1-dioxides. $^{+}$Results by JP. $^{++}$Results by LR……163
Scheme 4.19. (A) General access to cyclopropylamines by using a ketene acetal/sulfonyl chloride [2+2] strategy and (B) successful synthesis of cyclopropyl ketal **4.84**.164
Scheme 4.20. Failed attempts at the manipulation of the diethyl ketal group towards the installation of an amine moiety. $^{+}$Results by LR……166
Scheme 4.21. Dual photochemical approach to aryl cyclopropyl ketals such as **4.90**……...167
Scheme 4.22. Synthesis of α-bromo and α-chlorothietane-1,1-dioxides **4.95** and **4.96**…….168
Scheme 4.23. Attempts at installation of aryl groups using photoredox or metal catalyzed coupling approaches……169
Scheme 4.24. Thiete-1,1-dioxides as a platform for introducing diversity……170
Scheme 4.25. Failed access to thiete-1,1-dioxide by the elimination of chloride……..171
Scheme 4.26. Low yielding synthesis of thiete-1,1-dioxide by the elimination of an azide. $^{+}$Result by JP……172
Scheme 4.27. Efficient synthesis of thiete-1,1-dioxide **4.99** starting from thietan-3-one **4.115**……173

Scheme 4.28. Successful use of 2-arylated thiete-1,1-dioxides as electrophiles for the introduction of diversity at the β position (*C*3)……174
Scheme 4.29. General and modular synthesis of photochemical substrates……..176
Scheme 4.30. Synthesis and unsuccessful photochemical ring contraction of heteroaromatic substrate **4.175**. [+]Result by JP……..179
Scheme 4.31. Low yielding irradiation of trisubstituted thietane-1,1-dioxide substrates **4.178**–**4.180**. [+]Results by JP……...180
Scheme 4.32. A flow chemistry process for the more efficient synthesis of cyclopropane building blocks using high energy UV light……181
Scheme 4.33. Ring contraction of thietane-1,1-dioxides under conditions of triplet-energy transfer (EnT)……...181

LIST OF TABLES

Table 2. Preliminary attempts for the desired C-H functionalization reaction……..….45

Table 2.1. Further tests utilizing protected amines to validate the desired C-H functionalization reaction……...48

Table 2.2. Initial hit for the desired C-H functionalization reaction……...52

Table 2.3. Ligand optimization for the Au(I) catalyzed reaction of model substrate **2.103**...54

Table 2.4. Solvent optimization for the Au(I) catalyzed reaction of model substrate **2.103**..57

Table 2.5. Additive optimization for the Au(I) catalyzed reaction of model substrate **2.103**……...60

Table 2.6. Catalyst loading optimization for the Au(I) catalyzed reaction of model substrate **2.103**……...61

Table 2.7. Assessing the steric, electronic, and conformational effects of the malonate group on the outcome of the desired Au(I) catalyzed Csp^3-H functionalization reaction……...64

Table 2.8. Hydride donor scope for the Au(I) catalyzed α-Csp^3-H functionalization of tertiary amines……68

Table 2.9. Hydride donor scope continued……69

Table 2.10. Arylazide scope for the Au(I) catalyzed α-Csp^3-H functionalization of tertiary amines……70

Table 2.11. Optimization for the dealkoxycarbonylation reaction of model product **2.104** to give monoester product **2.187**……76

Table 2.12. Optimization for the formation of doubly oxidized product **2.192** from indole **2.104**……...78

Table 2.13. Oxidative conditions for the synthesis of pseudoindoxyl product **2.191a** and halogenated aminal products **2.194** and **2.195** from indole **2.104**…….80

Table 3. Propargylation attempts on PMB-protected diketopiperazine substrate **3.58**…..113

Table 3.1. Propargylation attempts using acetonides **3.79** and **3.81**…….122

Table 3.2. Finding conditions for the *N*-phthaloylation of **3.98**·TFA……...126

Table 3.3. Optimization of the coupling conditions with imine **3.21**……...128

Table 3.4. Optimization of the Au(I) catalyzed rearrangement of acetate protected diketopiperazine **3.104** into pseudoindoxyl **3.105**……...130

Table 3.5. Optimization of the solvent and temperature for the Au(I) catalyzed rearrangement of linear precursor **3.103** into pseudoindoxyl **3.106**……133

Table 3.6. Optimization of the catalyst and ligand for the Au(I) catalyzed rearrangement of linear precursor **3.103** into pseudoindoxyl **3.106**…….134

Table 4. Optimization of the photochemical ring contraction for thietane-1,1-dioxide model substrate **4.72**……160

Table 4.1. Failed attempts at cross-coupling between 2-bromothiete-1,1-dioxide **4.122** and heteroaromatic rings…….175

Table 4.2. Nucleophile and aryl ring scope for the photochemical ring contraction of thietane-1,1-dioxide derivatives……...177

Table 4.3. Unsuccessful irradiation of substrates **4.159**–**4.165** with different β substitution……...178

Table 6: Comparison of ^{1}H-NMR data of our synthetic sample of (±)-brevianamide A (**3**) to the sample prepared by the group of Lawrence……...377

Table 6.1: Comparison of ^{13}C-NMR data of our synthetic sample of (±)-brevianamide A (**3**) to the sample prepared by the group of Lawrence……...378

LIST OF ABBREVIATIONS

Δ – delta (heat)

γ – gamma (three atoms away)

ΔG – standard Gibbs free energy

[Au] – gold complex

[H] – general reduction reaction

[M] – generic organometallic complex

[O] – general oxidation reaction

°C – degrees Celsius

‡ – transition state symbol

1,2-DCE – 1,2-dichloroethane

1,2-DIE – 1,2-diiodoethane

1,2-DME – 1,2-dimethoxyethane

$^1O_2$ – singlet oxygen

2,6-lut. – 2,6-lutidine

3° - tertiary group

9-BBN – 9-borabicyclo[3.3.1]nonane

Å – angstrom

Ac – acetyl

Ad – adamantyl

aq. – aqueous

Ar – generic aromatic group

BArF – tetrakis[3,5-*bis*(trifluoromethyl)phenyl]borate

BDE – bond dissociation energy

Bn – benzyl

Boc – *tert*-butyloxycarbonyl

Boc_2O – di-*tert*-butyl dicarbonate

BrettPhos – 2-(dicyclohexylphosphino)-3,6-dimethoxy-2’,4’,6’-tri-*iso*-propyl-1,1’-biphenyl

Bz – benzoyl

Bz_2O_2 – dibenzoyl peroxide

CAAC – cyclic alkyl amino carbene

CAN – ceric ammonium nitrate

CBz – benzyloxycarbonyl

CF_3 – trifluoromethyl

CN – cyano

conc. – concentrated

conv. – conversion

CPhos – 2-dicyclohexylphosphino-2’,6’-*bis*(*N*,*N*-dimethylamino)biphenyl

C_q – quaternary carbon

Cy – cyclohexyl

d.r. – diastereomeric ratio

DABCO – 1,4-diazabicyclo[2.2.2]octane

DABSO – 1,4-diazabicyclo[2.2.2]octane *bis*(sulfur dioxide) adduct

dba – dibenzylideneacetone

DBU – 1,8-diazabicyclo[5.4.0]undec-7-ene

DCC – *N*,*N*’-dicyclohexylcarbodiimide

DCM – dichloromethane

DEAD – diethyl azodicarboxylate

DFT – density functional theory

DIPEA – *N*,*N*-di-*iso*-propylethylamine

DMA – *N*,*N*-dimethylacetamide

DMAP – 4-(*N*,*N*-dimethylamino)pyridine

DMDO – dimethyldioxirane

DMF – *N*,*N*-dimethylformamide

DMP – Dess-Martin periodinane

DMS – dimethyl sulfide

DMSO – dimethyl sulfoxide

dppm – *bis*(diphenylphosphino)methane

E – generic ester group

E^+ – generic electrophile

EDC – *N*-(3-dimethylaminopropyl)-*N*'-ethylcarbodiimide

EDTA – ethylenediaminetetraacetic acid

ee – enantiomeric excess

e.r. – enantiomeric ratio

epi – epimer

equiv. – equivalents

Et – ethyl

Et_2O – diethyl ether

Et_3N – triethylamine

EtOAc – ethyl acetate

EtOH – ethanol

EWG – generic electron-withdrawing group

FG – generic functional group

FGI – functional group interconversion

gem – geminal

GPhos – (3-(*tert*-butoxy)-2',6'-di-*iso*-propyl-6-methoxy-[1,1'-biphenyl]-2-yl)dicyclohexylphosphane

*h*ν – light

H^+ – proton or hydronium ion

HATU – hexafluorophosphate azabenzotriazole tetramethyl uronium

HMDS – hexamethyldisilazane

HOBt – hydroxybenzotriazole

HOMO – highest occupied molecular orbital

h – hour

Im. – imidazole

IMes – 1,3-*bis*(2,4,6-trimethylphenyl)imidazol-2-ylidene

IPent – 1,3-*bis*(2,6-di-3-pentylphenyl)imidazole-2-ylidene

IPr – 1,3-*bis*-(2,6-di-*iso*-propylphenyl)imidazole-2-ylidene

i-Pr – *iso*-propyl

i-PrOH – *iso*-propanol

I*t*-Bu – 1,3-di-*tert*-butylimidazol-2-ylidene

JohnPhos – 2-(di-*tert*-butylphosphino)biphenyl

kcal – kilocalorie

KO*t*-Bu – potassium *tert*-butoxide

L – generic ligand

LAH – lithium aluminum hydride

LDA – lithium di-*iso*-propylamide

LG – generic leaving group

LiHMDS – lithium hexamethyldisilazane

LLS – longest-linear sequence

LUMO – lowest unoccupied molecular orbital

m – meta

M – molar

m-CPBA – *m*-chloroperoxybenzoic acid

Me – methyl

MeCN – acetonitrile

$MeNO_2$ – nitromethane

MeOH – methanol

mM – millimolar

mmol – millimole

mol – mole

mol% – mole percentage

MoOPH – oxodiperoxymolybdenum(pyridine)(hexamethylphosphorictriamide)

MorDalPhos – di(1-adamantyl)-2-morpholinophenylphosphine

Ms – methanesulfonyl

MS – molecular sieves

N – nitrogen or normal (concentration)

n – non-bonding orbital

N_3 – azido

NaHMDS – sodium hexamethyldisilazane

NBS – *N*-bromosuccinimide

n-Bu – butyl

n-BuLi – *n*-butyllithium

NCS – *N*-chlorosuccinimide

NHP – *N*-hydroxyphthalimide

nm – nanometer

NMO – *N*-methylmorpholine *N*-oxide

n-Pr – propyl

NTf_2 – *bis*(trifluoromethanesulfonyl)imidate

Nuc – generic nucleophile

o – ortho

Oxone® – $2KHSO_5 \bullet KHSO_4 \bullet K_2SO_4$

OTf – trifluoromethanesulfonate

p – para

PCy_3 – tricyclohexylphosphine

Ph – phenyl

$PhCF_3$ – trifluorotoluene

PhCHO – benzaldehyde

PhCl – chlorobenzene

$PhCO_2H$ – benzoic acid

PhH – benzene

PhMe – toluene

Phth – phthaloyl

Pic. – picolinate

PIFA – [*bis*(trifluoroacetoxy)iodo]benzene

Pip. – piperidine

Piv – pivaloyl

PMB – *p*-methoxybenzyl

PMP – *p*-methoxyphenyl

PPh_3 – triphenylphosphine

Pro – proline

p-TsOH – *p*-toluenesulfonic acid

Pyr. – pyridine

quant. – quantitative

R – any generic carbon-based group

r.r. – regioisomeric ratio

rt – room temperature

SCN – thiocyanate

SDD – Stuttgart/Dresden basis set

SIPr – 1,3-*bis*(2,6-di-*iso*-propylphenyl)-4,5-dihydroimidazol-2-ylidene

S_N2 – substitution nucleophilic bimolecular

SPhos – 2-dicyclohexylphosphino-2',6'-dimethoxybiphenyl

TBS – *tert*-butylsilyl

t-Bu – *tert*-butyl

t-BuOCl – *tert*-butyl hypochlorite

Tf_2NH – trifluoromethanesulfonimide

TFA – trifluoroacetic acid

TFE – trifluoroethanol

TfOH – trifluoromethanesulfonic acid

TFP – *tris*(*o*-furyl)phosphine

THF – tetrahydrofuran

TLC – thin-layer chromatography

TLC/MS – thin-layer chromatography mass spectrometry

TMS – trimethylsilyl

Trp – tryptophan

Ts – *p*-toluenesulfonyl

TS – transition state

VPhos – 2-dicyclohexylphosphino-2'-methoxy-4',6'-di-*tert*-butylbiphenyl

wt% – weight percentage

X_C – generic chiral auxiliary

XPhos – 2-dicyclohexylphosphino-2',4',6'-tri-*iso*-propylbiphenyl

α – alpha (one atom away)

β – beta (two atoms away)

δ – delta (chemical shift or partial charge)

ΔG‡ – standard Gibbs free energy of activation

η – eta (ligand hapticity)

μm – micrometre

μW – microwave

π – pi (orbital)

σ – sigma (orbital)

PART I

Strategic Utilization of Au(I) catalysis for the Synthesis of Polycyclic Indole and Nitrogen Containing Heterocycles

CHAPTER 1

Introduction to Homogeneous Gold Catalysis

1.1 A golden revolution

Group 11 on the periodic table (copper, silver, and gold), also referred to as the "coinage metals" have always been of interest to mankind. These metals were probably some of the first to ever be used and discovered by ancient humans since all three exist naturally as their elemental form on Earth.[a] Gold has been utilized extensively in ancient civilizations such as Egypt for its appearance and malleability.[b] Nowadays with the rise in the price of metals, gold and silver are no longer being used in standard currency. However, copper remains as a common metal used in coins to this day. Elemental gold is remarkably resistant to atmospheric oxygen, chemical degradation, and does not tarnish over time. Therefore, it has been widely regarded as unreactive and possessing no promising features for catalytic applications and synthetic utility.[1] This longstanding belief had unfortunately delayed the evolution of gold chemistry in general, but the situation has drastically changed since then. Homogeneous gold catalysis is a blossoming field and continues to grow and expand every day. Ever since the first use of gold in catalytic applications by Ito and Hayashi[2] to the renaissance of homogeneous gold catalysis from the 2000's and 2010's[3, 4] – Au(I) complexes have now become the most effective catalysts for the electrophilic activation of alkynes with a plethora of synthetic tools developed for the formation of C-C and C-X bonds.[5]

1.2 Gold catalysis in the activation of carbon π-systems

1.2.1 Relativistic effect and binding mode of gold-alkyne complexes

In order to best understand the behaviour of Au(I) complexes as soft Lewis acids towards alkynes and other carbon π-systems, one needs to take into account the prominent relativistic effect observed with the gold atom.[6] Au(0) possesses the electronic configuration [Xe]$4f^{14}5d^{10}6s^{1}$, where there is one electron which resides in the most external 6*s* orbital. Due to quantum mechanics and special relativity, the electronic structure of heavy elements such as gold can differ significantly from their lighter relatives such as silver and copper. With gold, the electrons in the 1*s* orbital exhibit increased velocity and therefore this leads to an increase in their mass. Consequently, the Bohr radius of the atom will decrease (radius is inversely proportional to mass) causing a

[a]Greenwood, N. N.; Earnshaw, A. In *Chemistry of the Elements*, 2nd edition; Butterworth-Heinemann: 1997.
[b]Britannica, The Editors of Encyclopedia. Gold. In *Encyclopedia Britannica*, 2024.

contraction of *s*- and *p*-orbitals, bringing those electrons closer to the nucleus. This shields the electrons and their charge from the outer electrons in *d*- and *f*-orbitals, causing an expansion of these orbitals (Figure 1A). Contraction of the 6*s* orbital (LUMO in Au(I) catalysis) is stabilizing, resulting in improved Lewis acidic properties *via* LUMO-lowering which could not be explained using non-relativistic models. This also explains the apparent "alkynophilicity" of cationic Au(I) complexes when compared to other coinage metals.[6] Alkynes possess a lower lying HOMO and LUMO in comparison to alkenes which are more nucleophilic but less electrophilic. Au(I)-alkyne complexes should then have a lower lying LUMO which is more favorable for the addition of a nucleophile HOMO as compared to Au(I)-alkene complexes, explaining this selectivity. On the other hand, expansion of the 5*d* orbital (HOMO in Au(I) catalysis) results in an increase in its energy due to less electron/electron repulsion, resulting in a higher HOMO and accounting for better back-bonding with alkyne ligands and the stabilization of positive charges in reaction intermediates.[7] Despite being slightly higher in energy due to relativistic expansion, the gold 5*d* orbital is still lower in energy as compared to the higher energy 3*d* orbital in copper for example. This helps to explain why Au(I) species are not as nucleophilic as the related Cu(I) species and why they do not undergo oxidative addition from Au(I) to Au(III) as easily as Cu(I) to Cu(III).[8]

The interaction between the π-system of an alkyne and an LAu^+ fragment can be discussed within the framework of the Dewar-Chatt-Duncanson (DCD) model (Figure 1B).[7, 9] In general, the DCD model assumes a σ-type interaction between the filled π-orbitals of the alkyne with a vacant metal orbital of appropriate symmetry (in this case the *d*-orbitals of the gold atom). There is also a π-accepting interaction between the occupied *d*-orbitals of the metal center, with the vacant antibonding π*-orbitals of the alkyne ligand. Separate calculations also suggest that there is a significant electrostatic factor at play in the total bonding force, contributing to the stability of these metal-alkyne complexes. Isolated coinage metal η^2-alkyne complexes showed that for gold in particular, binding to the alkyne is not symmetrical, but rather slightly skewed to one side over another. Additionally, there is much more pronounced σ-donation than π-accepting character in gold-alkyne complexes as compared to the other coinage metals based on DFT calculations performed by the group of Toste.[10] This can be attributed to the prominent relativistic effect as described above in conjunction with the higher energy alkyne π*-orbitals. All these phenomena

taken together help to paint an overall picture on the superb "alkynophilicity" of Au(I) complexes as compared to the related copper and silver complexes.

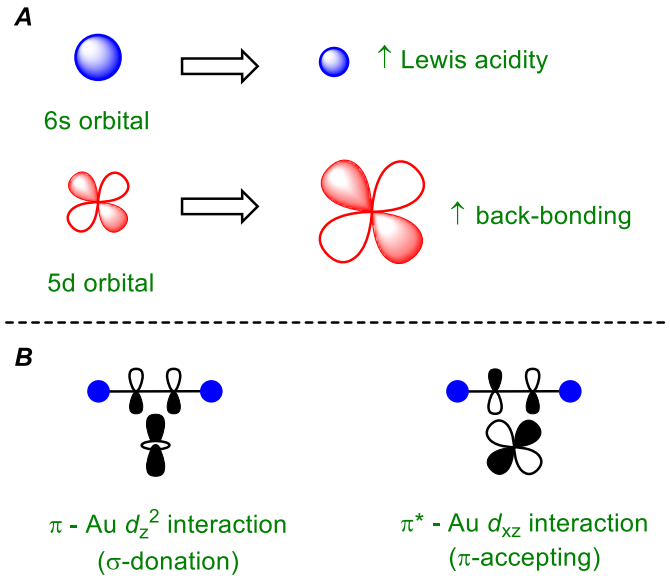


Figure 1. (A) Schematic representation of the relativistic contraction and expansion of the gold 6s and 5d orbitals and (B) overview of the DCD model for gold-alkyne complexes

1.2.2 Counterion and ligand effects

In general, gold catalysts can be grouped as either Au(I) or Au(III) salts and complexes. Some of the earliest examples used the corresponding chloride salts,[11] however since then there has been much work published on the effects of ligands and counterions on the activity of gold catalysts, especially when it comes to Au(I) catalysis.[5, 12, 13] Au(III) complexes adopt a square planar geometry and can include more simple salts based on the tetrachloroaurate anion ($NaAuCl_4$) or complexes such as the commonly used $PicAuCl_2$ catalyst (Figure 1.1). Au(I) complexes on the other hand typically exhibit a linear geometry with a ligand that is necessary to help stabilize the complex and a counterion to balance the formal positive charge, bearing the general formula [LAuX].[5] For Au(I) catalysis, the most common ligands employed are phosphines and their derivatives such as phosphites, and *N*-heterocyclic carbenes (NHC). The counterion (X) can vary and has a marked impact on the catalyst stability and activity. Some examples are shown below in Figure 1.1.

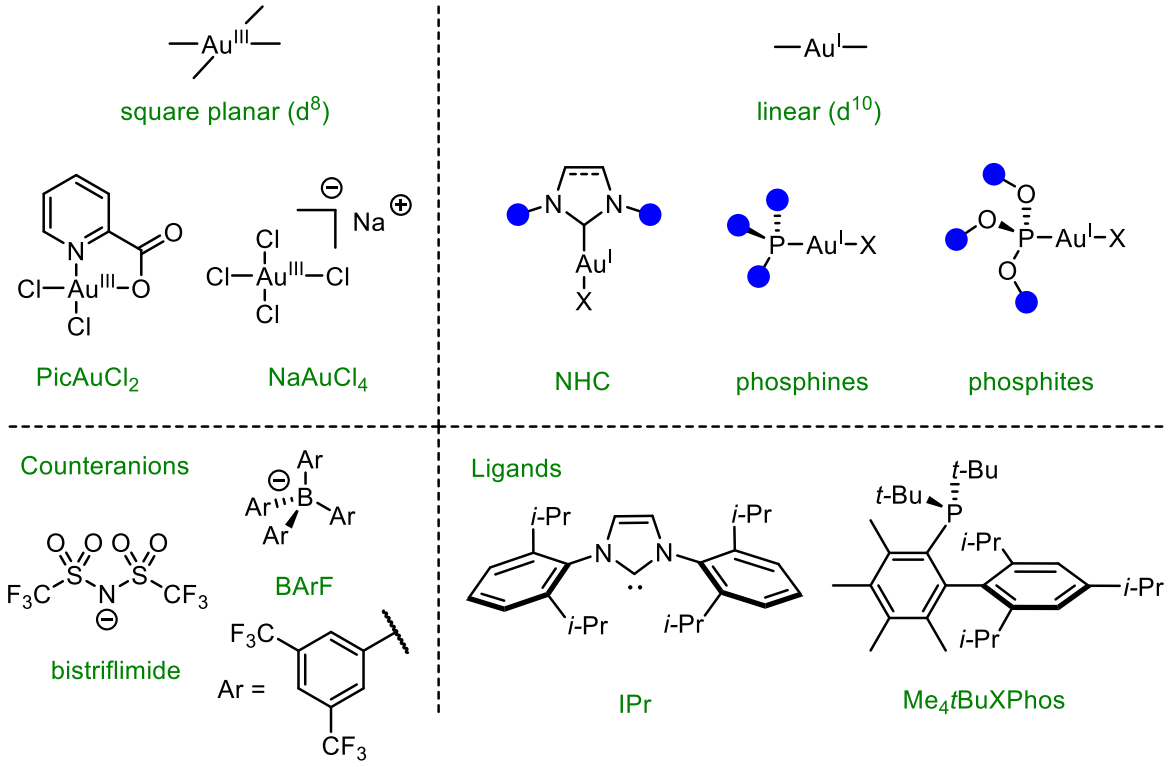


Figure 1.1. Examples of some generally common Au(I) and Au(III) catalyst structures and ligands/counteranions

Catalytic activity can be highly dependant on the counteranion[11, 14] and ligand[13, 15] used. In catalytically active complexes, the X-type counterion is usually a weakly coordinating anion such as SbF_6, NTf_2, or BArF instead of the typical chloride which is more stable but not as active.[15] The more coordinating the counteranion is to the cationic Au(I) center, the less active the catalyst. This is the case with counteranions such as halides or carboxylates where the negative charge is more localized. Counteranions that are much larger such as SbF_6 or BArF bear a negative charge that is more delocalized and are therefore less coordinating (Figure 1.2A). These trends are nicely illustrated by previous publications from the groups of Echavarren[12] and Kirsch.[16] Most active complexes are typically generated from the less active LAuCl either *in-situ* or beforehand and employ the use of a silver salt to abstract the chloride (Figure 1.2B). Complexes with non-coordinating anions are typically more "naked" and so are generally less stable and more reactive, requiring their formation *in-situ*[5] as opposed to being stored on the bench such as the more stable $LAuNTf_2$ salts developed by the group of Gagosz which utilizes the weakly coordinating *bis*-triflimide anion.[17, 18] Another breakthrough in catalyst synthesis came from the groups of

Echavarren[19] and Nolan[20] which showed that abstraction of the chloride using $AgSbF_6$ in the presence of acetonitrile led to isolable $LAu(MeCN)SbF_6$ catalysts that had a non-coordinating counteranion but was stabilized by the weakly donating acetonitrile (Figure 1.2B). When considering the ligand, the most important factors influencing catalytic activity are the electronic and steric nature of the ligand. Phosphine ligands are good σ-donors and π-acceptors, while NHC ligands are typically much better σ-donors as compared to phosphines. This typically renders most NHC Au(I) catalysts as less electrophilic as compared to Au(I) phosphine catalysts but can consequently stabilize cationic intermediates more easily. Phosphite ligands represent the other extreme where they are poor σ-donors but are very good π-acceptors. This renders them extremely electrophilic and therefore much more reactive (Figure 1.2A).

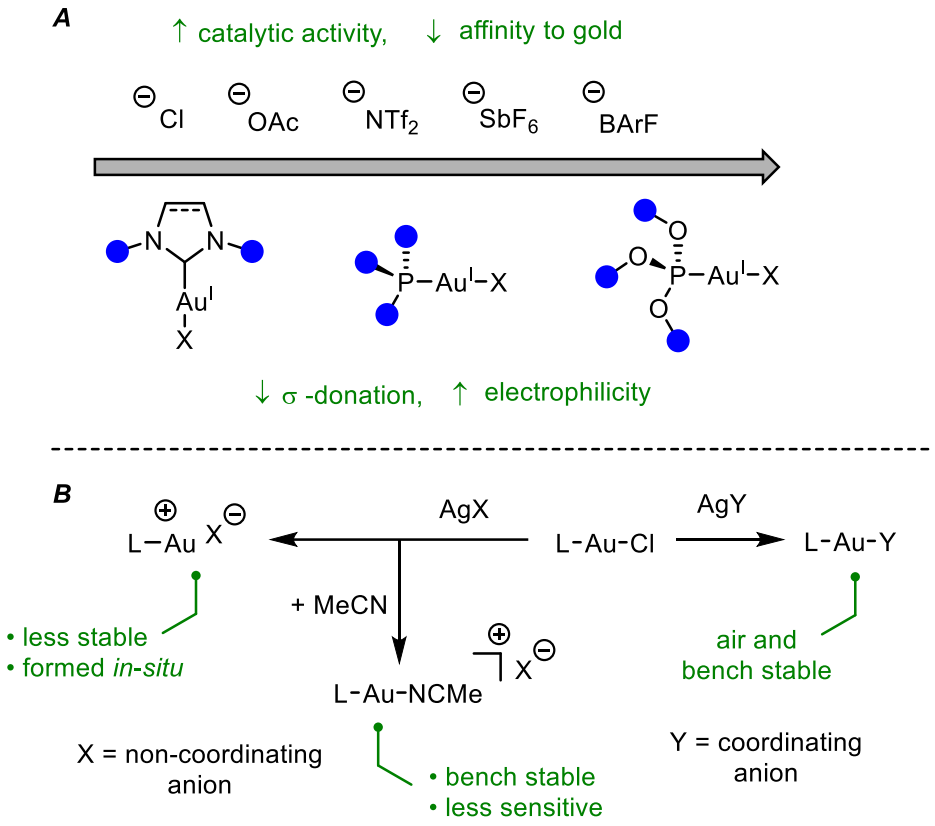


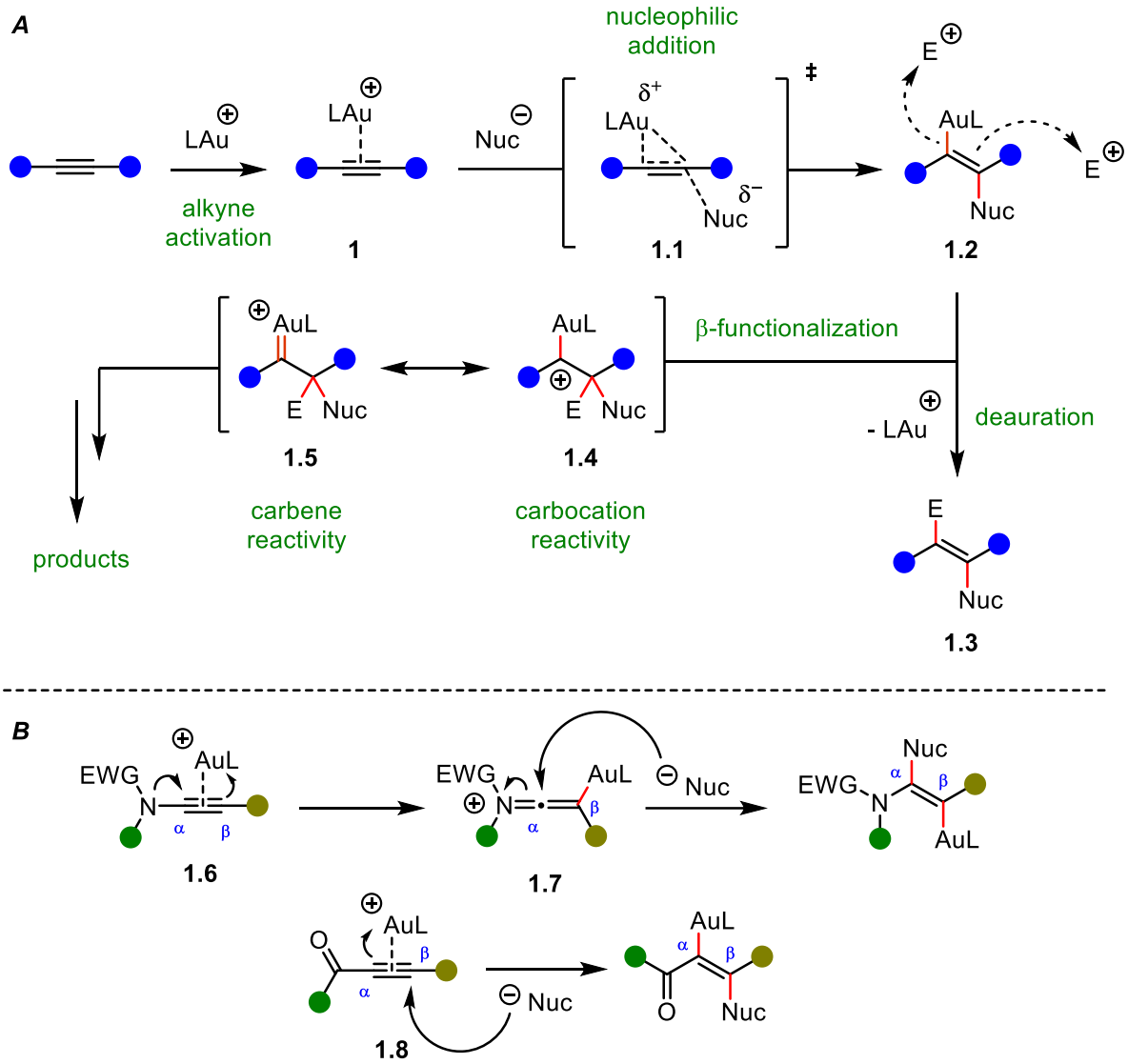
Figure 1.2. (A) Counterion and ligand trends in Au(I) catalysis and (B) formation of catalytically active and stable Au(I) catalysts from LAuCl complexes and silver salts

1.2.3 General reactivity modes in Au(I) catalysis

As discussed above, cationic Au(I) complexes are exceptional soft Lewis acids for the interaction with carbon π-systems such as alkynes. Due to the linear geometry of Au(I), the first step upon interaction with the alkyne is a ligand exchange with counteranion X, forming a η^2-Au(I)-alkyne complex **1** that is now sufficiently activated towards attack by all manner of nucleophiles (Scheme 1A). Nucleophilic attack onto an activated Au(I)-alkyne complex takes place in a *trans*-fashion, generating a vinyl gold intermediate **1.2**. It has also been shown that addition of nucleophiles to **1** proceeds with "slippage" of the Au(I)-alkyne species from a symmetrical η^2 to a non-symmetrical η^1-complex as illustrated by transition state **1.1**.[7] Vinyl gold intermediate **1.2** undergoes deauration in the presence of an electrophile to give the product **1.3** and regenerate the Au(I) catalyst. Depending on the kind of electrophile, more versatile transformations such as isomerizations and rearrangement reactions can be made possible. Besides functionalization of the α-carbon, the β-carbon to gold can also be functionalized by a suitable electrophile and this produces a carbocationic intermediate **1.4**. There is evidence that this type of reactive intermediate may exist on a cation-carbene spectrum since there is the possibility of back-donation by the gold atom in order to stabilize the positive charge and form a Au(I)-carbene **1.5**.[6, 7, 21] These two forms can be viewed as resonance extremes and the predominant form is likely dependant on the ligand being used.[22] Phosphite ligands are more π-accepting, likely destabilizing the carbocation form through reduction of electron density on the gold atom. On the other hand, NHC ligands that are strongly σ-donating can provide the gold atom with a higher electron density, better stabilizing the positive charge and favoring the carbene. This dual behaviour opens another dimension of Au(I) catalysis which will be discussed in later sections.

In cases where the alkyne ligand is non-symmetrical, an issue of regioselectivity can arise when it comes to nucleophilic addition onto complex **1**. In these cases, regioselectivity is typically governed by electronics (most common) of the substrate or by the steric crowding of the ligand being used. One such strategy to bias the system is to use alkynes which are specially activated or polarized (Scheme 1B). Two common examples of this are to use heteroatom substituted alkynes such as ynamides **1.6** or to use alkynes substituted with an electron-withdrawing group such as ynones **1.8**.[23] In the case of ynamides, the electron donating nitrogen will direct addition of Au(I) to the β-position, forming a keteniminium **1.7** which is activated towards nucleophilic addition at

the α-position. On the other hand, ynones exhibit the reverse polarization, and nucleophilic attack is intrinsically directed towards the β-position.

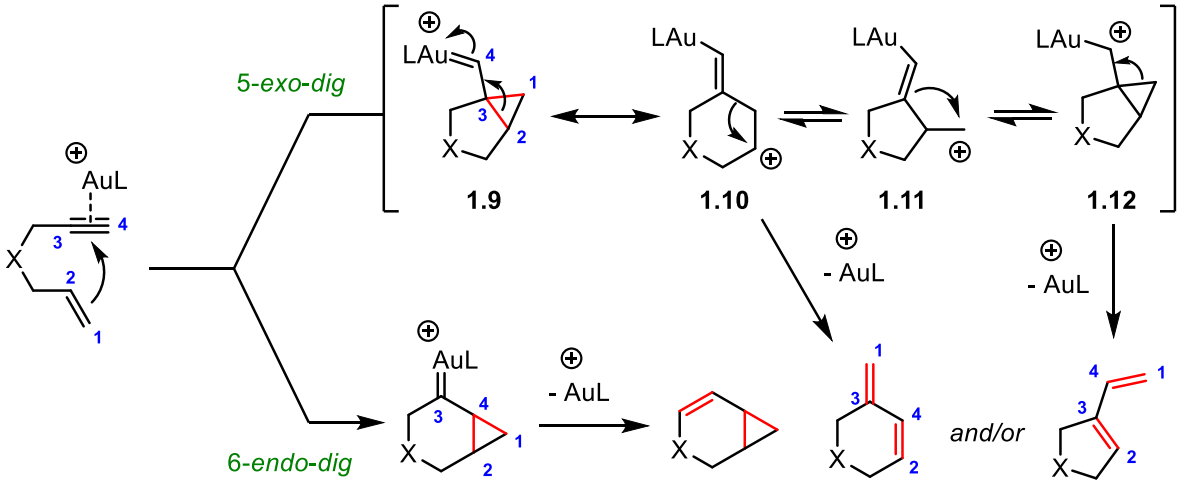


Scheme 1. General mechanistic summary for the Au(I) catalyzed functionalization of alkynes which are (A) non-polarized and (B) polarized

1.2.4 Addition of *C*-, *O*-, and *N*-nucleophiles to alkynes

In the addition of carbon-based nucleophiles, the cycloisomerization of 1,6-enynes is perhaps the most well known. These transformations have proven to be exceptionally useful as they provide an easy means of building molecular complexity quickly from much simpler and

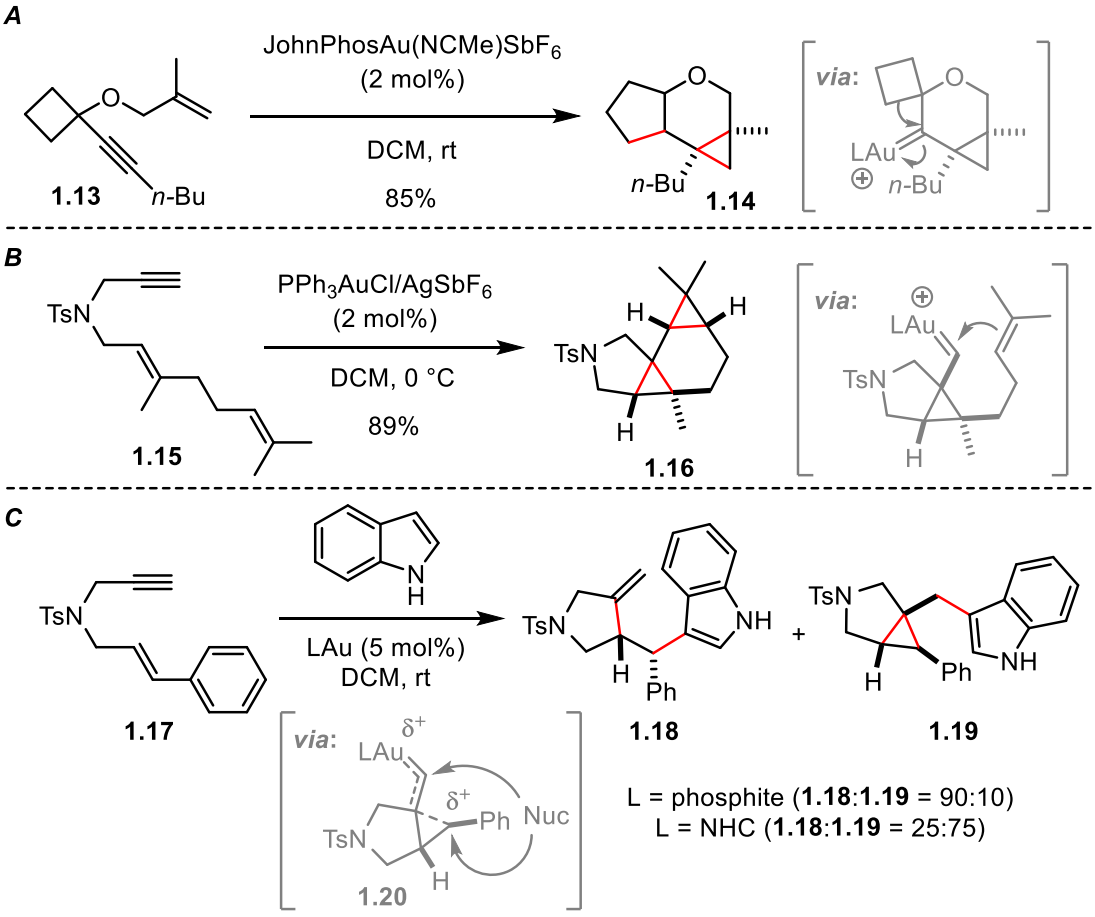
readily accessible building blocks.[5] In these transformations, the Au(I)-activated alkyne is intercepted by a pendant alkene as a nucleophile, generating a new C-C bond and the formation of a cyclopropyl gold carbene **1.9** (Scheme 1.1). The alkene can form a new C-C bond in either a 5-*exo* or 6-*endo* manner, undergoing different skeletal rearrangements. This reaction exhibits quite a complex mechanism, and it is important to realize that the intermediate cyclopropyl gold carbene can also exist as highly delocalized and stabilized carbocations such as the secondary carbocation, homoallyl, and cyclopropylmethyl cations **1.10**, **1.11**, and **1.12** respectively.[19] These pathways often compete with one another and can be highly dependent on the choice of ligand being used, particularly with respect to the steric environment of the ligand influencing the regioselectivity.



Scheme 1.1. General mechanism for the Au(I) catalyzed 1,6-enyne cycloisomerization

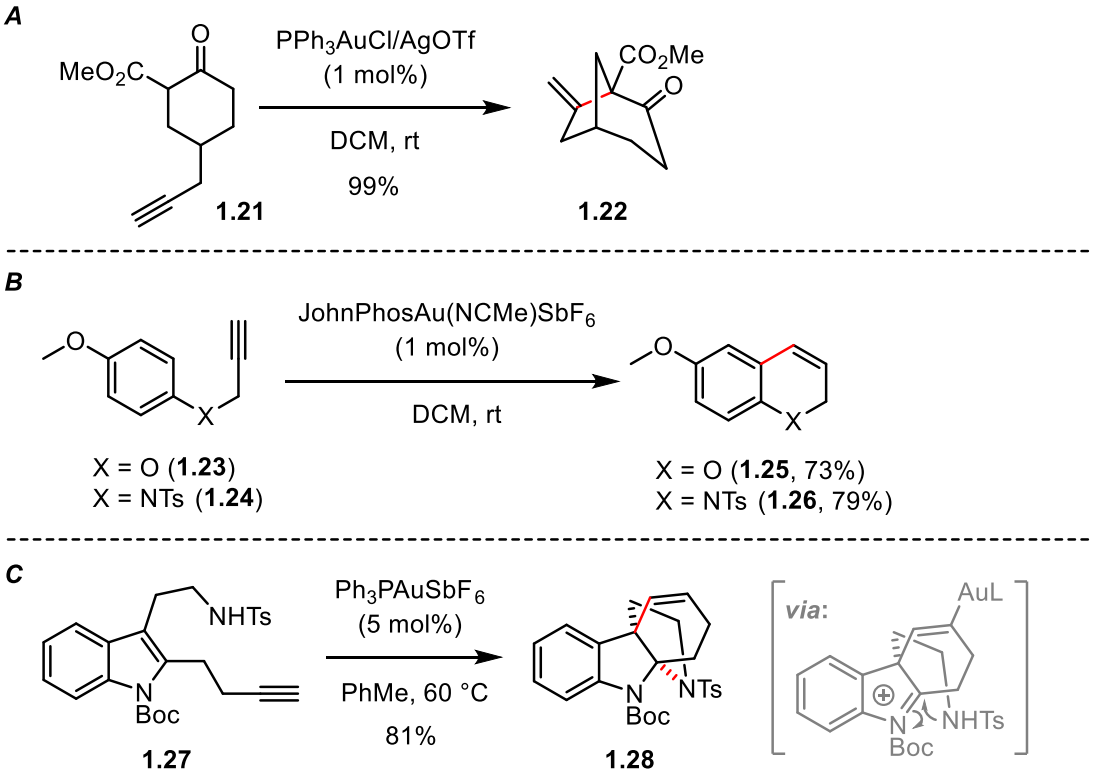
The literature encompassing Au(I) catalyzed cycloisomerizations is vast,[24-28] therefore only a few examples showcasing the utility of this transformation for building molecular complexity will be discussed. The group of Fensterbank demonstrated that 1,6-enynes **1.13** which contained an ether tether and a strained ring could undergo the desired cycloisomerization with subsequent ring expansion and protodeauration to give highly functionalized tricyclic molecules **1.14** that can be elaborated to natural products (Scheme 1.2A).[29] Another interesting example of this transformation and in taking advantage of the transient gold carbene intermediate was demonstrated by Echavarren and coworkers (Scheme 1.2B).[30] Using dienyne **1.15**, the 1,6-enyne cycloisomerization is carried out and followed by an intramolecular cyclopropanation reaction with the gold carbene intermediate, ultimately providing highly congested tetracycle **1.16**. This

represents a rapid increase in complexity from simple linear starting material. Additionally, the enyne cycloisomerization can also be interrupted if there is an exogenous nucleophile added to the reaction mixture, such as an electron rich heteroarene like indole. Echavarren and coworkers found that depending on the choice of ligand used for the catalyst, differing ratios of products could be obtained when using substrate **1.17** (Scheme 1.2C).[31] If the catalyst contains the poorly σ-donating phosphite ligands, then the major product formed is alkene product **1.18**. On the other hand, using the more σ-donating NHC ligands reverses the selectivity of the reaction, and now the cyclopropyl product **1.19** is the major compound. This result can be rationalized by the NHC ligands being able to provide enhancement of the carbene-like character in the intermediate of this reaction (**1.20**), which ultimately can exist as either the carbene or homoallylic cation resonance forms as shown by the hybrid structure.



Scheme 1.2. Examples of 1,6-enyne cycloisomerization reactions under homogeneous Au(I) catalysis

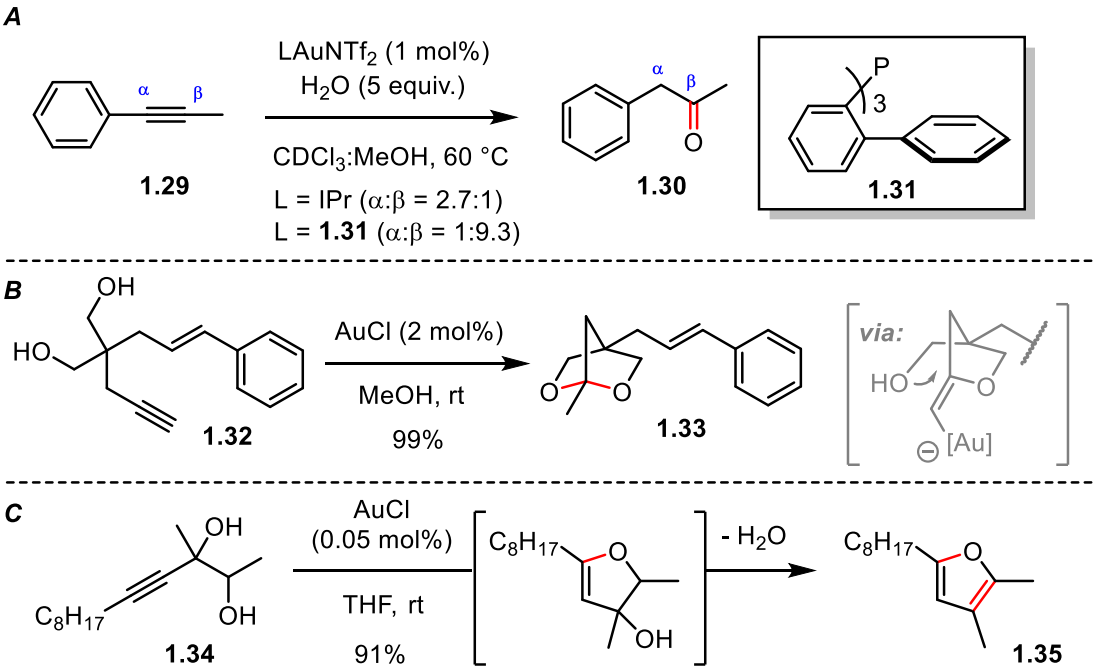
Besides cycloisomerization reactions using alkene nucleophiles, other *C*-based nucleophiles such as β-ketoesters and arenes have also been used to add onto Au(I)-activated alkynes as shown below. The group of Toste[32] demonstrated the Conia-ene reaction of β-ketoesters **1.21** with alkynes in the synthesis of highly functionalized carbocycles such as **1.22** (Scheme 1.3A) and the group of Banwell have shown that an intramolecular hydroarylation is possible in the synthesis of 2*H*-chromenes **1.25** and dihydroisoquinolines **1.26** (Scheme 1.3B) from aryl propargyl ethers **1.23** and sulfonamides **1.24**.[33] Iminium species which are generated *via* the hydroarylation of indoles at their *C3*-position can also be trapped by tethered nucleophiles, further increasing molecular complexity. The group of Wang demonstrated that alkynyl indoles **1.27** bearing a tethered nucleophile, could undergo tandem cyclizations to form indolines **1.28** which are often found in akuammiline alkaloids (Scheme 1.3C).[34]



Scheme 1.3. Addition of *C*-based nucleophiles using homogeneous Au(I) catalysis

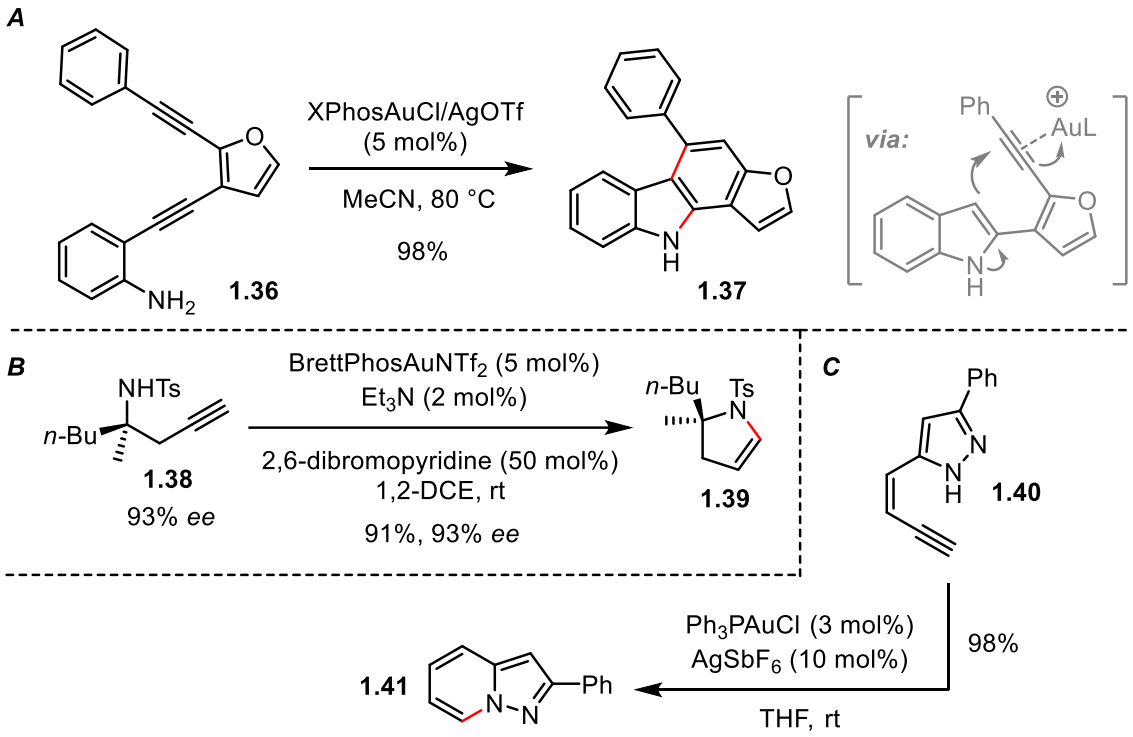
The addition of heteroatom nucleophiles such as oxygen and nitrogen have also been extensively studied in the context of Au(I) catalysis.[3, 4, 35, 36] In the context of *O*-nucleophiles, the low oxophilicity of gold has proven to be an advantage since many gold catalysts are compatible

with ambient conditions and can activate alkynes towards attack by nucleophilic oxygen species in the presence of water and oxygen gas without catalyst quenching. The hydration of alkynes is an industrially relevant process in the synthesis of ketones and gold catalysis can offer a much more benign alternative to this important reaction as compared to the more classical use of Hg(II) salts.[37] In the hydration of alkynes, regioselectivity can prove to be an issue with unsymmetrical alkynes, however the steric properties of the ligand being used have been shown to improve selectivity. Recent work by the Gagosz group utilized bulky *tris*-biarylphosphines as ligands to affect a highly regioselective hydration of alkynes **1.29** to synthesize ketones **1.30** (Scheme 1.4A).[38] The typical selectivity in alkyne hydration is Markovnikov when using classical NHC ligands, however the use of the bulky phosphine ligand **1.31** reversed this selectivity and led to *anti*-Markovnikov products. Another interesting approach is the use of geminal substituted diols **1.32** as nucleophiles with Au(I) activated alkynes (Scheme 1.4B). In this case, acetalization takes place and this has been used in the synthesis of strained acetals such as **1.33** by the groups of Michelet and Genêt.[39] In 2009, the groups of Aponick studied the intramolecular cyclization of vicinal diols **1.34** for the synthesis of furan building blocks **1.35** under mild conditions and with catalyst loadings as low as 0.05 mol% (Scheme 1.4C).[40]



Scheme 1.4. Examples for the addition of *O*-nucleophiles to Au(I) activated alkynes

For *N*-based nucleophiles, the intramolecular hydroamination of alkynes is a desirable tool for heterocyclic synthesis. In 2011, the groups of Fujii and Ohno demonstrated the facile synthesis of aryl fused carbazoles **1.37** through a hydroamination/hydroarylation cascade from aniline diynes **1.36** (Scheme 1.5A).[41] Utilizing chiral propargyl sulfonamide **1.38**, Ye and coworkers were able to synthesize important scaffolds based on dihydropyrrole **1.39** which could easily serve as a precursor for antifungal alkaloids and as a springboard for the construction of complex molecules owing to the nucleophilic enamine moiety (Scheme 1.5B).[42] Additionally, pyrazolopyridines **1.41** which are valuable heterocyclic scaffolds in the pharmaceutical industry were easily accessible from the corresponding alkynyl pyrazoles **1.40** (Scheme 1.5C).[43] Notably, Wu and coworkers found that the use of gold was necessary as it was the only metal which could affect this transformation in good yield and full conversion. Other metals such as platinum, copper, and silver failed to do so.

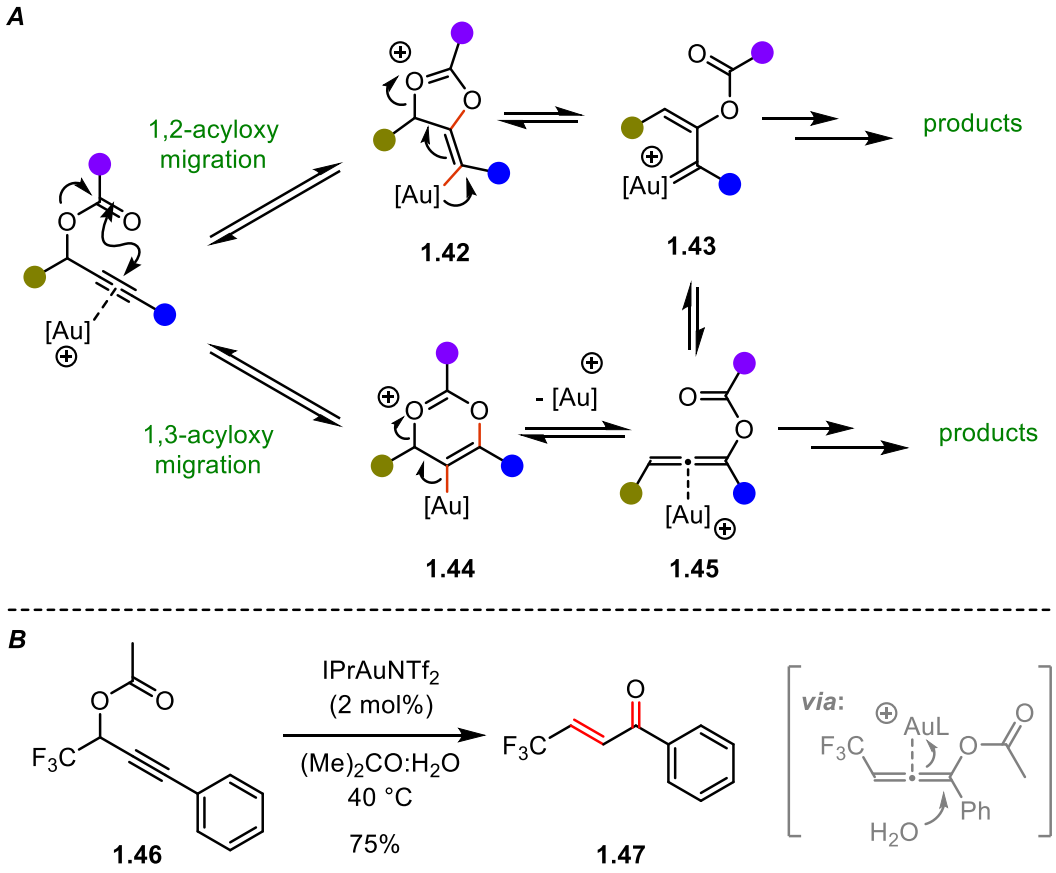


Scheme 1.5. Examples of Au(I) catalyzed hydroamination reactions of alkynes

1.2.5 Miscellaneous reactions

Since the initial publication using gold as a catalyst for organic transformations, the field has seen an exponential increase in growth. Au(I) and Au(III) complexes are now some of the most investigated for homogeneous catalysis and arguably the current "gold" standard for activation of carbon π-systems. In previous sections, the classical reactivity of nucleophilic additions to Au(I)-activated alkynes was outlined, but in no means was a comprehensive overview of such a large field. In this section, a few other meaningful and miscellaneous transformations mediated by Au(I) will be covered that have been of interest in the field.

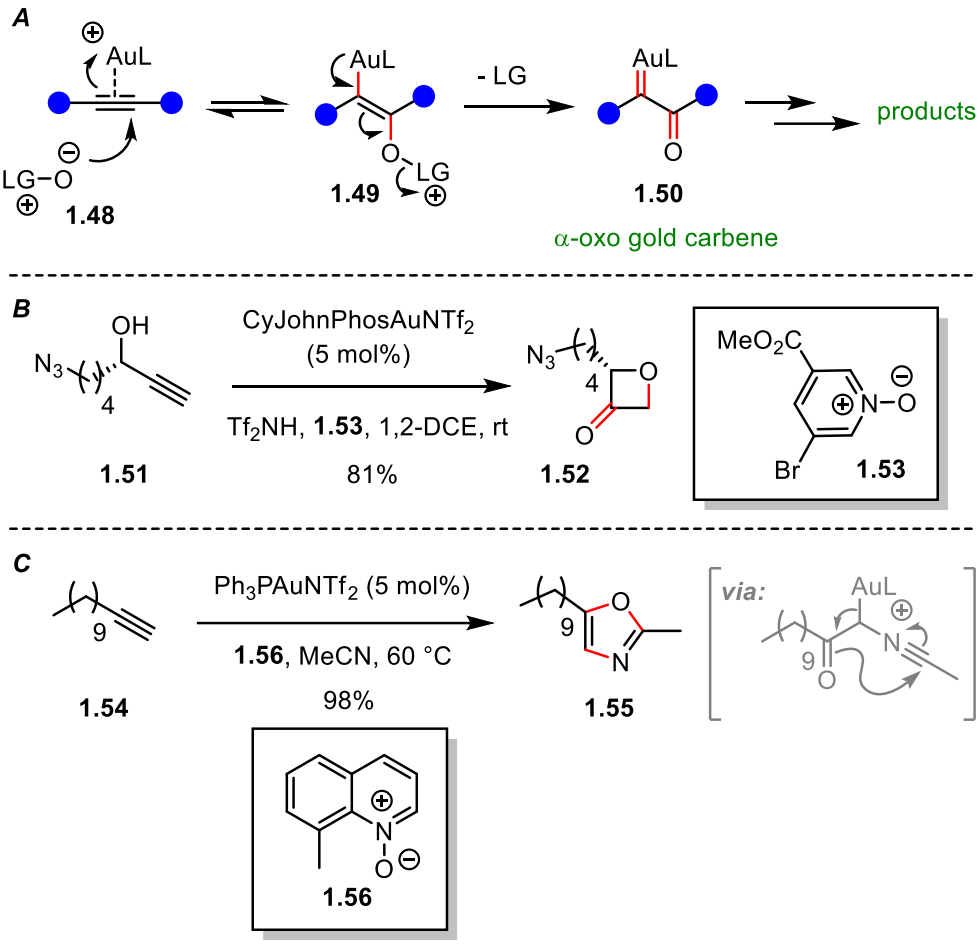
The rearrangement of propargylic esters such as acetates using Au(I) catalysis has received considerable attention from the synthetic community.[44] Like the enyne cycloisomerization discussed previously, the mechanistic aspects of this rearrangement reaction are complex and can depend on several factors such as the type of catalyst being used, the ligand, and the identity of the substrate. Upon coordination of the gold catalyst to the alkyne, the alkyne undergoes an intramolecular nucleophilic addition by the acetate group in either a 5-*exo*-*dig* or 6-*endo*-*dig* fashion, also referred to as 1,2-acyloxy or 1,3-acyloxy migrations respectively (Scheme 1.6A). The outcome of this step is typically dependant on the structure of the substrate and the reaction conditions being used, with sometimes the two pathways being competitive.[45, 46] After the 1,2-acyloxy migration, the corresponding vinyl gold species **1.42** can then form a gold carbene **1.43**, breaking the initial C-O bond in the substrate. Gold carbene **1.43** can then go on to form various kinds of products. In the case of 1,3-acyloxy migration, the vinyl gold intermediate **1.44** can undergo deauration and form a Au-activated allene intermediate **1.45** which can also lead to a variety of products being formed. There have also been proposals that gold coordinated allene **1.45** and gold carbene **1.43** have the potential to interconvert, adding an extra layer to this mechanism. Previous work from the Gagosz group took advantage of this reactivity by demonstrating the efficient synthesis of highly reactive and useful β-trifluoromethylated enones **1.47** from trifluoromethyl substituted propargylic acetates **1.46** (Scheme 1.6B).[47] The product is formed *via* the 1,3-acyloxy migration pathway, where the Au(I)-activated allene suffers nucleophilic addition by water under the reaction conditions. The corresponding products were also shown to nicely participate in Diels-Alder reactions in the same pot.



Scheme 1.6. (A) General mechanism for the Au(I) catalyzed rearrangement of propargylic acetates and (B) one pot synthesis of β-CF_3-enones

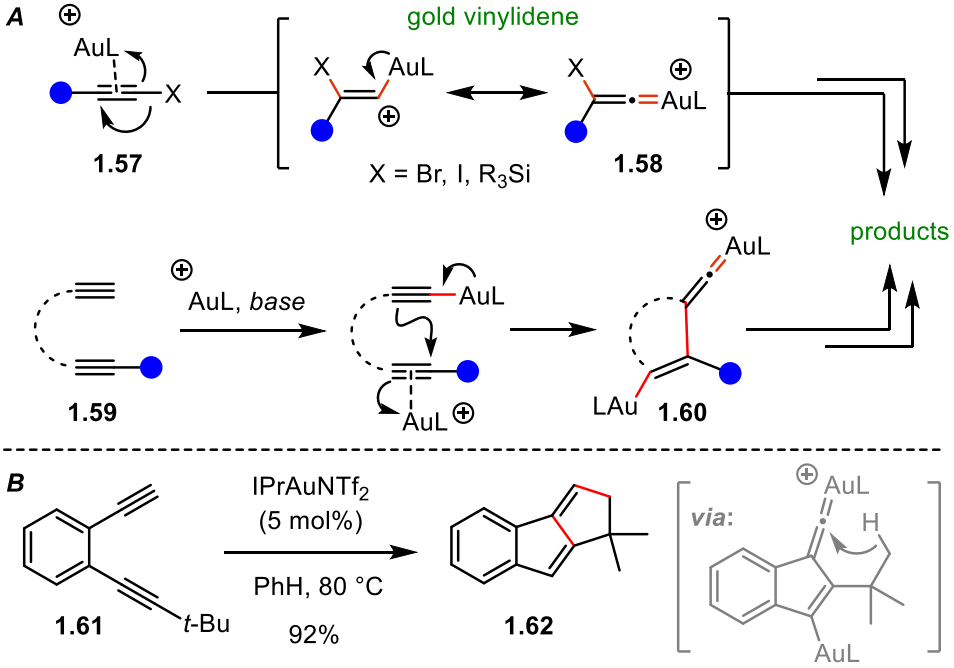
As shown previously, gold carbene intermediates may be generated through isomerization reactions, however they can also be generated in an oxidative manner from Au(I)-activated alkynes. Formation of gold carbenes in this manner has been studied extensively over the last decade by several research groups.[48, 49] Utilization of a nucleophilic oxidant such as **1.48** which bears a weak O-LG bond is critical to the success of this type of transformation (Scheme 1.7A). After the Au(I)-alkyne complex undergoes addition and forms alkenylgold species **1.49**, a subsequent fragmentation reaction of the weak O-LG bond may take place, forming an α-oxo gold carbene intermediate **1.50** that can participate in a variety of reactions owing to its high reactivity. Importantly this method avoids the synthesis of analogous α-diazo carbonyl compounds as carbene precursors since they can pose as a potential explosion hazard. Additionally, if a nucleophile containing a weak N-LG bond is used, the resulting product is known as an α-imino gold carbene and these will be discussed further in Chapter 2 of this thesis. Various kinds of nucleophilic

oxidants may be used to do this chemistry such as pyridine/quinoline *N*-oxides, nitro groups, nitrones, and sulfoxides. Early work from the group of Zhang showed that using pyridine *N*-oxide **1.53** as an oxidant with chiral propargylic alcohol substrate **1.51** led to the efficient synthesis of pharmaceutically relevant and enantiomerically enriched oxetan-3-ones **1.52** (Scheme 1.7B).[50] Acid additives are usually necessary when using these oxidants in order to neutralize the pyridine by-products which may otherwise impede catalysis. Nucleophilic trapping of α-oxo gold carbenes can also trigger other transformations if the appropriate nucleophile is used. For example, using acetonitrile as solvent, the group of Zhang was able to show that the α-oxo gold carbene generated from the reaction of terminal alkyne **1.54** with a quinoline *N*-oxide **1.56** as the oxidant could lead to the rapid synthesis of 2,5-disubstituted oxazoles **1.55** in one step (Scheme 1.7C).[51]



Scheme 1.7. (A) Formation of α-oxo gold carbenes and (B) examples using *N*-oxides as oxidants

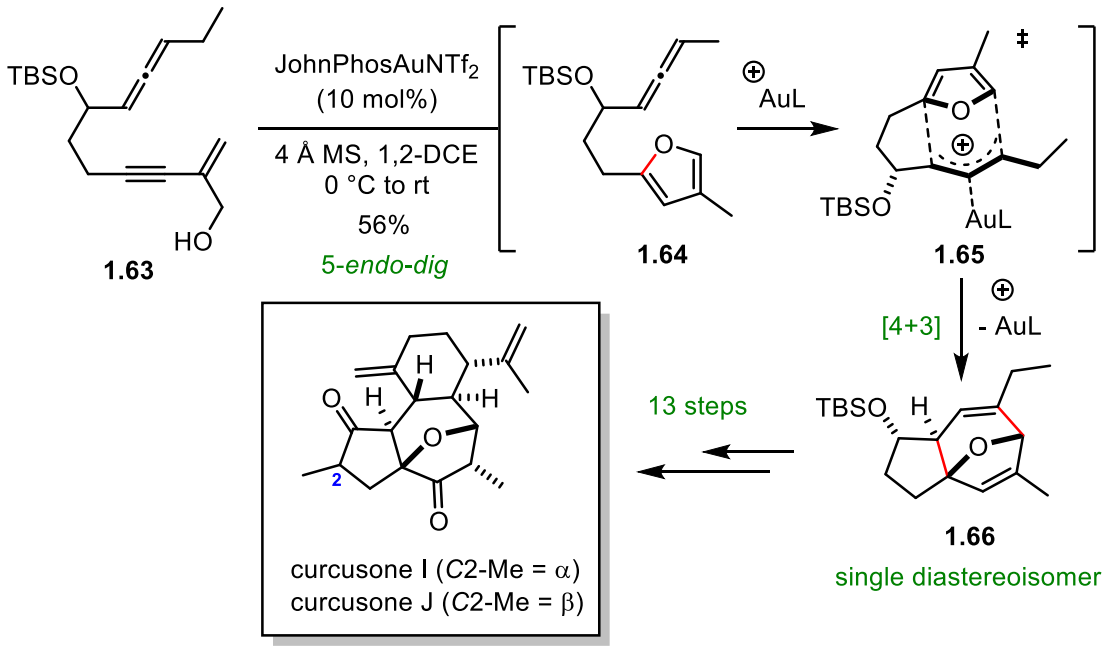
Like the generation of gold carbenes as reactive intermediates, another area of gold catalysis is in the generation of intermediates known as gold vinylidenes. These highly reactive species have garnered interest in recent years, despite being known since 2004.[52] Unlike the plethora of methods that may be used to access gold carbenes,[53, 54] access to gold vinylidenes is not as well developed, which may have limited their use in the past. In general, two main modes exist for generating gold vinylidene intermediates. The first is through the 1,2-migration of substituted alkynes **1.57** (Scheme 1.8A) to give gold vinylidene **1.58**. The second and more common method is through taking advantage of dual-gold catalysis which is based on the use of diyne substrates such as **1.59**. Here, the initial generation of a nucleophilic Au(I)-acetylide is required to engage with an electrophilic Au(I)-alkyne complex on the same substrate, forming the corresponding Au(I)-vinylidene **1.60**. Once the gold vinylidene intermediates are formed, they have been known to engage in C-H insertion reactions,[55, 56] nucleophilic additions,[57, 58] and cyclopropanation cascades.[59] An example of gold vinylidene generation using dual-gold catalysis from the group of Hashmi is shown below (Scheme 1.8B). In their case, the use of diyne **1.61** allowed for the synthesis of benzofulvenes **1.62** *via* a gold vinylidene intermediate which formally inserted into the C-H bond of the pendant *tert*-butyl group on the substrate.



Scheme 1.8. Generation and reactions of Au(I)-vinylidene intermediates

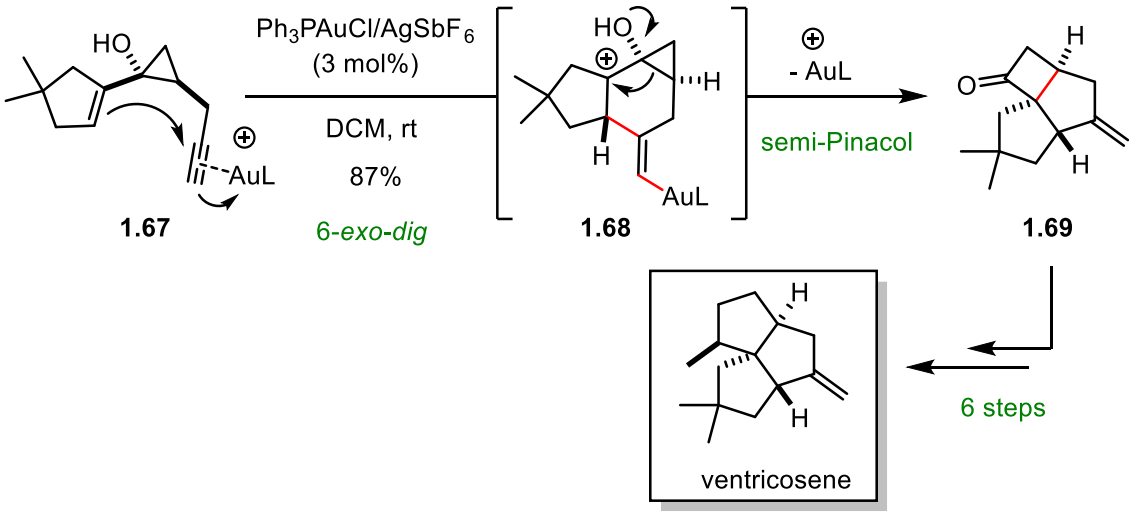
1.3 Gold catalysis in total synthesis

Au(I) catalysis has been applied extensively to total synthesis in the literature owing to its ease of use and functional group compatibility.[5, 60] In this context, gold catalysis is often used during the key step of a synthetic sequence to access a core scaffold for various natural products. Gold has the unique ability to mediate a myriad of complex transformations, particularly through cascade reactions and it is of no surprise that this has been taken advantage of for the synthesis of complex molecules. A few examples which showcase this type of reactivity will be discussed below. In 2017, the group of Dai reported on the racemic synthesis of two rhamnofolane diterpenoids curcusones I and J utilizing a novel Au(I)-cascade reaction of furan formation and furan-allene [4+3] cycloaddition (Scheme 1.9).[61] Despite the synthesis revealing the misassignment of the structures for curcusones I and J, the tandem Au(I)-cascade proved to be broadly tolerant and scalable, highlighting the usefulness of gold catalysis in general. It allowed the authors to construct the complex core 5-6-5 ring system of the natural product in one step from starting material **1.63**. When **1.63** was exposed to JohnPhosAuNTf$_2$ as a catalyst, this induced the formation of the furan ring *via* an initial nucleophilic attack of the pendant alcohol followed by isomerization and catalyst regeneration to give furan intermediate **1.64**. Like alkynes, allenes are also highly susceptible to activation by cationic Au(I) complexes (for much the same reasons) and this prompted a furan-allene [4+3] cycloaddition to take place *via* transition state **1.65** to give the final product **1.66** in good yield and excellent diastereoselectivity.



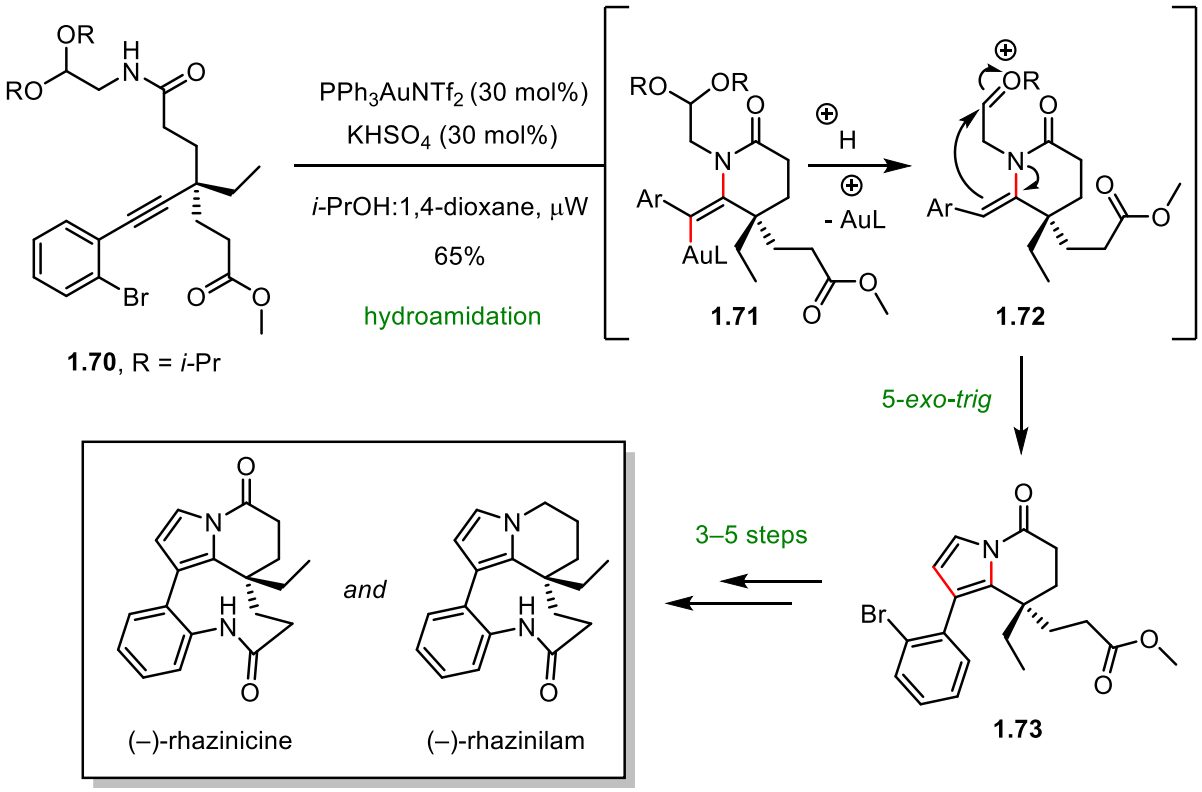
Scheme 1.9. Tandem Au(I) catalyzed furan formation/furan-allene [4+3] cycloaddition cascade for the core synthesis of the reported structures of curcusones I and J

As mentioned previously, the 1,6-enyne cycloisomerization is a powerful method in the Au(I) catalysis repertoire for rapid access to structures of high complexity. The group of Toste found that 1,6-enyne substrate **1.67** which contained an appended cyclopropanol could be used to effectively generate cyclopropylmethyl cation intermediate **1.68** *via* a 6-*exo*-*dig* cyclization, which then underwent semi-Pinacol rearrangements to form cyclobutanone **1.69** in a highly diastereoselective manner and in an 87% yield. They applied this unique methodology to the total synthesis of an angular triquinane known as ventricosene (Scheme 1.10).[62]



Scheme 1.10. Au(I) catalyzed 1,6-enyne cycloisomerization for rapid access to the angular diquinane core of ventricosene

Au(I) catalysis has also been exploited in the protecting group free synthesis of the natural products (–)-rhazinicine and (–)-rhazinilam by the group of Tokuyama.[63] The key step in the synthesis focused on a Au(I) catalyzed intramolecular secondary amide hydroamidation/enamide cyclization cascade in order to construct the indolizinone core (Scheme 1.11). Starting from sterically congested alkyne **1.70**, the authors were able to perform a hydroamidation reaction of the alkyne under their optimized conditions at 80 °C but found the yield of the desired indolizinone product **1.73** to be low. Ultimately, they found using microwave irradiation under acidic conditions was optimal to achieve the product in good yield (65%). Upon gold activation, the hydroamidation of the amide took place in a 6-*exo*-*dig* fashion to give enamide **1.71**. Under the acidic conditions of the reaction, an oxonium ion **1.72** could form, which was followed by spontaneous cyclization of the enamide function and aromatization to give the desired product **1.73**.



Scheme 1.11. Intramolecular hydroamidation/enamide cyclization cascade as a key step towards the total synthesis of (–)-rhazinicine and (–)-rhazinilam

1.4 Conclusion

The field of homogeneous gold catalysis has expanded exponentially over the last three decades, what is termed the so called "gold rush". Over the years, several kinds of transformations have been developed including the addition of various kinds of nucleophiles, rearrangement reactions, oxidations and cycloisomerizations. The overall advantage of gold in synthesis and catalysis is highlighted through its ease of use (air and moisture tolerant), high atom economy/functional group compatibility and often a tremendous increase in molecular complexity is achieved from much simpler building blocks when compared to other transition metals as highlighted by several examples of using gold in the context of total synthesis.

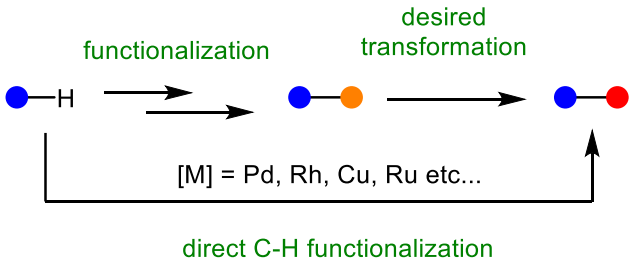
CHAPTER 2

Au(I) Catalysis in the α-C-H Functionalization of Tertiary Amines

2.1 Introduction

2.1.1 Csp^3-H functionalization

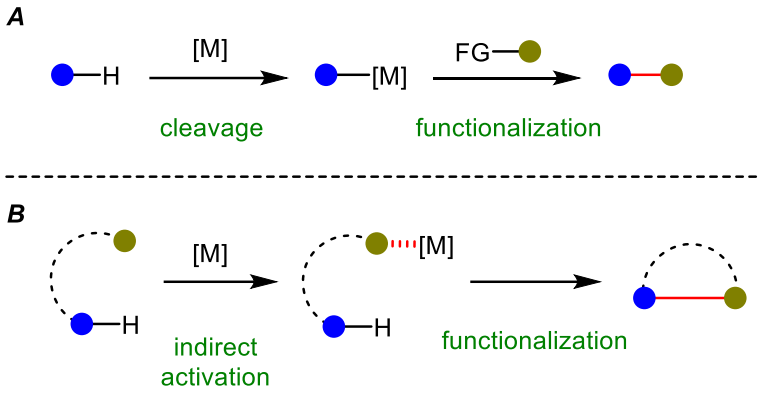
The formation of new C-C and C-X bonds using electrophilic activation has been the driving force for much of the early work in the field of homogeneous gold catalysis. Alkane Csp^3-H bonds are ubiquitous in organic chemistry but are notorious for their high thermodynamic stability, low chemical reactivity, and are not always thought of as being an appropriate functional group for direct functionalization reactions. In classical methods, a substrate is typically pre-functionalized with a reactive group (often taking several steps to make) and is then used to accomplish an intended transformation. Using the C-H bond as a reactive center would bypass the additional steps of pre-functionalization and allow for a highly desirable and direct access to new C-C and C-X bonds (Scheme 2). Within the literature, various transition metals such as palladium,[64, 65] copper,[66] and rhodium[67] have been used to accomplish this chemistry, however gold has not received nearly as much attention.[68] This is due to the innate Lewis acidic properties of Au(I) and Au(III) complexes for the electrophilic activation of carbon π-systems and as such, the direct functionalization of Csp^3-H bonds (while highly desirable) remains a challenge using gold catalysis.



Scheme 2. Classical functional group interconversion as compared to more direct C-H functionalization pathway

Most transition metal catalyzed C-H functionalizations proceed through one of two mechanisms: "inner sphere" or "outer sphere".[69] Mechanisms where the metal-mediated abstraction of the C-H bond leads to a new C-M bond are considered "inner sphere" (Scheme 2.1A). On the other hand, reactions that do not involve the need for direct interaction with the C-

H bond are considered “outer sphere”, which is mostly the case with mechanisms involving Au(I) (Scheme 2.1B) and what will be reviewed in this section.

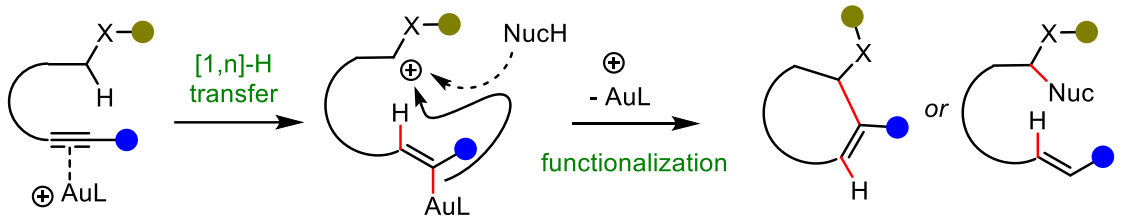


Scheme 2.1. General representation of (A) “inner sphere” and (B) “outer sphere” mechanisms for transition metal catalyzed C-H functionalization reactions

2.1.2 Au(I) catalyzed redox-neutral hydrogen atom transfer

As was mentioned above, processes which involve Csp^3-H bond activation using Au(I) catalysis typically take place *via* an “outer sphere” mechanism. These reactions are typically intramolecular and occur through hydride transfer which is initiated from the classical electrophilic activation mode of Au(I) with alkynes (Scheme 2.2). Furthermore, intramolecular hydride transfers to carbon based π-systems represents an interesting approach to promote C-H functionalization reactions through a redox-neutral pathway.[70] Previous C-H functionalization strategies have traditionally relied on the use of external or internal oxidants (usually a high valent transition metal) which are directed to activate the C-H bond of interest (similar to what is shown in Scheme 2.1B).[71] The hydride transfer approach is an alternative to this method since it does not rely on the installation/removal of directing groups and no additional redox reagents are required, rendering the overall process far more green and atom economical.[72] Intramolecular hydride transfers onto π-unsaturation’s also offers the opportunity to perform further chemical derivatization downstream. The appropriate hydride donor in this reaction is formally oxidized and becomes electrophilic in nature. When the Au(I) activated alkyne accepts the hydride, it is then formally reduced. Therefore, the resulting intermediate from this process can undergo further

functionalization (usually at the site of the C-H bond), which represents a unique opportunity to further build complexity in a cascade process.



Scheme 2.2. C-H functionalization using Au(I) catalysis by means of redox-neutral [1,n]-H transfer strategies

A variety of hydride donors can also be used to accomplish this transformation. Typically, they will have heteroatoms (nitrogen, oxygen) α to the migrating hydrogen atom or aryl/alkyl groups can also be used but are less common (Figure 2A). Utilizing donors which possess a heteroatom is advantageous due to stabilization of carbocation character from resonance.[73] Thus, substituted amines and ethers are both excellent hydride donors. Migrations can also occur from hydrogen atoms α to aryl and *tert*-alkyl groups but to a lesser extent. Negative hyperconjugation effect is another advantage (Figure 2B). Interaction of the heteroatom lone pair with the σ* antibonding orbital of the Csp^3-H bond helps to not only weaken the bond, but to also increase the hydridic character of the hydrogen atom with more electron density.

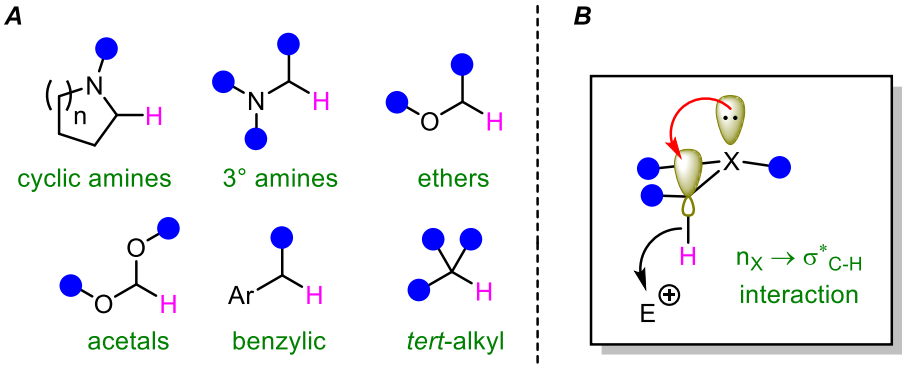
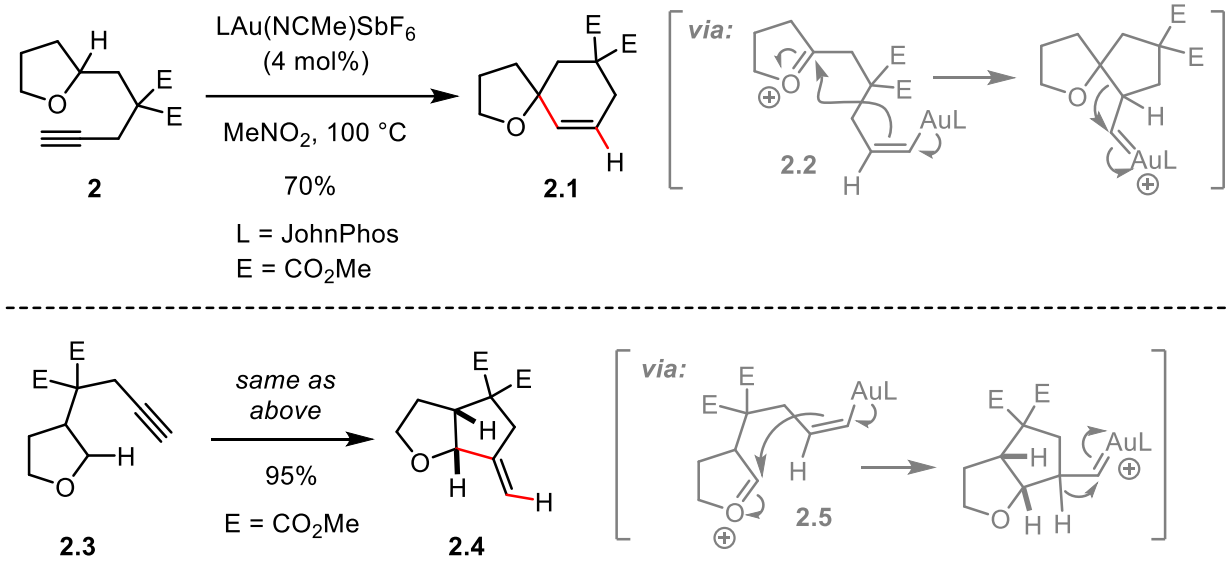


Figure 2. (A) Classical hydride donors and (B) orbital diagram for heteroatom assisted hydrogen atom migration

2.1.2.1 Dialkyl ether and benzyl ether hydride donors

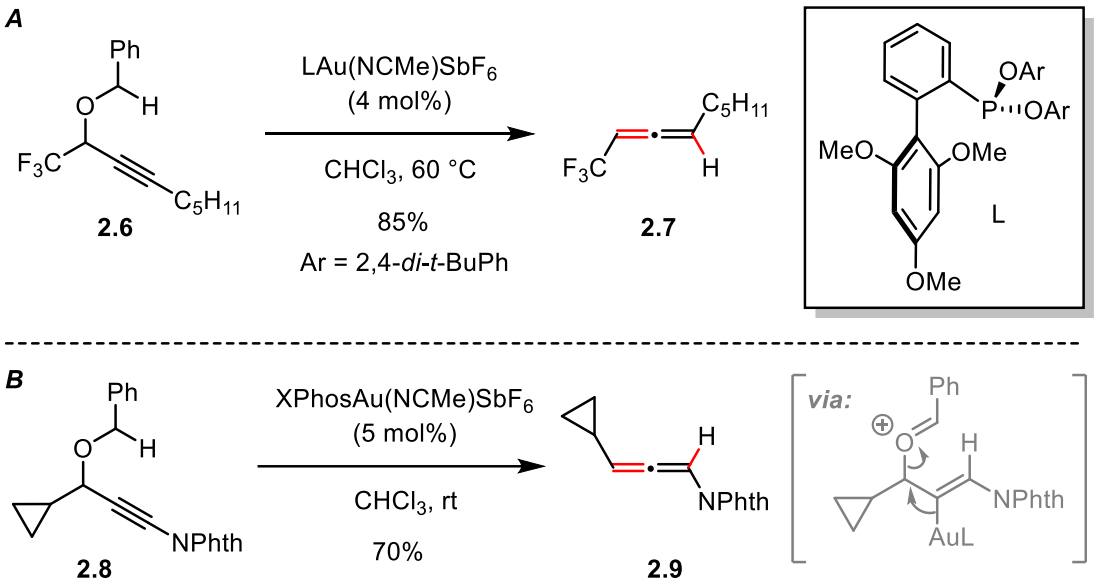
In the context of Au(I) catalysis, hydride transfer from ether donors is well documented with several pioneering contributions from the Gagosz group demonstrating this reactivity. A few of these examples will be discussed here. Gagosz and co-workers were able to perform a Au(I) catalyzed hydroalkylation reaction using alkynyl ethers *via* a [1,5]-H transfer/cyclization cascade sequence (Scheme 2.3).[74] If the alkynyl ether being used possessed a secondary or tertiary Csp^3-H bond (**2.3** or **2**), they were able to obtain either 5-*exo*-alkenylation or 6-*endo*-alkenylation products **2.4** and **2.1** respectively. The authors also found that selectivity of the reaction was highly dependent on steric factors as well as substitution of the alkyne. Based on deuterium labelling experiments, the mechanism for formation of either **2.1** or **2.4** is believed to begin with a [1,5]-H transfer onto the Au(I) activated alkyne giving oxonium ions **2.2** or **2.5**. After subsequent cyclization, a [1,2]-alkyl or H-shift gives the final products.



Scheme 2.3. Hydroalkylation of alkynyl ethers *via* a Au(I) catalyzed [1,5]-H transfer/cyclization cascade

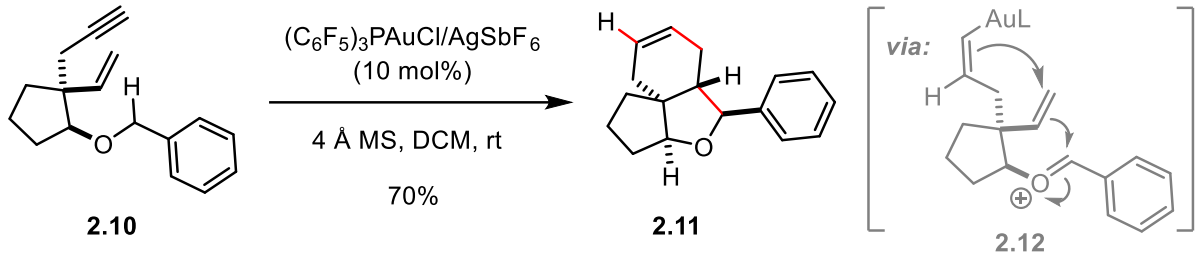
In cases where recombination is not favored (ie: cyclization to form small rings), a fragmentation pathway can be preferred. This has also been demonstrated by the Gagosz group in several publications, where they use a hydride transfer/fragmentation sequence to synthesize different allene building blocks.[75-77] Two examples of this include the synthesis of

trifluoromethylated allene **2.7** (Scheme 2.4A) and allenamide **2.9** (Scheme 2.4B) from α-CF_3 propargyl benzyl ether **2.6** and an ynamide **2.8** that has a benzyl ether at the propargylic carbon. In both instances, after the migration of the hydride in a [1,5] fashion, elimination and regeneration of the gold catalyst affords the substituted allene products in addition to one equivalent of benzaldehyde.



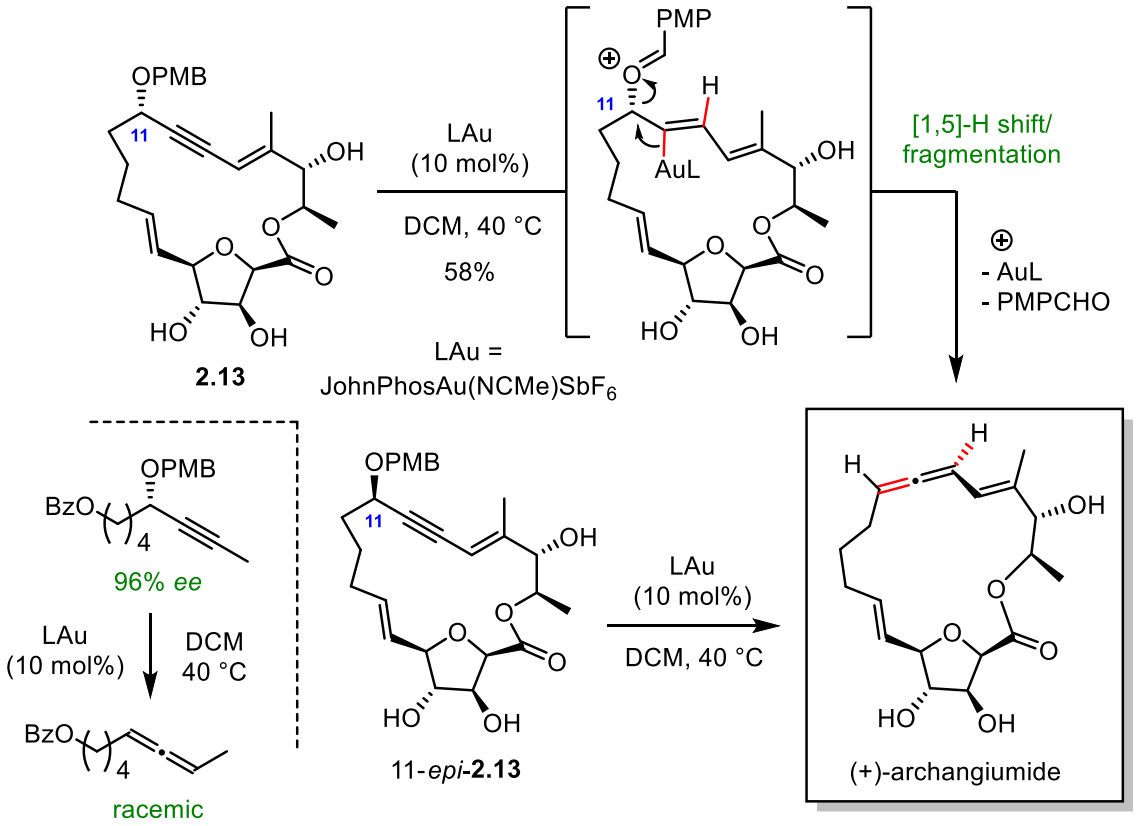
Scheme 2.4. Synthesis of allene building blocks by Gagosz and co-workers using a Au(I) catalyzed [1,5]-H transfer/fragmentation cascade

In 2018, the groups of Wong and Peng reported a tandem cycloisomerization protocol that hinged on a key hydrogen transfer event onto a gold activated alkyne complex.[78] They used 1,5-enyne substrate **2.10** which contained a benzyl ether group (Scheme 2.5). According to their deuterium labelling studies, they propose a [1,6]-H transfer event that is triggered by the electrophilic gold-alkyne complex to give oxonium ion **2.12**. Next, double cyclization in a Prins-like manner and subsequent elimination of the gold catalyst afforded the tricyclic product **2.11**. Remarkably, benzyl ether hydride donors are not required for this cascade process and even less activated dialkyl ethers can be used with modest success.



Scheme 2.5. Tandem Au(I) catalyzed cycloisomerization triggered by a [1,6]-H transfer

A novel utilization of benzyl ethers as potent hydride donors has been very recently demonstrated by the group of Fürstner in their total synthesis (+)-archangiumide (Scheme 2.6).[79] This unique polyketide natural product contains an endocyclic allene within a 17-membered macrolactone ring. The Fürstner group accomplished this total synthesis by using the Au(I) catalyzed rearrangement of propargyl benzyl ethers into allenes as a key step. They used the macrocylic alkyne **2.13** and found the rearrangement to proceed with good efficiency and isolated the natural product as a single diastereomer. Curious about the stereochemical outcome of the rearrangement, the authors also synthesized 11-*epi*-**2.13** and submitted it to their optimized conditions. They found that despite the inverted stereocenter at *C*11, they only obtained (+)-archangiumide as the sole product. A separate control experiment using a stereodefined yet truncated version of the substrate showed that all stereochemical information was lost during the gold catalyzed rearrangement. This led the authors to conclude that the formation of (+)-archangiumide is under thermodynamic control with the stereochemical outcome being dictated by the conformation of the macrocycle.

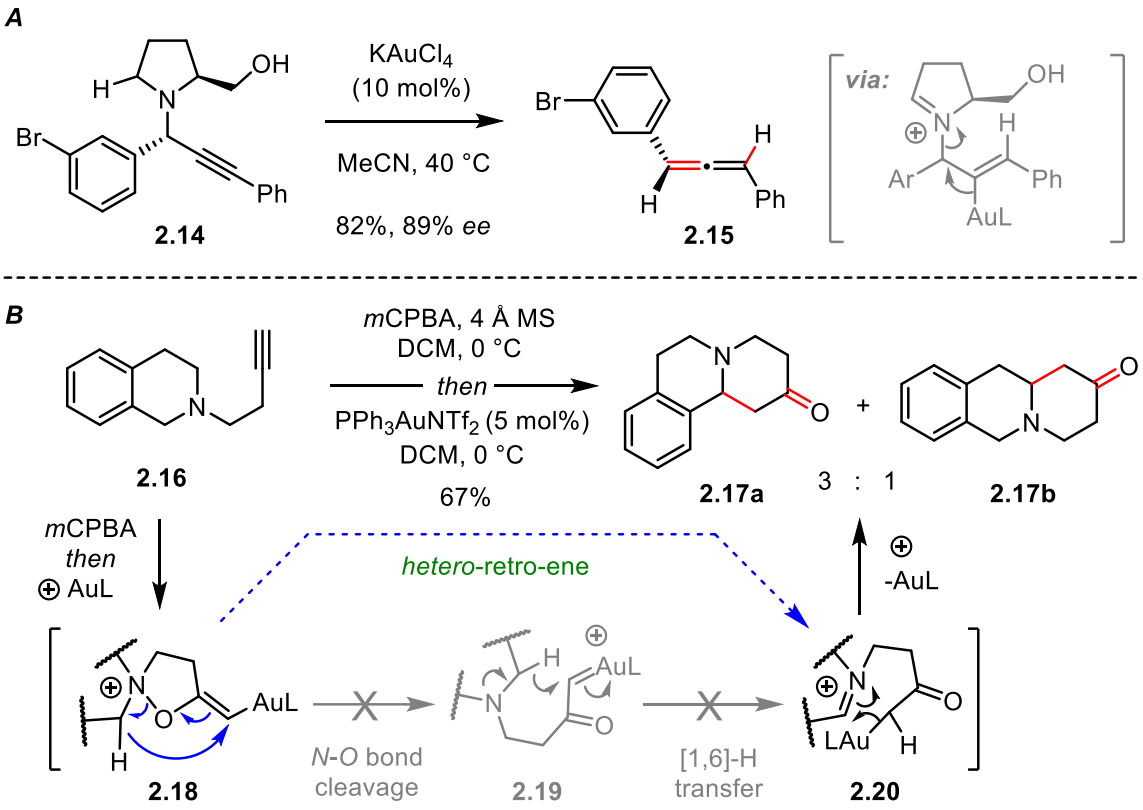


Scheme 2.6. Total synthesis of (+)-archangiumide using Au(I) catalyzed hydride transfer as a key step

2.1.2.2 Tertiary amine hydride donors

Unlike reactions involving ether hydride donors, Au(I) catalyzed C-H functionalization reactions on free amine substrates present a different challenge. Free amines are well-established as coordinating freely to Lewis acidic Au(I) and Au(III) complexes, rendering this sort of transformation difficult and preventing catalysis from happening. To the best of our knowledge, only a handful of reports demonstrating this kind of reactivity with free amines have been published to date and will be touched upon in this section. An early report from the group of Che and Wong showed that axially chiral allene **2.15** could be synthesized from chiral propargyl amine **2.14** using a Au(III) catalyst (Scheme 2.7A).[80] Based on some deuterium labelling and cross-over experiments, they proposed a tentative mechanism of [1,5]-H transfer exclusively from the least substituted position, followed by fragmentation to the allene. While this report does not involve the subsequent functionalization of the C-H bond of interest, it still demonstrates the feasibility of

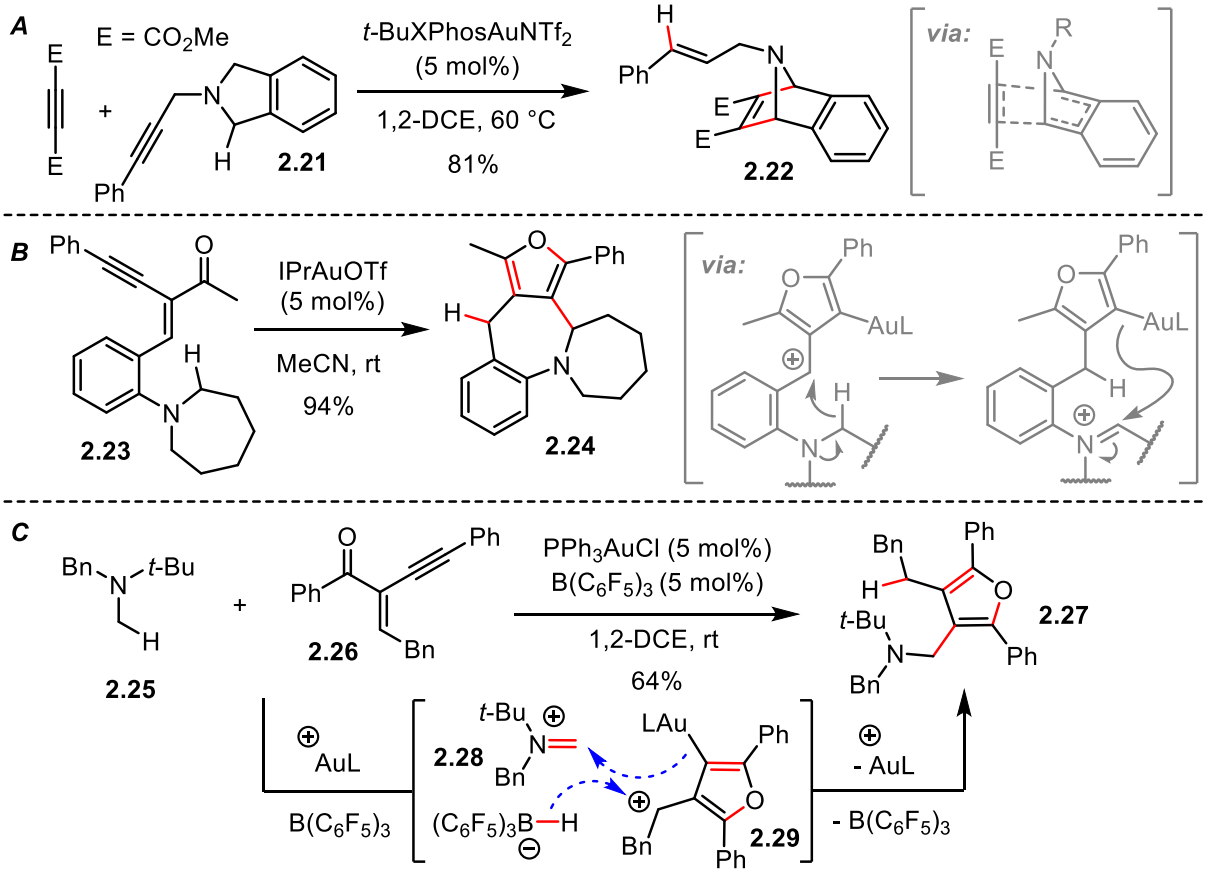
performing such a transformation. A different approach to this challenge was shown by the groups of Zhang and Houk who used *in-situ* formed *N*-oxides as substrates to synthesize regioisomeric 4-piperidone products **2.17a** and **2.17b** (Scheme 2.7B).[81, 82] The *N*-oxide was synthesized from homopropargyl amine **2.16** using *m*CPBA as an oxidant and then PPh_3AuNTf_2 was added as a catalyst *in-situ*. In the initial publication, the mechanism was believed to involve the formation of an α-oxo gold carbene intermediate **2.19** (generated from *N*-oxide adduct **2.18**), [1,6]-H transfer onto the gold carbene to form iminium **2.20**, and subsequent recombination. Computational evidence later showed that the more likely mechanism was a concerted hydrogen atom transfer event from adduct **2.18** that likely involves a *hetero*-retro-ene process.



Scheme 2.7. Au(I) catalyzed reactions of tertiary amine derivatives

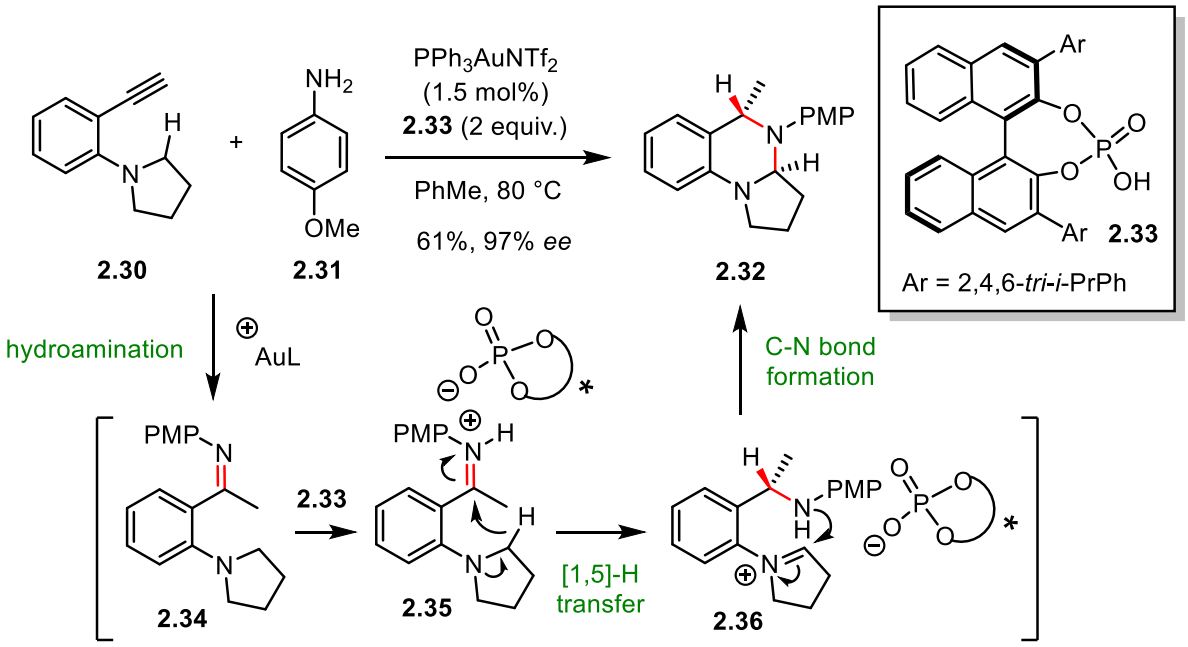
Previous studies of Au(I) catalyzed hydride transfers onto alkynes have shown [1,5]-H transfer processes in tandem with simple recombination's to form a new C-C bond or eliminations to form allenes. Gong and coworkers have demonstrated that other cascade reactions are possible after the initial [1,5]-H transfer event.[83] They showed that alkynyl indoline substrate **2.21** could

undergo a [1,5]-H transfer/isomerization/Diels-Alder cascade to synthesize bridged bicyclic products such as **2.22** (Scheme 2.8A). This is made possible through the propensity of the indoline motif to behave as a masked diene, triggering the [4+2] reaction with a suitable dienophile such as DMAD as shown below. The group of Zhang have also shown that yne-enone **2.23** with a tertiary amine could undergo a domino Au(I) catalyzed process involving furan formation/[1,5]-H transfer/cyclization to afford furanyl tetrahydroazepine **2.24** (Scheme 2.8B).[84] Using a chiral phosphine ligand, the resulting product **2.24** could be obtained in good yield with satisfying levels of enantioselectivity.[85] Most recently, the group of Wang has also shown that the C-H functionalization of tertiary amines could be realized through a borane and Au(I) co-catalytic system (Scheme 2.8C).[86] In the presence of the borane co-catalyst $B(C_6F_5)_3$, tertiary amine substrate **2.25** is proposed to undergo hydride abstraction and generates a stable iminium-borohydride ion pair **2.28**. This species then forms a C-C bond with furanyl gold intermediate **2.29** (generated separately from yne-enone **2.26** under Au(I) catalysis) to afford α-furan product **2.27**.



Scheme 2.8. Cascade processes for the Au(I) catalyzed C-H functionalization of tertiary amines

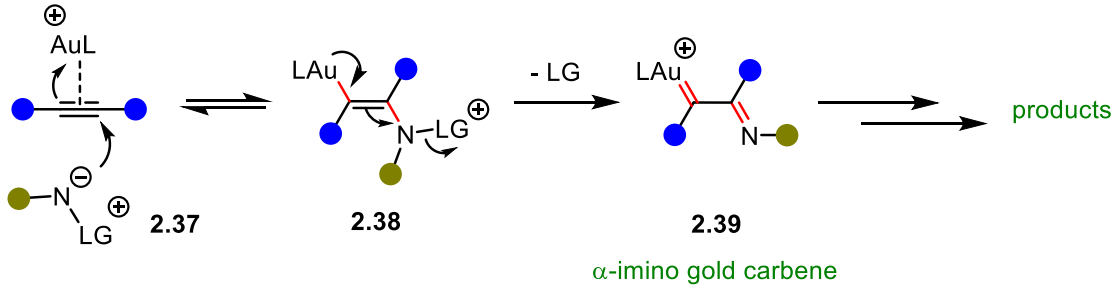
Besides the work done by the group of Zhang on enantioselective Au(I) catalyzed Csp^3-H functionalization reactions, the only other example of enantioselective amine functionalization was done by the group of Gong in 2013 (Scheme 2.9). Gong and co-workers developed a Au(I)/Brønsted acid catalyzed synthesis of cyclic aminals like **2.32** from readily available *ortho*-alkynyl aniline **2.30** in addition to exogenous aniline nucleophile **2.31**.[87] To make the reaction enantioselective, they employed the use of a chiral phosphoric acid such as **2.33**. Unfortunately, they found that catalytic quantities of **2.33** were not sufficient to afford high *ee* values and so a stoichiometric amount (2 equiv.) was used. As for the mechanism, the authors propose an initial intermolecular hydroamination of aniline **2.31** onto the Au(I) activated substrate **2.30** to form an intermediate imine **2.34**. In the presence of **2.33**, **2.34** is protonated and forms a chiral ion-pair complex **2.35**, suffering intramolecular [1,5]-H shift and giving a new iminium **2.36** which undergoes recombination to form the aminal product **2.32**.



Scheme 2.9. Cascade hydroamination/[1.5]-H transfer for the enantioselective synthesis of cyclic aminals

2.2 Au(I) catalyzed formal nitrene transfer reactions

Transition metal catalyzed nitrene transfer reactions have emerged as a highly versatile tool for the synthesis of nitrogen containing heterocycles.[88-90] Heterocycles are recurring scaffolds found in all manner of natural products and biological molecules. Their structural diversity is vast and new strategies towards these molecules is of utmost importance. In this regard, gold catalyzed formal nitrene transfers have become especially useful in the pursuit of efficient *N*-heterocycle synthesis throughout the last decade.[49, 91-95] The typical reaction profile for this type of formal nitrene transfer is shown below (Scheme 2.10). In the presence of an electrophilic Au(I)-alkyne complex, a nitrene-transfer reagent (or nucleophilic nitrenoid) such as **2.37** can interact in a reversible manner and form a vinylgold species **2.38**. Nitrene-transfer reagent is an umbrella term for a variety of *N*-containing compounds which can donate an electron pair and then lose a nucleofuge, generating carbenoid like character throughout the reaction. This typically manifests in the form of a reagent with a weak N-LG bond as shown below and that can be viewed as a synthon for a nitrene. From vinylgold intermediate **2.38**, cleavage of the labile N-LG bond can take place which would lead to the formation of key α-imino gold carbene species **2.39** that can evolve in several ways depending on the reaction conditions to produce the final *N*-heterocycle. Some of these can include 1,2-migrations, X-H insertions, and annulation reactions. This process is analogous to the formation of the more common α-oxo gold carbenes which were discussed briefly in Chapter 1. While the two are similar, there is the possibility of placing an extra substituent on the imino motif of carbene **2.39** that is not possible in the oxo derivative. This can open opportunities for additional diversity, further showcasing the usefulness of α-imino gold carbenes for heterocyclic synthesis.



Scheme 2.10. General mechanism for Au(I) catalyzed formal nitrene transfer onto activated alkynes

Throughout the literature, an increasing number of nitrene-transfer reagents utilized in gold catalysis have been discovered (Figure 2.1).[23] These can include cyclic aza-heterocycles such as isoxazoles, anthranils (benzisoxazoles), and 2*H*-azirines. Besides being cyclic, nitrene-transfer reagents can also be ylides such as *N*-pyridiniums and sulfilimines. Azides have also been extensively used as a highly convenient nucleophilic nitrenoid. For the remainder of this section, some representative examples of α-imino gold carbene formation will be discussed using different kinds of nitrene-transfer reagents but is by no means an exhaustive list.

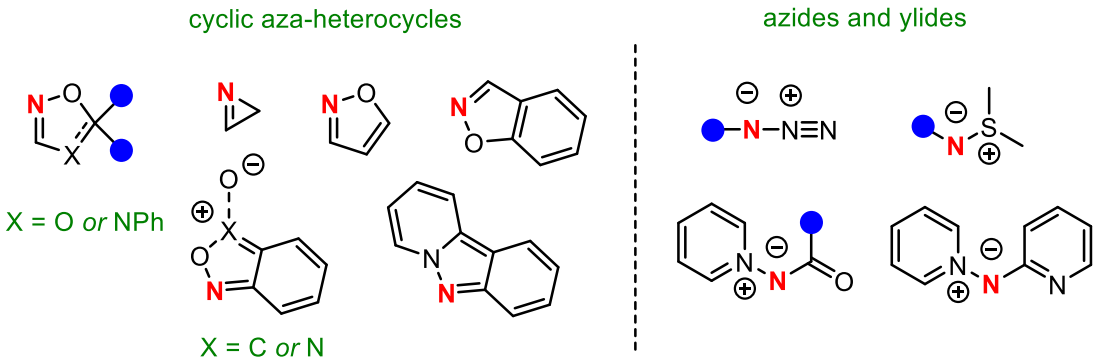
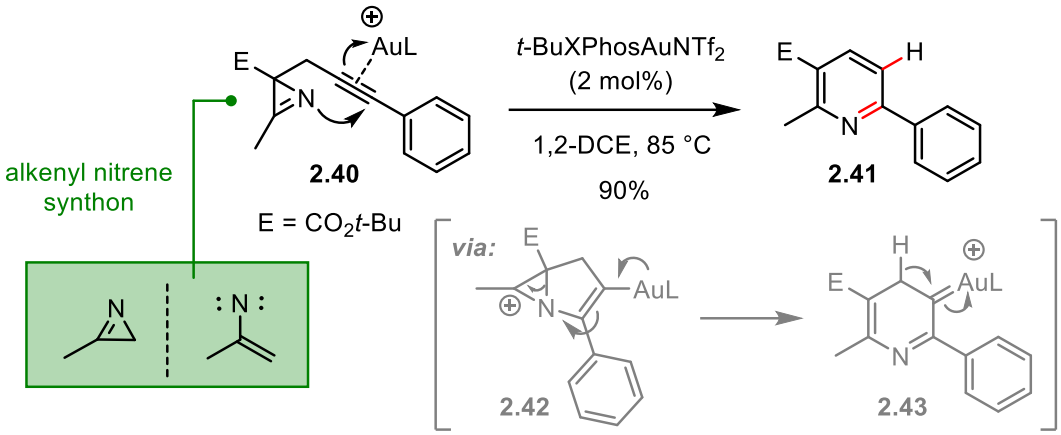


Figure 2.1. Structures for various types of nitrene-transfer reagents

2.2.1 Azirines

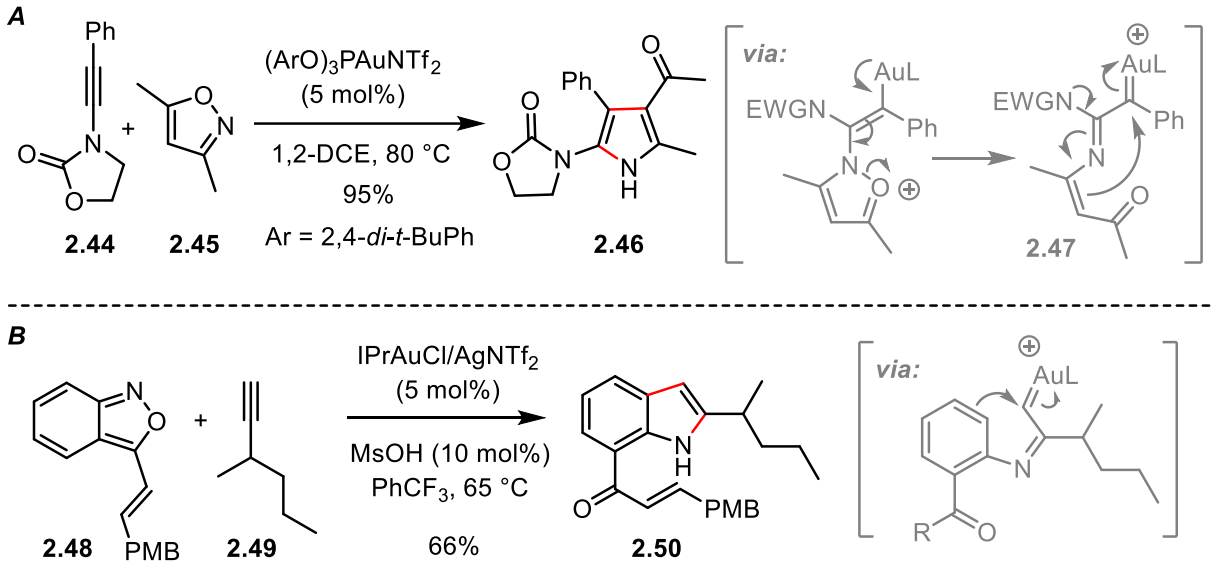
Work from the Gagosz lab has demonstrated that 2*H*-azirines can behave as competent precursors *en-route* to α-imino gold carbene intermediates. 2*H*-Azirines are strained three-membered heterocycles which serve as alkenyl nitrene equivalents (Scheme 2.11) and react in an unprecedented manner with alkynes. Gagosz and co-workers found that upon heating of propargyl 2*H*-azirine **2.40** in the presence of a gold catalyst resulted in the efficient synthesis of highly desirable tetrasubstituted pyridine building blocks such as **2.41**.[96] Mechanistically, the reaction is believed to begin with the initial 5-*endo*-*dig* cyclization of the 2*H*-azirine motif onto the Au(I)-alkyne complex, giving intermediate **2.42**. Next, opening of the azirine ring could take place with concomitant formation of the α-imino gold carbene intermediate **2.43**. A subsequent [1,2]-H migration and elimination of Au(I) would give the final product. Based on experimental results, the authors also proposed an alternative mechanism involving a concerted ring opening/[1,2]-H migration pathway, however this mechanism seems to be unlikely based on separate and further computational work done by the groups of Wu and Zhao.[97]



Scheme 2.11. Intramolecular synthesis of highly functionalized pyridines from 2*H*-azirines as masked alkenyl nitrenes

2.2.2 Isoxazoles and related derivatives

Owing to their weak N-O bond, isoxazoles and benzisoxazoles have also been used as nitrene-transfer reagents in gold catalyzed electrophilic cyclization reactions. Most of the work done with this class of nucleophilic nitrenoid has been with specially activated alkynes such as ynamides, owing to their poorer nucleophilicity. Furthermore, there is the possibility for nucleophilic addition from either oxygen or nitrogen and this can be dependent on the conditions of the reaction.[91] Additions from oxygen are beyond the scope of this thesis. In 2015, the groups of Ye and Lu reported on the formal [3+2] cycloaddition between ynamide substrate **2.44** and isoxazole **2.45**, giving rise to tetrasubstituted 2-aminopyrrole **2.46** (Scheme 2.12A).[98] The authors propose that after initial complexation of **2.44** with the gold catalyst, addition of **2.45** may take place to form α-imino gold carbene **2.47** *via* N-O bond cleavage. Subsequently, cyclization/loss of Au(I)/rearomatization occurs to give the product. Along the same theme, utilizing the benzisoxazole version can lead to a different outcome of the process and synthesis of a completely new heterocycle. Hashmi and co-workers have reported on the synthesis of indole products like **2.50** from terminal alkyne **2.49** and benzisoxazole **2.48** (Scheme 2.12B).[99] In this case, after formation of the α-imino gold carbene, it is intercepted by the aromatic ring of **2.48** which results in arylation and formation of the indole scaffold. Remarkably, product **2.50** happens to be a key precursor to the synthesis of pyrroloquinoline derivatives which demonstrate a wide range of biological activity.[100]

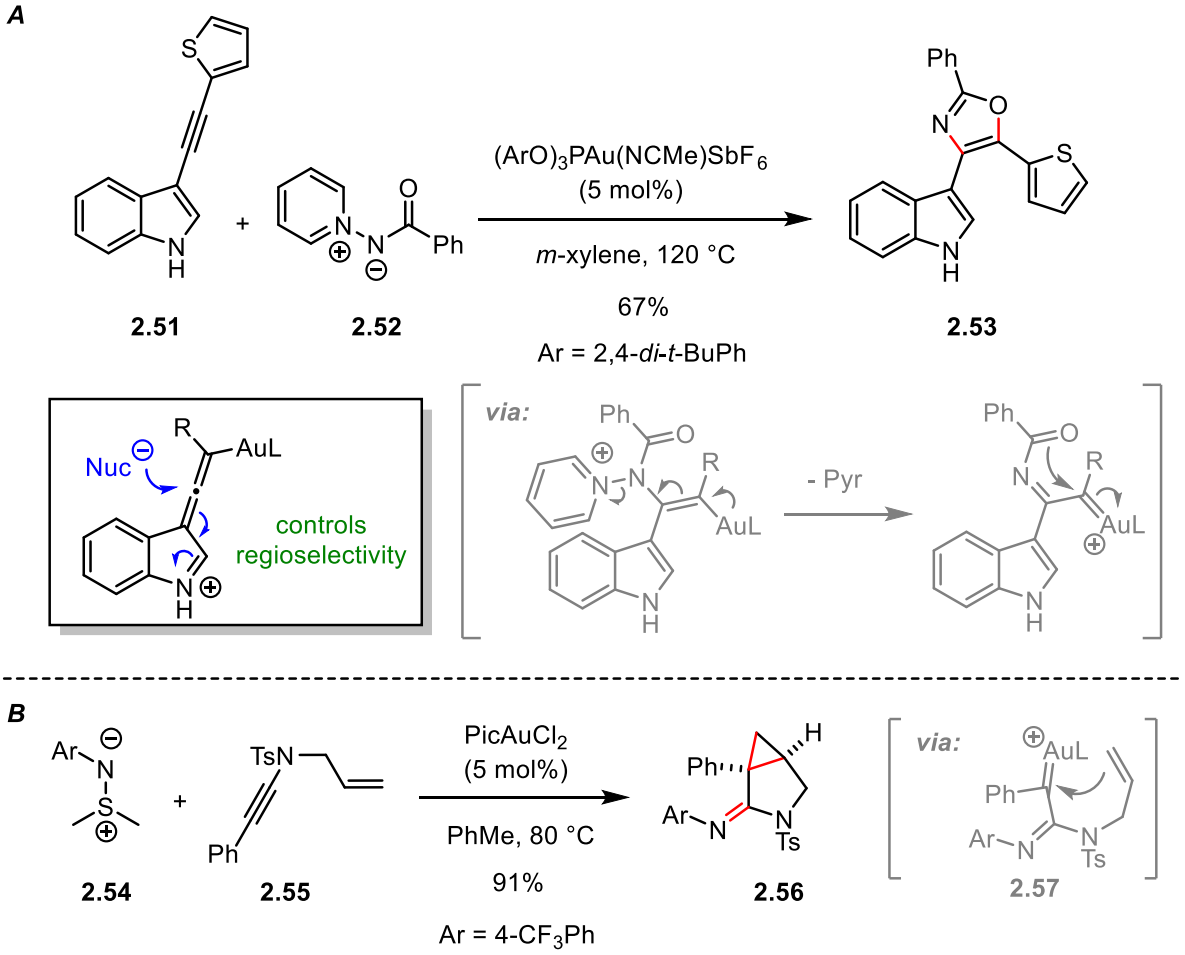


Scheme 2.12. Intermolecular synthesis of (A) tetrasubstituted pyrroles and (B) acyl indoles using isoxazoles and benzisoxazoles as nucleophilic nitrenoid precursors

2.2.3 *N*-pyridinium and sulfilimine ylides

N-Pyridinium and sulfilimine ylides have shown great promise as 1,3-dipole equivalents in gold catalyzed formation of α-imino gold carbenes and participating in formal [3+2] cycloaddition strategies. In this regard, Davies and co-workers have reported on the synthesis of fully substituted 2,4,5-triaryl oxazoles such as **2.53** from alkynyl indole **2.51** and an *N*-pyridinium salt **2.52** through a formal [3+2] cycloaddition, demonstrating excellent regioselectivity (Scheme 2.13A).[101] The regioselectivity is attributed to the polarization of the alkyne by the electron rich indole, directing addition of **2.52** to form the α-imino gold carbene after loss of pyridine. Further cyclization by the pendant acyl group onto the gold carbene and deauration afford the oxazole product. In this way, *N*-pyridinium **2.52** was able to function as a 1,3-*N*,*O*-dipole equivalent but other examples by Davies have also shown that these reagents are able to function as 1,3-*N*,*N*-dipole equivalents[102] as well, leading to different kinds of heterocycles. While *N*-pyridinium ylides have been used since 2011, sulfilimines did not find use until very recently by the group of Hashmi in 2019.[103] Employing a Au(III) catalyst, Hashmi and co-workers synthesized a variety of heterocycles including 2-aminoindoles, bicyclic pyrrolidines, quinolines, and imidazoles by varying slightly the structure of either the sulfilimine reagent **2.54** or the ynamide starting material **2.55**. A representative example for the synthesis of bicyclic pyrrolidine **2.56** will be shown

(Scheme 2.13B). From a mechanistic perspective, α-imino gold carbene **2.57** is formed *via* N-S bond cleavage and loss of dimethylsulfide. From there, cyclopropanation of the allyl group on ynamide **2.55** gives the final product **2.56**. The group of Hashmi later went on to publish several other reports of using sulfilimines in heterocyclic synthesis.[104-106]

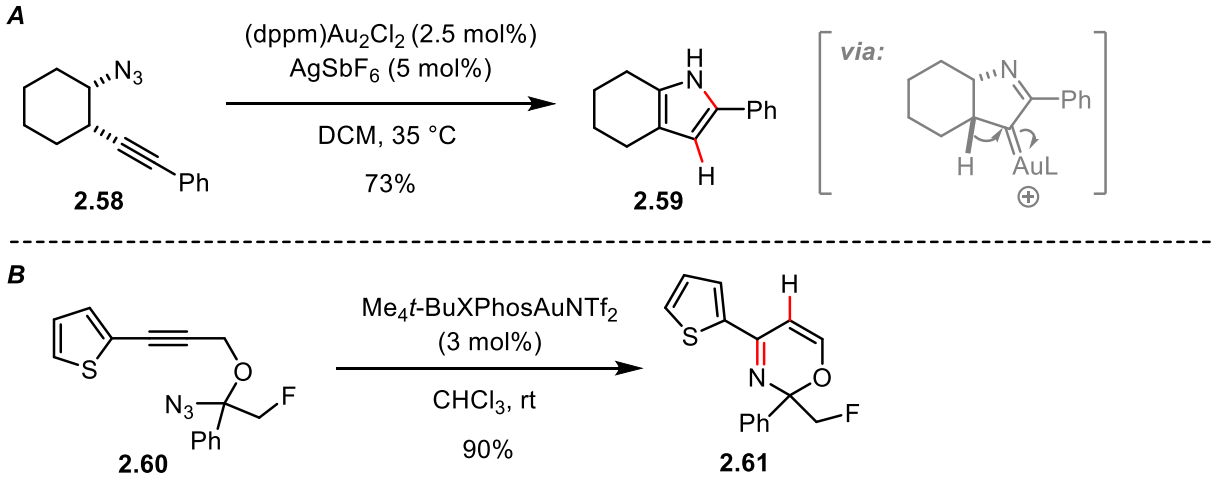


Scheme 2.13. Utilization of *N*-pyridinium and sulfilimine ylides for heterocyclic synthesis

2.2.4 Azides

The use of azides as nitrene-transfer reagents has been well documented for both inter- and intramolecular reactions. Azides are particularly attractive as nitrene precursors because they lose nitrogen gas during the reaction as a traceless and easy to remove by-product. The first example of using azides in the formation of α-imino gold carbenes was reported by Toste and co-workers in 2005 (Scheme 2.14A).[107] This acetylenic Schmidt reaction used *homo*-propargyl azide **2.58** in

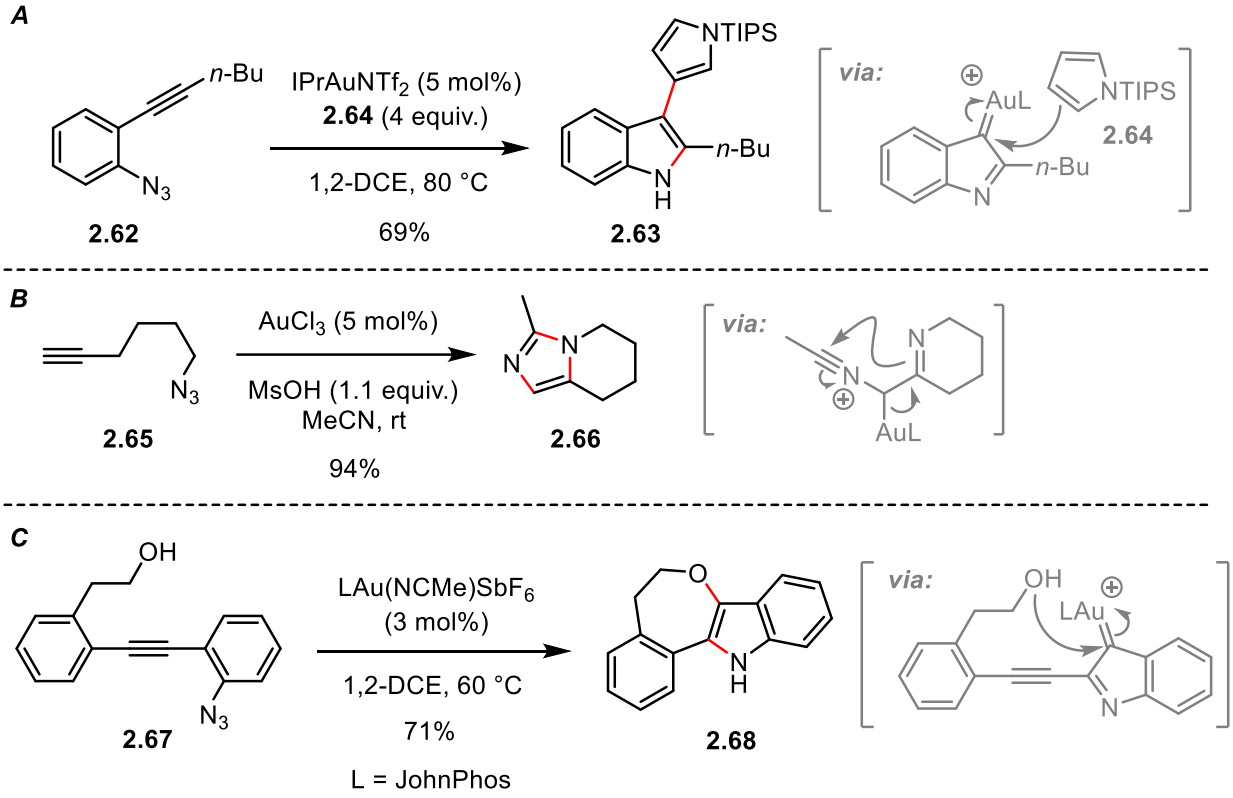
addition to a dimeric gold catalyst to synthesize pyrrole **2.59**. After nucleophilic addition of the azide (5-*endo*-*dig*) and extrusion of nitrogen gas, a [1,2]-H migration led to the final product. Gagosz and co-workers applied a similar strategy to form 1,3-oxazine **2.61** from alkyne **2.60** (Scheme 2.14B).[108] While most intramolecular additions of azides to alkynes occur in a 5-*endo* manner, substrate bias in **2.60** afforded 6-*endo* products which were not as common.



Scheme 2.14. Azides as nitrene-transfer agents in Au(I) catalysis with [1,2]-H migration onto α-imino gold carbenes

With azides, trapping of the transient α-imino gold carbene intermediate with either external or internal nucleophiles is a popular strategy for building complexity. Back-to-back, the groups of Zhang[109] and Gagosz[110] disclosed the synthesis of 3-substituted indoles like **2.63** from *ortho*-alknyl arylazide **2.62** (Scheme 2.15A). After the formation of the α-imino gold carbene, Zhang and co-workers focused on the addition of external arenes such as **2.64**. This effectively constituted an umpolung strategy to the indole nucleus since it reverses the naturally nucleophilic behaviour of the *C*3 position to electrophilic. Gagosz and co-workers focused on using allylic alcohols as the external nucleophiles. This report will be discussed in more detail during Chapter 3 of this thesis. Nitriles have also been used as external nucleophiles to trap α-imino gold carbenes. Zhang and co-workers devised a method towards an efficient synthesis of bicyclic imidazoles like **2.66** from alkynylazide **2.65** using acetonitrile as solvent/trap with an acid additive (Scheme 2.15B).[111] The acid was used to suppress unwanted Huisgen cycloaddition and favor the formation of **2.66** resulting from the interrupted acetylenic Schmidt reaction. Another approach is to tether a

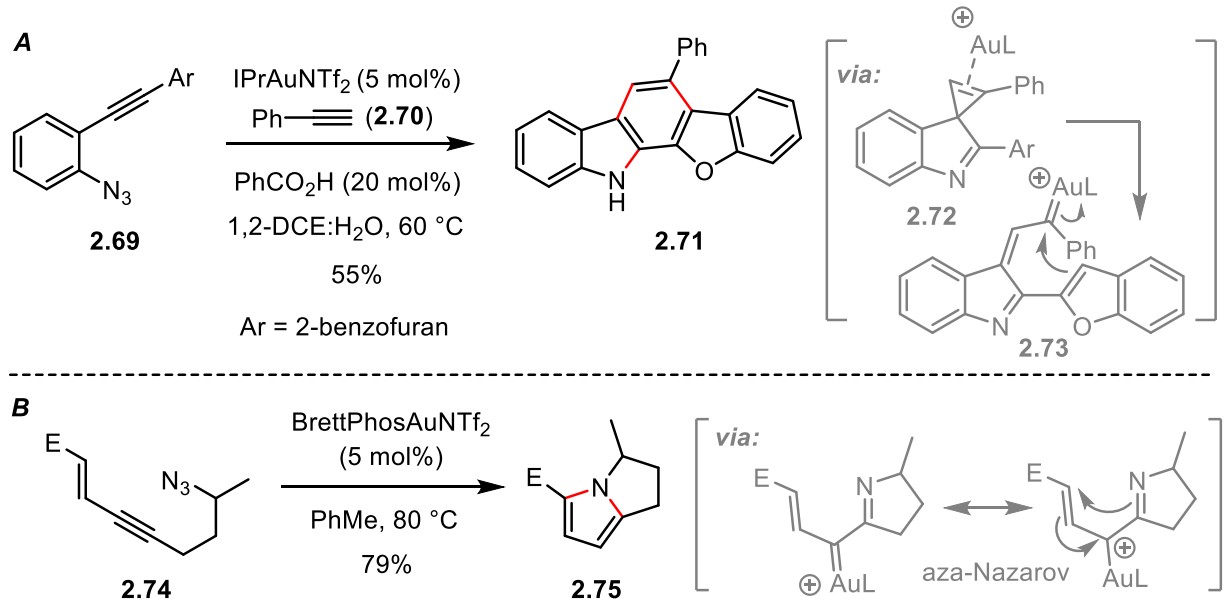
nucleophile to the alkyne, which is the strategy used by the groups of Xu and Qiu.[112] They synthesized polycyclic fused indole **2.68** using diaryl azido alkyne **2.67** that had a nucleophilic *homo*-benzylic alcohol handle (Scheme 2.15C). Trapping of the α-imino gold carbene by this alcohol led to the desired products.



Scheme 2.15. Azides as nitrene-transfer agents in Au(I) catalysis with trapping of α-imino gold carbenes

α-Imino gold carbenes generated from azides have also been known to participate in cyclopropanation and pericyclic cascades. For example, the groups of Gong and Han showed that aryl-annulated carbazole **2.71** can be directly accessed from easy to synthesize *ortho*-alkynyl arylazide **2.69** and an exogenous terminal alkyne **2.70** (Scheme 2.16A).[113] Carbazoles in general are of importance to the pharmaceutical and materials industry. They propose that a cyclopropenation takes place with the external alkyne and the α-imino gold carbene to give Au(I)-cyclopropene complex **2.72**, which rearranges to alkenyl gold carbene **2.73**. **2.73** is then subsequently hydroarylated by the nearby aryl ring to give the final product. Another unique

approach is using the α-imino gold carbene in conjunction with a pericyclic reaction such as a 4π-electrocyclization, effectively resulting in an aza-Nazarov reaction. Zhang and co-workers demonstrated this by the direct synthesis of *N*-fused pyrroles (dihydropyrrolizine **2.75**) from azido enyne **2.74** that had an electron-withdrawing group to bias the substrate for regioselective 5-*exo-dig* instead of 6-*endo-dig* cyclization (Scheme 2.16B).[114] A few years later, an intramolecular variant of this chemistry was done by Ye, Lu, and co-workers and used ynamides.[115]

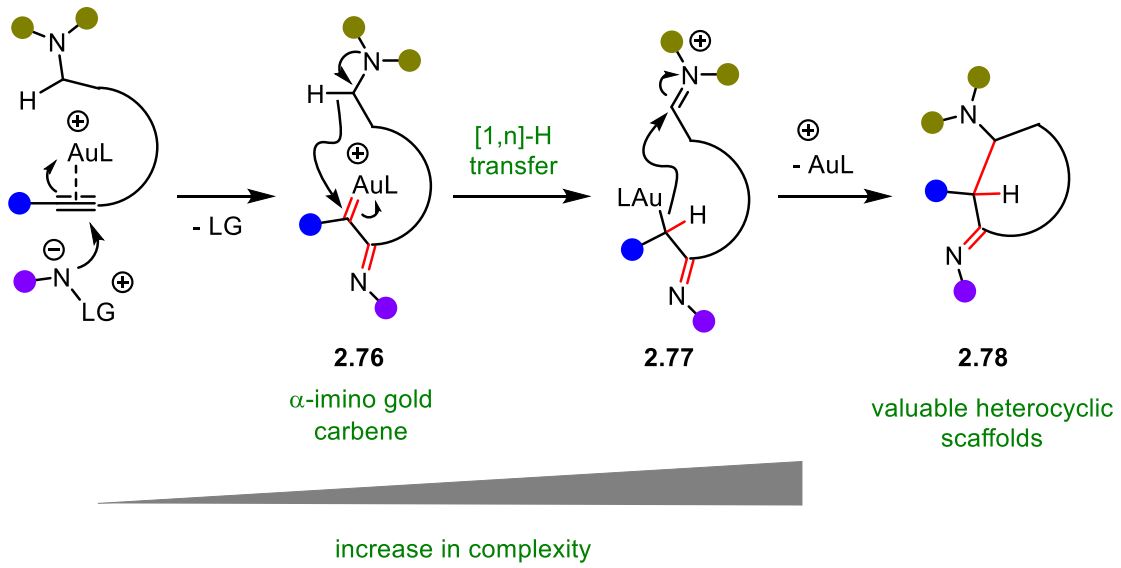


Scheme 2.16. Cascade reactions of α-imino gold carbenes generated from azides as nitrene-transfer reagents

2.3 Objective of the project

In line with our groups continued interest in the development of new catalytic methods in the field of homogeneous gold catalysis, we sought out a novel approach towards the Au(I) catalyzed α-C*sp*^{3}-H functionalization of tertiary amine substrates. The C-H functionalization of tertiary amine substrates is rare as compared to the well documented ether substrates. Therefore, having new methods to access functionalized amines (particularly for cyclic amines) is important since this can lead to alternative strategies in heterocyclic synthesis. Our approach to this challenge relied on combining and leveraging the unique reactivity of highly electrophilic α-imino gold carbene intermediates with redox-neutral hydrogen atom transfer. As we have discussed

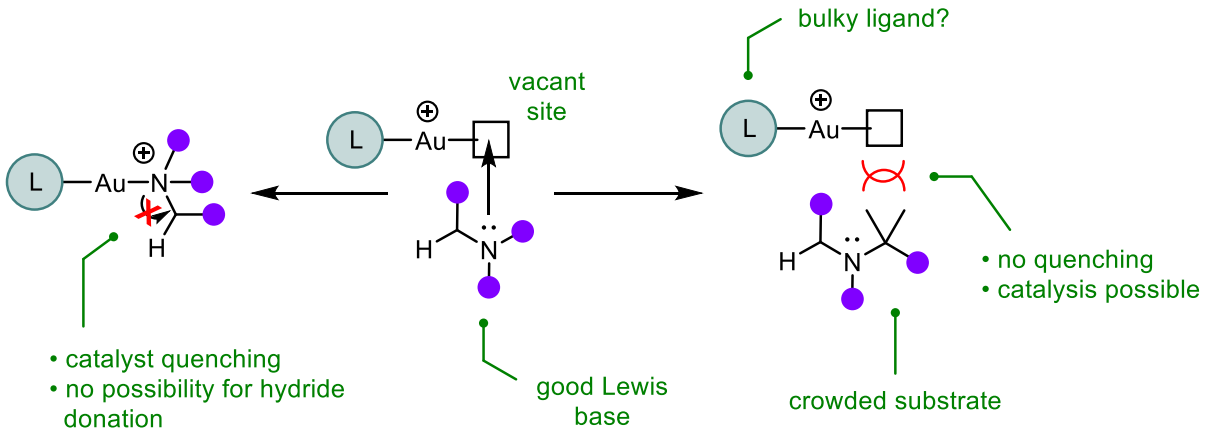
previously, α-imino gold carbene intermediates can be easily generated from alkynes and a nitrene-transfer reagent. To the best of our knowledge, no such reports of these intermediates have been used in tandem with the Csp^3-H functionalization of tertiary amines despite having been used in numerous other transformations with many different nucleophiles. In conceptualizing the project, we believed that a substrate bearing a suitable handle for Csp^3-H functionalization like a tertiary amine in conjunction with a nitrene-transfer reagent would allow us to realize this goal (Scheme 2.17). The process would be initiated by alkyne coordination from cationic Au(I), addition of the nitrene-transfer reagent, and formation of electrophilic α-imino gold carbene **2.76**. In the event that a [1,n]-H transfer is able to take place, hydride migration would occur onto the α-imino gold carbene, resulting in ambiphilic intermediate **2.77**. The subsequent recombination of the nucleophilic imino gold group with the iminium from hydride migration would deliver us the desired Csp^3-H functionalized product **2.78**. This would allow us to access valuable *N*-based heterocyclic scaffolds with increased molecular complexity.



Scheme 2.17. A new approach towards the Au(I) catalyzed C-H functionalization of tertiary amines

We were also cognizant of the favorable coordination ability of Lewis basic tertiary amines with Lewis acidic cationic Au(I) complexes. This sort of interaction would likely prevent catalysis from taking place not only from an electrophilic activation standpoint, but also from the

perspective of hydride migration since the donor ability of the amine would be greatly reduced in this case (Scheme 2.18). Instead, a work around to this problem will need to be rationally designed and implemented for this strategy to be successful. Sterics could prove to be an important factor here, either *via* the ligand on the gold catalyst or on the substrate itself which may prevent coordination. In this chapter, the successful implementation of this method for the C-H functionalization of tertiary amines using Au(I) catalysis will be discussed.



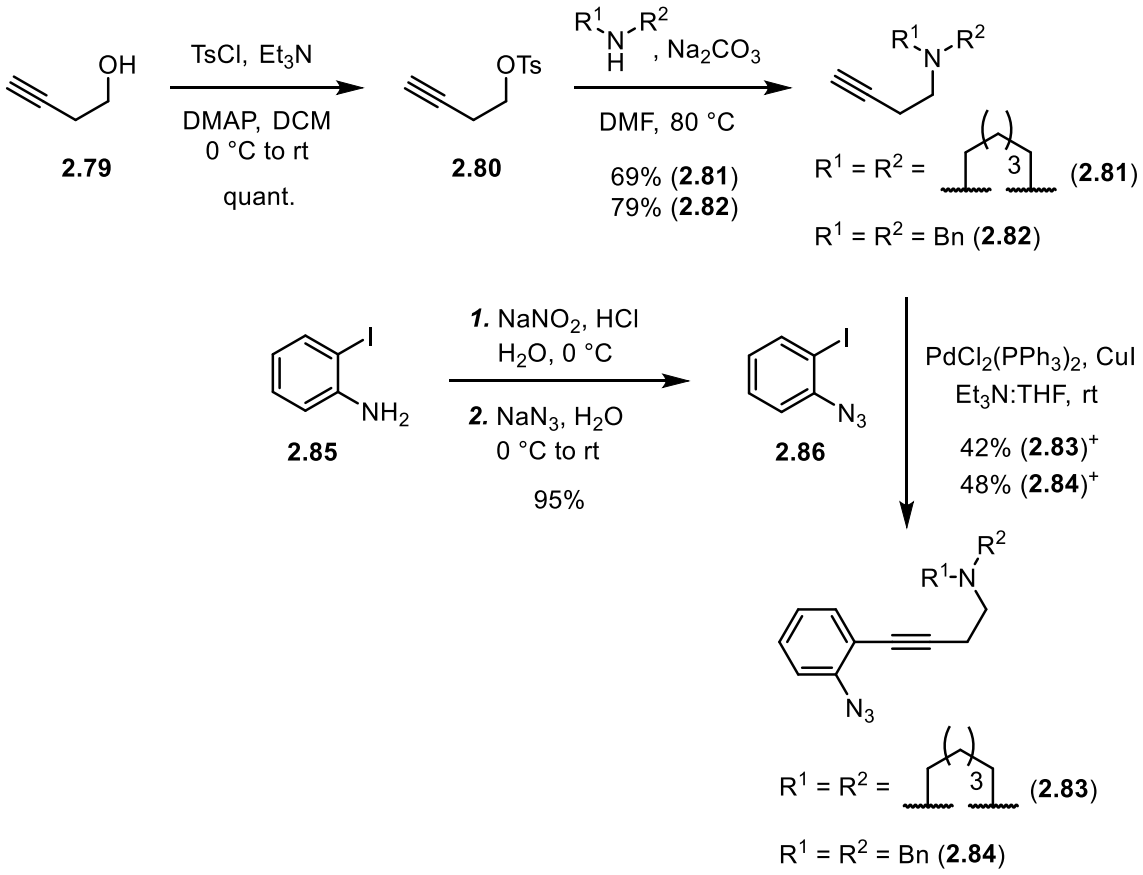
Scheme 2.18. Potential challenges associated with the Au(I) catalyzed C-H functionalization of tertiary amines

2.4 Substrate synthesis and intrinsic hydride donor reactivity studies

2.4.1 Preliminary experiments and challenges with reactivity

Before beginning our investigations, we sought to use the azide group as a form of nitrene-transfer reagent as this would produce a traceless by-product in the form of nitrogen gas. Additionally, utilization of *ortho*-alkynyl arylazides have been well documented in the literature (by our own group and others) to form unique indole-type scaffolds intramolecularly.[116] Given the ubiquitous presence of the indole nucleus in numerous natural products and drug candidates, this would also offer an opportunity to access interesting molecular architectures if combined with the α-C-H functionalization of tertiary amines. Therefore, the first series of experiments revolved around understanding the hydride donor capabilities of several substrates containing different tertiary amine groups (cyclic and acyclic).

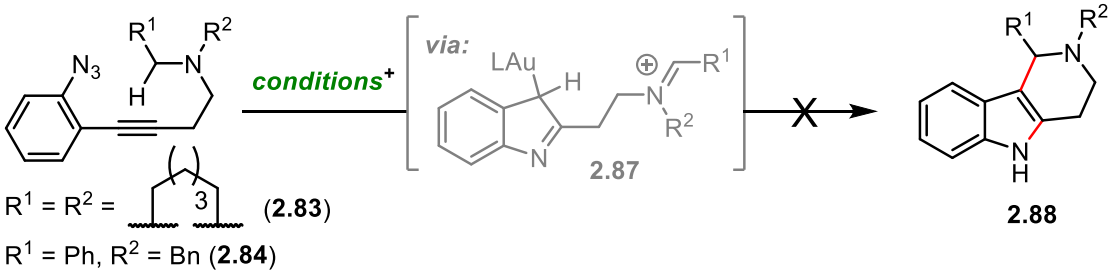
Initially, we chose to evaluate *homo*-propargyl piperidine and dibenzylamine groups, seeing as these were well established in the literature as highly effective hydride donors. Substrates **2.83** and **2.84** were easily synthesized in three steps from commercially available 3-butyn-1-ol **2.79** (Scheme 2.19). The synthesis was initiated with tosylation of the alcohol to give tosylate **2.80** in quantitative yield. Substitution of the tosyl group was then done with either piperidine or dibenzylamine under basic conditions to give substrates **2.81** and **2.82** in 69% and 79% yield respectively. Next, Sonogashira couplings using 1-azido-2-iodobenzene **2.86** as the partner was done by David and gave the desired products **2.83** and **2.84** in 42% and 48% yield respectively. Azide **2.86** was then synthesized *via* a Sandmeyer-type reaction from 2-iodoaniline **2.85** under acidic conditions using sodium nitrite and sodium azide in 95% yield.



Scheme 2.19. Three step synthesis of initial *homo*-propargyl piperidine and dibenzylamine substrates **2.83** and **2.84**. $^{+}$Results by DFLR

With both substrates in hand, we sought to validate our approach using catalytic conditions which had previously been shown to successfully generate indoles and trap α-imino gold carbene intermediates using similar arylazide substrates.[109, 117] If successful, the intermediate α-imino gold carbene **2.87** would react with the C*sp*^{3}-H bond α to nitrogen on the piperidine ring or dibenzylamine in a [1,6] fashion. This would afford us desired indoles of type **2.88** (Table 2). It should also be mentioned that due to the planarity of α-imino gold carbene **2.87**, we decided to use *homo*-propargyl substrates instead of propargyl substrates to perform a [1,6]-H transfer instead of the more common [1,5]-H transfer. This was due to the poor alignment of the σ-orbital for the hydridic C-H bond with the π*-antibonding orbital of the gold carbene center in the [1,5] case as seen from a molecular model analysis. The Au(I) catalyzed reactions were conducted by David using catalysts possessing the NHC ligand IPr and a phosphine ligand JohnPhos (Table 2). With both substrates, low conversions between 20–40% were observed across the board. In general, these reactions were completely unproductive and gave no trace of the desired C-H functionalization products. Instead, crude NMR analysis revealed significant decomposition or polymerization of the substrates. Additionally, these reactions became significantly colored over time as deep red or purple-blue solutions. This heavily implies degradation of the Au(I) catalysts to gold nanoparticles such as colloidal gold.[118]

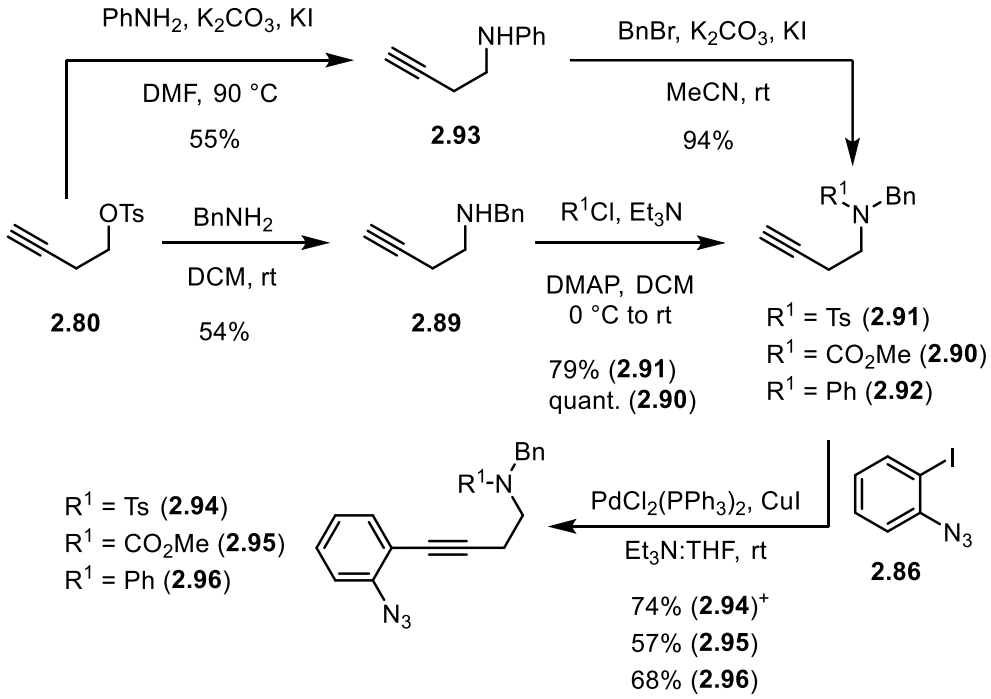
Table 2. Preliminary attempts for the desired C-H functionalization reaction



Entry[a]	Substrate	Catalyst (10 mol%)	Solvent	Temperature (°C)[b]	Time (h)	Conversion (%)[c]
1	**2.84**	JohnPhosAuNTf$_2$	1,2-DCE	85	4.5	40
2	**2.84**	IPrAuNTf$_2$	1,2-DCE	85	4.5	32
3	**2.83**	JohnPhosAuNTf$_2$	1,2-DCE	85	6	21
4	**2.83**	IPrAuNTf$_2$	1,2-DCE	85	6	20

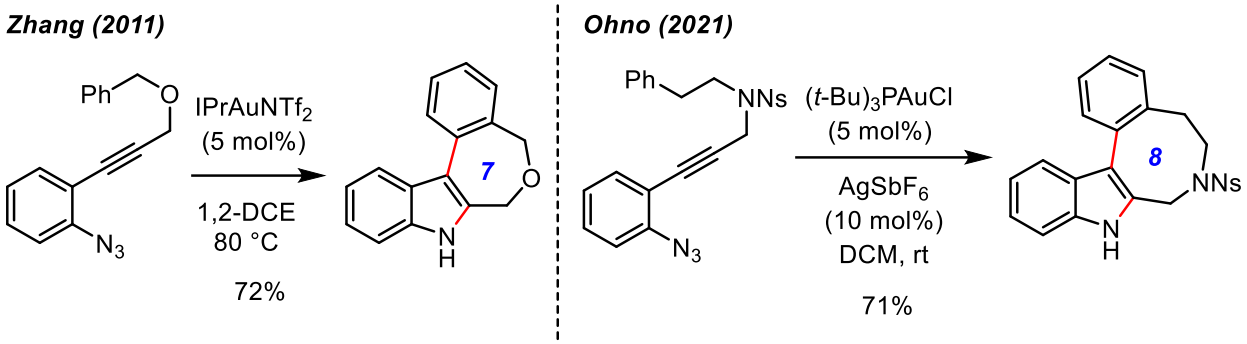
[a] Unless otherwise noted, all reactions were carried out using screw-cap test tubes with 0.06 mmol of the substrate at a concentration of 0.1 M in the indicated solvent. [b] Internal temperature. [c] Conversion was determined from the crude ^{1}H-NMR analysis using mesitylene as an internal standard.$^+$Results by DFLR.

With these negative results, we reasoned that the most probable cause of Au(I) catalyst degradation was likely occurring by reduction of the catalyst. To help alleviate this issue, we thought of replacing one of the benzyl groups in **2.84** with an electron-withdrawing group (EWG) to help temper the Lewis basicity of the tertiary amine, thereby limiting its interaction with the Au(I) catalyst. Synthesis of substrates **2.94**–**2.96** which had carbamate, tosyl, and phenyl groups on the amine center was done by me according to what is shown in Scheme 2.20. Here, the sequence of steps is like what was shown previously starting from tosylate **2.80**. Substrates **2.94** and **2.95** could be made from the common *homo*-propargyl benzylamine **2.89** which was protected with TsCl or methyl chloroformate to give methyl carbamate **2.90** and tosylamide **2.91** in good overall yields. Substrate **2.96** on the other hand required a different order and was synthesized by first substitution with aniline to give *homo*-propargyl aniline **2.93**, and then benzyl protected to afford **2.92** in 52% yield over both steps. Sonogashira coupling then delivered the required starting materials **2.94**–**2.96** in 57–74% yield, with the coupling reaction of terminal alkyne **2.91** being done by David.



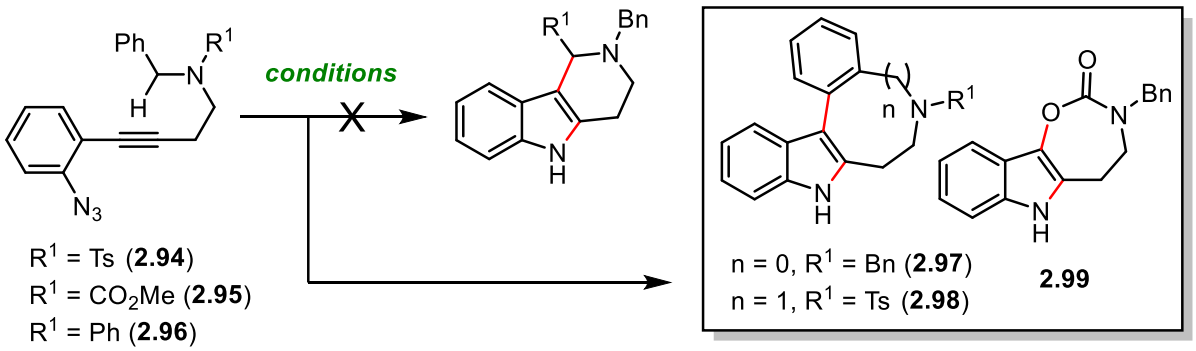
Scheme 2.20. Synthesis of tosyl, carbamate, and phenyl protected substrates **2.94**–**2.96**. $^{+}$Results by DFLR

Having made these new substrates, they were reacted under similar catalytic conditions as the initial non-protected versions **2.83** and **2.84** (Table 2.1). We were pleased to see that starting material conversion for all substrates was largely improved, however we were disappointed to find that still no products resulting from the α-C-H functionalization could be detected. Instead, we were able to isolate different products which originated from the result of intercepting the α-imino gold carbene from a different group and not by a hydride. In the case of substrate **2.96** which had a phenyl ring (Entries 1–2), the main product isolated was the 7-membered indole **2.97**. The nitrogen atom was made less basic by the phenyl ring, but it seems the delocalization of electrons was favored into the aromatic ring, leading to a hydroarylation reaction to occur with the *in-situ* generated α-imino gold carbene. Only 50% conversion was observed when using IPrAuNTf$_2$, with significant amounts of decomposition and a low NMR yield of **2.97**. JohnPhosAuNTf$_2$ led to full conversion but still a messy reaction profile. It allowed for the isolation of the 7-membered product **2.97** in 24% yield. For substrate **2.94** (catalysis done by David) which contains the tosyl group (Entries 3–4), the amine is completely deactivated in this case and the product isolated was the 8-membered indole **2.98**, resulting from hydroarylation of the benzyl groups aromatic ring with the gold carbene. Full conversion was observed with both catalysts in this case, however the reaction using JohnPhos did not exhibit as much decomposition of the substrate, leading to an isolated yield of 54% for **2.98**. The results observed from both substrates **2.94** and **2.96** are not entirely surprising, since the synthesis of these kinds of medium-sized benzannulated products *via* α-imino gold carbenes have some precedent in the literature (Scheme 2.21).[109, 112, 119, 120] On the other hand, when employing substrate **2.95** bearing a methyl carbamate (Entries 5–6), no product from C-H functionalization and perhaps only very trace hydroarylation could be observed. With both catalysts, extensive decomposition took place and only a small amount of an unidentified product could be isolated from the reaction mixture. This product is hypothesized to be the cyclic carbamate **2.99**, however due to the scale and negative outcome of the reaction, no further data was collected to support this structural assignment.



Scheme 2.21. Examples of benzannulation reactions in the synthesis of medium-sized rings

Table 2.1. Further tests utilizing protected amines to validate the desired C-H functionalization reaction



Entry[a]	Substrate	Catalyst (10 mol%)	Solvent	Temperature (°C)[b]	Time (h)	Conversion (%)[c]	Yield (%)[c]
1	**2.96**	JohnPhosAuNTf$_2$	1,2-DCE	85	6	100	24[d]
2	**2.96**	IPrAuNTf$_2$	1,2-DCE	85	6	50	20
3$^+$	**2.94**	JohnPhosAuNTf$_2$	1,2-DCE	85	1	100	53, 54[d]
4$^+$	**2.94**	IPrAuNTf$_2$	1,2-DCE	85	2	100	24
5	**2.95**	JohnPhosAuNTf$_2$	1,2-DCE	85	6	68	15
6	**2.95**	IPrAuNTf$_2$	1,2-DCE	85	6	85	23

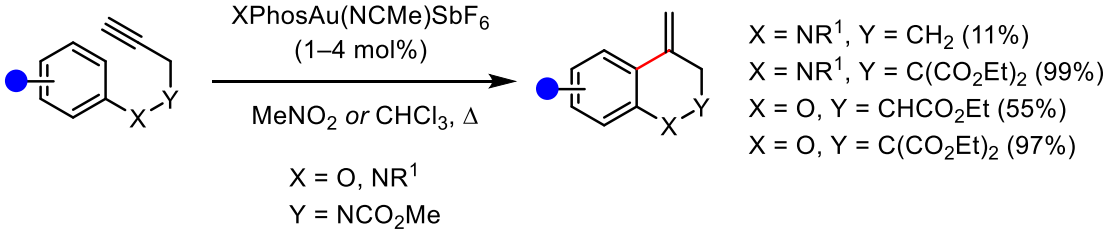
[a] Unless otherwise noted, all reactions were carried out using screw-cap test tubes with 0.06 mmol of the substrate at a concentration of 0.1 M in the indicated solvent. [b] Internal temperature. [c] Conversion and NMR yields were determined from the crude ^{1}H-NMR analysis using mesitylene as an internal standard. [d] Isolated yield. $^+$Results by DFLR.

2.4.2 Rational incorporation of a malonate blocking group

Realizing that arylation seemed like a more favorable process when the nitrogen atom is blocked with an electron-withdrawing group, we decided to introduce a malonate blocking group within the tether of substrate **2.83**, keeping the piperidine as a potent hydride donor. We rationalized the decision to keep the piperidine and install a malonate based on a few factors:

- From an entropy perspective, the piperidine group is more favorable (no free rotation in the 6-membered ring). Despite the benzyl group being a better donor by virtue of greater iminium stabilization, the flexible chain would result in an increased entropic penalty.

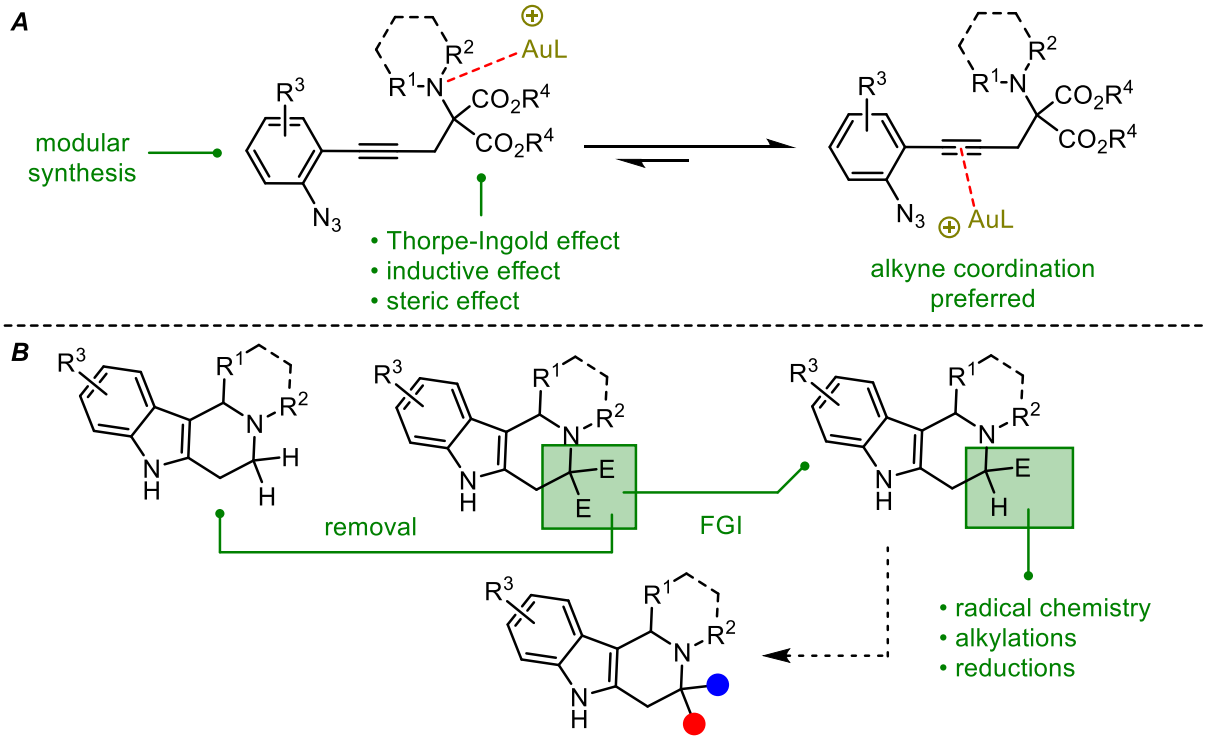
- Precedent from our group has demonstrated that using a malonate or related blocking group as a rational structural modification has helped kick-start or improve reactivity using Au(I) catalysis (Scheme 2.22).[121] In previous publications, our group was interested in the efficient synthesis of dihydroquinoline derivatives through a Au(I) catalyzed hydroarylation reaction. In the case where Y was a methylene group and X was a basic NR^1 group, little to no hydroarylation products were observed. Reactivity was only observed when the methylene was replaced with a diethylmalonate, regardless of the R^1 group on nitrogen. The improvement was attributed to the malonate weakening the interaction of the catalyst with nitrogen. This type of structural modification was also applied to our groups publications on the synthesis of chromene[122] and cinnoline[123] derivatives using similar starting materials.



Scheme 2.22. Previous application of a malonate blocking group by our lab in Au(I) catalyzed hydroarylation reactions

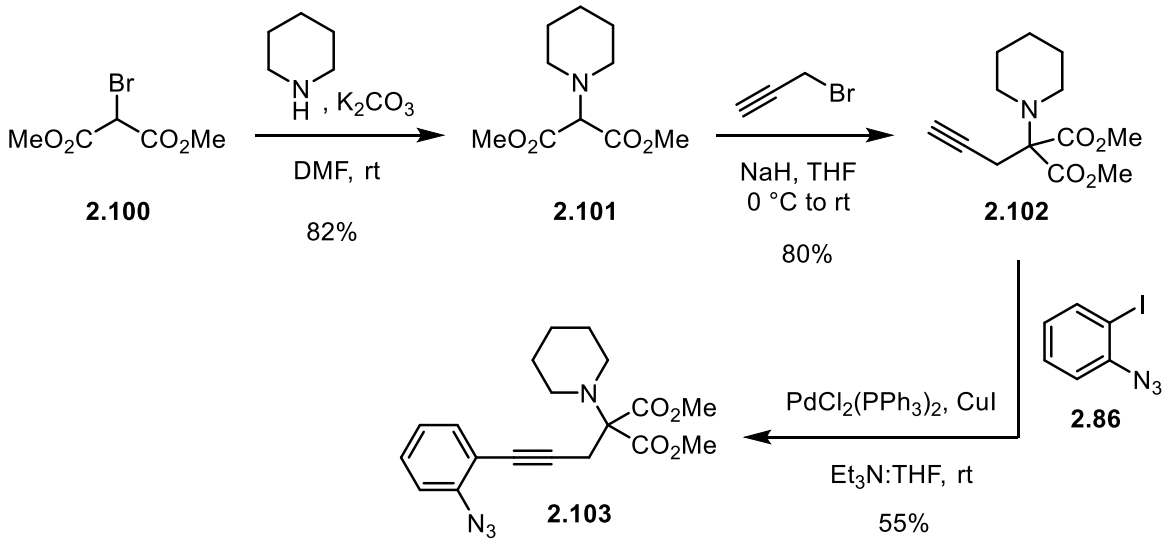
- The malonate moiety would introduce conformational, steric, and electronic effects into the system which may increase the possibility of realizing our desired C-H functionalization reaction. (Scheme 2.23A). Electronically, the malonate can lower the electron density on the nitrogen atom through the inductive effect. Sterically, the geminal substitution of the malonate provides crowding around the nitrogen atom, reducing its coordination to the gold complex. This effect could also be made even more pronounced if a sterically demanding ligand on the gold catalyst is used in unison. Finally, geminal substitution can induce a Thorpe-Ingold effect to cause a conformational change in the substrate, helping to favor the postulated [1,6]-H transfer to occur.

- Synthesis of substrates containing the malonate would still be straightforward and modular, easily allowing for diversification. Additionally, malonates are versatile structural handles and can be manipulated in a variety of ways to enable for derivatization of our desired C-H functionalization products (Scheme 2.23B).[124, 125]



Scheme 2.23. (A) Synergistic conformational, electronic, and steric effect by the malonate blocking group. (B) Using the malonate as a versatile synthetic handle for product derivatization

Based on this rationale, we set out to synthesize model substrate **2.103** where we thought it would be best to install the malonate on the two-carbon tether α to the piperidine nitrogen. This was initially chosen due to ease of synthesis since **2.103** can be made in three steps starting from commercially available dimethyl bromomalonate **2.100** (Scheme 2.24). However, positioning the malonate within the piperidine ring is also a possibility and may produce similar effects which could potentially afford new substrates of greater synthetic interest. The bromide of **2.100** was found to be easily substituted under basic conditions using piperidine in DMF to give piperidino malonate **2.101** in 82% yield. Next, deprotonation of the acidic malonate C-H bond with NaH allows for alkylation with propargyl bromide to give terminal alkyne **2.102** in 80% yield. Finally, Sonogashira coupling as shown before with arylazide **2.86** affords us the model substrate **2.103** in 55% yield.

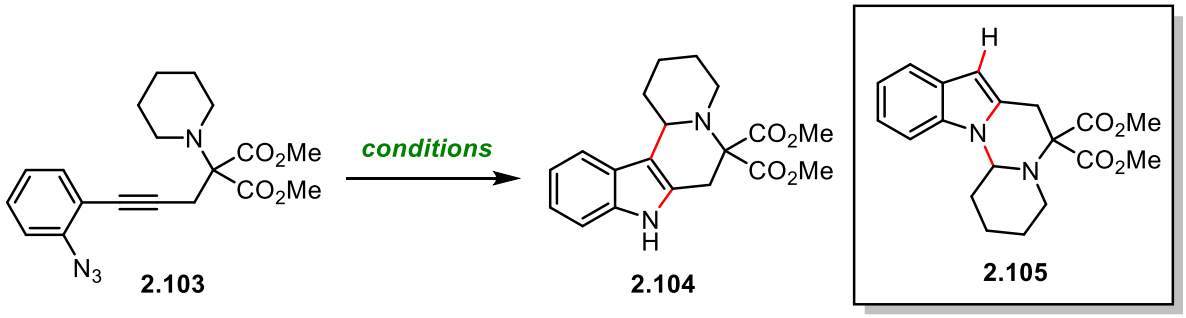


Scheme 2.24. Synthesis of model substrate **2.103** containing a dimethyl malonate group in the linker

With substrate **2.103** in hand, we were able to react it under the very same conditions as used previously with IPrAuNTf$_2$ and JohnPhosAuNTf$_2$ as catalysts (Table 2.2). To our delight, incorporation of the malonate led to our initial hit, and we could finally observe formation of the desired indole product **2.104**. When **2.103** was treated with IPrAuNTf$_2$ in refluxing 1,2-DCE, we observed 67% conversion for the starting material and a 30% NMR yield of indole **2.104** with no observable change by TLC/MS after a few hours. Interestingly, when **2.103** was treated instead

with JohnPhosAuNTf$_2$, we observed a similar conversion (66%) and NMR yield (36%), but also a new product in the mixture. We assigned the identity of this new product as aminal **2.105** which is the result of C-N bond formation instead of C-C formation. **2.105** was present as the minor component and in a 10:1 ratio with the major indole product **2.104**. This suggests the possible interconversion of the two in the reaction mixture since the gold catalyst may function as a competent Lewis acid affecting this isomerization.

Table 2.2. Initial hit for the desired C-H functionalization reaction



Entry[a]	Catalyst (10 mol%)	Solvent	Temperature (°C)[b]	Time (h)	Conversion (%)[c]	Combined Yield (%)	Ratio 2.104:2.105
1	IPrAuNTf$_2$	1,2-DCE	85	4.5	67	30	1:0
2	JohnPhosAuNTf$_2$	1,2-DCE	85	4.5	66	36	10:1

[a] Unless otherwise noted, all reactions were carried out using screw-cap test tubes with 0.06 mmol of the substrate at a concentration of 0.1 M in the indicated solvent. [b] Internal temperature. [c] Conversion and NMR yields were determined from the crude ^{1}H-NMR analysis using mesitylene as an internal standard.

2.5 Optimization of the catalytic system

Having demonstrated the feasibility of the proposed Au(I) catalyzed α-imino gold carbene formation/[1,6]-H transfer cascade, we now focused our efforts on optimizing the reaction in order to improve its efficiency and selectivity towards the formation of desired indole product **2.104** *vs* aminal side-product **2.105**. This included a thorough optimization campaign for the ligands and catalysts (Table 2.3, Scheme 2.25), solvent (Table 2.4), addition of additives (Table 2.5), and catalyst loading (Table 2.6).

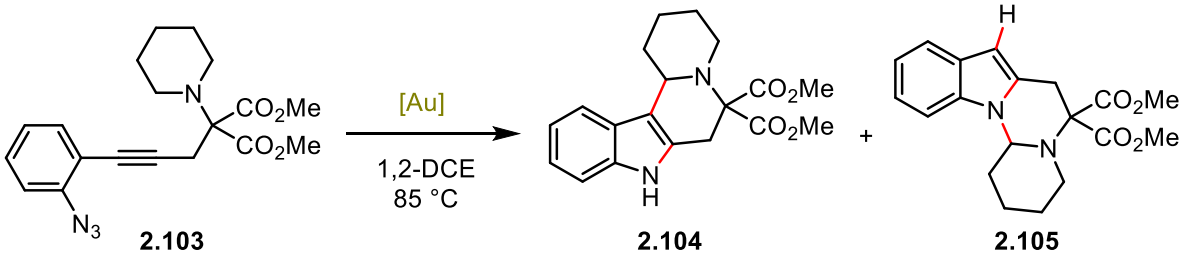
2.5.1 Ligand and catalyst optimization

Based on our initially promising result with JohnPhos as a ligand (Table 2.2), we first tested a variety of other Au(I)-phosphine *bis*-triflimide complexes as potential catalysts for this cascade process. As compared to JohnPhos (Entry 1), using other common Buchwald ligands such as XPhos and *t*-BuXPhos (Entries 2–3) did not significantly improve the efficiency of the process as conversions and overall NMR yields for **2.103** and **2.104** continued to hover around similar values (62–64% conversion and 21–27% NMR yield) with the bulkier *t*-BuXPhos performing better in terms of yield. Using the more electron rich BrettPhos (Entry 4) showed a decent improvement in NMR yield (doubling from 27% to 48%) despite conversions remaining relatively unchanged (67%). Seeing as increasing the electron richness and steric bulk of the ligand seemed to help the overall yield, we next tried to use *t*-BuBrettPhos complex (Entry 5) and were pleased to find that in three hours of reaction time, a significantly improved overall NMR yield of 60% was obtained with a slight increase in conversion (78%). Moving to the bulkier Me$_4$*t*-BuXPhos (Entry 6) proved to be even more beneficial, allowing us to achieve full conversion in the same amount of time and an overall NMR yield of 79%. As was briefly alluded to, the increase in overall yield and conversion seen in entries 5–6 is likely due to the increased electron richness and sterics of the ligand exerting an effect on the gold atom. Increasing the electron density on the ligand could help to better stabilize the α-imino gold carbene or other cationic reaction intermediates. Increasing the group size around phosphorous in the ligand would also push it closer to the second *ortho*-aryl ring, causing more steric bulk around the gold center and minimizing competitive coordination to nitrogen.

Testing other phosphine ligands (Entries 7–10) such as CPhos, VPhos, MorDalPhos, and simple PPh_3 did not show any improvement as compared to using Me$_4$*t*-BuXPhos. These ligands all had varying degrees of electron richness and steric bulk but were not as successful. Using very bulky ligands such as the NHC IPr* (Entry 11) or a *tris*-biaryl phosphine **2.106** (KarimPhos, Entry 12) developed in our own lab[38] also performed poorly. Highly electrophilic phosphite complexes (Entries 13–14) and simple PPh_3AuNTf_2 complexes stood out as being completely unproductive, forming no product and only leading to substrate/catalyst degradation being observed. Control experiments were also conducted using purely thermal conditions or using $AgNTf_2$ as a catalyst (Entries 15–16) and these confirmed that the gold catalyst was indeed necessary for reactivity.

Ultimately, Me$_4$*t*-BuXPhos was found to be the ligand of choice for this process among other phosphine, phosphite, and NHC ligands tested.

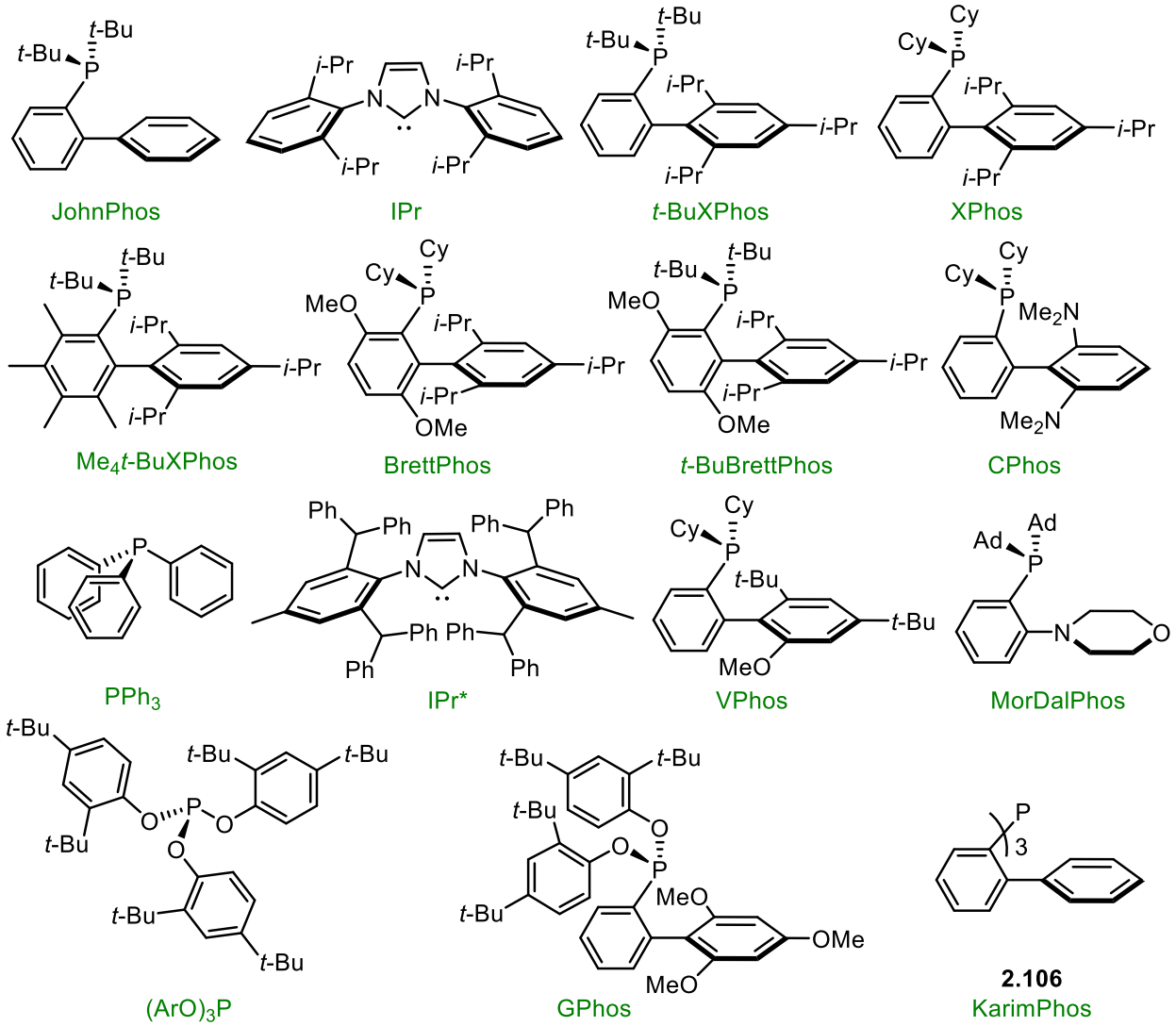
Table 2.3. Ligand optimization for the Au(I) catalyzed reaction of model substrate **2.103**



2.103 **2.104** **2.105**

Entry[a]	Catalyst (10 mol%)	Time (h)	Conversion (%)[c]	Combined Yield (%)	Ratio **2.104**:**2.105**
1	JohnPhosAuNTf$_2$	4.5	66	36	10:1
2	XPhosAuNTf$_2$	3	64	21	9:1
3$^+$	*t*-BuXPhosAuNTf$_2$	3	62	27	2:1
4$^+$	BrettPhosAuNTf$_2$	3	67	48	5.4:1
5	*t*-BuBrettPhosAuNTf$_2$	3$^+$	78	60	1.1:1
		6	88	59	2:1
6$^+$	Me$_4$*t*-BuXPhosAuNTf$_2$	1	87	79	2:1
		3	100	79	3.5:1
7$^+$	CPhosAuNTf$_2$	3	51	<5	0:1
8	VPhosAuNTf$_2$	3	58	23	8:1
9$^+$	MorDalPhosAuNTf$_2$	3	65	39	11:1
10$^+$	PPh$_3$AuNTf$_2$	3	28	--	--
11	IPr*AuNTf$_2$	3.5	40	13	2:1
12	(**2.106**)Au(NCMe)SbF$_6$	3	51	20	10:1
13$^+$	GPhosAuNTf$_2$	3	44	--	--
14$^+$	(ArO)$_3$PAuNTf$_2$	3	23	--	--
15	AgNTf$_2$	3	18	--	--
16	--	3	10	--	--

[a] Unless otherwise noted, all reactions were carried out using screw-cap test tubes with 0.06 mmol of the substrate at a concentration of 0.1 M in the indicated solvent. [b] Internal temperature. [c] Conversion and NMR yields were determined from the crude ^{1}H-NMR analysis using mesitylene as an internal standard. $^+$Results by DFLR.



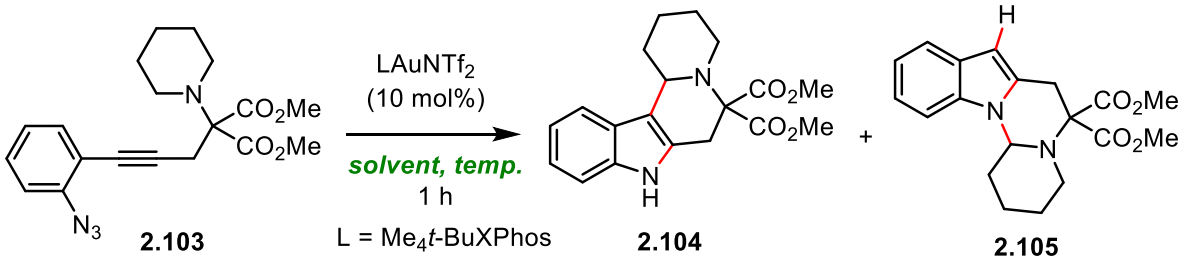
Scheme 2.25. Ligands used for the Au(I) catalyzed reaction of model substrate **2.103**

2.5.2 Solvent optimization

Having identified an optimal catalyst for this transformation, we next varied the solvent used to see what kind of influence that would have on the reaction. Conducting the reaction at room temperature does not produce any desired product, therefore we focused on solvents which could be used to conduct the reaction at temperatures of 50 °C or higher based on our group's previous work. We first tried another chlorinated solvent such as chloroform (Entry 2), and while the reaction works to give a modest 52% overall NMR yield of **2.104** and **2.105**, we were only able to see 80% conversion at reflux. We then screened other higher boiling polar and non-polar solvents. Toluene and 1,4-dioxane were tested next at 100 °C (Entries 3–4). Conversion and yields

in toluene were poor, while in 1,4-dioxane the reaction seemed to be as efficient as when conducted in chloroform despite the higher temperature and lower conversion. In general, it seems more polar solvents are beneficial. We next tried refluxing acetonitrile (Entry 5), and this greatly affected the reaction since we were no longer able to observe the desired indole product **2.104**. Instead, aminal **2.105** was obtained in a low 9% NMR yield despite 53% conversion. This is likely due to the well-established coordination ability of acetonitrile to the gold catalyst when used in solvent quantities. Therefore, a polar solvent which is not as coordinating is better in this case. On the other hand, using trifluoroethanol at 80 °C (Entry 6) gave excellent results and was an efficient reaction. Surprisingly, no aminal **2.105** was observed using this solvent. We believe this is likely due to the increased acidity of trifluoroethanol (pK_a ~12) which may help to catalyze the formation of indole **2.104** from aminal **2.105** during the reaction. Finally, we thought of trying nitromethane as a solvent which at first may seem like an unusual choice, however, has been used quite frequently as a solvent for gold catalyzed transformations by our group and others. We initially ran the reaction at 85 °C in nitromethane (Entry 7) and were pleased to see almost quantitative conversion (>95%) and an even greater NMR yield (82%) as compared to the reaction in refluxing 1,2-DCE (Entry 1). We repeated this reaction but this time at a higher temperature of 100 °C (Entry 8) and found the results to be similar with 94% conversion and a 78% NMR yield of **2.104**. Gratifyingly, when **2.104** is isolated by chromatography, a yield of 77% was obtained. 1,2-DCE and nitromethane could both be employed for this reaction and would be further evaluated under different conditions. Despite the promising results from using trifluoroethanol, it was not considered because of its potential to act as a nucleophile which may react with the gold carbene intermediate.

Table 2.4. Solvent optimization for the Au(I) catalyzed reaction of model substrate **2.103**



2.103 **2.104** **2.105**

Entry[a]	Solvent	Temperature (°C)[b]	Conversion (%)[c]	Combined Yield (%)	Ratio **2.104**:**2.105**
1	1,2-DCE	85	100	79, 64[d]	3.5:1
2[+]	$CHCl_3$	65	80	52	20:1
3	PhMe	100	54	32	1:1.5
4	1,4-dioxane	100	71	51	1:1
5[+]	MeCN	85	53	9	0:1
6	TFE	75	91	75, 72[d]	1:0
7	$MeNO_2$	85	95	82	5:1
8	$MeNO_2$	100	94	78, 77[d]	5:1

[a] Unless otherwise noted, all reactions were carried out using screw-cap test tubes with 0.06 mmol of the substrate at a concentration of 0.1 M in the indicated solvent. [b] Internal temperature. [c] Conversion and NMR yields were determined from the crude ^{1}H-NMR analysis using mesitylene as an internal standard. [d] Isolated yield. [+]Results by DFLR.

2.5.3 Additive optimization

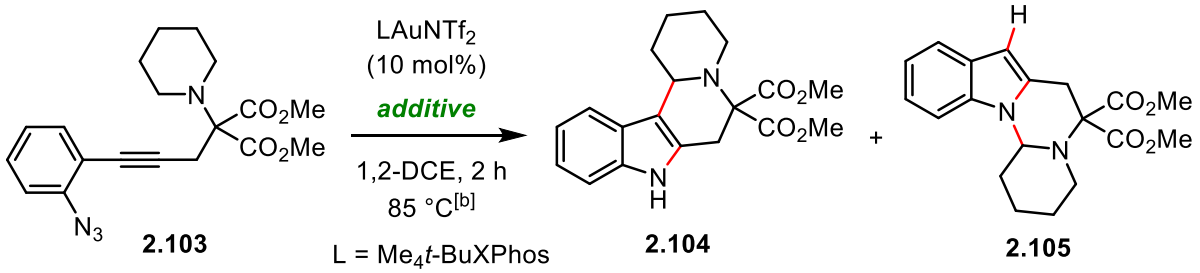
Throughout this optimization campaign, various ratios of **2.104**:**2.105** have been obtained depending on the catalyst and solvent being used. Interestingly, we have also observed that the ratio of **2.104**:**2.105** was found to change when the reaction was left to age longer, forming more indole **2.104** with respect to aminal **2.105** (see Table 2.3, Entries 5–6). This suggests an *in-situ* conversion of aminal **2.105** into indole **2.104** and indeed reaction monitoring by both TLC, TLC/MS, and NMR confirmed this hypothesis. Considering that indole **2.104** and aminal **2.105** are regioisomers, the Lewis acidic Au(I) complex or trace acids in the reaction medium could potentially catalyze their conversion. Nonetheless, to promote and study the selective formation of indole **2.104** while starting from model substrate **2.103**, a series of additives were tested.

We first tested several different acid additives that had a wide range of pK_a values. We believed a stoichiometric amount of a weak acid should help the process, and so we employed AcOH (Entry 2). Compared to no additive (Entry 1), we were pleased to see that in the presence of acid, the reaction was still highly efficient (100% conversion and 75% NMR yield) but was now completely selective for the formation of indole **2.104**. Additionally, no competitive gold carbene trapping was observed by the weakly nucleophilic acetate. Capitalizing on this result, we tested several other acids within a similar pK_a range (Entries 3–5) such as PivOH, $PhCO_2H$, and pyruvic acid. While these additives still gave exclusive formation of **2.104**, somewhat disappointingly they all varied with conversion and yield as compared to AcOH. None of them gave full conversion despite good reaction efficiency (NMR yields between 60–80%). HCO_2H (formic acid) was also added (Entry 6) but was completely unproductive. No reactivity was observed with only traces (<5%) of product, very low conversion (15%) and clear signs of catalyst degradation. This may be due to the propensity of formic acid to decompose at higher temperatures and poison the reaction. We also tried stoichiometric amounts of much stronger acids like TFA, MsOH, and TfOH (Entries 7–9). In this case, no reactivity was observed in addition to decomposition and only protonation of starting material **2.103** took place, completely preventing the hydride transfer event. To restore reactivity, we wondered if we could use a catalytic amount of an acid additive. We first tested this by trying to use 5 mol% of AcOH (Entry 10) and found no change in conversion or efficiency, only the ratio of **2.104**:**2.105** (~9:1). When a lower amount of the weak acid is used, the conversion of **2.105** into **2.104** is not complete. This opened the possibility to do the same with stronger acids to achieve better selectivity and so a catalytic quantity of strong acids TFA and MsOH was used first (Entries 11–12). As we expected, this restored reactivity, and we started seeing product forming. While the efficiency of the reaction with TFA or MsOH was modest (63% and 56% respectively), using 5 mol% TfOH showed excellent results (Entry 13). TfOH is roughly 10 pK_a units lower than TFA and MsOH, making it an even stronger acid. With catalytic TfOH, the reaction efficiency improved even further from 79% to 87% and showed full conversion.

Finally, we wanted to see if we could suppress the conversion of aminal **2.105** to the desired product *via* the addition of a stoichiometric basic additive. Using the highly basic proton sponge (Entry 14) demonstrated this to be true despite the severe reduction in reaction efficiency (38%

conversion and 9% NMR yield). Only aminal **2.105** could be detected from this experiment. Switching the additive to something less basic and coordinating should help the process. Therefore, we chose to try using a hindered pyridine base such as 2,6-*di*-*tert*-butylpyridine (2,6-DTBP) that would not coordinate to the Au(I) complex very well, but still result in a basic reaction mixture (Entry 15). This switch proved to be beneficial, since 2,6-DTBP did not affect the progress of the reaction but rather limited the isomerization of **2.105** into **2.104** (1.5:1 ratio). An interesting experiment was also conducted in Entry 16. If you add both one equivalent of AcOH and 2,6-DTBP, the reaction is still very efficient and selective towards the formation of indole **2.104**. Taken together, these experiments help to support our hypothesis that **2.105** is converted into **2.104** *via* acid-catalysis *in-situ*. After a lengthy additive screen, we decided on using TfOH (5 mol%) as it was the most efficient additive in terms of yield and conversion.

Table 2.5. Additive optimization for the Au(I) catalyzed reaction of model substrate **2.103**



Entry[a]	Additive (*x* equiv.)	Conversion (%)[c]	Combined Yield (%)	Ratio 2.104:2.105
1	--	100	79	3.5:1
2+	AcOH (1)	100	75	1:0
3	PivOH (1)	86	79	1:0
4	$PhCO_2H$ (1)	86	80	1:0
5	pyruvic acid (1)	80	62	1:0
6+	HCO_2H (1)	15	<5	--
7+	TFA (1)	60	18[e]	--
8+	MsOH (1)	33	--[e]	--
9	TfOH (1)	--	--[e]	--
10+	AcOH (0.05)	100	75	9:1
11+	TFA (0.05)	81	63	1:0
12+	MsOH (0.05)	69	56	1:0
13+	TfOH (0.05)	100	84, 87[d]	1:0
14+	Proton sponge (1)	38	9	0:1
15	2,6-DTBP (1)	79	66	1:1.5
16+	AcOH (1) + 2,6-DTBP (1)	84	69	20:1

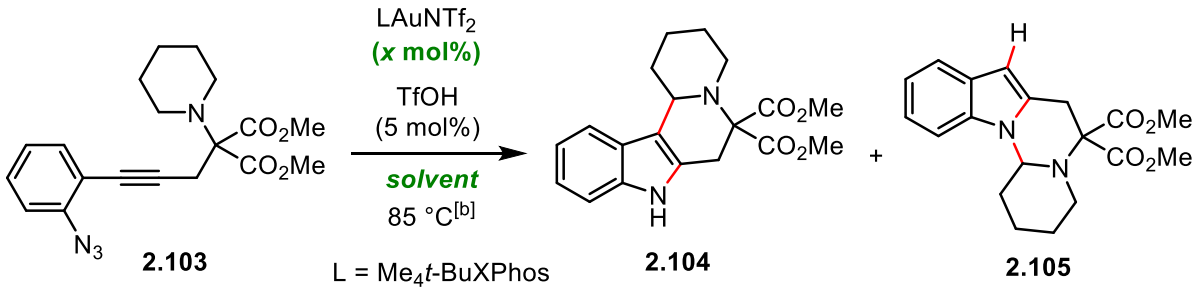
[a] Unless otherwise noted, all reactions were carried out using screw-cap test tubes with 0.06 mmol of the substrate at a concentration of 0.1 M in the indicated solvent. [b] Internal temperature. [c] Conversion and NMR yields were determined from the crude ^{1}H-NMR analysis using mesitylene as an internal standard. [d] Isolated yield. [e] Recovered protonated versions of the starting material. +Results by DFLR.

2.5.4 Catalyst loading optimization

With an appropriate ligand, additive, and set of solvents established, we set out to try and reduce the catalytic loading of the process. Dropping the catalyst loading from 10 mol% to 5 mol% in either nitromethane or 1,2-DCE at 85 °C (Entries 2–3) resulted in incomplete conversions, lower NMR yields, and significantly longer reaction times (one hour to six hours). Using 5 mol% of the gold catalyst in refluxing nitromethane however helped to improve the reaction in all areas, resulting in an 81% isolated yield of **2.104** in three hours of reaction time (Entry 4). Moving up a

bit to a loading of 7.5 mol% seemed to be ideal. At this loading, there is not much of a difference observed between nitromethane and 1,2-DCE (Entries 5–6) since indole **2.104** was isolated in 87% and 86% yield respectively. Ultimately, the experimental conditions chosen to continue moving forward and evaluate the reaction further are those shown in Entry 6. Despite 1,2-DCE being an equally good solvent as nitromethane, we preferred nitromethane since it would allow us to access higher temperatures in more difficult cases where substrates may not be as favorable.

Table 2.6. Catalyst loading optimization for the Au(I) catalyzed reaction of model substrate **2.103**



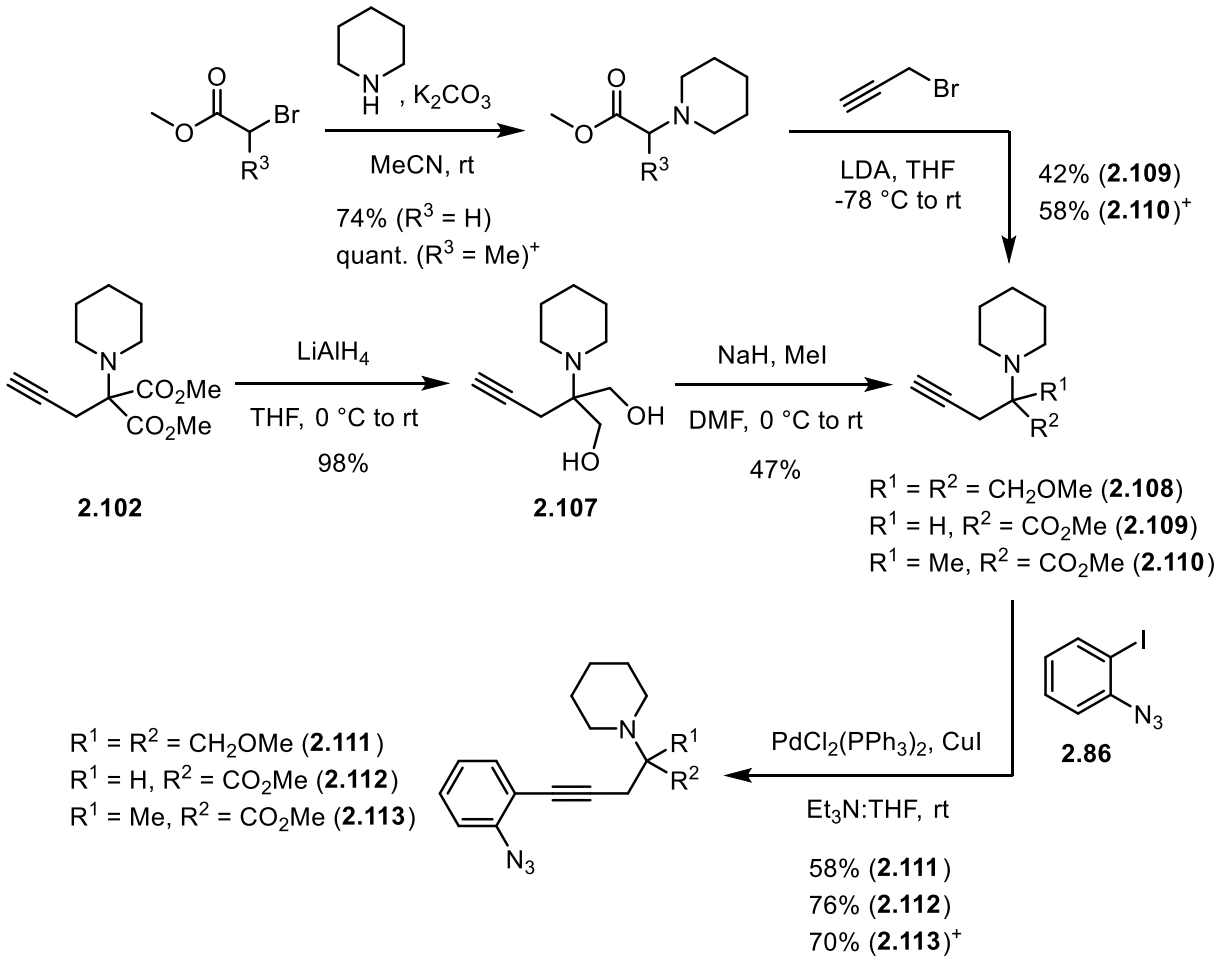
Entry[a]	Catalyst Loading (*x* mol%)	Solvent	Time (h)	Conversion (%)[c]	Combined Yield (%)	Ratio **2.104**:**2.105**
1[+]	10	1,2-DCE	1	100	84, 87[d]	1:0
2[+]	5	1,2-DCE	6	70	57	1:0
3[+]	5	$MeNO_2$	6	81	69	1:0
4[e][+]	5	$MeNO_2$	3	97	76, 81[d]	1:0
5	7.5	1,2-DCE	1.5	100	88, 86[d]	1:0
6	7.5	$MeNO_2$	1.5	100	85, 87[d]	1:0

[a] Unless otherwise noted, all reactions were carried out using screw-cap test tubes with 0.06 mmol of the substrate at a concentration of 0.1 M in the indicated solvent. [b] Internal temperature. [c] Conversion and NMR yields were determined from the crude ^{1}H-NMR analysis using mesitylene as an internal standard. [d] Isolated yield. [e] This entry was done with an internal temperature of 100 °C. [+]Results by DFLR.

2.6 Evaluating the effect of the malonate blocking group

With the optimized set of reaction conditions, we decided to study the role the malonate group was playing in allowing us to observe our desired reactivity. To do this, we synthesized three other substrates (**2.111**–**2.113**) which were derivatives of model substrate **2.103**. These

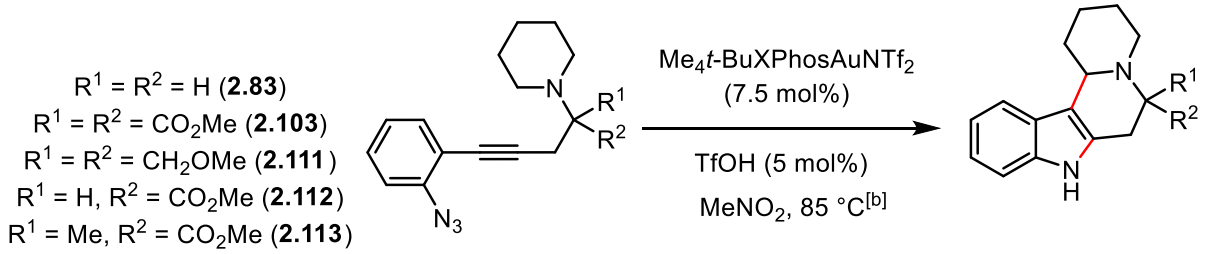
substrates were modified at the diester group and were synthesized according to Scheme 2.26 below. To assess the electronic impact of the malonate, *gem*-methoxymethyl substrate **2.111** was synthesized starting from terminal alkyne **2.102**. Reduction with LAH gave the diol **2.107** in 98% yield, and then dimethylation with NaH and methyl iodide gave **2.108** in 47% yield. To assess geometric and steric features, substrates which had one ester group replaced with either a methyl (**2.113**, synthesized by David) or hydrogen (**2.112**) were synthesized as well. Both substrates were synthesized starting from different methyl bromoacetates by a sequence of substitution with piperidine followed by alkylation with propargyl bromide at -78 °C using a strong base like LDA to give alkynes **2.109** and **2.110**. Finally, standard Sonogashria coupling delivers test substrates **2.111**–**2.113** in good overall yields.



Scheme 2.26. Synthesis of substrates **2.111**, **2.112**, and **2.113**. $^+$Results by DFLR

With compounds **2.111**–**2.113** in hand, we tested them in parallel with compound **2.83** which has the simple methylene and compared all substrates to the reactivity of the model **2.103** under our optimized catalytic conditions from above (Table 2.7). Unsurprisingly, using **2.83** (Entry 1) led to no product being formed under our optimized conditions and showed only catalyst decomposition. Similarly, using **2.111** (Entry 3) which does not have the same inductive effect as **2.103** did not result in any of the desired C-H functionalization product **2.114**, even when switching to the forcing conditions and performing the reaction with high catalyst loading (10 mol%) and in refluxing nitromethane (100 °C). Substrate decomposition was observed here in addition to recovering unchanged starting material. Remarkably, using **2.112** and **2.113** which both lack one ester group and have a reduced inductive effect showed little to no reactivity. In the case of **2.112**, which has only one ester group and no significant steric crowding, no formation of the product could be detected. This was not the case with substrate **2.113** which differed by simple methyl substitution. Using the forcing conditions, the desired indole product could be isolated in a modest 37% yield and in a 4:1 diastereomeric ratio from **2.113**. Under these conditions, we were only able to achieve 58% conversion after six hours of reaction time, with mostly remaining starting material. A Thorpe-Ingold effect could be invoked to help explain the success of this substrate in addition to sterics, however, these two effects are not the only ones in play since no transformation was seen with **2.111** which still has geminal substitution/steric bulk but lacks the inductive effect of the ester.

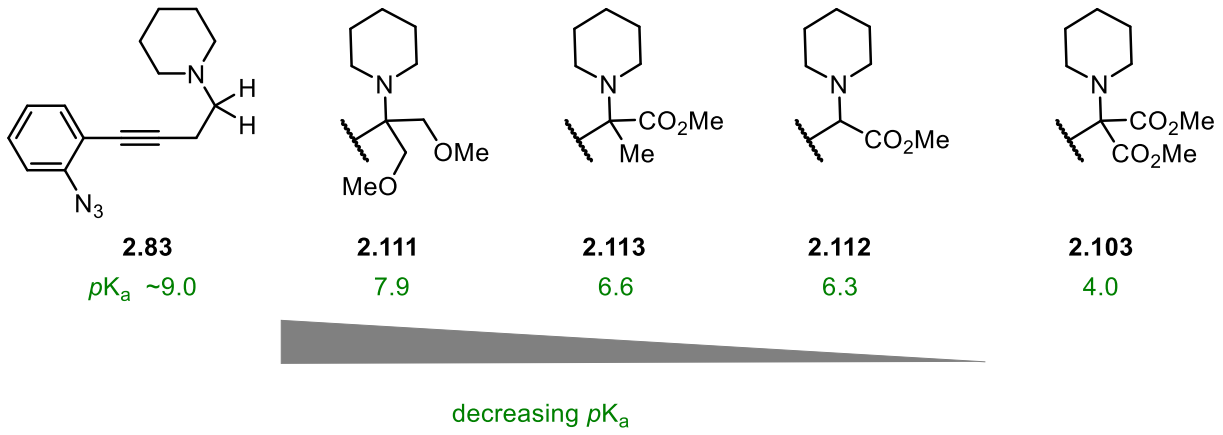
Table 2.7. Assessing the steric, electronic, and conformational effects of the malonate group on the outcome of the desired Au(I) catalyzed Csp^3-H functionalization reaction



Entry[a]	Substrate	Time (h)	Conversion (%)[c]	Yield (%)
1+	**2.83**	1.5	--	--[e]
2	**2.103**	1.5	100	87[d]
3	**2.111**	1.5	12	--
4	**2.112**	1.5	<5	--[f]
5+	**2.113**	1.5	49	<5
6[g]+	**2.113**	5	58	37[h]

[a] Unless otherwise noted, all reactions were carried out using screw-cap test tubes with 0.06 mmol of the substrate at a concentration of 0.1 M in the indicated solvent. [b] Internal temperature. [c] Conversion and NMR yields were determined from the crude ^{1}H-NMR analysis using mesitylene as an internal standard. [d] Isolated yield. [e] Complete degradation. [f] Recovered protonated starting material. [g] 10 mol% [Au] and 100 °C internal temperature. [h] *d.r.* = 4:1. +Results by DFLR.

Furthermore, Professor Fabien Gagosz also computed the predicted *p*K$_a$ values for the conjugate acids of all substrates **2.83**, **2.103**, and **2.111**–**2.113** to approximately compare their respective basicity with one another and help us to gauge their level of coordination to the gold catalyst (Scheme 2.27). The reaction was demonstrated to work with compounds **2.103** and **2.113** whose conjugate acid *p*K$_a$ values are low (*p*K$_a$ ~4 and 6.6 respectively). This really highlights the poor basicity of model substrate **2.103**, whose basicity is on-par with that of AcOH. However, **2.112** has a conjugate acid *p*K$_a$ very similar to that of **2.113** (*p*K$_a$ ~6.3) but differs by only a methyl group. This helps to show that electronic factors alone cannot account for the observed reactivity of **2.112** *vs* **2.113**. Ultimately, the malonate group clearly plays an important role in the success of this transformation which seems to come from a combination of steric, electronic, and conformational effects.

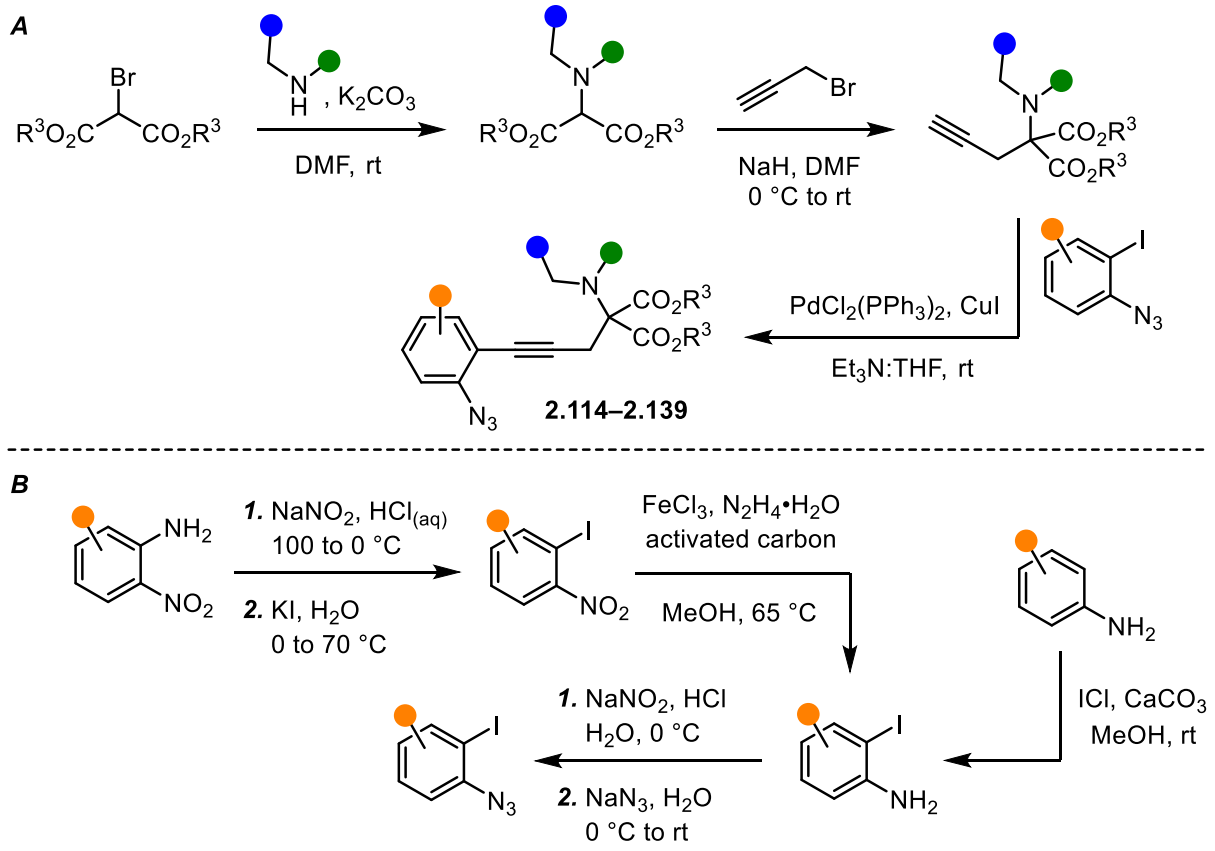


Scheme 2.27. Computed and predicted pK_a values for the conjugate acid of substrates **2.83**, **2.103**, and **2.111**–**2.113**

2.7 Methodology for the α-Csp^3-H functionalization of tertiary amines

2.7.1 Successful scope examples

The key *ortho*-alkynyl arylazide substrates **2.114**–**2.139** were synthesized according to the general scheme shown below (Scheme 2.28A) using either acyclic or cyclic hydride donors. As has been discussed previously in this thesis, a straightforward and modular three step sequence of substitution, propargylation, and Sonogashira coupling has been employed to introduce diversity to the amine and malonate motifs. To access a variety of different iodoarylazides, a few different approaches were used to access iodoanilines from substituted anilines or *ortho*-nitroanilines (Scheme 2.28B). If *ortho*-nitroanilines are used, a Sandmeyer reaction is used to access iodonitroarenes, which are then reduced to iodoanilines. If starting from aniline building blocks, the aromatic ring is iodinated to give the corresponding iodoanilines. Finally, the iodoanilines are converted to the iodoarylazides *via* another Sandmeyer-like reaction.

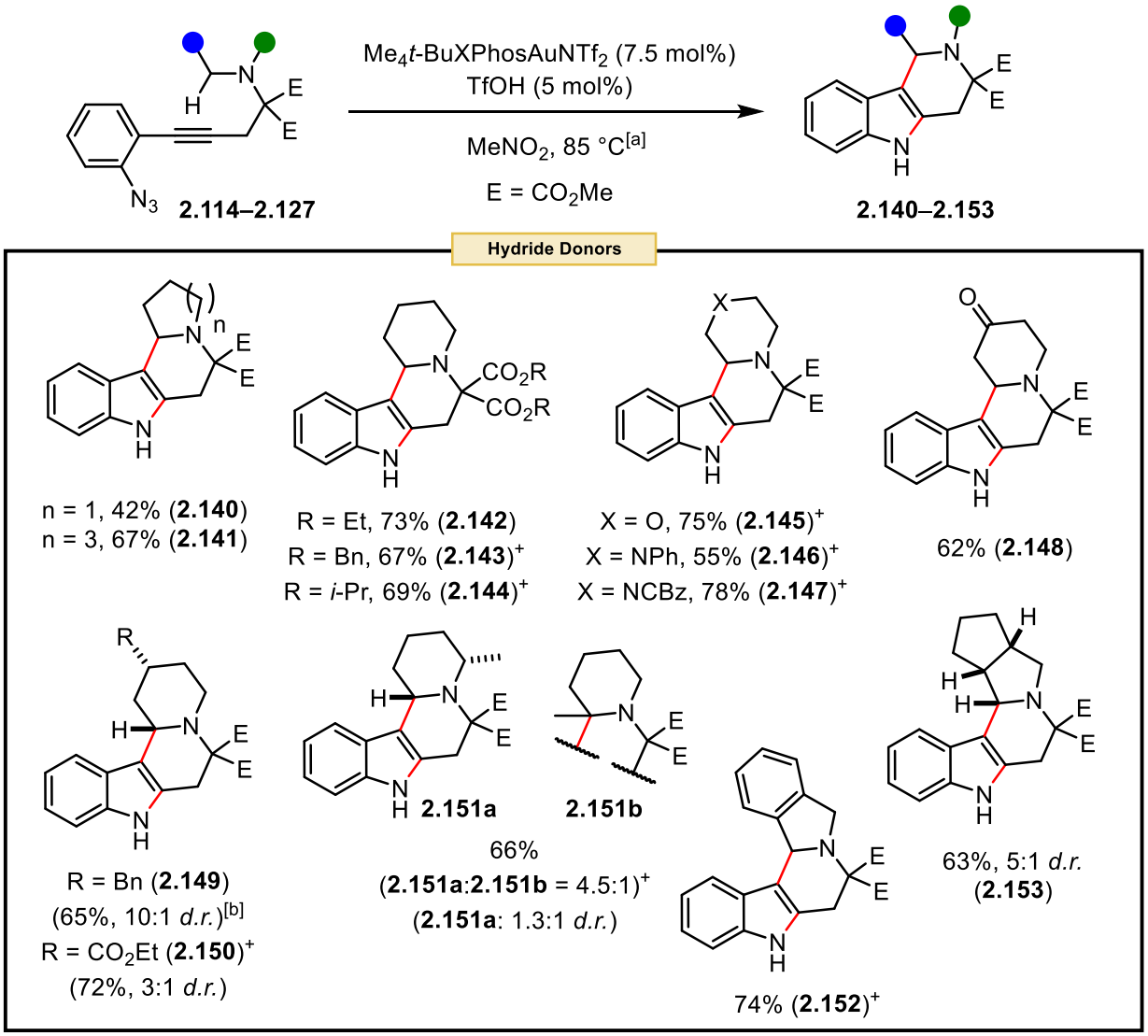


Scheme 2.28. Different routes used to access substrates **2.114**–**2.139** in a modular manner

As can be seen in Tables 2.8–2.10, a large variety of *ortho*-alkynyl arylazide substrates **2.114**–**2.139** were found to be effectively converted into valuable indole scaffolds **2.140**–**2.165** which are also considered tetrahydro-γ-carbolines. Different primary and secondary alkyl malonates **2.116**–**2.118** all reacted smoothly under the optimized reaction conditions to give indoles **2.142**–**2.144** in 67–73% yield. Importantly, 6-membered heterocycles like piperidine are not the only ones capable of transferring hydride, but other rings such as the 5-membered pyrrolidine derivatives and 7-membered azepine can do so as well. The 7-membered azepine indole product **2.141** was formed in 67% yield, while the smaller pyrrolidine indole product **2.140** was formed in a more modest 42% yield. Despite this, other pyrrolidine derivatives such as **2.126**–**2.127** and **2.129** are also competent substrates as seen by the formation of products **2.152**–**2.153** and **2.155** in 62–74% yield. The 3-substituted derivative **2.155** yielded an almost equal mixture of regioisomers **2.155a** and **2.155b** (1.1:1). Regioisomer **2.155b** where the hydride was transferred between the nitrogen and the pivaloyloxy group at the 3-position was formed as essentially a single

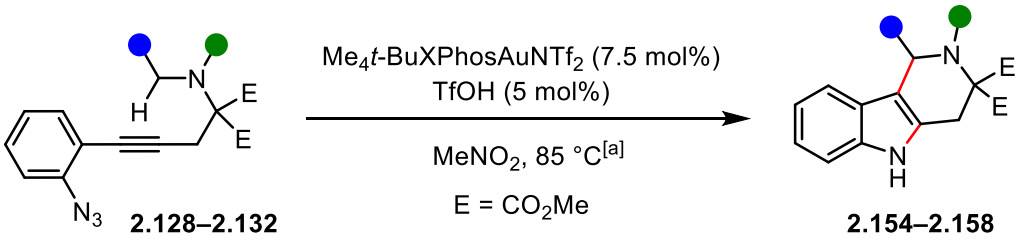
diastereomer (>16:1) whereas regioisomer **2.155a** that underwent hydride transfer from the opposite side was formed as a mixture (*d.r.* = 1.4:1). On the other hand, bicyclic pyrrolidine product **2.153** was formed in a good 5:1 diastereomeric ratio owing to the more favorable *cis*-fused ring junction. Substitution on the piperidine ring at *C*2, *C*3, and *C*4 was also found to be well tolerated. When using the *C*2 methyl substituted piperidine, the product formed as a 4.5:1 mixture of regioisomers (**2.151a** and **2.151b**, 66% combined yield) favoring the less substituted position of the piperidine. Difficulties in isolation made determining the *d.r.* difficult but based on the crude sample, the major regioisomer **2.151a** was formed in a 1.3:1 diastereomeric ratio. Reactions with *C*3 substituted piperidines to give indoles **2.156**–**2.158** were all successful (60–82% yield) but exhibited low to modest regio- and diastereoselectivity. Generally, reactivity took place at the least hindered position. Substrate **2.154** which used a tetrahydroisoquinoline donor showed improved regioselectivity for hydride donation (77% yield, 2.3:1 *d.r.*) to afford regioisomers **2.154a** and **2.154b**. This result can be rationalized from the increased stability of the iminium formed at the benzylic position, favoring the formation of regioisomer **2.154a**. Substrates with *C*4 substitution on piperidine also demonstrated good yields and diastereoselectivity in favor of the equatorial products such as **2.149** and **2.150** (10:1 and 3:1 *d.r.* respectively). The ketone product **2.148** formed in 62% yield is especially useful for further derivatization. Other heterocyclic donors such as morpholine (**2.145**) or *N*-substituted piperazines (**2.146** and **2.147**) did not affect the reactivity as shown by the formation of the indole derivatives in good to high yields (55–78%). Substitution on the arylazide portion was also general. Electron-withdrawing (CO_2Me, CF_3), electron-donating (OMe), and halogens (F, Cl) could be introduced onto the arene, and the desired products obtained in good to excellent yields (61–92%).

Table 2.8. Hydride donor scope for the Au(I) catalyzed α-Csp^3-H functionalization of tertiary amines

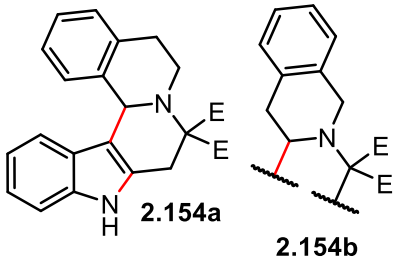


[a] Unless otherwise noted, all reactions were carried out using screw-cap test tubes at a concentration of 0.1 M in the indicated solvent and temperature. [b] All diastereomeric ratios (*d.r.*) and regioisomeric ratios were determined from the crude ^{1}H-NMR analysis using mesitylene as an internal standard. The major diastereomer is represented here. $^+$Results by DFLR.

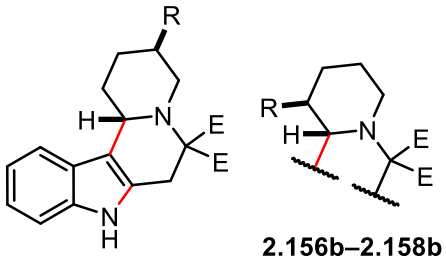
Table 2.9. Hydride donor scope continued



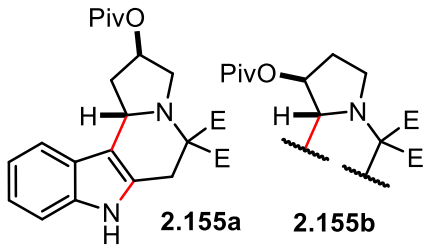
Hydride Donors cont'd



77%
(**2.154a**:**2.154b** = 2.3:1)[+]



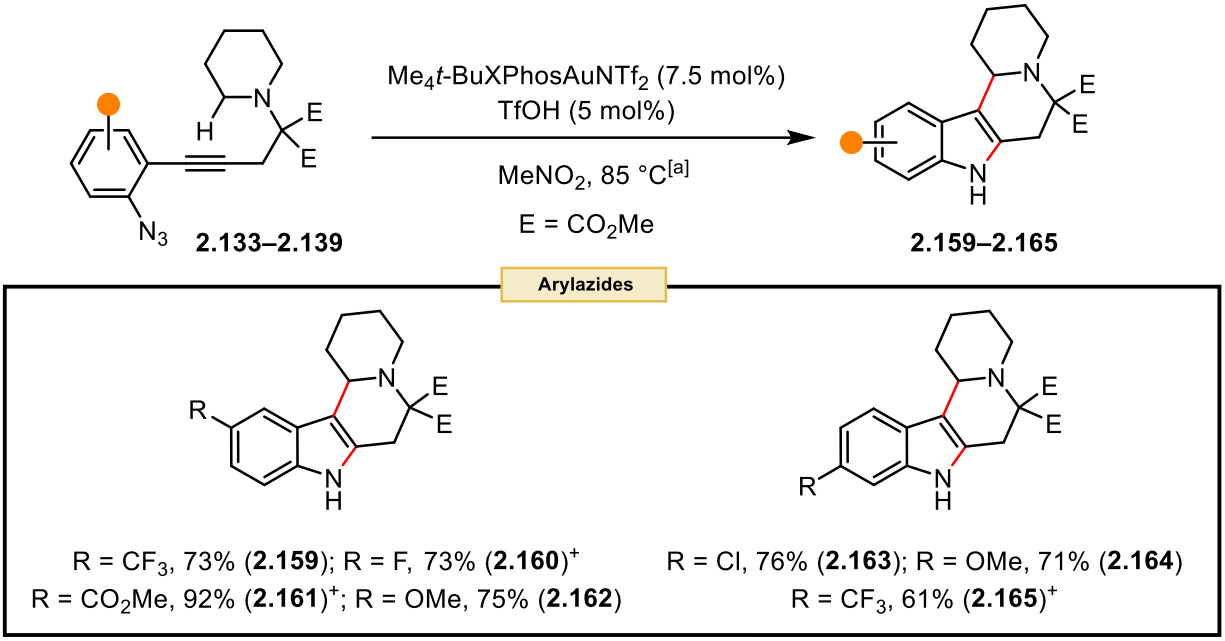
R = CO_2Me, 82%
(**2.156a**:**2.156b**[b] = 1.7:1)[+]
(**2.156a**: 3:1 *d.r.*, **2.156b**: 10:1 *d.r.*)
R = OAc, 60%
(**2.157a**:**2.157b** = 1:1)
(**2.157a**: 2:1 *d.r.*, **2.157b**: 2:1 *d.r.*)
R = CH_2OAc, 72%
(**2.158a**:**2.158b** = 1.6:1)[+]
(**2.158a**: 2:1 *d.r.*, **2.158b**: 1.5:1 *d.r.*)



62%
(**2.155a**:**2.155b** = 1.1:1)[+]
(**2.155a**: 1.4:1 *d.r.*, **2.155b**: 16:1 *d.r.*)

[a] Unless otherwise noted, all reactions were carried out using screw-cap test tubes at a concentration of 0.1 M in the indicated solvent and temperature. [b] All diastereomeric ratios (*d.r.*) and regioisomeric ratios were determined from the crude ^{1}H-NMR analysis using mesitylene as an internal standard. The major diastereomer is represented here. [+]Results by DFLR.

Table 2.10. Arylazide scope for the Au(I) catalyzed α-Csp^3-H functionalization of tertiary amines

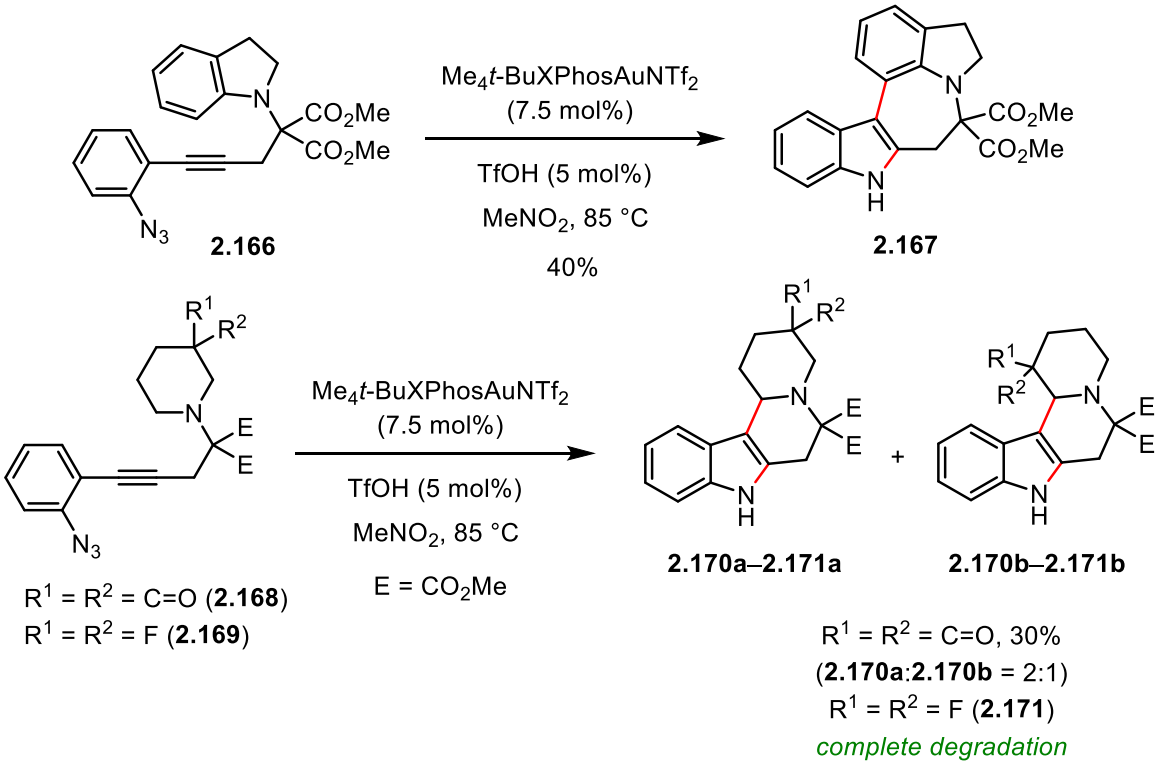


[a] Unless otherwise noted, all reactions were carried out using screw-cap test tubes at a concentration of 0.1 M in the indicated solvent and temperature. +Results by DFLR.

2.7.2 Limitations and failed examples

Not all substrates were able to be accessed or successful when using this methodology. To probe the regioselectivity of the hydride transfer event, we were interested in the synthesis of a few substrates which contained electron-withdrawing groups on the hydride donor at either the *C*2 or *C*3 positions and were synthesized by me. 3-Piperidinone substrate **2.168** should have allowed us to selectively access indole **2.170** where the hydride in between the carbonyl and nitrogen is likely not activated enough, and so we would expect reactivity exclusively from the other side. Similarly, we used the difluoro derivative **2.169** to probe the same kind of result. Substrates **2.166** and **2.168** were synthesized according to Scheme 2.28A using 3-piperidinone and indoline. Substrate **2.169** was synthesized by the same route as monoester substrate **2.112** using 3,3-difluoropiperidine (see Scheme 2.26). Substrates **2.168** and **2.169** ultimately ended up being problematic and were not very well tolerated in this transformation (Scheme 2.29). Using 3-piperidinone substrate **2.168** gave indole products **2.170a** and **2.170b** in a low 30% yield. Regioselectivity was not excellent but a modest 2:1 *r.r.* was obtained in favor of the more activated

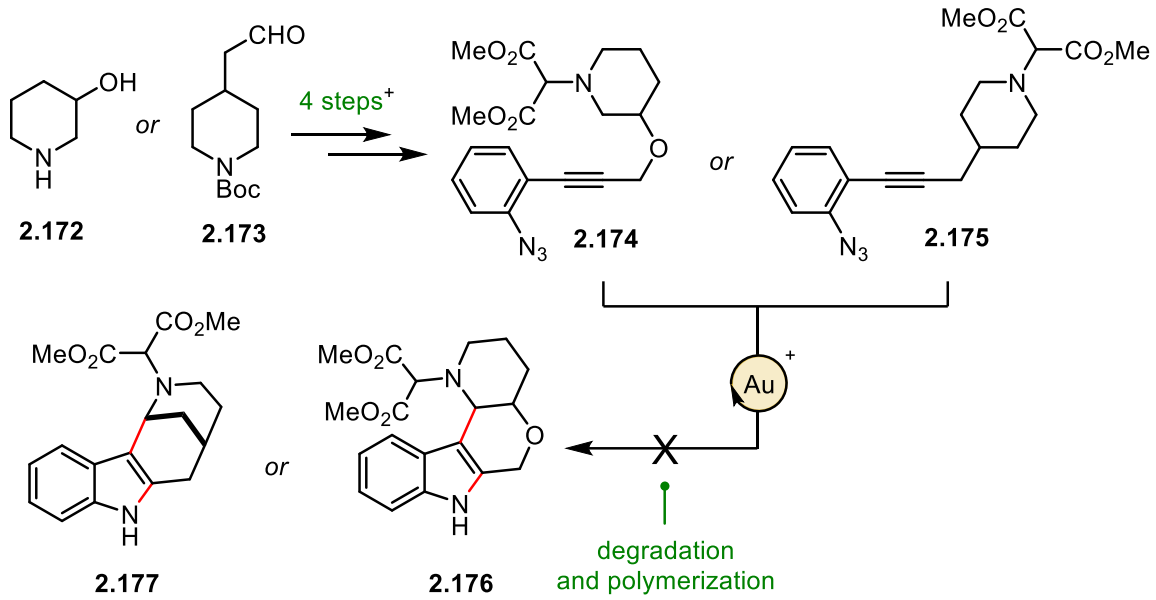
position, similar to the result obtained with the tetrahydroisoquinoline substrate **2.154**. Unfortunately, significant degradation was observed with this substrate and purification of the two regioisomeric products was complicated. Using the difluoro substrate **2.169** was completely unsuccessful. **2.169** was not formed in high yield after the Sonogashira coupling and was unable to be obtained in pure form since we observed rapid degradation upon standing. Nonetheless, we attempted the catalysis and were unfortunately only able to observe complete degradation of the substrate. Indoline substrate **2.166** was also unsuccessful. Rather than transferring a hydride, cyclization from the electron-rich aromatic ring intercepted the carbene, forming product **2.167** in 40% isolated yield.



Scheme 2.29. Unsuccessful hydride donor substrates

In parallel, we were also working on the synthesis of substrates which had the malonate group in a position other than the two-carbon tether. We were particularly interested in trying to access substrates which would map out nicely onto specific natural products and/or biologically relevant scaffolds after the desired C-H functionalization reaction. To this end we set out to synthesize substrates **2.174** and **2.175** which both had the malonate group on the nitrogen of the

piperidine ring. If successful, substrate **2.174** would be expected to form indole **2.176** which has a skeletal arrangement like that of members in the *Aspidosperma* family of monoterpene indole alkaloids. **2.175** would result in a bridged bicyclic indole product **2.177** which resembles the skeleton of the known toxin strychnine and has long been used as a benchmark for strategies in alkaloid total synthesis.[126] **2.174** and **2.175** were synthesized in four steps starting from piperidin-3-ol **2.172** or *N*-Boc-4-piperidineacetaldehyde **2.173** respectively (Scheme 2.30). To our disappointment, neither **2.174** nor **2.175** resulted in the formation of any desired C-H functionalization products under optimized or forcing conditions that we have developed. For the most part, these reactions underwent significant polymerization and degradation based on analysis of the crude NMR.

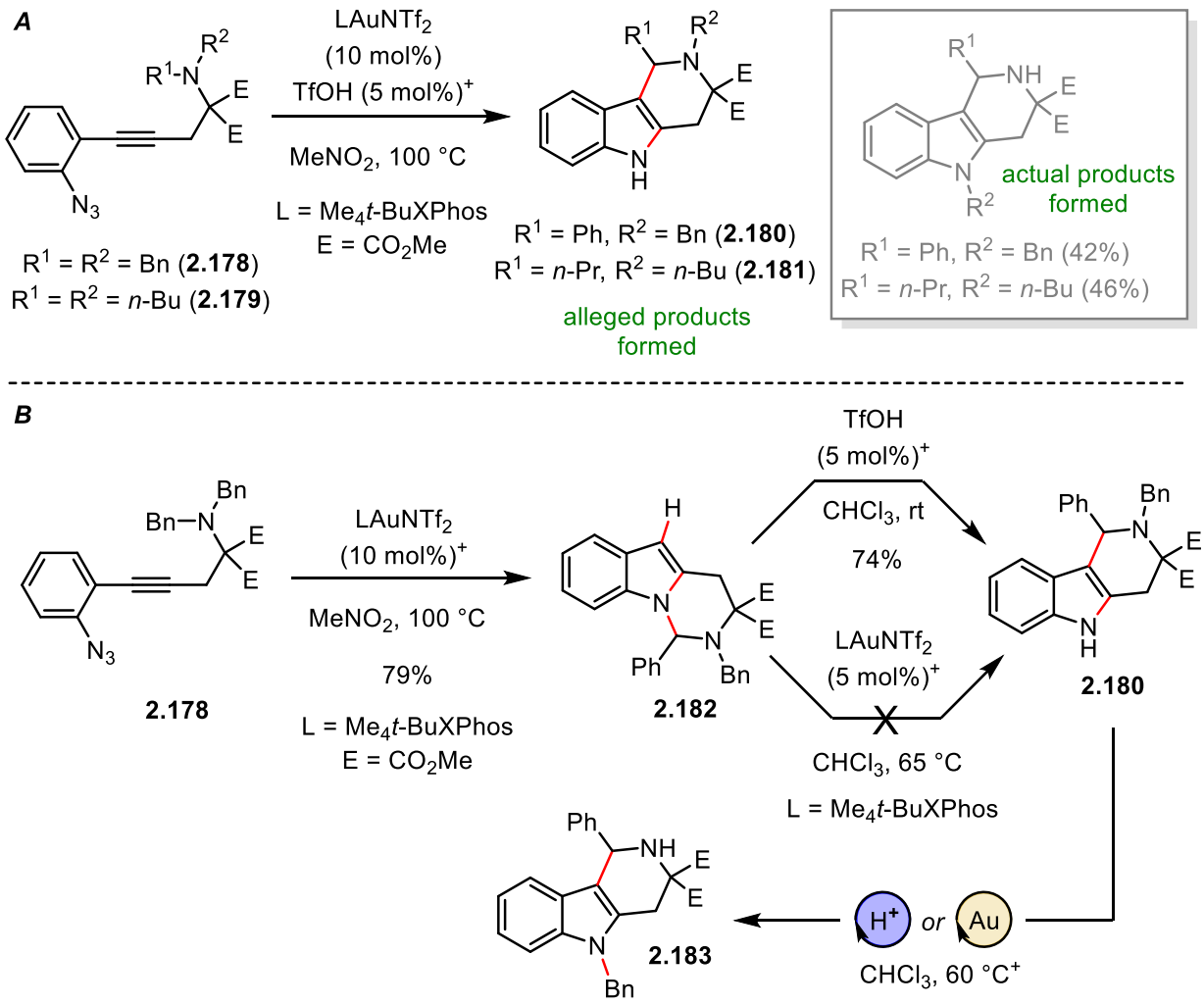


Scheme 2.30. Unsuccessful substrates with the malonate group not on the two-carbon linker. [+]Results by DFLR

2.7.3 Unexpected results when using acyclic hydride donor substrates

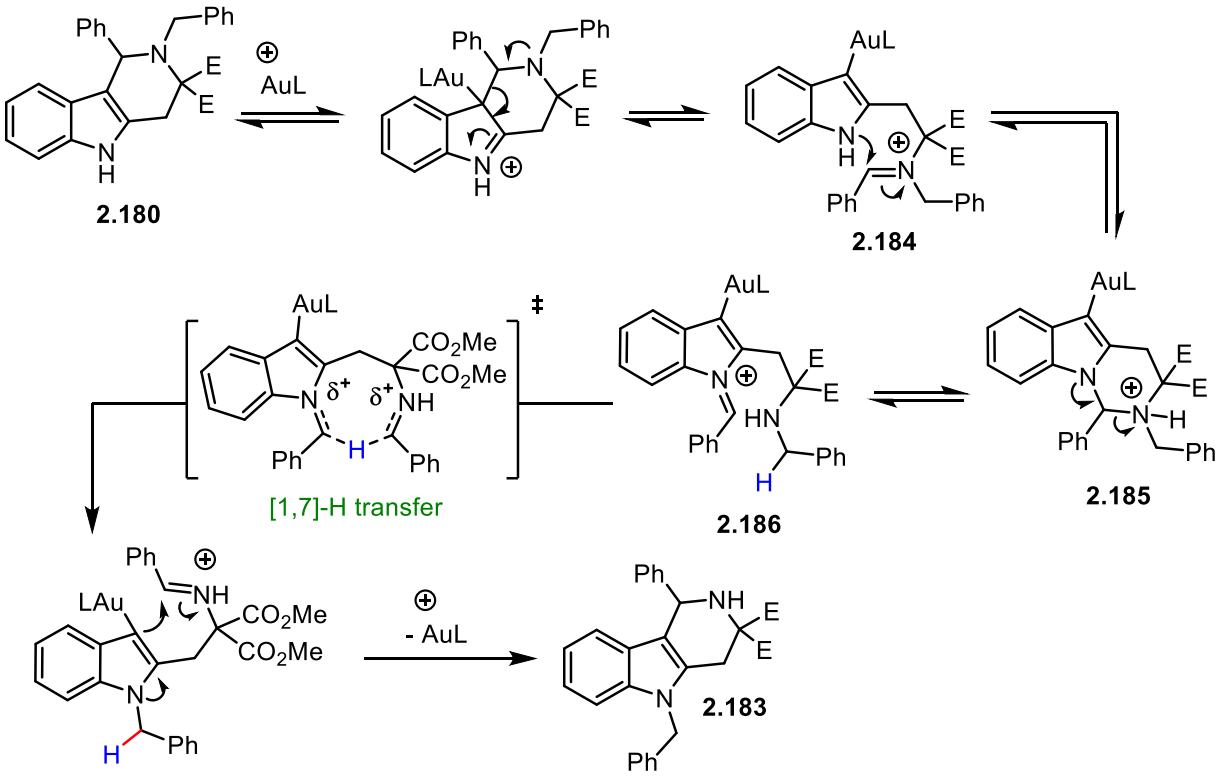
Substrates which possessed acyclic hydride donors that were commercially available were synthesized by David in an identical manner to substrates that contain cyclic hydride donors as shown above in Scheme 2.28A. When submitting these substrates to our forcing conditions, it was found that synthetically useful yields of product were only being obtained from symmetrical acyclic amine donors. Non-symmetrical donors generally underwent decomposition or formed

several side-products, likely because of competitive hydride donation from equally activated positions. Both dibenzyl **2.178** and dibutyl **2.179** worked reasonably well to deliver product in 42% and 46% isolated yield respectively (Scheme 2.31A). These products were initially assigned as indole products **2.180** and **2.181**. Further experimentation later showed this structural assignment to be false. To isolate the aminal intermediate **2.182**, dibenzyl substrate **2.178** was reacted by David under our best conditions but excluded the acid (Scheme 2.31B). Under these conditions, aminal **2.182** was isolated in 79% yield. Subjecting **2.182** to catalytic quantities of TfOH (5 mol%) in chloroform at room temperature led to the isolation of a different product in 74% yield. After thorough spectral analysis, this compound was confirmed to be the desired indole product **2.180**. The ^{1}H-NMR spectrum of desired **2.180** did not match the spectrum of the original product isolated from reacting dibenzyl substrate **2.178** in the presence of the gold catalyst ***and*** TfOH (Scheme 2.31A). This product was instead assigned as the rearranged product **2.183** which showed one benzyl group migration from the tertiary amine to the indole nitrogen. Further experimentation by David showed that desired indole **2.180** can also be converted to rearranged product **2.183** using ***only the gold catalyst*** or ***only TfOH*** in refluxing chloroform (Scheme 2.31B). Remarkably, aminal **2.182** does not isomerize to the indole product **2.180** in the presence of only the gold catalyst, explaining why **2.183** was only observed when acid was added. This is in stark contrast to the cyclic hydride donor substrates, which form mixtures of aminal and indole depending on the reaction conditions. These results were highly unexpected and represent an unprecedented turn of events that warrant further study. While incredibly interesting, only a brief discussion of these observations will be discussed since this work is beyond the scope of this thesis.



Scheme 2.31. Unexpected formation of a new rearranged product **2.183** from dibenzyl and dibutyl substrates **2.178** and **2.179**. $^{+}$Results by DFLR

To try and explain the formation of rearranged product **2.183**, the following tentative and preliminary mechanism is proposed below (Scheme 2.32). This mechanism is informed by the small number of experiments discussed above. Indole **2.180** in the presence of Au(I) is metalated at the *C*3 position, triggering a C-C bond fragmentation that gives iminium **2.184**. This iminium species is trapped by the indole nitrogen to give a new *C*3-aurated aminal **2.185** which following proton transfer can undergo further fragmentation to form a new iminium intermediate **2.186**. From here, a [1,7]-H transfer, followed by new C-C bond formation and loss of Au(I) could deliver the observed product.



Scheme 2.32. Preliminary mechanism explaining the formation of rearranged product **2.183** from indole **2.180** in the presence of Au(I) and acid

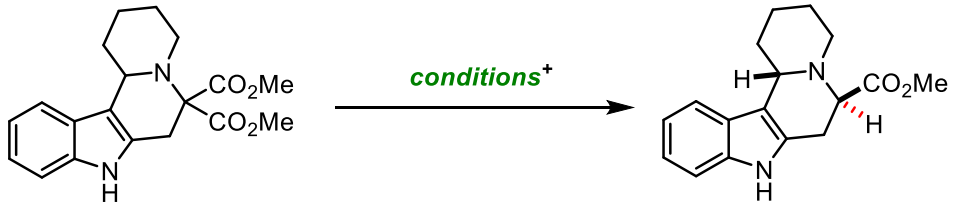
2.8 Product derivatization

2.8.1 Derivatization of the malonate blocking group

We next turned our attention to functionalizing the malonate group of the indole model product **2.104**. As was briefly alluded to above in Scheme 2.23, the malonate group can function as a useful synthetic handle for further functionalization. Classical transformations of malonates include the selective removal of one ester or both, usually under strongly basic or acidic conditions. The results of this study are summarized in Table 2.11 and were performed by David. Our first attempts at functionalization used an excess of KOH in EtOH (Entries 1–2). At 85 °C, our goal was to simultaneously saponify and decarboxylate, however only decomposition of the substrate was observed at high temperatures. Switching to room temperature was beneficial but we only obtained the ethyl ester derivative of our substrate (50% NMR yield), likely because of transesterification. Modifying the conditions slightly to using aqueous base showed promise.

Using LiOH in a 1:1 mixture of THF and H_2O resulted in the desired dealkoxycarbonylation occuring, albeit in a low 31% yield with modest diastereoselectivity (Entry 3). Switching the base back to KOH and using a phase transfer agent led to much better yields (Entry 4–5). Now, the monoester product **2.187** could be obtained in 67% isolated yield with a slight drop in diastereoselectivity. Notably, 30 equivalents of KOH were needed here. Using less resulted in incomplete conversions and lower yields. We also attempted the same under acidic conditions instead (Entry 6). No reactivity took place using concentrated HCl below 100 °C (salt formation). At temperatures >100 °C, decomposition of the substrate took place. Conditions to affect the Krapcho decarboxylation were also tried (Entry 7) but lead to decomposition over-time despite the initial observation of product formation when monitoring the reaction by TLC/MS.

Table 2.11. Optimization for the dealkoxycarbonylation reaction of model product **2.104** to give monoester product **2.187**



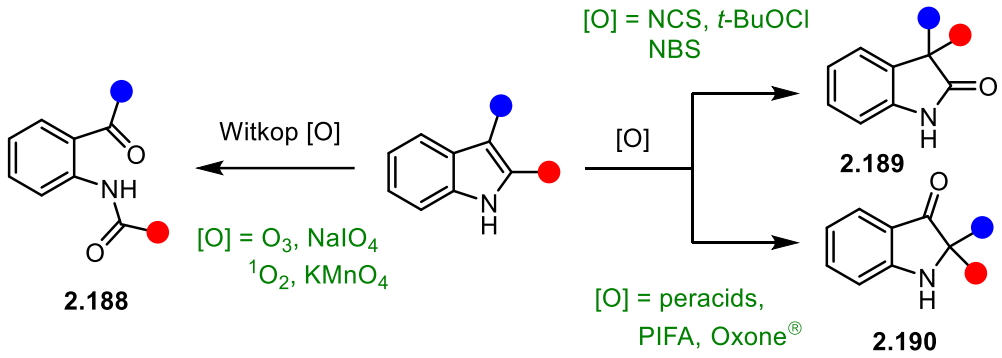
2.104 **2.187**[a]

Entry	Base (*x* equiv.)	Additive (*x* equiv.)	Temperature (°C)	Solvent[f]	Yield (%)	*d.r.*[b]
1	KOH (5)	--	85	EtOH	--[d]	--
2	KOH (5)	--	23	EtOH	50	--
3	LiOH (2)	--	50	THF:H_2O	31[c]	3.6:1
4	$KOH_{(aq)}$ (5)	$BnEt_3NCl$ (0.5)	50	THF	50[c]	1.8:1
5	$KOH_{(aq)}$ (30)	$BnEt_3NCl$ (0.5)	50	THF	67[c]	2.2:1
6	*conc.* HCl (50)	--	50	H_2O	--[d,e]	--
7	--	LiBr (10)	85	DMA	--[d]	--

[a] The major diastereoisomer is shown. [b] NMR yields and diastereomeric ratios (*d.r.*) were determined from the crude ^{1}H-NMR analysis using mesitylene as an internal standard. [c] Isolated yield. [d] Total degradation. [e] Recovered protonated starting material. [f] 0.1 M concentration. $^+$Results by DFLR.

2.8.2 Oxidative derivatization of the indole skeleton

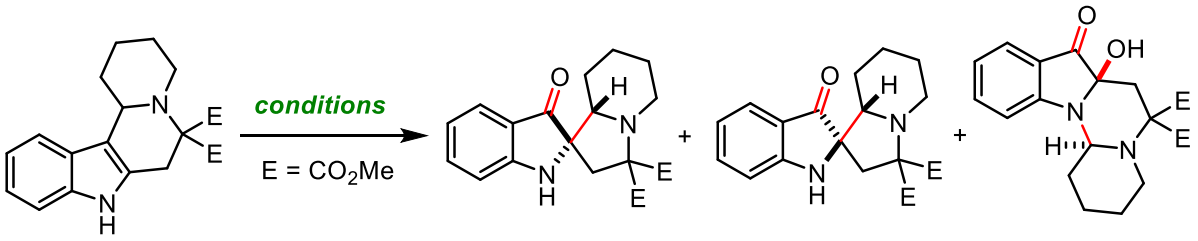
Indole oxidations are a fundamental transformation in organic chemistry and can deliver a variety of pharmaceutically relevant and synthetically useful compounds.[127] In particular, indoles will often undergo oxidative rearrangement or cleavage reactions, however these transformations are usually hard to control. This is mostly due to the electron-rich property of indoles, allowing them to be easily oxidized using numerous oxidants with competitive nitrogen, *C*2 and/or *C*3 oxidations taking place depending on the choice of oxidant.[128] In general, three major types of indole oxidations can take place (Scheme 2.33): oxidative rearrangement to 2-oxindoles **2.189**, oxidative rearrangement to 3-oxindoles **2.190** (also called pseudoindoxyls), and oxidative cleavage *via* the Witkop oxidation to give *ortho*-keto acetanalides **2.188**. Which pathway is chosen is generally highly dependant on the oxidant used, the reaction conditions, and on the substituents on either the *C*2 or *C*3 positions.



Scheme 2.33. Common pathways for the oxidation of indole scaffolds

We began by screening several oxidants which have been known to form either the 2- or 3-oxindole skeletons *via* oxidative rearrangements (Table 2.12). Initially attempting PIFA and Bz_2O_2 (Entries 1–2) were unsuccessful, mostly resulting in decomposition of the substrate or return of the starting material. Our first hit came with using *m*-CPBA as the oxidant (Entry 3), resulting in the formation of pseudoindoxyl product **2.191a** in 13% isolated yield and as a single diastereoisomer. Next, we tried using Oxone® as the oxidant in acetone to generate highly reactive DMDO *in-situ* (Entry 4). This resulted in a combined yield of 40% for both pseudoindoxyl diastereomers **2.191a** and **2.191b**. Capitalizing on this result, we decided to try other attempts utilizing Oxone® and other reagents besides acetone to see if we could improve selectivity.

Table 2.12. Optimization for the formation of doubly oxidized product **2.192** from indole **2.104**

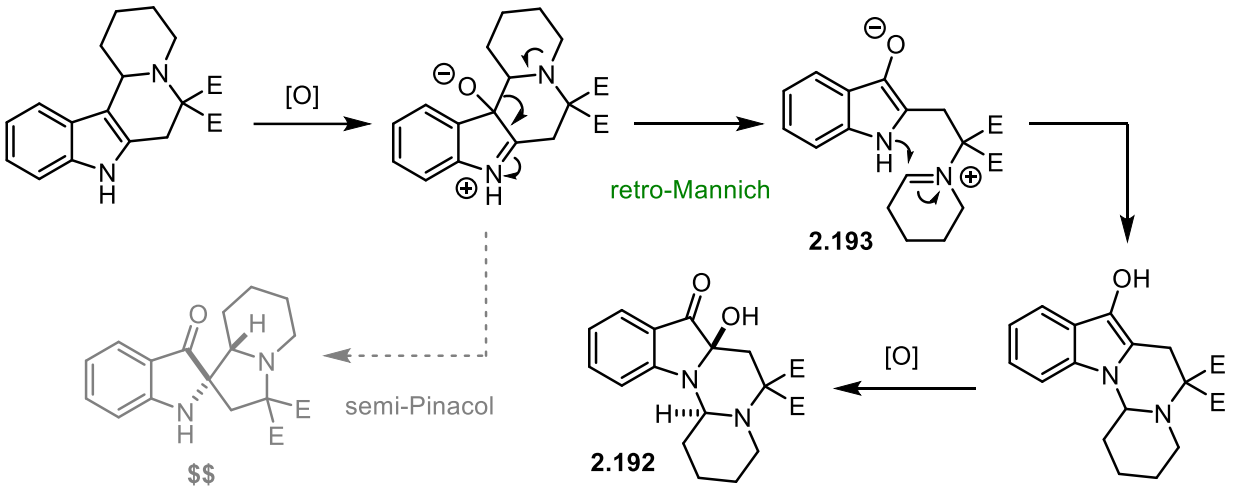


Entry	Oxidant (*x* equiv.)	Additive (*x* equiv.)	Temperature (°C)	Solvent[d]	Yield (%)[a] 2.191a	2.191b	2.192
1	PIFA (1.1)	--	0	MeCN:H_2O	--	--	--
2	Bz_2O_2 (1)	--	23	$CHCl_3$	--	--	--
3	*m*-CPBA (1)	--	23	DCM	13	--	--
4	Oxone® (2)	$NaHCO_{3(aq)}$ (10)	0	$(CH_3)_2CO$	20	20	--
5	Oxone® (2)	$NaHCO_{3(aq)}$ (10)	0	cyclohexanone	19	--	--
6	Oxone® (2)	$CF_3(CO)CH_3$ (2.2) $NaHCO_{3(aq)}$ (10)	0	MeCN	<5	--	--
7	Oxone® (2)	Shi's ketone (2.2) $NaHCO_{3(aq)}$ (10)	0	MeCN	--	--	--
8[b]	Oxone® (5)	cyclohexanone (2.2) $NaHCO_3$ (8)	0 to 23	MeCN	<5	<5	--
9[c]	Oxone® (10)	cyclohexanone (10) $BnEt_3NCl$ (0.1)	0	DCM:MeOH	--	--	70
10[c]	Oxone® (10)	$BnEt_3NCl$ (0.1)	0 to 23	$(CH_3)_2CO$	--	--	69
11	Oxone® (5)	--	0	MeOH:H_2O	--	--	70

[a] Isolated yield. [b] Using a 4 mM EDTA buffer (pH ~7). [c] Using a 0.5 M phosphate buffer (pH ~7). [d] 0.02 M concentration.

Various ketones (cyclohexanone, trifluoroacetone, Shi's ketone) and additives to help neutralize and buffer the reaction were used but to not much better success (Entries 5–8). Unbuffered (Entry 5), the reaction gave 19% yield of **2.191a** with no trace of **2.191b** employing cyclohexanone. Oxone® in the presence of trifluoroacetone or Shi's ketone was unproductive. Using an EDTA buffer with cyclohexanone (Entry 8) gave traces of product but switching to a

phosphate buffer (Entry 9) gave a new doubly oxidized product **2.192** in 70% isolated yield and as a single diastereoisomer. **2.192** is believed to form under neutral conditions, where after the first oxidation of the indole, a C-C bond fragmentation occurs forming an intermediate iminium species **2.193** (Scheme 2.34). Cyclization from the indole nitrogen, followed by a second oxidation affords **2.192**. For easier purification and work-up, the same reaction was repeated using acetone and **2.192** was again formed in 69% yield (Entry 10). We then found that the buffer and acetone were unnecessary (Entry 11). Simply conducting the reaction in MeOH with the addition of Oxone® in water was sufficient and resulted in isolation of **2.192** in high yield and purity.

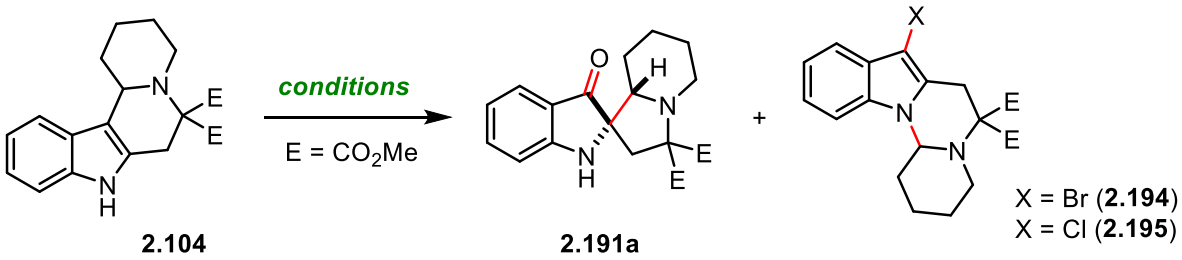


Scheme 2.34. Possible mechanism explaining the formation of **2.192**

In continuing our efforts to synthesize oxidative derivatization products of the indole nucleus, we also attempted oxidations mediated by halogenation reagents that have shown to be able to access 2-oxindoles (Table 2.13). Based on a recent report by Tong,[128] we employed Oxone® in the presence of KBr and AcOH as an alternative means of generating "Br+" (Entry 1). Using these conditions, it was expected we could form the 2-oxindole product; however, we ended up isolating the same pseudoindoxyl **2.191a** as a single diastereoisomer and in 18% yield. Other halogenating reagents such as NBS and NCS gave decomposition of the starting material (Entries 2–3). Re-trying the conditions by Tong but excluding the acid (Entry 4) resulted in the formation of another new compound that was found to be the bromoaminal **2.194** in 42% yield (most likely formed by a similar mechanism that led to **2.192**). Similarly, the use of *t*-BuOCl in place of NCS also led to the formation of chloroaminal **2.195** in good yield (Entry 5). Based on these

experiments, it seems the position of the nitrogen atom in our system is nicely poised to promote the key C-C bond fragmentation that is leading to oxidized aminal products **2.192**, **2.194**, and **2.195**. This implies that formation of 2-oxindole products will be difficult, however the formation of pseudoindoxyl products is still possible based on the result from Entry 1. The acidic conditions of that reaction likely helped prevent the C-C bond fragmentation by means of nitrogen protonation. With the ammonium unable to promote bond cleavage, the 1,2-migration pathway became preferred and led to the formation of **2.191a**. With this in mind, we preemptively protonated our substrate using a stronger acid such as TFA and then introduced the Oxone® (Entry 6). Gratifyingly, this led to the successful isolation of pseudoindoxyl **2.191a** in 76% yield with excellent selectivity (*d.r.* = 15:1).

Table 2.13. Oxidative conditions for the synthesis of pseudoindoxyl product **2.191a** and halogenated aminal products **2.194** and **2.195** from indole **2.104**



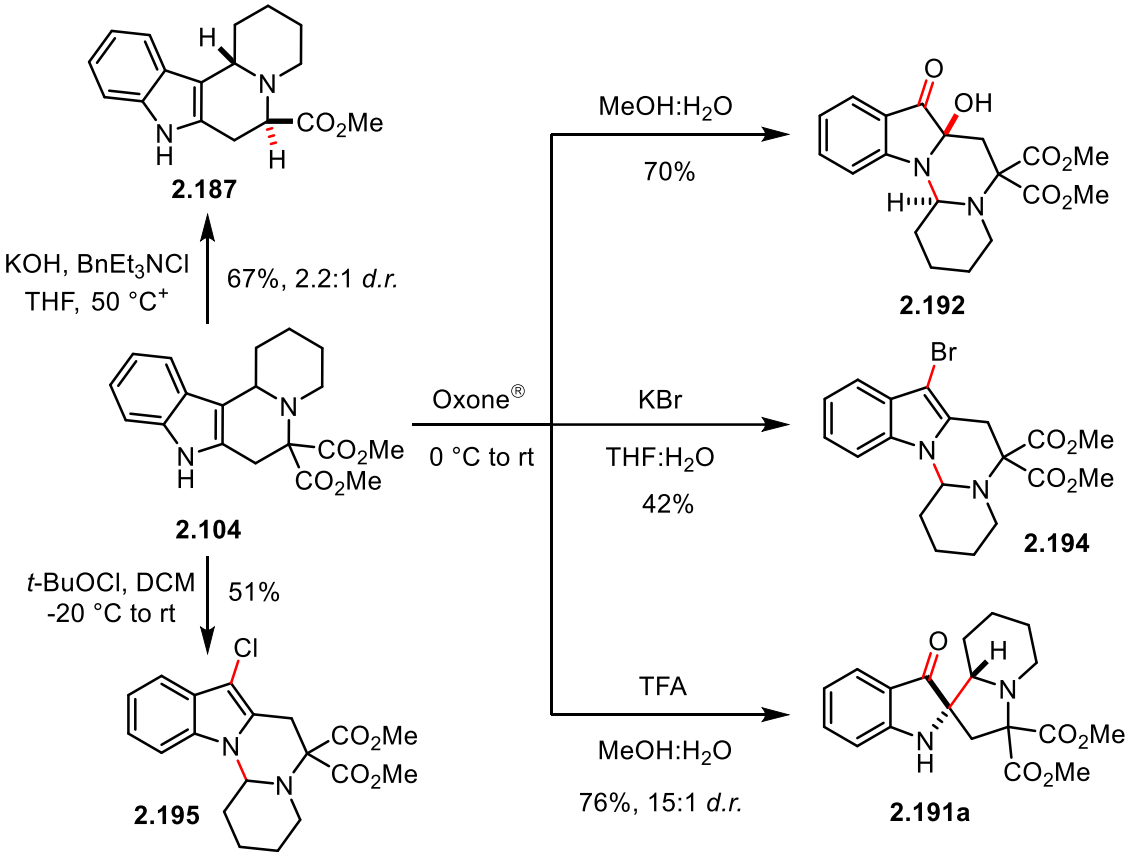
2.104 **2.191a**

Entry	Oxidant (*x* equiv.)	Additive (*x* equiv.)	Temperature (°C)	Solvent[b]	Yield (%)[a] 2.191a	2.194	2.195
1	Oxone® (1.2)	KBr (0.1)	0 to 23	THF:H_2O:AcOH	18	--	--
2	NBS (1)	--	23	$(CH_3)_2CO$	--	--	--
3	NCS (1.3)	--	-40 to 23	DCM	--	--	--
4	Oxone® (1.2)	KBr (1)	0 to 23	THF:H_2O	--	42	--
5	*t*-BuOCl (1.1)	--	-20 to 23	DCM	--	--	51
6	Oxone® (3.2)	TFA (1.2)	0	MeOH:H_2O	76	--	--

[a] Isolated yield. [b] 0.02 M concentration.

Interestingly, doubly oxidized aminal **2.192** and pseudoindoxyl **2.191a** possess the core structure of two indole alkaloid natural products vernavosine[129] and mitragynine pseudoindoxyl that has been recently synthesized.[130] Given the rapid access of these scaffolds using our

methodology, an opportunity for chemical synthesis or analogue development is possible. The results of our efforts towards the derivatization of indole **2.104** are summarized in Scheme 2.35 below.



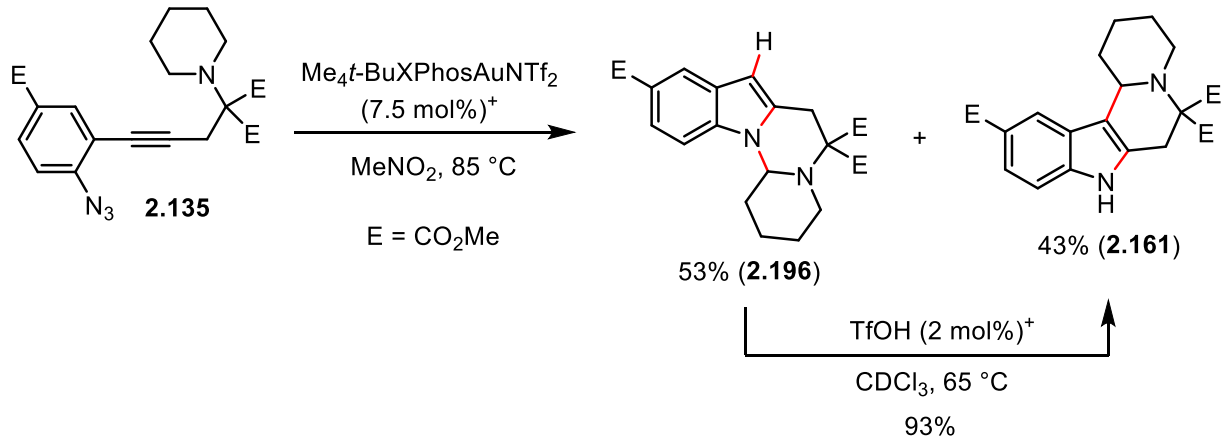
Scheme 2.35. Summary of indole product derivatization post C-H functionalization. [+]Result by DFLR

2.9 Mechanistic studies

2.9.1 Isolation of reaction intermediates

To probe for the existence of the aminal intermediate, we set out to isolate this compound from the reaction mixture (Scheme 2.36). During our scope evaluation, David found that substrate **2.135** which possessed a methyl ester on the arylazide (*para* relationship) gave appreciable amounts of the aminal by-product **2.196** in the absence of the Brønsted acid additive. The aminal **2.196** could be easily separated from the indole **2.161** (43% yield), therefore it was isolated in 53% yield and fully characterized. Subjecting aminal **2.196** with a catalytic amount of TfOH in $CDCl_3$

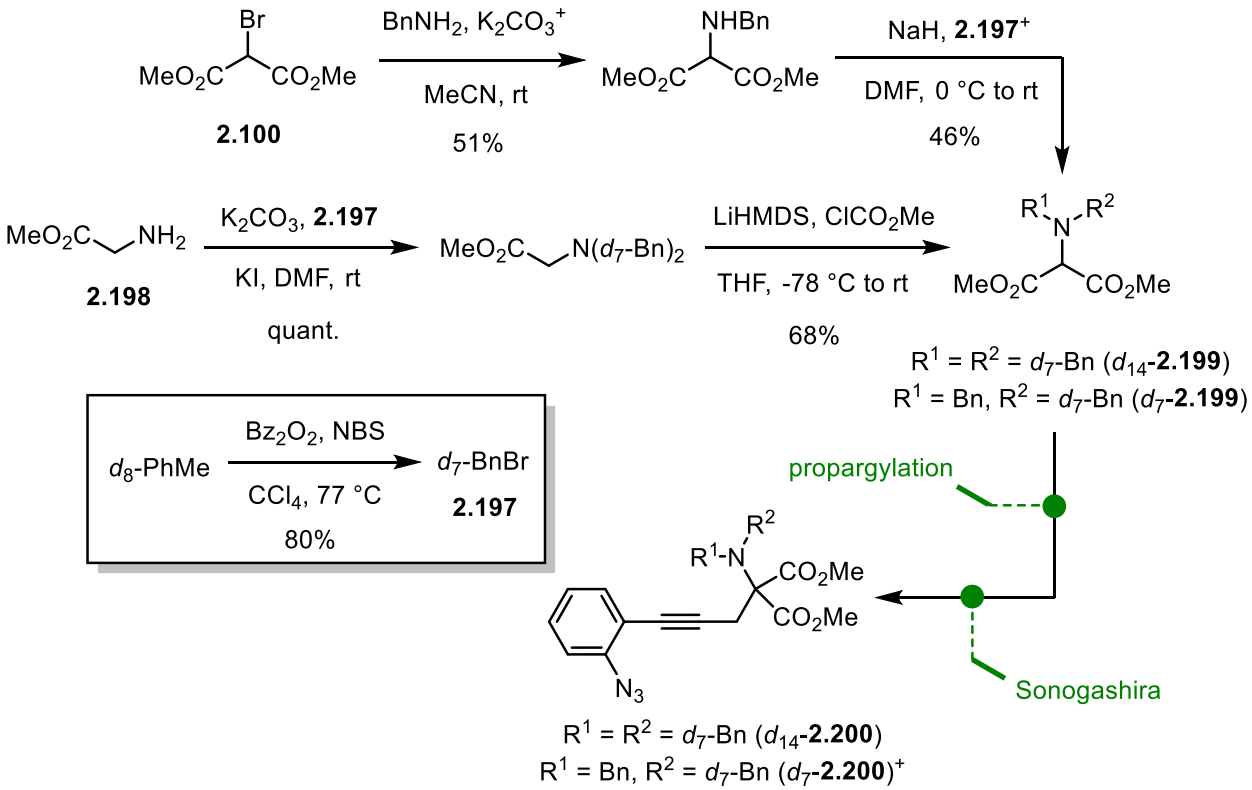
demonstrated full conversion to indole **2.161** in 93% yield, supporting the intermediacy of aminal **2.196** in this reaction.



Scheme 2.36. Successful isolation, characterization, and conversion of aminal **2.196** into indole product **2.161** supporting its role as a reactive intermediate. [+]Results by DFLR

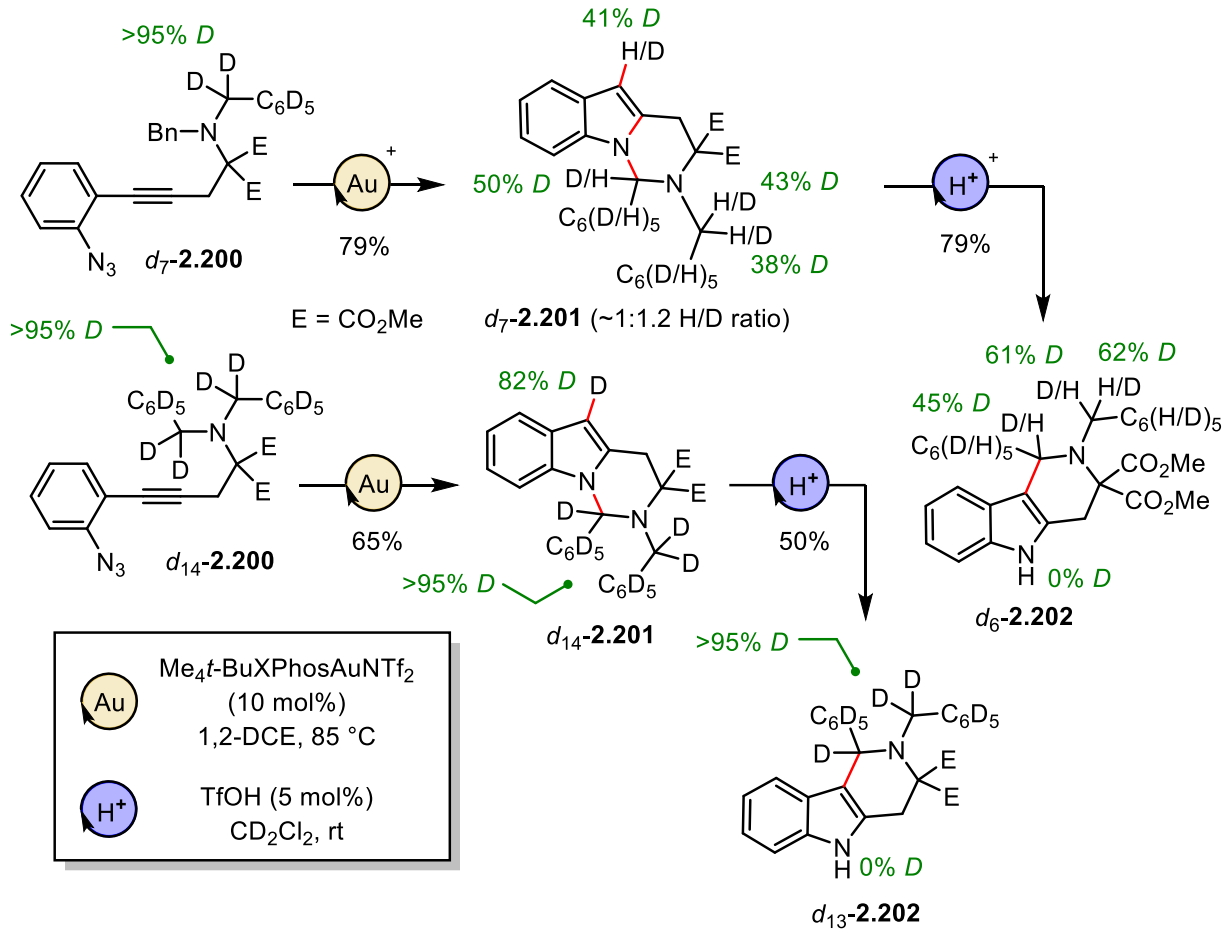
2.9.2 Deuterium labelling experiments

To help support the [1,6]-H transfer mechanism, we conducted a series of deuterium labelling experiments. We chose to use dibenzyl substrate **2.178** as our probe since we have shown it is possible to access both the aminal intermediate **2.182** and the indole product **2.180** in a stepwise manner, making tracking the movement of deuterium more feasible. We began by synthesizing d_7-**2.200** and d_{14}-**2.200** which are deuterated versions of **2.178** with one or both benzyl groups fully deuterated (Scheme 2.37). The deuterated benzyl groups were introduced *via* substitution using d_7-BnBr **2.197** which was synthesized by radical bromination of d_8-PhMe with NBS and Bz_2O_2 in refluxing carbon tetrachloride (80% yield). Glycine methyl ester **2.198** was then dibenzylated with **2.197** and carbonylated with methyl chloroformate to make d_{14}-malonate (d_{14}-**2.199**) in 68% yield over two steps. In parallel, substitution of methyl bromomalonate **2.100** with benzylamine followed by amine benzylation with **2.197** gave d_7-malonate (d_7-**2.199**) in good yield. Subsequently, both d_7-**2.199** and d_{14}-**2.199** underwent propargylation and Sonogashira coupling with arylazide **2.86** as seen previously to afford substrates d_7-**2.200** and d_{14}-**2.200**.



Scheme 2.37. Synthesis of partially and fully deuterated substrates d_7-**2.200** and d_{14}-**2.200**. [+]Results by DFLR

Submitting both substrates to our optimized catalysis conditions in 1,2-DCE as solvent led to the smooth transfer of the benzylic deuterium atoms to the *C*3 position of the intermediate d_7- and d_{14}-aminals (d_7-**2.201** and d_{14}-**2.201**) respectively (Scheme 2.38). 82% deuterium incorporation was observed at *C*3 for d_{14}-**2.201** and it was isolated in 65% yield. In the case of d_7-**2.201**, it was isolated in 79% yield as a ~1:1.2 mixture of hydrogen *vs* deuterium transfer products. 33% deuterium incorporation was observed at the *C*3 position. The slightly reduced labelling observed at the *C*3 position is likely due to residual water favoring deuterium to hydrogen exchange. In a separate experiment, we had also observed gradual deuteration of the aminal *C*3 position when reacting non-deuterated dibenzyl substrate **2.178** in d_3-$MeNO_2$. This implies the facile exchange that may occur at position *C*3 with acidic and/or exchangeable protons. Subjecting both d_7-**2.201** and d_{14}-**2.201** to acidic rearrangement resulted in the complete loss of deuteration at *C*3 in the final indole products d_6-**2.202** and d_{13}-**2.202**. As expected, labelling at the benzylic positions remained similar in both products.

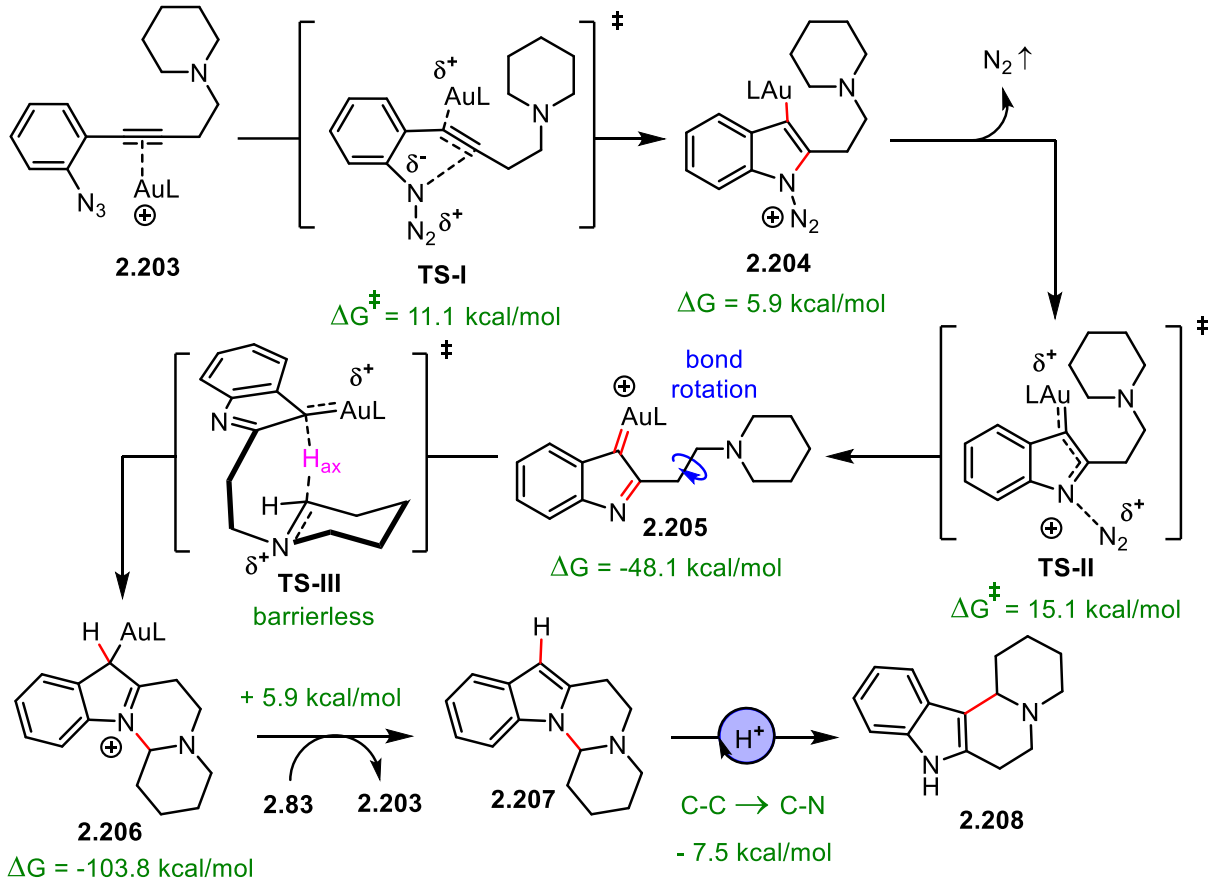


Scheme 2.38. Deuterium labelling experiments. [+]Results by DFLR

2.9.3 DFT studies and calculations

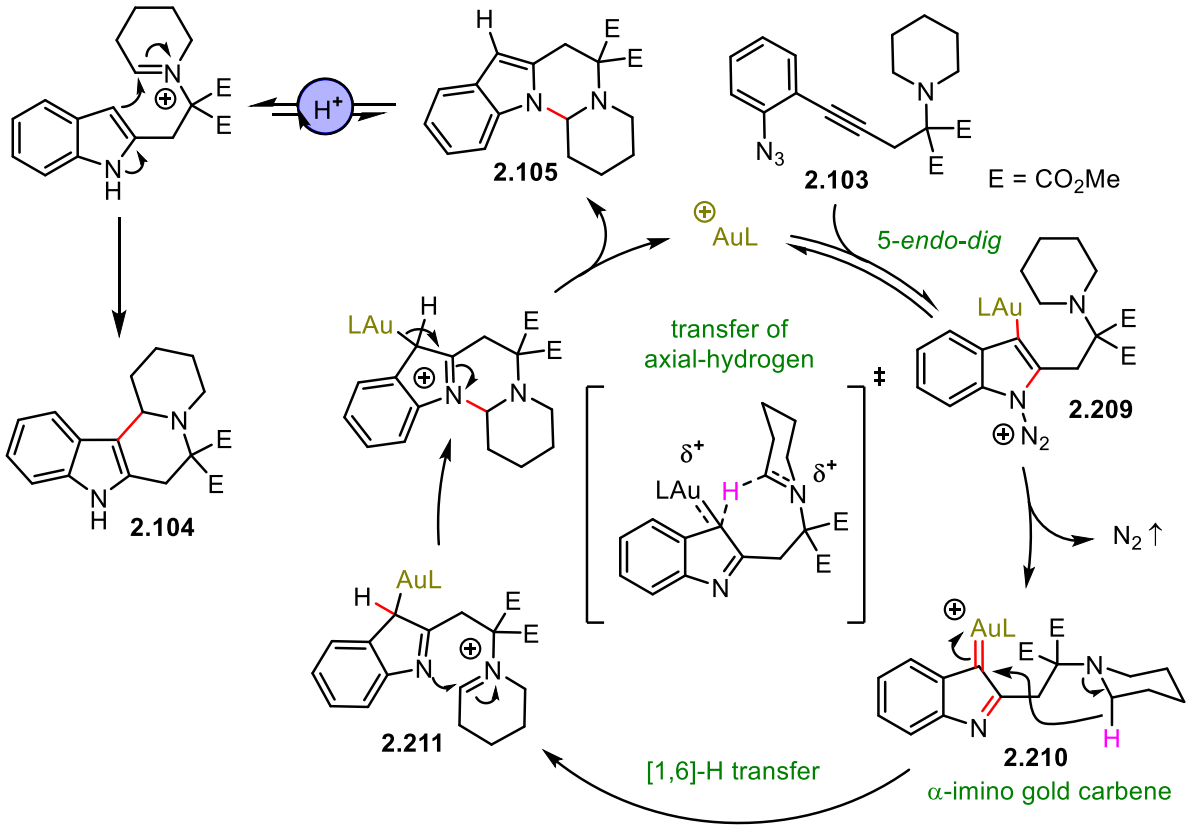
To gain better insight into the relative energy profile of the reaction, density functional theory (DFT) calculations were performed by Professor Gagosz. These calculations were performed at the M06/6-31G(d,p) level of theory for *C*, *H*, *N*, and *P* atoms and SDD for the Au basis set. To account for the use of 1,2-DCE and $MeNO_2$, the solvation model based on density (SMD) was used. For convenience and to make computation a little easier and less demanding, piperidine substrate **2.83** lacking the malonate was used in addition to PH_3 as the ligand (Scheme 2.39). According to calculations, the initial steps of the reaction are initiated by the nucleophilic azide attacking the activated Au(I)-alkyne complex **2.203** through transition state **TS-I**, forming intermediate **2.204** that is higher in energy by 11.1 kcal/mol. This unfavorable increase in energy is then compensated for by successive exergonic steps, first of which involving the highly

favorable and irreversible loss of nitrogen gas from intermediate **2.204** (through **TS-II**) with concomitant formation of α-imino gold carbene **2.205** that is 38.9 kcal/mol lower in energy than intermediate **2.204**. Next, a low energy bond rotation helps α-imino gold carbene **2.205** reach the correct conformation for the [1,6]-H transfer to occur. The hydride transfer event appeared to be virtually barrierless since the transition state for this process (**TS-III)** was located on a very flat potential energy surface. The iminium from the hydride transfer step is trapped and then shown to result in *C*3-Au(I) complex **2.206** in a highly favorable process. The catalytic cycle is closed *via* exchange with another molecule of substrate and loss of gold to liberate aminal **2.207** that is then isomerized to the indole product **2.208**. Interestingly, forming aminal **2.207** was found to be unfavorable by 5.9 kcal/mol, since calculations showed that transfer of Au(I) from **2.206** onto a new molecule of substrate **2.83** was needed. In the presence of acid, this increase in energy is likely offset by the formation of the thermodynamically more stable indole which was calculated to be 7.9 kcal/mol more stable (agreeing with our experimental observations).



Scheme 2.39. Computational analysis of the free energy reaction profile

Overall, the DFT calculations in addition to the other mechanistic experiments support the catalytic cycle proposed in Scheme 2.40. An initial 5-*endo-dig* cyclization of the azide onto the Au(I)-alkyne complex produces intermediate **2.209** in a reversible manner. Loss of nitrogen occurs with formation of the α-imino gold carbene **2.210** that subsequently undergoes the key [1,6]-H transfer. The resulting iminium **2.211** evolves to yield aminal **2.105** after loss of the catalyst and exchange with another molecule of substrate **2.103** to restart the cycle. Finally, aminal **2.105** can be isomerized to the more stable indole **2.104** under acid catalysis.



Scheme 2.40. Proposed mechanism for the Au(I) catalyzed α-C-H functionalization of tertiary amines

2.10 Conclusion

To summarize this chapter, we have developed a new process for the Au(I) catalyzed Csp^3-H bond functionalization of free tertiary amines. As discussed throughout this chapter, this type of transformation has seen little progress owing to the general incompatibility between Lewis acidic Au(I) complexes and basic nitrogen atoms. We uniquely overcame this challenge through the

rational incorporation of a malonate blocking group α the nitrogen atom. A thorough optimization series and a meticulous structure-activity relationship campaign helped to show that the malonate exerts steric, electronic, and conformational effects. Importantly, these effects seemed to be operating in synergy rather than in competition with one another. We also demonstrated that this reaction is broadly applicable, tolerates different functional groups, and affords us valuable products that can be selectively functionalized to result in biologically and synthetically relevant structural motifs. Finally, we studied the mechanism of this reaction both experimentally and computationally, being able to isolate key reaction intermediates and show evidence for intramolecular hydride transfer through deuterium labelling.

CHAPTER 3

Total Synthesis of (±)-Brevianamide A

3.1 Introduction

3.1.1 Fungal derived prenylated indole alkaloids

Natural products derived from marine and terrestrial fungal sources have been an area of intense research and are known to serve as medicines for human, veterinary, and agricultural diseases.[131, 132] In particular, isolation of natural products from fungal species such as *Aspergillus* and *Penicillium* have led to the discovery of a wide variety of structurally unique prenylated indole alkaloids.[131] These alkaloids all share a bridging bicyclo[2.2.2]diazaoctane ring system (Figure 3) in addition to functionalized indole, hydroxy-indolenine, oxindole, or pseudoindoxyl units.[133] The bicyclo[2.2.2]diazaoctane core can possess either the *anti*- or *syn*-configuration and is thought to arise *via* an intramolecular Sammes-type *hetero*-Diels-Alder (IMDA) reaction.[134] The nomenclature of *syn* or *anti* refers to the relative orientation of the bridging C-H group and the nearby diketopiperazine nitrogen. In general, the *anti*-configuration is rare, with most bicyclo[2.2.2]diazaoctane alkaloids retaining the *syn*-configuration.[131] Similarly, the indole and oxindole motifs are common as compared to the more rare hydroxy-indolenine and pseudoindoxyl structures. Prominent representatives of this family of alkaloids can be categorized into two biosynthetically distinct sub-families: the monooxopiperazines and the dioxopiperazines.[135]

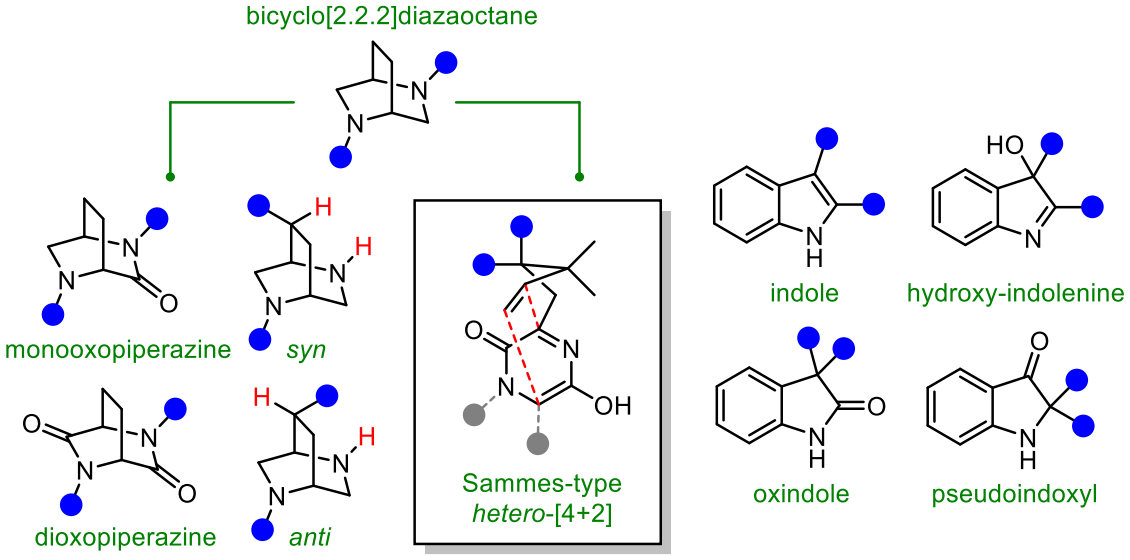


Figure 3. Key structural features of the bicyclo[2.2.2]diazaoctane family of alkaloids

Examples of the monooxopiperazine subfamily can include the paraherquamides,[136] asperparalines,[137] and malbrancheamides.[138, 139] Examples within the dioxopiperazine sub-family can include the brevianamides,[140] notoamides,[141] stephacidins,[142] and the taichunamides.[143] For decades, alkaloids within these classes have drawn considerable attention from the synthetic chemistry and biological communities owing to their plethora of important biological activities, intriguing biosynthesis, and complex molecular architectures. Many of these alkaloids have been reported to demonstrate anticancer,[141, 142] antihelmintic (antiparasitic),[144] neuroprotective,[145] and calmodulin inhibitory effects (Figure 3.1).[139] An example of a currently used formulation is the oral antihelmintic solution STARTECT™.[146] This veterinary medicine is used to treat and control gastrointestinal nematode and lungworm infections in sheep. It contains a mixture of the macrocyclic lactone abamectin in addition to (–)-2-deoxy-paraherquamide.

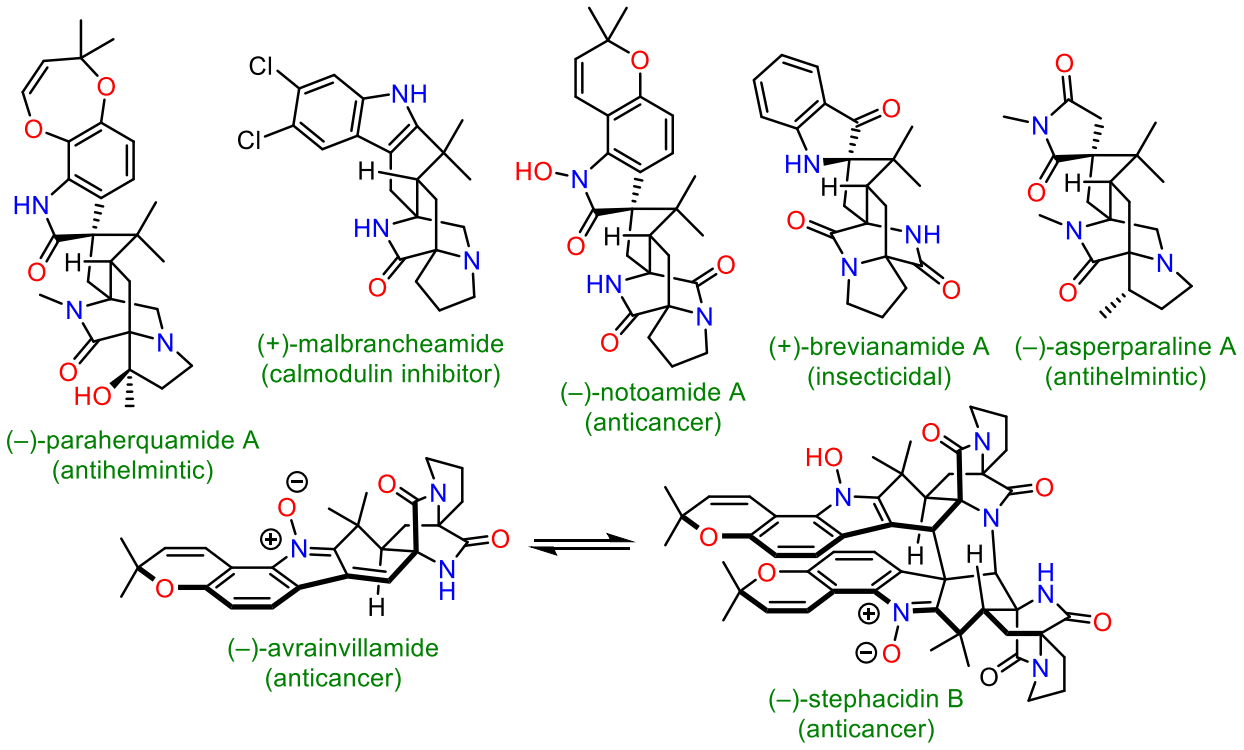


Figure 3.1. Representative examples and biological activity of prominent members within both monooxo- and dioxopiperazine sub-families

3.1.2 The brevianamides

The brevianamides are a group of fungal secondary metabolites that are mainly isolated from the genera *Penicillium* and *Aspergillus*. They are comprised of a relatively small group but are structurally interesting with several members having been reported since their initial isolation in 1969 by Birch and Wright.[147] Between the years of 1969 and 1972, Birch and co-workers isolated six brevianamides (A–F) from *Penicillium brevicompactum* (Figure 3.2).[131] Of these new compounds, four possessed the flagship bicyclo[2.2.2]diazaoctane core, with (+)-brevianamide A being the major fluorescent metabolite produced by this species of fungi. (+)-brevianamide A has also been isolated from the fungus *P. viridicatum*, of which it is now a known producer. At the time, this was the first instance where the bicyclo[2.2.2]diazaoctane core had been discovered in fungi, but since then greater than 100 fungal-derived prenylated indole alkaloids containing this ring system have been discovered.[148]

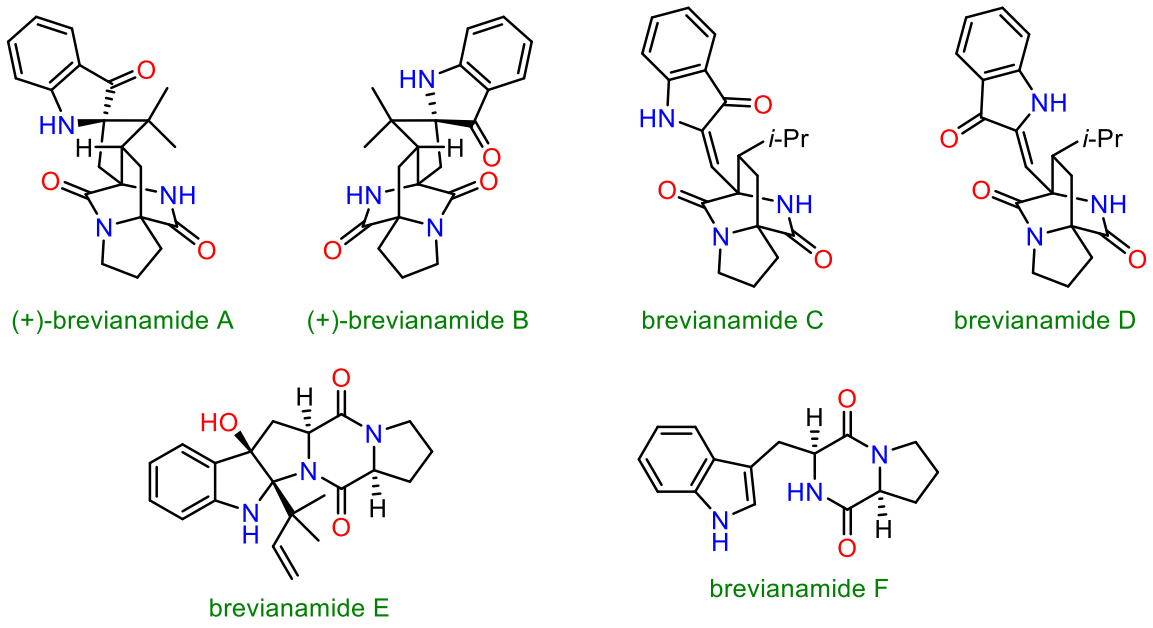
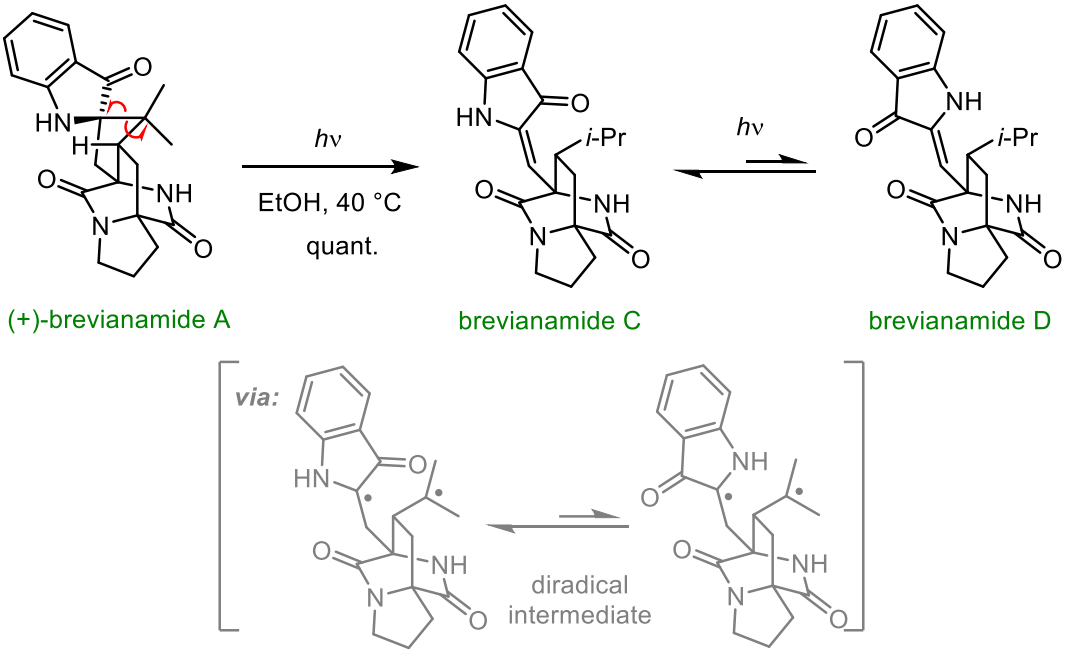


Figure 3.2. Structures of brevianamides A–F

Additional research by Birch and Russell found that brevianamides C and D were not metabolites of enzymatic origin, but rather were photochemical artifacts of isolation (Scheme 3).[149] Hypothesizing that (+)-brevianamides A and B were biosynthetic precursors to brevianamides C and D, they initially tried thermal treatment of (+)-brevianamides A and B to induce ring cleavage

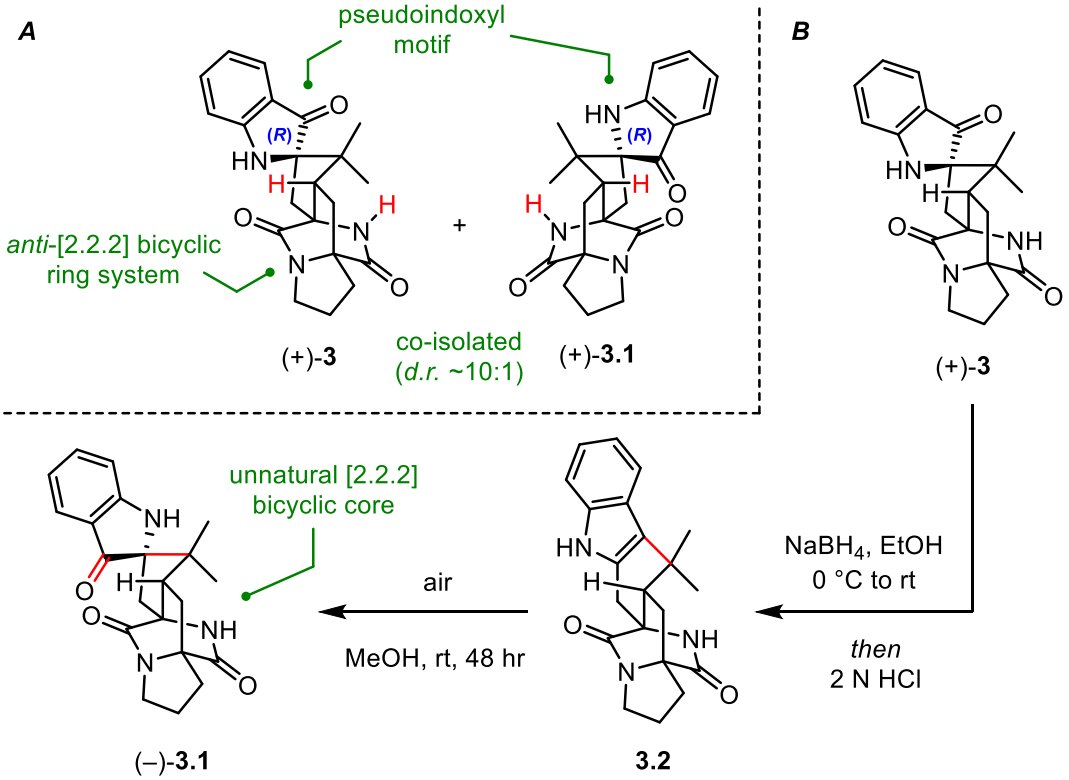
but found no success. They next considered a photochemical conversion, finding that irradiation of ethanolic solutions of (+)-brevianamide A led to an equilibrating mixture of brevianamides C and D in quantitative yield. This facile photolysis process can be explained through initial C-C bond homolysis to a diradical, hydrogen atom transfer, and then radical recombination. Intrigued by this result, they decided to grow cultures of *P. brevicompactum* in the dark. Remarkably, only (+)-brevianamides A and B were isolated with no traces of brevianamides C or D, verifying the hypothesis that the two are artifacts due to light exposure.



Scheme 3. Birch and Russell's photolysis studies on (+)-brevianamide A

As was mentioned before, (+)-brevianamide A (**3**) is the major metabolite produced by *P. brevicompactum* and is a prototypical dioxopiperazine indole alkaloid. Its structure and absolute stereochemistry were unambiguously solved through X-ray crystallography of the derivative (+)-5-bromobrevianamide A.[150] Exhibiting a unique (*R*)-configured *spiro*-pseudoindoxyl moiety and an *anti*-configured bicyclo[2.2.2]diazaoctane core, (+)-**3** is isolated as an approximate 10:1 mixture with another minor metabolite sharing the same structural features (Scheme 3.1A).[151] This minor component was deduced to be (+)-brevianamide B (**3.1**) and was assigned as the epimer of (+)-**3** at the *C*2 spirocyclic center. This structural assignment was confirmed *via* the semi-synthesis of (–)-**3.1** from natural sources of (+)-**3** (Scheme 3.1B).[149, 152] Sodium borohydride reduction

followed by acidic rearrangement gave the indole deoxybrevianamide A (**3.2**) that was oxidized under air to yield the unnatural and unexpected enantiomer (–)-**3.1** as the only product. At the time, the absolute configuration of brevianamide B produced under these conditions was not determined and this would later prove to be the crux of an interesting stereochemical puzzle which has its answer firmly rooted in the biogenesis of both (+)-**3**/**3.1**. This will be briefly discussed in the upcoming section.

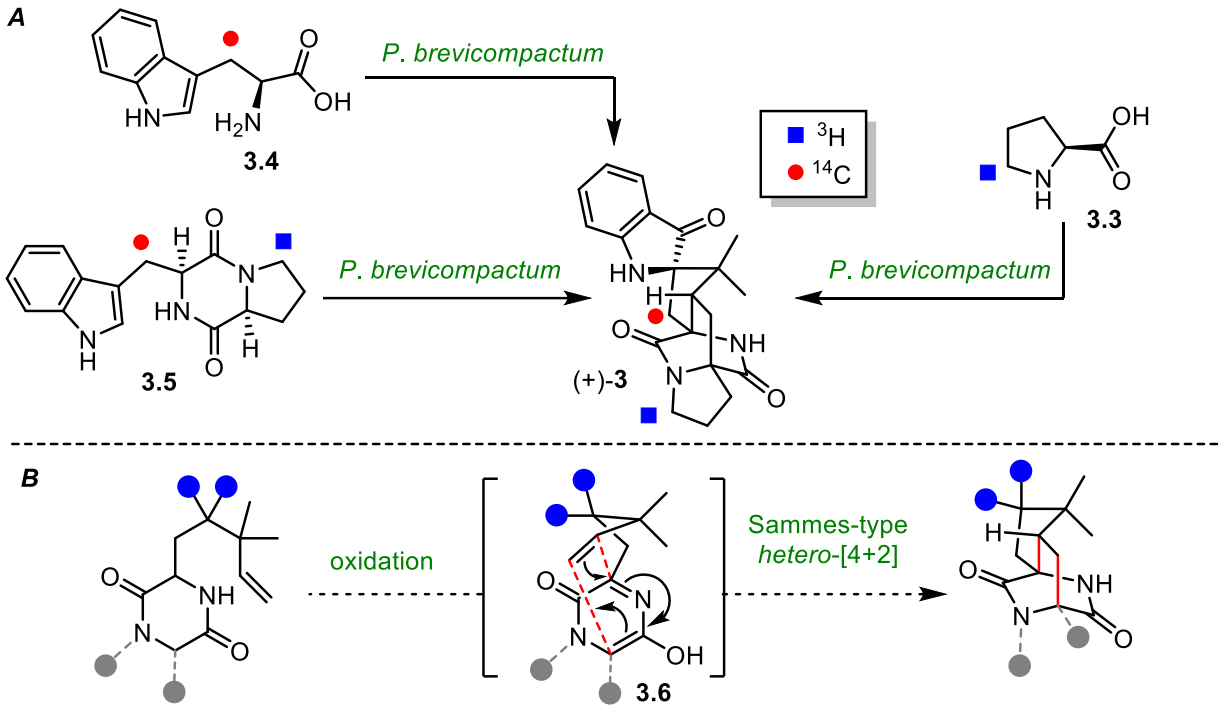


Scheme 3.1. (A) (+)-brevianamides A and B are co-isolated in ~10:1 *d.r.* from *P. brevicompactum* and (B) semi-synthesis of unnatural (–)-brevianamide B from natural (+)-brevianamide A

(+)-**3** is also a potent antifeedant and demonstrates insecticidal activity against the insect larvae of *Spodoptera frugiperda* (fall armyworm) and *Heliothis virescens* (tobacco budworm).[135, 153] As of yet, no reported biological activity has been demonstrated for (+)-**3.1** but the photolysis product brevianamide D showed promise as an antifeedant, albeit with weaker activity. However, brevianamide D was exceptionally good at causing weight loss in both larvae tested.

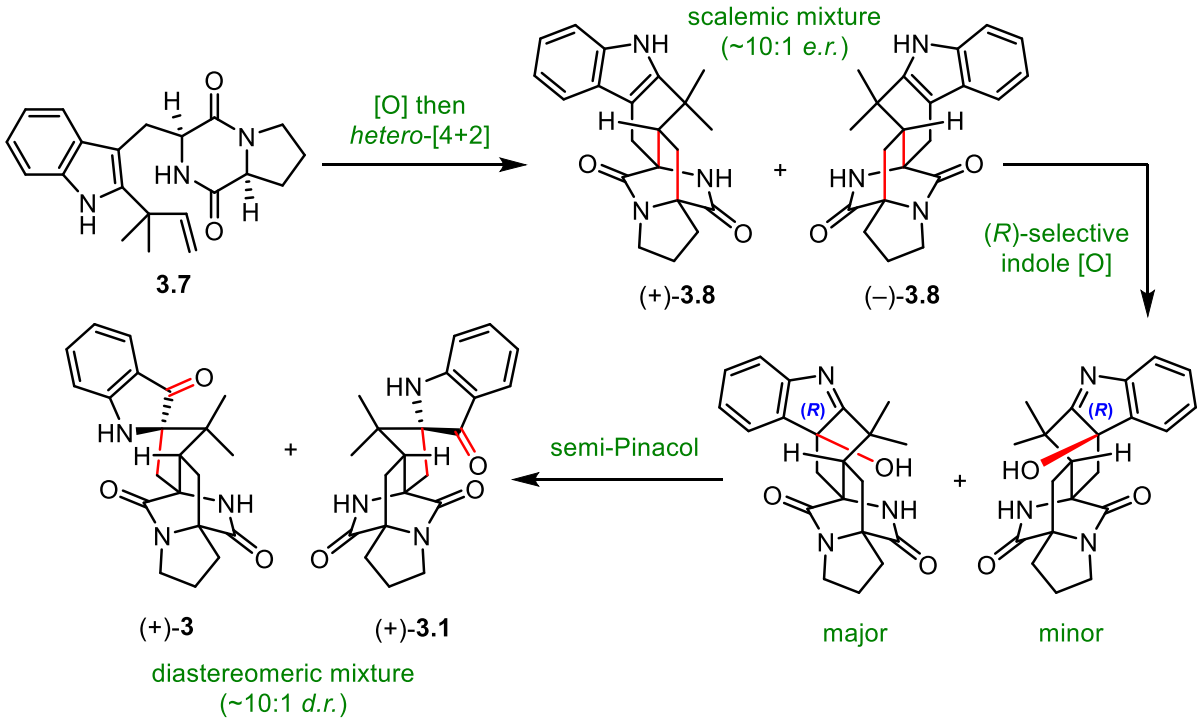
3.2 Studies toward the biosynthetic origins of (+)-brevianamides A and B

Early work from Birch and co-workers focused on elucidating the early stages of biosynthesis through several radiolabeling and incorporation studies (Scheme 3.2A).[154] They demonstrated that brevianamides are derived from naturally occurring amino acids *L*-proline (**3.3**) and *L*-tryptophan (**3.4**), giving rise to brevianamide F (**3.5**). Radiolabeled **3.3**, **3.4**, and **3.5** were fed to cultures of *P. brevicompactum* and shown to incorporate and be precursors to (+)-**3**. Reverse prenylation is then proposed to afford deoxybrevianamide E which is itself a natural product[155] and believed to be the common intermediate leading to all brevianamides. As for the bicyclo[2.2.2]diazaoctane core, Porter and Sammes suggested early on that this core may result from a *hetero*-intramolecular Diels-Alder (IMDA) reaction (Scheme 3.2B) with model studies to help support their claim.[156] They postulated the formation of an azadiene oxidized form (**3.6**) of the diketopiperazine which engages with the tethered dienophile in a [4+2] cycloaddition. This hypothesis dominated the literature and has been applied to other bicyclo[2.2.2]diazaoctane alkaloids.[133] Other proposals such as Birch's bridging disulfide intermediate were refuted due to lack of evidence for any sulfur incorporation in feeding studies.[157]



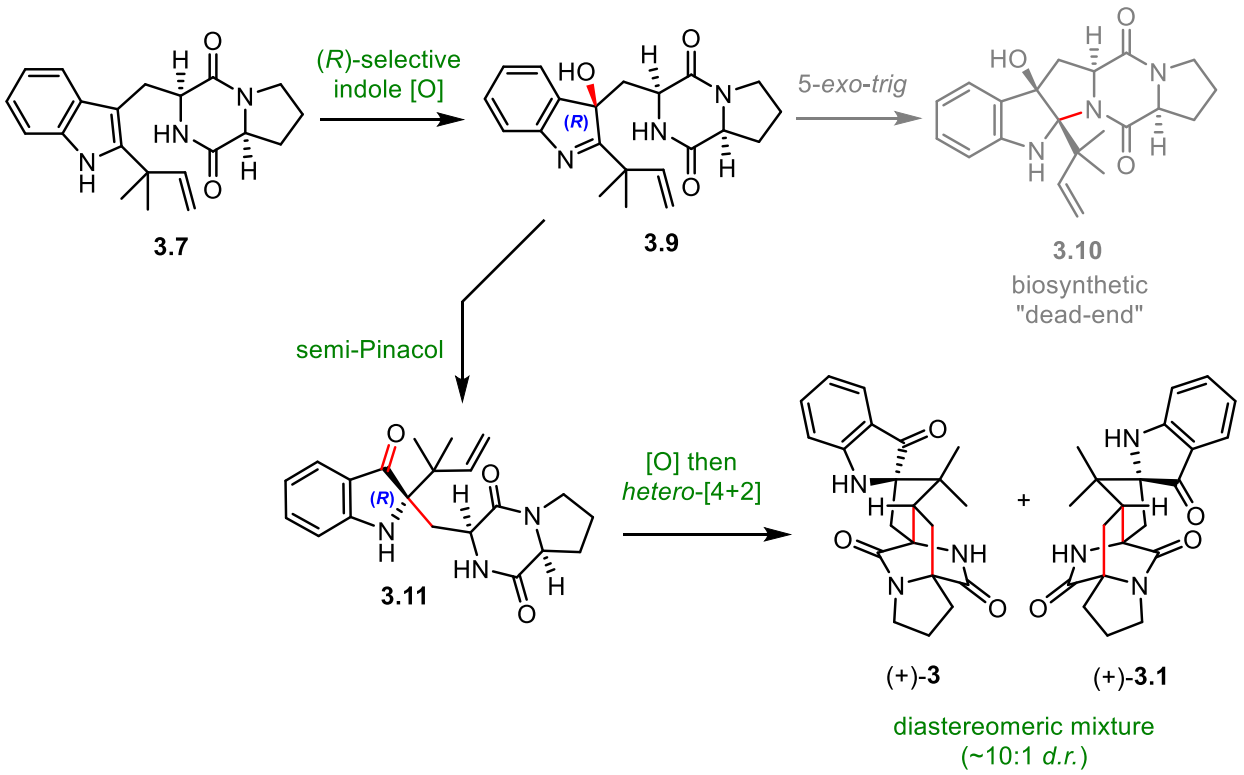
Scheme 3.2. (A) Birch's early labelling/incorporation studies and (B) Sammes and Porters proposed *hetero*-IMDA reaction

The group of Williams later came up with their own biosynthetic proposals for (+)-**3**/**3.1** building upon the pioneering work by the groups of Birch and Sammes. Several years of research involving labeling/incorporation studies in addition to semi-synthesis and total synthesis efforts led to the development of the two proposals shown below in Schemes 3.3 and 3.4. Williams and co-workers first-generation biosynthetic proposal (Scheme 3.3) was informed by their first synthesis of asymmetric (–)-**3.1**.[158] This synthesis revealed an unusual *pseudo*-enantiomeric relationship between (+)-**3**/**3.1** with respect to the bicyclo[2.2.2]diazaoctane core, even though (+)-**3**/**3.1** are technically diastereoisomers of one another. To accommodate this fact, bicyclo[2.2.2]diazaoctane formation from deoxybrevianamide E (**3.7**) was initially hypothesized to precede oxidative rearrangement to (+)-**3**/**3.1**.[159] This sequence of steps would lead to an initial ~10:1 scalemic mixture of cycloadducts (+)-**3.8** and (–)-**3.8** to account for the "enantiomeric" relationship observed. Subsequent (*R*)-selective oxidative rearrangement would account for the observed ~10:1 diastereomeric mixture of (+)-**3**/**3.1**. This first-generation proposal was ultimately disproven based on labeling, synthetic, and computational experiments. Radiolabeled cycloadducts (+)-**3.8** and (–)-**3.8** were not successfully incorporated into either (+)-**3** or (+)-**3.1**, making them unlikely as biosynthetic intermediates.[160] Computationally, Domingo and co-workers (in collaboration with Williams) had provided evidence that the *hetero*-IMDA reaction from deoxybrevianamide E (**3.7**) was not expected to be *anti*-selective.[161] Instead, the reaction would favor the *syn*-configured bicyclo[2.2.2]diazaoctane ring system that is opposite to what is observed in natural (+)-**3**/**3.1**. This was also verified experimentally by Williams and co-workers through total synthesis, affording a 2:1 mixture of *syn*:*anti* bicycles, favoring the *syn*-configuration.[162]



Scheme 3.3. Williams and co-workers' first-generation biosynthetic proposal

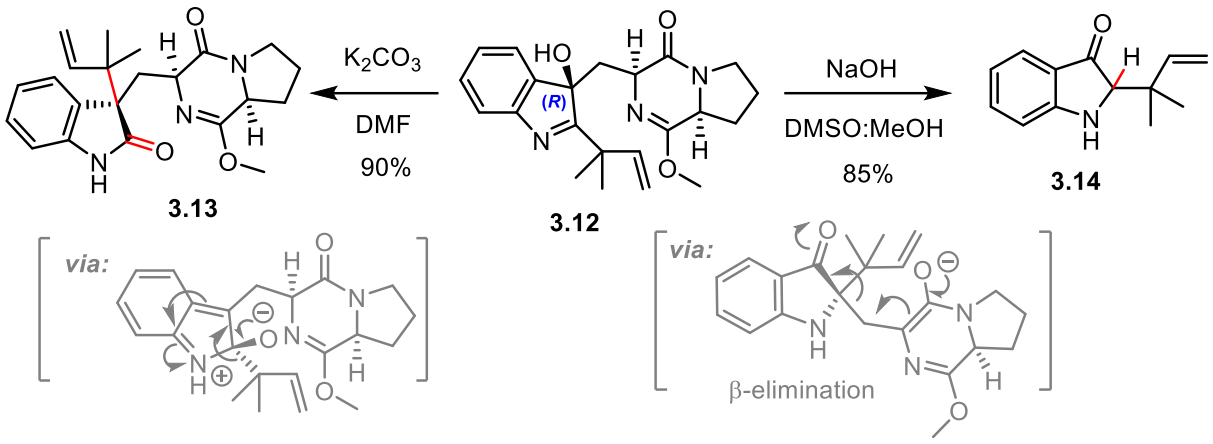
Based on the findings above, Williams and co-workers then put forth a new proposal with the inclusion of hydroxy-indolenine intermediate **3.9** which is believed to be the precursor to brevianamide E (**3.10**) that is also isolated from *P. brevicompactum* (Scheme 3.4).[140, 163] An initial (*R*)-selective oxidation of deoxybrevianamide E (**3.7**) to hydroxy-indolenine (**3.9**) is followed by semi-Pinacol rearrangement to afford (*R*)-pseudoindoxyl intermediate **3.11** which has never been identified before. From **3.11**, the *hetero*-IMDA reaction is expected to occur after two electron oxidation of the diketopiperazine, accounting for the observed ~10:1 ratio of (+)-**3**/**3.1**. Radiolabeled deoxybrevianamide E (**3.7**) was shown to incorporate into brevianamide E (**3.10**), (+)-**3**, and (+)-**3.1** in high radiochemical yields, supporting this pathway. Despite this, radiolabeled brevianamide E (**3.10**) was not shown to incorporate into either (+)-**3** or (+)-**3.1**, indicating that brevianamide E may be a biosynthetic "dead end".[160, 164] A point of uncertainty in this proposal was the order in which the sequence of azadiene formation, semi-Pinacol, and the *hetero*-IMDA events took place. What is depicted in Scheme 3.4 is first semi-Pinacol, azadiene formation, then *hetero*-IMDA. One could also envision that **3.9** could first undergo azadiene formation, then semi-Pinacol, and finally *hetero*-IMDA to arrive at the same result.



Scheme 3.4. Williams and co-workers' second-generation biosynthetic proposal

Williams and co-workers tried to validate this proposal through synthesis by accessing pseudoindoxyl **3.11** (Scheme 3.5).[c] Unfortunately, any attempt at rearranging late-stage hydroxy-indolenine substrate **3.12** under basic conditions led to the formation of undesired 2-oxindole **3.13** or fragmentation product **3.14**. Several other attempts by the authors on different substrates and using different oxidants never led to the successful isolation of any pseudoindoxyl intermediates and mostly oxindole products were recovered. This was speculated to be due to the greater thermodynamic stability of the oxindole as compared to the pseudoindoxyl.

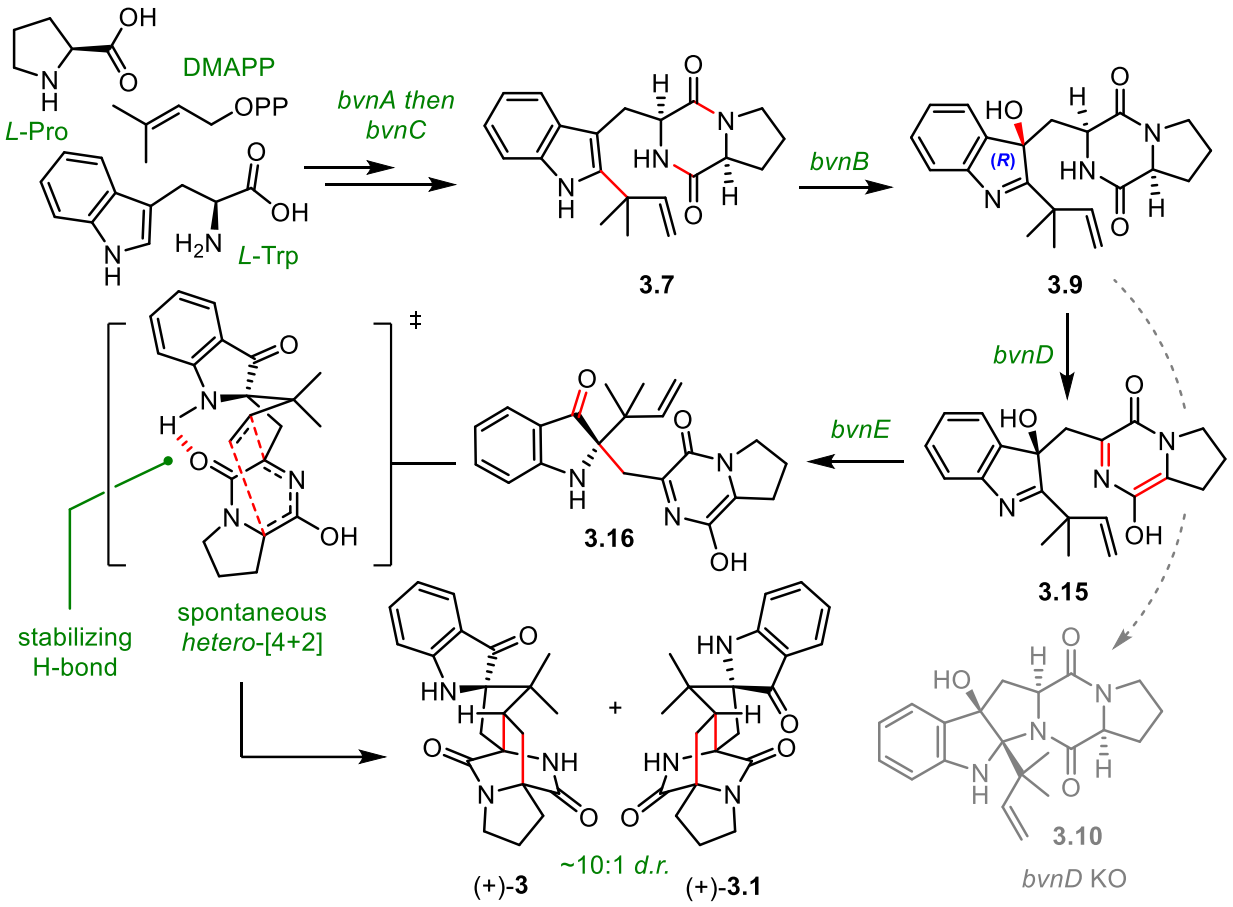
[c]Information was obtained from a preprint version of the published article: *Nat. Catal.* **2020**, *3*, 497–506 (preprint: *ChemRxiv*, **2019**, doi:10.26434/chemrxiv.9122009.v1). The illustrated schemes are also found in the Ph.D. dissertation: Halligan, K. M. Synthetic and Biosynthetic Studies of the Brevianamides. Ph.D dissertation, Colorado State University, Fort Collins, CO, 2000.



Scheme 3.5. Attempts by Williams and co-workers to rearrange hydroxy-indolenine **3.12** *via* late-stage semi-Pinacol to access pseudoindoxyl intermediates

Very recently, a multi-disciplinary effort between the groups of Williams, Sherman, and Li finally helped to shed some much-needed light on this old biosynthetic conundrum.[165] Their combined synthetic, biochemical, genomic, and computational study led to the identification of the (+)-brevianamide A biosynthetic gene cluster (*bvn*) and the discovery of an essential isomerase/semipinacolase enzyme named *bvnE*. Analysis of the gene cluster *bvn* revealed several enzymes (*bvnA*–*E*) that catalyzed individual steps within the biosynthetic pathways proposed by Birch, Sammes, and Williams over the last 50 years. To probe the function of each enzyme within *bvn*, gene deletion/expression experiments in addition to synthetic and quantum chemical calculations were performed. The data obtained from these experiments ultimately led to the fully revised biogenesis of (+)-**3**/**3.1** and considers the enantiomorphic nature of these two natural products (Scheme 3.6). *bvn*A is a non-ribosomal peptide synthase (NRPS) that catalyzes the formation of brevianamide F (**3.5**) from *L*-Pro and *L*-Trp. Reverse prenylation at *C*2 of the indole with dimethylallyl pyrophosphate (DMAPP) is then mediated by a prenyltransferase (*bvn*C) to give deoxybrevianamide E (**3.7**). Next, two oxidations occur (*bvnB* → *bvnD*) *via* an initial (*R*)-selective oxidation to the hydroxy-indolenine **3.9** followed by oxidation of the diketopiperazine to give azadiene intermediate **3.15**. Deletion of *bvnD* led to the unproductive accumulation of brevianamide E (**3.10**), supporting Williams and co-workers' earlier proposal. From azadiene **3.15**, *bvnE* is proposed as the key isomerase that catalyzes the semi-Pinacol rearrangement to pseudoindoxyl **3.16**. Strikingly, the final *hetero*-IMDA reaction was found to be spontaneous and non-catalyzed with facial selectivity of the cycloaddition (~10:1) being highly dependent on the

presence of *bvn*E. Furthermore, computational work from the groups of Domingo and the groups of Williams, Sherman, and Li also demonstrated that the putative *hetero*-IMDA from pseudoindoxyl **3.16** should occur with high selectivity based on a favorable intramolecular hydrogen bond between the pseudoindoxyl N-H and the proximal amide carbonyl of the diketopiperazine.[165, 166] This interaction stabilizes the transition state forming (+)-**3** relative to (+)-**3.1** by about 6–7 kcal/mol, accounting for the greater ratio of (+)-**3** observed during isolation. Additionally, deletion of *bvn*E led to the isolation of numerous products in addition to (+)-**3**/**3.1** being formed in a ~1:1 ratio and in significantly lesser amounts.

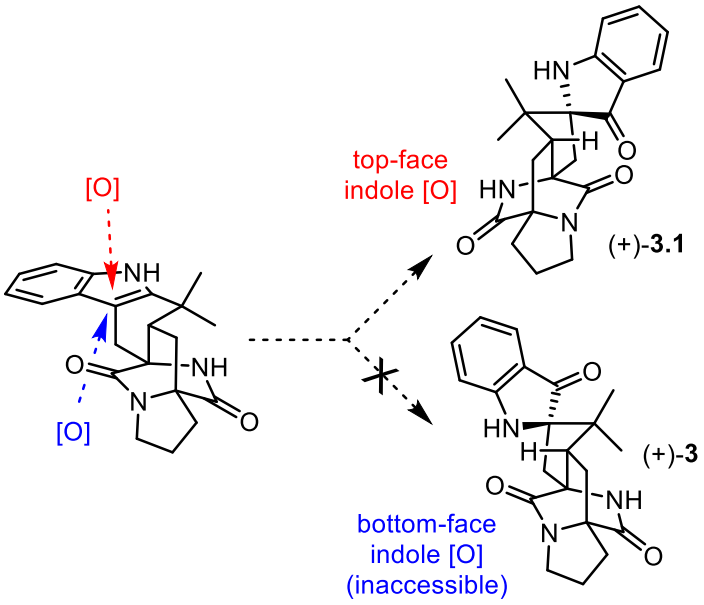


Scheme 3.6. Williams, Sherman, and Li's revised and most recent biosynthetic proposal

3.3 Previous syntheses of brevianamide A

Over the last several decades of synthetic and biochemical research, the overwhelming majority of brevianamide alkaloid total syntheses have been on the minor diastereomer

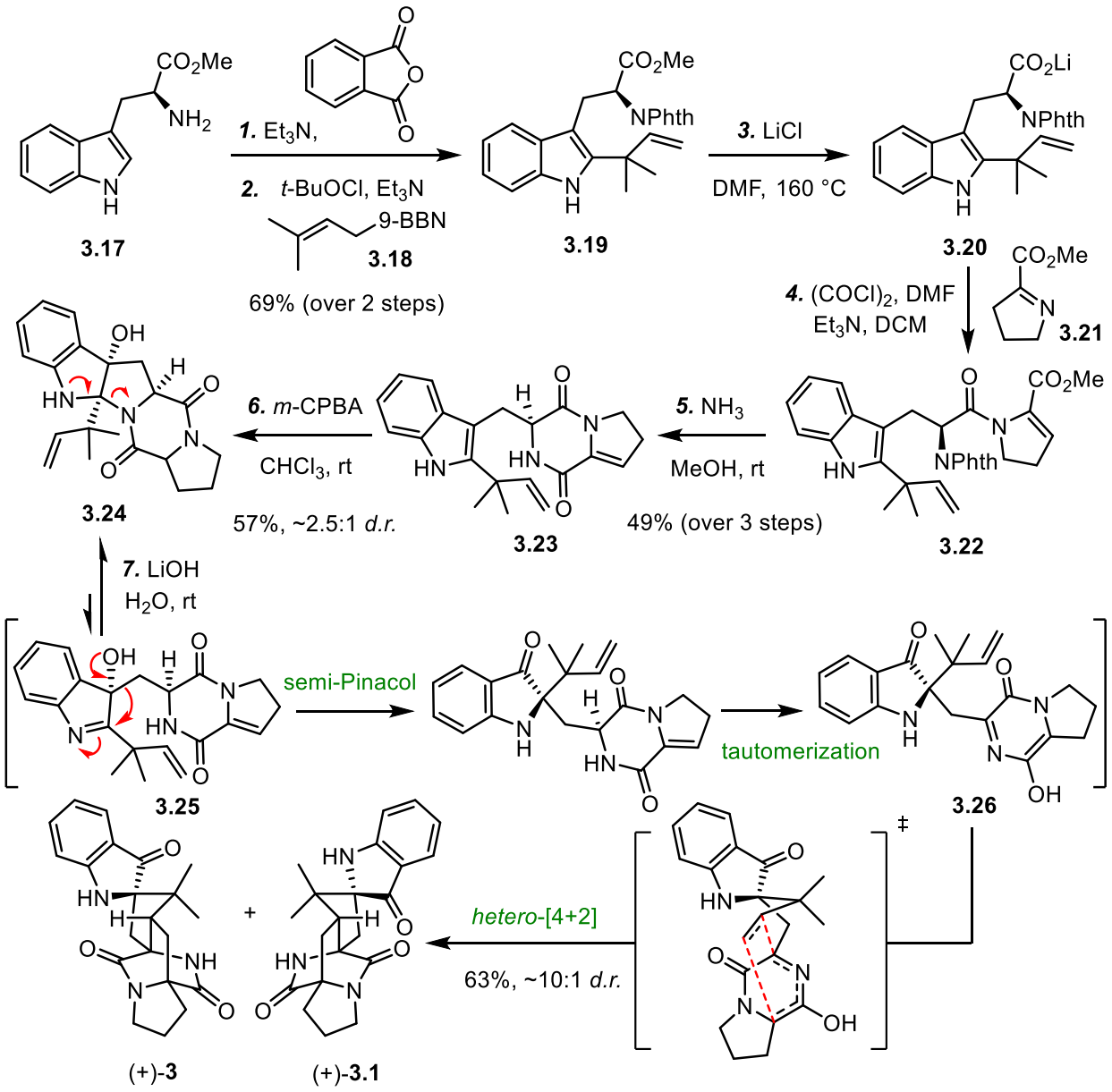
brevianamide B. The group of Williams has been a key player in this field, developing several asymmetric, racemic, and biomimetic syntheses of brevianamide B. Despite the similarities, the total synthesis of the major diastereomer brevianamide A had remained largely inaccessible for a long time. Major issues of stereoselectivity and reactivity consistently afforded brevianamide B, especially when one considers that past syntheses relied on a common end-game strategy that was unsuccessful. This strategy depended on the stereoselective oxidative rearrangement of an advanced hexacyclic indole precursor which had already undergone the biomimetic Sammes-type *hetero*-IMDA reaction. Unfortunately, all iterations of this late-stage process resulted in the exclusive formation of brevianamide B since oxidation of the indole always occurred from the least sterically demanding face of the double bond (Scheme 3.7). When considering the newly revised biosynthesis of (+)-**3**/**3.1**, oxidative tailoring of the indole framework into the pseudoindoxyl motif is believed to precede the *hetero*-IMDA reaction (not the opposite), resulting in the predominant formation of (+)-**3** by the organism. Therefore, this sequence of steps should have major implications towards the development of a successful total synthesis of brevianamide A. Despite the initially discouraging results by the group of Williams (see Scheme 3.5), 20 years later this type of strategy ultimately proved to be successful and allowed brevianamide A to finally succumb to total synthesis.



Scheme 3.7. Failed end-game strategy for oxidative access to brevianamide A

3.3.1 Lawrence's total synthesis of (+)- and (–)-brevianamide A

In 2020, brevianamide A finally succumbed to synthesis by the group of Lawrence using a biomimetic route to this natural product.[135] This synthesis was inspired by a slightly modified biosynthetic proposal compared to the second-generation proposal put forth by the group of Williams. Their elegant strategy relied on a late-stage domino sequence involving a stereospecific semi-Pinacol rearrangement and a *hetero*-IMDA reaction to afford both enantiomers of brevianamide A in seven steps (Scheme 3.8). The synthesis commenced with the formation of *N*-phthalimide protected *L*-tryptophan methyl ester, followed by *C*2 reverse prenylation of the indole using 9-BBN reagent **3.18** to give reverse prenylated indole **3.19** in 69% yield over the two steps. The methyl ester was then converted into the lithium carboxylate **3.20** using LiCl in refluxing DMF. **3.20** is then used as a competent substrate to form an enamide **3.22** in an amide coupling reaction with cyclic imine reagent **3.21**. From here, deprotection of the phthalimide took place under basic conditions which directly afforded the cyclized diketopiperazine product **3.23** in 49% yield over the three steps. Oxidation of **3.23** with one equivalent of *m*-CPBA afforded key pentacyclic intermediate **3.24** as a mixture of diastereoisomers in 57% yield. Subjecting the major diastereoisomer shown to strongly basic conditions (aqueous LiOH) initiated the biomimetic cascade leading to (+)-**3** in high yield with (+)-**3.1** also able to be isolated from the reaction mixture. Additionally, if the minor diastereoisomer of **3.24** is used, Lawrence and co-workers have shown that they were able to obtain the unnatural enantiomers of (+)-**3** and (+)-**3.1** (not shown). This domino process takes place through the reversible opening of the pentacyclic intermediate to give hydroxy-indolenine **3.25** that suffers stereospecific semi-Pinacol rearrangement and spontaneous *hetero*-IMDA from azadiene **3.26**. Importantly, no additional redox steps are required here since the diketopiperazine motif is already at the correct oxidation state. Therefore, only tautomerization is required to reveal the azadiene. This process also results in the production of brevianamides A and B with a distribution that mirrors closely that which is observed from natural sources (~10:1). This result is in agreement with the finding that the cycloaddition step is indeed a spontaneous process and not enzyme mediated.[165]

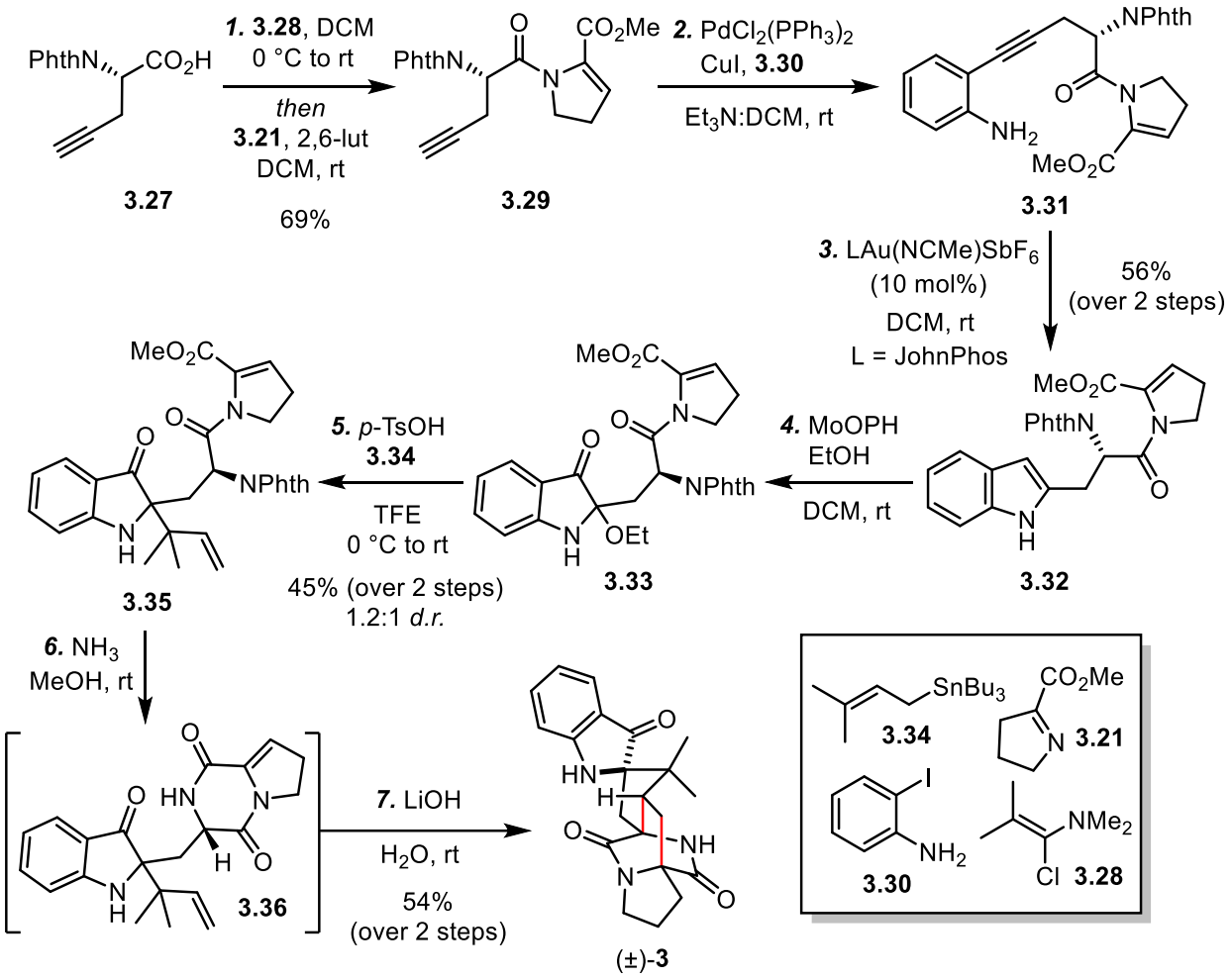


Scheme 3.8. Lawrence's 2020 biomimetic total synthesis of (+)/(–)-brevianamides A and B

3.3.2 Smith's total synthesis of (±)-brevianamide A

One year after Lawrence's synthesis, Smith and co-workers accomplished a synthesis of racemic brevianamide A (Scheme 3.9). Relying on a similar end-game strategy, they achieved the synthesis of racemic brevianamide A with the same step-count as Lawrence's synthesis but with a lower overall efficiency.[167] As one of the key steps in their synthesis, the group of Smith showcases their methodology for the synthesis of *C*2 substituted pseudoindoxyls from indoles. Their synthesis

began with the *N*-phthalimide protected propargyl glycine **3.27** which they subjected to amide coupling with cyclic imine **3.21** to afford enamide **3.29** in 63% yield. Next, Sonogashira coupling gave alkynyl aniline **3.31** that was submitted to Au(I)-catalysis to form indole **3.32** in 56% yield over two steps. To obtain the necessary *C*2 reverse prenylated pseudoindoxyl **3.35**, the indole is first oxidized in the presence of excess MoOPH to 2-ethoxypseudoindoxyl **3.33**. Under acidic conditions, **3.33** is subsequently treated with excess stannane reagent **3.34** to enable the reverse prenylation reaction. This results in the formation of **3.35** in 45% yield over the two steps and as a mixture of diastereoisomers (1.2:1 *d.r.*). Carrying forward both diastereoisomers, Smith and co-workers now applied the end-game strategy used by Lawrence and co-workers to synthesize brevianamide A. Deprotection with ammonia resulted in cyclization to the diketopiperazine **3.36** which was not isolated. Solvent swap and addition of aqueous LiOH according to Lawrence's report led to the synthesis and isolation of racemic brevianamide A in 54% yield. In this case, Smith and co-workers do not report on the isolation of brevianamide B from the same reaction mixture.

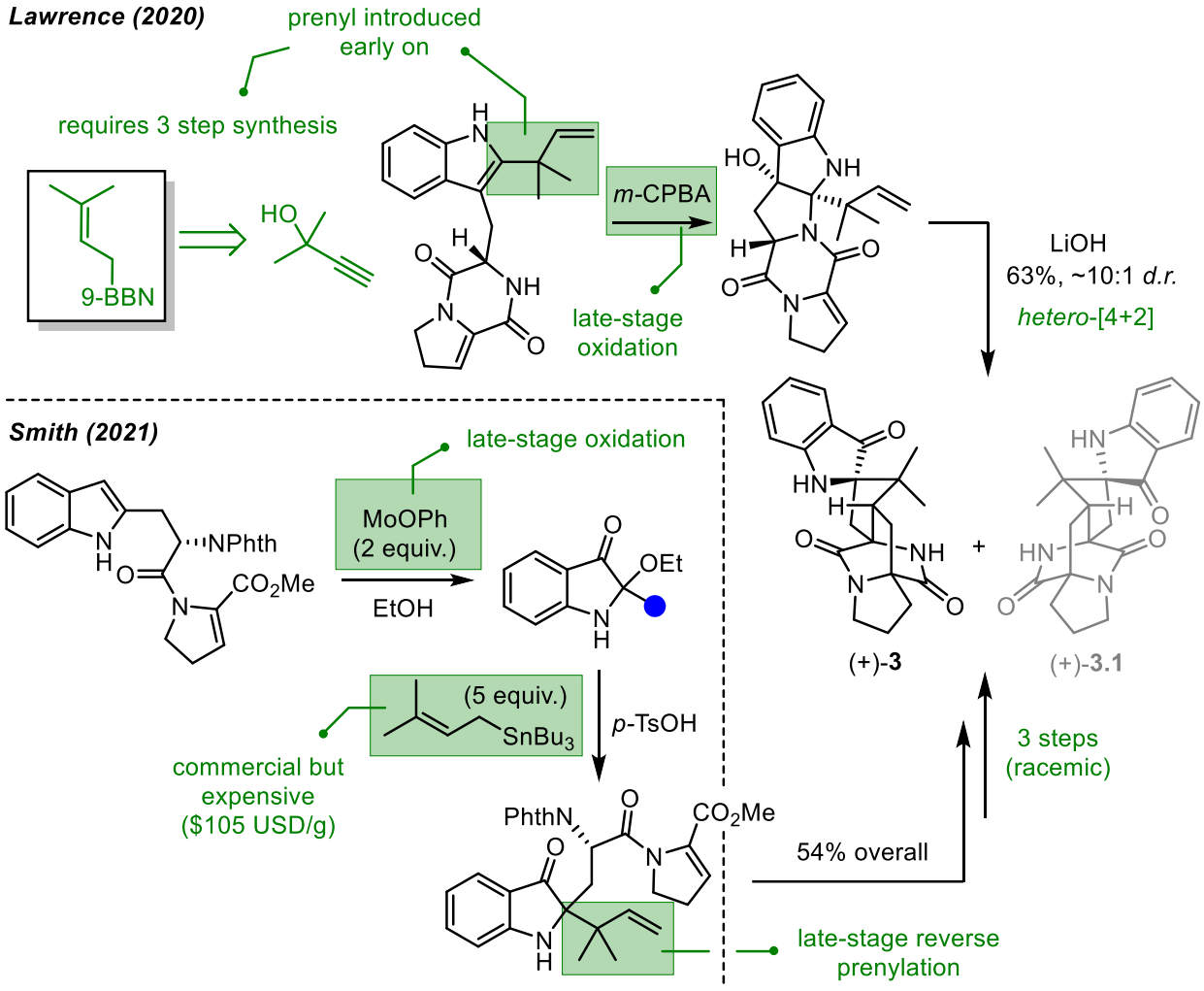


Scheme 3.9. Smith's 2021 total synthesis of (±)-brevianamide A

3.4 Objective of the project

Both the Lawrence and Smith syntheses of brevianamide A are concise and efficient routes with low step-count and good overall efficiency (11% and 6% overall yield respectively, Scheme 3.10). Despite this, we saw room for improvement when it came to step and atom economy, particularly for the introduction of the reverse prenyl moiety and the indole oxidation step since both steps are critical to the success of the *hetero*-IMDA reaction. The synthesis by Lawrence and co-workers introduced the reverse prenyl group early on in their synthesis through an oxidative process that used *t*-BuOCl and an excess of a 9-BBN reagent. While this process was efficient (69% yield), this reagent was not commercial and required a three-step synthesis that was reported as being inefficient (32% overall yield). Additionally, oxidation of the indole then occurred late-

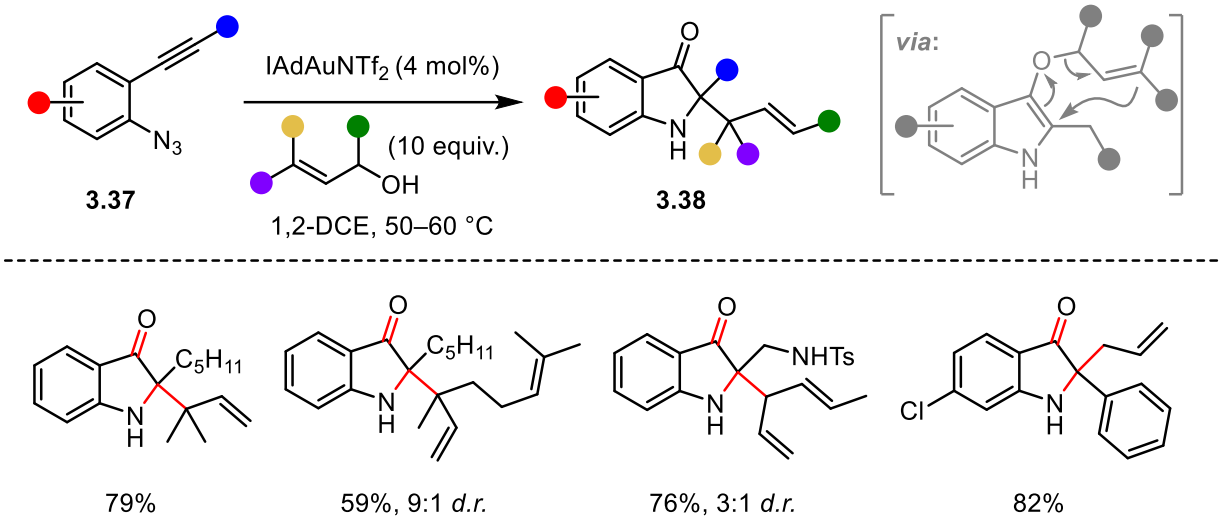
stage using *m*-CPBA, affording their key pentacyclic intermediate in good levels of diastereoselectivity and yield. In the work by the group of Smith, the indole oxidation and reverse prenylation occurred successively and late-stage. A two-fold excess of a molybdenum-based oxidant (MoOPH) is used to access the pseudoindoxyl motif and is then treated with a large excess (five equivalents) of a commercial but expensive stannane reagent under acidic conditions, affording their key intermediate as essentially a statistical mixture.



Scheme 3.10. Limitations associated with previous syntheses of brevianamide A by the groups of Lawrence and Smith

With these aspects in mind, we reasoned that we would be able to simplify and improve access to the key reverse prenylated pseudoindoxyl intermediate **3.36** and develop a new synthetic

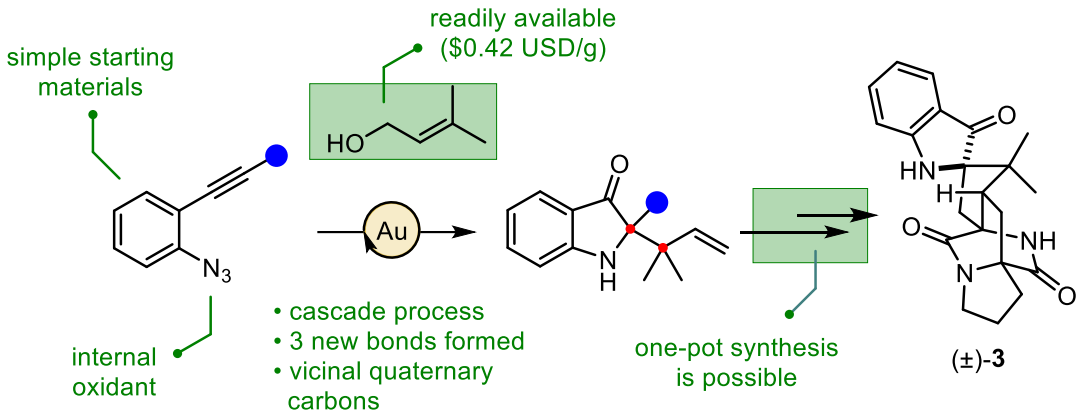
approach towards racemic brevianamide A. To do this, we sought to take advantage of the powerful ability of gold catalysis to help build molecular complexity in a rapid and efficient manner. Previously developed work in our group focused on the synthesis of pseudoindoxyl products of type **3.38** and we considered this as an ideal tool in helping us bring this new synthesis to fruition (Scheme 3.11).[117] During this work, *ortho*-alkynyl arylazides **3.37** were used to generate highly electrophilic α-imino gold carbene intermediates that would then be trapped by a nucleophile. Upon using an allylic alcohol as a nucleophile, the expected 3-alkoxyindole that would result from nucleophilic addition to the carbene was not isolated. Instead, 2,2-disubstituted reverse prenylated pseudoindoxyl products **3.38** were isolated in high yields. These products are believed to be the result of a Claisen rearrangement taking place under the conditions of the reaction. Using this methodology, a wide range of allylic alcohols were employed as nucleophiles and resulted in the formation of pseudoindoxyl products in good to excellent yields (59–92%).



Scheme 3.11. Previous work from the Gagosz lab on the synthesis of 2,2-disubstituted pseudoindoxyl products using Au(I)-catalysis

In this scenario and in-line with our objectives for this project, the indole oxidation and reverse prenylation could occur in a single operation through a cascade process (Scheme 3.12). This gold catalyzed transformation would allow for a significant increase in molecular complexity with the formation of the pseudoindoxyl moiety, several new C-C and C-X bonds, and vicinal quaternary centers (non-trivial). Furthermore, this new synthesis would be highly atom and step

economical, requiring no additional oxidant for this transformation to take place, simpler starting materials, and the source of the prenyl group would be derived from prenyl alcohol (a costless commodity chemical). This is in stark contrast to the previous routes used by the groups of Lawrence and Smith. However, similar to the Lawrence and Smith syntheses, we opted to retain the biomimetic *hetero*-IMDA reaction for the end-game since this is an incredibly powerful disconnection that would afford the bicyclo[2.2.2]diazaoctane core. Moreover, the conditions necessary to affect this cycloaddition should be compatible with the conditions used in gold catalysis, allowing for the development of a one-pot process, further streamlining our new approach towards this natural product. In this chapter, the successful implementation of this strategy will be discussed with respect to the synthesis and development of two concise and complementary approaches to racemic brevianamide A.

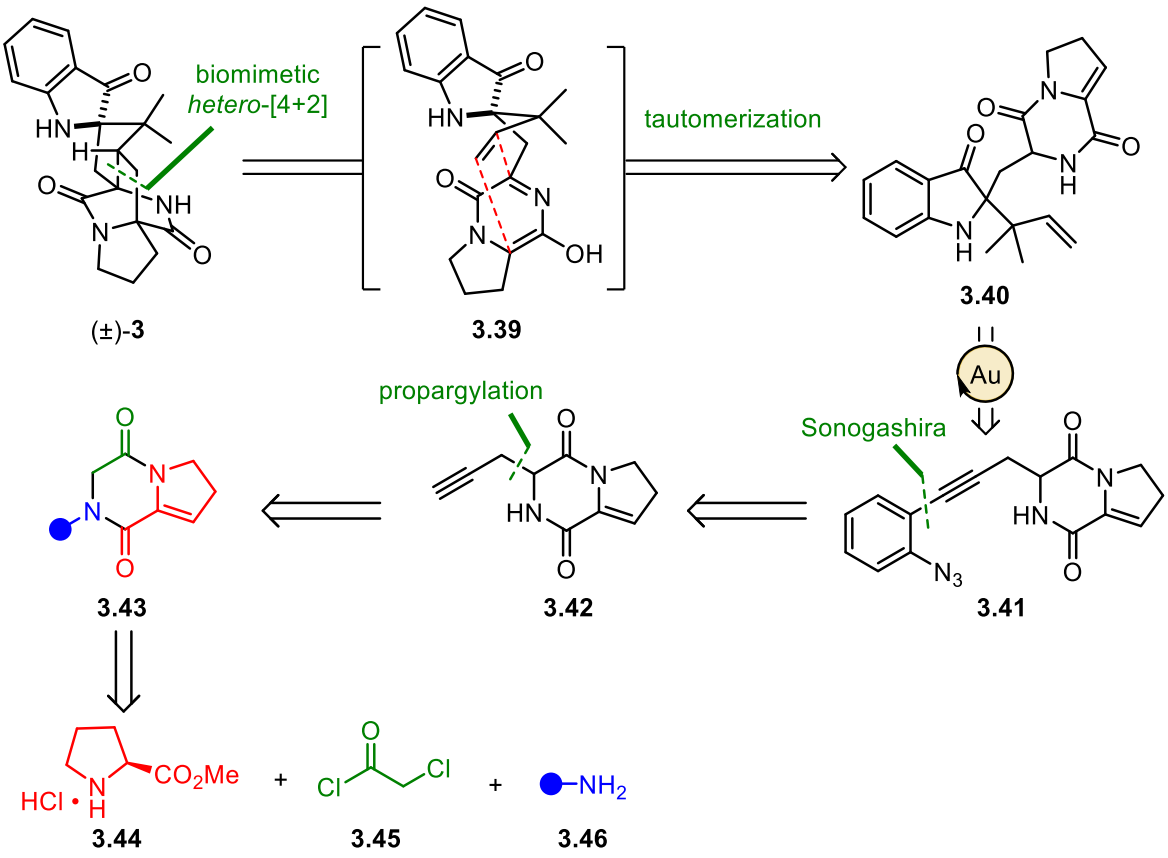


Scheme 3.12. Our groups approach towards an expedited synthesis of racemic brevianamide A using Au(I) catalysis

3.5 Initial retrosynthetic analysis

When first examining (±)-**3**, we sought to take advantage of the well-established biosynthetic *hetero*-IMDA reaction as an end-game strategy. As was mentioned above, this is an incredibly powerful and simplifying disconnection for this natural product and it would be remiss if we did not take advantage of this (Scheme 3.13). This would lead us back to transient azadiene **3.39** which should arise from tautomerism of advanced pseudoindoxyl intermediate **3.40** bearing a diketopiperazine motif at the correct oxidation state. The advantage of having the proline unsaturation pre-installed is to no longer need a separate redox step to reveal the azadiene.

Additionally, it helps to minimize functional group manipulations in later stages of the synthesis. We then envisioned that the 2,2-disubstituted pseudoindoxyl possessing two adjacent quaternary centers could be generated from the *ortho*-alkynyl arylazide **3.41** using the Au(I) methodology developed previously in our group, a process that has the potential to be used in tandem with the diketopiperazine tautomerization/*hetero*-IMDA sequence (**3.41**→**3.40**→**3.39**). The successful development of this one-pot process would enable efficient and rapid entry into the complex brevianamide A skeleton. The arylazide moiety can be installed through a classical palladium catalyzed Sonogashira cross-coupling, bringing us back to propargylated N-H diketopiperazine **3.42**. **3.42** should be able to be obtained from the propargylation of a suitably protected diketopiperazine such as **3.43**. Finally, the formation of **3.43** can be seen as coming from the combination of proline methyl ester (**3.44**), chloroacetyl chloride (**3.45**) and a suitable amine nucleophile (**3.46**) that are all readily available building blocks. This might occur through a series of acylation and substitution reactions.

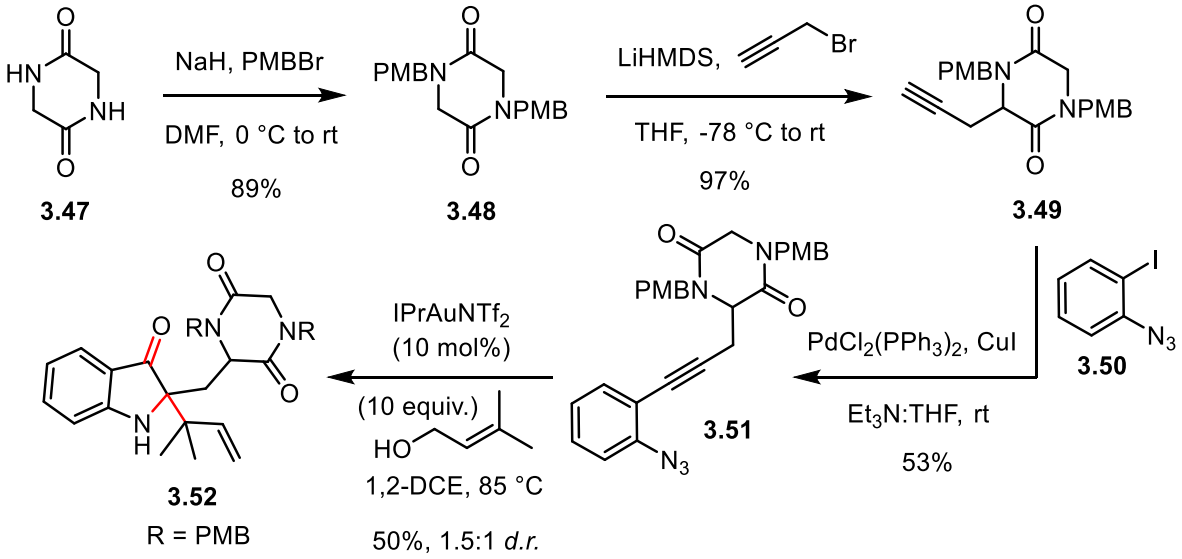


Scheme 3.13. Initial retrosynthetic analysis of (±)-brevianamide A

3.6 Forward synthesis (first-generation)

3.6.1 Model study on a truncated Au(I) catalysis precursor

Before beginning the synthesis, we decided to test our proposed Au(I) catalyzed reaction on a simpler substrate **3.51** which did not contain the proline pyrrolidine ring (Scheme 3.14). To obtain **3.51**, glycine anhydride **3.47** was *bis*-protected with PMB groups under basic conditions in 89% yield. From there, propargylation of **3.48** using LiHMDS at -78 °C resulted in the formation of compound **3.49** in very high yield (97%). Sonogashira coupling then delivered the arylazide **3.51** in 53% yield. To our delight, treating **3.51** with $IPrAuNTf_2$ and a large excess of prenyl alcohol (10 equivalents) led to the smooth isolation of pseudoindoxyl product **3.52** as an inconsequential mixture of diastereoisomers (~1.5:1 *d.r.*) and in 50% combined yield. Having confirmed the feasibility of the Au(I) catalyzed rearrangement, we proceeded with the rest of the total synthesis.

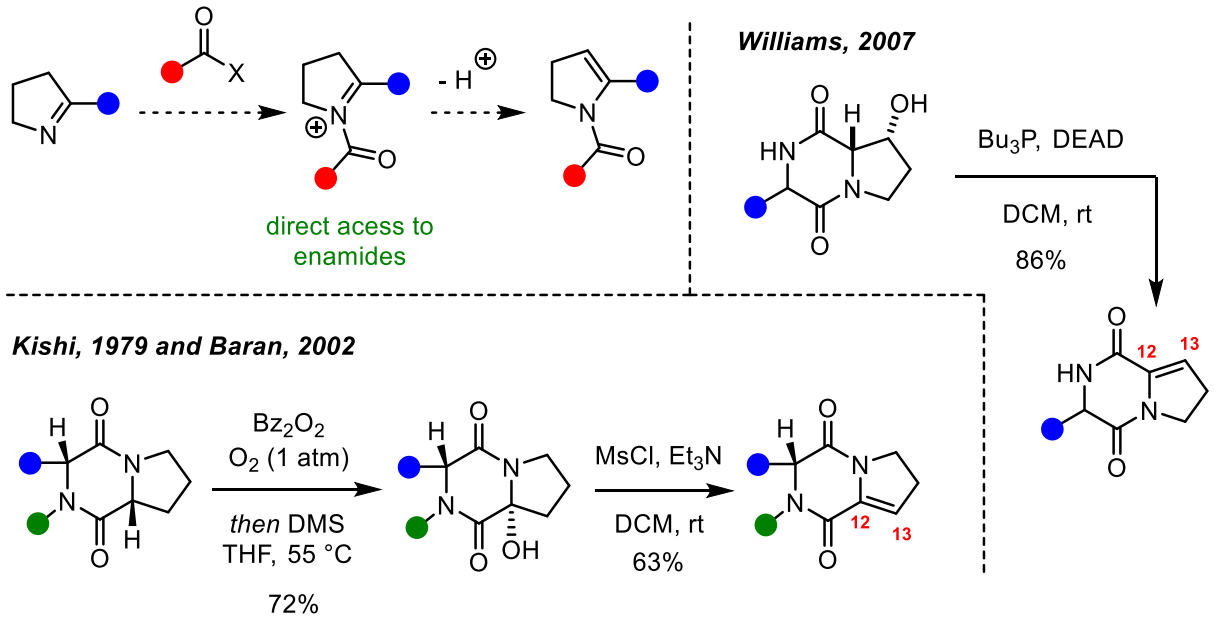


Scheme 3.14. Model study towards testing our proposed Au(I) catalyzed cascade process

3.6.2 Efforts toward the synthesis of free amide Au(I) catalysis precursor

We first began this study with the synthesis of the imine reagent **3.21** that was initially used in Lawrence and co-workers' synthesis of (+)-**3**. We chose to utilize this imine as a means of generating the requisite *C*12-*C*13 unsaturation in protected diketopiperazine **3.43** since this would

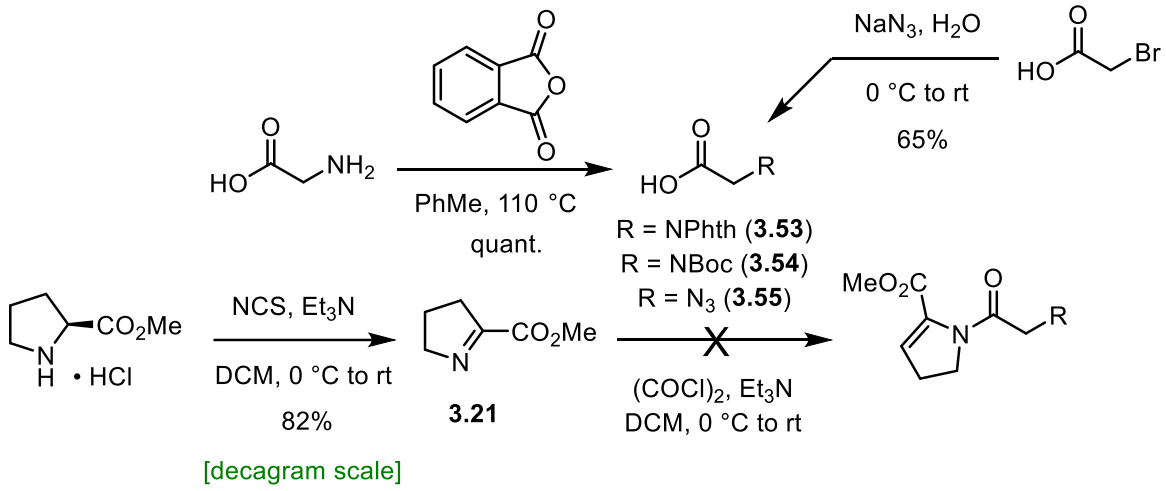
significantly simplify its installation by means of direct imine acylation with an activated carboxylic acid partner. This would lead directly to the desired *N*-acyl enamine or enamide functionality, otherwise other discrete steps would be necessary to install this unsaturation (Scheme 3.15). For example, previous work from one of Williams' total syntheses of (±)-stephacidin A/brevianamide B required a separate Mitsunobu-type dehydration of a 3-hydroxyproline intermediate to form the double bond.[168] 3-Hydroxyproline is also not widely available and required four steps to synthesize. Imine **3.21** on the other hand can be readily synthesized from *L*-proline methyl ester hydrochloride in one step and high yield according to the procedure by the group of Schmalz.[169] Work by the groups of Kishi[170] and Baran[171] on a related but different natural product (austamide) also sought to install the same unsaturation. To accomplish this, they needed two additional steps involving radical oxidation of the activated *C*12 methine, followed by elimination.



Scheme 3.15. One step enamide synthesis from imine acylation as compared to other methods

Repeating Schmalz and co-workers' conditions, *L*-proline methyl ester hydrochloride was reacted with NCS in the presence of triethylamine at 0 °C to afford a crude solution of imine **3.21**. Following the group of Lawrence's procedure, we directly isolated imine **3.21** from the crude reaction mixture by distillation under reduced pressure (Scheme 3.16). This consistently afforded

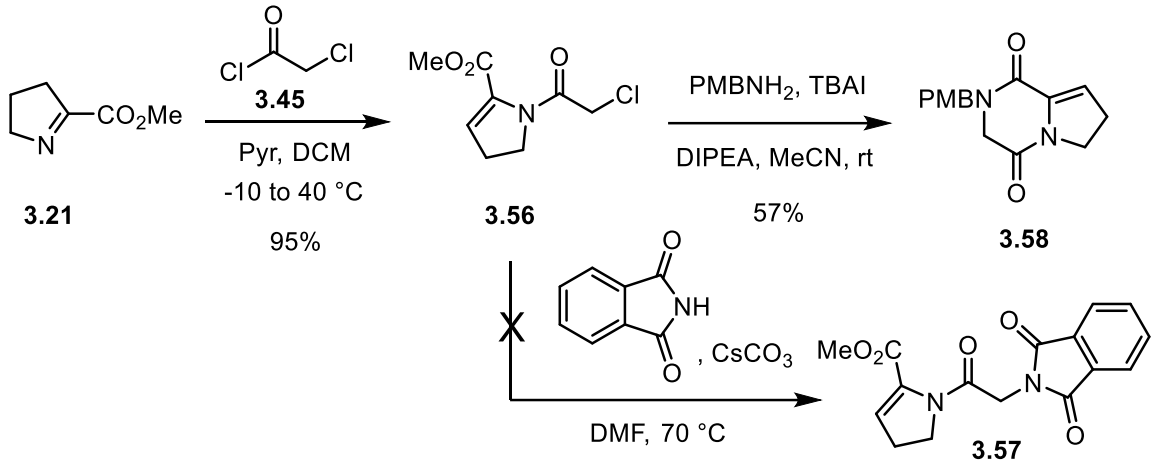
us imine **3.21** of high purity and yield (82%) on decagram scales (>20 grams). To test Lawrence and co-workers reported procedure for the imine acylation,[135] we first synthesized *N*-phthaloylglycine (**3.53**). Repeating their conditions exactly with the formation of acyl chloride *in-situ* and triethylamine as base led to mostly decomposition with the desired enamide not being formed. Trying different protecting groups and using Boc-glycine (**3.54**) or azidoacetic acid (**3.55**) gave decomposition instead.



Scheme 3.16. Synthesis and attempted acylation reactions of imine **3.21**

Trying preformed acyl chlorides as electrophiles (reported by Schmalz and co-workers) thankfully solved this problem. Using pyridine, we were able to obtain the enamide product in essentially quantitative yield with ^{1}H-NMR data that is in good agreement with the literature. Having found conditions which successfully resulted in acylation of imine **3.21**, we proceeded forward with the synthesis (Scheme 3.17). Reacting imine **3.21** with chloroacetyl chloride **3.45** in the presence of pyridine as base gratifyingly led to the isolation of chloroenamide **3.56** in near quantitative yield. Our next step was to introduce a protected amine nucleophile to perform an S_N2 reaction with the activated chloride. Once that was complete, our goal was to then hydrolyze the methyl ester to the carboxylic acid and perform an intramolecular amide coupling reaction over two steps. We first tried the addition of phthalimide since the resulting product **3.57** could be easily deprotected using hydrazine. Surprisingly, this addition did not work and resulted in the complete degradation of the substrate. However, when we added excess *p*-methoxybenzylamine ($PMBNH_2$) to a solution of chloroenamide **3.56**, we found that substitution of the chloride took place, followed

by an intramolecular transamidation reaction to afford us PMB-protected diketopiperazine **3.58** in 57% yield.

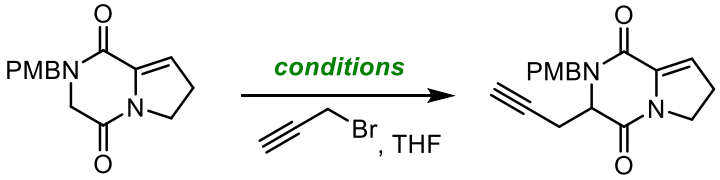


Scheme 3.17. Synthesis of PMB-protected diketopiperazine **3.58**

With this positive result, we turned our attention towards the introduction of the propargyl group to synthesize propargylated diketopiperazine **3.59** (Table 3). At first glance, this seemed like a trivial task since there were examples in the literature which indicated this type of alkylation would be possible.[172, 173] Unfortunately, when we tried to deprotonate the substrate with LDA at -78 °C (Entry 1) followed by alkylation with propargyl bromide, we only formed trace amounts of product. We first thought that perhaps degradation of the substrate was taking place when warming to higher temperatures but conducting the reaction entirely at -78 °C led to no product being formed whatsoever (Entry 2). Only upon the addition of a LiCl additive did we start to see product formation (Entry 3). According to TLC analysis, full consumption of the starting material took place. Despite this promising result, we were only ever able to obtain a low 25–30% yield of product after column chromatography. We believed the low yield of this step may be due to solubility issues of the diketopiperazine lithium enolate since we observed precipitation during this step and observed slightly higher yields on larger scales. This might also help to explain why product formation was observed upon addition of LiCl. Lithium halide salts have often been used in organolithium reactions to help with aggregation. In our attempt to fix this issue, we conducted the deprotonation at higher temperatures and then added electrophile (Entry 4). Unfortunately, this simply led to decomposition. Switching the base to LiHMDS instead of LDA gave similar results

with a slightly lower yield (Entry 5). Despite the low yield of the propargylation, the yield was reproducible and was consistent on larger scales. To test if our proposed gold catalyzed rearrangement was feasible, we continued onward with the synthesis.

Table 3. Propargylation attempts on PMB-protected diketopiperazine substrate **3.58**

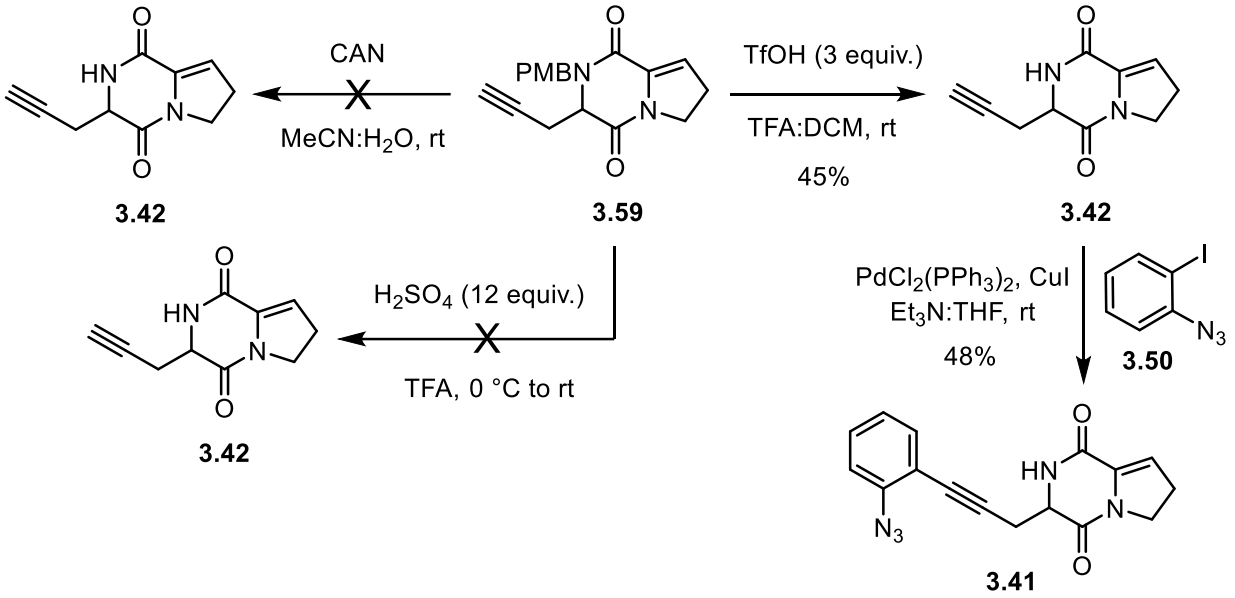


3.58 **3.59**

Entry[a]	Base	Temperature (°C)	Additive	Yield (%)[b]
1	LDA[d]	-78 to 23	--	traces
2	LDA	-78	--	--
3	LDA	-78	LiCl	25, 30[c]
4	LDA	0 to 23	LiCl	--
5	LiHMDS	-78	LiCl	27

[a] Unless otherwise noted, all reactions were carried out in anhydrous THF at a substrate concentration of 0.2 M. [b] Isolated yields. [c] Reaction conducted on a 25 mmol scale. [d] LDA was generated *in-situ* by deprotonation of (*i*-Pr)$_2$NH with *n*-BuLi.

Removal of the PMB protecting group was carried out next (Scheme 3.18). Classical oxidative conditions were carried out as a first attempt. Using CAN as the oxidant resulted in cleavage of the PMB group (*p*-anisaldehyde signals were present by crude ^{1}H-NMR), however we also observed significant decomposition of the proline unit in the diketopiperazine ring system. We next carried out the deprotection under strongly acidic conditions. Addition of H_2SO_4 to the substrate in TFA only resulted in recovery of the starting material. Changing to a stronger acid (TfOH) led to the smooth removal of the PMB group allowing us to isolate the free N-H diketopiperazine **3.42** in 30% yield (45% yield on larger scale). Issues were experienced during basic work-up and we found **3.42** to have significant water solubility and was difficult to recover from the aqueous phase. Nonetheless, all that was left was to perform a Sonogashira coupling on substrate **3.42** which smoothly afforded us the arylazide **3.41** in a good 48% yield.

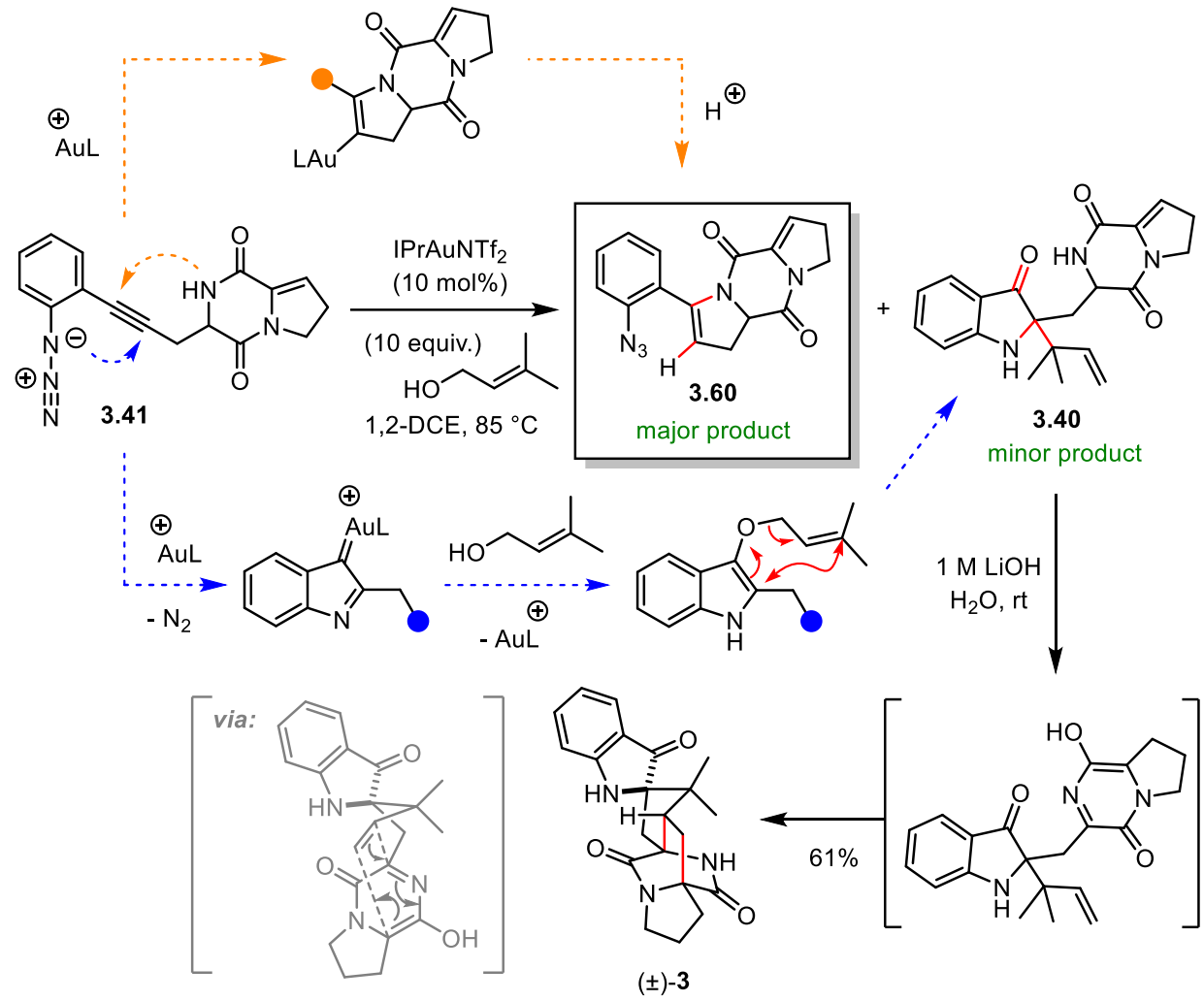


Scheme 3.18. Synthesis of Au(I) catalysis precursor **3.41**

3.6.3 Completion of the synthesis (first-generation)

With arylazide substrate **3.41** in hand, we were finally able to test our key Au(I) catalyzed rearrangement (Scheme 3.19). Initial results by TLC analysis seemed to be incredibly promising, however subjecting **3.41** to our group's previously optimized conditions for the formation of the pseudoindoxyl motif did not afford us the pseudoindoxyl **3.40** as the major product. Rather, the major product of this reaction was the corresponding hydroamidation product **3.60** (75% yield). We believe **3.60** is formed *via* 5-*endo-dig* cyclization of the free amide onto the activated Au(I)-alkyne complex rather than cyclization by the azide group. The desired product **3.40** was isolated in ~18% yield as a mixture of diastereoisomers and as the minor product of the reaction. Our attempts to properly purify **3.40** for full characterization were unsuccessful due to its instability on a silica column. To confirm we had made pseudoindoxyl compound **3.40** and to test if this intermediate can be successfully converted into (±)-**3**, we synthesized more of **3.40** on slightly larger scale and repeated the conditions reported by Lawrence and co-workers. We were delighted to find that subjecting pseudoindoxyl **3.40** to aqueous LiOH at room temperature led to the isolation of (±)-**3** in a good 61% yield and had ^{1}H- and ^{13}C-NMR spectra that were in good agreement with brevianamide A spectra produced by the group of Lawrence (see Tables 6 and 6.1

in the Supporting Information). Unlike Lawrence and co-workers however, we were unable to detect any trace of brevianamide B from this reaction.

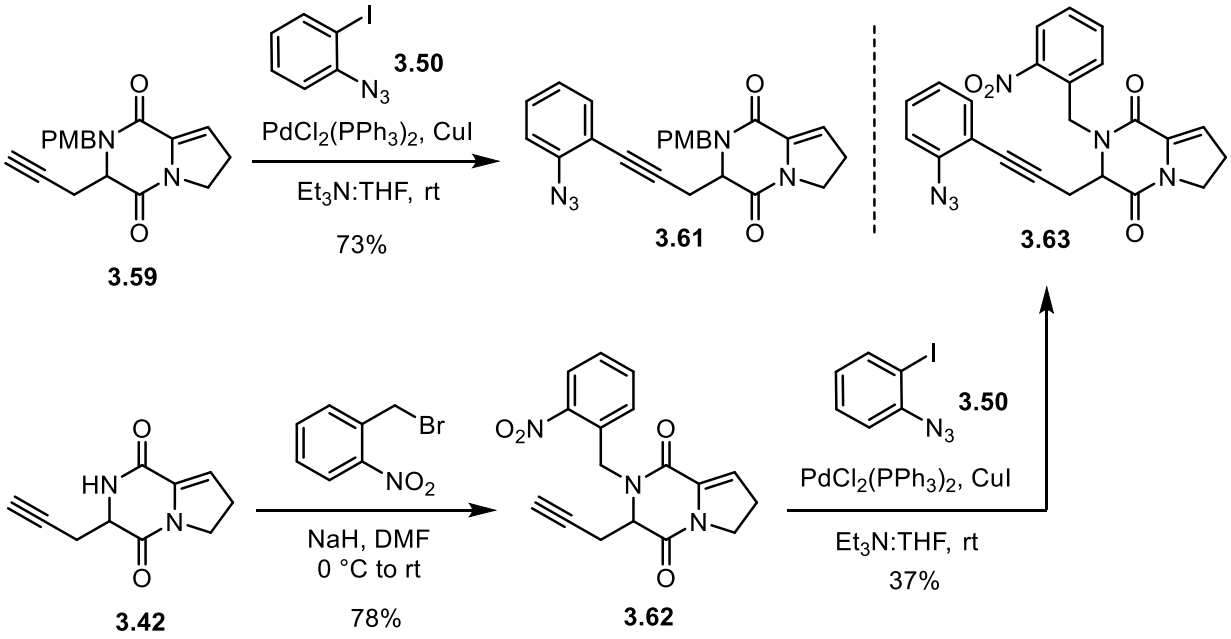


Scheme 3.19. First-generation synthesis of (±)-brevianamide A

3.6.4 Manipulation of the protecting group for the Au(I) catalysis precursor

While disappointed by the lack of selectivity in the Au(I) catalyzed rearrangement of arylazide **3.41**, we reasoned that the competing 5-*endo*-*dig* pathway of the free amide should be shut down if a suitable protecting group is used. This would allow for formation of the pseudoindoxyl in more synthetically useful yields and a subsequent deprotection could afford us access to brevianamide A in one-pot. For these tests, we chose to use PMB and *ortho*-nitrobenzyl (*o*-NB) protecting groups for the amide since there is precedent for the removal of these groups

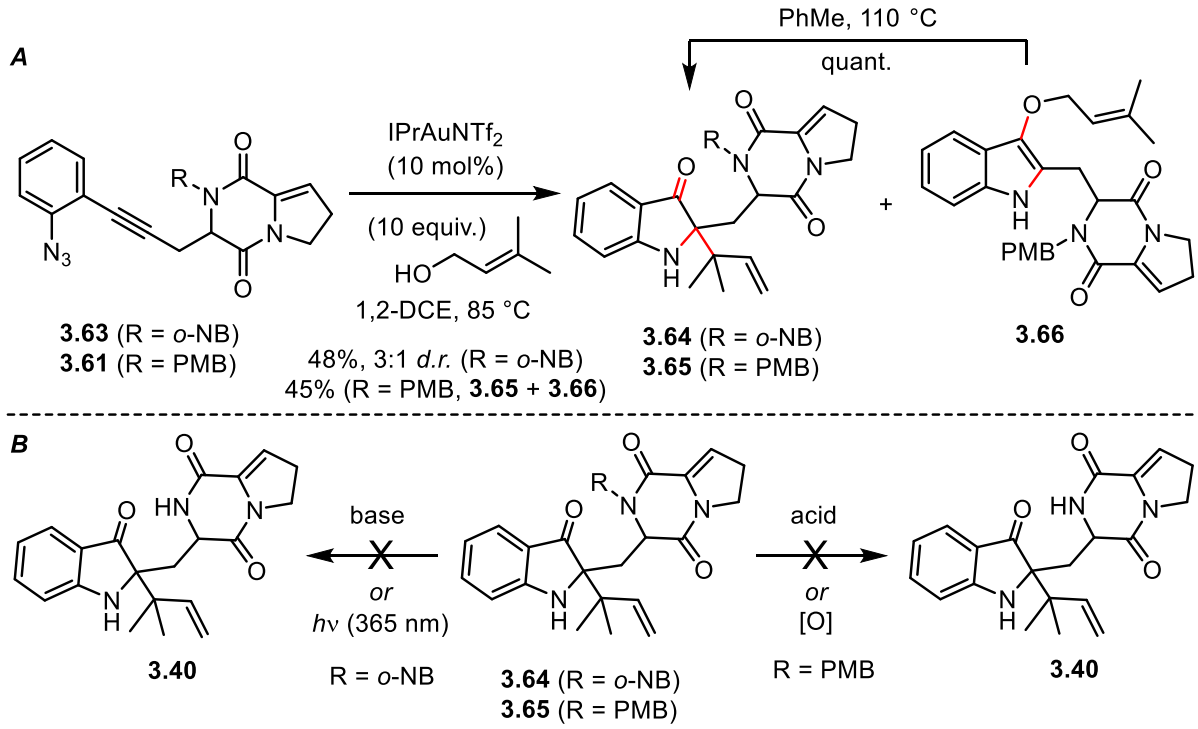
under relatively mild reaction conditions. The synthesis of these substrates began from diketopiperazines **3.59** and **3.42** (Scheme 3.20). To get the PMB-protected arylazide substrate **3.61**, a Sonogashira reaction was performed that proceeded in a good 73% yield. To obtain *o*-NB-protected arylazide **3.63**, free diketopiperazine **3.42** underwent benzylation with 2-nitrobenzylbromide using NaH (78% yield) to afford **3.62**. Finally, another Sonogashira coupling delivered us **3.63** in 37% yield.



Scheme 3.20. Synthesis of PMB- and *o*-NB-protected arylazide substrates **3.61** and **3.63** respectively

Interestingly, both substrates reacted slightly differently in the presence of the Au(I) catalyst (Scheme 3.21A). **3.63** gave the correct pseudoindoxyl product **3.64** as a mixture of diastereoisomers (3:1 *d.r.*) in a combined 48% yield. On the other hand, **3.61** underwent partial Claisen rearrangement to form the pseudoindoxyl product **3.65** with the rest of the substrate being consumed and forming the 3-allyloxyidole product **3.66** (combined yield is 45%, ratio not determined due to overlapping signals). This is an interesting observation that was not observed in our group's previous publication or in our initial model studies (see Schemes 3.11 and 3.14). Those substrates underwent complete conversion to the pseudoindoxyl products, with no 3-allyloxyindole products observed. The only instance was with a previous example using a

sterically hindered allylic alcohol was used as a nucleophile, but this did not rearrange and formed only the nucleophilic addition product. To confirm our structural assignment, the mixture of products was dissolved in toluene and heated to reflux. TLC and crude ^{1}H-NMR analysis indicated smooth conversion of the 3-allyloxyindole **3.66** (short-wave 254 nm UV) to the more polar and fluorescent (long-wave 366 nm) pseudoindoxyl diastereoisomers **3.65**. To our dismay, attempts to cleave these protecting groups from the pseudoindoxyl products led to degradation in all cases (Scheme 3.21B). The PMB protecting group was subjected to oxidative and strongly acidic conditions as we had done previously but led to mostly decomposition. Similarly, the *o*-NB group is known to be labile under strongly basic conditions or under irradiation with visible light (365 nm). In both cases, degradation was also observed. Regardless of the protecting group, acidic or basic conditions led to the observation of a highly fluorescent product by TLC. The formation of this compound may be the result of β-fragmentation of the diketopiperazine ring system, which has been observed previously by Williams and co-workers (see Scheme 3.5). With these failures, we decided that it would be best to shift gears and focus on a different strategy, allowing us to reevaluate our approach towards the synthesis of brevianamide A.



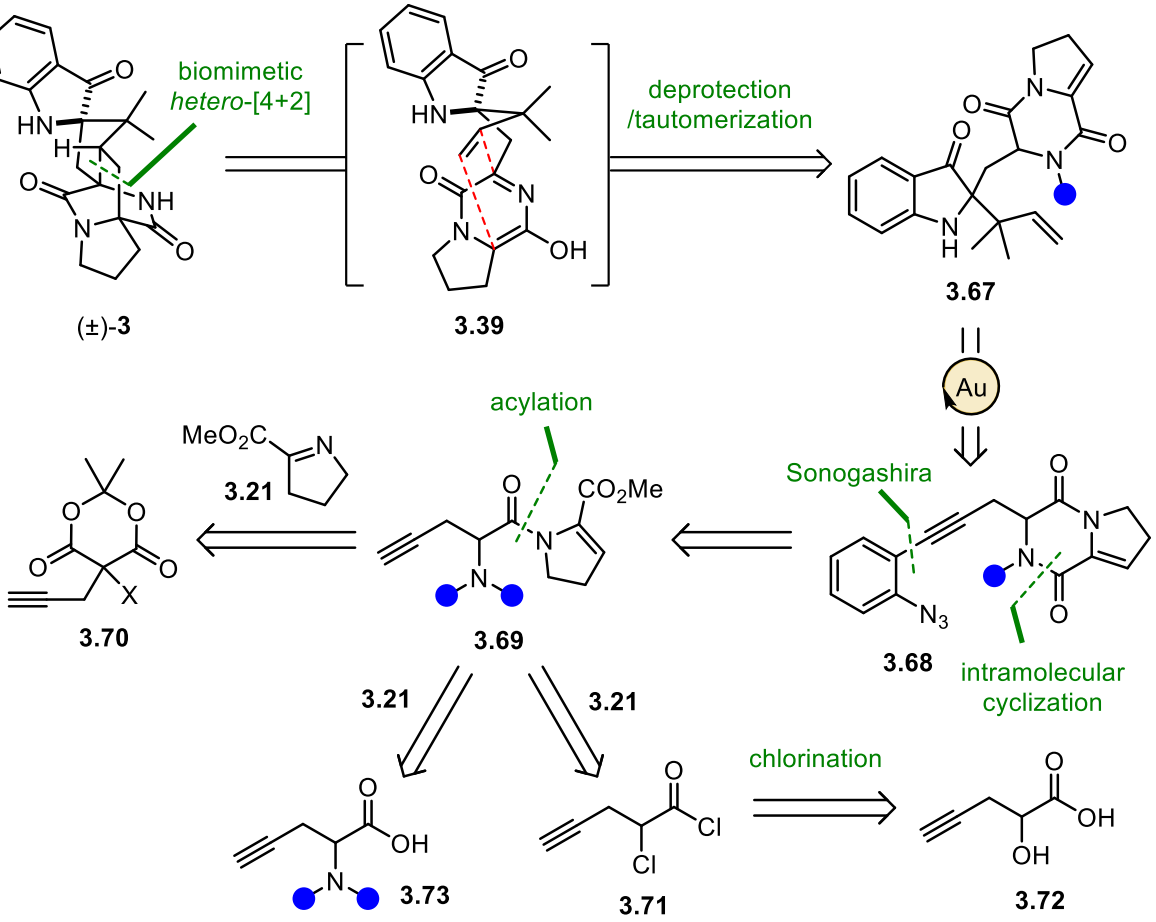
Scheme 3.21. (A) Formation of protected pseudoindoxyl products **3.64** and **3.65** using Au(I) catalysis and (B) unsuccessful attempts at protecting group removal

3.7 Revised retrosynthetic analysis

From our initial studies, we were able to complete the synthesis of racemic brevianamide A in a total of eight steps (one step shorter than the synthesis by Lawrence and co-workers). This is thanks to the use of gold catalysis, which helped to greatly shortcut the synthesis of this natural product by allowing for a rapid increase in molecular complexity. Despite this, our current synthesis of brevianamide A has a much lower overall efficiency and faces problems during multiple steps of the synthesis. One major problem is the introduction of the propargyl group which is low yielding and represents a bottleneck early on in our synthesis. Substrate solubility may be an issue here and can be a difficult problem to solve. A more pressing concern is the issues associated with protecting group manipulation and removal. These steps will be of utmost importance due to the inherent selectivity issue in the Au(I) catalyzed reaction with the free N-H substrate **3.41**. Taken together, these problems render our current synthesis far from ideal, leaving plenty of room for improvement. To address these challenges, we have revised our initial retrosynthetic analysis.

In our new retrosynthesis, the biomimetic *hetero*-IMDA reaction is retained and can be traced back as occurring from a suitably protected arylazide substrate **3.68** (Scheme 3.22). Rather than modifying the periphery and bringing in the propargyl group after diketopiperazine formation, we thought it would be best to consider a disconnection where the alkyne was already installed. Therefore, we chose to disconnect one of the C-N amide bonds which would result in a more linear starting material. As before, the arylazide moiety can still be installed through a Sonogashira cross-coupling, bringing us back to α-propargyl enamide **3.69**. From **3.69**, we considered several possibilities that could allow us to form the enamide motif from a previously propargylated building block. One possibility was to use a propargylated Meldrum's acid derivative **3.70**. Meldrum's acid is well known to thermally decompose into acetone, carbon dioxide, and one equivalent of a ketene derivative. The hypothesis is that the ketene should be a strong enough electrophile to trap the weakly nucleophile imine **3.21**, resulting in a one step access to the enamide **3.69**. The remaining handle (X) might be used to complete the cyclization to the diketopiperazine ring system. Another possibility is to utilize propargylated α-hydroxy acid **3.72**. Our idea here was to convert compounds like **3.72** into chloroacyl chlorides like **3.71**, which should function as

competent acylating agents in the same way as chloroacetyl chloride from our first-generation synthesis. A final possibility was to use a suitably protected propargyl glycine **3.73**. The advantage of this route is the commercial availability of *D,L*-propargyl glycine, however we would likely need to contest the issue of coupling a carboxylic acid with a weakly nucleophilic imine. This would require further experimentation than previous attempts (see Scheme 3.16).



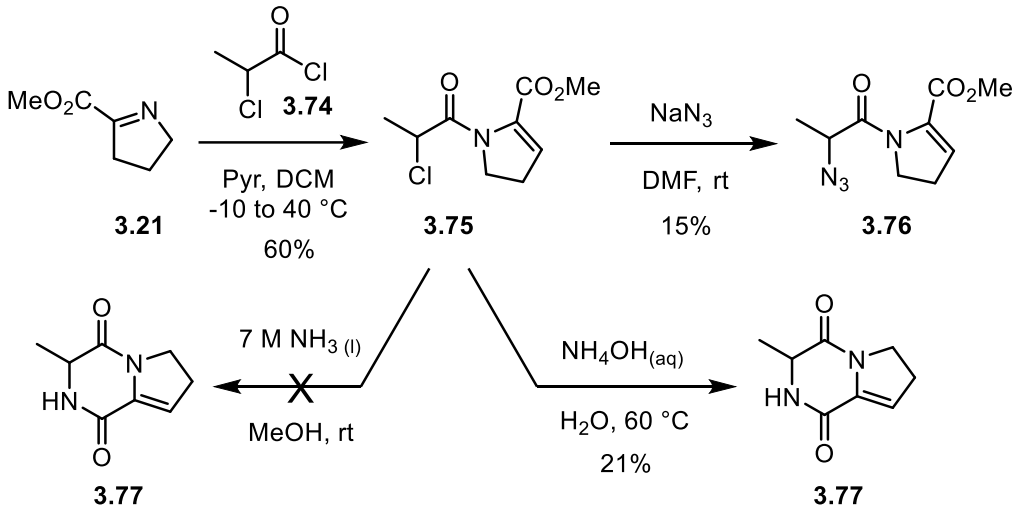
Scheme 3.22. Revised retrosynthetic analysis of (±)-brevianamide A

3.8 Efforts towards the synthesis of a propargylated enamide substrate

3.8.1 α-hydroxy acid route

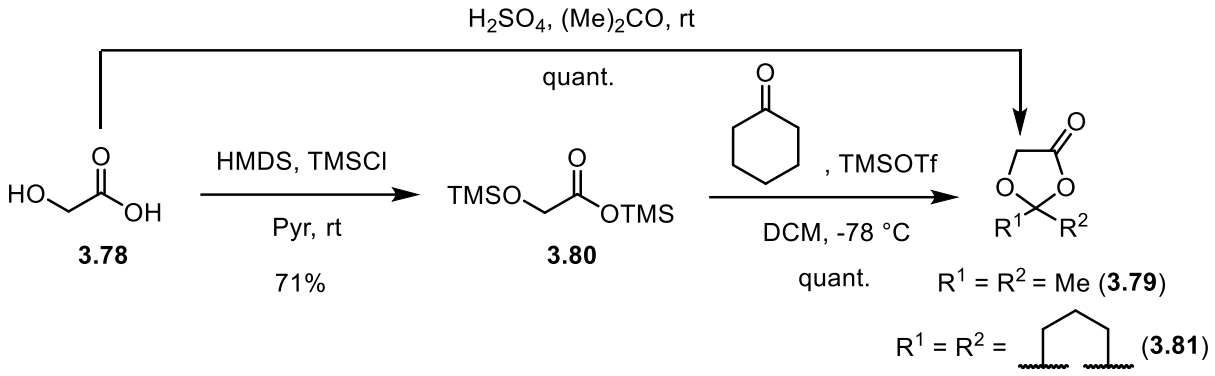
Our plan with this disconnection involved the coupling of imine **3.21** with acyl chloride **3.71** (Scheme 3.23). We initially began by trying a model study using 2-chloropropionyl chloride

3.74 as the acylating agent (methyl instead of propargyl) to assess if alkyl substitution α to the acid chloride would affect reactivity. We were pleased to see that the enamide **3.75** was formed in 60% yield. Next, we wanted to see if we could substitute this chloride with a suitable nucleophile. We first attempted substitution with NaN_3, and this resulted in a low yield of the product **3.76** with significant amounts of decomposition. Our next attempt was with different sources of ammonia. Using methanolic ammonia led to complete degradation, however aqueous ammonia was more successful. Using a solution of NH_4OH allowed for the isolation of the N-H diketopiperazine **3.77** in 21% yield. We attribute this low yield due to issues during chromatographic purification but the fact that we could isolate **3.77** from the reaction mixture was promising.



Scheme 3.23. Initial test reactions

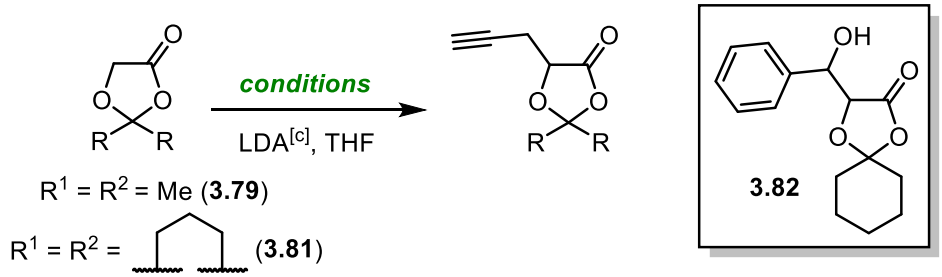
To synthesize the propargylated α-hydroxy acid **3.72**, we started from glycolic acid **3.78** and protected both the alcohol and carboxylic acid groups as the dimethyl and cyclohexyl acetonides **3.79** and **3.81** respectively (Scheme 3.24). Dimethyl acetonide **3.79** was synthesized from glycolic acid using catalytic H_2SO_4 with acetone. To synthesize cyclohexyl acetonide **3.81**, glycolic acid was first converted to trimethylsilyl trimethylsiloxyacetate **3.80** (71% yield) and then converted to the acetonide with cyclohexanone in the presence of catalytic TMSOTf. Both **3.79** and **3.81** were synthesized in quantitative yields.



Scheme 3.24. Synthesis of acetonides **3.79** and **3.81**

Our first attempts at introducing the propargyl group started with dimethyl acetonide **3.79** (Table 3.1). Deprotonation with LDA at -78 °C and warming to room temperature after quenching with propargyl bromide surprisingly led to decomposition of the substrate (Entry 1). Over time, the reaction developed a black color and formed significant amounts of precipitate. Keeping the reaction at -78 °C was somewhat helpful, allowing for the product to form in about 10% yield (Entry 2). Repeating the same using the more stable cyclohexyl acetonide **3.81** (Entries 3–4) gave similar results, with traces of product being formed in addition to large amounts of cyclohexanone, indicating some sort of decomposition pathway under the reaction conditions. Repeating this reaction at -100 °C (Entry 5) led to roughly the same outcome. Thinking it might be an issue with the electrophile, we instead tried to quench the enolate of **3.81** with benzaldehyde at -100 °C (Entry 6). This change led to the formation of diastereomeric aldol adducts **3.82** in a combined 54% yield. The rest of the material observed by ^{1}H-NMR was cyclohexanone. This indicated to us that propargyl bromide is not a suitable electrophile for this process in addition to the apparent instability of the lithium enolate. Because of this, we decided to abandon this route.

Table 3.1. Propargylation attempts using acetonides **3.79** and **3.81**



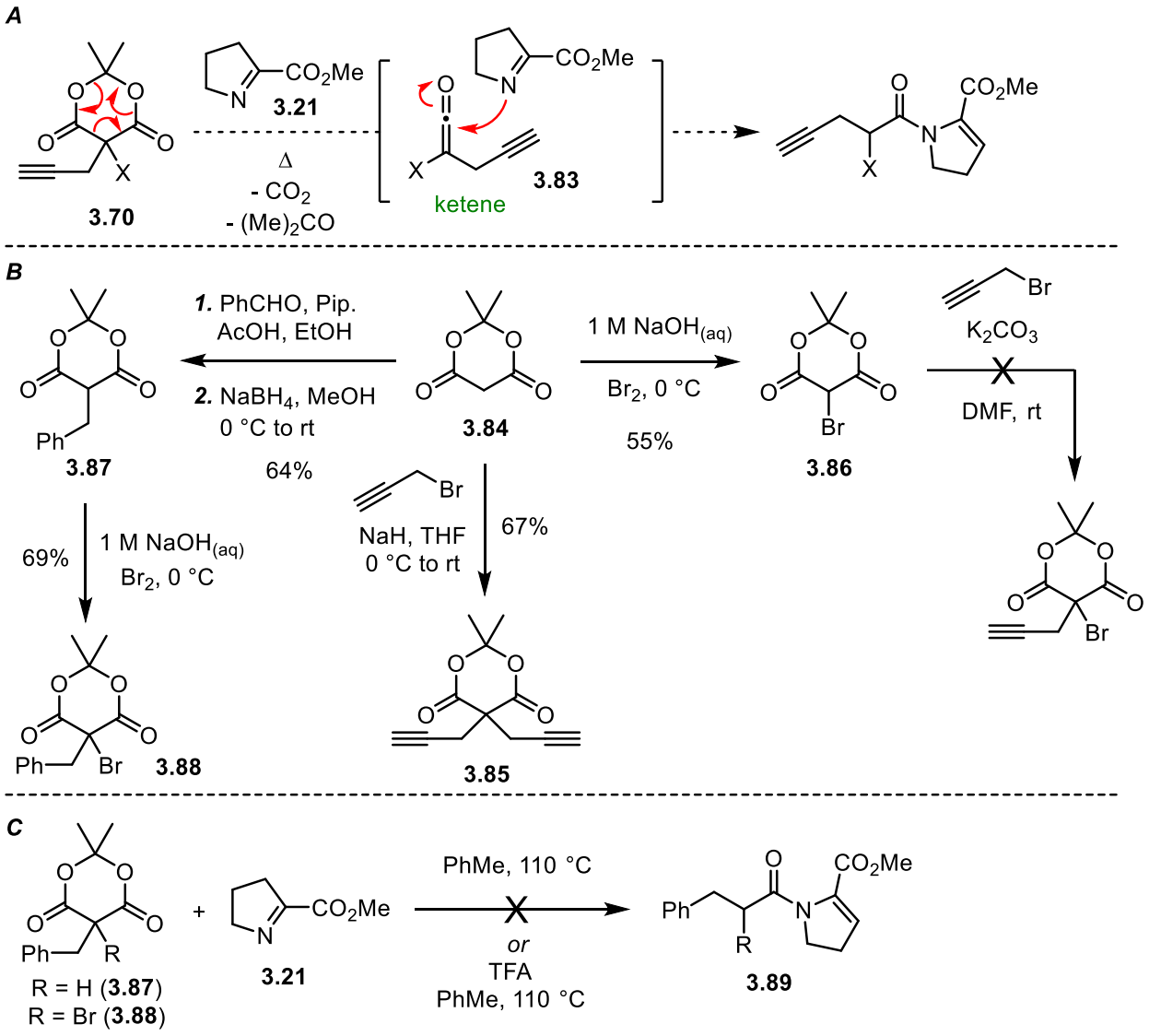
Entry[a]	Substrate	Temperature (°C)	Electrophile	Yield (%)[b]
1	**3.79**	-78 to 23	Br	--
2	**3.79**	-78	Br	10
3	**3.81**	-78 to 23	Br	traces
4	**3.81**	-78	Br	12
5	**3.81**	-100	Br	13
6	**3.81**	-100	PhCHO	54[d]

[a] Unless otherwise noted, all of the reactions were carried out in anhydrous THF at a substrate concentration of 0.2 M. [b] Isolated yields. [c] LDA is generated *in-situ* by deprotonation of $(i\text{-Pr})_2NH$ with *n*-BuLi. [d] Formed product **3.82**.

3.8.2 Meldrum's acid route

Our plan with this disconnection involved the reaction of imine **3.21** with *in-situ* formed ketene derivative **3.83** from a disubstituted Meldrum's acid such as **3.70** (Scheme 3.25A). We began by attempted propargylation of Meldrum's acid **3.84** (Scheme 3.25B). Our first try using NaH led exclusively to the isolation of the *bis*-propargyl product **3.85**, regardless of the amount of base used. This is probably attributed to the significantly increased acidity of Meldrum's acid as compared to other acyclic malonates. To address this issue, we attempted a two-step procedure. First, bromination of Meldrum's acid took place to give **3.86** in 55% yield. Second, propargylation was attempted using a weak base such as potassium carbonate with the addition of propargyl bromide. This was unsuccessful and only led to degradation of the starting material. Given the propensity of Meldrum's acid to undergo *bis*-alkylation, we used a Knoevenagel condensation instead with benzaldehyde, and formed the benzylidene product in quantitative yield. Reduction

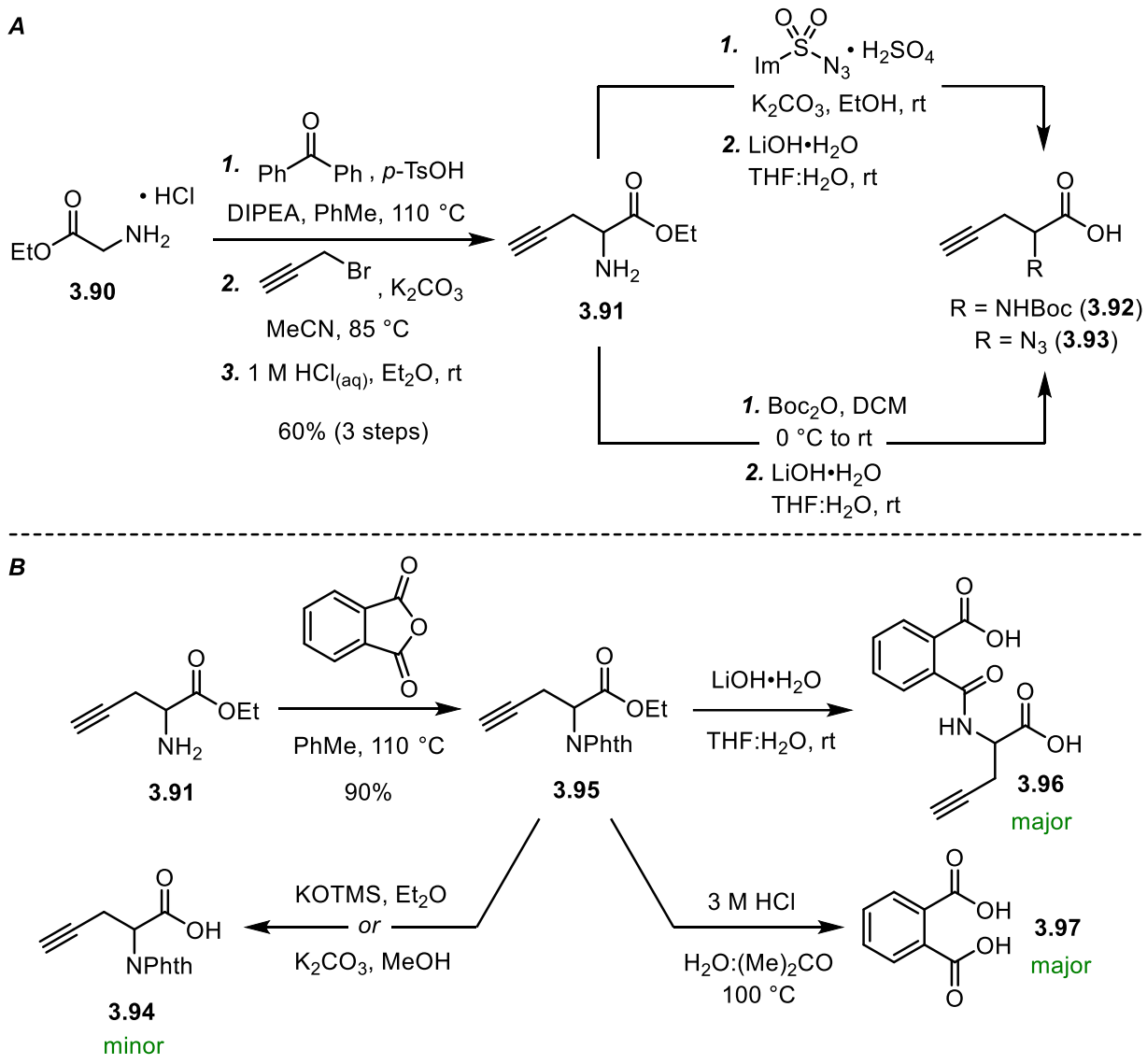
of this highly activated double bond with $NaBH_4$ gave the monoalkylated Meldrum's acid **3.87** in 64% yield. We were also able to brominate **3.87** using bromine and aqueous NaOH, affording us brominated derivative **3.88** in 69% yield. Despite being unable to install the propargyl group for the moment, we used **3.87** and **3.88** as test substrates to find conditions which could affect the formation of enamide **3.89** (Scheme 3.25C). Disappointingly, all attempts at thermal ketene generation in the presence of imine **3.21** using either Meldrum's acid derivative **3.87** or **3.88** led to complete decomposition. No traces of enamide product could be detected.



Scheme 3.25. Unsuccessful attempts at manipulating Meldrum's acid derivatives in the formation of enamide products

3.8.3. Propargyl glycine route

We next looked towards using propargyl glycine as a building block for the synthesis of desired enamide **3.69**, requiring us to revisit our attempts at coupling of a carboxylic acid derivative with imine **3.21**. Despite the commercial availability of propargyl glycine, we opted to synthesize it ourselves to obtain very large quantities for our studies (Scheme 3.26A). The synthesis began with glycine ethyl ester hydrochloride **3.90** that was converted to propargyl glycine ethyl ester **3.91** in an excellent 60% yield over three steps by a sequence of nitrogen protection, propargylation, and deprotection. A protecting group swap to Boc, followed by hydrolysis of the ethyl ester afforded Boc-propargyl glycine **3.92** in quantitative yield. To assess different protecting groups in the coupling reaction, we also set out to synthesize *N*-phthaloyl (**3.94**) and azidopropargyl glycine **3.93**. **3.93** was synthesized starting from **3.91** in a two-step procedure. First, the H_2SO_4 salt of diazo-transfer reagent imidazole-1-sulfonyl azide[174] was used to convert the primary amine to the azide and subsequent saponification then delivered azidopropargyl glycine **3.93** in 35% yield over two steps. The *N*-phthaloyl derivative was also synthesized by refluxing **3.91** with phthalic anhydride in toluene to afford **3.95** in 90% yield (Scheme 3.26B). However, our attempts at hydrolysis of the ethyl ester were met with some failure. Saponification of **3.95** with LiOH resulted in the isolation of *bis*-carboxylic acid **3.96**, where the phthalimide group had been ring opened. More mild conditions such as using K_2CO_3 in MeOH or using potassium trimethylsilanolate (KOTMS) resulted in mixtures of left-over starting material and phthalimide opening, with minor quantities of ester hydrolysis product **3.94**. Acidic hydrolysis was successful on small scale (<1 mmol) but on larger scales (>5 mmol), complete hydrolysis took place resulting in the isolation of phthalic acid **3.97**.

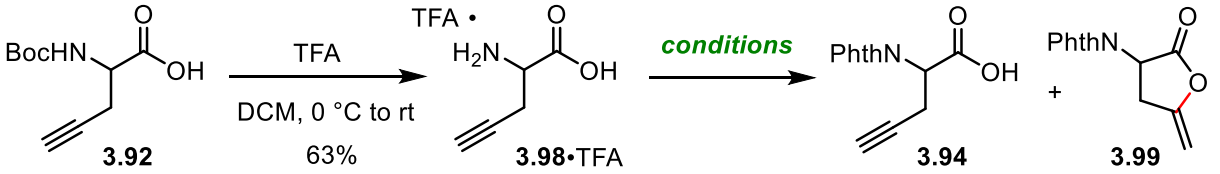


Scheme 3.26. Efforts towards the synthesis of protected propargyl glycine derivatives **3.92–3.94**

To access the phthalimide protected derivative, we deprotected the Boc group from **3.92** using an excess of TFA and obtained the TFA salt of propargyl glycine (**3.98**·TFA) in 65% yield. From there, several conditions were attempted to install the phthalimido protecting group (Table 3.2). Our first attempt (Entry 1) was to reflux **3.98**·TFA in the presence of phthalic anhydride. Full conversion was achieved; however, we did not obtain the desired product **3.94**. Instead, we obtained lactone **3.99** resulting from 5-*exo*-*dig* cyclization by the free carboxylic acid. Conducting the reaction in the presence of base (Entry 2) was unhelpful, resulting in the formation of the same side-product **3.99**. Changing the solvent to water and performing the reaction at reflux formed

minor amounts of **3.94** (17%) but led predominantly to hydrolysis of the phthalic anhydride and returned **3.98**·TFA (Entry 3). Hypothesizing that acidic activation was an issue here, we decided to free base the substrate before the addition of phthalic anhydride (Entries 4–6). This maneuver was somewhat successful, resulting in inconsistent mixtures of desired product **3.94** to the undesired lactone **3.99**. We next tried using phthaloyl chloride (Entry 7) as a milder means of introducing the protecting group. This led to decomposition of the mixture. As an alternative reagent that is used frequently in peptide chemistry, *N*-carbethoxyphthalimide[175] was used which turned out to be the reagent of choice (Entry 8) and allowed us to isolate **3.94** in 82% yield with no trace of lactone **3.99** being formed. This result was also confirmed on a sample of the free amino acid (**3.98**) that was commercially available. We also decided to test the related MSB as an *N*-phthaloylation reagent (Entry 9).[176] This reagent also worked well to introduce the phthalimide protecting group in 70% yield. Ultimately, *N*-carbethoxyphthalimide was chosen due to its commercial availability.

Table 3.2. Finding conditions for the *N*-phthaloylation of **3.98**·TFA



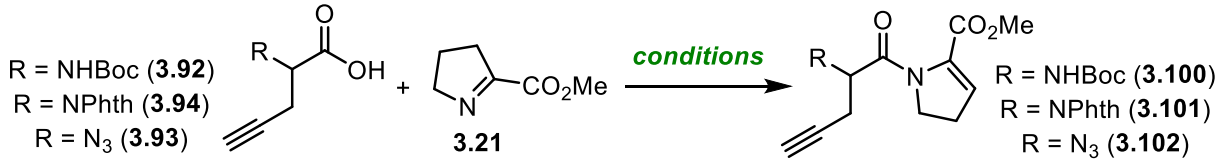
3.92 **3.98•TFA** **3.94** **3.99**

Entry[a]	Reagent	Base Additive	Temperature (°C)	Solvent	Yield (%)[b] 3.94	3.99
1	Phthalic anhydride	--	110	PhMe	--	98
2	Phthalic anhydride	Et_3N	110	PhMe	--	98
3	Phthalic anhydride	--	100	H_2O	17	--
4	Phthalic anhydride	Et_3N[c]	23 to 110	PhMe	--	96
5	Phthalic anhydride	1 M $NaOH_{(aq)}$[c]	23 to 110	PhMe	48	52
6	Phthalic anhydride	1 M $KOH_{(aq)}$[c]	23 to 110	PhMe	29	70
7	Phthaloyl chloride	Et_3N	0 to 23	DCM	--	--
8	NPhthCO_2Et[d]	Na_2CO_3	23	H_2O	82	--
9	MSB[e]	Na_2CO_3	23	MeCN:H_2O	70	--

[a] All reactions were conducted in the indicated solvent at concentrations between 0.1–0.4 M. [b] Isolated yield. [c] Base was added to **3.98**•TFA prior to the addition of the phthaloylation reagent and stirred for ~10 min. [d] *N*-carbethoxyphthalimide. [e] Methyl 2-((succinimidooxy)carbonyl)benzoate.

With protected propargyl glycine derivatives in hand, we could now initiate our studies towards finding suitable conditions that would allow us to synthesize the desired enamide **3.69** from the coupling of imine **3.21** with a carboxylic acid (Table 3.3). We started by using the Boc derivative **3.92**, repeating the conditions reported by Lawrence and co-workers (Entry 1). Similarly to what was observed with Boc-glycine **3.54**, no product was detected and only decomposition of the substrate took place. Using pyridine as the base did not restore reactivity (Entry 2). Using $SOCl_2$ in-place of $(COCl)_2$ for generating the acyl chloride *in-situ* also resulted in decomposition (Entry 3). Conventional activation with peptide coupling reagents such as EDC, DCC, or HATU with the addition of additives such as DMAP or HOBt were unsuccessful (Entries 4–6). Under these conditions, no reaction took place and led to full recovery of the starting material, likely due to the generation of an electrophile that was not reactive enough to addition by the weakly nucleophilic imine **3.21**. The same results were observed using either the azido (**3.93**) or *N*-phthaloyl (**3.94**) propargyl glycine derivatives. As a set of control experiments, we repeated the conditions of carbodiimide and acid chloride activation with more nucleophilic secondary amine nucleophiles (Entry 7–8). With carbodiimide activation, *L*-proline methyl ester coupled well with Boc-propargyl glycine **3.92** in 83% yield. However, under acid chloride activation, no product from coupling with pyrrolidine could be detected. It was noticed that the Boc group was no longer present in the crude ^{1}H-NMR analysis, presumably due to the rapid formation of an oxazolium intermediate that could decompose under the acidic conditions of the reaction. This result implies that perhaps a more mild or different reagent for acid chloride generation is needed. Inspired by Li and Seiple's work on the total synthesis of virginiamycin M1,[177] we utilized the Ghosez reagent[178] (1-chloro-*N*,*N*-2-trimethylpropenylamine) as a means of generating the acyl chloride under strictly neutral conditions (Entry 9).[179] While not the result we were expecting, using the Ghosez reagent allowed us to finally observe traces of the desired coupling product (from **3.92**) with mostly decomposition taking place. To our delight, switching to *N*-phthaloyl propargyl glycine **3.94** finally allowed us to isolate enamide **3.101** and in an excellent 96% yield (Entry 10). To compare, utilizing the azido derivative **3.93** only led to degradation (Entry 11).

Table 3.3. Optimization of the coupling conditions with imine **3.21**



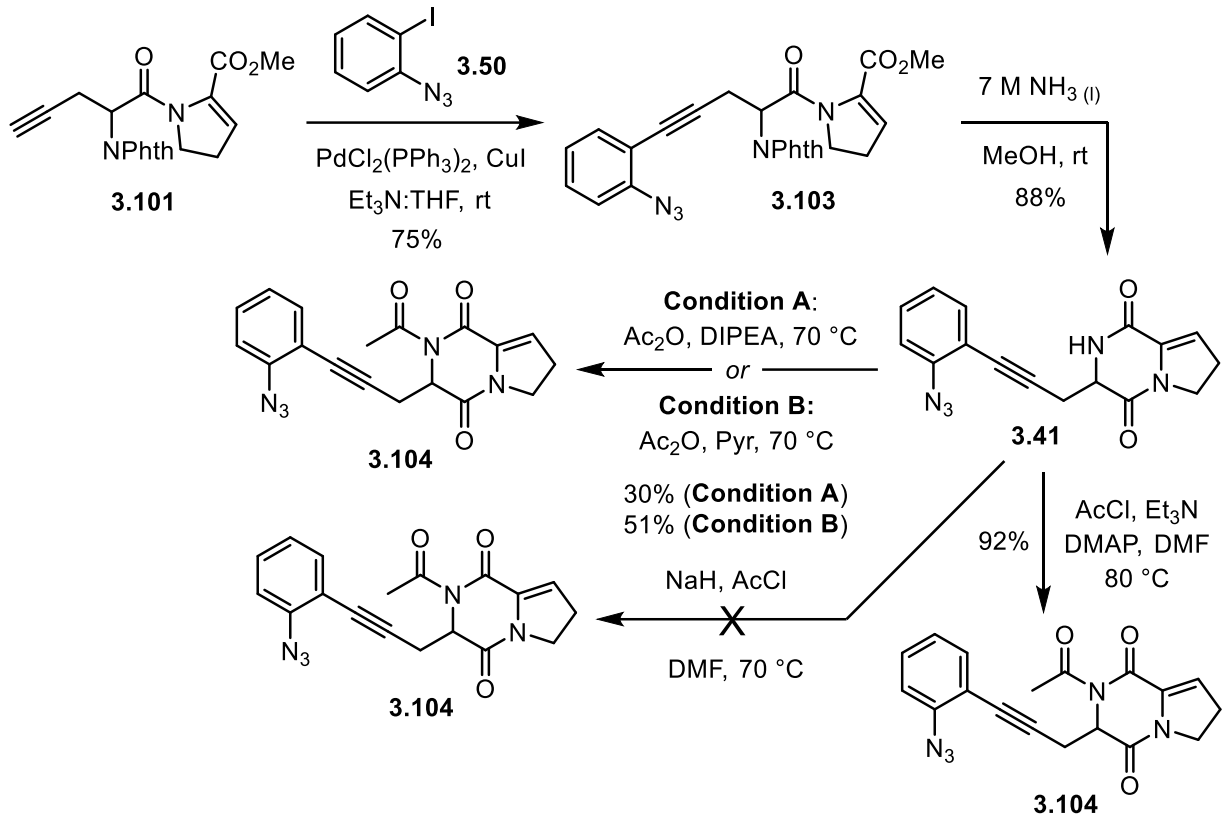
Entry[a]	Substrate	Nucleophile	Base/ Additive	Activating Agent	Temperature (°C)	Solvent	Yield (%)[b]
1	**3.92–3.94**	**3.21**	Et_3N	$(COCl)_2$, DMF	0 to 23	DCM	--
2	**3.92–3.94**	**3.21**	Pyridine	$(COCl)_2$, DMF	0 to 23	DCM	--
3	**3.92–3.94**	**3.21**	DIPEA	$SOCl_2$	23	DCM	--
4	**3.92–3.94**	**3.21**	Et_3N/HOBt	EDC•HCl	0 to 23	DCM	--[c]
5	**3.92–3.94**	**3.21**	DIPEA	HATU	23	DMF	--[c]
6	**3.92–3.94**	**3.21**	DIPEA	DCC	23	DCM	--[c]
7	**3.92**	*L*-Pro-CO_2Me	DIPEA/HOBt	EDC•HCl	0 to 23	DCM	83[d]
8	**3.92**	Pyrrolidine	Et_3N	$(COCl)_2$, DMF	0 to 23	DCM	--
9	**3.92**	**3.21**	2,6-lutidine	Ghosez reagent	0 to 60	DCM	traces
10	**3.94**	**3.21**	2,6-lutidine	Ghosez reagent	0 to 60	DCM	96
11	**3.93**	**3.21**	2,6-lutidine	Ghosez reagent	0 to 60	DCM	traces

[a] All reactions were conducted in the indicated solvent at concentrations of 0.2 M. [b] Isolated yield. [c] Starting material was fully recovered. [d] Product is *tert*-butyl *N*-[1-oxo-1-(pyrrolidin-1-yl)pent-4-yn-2-yl] carbamate.

3.9 Completion of the synthesis (second-generation)

Having finally developed reliable and scalable access to enamide **3.101**, we moved towards diketopiperazine installation (Scheme 3.27). Sonogashira coupling to install the arylazide proceeded smoothly to give **3.103** in 75% yield. Using the conditions reported by Lawrence and co-workers for phthalimide deprotection (methanolic ammonia) also afforded us the cyclized free N-H diketopiperazine **3.41** in 88% yield. When selecting a protecting group for the diketopiperazine, we initially elected to use an acetyl protecting group since it could likely be cleaved under the same conditions required for the end-game *hetero*-IMDA sequence. Classical conditions for installation of the acetate involved heating in acetic anhydride as solvent but solubility issues of **3.103** resulted in lower yields. Switching to DMF helped with solubility but using a strong base like NaH gave decomposition. Et_3N as a milder base was beneficial and gave

the protected diketopiperazine **3.104** in 92% yield, allowing us to set the stage for our key Au(I) catalyzed transformation to the desired pseudoindoxyl scaffold.

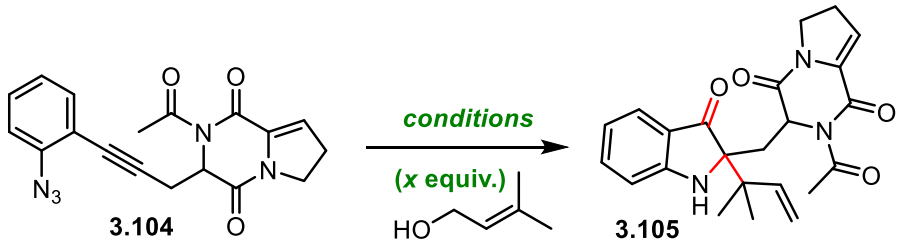


Scheme 3.27. Synthesis of acetate protected diketopiperazine **3.104** as the precursor to our key Au(I) catalyzed transformation

Based on our group's previous experience with this type of Au(I) catalyzed transformation, highly σ-donating NHC ligands were most beneficial as compared to Buchwald-type phosphine ligands. We therefore screened several NHC-Au(I) complexes to optimize this process (Table 3.4). Using the prototypical IPr ligand (Entry 1) in 1,2-DCE and with a large excess of prenyl alcohol (10 equivalents) led to full conversion of **3.104** and a promising 38% NMR-yield of pseudoindoxyl **3.105** as an inconsequential mixture of diastereoisomers in addition to unidentified impurities and some decomposition. Assessment of the diastereoselectivity for the Au(I) catalyzed rearrangement was only analyzed in the context of our optimal reaction conditions. Based on the crude ^{1}H-NMR analysis, pseudoindoxyl **3.105** was formed in a 5:1 diastereomeric ratio. Attempts to improve this process were unfortunately unsuccessful, and a 38% NMR yield was the best that could be

achieved. Using the fully saturated SIPr ligand (Entries 2–3) performed similarly (35% and 36% NMR-yield) and the bulkier IMes and IPr* were only slightly lower in the observed yield (Entries 4–5). The alkyl derivative IPent did not show any significant improvement (Entry 6). For comparison, we also tested Buchwald ligands (Entries 7–9). The richer RuPhos did not perform well, and bulkier phosphines *t*-BuXPhos and JohnPhos were comparable to most of the NHC ligands tested. We tried to vary the solvent using IPr as the ideal ligand and did not find much improvement as compared to 1,2-DCE (Entries 10–11). Prenyl alcohol in solvent level quantities led to essentially full conversion, but only gave traces of the desired product because of acetate cleavage and subsequent substrate decomposition.

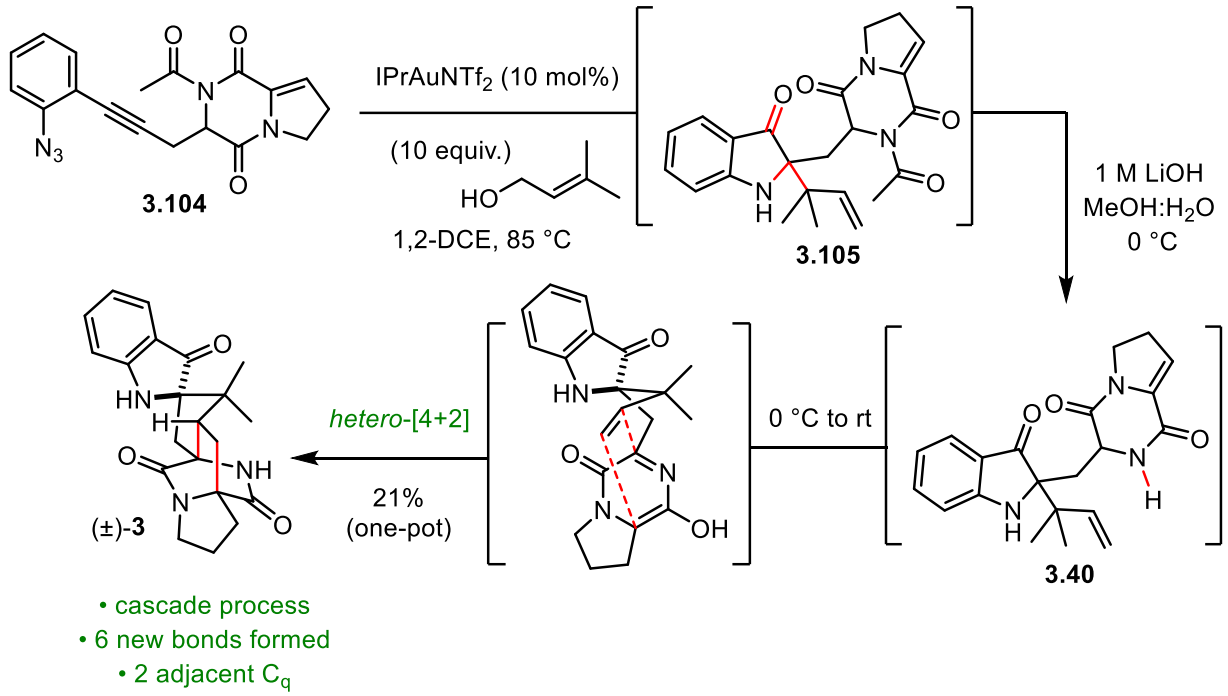
Table 3.4. Optimization of the Au(I) catalyzed rearrangement of acetate protected diketopiperazine **3.104** into pseudoindoxyl **3.105**



Entry[a]	Catalyst (10 mol%)	Prenyl alcohol (x equiv.)	Solvent	Time (min)	Temperature (°C)[b]	Conversion (%)[c]	NMR-Yield (%)
1	$IPrAuNTf_2$	10	1,2-DCE	30	85	100	38
2	$SIPrAuNTf_2$	10	1,2-DCE	30	85	100	36
3	$SIPrAu(NCMe)SbF_6$	10	1,2-DCE	30	85	100	35
4	$IMesAuNTf_2$	10	1,2-DCE	30	85	100	31
5	IPr^*AuNTf_2	10	1,2-DCE	30	85	100	29
6	$IPentAu(NCMe)SbF_6$	10	1,2-DCE	30	85	100	33
7	$RuPhosAuNTf_2$	10	1,2-DCE	30	85	97	15
8	$JohnPhosAuNTf_2$	10	1,2-DCE	30	85	100	31
9	*t*-$BuXPhosAuNTf_2$	10	1,2-DCE	30	85	100	28
10	$IPrAuNTf_2$	10	$MeNO_2$	30	85	100	32
11	$IPrAuNTf_2$	100	--	30	85	96	traces

[a] Unless otherwise noted, all reactions were carried out using screw-cap test tubes with 0.05 mmol of the substrate at a concentration of 0.15 M in the indicated solvent. [b] Internal temperature. [c] Conversion and NMR yields were determined from the crude ^{1}H-NMR analysis using mesitylene as an internal standard.

Throughout this optimization, we noticed the significant instability of pseudoindoxyl **3.105**, especially during purification on silica. We saw this as an excellent opportunity to implement a one-pot access to (±)-**3** (Scheme 3.28). To our delight, *in-situ* treatment of the crude reaction mixture with LiOH in a mixture of water and methanol cleanly induced the cleavage of the acetate group. Interestingly, this cleavage can be easily monitored by TLC due to the drastic change in polarity of the substrate and if conducted exclusively at 0°C, no *hetero*-IMDA reaction towards brevianamide A is observed and only pseudoindoxyl **3.40** is formed. The tautomerization and [4+2] cycloaddition seems to only occur upon warming to room temperature. Conducting this one-pot sequence allowed us to isolate (±)-**3** in a 21% overall yield, starting from **3.104**.

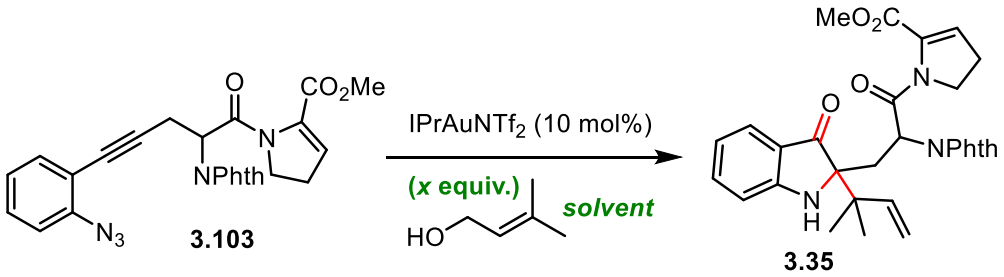


Scheme 3.28. One-pot synthesis of (±)-brevianamide A starting from acetate protected diketopiperazine **3.104**

We also recognized that Sonogashira product **3.103** could advantageously serve as a precursor for the key Au(I) catalyzed transformation, resulting in the same pseudoindoxyl intermediate that was accessed by the group of Smith in their total synthesis of (±)-**3**. We thus undertook a separate optimization of the key Au(I) step starting from linear precursor **3.103** (Table 3.5). From our experiences using precursor **3.104**, we began the optimization with $IPrAuNTf_2$ in

several solvents using a large excess of prenyl alcohol (10 equivalents). 1,2-DCE was worse in this case (Entry 1, 29% isolated yield) while $MeNO_2$ at 100 °C was particularly good affording a 41% isolated yield of pseudoindoxyl **3.35** as an ~1:1 inconsequential mixture of diastereoisomers (Entry 2). Surprisingly, the use of prenyl alcohol as the solvent (Entry 3) with substrate **3.103** was even more beneficial as compared to using **3.104**, thus allowing for the isolation of **3.35** in 47% yield (51% NMR-yield). We wondered if a specific ratio of $MeNO_2$ to prenyl alcohol as co-solvents would help (Entries 4–6), however lower ratios of prenyl alcohol were detrimental to the yield. Other solvents (Entries 7–11) such as $CHCl_3$, higher boiling aromatics, and 1,4-dioxane did not improve the yield. We also found that increasing the temperature further (120 °C) led to an almost 20% reduction in NMR-yield (Entry 12) and lowering to 80 °C (Entry 13) was comparable to conducting the reaction at 100 °C in prenyl alcohol as the solvent. Moving forward, we used prenyl alcohol as the solvent of the reaction and evaluated different ligands and catalysts for this process (Table 3.6). In general, Buchwald type ligands (Entries 3–8) performed better as compared to the reaction with **3.104** but were not as good as using NHC ligand IPr (Entry 1–2). More sterically demanding phosphines seemed to improve the yield (JohnPhos *vs* *t*-BuXPhos), but increasing steric bulk further was detrimental (Me_4*t*-BuXPhos *vs* *t*-BuXPhos). Other NHC ligands were also tested (Entries 9–12) and performed with similar efficiencies to most of the Buchwald ligands tested. A similar issue with sterics was also observed in this case. A catalyst bearing a bicyclic CAAC ligand (**3.106**) was particularly ineffective, affording traces of the desired product and decomposition (Entry 13).

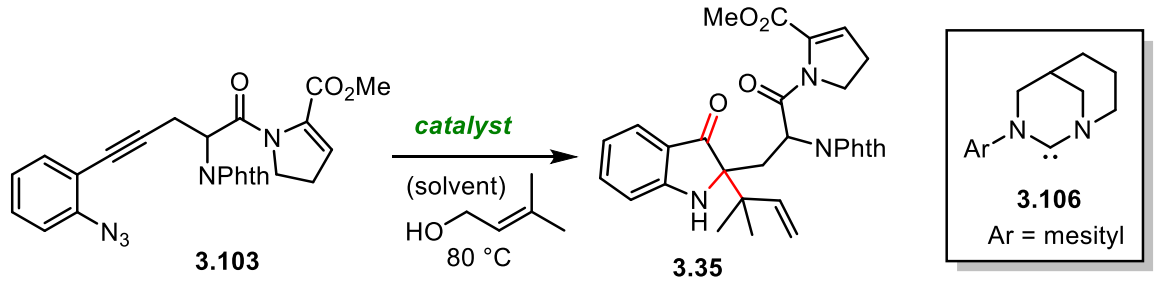
Table 3.5. Optimization of the solvent and temperature for the Au(I) catalyzed rearrangement of linear precursor **3.103** into pseudoindoxyl **3.35**



Entry[a]	Prenyl alcohol (x equiv.)	Solvent	Time (h)	Temperature (°C)[b]	Conversion (%)[c]	NMR-Yield (%)
1	10	1,2-DCE	2	100	96	27, 29[d]
2	10	$MeNO_2$	2	100	100	39, 41[d]
3	100	--	2	100	100	51, 47[d]
4	25[e]	$MeNO_2$	2	100	100	36
5	50[f]	$MeNO_2$	2	100	100	39
6	75[g]	$MeNO_2$	2	100	100	42
7	10	$CHCl_3$	2	100	70	20
8	10	1,4-dioxane	2	100	100	31
9	10	PhMe	2	100	100	16
10	10	$PhCF_3$	2	100	100	15
11	10	PhCl	2	100	100	22
12	100	--	2	120	100	32
13	100	--	2	80	100	49

[a] Unless otherwise noted, all reactions were carried out using screw-cap test tubes with 0.06 mmol of the substrate at a concentration of 0.15 M in the indicated solvent. [b] Internal temperature. [c] Conversion and NMR yields were determined from the crude ^{1}H-NMR analysis using mesitylene as an internal standard. [d] Isolated yield. [e] 2:1 ratio of $MeNO_2$:prenyl alcohol. [f] 1:1 ratio of $MeNO_2$:prenyl alcohol. [g] 1:2 ratio of $MeNO_2$:prenyl alcohol.

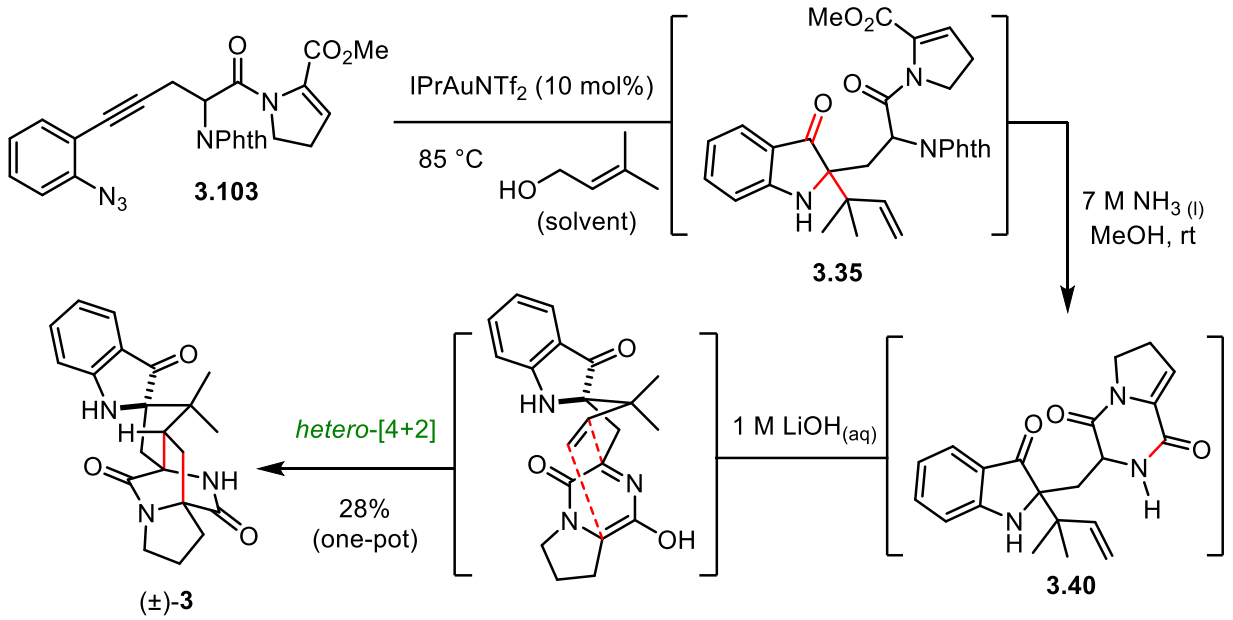
Table 3.6. Optimization of the catalyst and ligand for the Au(I) catalyzed rearrangement of linear precursor **3.103** into pseudoindoxyl **3.35**



Entry[a]	Catalyst (10 mol%)	Time (h)	Temperature (°C)[b]	Conversion (%)[c]	NMR-Yield (%)
1	$IPrAuNTf_2$	2	80	100	51, 47[d]
2	$IPrAu(NCMe)SbF_6$	2	80	100	39
3	$RuPhosAuNTf_2$	2	80	100	34
4	$JohnPhosAuNTf_2$	2	80	100	32
5	*t*-$BuXPhosAuNTf_2$	2	80	100	43
6	Me_4*t*-$BuXPhosAuNTf_2$	2	80	100	32
7	*t*-$BuXPhosAu(NCMe)SbF_6$	2	80	97	28
8	$MorDalPhosAuNTf_2$	2	80	100	20
9	$IPr^*(NCMe)SbF_6$	2	80	70	17
10	IPr^*AuNTf_2	2	80	82	28
11	I*t*-$BuAuNTf_2$	2	80	100	31
12	$IPent(NCMe)SbF_6$	2	80	100	39
13	**3.106**$AuNTf_2$	2	80	34	traces

[a] Unless otherwise noted, all reactions were carried out using screw-cap test tubes with 0.05 mmol of the substrate at a concentration of 0.15 M in the indicated solvent. [b] Internal temperature. [c] Conversion and NMR yields were determined from the crude ^{1}H-NMR analysis using mesitylene as an internal standard. [d] Isolated yield.

Having identified optimal conditions for the conversion of **3.103** into **3.35** using Au(I) catalysis, we once again attempted a one-pot conversion into (±)-**3** (Scheme 3.29). Gratifyingly, this could be achieved by treating the crude reaction mixture containing **3.35** with ammonia in MeOH to induce the deprotection of the phthalimido group and result in formation of the diketopiperazine ring system (monitored by TLC). Once the reaction was complete, an aqueous solution of LiOH was added directly and ultimately furnished (±)-**3** in 28% overall isolated yield.

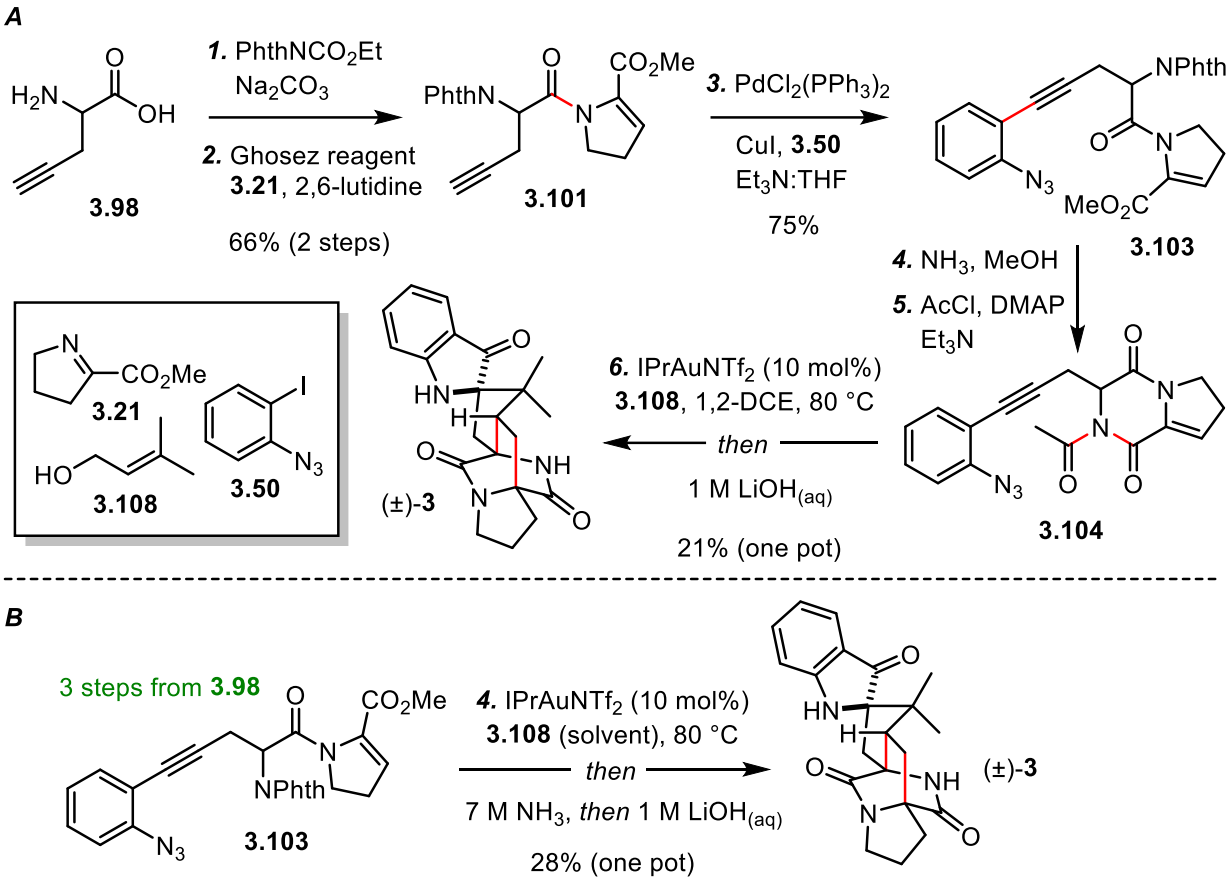


Scheme 3.29. One-pot synthesis of (±)-brevianamide A starting from linear arylazide precursor **3.103**

3.10 Conclusion

We have developed two concise and complementary routes towards the natural product (±)-brevianamide A that have been summarized in Scheme 3.30 below. Our initial efforts led to the first-generation synthesis of (±)-**3** in a total of seven steps, however the efficiency of the process was very low and left much to be desired. Low yields and reproducibility issues led to a bottleneck in the early stages of our synthesis and the key Au(I) catalyzed rearrangement exhibited poor efficiency and chemoselectivity. Forced back to the drawing board, we reevaluated our retrosynthetic analysis and developed the successful synthesis of a propargylated enamide building block **3.101** which allowed us to overcome our earlier issues. Elaboration from this point allowed us to access (±)-**3** in a one-pot manner from two separate intermediates. Using acetyl protected diketopiperazine **3.104**, we synthesized (±)-**3** in six steps as the LLS and in an 8% overall yield (Scheme 3.30A). With this result we have shortened the syntheses reported by the groups of Lawrence and Smith by one step and have achieved a comparable level of efficiency. On the other hand, using substrate **3.103** allowed us to shorten the synthesis of (±)-**3** even further (four steps as the LLS) and in a 14% overall yield (Scheme 3.30B). With this new result, we have achieved the shortest and highest yielding synthesis of (±)-**3** to date. Overall, the success of this approach is

thanks to the use of a Au(I) catalyzed cascade process that installed key elements of the natural product in a single step.



Scheme 3.30. Overview of the total synthesis of (±)-**3** from (A) acetyl protected diketopiperazine **3.104** and (B) linear arylazide intermediate **3.103**

PART II

Synthesis of Cyclopropane Building Blocks *via* the Photochemical Extrusion of Sulfur Dioxide (SO_2)

CHAPTER 4

Photochemical Ring Contraction of Thietane-1,1-dioxide Derivatives

4.1 Introduction

4.1.1 Importance and properties of the cyclopropane ring

As the smallest possible carbocycle, cyclopropanes have always interested organic chemists and demonstrates interesting characteristics (Figure 4).[180] Notably, the cyclopropane ring exhibits high ring-strain of about 27 kcal/mol as compared to other cyclic alkanes and possesses a highly rigid framework with unusual bond angles of around 60°, deviating greatly from the standard tetrahedral bond angles of 109.5° in other alkanes.[181] Perhaps somewhat counterintuitive, the cyclopropane ring also more closely resembles alkenes and is said to possess "double bond character" which is not the case for the slightly larger cyclobutane ring.[182] The C-C bonds of the cyclopropane ring possess more *p*-orbital character which helps to offset any destabilization associated with decreased bond angles. From an orbital perspective, this leads to the concept of "bent bonds" where instead of electron density being positioned along the internuclear C-C bond axis, much of the electron density lies off the C-C bond axis.[183] Consequently, the C-H bonds then possess more *s*-orbital character, resulting in bonds that are shorter (1.08 Å) and stronger (BDE = 106 kcal/mol) than typical alkane C-H bonds (1.09 Å and BDE = 98 kcal/mol). This also manifests spectroscopically, resulting in diagnostically up-field chemical shift values (δ = 0–1 ppm) for the cyclopropane C-H resonances as compared to other alkane C-H bonds.[184]

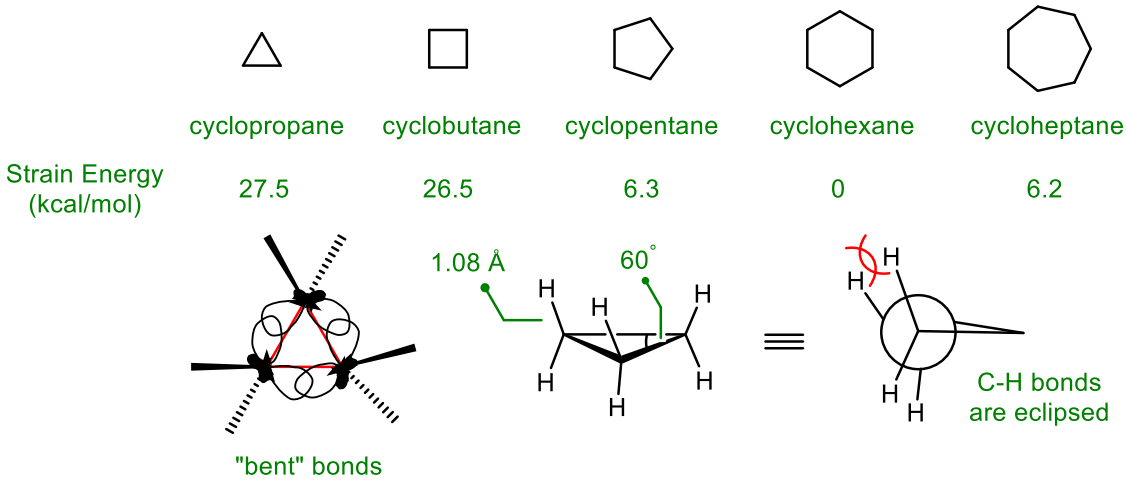


Figure 4. Physical properties of the cyclopropane ring

Despite being stable compounds in general, the C-C single bonds of cyclopropanes are weaker due to ring-strain and this has been taken advantage of to affect ring opening or expansion reactions in the literature.[185, 186] Additionally, the rigidity of the three-membered ring allows for organization of substituents which are well-defined in 3D space with increased lipophilicity as well as metabolic stability.[187] As a result, the cyclopropyl motif has become a privileged scaffold in medicinal chemistry, receiving significant attention as a bioisostere. A bioisostere is a functional unit that is used to replace a different substructure within a parent molecule. The new molecule containing the bioisostere should then ideally possess similar or improved biological properties with respect to factors such as potency, pharmacokinetics, and toxicity among other things. Cyclopropane rings are found in the core structure of many natural products, pharmaceutical drugs, agrochemicals, and even fragrances for the perfume industry (Figure 4.1).[188-191] In fact, the cyclopropane ring was present in 12 of the 200 best-selling small molecule drugs in the year 2022.[192]

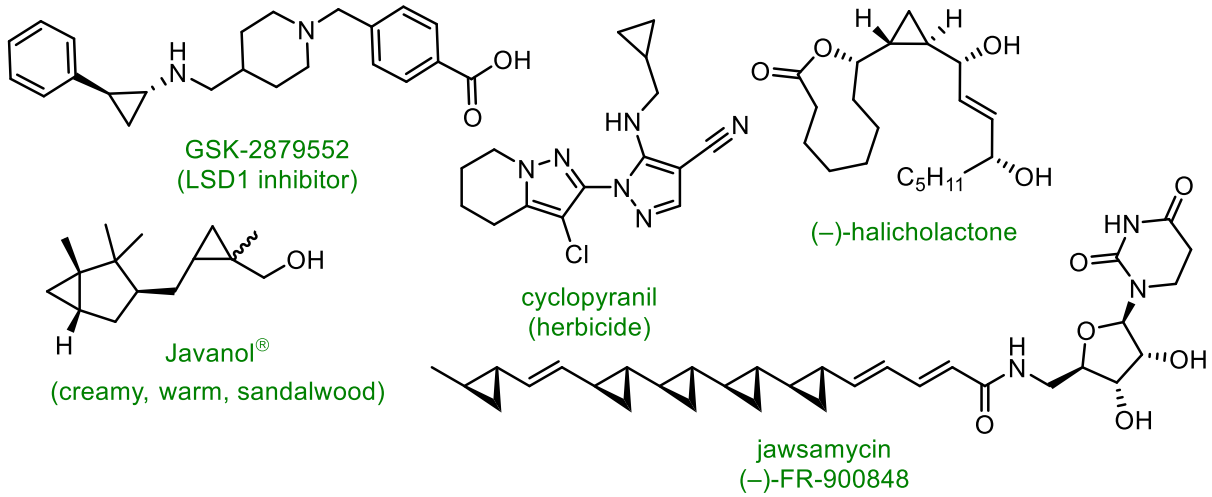
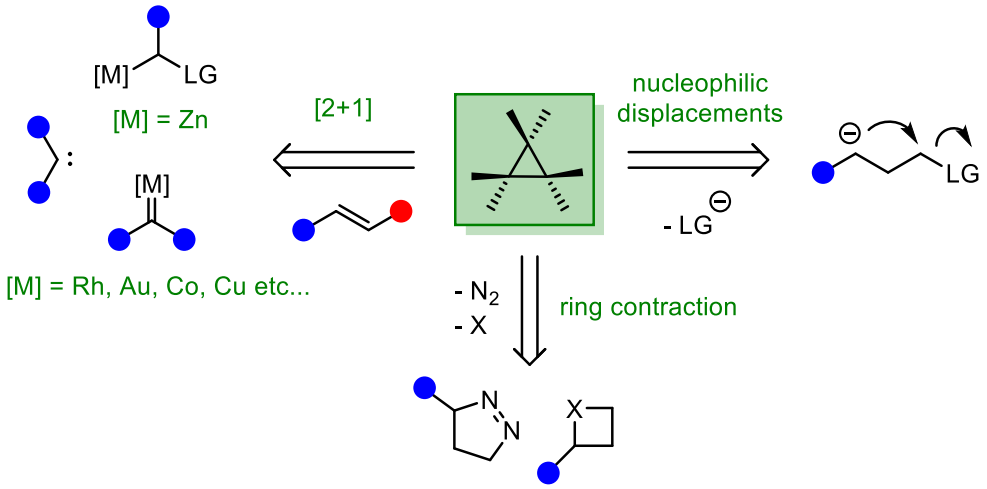


Figure 4.1. Examples of compounds which feature the cyclopropane ring

4.1.2 Methods for the synthesis of the cyclopropyl motif

Different methods exist for the synthesis of cyclopropane rings, however most of these strategies fall into a small handful of reaction types which are consistently used (Scheme 4). As a result, extensive efforts have been dedicated to achieving the synthesis of highly substituted cyclopropanes in high yields and selectivity.[193-195] In general, the synthesis of small ring systems

such as cyclopropanes is dominated by two main strategies: cycloaddition/carbene and nucleophilic displacement processes. Additionally, a highly underutilized approach to cyclopropanes is a ring contraction strategy from larger four- or five-membered ring systems. Other miscellaneous syntheses of the cyclopropane ring such as through radical addition[196] or the Kulinkovich reaction and variations thereof[197] have been documented but will not be discussed in this section. Given the size and scope of this important field, a non-comprehensive account and discussion of the main reactions used to make cyclopropanes will be discussed.



Scheme 4. Current strategies towards the synthesis of cyclopropanes

4.1.2.1 Formal [2+1] cycloaddition strategies

The most common strategy used to make cyclopropanes is through a formal [2+1] cycloaddition using free or metal-stabilized carbenes and carbenoids in conjunction with an alkene partner. A carbene is a neutral and divalent species with the general formula :CR_2 which contains two unshared valence electrons (Figure 4.2). Carbenes can exist in either the singlet or triplet state depending on their electronic structure. Singlet carbenes are spin-paired, possessing a sp^2-orbital containing both unshared valence electrons in addition to an unoccupied *p*-orbital. Triplet carbenes have two unpaired electrons of the same spin, each occupying its own orbital. Carbenes can exist either in their free form or can be stabilized by various transition metals. Carbenoids on the other hand are distinct species and are often confused with carbenes in the literature.[22] The general formula of a carbenoid is that of an organometallic species that bears a good leaving group

[L_nMCH_2X], thus exhibiting similar reactivity to that of carbenes in terms of nucleophilic addition and electrophilicity.

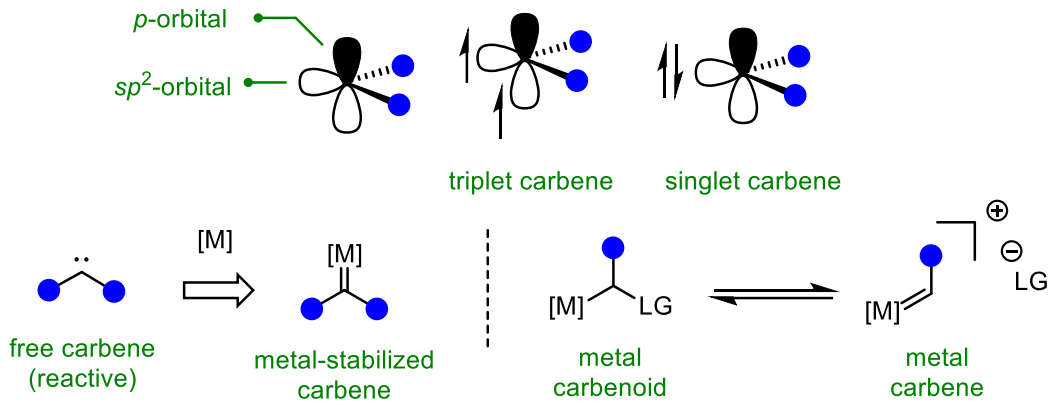
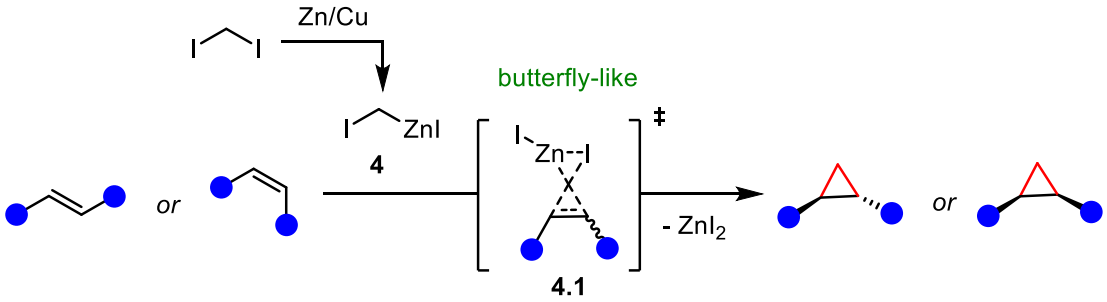


Figure 4.2. Representative structures of free or metal-stabilized carbenes/carbenoids

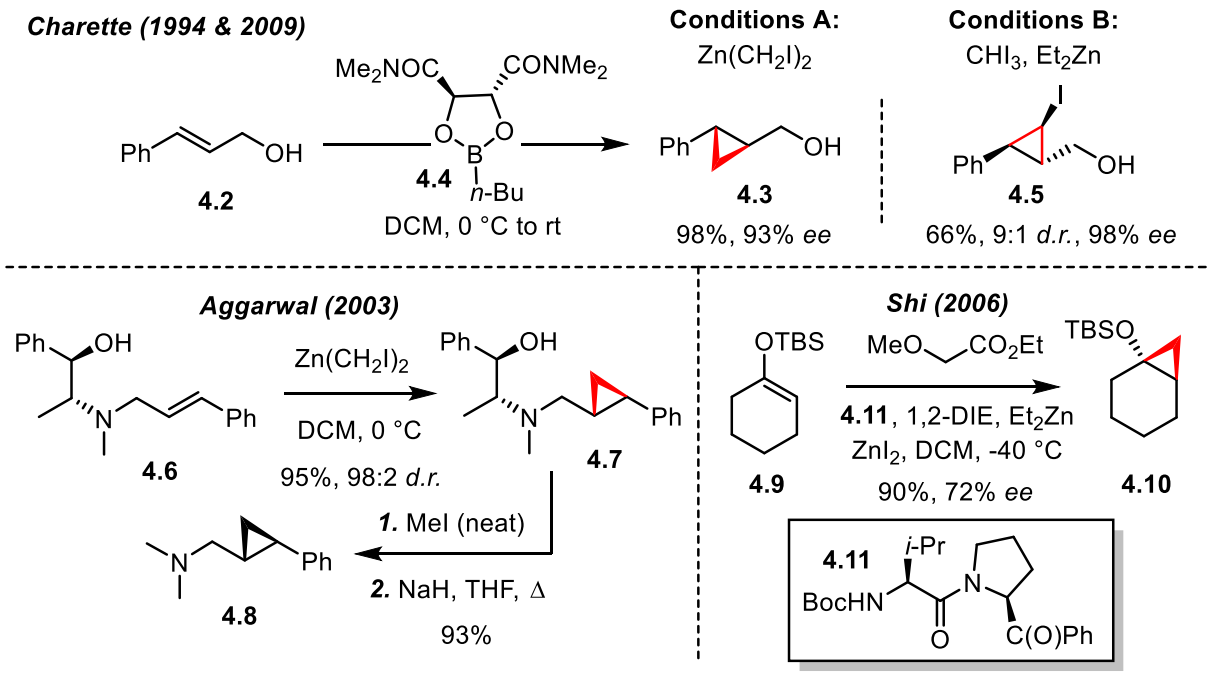
Perhaps the most well-known application of the formal [2+1] cycloaddition approach is the Simmons-Smith cyclopropanation reaction (Scheme 4.1). Classically, this reaction utilizes the carbenoid species (iodomethyl)zinc iodide **4** (generated from diiodomethane and a zinc-copper (Zn/Cu) couple to stereospecifically convert olefins into cyclopropanes. Mechanistically, this reaction is believed to proceed through a formal [2+1] cycloaddition that is concerted and has a three-centered "butterfly-like" transition state **4.1**.



Scheme 4.1. General mechanism for the Simmons-Smith cyclopropanation

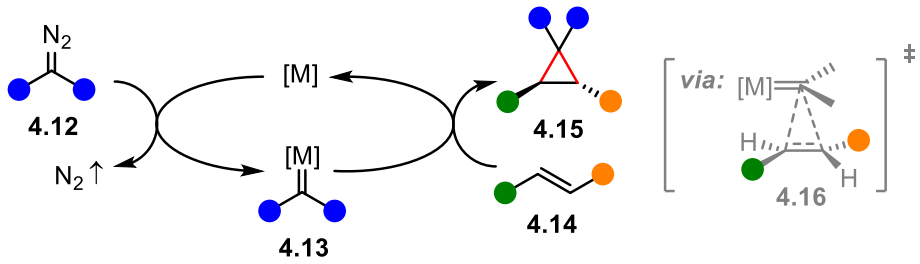
Using this method, cyclopropanations of basic olefins occur at a modest rate. However, significant rate enhancement can be observed in the presence of an oxygen based directing group.[198] This led to the development of several diastereoselective and enantioselective

cyclopropanation reactions (Scheme 4.2). Work from the group of Charette demonstrated the enantioselective cyclopropanation of allylic alcohol substrates which did not rely on pre-installed chiral auxiliaries.[199] The group of Charette used a stoichiometric amount of a chiral and bifunctional dioxaborolane ligand **4.4** to enable the synthesis of cyclopropylmethanol product **4.3** (from allylic alcohols **4.2**) with high enantioselectivity. This method could also be extended to performing an enantioselective iodocyclopropanation reaction (giving product **4.5**) by utilizing a zinc carbenoid derived from iodoform instead of diiodomethane.[200] Similarly, work by the group of Aggarwal showed that it was possible to cyclopropanate allylic amine substrate **4.6** using a pendant alcohol as a chelating group for the active zinc carbenoid.[201] Removal of this chelate led to failure since the predominant pathway became coordination of the amine to the zinc carbenoid, forming stable adducts. If pseudoephedrine is used as the chelating group, Aggarwal and co-workers observed high levels of diastereoselectivity and yield for the product **4.7**. The pseudoephedrine auxiliary could also be removed in a simple two step process affording aminomethyl cyclopropane **4.8**. Taking a different approach, the group of Shi demonstrated the enantioselective Simmons-Smith cyclopropanation of highly electron rich silyl enol ether **4.9** using a chiral peptide additive **4.11**.[202] This consistently afforded the authors silyl-protected cyclopropanol products **4.10** in excellent yields and enantioselectivities.



Scheme 4.2. Representative asymmetric Simmons-Smith cyclopropanation reactions

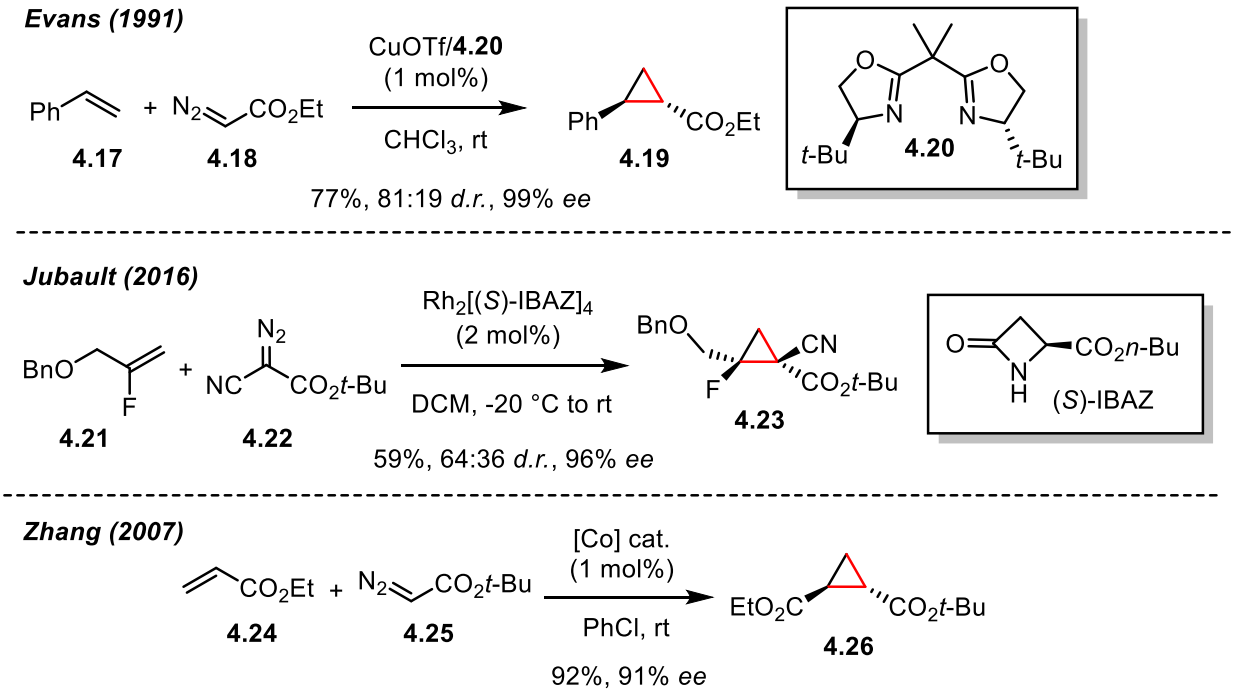
Other strategies towards the cyclopropanation of alkenes involve using free or metal-stabilized carbenes as opposed to zinc carbenoid species. Methods utilizing metal-stabilized carbenes are very common as compared to free carbenes since the transition metal helps to tame the incredibly high reactivity of free carbenes in solution. Reactions of metal-stabilized carbenes typically employ diazo substrates like **4.12** as carbene precursors (Scheme 4.3) that are either formed separately or *in-situ*.[203] It is accepted that interaction of **4.12** with a transition-metal results in the loss of nitrogen gas and the formation of a metal-stabilized carbene (**4.13**) that is electrophilic. Reaction with an alkene **4.14** then produces the cyclopropane product **4.15** *via* a concerted three-membered transition state **4.16**.[194, 204] Chemo-, enantio-, and diastereoselectivity in these reactions are typically governed by the transition-metal used, the chiral ligand, and the specific substituents on either the alkene, diazo compound, or both. Therefore, this strategy requires a more nuanced assessment of the reaction to achieve a desired outcome.



Scheme 4.3. General catalytic cycle for the transition-metal catalyzed cyclopropanation of alkenes *via* the decomposition of diazo compounds

Several transition-metals such as rhodium, ruthenium, copper, gold, and cobalt are known to participate in this chemistry and lead to stabilized carbene species.[193, 195] A few interesting examples will be mentioned below (Scheme 4.4). Work from the group of Evans first introduced C_2-symmetric Cu(I) oxazoline complex **4.20** for the enantioselective cyclopropanation of styrene **4.17** using ethyl diazoacetate **4.18** with great diastereoselectivity, favoring *trans*-isomer **4.19**.[205] Jubault and co-workers have also reported on the asymmetric synthesis of biologically relevant[206] fluorocyclopropane **4.23** using a Rh(II) catalyst and highly electrophilic diazo substrate **4.22** bearing two electron-withdrawing groups.[207] This method is also amenable to the synthesis of chloro, bromo, and iodocyclopropanes which are incredibly useful as synthetic intermediates in general. While most Rh-catalyzed cyclopropanations occur with more electron-rich alkene

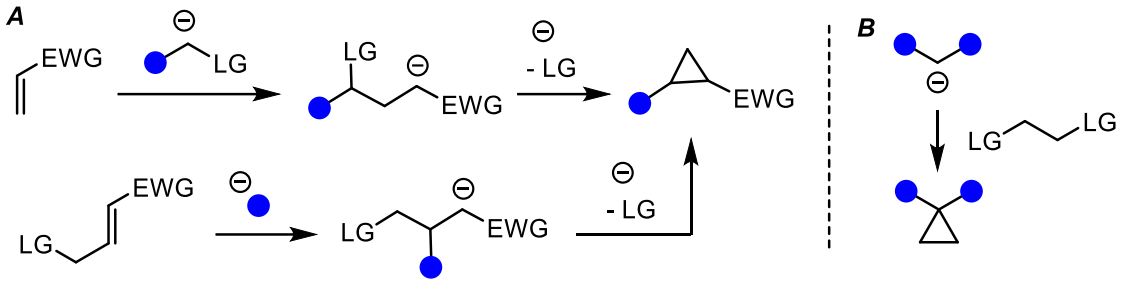
substrates, the group of Zhang demonstrated that Co(II)-porphyrin complexes are capable of cyclopropanating more electron-poor alkenes such as ethyl acrylate (**4.24**) with excellent yields and enantioselectivity, forming the *trans*-cyclopropane isomers **4.26**.[208] An interesting solvent effect was observed in this case where simply switching from toluene to chlorobenzene led to a dramatic increase in reaction yield by ~20%.



Scheme 4.4. Representative examples of transition-metal catalyzed cyclopropanation reactions *via* metal-stabilized carbenes

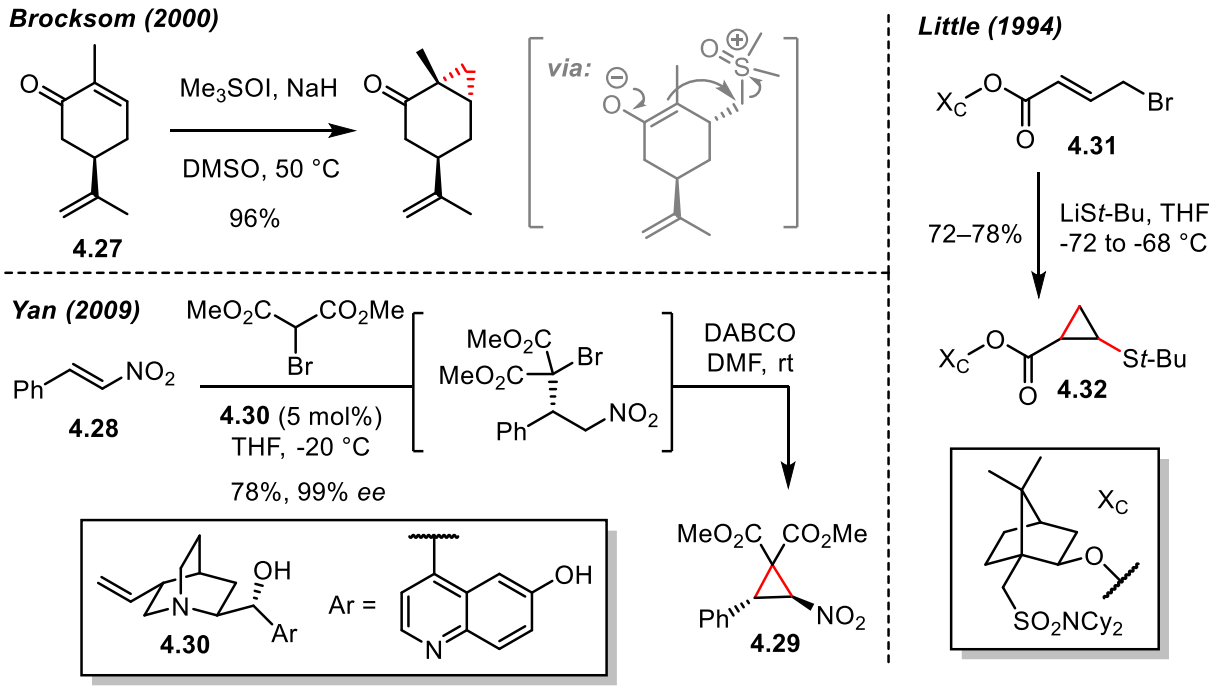
4.1.2.2 Nucleophilic displacement strategies

While transition-metal catalysis has been a powerful tool for cyclopropane synthesis, metal free approaches are also common strategies which fall into the broad category of nucleophilic displacement reactions. One such strategy has been termed Micheal Initiated Ring Closure (MIRC), which consists of the 1,4-addition of a nucleophile onto a Michael acceptor, followed by ring closure *via* the nucleophilic displacement of a leaving group (Scheme 4.5).[193, 194] More direct alkylative approaches involving strong bases and carbanion nucleophiles have also been utilized, albeit to a lesser extent which is likely due to the lower functional group tolerance.[194, 209]



Scheme 4.5. (A) MIRC and (B) carbanion strategies towards the synthesis of cyclopropane rings

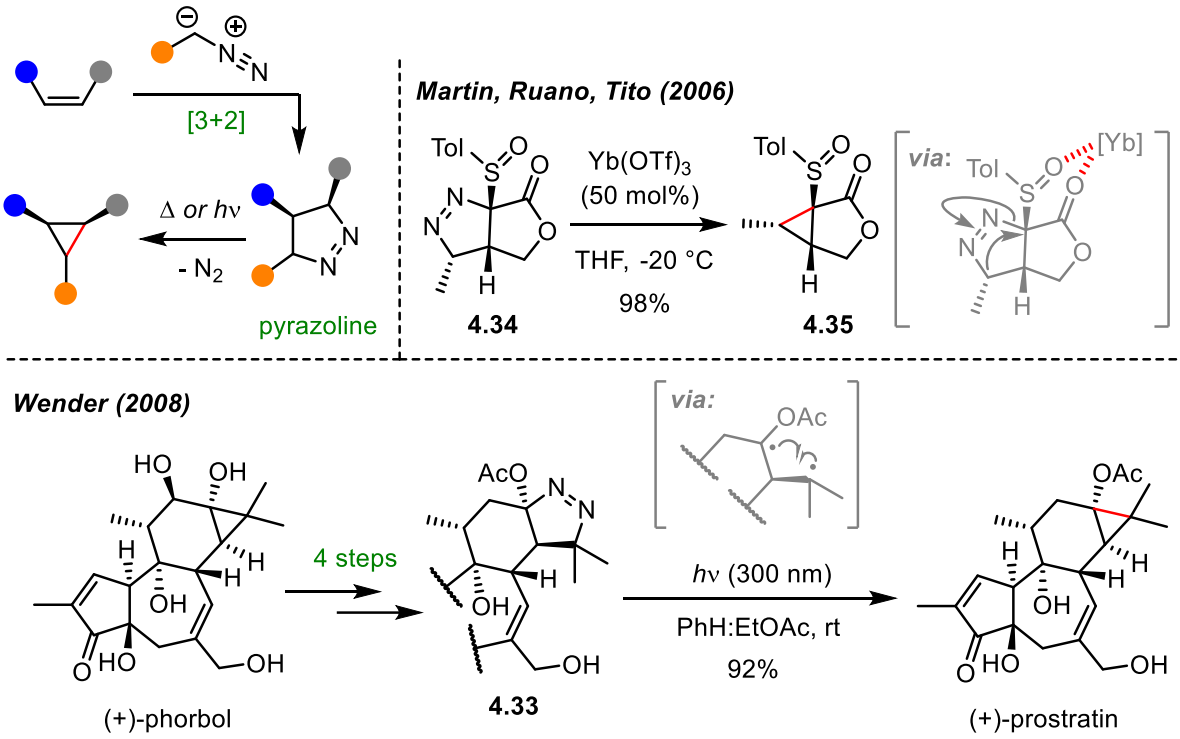
MIRC has become a very successful method for the synthesis of cyclopropanes and is exemplified in the well-known Corey-Chaykovsky reaction which utilizes sulfur-ylides as nucleophiles (Scheme 4.6).[210] The Corey-Chaykovsky reaction is known to be sensitive to steric effects. For example, the cyclopropanation of (*R*)-carvone **4.27** with trimethylsulfoxonium iodide (Me_3SOI) proceeds with high diastereoselectivity due to the presence of the isopropenyl group blocking the top face of the enone.[211] The MIRC strategy is also particularly useful in the synthesis of nitrocyclopropanes which are convenient precursors to cyclopropylamine motifs that are present in many pharmaceuticals.[212] Yan and co-workers found that reaction of dimethyl bromomalonate with nitroalkene **4.28** gave nitrocyclopropane **4.29** in good yields and enantioselectivities if a chiral Cinchona alkaloid catalyst **4.30** is employed.[213] The MIRC strategy can also be considered if the Michael acceptor possesses a leaving group at the γ position. Little and co-workers studied the addition of lithium *tert*-butyl thiolate to bromoester **4.31** which had a chiral auxiliary.[214] After extensive optimization, only low to modest levels of chiral induction was achieved despite good yields in the formation of cyclopropane **4.32**.



Scheme 4.6. Representative examples of cyclopropane synthesis employing nucleophilic displacement strategies

4.1.2.3 Ring contraction strategies

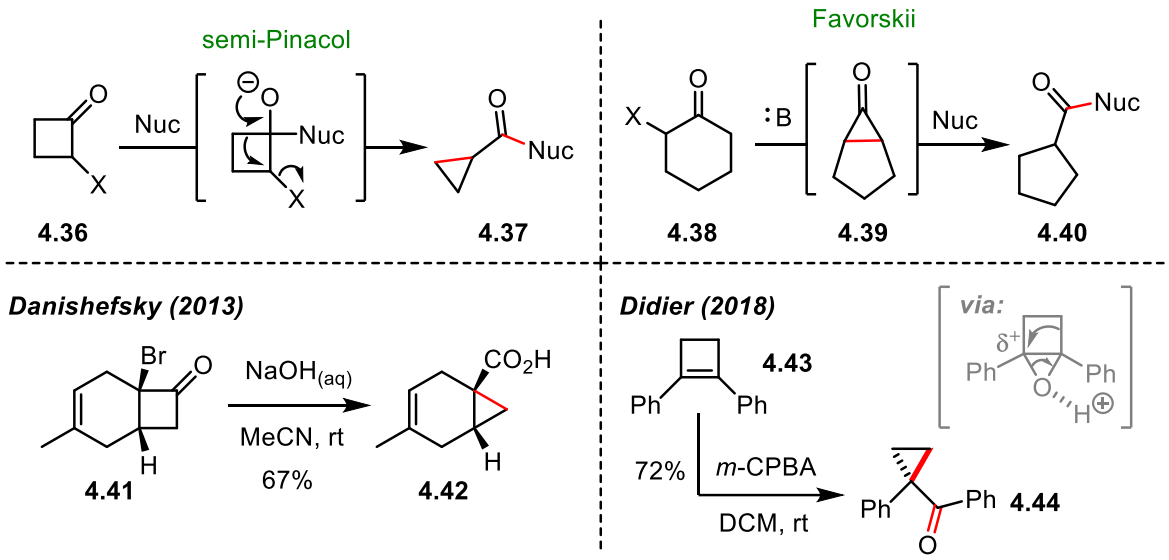
Ring contraction strategies towards the synthesis of cyclopropyl motifs are few and far between. Of notable use is the ring contraction of pyrazolines through the extrusion of nitrogen gas and formation of cyclopropanes (Scheme 4.7).[215] The pyrazolines are typically synthesized from the dipolar cycloaddition of olefins and diazaoalkanes. This process has been known since the 1970's and represents a unique method for cyclopropane synthesis either thermally or photochemically. Photochemical induced ring contractions of pyrazolines are more common in the literature owing to higher levels of selectivity and have even been used in the context of total synthesis. Wender and co-workers installed the key cyclopropane ring of the natural product (+)-prostratin through the irradiation of a benzene/ethyl acetate solution of precursor **4.33** using 300 nm UV light.[216] On the other hand, thermal processes often suffer from significant olefin formation at the temperatures required for ring contraction to occur (>100 °C). However, this unwanted cycloreversion process can be suppressed using an appropriate Lewis acid catalyst. The groups of Martin, Tito, and Ruano showed that bicyclic pyrazoline **4.34** can be efficiently converted to the cyclopropane **4.35** using $Yb(OTf)_3$ at low temperatures.[217]



Scheme 4.7. Cyclopropane synthesis through the ring contraction of pyrazoline derivatives

Interestingly, cyclopropanes have also been synthesized under basic conditions using α-halo cyclobutanones, cyclobutanols, and cyclobutanone ketals.[218] This reaction can be viewed in a similar manner to the Favorskii rearrangement in terms of the reaction outcome (ring contraction) but with a slightly different mechanism (Scheme 4.8). The Favorskii rearrangement is known to proceed *via* a strained cyclopropanone intermediate **4.39** that is formed from the treatment of α-halo cyclohexanones **4.38** with strong base. **4.39** is ring opened by a nucleophile to give the indirect ring contraction cyclopentane product **4.40**. With α-halo cyclobutanones **4.36**, nucleophilic addition results in a direct ring contraction to give cyclopropanes **4.37**, resembling that of a semi-Pinacol rearrangement. Notably, α-halo cyclopentanones do not undergo rearrangement under the same conditions. This reaction is nicely demonstrated by the group of Danishefsky where they converted angularly brominated cyclobutanone **4.41** into cyclopropane carboxylic acids **4.42** in the presence of NaOH.[219] A related approach to cyclopropanes from cyclobutene derivatives has also been reported by the group of Didier.[220] In this case, cyclobutene **4.43** is converted to cyclopropyl ketone **4.44** using *m*-CPBA as an oxidant.

This reaction is believed to proceed through the intermediacy of a cyclobutene oxide, which are known to rearrange under acidic conditions to give ring contraction products.[218]



Scheme 4.8. Cyclopropane synthesis through the ring contraction of cyclobutyl derivatives

4.1.3 Fundamentals of photochemistry

Photochemistry is defined as the branch of chemistry which relates to the chemical changes associated with molecules upon their interaction with a photon of either ultraviolet (UV) or visible light. Photochemical reactions occur everywhere and are an important feature of vital chemical processes in living organisms. In humans for instance, adequate skin exposure to UVB light is necessary for the biosynthesis of vitamin D_3, a vital precursor molecule that is used in several downstream biological functions.[221] Photochemistry of organic molecules involves the overall process: R + *hν* → R* → I → P, where the absorption of a photon (*hν*) is required to access an electronically excited state (R*), leading eventually to product (P) through an intermediate (I).[d] Absorption of a photon with a specific frequency (*ν*) or wavelength (λ) therefore implies that the organic substrate (R) possesses a chromophore which can absorb that light. All molecules possess a maximum absorption wavelength (λ_{max}). For most organic molecules, this value will typically fall within the UV (~200–400 nm) range. Few organic molecules absorb within the visible light

[d]Turro, N. J.; Scaiano, J. C.; Ramamurthy, V. In *Principles of Molecular Photochemistry: An Introduction Series*, 1st edition; University Science Books: 2008.

ranges (~380–700 nm). Photons within these two regions typically possess energies between ~40–110 kcal/mol.[e] This energy range is sufficiently capable of forming an excited state and allowing for photochemistry to take place, thereby allowing for reactions to happen which are not thermally accessible. Outside of these ranges, the energies of the incoming photons are either too high or too low to allow for any productive event to occur.

The formation of an excited state can be explained from a molecular orbital perspective, with the electronic transitions being conveniently illustrated through a Jablonski diagram (Figure 4.3).[222] Upon the absorption of a photon (*hv*) with a specific wavelength, one electron in the molecules ground state singlet orbital (HOMO, S_0) is promoted to a higher energy singlet excited state orbital (LUMO, S_1), retaining its original spin. Depending on the energy of the incoming photon, several excited state energy levels may be accessed. However, they will all eventually relax to the lowest energy S_1 state within picoseconds. From the S_1 excited state, several fates are possible which include radiative and non-radiative pathways. Intersystem crossing (ISC) is a non-radiative event in which the electron converts to a lower energy triplet excited state (T_1) with opposite spin. Like S_1, different radiative and non-radiative pathways are available to the electron from T_1. Productive photochemical transformations are typically able to occur from the S_1 and T_1 excited states owing to their extended lifetimes (nanoseconds to milliseconds).[223] These singlet or triplet reactions lead to intermediates (I) that evolve into an observed product.

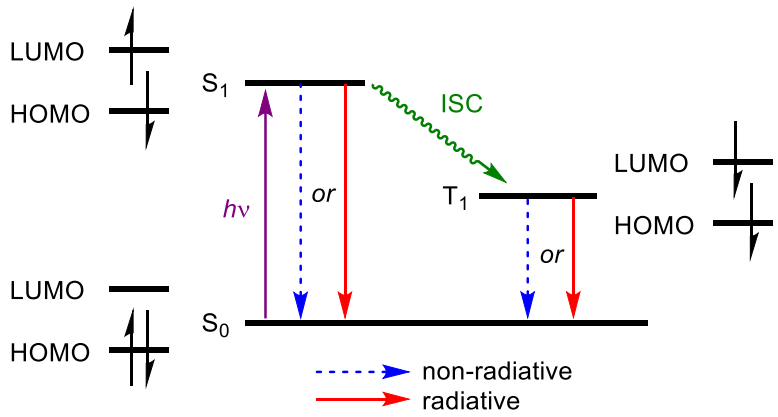
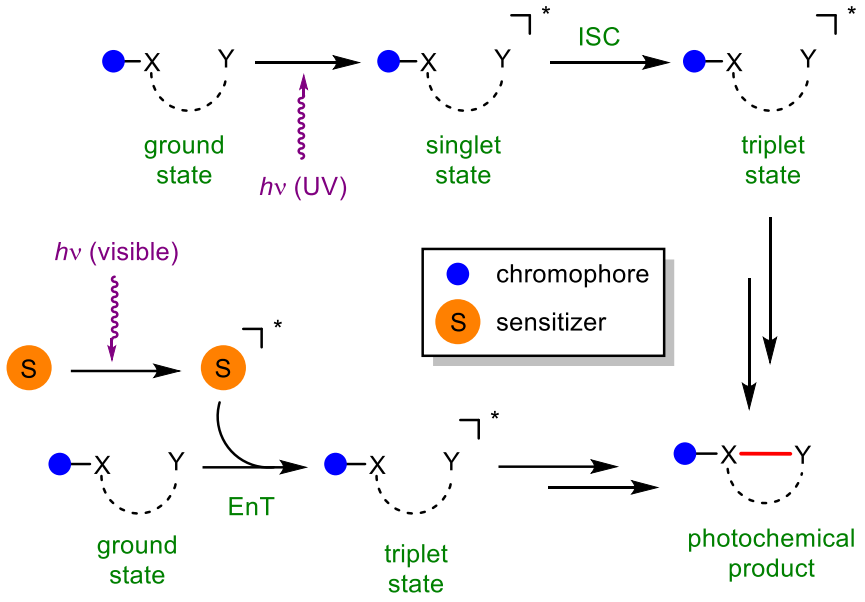


Figure 4.3. Simplified Jablonski diagram illustrating the formation of a molecules excited state from its ground state

[e]Wardle, B. In *Principles and Applications of Photochemistry*, 1st edition; John Wiley & Sons: 2009.

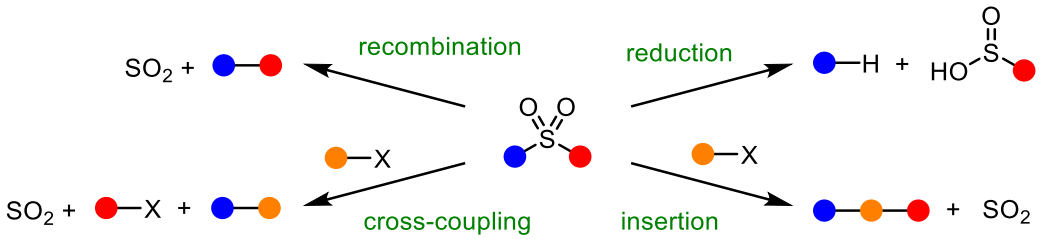
The absorption of light by simpler organic molecules is typically dependent on the value of λ_{max}, however in more complex molecules other factors such as the type of functional groups present can have an impact. This will determine what energy of the incoming light is needed to promote an electronic transition to occur within the molecule. Typically, molecules which contain more π-electron functional groups and extended conjugation absorb light more easily and these groups are known as chromophores. Absorption of light for organic molecules can take place in either a direct or indirect manner that is also called photosensitization (Scheme 4.9).[223, 224] For most organic molecules, UV light irradiation is typically required to access excited states *via* ***direct excitation*** of functional groups such as aromatic rings, olefins, halogens, or carbonyls.[225] The process is like what has already been described above where a substrate at its ground state and possessing a chromophore absorbs light of appropriate energy to access a higher energy singlet excited state.[224] Rapid ISC then affords a triplet excited state from which the observed photochemical product can be formed. The lack of visible light absorption by most organic molecules has limited the use of photochemistry in organic synthesis. This is mainly due to the high energy associated with UV light, limiting functional group compatibility and reducing reaction efficiencies.[226] To combat this issue, ***indirect excitation*** through photocatalysis was developed. In this case, photochemical transformations are mediated by a photocatalyst or sensitizer that is capable of absorbing lower energy visible light.[227] The majority of photocatalysts utilized in contemporary organic photochemistry are based on transition-metal complexes, however several organic-based dyes are also capable of functioning as sensitizers and have classically been extensively utilized. In this process, the sensitizer or photocatalyst is excited to its own singlet ***or*** triplet excited states by the same process as above. Rather than reacting to form product, the sensitizer relaxes to its ground state by simultaneously transferring its energy to a molecule of substrate, propelling it directly to its own excited state and regenerating the active sensitizer. The excited state of the substrate can then evolve into the photochemical product. If the sensitizer is excited as the triplet, this process overall is also known as triplet energy transfer (EnT) or triplet-triplet energy transfer (TTEnT) and is especially useful if the substrate cannot absorb visible light itself but can exhibit excited state triplet reactivity.



Scheme 4.9. Direct *vs* indirect photoexcitation of organic molecules

4.1.4 Radical chemistry of sulfone derivatives

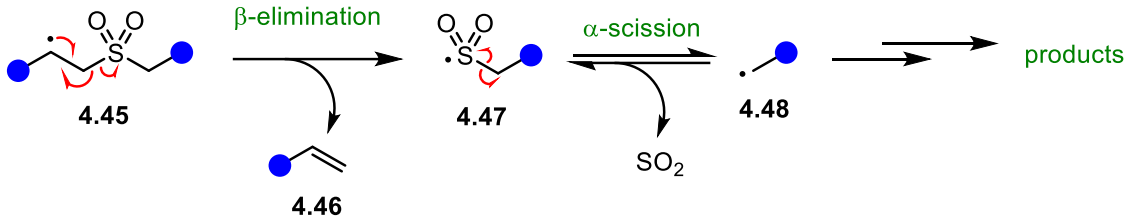
The sulfone group has been described as a "chemical chameleon" since it can function to both stabilize carbanions at the α position (through induction) in addition to behaving as a competent leaving group.[228] Comparable to the carbonyl group, sulfones are incredibly useful in organic synthesis. Particularly useful are desulfonylative radical processes that have been extensively used for the general construction of new C-C single bonds (Scheme 4.10). Reduction, cross-coupling, recombination, and insertion processes have all been demonstrated in the literature.[229]



Scheme 4.10. Some examples of desulfonylative radical reaction modes

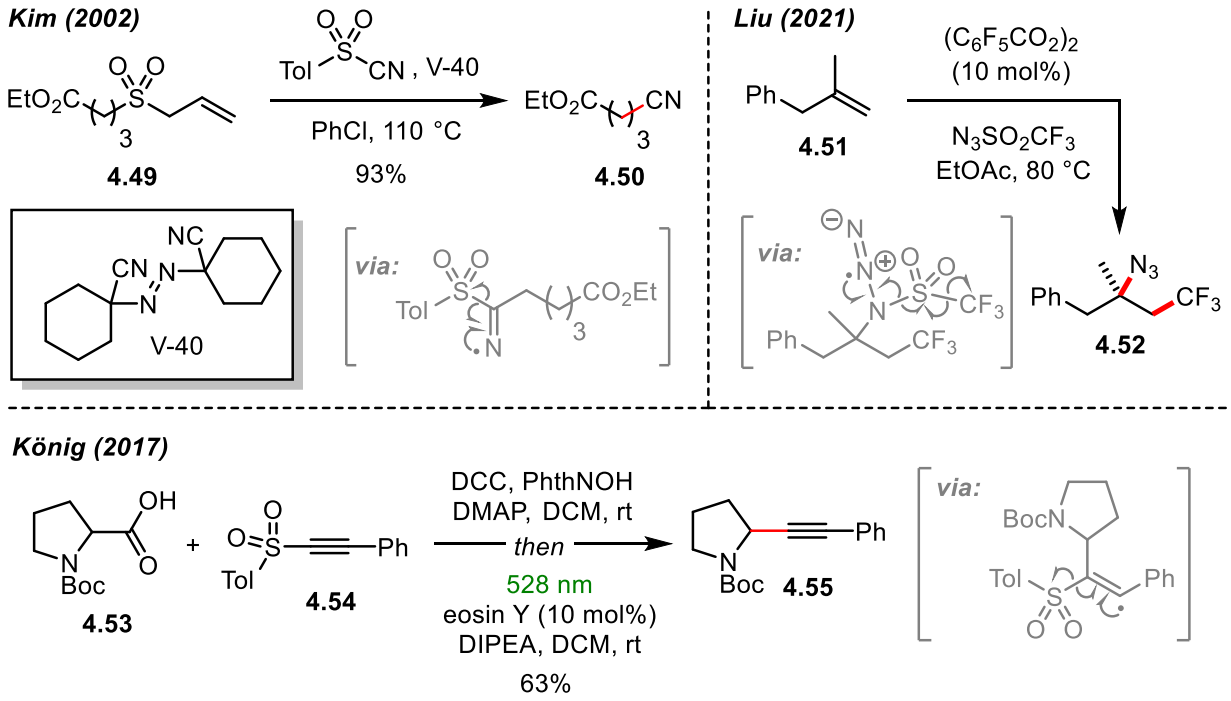
From a general mechanistic perspective, formation of a radical (thermally or photochemically) at the β position for sulfones of type **4.45** initiates the process (Scheme 4.11).[230] A facile β-elimination takes place to afford a sulfonyl radical intermediate **4.47** and an olefin

product **4.46**. The sulfonyl radical can then undergo a process termed α-scission, extruding SO_2 and a new radical **4.48** which can go on to perform further chemistry depending on the conditions of the reaction. The SO_2 extrusion step is known to be reversible, with the equilibrium typically favoring the position of the sulfonyl radical **4.47**. However, depending on certain reaction conditions or the stability of the resulting radical **4.48**, the equilibrium may be shifted towards the liberation of SO_2.[231]



Scheme 4.11. General mechanism for radical desulfonylation

For example, Kim and co-workers demonstrated that alkyl allyl sulfone **4.49** functioned as a competent source of alkyl radical intermediate which could be trapped in transition-metal free cyanation reactions, forming nitrile product **4.50** (Scheme 4.12).[232] Activated sulfones such as *p*-toluenesulfonyl cyanide were used as trapping agents for the alkyl radicals, resulting in the regeneration of arylsulfonyl radicals for propagation *via* a radical chain process. The group of König developed a decarboxylative alkynylation reaction from redox active NHP esters and used acetylenic sulfone **4.54** as the alkyne source.[233] Utilizing eosin Y as an organic photocatalyst, the authors were able to perform single-electron transfer (SET) with the NHP ester (generated *in-situ* from carboxylic acid **4.53**) under green light irradiation (528 nm). This resulted in the generation of an alkyl radical which upon addition to the substrate **4.54** gave a β vinylic radical that eliminated the arylsulfonyl group and formed the alkyne product **4.55**. In a different approach, Liu and co-workers attempted the difunctionalization of unactivated alkene substrate **4.51** using trifluoromethanesulfonyl azide as a bifunctional reagent in the presence of a radical initiator pentafluorobenzoyl peroxide.[234] The mechanism is believed to occur by a radical chain process through the recurring generation of a trifluoromethylsulfonyl radical that liberates SO_2 and trifluoromethyl radical. Subsequent radical addition to the alkene substrate and azidation by $N_3SO_2CF_3$ delivers the vicinal trifluoromethyl azide product **4.52**.

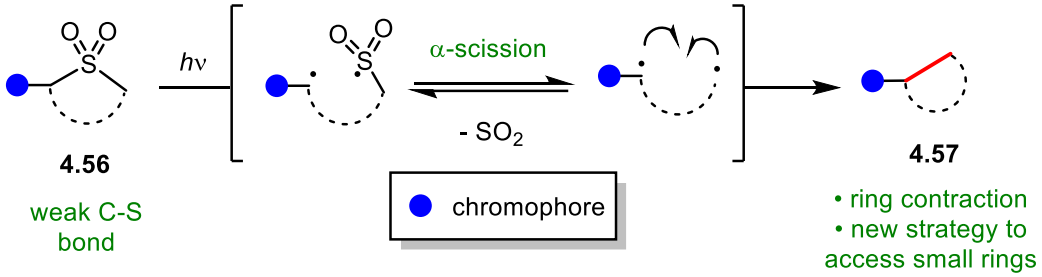


Scheme 4.12. Examples of radical processes involving extrusion of the sulfonyl group for the formation of new C-C bonds

4.2 Objective of the project

Owing to the resulting thermodynamic instability associated with highly strained rings, methods for their formation typically require the use of high energy intermediates or reagents. This creates several issues in terms of atom economy, scalability, functional group compatibility, and reduces the overall "greenness" of the process. This is especially true with the current state-of-the-art regarding small ring synthesis, particularly with respect to the cyclopropyl motif. General and direct strategies which do not rely on highly reactive intermediates such as metal-stabilized carbenes or metal carbenoids are rare. Recently, there has been a large push towards more sustainable and environmentally friendly synthetic methods. This has been the case with green chemistry and in this context, photochemistry and photocatalysis have emerged as incredibly powerful tools for the formation of new bonds.[235] Light is a cheap and renewable energy source, showing potential to provide new avenues for synthesis as compared to traditional methods which have been more wasteful and impactful towards the environment.

In this context, the goal for this project was to develop a new photochemical method towards the synthesis of cyclopropane building blocks *via* an uncommon ring contraction strategy. We saw this as an incredibly useful and direct strategy to access these important structures. Small ring systems such as three- and four-membered rings like cyclopropanes or azetidines also exhibit much higher three-dimensionality and represent a departure from the more common "flatland" philosophy of drug design.[236] In this way, these ring systems can also function as privileged structures for the design of new and useful subunits in medicinal chemistry. To do this, we considered using cyclic sulfone derivatives (**4.56**) as precursors to ring contraction products (**4.57**) under photochemical conditions (Scheme 4.13). This concept relies on the presence of a chromophore on the substrate **4.56** in addition to the unique behaviour of sulfone derivatives under radical conditions, where extrusion of SO_2 is known to be a facile process. If successful, this type of strategy could enable the synthesis of a range of building blocks (including cyclopropanes) that are pharmaceutically relevant. In this chapter, the successful implementation of this ring contraction strategy using four-membered cyclic sulfones (thietane-1,1-dioxides) will be presented and will include the results obtained prior to the writing of this thesis. A brief outlook section on the future directions of the project will also be discussed.

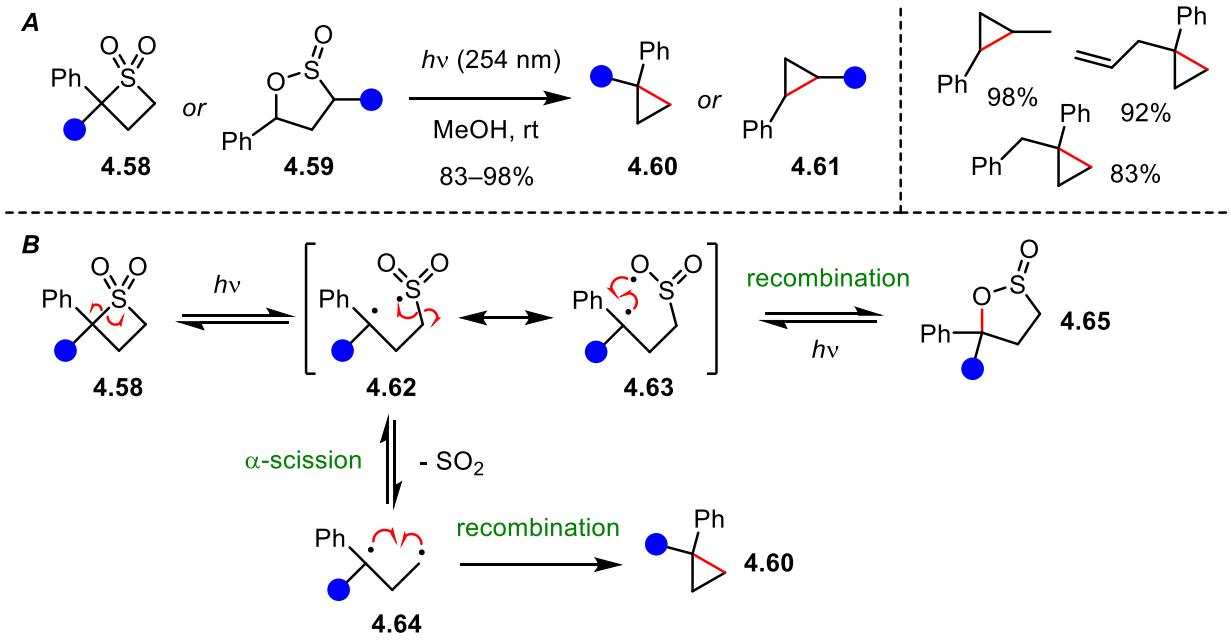


Scheme 4.13. Utilizing cyclic sulfones under photochemical conditions to affect a ring contraction strategy *via* SO_2 extrusion

4.3 Precedent, initial results, and reaction optimization

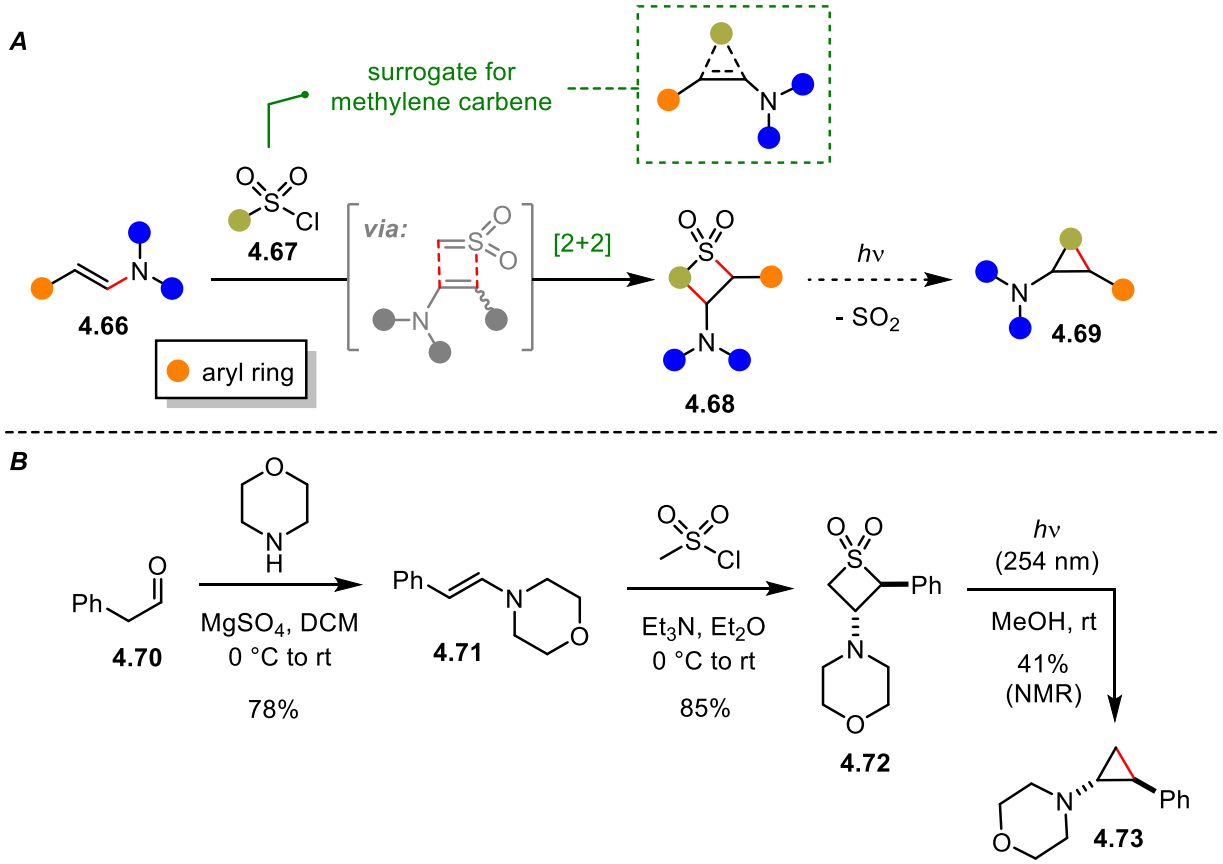
As was mentioned above, general strategies for the thermal and photochemical extrusion of SO_2 are well documented. However, photochemical strategies for the ring contraction of cyclic sulfones are very rare. This type of reactivity was first documented almost 50 years ago by the groups of Durst and Smith, giving us confidence in the success of our proposed approach (Scheme

4.14A).[237, 238] Their work showed that cyclopropanes **4.60** could be accessed by the irradiation of thietane-1,1-dioxides bearing a phenyl ring chromophore at the 2-position (**4.58**). Under direct UV irradiation, C-S bond cleavage is proposed to occur and give rise to a sulfonyl radical intermediate that can exist as either *S*- or *O*-centered sulfonyl radicals **4.62** and **4.63** respectively (Scheme 4.14B). Loss of SO_2 then occurs through α-scission, affording diradical intermediate **4.64** that undergoes recombination to deliver the cyclopropane products. Notably, the same transformation was also shown to occur starting from 5-phenyl γ-sultine substrates **4.59**. This implies that **4.58** and **4.65** are likely in equilibrium with one another under the conditions of the reaction, with both substrates proceeding through the intermediacy of either *O*- or *S*-centered sulfonyl radicals prior to SO_2 extrusion. Unfortunately, the scope of their transformation was limited and included only alkyl substitutions in addition to a lack of evaluation for substituents at the β or γ position of the thietane ring system. We initially sought to improve upon this work and extend the proposed methodology towards the generalized synthesis of cyclopropane buildings blocks that contained varied substitution patterns, and which are relevant to the pharmaceutical industry (such as cyclopropylamines).



Scheme 4.14. (A) Scope of the photolysis of thietane-1,1-dioxides and γ-sultines towards cyclopropanes by Durst and Smith and (B) the proposed mechanism

We initiated our study by synthesizing precursors to cyclopropylamine derivatives **4.69** such as 3-aminothietane-1,1-dioxides **4.68** (Scheme 4.15A). These substrates were chosen due to their well documented preparation and ease of synthesis.[239] Compounds such as **4.68** are typically synthesized by the [2+2] cycloaddition of an electron rich enamine **4.66** and a sulfene intermediate which is generated *in-situ* from a sulfonyl chloride **4.67**. This method was independently discovered by the two groups of Stork and Borowitz[240] and Opitz and Adolph[241] in 1962 and since then has been extensively used in the synthesis of various thietane-1,1-dioxide derivatives.[239] This was important to us since the development of a new photochemical ring contraction methodology would require that accessing the corresponding precursors be a modular and straightforward process. As a model substrate, we chose the 2-phenyl-3-morpholino derivative **4.72**. The synthesis of the substrate commenced with the condensation of morpholine onto phenylacetaldehyde **4.70**, affording the morpholino enamine **4.71** as a crystalline solid in 78% yield (Scheme 4.15B). Next, the [2+2] cycloaddition between enamine **4.71** and methanesulfonyl chloride (MsCl) could be carried out by the slow addition of MsCl to an ethereal solution of enamine **4.71** and triethylamine as a base. Gratifyingly, the photochemical substrate **4.72** was able to be isolated in an excellent 85% yield and as a single *trans*-isomer. We now turned our attention to the photochemical ring contraction. To our delight, our first attempt with reproducing the conditions reported by Durst and Smith (see Scheme 4.14 above) were successful. We were able to isolate the corresponding morpholino cyclopropane **4.73** as the *trans*-isomer in a 41% NMR-yield. A significant amount of decomposition was occurring as we were able to identify aldehyde peaks within the crude NMR, indicating possible issues with the amino group. With this result, we have shown that we are able to access privileged cyclopropylamines in a direct manner while also allowing us to view the overall process as the formal cyclopropanation of electron rich enamines (non-trivial). In this way, MsCl can be seen as behaving like a surrogate for the highly reactive methylene carbene. Furthermore, the [2+2] cycloaddition approach would allow for a modular access to various cyclopropylamine building blocks, allowing us to easily differentiate the amine and aryl ring moieties.

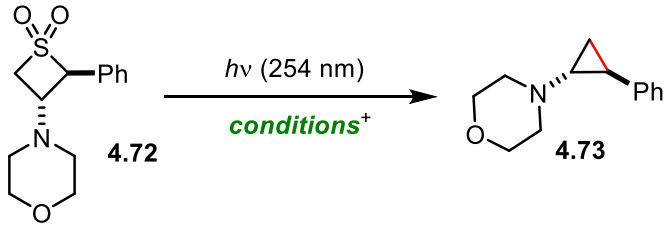


Scheme 4.15. (A) General access to cyclopropylamines and (B) synthesis and evaluation of a model substrate under photochemical conditions

With confirmation that our photochemical ring contraction method was feasible and tolerated substitution at the 3-position, an optimization of the process was attempted by Jessica since our initial result led to a modest yield of product. We began by evaluating different solvents which were used in similar reactions previously (Table 4). Changing the solvent from methanol (Entry 1) to either benzene or acetone (Entries 2–3) was unsuccessful and led to only degradation of the substrate and no traces of cyclopropane product being formed. Taking inspiration from a recent publication by Mansson and Burns,[242] we evaluated water as a solvent for the photochemical reaction (Entry 4). To solubilize the substrate, one equivalent of a Brønsted acid (H_2SO_4) was added and this resulted in a slight increase in the NMR yield of the product (51% as compared to 43% in MeOH). Under these conditions, a cleaner reaction profile was observed with less aldehyde impurities being formed (likely due to amine protonation). The reaction in water was done under an atmosphere of nitrogen and we applied the same to the reaction in MeOH, observing a further

increase to 48% NMR yield as compared to the original reaction done under air (Entry 5 *vs* Entry 1). This increase in yield is most likely due to deleterious side reactions occurring in the presence of oxygen reacting with radicals generated in solution or with the tertiary amine. Cognizant of the reversible SO_2 extrusion process, we next investigated the effects of different SO_2 trapping agents to help drive the equilibrium towards the formation of product. Trapping agents such as water, NMO, MnO, and DABCO were evaluated (Entries 6–9). Water was added as a means of trapping SO_2 by forming H_2SO_3 in solution, however this led to a significant decrease in NMR yield (Entry 6, 20%). *N*-oxides such as NMO were also employed since they are known to form stable sulfur trioxide adducts,[243] however this was also not beneficial (Entry 7). Oxidative degradation of the SO_2 was tested using MnO (Entry 8), however this did not result in significant improvement, and we obtained the cyclopropane in 50% NMR yield. The reaction was also conducted in the presence of one equivalent of DABCO (Entry 9), a known SO_2 trap that results in the formation of the stable adduct DABSO.[244] In this case, we obtained the highest yield of cyclopropane so far (53% NMR yield), the cleanest reaction profile, and we observed a slightly longer reaction time. We noticed the precipitation of a white solid during irradiation (most likely DABSO) which may have resulted in decreased penetration by the UV light. Given the success of using DABCO, we also tried to use it as an additive in an unsuccessful solvent such as benzene (Entry 10), however the same outcome of decomposition was observed. With DABCO as an additive, we next varied the concentration of the reaction since this can also have a marked impact on the efficiency of a photochemical process. Increasing the concentration to a standard 0.1 M (Entry 11) was unproductive, resulting in a decrease to a 33% NMR yield. Running the reaction at 0.05 M instead of 0.03 M (Entry 12 *vs* Entry 9) was roughly the same. However, diluting the reaction further to 0.01 M (Entry 13) was more beneficial and led to a 61% NMR yield of the cyclopropane being formed with no increase in reaction time. Moving forward, we decided to use the conditions shown in Entry 9 as optimal. Despite the increase in yield observed by running the reaction 3x more dilute, we were limited by the size of the quartz vials that we were using to perform the reaction.

Table 4. Optimization of the photochemical ring contraction for thietane-1,1-dioxide model substrate **4.72**



Entry[a]	Solvent	Time (h)	Concentration (M)	Additives[b]	Atmosphere	NMR-Yield (%)
1	MeOH	4	0.03	--	air	43
2	PhH	5	0.03	--	air	--
3	$(Me)_2CO$	7	0.03	--	air	--
4	H_2O	3	0.03	H_2SO_4	N_2[e]	51
5	MeOH	4	0.03	--	N_2	48
6	MeOH	6	0.03	H_2O	N_2	20
7	MeOH	8	0.03	NMO	N_2	31
8	MeOH	6	0.03	MnO	N_2	50
9	MeOH	6	0.03	DABCO	N_2	53, 52[d]
10	PhH	16	0.03	DABCO	N_2	--
11	MeOH	4	0.1	DABCO	N_2	33
12	MeOH	4	0.05	DABCO	N_2	51
13	MeOH	4	0.01	DABCO	N_2	61

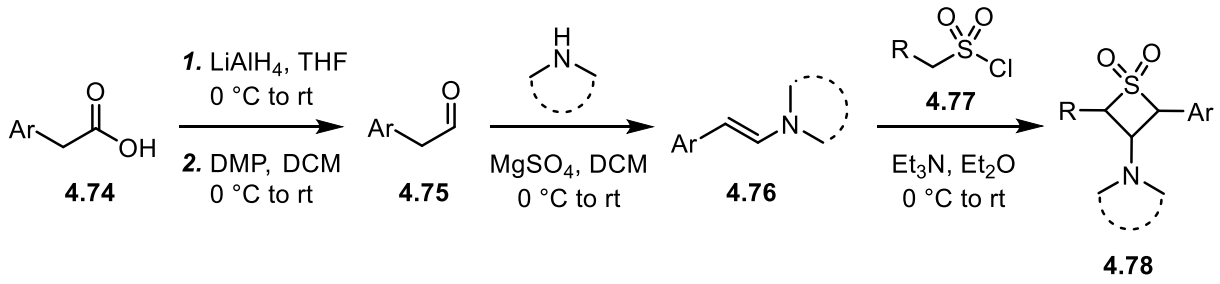
[a] Unless otherwise noted, all reactions were carried out using 3.5 mL screw-cap quartz vials with 0.09 mmol of substrate and irradiated in a Rayonet photochemical reactor. [b] One equivalent of additive was added unless otherwise noted. [c] NMR yields were determined from the crude ^{1}H-NMR analysis using mesitylene as an internal standard. [d] Isolated yield. [e] Nitrogen gas was bubbled through the solution for approx. two to three minutes. $^+$Results by JP.

4.4 Issues with substrate access and evaluation

4.4.1 Enamine/sulfonyl chloride [2+2] strategy

Depending on the desired substitution pattern, different sulfonyl chlorides **4.77** and enamines **4.76** were utilized for the synthesis of various 2-aryl-3-aminothietane-1,1-dioxides **4.78**

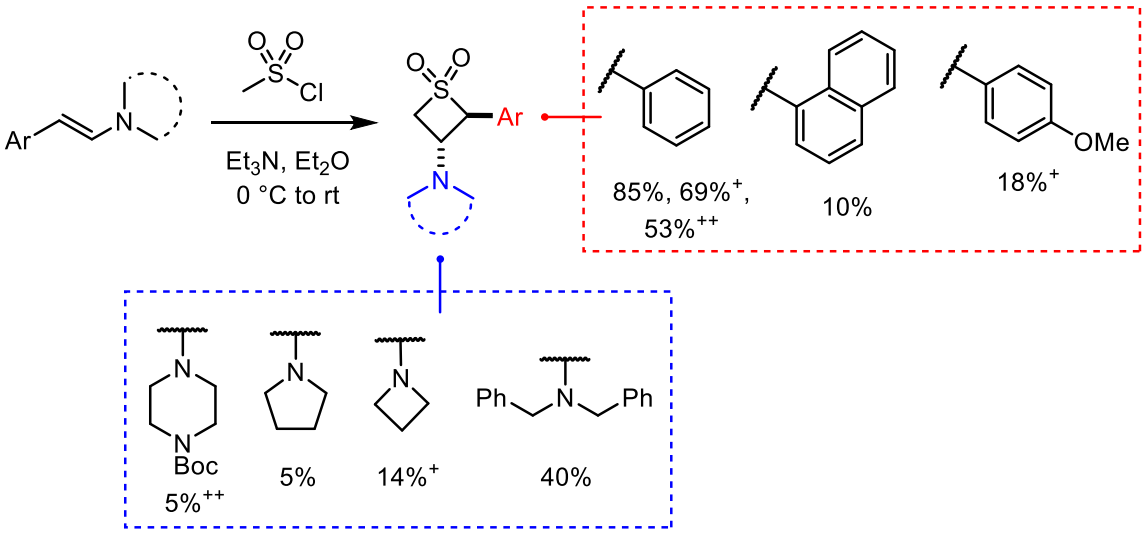
(Scheme 4.16). Arylacetaldehydes **4.75** were synthesized by complete reduction of the arylacetic acids **4.74** using $LiAlH_4$, followed by oxidation of the alcohol to the aldehyde using DMP. Formation of the enamine was then accomplished *via* condensation onto an appropriate aldehyde substrate using a weak Lewis acid and desiccant such as $MgSO_4$. To obtain the 2-aryl-3-aminothietane-1,1-dioxides **4.78**, the [2+2] cycloaddition was carried out.



Scheme 4.16. Synthesis of different 2-aryl-3-aminothietane-1,1-dioxides by the enamine/sulfonyl chloride [2+2] strategy

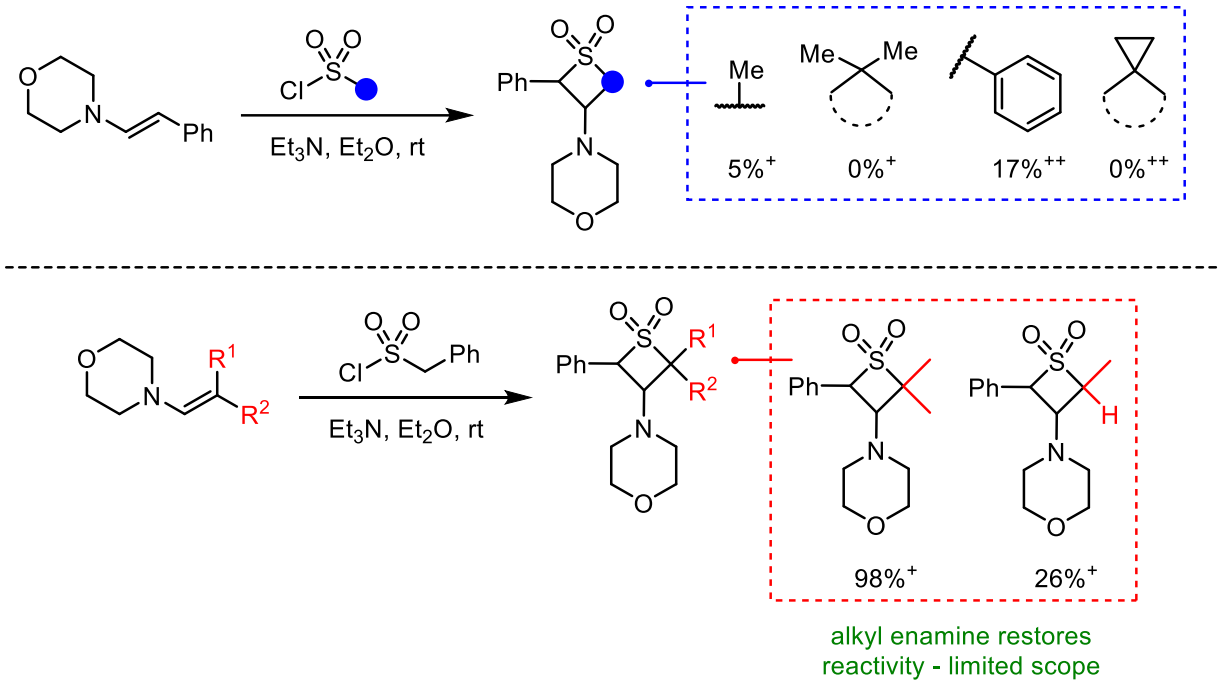
During our synthesis efforts towards evaluating a scope for the process, we unfortunately encountered several issues with the [2+2] cycloaddition of enamines and sulfonyl chlorides:

- The identity of the amine on the enamine component is important and has a marked impact on the reaction (Scheme 4.17). Morpholine seems to be the most successful choice and thietane-1,1-dioxides derived from enamines bearing other seemingly similar cyclic amines such as pyrrolidine or piperazine do not behave well when used. Variation in the aryl ring is also problematic since switching from phenyl to electron rich anisole or naphthalene rings led to a complete loss of reaction efficiency, resulting in yields which were not synthetically useful. Additionally, reproducibility is another issue. When the model substrate **4.72** was synthesized by three different researchers, three very different yields were obtained for the product.



Scheme 4.17. Issues with varying the enamine component in the [2+2] cycloaddition towards thietane-1,1-dioxides. $^{+}$Results by JP. $^{++}$Results by LR

- Even when morpholine is used as the amine on the enamine component, the reaction is still highly dependent on the substitution pattern of the sulfonyl chloride as was seen by Jessica and Loïc (Scheme 4.18). In general, an increase in steric bulk α to the sulfonyl chloride led to no reactivity. In some cases, reactivity could be restored if using an enamine which was not aryl substituted (ie: more electron rich) in conjunction with phenylmethanesulfonyl chloride ($BnSO_2Cl$) instead of MsCl. However, this was also linked to the stability of the alkyl enamine being used, since thietane-1,1-dioxides derived from less substituted enamines were much lower yielding.



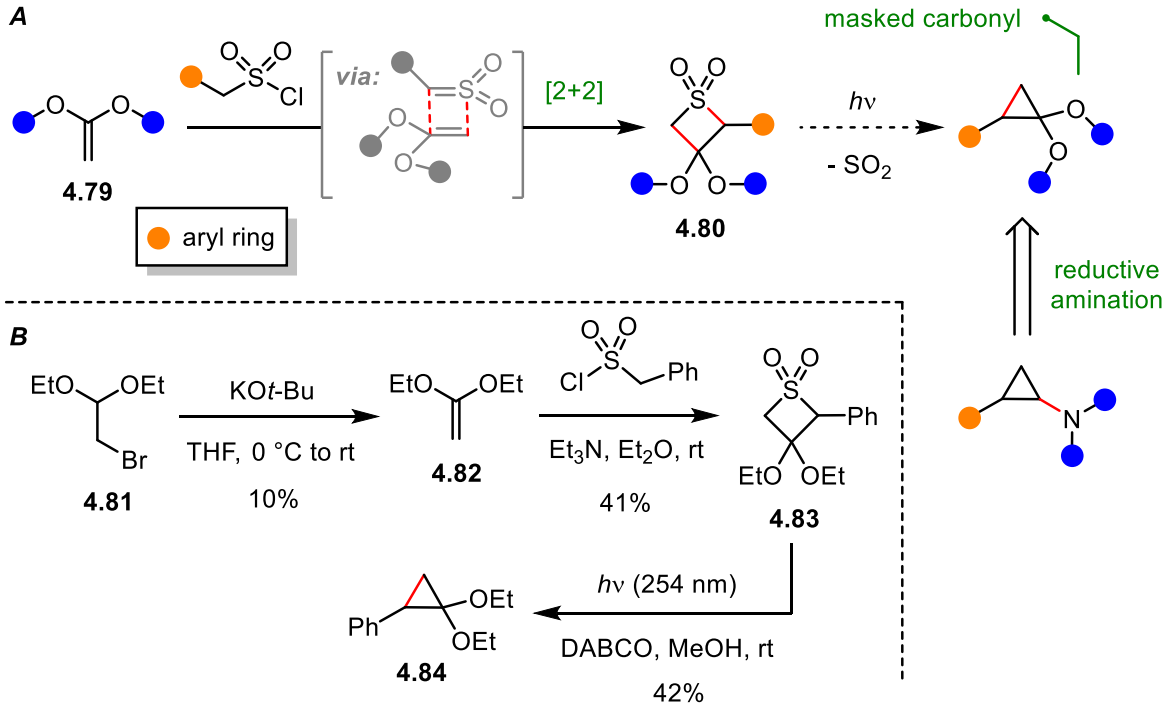
Scheme 4.18. Issues with varying the sulfonyl chloride component in the [2+2] cycloaddition towards thietane-1,1-dioxides. $^{+}$Results by JP. $^{++}$Results by LR

Most of the reactions we tested led to significant discoloration of the reaction mixtures and observation of insoluble black "tars" forming. We also observed significant amounts of enamine hydrolysis in addition to the formation of sulfonamide by-products. A small optimization campaign was performed by Jessica in which she varied the base being used, the reaction concentration, and the temperature. Ultimately, this optimization was unsuccessful and did not lead to any improvement. The failure associated with these reactions is likely due to the difference in reactivity between the enamine and sulfonyl chloride. This process is inherently a nucleophile/electrophile reaction where an appropriately nucleophilic and electron rich enamine must react with an appropriately electrophilic sulfene intermediate. If enamine addition to the sulfene does not happen within a reasonable rate, then the highly reactive sulfene intermediate will begin to participate in unproductive side reactions.

4.4.2 Ketene acetal/sulfonyl chloride [2+2] strategy

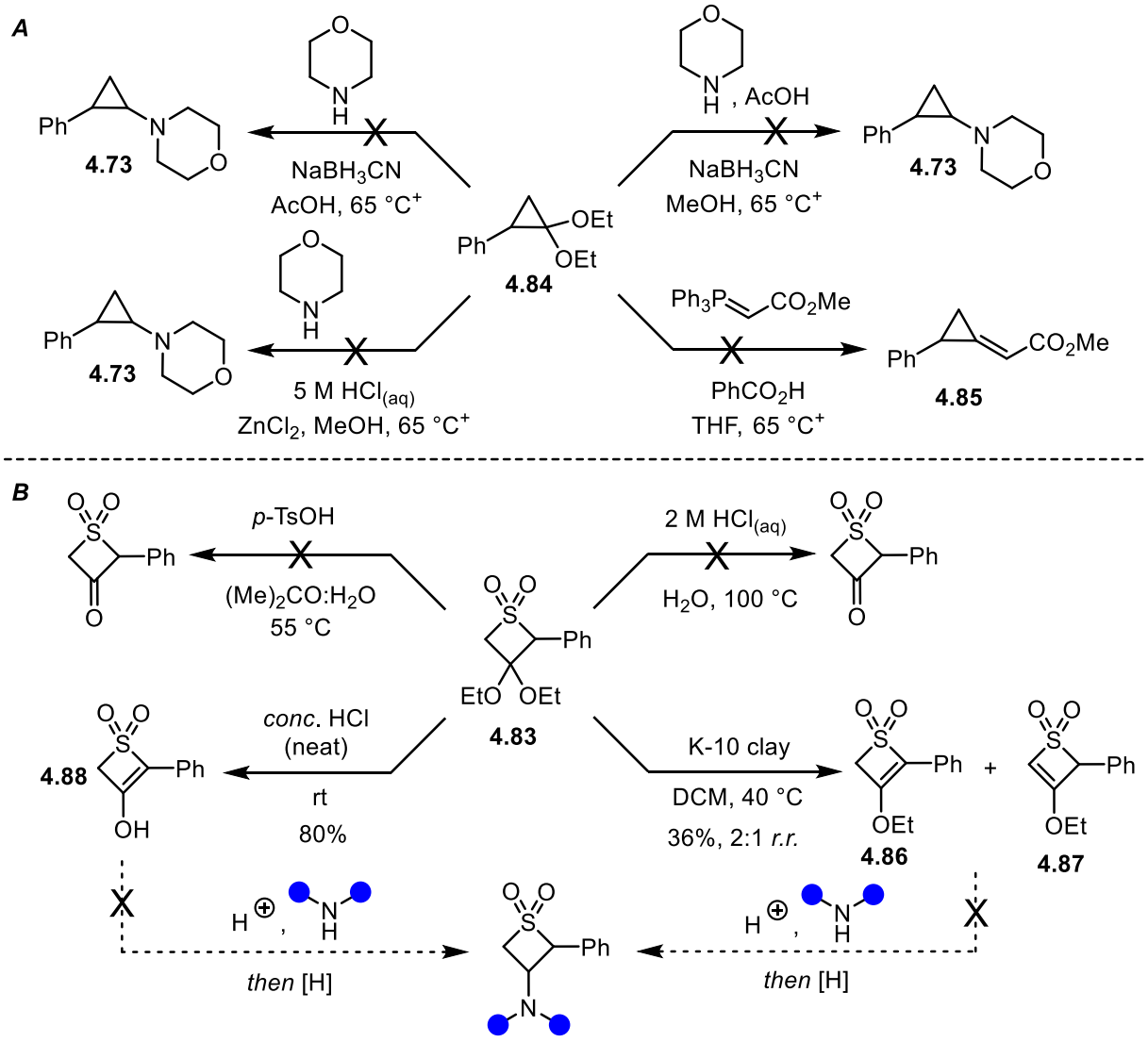
At first glance, the [2+2] cycloaddition between enamines and sulfonyl chlorides seemed like a highly desirable route towards the modular synthesis of various cyclopropylamines.

Unfortunately, issues of reactivity and reproducibility rendered this strategy inappropriate for our goals. In the hope of finding a solution, we turned our attention to a similar [2+2] cycloaddition that had been developed by the group of Truce and Abraham.[245] This strategy uses ketene acetals **4.79** (instead of enamines) as reactive partners in the cycloaddition with sulfene intermediates and is otherwise very similar, differing in the production of 3,3-dialkoxythietane-1,1-dioxides **4.80** instead (Scheme 4.19A). With **4.80**, our strategy is to utilize the ketal functionality as a masked carbonyl. This would allow us to use the carbonyl as a springboard to perform classical chemistry such as reductive amination, restoring us access to privileged cyclopropylamines. Before attempting this strategy, we first needed to confirm that substrate **4.84** was competent under our optimized photochemical conditions (Scheme 4.19B). To begin, diethyl ketene acetal **4.82** was synthesized in 10% yield (volatile) from commercially available bromoacetaldehyde diethyl acetal **4.81** using potassium *tert*-butoxide. Next the [2+2] cycloaddition was performed as reported, affording the desired product **4.83** in 41% yield. To our delight, we were able to isolate the cyclopropyl ketal **4.84** in 42% yield after submitting precursor **4.83** to irradiation at 254 nm in the presence of DABCO.



Scheme 4.19. (A) General access to cyclopropylamines by using a ketene acetal/sulfonyl chloride [2+2] strategy and (B) successful synthesis of cyclopropyl ketal **4.84**

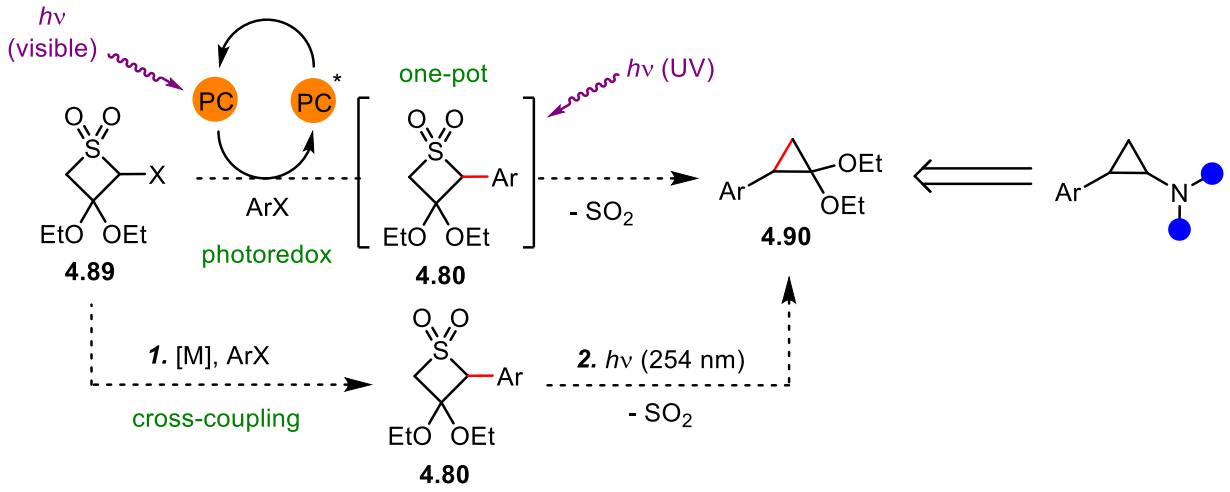
With **4.84** in hand, we turned our attention to functionalization of the ketal group by replacing it with an amino functionality and this was done by Loïc (Scheme 4.20A). Unfortunately, **4.84** did not behave as we expected under the conditions of reductive amination and resulted in failed attempts to functionalize the diethyl ketal. Utilizing MeOH with stoichiometric AcOH or as solvent led to mostly decomposition with varying amounts of starting material recovered. Switching to using aqueous HCl with a Lewis acid such as $ZnCl_2$ led to exclusive decomposition. We also attempted an *in-situ* Wittig reaction under acidic conditions which had been reported on a similar dimethyl ketal substrate. Unfortunately, this method also led to full degradation of the substrate. With these results, we decided to take a step back and unmask the carbonyl at an earlier point in our synthesis by deprotecting the diethyl ketal in thietane-1,1-dioxide **4.83** and this was done by me (Scheme 4.20B). We first attempted classical conditions for ketal deprotection using *p*-TsOH in a 10:1 mixture of acetone:water but found we were only able to recover the starting material unchanged. Using a heterogeneous reagent such as K-10 clay resulted in full consumption of the starting material but only resulted in partial deprotection. Isomeric thiete-1,1-dioxides **4.86** and **4.87** were isolated in a 36% combined yield and in a 2:1 ratio favoring thiete **4.86**. Partial deprotection may have been a result of low water content in the clay being used. Changing to aqueous 2 M HCl was not beneficial. No reactivity was taking place at room temperature and heating to reflux led to decomposition. Interestingly, the use of concentrated HCl (37.5 wt%) as solvent led to clean deprotection of the diethyl ketal, resulting in the isolation of enol **4.88** in 80% yield. According to ^{1}H-NMR analysis, **4.88** possesses zero ketone character and instead exists exclusively as the enol tautomer. To our dismay, enol **4.88** was found to be completely inert to conditions of reductive amination and starting material was returned in all attempts. We also attempted the functionalization of thiete-1,1-dioxides **4.86** and **4.87** under the same conditions, but no exchange of the ethoxy group for an amino group was observed.



Scheme 4.20. Failed attempts at the manipulation of the diethyl ketal group towards the installation of an amine moiety. [+]Results by LR

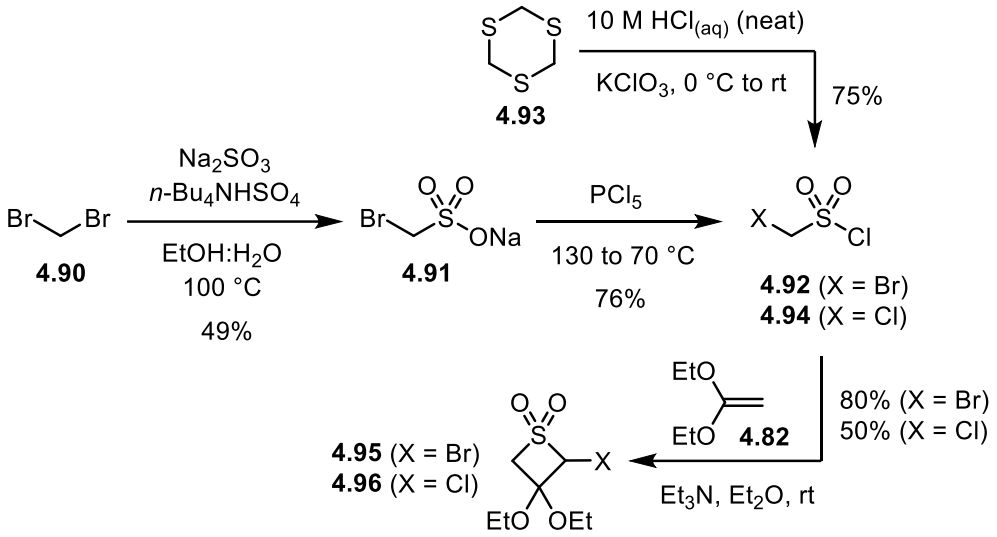
In parallel, a strategy was also being tested which would allow for the modular installation of aryl groups, followed by photochemical ring contraction to occur. The idea with this approach was to avoid the cumbersome synthesis of various arylmethanesulfonyl chlorides and rather rely on the abundant feedstock of aryl halides. We initially turned to photoredox catalysis to realize this strategy, which could offer a highly streamlined access to cyclopropanes *via* a one-pot process and starting from α-halo thietane-1,1-dioxides **4.89** (Scheme 4.21). Photoredox catalysis would proceed using visible light to install the aryl group to give compounds such as **4.80** and therefore would not have enough energy to excite the product towards ring contraction. Once the aryl ring

is installed, a wavelength switch to higher energy UV light would then promote the ring contraction to occur to give cyclopropanes such as **4.90**. Alternatively, cross-electrophile or classical cross-coupling approaches could also be utilized but in a two-step manner.



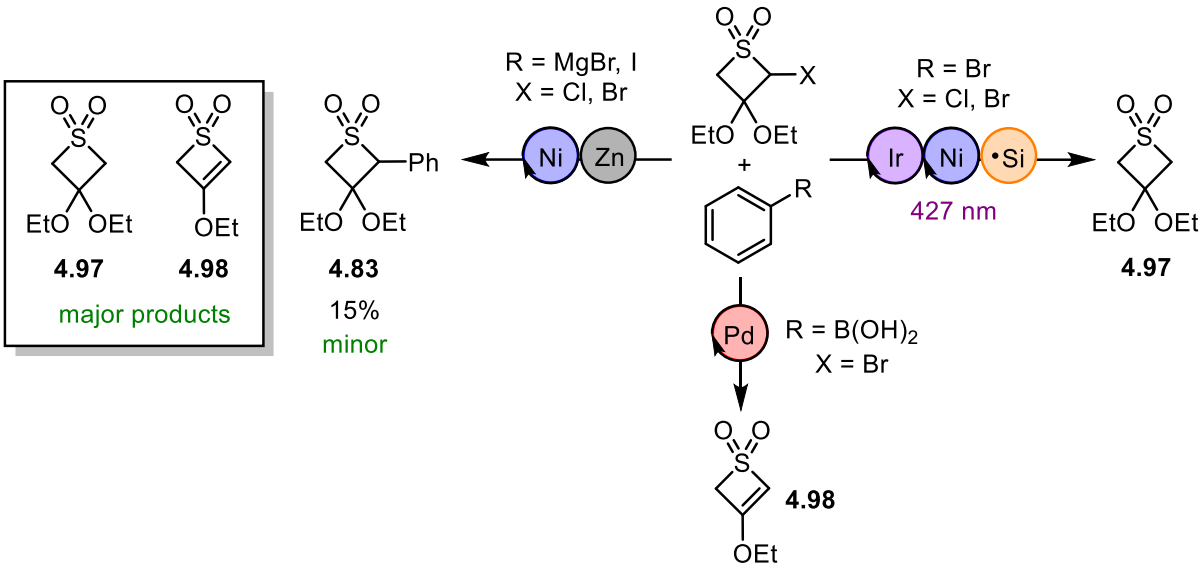
Scheme 4.21. Dual photochemical approach to aryl cyclopropyl ketals such as **4.90**

To test our approach, we began by synthesizing α-bromo or α-chlorothietane-1,1-dioxides **4.95** and **4.96** (Scheme 4.22). Both substrates could be accessed in 50% or 80% yield using the same [2+2] cycloaddition between diethyl ketene acetal **4.82** and the corresponding bromomethanesulfonyl and chloromethanesulfonyl chlorides **4.92** and **4.94** respectively. Chloromethanesulfonyl chloride **4.94** was synthesized in one step from 1,3,5-trithiane **4.93** by aqueous chlorination in 75% yield. The synthesis of bromomethanesulfonyl chloride **4.92** starts from dibromomethane **4.90**, where it undergoes substitution with sodium sulfite in 49% yield to give the sodium sulfonate salt **4.91**. Chlorination of the sulfonate group with PCl_5 then affords **4.92** in 76% yield.



Scheme 4.22. Synthesis of α-bromo and α-chlorothietane-1,1-dioxides **4.95** and **4.96**

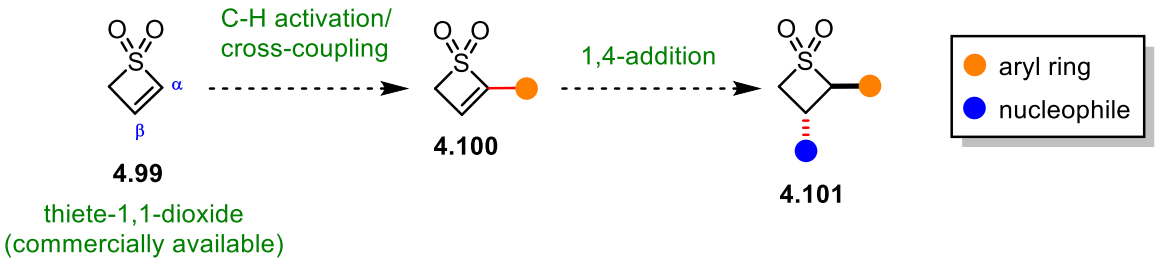
Applying photoredox conditions for the coupling of aryl bromides with alkyl chlorides/bromides α to EWG's led to the complete consumption of starting material but with no formation of product (Scheme 4.23). Instead, reduction of the C-X bond for both substrates took place, giving rise to the reduced thietane-1,1-dioxide product **4.97**. In the less active chloride substrate, significant amounts of starting material also remained. A sp^3-sp^2 palladium catalyzed Suzuki cross-coupling was also attempted. These conditions had been reported on similarly crowded acyclic substrates but also proved to be unsuccessful, affording instead a high yield (88%) of 3-ethyoxythiete-1,1-dioxide **4.98**. Similar results were observed using nickel catalysis in conjunction with a stoichiometric zinc reductant for a cross-electrophile coupling approach where varying mixtures of **4.97** and **4.98** are formed. Thiete **4.98** likely forms due to overreduction and elimination of ethoxide. Desired product **4.83** was observed in the case of chloride substrate **4.96** albeit in a low 15% yield as a minor component. However, considering the failure observed with the subsequent functionalization of the diethyl ketal group, we chose not to pursue this route any longer.



Scheme 4.23. Attempts at installation of aryl groups using photoredox or metal catalyzed coupling approaches

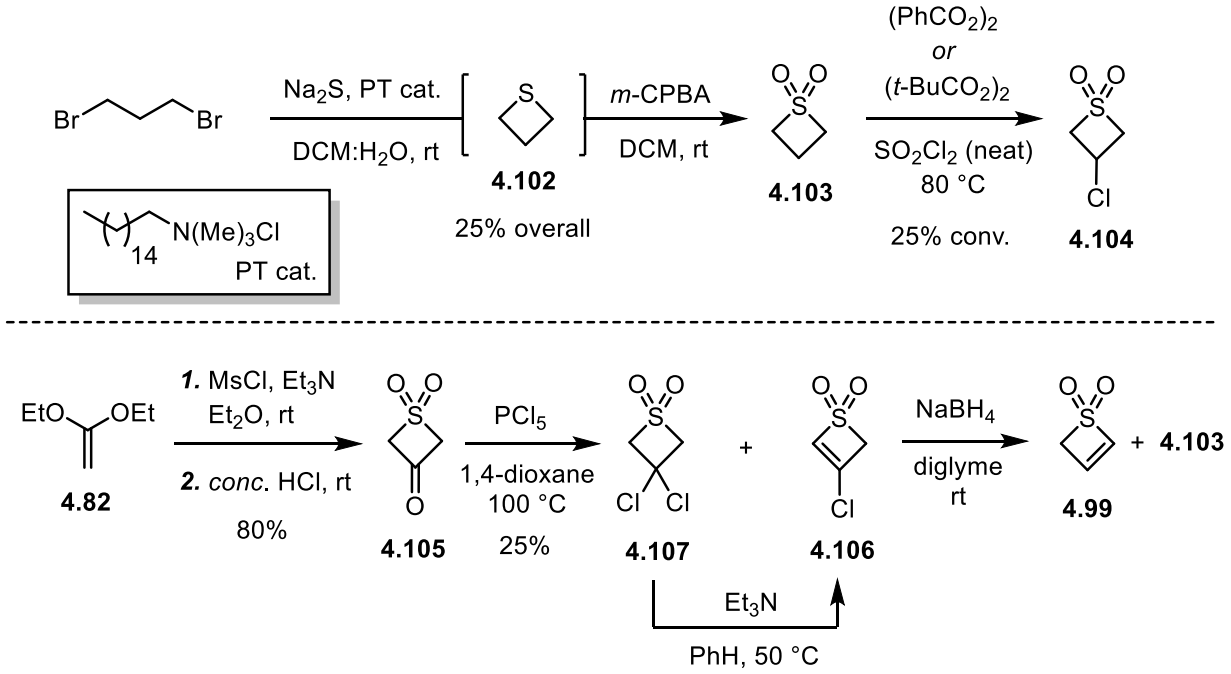
4.5 Synthesis and evaluation of 2-bromothiete-1,1-dioxide as a platform for diversity

Seeking a more modular approach, we thought about using the corresponding thiete-1,1-dioxides **4.100** as an activated platform for the introduction of nucleophiles (Scheme 4.24). Unlike the fully saturated thietane-1,1-dioxide, thiete-1,1-dioxides (containing an activated double bond) have received considerably less attention and have fewer reports on their modifications and synthesis in general. Most methods concerning the synthesis of thiete-1,1-dioxides proceed first through the preparation of an appropriately substituted thietane-1,1-dioxide. The corresponding thiete-1,1-dioxides are then typically formed *via* elimination reactions. Addition of nucleophiles to the β position of **4.100** is a relatively well documented process to give thietane-1,1-dioxide **4.101**, particularly when substitution is present at the α position.[239] Nucleophilic addition to the thiete-1,1-dioxide double bond with β substitution already present is less common and typically not as favorable.[246] Furthermore, recent work from the group of Didier has also looked at the α-arylation of β-substituted thiete-1,1-dioxide substrates under metal catalyzed or basic conditions.[247, 248] With these features in mind, we saw this route as a modular and an attractive alternative to the initially proposed enamine/sulfonyl chloride [2+2] approach.



Scheme 4.24. Thiete-1,1-dioxides as a platform for introducing diversity

The parent thiete-1,1-dioxide (α = β = H) is a commercially available compound, however for our purposes we thought it would be best to synthesize it ourselves since we would likely need very large quantities to support our studies, and this was done by myself. Our first attempts at accessing **4.99** relied on the radical halogenation of the parent thietane-1,1-dioxide **4.103** which was easily accessible in one step (Scheme 4.25). 1,3-dibromopropane is cyclized to the highly volatile thietane **4.102** using sodium sulfide under phase-transfer conditions and then oxidized to **4.103** *in-situ* using *m*-CPBA. The photochemical radical chlorination and bromination of **4.103** has been previously reported but uses toxic chlorine gas. Therefore, we opted for a safer alternative employing sulfuryl chloride and a radical initiator under thermal conditions. Despite our efforts, this chlorination reaction was very inefficient, and greater than 25% conversion of the substrate could never be achieved. Separation of the desired product **4.104** from the starting material was not possible and so a different approach was used. Instead, we synthesized 3-ketothietane-1,1-dioxide **4.105** from the [2+2] reaction between diethyl ketene acetal **4.82** and MsCl, followed by acidic deprotection with concentrated HCl. Manipulation of **4.105** proved to be rather challenging due to its insolubility in most organic solvents other than DMSO and 1,4-dioxane. However, we were able to chlorinate **4.105** by using PCl_5 to give a mixture of vinyl chloride (**4.106**) and *gem*-dichloro (**4.107**) compounds. Treating the mixture with Et_3N led to the isolation of vinyl chloride **4.106** in 25% yield over the two steps. Precedent in the literature indicated that a reduction/chloride elimination sequence using $NaBH_4$ was feasible towards accessing the parent thiete-1,1-dioxide **4.99**. Unfortunately, in our hands this led to a mixture of compounds including **4.99** and the saturated analog **4.103** which likely formed due to over reduction. Due to these failures, this route was abandoned.

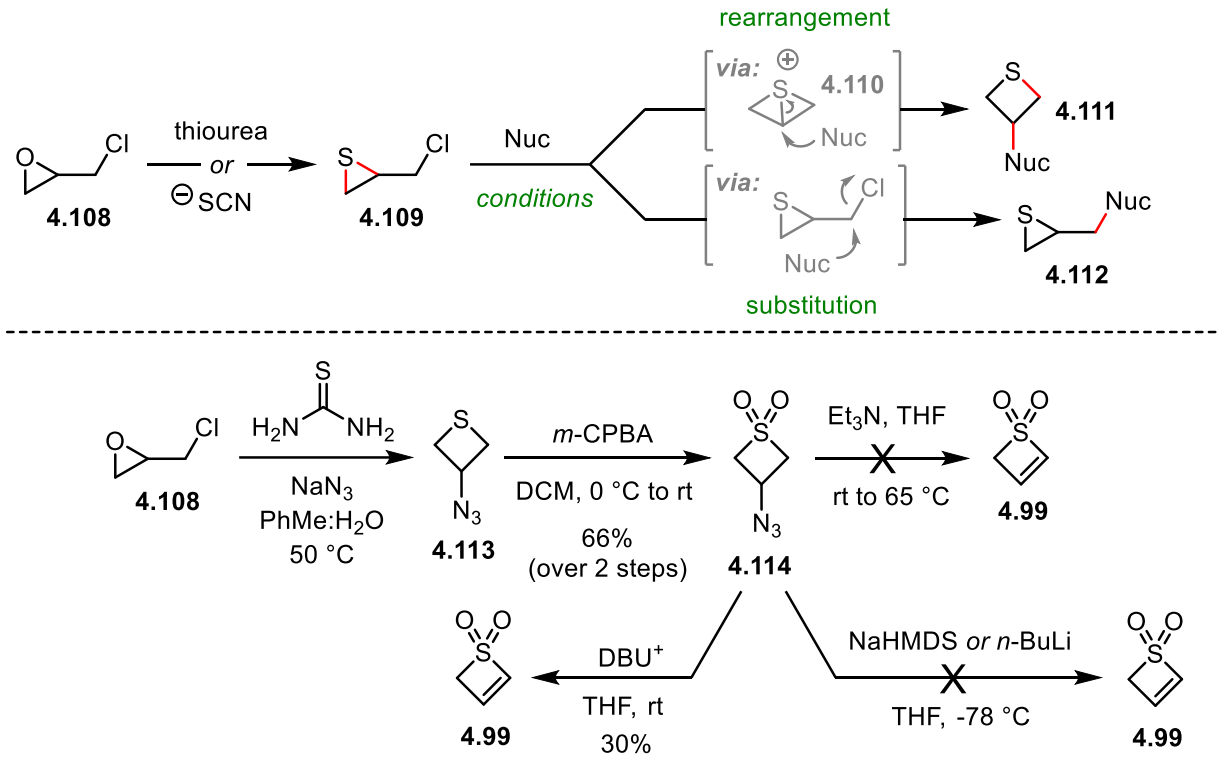


Scheme 4.25. Failed access to thiete-1,1-dioxide by the elimination of chloride

Our next attempt at accessing thietane-1,1-dioxides with a leaving group at the β position used epichlorohydrin **4.108** as a starting material (Scheme 4.26). In the presence of either thiourea or thiocyanate, **4.108** is known to convert into (chloromethyl)thiirane **4.109**.[249] Depending on the reaction conditions and in the presence of an appropriate nucleophile, **4.109** can engage in two pathways: a rearrangement *via* the bicyclic sulfonium **4.110** which leads to β substituted thietanes such as **4.111**; or S_N2 reaction to give substituted thiirane **4.112**.[250] Oxidation of **4.111** to the dioxide would then allow for a facile elimination to the thiete ring system. Based on this precedent, **4.108** was reacted with thiourea/sodium azide to result in the 3-azidothietane **4.113**.[f] Oxidation of **4.113** to the dioxide **4.114** was successful and proceeded in good yield (66% over two steps). Moving forward with **4.114**, different bases were used to affect the elimination. Triethylamine was ineffective as base (returning starting material) and using a much stronger base such as NaHMDS led to complete degradation. Alkylation of thietane-1,1-dioxides at the α position is known, however deprotonation of **4.114** with *n*-BuLi and attempted trapping of the anion resulted in complete degradation with a TLC profile like what was observed using NaHMDS. Interestingly,

[f]Cassayre, J. V.; Godineau, E.; Boussemghoune, M. A.; Smits, H. PROCESS FOR THE PREPARATION OF THIETANAMINE. International Patent WO 2013007582A2, January 17, 2013.

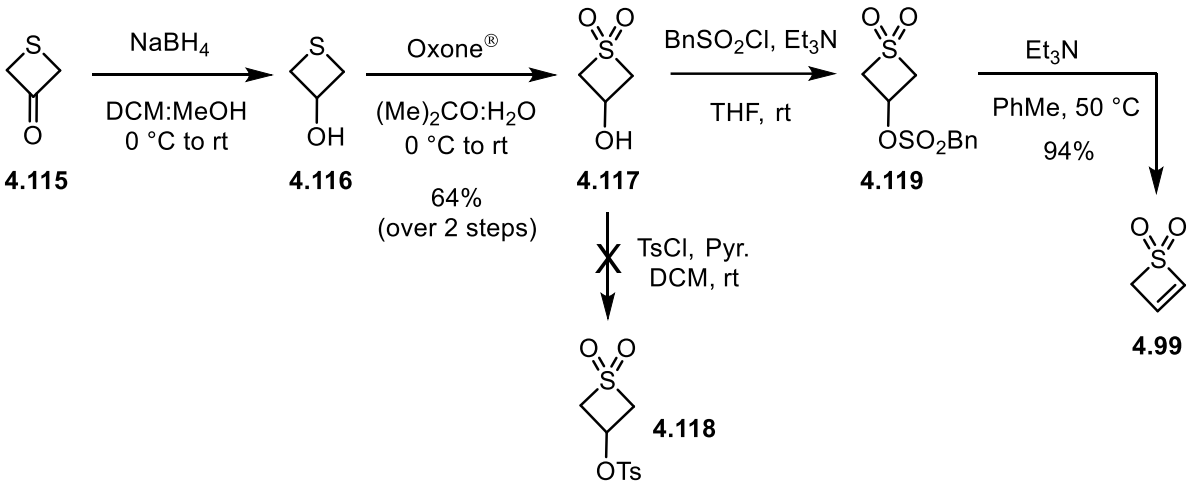
Jessica found that DBU seemed to be a mild enough base and led to the formation of **4.99** albeit in a low 30% yield. It is likely that after the formation of the thiete, further degradation is taking place under basic conditions.



Scheme 4.26. Low yielding synthesis of thiete-1,1-dioxide by the elimination of an azide. [+]Result by JP

Taking inspiration from the groups of Smith[251] and Christy and Dittmer,[252] we sought access to 3-hydroxythietane-1,1-dioxide **4.117** so that we could transform the alcohol into a better leaving group, hopefully achieving higher yields in the elimination reaction as compared to using substrate **4.114** (Scheme 4.27). The synthesis began from the commercially available and cheap thietan-3-one **4.115** that was reduced in the presence of $NaBH_4$, affording somewhat volatile thietan-3-ol **4.116** which was used as a crude solution without purification. Next, oxidation of the sulfide took place using Oxone® and gave **4.117** in 64% yield over two steps. To eliminate the alcohol, **4.117** was reacted in the presence of *p*-toluenesulfonyl chloride (TsCl) and pyridine. Surprisingly, these conditions led to decomposition of the substrate with no tosyl product **4.118** observed. Gratifyingly, switching to $BnSO_2Cl$ and triethylamine gave a positive result that allowed

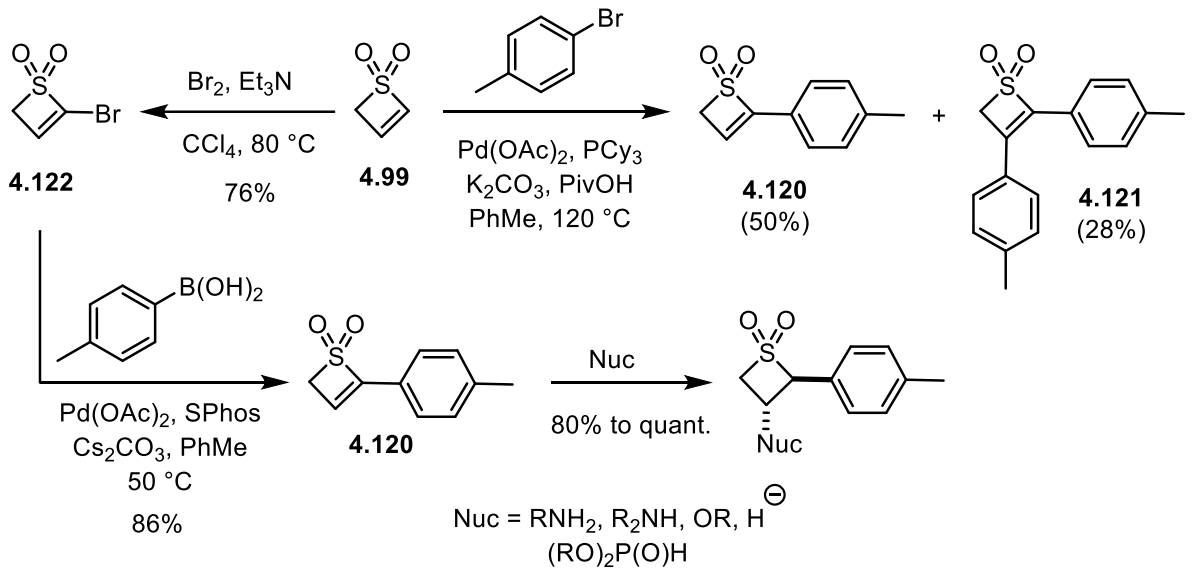
us to isolate the benzylsulfonate **4.119** without any purification. Finally, elimination of the benzylsulfonate took place by simply using triethylamine as a weak base, affording the thiete-1,1-dioxide **4.99** in an excellent 94% yield. Moving forward, we chose to use this route to access **4.99** as it is high yielding, required one purification step at the end of the sequence, and could deliver multi-gram quantities (3 grams) of **4.99** in a single pass.



Scheme 4.27. Efficient synthesis of thiete-1,1-dioxide **4.99** starting from thietan-3-one **4.115**

With **4.99** in hand, we were ready to test the possibility of installing an aryl group at the 2-position of the thiete ring (Scheme 4.28). We first tested the conditions of C-H activation which were reported by Didier. Under these conditions, we saw consumption of **4.99** and formation of the desired 2-tolylthiete-1,1-dioxide **4.120**. We also observed the formation of a side product, which we identified as the *bis*-arylated product **4.121**. These two compounds were formed in a ~3.5:1 ratio in favor of **4.120**. While we were pleased to see that the C-H activation was successful in providing a modest yield of **4.120**, the formation of **4.121** was undesirable. The ratio of **4.120**:**4.121** would likely change with the coupling of different aryl groups and may even worsen when using more electrophilic aryl groups as well. Furthermore, this would likely become a major issue when introducing heteroaromatic groups as well. To avoid this problem, we reasoned the introduction of a bromide for selective cross-coupling would solve our issue. Additionally, 2-bromothiete-1,1-dioxide (**4.122**) is a known compound and can be synthesized by a dibromination/elimination sequence in high yield (76%). To our delight, subjecting **4.122** to conditions of Suzuki coupling afforded us arylated product **4.120** in an excellent 86% yield. From

this point, we were able to show that **4.120** is a highly competent electrophile for the introduction of various nucleophiles including amines, alcohols, thiols, phosphites, hydrides, heteroaromatics, and even carbon nucleophiles.

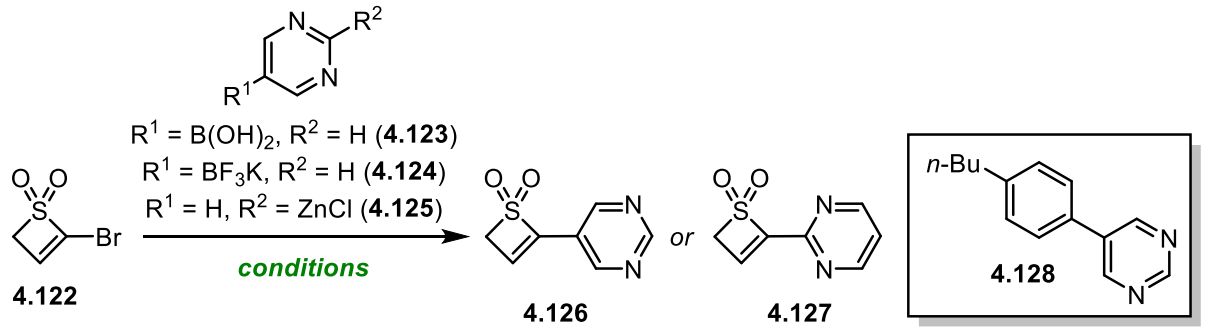


Scheme 4.28. Successful use of 2-arylated thiete-1,1-dioxides as electrophiles for the introduction of diversity at the β position (*C*3)

Having established diversity at the β position, we next focused on differentiating the α position with respect to the aryl rings used. We found that for the most part, aryl boronic acids were competent partners in the Suzuki coupling reaction of **4.122**. However, this reactivity could not be translated to the corresponding heteroaromatic boronic acids such as furan, pyridine, or pyrimidine as was seen initially by Jessica. Disappointed by this, we tested different conditions in an attempt to successfully perform this coupling reaction (Table 4.1). Under the standard conditions for aryl boronic acids (Entry 1), no product was observed using pyrimidine-5-boronic acid (**4.123**) despite full conversion of substrate **4.122**. Noticing the poor solubility of **4.123**, 20% water was added as solvent (Entry 2). Despite the better solubility, the same outcome was unfortunately observed. Additionally, switching the catalytic system (Entries 3–4) to $Na_2CO_3/Pd(PPh_3)_4$ or $K_2CO_3/PdCl_2(PPh_3)_2$ in different solvents was not beneficial and neither was switching to the more active potassium pyrimidine-5-trifluoroborate salt **4.124** (Entry 5). Moving away from the Suzuki coupling and inspired by the groups of Knochel and Hevia,[253] we also

attempted a Negishi coupling with an *in-situ* generated pyrimidine-2-zincate species (**4.125**) that was unsuccessful (Entry 6). As a final control experiment (Entry 7), a coupling reaction was done with pyrimidine-5-boronic acid **4.123** and 1-bromo-4-butylbenzene. This reaction gave the biaryl product **4.128** in 64% yield, indicating the problem was likely due to the substrate **4.122**. In general, all the reactions tested led to complete degradation of the substrate **4.122**.

Table 4.1. Failed attempts at cross-coupling between 2-bromothiete-1,1-dioxide **4.122** and heteroaromatic rings



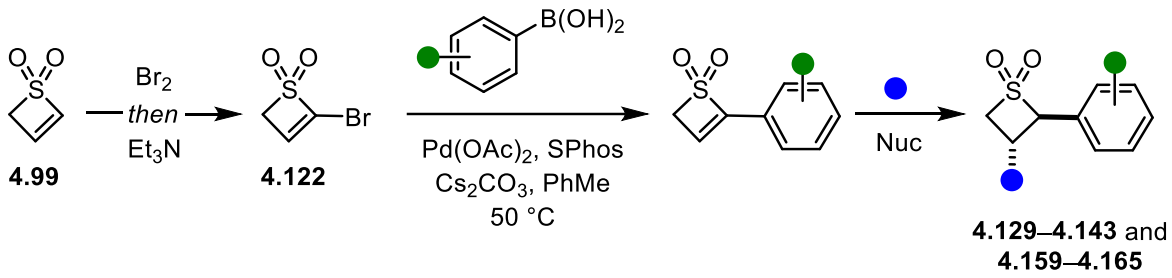
Entry[a]	Coupling Partner	Catalyst	Ligand	Base	Temperature (°C)[b]	Solvent	Yield (%)[c]
1+	**4.123**	$Pd(OAc)_2$	SPhos	Cs_2CO_3	50	PhMe	--[e]
2+	**4.123**	$Pd(OAc)_2$	SPhos	Cs_2CO_3	50	PhMe:H_2O	--
3+	**4.123**	$Pd(PPh_3)_4$	--	Na_2CO_3	85	1,2-DME	--
4+	**4.123**	$PdCl_2(PPh_3)_2$	--	K_2CO_3	120	DMF	--
5+	**4.124**	$Pd(OAc)_2$	SPhos	Cs_2CO_3	50	PhMe:H_2O	--
6	**4.125**[d]	$Pd(dba)_2$	TFP	--	23	THF	--[g]
7[f]	**4.123**	$Pd(PPh_3)_4$	--	Na_2CO_3	100	THF:H_2O	64

[a] Unless otherwise noted, all reactions were carried out using screw-cap test tubes at a concentration of 0.2 M in the indicated solvent. [b] Internal temperature. [c] Yields for **4.126**. [d] The zincate **4.125** was made by the *in-situ* deprotonation of pyrimidine using TMPZnCl as a base. [e] Degradation observed. [f] A control reaction using 1-bromo-4-butylbenzene and **4.123**. [g] Yield for **4.127**. +Results by JP.

4.6 Methodology for the photochemical ring contraction of thietane-1,1-dioxides

Thietane-1,1-dioxides which are substituted at the β position and contain an aryl ring chromophore at the α position were synthesized according to the general scheme shown below

(Scheme 4.29). 2-bromothiete-1,1-dioxide **4.122** (available in two steps from **4.99**) is arylated with different aryl boronic acids by a Suzuki coupling reaction to give 2-arylthiete-1,1-dioxides. Nucleophilic addition with various nucleophiles then affords the photochemical precursors **4.129**–**4.143** and **4.159**–**4.165**.

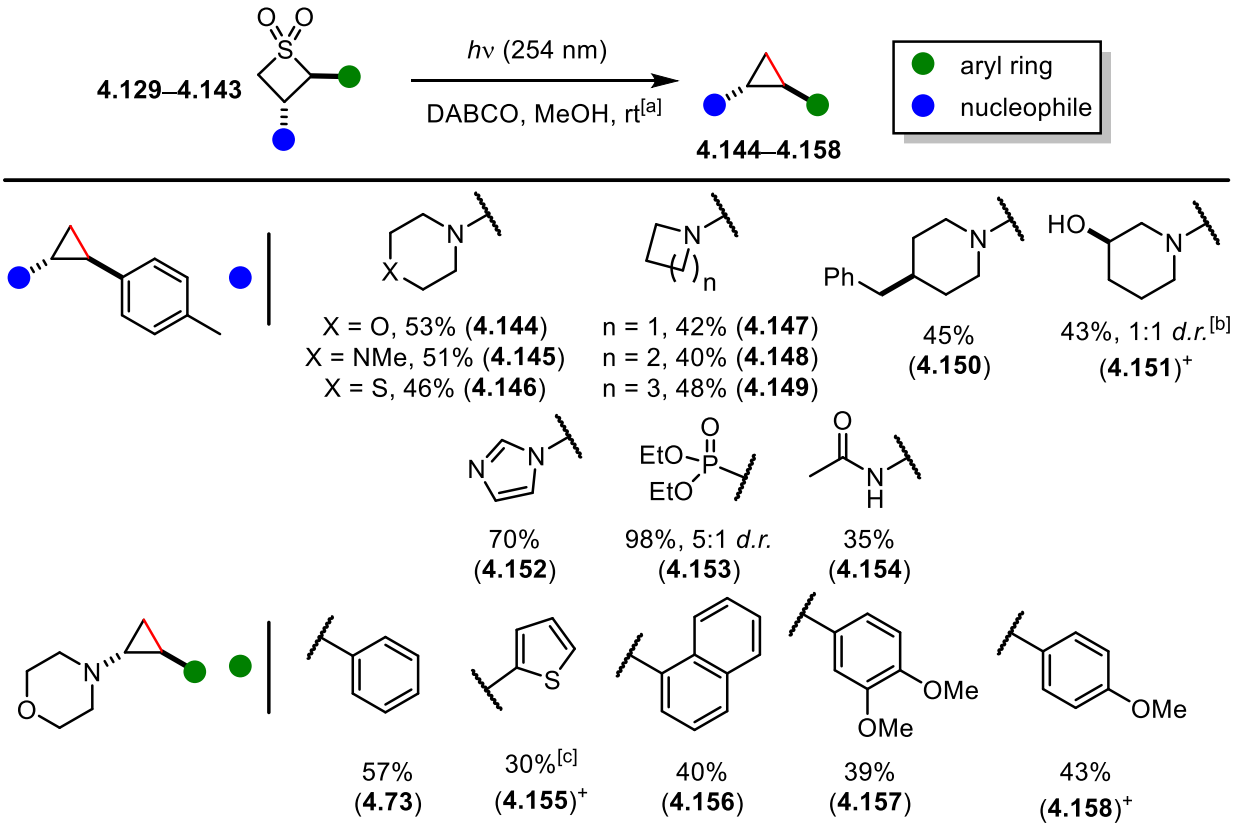


Scheme 4.29. General and modular synthesis of photochemical substrates

4.6.1 Successful scope examples thus far

As shown in Table 4.2, several different thietane-1,1-dioxides were successfully converted to cyclopropane products **4.144**–**4.158** under conditions of UV irradiation (254 nm) and in the presence of DABCO. The ring contraction protocol is tolerant to several groups at the β position of the thietane-1,1-dioxide ring system. Cyclic amines **4.147**–**4.149** of various ring sizes were well tolerated with yields between 42–48%. Importantly, product **4.147** incorporates the four-membered azetidine ring that has also been shown as a privileged structure in medicinal chemistry. Other heterocyclic amines such as morpholine (**4.144**), thiomorpholine (**4.146**), or N-methylpiperazine (**4.145**) did not impact reactivity as shown by the formation of the cyclopropanes in good yields (46–53%). Similarly, substituted piperidine rings were also tolerated under the photochemical conditions including 4-benzyl (**4.150**) and the free alcohols at the 3-position (**4.151**). Notably, the heteroaromatic imidazole ring (**4.152**) was also well tolerated, resulting in a 70% yield of the product. Amides (NHAc, **4.154**) also gave the product in a 35% yield. More exotic diethyl phosphonate (**4.153**) resulted in near quantitative conversion, affording the cyclopropane product in 5:1 *d.r.* and 98% yield. Typically, the ring contraction results in the trans-cyclopropane products, however this is the only example thus far where this is not the case. Finally, the photochemical reaction can also tolerate other aryl rings such as those which are more electron rich (**4.157**–**4.158**), naphthyl (**4.156**), and the heteroaromatic thiophene ring (**4.155**) as well.

Table 4.2. Nucleophile and aryl ring scope for the photochemical ring contraction of thietane-1,1-dioxide derivatives



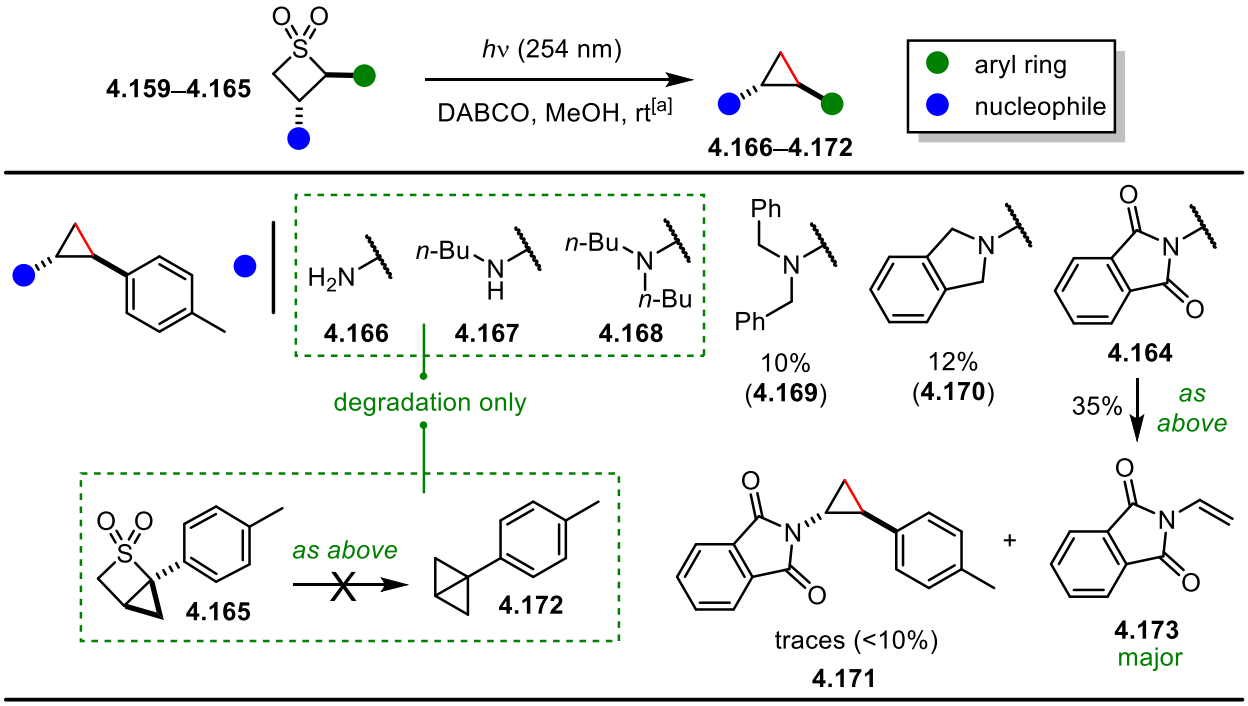
[a] Unless otherwise noted, reactions were carried out using 3.5 mL screw-cap quartz vials with 0.09 mmol of substrate in the indicated solvent at a concentration of 0.03 M. Reactions were degassed with nitrogen for approx. two to three minutes and irradiated in a Rayonet photochemical reactor. [b,c] NMR-yields and diastereomeric ratios (*d.r.*) were determined from the crude ^{1}H-NMR analysis using mesitylene as an internal standard. $^{+}$Results by JP.

4.6.2 Limitations and failed examples

Throughout the scope evaluation, we came across several examples of substrates which were not very compatible under our optimized conditions (Table 4.3). Unlike cyclic amines which were well tolerated across the board, acyclic amines proved to be particularly problematic. Free, primary, secondary, and even tertiary acyclic amines **4.166**–**4.168** resulted in complete degradation under photochemical conditions. More activated amines such as dibenzylamine (**4.169**) or isoindoline (**4.170**) were not competent substrates for this reaction. While the cyclopropane products could be isolated (10% and 12% yield), irradiation resulted in significant degradation and

polymerization. We believe these issues may be due competitive HAT events taking place or even amine oxidation under the conditions of the reaction that is leading to degradation. The substrates tested contained longer *n*-butyl chains, however it would be interesting to see how simple methyl substitution affects the outcome of the reaction. Protecting the amine as the amide (see **4.154**) seemed to help restore reactivity, however a different protecting group such as phthalimide (**4.171**) was attempted and was unsuccessful. Interestingly, this resulted in what appeared to be a *retro*-[2+2] reaction, giving vinyl phthalimide **4.173** as the major product in 35% yield with what seemed to be trace formation (<10%) of the desired cyclopropane **4.171**. Cyclopropyl thietane-1,1-dioxide **4.165** was also an unsuccessful substrate and did not deliver the bicyclobutane (BCB) product **4.172**. Aside from incomplete conversion, mostly decomposition took place with olefinic signals in the crude ^{1}H-NMR that indicates potential cyclopropane ring opening taking place.

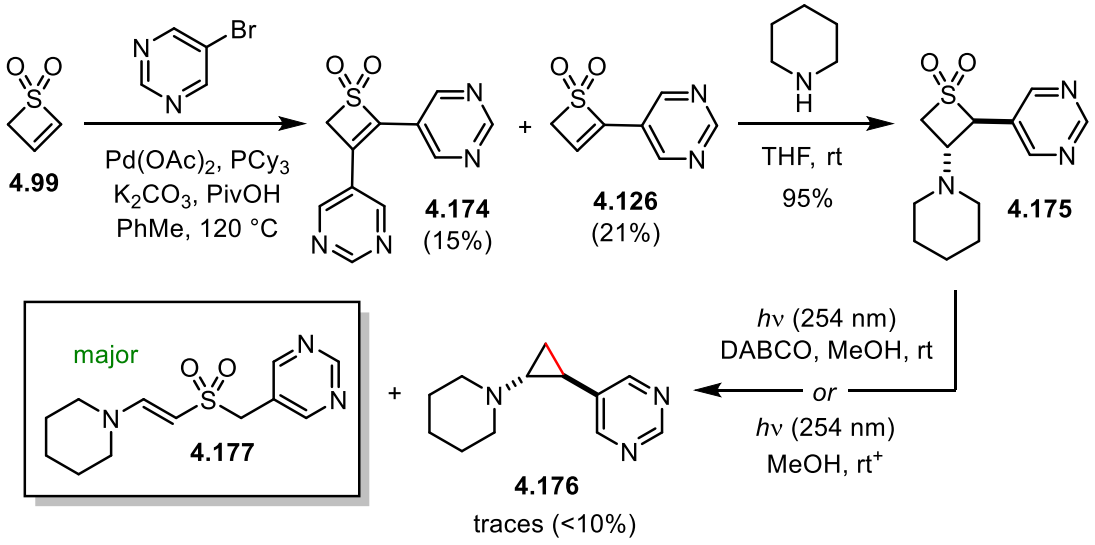
Table 4.3. Unsuccessful irradiation of substrates **4.159**–**4.165** with different β substitution



[a] Unless otherwise noted, reactions were carried out using 3.5 mL screw-cap quartz vials with 0.09 mmol of substrate in the indicated solvent at a concentration of 0.03 M. Reactions were degassed with nitrogen for approx. two to three minutes and irradiated in a Rayonet photochemical reactor.

As was discussed above, thietane-1,1-dioxide derivatives bearing heteroaromatic chromophores were difficult to access using cross-coupling methods and so we revisited the

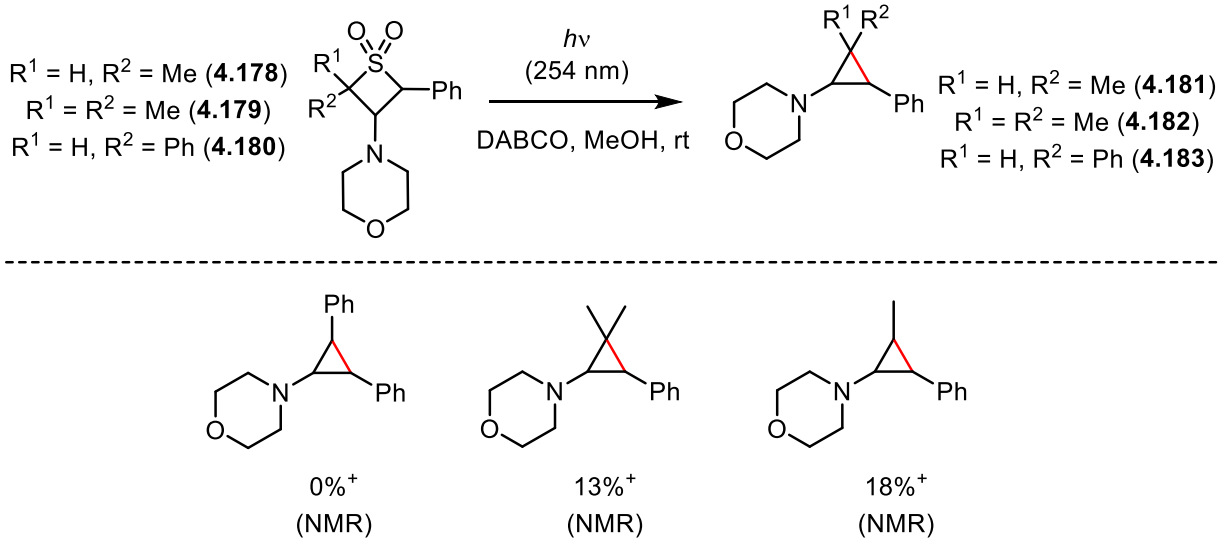
possibility of accessing compound **4.126** by C-H activation. Starting from the parent thiete-1,1-dioxide **4.99** and 5-bromopyrimidine, we were able to access compound **4.126** using the C-H activation strategy (Scheme 4.30). However, **4.126** was again accompanied by the formation of *bis*-arylated product **4.174** and the overall yield of the two compounds was modest (21% **4.126** and 15% **4.174**). The remainder was starting material that did not react further. Despite the low yield, we decided to push forward to test the reactivity of these substrates towards ring contraction. Nucleophilic addition with piperidine to give adduct **4.175** proceeded in an excellent 95% yield. To our disappointment however, irradiation of **4.175** gave trace amounts of cyclopropane **4.176** (<10%) and instead afforded near quantitative formation of the ring opened product **4.177**. Reasoning that this may be due to DABCO functioning as a base, the reaction was run again by Jessica in the absence of DABCO. Unfortunately, this resulted in the same outcome which indicated the instability of these kinds of substrates to the reaction conditions. Substrate **4.175** may be predisposed to favorable ring-opening in MeOH due to the overall electron richness of the system. Testing a similar substrate lacking the electron rich piperidine ring may disfavour ring-opening and favor cyclopropane formation instead.



Scheme 4.30. Synthesis and unsuccessful photochemical ring contraction of heteroaromatic substrate **4.175**. [+]Result by JP

Additionally, variously substituted thietane-1,1-dioxides such as **4.178**–**4.180** that were synthesized by the previous [2+2] reaction also failed to afford cyclopropane products in good

yields and was done by Jessica (Scheme 4.31). 3-methyl (**4.178**) and 3,3-dimethyl (**4.179**) substrates gave cyclopropanes **4.181** and **4.182** in 18% and 13% yield respectively. On the other hand, 2,3-diphenyl substrate **4.180** resulted in complete degradation with no cyclopropane **4.183** being observed. These substrates also required significantly longer irradiation times (6–13 hrs) for complete conversion.

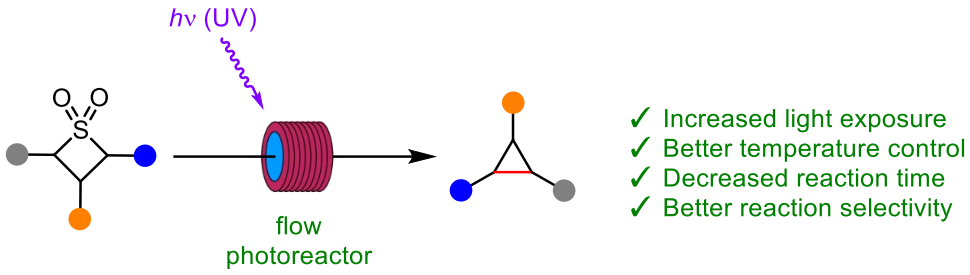


Scheme 4.31. Low yielding irradiation of trisubstituted thietane-1,1-dioxide substrates **4.178**–**4.180**. [+]Results by JP

4.7 Outlook and future directions

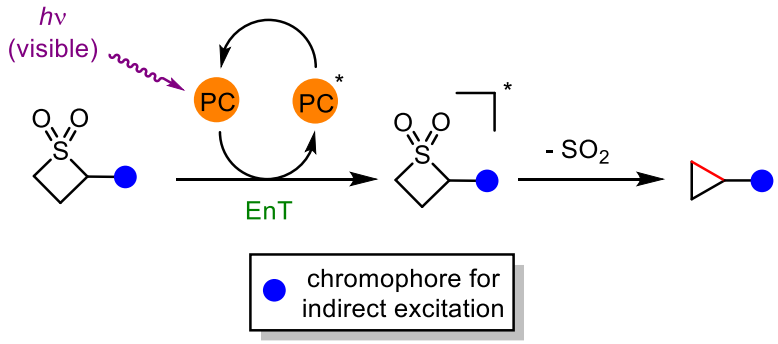
This study has demonstrated the photochemically induced ring contraction of thietane-1,1-dioxide substrates bearing an aryl ring chromophore as a viable approach towards the synthesis of substituted cyclopropane building blocks. These include cyclopropylamines which are of interest in medicinal chemistry. Thanks to the use of thiete-1,1-dioxides as a platform for diversity, a variety of substrates are accessible to study and will be tested in due course in addition to product derivatization and mechanistic studies. Our current approach should offer new possibilities for the synthesis of a range of privileged structures and for the design of new types of bioisosteres. The current methodology is however limited by reactivity issues associated with acyclic or free amines, heteroaromatic rings, and variously substituted substrates. Product and substrate degradation is a major problem in these examples, and this is likely due to the use of high energy UV light. A

potential solution to this problem is through the implementation of a flow chemistry process (Scheme 4.32). Flow chemistry can mitigate common problems associated with batch photochemistry such as light penetration, reaction times, energy consumption, and reaction selectivity (chemo-, stereo-, regioselectivity).[254]



Scheme 4.32. A flow chemistry process for the more efficient synthesis of cyclopropane building blocks using high energy UV light

Moreover, a logical extension to our proposed methodology is to move away from high energy UV light and to focus on the use of triplet-energy transfer (EnT) with lower energy visible light as a more mild, efficient, and selective method for the photochemical ring contraction of thietane-1,1-dioxides (Scheme 4.33). As a result, a different chromophore other than aryl rings will need to be used in conjunction with a photocatalyst which can absorb the visible light as shown below.

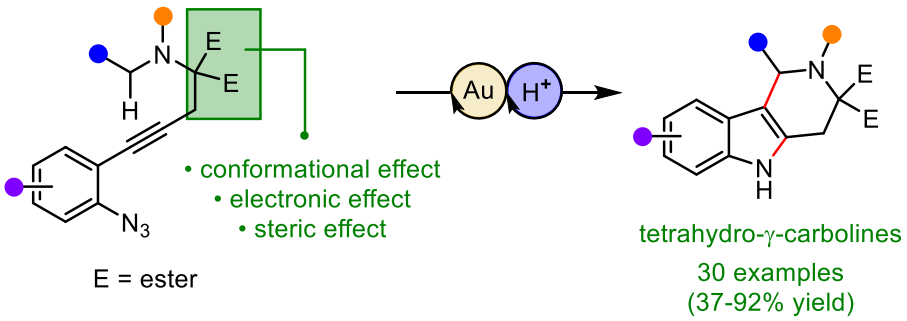


Scheme 4.33. Ring contraction of thietane-1,1-dioxides under conditions of triplet-energy transfer (EnT)

CHAPTER 5

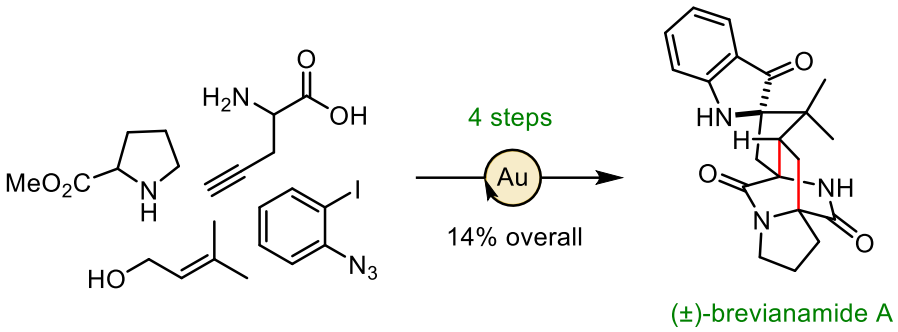
Conclusion

Overall, the work presented in Part I of this thesis exemplifies the usefulness and utility of Au(I) catalysis for the generation of molecular complexity and diversity. In Chapter 2, an in-depth study on the net Au(I) catalyzed Csp^3-H bond functionalization of free tertiary amines is presented. This rare transformation has been considered difficult owing to the general incompatibility of Lewis acidic Au(I) complexes and electron rich amines which are prone to coordination. Key to our success was through the rational incorporation of a malonate blocking group that demonstrated steric, electronic, and conformational effects which limited the interaction between the amine and the Au(I) center, thereby favoring hydride transfer to occur through bringing the hydride donor near the electrophilic and transient α-imino gold carbene. Thanks to this, we were also able to demonstrate that this reaction can be applied to a variety of substrates and represents a valuable approach to tetrahydro-γ-carboline scaffolds that can be rearranged under oxidative conditions into structural motifs that are found in several bioactive alkaloid natural products. Our current methodology is limited to cyclic hydride donors (see Section 2.7.3) and produces racemic products. However, our approach can potentially be made asymmetric using chiral catalysts or additives such as chiral Brønsted acids. An asymmetric synthesis of tetrahydro-γ-carbolines would therefore be of great interest for total synthesis and heterocyclic chemistry, underscoring the promising advance our method has demonstrated in the field of Au(I) catalysis.



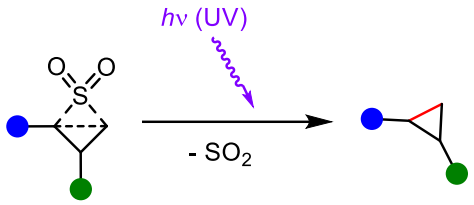
In Chapter 3, two complementary routes towards the natural product (±)-brevianamide A were accomplished. A first-generation synthesis of a total of seven steps was initially achieved and resulted in very low overall yields of (±)-brevianamide A being produced, leaving plenty of room for improvement. In our second-generation synthesis, we achieved the shortest (four steps LLS) and highest yielding (14% overall) synthesis of (±)-brevianamide A to date. The success of this synthesis hinged on the use of a Au(I) cascade process that forged the pseudoindoxyl motif of the

natural product in a single step and utilized prenyl alcohol as a simple and readily available commodity as the source of the reverse prenyl group. Furthermore, this process also allowed for the challenging installation of two adjacent quaternary centers that are found in the natural product. Owing to the general compatibility of the Au(I) catalyzed steps with basic media, we were ultimately able to fully telescope the synthesis of (±)-brevianamide A such that no purification or isolation of late-stage intermediates was required. The successful execution of this synthesis further highlights the molecular complexity which can be achieved using Au(I) catalysis and contributes greatly to the field of alkaloid total synthesis.



Part II of this thesis shifts gears and focuses on the preliminary introduction of thietane-1,1-dioxide substrates as viable substrates for the execution of a ring contraction methodology through the extrusion of sulfur dioxide gas. This leads to the synthesis of cyclopropane building blocks that are of interest to medicinal chemistry and the pharmaceutical sectors. Initial access to the thietane-1,1-dioxide substrates seemed trivial, however upon further experimentation it was found that this was not the case. As a result, further experimentation towards the synthesis of new precursors for accessing the desired thietane-1,1-dioxide substrates were undertaken. This led to the use of thiete-1,1-dioxides as a platform for diversity. While reports on the synthesis and use of thiete-1,1-dioxides were scarce in the literature, we found that a variety of thietane-1,1-dioxide substrates were easily able to be accessed and studied from them, allowing us to test them in our ring contraction method. Therefore, this new ring contraction approach should offer several possibilities for the synthesis of a range of privileged cyclopropane structures and for the design of new types of bioisosteres in medicinal chemistry. In particular, we have shown that pharmaceutically relevant cyclopropylamine building blocks are easily synthesized using our

method as compared to previous routes and this further showcases the advance and importance of this work in the broader field of medicinal chemistry as a whole.



In general, the research discussed in Parts I and II of this thesis demonstrate the positive outcomes that can be achieved through using catalysis and photochemistry. The unique reactivity of electrophilic Au(I) complexes has led to the realization of the challenging Csp^3-H bond functionalization of free tertiary amine substrates in addition to the expedited total synthesis of the complex natural product (±)-brevianamide A, affording the shortest and highest yielding synthesis to date. By leveraging light as a renewable and green energy source, we have also been able to synthesize important cyclopropane building blocks in a new and environmentally friendly manner, foregoing the use of higher energy and toxic reagents that have been used previously. It is our hope that these findings will spur continuous advancement in both the fields of Au(I) catalysis and photochemistry, such that new methodologies will be unlocked to allow for access to unique and interesting structures.

CHAPTER 6

Supporting Information

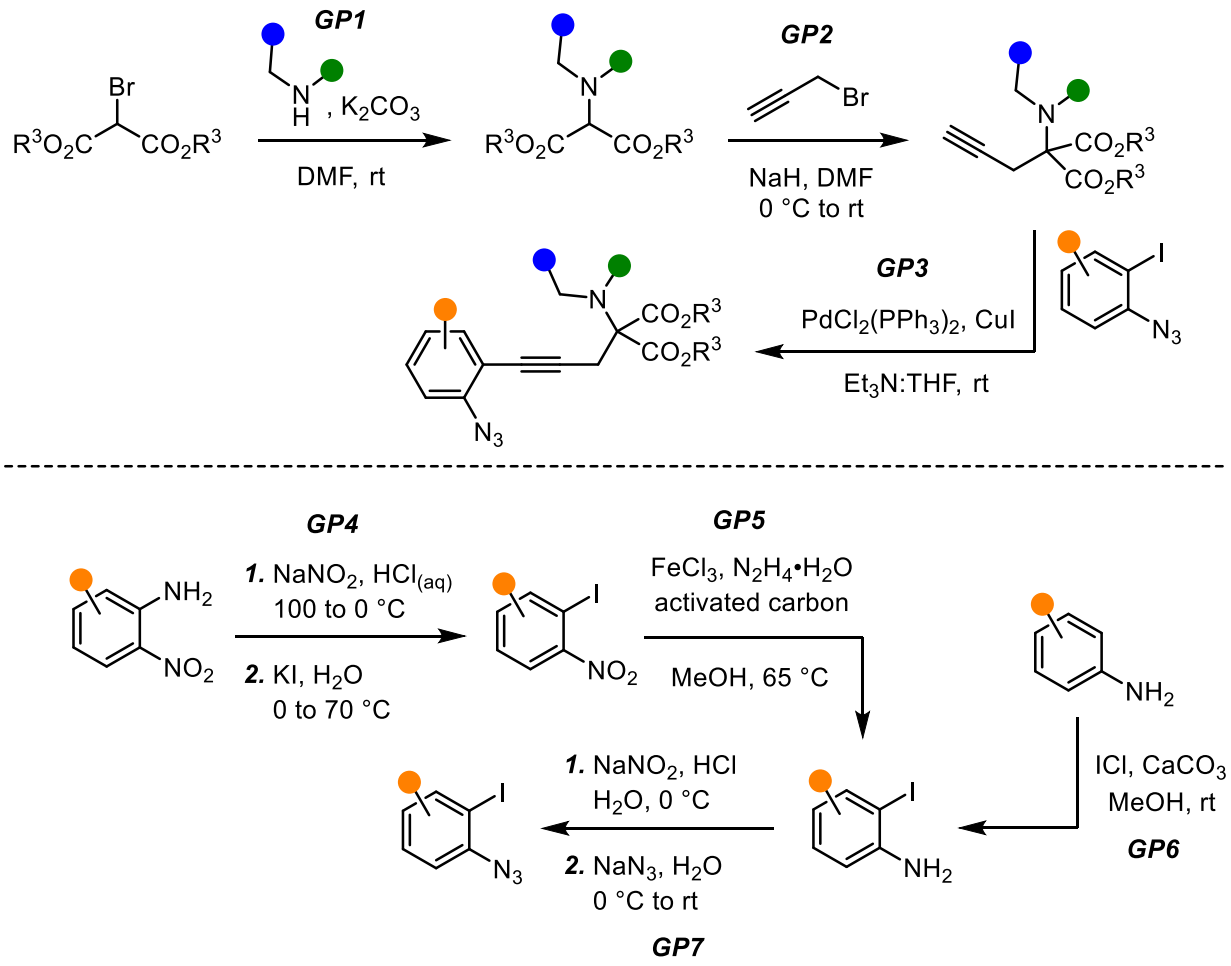
6.1 General information

Commercially available reagents were purchased from Sigma-Aldrich, Alfa-Aesar, Oakwood Chemicals, TCI America, Thermo Fisher Scientific, Combi-Blocks or Ambeed chemical suppliers and were used as received without further purification. Anhydrous solvents were obtained from an MB-SPS 800 or dried over 4 Å molecular sieves and kept under an inert atmosphere of nitrogen gas. All reactions were performed in flame-dried Synthware™ round-bottom flasks or round-bottom pressure vessels fitted with a rubber septum/Teflon screwcap under a positive pressure of nitrogen gas with magnetic stirring, unless otherwise stated. Photochemical reactions were conducted in screw-cap quartz vials and irradiated at 254 nm in a Rayonet photochemical reactor. Reaction temperatures performed above room temperature (21–24 °C) were controlled using an IKA® temperature probe and heated using a silicone oil bath situated on an IKA® stir-plate. Liquids and solutions were transferred *via* syringe or stainless-steel cannula. Organic solutions were concentrated under reduced pressure on temperature- and pressure-controlled Buchi rotary evaporators equipped with an ice condenser. Thin-layer chromatography was performed on aluminum backed TLC Silica gel 60 F254 plates (thickness: 175–225 μm) and visualized by fluorescent quenching at 254/366 nm or stained using potassium permanganate ($KMnO_4$) solution, p-anisaldehyde solution, iodine stain and ninhydrin solution followed by heating with a heat gun. Flash-column chromatography was carried out on silica gel using a forced flow of eluents with reagent-grade solvents in glass columns. Nuclear magnetic resonance (NMR) spectra were recorded at room temperature in the given deuterated solvent on 300, 400, 500, and 600 megahertz (MHz) Bruker instruments for the specified nucleus. Chemical shifts (δ) are given in parts per million (ppm) and are internally referenced to the residual $CDCl_3$ (δ 7.26 ppm ^1H and δ 77.16 ppm ^{13}C), d_4-MeOH (δ 3.31 ppm ^1H and 49 ppm ^{13}C), d_6-DMSO (δ 2.50 ppm ^1H and δ 39.52 ppm ^{13}C), and $(CD_3)_2CO$ (δ 2.05 ppm ^1H and 29.8, 206.3 ppm ^{13}C) resonances. Coupling constants (J) are given in hertz (Hz). Signal multiplicities are depicted using the following abbreviations: s = singlet, d = doublet, t = triplet, q = quartet, p = quintet, m = multiplet, dd = doublet of doublet, dt = doublet of triplet, tt = triplet of triplet, td = triplet of doublet, dq = doublet of quartet, qd = quartet of doublet, ddd = doublet of doublet of doublet, ddt = doublet of doublet of triplet, dddd = doublet of doublet of doublet of doublet, and br s = broad singlet. Infrared (IR) spectra were recorded with an Agilent Technologies Cary 630 Fourier transform infrared (FT-IR) spectrometer equipped with a diamond attenuated total reflection (ATR) module. High-resolution

mass spectrometry by electron impact (HRMS-EI) was performed on a JEOL JMCGCmate II mass spectrometer and fragment signals are given in a mass per charge ratio (*m/z*). High-resolution mass spectrometry by electrospray ionization (HRMS-ESI) was performed on a Micromass Q-Tof II mass spectrometer and fragment signals are given in a mass per charge ratio (*m/z*). Low resolution mass spectrometry was performed on an Advion Interchim Scientific expression® compact mass spectrometer (CMS) using an atmospheric pressure chemical ionization (APCI) probe and fragment signals are given in a mass per charge ratio (*m/z*).

6.2 Supporting information for Chapter 2

6.2.1 Experimental procedures



GP1:

Dimethyl bromomalonate (5 mmol, 1 equiv.) was added in one portion to a vigorously stirred slurry of secondary amine (5 mmol, 1 equiv.) and solid K_2CO_3 (6 mmol, 1.2 equiv.) in DMF (5 mL). The reaction mixture was stirred at room temperature and aged for 3–4 hours at which point TLC analysis indicated complete consumption of the starting material. The reaction mixture was quenched with a saturated aqueous solution of NH_4Cl (2 mL), extracted with Et_2O (20 mL), and the organic phase washed multiple times with H_2O to remove any residual DMF. The organic phase was collected and dried over anhydrous $MgSO_4$, filtered, and concentrated to afford crude amino malonate.

GP2:

Amino malonate (2.7 mmol, 1 equiv.) was added dropwise as a solution in THF (2.7 mL) to a vigorously stirred suspension of NaH (60 wt% in mineral oil, 6.7 mmol, 2.5 equiv.) in THF (2.7 mL) that had been cooled to 0 °C. The reaction mixture was aged for 10–15 minutes at that temperature, at which point propargyl bromide (80 wt% in PhMe, 5.4 mmol, 2 equiv.) was added dropwise and the reaction mixture was warmed to room temperature and aged for 2–4 hours. After TLC analysis indicated complete consumption of the starting material, the reaction was quenched with a saturated aqueous solution of NH_4Cl (5 mL) in an ice bath and extracted with EtOAc (3x 10 mL). The organic phase was collected and dried over anhydrous $MgSO_4$, filtered, and concentrated to afford crude terminal alkyne which was purified by flash-column chromatography.

GP3:

$PdCl_2(PPh_3)_2$ (0.01 mmol, 2.5 mol%) and CuI (0.02 mmol, 5 mol%) were added to a stirring solution of terminal alkyne (0.4 mmol, 1 equiv.) and iodoarylazide (0.44 mmol, 1.1 equiv.) at room temperature in a 1:1 mixture of Et_3N:THF (1.5 mL) that had been degassed using a strong flow of nitrogen gas. Once TLC analysis indicated complete consumption of the starting material, the reaction mixture was diluted with H_2O (3 mL) and extracted with EtOAc (3x 5 mL). The organic phase was collected and dried over anhydrous $MgSO_4$, filtered, and concentrated to afford crude *ortho*-alkynyl arylazide which was purified by flash-column chromatography.

GP4:

Ortho-nitroaniline (5 mmol, 1 equiv.) was added in one portion to a stirred flask containing concentrated HCl (5 mL) and heated to 100 °C in an oil bath for 10 minutes. After 10 minutes, the reaction mixture was cooled to room temperature and transferred to an ice bath to cool to 0 °C, at which point a solution of $NaNO_2$ (6 mmol, 1.2 equiv.) in H_2O (1 mL) was added dropwise and the reaction mixture was aged at that temperature for another 30 minutes to 1 hour. After, a solution of KI (7.5 mmol, 1.5 equiv.) in H_2O (1 mL) was added dropwise and the reaction mixture was transferred to an oil bath to be warmed to 70 °C and left to age for 2–4 hours. The reaction mixture was diluted with H_2O (5 mL) and extracted with EtOAc (3x 10 mL). The organic phase was collected and dried over anhydrous $MgSO_4$, filtered, and concentrated to afford crude iodonitroarene which was purified by flash-column chromatography.

GP5:

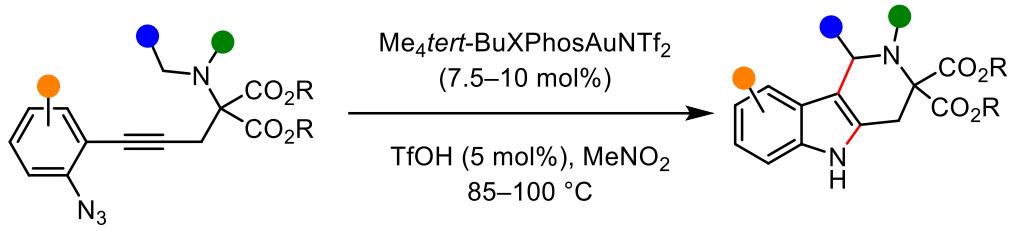
Iodonitroarene (2.5 mmol, 1 equiv.) was added as a solution in anhydrous MeOH (4 mL) to a stirring solution of $FeCl_3$ (0.04 mmol, 1.5 mol%) in anhydrous MeOH (8 mL). Activated carbon (0.5 mmol, 20 mol%) was added to the flask in one portion and the entire flask was placed in an oil bath and heated to reflux. Once at reflux, hydrazine monohydrate (5 mmol, 2 equiv.) was added all at once and the reaction mixture left under reflux overnight. After, the reaction mixture was filtered over a pad of silica gel/celite and concentrated to afford crude iodoaniline which was purified by flash-column chromatography.

GP6:

$CaCO_3$ (10 mmol, 2 equiv.) and ICl (6 mmol, 1.2 equiv.) were added to a stirred solution of aniline (5 mmol, 1 equiv.) in anhydrous MeOH (25 mL) at room temperature. The reaction mixture was covered from light and allowed to age overnight. The next day, TLC analysis indicated complete consumption of the starting material and the reaction mixture was quenched with a saturated aqueous solution of $Na_2S_2O_3$ (10 mL) and extracted with EtOAc (3x 20 mL). The organic phase was collected and dried over anhydrous $MgSO_4$ filtered, and concentrated to afford crude iodoaniline which was purified by flash-column chromatography.

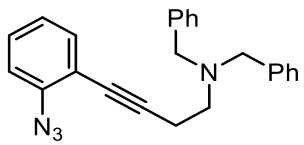
GP7:

Iodoaniline (2 mmol, 1 equiv.) was added in one portion to a stirred flask containing concentrated HCl (20 mmol, 10 equiv.) in H_2O (2 mL) that had been cooled to 0 °C and stirred for 10 minutes. After 10 minutes, a solution of $NaNO_2$ (2.4 mmol, 1.2 equiv.) in H_2O (0.5 mL) was added dropwise and the reaction mixture was aged at 0 °C for another 30 minutes to 1 hour. After, a solution of NaN_3 (2.4 mmol, 1.2 equiv.) in H_2O (0.5 mL) was added dropwise and the reaction mixture was warmed to room temperature and left for 1 hour. The reaction mixture was diluted with H_2O (5 mL) and extracted with EtOAc (3x 10 mL). The organic phase was collected and dried over anhydrous $MgSO_4$, filtered, and concentrated to afford crude iodoarylazide that was purified by flash-column chromatography.



GP8:

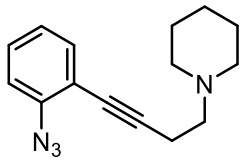
Me_4*t*-BuXPhosAuNTf$_2$ (0.005–0.006 mmol, 7.5–10 mol%) and a solution of TfOH in anhydrous $MeNO_2$ (0.5 M, 0.003 mmol, 5 mol%) were added to a solution of *ortho*-alkynyl arylazide (0.06 mmol, 1 equiv.) in anhydrous $MeNO_2$ (0.6 mL) and stirred at 85–100 °C in an oil bath until TLC analysis indicated full consumption of the starting material. Once the reaction was complete, the reaction mixture was taken out of the oil bath to cool to room temperature, quenched with a few drops of Et_3N, and concentrated to afford crude indole which was purified by flash-column chromatography.



2.84

Prepared from *N*,*N*-dibenzylbut-3-yn-1-amine (133 mg, 0.53 mmol) and 1-azido-2-iodobenzene (144 mg, 0.59 mmol) following GP3. Purification over silica (eluent: Et_2O/Hexanes). Arylazide **2.84** was obtained as a green oil: 93.4 mg, 48% yield.

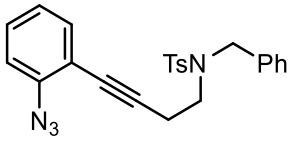
^{1}H-NMR (400 MHz, $CDCl_3$): δ 7.46–7.40 (m, 4H), 7.37 (dd, *J* = 7.7, 1.6 Hz, 1H), 7.35–7.21 (m, 7H), 7.11–7.04 (m, 2H), 3.69 (s, 4H), 2.82 (t, *J* = 7.2 Hz, 2H), 2.67 (t, *J* = 7.2 Hz, 2H).
^{13}C-NMR (100 MHz, $CDCl_3$): δ 140.8, 139.7, 133.9, 129.0, 128.9, 128.4, 127.0, 124.7, 118.8, 116.2, 95.4, 77.1, 58.3, 52.2, 18.5.
IR (ATR): ῡ 3025 (w), 2921 (w), 2795 (m), 2125 (s), 2091 (s), 1567 (w), 1486 (s), 1444 (s), 1364 (m), 1121 (m), 1095 (m), 1024 (m), 972 (m), 907 (m), 812 (w) cm^{-1}.
HRMS (ESI): Calculated for $C_{24}H_{23}N_4$ $[M+H]^+$: 367.1917; found: *m/z* 367.1928.



2.83

Prepared from 1-(but-3-yn-1-yl)piperidine (102 mg, 0.74 mmol) and 1-azido-2-iodobenzene (200 mg, 0.82 mmol) following GP3. Purification over silica (eluent: EtOAc/Hexanes). Arylazide **2.83** was obtained as a brown oil: 79.9 mg, 42% yield.

^{1}H-NMR (400 MHz, $CDCl_3$): δ 7.37 (dd, *J* = 7.6, 1.6 Hz, 1H), 7.32–7.23 (m, 1H), 7.09–7.02 (m, 2H), 2.67 (h, *J* = 2.4 Hz, 4H), 2.47 (t, *J* = 5.3 Hz, 4H), 1.59 (p, *J* = 5.6 Hz, 4H), 1.44 (tq, *J* = 8.9, 5.8, 4.6 Hz, 2H).
^{13}C-NMR (100 MHz, $CDCl_3$): δ 140.8, 133.9, 129.0, 124.7, 118.8, 116.1, 95.2, 77.0, 58.0, 54.3, 26.1, 24.4, 18.0.
IR (ATR): ῡ 2930 (s), 2851 (m), 2799 (m), 2130 (s), 2090 (s), 1562 (w), 1485 (m), 1439 (m), 1299 (s), 1154 (m), 1038 (m), 991 (w), 938 (w), 860 (m), 748 (s) cm^{-1}.
HRMS (ESI): Calculated for $C_{15}H_{19}N_4$ $[M+H]^+$: 255.1604; found: *m/z* 255.1600.



2.94

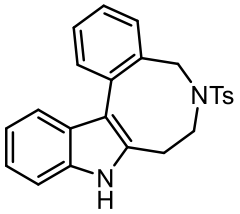
Prepared from *N*-benzyl-*N*-(but-3-yn-1-yl)-4-methylbenzenesulfonamide (151 mg, 0.48 mmol) and 1-azido-2-iodobenzene (130 mg, 0.53 mmol) following GP3. Purification over silica (eluent: Et_2O/Hexanes). Arylazide **2.94** was obtained as a brown solid: 153.1 mg, 74% yield.

^{1}H-NMR (400 MHz, $CDCl_3$): δ 7.77 (d, *J* = 8.3 Hz, 2H), 7.36–7.23 (m, 9H), 7.09–7.00 (m, 2H), 4.44 (s, 2H), 3.39 (dd, *J* = 8.3, 6.9 Hz, 2H), 2.53 (dd, *J* = 8.2, 6.9 Hz, 2H), 2.42 (s, 3H).

^{13}C-NMR (100 MHz, $CDCl_3$): δ 143.6, 140.8, 137.1, 136.3, 133.9, 129.9, 129.3, 128.8, 128.4, 128.1, 127.3, 124.7, 118.8, 115.6, 92.9, 78.0, 52.5, 46.7, 21.7, 20.3.

IR (ATR): ῡ 2920 (w), 2128 (m), 2092 (m), 1595 (w), 1568 (w), 1487 (m), 1441 (m), 1334 (s), 1300 (s), 1233 (m), 1149 (s), 1097 (s), 985 (m), 938 (m), 902 (m), 815 (m), 743 (s), 721 (s) cm^{-1}.

HRMS (ESI): Calculated for $C_{24}H_{21}N_4NaO_2S$ $[M+Na]^+$: 453.1356; found: *m/z* 453.1366.



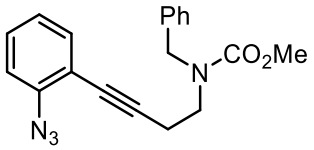
2.98

Prepared from arylazide **2.94** (26 mg, 0.06 mmol) using $IPrAuNTf_2$ as a catalyst (5.2 mg, 0.006 mmol) and 1,2-DCE (0.6 mL) as a solvent. Reaction time: 1 hr. Purification over silica (eluent: EtOAc/Hexanes + Et_3N). Indole **2.98** was obtained as a brown solid: 13.1 mg, 54% yield.

^{1}H-NMR (400 MHz, $CDCl_3$): δ 8.02 (bs, 1H), 7.73 (d, *J* = 7.5 Hz, 1H), 7.68 (d, *J* = 8.3 Hz, 2H), 7.60 (dd, *J* = 7.6, 1.2 Hz, 1H), 7.55 (d, *J* = 7.9 Hz, 1H), 7.44 (td, *J* = 7.5, 1.4 Hz, 1H), 7.36 (td, *J* = 7.5, 1.3 Hz, 1H), 7.32 (d, *J* = 8.0 Hz, 1H), 7.26 (d, *J* = 8.1 Hz, 2H), 7.18 (td, *J* = 7.4, 1.2 Hz, 1H), 7.11 (td, *J* = 7.6, 1.0 Hz, 1H), 4.83 (d, *J* = 13.9 Hz, 1H), 3.87 (dd, *J* = 12.8, 7.8 Hz, 1H), 3.49 (d, *J* = 13.9 Hz, 1H), 3.04–2.86 (m, 2H), 2.74 (dd, *J* = 16.0, 9.3 Hz, 1H), 2.39 (s, 3H).

^{13}C-NMR (100 MHz, $CDCl_3$): δ 143.4, 136.9, 135.4, 135.1, 134.5, 134.0, 131.8, 130.0, 129.9, 128.2, 128.0, 127.3, 127.2, 122.3, 120.4, 119.1, 113.3, 110.7, 50.7, 44.5, 28.7, 21.6.

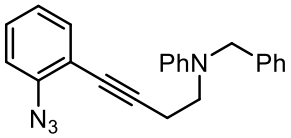
IR (ATR): ῡ 3322 (m), 2079 (w), 1596 (m), 1559 (w), 1491 (m), 1453 (m), 1316 (s), 1245 (m), 1147 (s), 1088 (s), 1062 (m), 1011 (m), 947 (m), 878 (m), 812 (s), 746 (s), 718 (s) cm^{-1}.
HRMS (EI): Calculated for $C_{24}H_{22}N_2O_2S$ $[M]^+$: 402.1396; found: *m/z* 402.1434.



2.95

Prepared from methyl benzyl(but-3-yn-1-yl)carbamate (172 mg, 0.79 mmol) and 1-azido-2-iodobenzene (233 mg, 0.95 mmol) following GP3. Purification over silica (eluent: EtOAc:hexanes). Arylazide **2.95** was obtained as an amber oil: 152 mg, 57% yield.

^{1}H-NMR (300 MHz, $CDCl_3$): δ 7.39–7.21 (m, 7H), 7.12–7.03 (m, 2H), 4.57 (s, 2H), 3.76 (s, 3H), 3.39–3.35 (m, 2H), 2.70 (dt, *J* = 23.8, 7.0 Hz, 2H), 1.97 (t, *J* = 2.0 Hz, 1H).
^{13}C-NMR (101 MHz, $CDCl_3$): δ 157.6, 157.2, 141.2, 138.2, 134.1, 129.6, 129.1, 128.3, 127.9, 127.6, 125.1, 119.1, 115.6, 94.2, 93.7, 77.8, 77.5, 77.2, 53.3, 51.5, 46.5, 45.6, 20.1, 19.6.
HRMS (ESI): Calculated for $C_{19}H_{18}N_4NaO_2$ $[M+Na]^+$: 357.1327; found: *m/z* 357.1352.

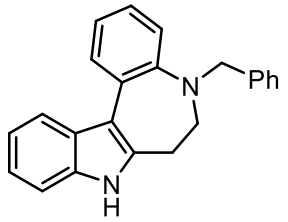


2.96

Prepared from *N*-benzyl-*N*-(but-3-yn-1-yl)aniline (179 mg, 0.76 mmol) and 1-azido-2-iodobenzene (205 mg, 0.84 mmol) following GP3. Purification over silica (eluent: Et_2O:hexanes). Arylazide **2.96** was obtained as a yellow oil: 182 mg, 68% yield.

^{1}H-NMR (500 MHz, $CDCl_3$): δ 7.36–7.28 (m, 4H), 7.26–7.19 (m, 5H), 7.09 (dd, *J* = 8.1, 1.1 Hz, 1H), 7.06 (td, *J* = 7.5, 1.1 Hz, 1H), 6.76 (d, *J* = 8.2 Hz, 2H), 6.72 (t, *J* = 7.2 Hz, 1H), 4.67 (s, 2H), 3.77 (t, *J* = 7.3 Hz, 2H), 2.82 (t, *J* = 7.3 Hz, 2H).
^{13}C-NMR (101 MHz, $CDCl_3$): δ 148.3, 141.2, 139.1, 134.2, 129.8, 129.5, 129.1, 127.3, 127.0, 125.1, 119.1, 117.2, 116.2, 112.8, 94.3, 78.1, 55.1, 50.7, 18.8.

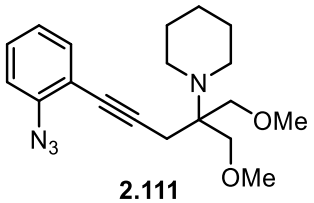
HRMS (ESI): Calculated for $C_{23}H_{21}N_4$ $[M+H]^+$: 353.1766; found: *m/z* 353.1758.



2.97

Prepared from arylazide **2.96** (25.4 mg, 0.07 mmol) using JohnPhosAuNTf$_2$ (5.4 mg, 0.007 mmol) as a catalyst and 1,2-DCE as solvent (0.7 mL). Purification over silica (eluent: EtOAc:hexanes). Indole **2.97** was obtained as an oil: 5.5 mg, 24% yield.

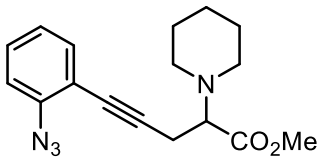
^{1}H-NMR (300 MHz, CDCl$_3$): δ 8.14–8.06 (m, 2H), 7.99 (bs, 1H), 7.41–7.11 (m, 11H), 4.49 (s, 2H), 3.31 (t, *J* = 6.0 Hz, 2H), 2.95 (t, *J* = 5.9 Hz, 2H).
^{13}C-NMR (101 MHz, CDCl$_3$): δ 151.6, 139.0, 136.2, 129.2, 128.7, 128.4, 127.8, 127.3, 127.2, 125.3, 121.8, 121.3, 120.3, 119.9, 117.1, 111.6, 110.3, 57.5, 51.3, 30.7.
HRMS (EI): Calculated for $C_{23}H_{20}N_2$ $[M]^+$: 324.1626; found: *m/z* 324.1629.



2.111

Prepared from 1-(1-methoxy-2-(methoxymethyl)pent-4-yn-2-yl)piperidine (79 mg, 0.35 mmol) and 1-azido-2-iodobenzene (95 mg, 0.38 mmol) following GP3. Purification over silica (eluent: EtOAc:hexanes:Et$_3$N). Arylazide **2.111** was obtained as a pale-yellow oil: 69 mg, 58% yield.

^{1}H-NMR (300 MHz, CDCl$_3$): δ 7.38 (dd, *J* = 7.7, 1.6 Hz, 1H), 7.32–7.28 (m, 1H), 7.12–7.03 (m, 2H), 3.58 (s, 4H), 3.36 (s, 6H), 2.79–2.73 (m, 4H), 2.69 (s, 2H), 1.61–1.52 (m, 4H), 1.48–1.39 (m, 2H).
^{13}C-NMR (101 MHz, CDCl$_3$): δ 140.7, 133.4, 128.5, 124.4, 118.5, 116.2, 94.3, 77.8, 73.5, 62.7, 59.1, 48.0, 26.9, 24.9, 21.4.
HRMS (ESI): Calculated for $C_{19}H_{26}N_4NaO_2$ $[M+Na]^+$: 365.1953; found: *m/z* 365.1941.



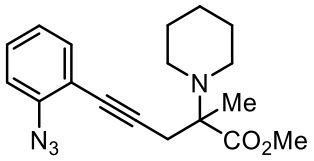
2.112

Prepared from methyl 2-(piperidin-1-yl)pent-4-ynoate (163 mg, 0.84 mmol) and 1-azido-2-iodobenzene (226 mg, 0.92 mmol) following GP3. Purification over silica (eluent: EtOAc:hexanes). Arylazide **2.112** was obtained as an amber oil: 198 mg, 76% yield.

^{1}H-NMR (300 MHz, $CDCl_3$): δ 7.35 (ddd, *J* = 7.6, 1.6, 0.6 Hz, 1H), 7.32–7.25 (m, 1H), 7.09–7.01 (m, 2H), 3.76 (s, 3H), 3.53 (dd, *J* = 9.0, 5.8 Hz, 1H), 2.96 (dd, *J* = 16.6, 9.0 Hz, 1H), 2.78 (dd, *J* = 16.6, 5.8 Hz, 1H), 2.58 (dh, *J* = 16.5, 5.1 Hz, 4H), 1.67–1.52 (m, 4H), 1.43 (p, *J* = 5.8 Hz, 2H).

^{13}C-NMR (101 MHz, $CDCl_3$): δ 171.4, 140.9, 133.9, 129.2, 124.7, 118.8, 116.0, 93.1, 78.1, 67.8, 51.6, 51.2, 26.5, 24.6, 20.5.

HRMS (ESI): Calculated for $C_{17}H_{21}N_4O_2$ $[M+H]^+$: 313.1665; found: *m/z* 313.1675.



2.113

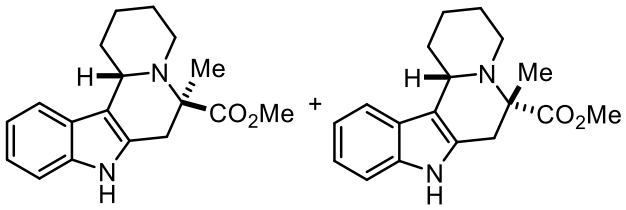
Prepared from methyl 2-methyl-2-(piperidin-1-yl)pent-4-ynoate (234 mg, 1.12 mmol) and 1-azido-2-iodobenzene (301 mg, 1.23 mmol) following GP3. Purification over silica (eluent: EtOAc/Hexanes). Arylazide **2.113** was obtained as a yellow oil: 256.8 mg, 70% yield.

^{1}H-NMR (400 MHz, $CDCl_3$): δ 7.35 (dd, *J* = 7.7, 1.2 Hz, 1H), 7.31–7.25 (m, 1H), 7.10–7.02 (m, 2H), 3.74 (s, 3H), 2.98 (d, *J* = 16.6 Hz, 1H), 2.81 (d, *J* = 16.6 Hz, 1H), 2.55 (hept, *J* = 6.0, 5.5 Hz, 4H), 1.58 (p, *J* = 5.5 Hz, 4H), 1.51 (s, 3H), 1.43 (p, *J* = 5.9, 5.4 Hz, 2H).

^{13}C-NMR (100 MHz, $CDCl_3$): δ 173.7, 140.9, 133.9, 129.0, 124.6, 118.7, 116.1, 93.2, 78.8, 66.8, 51.8, 48.4, 27.7, 26.9, 24.8, 19.8.

IR (ATR): ῡ 2981 (w), 2931 (m), 2850 (w) 2807 (w), 2125 (s), 2093 (s), 1723 (s), 1594 (w), 1569 (w), 1487 (m), 1438 (m), 1374 (w), 1294 (s), 1210 (s), 1162 (m), 1095 (s), 1062 (w), 1032 (w), 980 (w), 960 (w), 921 (w), 858 (w), 822 (w), 749 (s) cm^{-1}.

HRMS (ESI): Calculated for $C_{18}H_{23}N_4O_2$ $[M+H]^+$: 327.1815; found: *m/z* 327.1824.



2.113a **2.113b**

Prepared from arylazide **2.113** (32.7 mg, 0.10 mmol) following GP8 with 10 mol% catalyst and at 100 °C. Reaction time: 5 hr. Overall NMR-yield[g] = 37% and *d.r.* = 4:1. Purification over silica (eluent: EtOAc/Hexanes). Major diastereoisomer **2.113a** was obtained as a yellow solid: 8.3 mg, 28% yield. An analytical sample of the minor diastereoisomer **2.113b** was unable to be obtained after purification.

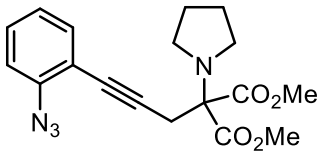
^{1}H-NMR (400 MHz, $CDCl_3$): δ 7.79 (bs, 1H), 7.50 (d, *J* = 7.8 Hz, 1H), 7.27 (d, *J* = 8.2 Hz, 1H), 7.09 (td, *J* = 7.5, 7.5, 1.1 Hz, 1H), 7.04 (td, *J* = 7.5, 7.1, 1.1 Hz, 1H), 3.91 (d, *J* = 10.7 Hz, 1H), 3.53 (s, 3H), 3.37 (d, *J* = 10.7 Hz, 1H), 3.22 (dd, *J* = 15.4, 1.4 Hz, 1H), 2.96 (t, *J* = 10.6 Hz, 1H), 2.89 (d, *J* = 14.6 Hz, 1H), 2.57 (d, *J* = 13.4 Hz, 1H), 1.87–1.81 (m, 1H), 1.76 (d, *J* = 8.7 Hz, 1H), 1.67–1.53 (m, 2H), 1.53 (s, 3H), 1.46–1.36 (m, 1H).

^{13}C-NMR (100 MHz, $CDCl_3$): δ 175.7, 136.4, 131.2, 125.9, 120.9, 119.1, 112.1, 110.9, 62.5, 57.2, 51.5, 47.2, 36.0, 33.7, 27.6, 25.8, 24.9.[h]

IR (ATR): ῡ 2933 (w), 2841 (w), 1727 (s), 1623 (w), 1465 (m), 1451 (m), 1328 (w), 1311 (w), 1270 (m), 1216 (m), 1192 (m), 1167 (m), 1127 (m), 1090 (m), 1056 (w), 1024 (w), 982 (w), 886 (w), 860 (w), 823 (w) cm^{-1}.

HRMS (EI): Calculated for $C_{18}H_{22}N_2O_2$ $[M]^+$: 298.1681; found: *m/z* 298.1678.

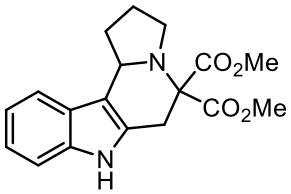
[g]NMR-yield, regioisomeric ratio (*r.r.*), and diastereomeric ratio (*d.r.*) were calculated from the crude ^{1}H-NMR using mesitylene as internal standard.
[h]Carbon signal overlap at 119.1 ppm.



2.114

Prepared from dimethyl 2-(prop-2-yn-1-yl)-2-(pyrrolidin-1-yl)malonate (206 mg, 0.86 mmol) and 1-azido-2-iodobenzene (232 mg, 0.95 mmol) following GP3. Purification over silica (eluent: EtOAc:hexanes). Arylazide **2.114** was obtained as an amber oil: 139 mg, 45% yield.

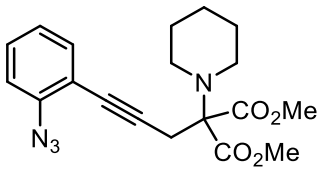
^{1}H-NMR (300 MHz, $CDCl_3$): δ 7.34 (ddd, *J* = 7.7, 1.6, 0.5 Hz, 1H), 7.32–7.26 (m, 1H), 7.09–7.01 (m, 2H), 3.81 (s, 6H), 3.24 (s, 2H), 3.03–2.88 (m, 4H), 1.89–1.74 (m, 4H).
^{13}C-NMR (101 MHz, $CDCl_3$): δ 169.2, 141.0, 134.1, 129.3, 124.6, 118.7, 115.7, 91.3, 79.1, 73.4, 52.6, 48.3, 26.4, 24.3.
HRMS (ESI): Calculated for $C_{18}H_{20}N_4NaO_4$ $[M+Na]^+$: 379.1382; found: *m/z* 379.1375.



2.140

Prepared from arylazide **2.114** (23 mg, 0.06 mmol) following GP8. Reaction time: 21 hr. Purification over silica (eluent: EtOAc:hexanes). Indole **2.140** was obtained as a light orange oil: 9.1 mg, 42% yield.

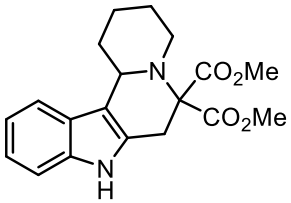
^{1}H-NMR (300 MHz, $CDCl_3$): δ 7.86 (bs, 1H), 7.45 (d, *J* = 7.7 Hz, 1H), 7.31 (d, *J* = 8.0 Hz, 1H), 7.19–7.04 (m, 2H), 4.90–4.82 (m, 1H), 3.86 (s, 3H), 3.69 (s, 3H), 3.55–3.39 (m, 2H), 2.99 (td, *J* = 8.1, 4.2 Hz, 1H), 2.70 (q, *J* = 8.0 Hz, 1H), 2.59–2.46 (m, 1H), 2.13–1.90 (m, 2H), 1.83–1.68 (m, 1H).
^{13}C-NMR (101 MHz, $CDCl_3$): δ 169.5, 169.5, 136.1, 128.7, 125.6, 121.8, 119.6, 118.7, 111.8, 111.0, 71.3, 55.2, 53.6, 53.4, 47.1, 30.1, 24.0, 23.1.
HRMS (EI): Calculated for $C_{18}H_{20}N_2O_4$ $[M]^+$: 328.1423; found: *m/z* 328.1426.



2.103

Prepared from dimethyl 2-(piperidin-1-yl)-2-(prop-2-yn-1-yl)malonate (547 mg, 2.16 mmol) and 1-azido-2-iodobenzene (582 mg, 2.38 mmol) following GP3. Purification over silica (eluent: EtOAc:hexanes). Arylazide **2.103** was obtained as an amber solid: 438 mg, 55% yield.

^{1}H-NMR (300 MHz, $CDCl_3$): δ 7.38–7.27 (m, 2H), 7.11–7.00 (m, 2H), 3.80 (s, 6H), 3.23 (s, 2H), 2.66 (t, *J* = 5.3 Hz, 4H), 1.73–1.57 (m, 4H), 1.46 (p, *J* = 5.5, 4.9 Hz, 2H).
^{13}C-NMR (101 MHz, $CDCl_3$): δ 169.0, 141.0, 134.1, 129.3, 124.7, 118.7, 115.8, 91.3, 79.3, 76.0, 52.6, 49.7, 26.7, 24.9, 24.7.
HRMS (ESI): Calculated for $C_{19}H_{22}N_4NaO_4$ $[M+Na]^+$: 393.1533; found: 393.1534.

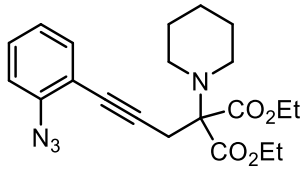


2.104

Prepared from arylazide **2.103** (22.3 mg, 0.06 mmol) following GP8. Reaction time: 1.5 hr. Purification over silica (eluent: EtOAc:hexanes). Indole **2.104** was obtained as a yellow solid: 17.8 mg, 87% yield.

^{1}H-NMR (400 MHz, $CDCl_3$): δ 7.91 (bs, 1H), 7.49 (d, *J* = 7.8 Hz, 1H), 7.28 (d, *J* = 8.0 Hz, 1H), 7.12 (td, *J* = 8.1, 7.6, 1.2 Hz, 1H), 7.06 (td, *J* = 7.5, 1.1 Hz, 1H), 3.98 (d, *J* = 9.1 Hz, 1H), 3.84 (s, 3H), 3.63 (s, 3H), 3.50–3.37 (m, 2H), 3.24 (td, *J* = 11.0, 3.5 Hz, 1H), 2.89 (d, *J* = 11.8 Hz, 1H), 2.54 (d, *J* = 13.3 Hz, 1H), 1.92–1.83 (m, 1H), 1.76–1.46 (m, 4H).
^{13}C-NMR (101 MHz, $CDCl_3$): δ 170.9, 170.5, 136.5, 129.3, 125.6, 121.3, 119.3, 119.1, 111.5, 111.0, 73.6, 56.9, 53.3, 52.2, 51.2, 33.4, 32.5, 27.2, 25.1.
IR (ATR): $\tilde{\nu}$ 3384 (m), 2930 (m), 2848 (m), 1728 (s), 1622 (w), 1431 (m), 1373 (w), 1252 (s), 1193 (s), 1052 (s), 1014 (m), 958 (w), 916 (m), 828 (m), 738 (s) cm^{-1}.

HRMS (EI): Calculated for $C_{19}H_{22}N_2O_4$ $[M]^+$: 342.1579; found: 342.1551.



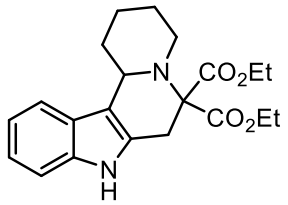
2.116

Prepared from diethyl 2-(piperidin-1-yl)-2-(prop-2-yn-1-yl)malonate (155 mg, 0.56 mmol) and 1-azido-2-iodobenzene (149 mg, 0.61 mmol) following GP3. Purification over silica (eluent: EtOAc:hexanes). Arylazide **2.116** was obtained as a yellow oil: 148 mg, 67% yield.

^{1}H-NMR (300 MHz, $CDCl_3$): δ 7.37–7.25 (m, 2H), 7.09–7.00 (m, 2H), 4.27 (q, *J* = 7.1 Hz, 4H), 3.22 (s, 2H), 2.69 (t, *J* = 5.2 Hz, 4H), 1.65 (p, *J* = 5.6 Hz, 4H), 1.52–1.41 (m, 2H), 1.29 (t, *J* = 7.1 Hz, 6H).

^{13}C-NMR (101 MHz, $CDCl_3$): δ 168.6, 140.9, 134.0, 129.2, 124.7, 118.7, 115.9, 91.6, 79.1, 75.6, 61.6, 49.7, 26.7, 24.8, 24.6, 14.3.

HRMS (ESI): Calculated for $C_{21}H_{26}N_4NaO_4$ $[M+Na]^+$: 421.1852; found: *m/z* 421.1870.



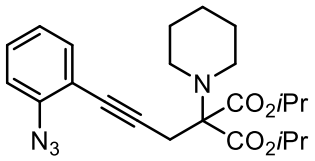
2.142

Prepared from arylazide **2.116** (25 mg, 0.06 mmol) following GP8. Reaction time: 4.5 hr. Purification over silica (eluent: EtOAc:hexanes). Indole **2.142** was obtained as an amber oil: 16.4 mg, 73% yield.

^{1}H-NMR (300 MHz, $CDCl_3$): δ 7.87 (bs, 1H), 7.48 (d, *J* = 7.6 Hz, 1H), 7.31–7.27 (m, 1H), 7.08 (dtd, *J* = 18.5, 7.2, 1.3 Hz, 2H), 4.31 (qd, *J* = 7.2, 2.9 Hz, 2H), 4.09 (qt, *J* = 7.2, 3.7 Hz, 2H), 4.03–3.95 (m, 1H), 3.49–3.36 (m, 2H), 3.30–3.18 (m, 1H), 2.95 (dd, *J* = 11.9, 3.8 Hz, 1H), 2.53 (d, *J* = 12.2 Hz, 1H), 1.94–1.83 (m, 1H), 1.76–1.55 (m, 4H), 1.33 (t, *J* = 7.1 Hz, 3H), 1.15 (t, *J* = 7.1 Hz, 3H).

^{13}C-NMR (101 MHz, $CDCl_3$): δ 170.5, 170.0, 136.5, 129.5, 125.6, 121.2, 119.3, 119.0, 111.6, 111.0, 73.4, 62.2, 61.1, 57.0, 51.2, 33.5, 32.6, 27.3, 25.2, 14.3, 14.2.

HRMS (EI): Calculated for $C_{21}H_{26}N_2O_4$ $[M]^+$: 370.1893; found: *m/z* 370.1880.



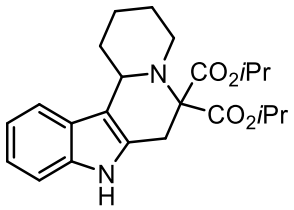
2.118

Prepared from diisopropyl 2-(piperidin-1-yl)-2-(prop-2-yn-1-yl)malonate (282 mg, 0.91 mmol) and 1-azido-2-iodobenzene (268 mg, 1.09 mmol) following GP3. Purification over silica (eluent: EtOAc/Hexanes). Arylazide **2.118** was obtained as an amber solid: 293.6 mg, 76% yield.

^{1}H-NMR (400 MHz, $CDCl_3$): δ 7.34 (dd, *J* = 7.7, 1.5 Hz, 1H), 7.31 – 7.25 (m, 1H), 7.08 – 7.01 (m, 2H), 5.12 (hept, *J* = 6.2 Hz, 2H), 3.20 (s, 2H), 2.70 (bs, 4H), 1.71 – 1.58 (m, 4H), 1.47 (q, *J* = 5.7 Hz, 2H), 1.28 (d, *J* = 1.7 Hz, 6H), 1.26 (d, *J* = 1.7 Hz, 6H).

^{13}C-NMR (100 MHz, $CDCl_3$): δ 168.1, 140.9, 134.0, 129.1, 124.6, 118.7, 116.0, 91.7, 78.9, 75.1, 69.3, 49.6, 26.8, 24.9, 24.7, 21.9, 21.8.

HRMS (ESI): Calculated for $C_{23}H_{30}N_4NaO_4$ $[M+Na]^+$: 449.2165; found: *m/z* 449.2162.



2.144

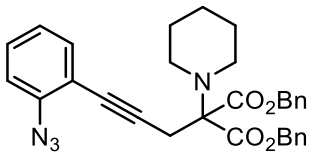
Prepared from arylazide **2.118** (42.7 mg, 0.10 mmol) following GP8. Reaction time: 1.5 hr. Purification over silica (eluent: EtOAc/Hexanes). Indole **2.144** was obtained as orange solid: 27.4 mg, 69% yield.

^{1}H-NMR (400 MHz, $CDCl_3$): δ 7.88 (bs, 1H), 7.48 (d, *J* = 7.7 Hz, 1H), 7.27 (d, *J* = 9.2 Hz, 1H), 7.10 (t, *J* = 7.4 Hz, 1H), 7.04 (t, *J* = 7.4 Hz, 1H), 5.17 (hept, *J* = 6.2 Hz, 1H), 4.92 (hept, *J* = 6.3 Hz, 1H), 3.97 (d, *J* = 10.6 Hz, 1H), 3.38 (s, 2H), 3.27–3.17 (m, 1H), 3.02 (d, *J* = 11.8 Hz, 1H),

2.52 (d, *J* = 11.9 Hz, 1H), 1.88 (d, *J* = 11.3 Hz, 1H), 1.74–1.45 (m, 4H), 1.31 (t, *J* = 6.3 Hz, 6H), 1.20 (d, *J* = 6.2 Hz, 3H), 1.06 (d, *J* = 6.2 Hz, 3H).

^{13}C-NMR (100 MHz, $CDCl_3$): δ 169.9, 169.5, 136.5, 129.8, 125.7, 121.1, 119.2, 118.9, 111.5, 111.0, 73.2, 69.9, 68.7, 57.1, 51.2, 33.6, 32.7, 27.3, 25.4, 22.0, 21.8, 21.7, 21.7.

HRMS (ESI): Calculated for $C_{23}H_{30}N_2NaO_4$ $[M+Na]^+$: 421.2103; found: *m/z* 421.2104.



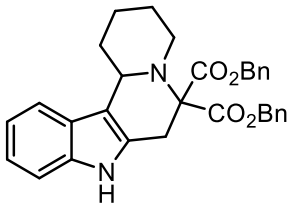
2.117

Prepared from diisopropyl 2-(piperidin-1-yl)-2-(prop-2-yn-1-yl)malonate (361 mg, 0.89 mmol) and 1-azido-2-iodobenzene (262 mg, 1.07 mmol) following GP3. Purification over silica (eluent: EtOAc/Hexanes). Arylazide **2.117** was obtained as a yellow oil: 293.1 mg, 63% yield.

^{1}H-NMR (400 MHz, $CDCl_3$): δ 7.34–7.25 (m, 11H), 7.22 (dd, *J* = 7.7, 1.3 Hz, 1H), 7.08–6.98 (m, 2H), 5.25–5.14 (m, 4H), 3.27 (s, 2H), 2.71–2.62 (m, 4H), 1.60 (p, *J* = 5.7 Hz, 4H), 1.43 (p, *J* = 5.8 Hz, 2H).

^{13}C-NMR (100 MHz, $CDCl_3$): δ 168.4, 141.0, 135.5, 134.1, 129.2, 128.6, 128.4, 128.3, 124.6, 118.6, 115.8, 91.2, 79.4, 75.9, 67.3, 49.6, 26.8, 25.2, 24.7.

HRMS (ESI): Calculated for $C_{31}H_{30}N_4NaO_4$ $[M+Na]^+$: 545.2165; found: *m/z* 545.2175.



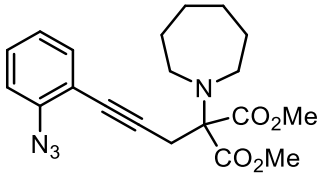
2.143

Prepared from arylazide **2.117** (53.0 mg, 0.10 mmol) following GP8. Reaction time: 4 hr. Purification over silica (eluent: EtOAc/Hexanes). Indole **2.143** was obtained as yellow solid: 33.2 mg, 67% yield.

^{1}H-NMR (400 MHz, $CDCl_3$): δ 7.76 (bs, 1H), 7.47 (d, *J* = 7.8 Hz, 1H), 7.36 (s, 5H), 7.27 (d, *J* = 8.7 Hz, 1H), 7.20–7.10 (m, 2H), 7.11–7.05 (m, 1H), 7.01 (t, *J* = 7.7 Hz, 2H), 6.88 (d, *J* = 7.5 Hz, 2H), 5.30 (d, *J* = 12.2 Hz, 1H), 5.22 (d, *J* = 12.2 Hz, 1H), 5.13 (d, *J* = 12.5 Hz, 1H), 4.94 (d, *J* = 12.5 Hz, 1H), 3.98 (d, *J* = 9.1 Hz, 1H), 3.46 (dd, *J* = 15.0, 2.3 Hz, 1H), 3.39 (d, *J* = 15.0 Hz, 1H), 3.28–3.16 (m, 1H), 2.87 (d, *J* = 11.4 Hz, 1H), 2.49 (d, *J* = 11.9 Hz, 1H), 1.88–1.80 (m, 1H), 1.65–1.46 (m, 4H).

^{13}C-NMR (100 MHz, $CDCl_3$): δ 170.1, 169.5, 136.5, 135.7, 135.2, 129.3, 128.7, 128.6, 128.4, 128.4, 128.0, 127.6, 125.6, 121.3, 119.4, 119.1, 111.8, 111.0, 73.6, 67.7, 66.7, 57.1, 51.2, 33.5, 32.8, 27.2, 25.2.

HRMS (ESI): Calculated for $C_{23}H_{30}N_2NaO_4$ $[M+Na]^+$: 421.2103; found: *m/z* 421.2104



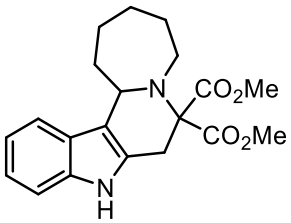
2.115

Prepared from dimethyl 2-(azepan-1-yl)-2-(prop-2-yn-1-yl)malonate (206 mg, 0.77 mmol) and 1-azido-2-iodobenzene (208 mg, 0.85 mmol) following GP3. Purification over silica (eluent: EtOAc:hexanes). Arylazide **2.115** was obtained as a yellow oil: 197 mg, 67% yield.

^{1}H-NMR (300 MHz, $CDCl_3$): δ 7.37 (dd, *J* = 7.6, 1.8 Hz, 1H), 7.32–7.26 (m, 1H), 7.09–7.01 (m, 2H), 3.79 (s, 6H), 3.20 (s, 2H), 2.79 (t, *J* = 5.6 Hz, 4H), 1.72–1.56 (m, 8H).

^{13}C-NMR (101 MHz, $CDCl_3$): δ 170.0, 140.9, 134.0, 129.2, 124.7, 118.7, 115.9, 91.5, 79.1, 52.5, 51.4, 29.9, 26.9 (2C).

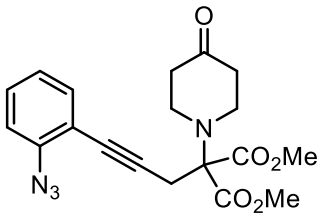
HRMS (ESI): Calculated for $C_{20}H_{24}N_4NaO_4$ $[M+Na]^+$: 407.1695; found: 407.1689.



2.141

Prepared from arylazide **2.115** (24 mg, 0.06 mmol) following GP8. Reaction time: 21 hr. Purification over silica (eluent: EtOAc:hexanes). Indole **2.141** was obtained as a yellow solid: 14.9 mg, 67% yield.

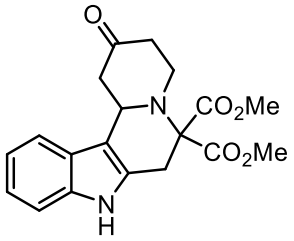
^{1}H-NMR (300 MHz, $CDCl_3$): δ 7.86 (bs, 1H), 7.47 (d, *J* = 7.6 Hz, 1H), 7.29 (d, *J* = 7.5 Hz, 1H), 7.09 (dtd, *J* = 18, 7.2, 1.3 Hz, 2H), 4.21–4.11 (bs, 1H), 3.84 (s, 3H), 3.60 (s, 3H), 3.47–3.32 (m, 2H), 3.10–2.93 (m, 2H), 2.64–2.48 (m, 1H), 1.87–1.51 (m, 7H).
^{13}C-NMR (101 MHz, $CDCl_3$): δ 171.0, 170.8, 136.5, 129.5, 125.8, 121.3, 119.4, 119.1, 113.2, 111.0, 75.2, 59.2, 53.1, 52.8, 52.5, 38.4, 31.4, 29.1, 27.5, 24.4.
HRMS (EI): Calculated for $C_{20}H_{24}N_2O_4$ $[M]^+$: 356.1736; found: 356.17369.



2.122

Prepared from dimethyl 2-(4-oxopiperidin-1-yl)-2-(prop-2-yn-1-yl)malonate (82.4 mg, 0.31 mmol) and 1-azido-2-iodobenzene (83.2 mg, 0.34 mmol) following GP3. Purification over silica (eluent: EtOAc:hexanes). Arylazide **2.122** was obtained as an amber oil: 54.3 mg, 46% yield.

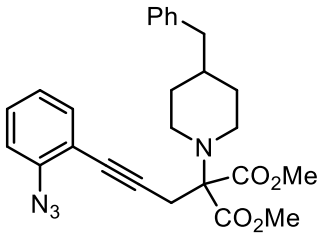
^{1}H-NMR (400 MHz, $CDCl_3$): δ 7.37–7.27 (m, 2H), 7.11–7.02 (m, 2H), 3.82 (s, 6H), 3.31 (s, 2H), 3.05 (t, *J* = 5.9 Hz, 4H), 2.55 (t, *J* = 5.8 Hz, 4H).
^{13}C-NMR (100 MHz, $CDCl_3$): δ 208.8, 168.7, 141.1, 134.0, 129.6, 124.8, 118.8, 115.3, 89.9, 79.8, 74.6, 52.9, 48.1, 42.3, 25.5.
HRMS (ESI): Calculated for $C_{19}H_{20}N_4NaO_5$ $[M+Na]^+$: 407.1331; found: *m/z* 407.1339.



2.148

Prepared from arylazide **2.122** (12.4 mg, 0.032 mmol) following GP8. Reaction time: 4.5 hr. Purification over silica (eluent: EtOAc:hexanes). Indole **2.148** was obtained as a yellow solid: 6.9 mg, 62% yield.

^{1}H-NMR (300 MHz, $CDCl_3$): δ 7.95 (bs, 1H), 7.43 (d, *J* = 7.8 Hz, 1H), 7.32 (d, *J* = 8.1 Hz, 1H), 7.13 (dtd, *J* = 21.5, 7.2, 1.2 Hz, 2H), 4.31 (dd, *J* = 11.5, 2.6 Hz, 1H), 3.89 (s, 3H), 3.63 (s, 3H), 3.58–3.46 (m, 3H), 3.27–3.15 (m, 2H), 2.71 (td, *J* = 13.6, 13.0, 6.7 Hz, 1H), 2.57–2.41 (m, 2H).
^{13}C-NMR (101 MHz, $CDCl_3$): δ 208.6, 170.5, 170.0, 136.4, 129.2, 124.8, 121.9, 120.0, 118.7, 111.2, 110.0, 72.9, 55.6, 53.6, 52.6, 49.4, 49.2, 43.0, 32.7.
HRMS (EI): Calculated for $C_{19}H_{20}N_2O_5$ $[M]^+$: 356.1372; found: *m/z* 356.1375.

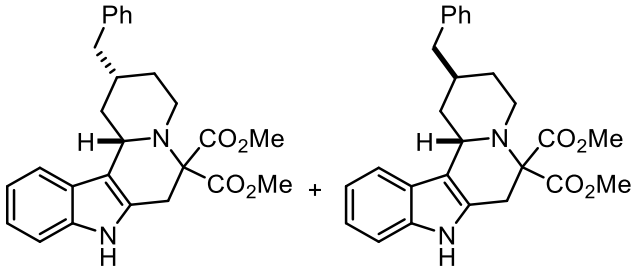


2.123

Prepared from dimethyl 2-(4-benzylpiperidin-1-yl)-2-(prop-2-yn-1-yl)malonate (198 mg, 0.58 mmol) and 1-azido-2-iodobenzene (157 mg, 0.63 mmol) following GP3. Purification over silica (eluent: EtOAc:hexanes). Arylazide **2.123** was obtained as an amber oil: 232 mg, 87% yield.

^{1}H-NMR (300 MHz, $CDCl_3$): δ 7.35–7.28 (m, 2H), 7.27–7.23 (m, 2H), 7.21–7.01 (m, 5H), 3.79 (s, 6H), 3.22 (s, 2H), 3.03 (d, *J* = 11.2 Hz, 2H), 2.53 (d, *J* = 6.6 Hz, 2H), 2.30 (t, *J* = 11.1 Hz, 2H), 1.65 (d, *J* = 13.2 Hz, 2H), 1.60–1.50 (m, 1H), 1.43 (td, *J* = 11.7, 3.6 Hz, 2H).
^{13}C-NMR (101 MHz, $CDCl_3$): δ 169.0, 141.0, 140.8, 134.0, 129.3, 129.2, 128.3, 125.9, 124.7, 118.7, 115.7, 91.2, 79.3, 75.7, 52.6, 48.9, 43.2, 38.1, 32.8, 24.8.

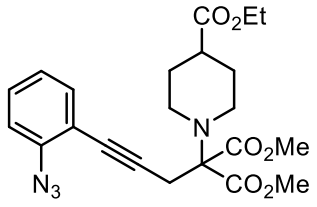
HRMS (ESI): Calculated for $C_{26}H_{28}N_4NaO_4$ $[M+Na]^+$: 483.2008; found: *m/z* 483.2026.



2.149a **2.149b**

Prepared from arylazide **2.123** (29.7 mg, 0.065 mmol) following GP8. Reaction time: 1 hr. Overall NMR-yield = 76% and *d.r.* = 10:1. Purification over silica (eluent: Et_2O:hexanes). *Anti*-diastereoisomer **2.149a** was obtained as an off-white solid: 18 mg, 65% yield. An analytical sample of *syn*-diastereoisomer **2.149b** was unable to obtained after purification.

^{1}H-NMR (300 MHz, $CDCl_3$): δ 7.83 (bs, 1H), 7.37 (d, *J* = 7.8 Hz, 1H), 7.34–7.00 (m, 8H), 3.95 (dd, *J* = 11.2, 2.3 Hz, 1H), 3.84 (s, 3H), 3.61 (s, 3H), 3.51–3.38 (m, 2H), 3.21 (td, *J* = 12.0, 2.3 Hz, 1H), 2.88 (dt, *J* = 11.8, 3.5 Hz, 1H), 2.72–2.48 (m, 3H), 1.96 (ddd, *J* = 11.5, 7.5, 4.0 Hz, 1H), 1.69 (d, *J* = 12.9 Hz, 1H), 1.47–1.27 (m, 2H).
^{13}C-NMR (101 MHz, $CDCl_3$): δ 170.9, 170.4, 140.7, 136.5, 129.3, 129.3, 128.3, 126.0, 125.5, 121.3, 119.4, 119.0, 111.4, 111.0, 73.3, 56.3, 53.3, 52.2, 50.6, 43.5, 39.8, 38.8, 33.3, 32.7.
HRMS (EI): Calculated for $C_{26}H_{28}N_2O_4$ $[M]^+$: 432.2049; found: *m/z* 432.2063.



2.124

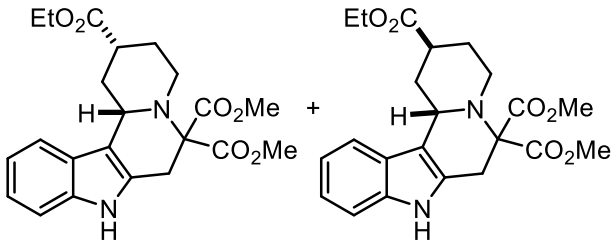
Prepared from dimethyl 2-(4-(ethoxycarbonyl)piperidin-1-yl)-2-(prop-2-yn-1-yl)malonate (331 mg, 1.02 mmol) and 1-azido-2-iodobenzene (299 mg, 1.22 mmol) following GP3. Purification over silica (eluent: EtOAc/Hexanes). Arylazide **2.124** was obtained as an orange oil: 276 mg, 61% yield.

^{1}H-NMR (400 MHz, $CDCl_3$): δ 7.34 (dd, *J* = 7.7, 1.5 Hz, 1H), 7.29 (td, *J* = 7.8, 1.6 Hz, 1H), 7.10–7.01 (m, 2H), 4.11 (q, *J* = 7.1 Hz, 2H), 3.79 (s, 6H), 3.23 (s, 2H), 3.07 (dt, *J* = 10.8, 3.4 Hz, 2H), 2.40 (td, *J* = 11.3, 2.7 Hz, 2H), 2.31 (tt, *J* = 10.9, 4.4 Hz, 1H), 1.98–1.77 (m, 4H), 1.23 (t, *J* = 7.1 Hz, 3H).

^{13}C-NMR (100 MHz, $CDCl_3$): δ 175.0, 168.9, 141.0, 134.0, 129.3, 124.7, 118.7, 115.6, 90.7, 79.4, 75.4, 60.4, 52.7, 48.1, 41.4, 28.9, 25.1, 14.3.

IR (ATR): ῡ 2951 (w), 2126 (m), 2095 (m), 1724 (s), 1569 (w), 1487 (m), 1438 (m), 1378 (w), 1290 (m), 1254 (m), 1232 (m), 1199 (m), 1173 (m), 1142 (m), 1096 (w), 1041 (m), 941 (w), 860 (w), 812 (w), 750 (s) cm^{-1}.

HRMS (ESI): Calculated for $C_{22}H_{26}N_4NaO_6$ $[M+Na]^+$: 465.1750; found: *m/z* 465.1726.



2.150a **2.150b**

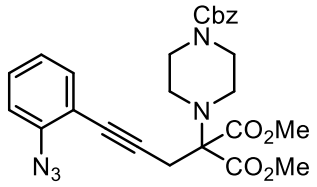
Prepared from arylazide **2.124** (44.3 mg, 0.10 mmol) following GP8. Reaction time: 4 hr. Overall NMR-yield = 81% and *d.r.* = 3:1. Purification over silica (eluent: EtOAc/Hexanes). The mixture of diastereoisomers **2.150a,b** (30 mg, 72% isolated yield) were obtained as a yellow solid.

^{1}H-NMR (400 MHz, $CDCl_3$): δ 7.96 (s, 1H), 7.56 (d, *J* = 7.7 Hz, 1H, **2.150b**), 7.51 (d, *J* = 7.8 Hz, 1H), 7.29 (d, *J* = 8.4 Hz, 1H), 7.13 (ddd, *J* = 8.1, 7.1, 1.3 Hz, 1H), 7.08 (ddd, *J* = 8.1, 7.1, 1.2 Hz, 1H), 4.28 (dddd, *J* = 17.9, 10.8, 7.1, 3.7 Hz, 2H, **2.150b**), 4.13 (q, *J* = 7.1 Hz, 2H), 4.01 (dt, *J* = 11.3, 2.1 Hz, 1H), 3.85 (s, 3H), 3.84 (s, 3H, **2.150b**), 3.62 (s, 3H, **2.150b**), 3.62 (s, 3H), 3.50–3.38 (m, 2H), 3.29 (td, *J* = 12.1, 2.5 Hz, 1H), 2.96 (ddd, *J* = 11.8, 4.2, 2.8 Hz, 1H), 2.84–2.77 (m, 1H), 2.70 (tt, *J* = 12.4, 4.0 Hz, 1H), 2.20 (d, *J* = 13.6 Hz, 1H, **2.150b**), 2.00 (ddd, *J* = 12.9, 4.4, 2.3 Hz, 1H), 1.86 (td, *J* = 12.5, 4.2 Hz, 1H), 1.65 (td, *J* = 12.7, 11.2 Hz, 1H), 1.36 (t, *J* = 7.1 Hz, 3H, **2.150b**), 1.24 (t, *J* = 7.1 Hz, 3H).

^{13}C-NMR (100 MHz, $CDCl_3$): δ 174.9, 174.8, 170.7, 170.5, 170.4, 136.5, 129.6, 129.4, 125.5, 125.3, 121.5, 119.6, 119.5, 118.9, 111.1, 110.6, 110.3, 73.4, 73.2, 60.6, 60.5, 55.9, 53.6, 53.3, 52.5, 52.3, 50.0, 47.4, 42.4, 38.3, 35.7, 34.0, 32.6, 29.6, 28.2, 14.6, 14.4.[i]

IR (ATR): ῡ 3390 (w), 2951 (w), 2841 (w), 1724 (s), 1624 (w), 1456 (m), 1433 (m), 1374 (w), 1329 (w), 1248 (s), 1178 (s), 1157 (m), 1093 (w), 1048 (m), 1030 (m), 962 (w), 917 (w), 892 (w), 858 (w), 802 (w), 775 (w), 744 (s), 693 (w) cm^{-1}.

HRMS (EI): Calculated for $C_{22}H_{26}N_2O_6$ $[M]^+$: 414.1791; found: *m/z* 414.1790.



2.121

Prepared from dimethyl 2-(4-((benzyloxy)carbonyl)piperazin-1-yl)-2-(prop-2-yn-1-yl)malonate (394 mg, 1.01 mmol) and 1-azido-2-iodobenzene (273 mg, 1.12 mmol) following GP3. Purification over silica (eluent: EtOAc/Hexanes). Arylazide **2.121** was obtained as an orange/brown oil: 338.6 mg, 66% yield.

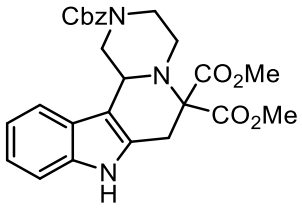
^{1}H-NMR (400 MHz, $CDCl_3$): δ 7.39–7.28 (m, 7H), 7.10–7.02 (m, 2H), 5.13 (s, 2H), 3.80 (s, 6H), 3.64–3.55 (m, 4H), 3.25 (s, 2H), 2.74 (bs, 4H).

^{13}C-NMR (100 MHz, $CDCl_3$): δ 168.5, 155.3, 141.1, 136.8, 134.0, 129.5, 128.6, 128.1, 128.0, 124.7, 118.7, 115.4, 90.0, 79.7, 74.7, 67.3, 52.8, 48.2, 44.5, 24.9.

IR (ATR): ῡ 2950 (w), 2832 (s), 2126 (s), 2095 (s), 1728 (s), 1695 (s), 1569 (w), 1487 (m), 1429 (s), 1361 (w), 1286 (m), 1222 (s), 1144 (m), 1114 (m), 1025 (m), 969 (m), 912 (w), 912 (w), 860 (w), 749 (s) cm^{-1}.

HRMS (ESI): Calculated for $C_{26}H_{28}N_5NaO_6$ $[M+Na]^+$: 528.1853; found: *m/z* 528.1870.

[i]Some carbon signals of compound **2.150b** are missing due to overlap.



2.147

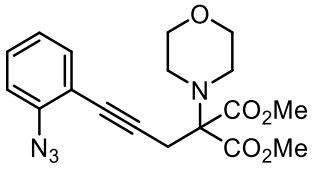
Prepared from arylazide **2.121** (50.3 mg, 0.10 mmol) following GP8. Reaction time: 4 hr. Purification over silica (eluent: EtOAc/Hexanes). Indole **2.147** was obtained as a yellow solid: 37 mg, 78% yield.

^{1}H-NMR (400 MHz, $CDCl_3$): δ 8.12 (bs, 1H), 7.67–7.28 (m, 7H), 7.19–7.11 (td, *J* = 7.5, 1.0 Hz, 1H), 7.06 (bs, 1H), 5.38–5.15 (m, 2H), 4.90 (dd, *J* = 35.2, 13.4 Hz, 1H), 4.27–3.97 (m, 2H), 3.85 (s, 3H), 3.63 (s, 3H), 3.47 (d, *J* = 1.8 Hz, 2H), 3.36 (t, *J* = 11.4 Hz, 1H), 3.12 (d, *J* = 12.2 Hz, 1H), 2.85 (bs, 2H).

^{13}C-NMR (100 MHz, $CDCl_3$): δ 170.1 (2C), 155.3, 136.9, 136.4, 130.4, 130.2, 128.6, 128.2, 128.0, 125.0, 121.7, 119.8, 119.0, 118.4, 111.2, 107.3, 72.7, 67.4, 55.9, 53.4, 52.5, 50.0, 49.5, 45.1, 32.5.

IR (ATR): ῡ 3390 (m), 2954 (w), 2852 (w), 1719 (s), 1694 (s), 1494 (w), 1454 (m), 1430 (s), 1356 (w), 1316 (w), 1301 (w), 1269 (m), 1255 (m), 1217 (s), 1178 (w), 1162 (w), 1112 (m), 1068 (w), 1046 (m), 995 (w), 962 (w), 902 (w), 862 (w), 846 (w), 802 (w), 704 (m) cm^{-1}.

HRMS (EI): Calculated for $C_{26}H_{27}N_3O_6$ $[M]^+$: 477.1900; found: *m/z* 477.1892.



2.119

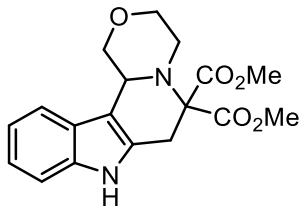
Prepared from dimethyl 2-morpholino-2-(prop-2-yn-1-yl)malonate (177 mg, 0.69 mmol) and 1-azido-2-iodobenzene (204 mg, 0.83 mmol) following GP3. Purification over silica (eluent: EtOAc/Hexanes). Arylazide **2.119** was obtained as an orange/brown oil: 150.8 mg, 58% yield.

^{1}H-NMR (400 MHz, $CDCl_3$): δ 7.35 (dd, *J* = 7.7, 1.4 Hz, 1H), 7.30 (td, *J* = 8.1, 1.5 Hz, 1H), 7.10–7.02 (m, 2H), 3.81 (s, 6H), 3.80–3.76 (m, 4H), 3.24 (s, 2H), 2.80–2.73 (m, 4H).

^{13}C-NMR (100 MHz, $CDCl_3$): δ 168.5, 141.0, 134.0, 129.4, 124.7, 118.7, 115.5, 90.2, 79.6, 74.7, 67.6, 52.7, 48.8, 24.7.

IR (ATR): ῡ 2952 (w), 2862 (w), 2833 (w), 2128 (s), 2093 (s), 1750 (s), 1719 (s), 1567 (w), 1484 (m), 1437 (s), 1301 (m), 1268 (m), 1238 (s), 1200 (s), 1179 (m), 1144 (m), 1112 (m), 1079 (w), 1051 (m), 1020 (w), 938 (m), 856 (m), 810 (w), 642 (s) cm^{-1}.

HRMS (ESI): Calculated for $C_{18}H_{20}N_4NaO_5$ $[M+Na]^+$: 395.1326; found: *m/z* 395.1352.



2.145

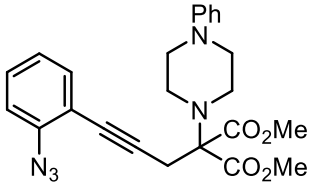
Prepared from arylazide **2.119** (37.3 mg, 0.10 mmol) following GP8. Reaction time: 24 hr. Purification over silica (eluent: EtOAc/Hexanes). Indole **2.145** was obtained as a yellow solid: 25.8 mg, 75% yield.

^{1}H-NMR (400 MHz, $CDCl_3$): δ 8.13 (bs, 1H), 7.44 (d, *J* = 7.7 Hz, 1H), 7.29 (d, *J* = 7.9 Hz, 1H), 7.14 (td, *J* = 7.6, 1.2 Hz, 1H), 7.08 (td, *J* = 7.4, 1.2 Hz, 1H), 4.59 (dd, *J* = 10.9, 2.6 Hz, 1H), 4.25 (dd, *J* = 9.9, 2.1 Hz, 1H), 3.93 (d, *J* = 10.6 Hz, 1H), 3.85 (s, 3H), 3.77 (td, *J* = 11.2, 2.5 Hz, 1H), 3.68 (s, 3H), 3.54 (td, *J* = 11.7, 3.1 Hz, 1H), 3.51–3.42 (m, 3H), 2.77 (d, *J* = 11.7 Hz, 1H).

^{13}C-NMR (100 MHz, $CDCl_3$): δ 170.2, 170.1, 136.3, 130.4, 125.1, 121.6, 119.8, 118.7, 111.2, 106.4, 72.3, 72.0, 68.1, 56.2, 53.4, 52.4, 49.9, 32.4.

IR (ATR): ῡ 3350 (m), 2850 (w), 2804 (w), 1754 (s), 1718 (s), 1495 (w), 1456 (m), 1427 (m), 1330 (w), 1275 (m), 1251 (m), 1239 (m), 1211 (m), 1147 (w), 1115 (s), 1065 (m), 1049 (m), 981 (m), 953 (m), 935 (w), 892 (m), 868 (w), 848 (w), 771 (w), 717 (w) cm^{-1}.

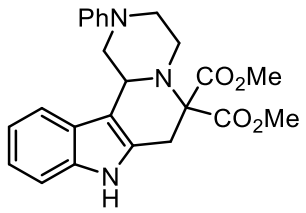
HRMS (EI): Calculated for $C_{18}H_{20}N_2O_5$ $[M]^+$: 344.1372; found: *m/z* 344.1380.



2.120

Prepared from dimethyl 2-(4-phenylpiperazin-1-yl)-2-(prop-2-yn-1-yl)malonate (312 mg, 0.94 mmol) and 1-azido-2-iodobenzene (278 mg, 1.13 mmol) following GP3. Purification over silica (eluent: EtOAc/Hexanes). Arylazide **2.120** was obtained as an orange oil: 214.8 mg, 51% yield.

^{1}H-NMR (400 MHz, $CDCl_3$): δ 7.35 (dd, *J* = 7.7, 1.3 Hz, 1H), 7.32–7.22 (m, 3H), 7.10–7.01 (m, 2H), 6.93 (d, *J* = 7.9 Hz, 2H), 6.86 (t, *J* = 7.3 Hz, 1H), 3.83 (s, 6H), 3.30 (s, 2H), 3.29–3.25 (m, 4H), 2.97–2.91 (m, 4H).
^{13}C-NMR (100 MHz, $CDCl_3$): δ 168.6, 151.4, 141.0, 134.1, 129.4, 129.2, 124.7, 119.9, 118.7, 116.2, 115.5, 90.3, 79.6, 74.8, 52.7, 49.9, 48.3, 24.9.
IR (ATR): ῡ 2950 (w), 2826 (w), 2125 (s), 2094 (s), 1726 (s), 1597 (m), 1488 (s), 1436 (m), 1385 (w), 1291 (m), 1271 (m), 1231 (s), 1203 (m), 1144 (s), 1096 (w), 1047 (m), 1023 (m), 990 (w), 939 (w), 842 (w), 813 (w), 749 (s) cm^{-1}.
HRMS (ESI): Calculated for $C_{24}H_{25}N_5NaO_4$ $[M+Na]^+$: 470.1804; found: *m/z* 470.1789.



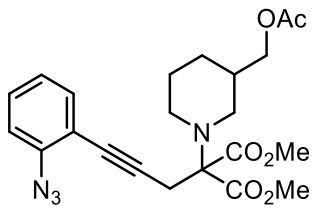
2.146

Prepared from arylazide **2.120** (45.4 mg, 0.10 mmol) following GP8. Reaction time: 24 hr. Purification over silica (eluent: EtOAc/Hexanes). Indole **2.146** was obtained as a yellow solid: 22.9 mg, 55% yield.

^{1}H-NMR (400 MHz, $CDCl_3$): δ 8.04 (bs, 1H), 7.56 (d, *J* = 7.5 Hz, 1H), 7.36–7.27 (m, 3H), 7.20–7.10 (m, 2H), 7.03 (d, *J* = 8.2 Hz, 2H), 6.90 (t, *J* = 7.3 Hz, 1H), 4.38 (d, *J* = 11.4 Hz, 1H), 4.31 (dd, *J* = 10.1, 2.0 Hz, 1H), 3.88 (s, 3H), 3.72–3.55 (m, 5H), 3.50 (s, 2H), 3.06–2.96 (m, 2H), 2.77 (t, *J* = 10.8 Hz, 1H).
^{13}C-NMR (100 MHz, $CDCl_3$): δ 170.4, 170.3, 151.4, 136.5, 130.4, 129.3, 125.2, 121.6, 120.0, 119.8, 118.7, 116.5, 111.3, 108.1, 72.6, 55.7, 55.3, 53.4, 52.4, 50.7, 49.6, 32.6.

IR (ATR): ῡ 3389 (w), 3339 (w), 2951 (w), 1725 (s), 1708 (s), 1599 (m), 1499 (m), 1456 (m), 1431 (m), 1369 (w), 1257 (m), 1221 (s), 1191 (m), 1130 (w), 1054 (m), 1042 (m), 999 (w), 960 (m), 927 (m), 844 (w), 802 (w) cm^{-1}.

HRMS (EI): Calculated for $C_{24}H_{25}N_3O_4$ $[M]^+$: 419.1845; found: *m/z* 419.1848.



2.132

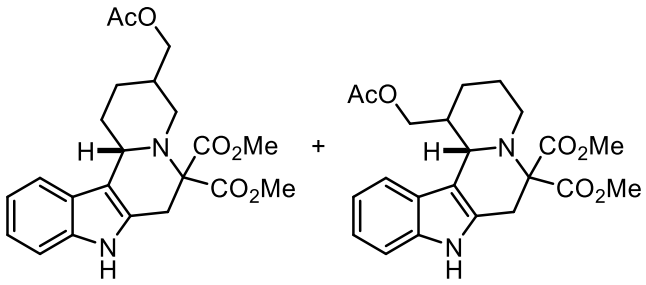
Prepared from dimethyl 2-(3-(acetoxymethyl)piperidin-1-yl)-2-(prop-2-yn-1-yl)malonate (352 mg, 1.08 mmol) and 1-azido-2-iodobenzene (318 mg, 1.30 mmol) following GP3. Purification over silica (eluent: EtOAc/Hexanes). Arylazide **2.132** was obtained as an orange oil: 197.2 mg, 44% yield.

^{1}H-NMR (400 MHz, $CDCl_3$): δ 7.35 (dd, *J* = 7.7, 1.4 Hz, 1H), 7.29 (td, *J* = 8.2, 1.5 Hz, 1H), 7.10–7.01 (m, 2H), 4.03 (dd, *J* = 10.9, 5.8 Hz, 1H), 3.94 (dd, *J* = 10.9, 7.6 Hz, 1H), 3.80 (s, 6H), 3.23 (d, *J* = 1.0 Hz, 2H), 3.00 (d, *J* = 10.9 Hz, 1H), 2.88 (dt, *J* = 11.0, 4.2 Hz, 1H), 2.42 (td, *J* = 9.5, 2.5 Hz, 1H), 2.26 (dd, *J* = 10.5, 9.2 Hz, 1H), 2.11–1.95 (m, 4H), 1.79–1.54 (m, 4H).

^{13}C-NMR (100 MHz, $CDCl_3$): δ 171.2, 169.0, 168.9, 140.9, 134.1, 129.3, 124.7, 118.7, 115.6, 90.7, 79.4, 75.5, 67.0, 52.6 (2C), 52.0, 49.2, 36.2, 27.3, 25.3, 25.0, 21.0.

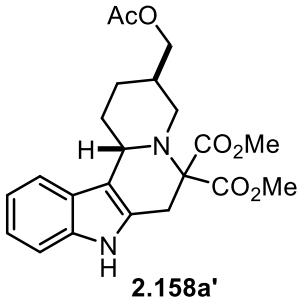
IR (ATR): ῡ 2947 (w), 2849 (w), 2126 (m), 2095 (m), 1726 (s), 1569 (w), 1487 (m), 1437 (m), 1364 (w), 1292 (m), 1231 (s), 1177 (m), 1116 (w), 1032 (m), 987 (w), 857 (w), 816 (w), 751 (s) cm^{-1}.

HRMS (ESI): Calculated for $C_{22}H_{26}N_4NaO_6$ $[M+Na]^+$: 465.1750; found: *m/z* 465.1754.



2.158a **2.158b**

Prepared from arylazide **2.132** (44.6 mg, 0.10 mmol) following GP8. Reaction time: 1.5 hr. Overall NMR-yield = 78%, *r.r.* = 1.6:1, *d.r.* (**2.158a**) = 2:1, and *d.r.* (**2.158b**) = 1.5:1. Purification over silica (eluent: EtOAc/Hexanes). Overall mass obtained was 30.3 mg (72% isolated yield). Purification was difficult and only an analytical sample of the major regioisomeric *syn*-diastereoisomer **2.158a'** (yellow solid) was able to be obtained for characterization.



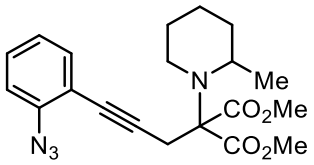
2.158a'

^{1}H-NMR (400 MHz, $CDCl_3$): δ 7.88 (bs, 1H), 7.47 (d, *J* = 7.8 Hz, 1H), 7.30 (d, *J* = 7.9 Hz, 1H), 7.13 (td, *J* = 7.2, 1.2 Hz, 1H), 7.07 (td, *J* = 7.6, 1.1 Hz, 1H), 4.01 (dd, *J* = 11.0, 5.4 Hz, 1H), 3.93 (dq, *J* = 10.9, 2.0 Hz, 1H), 3.91–3.80 (m, 4H), 3.62 (s, 3H), 3.45 (s, 2H), 3.03–2.93 (m, 2H), 2.60 (dq, *J* = 9.5, 3.0 Hz, 1H), 2.13–1.98 (m, 4H), 1.92 (dd, *J* = 12.5, 3.1 Hz, 1H), 1.56–1.47 (m, 1H), 1.40 (qd, *J* = 13.3, 12.8, 3.7 Hz, 1H).

^{13}C-NMR (100 MHz, $CDCl_3$): δ 171.2, 170.8, 170.5, 136.5, 129.2, 125.5, 121.4, 119.5, 118.9, 111.1 (2C), 73.4, 67.3, 56.7, 54.2, 53.2, 52.3, 37.3, 32.6, 28.2, 21.0.[j]

HRMS (EI): Calculated for $C_{22}H_{26}N_2O_6$ $[M]^+$: 414.1791; found: *m/z* 414.1784.

[j]One carbon signal is missing due to peak overlap at 32.6 ppm.



2.125

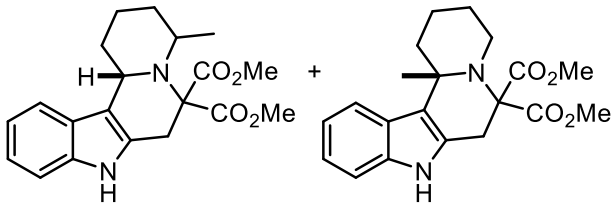
Prepared from dimethyl 2-(2-methylpiperidin-1-yl)-2-(prop-2-yn-1-yl)malonate (273 mg, 1.02 mmol) and 1-azido-2-iodobenzene (300 mg, 1.23 mmol) following GP3. Purification over silica (eluent: EtOAc/Hexanes). Arylazide **2.125** was obtained as an orange oil: 234.6 mg, 60% yield.

^{1}H-NMR (400 MHz, $CDCl_3$): δ 7.37 (dd, *J* = 7.6, 1.5 Hz, 1H), 7.29 (ddd, *J* = 8.9, 7.8, 1.6 Hz, 1H), 7.10–7.02 (m, 2H), 3.77 (s, 3H), 3.77 (s, 3H), 3.56–3.44 (m, 1H), 3.29 (d, *J* = 17.4 Hz, 1H), 3.19 (d, *J* = 17.4 Hz, 1H), 2.88 (td, *J* = 11.7, 10.8, 3.3 Hz, 1H), 2.79 (dt, *J* = 12.6, 3.5 Hz, 1H), 1.85 (tt, *J* = 12.3, 5.9 Hz, 1H), 1.68–1.47 (m, 4H), 1.44 (d, *J* = 13.3 Hz, 1H), 1.00 (d, *J* = 6.7 Hz, 3H).

^{13}C-NMR (100 MHz, $CDCl_3$): δ 170.9, 170.8, 140.9, 134.2, 129.2, 124.7, 118.7, 115.8, 91.1, 79.2, 74.7, 52.8, 52.2, 48.3, 43.9, 33.4, 27.1, 26.3, 19.4, 12.3.

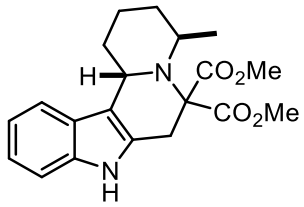
IR (ATR): ῡ 2933 (m), 2848 (w), 2126 (s), 2093 (s), 1725 (s), 1569 (w), 1487 (m), 1437 (m), 1373 (w), 1299 (m), 1225 (s), 1195 (s), 1162 (s), 1140 (m), 1097 (m), 1040 (m), 992 (w), 964 (w), 863 (w), 82. (w), 749 (s) cm^{-1}.

HRMS (ESI): Calculated for $C_{20}H_{24}N_4NaO_4$ $[M+Na]^+$: 407.1695; found: *m/z* 407.1673.



2.151a **2.151b**

Prepared from arylazide **2.125** (38.8 mg, 0.10 mmol) following GP8. Reaction time: 4 hr. Overall NMR-yield = 72%, *r.r.* = 4.5:1, and *d.r.* (**2.151a**) = 1.3:1. Purification over silica (eluent: EtOAc/Hexanes). Overall mass obtained was 23.8 mg (66% isolated yield). Analytical samples of the major *syn*-diastereoisomer **2.151a'** (yellow solid) and an inseparable mixture of the minor *anti*-diastereoisomer **2.151a''** and minor regioisomer **2.151b** were obtained for characterization.



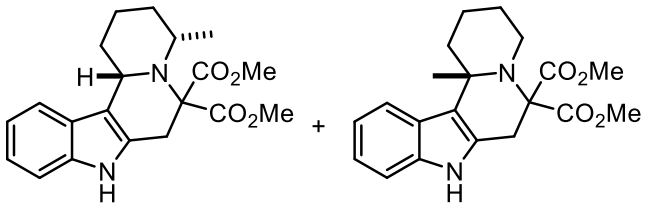
2.151a'

^{1}H-NMR (400 MHz, $CDCl_3$): δ 7.75 (bs, 1H), 7.48 (d, *J* = 7.8 Hz, 1H), 7.27 (d, *J* = 8.4 Hz, 1H), 7.12 (td, *J* = 8.1, 7.6, 1.3 Hz, 1H), 7.06 (td, *J* = 7.6, 1.1 Hz, 1H), 4.70 (d, *J* = 11.1 Hz, 1H), 3.84 (s, 3H), 3.57 (dd, *J* = 14.9, 2.3 Hz, 1H), 3.52 (s, 3H), 3.34 (dd, *J* = 14.9, 1.4 Hz, 1H), 3.22 – 3.12 (m, 1H), 2.44 (d, *J* = 12.2 Hz, 1H), 1.87 (tdd, *J* = 21.8, 9.9, 6.2 Hz, 2H), 1.70–1.46 (m, 2H), 1.41–1.24 (m, 4H).

^{13}C-NMR (100 MHz, $CDCl_3$): δ 171.0, 170.5, 136.4, 129.0, 125.8, 121.2, 119.3, 119.0, 113.2, 110.9, 73.5, 53.0, 52.3, 52.2, 49.3, 34.7, 34.5, 33.9, 19.7, 15.4.

IR (ATR): ῡ 3401 (w), 2931 (w), 2851 (w), 1729 (s), 1456 (m), 1433 (m), 1259 (m), 1227 (s), 1193 (m), 1171 (m), 1139 (m), 1096 (w), 1057 (m), 1029 (m), 966 (w), 899 (w), 740 (s), 713 (w) cm^{-1}.

HRMS (EI): Calculated for $C_{20}H_{24}N_2O_4$ $[M]^+$: 356.1736; found: *m/z* 356.1738.



2.151a'' **2.151b**

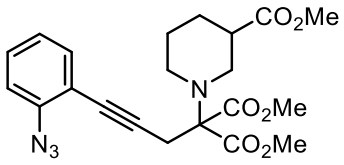
^{1}H-NMR (400 MHz, $CDCl_3$): δ 7.79 (bs, *J* = 4.4 Hz, 2H), 7.50 (d, *J* = 7.9 Hz, 1H, **2.151b**), 7.45 (d, *J* = 7.9 Hz, 1H, **2.151a''**), 7.29 (d x2, *J* = 8.0, 2H), 7.08 (m, 5H), 3.91 (d, *J* = 11.4 Hz, 1H, **2.151a''**), 3.83 (s, 3H, **2.151b**), 3.81 (s, 3H, **2.151a''**), 3.67 (s, 3H, **2.151b**), 3.61 (s, 3H, **2.151a''**), 3.54–3.40 (m, 4H), 3.39–3.29 (m, 1H, **2.151b**), 3.25 (d, *J* = 15.2 Hz, 2H, **2.151b**), 2.85 (dt, *J* = 14.0, 3.6 Hz, 1H, **2.151b**), 2.51 (d, *J* = 14.1 Hz, 1H, **2.151a''**), 2.37 (d, *J* = 11.0 Hz, 1H), 1.93–1.51 (m, 10H), 1.38 (s, 3H, **2.151b**), 1.18 (d, *J* = 6.7 Hz, 3H, **2.151a''**).[k]

[k]HSQC and COSY experiments were performed to corroborate the assignments.

^{13}C-NMR (100 MHz, $CDCl_3$): δ 172.8, 172.3, 172.2, 170.7, 136.6 (2C), 129.1, 127.2, 125.7, 125.1, 121.3, 121.1, 119.5, 119.4, 119.2, 118.8, 117.2, 111.6, 111.1, 71.6, 71.3, 60.3, 59.5, 56.1, 53.2, 53.0, 52.3, 52.0, 45.8, 39.9, 36.2, 34.8, 33.7, 31.6, 27.6, 24.6, 21.4, 21.3, 17.6.[l]

IR (ATR): ῡ 3390 (w), 2928 (w), 1729 (s), 1457 (m), 1432 (m), 1368 (w), 1326 (w), 1296 (w), 1265 (m), 1227 (s), 1207 (s), 1096 (w), 1055 (m), 953 (w), 856 (w), 970 (w), 741 (s), 707 (w) cm^{-1}.

HRMS (EI): Calculated for $C_{20}H_{24}N_2O_4$ $[M]^+$: 356.1736; found: *m/z* 356.1735.



2.130

Prepared from dimethyl 2-(3-(methoxycarbonyl)piperidin-1-yl)-2-(prop-2-yn-1-yl)malonate (399 mg, 1.28 mmol) and 1-azido-2-iodobenzene (377 mg, 1.54 mmol) following GP3. Purification over silica (eluent: EtOAc/Hexanes). Arylazide **2.130** was obtained as an orange oil: 285.6 mg, 56% yield.

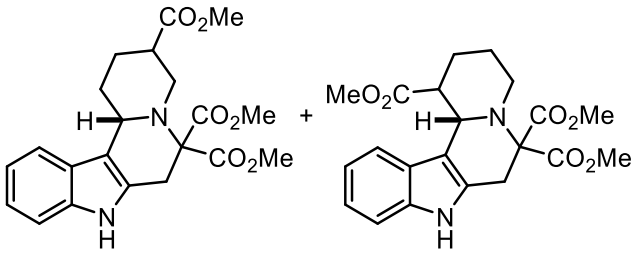
^{1}H-NMR (400 MHz, $CDCl_3$): δ 7.35 (dd, *J* = 7.7, 1.4 Hz, 1H), 7.29 (ddd, *J* = 8.9, 7.8, 1.5 Hz, 1H), 7.09–7.02 (m, 2H), 3.80 (s, 6H), 3.65 (s, 3H), 3.30–3.20 (m, 3H), 2.98 (d, *J* = 11.3 Hz, 1H), 2.70 (tt, *J* = 10.7, 3.7 Hz, 1H), 2.51 (t, *J* = 10.6 Hz, 1H), 2.35 (td, *J* = 10.9, 2.8 Hz, 1H), 1.97 (dd, *J* = 12.9, 3.7 Hz, 1H), 1.81–1.59 (m, 2H), 1.48 (qd, *J* = 11.5, 4.5 Hz, 1H).

^{13}C-NMR (100 MHz, $CDCl_3$): δ 174.5, 168.8 (2C), 141.0, 134.1, 129.3, 124.7, 118.7, 115.7, 90.6, 79.4, 75.4, 52.7, 51.7, 50.9, 48.9, 42.5, 27.3, 25.4, 25.3.

IR (ATR): ῡ 2946 (w), 2650 (w), 2131 (m), 2092 (s), 1716 (s), 1568 (w), 1483 (m), 1436 (s), 1335 (w), 1308 (s), 1279 (m), 1231 (m), 1203 (s), 1178 (m), 1157 (m), 1142 (m), 1084 (w), 1057 (s), 1017 (w), 981 (w), 958(w), 915 (w), 877 (w), 853 (w), 809 (w), 753 (s) cm^{-1}.

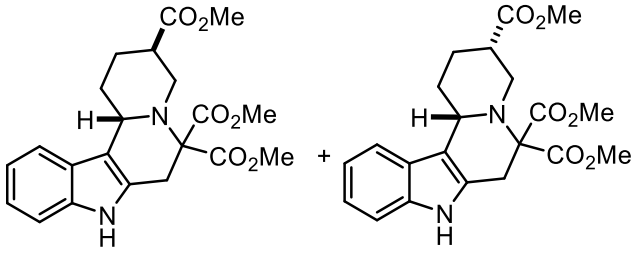
HRMS (ESI): Calculated for $C_{21}H_{24}N_4NaO_6$ $[M+Na]^+$: 451.1593; found: *m/z* 451.1576.

[l]One carbon signal missing due to overlap at 111.0 ppm.



2.156a **2.156b**

Prepared from arylazide **2.130** (42.8 mg, 0.10 mmol) following GP8. Reaction time: 4 hr. Overall NMR-yield = 85%, *r.r.* = 1.7:1, *d.r.* (**2.156a**) = 3:1, and *d.r.* (**2.156b**) = 10:1. Purification over silica (eluent: EtOAc/Hexanes). Overall mass obtained was 32.6 mg (82% isolated yield). Analytical samples of regioisomers **2.156a** (yellow solid) and **2.156b** (yellow solid) as inseparable diastereomeric mixtures were obtained for characterization.

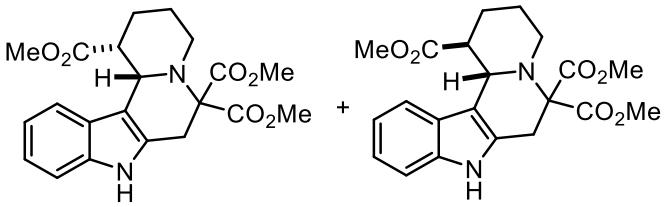


2.156a' **2.156a''**

^{1}H-NMR (400 MHz, $CDCl_3$): δ 7.83 (bs, 1H), 7.79 (bs, 1H), 7.46 (d, *J* = 7.7 Hz, 2H), 7.32–7.27 (m, 2H), 7.17–7.02 (m, 4H), 4.08 (d, *J* = 10.0 Hz, 1H), 3.93 (dd, *J* = 10.9, 2.1 Hz, 1H), 3.86 (s, 3H), 3.85 (s, 3H), 3.69 (s, 3H), 3.69 (s, 3H), 3.64 (s, 3H), 3.62 (s, 3H), 3.53–3.35 (m, 5H), 3.34–3.25 (m, 2H), 3.16 (ddd, *J* = 11.9, 4.3, 1.6 Hz, 1H), 2.71 (ddd, *J* = 15.6, 7.7, 3.9 Hz, 2H), 2.60 (dd, *J* = 13.1, 3.6 Hz, 1H), 2.39 (dd, *J* = 11.6, 4.2 Hz, 1H), 2.26–2.18 (m, 2H), 1.94–1.73 (m, 2H), 1.56–1.47 (m, 1H).

^{13}C-NMR (100 MHz, $CDCl_3$): δ 174.5, 174.2, 170.6, 170.5, 170.4, 170.2, 136.5, 136.4, 129.3, 129.1, 125.7, 125.5 (2C), 121.5, 121.4, 119.5 (2C), 118.9 (2C), 111.1, 111.0, 110.9, 73.4 (2C), 56.8, 56.4, 53.4, 53.2, 52.8, 52.4 (2C), 52.0, 51.8, 51.7, 43.3, 40.9, 32.7, 32.5, 31.4, 30.5, 28.2, 25.3.

HRMS (EI): Calculated for $C_{21}H_{24}N_2O_6$ $[M]^+$: 400.1634; found: *m/z* 400.1636.



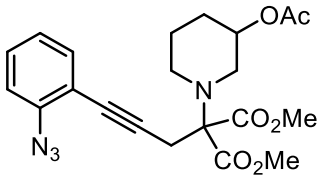
2.156b' **2.156b''**

^{1}H-NMR (400 MHz, $CDCl_3$): δ 7.97 (s, 1H), 7.88 (s, 1H), 7.40 (d, *J* = 7.7 Hz, 1H), 7.37 (d, *J* = 8.1 Hz, 1H), 7.31–7.22 (m, 2H), 7.16–6.96 (m, 3H), 4.32 (t, *J* = 2.6 Hz, 1H), 4.29 (d, *J* = 8.9 Hz, 1H), 3.83 (s, 3H), 3.82 (s, 3H), 3.57 (s, 3H), 3.54 (s, 3H), 3.48 (dd, *J* = 14.6, 2.4 Hz, 1H), 3.43 (s, 3H), 3.40–3.34 (m, 2H), 3.33 (s, 3H), 3.28 (td, *J* = 11.8, 2.6 Hz, 1H), 3.19 (td, *J* = 11.7, 3.0 Hz, 1H), 2.89 (d, *J* = 11.7 Hz, 1H), 2.63 (ddd, *J* = 11.2, 8.8, 4.0 Hz, 1H), 2.30 (dd, *J* = 13.6, 3.0 Hz, 2H), 2.14–1.93 (m, 2H), 1.87 (tt, *J* = 13.3, 4.4 Hz, 1H), 1.79–1.53 (m, 2H).

^{13}C-NMR (100 MHz, $CDCl_3$): δ 175.8, 172.5, 171.0, 170.9, 170.6, 170.5, 136.3, 136.1, 131.0, 130.5, 125.6, 125.5, 121.5, 121.2, 119.7, 119.4 (2C), 118.3, 111.1, 110.8, 109.7, 109.5, 73.8 (2C), 60.1, 58.4, 53.3, 53.2, 52.4, 52.2, 52.0, 51.5, 51.4, 51.1, 44.3, 33.1, 32.5, 29.6, 27.9, 25.8, 23.8.[m]

IR (ATR): ῡ 3355 (w), 2931 (w), 1727 (s), 1627 (w), 1496 (w), 1456 (w), 1436 (m), 1374 (w), 1312 (w), 1295 (w), 1262 (m), 1240 (w), 1187 (m), 1154 (m), 1066 (m), 1048 (m), 1015 (w), 983 (w), 916 (w), 805 (w), 777 (w), 762 (s), 752 (w) cm^{-1}.

HRMS (EI): Calculated for $C_{21}H_{24}N_2O_6$ $[M]^+$: 400.1634; found: *m/z* 400.1623.



2.131

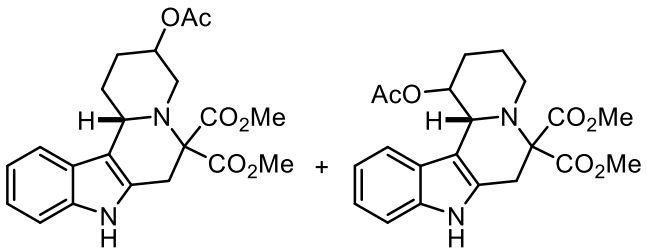
Prepared from dimethyl 2-(3-acetoxypiperidin-1-yl)-2-(prop-2-yn-1-yl)malonate (204 mg, 0.66 mmol) and 1-azido-2-iodobenzene (177 mg, 0.72 mmol) following GP3. Purification over silica (eluent: EtOAc:hexanes). Arylazide **2.131** was obtained as an amber oil: 191 mg, 68% yield.

[m]One carbon signal missing due to peak overlap at 51.5 ppm.

^{1}H-NMR (300 MHz, $CDCl_3$): δ 7.41–7.25 (m, 2H), 7.10–7.02 (m, 2H), 4.85 (sept, *J* = 4.1 Hz, 1H), 3.81 (s, 3H), 3.80 (s, 3H), 3.22 (s, 2H), 3.14–3.06 (m, 1H), 2.93–2.84 (m, 1H), 2.53–2.38 (m, 2H), 2.05–1.92 (m, 4H), 1.85–1.61 (m, 2H), 1.47–1.32 (m, 1H).

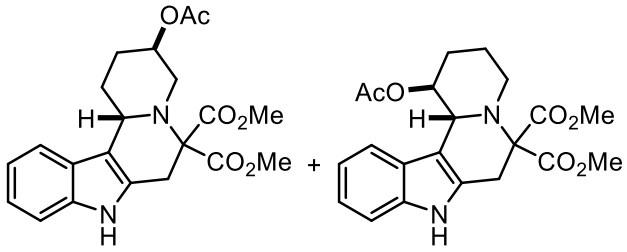
^{13}C-NMR (101 MHz, $CDCl_3$): δ 170.5, 168.8, 141.0, 134.1, 129.3, 124.7, 118.7, 115.6, 90.5, 79.5, 75.1, 70.1, 52.7, 52.8, 48.4, 30.0, 25.6, 23.7, 21.4.

HRMS (ESI): Calculated for $C_{21}H_{24}N_4NaO_6$ $[M+Na]^+$: 451.1594; found: *m/z* 451.1612.



2.157a **2.157b**

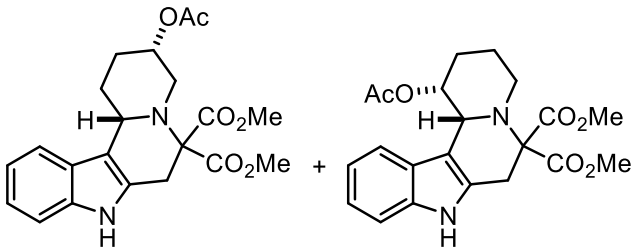
Prepared from arylazide **2.131** (25.5 mg, 0.060 mmol) following GP8. Reaction time: 1 hr. Overall NMR yield = 60%, *r.r.* = 1:1, and *d.r.* (**2.157a,b**) = 2:1. Purification over silica (eluent: Et_2O:hexanes). *Syn*-diastereoisomers **2.157a'** and **2.157b'** were obtained as an inseparable mixture of regioisomers as a yellow oil: 9.3 mg, 40% combined yield. *Anti*-diastereoisomers **2.157a''** and **2.157b''** were obtained as an inseparable mixture of regioisomers as a yellow oil: 4 mg, 20% combined yield.



2.157a' **2.157b'**

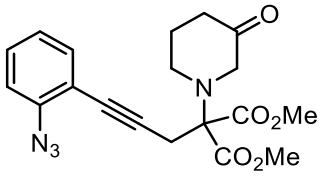
^{1}H-NMR (300 MHz, $CDCl_3$): δ 7.92 (bs, 1H), 7.89 (bs, 1H), 7.72 (d, *J* = 7.8 Hz 1H), 7.46 (d, *J* = 7.8 Hz, 1H), 7.32–7.22 (m, 2H), 7.18–6.98 (m, 4H), 4.83 (tt, *J* = 10.2, 4.9 Hz, 1H), 4.72 (ddd, *J* = 10.2, 9.1, 4.3 Hz, 1H), 4.08 (d, *J* = 9.4 Hz, 1H), 3.93 (dd, *J* = 10.8, 2.2 Hz, 1H), 3.88 (s, 3H), 3.84 (s, 3H), 3.64 (s, 3H), 3.54 (s, 3H), 3.50–3.33 (m, 4H), 3.19–3.04 (m, 3H), 2.86 (dt, *J* = 12.2, 3.1 Hz, 1H), 2.63–2.54 (m, 1H), 2.30–2.18 (m, 2H), 2.05 (s, 3H), 1.97 (s, 3H), 1.78–1.49 (m, 6H).

^{13}C-NMR (101 MHz, $CDCl_3$): δ 170.9, 170.5 (3C), 170.4, 170.3, 136.5, 136.3, 130.5, 129.2, 126.9, 125.5, 121.5, 121.5, 120.9, 119.6, 119.2, 118.8, 111.1, 110.8, 110.6, 108.9, 73.3, 70.8, 61.1, 56.2, 54.6, 53.5, 53.3, 52.4 (2C), 51.3, 33.2, 32.2, 32.0, 31.3, 30.8, 30.5, 29.9, 25.5, 21.9, 21.4.
HRMS (EI): Calculated for $C_{21}H_{24}N_2O_6$ $[M]^+$: 400.1634; found: *m/z* 400.1063.



2.157a" **2.157b"**

^{1}H-NMR (400 MHz, $CDCl_3$): δ 7.82 (bs, 1H), 7.81 (bs, 1H), 7.47 (d, *J* = 7.9 Hz, 2H), 7.33–7.24 (m, 2H), 7.17–7.01 (m, 4H), 5.70–5.66 (m, 1H), 4.91–4.86 (m, 1H), 4.30–4.27 (m, 1H), 4.08–4.01 (m, 1H), 3.85 (s, 3H), 3.80 (s, 3H), 3.62 (s, 3H), 3.60 (s, 3H), 3.53 (dd, *J* = 4.3, 2.3 Hz, 1H), 3.48 (dd, *J* = 4.5, 2.4 Hz, 1H), 3.45 (d, *J* = 1.6 Hz, 1H), 3.40 (d, *J* = 1.4 Hz, 1H), 3.35 (d, *J* = 1.7 Hz, 1H), 3.32–3.08 (m, 3H), 2.91 (dt, *J* = 11.5, 3.1 Hz, 1H), 2.43–2.34 (m, 1H), 2.16–2.08 (m, 4H), 2.01–1.96 (m, 1H), 1.92 (t, *J* = 3.5 Hz, 1H), 1.90–1.80 (m, 2H), 1.71 (s, 3H).
^{13}C-NMR (76 MHz, $CDCl_3$): δ 171.1, 170.7, 170.5, 170.6, 170.4, 170.3, 136.4, 136.2, 130.8, 129.1, 125.5, 125.4, 125.0, 121.4 (2C), 119.7, 119.4, 118.7, 118.6, 111.0, 110.7, 107.6, 73.6, 72.3, 69.4, 68.8, 59.3, 56.3, 53.1, 53.0, 52.2, 52.2, 50.7, 32.5, 32.0, 30.3, 29.7, 29.1, 28.9, 28.8, 22.1, 21.4.
HRMS (EI): Calculated for $C_{21}H_{24}N_2O_6$ $[M]^+$: 400.1634; found: *m/z* 400.1606.



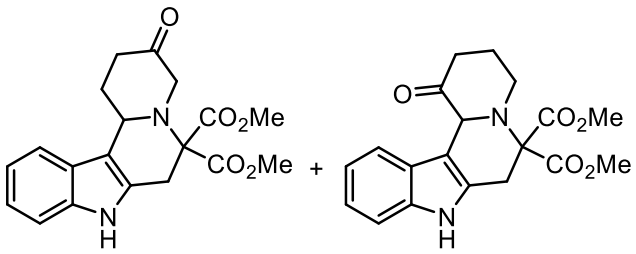
2.168

Prepared from dimethyl 2-(3-oxopiperidin-1-yl)-2-(prop-2-yn-1-yl)malonate (69.6 mg, 0.260 mmol) and 1-azido-2-iodobenzene (70.2 mg, 0.286 mmol) following GP3. Purification over silica (eluent: EtOAc:hexanes). Arylazide **2.168** was obtained as an amber oil: 38.3 mg, 38% yield.

^{1}H-NMR (300 MHz, $CDCl_3$): δ 7.36–7.27 (m, 2H), 7.10–7.02 (m, 2H), 3.82 (s, 6H), 3.43 (s, 2H), 3.25 (s, 2H), 3.01–2.95 (m, 2H), 2.44 (t, *J* = 7.0 Hz, 2H), 2.06–1.96 (m, 2H).

^{13}C-NMR (101 MHz, $CDCl_3$): δ 206.3, 168.5, 141.2, 134.0, 129.5, 124.7, 118.7, 115.4, 89.9, 79.9, 74.4, 59.9, 52.9, 47.3, 38.5, 25.5, 23.6.

HRMS (ESI): Calculated for $C_{19}H_{20}N_4NaO_5$ $[M+Na]^+$: 407.1331; found: *m/z* 407.1334.



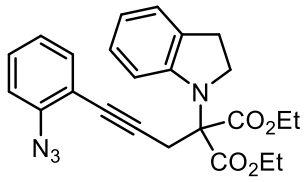
2.170a **2.170b**

Prepared from arylazide **2.168** (23.9 mg, 0.062 mmol) following GP8. Reaction time: 2 hr. Overall NMR yield = 35% and *r.r.* = 2:1. Purification over silica (eluent: Et_2O:hexanes). Regioisomer **2.170a** was obtained as a yellow oil: 4.5 mg, 18% yield. An analytical sample of the minor regioisomer **2.170b** was unable to be obtained for characterization.

^{1}H-NMR (300 MHz, $CDCl_3$): δ 7.88 (bs, 1H), 7.46 (dd, *J* = 7.6, 1.1 Hz, 1H), 7.31 (dt, *J* = 8.0, 0.9 Hz, 1H), 7.16 (ddd, *J* = 8.2, 7.1, 1.3 Hz, 1H), 7.09 (ddd, *J* = 8.1, 7.1, 1.2 Hz, 1H), 4.44–4.38 (m, 1H). 4.07 (d, *J* = 15.1 Hz, 1H), 3.84 (s, 3H), 3.62 (s, 3H), 3.54–3.42 (m, 2H), 3.37 (dd, *J* = 15.2, 1.2 Hz, 1H), 2.77 (ddt, *J* = 12.9, 6.1, 3.0 Hz, 1H), 2.71–2.58 (m, 2H), 1.85 (dtd, *J* = 13.1, 11.0, 7.0 Hz, 1H).

^{13}C-NMR (101 MHz, $CDCl_3$): δ 205.8, 170.0, 169.6, 136.5, 129.2, 125.4, 121.9, 119.9, 118.7, 111.2, 110.1, 72.4, 61.7, 55.1, 53.6, 52.6, 39.1, 32.1, 31.1.

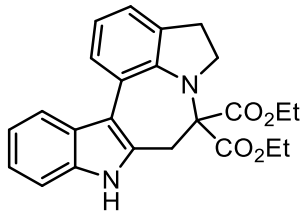
HRMS (EI): Calculated for $C_{19}H_{20}N_2O_5$ $[M]^+$: 356.1372; found: *m/z* 297.1239 (loss of CO_2Me).



2.166

Prepared from diethyl 2-(indolin-1-yl)-2-(prop-2-yn-1-yl)malonate (433 mg, 1.37 mmol) and 1-azido-2-iodobenzene (370 mg, 1.51 mmol) following GP3. Purification over silica (eluent: EtOAc:hexanes). Arylazide **2.166** was obtained as an amber solid: 479 mg, 81% yield.

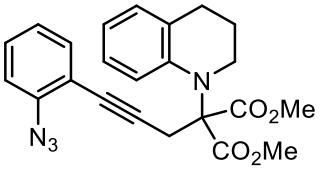
^{1}H-NMR (300 MHz, $CDCl_3$): δ 7.32 (td, *J* = 7.8, 1.6 Hz, 2H), 7.11–6.92 (m, 4H), 6.70 (t, *J* = 7.3 Hz, 1H), 6.48 (d, *J* = 8.1 Hz, 1H), 4.29 (q, *J* = 7.1 Hz, 4H), 3.83 (t, *J* = 8.3 Hz, 2H), 3.45 (s, 2H), 3.02 (t, *J* = 8.3 Hz, 2H), 1.24 (t, *J* = 7.1 Hz, 6H).
^{13}C-NMR (101 MHz, $CDCl_3$): δ 167.9, 148.9, 141.1, 134.0, 130.8, 129.4, 126.6, 124.7, 124.4, 119.0, 118.7, 115.5, 110.8, 90.5, 79.6, 71.6, 62.2, 50.8, 28.3, 27.0, 14.2.
HRMS (ESI): Calculated for $C_{24}H_{24}N_4NaO_4$ $[M+Na]^+$: 455.1695; found: *m/z* 455.1693.



2.167

Prepared from arylazide **2.166** (26.6 mg, 0.062 mmol) following GP8. Reaction time: 1 hr. Purification over silica (eluent: Et_2O:hexanes). Indole **2.167** was obtained as an amber solid: 10 mg, 42% yield.

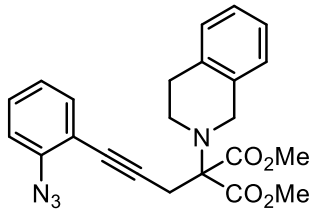
^{1}H-NMR (400 MHz, $CDCl_3$): δ 8.07–7.94 (m, 2H), 7.74 (d, *J* = 7.5 Hz, 1H), 7.31 (d, *J* = 7.8 Hz, 1H), 7.19–7.07 (m, 2H), 7.01 (d, *J* = 7.1 Hz, 1H), 6.88 (t, *J* = 7.5 Hz, 1H), 4.19–4.05 (m, 4H), 3.67 (t, *J* = 8.4 Hz, 2H), 3.57 (s, 2H), 3.05 (t, *J* = 8.4 Hz, 2H), 1.10 (t, *J* = 7.1 Hz, 6H).
^{13}C-NMR (126 MHz, $CDCl_3$): δ 168.7, 144.4, 136.4, 131.8, 131.8, 126.4, 125.9, 122.0, 121.8, 120.2, 120.0, 119.5, 118.2, 111.7, 111.1, 74.5, 62.1, 53.0, 35.7, 29.0, 14.1.
HRMS (EI): Calculated for $C_{24}H_{24}N_2O_4$ $[M]^+$: 404.1740; found: *m/z* 404.1716.



2.212

Prepared from dimethyl 2-(3,4-dihydroquinolin-1(2*H*)-yl)-2-(prop-2-yn-1-yl)malonate (104 mg, 0.35 mmol) and 1-azido-2-iodobenzene (93.2 mg, 0.38 mmol) following GP3. Purification over silica (eluent: EtOAc:hexanes). Arylazide **2.212** was obtained as an amber oil: 54.3 mg, 38% yield.

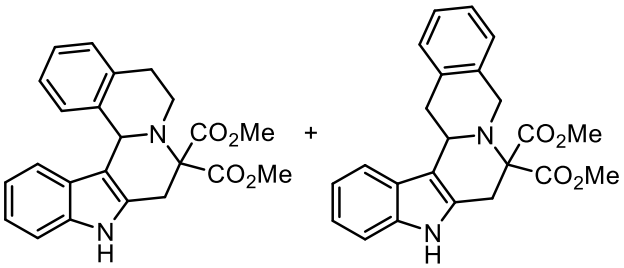
^{1}H-NMR (300 MHz, $CDCl_3$): δ 7.34–7.24 (m, 2H), 7.12–6.93 (m, 4H), 6.73 (t, *J* = 7.4 Hz, 1H), 6.51 (d, *J* = 8.2 Hz, 1H), 3.80 (s, 6H), 3.52 (s, 2H), 3.43 (t, *J* = 6.3 Hz, 2H), 2.74 (t, *J* = 6.6 Hz, 2H), 2.09–1.95 (m, 2H).
^{13}C-NMR (101 MHz, $CDCl_3$): δ 169.8, 144.5, 141.1, 134.0, 129.3, 128.8, 128.5, 126.1, 124.7, 118.9, 118.7, 115.7, 114.4, 91.0, 79.4, 73.8, 53.2, 47.2, 27.8, 27.2, 24.5.
HRMS (ESI): Calculated for $C_{23}H_{22}N_4NaO_4$ $[M+Na]^+$: 441.1539; found: *m/z* 441.1533.



2.128

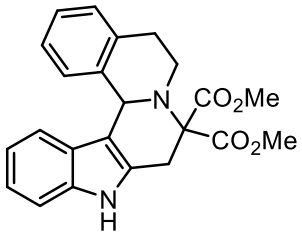
Prepared from dimethyl 2-(3,4-dihydroisoquinolin-2(1*H*)-yl)-2-(prop-2-yn-1-yl)malonate (448 mg, 1.49 mmol) and 1-azido-2-iodobenzene (437 mg, 1.78 mmol) following GP3. Purification over silica (eluent: EtOAc/Hexanes). Arylazide **2.128** was obtained as a brown solid: 515.6 mg, 83% yield.

^{1}H-NMR (400 MHz, $CDCl_3$): δ 7.30 (td, *J* = 7.5, 1.5 Hz, 1H), 7.26 (m, 1H), 7.15–7.07 (m, 3H), 7.07–6.99 (m, 3H), 3.99 (s, 2H), 3.82 (s, 6H), 3.35 (s, 2H), 3.05 (t, *J* = 5.6 Hz, 2H), 2.95 (t, *J* = 5.5 Hz, 2H).
^{13}C-NMR (100 MHz, $CDCl_3$): δ 168.9, 141.1, 134.7, 134.6, 134.0, 129.3, 128.9, 126.7, 126.2, 125.7, 124.6, 118.7, 115.6, 90.6, 79.6, 75.2, 52.8, 50.3, 47.1, 30.2, 25.3.
IR (ATR): ῡ 2951 (w), 2916 (w), 2131 (s), 2097 (s), 1752 (s), 1727 (s), 1571 (w), 1488 (m), 1431 (m).1393 (w), 1280 (m), 1239 (s), 1193 (m), 1170 (m), 1105 (m), 1073 (m), 1038 (m), 1013 (m), 985 (w), 961 (w), 932 (w), 915 (m), 854 (w), 830 (w), 754 (s), 732 (s) cm^{-1}.
HRMS (ESI): Calculated for $C_{23}H_{22}N_4NaO_4$ $[M+Na]^+$: 441.1533; found: *m/z* 441.1540.



2.154a **2.154b**

Prepared from arylazide **2.128** (41.9 mg, 0.10 mmol) following GP8. Reaction time: 1.5 hr. Overall NMR-yield = 78% and *r.r.* = 2.3:1. Purification over silica (eluent: EtOAc/Hexanes). Overall mass obtained was 30 mg (77% isolated yield). Analytical samples of the major regioisomer **2.154a** (orange solid) and minor regioisomer **2.154b** (orange solid) were obtained for characterization.



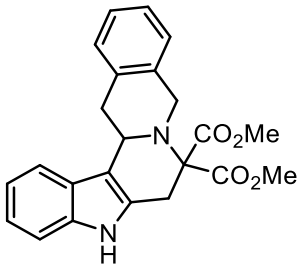
2.154a

^{1}H-NMR (400 MHz, $CDCl_3$): δ 8.07 (bs, 1H), 7.42 (d, *J* = 8.2 Hz, 2H), 7.31 (d, *J* = 8.1 Hz, 1H), 7.26–7.07 (m, 4H), 7.01 (t, *J* = 7.5 Hz, 1H), 5.41 (s, 1H), 3.74 (s, 3H), 3.72 (s, 3H), 3.54 (d, *J* = 15.9 Hz, 1H), 3.45 (dd, *J* = 15.9, 1.9 Hz, 1H), 3.37 (dd, *J* = 9.8, 5.7 Hz, 1H), 3.24–3.08 (m, 2H), 2.95–2.84 (m, 1H).

^{13}C-NMR (100 MHz, $CDCl_3$): δ 170.0, 169.8, 137.8, 136.2, 135.6, 130.3, 128.3, 127.5, 127.2, 126.8, 125.4, 121.5, 120.0, 119.7, 110.9, 108.9, 73.3, 56.2, 53.3, 53.2, 45.2, 29.2, 28.8.

IR (ATR): ῡ 3323 (m), 2861 (w), 1731 (s), 1496 (w), 1457 (m), 1429 (m), 1320 (w), 1286 (w), 1265 (m), 1245 (m), 1208 (s), 1142 (m), 1118 (w), 1101 (w), 1077 (m), 1056 (m), 1014 (w), 956 (w), 915 (w), 846 (w), 820 (w), 780 (w), 765 (w), 742 (s), 718 (w) cm^{-1}.

HRMS (EI): Calculated for $C_{23}H_{22}N_2O_4$ $[M]^+$: 390.1580; found: *m/z* 390.1580.



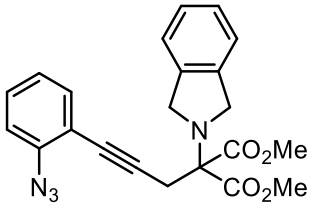
2.154b

^{1}H-NMR (400 MHz, $CDCl_3$): δ 7.89 (bs, 1H), 7.54 (d, *J* = 7.7 Hz, 1H), 7.34 (d, *J* = 8.1 Hz, 1H), 7.21 – 7.10 (m, 5H), 7.09 – 7.02 (m, 1H), 4.87 (d, *J* = 14.6 Hz, 1H), 4.54 (d, *J* = 11.4 Hz, 1H), 3.91 (d, *J* = 14.6 Hz, 1H), 3.90 (s, 3H), 3.63 (s, 3H), 3.62 – 3.49 (m, 3H), 2.91 (dd, *J* = 15.9, 11.5 Hz, 1H).

^{13}C-NMR (100 MHz, $CDCl_3$): δ 170.4, 170.3, 136.6, 134.8, 134.3, 129.3, 128.9, 126.3, 126.2, 125.9, 125.5, 121.7, 119.7, 118.9, 111.3, 111.1, 72.6, 53.4, 53.3, 52.4, 51.8, 37.7, 32.8.

IR (ATR): ῡ 3338 (w), 1723 (s), 1496 (w), 1453 (m), 1430 (m), 1375 (w), 1328 (w), 1270 (m), 1237 (m), 1199 (m), 1175 (m), 1106 (w), 1065 (m), 1041 (m), 1012 (w), 948 (w), 914 (w), 801 (w), 739 (s), 696 (w) cm^{-1}.

HRMS (EI): Calculated for $C_{23}H_{22}N_2O_4$ $[M]^+$: 390.1580; found: *m/z* 390.1579.



2.126

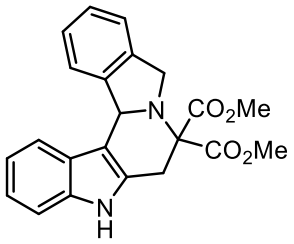
Prepared from dimethyl 2-(isoindolin-2-yl)-2-(prop-2-yn-1-yl)malonate (180 mg, 0.63 mmol) and 1-azido-2-iodobenzene (184 mg, 0.75 mmol) following GP3. Purification over silica (eluent: EtOAc/Hexanes). Arylazide **2.126** was obtained as a brown oil: 138.4 mg, 54% yield.

^{1}H-NMR (400 MHz, $CDCl_3$): δ 7.35 (dd, *J* = 7.7, 1.5 Hz, 1H), 7.29 (td, *J* = 8.0, 1.5 Hz, 1H), 7.20 (s, 4H), 7.09–7.01 (m, 2H), 4.44 (s, 4H), 3.83 (s, 6H), 3.36 (s, 2H).

^{13}C-NMR (100 MHz, $CDCl_3$): δ 169.0, 141.1, 138.8, 134.1, 129.4, 126.9, 124.6, 122.4, 118.7, 115.5, 90.7, 79.4, 73.0, 54.5, 52.8, 27.2.

IR (ATR): ῡ 2889 (w), 2856 (w), 2127 (s), 2093 (s), 1729 (s), 1571 (w), 1486 (m), 1464 (m), 1438 (m), 1419 (m), 1370 (w), 1288 (s), 1246 (s), 1195 (s) 1163 (s), 1140 (s), 1087 (m), 1068 (m), 1035 (m), 1000 (m), 977 (m), 938 (w), 920 (m), 847 (w), 778 (w), 741 (s) cm^{-1}.

HRMS (ESI): Calculated for $C_{22}H_{20}N_4NaO_4$ $[M+Na]^+$: 427.1377; found: *m/z* 427.1378.



2.152

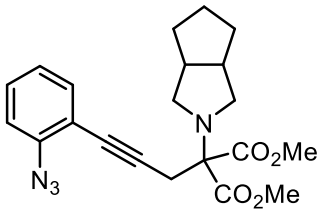
Prepared from arylazide **2.126** (40.6 mg, 0.10 mmol) following GP8. Reaction time: 22 hr. Purification over silica (eluent: EtOAc/Hexanes). Indole **2.152** was obtained as a yellow solid: 28 mg, 74% yield. **Note:** Isolated **2.152** is highly sensitive to air oxidation.

^{1}H-NMR (400 MHz, $CDCl_3$): δ 8.00 (bs, 1H), 7.86–7.77 (m, 2H), 7.31–7.22 (m, 2H), 7.21–7.08 (m, 4H), 6.22 (s, 1H), 4.19 (s, 2H), 3.92 (s, 3H), 3.76–3.68 (m, 4H), 3.47 (dd, *J* = 16.6, 1.6 Hz, 1H).

^{13}C-NMR (100 MHz, $CDCl_3$): δ 169.2, 169.0, 141.5, 137.4, 136.2, 128.9, 127.3, 127.1, 125.4, 123.6, 122.8, 121.9, 119.8, 119.4, 111.1, 110.2, 71.0, 62.4, 53.8, 53.7, 53.0, 23.5.

IR (ATR): ῡ 3310 (w), 2955 (w), 1730 (s), 1457 (m), 1430 (m), 1324 (w), 1277 (m), 1235 (m), 1211 (s), 1176 (m), 1118 (m), 1067 (m), 1019 (w), 950 (w), 867 (w), 825 (w), 741 (s), 691 (w) cm^{-1}.

HRMS (ESI): Calculated for $C_{22}H_{20}N_2NaO_4$ $[M]^+$: 399.1321; found: *m/z* 399.1340.

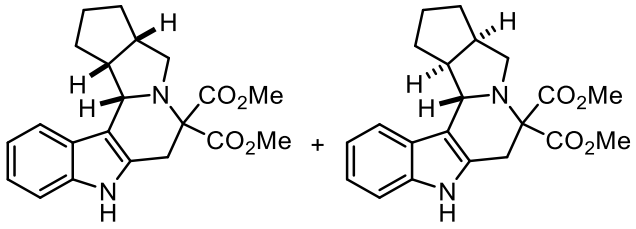


2.127

Prepared from dimethyl 2-(hexahydrocyclopenta[*c*]pyrrol-2(1*H*)-yl)-2-(prop-2-yn-1-yl)malonate (242 mg, 0.87 mmol) and 1-azido-2-iodobenzene (234 mg, 0.95 mmol) following GP3.

Purification over silica (eluent: EtOAc:hexanes). Arylazide **2.127** was obtained as an amber oil: 159 mg, 46% yield.

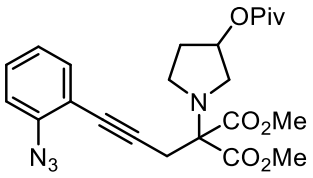
^{1}H-NMR (300 MHz, $CDCl_3$): δ 7.34 (dd, *J* = 7.6, 1.6 Hz, 1H), 7.32–7.25 (m, 1H), 7.10–7.01 (m, 2H), 3.78 (s, 6H), 3.22 (s, 2H), 2.99–2.90 (m, 2H), 2.63–2.51 (m, 4H), 1.74–1.59 (m, 3H), 1.52–1.38 (m, 3H).
^{13}C-NMR (101 MHz, $CDCl_3$): δ 168.8, 141.0, 134.1, 129.3, 124.7, 118.7, 115.8, 91.1, 79.1, 72.6, 55.3, 52.4, 41.7, 33.2, 26.3, 26.1.
HRMS (ESI): Calculated for $C_{21}H_{24}N_4NaO_4$ $[M+Na]^+$: 419.1695; found: *m/z* 419.1689.



2.153a **2.153b**

Prepared from arylazide **2.127** (24.7 mg, 0.062 mmol) following GP8. Reaction time: 21 hr. Overall NMR-yield = 85% and *d.r.* = 5:1. Purification over silica (eluent: EtOAc:hexanes). *Syn*-diastereoisomer **2.153a** was obtained as an off-white solid: 14.4 mg, 63% yield. An analytical sample of *anti*-diastereoisomer **2.153b** was unable to be obtained after purification.

^{1}H-NMR (300 MHz, $CDCl_3$): δ 7.86 (bs, 1H), 7.53 (dd, *J* = 7.3, 1.3 Hz, 1H), 7.29 (ddd, *J* = 8.4, 1.3, 0.6 Hz, 1H), 7.17–7.03 (m, 2H), 4.09 (dd, *J* = 4.7, 2.4 Hz, 1H), 3.85 (s, 3H), 3.60 (s, 3H), 3.54–3.35 (m, 2H), 3.11 (t, *J* = 8.1 Hz, 1H), 2.85 (tt, *J* = 9.0, 4.6 Hz, 1H), 2.73 (dd, *J* = 8.5, 4.7 Hz, 1H), 2.61 (dq, *J* = 8.9, 5.2, 4.6 Hz, 1H), 2.05 (ddt, *J* = 22.5, 12.6, 6.6 Hz, 2H), 1.79 (ddt, *J* = 19.4, 11.9, 6.9 Hz, 2H), 1.59 (qt, *J* = 10.5, 5.2 Hz, 2H).
^{13}C-NMR (101 MHz, $CDCl_3$): δ 169.9, 169.6, 136.1, 128.7, 125.8, 121.5, 119.5, 119.0, 111.5, 111.0, 70.5, 63.3, 54.3, 53.4, 52.8, 47.7, 42.0, 33.8, 32.9, 27.0, 26.9.
HRMS (EI): Calculated for $C_{21}H_{24}N_2O_4$ $[M]^+$: 368.1736; found: *m/z* 368.1720.



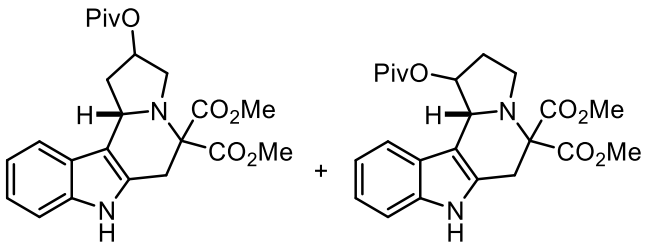
2.129

Prepared from dimethyl 2-(3-(pivaloyloxy)pyrrolidin-1-yl)-2-(prop-2-yn-1-yl)malonate (309 mg, 0.91 mmol) and 1-azido-2-iodobenzene (268 mg, 1.09 mmol) following GP3. Purification over silica (eluent: EtOAc/Hexanes). Arylazide **2.129** was obtained as an orange oil: 293 mg, 70% yield.

^{1}H-NMR (400 MHz, $CDCl_3$): δ 7.33 (dd, *J* = 7.7, 1.3 Hz, 1H), 7.31–7.26 (m, 1H), 7.08–7.00 (m, 2H), 5.17 (tt, *J* = 6.2, 3.0 Hz, 1H), 3.80 (s, 3H), 3.79 (s, 3H), 3.46 (dd, *J* = 10.8, 6.2 Hz, 1H), 3.23 (s, 2H), 3.08–3.02 (m, 2H), 2.95 (dd, *J* = 10.8, 2.9 Hz, 1H), 2.16 (dq, *J* = 14.6, 7.8 Hz, 1H), 1.90–1.80 (m, 1H), 1.16 (s, 9H).

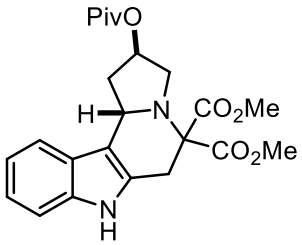
^{13}C-NMR (100 MHz, $CDCl_3$): δ 178.4, 168.8, 168.7, 141.0, 134.1, 129.3, 124.6, 118.7, 115.6, 90.8, 79.3, 73.4, 72.7, 54.1, 52.6, 52.6, 46.6, 38.6, 31.6, 27.2, 26.4.

HRMS (ESI): Calculated for $C_{23}H_{28}N_4NaO_6$ $[M+Na]^+$: 479.1906; found: *m/z* 479.1900.



2.155a **2.155b**

Prepared from arylazide **2.129** (45.4 mg, 1.00 mmol) following GP8. Reaction time: 1.5 hr. Overall NMR-yield = 66%, *r.r.* = 1:1, *d.r.* (**2.155a**) = 1.4:1, and *d.r.* (**2.155b**) = 16:1. Purification over silica (eluent: EtOAc/Hexanes). Overall mass obtained was 26.1 mg (62% isolated yield). Analytical samples of both *syn*- (**2.155a'**, green oil) and *trans*-diastereoisomers (**2.155a''**, yellow solid) of regioisomer **2.155a** and *trans*-diastereoisomer **2.155b'** (yellow solid) of regioisomer **2.155b** were obtained for characterization.

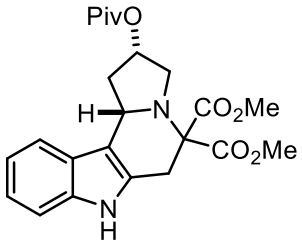


2.155a'

^{1}H-NMR (400 MHz, $CDCl_3$): δ 7.87 (bs, 1H), 7.45 (d, *J* = 7.8 Hz, 1H), 7.31 (d, *J* = 8.0 Hz, 1H), 7.15 (td, *J* = 6.9, 1.1 Hz, 1H), 7.08 (td, *J* = 7.7, 1.1 Hz, 1H), 5.09 (ddd, *J* = 12.5, 7.3, 4.7 Hz, 1H), 4.66 (tt, *J* = 6.0, 2.0 Hz, 1H), 3.85 (s, 3H), 3.71 (s, 3H), 3.47 (d, *J* = 2.0 Hz, 2H), 3.44 (dd, *J* = 10.7, 7.9 Hz, 1H), 3.07 (dd, *J* = 10.5, 4.2 Hz, 1H), 2.54–2.48 (m, 2H), 1.20 (s, 9H).

^{13}C-NMR (100 MHz, $CDCl_3$): δ 178.6, 169.3 (2C), 136.2, 129.4, 125.3, 121.9, 119.8, 118.5, 111.1, 110.2, 72.7, 70.4, 54.9, 53.6, 53.5, 53.1, 38.7, 36.4, 27.3, 26.6.

HRMS (EI): Calculated for $C_{23}H_{28}N_2O_6$ $[M]^+$: 428.1947; found: *m/z* 428.1968.

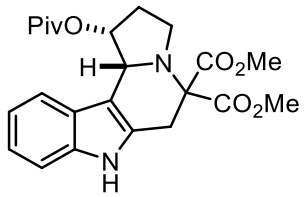


2.155a''

^{1}H-NMR (400 MHz, $CDCl_3$) δ 7.86 (bs, 1H), 7.42 (d, *J* = 7.8 Hz, 1H), 7.29 (d, *J* = 8.0 Hz, 1H), 7.13 (td, *J* = 7.3, 1.1 Hz, 1H), 7.06 (td, *J* = 7.9, 1.2 Hz, 1H), 5.28 (tt, *J* = 6.6, 3.3 Hz, 1H), 4.86 (dq, *J* = 7.2, 2.0 Hz, 1H), 3.87 (s, 3H), 3.70 (s, 3H), 3.54 (dd, *J* = 10.6, 6.4 Hz, 1H), 3.48 (d, *J* = 1.9 Hz, 2H), 2.84–2.72 (m, 2H), 2.32 (dt, *J* = 13.5, 3.1 Hz, 1H), 0.75 (s, 9H).

^{13}C-NMR (100 MHz, $CDCl_3$): δ 178.2, 169.1, 169.0, 136.2, 128.5, 125.6, 121.9, 119.7, 118.5, 111.2, 110.9, 73.2, 70.8, 55.0, 53.7, 53.5, 53.4, 38.4, 36.3, 26.7, 24.1.

HRMS (EI): Calculated for $C_{23}H_{28}N_2O_6$ $[M]^+$: 428.1947; found: *m/z* 428.1973.

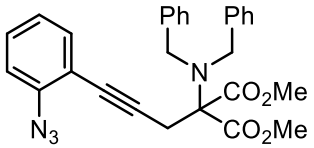


2.155b'

^{1}H-NMR (400 MHz, $CDCl_3$): δ 7.88 (bs, 1H), 7.52 (d, *J* = 7.9 Hz, 1H), 7.30 (d, *J* = 8.1 Hz, 1H), 7.15 (td, *J* = 7.3, 1.1 Hz, 1H), 7.07 (td, *J* = 7.9, 1.1 Hz, 1H), 5.27 (ddd, *J* = 7.4, 5.9, 3.3 Hz, 1H), 4.95 (q, *J* = 2.0 Hz, 1H), 3.87 (s, 3H), 3.67 (s, 3H), 3.54 – 3.35 (m, 2H), 3.12 (td, *J* = 8.2, 3.7 Hz, 1H), 2.83 (td, *J* = 8.8, 7.1 Hz, 1H), 2.37 (dtd, *J* = 13.0, 7.1, 3.6 Hz, 1H), 1.97 – 1.85 (m, 1H), 1.33 (s, 9H).

^{13}C-NMR (100 MHz, $CDCl_3$): δ 178.6, 169.3, 169.1, 136.1, 129.0, 125.4, 122.1, 120.0, 118.9, 111.0, 109.0, 79.1, 71.3, 61.0, 53.6, 53.5, 46.8, 38.9, 30.9, 27.4, 24.4.

HRMS (ESI): Calculated for $C_{23}H_{28}N_2NaO_6$ $[M+Na]^+$: 451.1845; found: *m/z* 451.1845.



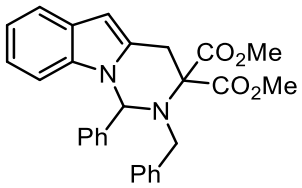
2.178

Prepared from dimethyl 2-(dibenzylamino)-2-(prop-2-yn-1-yl)malonate (397 mg, 1.57 mmol) and 1-azido-2-iodobenzene (461 mg, 1.88 mmol) following GP3. Purification over silica (eluent: EtOAc/Hexanes). Arylazide **2.178** was obtained as an orange solid: 322.6 mg, 43% yield.

^{1}H-NMR (400 MHz, $CDCl_3$): δ 7.41–7.28 (m, 6H), 7.22–7.04 (m, 8H), 4.01 (s, 4H), 3.64 (s, 6H), 3.31 (s, 2H).

^{13}C-NMR (100 MHz, $CDCl_3$): δ 169.8, 141.1, 139.5, 134.0, 129.3, 129.0, 128.0, 126.9, 124.7, 118.7, 115.7, 91.4, 79.5, 75.7, 55.6, 52.5, 27.0.

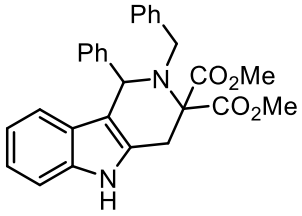
HRMS (ESI): Calculated for $C_{28}H_{26}N_4NaO_4$ $[M+Na]^+$: 505.1852; found: *m/z* 505.1860.



2.182

Prepared from arylazide **2.178** (48.5 mg, 0.10 mmol) following GP8 without using TfOH. Reaction time: 0.5 hr. Purification over silica (eluent: EtOAc/Hexanes). Aminal **2.182** was obtained as white solid: 37.6 mg, 83% yield.

^{1}H-NMR (400 MHz, $CDCl_3$): δ 7.53 (d, *J* = 7.8 Hz, 1H), 7.19 (td, *J* = 10.7, 9.8, 4.5 Hz, 10H), 7.03 (t, *J* = 7.4 Hz, 1H), 6.94 (t, *J* = 7.6 Hz, 1H), 6.81 (d, *J* = 8.2 Hz, 1H), 6.37 (s, 1H), 6.26 (s, 1H), 4.43 (d, *J* = 15.9 Hz, 1H), 4.13 (d, *J* = 15.9 Hz, 1H), 3.93 (d, *J* = 15.7 Hz, 1H), 3.67 (s, 3H), 3.63 (d, *J* = 15.7 Hz, 1H), 3.16 (s, 3H).
^{13}C-NMR (100 MHz, $CDCl_3$): δ 169.9, 169.0, 139.9, 139.0, 135.4, 132.0, 128.8, 128.6, 128.5, 128.4, 128.3, 128.0, 127.0, 120.9, 120.1, 120.0, 110.5, 98.8, 74.8, 70.3, 54.8, 52.8, 52.7, 31.7.
HRMS (EI): Calculated for $C_{28}H_{26}N_2O_4$ $[M]^+$: 454.1893; found: *m/z* 454.1903.

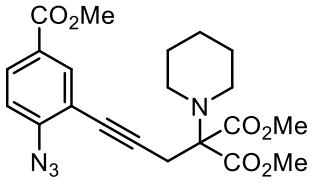


2.180

In a screw-cap NMR tube, to a solution of aminal **2.182** (16.3 mg, 0.04 mmol) in 0.6 mL of dry $CDCl_3$, 3.6 µL of a 0.5 M solution of TfOH in dry $CDCl_3$ was added and the mixture stirred at room temperature. Once finished as indicated by crude ^{1}H-NMR analysis, the reaction was quenched by the addition of a few drops of triethylamine. Purification over silica (eluent: EtOAc/Hexanes) gave indole **2.180** that was obtained as a yellow solid: 12 mg, 74% yield.

^{1}H-NMR (400 MHz, $CDCl_3$): δ 7.87 (bs, 1H), 7.42 (d, *J* = 7.3 Hz, 2H), 7.31–6.99 (m, 10H), 6.89–6.79 (m, 2H), 5.39 (s, 1H), 4.43 (d, *J* = 16.5 Hz, 1H), 4.13 (d, *J* = 16.5 Hz, 1H), 3.89 (d, *J* = 15.4 Hz, 1H), 3.70 (s, 3H), 3.49 (d, *J* = 15.4 Hz, 1H), 3.09 (s, 3H).

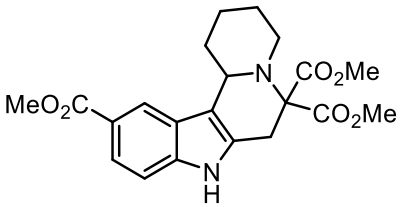
^{13}C-NMR (100 MHz, $CDCl_3$): δ 170.6, 169.6, 142.7, 140.6, 136.4, 130.0, 129.3, 128.1 (2C), 127.6, 127.5, 126.4, 126.1, 121.6, 119.6, 118.9, 112.1, 110.7, 72.5, 64.1, 55.0, 52.6, 52.5, 32.1.
HRMS (EI): Calculated for $C_{28}H_{26}N_2O_4$ $[M]^+$: 454.1893; found: *m/z* 454.1878.



2.135

Prepared from dimethyl 2-(piperidin-1-yl)-2-(prop-2-yn-1-yl)malonate (253 mg, 1.00 mmol) and methyl 4-azido-3-iodobenzoate (333 mg, 1.10 mmol) following GP3. Purification over silica (eluent: EtOAc/Hexanes). Arylazide **2.135** was obtained as an orange oil: 222.7 mg, 52% yield.

^{1}H-NMR (400 MHz, $CDCl_3$): δ 8.01 (d, *J* = 2.0 Hz, 1H), 7.94 (dd, *J* = 8.5, 2.0 Hz, 1H), 7.11 (d, *J* = 8.5 Hz, 1H), 3.90 (s, 3H), 3.81 (s, 6H), 3.23 (s, 2H), 2.66 (t, *J* = 5.1 Hz, 4H), 1.65 (p, *J* = 5.5 Hz, 4H), 1.47 (p, *J* = 6.3 Hz, 2H).
^{13}C-NMR (100 MHz, $CDCl_3$): δ 169.0, 165.9, 145.4, 135.5, 130.4, 126.6, 118.6, 115.8, 92.2, 78.4, 75.9, 52.6, 52.4, 49.7, 26.7, 24.9, 24.6.
IR (ATR): ῡ 2942 (w), 2808 (w), 2120 (s), 1757 (m), 1710 (s), 1594 (w), 1574 (m), 1490 (w), 1431 (s), 1398 (w), 1355 (w), 1311 (m), 1243 (s), 1225 (s), 1168 (m), 1156 (m), 1121 (m), 1033 (m), 1010 (m), 957 (w), 913 (w), 853 (w), 838 (w), 808 (w), 781 (w), 761 (s) cm^{-1}.
HRMS (ESI): Calculated for $C_{21}H_{24}N_4NaO_6$ $[M+Na]^+$: 451.1594; found: *m/z* 451.1591.



2.161

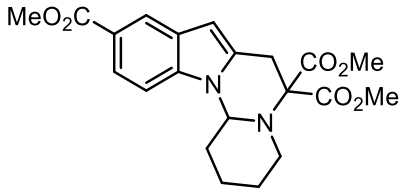
Prepared from arylazide **2.135** (43.4 mg, 0.10 mmol) following GP8. Reaction time: 6 hr. Purification over silica (eluent: EtOAc/Hexanes). Indole **2.161** was obtained as a yellow solid: 37.3 mg, 92% yield.

^{1}H-NMR (400 MHz, $CDCl_3$): δ 8.40 (bs, 1H), 8.23 (s, 1H), 7.81 (d, *J* = 8.5 Hz, 1H), 7.24 (d, *J* = 8.6 Hz, 1H), 3.96 (dd, *J* = 10.6, 2.0 Hz 1H), 3.92 (s, 3H), 3.82 (s, 3H), 3.64 (s, 3H), 3.40 (s, 2H), 3.20 (td, *J* = 10.9, 2.6 Hz, 1H), 2.89 (d, *J* = 11.4 Hz, 1H), 2.56 (d, *J* = 13.0 Hz, 1H), 1.93–1.83 (m, 1H), 1.77–1.45 (m, 4H).

^{13}C-NMR (100 MHz, $CDCl_3$): δ 170.7, 170.6, 168.3, 139.2, 130.8, 125.1, 122.8, 121.8, 121.3, 112.6, 110.7, 73.5, 56.7, 53.3, 52.3, 52.0, 51.2, 33.5, 32.5, 27.1, 25.0.

IR (ATR): ῡ 3450 (w), 2940 (w), 2845 (w), 1730 (s), 1710 (s), 1624 (w), 1473 (m), 1431 (s), 1374 (w), 1316 (m), 1261 (m), 1241 (s), 1224 (s), 1194 (s), 1120 (m), 1089 (m), 1052 (m), 1003 (m), 960 (w), 921 (w), 894 (w), 863 (w), 823 (w), 767 (s), 663 (w) cm^{-1}.

HRMS (EI): Calculated for $C_{21}H_{24}N_2O_6$ $[M]^+$: 400.1634; found: *m/z* 400.1618.



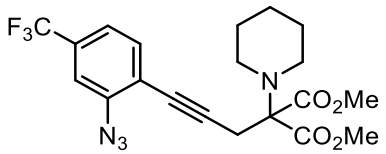
2.196

Prepared from arylazide **2.135** (43.4 mg, 0.10 mmol) following GP8 without the addition of TfOH. Reaction time: 1 hr. Purification over silica (eluent: EtOAc/Hexanes). Aminal **2.196** was obtained as yellow solid (17.5 mg, 53% yield).

^{1}H-NMR (400 MHz, $CDCl_3$): δ 8.27 (d, *J* = 1.4 Hz, 1H), 7.81 (dd, *J* = 8.7, 1.7 Hz, 1H), 7.29 (d, *J* = 8.7 Hz, 1H), 6.31 (s, 1H), 5.04 (dd, *J* = 9.5, 1.6 Hz, 1H), 3.91 (s, 3H), 3.86 (s, 3H), 3.58 (s, 2H), 3.55 (s, 3H), 3.27–3.17 (m, 1H), 2.98 (d, *J* = 12.7 Hz, 1H), 2.74 (d, *J* = 10.5 Hz, 1H), 1.96 (d, *J* = 12.0 Hz, 1H), 1.82–1.58 (m, 4H).

^{13}C-NMR (100 MHz, $CDCl_3$): δ 169.7, 169.4, 168.3, 136.8, 133.8, 128.7, 123.0, 122.0, 121.9, 110.2, 100.0, 72.4, 71.0, 53.4, 52.4, 51.9, 51.0, 34.0, 33.9, 26.4, 23.9.

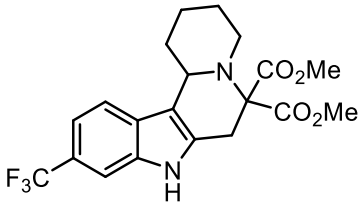
HRMS (EI): Calculated for $C_{21}H_{24}N_2O_6$ $[M]^+$: 400.1634; found: *m/z* 400.1629.



2.139

Prepared from dimethyl 2-(piperidin-1-yl)-2-(prop-2-yn-1-yl)malonate (270 mg, 1.07 mmol) and 2-azido-1-iodo-4-(trifluoromethyl)benzene (367 mg, 1.17 mmol) following GP3. Purification over silica (eluent: EtOAc/Hexanes). Arylazide **2.139** was obtained as an orange solid: 185.5 mg, 40% yield.

^{1}H-NMR (400 MHz, $CDCl_3$): δ 7.45 (d, *J* = 7.8 Hz, 1H), 7.28 (d, *J* = 8.5 Hz, 2H), 3.80 (s, 6H), 3.24 (s, 2H), 2.68–2.58 (m, 4H), 1.64 (p, *J* = 5.8 Hz, 4H), 1.47 (p, *J* = 6.0 Hz, 2H).
^{13}C-NMR (100 MHz, $CDCl_3$): δ 168.9, 141.7, 134.5, 131.2 (q, *J* = 33.4 Hz), 123.4 (q, *J* = 272.6 Hz), 121.3 (q, *J* = 3.7 Hz), 119.4, 115.8 (q, *J* = 3.8 Hz), 94.2, 78.2, 75.9, 52.6, 49.7, 26.7, 25.0, 24.6.
^{19}F-NMR (377 MHz, $CDCl_3$): δ -62.99 (s).
IR (ATR): ῡ 2930 (w), 2818 (w), 2109 (s), 1761 (m), 1721 (s), 1608 (w), 1565 (w), 1504 (w), 1434 (m), 1409 (m), 1328 (s), 1277 (s), 1237 (m), 1195 (w), 1166 (m), 1146 (m), 1117 (m), 1078 (m), 1050 (w), 1034 (m), 990 (w), 966 (w), 924 (w), 889 (w), 865 (w), 849 (m), 809 (w), 782 (w), 762 (w) cm^{-1}.
HRMS (ESI): Calculated for $C_{20}H_{21}F_3N_4NaO_4$ $[M+Na]^+$: 461.1413; found: *m/z* 461.1423.



2.165

Prepared from arylazide **2.139** (44.5 mg, 0.10 mmol) following GP8. Reaction time: 6 hr. Purification over silica (eluent: EtOAc/Hexanes). Indole **2.165** was obtained as yellow solid: 25.5 mg, 61% yield.

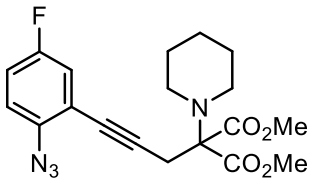
^{1}H-NMR (400 MHz, $CDCl_3$): δ 8.40 (bs, 1H), 7.54 (d, *J* = 8.6 Hz, 1H), 7.52 (s, 1H), 7.28 (dd, *J* = 8.6, 1.3 Hz, 1H), 3.96 (dd, *J* = 10.7, 1.9 Hz, 1H), 3.83 (s, 3H), 3.66 (s, 3H), 3.48–3.37 (m, 2H), 3.22 (td, *J* = 11.2, 3.1 Hz, 1H), 2.91 (d, *J* = 11.7 Hz, 1H), 2.50 (d, *J* = 13.1 Hz, 1H), 1.93–1.83 (m, 1H), 1.77–1.44 (m, 4H).

^{13}C-NMR (100 MHz, $CDCl_3$): δ 170.7, 170.6, 135.4, 132.3, 127.7, 125.3 (q, *J* = 271.3 Hz), 123.3 (q, *J* = 31.9 Hz), 119.2, 116.1 (q, *J* = 3.5 Hz), 111.7, 108.5 (q, *J* = 4.3 Hz), 73.5, 56.7, 53.3, 52.4, 51.2, 33.4, 32.6, 27.1, 25.0.

^{19}F-NMR (377 MHz, $CDCl_3$): δ -60.51 (s).

IR (ATR): ῡ 3344 (m), 2852 (w), 1755 (w), 1730 (s), 1592 (w), 1507 (w), 1477 (w), 1436 (m), 1341 (m), 1313 (w), 1266 (m), 1241 (m), 1224 (w), 1195 (m), 1165 (m), 1153 (m), 1110 (s), 1091 (m), 1053 (s), 1009 (m), 954 (w), 878 (m), 820 (m), 783 (w), 749 (w), 719 (w), 671 (w), 659 (w) cm^{-1}.

HRMS (EI): Calculated for $C_{20}H_{21}F_3N_2O_4$ $[M]^+$: 410.1453; found: *m/z* 410.1430.



2.134

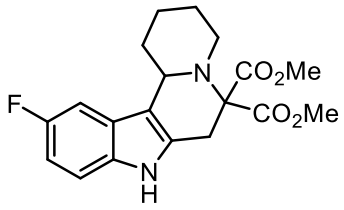
Prepared from dimethyl 2-(piperidin-1-yl)-2-(prop-2-yn-1-yl)malonate (259 mg, 1.02 mmol) and 1-azido-4-fluoro-2-iodobenzene (296 mg, 1.12 mmol) following GP3. Purification over silica (eluent: EtOAc/Hexanes). Arylazide **2.134** was obtained as an orange solid: 149.2 mg, 38% yield.

^{1}H-NMR (400 MHz, $CDCl_3$): δ 7.04 (dt, *J* = 8.6, 1.7 Hz, 1H), 7.00 (dd, *J* = 6.5, 1.9 Hz, 2H), 3.80 (s, 6H), 3.22 (s, 2H), 2.67–2.58 (m, 4H), 1.64 (p, *J* = 5.9 Hz, 4H), 1.46 (p, *J* = 5.8 Hz, 2H).

^{13}C-NMR (100 MHz, $CDCl_3$): δ 168.9, 159.2 (d, *J* = 245.0 Hz), 137.0 (d, *J* = 2.9 Hz), 120.4 (d, *J* = 24.0 Hz), 120.1 (d, *J* = 8.9 Hz), 117.2 (d, *J* = 9.9 Hz), 116.6 (d, *J* = 23.4 Hz), 92.5, 78.3 (d, *J* = 2.8 Hz), 75.9, 52.6, 49.7, 26.7, 24.9, 24.6.

^{19}F-NMR (377 MHz, $CDCl_3$): δ -117.85 (dt, *J* = 8.7, 6.1 Hz).

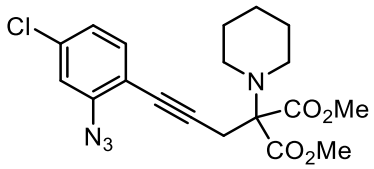
IR (ATR): ῡ 2926 (w), 2819 (w), 2113 (m), 1753 (s), 1725 (s), 1606 (w), 1488 (m), 1435 (m), 1412 (m), 1314 (w), 1288 (m), 1266 (m), 1234 (s), 1200 (s), 1166 (s), 1147 (m), 1111 (m), 1087 (w), 1050 (m), 1034 (w), 967 (w), 921 (w), 889 (w), 865 (m), 815 (w), 781 (w) cm^{-1}.
HRMS (ESI): Calculated for $C_{19}H_{21}FN_4NaO_4$ $[M+Na]^+$: 411.1444; found: *m/z* 411.1427.



2.160

Prepared from arylazide **2.134** (39.5 mg, 0.10 mmol) following GP8. Reaction time: 24 hr. Purification over silica (eluent: EtOAc/Hexanes). Indole **2.160** was obtained as yellow solid: 26.7 mg, 73% yield.

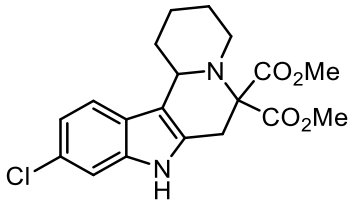
^{1}H-NMR (400 MHz, $CDCl_3$): δ 7.96 (bs, 1H), 7.15 (dd, *J* = 8.8, 4.5 Hz, 1H), 7.11 (dd, *J* = 10.0, 2.5 Hz, 1H), 6.84 (td, *J* = 9.0, 2.5 Hz, 1H), 3.91 (dd, *J* = 10.6, 2.2 Hz, 1H), 3.83 (s, 3H), 3.64 (s, 3H), 3.49–3.32 (m, 2H), 3.20 (td, *J* = 11.2, 3.3 Hz, 1H), 2.88 (d, *J* = 11.7 Hz, 1H), 2.45 (d, *J* = 13.2 Hz, 1H), 1.92–1.83 (m, 1H), 1.78–1.41 (m, 4H).
^{13}C-NMR (100 MHz, $CDCl_3$): δ 170.8, 170.5, 157.6 (d, *J* = 233.9 Hz), 132.9, 131.3, 125.8 (d, *J* = 9.9 Hz), 111.6 (d, *J* = 4.6 Hz), 111.4 (d, *J* = 9.8 Hz), 109.2 (d, *J* = 25.9 Hz), 104.3 (d, *J* = 24.1 Hz), 73.5, 56.7, 53.3, 52.3, 51.1, 33.1, 32.5, 27.1, 25.0.
^{19}F-NMR (377 MHz, $CDCl_3$): δ -124.80 (tt, *J* = 8.3, 3.7 Hz).
IR (ATR): ῡ 3362 (m), 2930 (w), 2847 (w), 1734 (m), 1713 (s), 1635 (m), 1594 (w), 1453 (m), 1430 (m), 1374 (w), 1321 (w), 1272 (m), 1248 (m), 1224 (s), 1178 (m), 1143 (w), 1099 (m), 1085 (m), 1067 (m), 1051 (m), 1007 (w), 961 (w), 923 (w), 860 (s), 822 (w), 792 (w), 778 (w), 762 (w), 742 (w) cm^{-1}.
HRMS (EI): Calculated for $C_{19}H_{21}FN_2O_4$ $[M]^+$: 360.1485; found: *m/z* 360.1486.



2.137

Prepared from dimethyl 2-(piperidin-1-yl)-2-(prop-2-yn-1-yl)malonate (164 mg, 0.65 mmol) and 2-azido-4-chloro-1-iodobenzene (200 mg, 0.71 mmol) following GP3. Purification over silica (eluent: EtOAc:hexanes). Arylazide **2.137** was obtained as an amber oil: 127 mg, 48% yield.

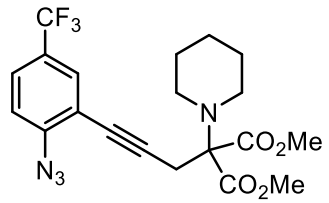
^{1}H-NMR (300 MHz, $CDCl_3$): δ 7.29–7.24 (m, 1H), 7.07–6.99 (m, 2H), 3.80 (s, 6H), 3.21 (s, 2H), 2.64 (t, *J* = 5.2 Hz, 4H), 1.70–1.58 (m, 4H), 1.52–1.42 (m, 2H).
^{13}C-NMR (101 MHz, $CDCl_3$): δ 169.0, 142.1, 134.8, 134.8, 125.1, 119.1, 114.4, 92.3, 78.3, 75.9, 52.6, 49.7, 26.7, 25.0, 24.7.
HRMS (ESI): Calculated for $C_{19}H_{21}ClN_4NaO_4$ $[M+Na]^+$: 427.1149; found: *m/z* 427.1151.



2.163

Prepared from arylazide **2.137** (25.1 mg, 0.062 mmol) following GP8. Reaction time: 2.5 hr. Purification over silica (eluent: EtOAc:hexanes). Indole **2.163** was obtained as a yellow solid: 18 mg, 76% yield.

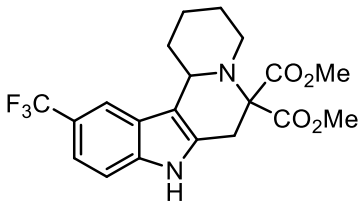
^{1}H-NMR (300 MHz, $CDCl_3$): δ 7.98 (bs, 1H), 7.37 (d, *J* = 8.5 Hz, 1H), 7.28–7.23 (m, 1H), 7.02 (dd, *J* = 8.5, 1.9 Hz, 1H), 3.97–3.89 (m, 1H), 3.85 (s, 3H), 3.65 (s, 3H), 3.46–3.32 (m, 2H), 3.26–3.16 (m, 1H), 2.93–2.84 (m, 1H), 2.51–2.41 (m, 1H), 1.92–1.81 (m, 1H), 1.75–1.46 (m, 4H).
^{13}C-NMR (101 MHz, $CDCl_3$): δ 170.7, 170.5, 136.9, 130.1, 127.2, 124.1, 120.0, 119.8, 111.5, 111.0, 73.5, 56.7, 53.3, 52.3, 51.1, 33.4, 32.4, 27.1, 25.0.
HRMS (EI): Calculated for $C_{19}H_{21}ClN_2O_4$ $[M]^+$: 376.1190; found: *m/z* 376.1175.



2.133

Prepared from dimethyl 2-(piperidin-1-yl)-2-(prop-2-yn-1-yl)malonate (203 mg, 0.80 mmol) and 1-azido-2-iodo-4-(trifluoromethyl)benzene (276 mg, 0.88 mmol) following GP3. Purification over silica (eluent: EtOAc:hexanes). Arylazide **2.133** was obtained as a pale-yellow oil: 59.3 mg, 17% yield.

^{1}H-NMR (300 MHz, $CDCl_3$): δ 7.59 (dt, *J* = 2.2, 0.7 Hz, 1H), 7.51 (ddd, *J* = 8.5, 2.2, 0.7 Hz, 1H), 7.15 (dt, *J* = 8.5, 0.7 Hz, 1H), 3.81 (s, 6H), 3.24 (s, 2H), 2.65 (t, *J* = 5.3 Hz, 4H), 1.65 (p, *J* = 5.6 Hz, 4H), 1.48 (q, *J* = 6.1 Hz, 2H).
^{13}C-NMR (101 MHz, $CDCl_3$): δ 168.8, 144.2, 131.0 (q, *J* = 3.8 Hz), 126.9 (q, *J* = 33.2 Hz), 125.8 (q, *J* = 3.8 Hz), 123.5 (q, *J* = 272.4 Hz), 118.9, 116.1, 92.9, 77.8, 75.7, 52.5, 49.5, 26.5, 24.8, 24.5.
^{19}F-NMR (471 MHz, $CDCl_3$): δ -62.5.
HRMS (ESI): Calculated for $C_{20}H_{21}F_3N_4NaO_4$ $[M+Na]^+$: 461.1413; found: *m/z* 461.1389.



2.159

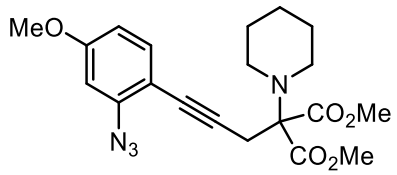
Prepared from arylazide **2.133** (25.6 mg, 0.058 mmol) following GP8. Reaction time: 3 hr. Purification over silica (eluent: Et_2O:hexanes). Indole **2.159** was obtained as a yellow solid: 17 mg, 73% yield.

^{1}H-NMR (300 MHz, $CDCl_3$): δ 8.16 (bs, 1H), 7.74 (dd, *J* = 1.7, 0.9 Hz, 1H), 7.38–7.29 (m, 2H), 3.96 (dd, *J* = 10.5, 2.2 Hz, 1H), 3.85 (s, 3H), 3.65 (s, 3H), 3.51–3.37 (m, 2H), 3.21 (td, *J* = 11.1, 3.5 Hz, 1H), 2.95–2.86 (m, 1H), 2.54–2.45 (m, 1H), 1.97–1.84 (m, 1H), 1.77–1.49 (m, 4H).

^{13}C-NMR (101 MHz, $CDCl_3$): δ 170.5, 170.4, 137.7, 131.1, 125.2 (q, *J* = 271.6 Hz), 124.8, 121.7 (q, *J* = 31.6 Hz), 118.0 (q, *J* = 3.7 Hz), 116.4 (q, *J* = 3.7 Hz), 112.2, 111.0, 73.3, 56.5, 53.2, 52.2, 51.1, 33.4, 32.4, 27.0, 24.9.

^{19}F-NMR (471 MHz, $CDCl_3$): δ -60.1.

HRMS (EI): Calculated for $C_{20}H_{21}F_3N_2O_4$ $[M]^+$: 410.1454; found: *m/z* 410.1451.



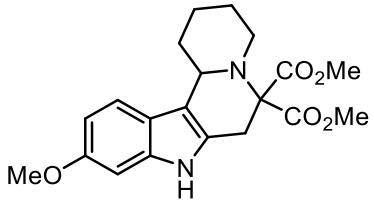
2.138

Prepared from dimethyl 2-(piperidin-1-yl)-2-(prop-2-yn-1-yl)malonate (39 mg, 0.15 mmol) and 2-azido-1-iodo-4-methoxybenzene (46 mg, 0.17 mmol) following GP3. Purification over silica (eluent: EtOAc:hexanes). Arylazide **2.138** was obtained as an amber oil: 37.2 mg, 55% yield.

^{1}H-NMR (300 MHz, $CDCl_3$): δ 7.25 (dd, *J* = 8.4, 0.4 Hz, 1H), 6.60 (dd, *J* = 8.5, 2.5 Hz, 1H), 6.56 (dd, *J* = 2.4, 0.6 Hz, 1H), 3.80 (s, 3H), 3.79 (s, 6H), 3.20 (s, 2H), 2.65 (t, *J* = 5.0 Hz, 4H), 1.70–1.57 (m, 4H), 1.46 (dt, *J* = 9.8, 5.1 Hz, 2H).

^{13}C-NMR (101 MHz, $CDCl_3$): δ 169.1, 160.4, 142.1, 135.0, 110.8, 108.3, 104.6, 89.5, 79.0, 76.0, 55.7, 52.6, 49.7, 26.7, 24.9, 24.7.

HRMS (ESI): Calculated for $C_{20}H_{24}N_4NaO_5$ $[M+Na]^+$: 423.1644; found: *m/z* 423.1652.



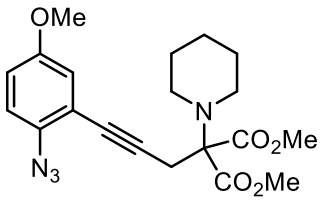
2.164

Prepared from arylazide **2.138** (15.8 mg, 0.039 mmol) following GP8. Reaction time: 3 hr. Purification over silica (eluent: EtOAc:hexanes). Indole **2.164** was obtained as an amber solid: 10.5 mg, 71% yield.

^{1}H-NMR (300 MHz, $CDCl_3$): δ 7.73 (bs, 1H), 7.34 (d, *J* = 8.6 Hz, 1H), 6.80 (dd, *J* = 2.3, 0.5 Hz, 1H), 6.72 (dd, *J* = 8.6, 2.3 Hz, 1H), 3.94 (dd, *J* = 10.2, 2.3 Hz, 1H), 3.84 (s, 3H), 3.81 (s, 3H), 3.63 (s, 3H), 3.47–3.33 (m, 2H), 3.22 (td, *J* = 11.2, 3.5 Hz, 1H), 2.86 (dd, *J* = 11.7, 3.7 Hz, 1H), 2.52–2.43 (m, 1H), 1.86 (d, *J* = 7.2 Hz, 1H), 1.74–1.48 (m, 4H).

^{13}C-NMR (101 MHz, $CDCl_3$): δ 170.9, 170.5, 155.9, 137.3, 127.9, 120.0, 119.5, 111.4, 108.7, 95.2, 73.6, 56.9, 55.7, 53.2, 52.2, 51.1, 33.4, 32.4, 27.2, 25.1.

HRMS (EI): Calculated for $C_{20}H_{24}N_2O_5$ $[M]^+$: 372.1685; found: *m/z* 372.1692.



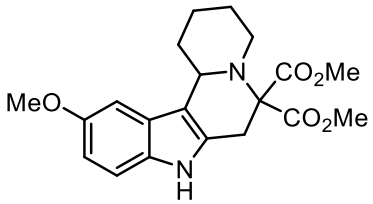
2.136

Prepared from dimethyl 2-(piperidin-1-yl)-2-(prop-2-yn-1-yl)malonate (112 mg, 0.44 mmol) and 1-azido-2-iodo-4-methoxybenzene (133 mg, 0.49 mmol) following GP3. Purification over silica (eluent: EtOAc:hexanes). Arylazide **2.136** was obtained as an amber oil: 126 mg, 71% yield.

^{1}H-NMR (300 MHz, $CDCl_3$): δ 6.97 (dd, *J* = 8.5, 0.8 Hz, 1H), 6.88–6.82 (m, 2H), 3.80 (s, 6H), 3.77 (s, 3H), 3.22 (s, 2H), 2.66 (t, *J* = 5.2 Hz, 4H), 1.65 (p, *J* = 5.6 Hz, 5H), 1.46 (p, *J* = 6.6 Hz, 2H).

^{13}C-NMR (100 MHz, $CDCl_3$): δ 169.0, 156.5, 133.7, 119.9, 118.4, 116.5, 115.9, 91.2, 79.2, 76.0, 55.8, 52.6, 49.7, 26.7, 24.9, 24.7.

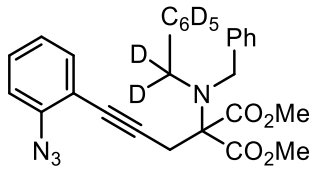
HRMS (ESI): Calculated for $C_{20}H_{24}N_4NaO_5$ $[M+Na]^+$: 423.1644; found: *m/z* 423.1667.



2.162

Prepared from arylazide **2.136** (23.5 mg, 0.059 mmol) following GP8. Reaction time: 2 hr. Purification over silica (eluent: Et_2O:hexanes). Indole **2.162** was obtained as a yellow solid: 16 mg, 75% yield.

^{1}H-NMR (400 MHz, $CDCl_3$): δ 7.74 (bs, 1H), 7.17 (dd, *J* = 8.7, 0.6 Hz, 1H), 6.93 (d, *J* = 2.4 Hz, 1H), 6.78 (dd, *J* = 8.7, 2.4 Hz, 1H), 3.94 (dd, *J* = 10.5, 2.2 Hz, 1H), 3.84 (s, 6H), 3.63 (s, 3H), 3.49–3.34 (m, 2H), 3.23 (td, *J* = 10.8, 3.7 Hz, 1H), 2.92–2.83 (m, 1H), 2.54–2.46 (m, 1H), 1.94–1.83 (m, 1H), 1.75–1.51 (m, 4H).
^{13}C-NMR (100 MHz, $CDCl_3$): δ 170.9, 170.5, 153.9, 131.6, 130.2, 126.0, 111.5, 111.3, 110.7, 101.9, 73.6, 57.0, 56.2, 53.2, 52.2, 51.2, 33.2, 32.6, 27.2, 25.1.
HRMS (EI): Calculated for $C_{20}H_{24}N_2O_5$ $[M]^+$: 372.1685; found: *m/z* 372.1666.

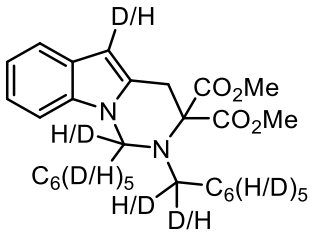


d$_7$-**2.200**

Prepared from dimethyl 2-(benzyl((phenyl-*d*$_5$)methyl-*d*$_2$)amino)-2-(prop-2-yn-1-yl)malonate (185 mg, 0.48 mmol) and 1-azido-2-iodobenzene (140 mg, 0.57 mmol) following GP3. Purification over silica (eluent: EtOAc/Hexanes). *d*$_7$-**2.200** was obtained as an orange solid: 163.7 mg, 70% yield.

^{1}H-NMR (500 MHz, $CDCl_3$): δ 7.39 (dd, *J* = 7.7, 1.3 Hz, 1H), 7.36 (d, *J* = 7.3 Hz, 2H), 7.31 (td, *J* = 8.1, 1.5 Hz, 1H), 7.19 (t, *J* = 7.4 Hz, 2H), 7.16 – 7.05 (m, 3H), 4.01 (s, 2H), 3.64 (s, 6H), 3.31 (s, 2H).
^{13}C-NMR (126 MHz, $CDCl_3$): δ 169.8, 141.0, 139.5, 139.2, 134.0, 129.3, 129.0, 128.6 (t, *J* = 23.0 Hz, 1H), 128.0, 127.5 (t, *J* = 24.0 Hz, 1H), 126.9, 126.4 (t, *J* = 24.0 Hz, 1H), 124.7, 118.7, 115.7, 91.4, 79.5, 75.7, 55.5, 54.8, 52.5, 26.9.[n]
HRMS (ESI): Calculated for $C_{28}H_{19}D_7N_4NaO_4$ $[M+Na]^+$: 512.2291; found: *m/z* 512.2301.

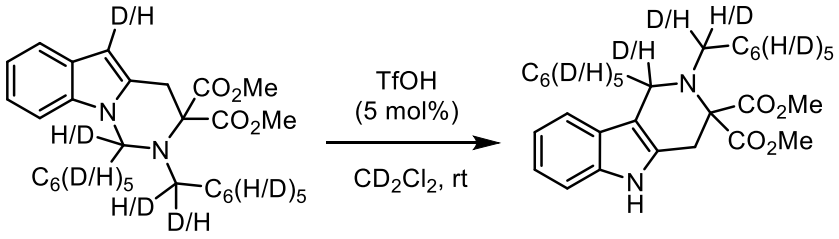
[n]The complete multiplicity for the signal at 54.8 ppm corresponding to CD_2 was not able to be clearly observed.



d$_7$-**2.201**

Prepared from *d*$_7$-**2.200** (24.7 mg, 0.05 mmol) following GP8 without using TfOH. Reaction time: 45 min. Purification over silica (eluent: EtOAc:hexanes). *d*$_7$-**2.201** was obtained as a white solid: 18 mg, 79% yield.

^{1}H-NMR (500 MHz, CD_2Cl_2): δ 7.51 (d, *J* = 7.9 Hz, 1H), 7.25–7.10 (m, 5H, 50% *D*), 7.02–6.98 (m, 1H), 6.91 (ddd, *J* = 8.2, 7.1, 1.1 Hz, 1H), 6.83 (d, *J* = 8.2 Hz, 1H), 6.36 (d, *J* = 0.8 Hz, 1H, 33% *D*), 6.26 (s, 1H, 48% *D*), 4.43 (d, *J* = 16.0 Hz, 1H, 54% *D*), 4.14 (d, *J* = 16.0 Hz, 1H, 56% *D*), 3.90 (dd, *J* = 15.7, 1.0 Hz, 1H), 3.65 (s, 2H), 3.63 (d, *J* = 15.8 Hz, 1H), 3.18 (s, 2H).
^{13}C-NMR (100 MHz, CD_2Cl_2): δ 170.4, 169.3, 140.7, 140.4, 139.6, 139.3, 135.6, 132.7, 132.6, 129.3, 129.2, 129.0, 128.9, 128.8, 128.6, 128.4, 127.4, 121.2, 120.4, 110.7, 110.6, 99.1, 75.3, 74.8 (t, *J* = 24.0 Hz), 70.7 (2C), 55.2, 53.1 (2C), 32.3 (2C).[o]
HRMS (EI): Calculated for $C_{28}H_{19}D_7N_2O_4$ $[M]^+$: 461.2332; found: *m/z* 461.2345.



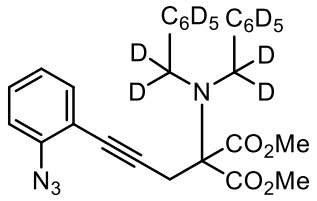
d$_7$-**2.201** *d*$_6$-**2.202**

Partially deuterated aminal *d*$_7$-**2.201** (9.5 mg, 0.021 mmol, 1 equiv.) was dissolved in CD_2Cl_2 (0.2 mL) and transferred to a screw-cap NMR tube[p] followed by the addition of TfOH (0.5 M solution in CD_2Cl_2, 1.0 μL, 0.0062 mmol, 0.05 equiv.) at room temperature. After 10 minutes, the reaction is quenched with triethylamine and concentrated under reduced pressure to afford a crude oil.

[o]Due to not enough sample, some deuterated signals were unable to be observed.
[p]Mesitylene was added as an internal standard.

Purification over silica (eluent: EtOAc/Hexanes). Partially deuterated indole d_6-**2.202** was obtained as a white solid (7.3 mg, 79% yield).

^{1}H-NMR (300 MHz, $CDCl_3$): δ 7.85 (bs, 1H), 7.42 (d, *J* = 6.8 Hz, 1H), 7.28–7.00 (m, 6H), 6.86–6.81 (m, 2H), 5.40–5.37 (m, 1H, 49% D), 4.42 (d, *J* = 16.4 Hz, 1H, 61% D), 4.12 (d, *J* = 16.3 Hz, 1H, 62% D), 3.89 (d, *J* = 15.5 Hz, 1H), 3.70 (s, 3H), 3.48 (d, *J* = 15.5 Hz, 1H), 3.08 (s, 3H).
^{13}C-NMR (76 MHz, $CDCl_3$): δ 170.6, 169.6, 142.7, 142.5, 140.6, 140.3, 136.4, 130.0, 129.3 (2C), 129.1, 128.4, 128.1 (2C), 127.7, 127.6, 127.5, 127.4, 126.4, 126.1, 121.6, 119.6, 118.9, 112.0, 111.9, 110.7, 72.4, 72.4, 64.0, 54.9, 53.57, 53.43, 52.6, 52.5, 32.1.[q]
HRMS (EI): Calculated for $C_{28}H_{19}D_7N_2O_4$ $[M]^+$: 461.2332; found: *m/z* 461.22981.

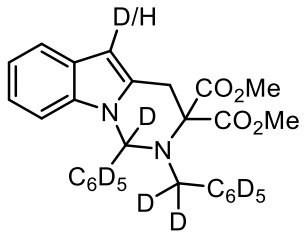


d_{14}-**2.200**

Prepared from dimethyl 2-(bis((phenyl-d_5)methyl-d_2)amino)-2-(prop-2-yn-1-yl)malonate (736.8 mg, 1.94 mmol) and 1-azido-2-iodobenzene (570.1 mg, 2.32 mmol) following GP3. Purification over silica (eluent: DCM:hexanes). Fully deuterated arylazide d_{14}-**2.200** was obtained as an amber solid: 571.4 mg, 59% yield.

^{1}H-NMR (300 MHz, $CDCl_3$): δ 7.40 (ddd, *J* = 7.7, 1.6, 0.6 Hz, 1H), 7.32 (ddd, *J* = 8.1, 7.4, 1.6 Hz, 1H), 7.14–7.04 (m, 2H), 3.64 (s, 6H), 3.32 (s, 2H).
^{13}C-NMR (126 MHz, $CDCl_3$): δ 169.7, 141.0, 139.1, 133.9, 129.2, 128.5 (t, *J* = 24.7 Hz), 127.4 (t, *J* = 24.7 Hz), 126.4 (t, *J* = 24.3 Hz), 124.6, 118.6, 115.6, 91.3, 79.4, 75.7, 54.6 (t, *J* = 20.6 Hz), 52.4, 26.8.
HRMS (ESI): Calculated for $C_{28}H_{12}D_{14}N_4O_4$ $[M+Na]^+$: 519.2741; found: *m/z* 519.2716.

[q]Due to not enough sample, some deuterated signals were unable to be observed.



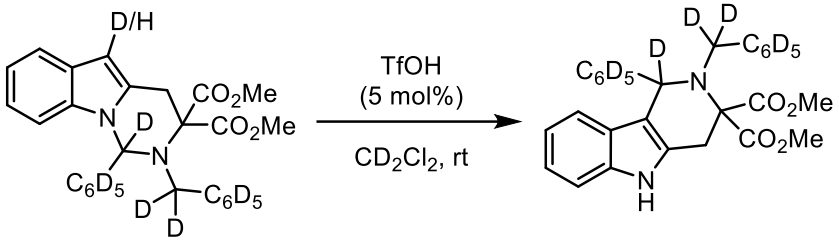
d_{14}-**2.201**

Prepared from fully deuterated arylazide d_{14}-**2.200** (30.8 mg, 0.06 mmol) following GP8 and without TfOH. Reaction time: 45 min. Purification over silica (eluent: EtOAc:hexanes). Fully deuterated aminal d_{14}-**2.201** was obtained as a white solid: 19 mg, 65% yield.

^{1}H-NMR (400 MHz, CD_2Cl_2): δ 7.52 (dt, *J* = 8.2, 0.9 Hz, 1H), 7.02 (ddd, *J* = 7.9, 7.0, 1.2 Hz, 1H), 6.93 (ddd, *J* = 8.2, 7.0, 1.3 Hz, 1H), 6.84 (dt, *J* = 8.1, 1.1 Hz, 1H), 6.38 (bs, 1H, 85% *D*). 3.91 (d, *J* = 15.8 Hz, 1H), 3.66 (s, 3H), 3.64 (d, *J* = 15.8 Hz, 1H), 3.19 (s, 3H).

^{13}C-NMR (100 MHz, CD_2Cl_2): δ 169.8, 168.7, 139.9, 138.8, 135.1, 132.1, 128.7, 128.3–126.9 (m)[r], 126.3 (t, *J* = 24.3 Hz), 120.6, 119.9 (2C), 110.1, 98.5, 98.3 (t, *J* = 26.4 Hz), 74.2 (t, *J* = 23.1 Hz), 70.1, 52.5, 52.5, 31.7.[s]

HRMS (EI): Calculated for $C_{28}H_{12}D_{14}N_2O_4$ $[M]^+$: 468.2771; found: *m/z* 468.2774.



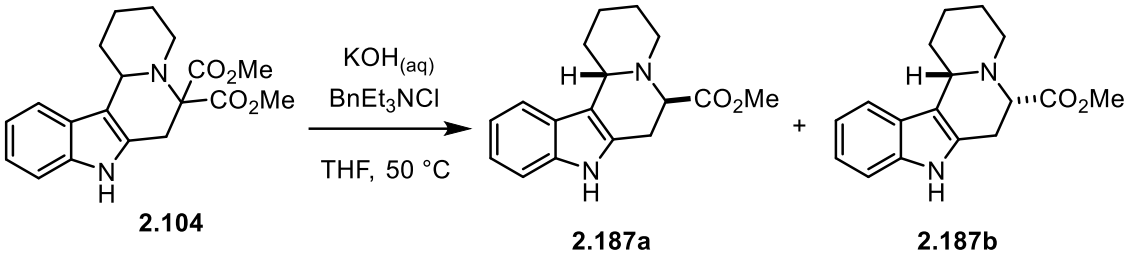
d_{14}-**2.202** d_{13}-**2.202**

Fully deuterated aminal d_{14}-**2.201** (40.3 mg, 0.086 mmol, 1 equiv.) was dissolved in CD_2Cl_2 (0.8 mL) and transferred to a screw-cap NMR tube,[t] followed by the addition of TfOH (0.5 M solution in CD_2Cl_2, 8.6 μL, 0.0043 mmol, 0.05 equiv.) at room temperature. After 10 minutes, the reaction is quenched with triethylamine and concentrated under reduced pressure to afford a crude oil.

[r]Multiple overlap of signals from 128.3–126.9 ppm due to C-D aromatic signals.
[s]Extra peaks due to an unexpected isotopic effect from the signals at 132.1 and 128.7 ppm.
[t]Mesitylene was added as an internal standard.

Purification over silica (eluent: EtOAc/Hexanes). Fully deuterated indole d_{13}-**2.202** was obtained as a white solid (20 mg, 50% yield).

^{1}H-NMR (400 MHz, $CDCl_3$): δ 7.92 (bs, 1H), 7.29–7.22 (m, 1H), 7.06 (ddd, *J* = 8.2, 4.8, 3.5 Hz, 1H), 6.89–6.80 (m, 2H), 3.90 (d, *J* = 15.5 Hz, 1H), 3.71 (s, 3H), 3.50 (d, *J* = 15.5 Hz, 1H), 3.10 (s, 3H).
^{13}C-NMR (100 MHz, $CDCl_3$): δ 170.6, 169.5, 142.4, 140.3, 136.3, 129.4 (t, *J* = 24.1 Hz), 129.3, 127.6 (2C, t, *J* = 23.1 Hz), 127.0 (2C, t, *J* = 24.0 Hz), 126.0, 125.8 (t, *J* = 24.1 Hz), 121.5, 119.5, 118.8, 111.8, 110.6, 72.3, 63.4 (t, *J* = 21.1 Hz), 54.1 (t, *J* = 20.4 Hz), 52.5, 52.4, 31.9.
HRMS (EI): Calculated for $C_{28}H_{13}D_{13}N_2O_4$ $[M]^+$: 467.2709; found: *m/z* 467.2715.



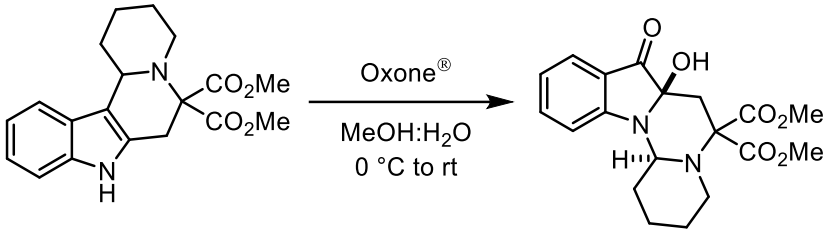
2.104 **2.187a** **2.187b**

Indole **2.104** (18.6 mg, 0.05 mmol, 1 equiv.), $BnEt_3NCl$ (6.2 mg, 0.03 mmol, 0.5 equiv.) and aqueous KOH (91 mg, 1.62 mmol, 30 equiv.) were dissolved in 0.5 mL of THF. The reaction mixture was heated to 50 °C and left to stir overnight. Afterwards, the mixture was cooled to room temperature and neutralized (pH ~6–7) by adding 1 M $HCl_{(aq)}$ dropwise, diluted with water, and extracted using EtOAc (3x 5 mL). The organic phase was dried under $MgSO_4$, filtered, concentrated *in-vacuo*, and purified by flash-column chromatography. Diastereomeric monoesters **2.187a** and **2.187b** were obtained as yellow solids and as an inseparable mixture: 9.3 mg, 67% yield, and *d.r.* = 2.2:1.

^{1}H-NMR (400 MHz, $CDCl_3$): δ 7.85 (bs, 1H, **2.187b**), 7.78 (bs, 1H, **2.187a**), 7.57 (d, *J* = 7.8 Hz, 1H, **2.187b**), 7.53 (d, *J* = 7.8 Hz, 1H, , **2.187a**), 7.30 (d, *J* = 8.4 Hz, 2H), 7.17–7.02 (m, 3H), 4.12 (dq, *J* = 11.0, 1.8 Hz, 1H, **2.187a**), 3.81 (s, 3H, **2.187b**), 3.79 (dd, *J* = 5.9, 1.1 Hz, 1H, **2.187a**), 3.66 (d, *J* = 5.9 Hz, 1H, **2.187b**), 3.60 (s, 3H, **2.187a**), 3.51 (dd, *J* = 11.1, 3.8 Hz, 1H, **2.187b**), 3.39–3.17 (m, 3H), 3.08 (d, *J* = 15.8 Hz, 1H, **2.187a**), 2.99–2.79 (m, 2H), 2.67–2.52 (m, 2H), 2.41 (td, *J* = 10.2, 9.6, 4.1 Hz, 1H, **2.187b**), 1.95–1.53 (m, 7H), 1.47–1.30 (m, 1H, **2.187b**).

^{13}C-NMR (100 MHz, $CDCl_3$): δ 173.3 (**2.187b**), 172.9, 136.3, 129.8, 125.8, 125.5 (**2.187b**), 121.1 (**2.187b**), 120.9, 119.4 (**2.187b**), 119.3 (**2.187b**), 119.1 (2C), 112.3, 110.8 (**2.187b**), 110.7, 64.8 (**2.187b**), 61.7, 60.9 (**2.187b**), 54.9, 53.8, 52.2 (**2.187b**), 51.2, 32.8, 31.0 (**2.187b**), 27.3, 26.8, 26.0 (**2.187b**), 24.9, 23.9 (**2.187b**).[u]

HRMS (ESI): Calculated for $C_{17}H_{20}N_2O_2$ $[M]^+$: 284.1525; found: *m/z* 284.1490.



2.104 **2.192**

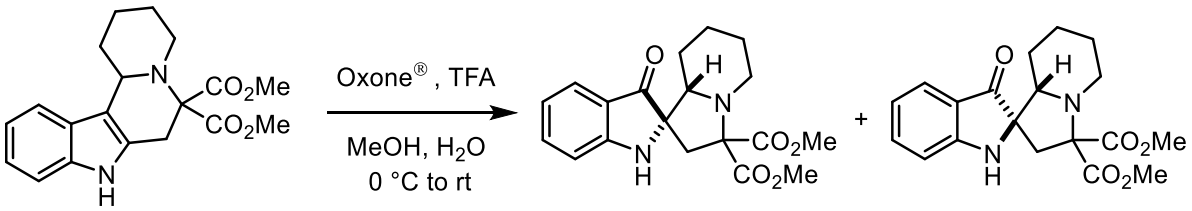
A solution of indole **2.104** (111 mg, 0.33 mmol, 1 equiv.) in MeOH (0.02 M, 16 mL) is cooled to 0 °C, at which point Oxone® (500 mg, 1.63 mmol, 5 equiv.) is added in H_2O (2 mL) dropwise. The reaction is warmed to room temperature and stirred till completion as indicated by TLC analysis. Once complete, the reaction is quenched with a saturated aqueous solution of $Na_2S_2O_5$ and extracted using DCM (3x 10 mL) and the collected organic fractions are washed with brine before being dried over anhydrous $MgSO_4$, filtered, and concentrated *in vacuo* to afford a crude, dark amber oil. **Note:** The hydroxy aminal **2.192** is acid sensitive, therefore any TLC analysis or chromatography should be conducted on deactivated silica using 1–2% Et_3N in the eluent. Purification over silica (eluent: EtOAc:Et_3N:hexanes followed by MeOH:Et_3N:DCM) gave hydroxy aminal **2.192** as a yellow solid: 78 mg, 64% yield and as a single diastereoisomer.

^{1}H-NMR (300 MHz, $CDCl_3$): δ 7.54–7.49 (m, 1H), 7.42 (ddd, *J* = 8.4, 7.0, 1.4 Hz, 1H), 6.91 (bs, 1H), 6.79 (dt, *J* = 8.3, 0.8 Hz, 1H), 6.71 (ddd, *J* = 7.9, 7.1, 0.9 Hz, 1H), 4.15–4.02 (m, 2H), 3.94–3.87 (m, 4H), 3.85 (s, 3H), 3.55 (d, *J* = 14.5 Hz, 1H), 2.58 (d, *J* = 14.5 Hz, 1H), 2.33 (tdd, *J* = 17.4, 8.7, 4.0 Hz, 1H), 2.17 (qd, *J* = 13.0, 4.0 Hz, 1H), 1.77–1.66 (m, 1H), 1.64–1.53 (m, 1H), 1.33 (ddd, *J* = 17.3, 8.6, 4.0 Hz, 1H), 1.25–1.13 (m, 1H).

^{13}C-NMR (101 MHz, $CDCl_3$): δ 199.8, 167.5, 163.2, 161.3, 138.4, 124.8, 118.6, 118.1, 111.7, 88.2, 78.9, 72.8, 60.6, 53.7, 53.6, 42.7, 21.5, 20.1, 19.9.

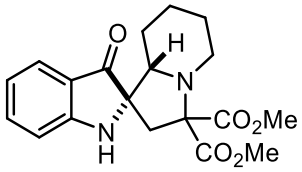
[u]Peak assignments were confirmed by HSQC and COSY experiments.

HRMS (ESI): Calculated for $C_{19}H_{22}N_2NaO_6$ $[M+Na]^+$: 397.1376; found: *m/z* 397.1375.



2.104 **2.191a** **2.191b**

A solution of indole **2.104** (33.1 mg, 0.10 mmol, 1 equiv.) in MeOH (0.02 M, 4.8 mL) is cooled to 0 °C, at which point TFA (8.9 μL, 0.12 mmol, 1.2 equiv.) is added and the reaction stirred at that temperature for 5 minutes. Subsequently, Oxone® (77 mg, 0.25 mmol, 2.5 equiv.) is added in H_2O (1 mL) dropwise. The reaction is warmed to room temperature and stirred till completion as indicated by TLC analysis. Once complete, the reaction is quenched with a saturated aqueous solution of $Na_2S_2O_5$, followed by a saturated aqueous solution of $NaHCO_3$ to neutralize the reaction mixture. The reaction is then extracted using DCM (3x 5 mL) and the collected organic fractions are washed with brine before being dried over anhydrous $MgSO_4$, filtered, and concentrated *in vacuo* to afford a crude, yellow oil. Overall NMR yield = 88% and *d.r.* = 15:1. Purification over silica (eluent: EtOAc:hexanes). Pseudoindoxyl **2.191a** was obtained as a yellow solid: 27.2 mg, 76% yield. The minor diastereomer pseudoindoxyl **2.191b** was obtained as a yellow solid: 2.2 mg, 6% yield.

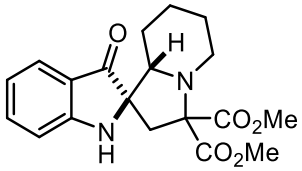


2.191a

^{1}H-NMR (300 MHz, $CDCl_3$): δ 7.56 (dd, *J* = 7.8, 1.4 Hz, 1H), 7.42 (ddd, *J* = 8.4, 7.0, 1.4 Hz, 1H), 6.84 (dt, *J* = 8.3, 0.8 Hz, 1H), 6.77 (ddd, *J* = 7.8, 7.1, 0.9 Hz, 1H), 5.15 (bs, 1H), 3.80 (s, 3H), 3.80 (s, 2H), 3.29–3.21 (m, 1H), 3.15 (dd, *J* = 10.1, 3.2 Hz, 1H), 2.91 (d, *J* = 13.9 Hz, 1H), 2.58–2.44 (m, 2H), 1.70–1.54 (m, 2H), 1.50–1.34 (m, 1H), 1.35–1.11 (m, 3H).

^{13}C-NMR (101 MHz, $CDCl_3$): δ 199.6, 171.6, 170.3, 160.8, 137.5, 124.6, 121.2, 118.7, 112.2, 73.5, 73.4, 68.6, 52.9, 52.4, 47.6, 43.9, 25.5, 24.9, 22.7.

HRMS (EI): Calculated for $C_{19}H_{22}N_2O_5$ $[M]^+$: 358.1530; found: *m/z* 358.1541.

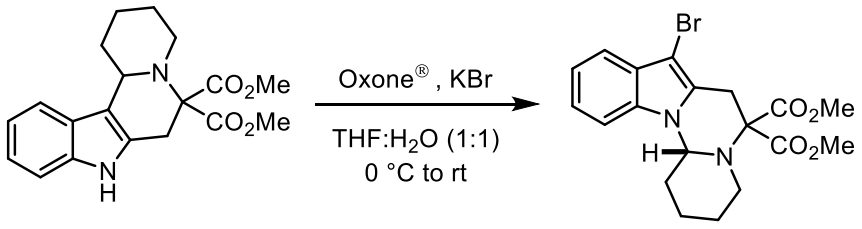


2.191b

^{1}H-NMR (300 MHz, $CDCl_3$): δ 7.54 (d, *J* = 7.8 Hz, 1H), 7.40 (ddd, *J* = 8.3, 7.0, 1.4 Hz, 1H), 6.80–6.70 (m, 2H), 5.37 (bs, 1H), 3.81 (s, 3H), 3.79 (s, 3H), 3.55–3.46 (m, 1H), 2.74 (dd, *J* = 11.3, 2.7 Hz, 1H), 2.56–2.41 (m, 2H), 1.99 (td, *J* = 10.6, 4.0 Hz, 1H), 1.79–1.67 (m, 1H), 1.67–1.49 (m, 2H), 1.39–1.24 (m, 2H), 1.17–1.01 (m, 1H).

^{13}C NMR (126 MHz, $CDCl_3$): δ 201.8, 169.8, 169.7, 160.3, 137.3, 124.8, 119.8, 118.5, 111.3, 74.5, 71.2, 70.2, 52.7, 52.2, 49.4, 44.1, 27.0, 25.0, 24.3.

HRMS (EI): Calculated for $C_{19}H_{22}N_2O_5$ $[M]^+$: 358.1530; found: *m/z* 358.1541.

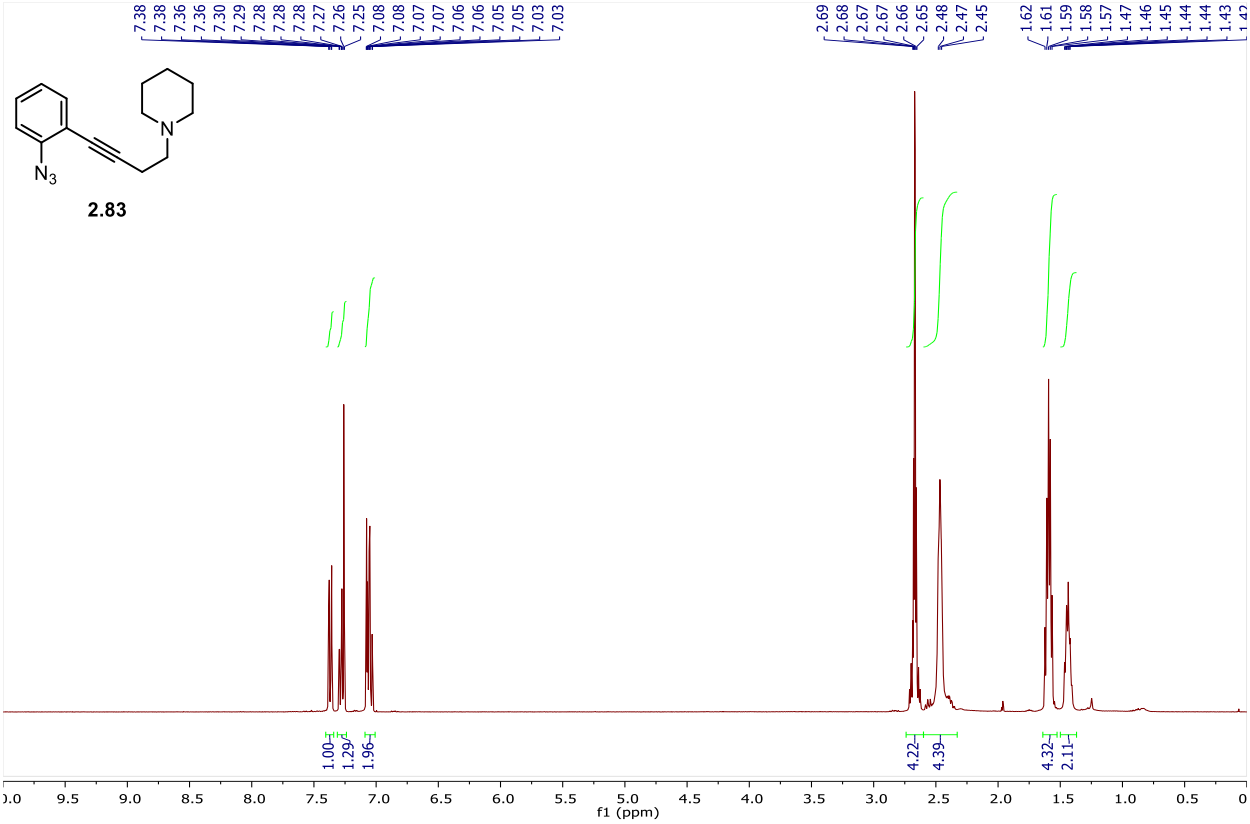


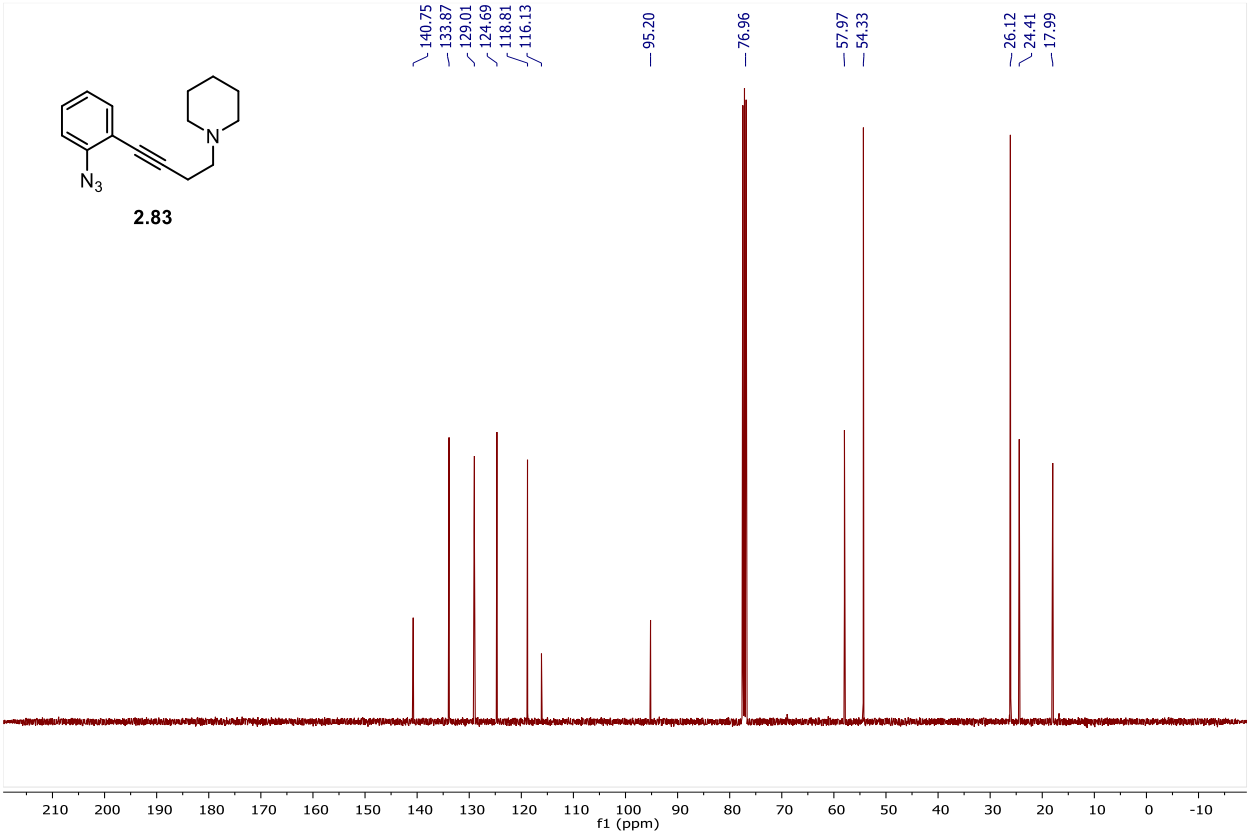
2.104 **2.194**

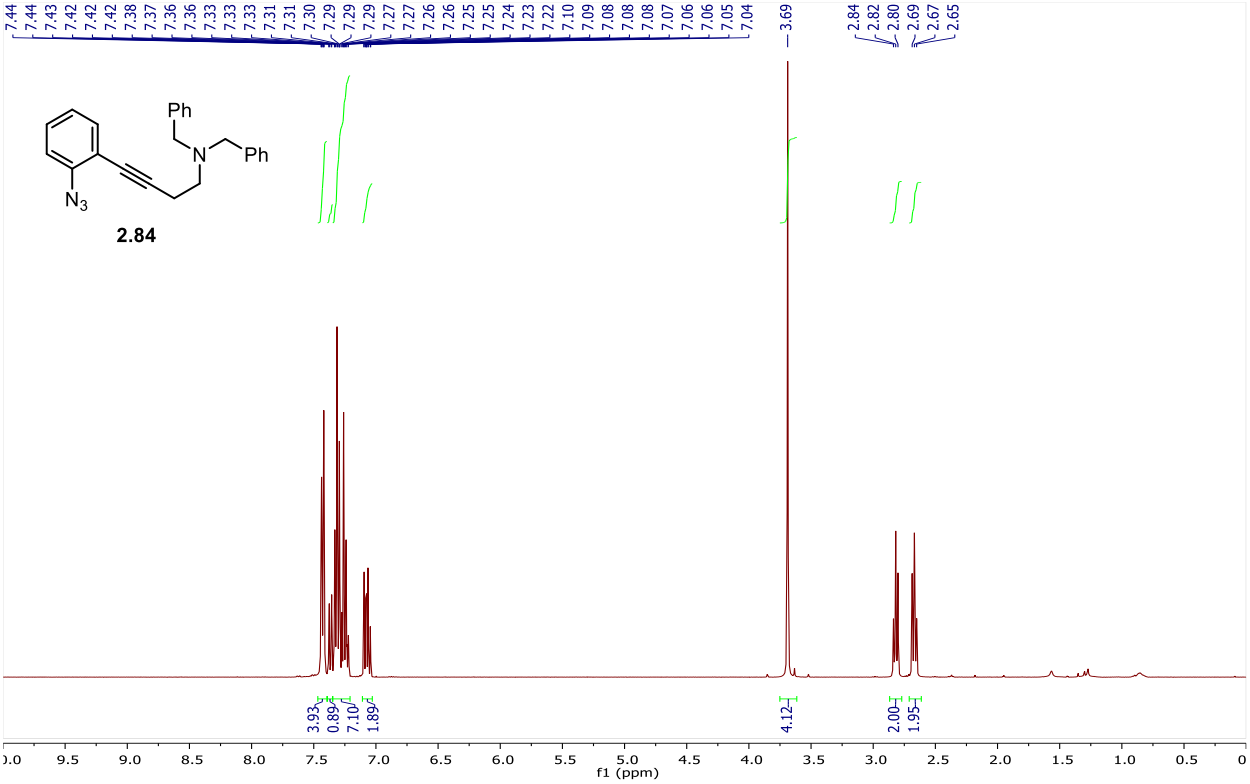
A solution of indole **2.104** (14.6 mg, 0.04 mmol, 1 equiv.) in THF:H_2O (1:1, 0.1 M, 0.5 mL) is cooled to 0 °C, at which point KBr (20.3 mg, 0.17 mmol, 4 equiv.) was added in H_2O (0.2 mL), followed by Oxone® (19.7 mg, 0.06 mmol, 1.5 equiv.) in H_2O (0.2 mL) dropwise. The reaction is warmed to room temperature and stirred till completion as indicated by TLC analysis. Once complete, the reaction is quenched with a saturated aqueous solution of $Na_2S_2O_5$. The reaction is then extracted using DCM (3x 5 mL) and the collected organic fractions are washed with brine before being dried over anhydrous $MgSO_4$, filtered, and concentrated *in vacuo* to afford a crude, yellow oil. Purification over silica (eluent: EtOAc:hexanes). Bromoaminal **2.194** was obtained as a clear oil: 6.9 mg, 42% yield.

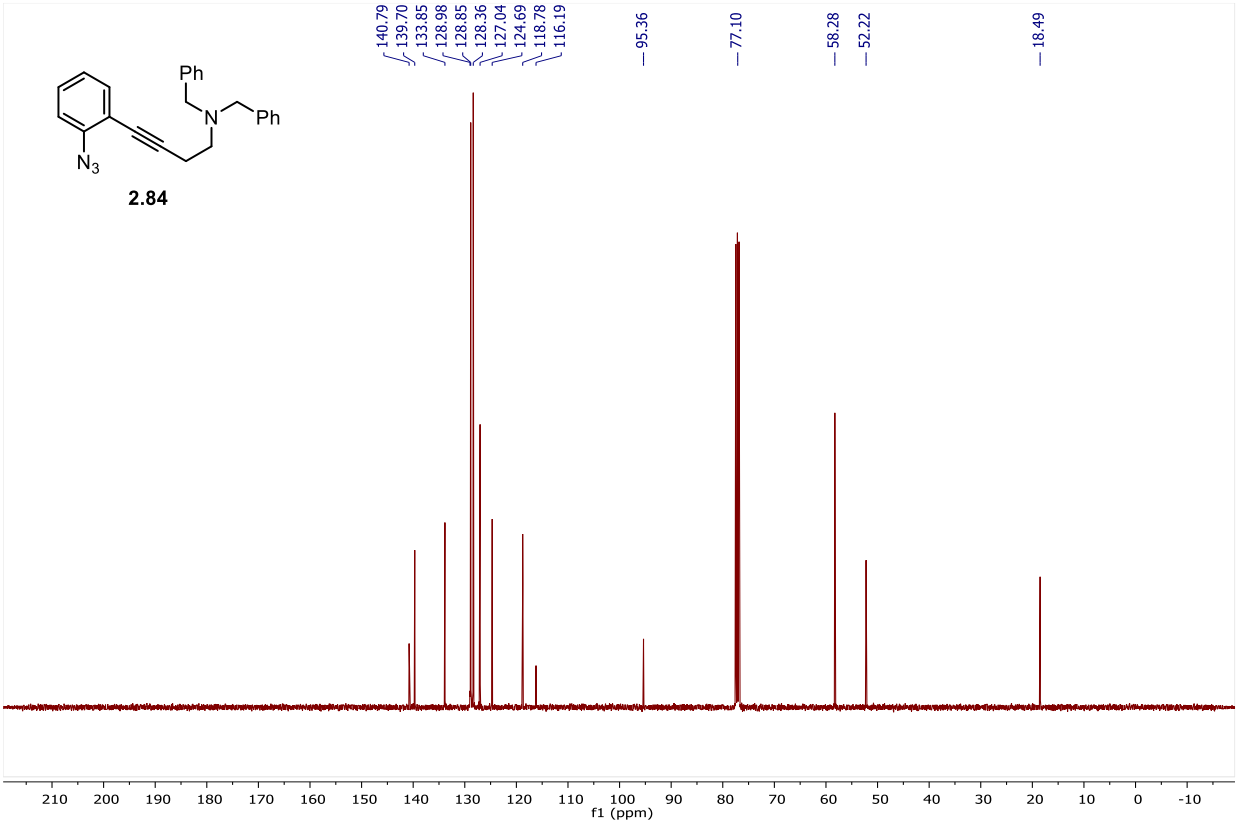
^{1}H-NMR (300 MHz, $CDCl_3$): δ 7.54–7.47 (m, 1H), 7.33–7.26 (m, 1H), 7.21–7.13 (m, 2H), 5.02 (d, *J* = 9.3 Hz, 1H), 3.88 (s, 3H), 3.67 (d, *J* = 15.4 Hz, 1H), 3.57 (s, 3H), 3.42 (d, *J* = 15.4 Hz, 1H), 3.29–3.16 (m, 1H), 3.05–2.94 (m, 1H), 2.80–2.68 (m, 1H), 2.00–1.89 (m, 1H), 1.78–1.57 (m, 4H).
^{13}C-NMR (126 MHz, $CDCl_3$): δ 169.6, 169.2, 133.7, 129.9, 128.0, 121.7, 120.5, 118.8, 111.0, 88.0, 72.5, 71.0, 53.5, 52.5, 50.8, 33.9, 32.5, 26.4, 23.7.
HRMS (ESI): Calculated for $C_{19}H_{21}BrN_2O_4$ $[M]^+$: 420.0680; found: *m/z* 420.0683.

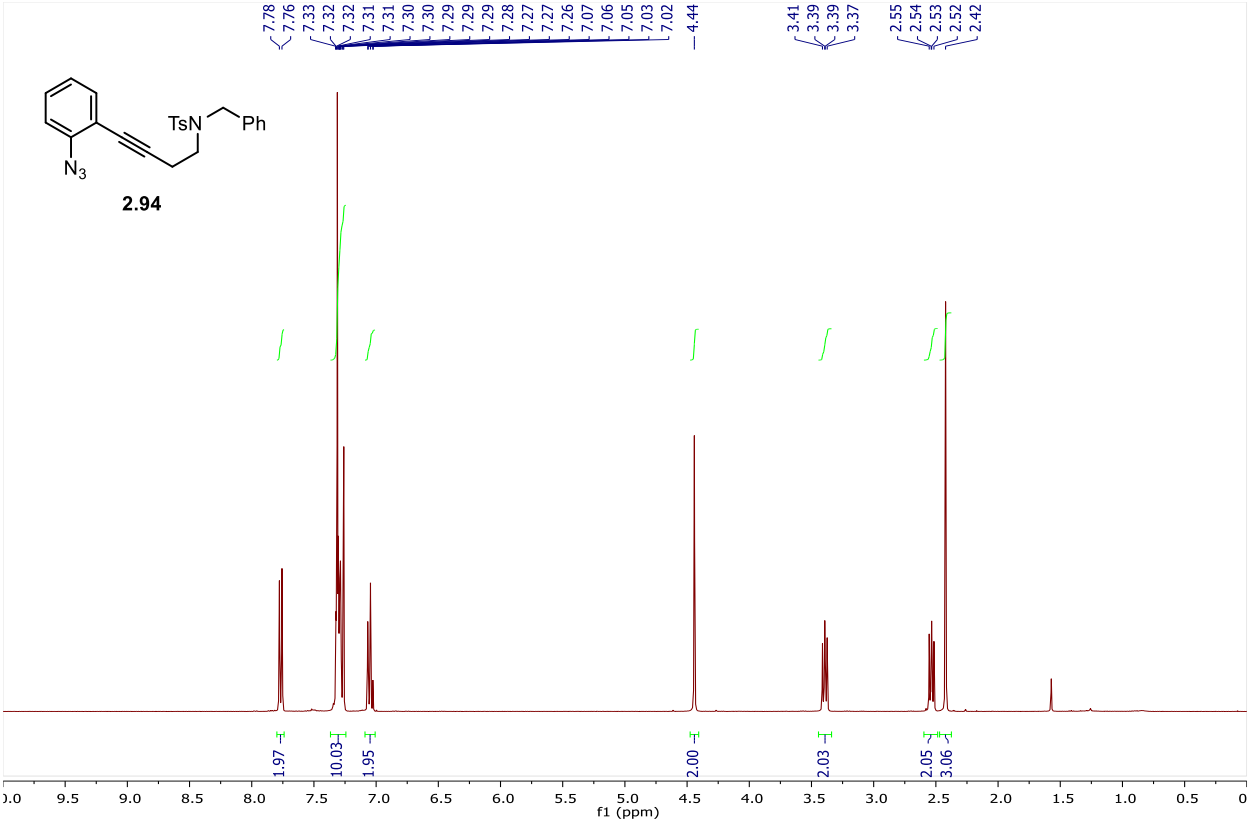
6.2.2 ^{1}H- and ^{13}C-NMR spectra

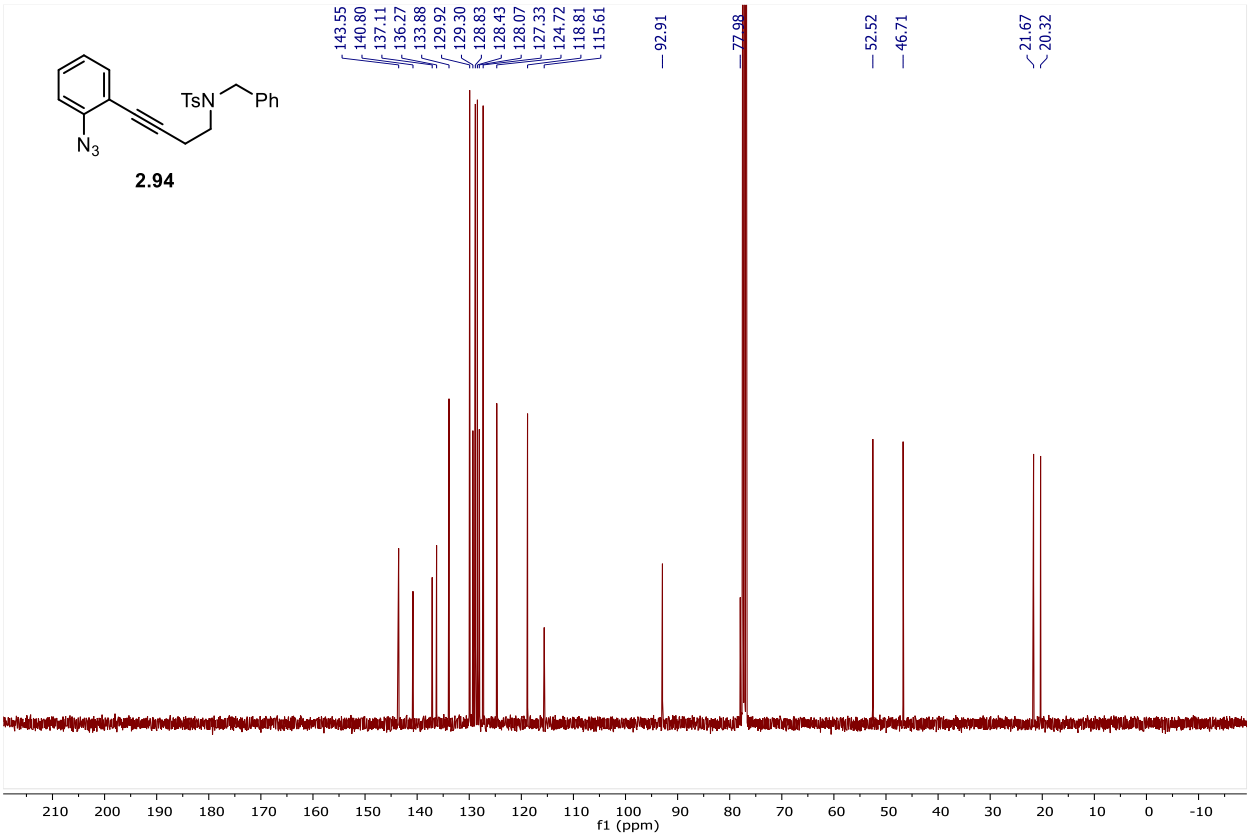


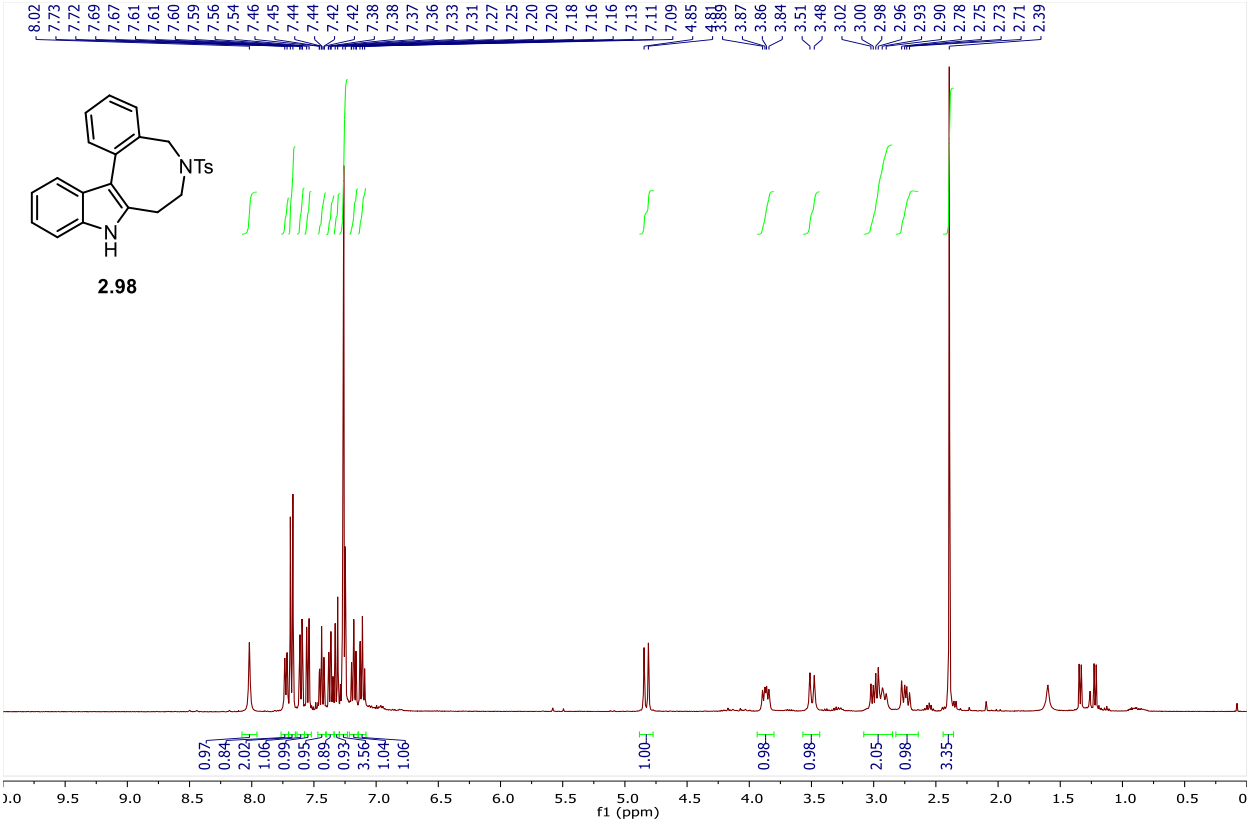


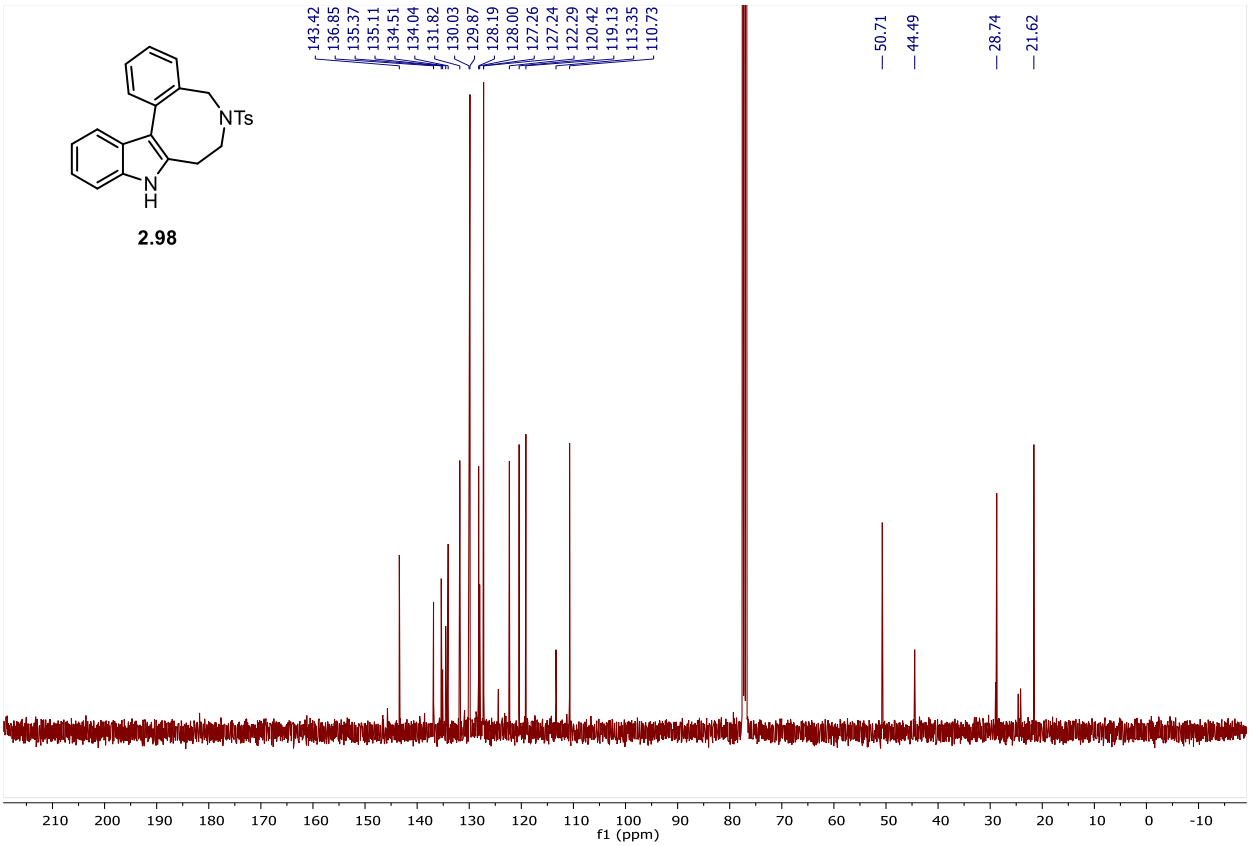

7.44 7.44 7.43 7.42 7.42 7.42 7.38 7.37 7.36 7.36 7.33 7.33 7.33 7.31 7.31 7.30 7.29 7.29 7.29 7.27 7.27 7.26 7.26 7.25 7.25 7.24 7.23 7.22 7.10 7.09 7.08 7.08 7.08 7.07 7.06 7.06 7.05 7.04
3.69
2.84 2.82 2.80 2.69 2.67 2.65
Ph
N
Ph
N3
2.84
3.93 0.89 7.10 1.89
4.12
2.00 1.95
f1 (ppm)

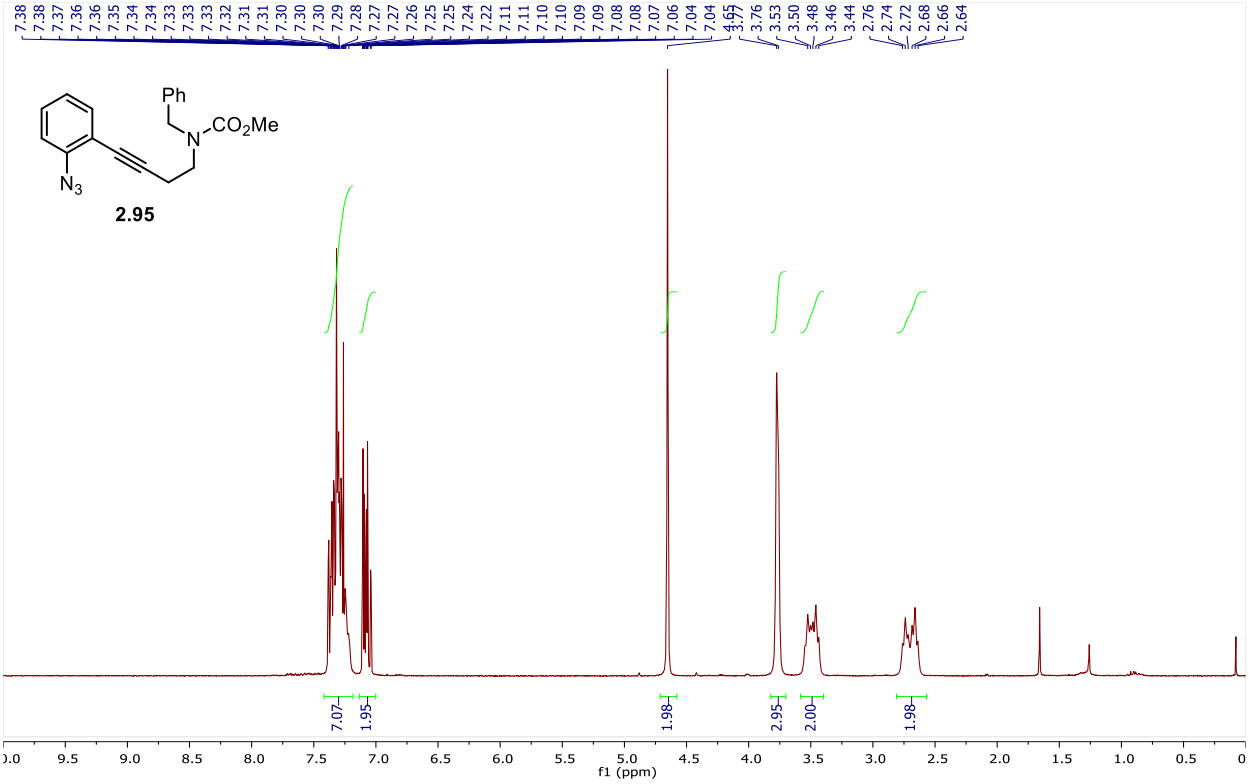

140.79 139.70 133.85 128.98 128.85 128.36 127.04 124.69 118.78 116.19
95.36
77.10
58.28
52.22
18.49
Ph
N
Ph
N3
2.84
f1 (ppm)

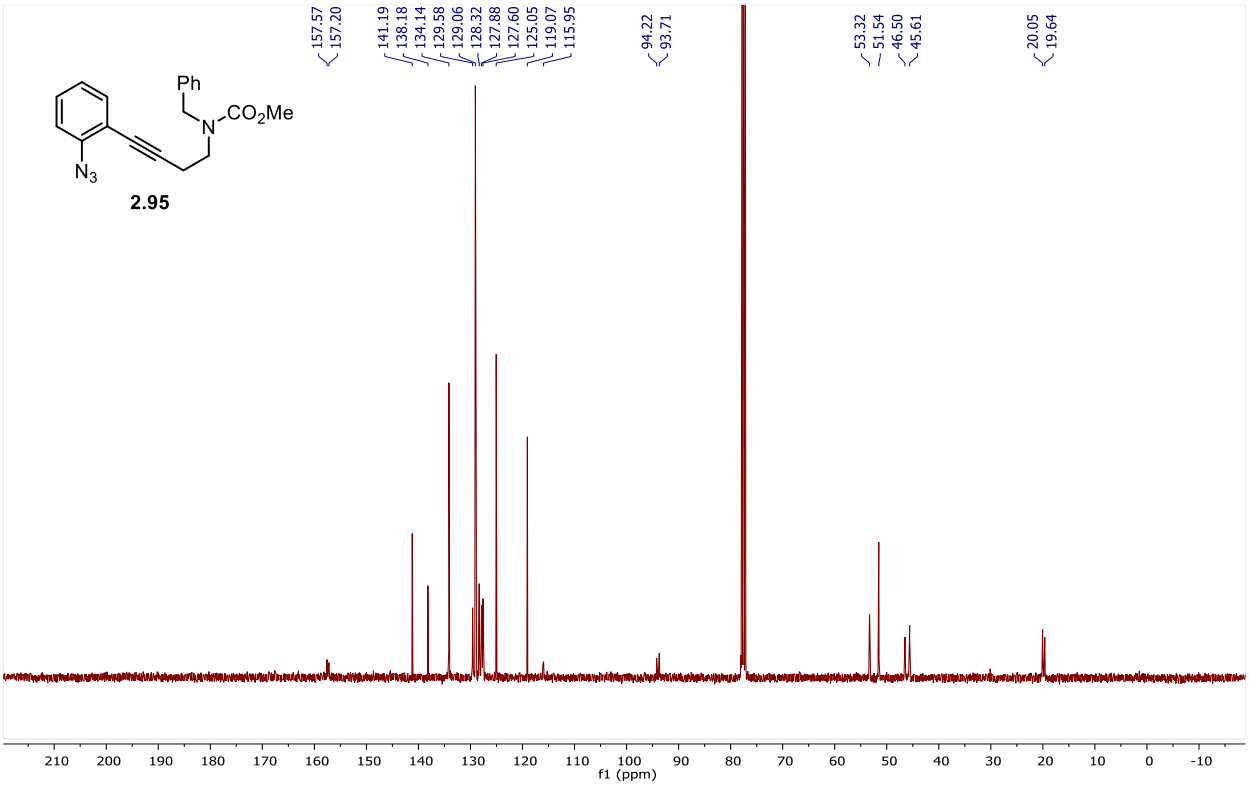

7.78
7.76
7.33
7.32
7.32
7.31
7.31
7.30
7.30
7.29
7.29
7.29
7.28
7.27
7.27
7.26
7.07
7.06
7.05
7.03
7.02
4.44
3.41
3.39
3.39
3.37
2.55
2.54
2.53
2.52
2.42
TsN
Ph
N3
2.94
1.97
10.03
1.95
2.00
2.03
2.05
3.06
f1 (ppm)

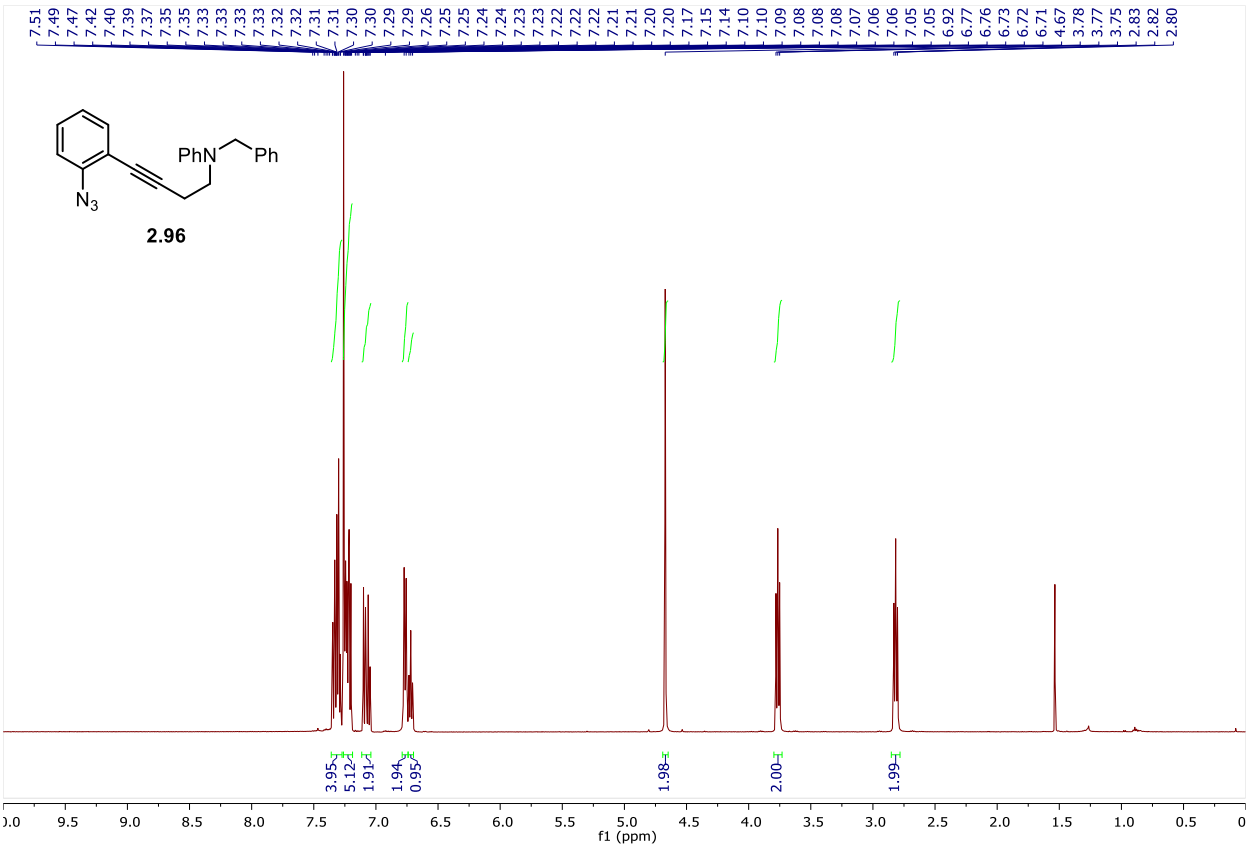

143.55
140.80
137.11
136.27
133.88
129.92
129.30
128.83
128.43
128.07
127.33
124.72
118.81
115.61
92.91
77.98
52.52
46.71
21.67
20.32
TsN
Ph
N3
2.94
f1 (ppm)

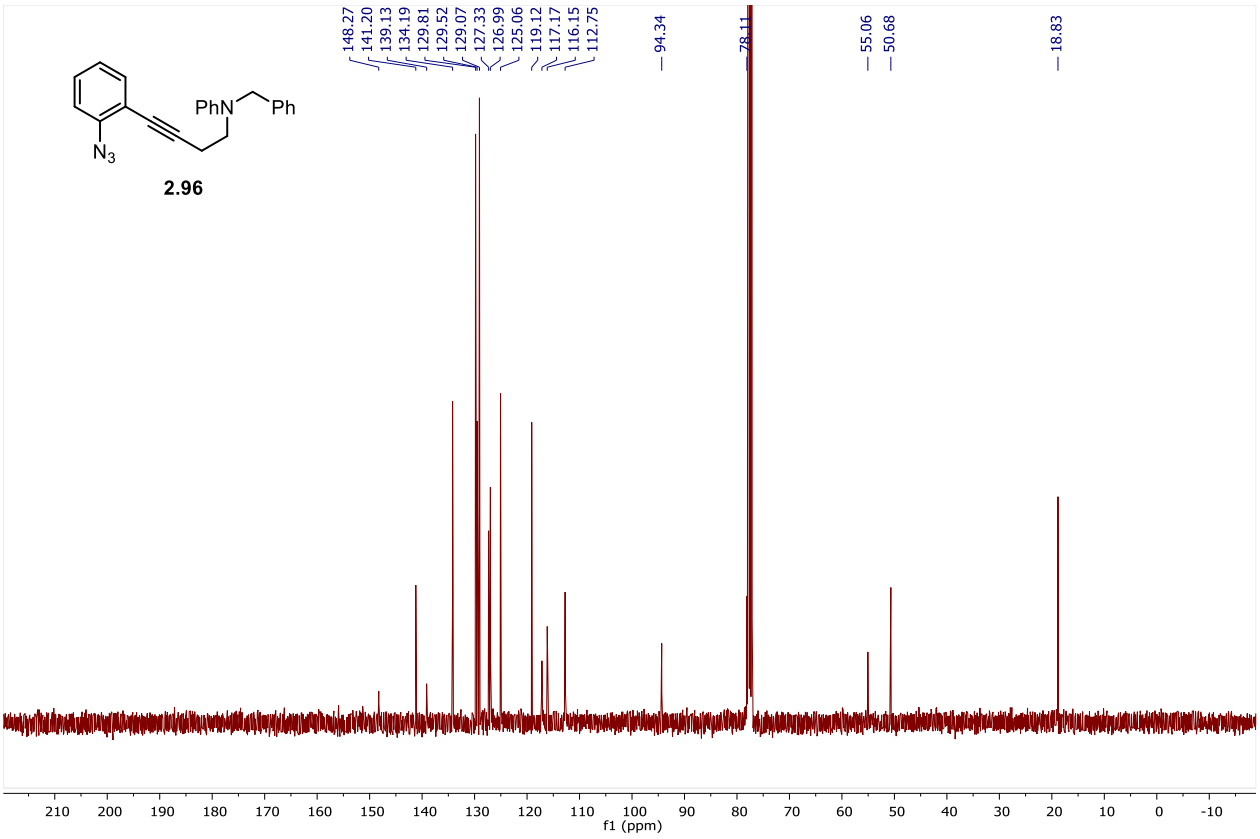

8.02 7.73 7.72 7.69 7.67 7.61 7.61 7.60 7.59 7.56 7.54 7.46 7.45 7.44 7.44 7.42 7.42 7.38 7.38 7.37 7.36 7.33 7.31 7.27 7.25 7.20 7.20 7.18 7.16 7.16 7.13 7.11 7.09 4.85 3.87 3.86 3.84 3.51 3.48 3.02 3.00 2.98 2.96 2.93 2.90 2.78 2.75 2.73 2.71 2.39
NTs
N
H
2.98
0.97 0.84 2.02 1.06 0.99 0.95 0.89 0.93 3.56 1.04 1.06 1.00 0.98 0.98 2.05 0.98 3.35
f1 (ppm)

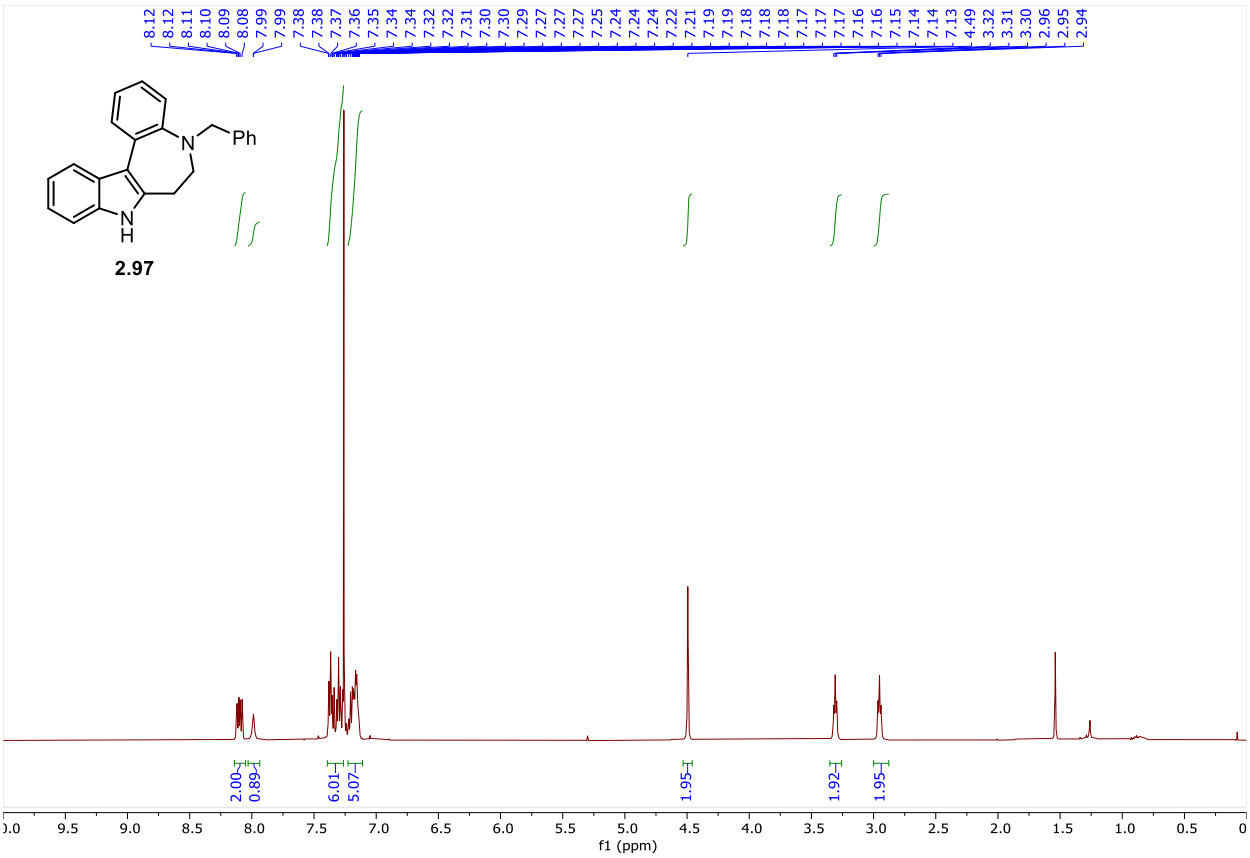

143.42 136.85 135.37 135.11 134.51 134.04 131.82 130.03 129.87 128.19 128.00 127.26 127.24 122.29 120.42 119.13 113.35 110.73
50.71 44.49 28.74 21.62
NTs
N
H
2.98
f1 (ppm)

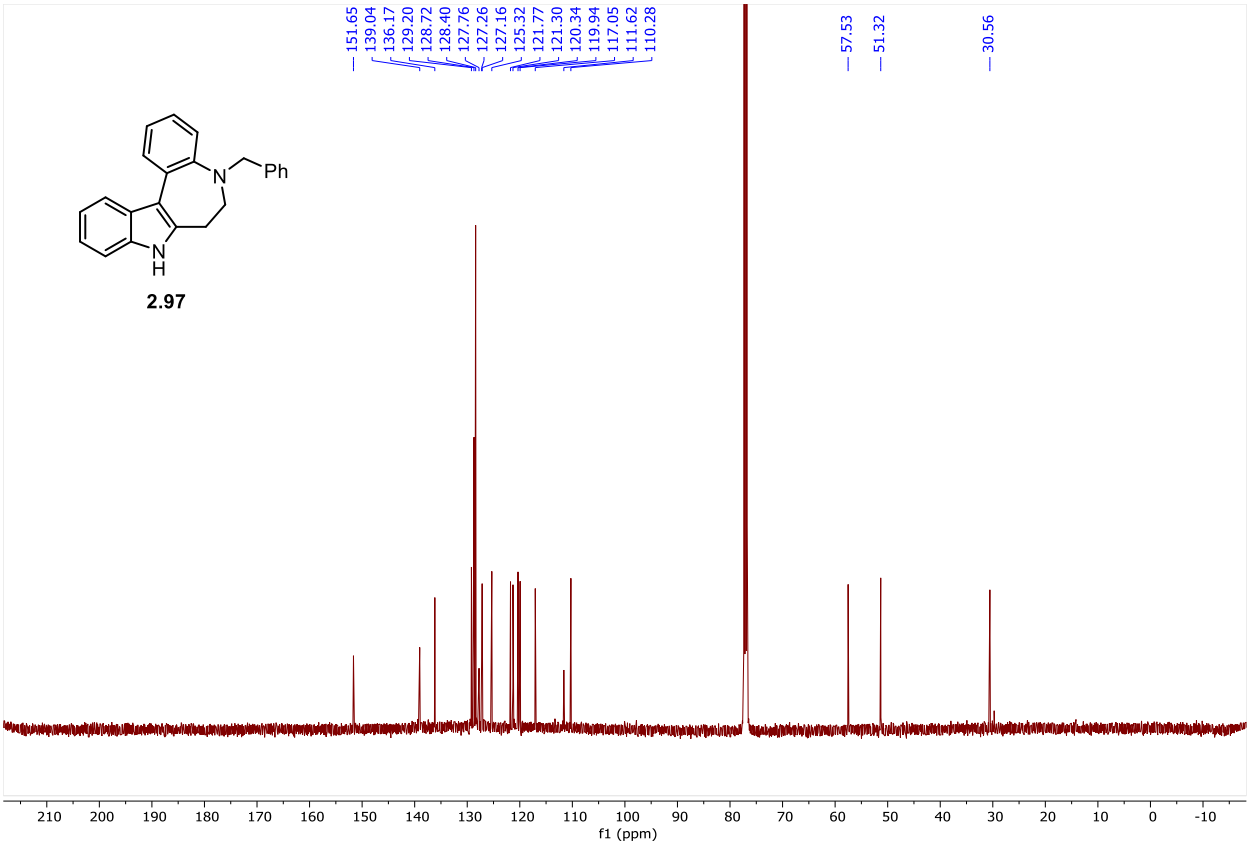

Ph
N
CO2Me
N3
2.95
f1 (ppm)

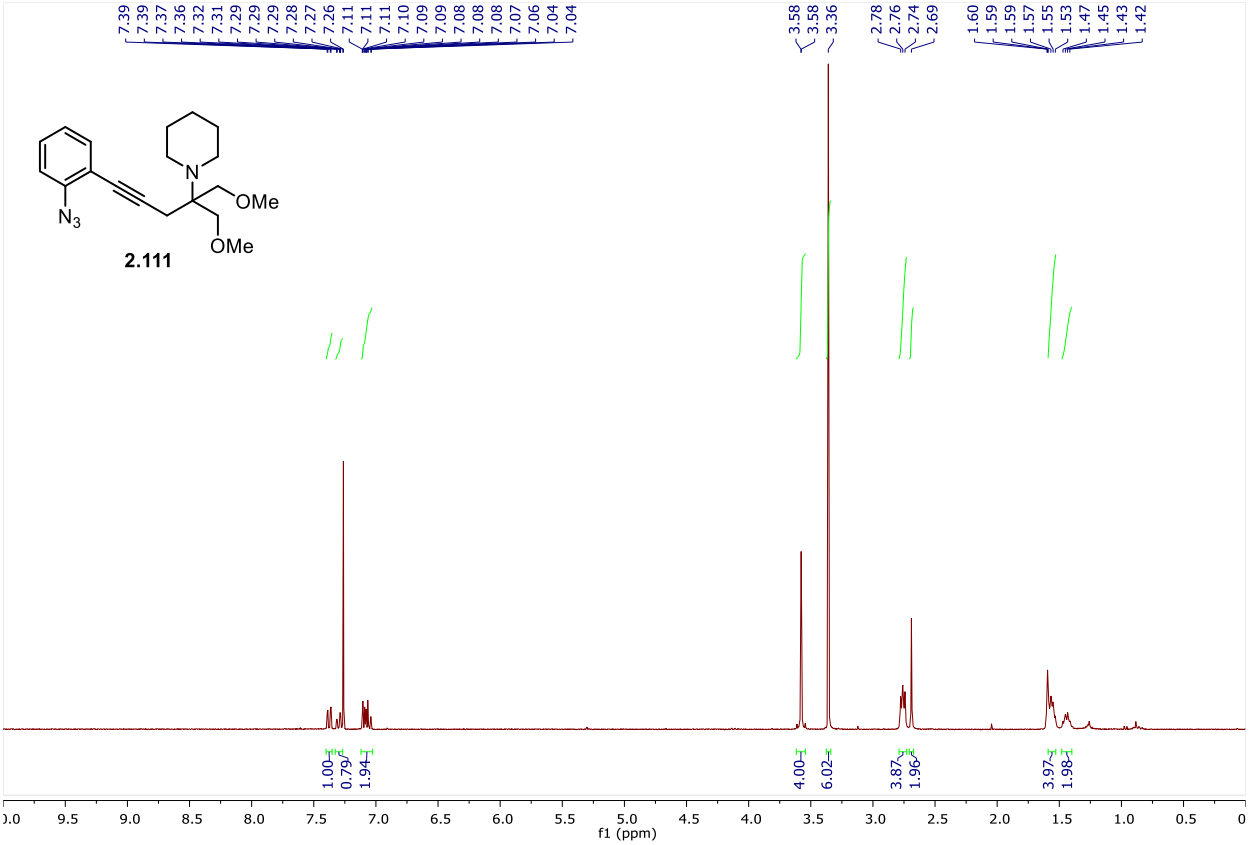

Ph
N
CO2Me
N3
2.95
f1 (ppm)

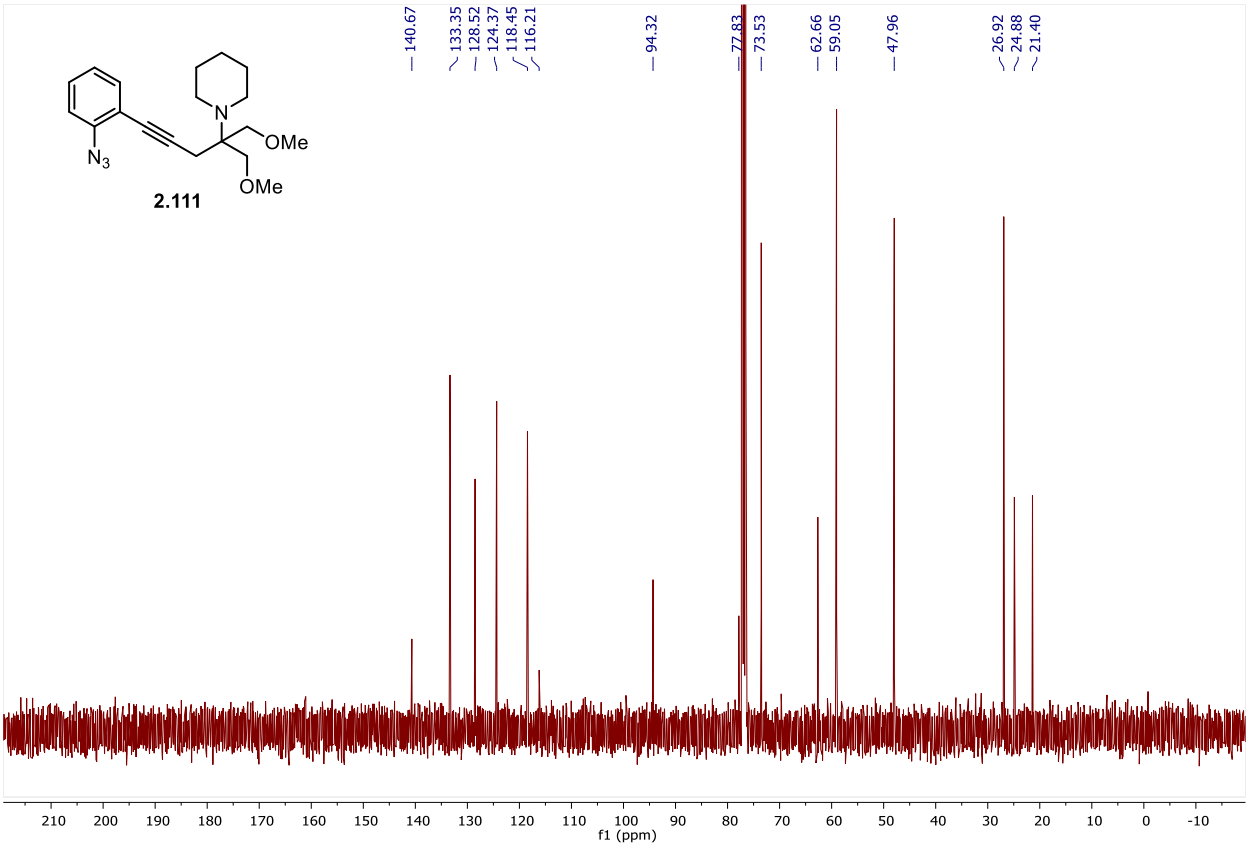

PhN
Ph
N3
2.96
f1 (ppm)

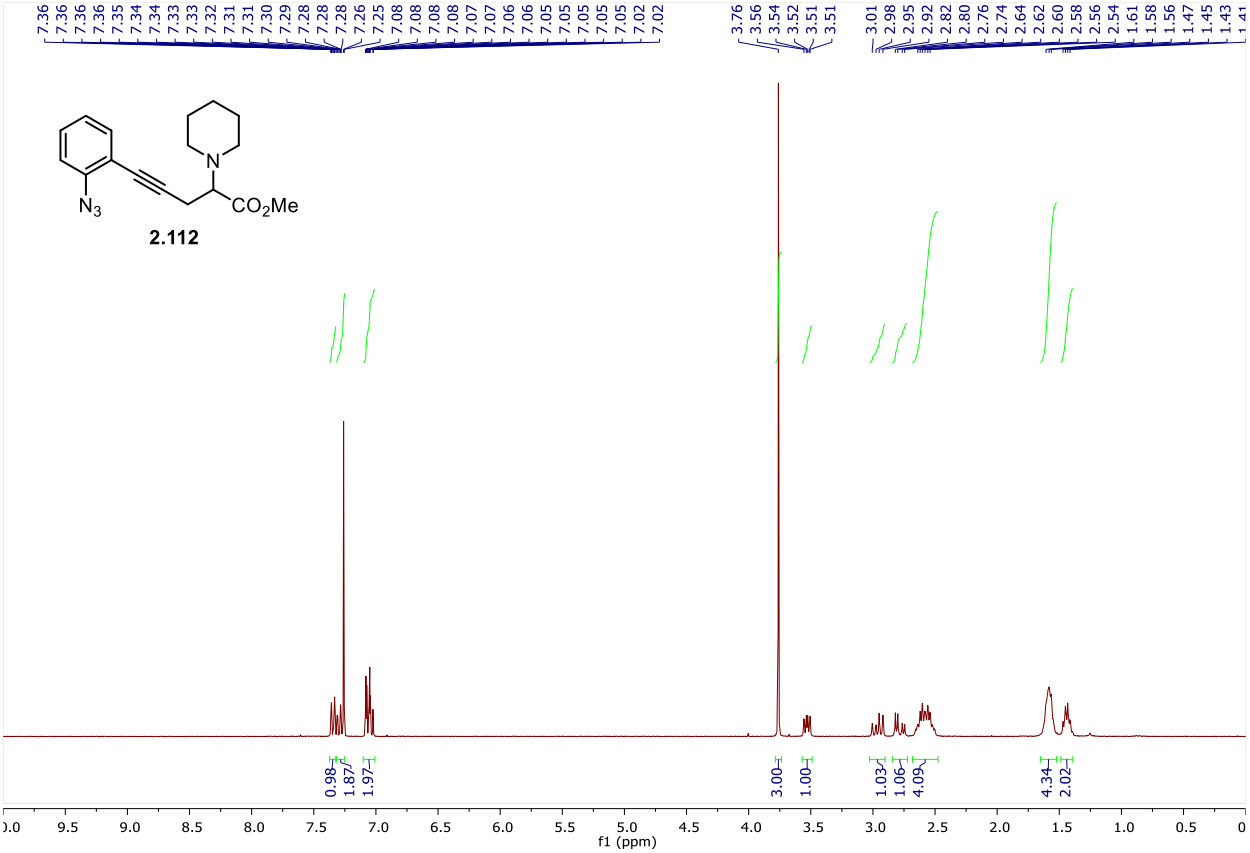

PhN
Ph
N3
2.96
f1 (ppm)

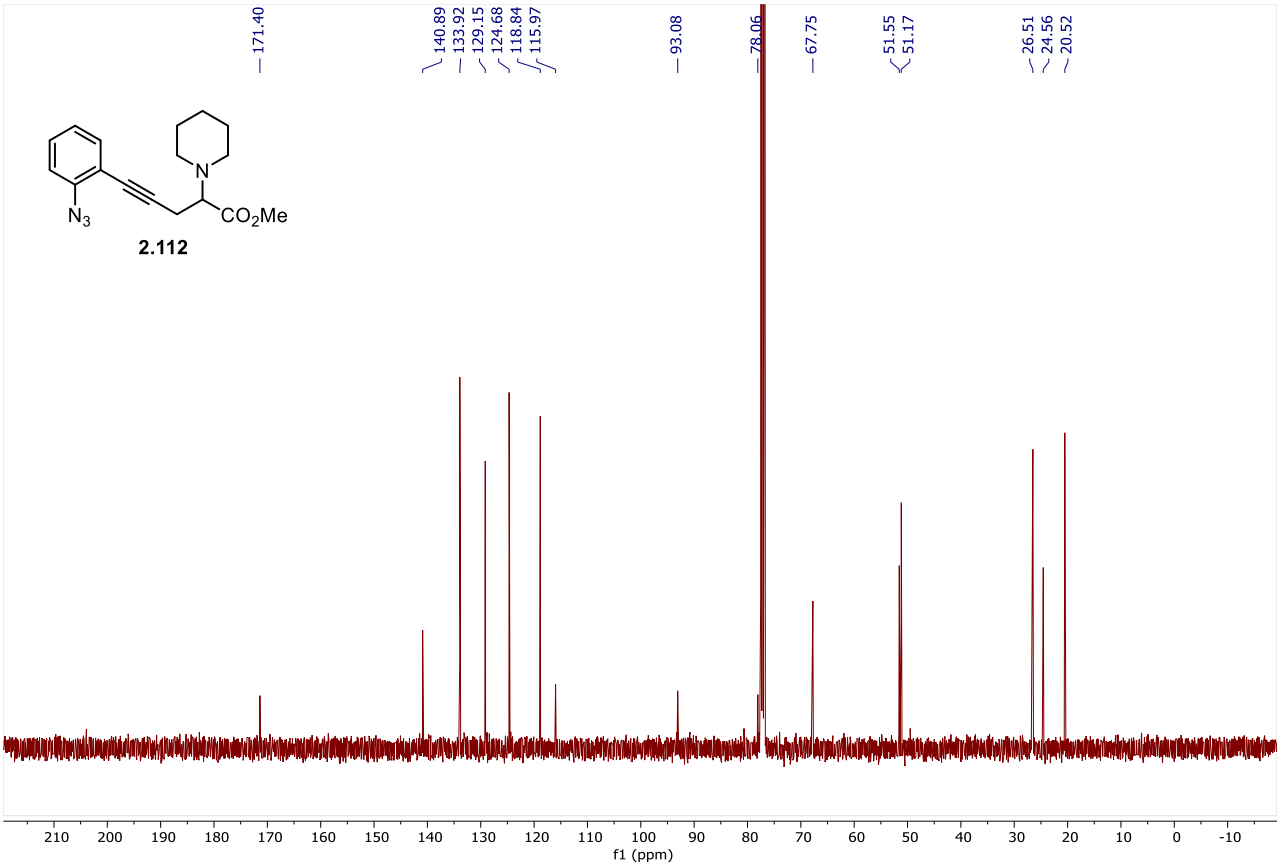

8.12 8.12 8.11 8.10 8.09 8.08 8.08 7.99 7.99 7.38 7.38 7.37 7.36 7.35 7.34 7.34 7.32 7.32 7.31 7.30 7.30 7.29 7.27 7.27 7.27 7.25 7.24 7.24 7.24 7.22 7.21 7.19 7.19 7.18 7.18 7.18 7.17 7.17 7.17 7.16 7.16 7.15 7.14 7.14 7.13 4.49 3.32 3.31 3.30 2.96 2.95 2.94
Ph
N
H
2.97
2.00 0.89 6.01 5.07 1.95 1.92 1.95
f1 (ppm)

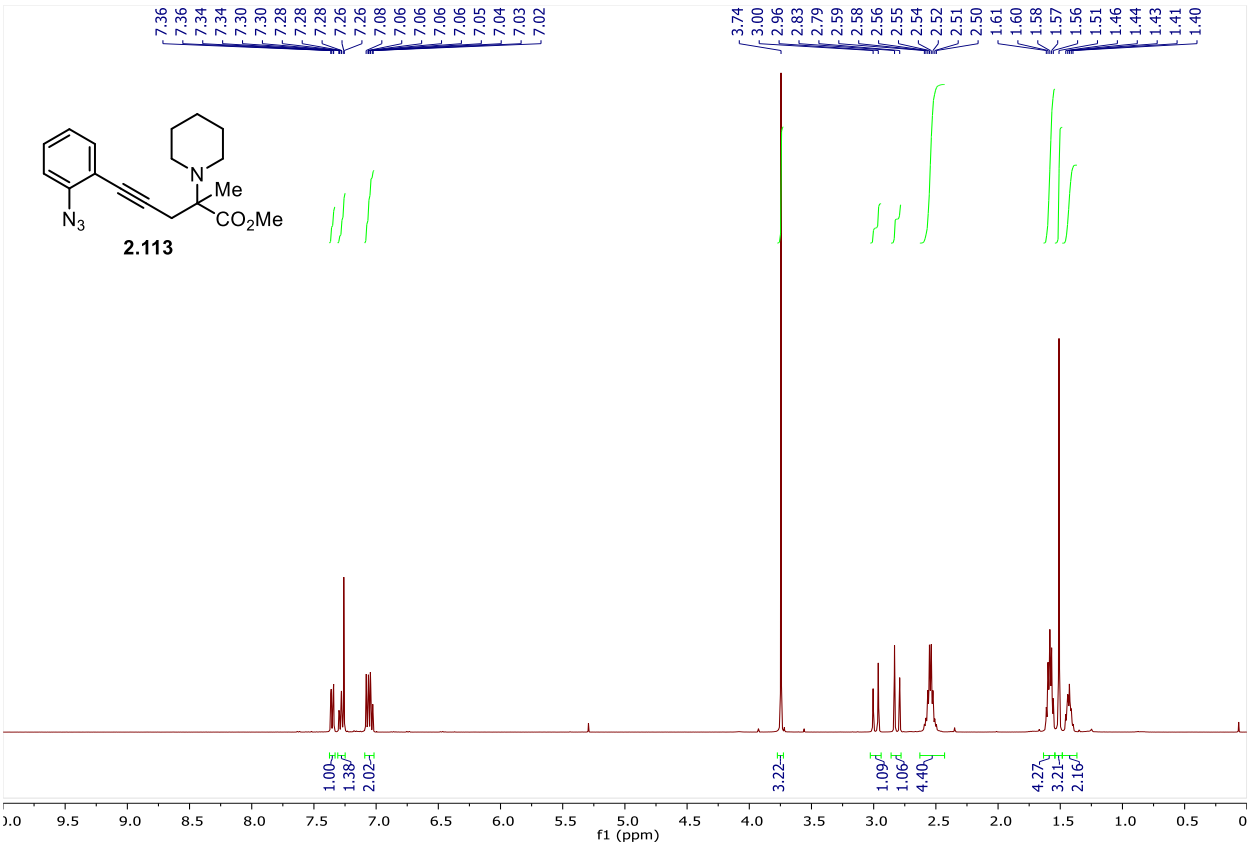

151.65 139.04 136.17 129.20 128.72 128.40 127.76 127.26 127.16 125.32 121.77 121.30 120.34 119.94 117.05 111.62 110.28
57.53 51.32 30.56
Ph
N
H
2.97
f1 (ppm)

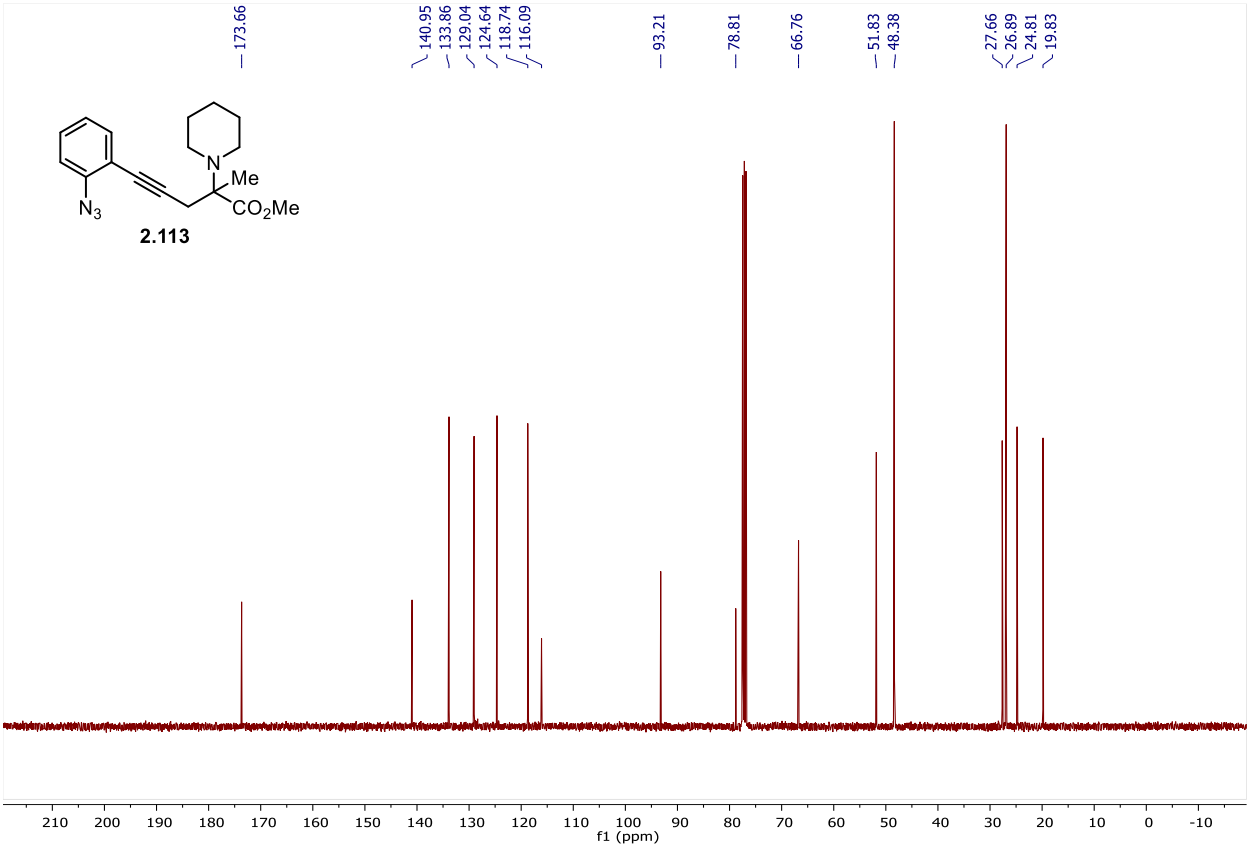

7.39 7.39 7.37 7.36 7.32 7.31 7.29 7.29 7.29 7.28 7.27 7.26 7.11 7.11 7.11 7.10 7.09 7.09 7.08 7.08 7.08 7.07 7.06 7.04 7.04
3.58 3.58 3.36
2.78 2.76 2.74 2.69
1.60 1.59 1.59 1.57 1.55 1.53 1.47 1.45 1.43 1.42
N
OMe
OMe
N3
2.111
1.00 0.79 1.94 4.00 6.02 3.87 1.96 3.97 1.98
f1 (ppm)

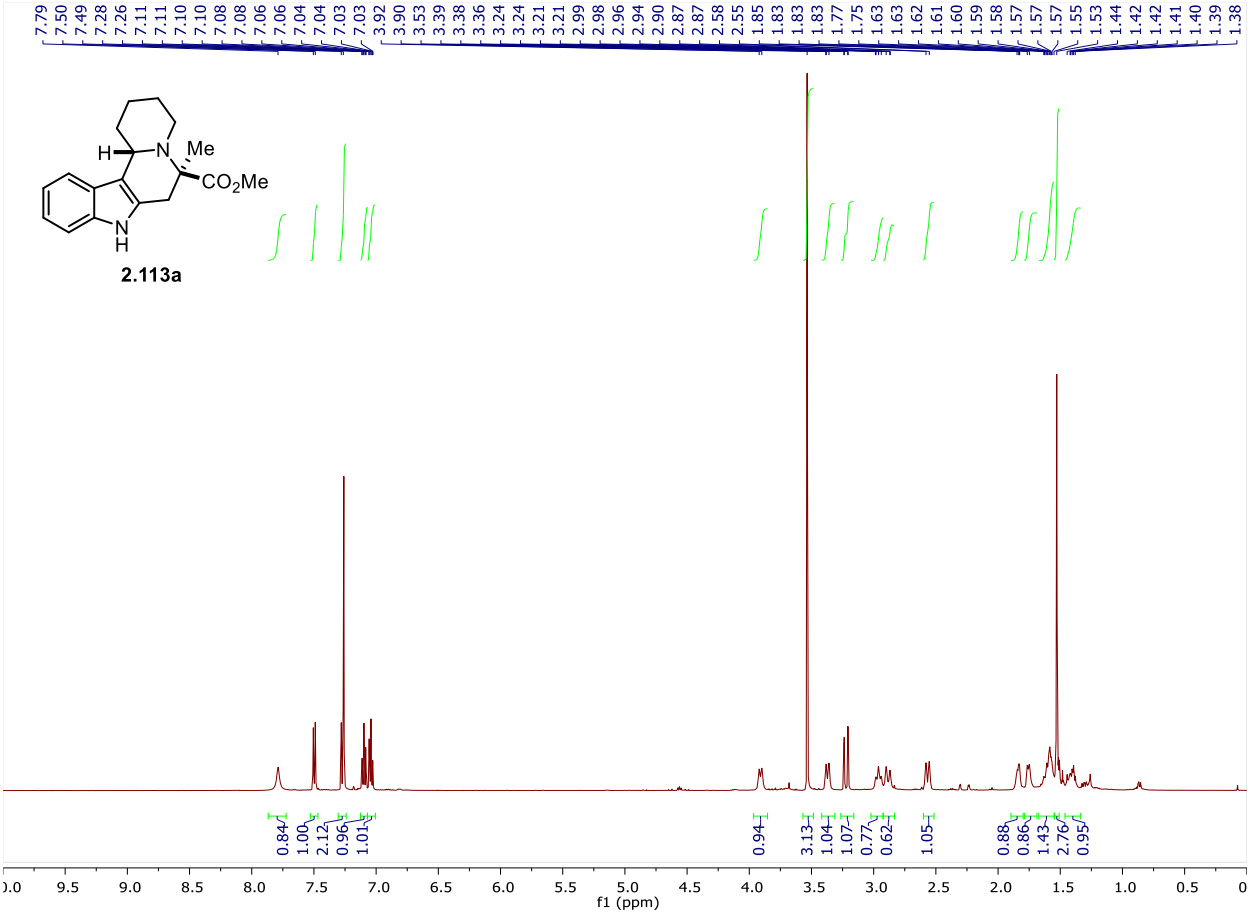

140.67 133.35 128.52 124.37 118.45 116.21 94.32 77.83 73.53 62.66 59.05 47.96 26.92 24.88 21.40
N
OMe
OMe
N3
2.111
f1 (ppm)

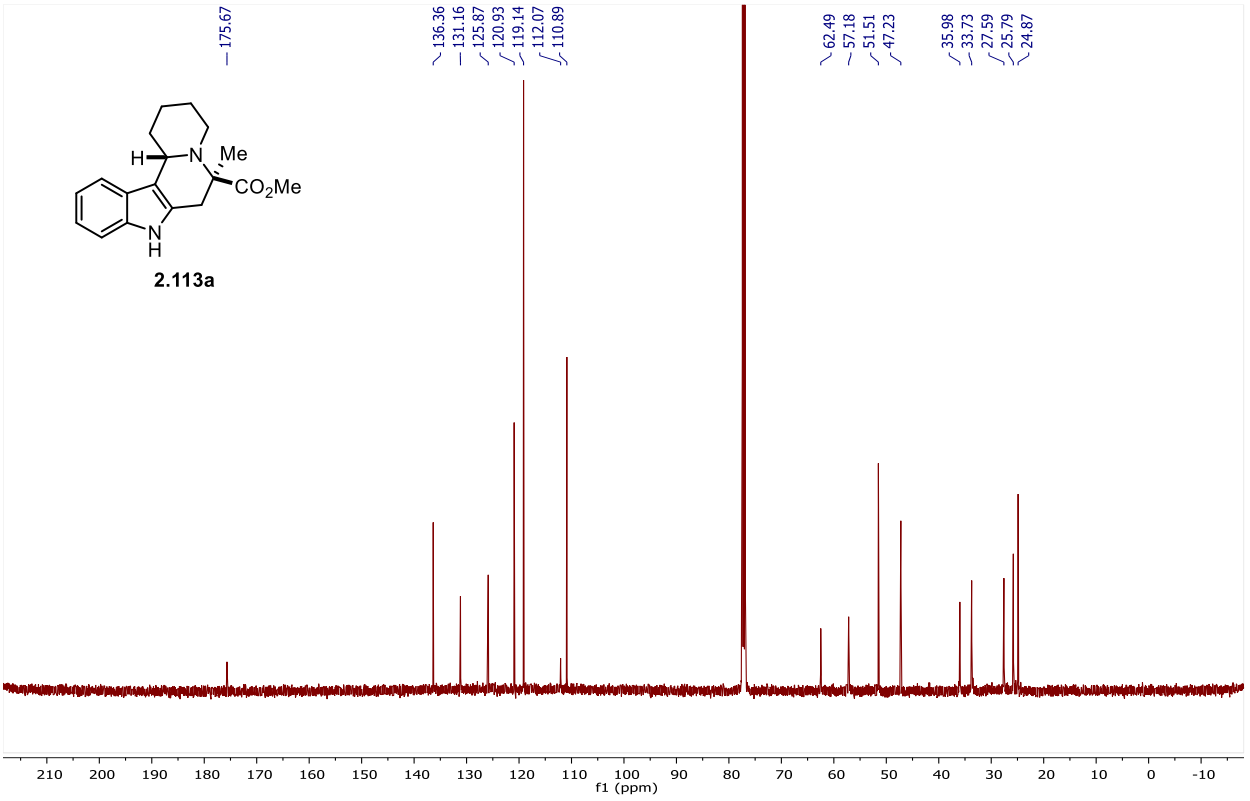

7.36 7.36 7.36 7.36 7.35 7.34 7.34 7.33 7.33 7.32 7.31 7.31 7.30 7.29 7.28 7.28 7.28 7.26 7.25 7.08 7.08 7.08 7.08 7.07 7.07 7.06 7.06 7.05 7.05 7.05 7.05 7.05 7.02 7.02
3.76 3.56 3.54 3.52 3.51 3.51
3.01 2.98 2.95 2.92 2.82 2.80 2.76 2.74 2.64 2.62 2.60 2.58 2.56 2.54 1.61 1.58 1.56 1.47 1.45 1.43 1.41
N
N3
CO2Me
2.112
0.98 1.87 1.97 3.00 1.00 1.03 1.06 4.09 4.34 2.02
f1 (ppm)

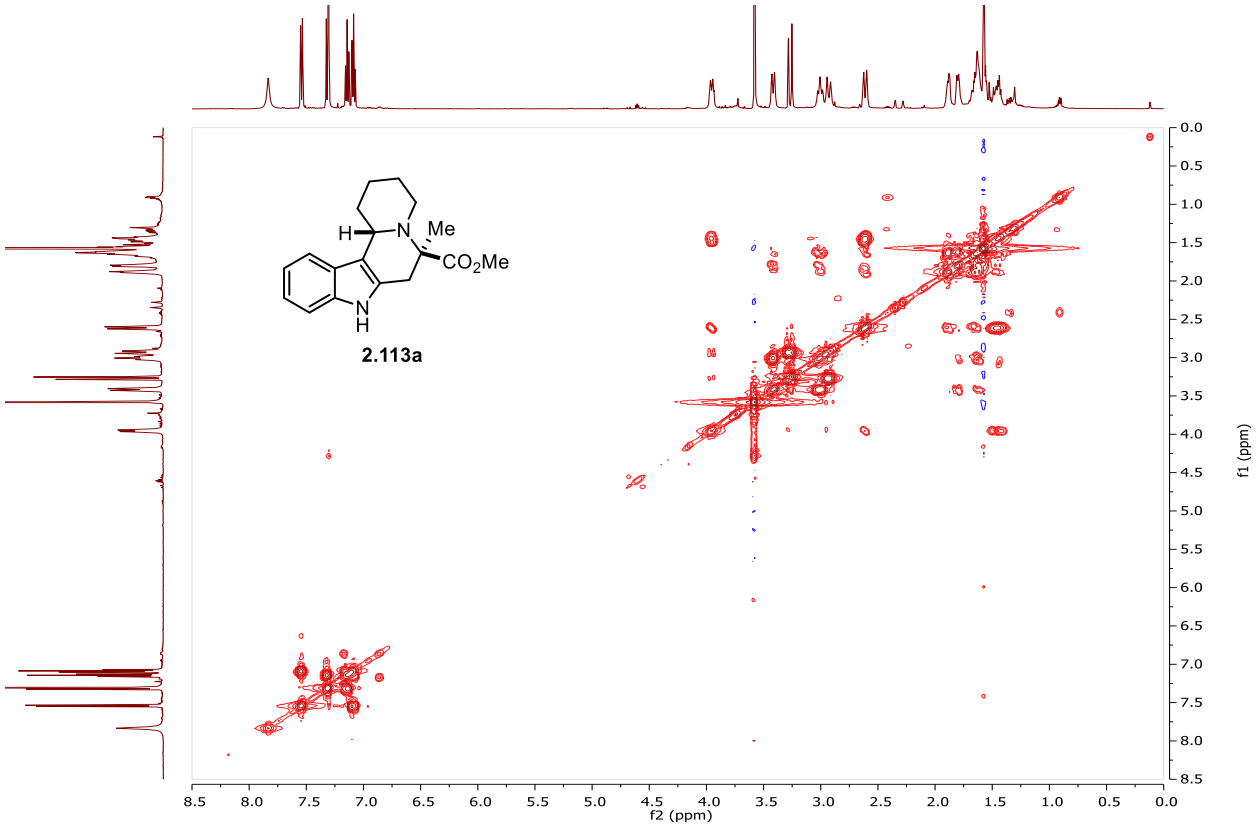

171.40
140.89 133.92 129.15 124.68 118.84 115.97
93.08
78.06
67.75
51.55 51.17
26.51 24.56 20.52
N
N3
CO2Me
2.112
f1 (ppm)

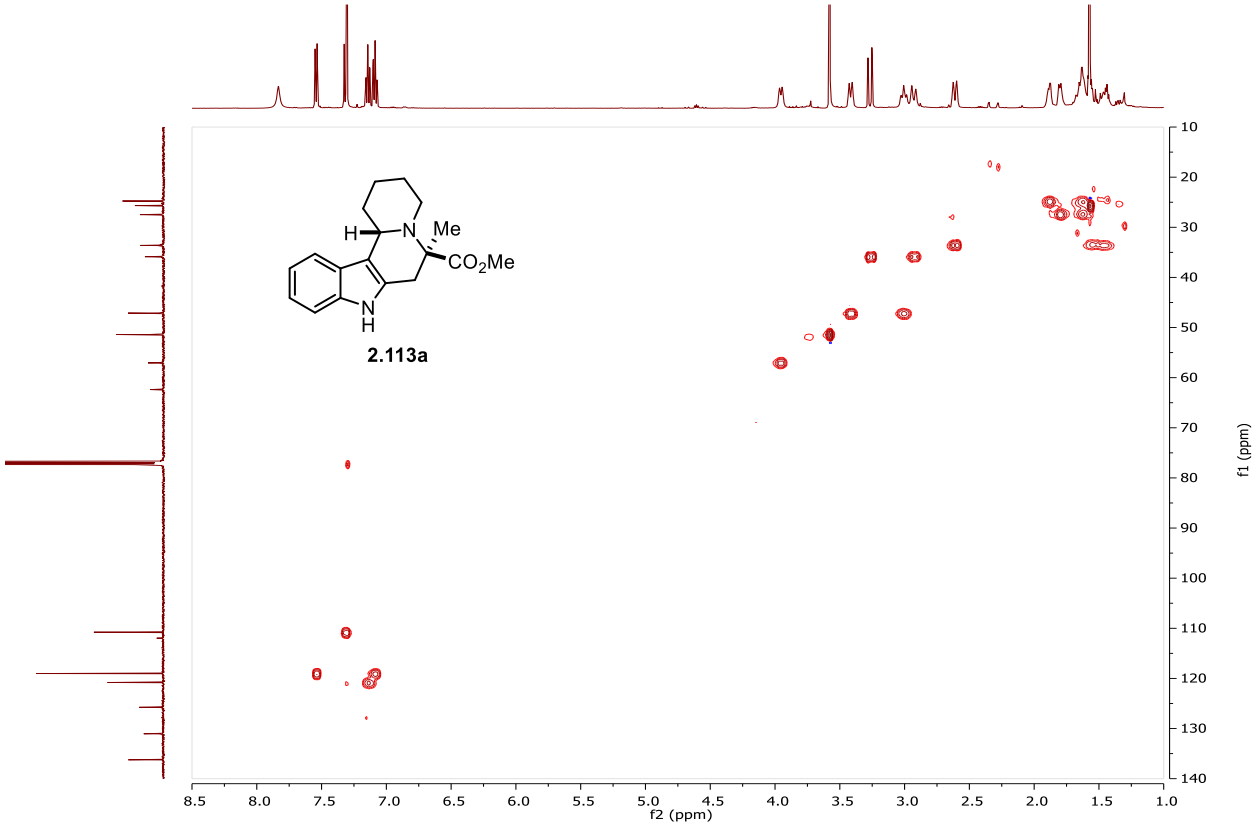

7.36 7.36 7.34 7.34 7.30 7.28 7.28 7.28 7.26 7.26 7.08 7.06 7.06 7.06 7.06 7.05 7.04 7.03 7.02
3.74 3.00 2.96 2.83 2.79 2.59 2.58 2.56 2.55 2.54 2.52 2.51 2.50 1.61 1.60 1.58 1.57 1.56 1.51 1.46 1.44 1.43 1.41 1.40
N
Me
CO2Me
N3
2.113
1.00 1.38 2.02 3.22 1.09 1.06 4.40 4.27 3.21 2.16
f1 (ppm)

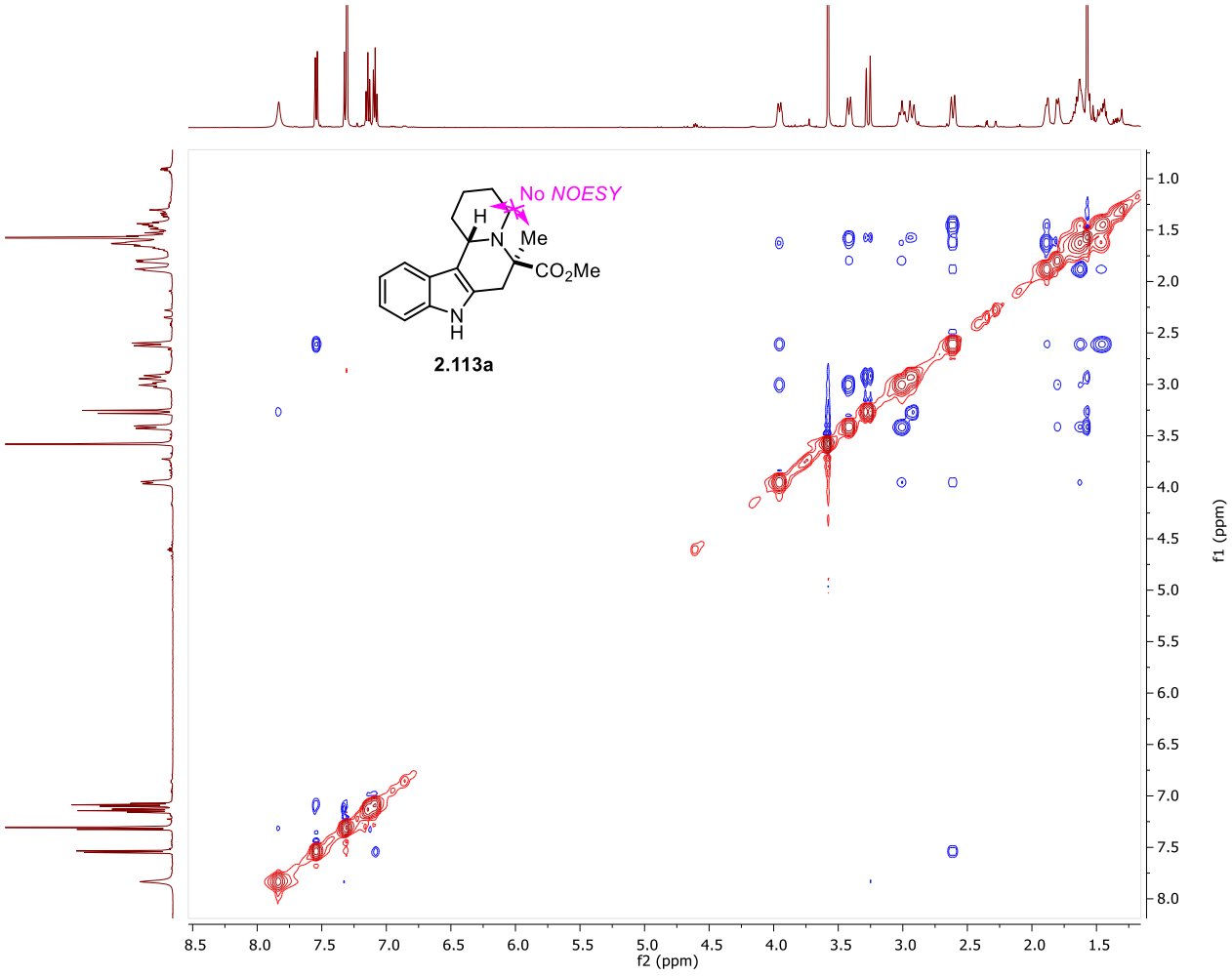

173.66
140.95 133.86 129.04 124.64 118.74 116.09
93.21
78.81
66.76
51.83 48.38
27.66 26.89 24.81 19.83
N
Me
CO2Me
N3
2.113
f1 (ppm)

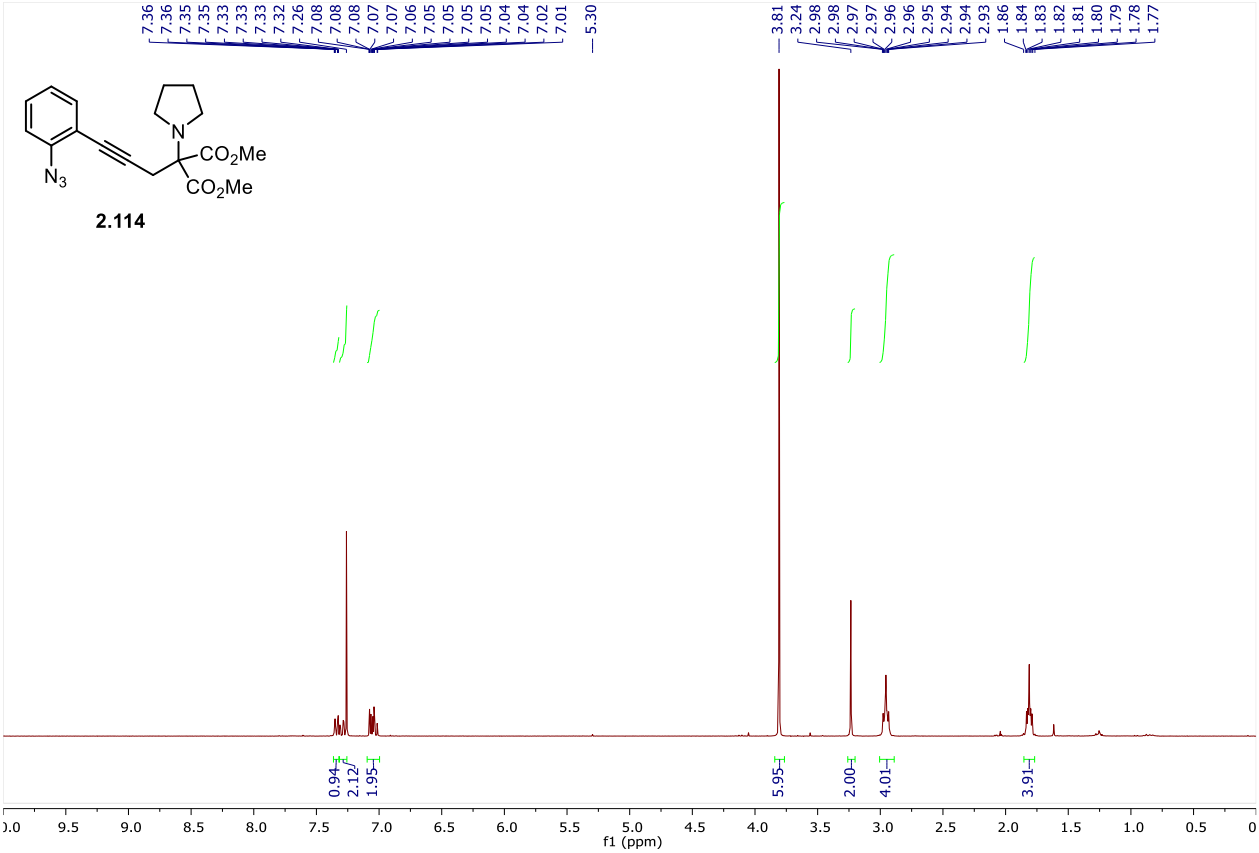

7.79 7.50 7.49 7.28 7.26 7.11 7.11 7.10 7.10 7.08 7.08 7.06 7.06 7.04 7.04 7.03 7.03 3.92 3.90 3.53 3.39 3.38 3.36 3.24 3.24 3.21 3.21 2.99 2.98 2.96 2.94 2.90 2.87 2.87 2.58 2.55 1.85 1.83 1.83 1.83 1.77 1.75 1.63 1.63 1.62 1.61 1.60 1.59 1.58 1.57 1.57 1.57 1.55 1.53 1.44 1.42 1.42 1.41 1.40 1.39 1.38
H
N
Me
CO2Me
N
H
2.113a
0.84 1.00 2.12 0.96 1.01 0.94 3.13 1.04 1.07 0.77 0.62 1.05 0.88 0.86 1.43 2.76 0.95
f1 (ppm)

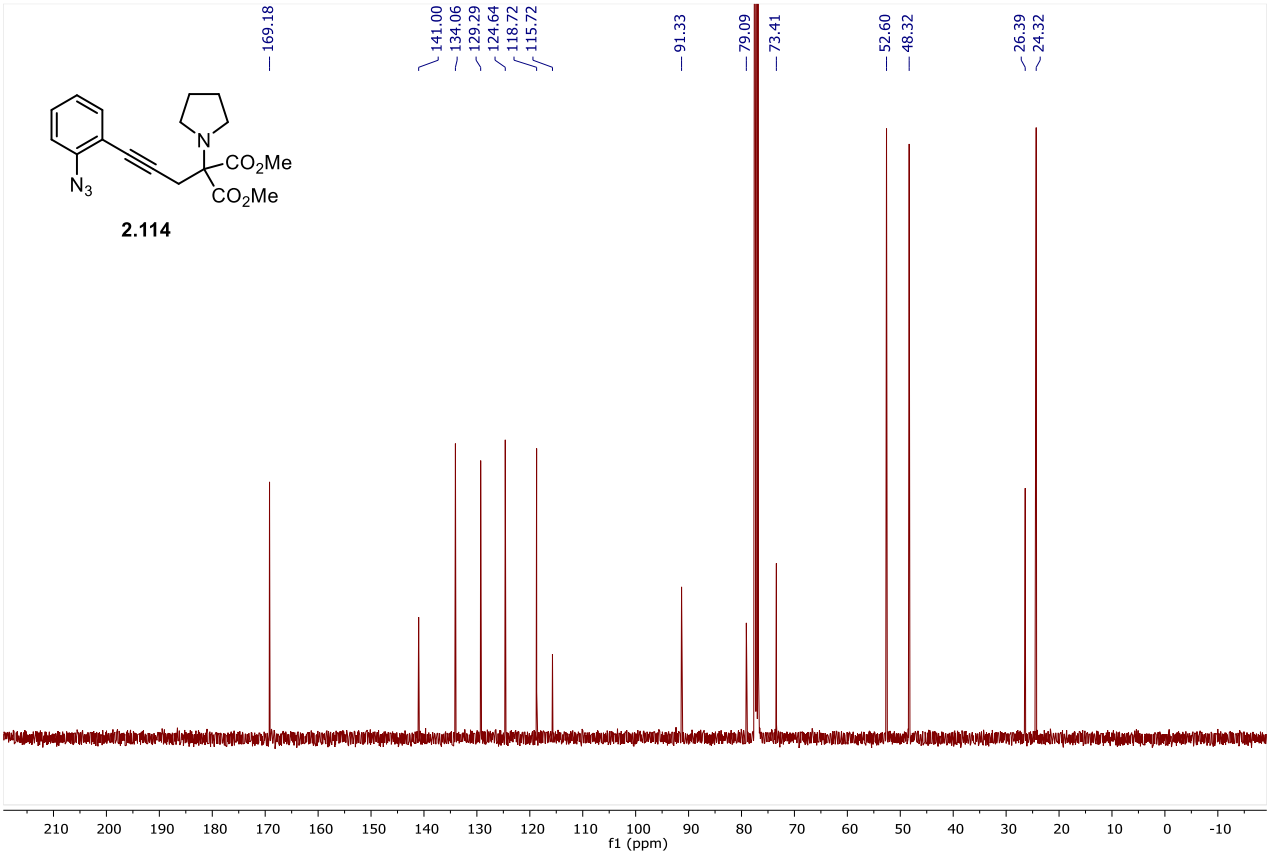

175.67
136.36 131.16 125.87 120.93 119.14 112.07 110.89
62.49 57.18 51.51 47.23
35.98 33.73 27.59 25.79 24.87
H
N
Me
CO2Me
N
H
2.113a
f1 (ppm)

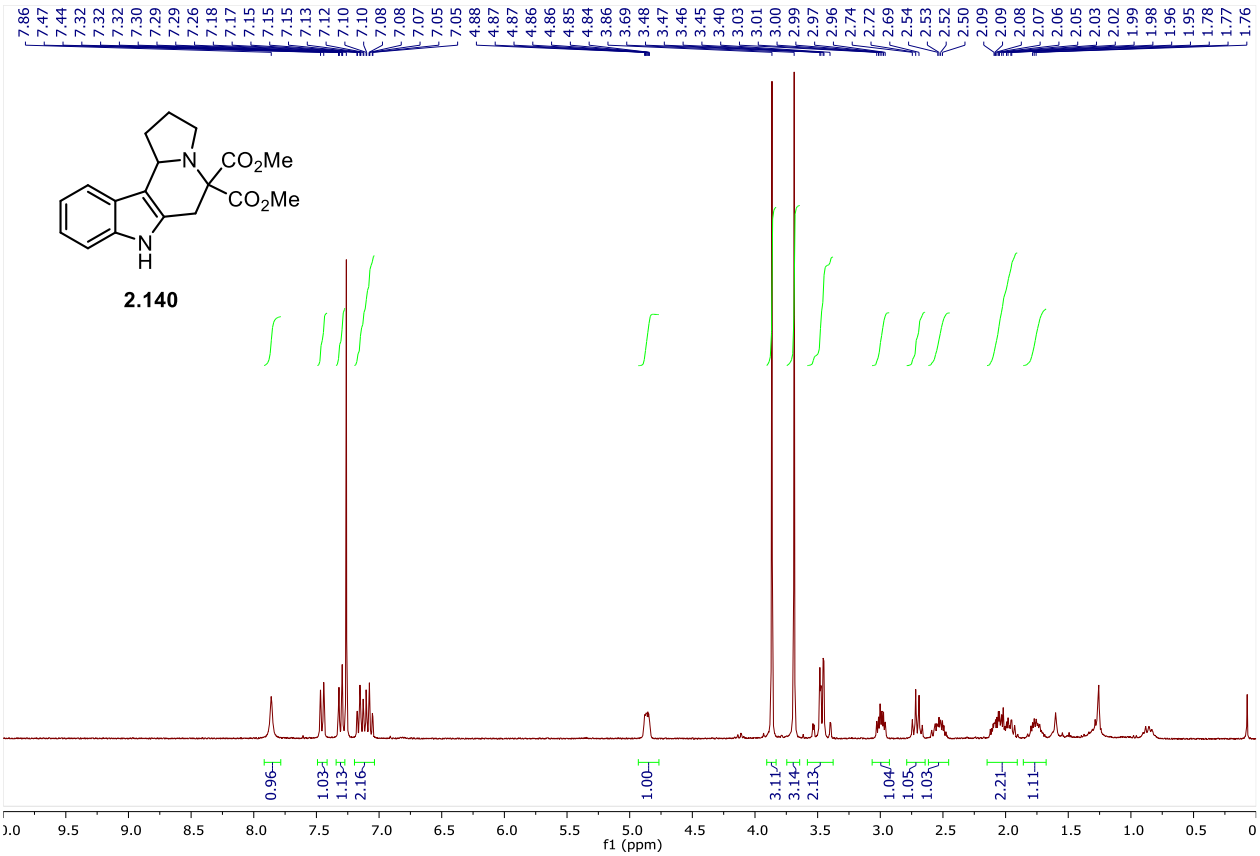

H
N
Me
CO2Me
N
H
2.113a
f2 (ppm)
f1 (ppm)

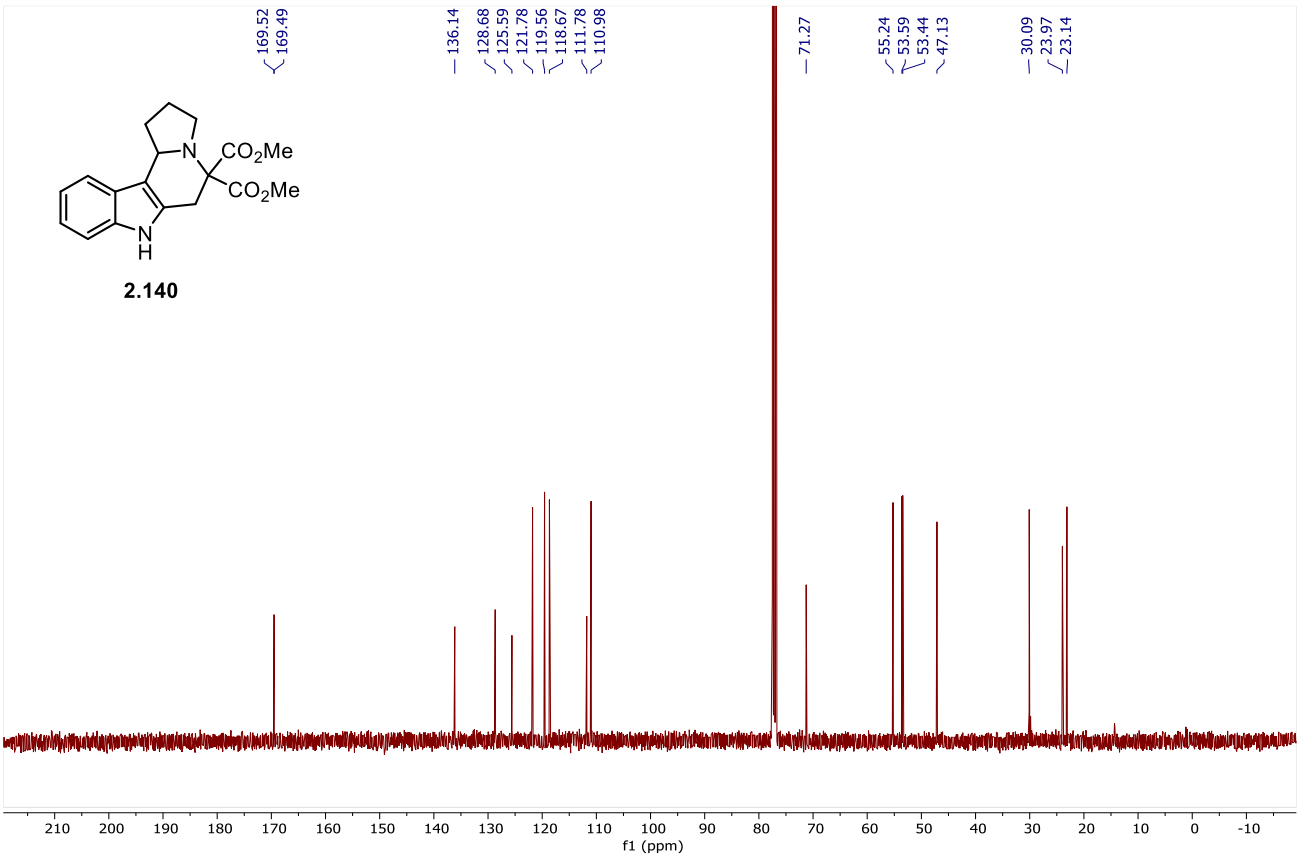

H
N
Me
CO2Me
N
H
2.113a
f2 (ppm)
f1 (ppm)

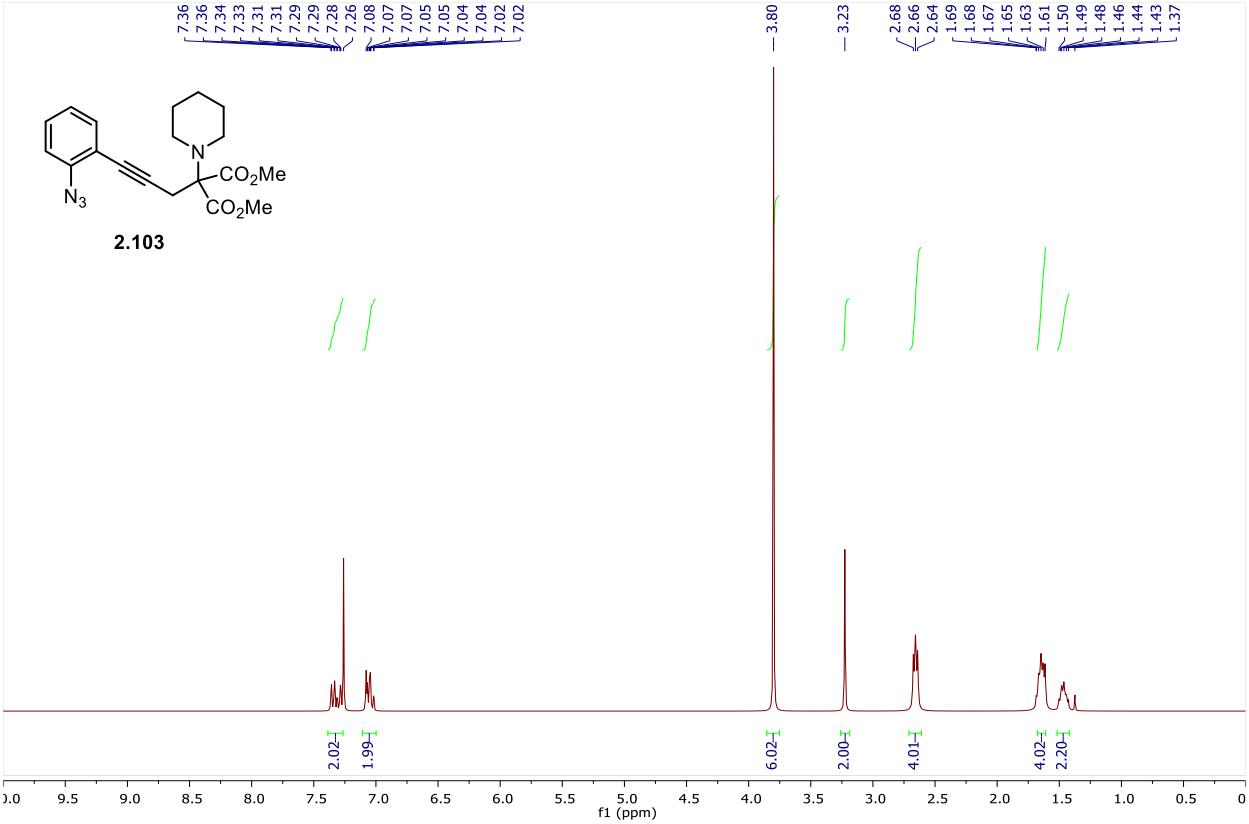

No NOESY
H
N
Me
CO2Me
N
H
2.113a
f2 (ppm)
f1 (ppm)

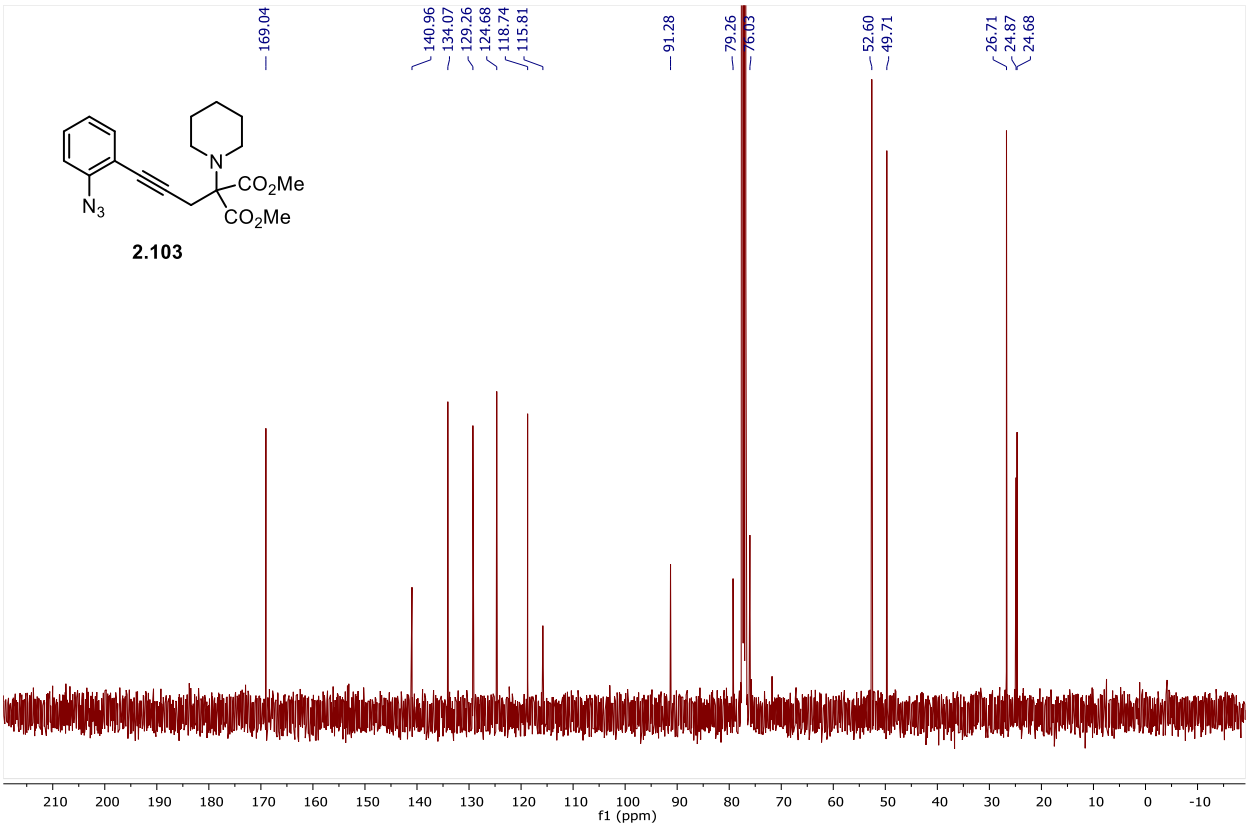

7.36
7.36
7.35
7.35
7.33
7.33
7.33
7.32
7.26
7.08
7.08
7.08
7.07
7.07
7.06
7.05
7.05
7.05
7.04
7.04
7.02
7.01
5.30
3.81
3.24
2.98
2.98
2.97
2.97
2.96
2.96
2.95
2.94
2.94
2.93
1.86
1.84
1.83
1.82
1.81
1.80
1.79
1.78
1.77
N
CO2Me
CO2Me
N3
2.114
0.94
2.12
1.95
5.95
2.00
4.01
3.91
f1 (ppm)

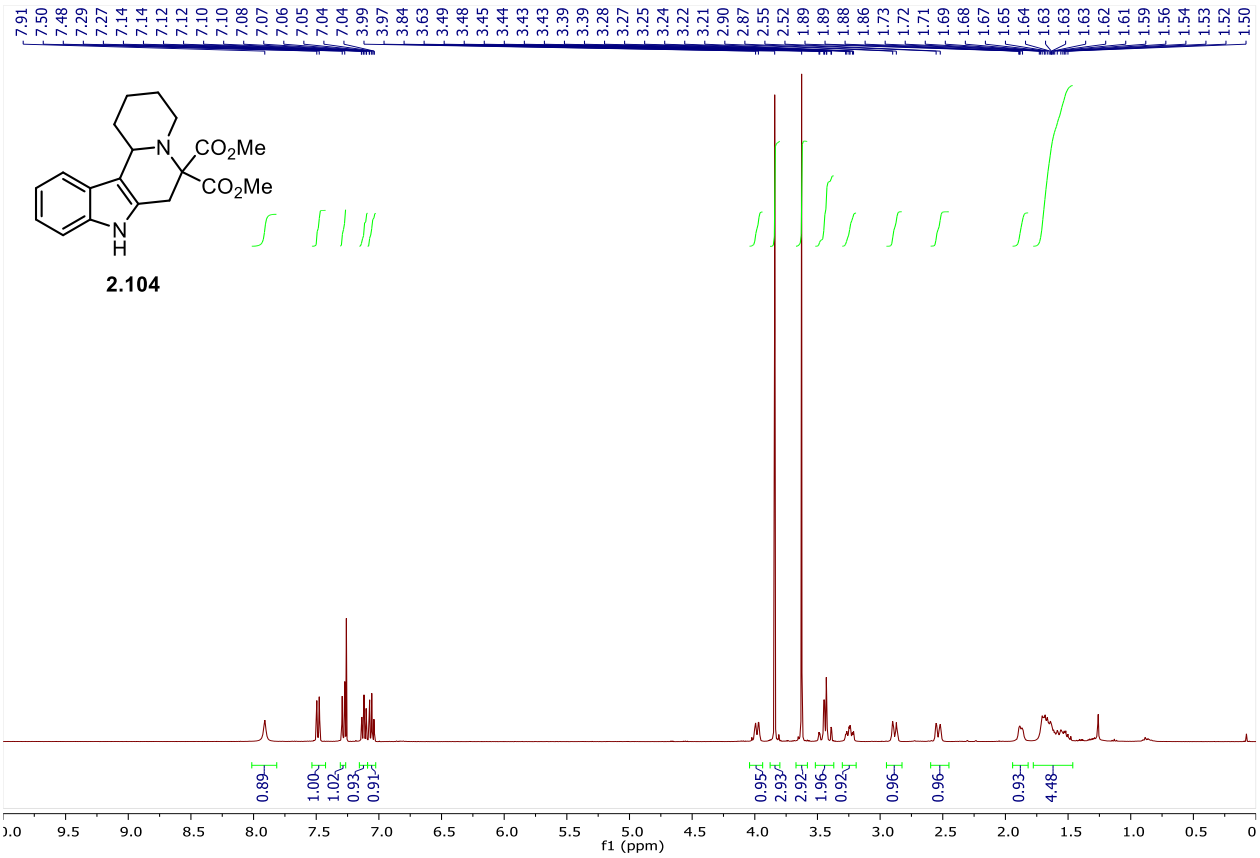

169.18
141.00
134.06
129.29
124.64
118.72
115.72
91.33
79.09
73.41
52.60
48.32
26.39
24.32
N
CO2Me
CO2Me
N3
2.114
f1 (ppm)

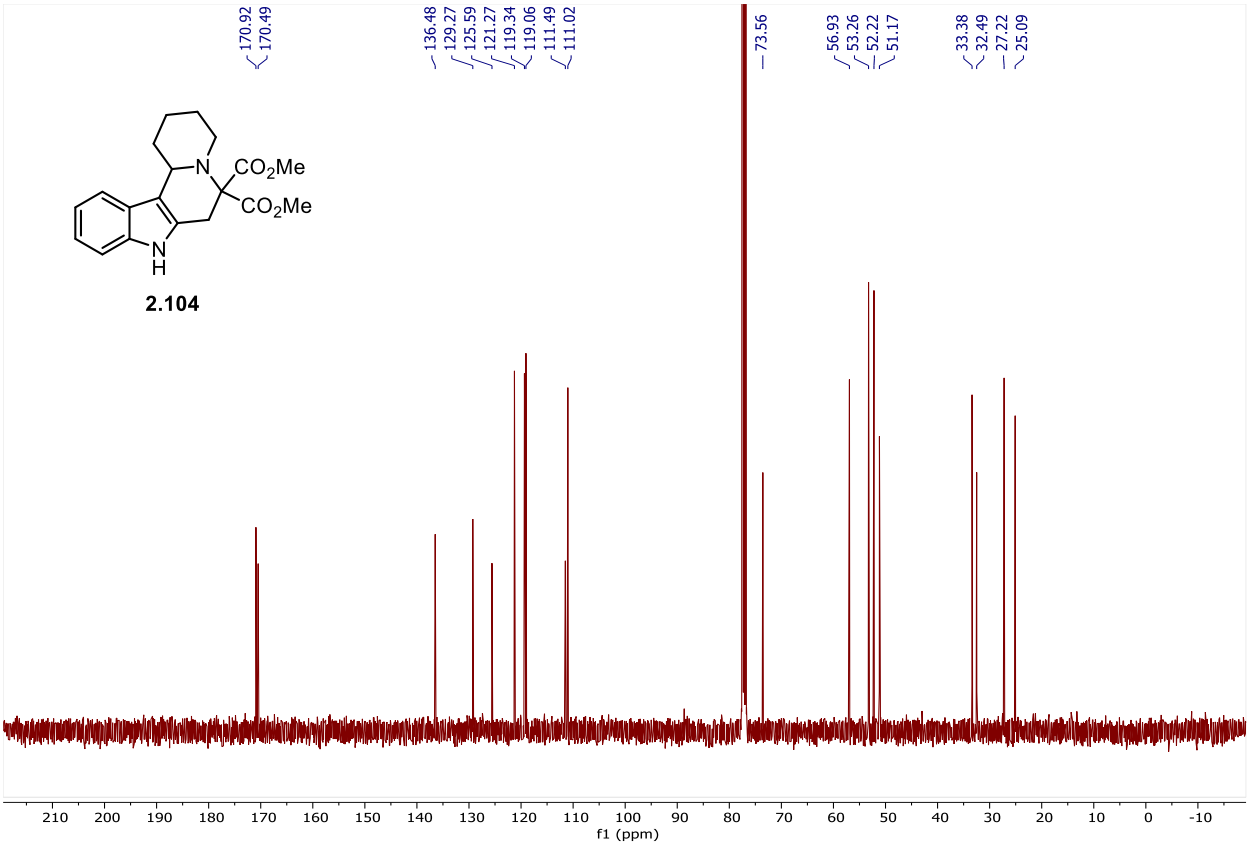

7.86 7.47 7.44 7.32 7.32 7.32 7.30 7.29 7.29 7.26 7.18 7.17 7.15 7.15 7.15 7.13 7.12 7.10 7.10 7.08 7.08 7.07 7.05 7.05
4.88 4.87 4.87 4.86 4.86 4.85 4.84 3.86 3.69 3.48 3.47 3.46 3.45 3.40 3.03 3.01 3.00 2.99 2.97 2.96 2.74 2.72 2.69 2.54 2.53 2.52 2.50 2.09 2.09 2.08 2.07 2.06 2.05 2.03 2.02 1.99 1.98 1.96 1.95 1.78 1.77 1.76
CO2Me
CO2Me
N
H
2.140
0.96 1.03 1.13 2.16 1.00 3.11 3.14 2.13 1.04 1.05 1.03 2.21 1.11
f1 (ppm)

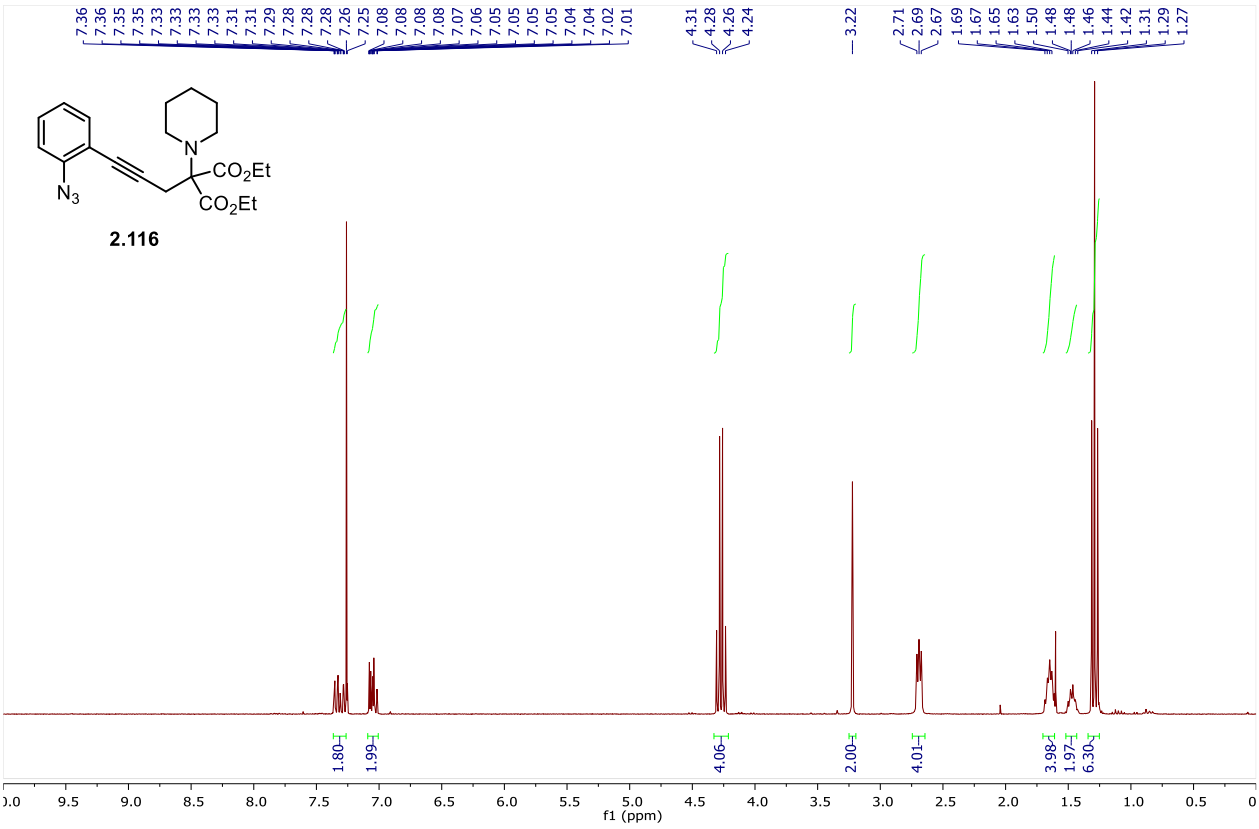

169.52 169.49 136.14 128.68 125.59 121.78 119.56 118.67 111.78 110.98 71.27 55.24 53.59 53.44 47.13 30.09 23.97 23.14
CO2Me
CO2Me
N
H
2.140
f1 (ppm)

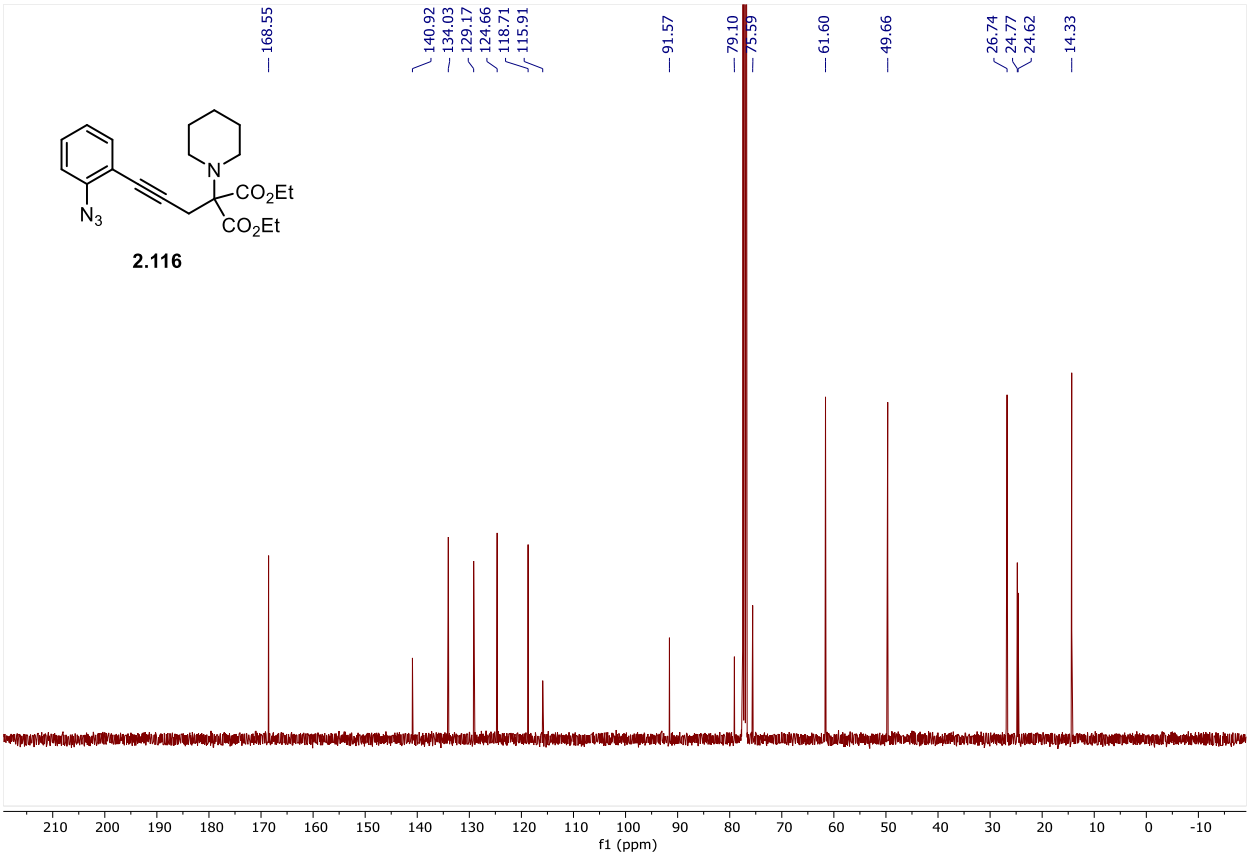

7.36
7.36
7.34
7.33
7.31
7.31
7.29
7.29
7.28
7.26
7.08
7.07
7.07
7.05
7.05
7.04
7.04
7.02
7.02
3.80
3.23
2.68
2.66
2.64
1.69
1.68
1.67
1.65
1.63
1.61
1.50
1.49
1.48
1.46
1.44
1.43
1.37
N
CO2Me
CO2Me
N3
2.103
2.02
1.99
6.02
2.00
4.01
4.02
2.20
f1 (ppm)

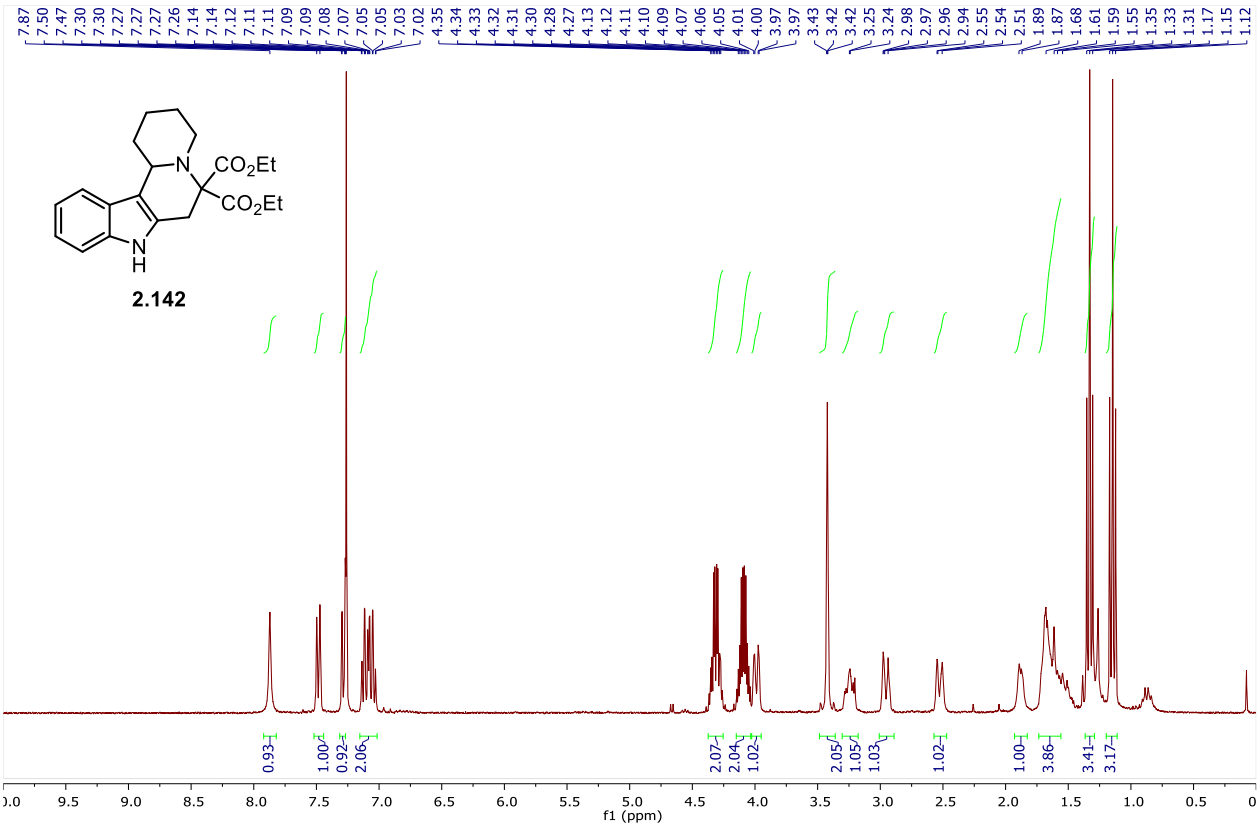

169.04
140.96
134.07
129.26
124.68
118.74
115.81
91.28
79.26
76.03
52.60
49.71
26.71
24.87
24.68
N
CO2Me
CO2Me
N3
2.103
f1 (ppm)

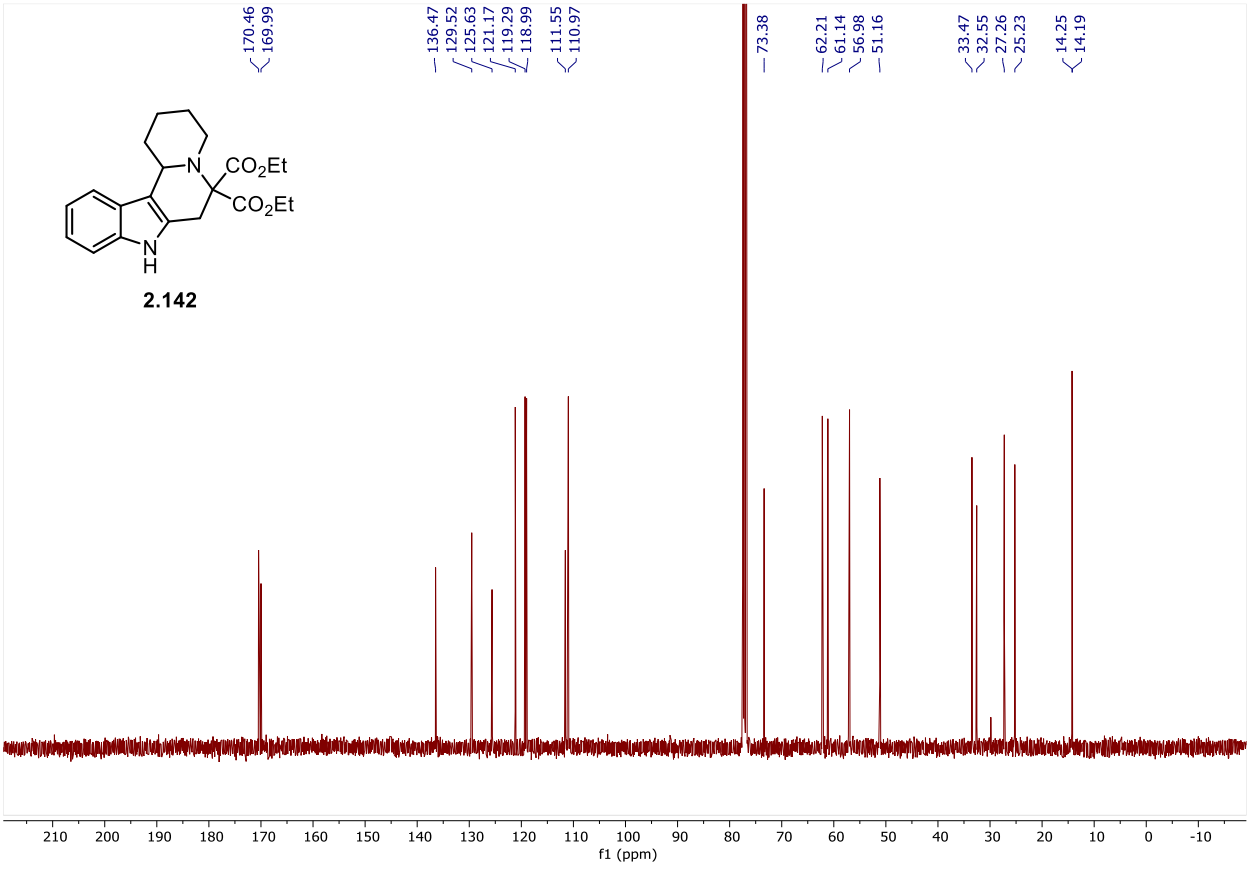

CO2Me
CO2Me
N
H
2.104
f1 (ppm)

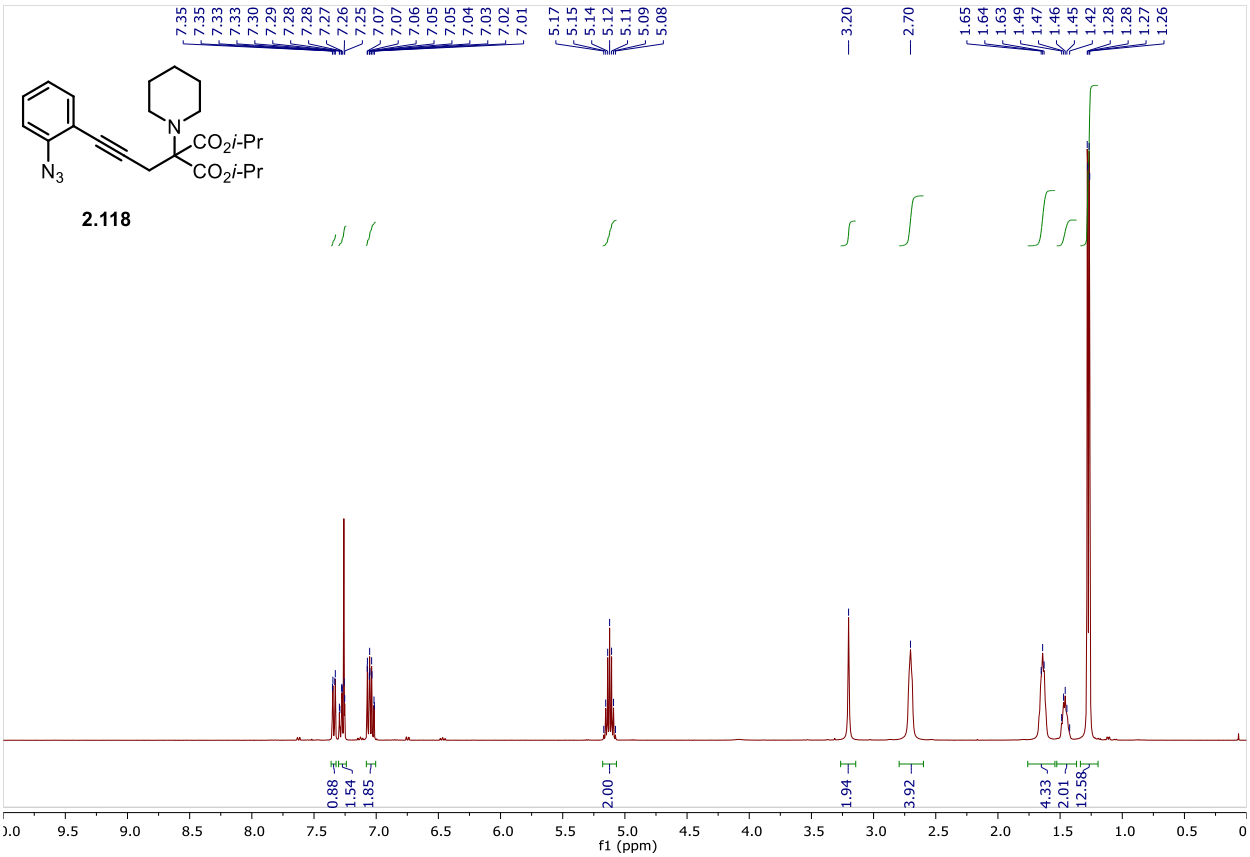

CO2Me
CO2Me
N
H
2.104
f1 (ppm)

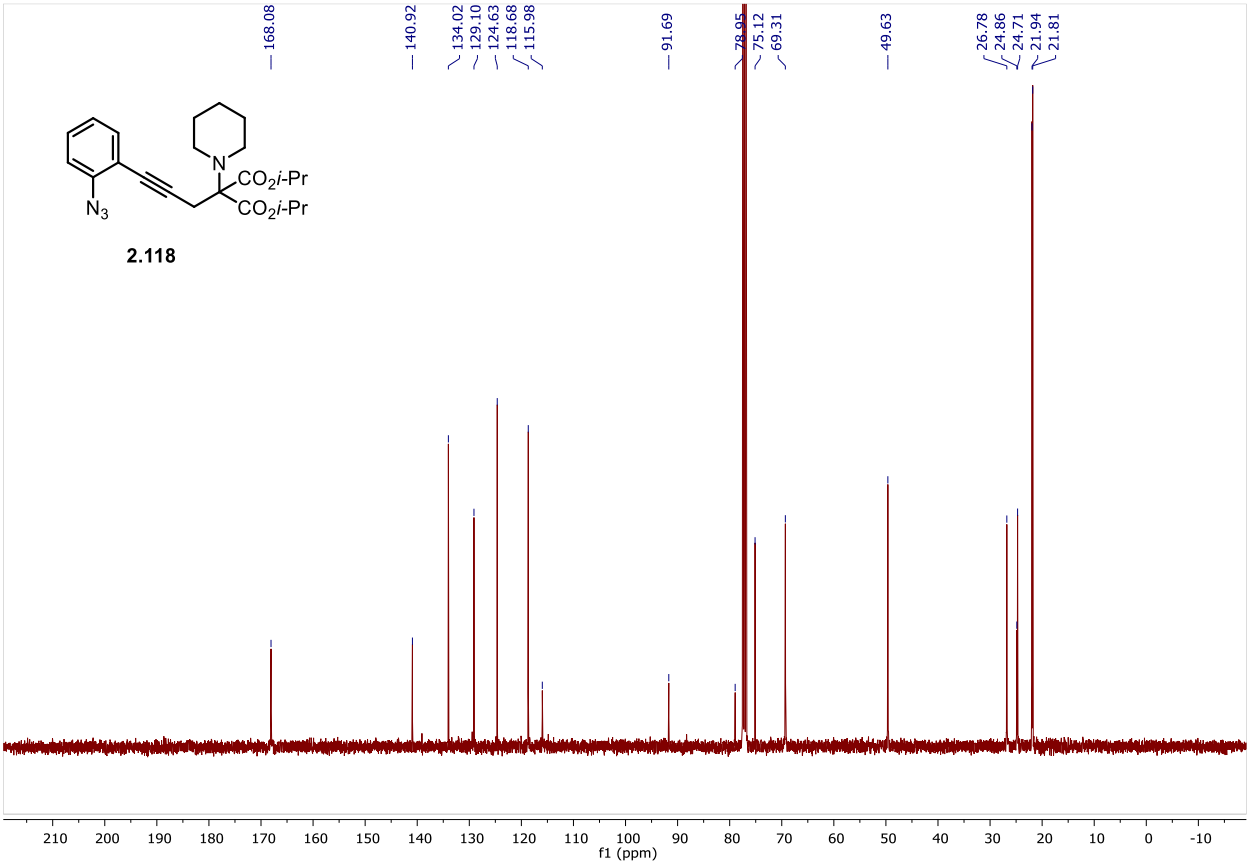

7.36 7.36 7.35 7.35 7.33 7.33 7.33 7.33 7.31 7.31 7.29 7.28 7.28 7.28 7.26 7.25 7.08 7.08 7.08 7.08 7.07 7.06 7.05 7.05 7.05 7.05 7.04 7.04 7.02 7.01
4.31 4.28 4.26 4.24
3.22
2.71 2.69 2.67
1.69 1.67 1.65 1.63 1.50 1.48 1.48 1.46 1.44 1.42 1.31 1.29 1.27
N
CO2Et
CO2Et
N3
2.116
1.80 1.99 4.06 2.00 4.01 3.98 1.97 6.30
f1 (ppm)

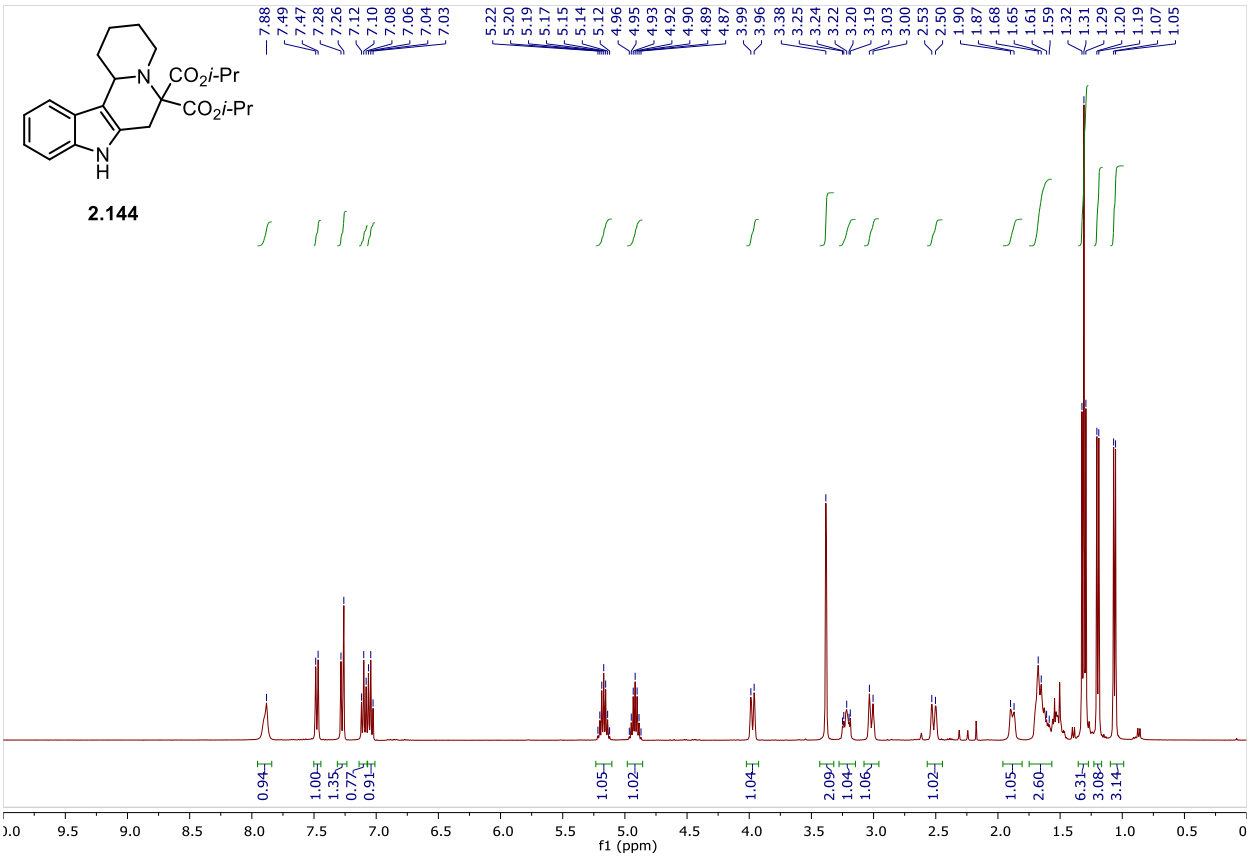

168.55
140.92 134.03 129.17 124.66 118.71 115.91
91.57
79.10 75.59
61.60
49.66
26.74 24.77 24.62
14.33
N
CO2Et
CO2Et
N3
2.116
f1 (ppm)

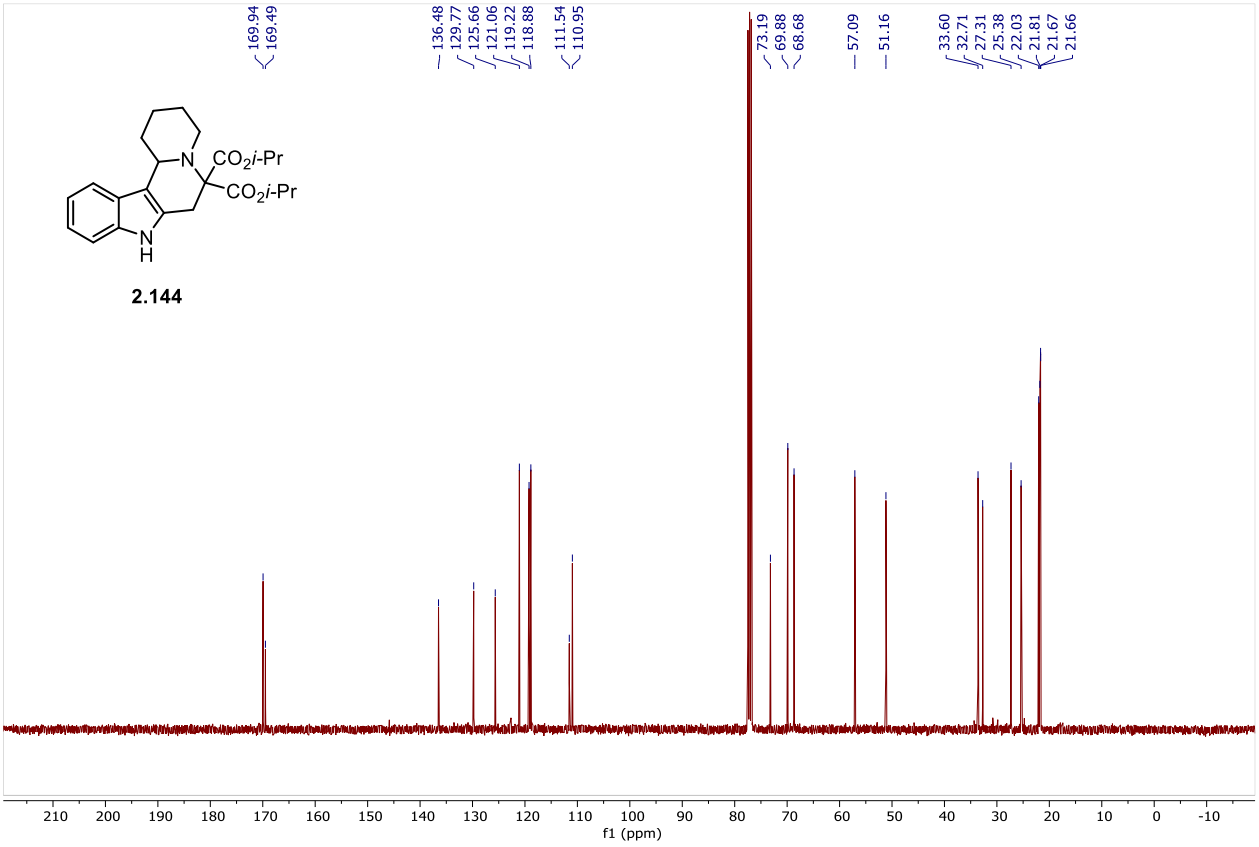

CO2Et
CO2Et
N
H
2.142
f1 (ppm)

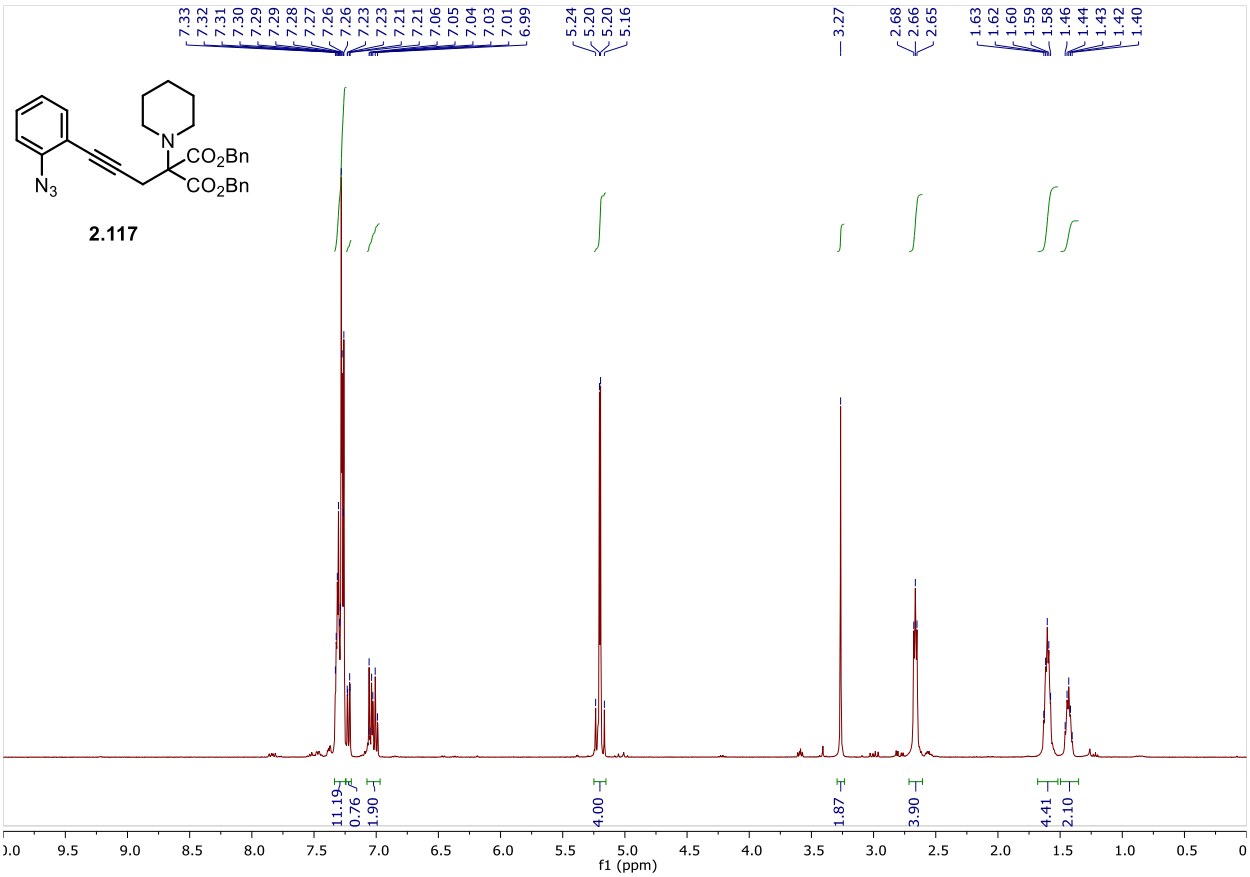

CO2Et
CO2Et
N
H
2.142
f1 (ppm)

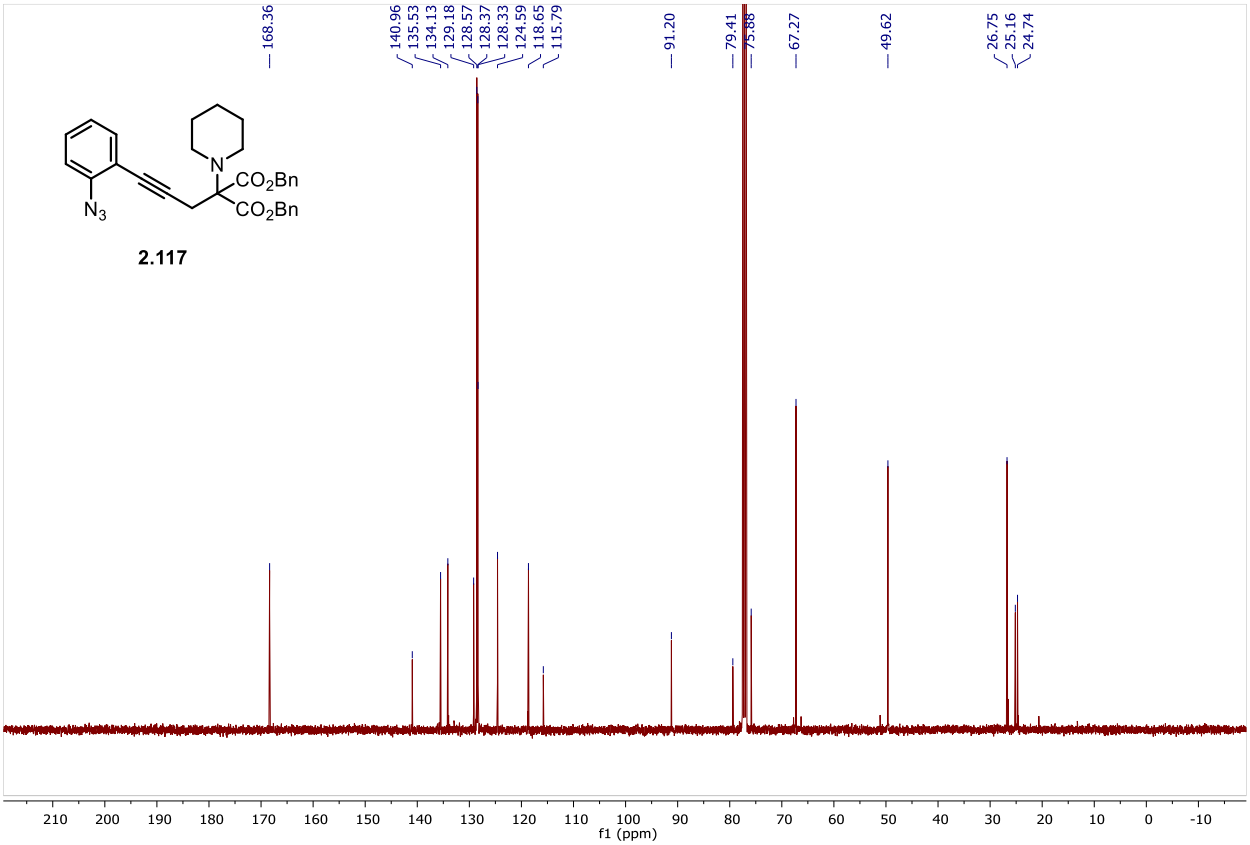

7.35 7.35 7.33 7.33 7.30 7.29 7.28 7.28 7.27 7.26 7.25 7.07 7.07 7.06 7.05 7.05 7.04 7.03 7.02 7.01
5.17 5.15 5.14 5.12 5.11 5.09 5.08
3.20
2.70
1.65 1.64 1.63 1.49 1.47 1.46 1.45 1.42 1.28 1.28 1.27 1.26
N
CO2i-Pr
CO2i-Pr
N3
2.118
0.88 1.54 1.85 2.00 1.94 3.92 4.33 2.01 12.58
f1 (ppm)

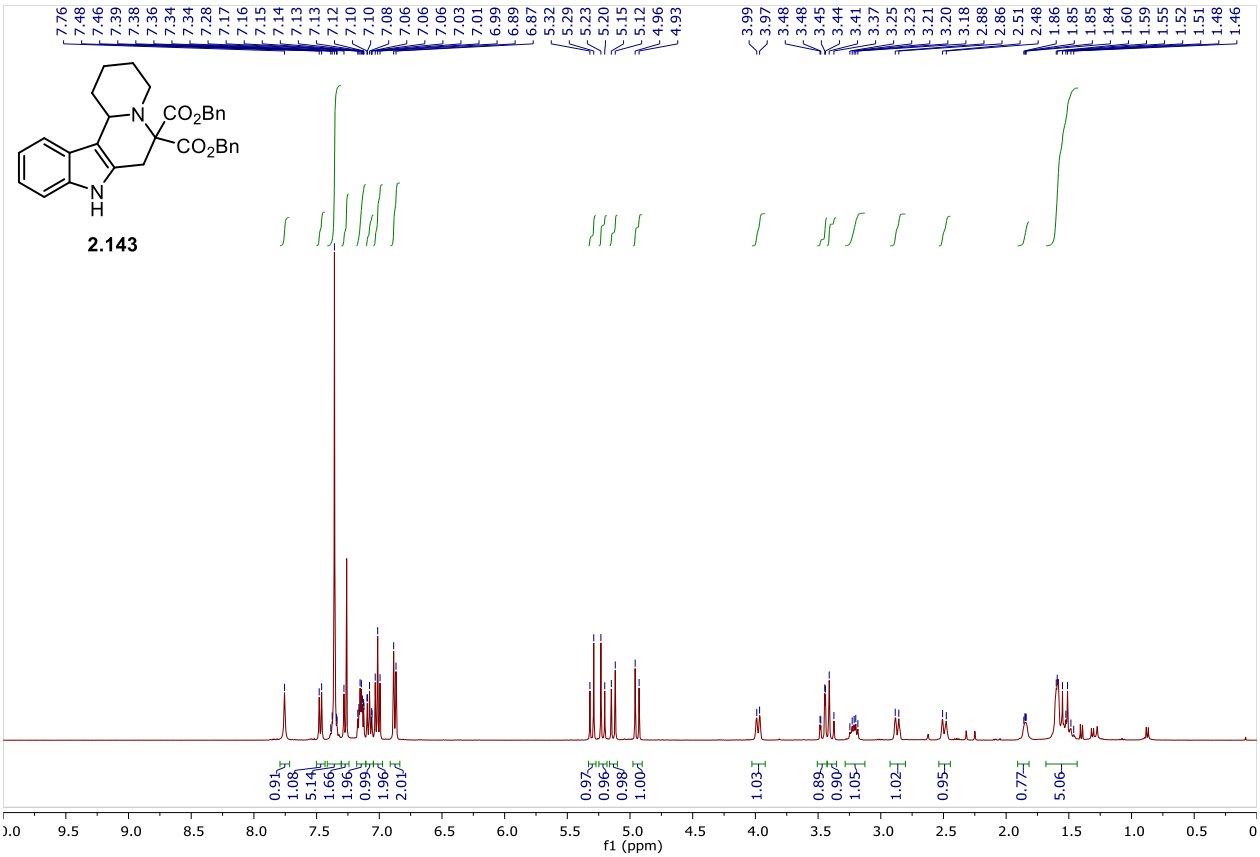

168.08
140.92
134.02 129.10 124.63 118.68 115.98
91.69
78.95 75.12 69.31
49.63
26.78 24.86 24.71 21.94 21.81
N
CO2i-Pr
CO2i-Pr
N3
2.118
f1 (ppm)

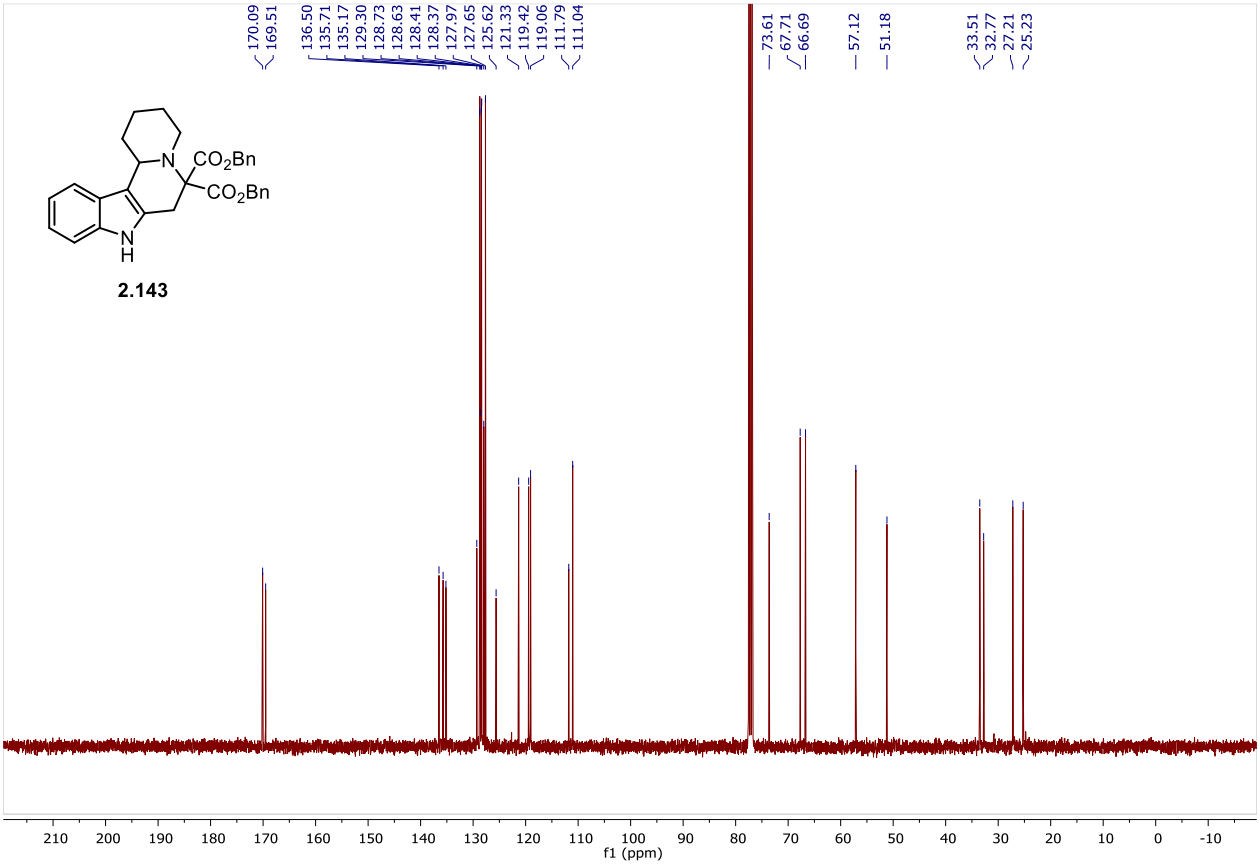

CO2i-Pr
CO2i-Pr
N
H
2.144
f1 (ppm)

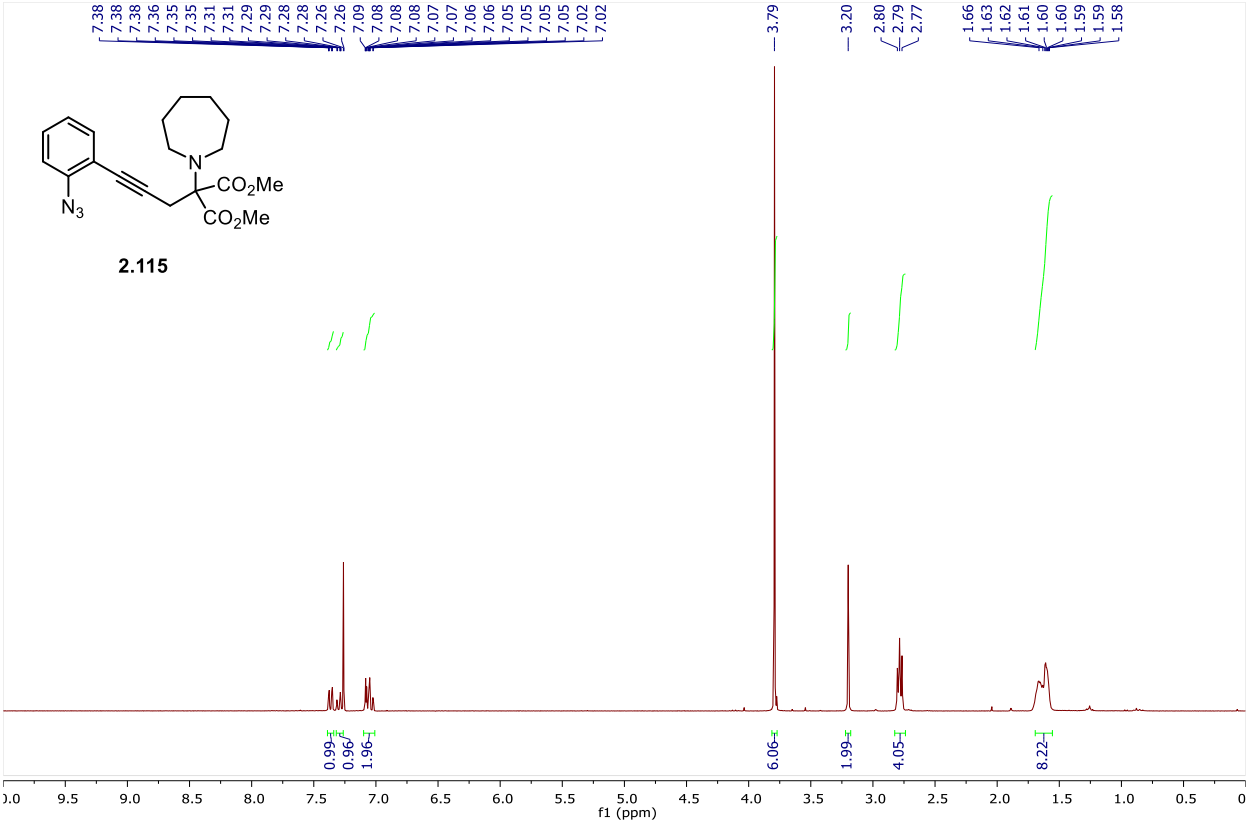

CO2i-Pr
CO2i-Pr
N
H
2.144
f1 (ppm)

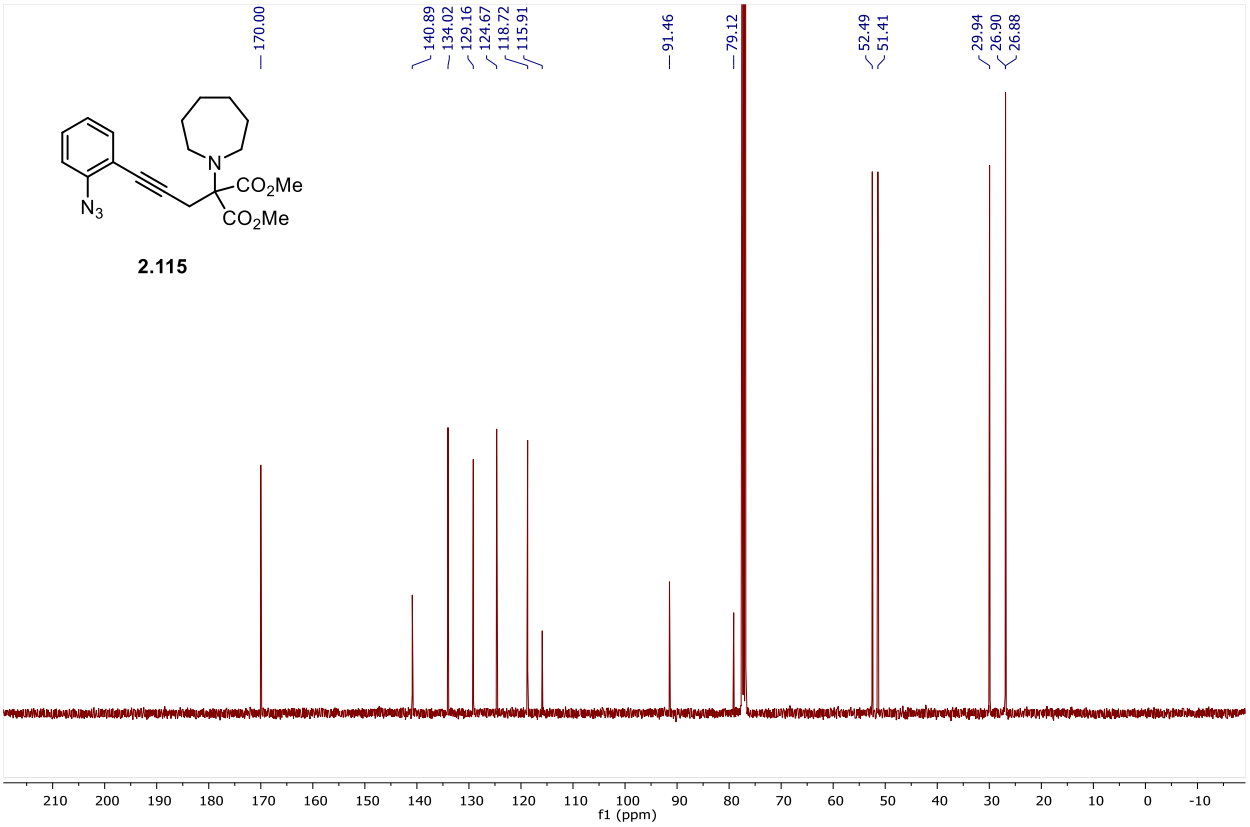

7.33 7.32 7.31 7.30 7.29 7.29 7.28 7.27 7.26 7.26 7.23 7.23 7.21 7.21 7.06 7.05 7.04 7.03 7.01 6.99
5.24 5.20 5.20 5.16
3.27
2.68 2.66 2.65
1.63 1.62 1.60 1.59 1.58 1.46 1.44 1.43 1.42 1.40
N
CO2Bn
CO2Bn
N3
2.117
11.19 0.76 1.90 4.00 1.87 3.90 4.41 2.10
f1 (ppm)

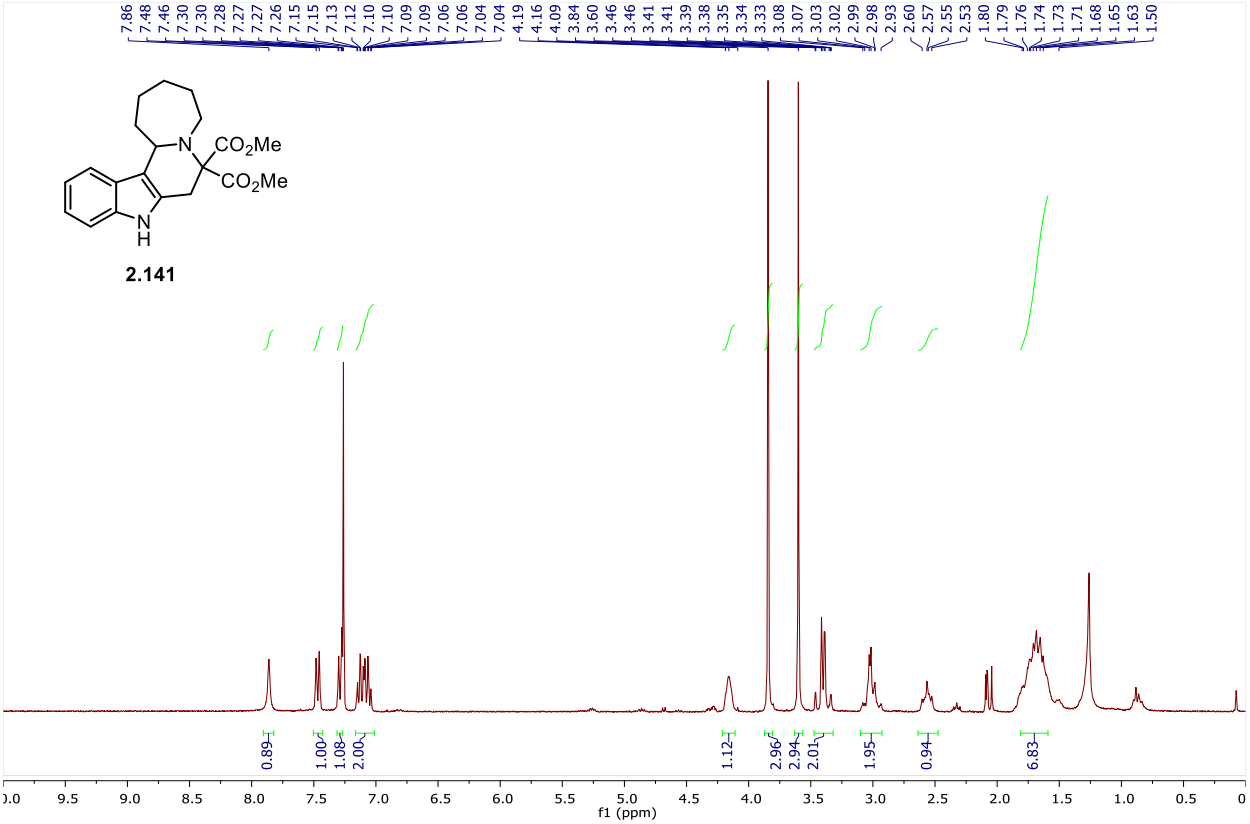

168.36
140.96 135.53 134.13 129.18 128.57 128.37 128.33 124.59 118.65 115.79
91.20
79.41 75.88
67.27
49.62
26.75 25.16 24.74
N
CO2Bn
CO2Bn
N3
2.117
f1 (ppm)

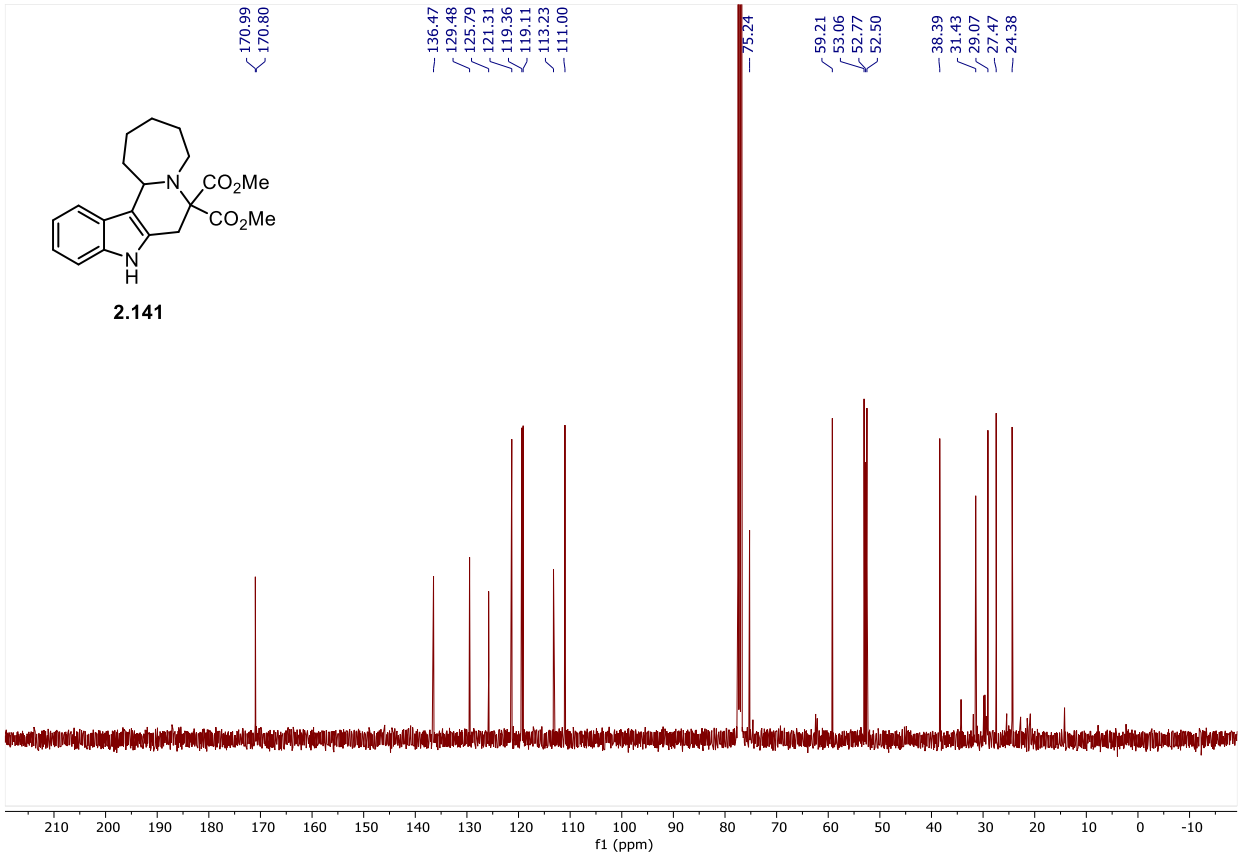

7.76 7.48 7.46 7.39 7.38 7.36 7.34 7.34 7.28 7.17 7.16 7.15 7.14 7.13 7.13 7.12 7.10 7.10 7.08 7.06 7.06 7.06 7.03 7.01 6.99 6.89 6.87
5.32 5.29 5.23 5.20 5.15 5.12 4.96 4.93
3.99 3.97 3.48 3.48 3.45 3.44 3.41 3.37 3.25 3.23 3.21 3.20 3.18 2.88 2.86 2.51 2.48 1.86 1.85 1.85 1.84 1.60 1.59 1.55 1.52 1.51 1.48 1.46
CO2Bn
CO2Bn
N
H
2.143
0.91 1.08 5.14 1.66 1.96 0.99 1.96 2.01
0.97 0.96 0.98 1.00
1.03
0.89 0.90 1.05
1.02
0.95
0.77
5.06
f1 (ppm)

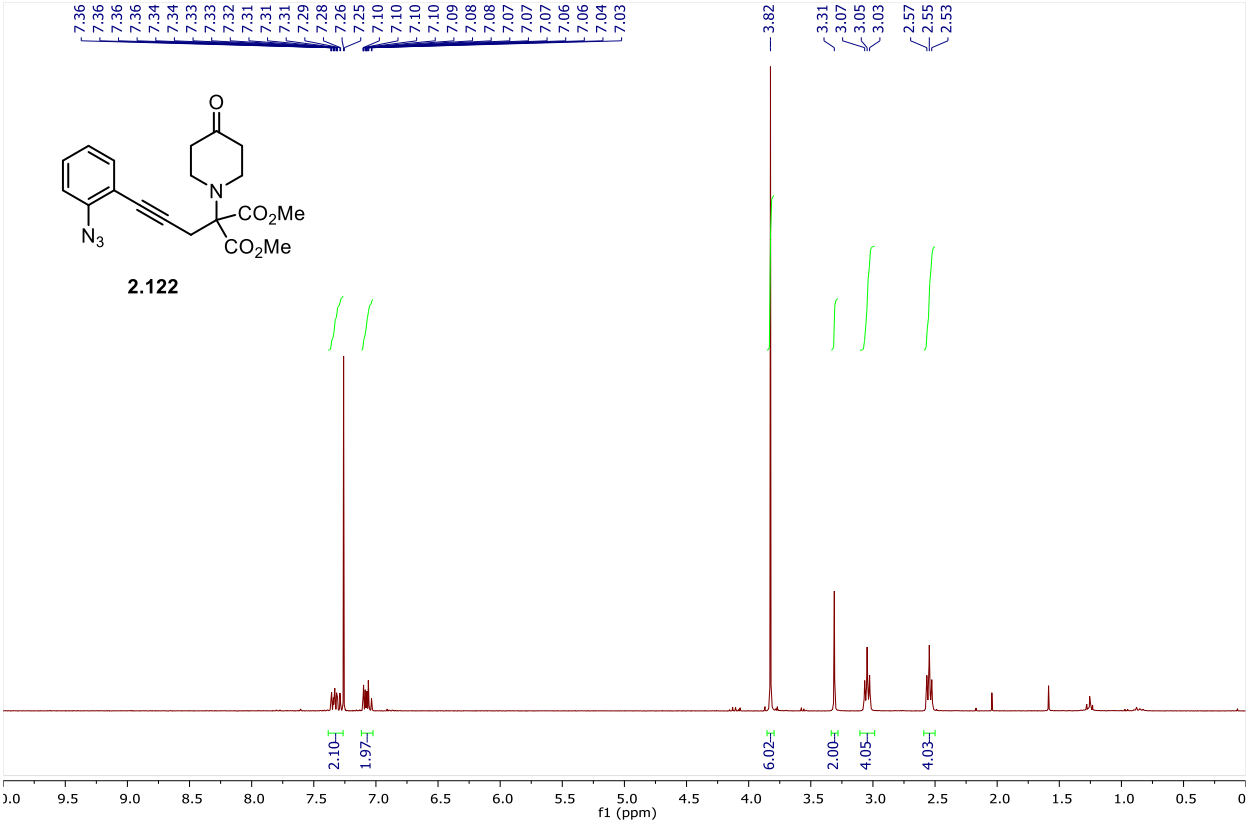

170.09 169.51
136.50 135.71 135.17 129.30 128.73 128.63 128.41 128.37 127.97 127.65 125.62 121.33 119.42 119.06 111.79 111.04
73.61 67.71 66.69
57.12
51.18
33.51 32.77 27.21 25.23
CO2Bn
CO2Bn
N
H
2.143
f1 (ppm)

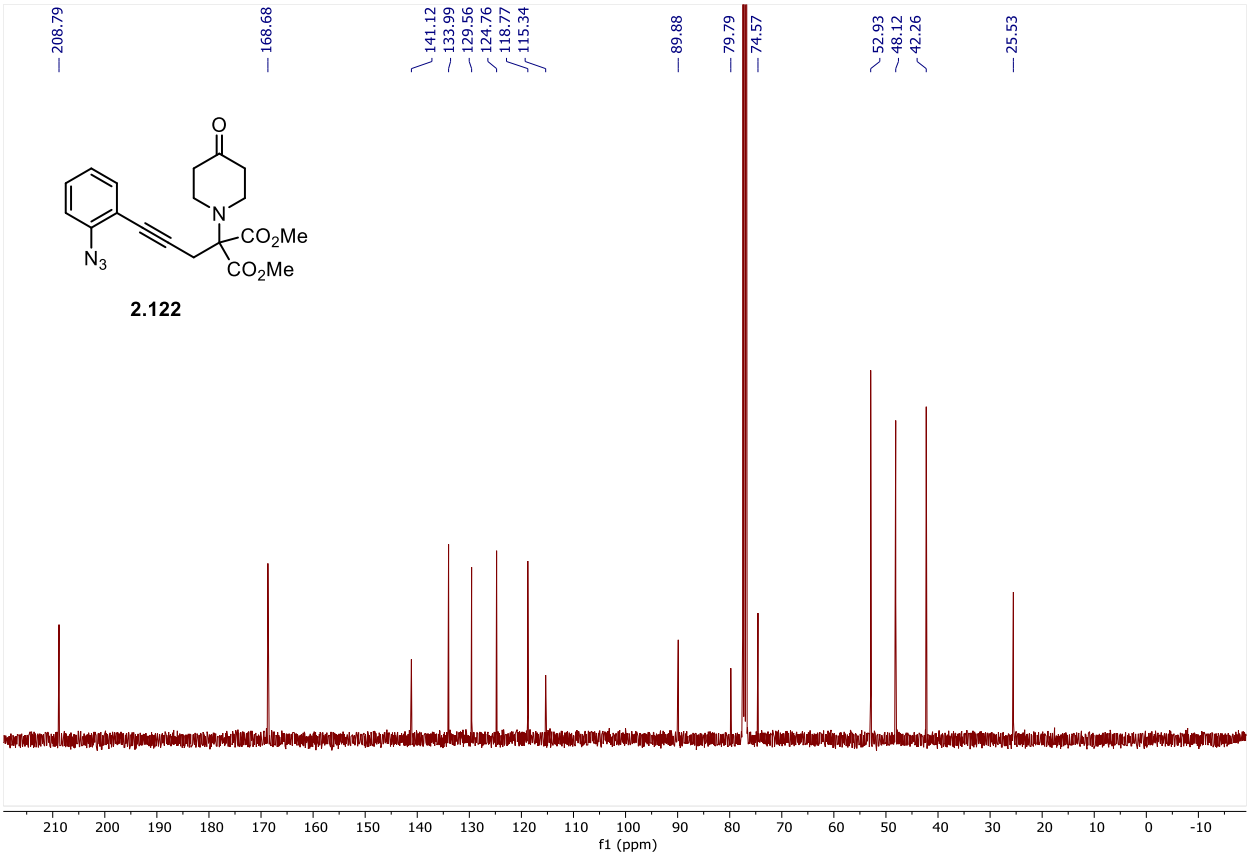

7.38 7.38 7.38 7.36 7.35 7.35 7.31 7.31 7.29 7.29 7.28 7.28 7.26 7.26 7.09 7.08 7.08 7.08 7.07 7.07 7.06 7.06 7.05 7.05 7.05 7.05 7.02 7.02
3.79
3.20
2.80 2.79 2.77
1.66 1.63 1.62 1.61 1.60 1.60 1.59 1.59 1.58
N
CO2Me
CO2Me
N3
2.115
0.99 0.96 1.96 6.06 1.99 4.05 8.22
f1 (ppm)

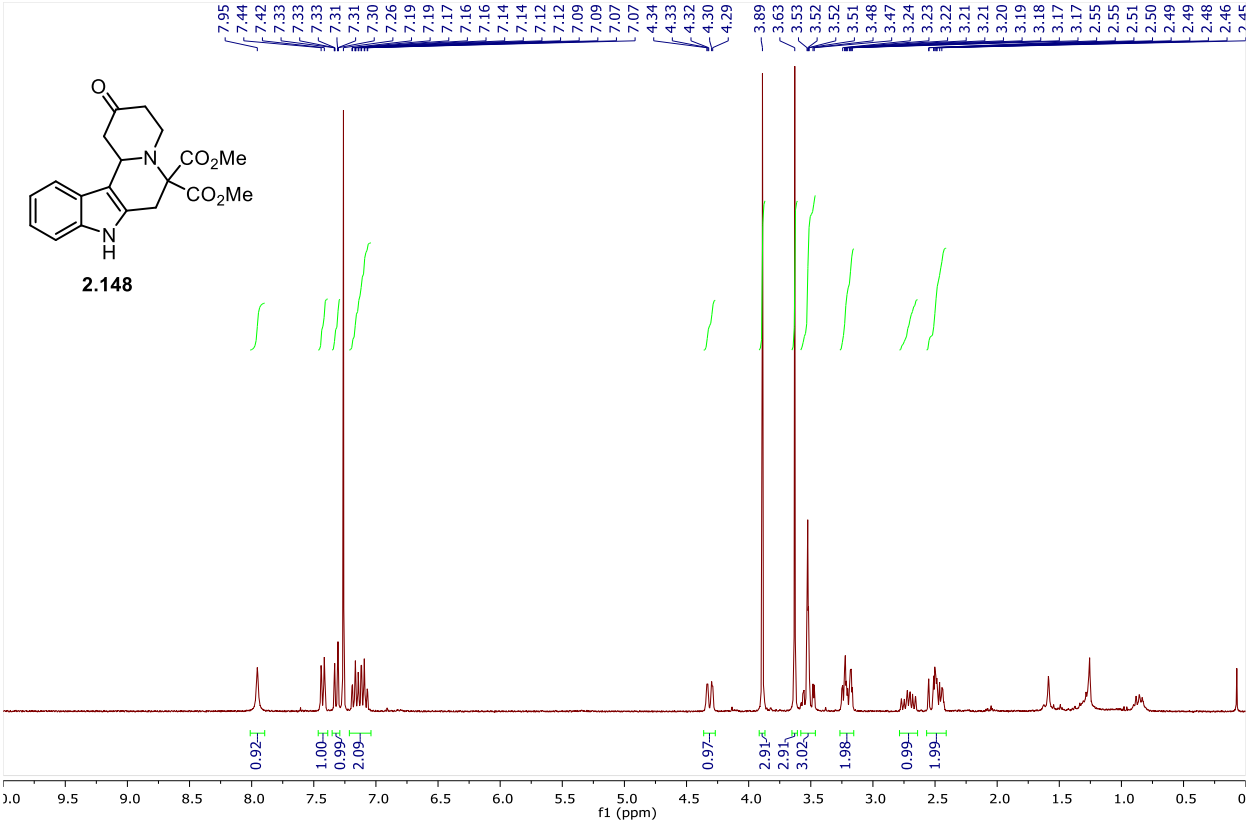

170.00
140.89 134.02 129.16 124.67 118.72 115.91
91.46
79.12
52.49 51.41
29.94 26.90 26.88
N
CO2Me
CO2Me
N3
2.115
f1 (ppm)

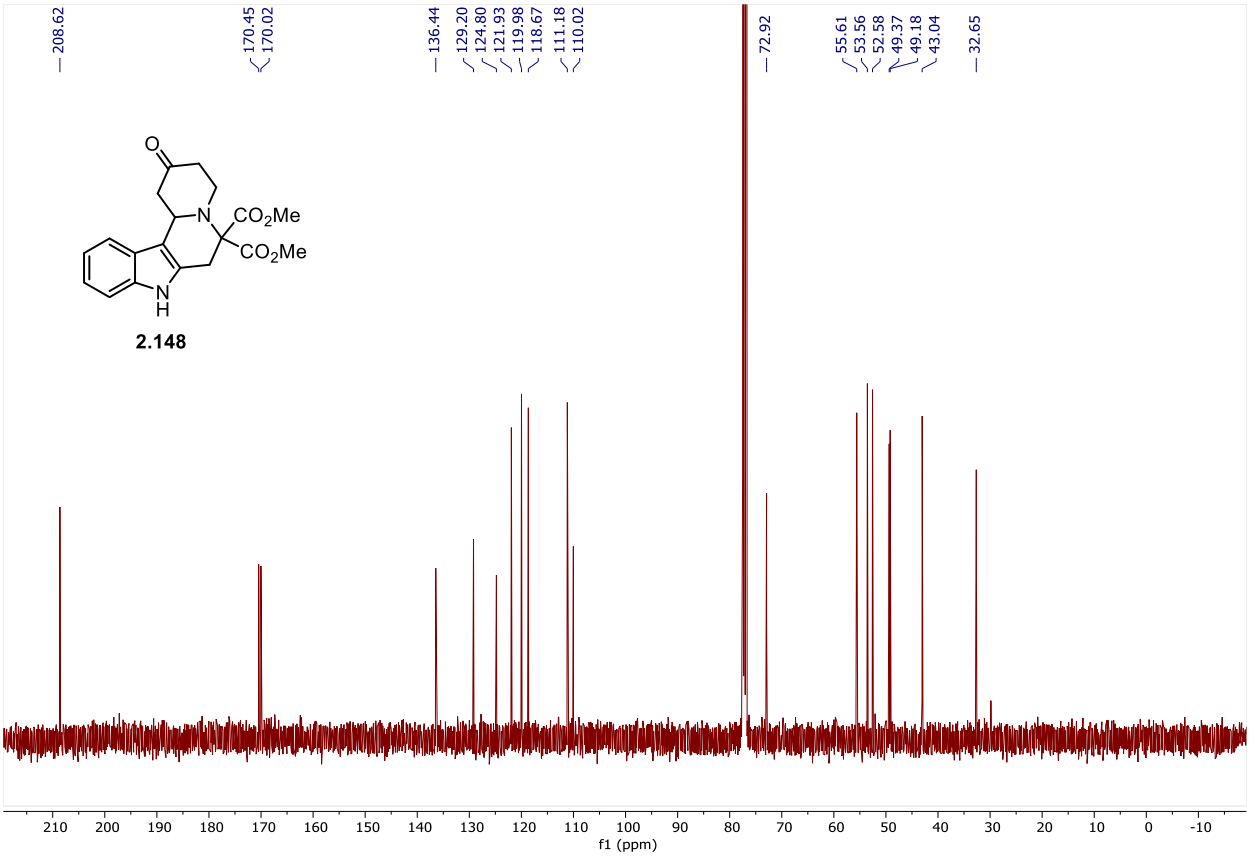

7.86 7.48 7.46 7.30 7.30 7.28 7.27 7.27 7.26 7.15 7.15 7.13 7.12 7.10 7.10 7.09 7.09 7.06 7.06 7.04 7.04 4.19 4.16 4.09 3.84 3.60 3.46 3.41 3.41 3.39 3.38 3.35 3.34 3.33 3.08 3.07 3.03 3.02 2.99 2.98 2.93 2.60 2.57 2.55 2.53 1.80 1.79 1.76 1.74 1.73 1.71 1.68 1.65 1.63 1.50
CO2Me
CO2Me
N
H
2.141
0.89 1.00 1.08 2.00 1.12 2.96 2.94 2.01 1.95 0.94 6.83
f1 (ppm)

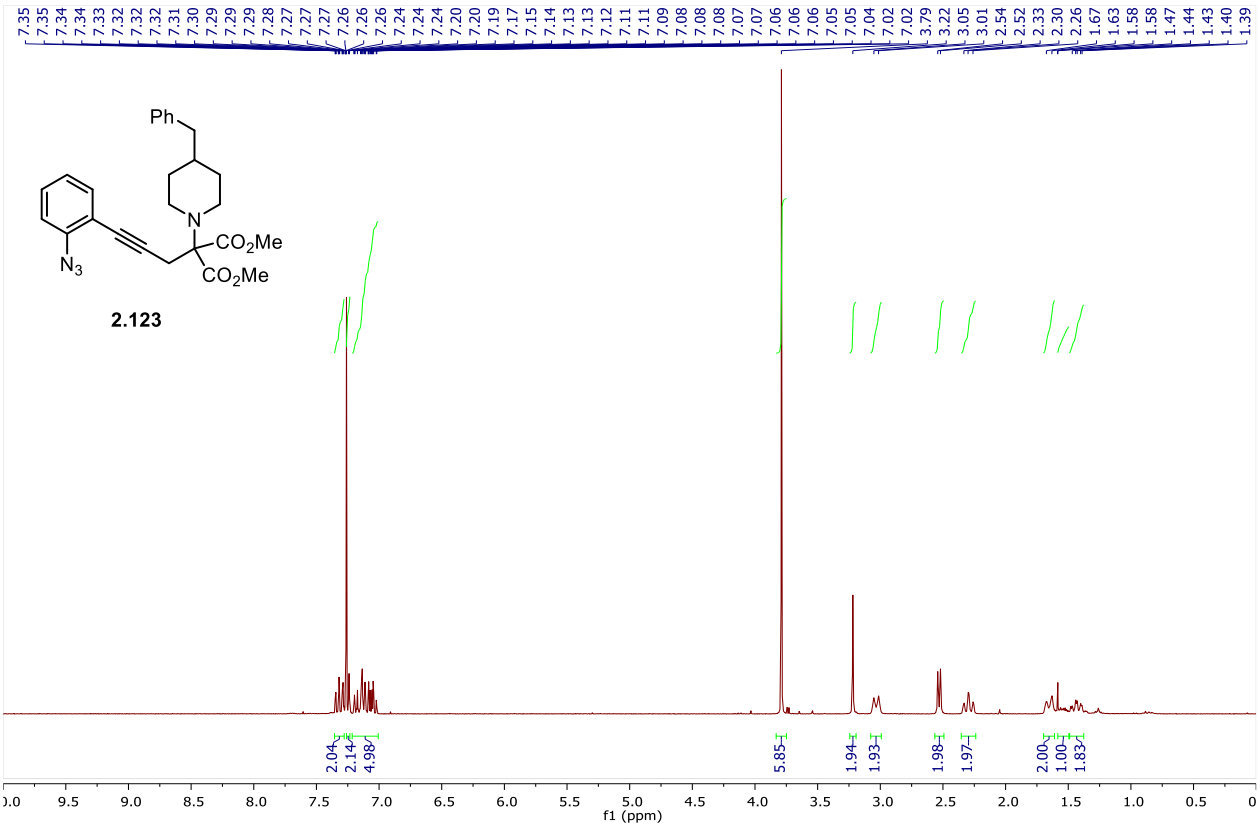

170.99 170.80 136.47 129.48 125.79 121.31 119.36 119.11 113.23 111.00 75.24 59.21 53.06 52.77 52.50 38.39 31.43 29.07 27.47 24.38
CO2Me
CO2Me
N
H
2.141
f1 (ppm)

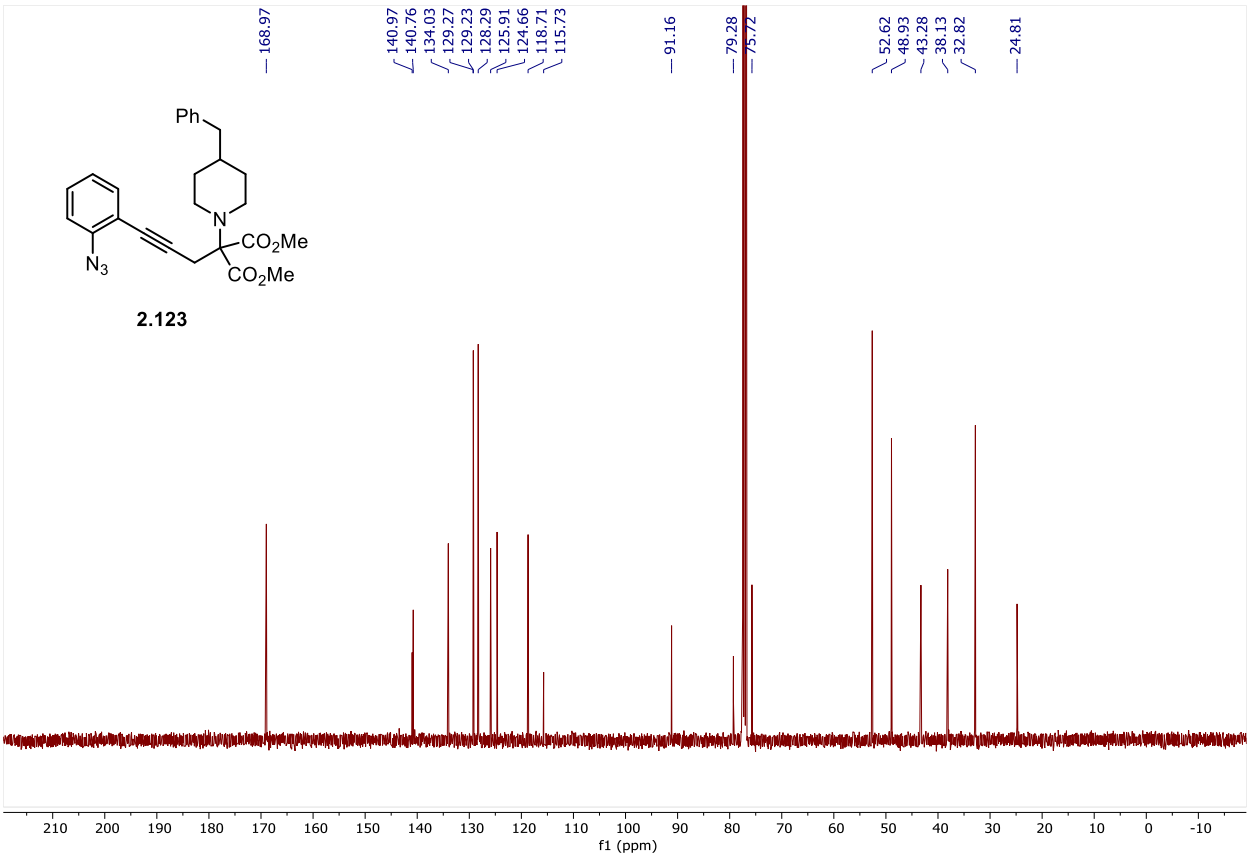

7.36 7.36 7.36 7.36 7.34 7.34 7.33 7.33 7.32 7.31 7.31 7.31 7.29 7.28 7.26 7.25 7.10 7.10 7.10 7.09 7.08 7.08 7.07 7.07 7.07 7.06 7.06 7.04 7.03
3.82
3.31 3.07 3.05 3.03
2.57 2.55 2.53
O
N
CO2Me
CO2Me
N3
2.122
2.10 1.97 6.02 2.00 4.05 4.03
f1 (ppm)

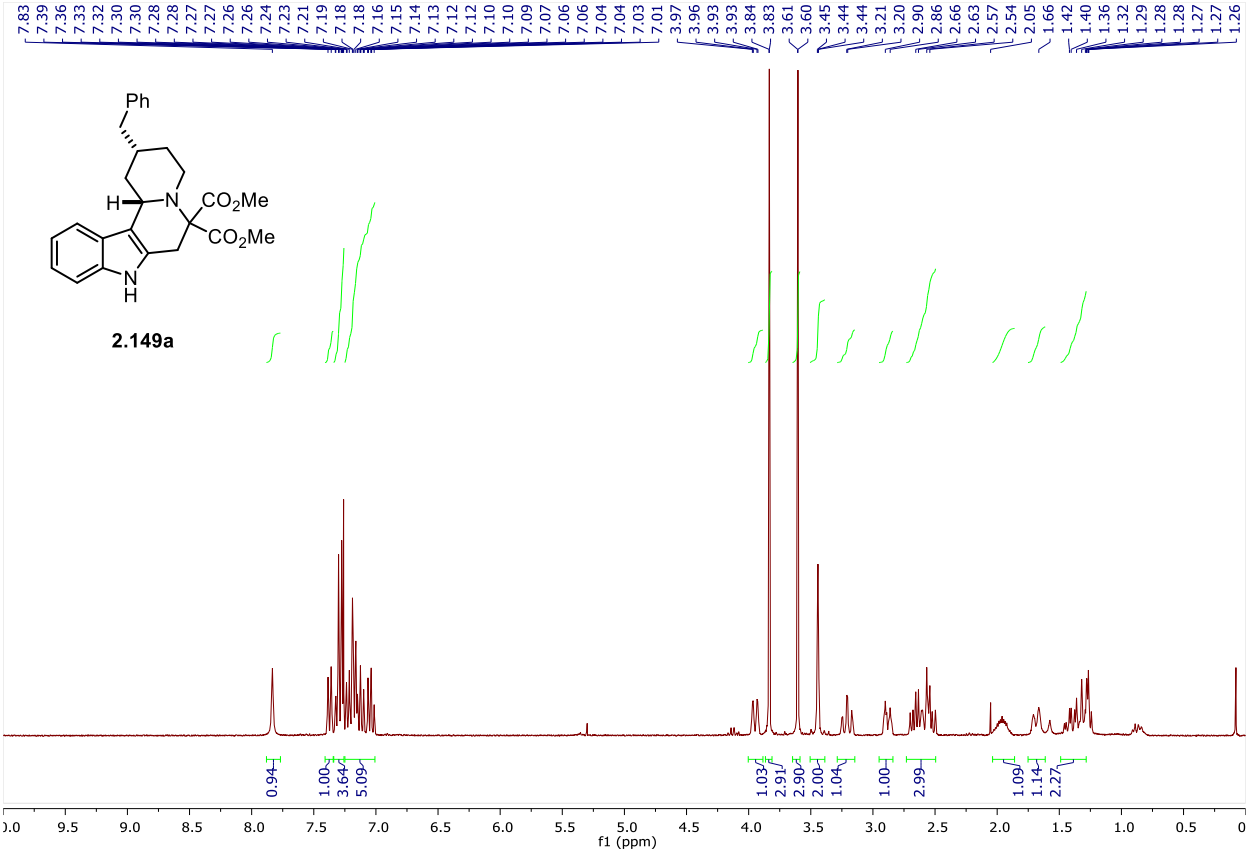

208.79
168.68
141.12 133.99 129.56 124.76 118.77 115.34
89.88
79.79
74.57
52.93 48.12 42.26
25.53
O
N
CO2Me
CO2Me
N3
2.122
f1 (ppm)

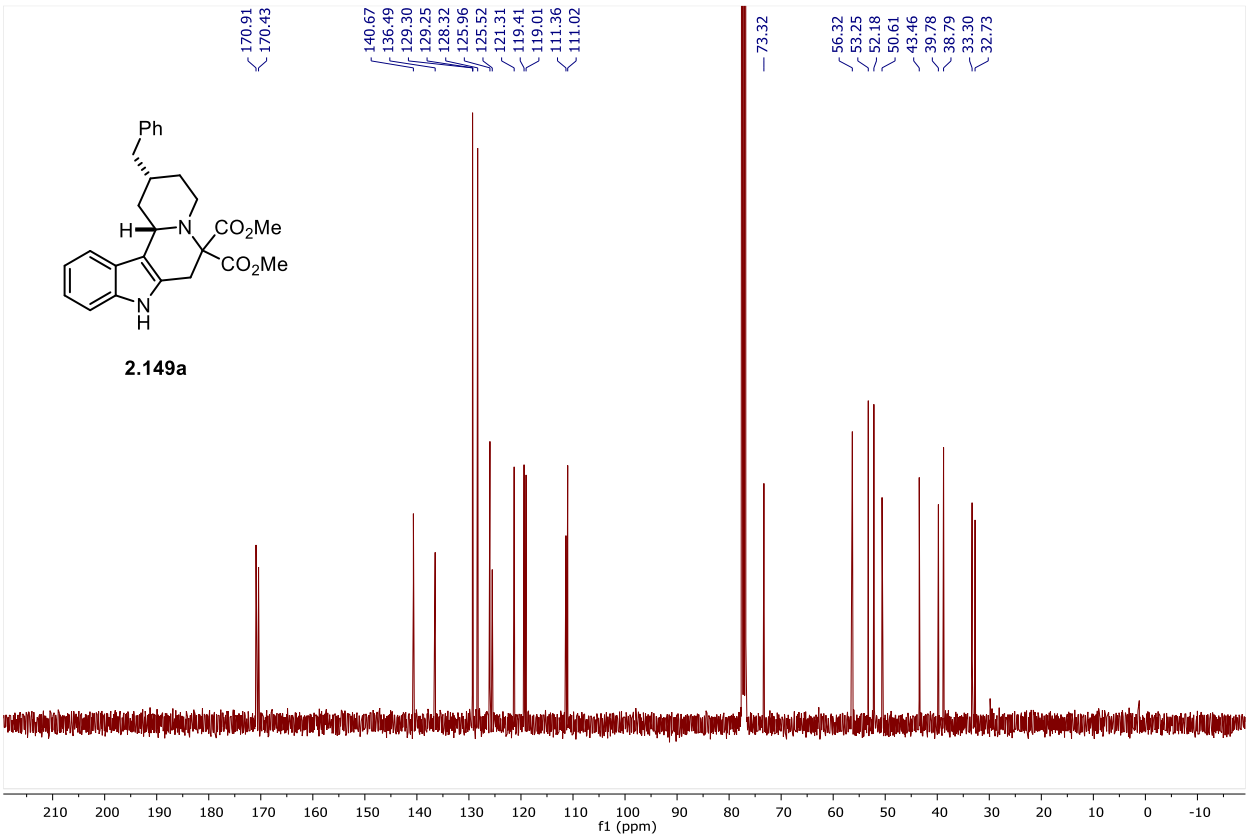

7.95 7.44 7.42 7.33 7.33 7.33 7.31 7.31 7.30 7.26 7.19 7.17 7.16 7.16 7.14 7.14 7.12 7.12 7.09 7.09 7.07 7.07 4.34 4.33 4.32 4.30 4.29 3.89 3.63 3.53 3.52 3.52 3.51 3.48 3.47 3.24 3.23 3.22 3.21 3.21 3.20 3.19 3.18 3.17 3.17 2.55 2.55 2.51 2.50 2.49 2.49 2.48 2.46
O
N
CO2Me
CO2Me
N
H
2.148
0.92 1.00 0.99 2.09 0.97 2.91 2.91 3.02 1.98 0.99 1.99
f1 (ppm)

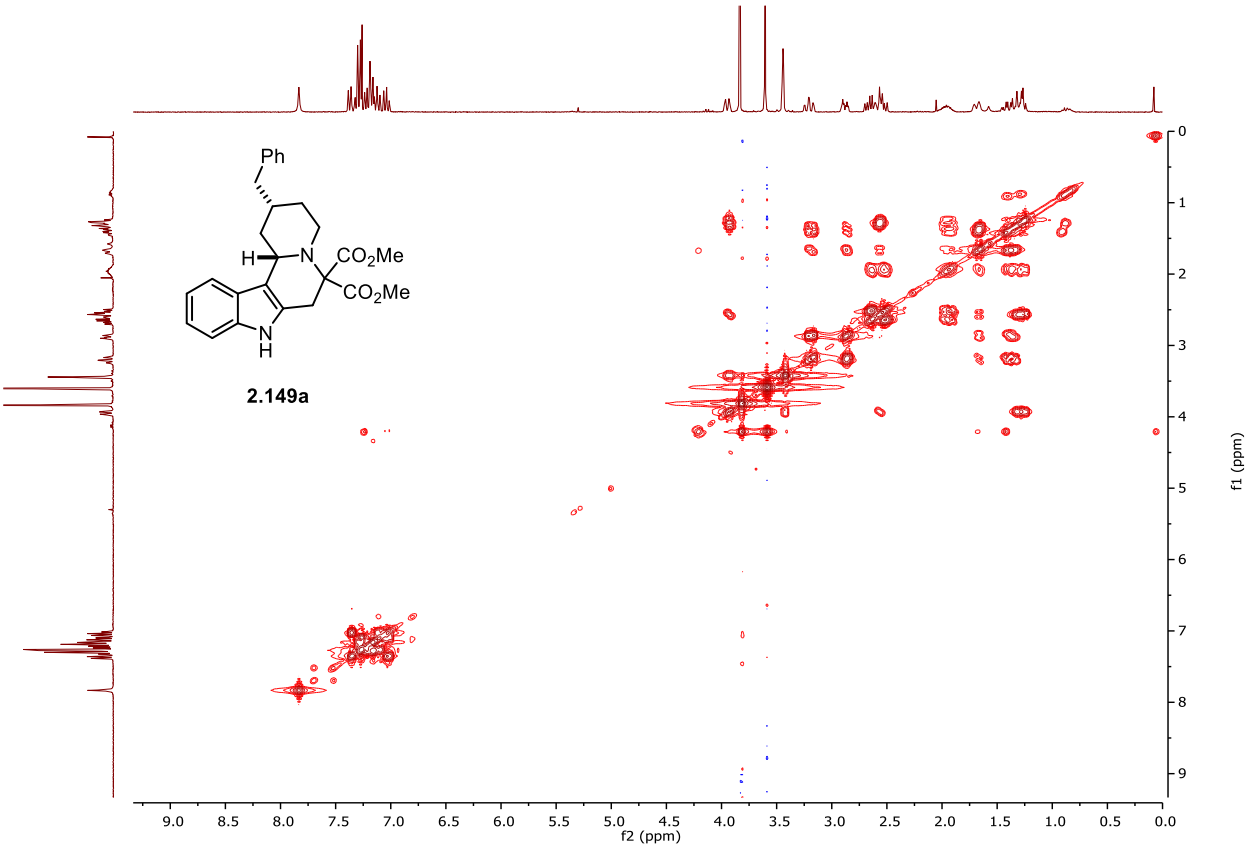

208.62 170.45 170.02 136.44 129.20 124.80 121.93 119.98 118.67 111.18 110.02 72.92 55.61 53.56 52.58 49.37 49.18 43.04 32.65
O
N
CO2Me
CO2Me
N
H
2.148
f1 (ppm)

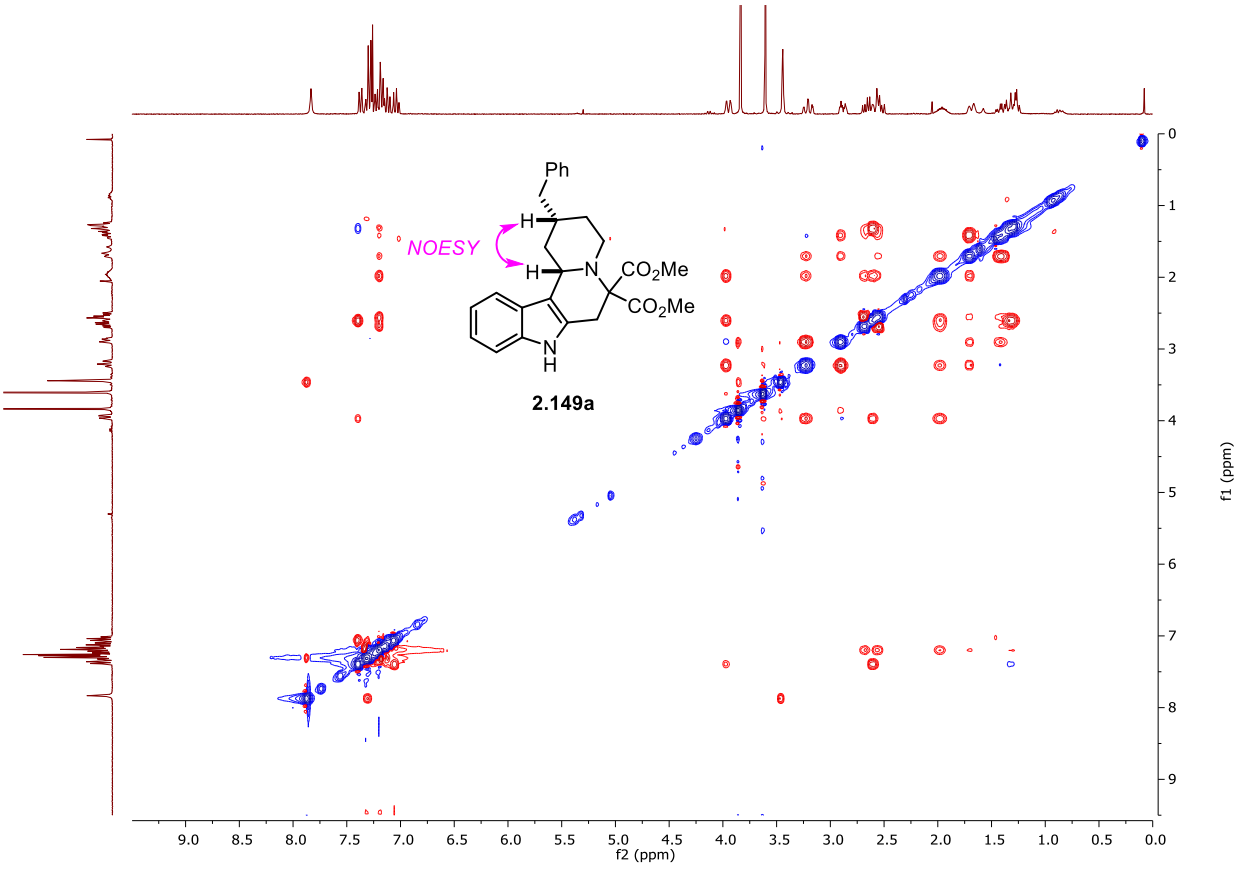

Ph
N
CO2Me
CO2Me
N3
2.123
f1 (ppm)

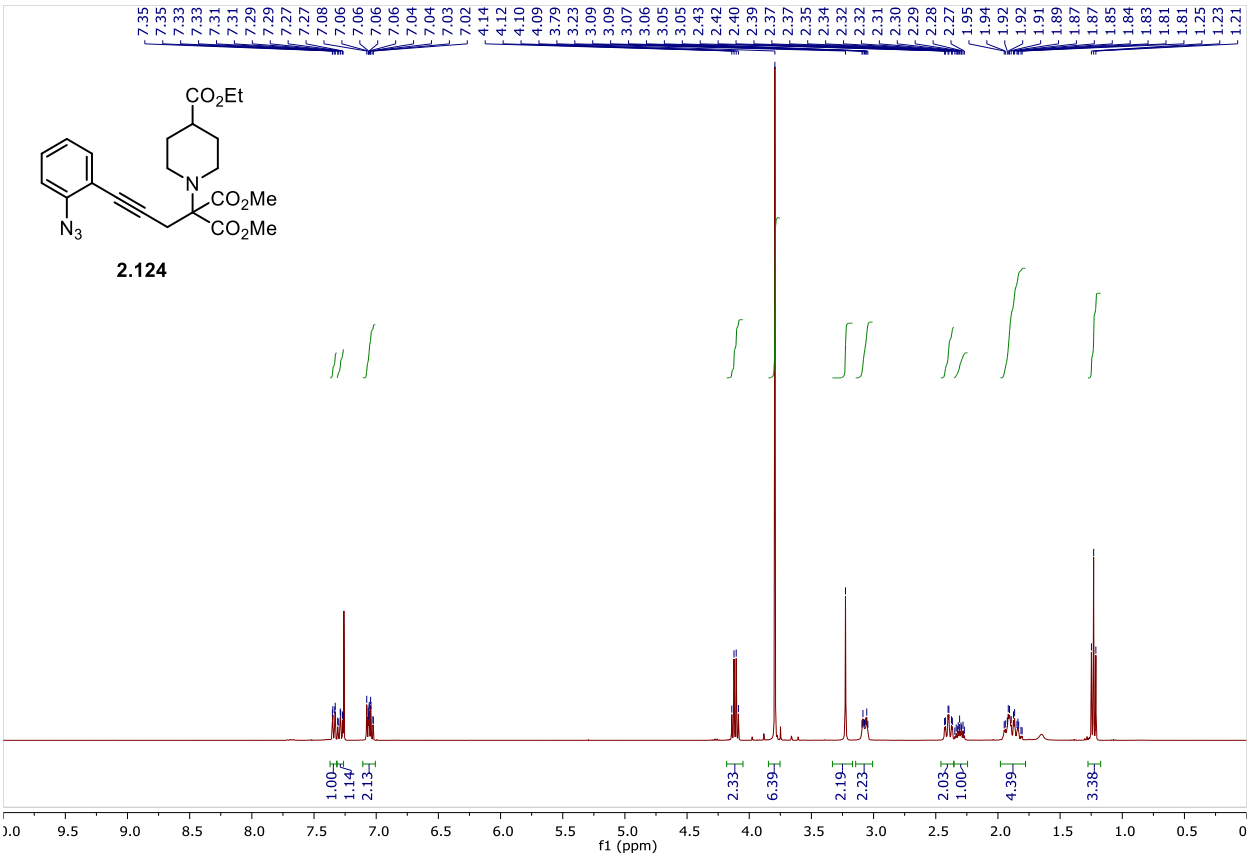

Ph
N
CO2Me
CO2Me
N3
2.123
f1 (ppm)

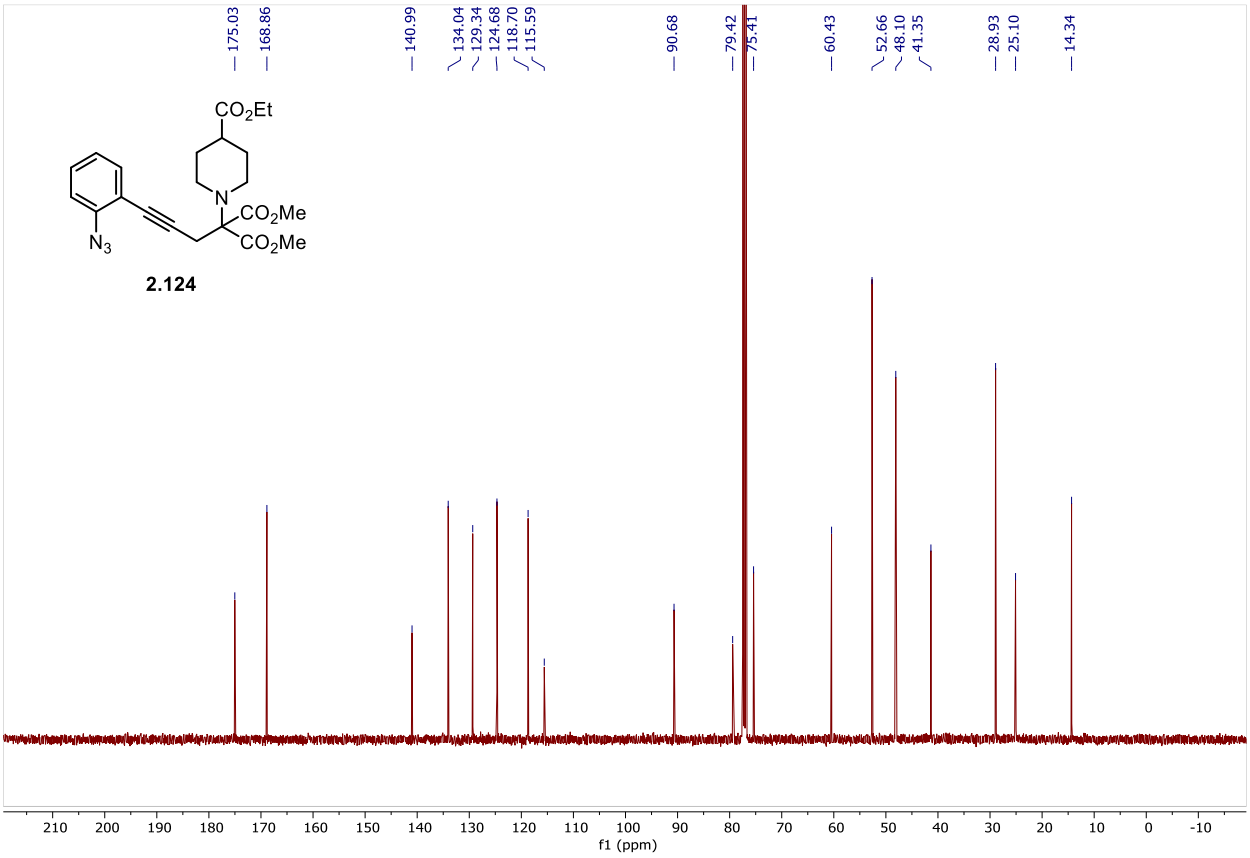

Ph
H
N
CO2Me
CO2Me
N
H
2.149a
f1 (ppm)

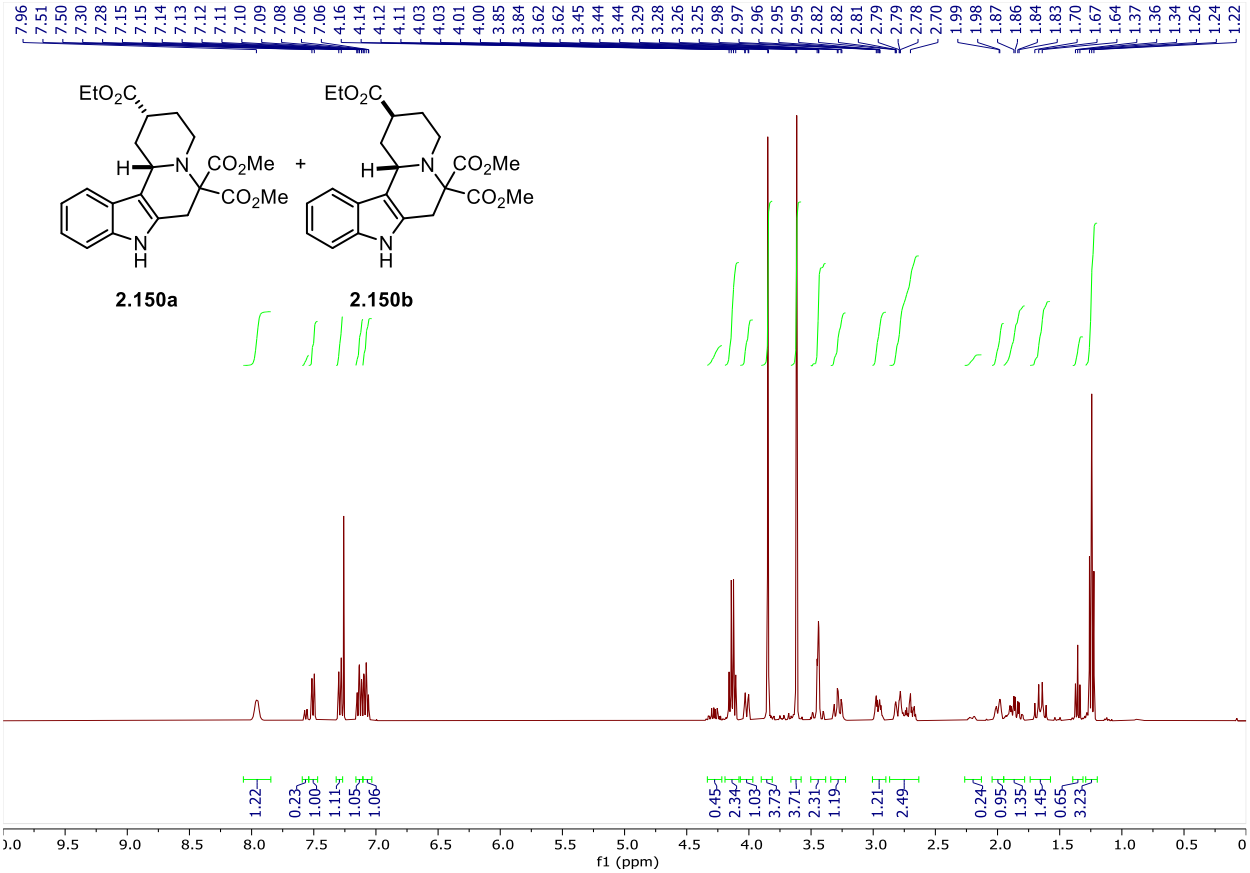

Ph
H
N
CO2Me
CO2Me
N
H
2.149a
f1 (ppm)

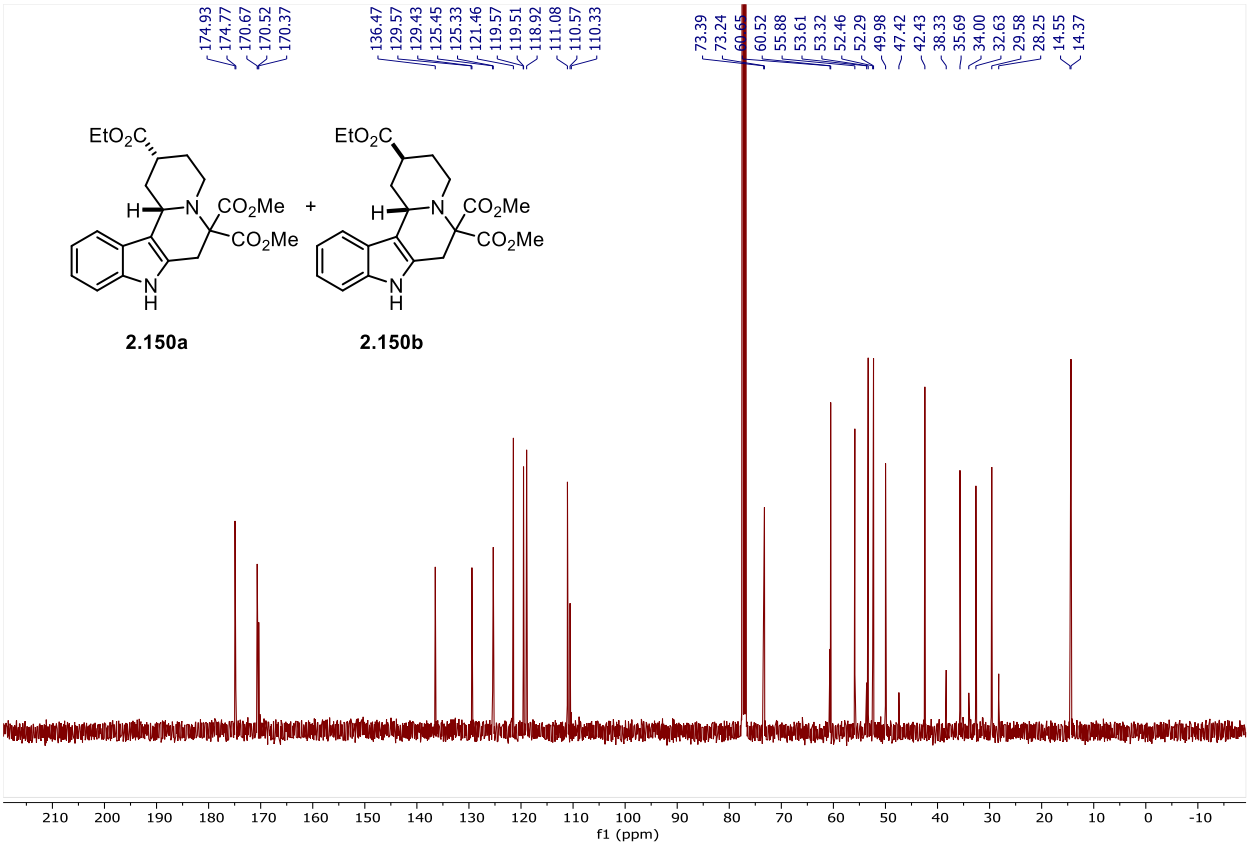

Ph
H
N
CO2Me
CO2Me
N
H
2.149a
f2 (ppm)
f1 (ppm)

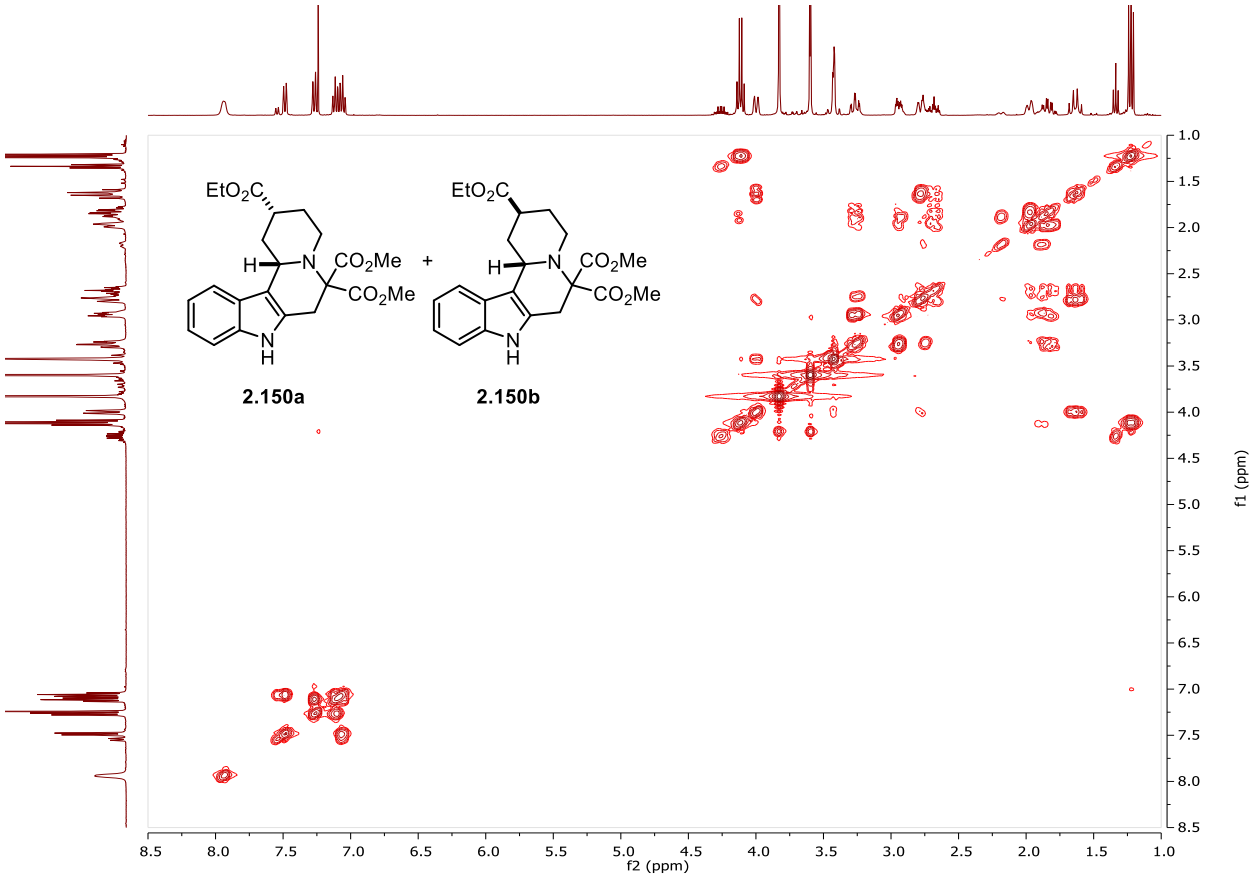

NOESY
Ph
H
H
N
CO2Me
CO2Me
N
H
2.149a
f2 (ppm)
f1 (ppm)

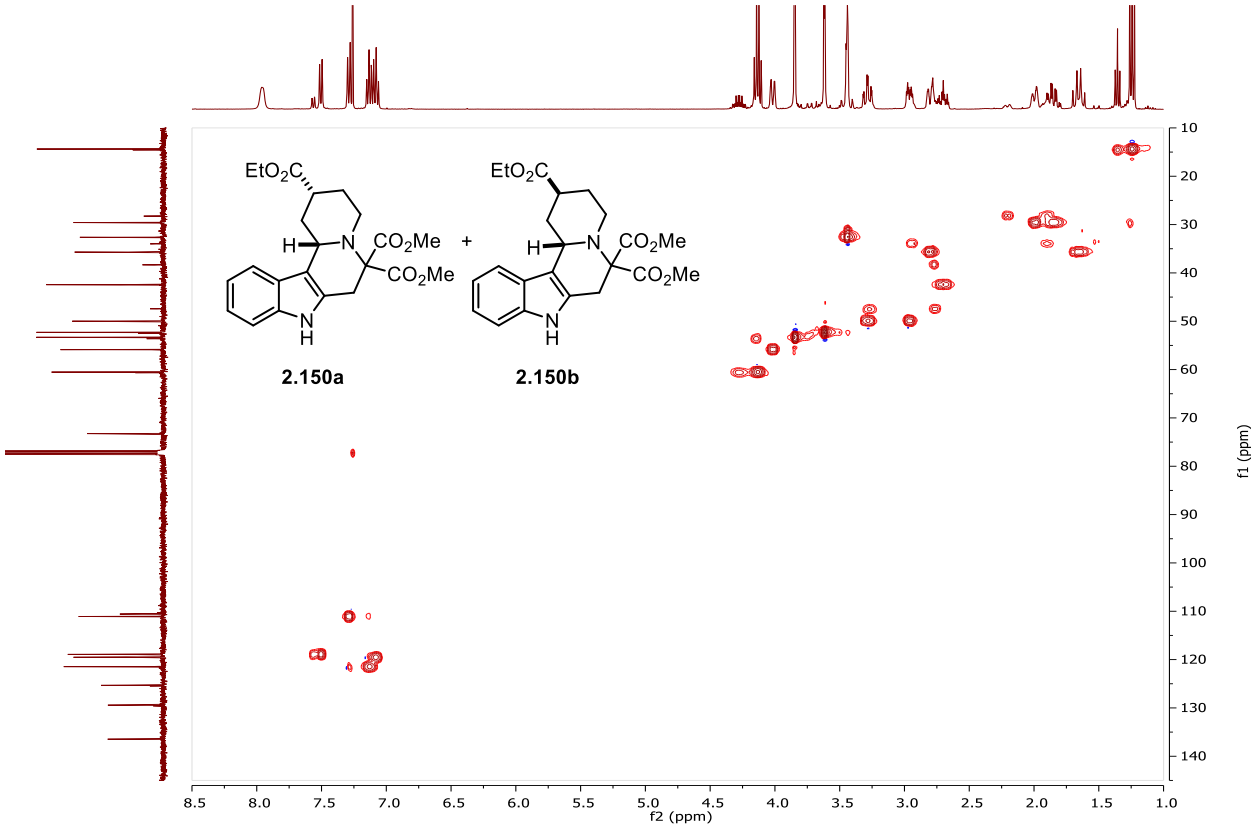

7.35 7.35 7.33 7.33 7.31 7.31 7.29 7.29 7.27 7.27 7.08 7.06 7.06 7.06 7.06 7.04 7.04 7.03 7.02 4.14 4.12 4.10 4.09 3.79 3.23 3.09 3.09 3.07 3.06 3.05 3.05 2.43 2.42 2.40 2.39 2.37 2.37 2.35 2.34 2.32 2.32 2.31 2.30 2.29 2.28 2.27 1.95 1.94 1.92 1.92 1.91 1.89 1.87 1.87 1.85 1.84 1.83 1.81 1.81 1.25 1.23 1.21
CO2Et
N
CO2Me
CO2Me
N3
2.124
1.00 1.14 2.13 2.33 6.39 2.19 2.23 2.03 1.00 4.39 3.38
f1 (ppm)

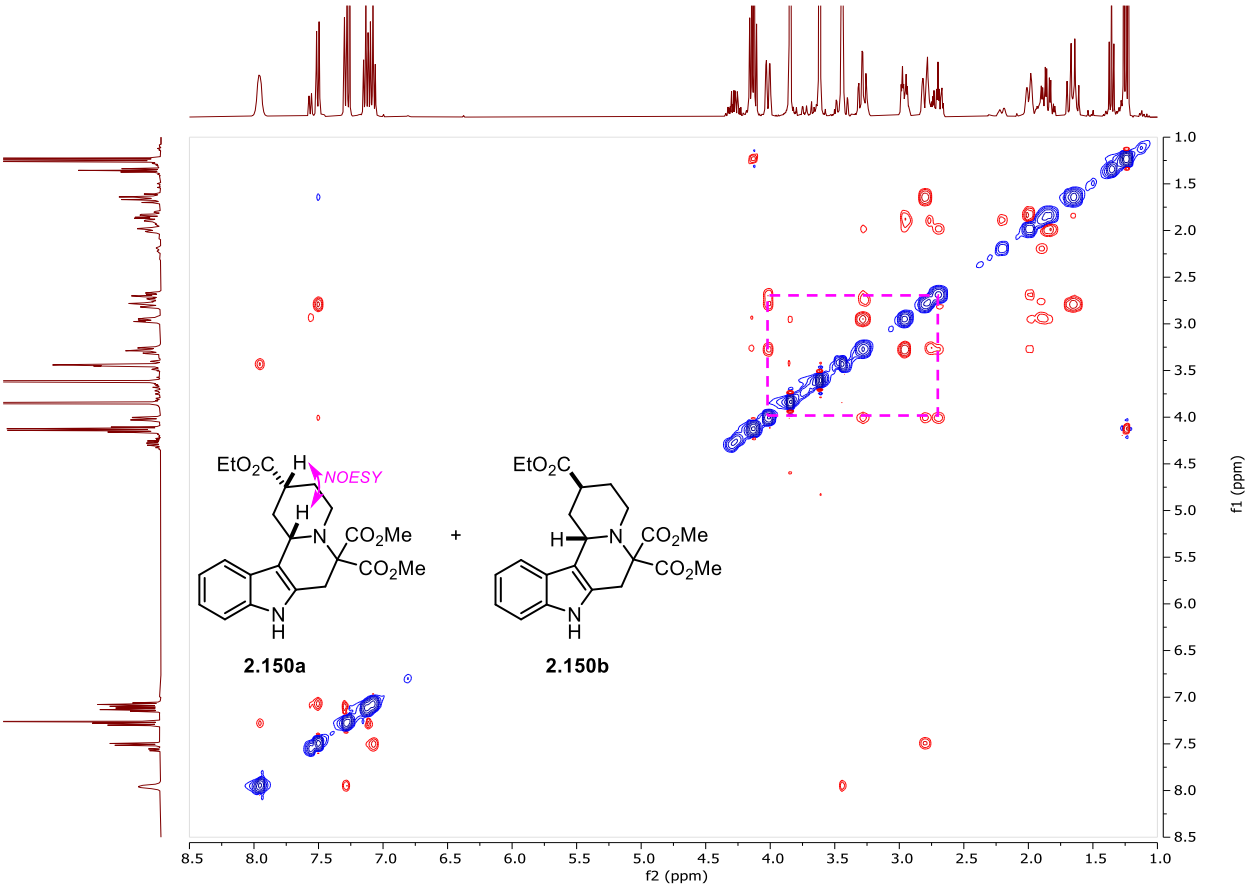

175.03 168.86 140.99 134.04 129.34 124.68 118.70 115.59 90.68 79.42 75.41 60.43 52.66 48.10 41.35 28.93 25.10 14.34
CO2Et
N
CO2Me
CO2Me
N3
2.124
f1 (ppm)

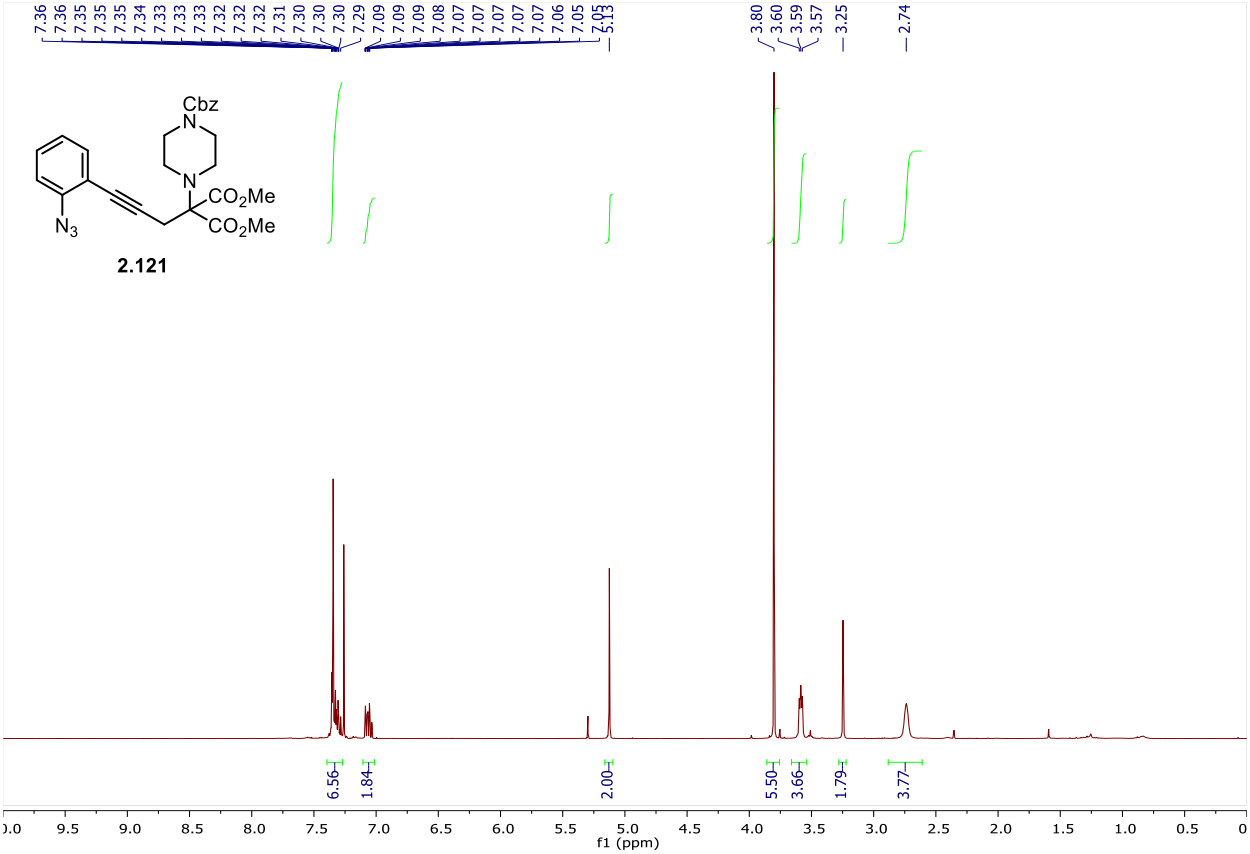

EtO2C
H
N
CO2Me
CO2Me
N
H
+
EtO2C
H
N
CO2Me
CO2Me
N
H
2.150a
2.150b
f1 (ppm)

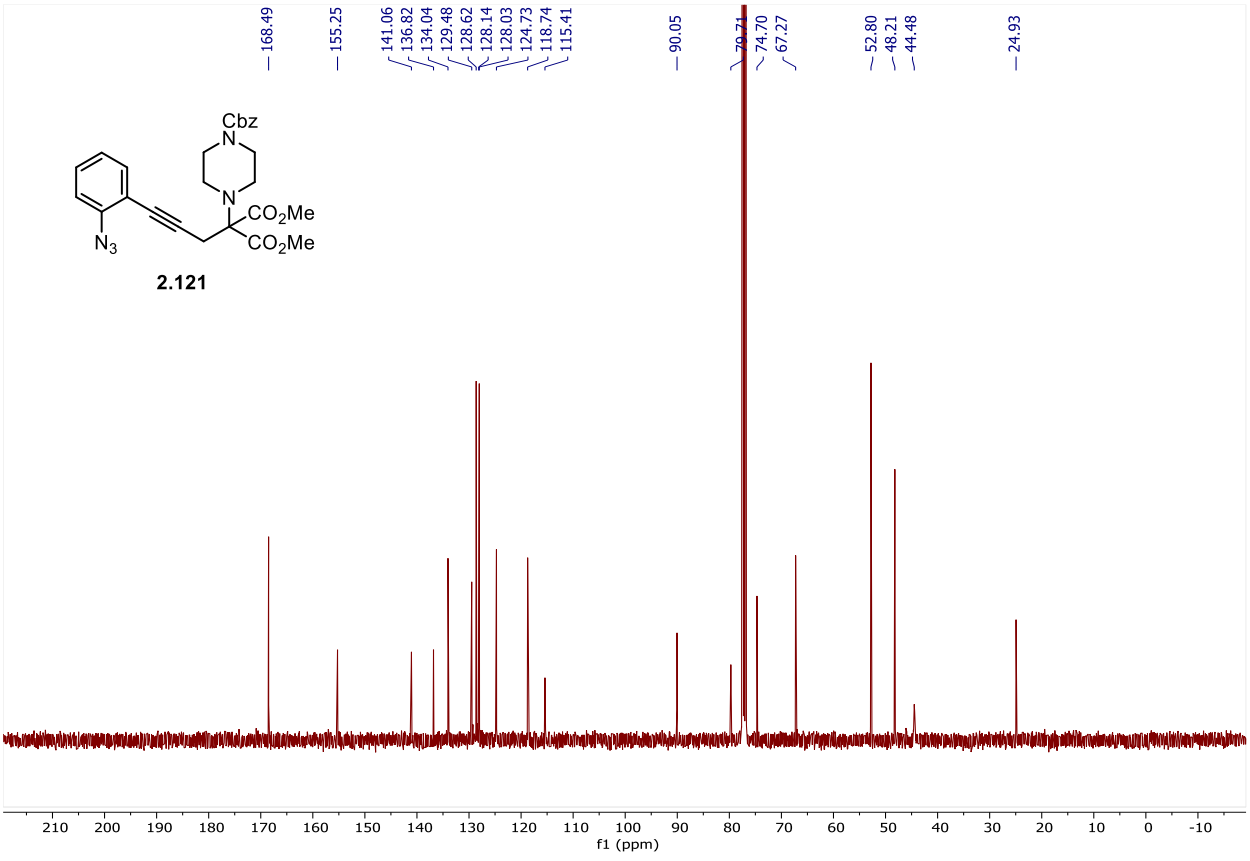

EtO2C
H
N
CO2Me
CO2Me
N
H
+
EtO2C
H
N
CO2Me
CO2Me
N
H
2.150a
2.150b
f1 (ppm)

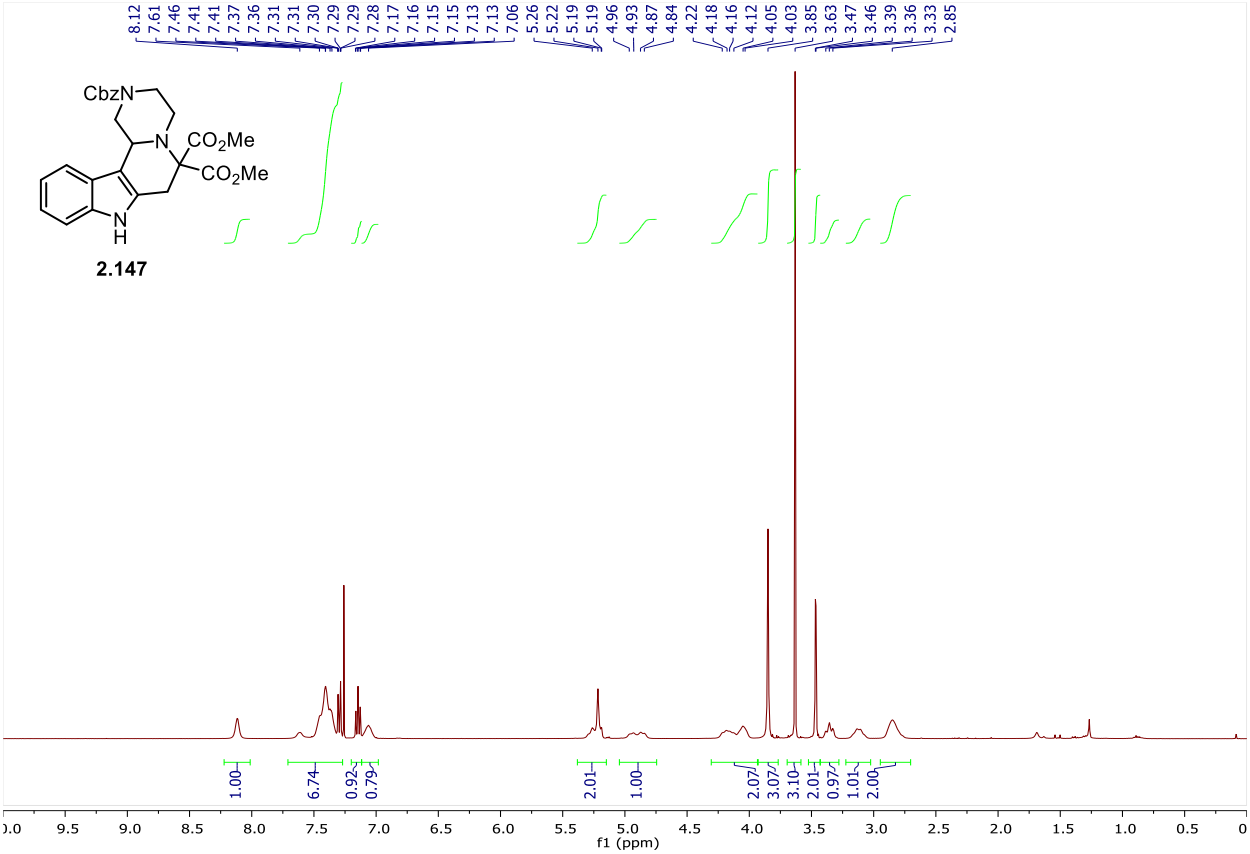

EtO2C
H
N
CO2Me
CO2Me
N
H
+
2.150a
2.150b
f2 (ppm)
f1 (ppm)

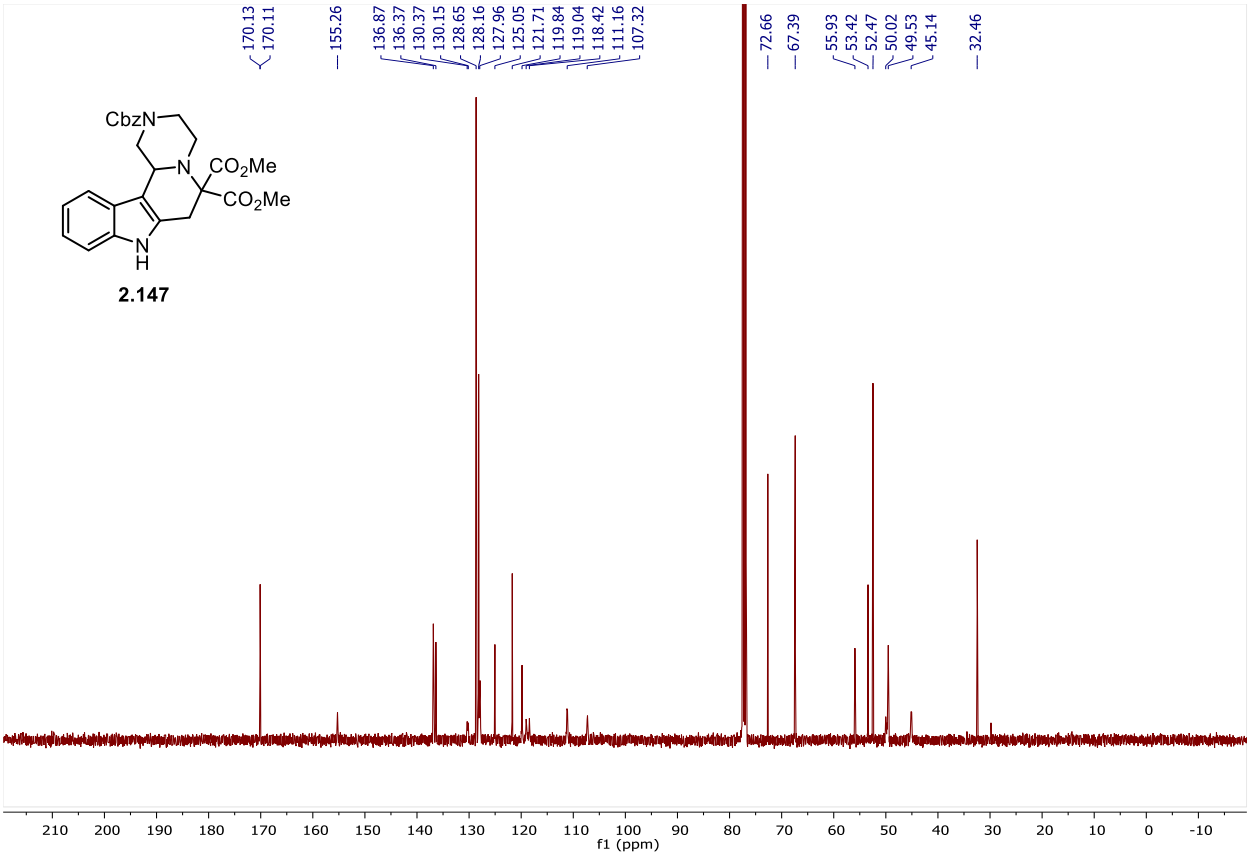

EtO2C
H
N
CO2Me
CO2Me
N
H
+
2.150a
2.150b
f2 (ppm)
f1 (ppm)

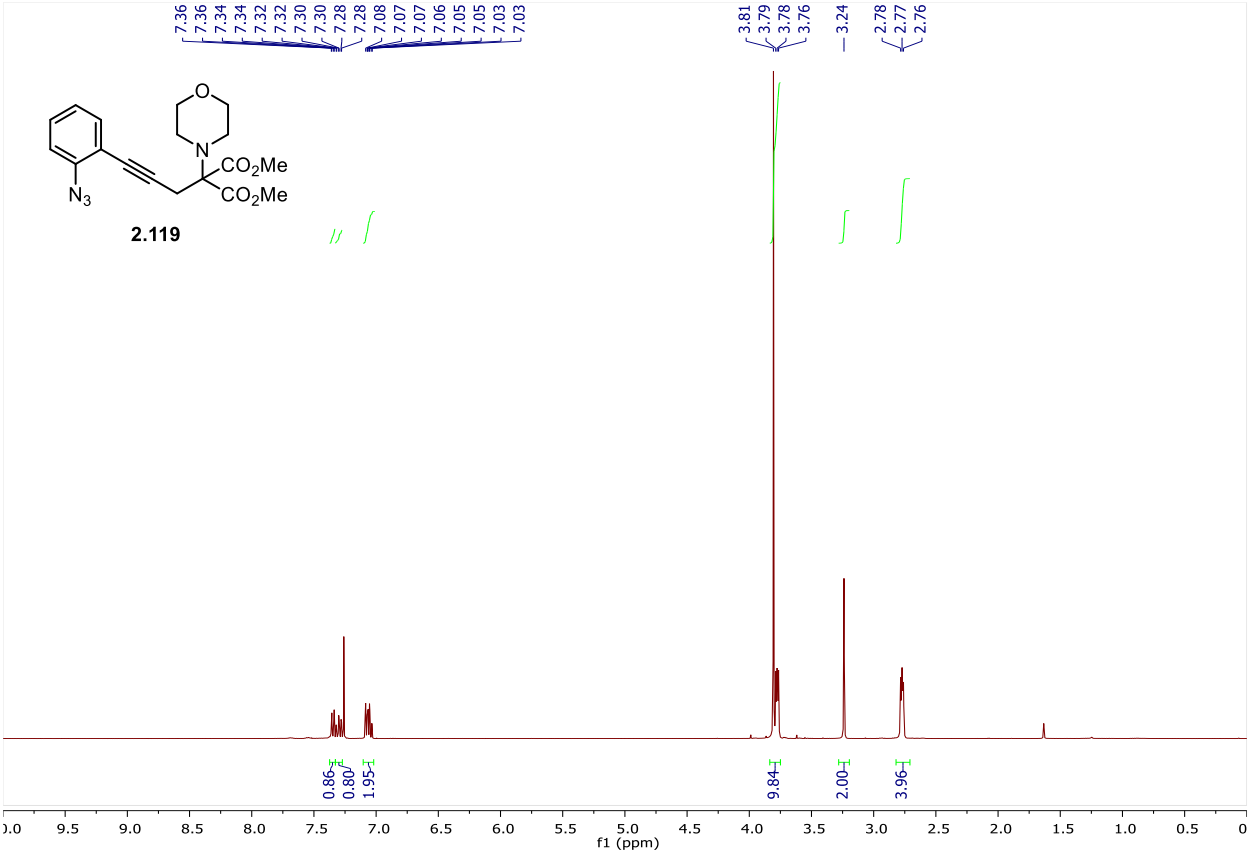

NOESY
EtO2C
H
CO2Me
CO2Me
N
H
+
2.150a
2.150b
f2 (ppm)
f1 (ppm)

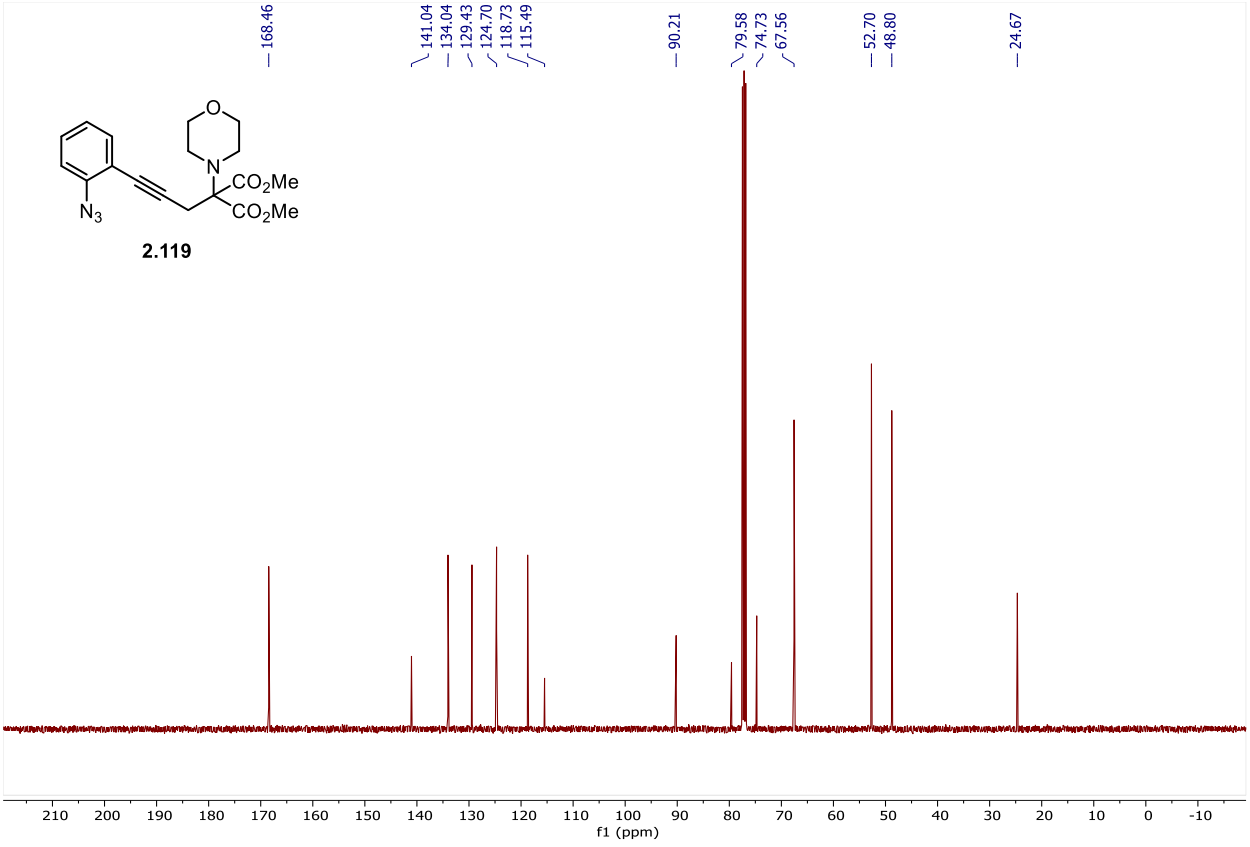

Cbz
N
N
CO2Me
CO2Me
N3
2.121
7.36
7.36
7.35
7.35
7.35
7.34
7.33
7.33
7.33
7.32
7.32
7.32
7.31
7.30
7.30
7.30
7.29
7.09
7.09
7.09
7.08
7.07
7.07
7.07
7.07
7.07
7.06
7.05
7.03
5.13
3.80
3.60
3.59
3.57
3.25
2.74
6.56
1.84
2.00
5.50
3.66
1.79
3.77
f1 (ppm)

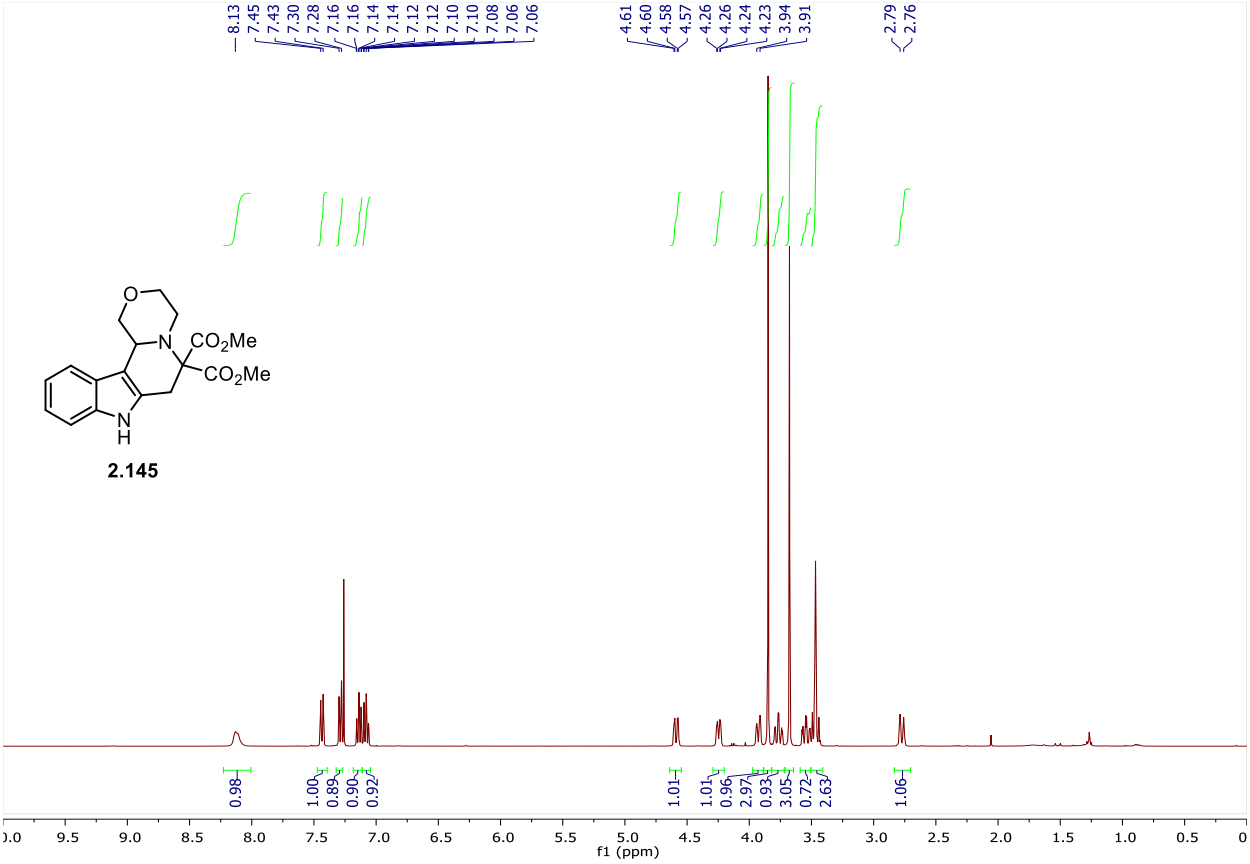

Cbz
N
N
CO2Me
CO2Me
N3
2.121
168.49
155.25
141.06
136.82
134.04
129.48
128.62
128.14
128.03
124.73
118.74
115.41
90.05
79.71
74.70
67.27
52.80
48.21
44.48
24.93
f1 (ppm)

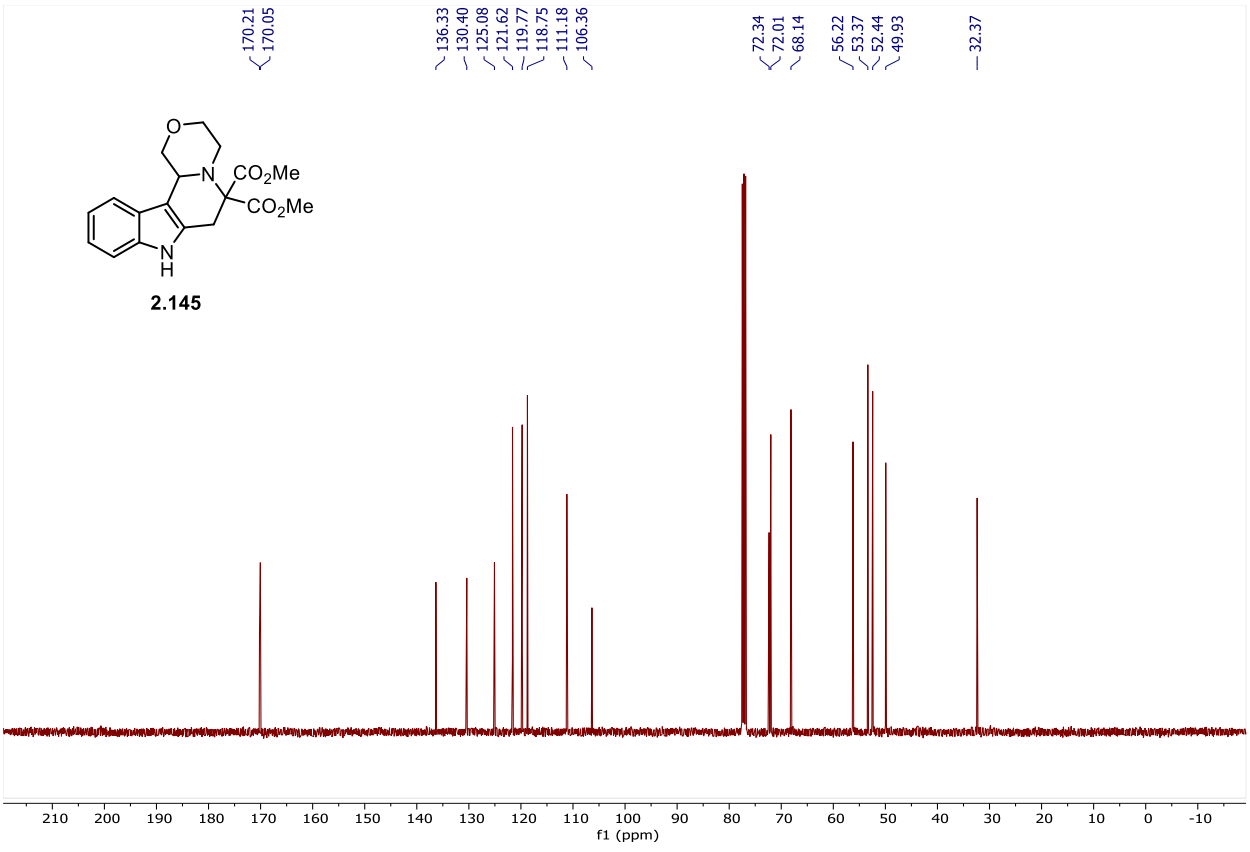

8.12 7.61 7.46 7.41 7.41 7.37 7.36 7.31 7.31 7.30 7.29 7.29 7.28 7.17 7.16 7.15 7.15 7.13 7.13 7.06 5.26 5.22 5.19 5.19 4.96 4.93 4.87 4.84 4.22 4.18 4.16 4.12 4.05 4.03 3.85 3.63 3.47 3.46 3.39 3.36 3.33 2.85
CbzN
N
CO2Me
CO2Me
N
H
2.147
1.00 6.74 0.92 0.79 2.01 1.00 2.07 3.07 3.10 2.01 0.97 1.01 2.00
f1 (ppm)

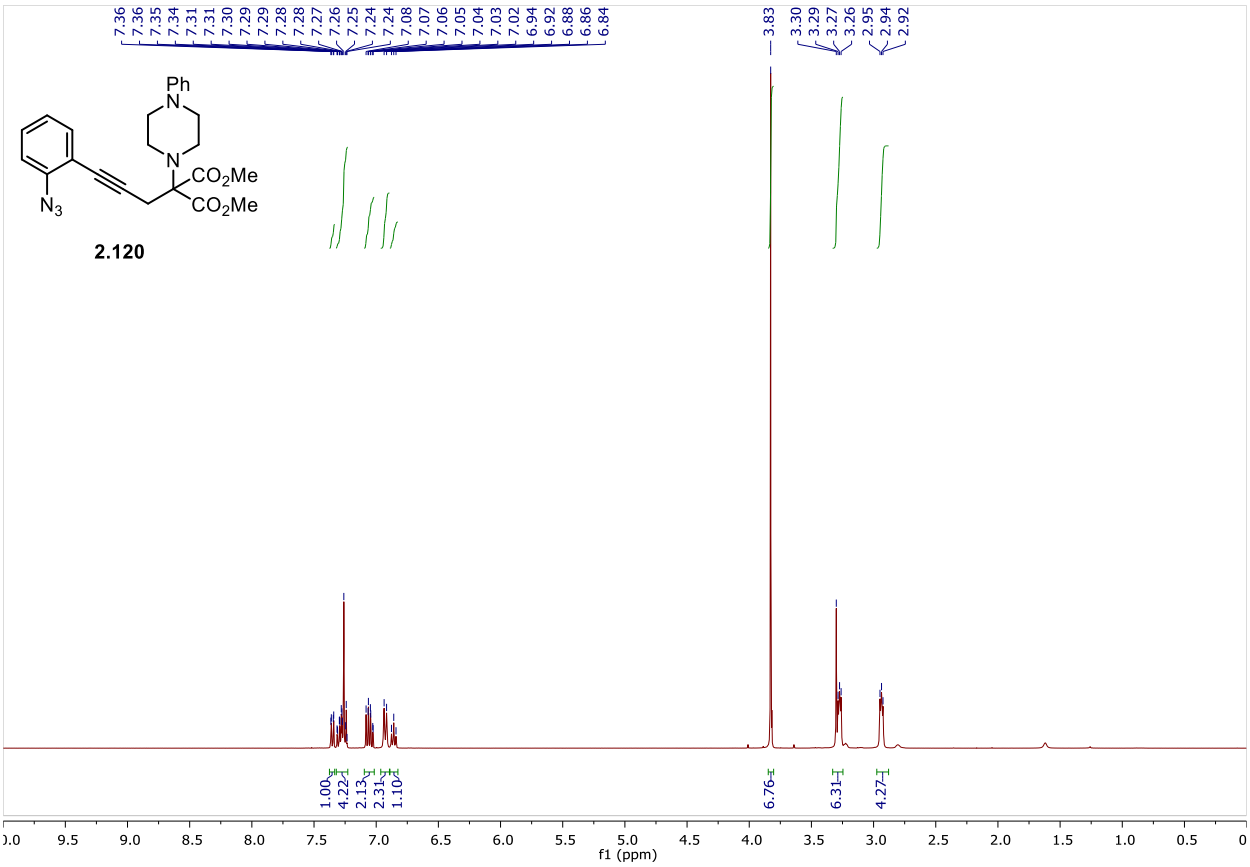

170.13 170.11 155.26 136.87 136.37 130.37 130.15 128.65 128.16 127.96 125.05 121.71 119.84 119.04 118.42 111.16 107.32 72.66 67.39 55.93 53.42 52.47 50.02 49.53 45.14 32.46
CbzN
N
CO2Me
CO2Me
N
H
2.147
f1 (ppm)

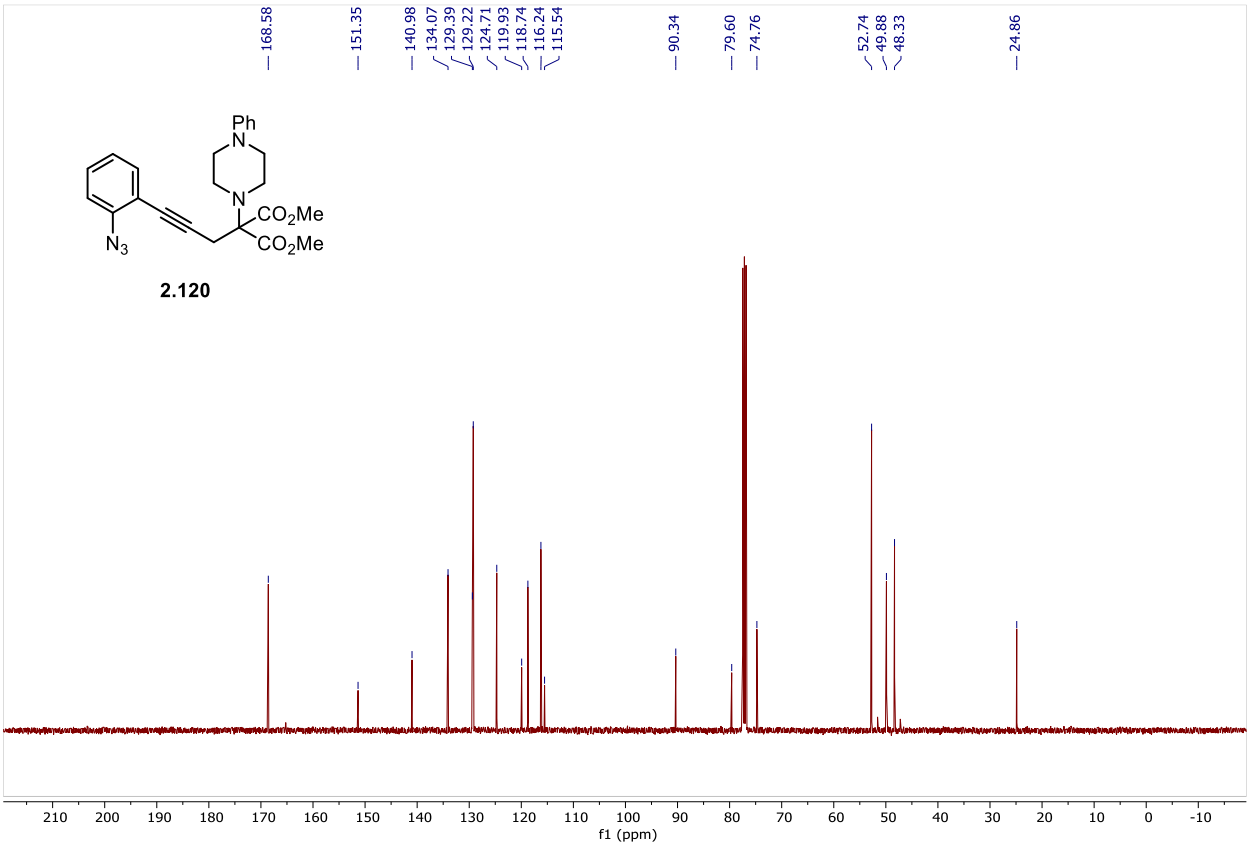

7.36
7.36
7.34
7.34
7.32
7.32
7.30
7.30
7.28
7.28
7.08
7.07
7.07
7.06
7.05
7.05
7.03
7.03
3.81
3.79
3.78
3.76
3.24
2.78
2.77
2.76
O
N
CO2Me
CO2Me
N3
2.119
0.86
0.80
1.95
9.84
2.00
3.96
f1 (ppm)

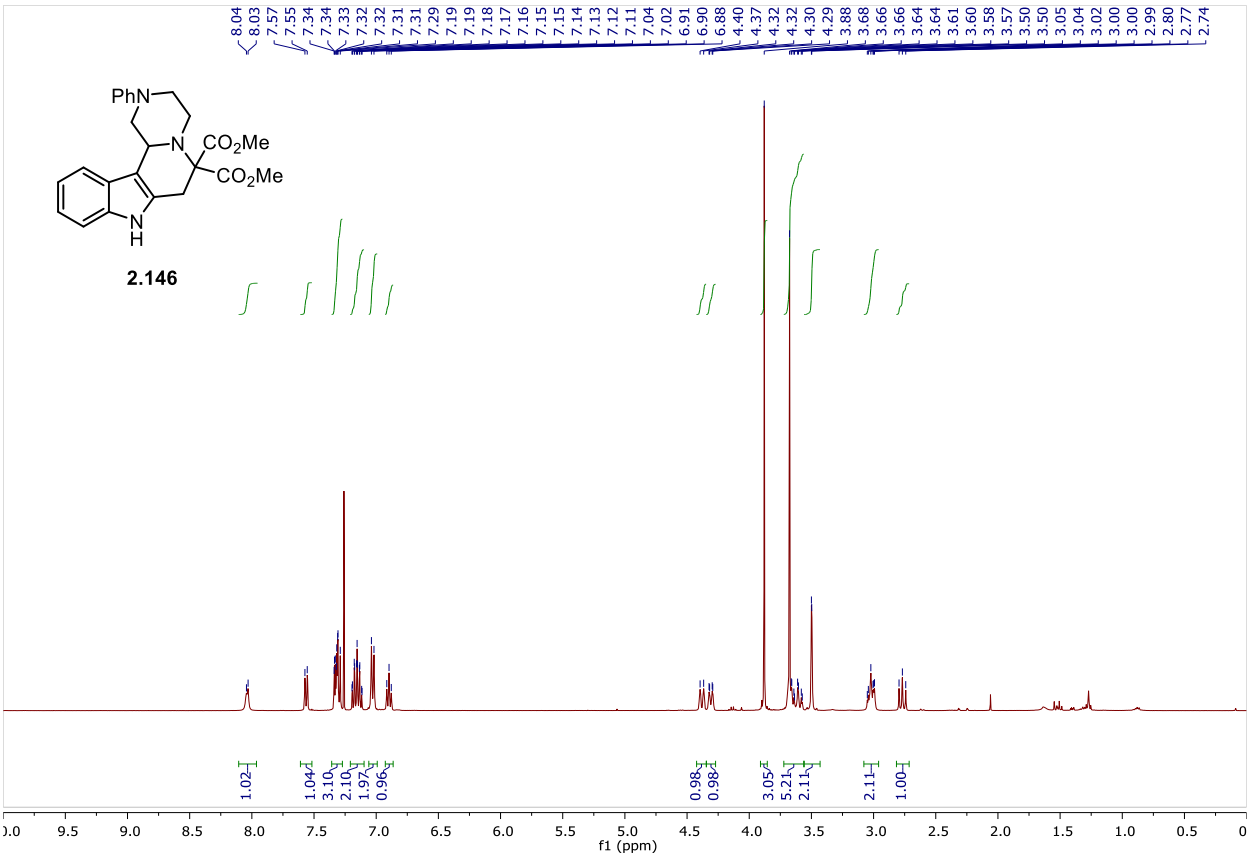

168.46
141.04
134.04
129.43
124.70
118.73
115.49
90.21
79.58
74.73
67.56
52.70
48.80
24.67
O
N
CO2Me
CO2Me
N3
2.119
f1 (ppm)

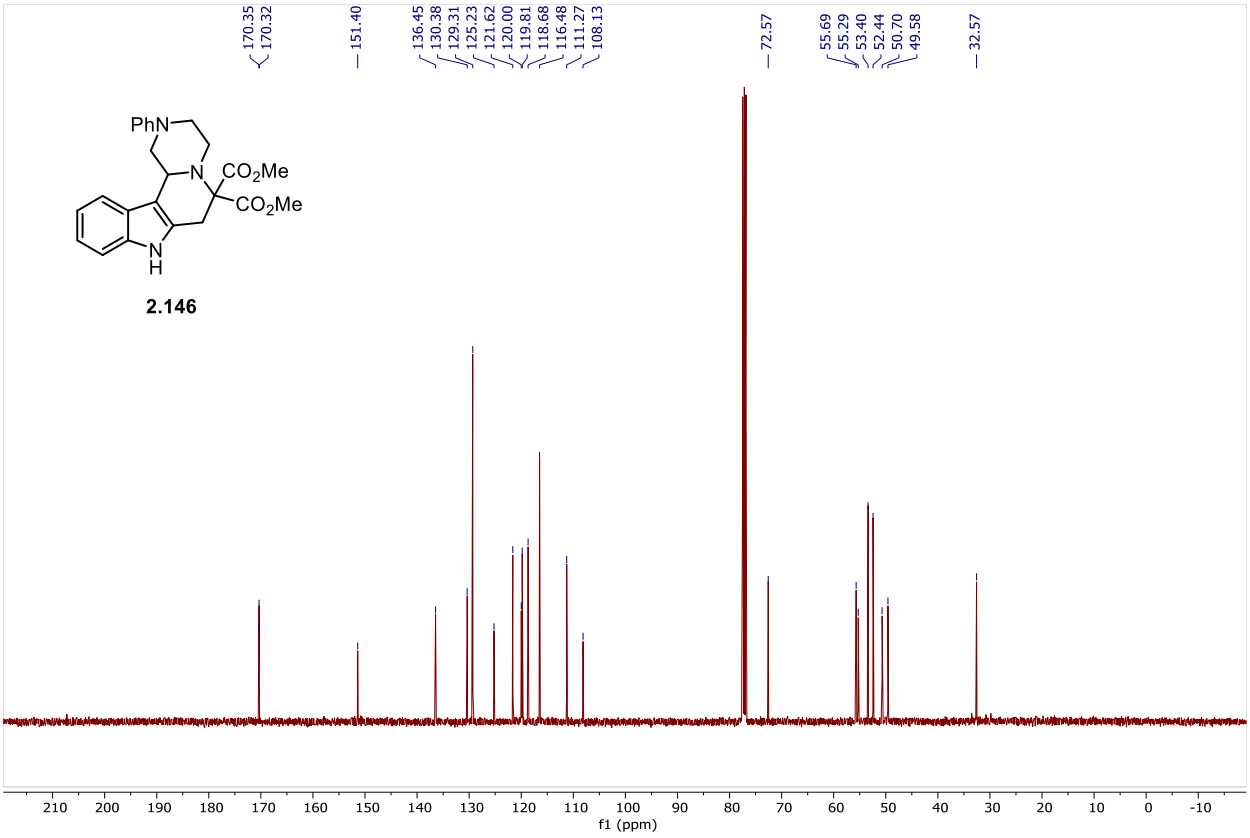

8.13
7.45
7.43
7.30
7.28
7.16
7.16
7.14
7.14
7.14
7.12
7.12
7.10
7.10
7.08
7.06
7.06
4.61
4.60
4.58
4.57
4.26
4.26
4.24
4.23
3.94
3.91
2.79
2.76
O
N
CO2Me
CO2Me
N
H
2.145
0.98
1.00
0.89
0.90
0.92
1.01
1.01
0.96
2.97
0.93
3.05
0.72
2.63
1.06
f1 (ppm)

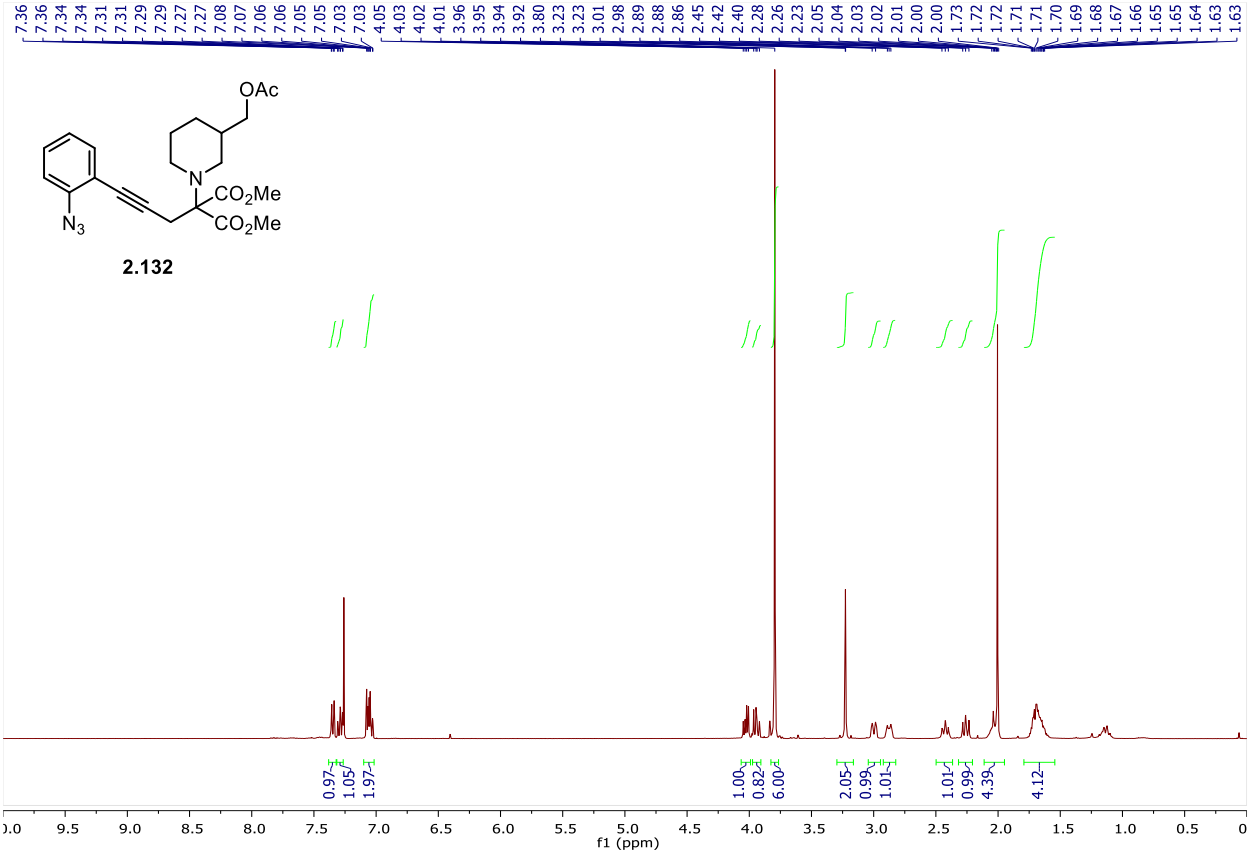

170.21
170.05
136.33
130.40
125.08
121.62
119.77
118.75
111.18
106.36
72.34
72.01
68.14
56.22
53.37
52.44
49.93
32.37
O
N
CO2Me
CO2Me
N
H
2.145
f1 (ppm)

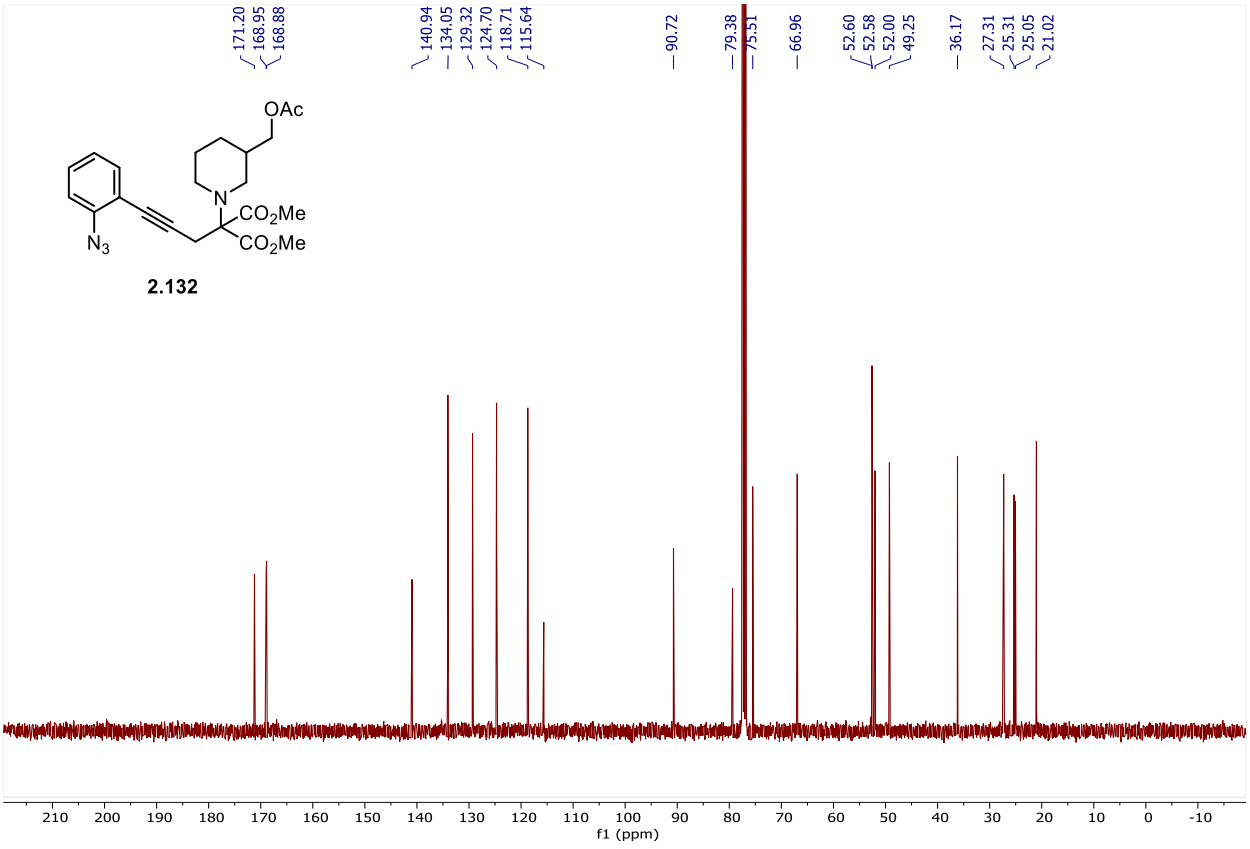

7.36
7.36
7.35
7.34
7.31
7.31
7.30
7.29
7.29
7.28
7.28
7.27
7.26
7.25
7.24
7.24
7.08
7.07
7.06
7.05
7.04
7.03
7.02
6.94
6.92
6.88
6.86
6.84
3.83
3.30
3.29
3.27
3.26
2.95
2.94
2.92
Ph
N
N
CO2Me
CO2Me
N3
2.120
1.00
4.22
2.13
2.31
1.10
6.76
6.31
4.27
f1 (ppm)

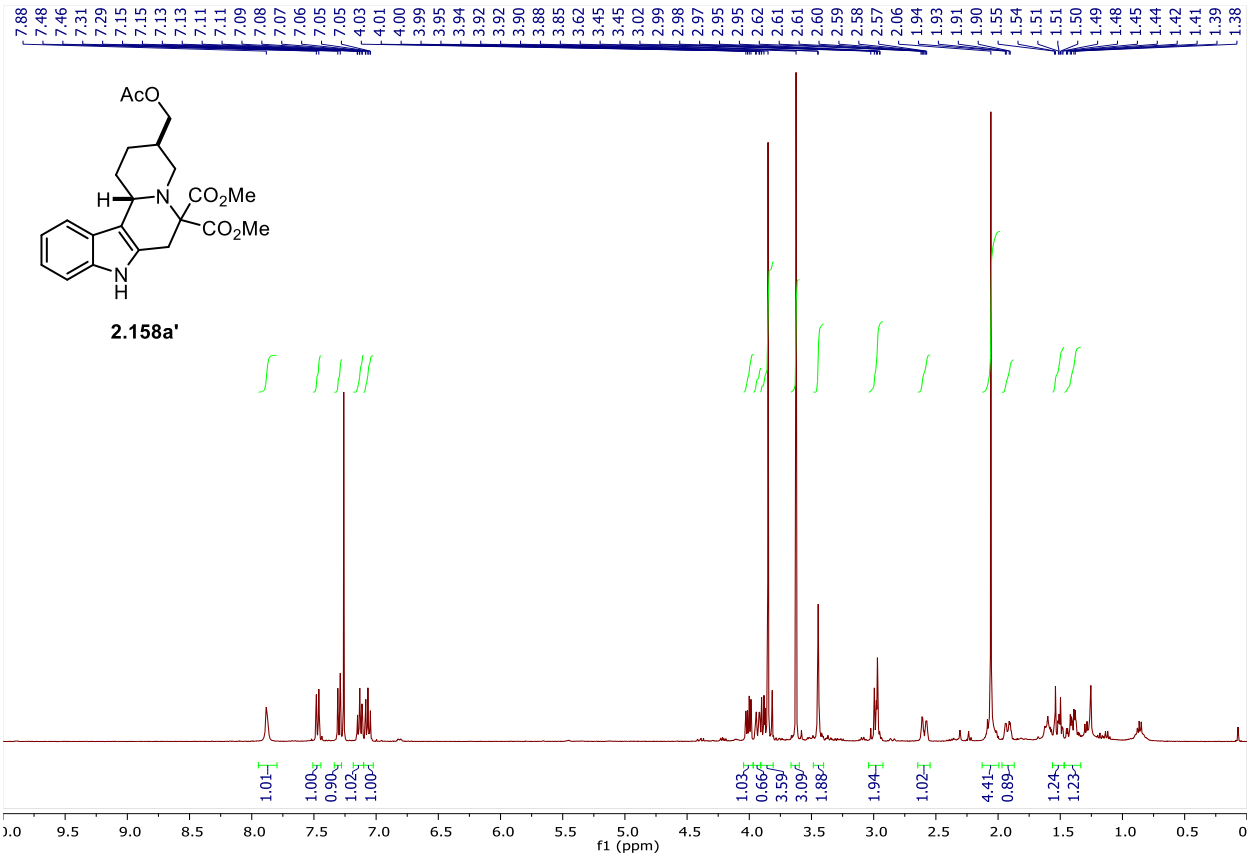

168.58
151.35
140.98
134.07
129.39
129.22
124.71
119.93
118.74
116.24
115.54
90.34
79.60
74.76
52.74
49.88
48.33
24.86
Ph
N
N
CO2Me
CO2Me
N3
2.120
f1 (ppm)

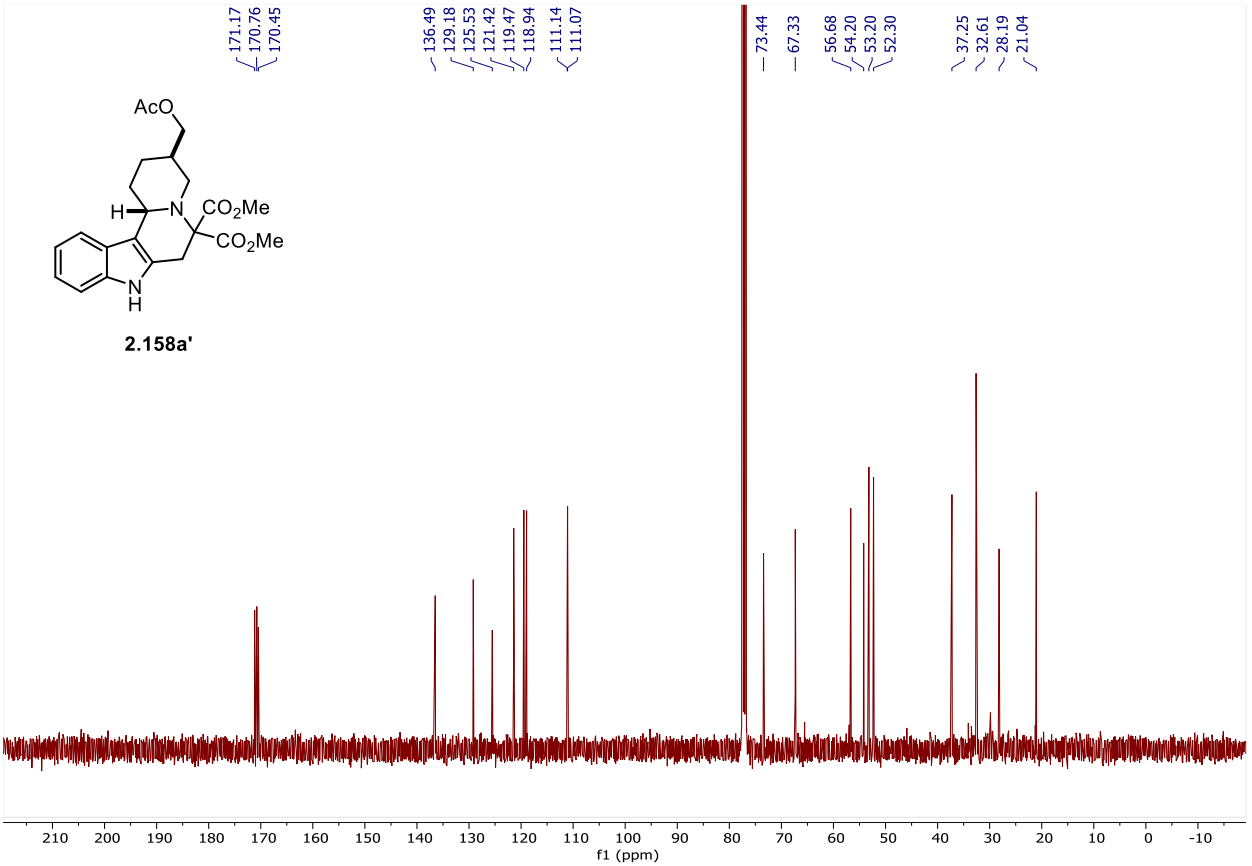

PhN
N
CO2Me
CO2Me
N
H
2.146
f1 (ppm)

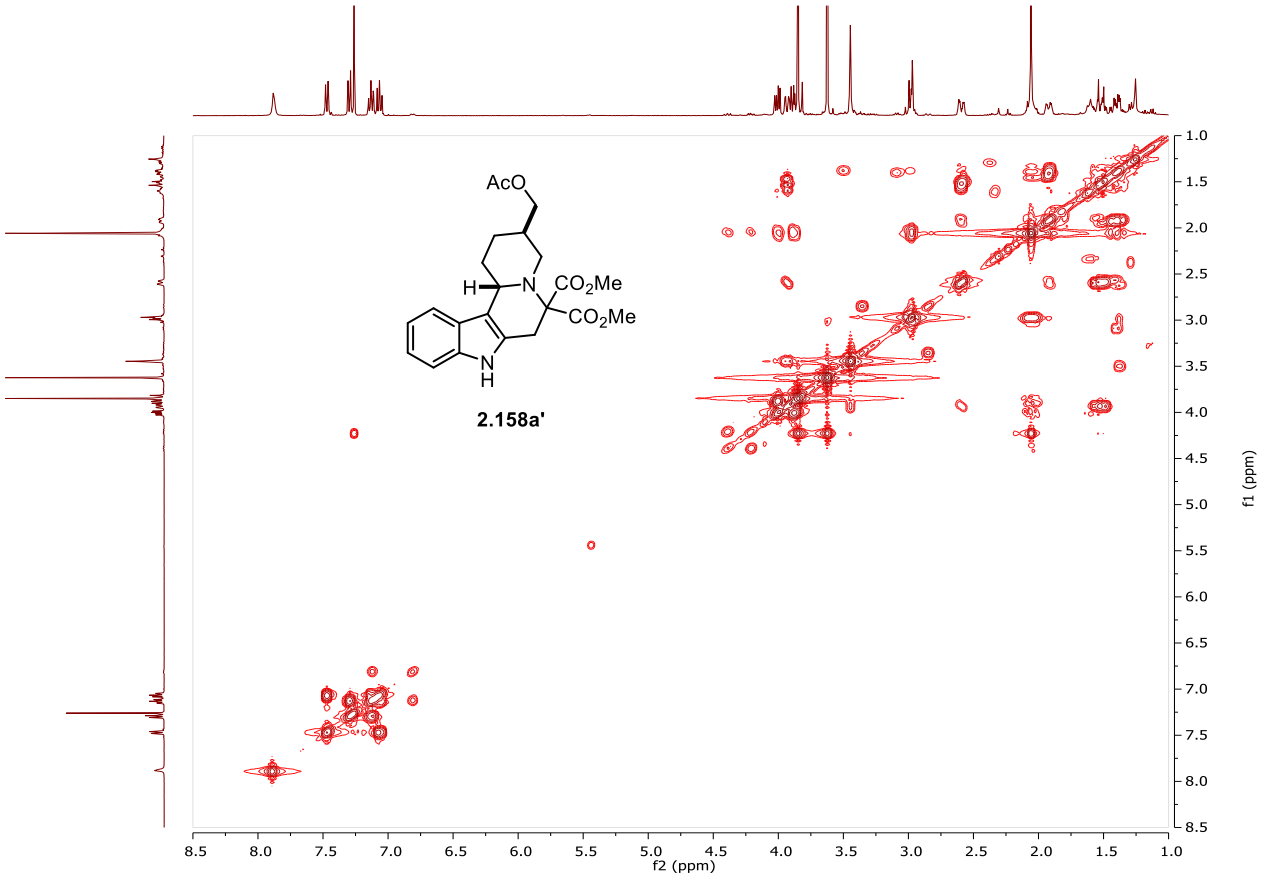

PhN
N
CO2Me
CO2Me
N
H
2.146
f1 (ppm)

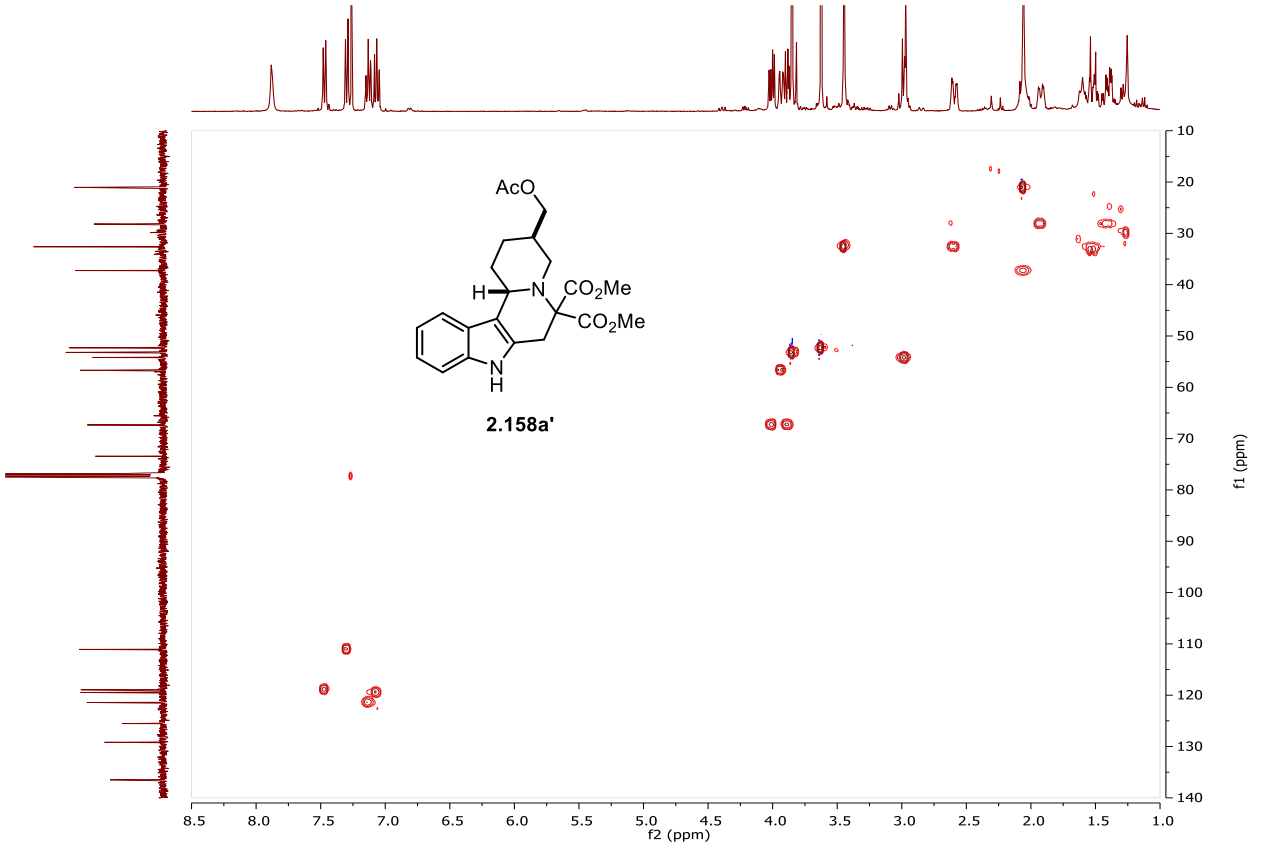

OAc
N
CO2Me
CO2Me
N3
2.132
f1 (ppm)

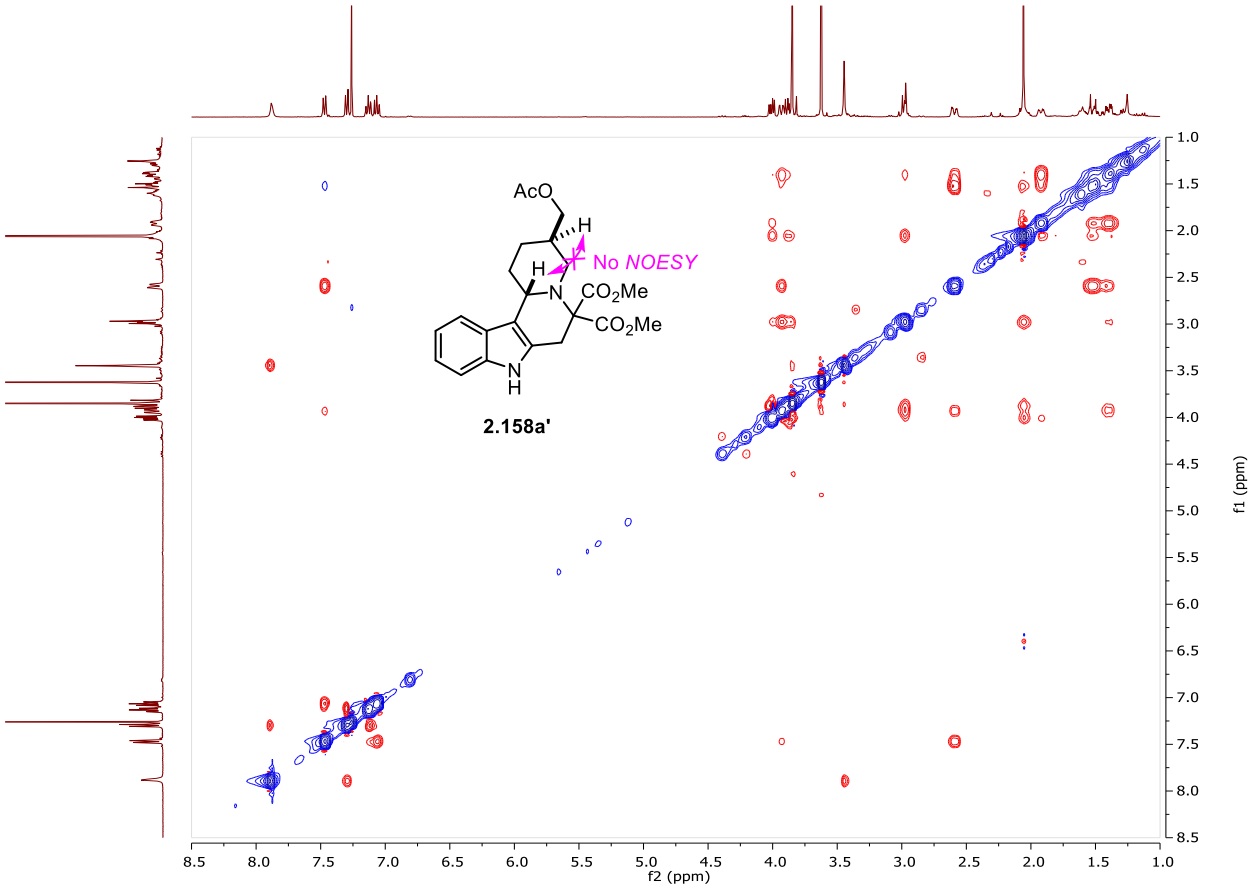

OAc
N
CO2Me
CO2Me
N3
2.132
f1 (ppm)

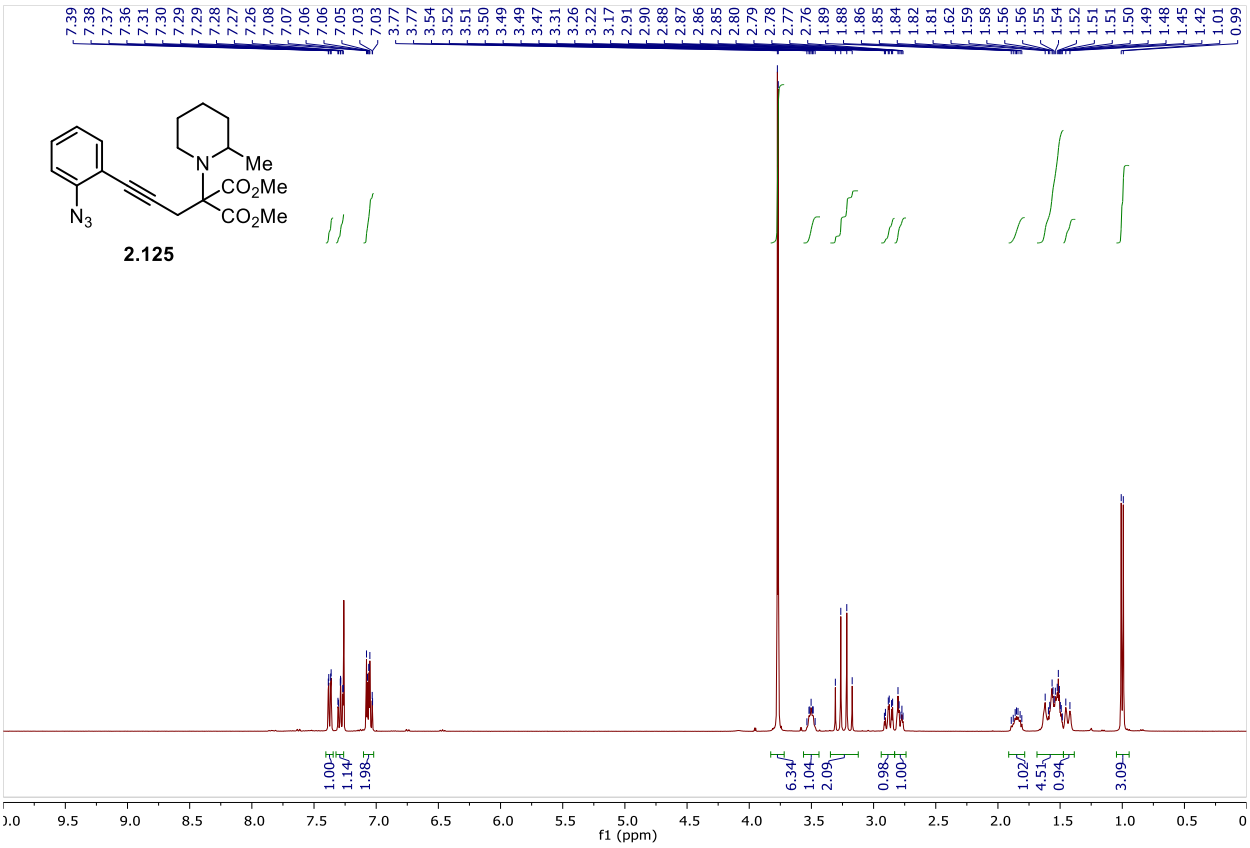

AcO
H
N
CO2Me
CO2Me
N
H
2.158a'
f1 (ppm)

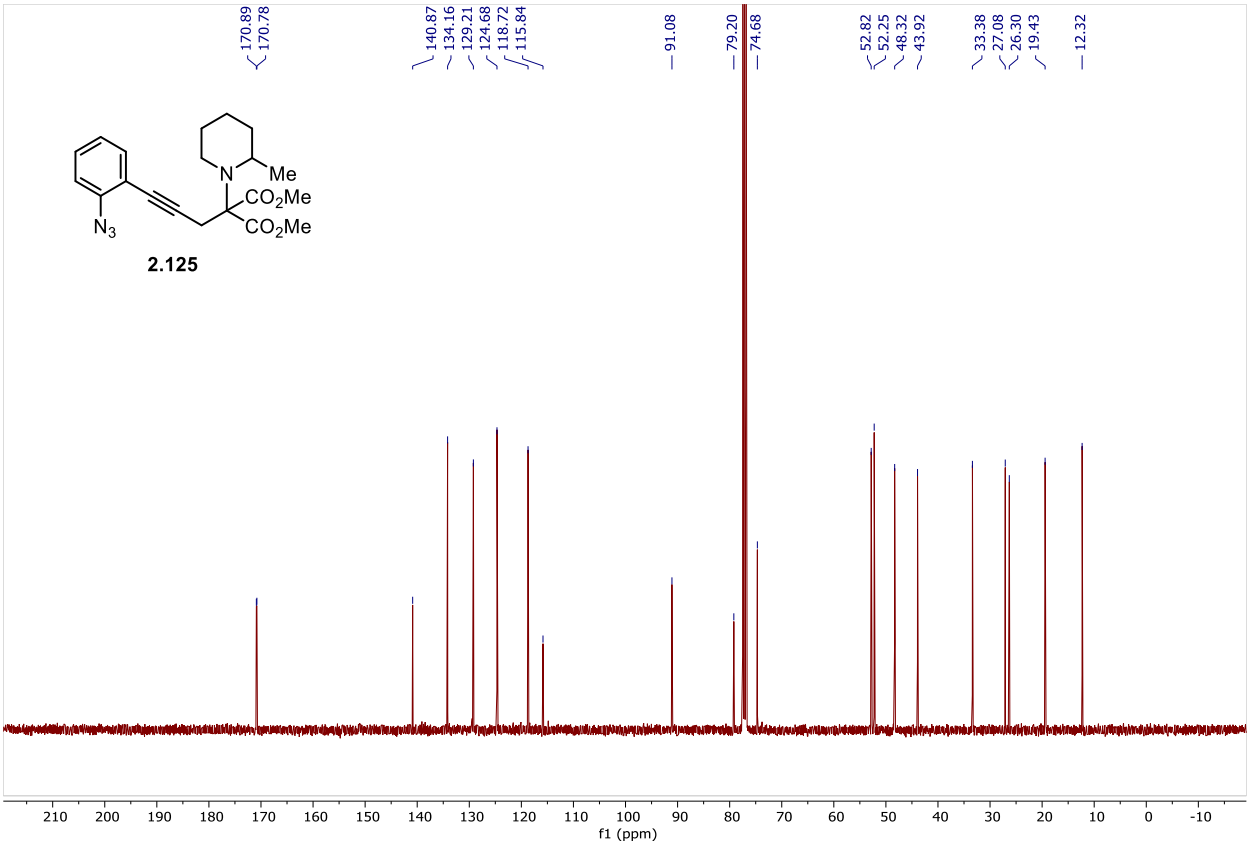

AcO
H
N
CO2Me
CO2Me
N
H
2.158a'
f1 (ppm)

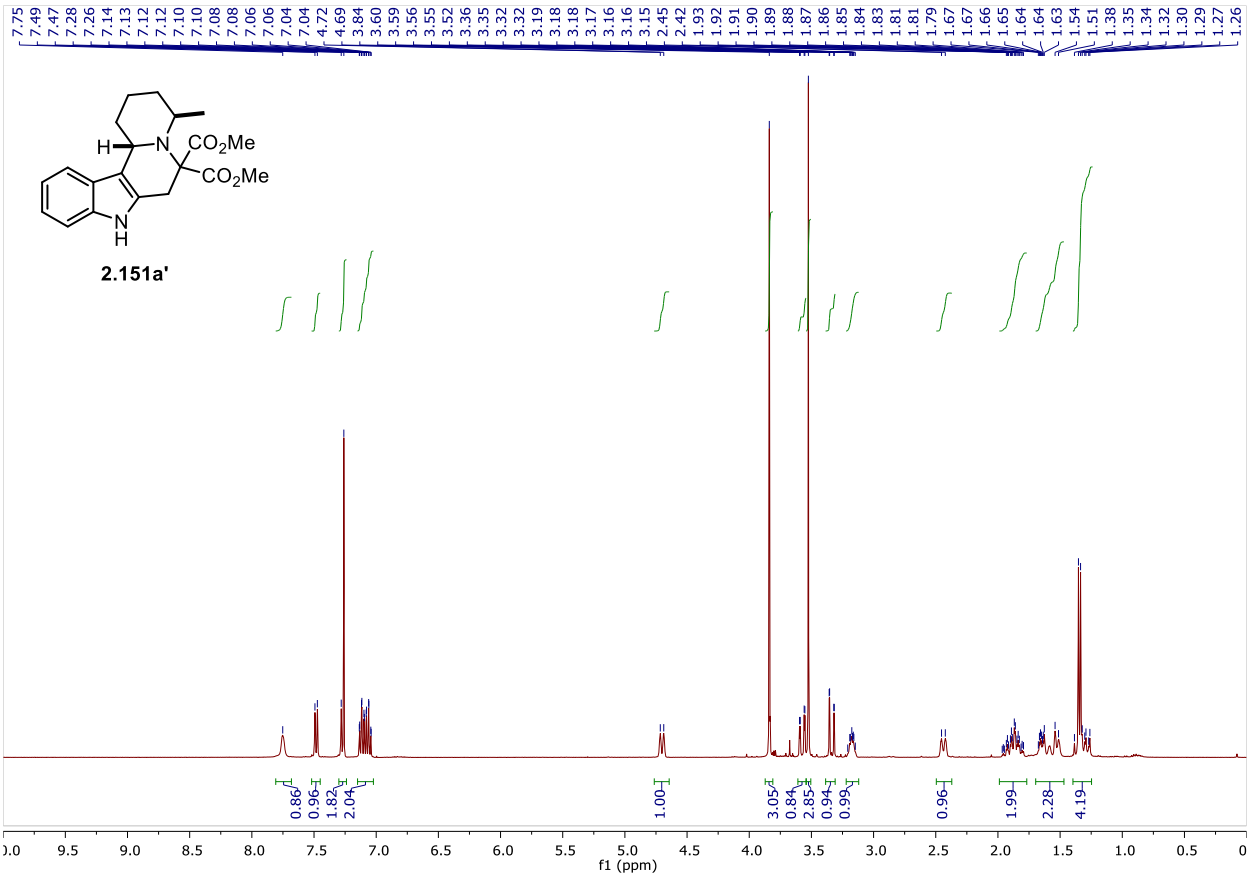

AcO
H
N
CO2Me
CO2Me
N
H
2.158a'
f2 (ppm)
f1 (ppm)

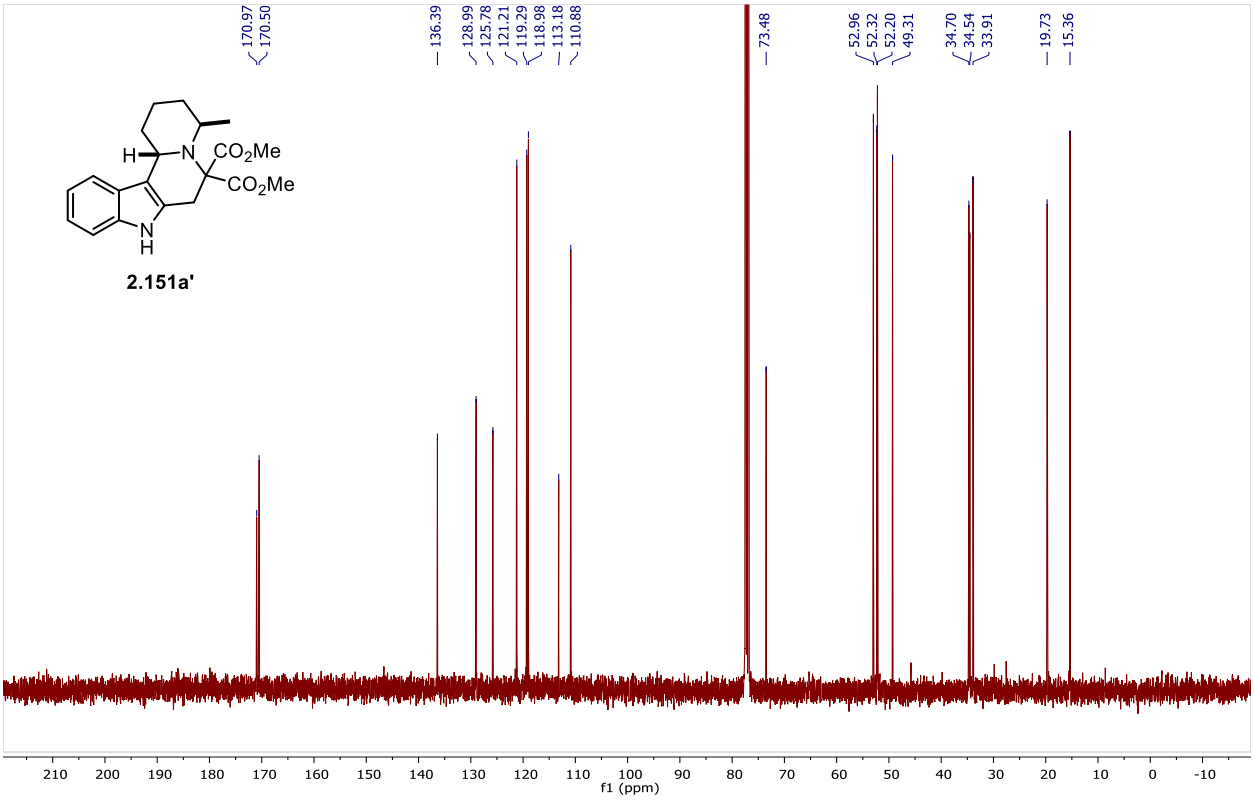

AcO
H
N
CO2Me
CO2Me
N
H
2.158a'
f2 (ppm)
f1 (ppm)

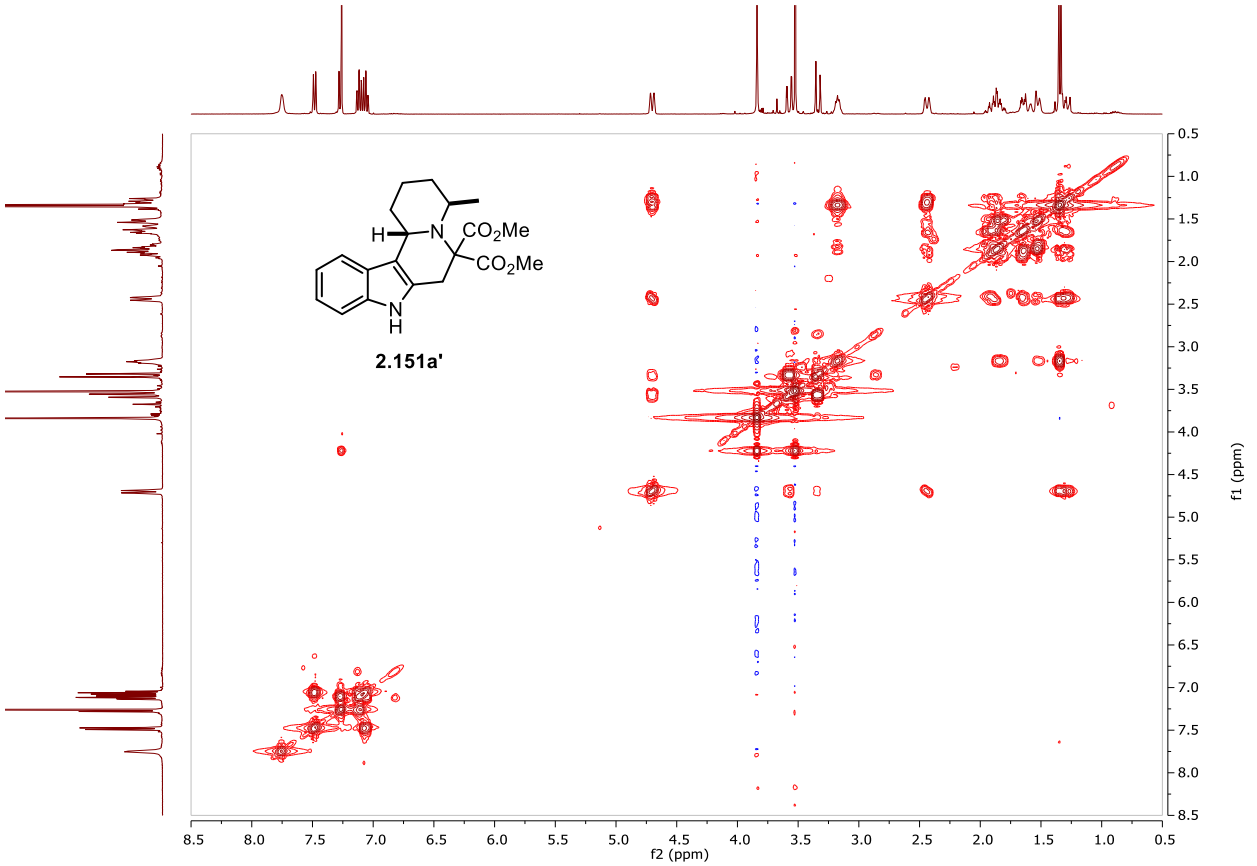

AcO
H
H
N
No NOESY
CO2Me
CO2Me
N
H
2.158a'
f2 (ppm)
f1 (ppm)

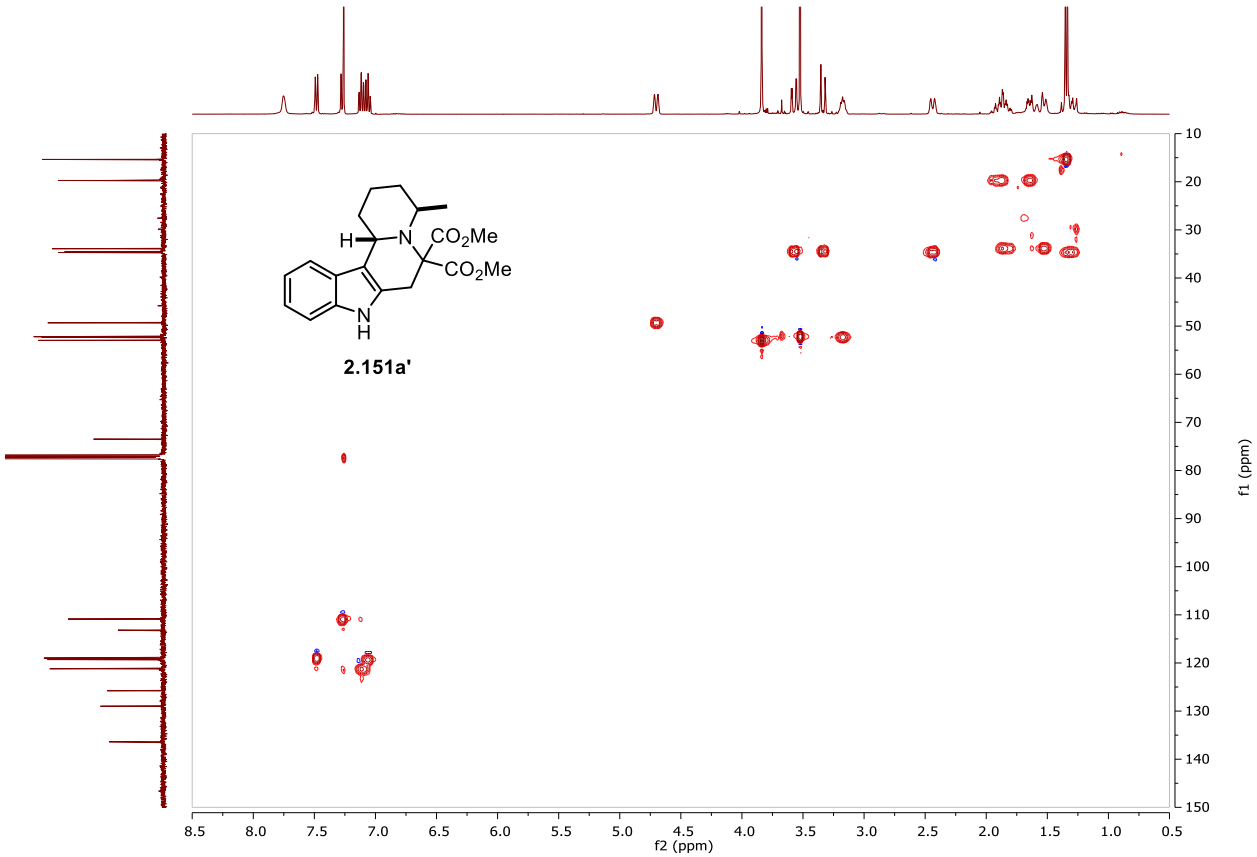

N
Me
CO2Me
CO2Me
N3
2.125
f1 (ppm)

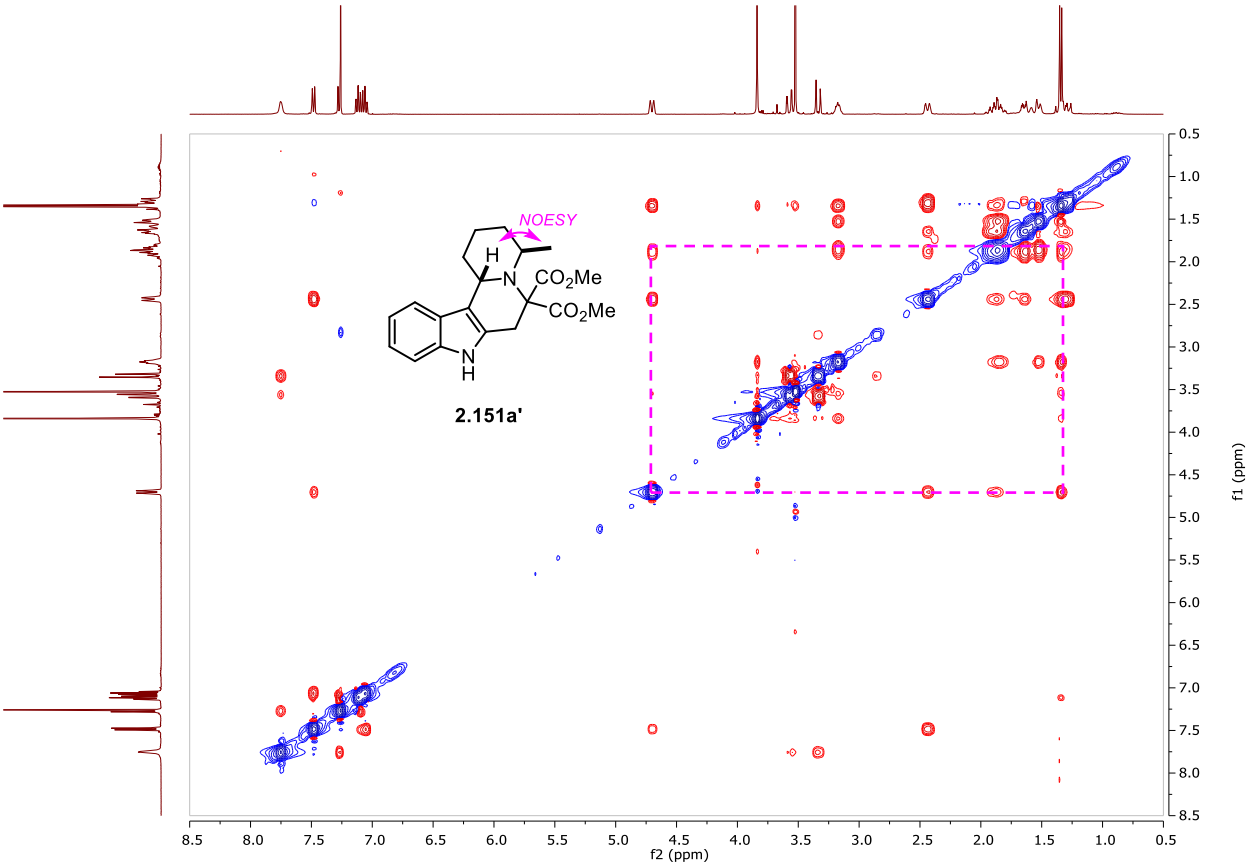

N
Me
CO2Me
CO2Me
N3
2.125
f1 (ppm)

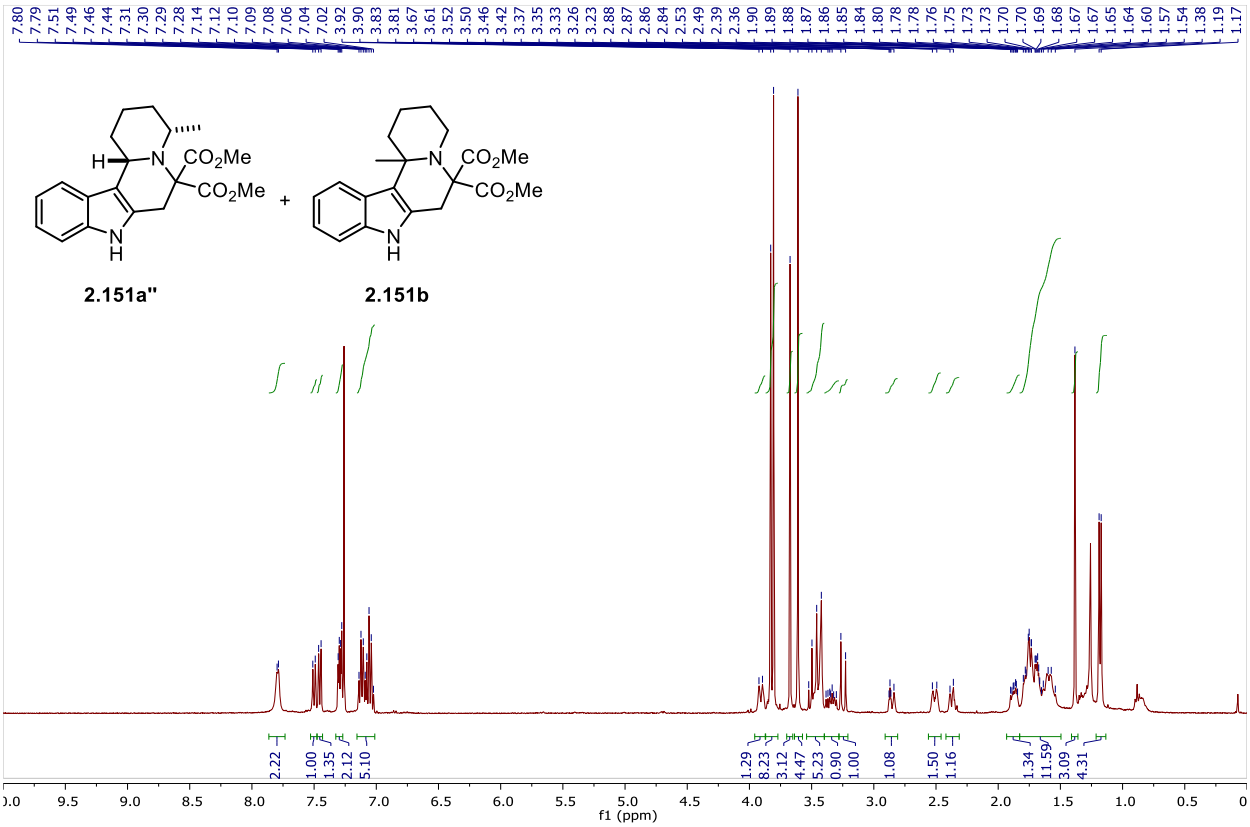

7.75 7.49 7.47 7.28 7.26 7.14 7.13 7.12 7.12 7.10 7.10 7.08 7.08 7.06 7.06 7.04 7.04 4.72 4.69 3.84 3.60 3.59 3.56 3.55 3.52 3.36 3.35 3.32 3.32 3.19 3.18 3.18 3.17 3.16 3.16 3.15 2.45 2.42 1.93 1.92 1.91 1.90 1.89 1.88 1.87 1.86 1.85 1.84 1.83 1.81 1.81 1.79 1.67 1.67 1.66 1.65 1.64 1.64 1.63 1.54 1.51 1.38 1.35 1.34 1.32 1.30 1.29 1.27 1.26
H
N
CO2Me
CO2Me
N
H
2.151a'
0.86 0.96 1.82 2.04 1.00 3.05 0.84 2.85 0.94 0.99 0.96 1.99 2.28 4.19
f1 (ppm)

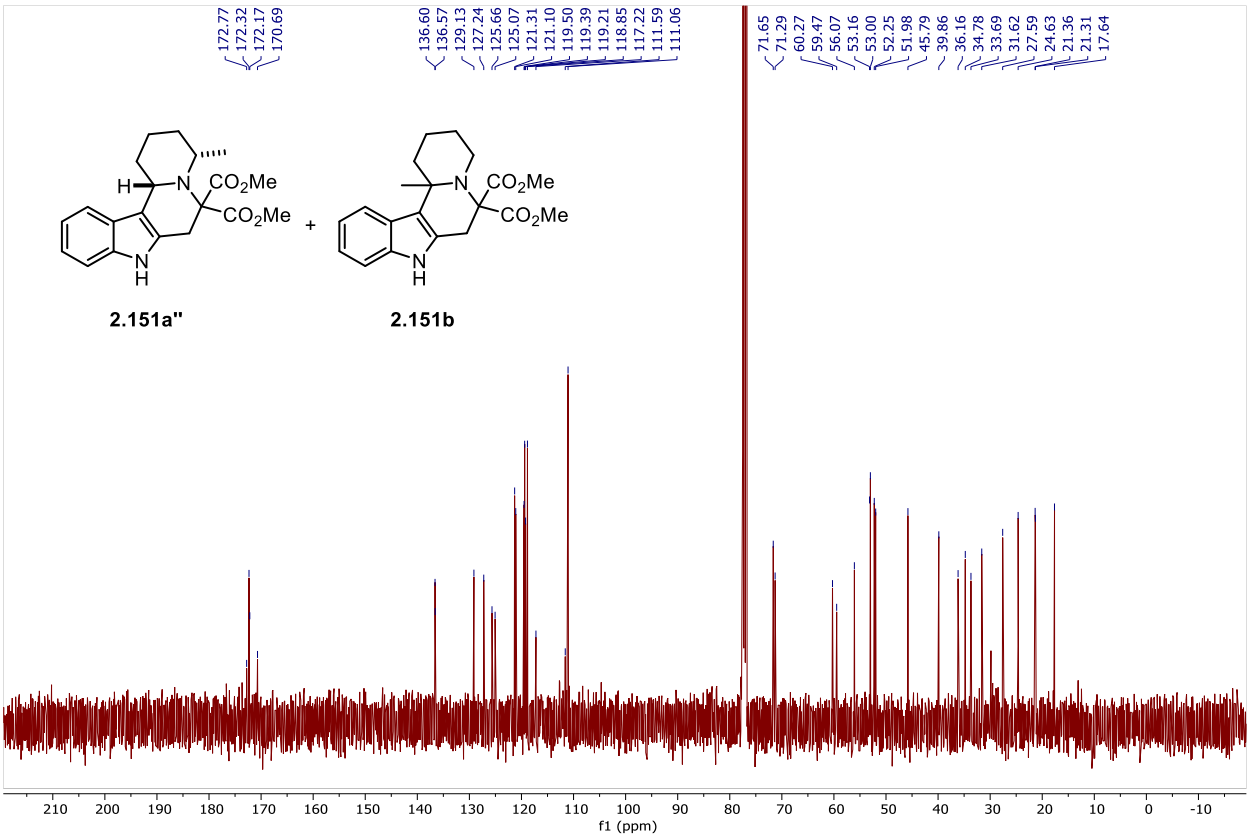

170.97 170.50 136.39 128.99 125.78 121.21 119.29 118.98 113.18 110.88 73.48 52.96 52.32 52.20 49.31 34.70 34.54 33.91 19.73 15.36
H
N
CO2Me
CO2Me
N
H
2.151a'
f1 (ppm)

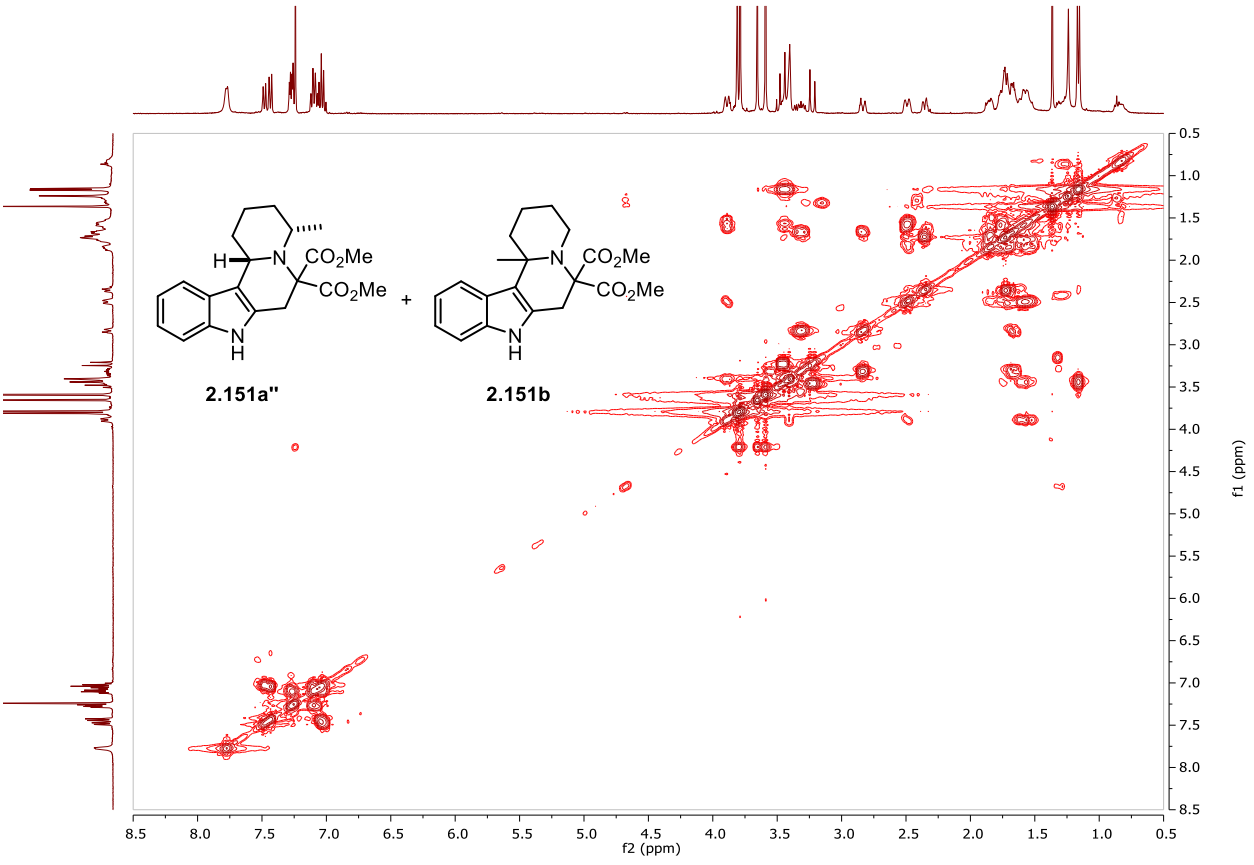

H
N
CO2Me
CO2Me
N
H
2.151a'
f2 (ppm)
f1 (ppm)

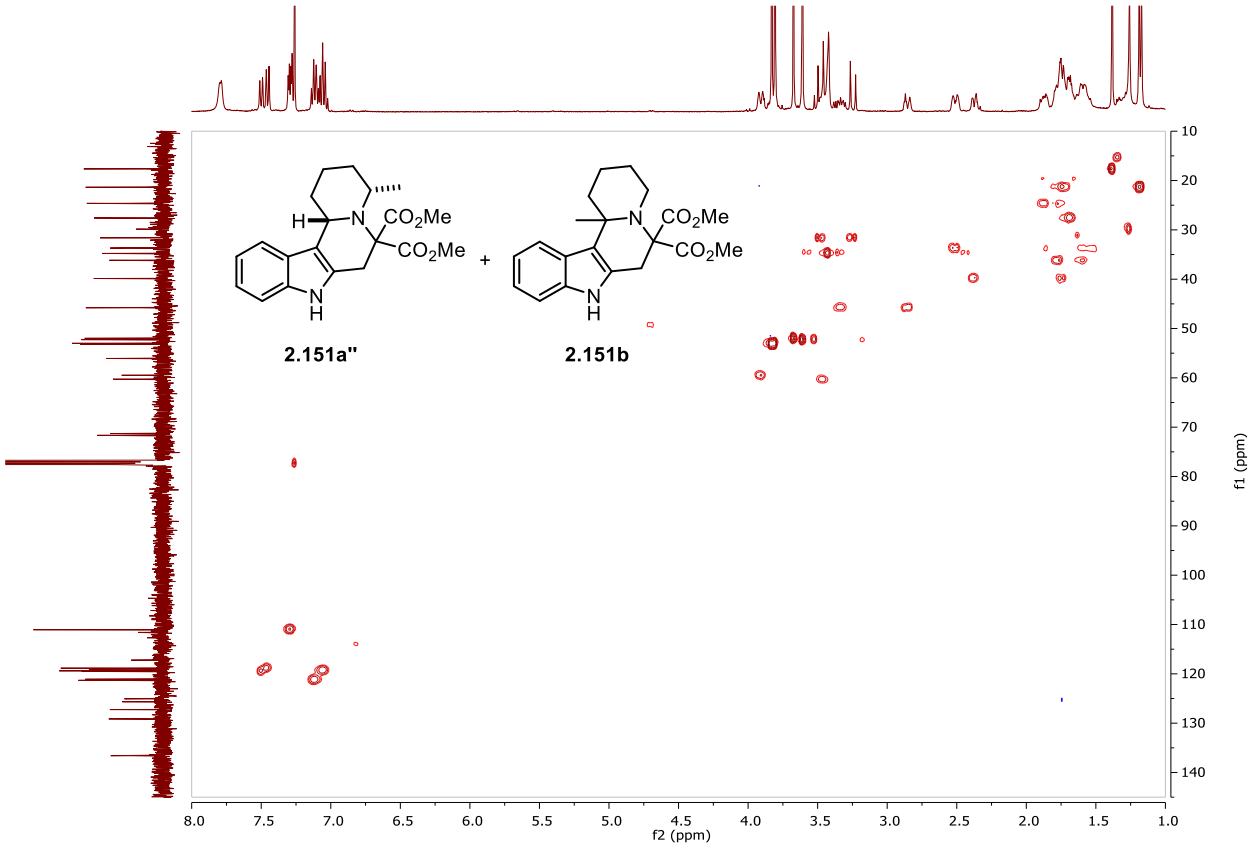

H
N
CO2Me
CO2Me
N
H
2.151a'
f2 (ppm)
f1 (ppm)

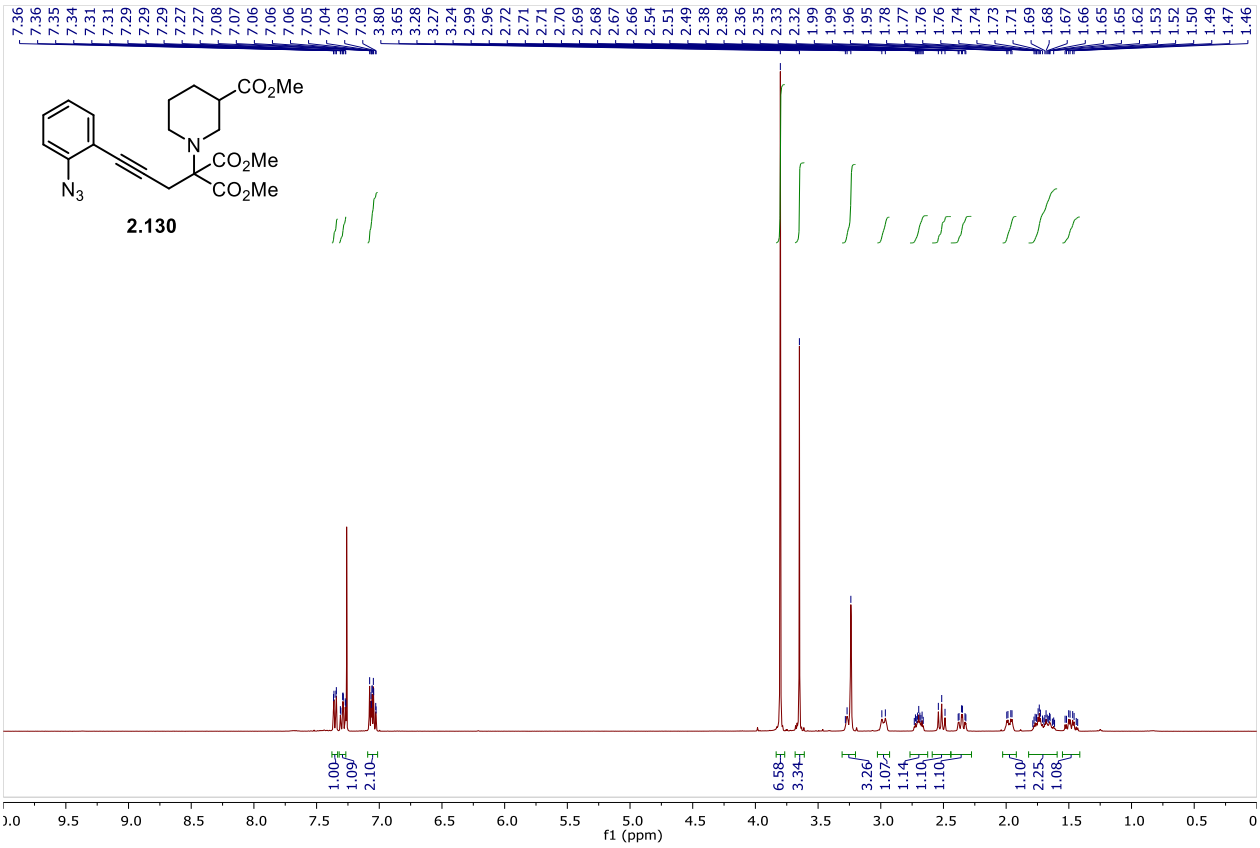

NOESY
H
N
CO2Me
CO2Me
N
H
2.151a'
f2 (ppm)
f1 (ppm)

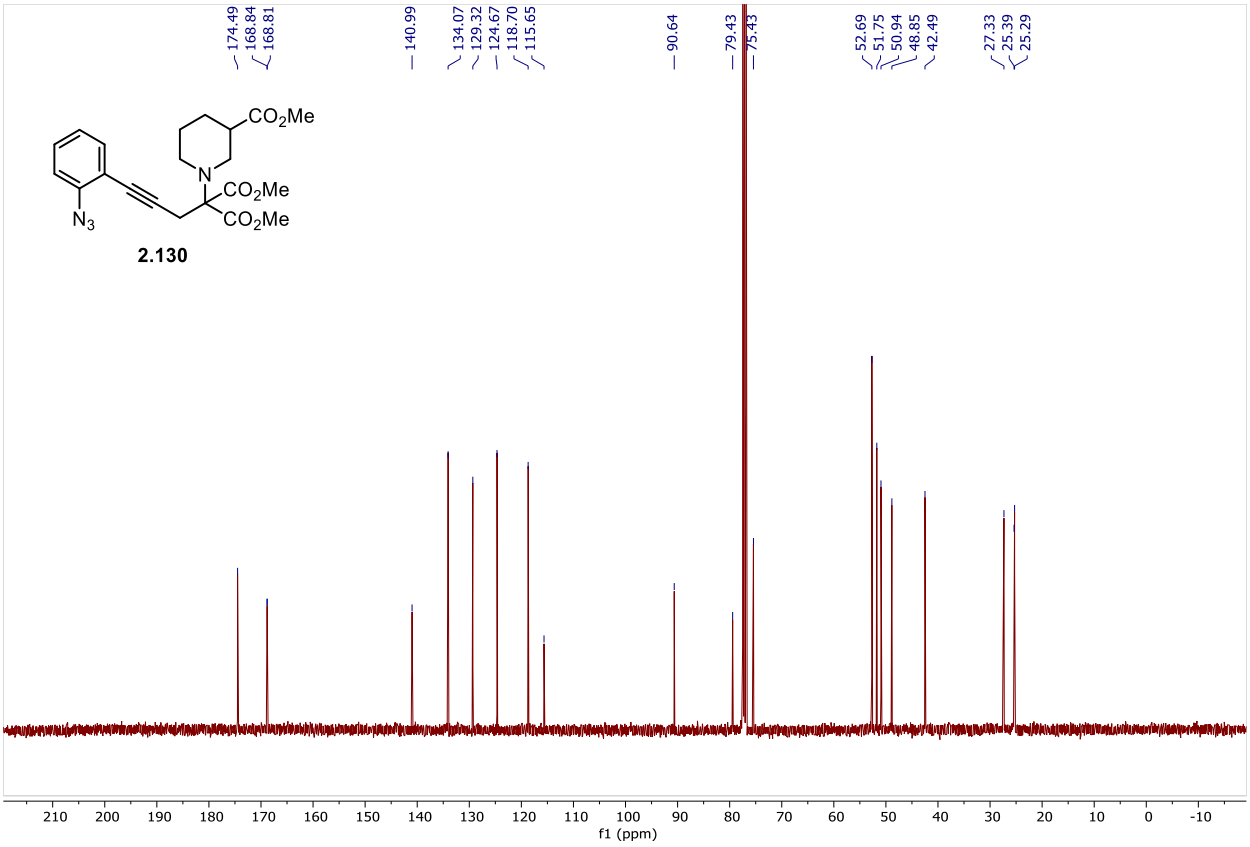

H
N
CO2Me
CO2Me
N
H
2.151a''
+
N
CO2Me
CO2Me
N
H
2.151b
f1 (ppm)

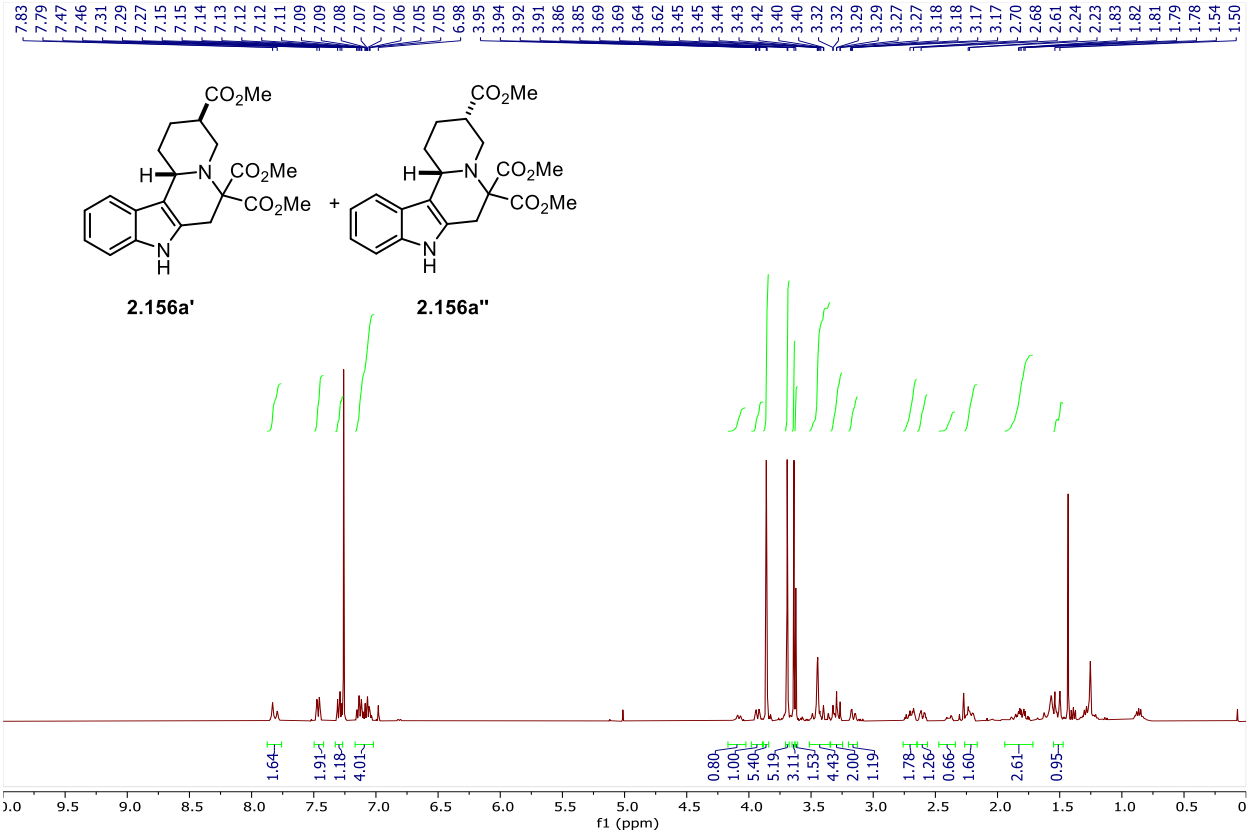

172.77
172.32
172.17
170.69
136.60
136.57
129.13
127.24
125.66
125.07
121.31
121.10
119.50
119.39
119.21
118.85
117.22
111.59
111.06
71.65
71.29
60.27
59.47
56.07
53.16
53.00
52.25
51.98
45.79
39.86
36.16
34.78
33.69
31.62
27.59
24.63
21.36
21.31
17.64
CO2Me
CO2Me
2.151a''
2.151b
f1 (ppm)

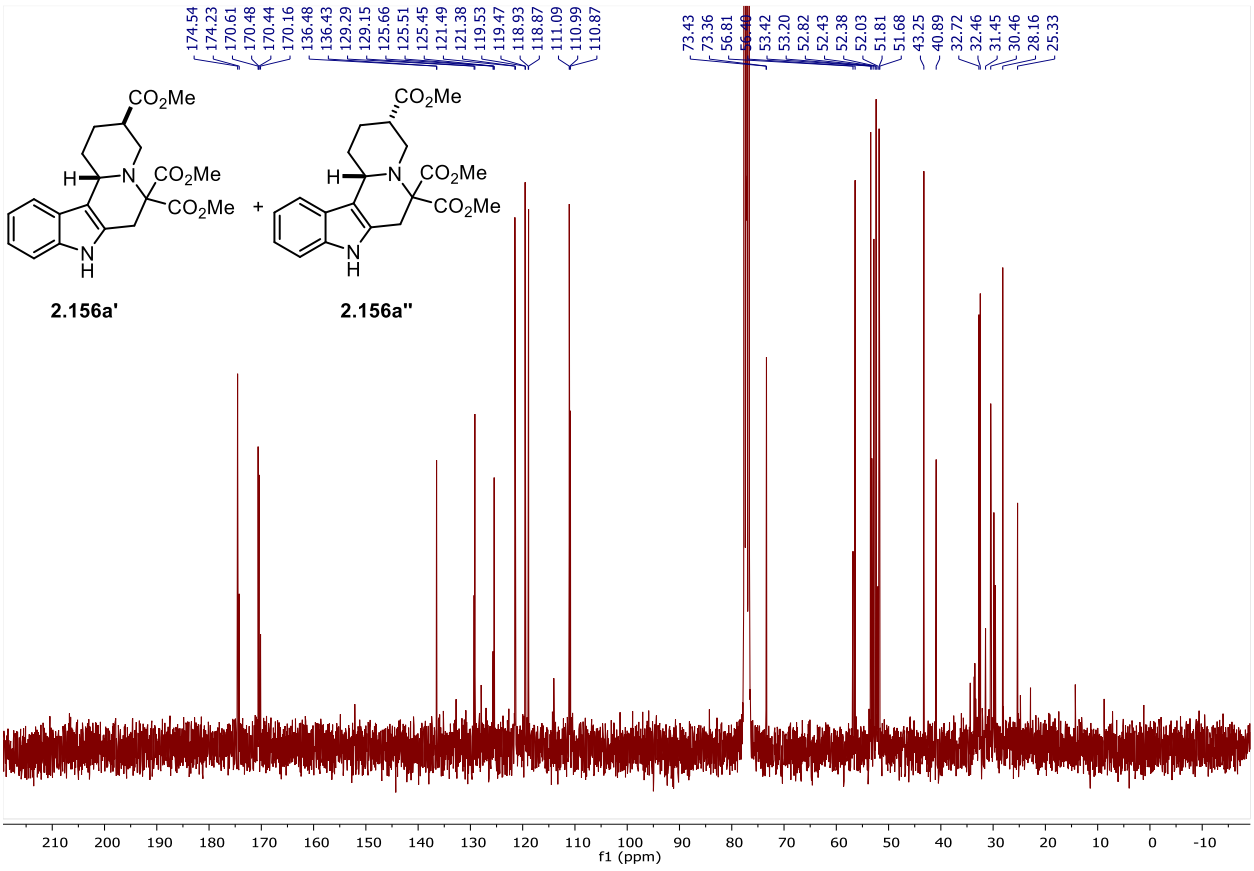

CO2Me
CO2Me
2.151a''
2.151b
f2 (ppm)
f1 (ppm)

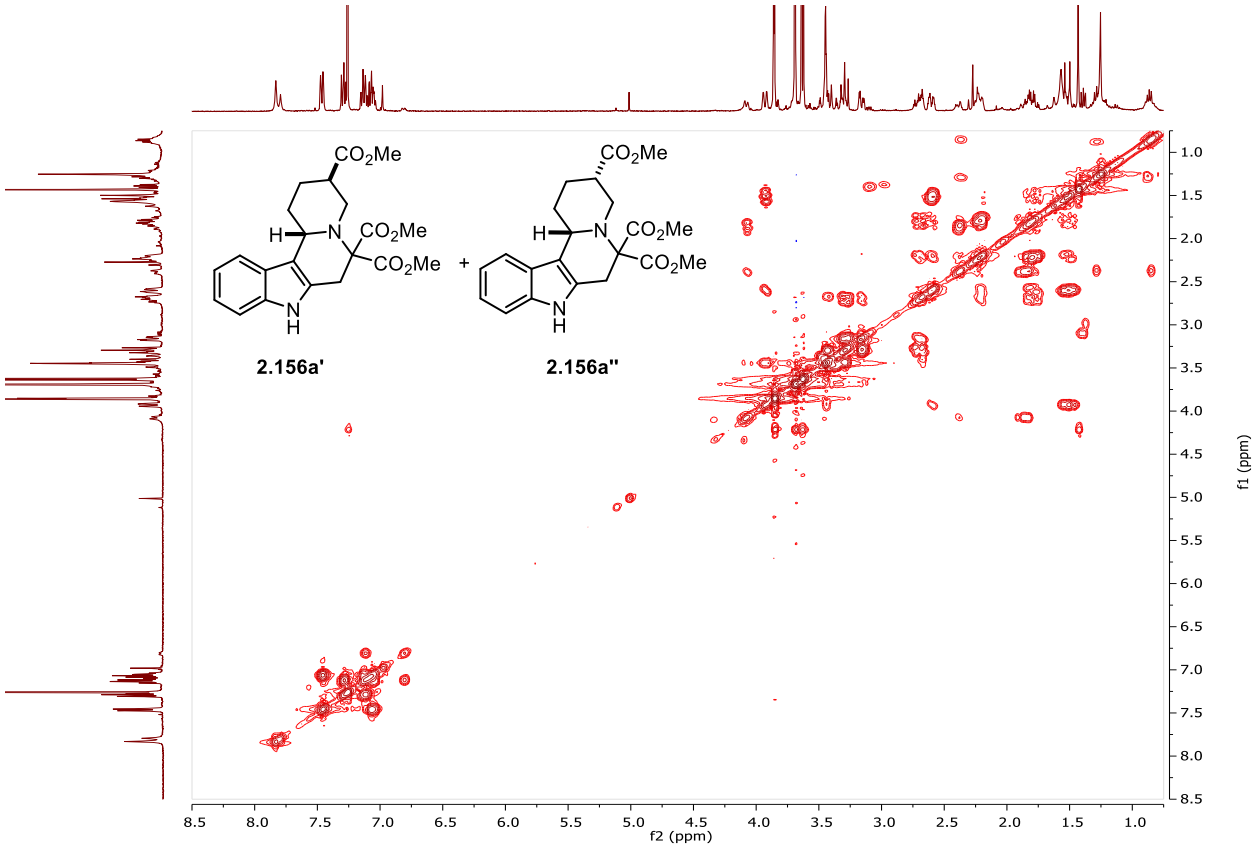

2.151a"
2.151b
f2 (ppm)
f1 (ppm)

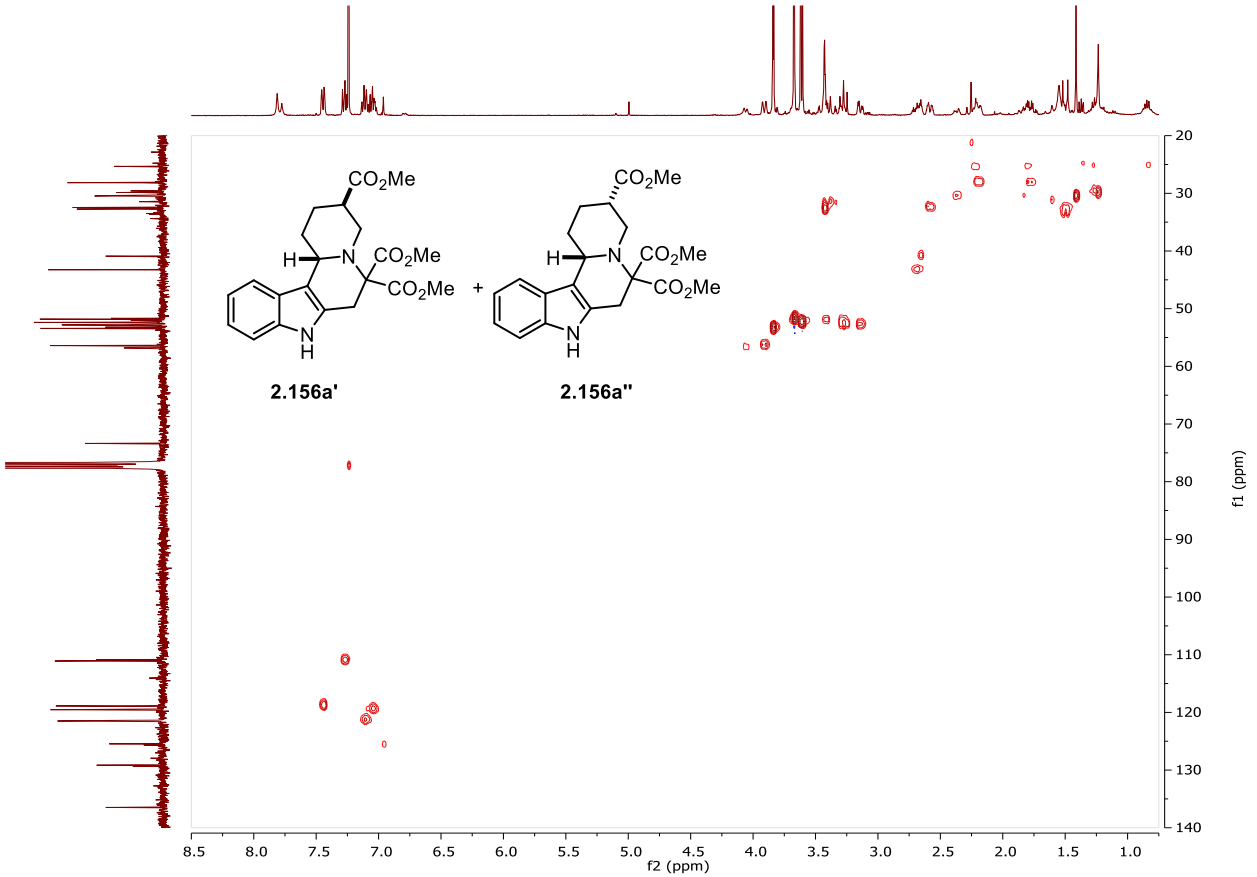

CO2Me
N
CO2Me
CO2Me
N3
2.130
f1 (ppm)

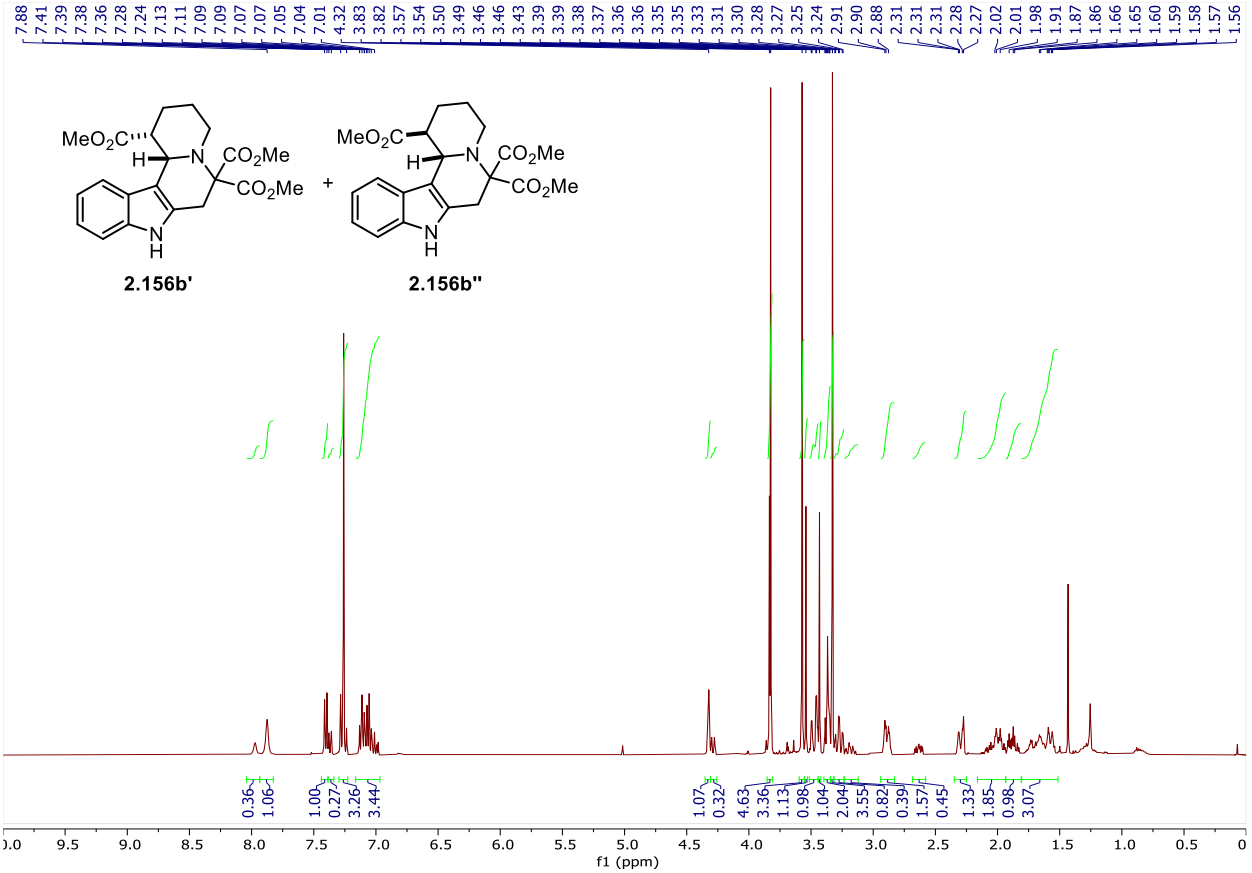

CO2Me
N
CO2Me
CO2Me
N3
2.130
f1 (ppm)

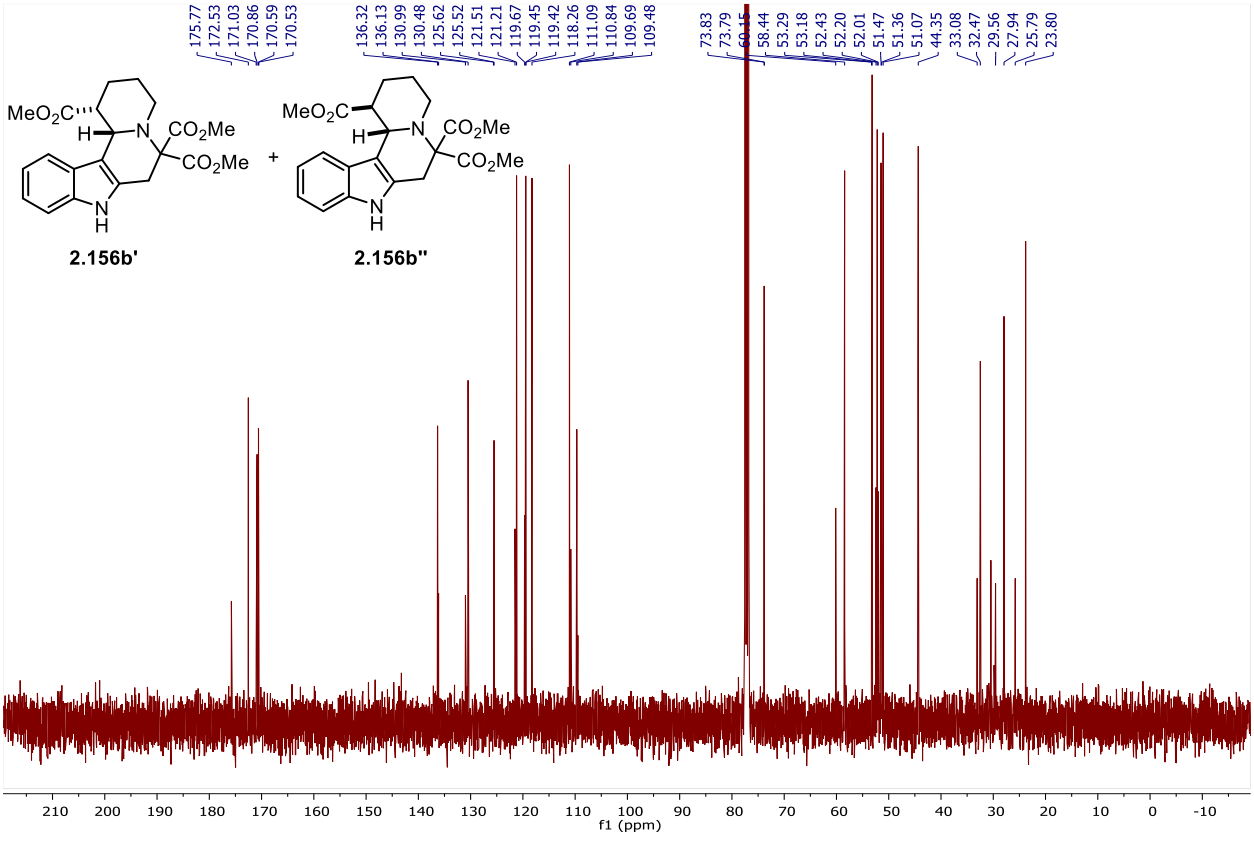

7.83 7.79 7.47 7.46 7.31 7.29 7.27 7.15 7.15 7.14 7.13 7.12 7.12 7.11 7.09 7.09 7.08 7.07 7.07 7.06 7.05 7.05 6.98
3.95 3.94 3.92 3.91 3.86 3.85 3.69 3.69 3.64 3.62 3.45 3.45 3.44 3.43 3.42 3.40 3.40 3.32 3.32 3.29 3.29 3.27 3.27 3.18 3.18 3.17 3.17 2.70 2.68 2.61 2.24 2.23 1.83 1.82 1.81 1.79 1.78 1.54 1.50
CO2Me
H
N
CO2Me
CO2Me
N
H
+
2.156a'
2.156a''
1.64 1.91 1.18 4.01
0.80 1.00 5.40 5.19 3.11 1.53 4.43 2.00 1.19 1.78 1.26 0.66 1.60 2.61 0.95
f1 (ppm)

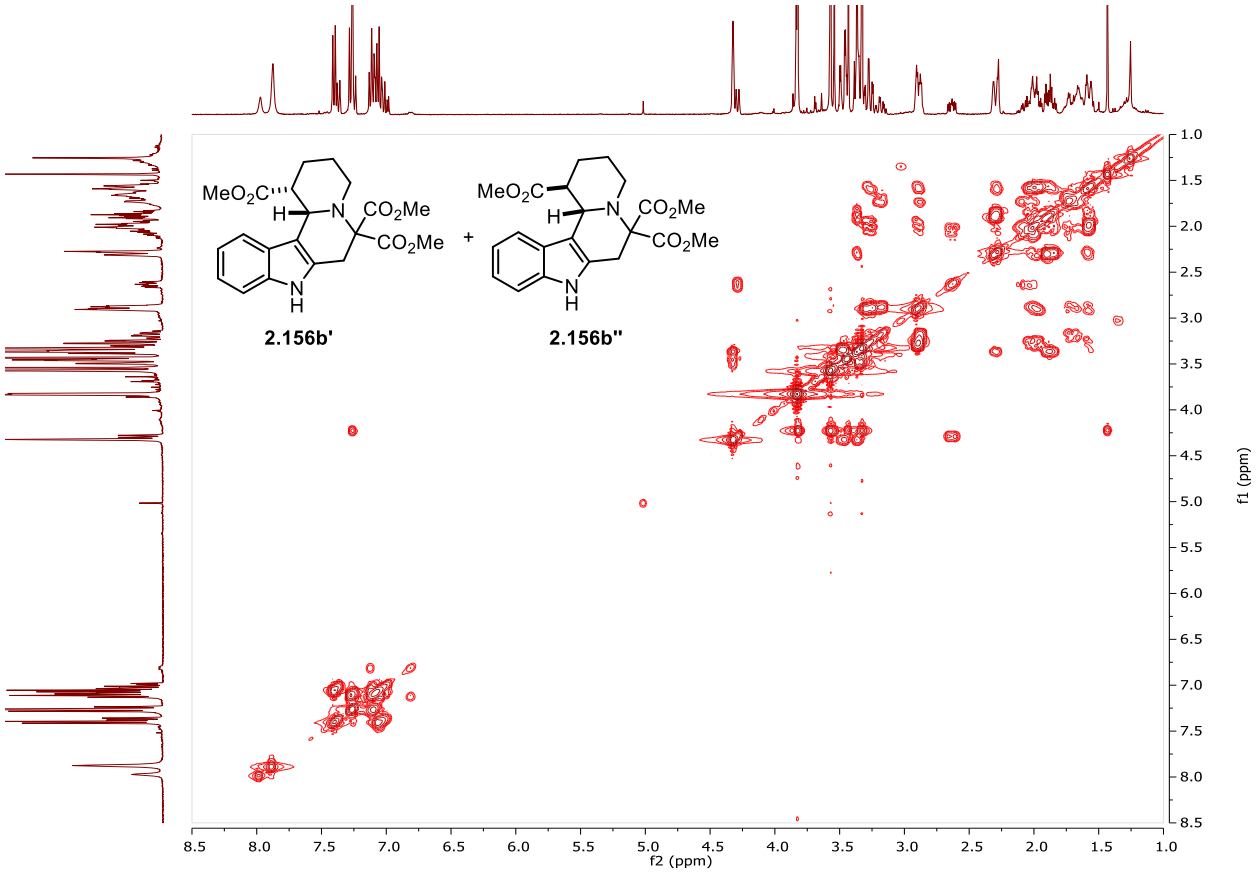

174.54 174.23 170.61 170.48 170.44 170.16 136.48 136.43 129.29 129.15 125.66 125.51 125.45 121.49 121.38 119.53 119.47 118.93 118.87 111.09 110.99 110.87
73.43 73.36 56.81 56.40 53.42 53.20 52.82 52.43 52.38 52.03 51.81 51.68 43.25 40.89 32.72 32.46 31.45 30.46 28.16 25.33
CO2Me
H
N
CO2Me
CO2Me
N
H
+
2.156a'
2.156a''
f1 (ppm)

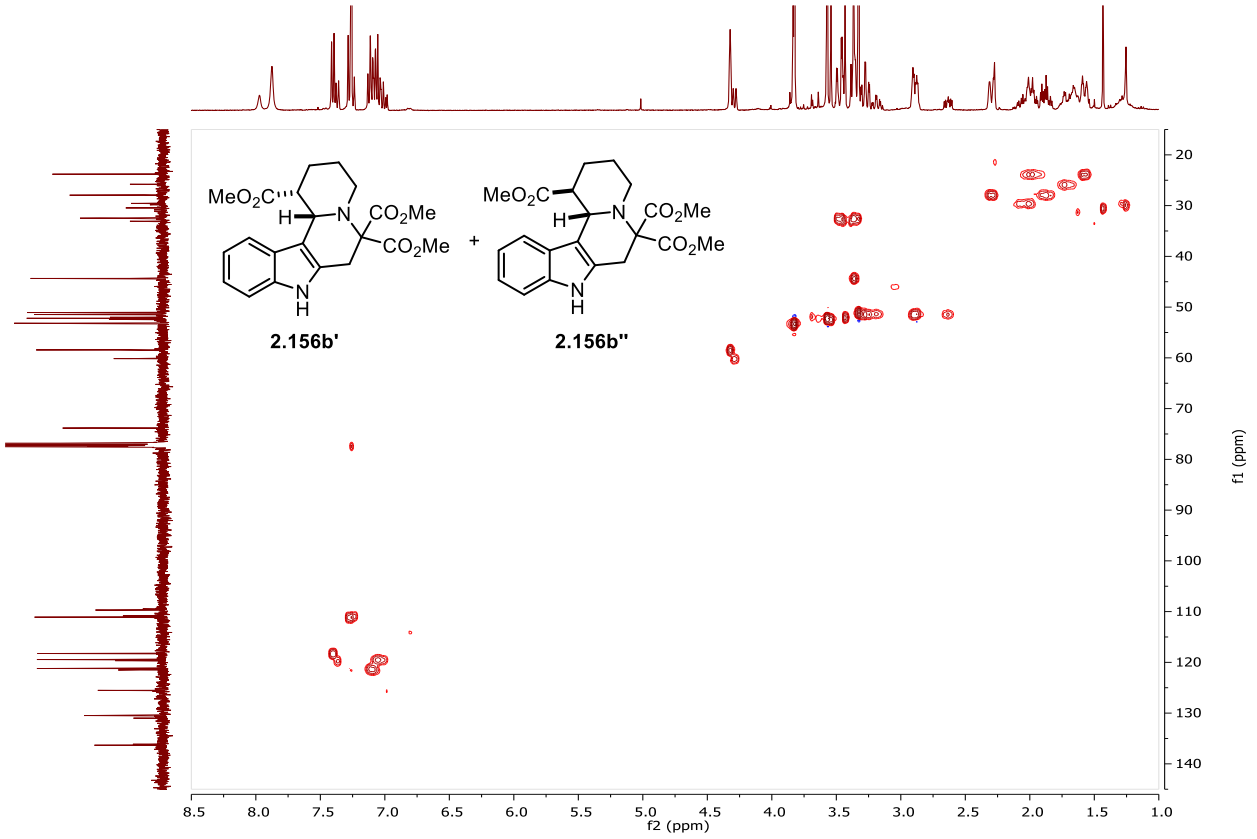

CO2Me
H
N
CO2Me
CO2Me
N
H
+
2.156a'
2.156a''
f1 (ppm)
f2 (ppm)

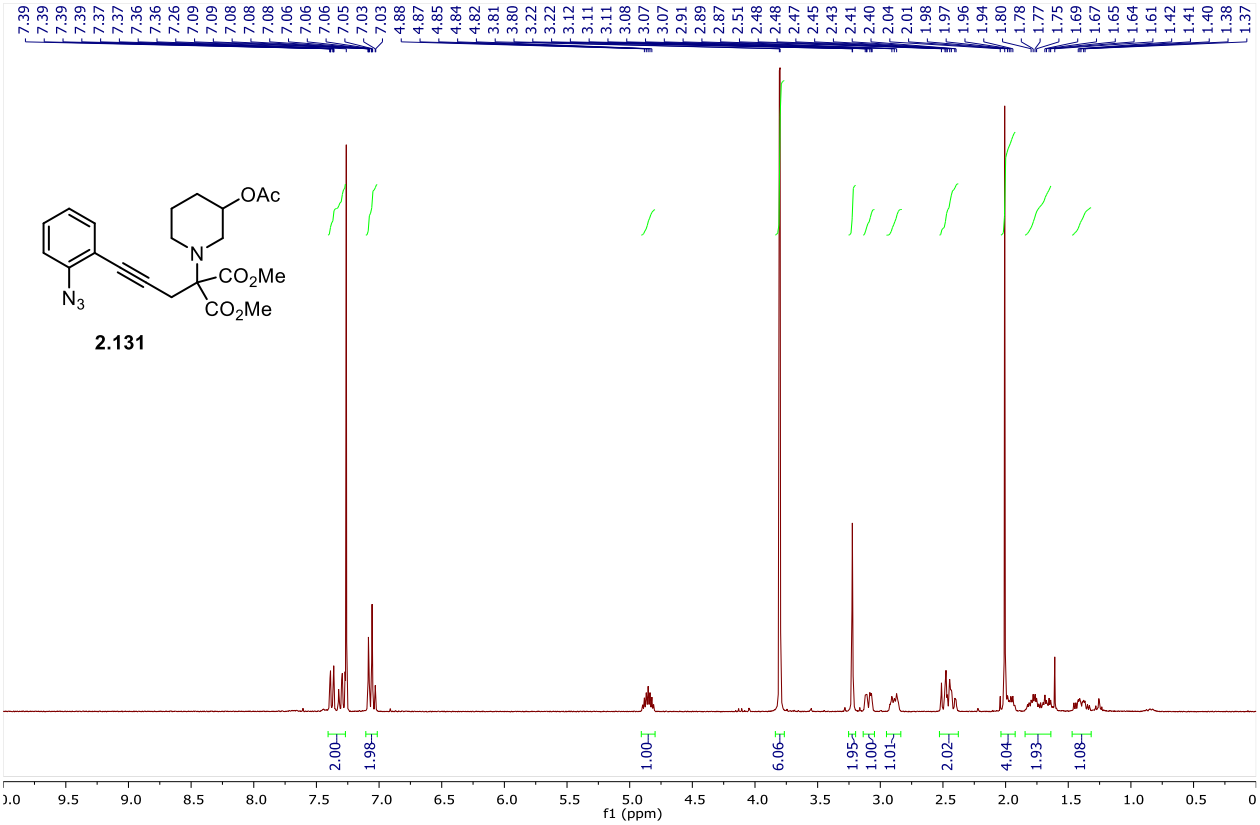

CO2Me
H
N
CO2Me
CO2Me
N
H
+
2.156a'
2.156a''
f1 (ppm)
f2 (ppm)

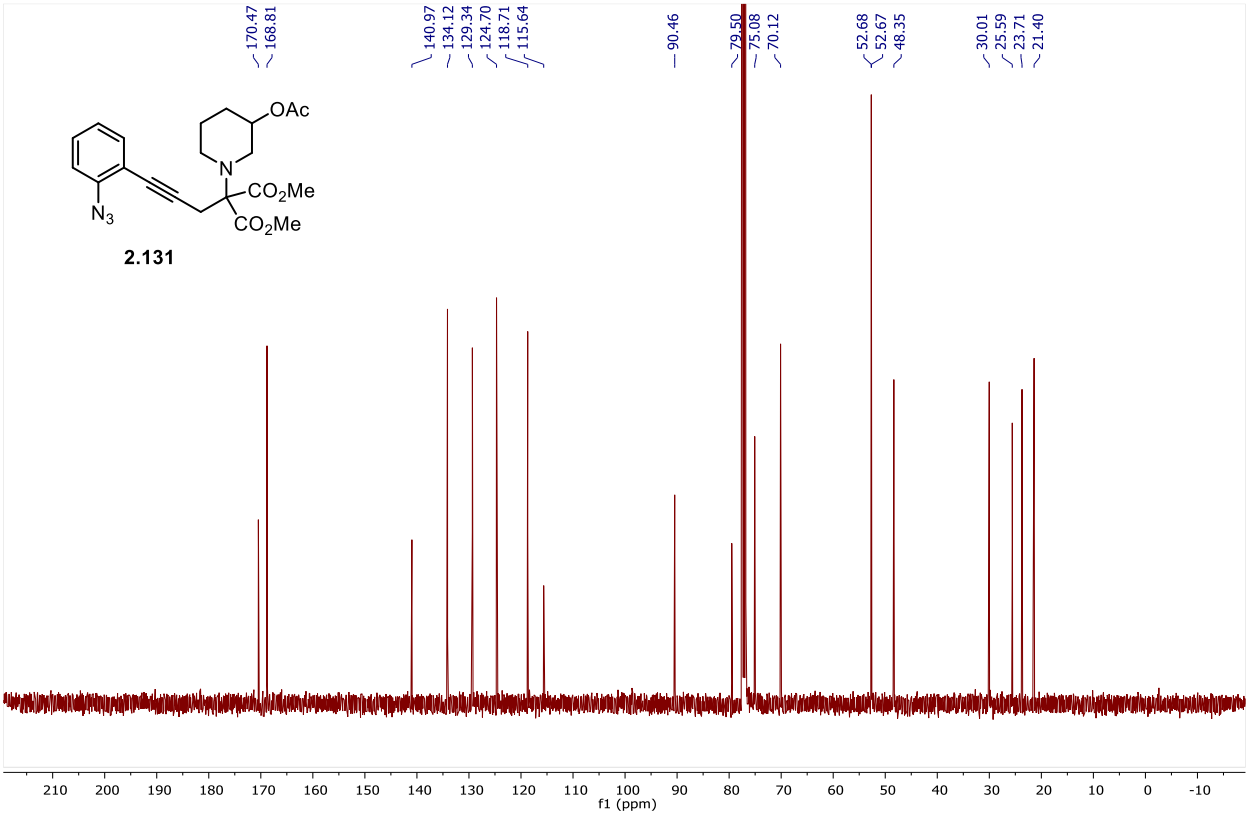

2.156b'
2.156b''
f1 (ppm)

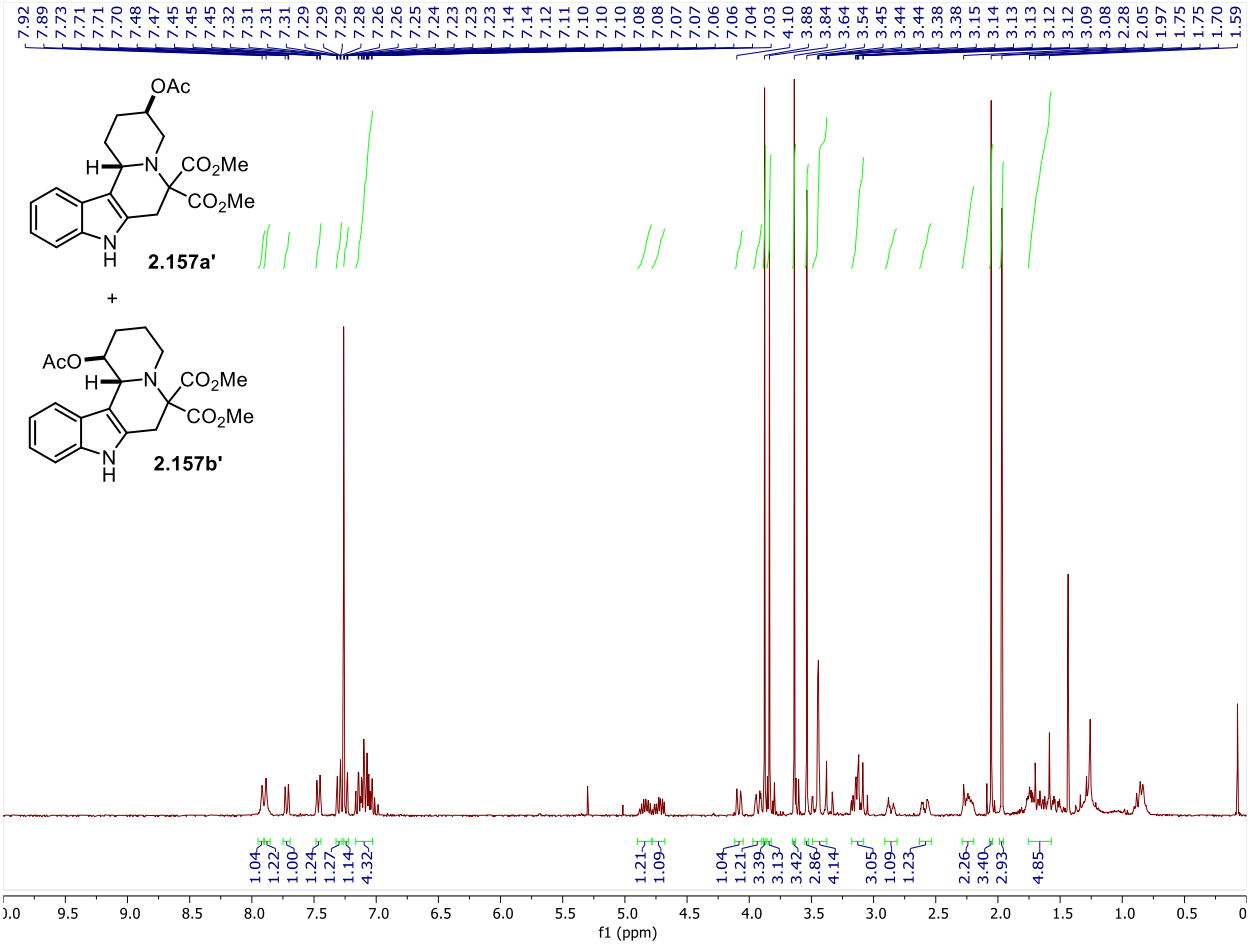

2.156b'
2.156b''
f1 (ppm)

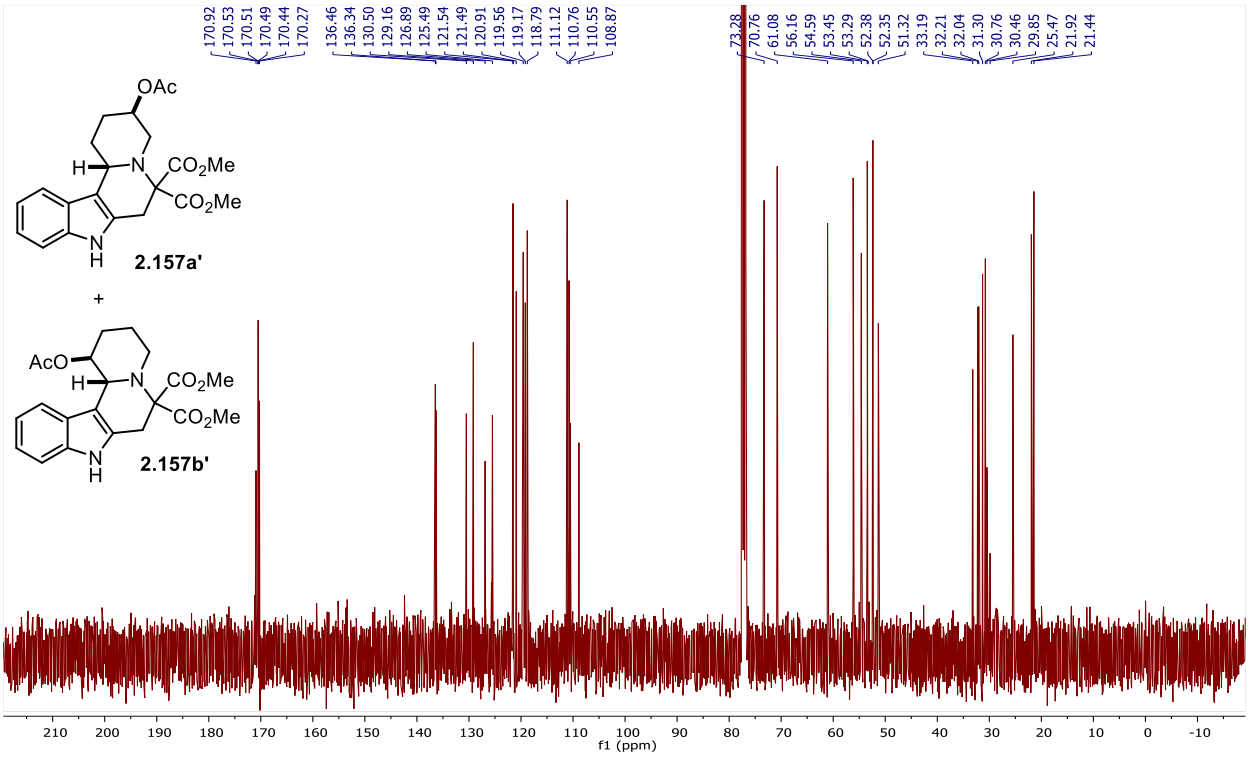

MeO2C
H
N
CO2Me
CO2Me
N
H
+
2.156b'
2.156b''
f1 (ppm)
f2 (ppm)

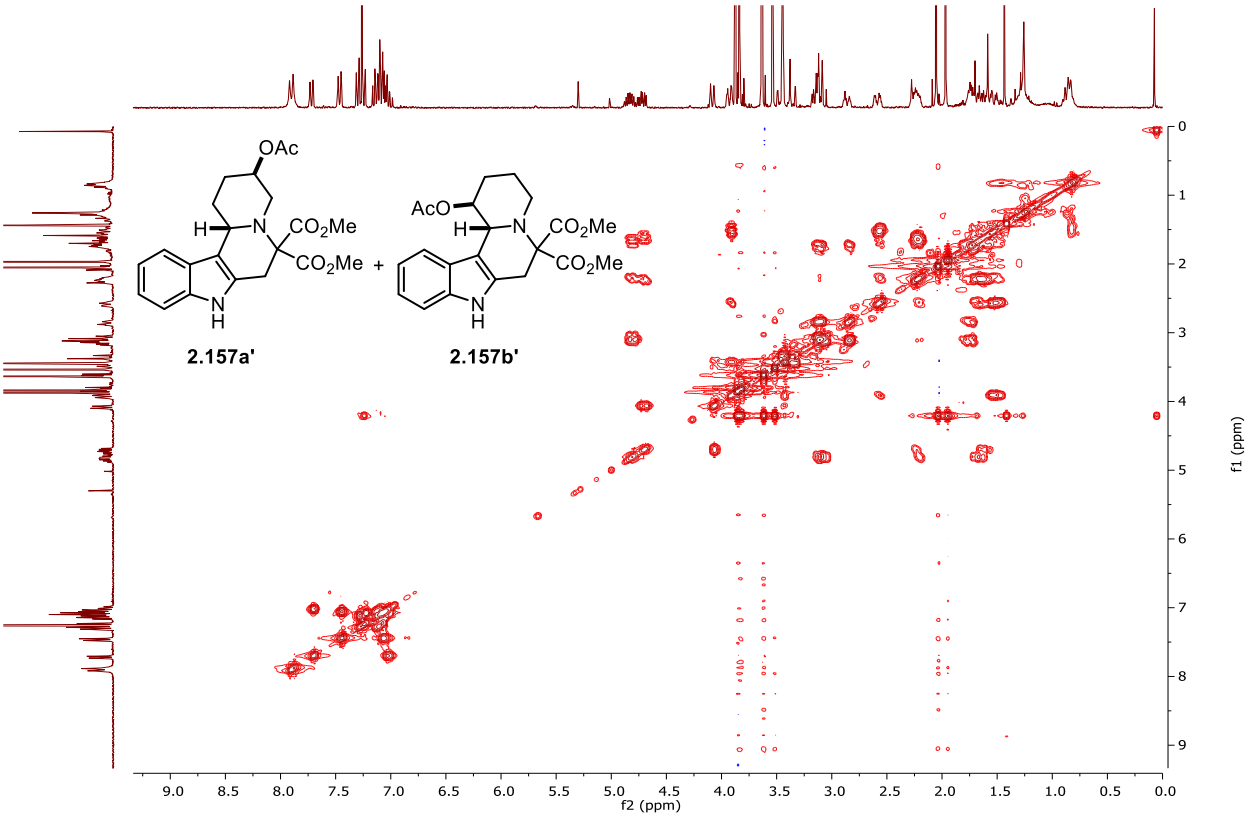

MeO2C
H
N
CO2Me
CO2Me
N
H
+
2.156b'
2.156b''
f1 (ppm)
f2 (ppm)

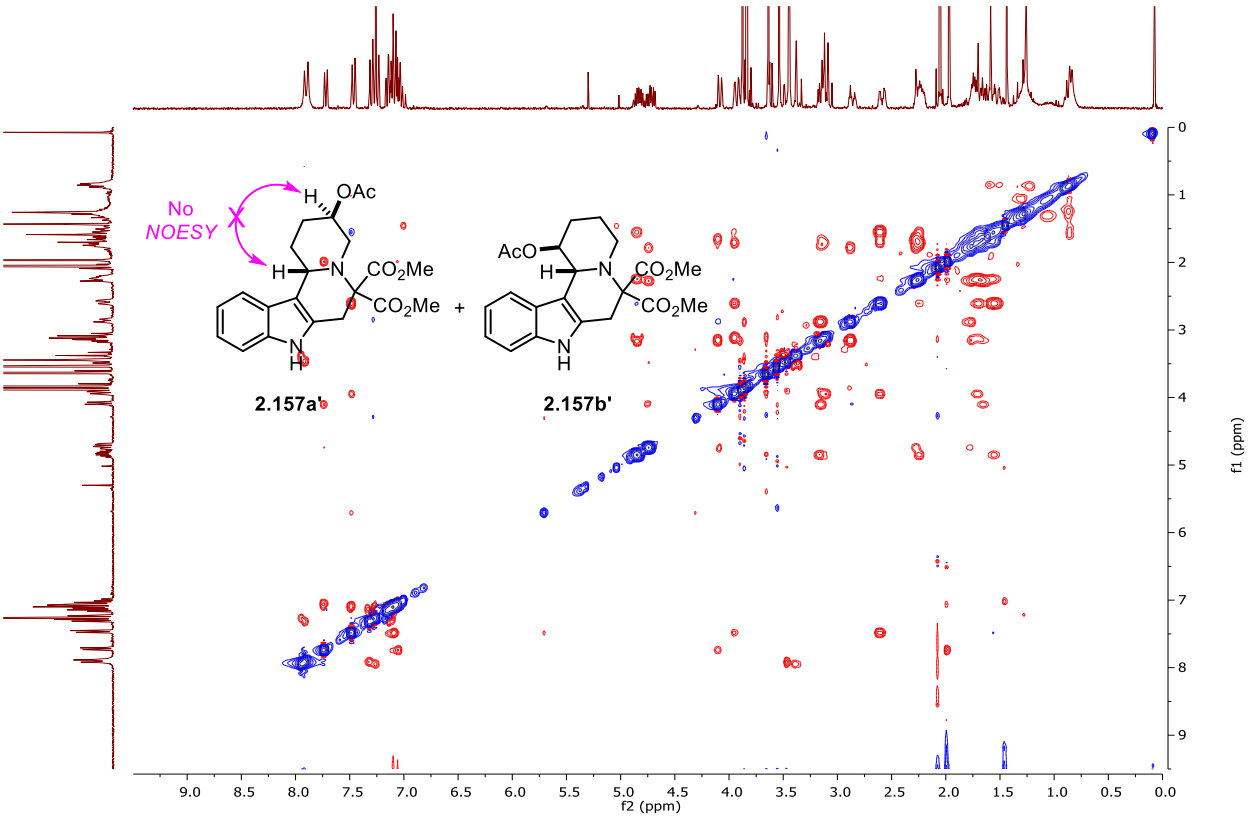

OAc
N
CO2Me
CO2Me
N3
2.131
f1 (ppm)

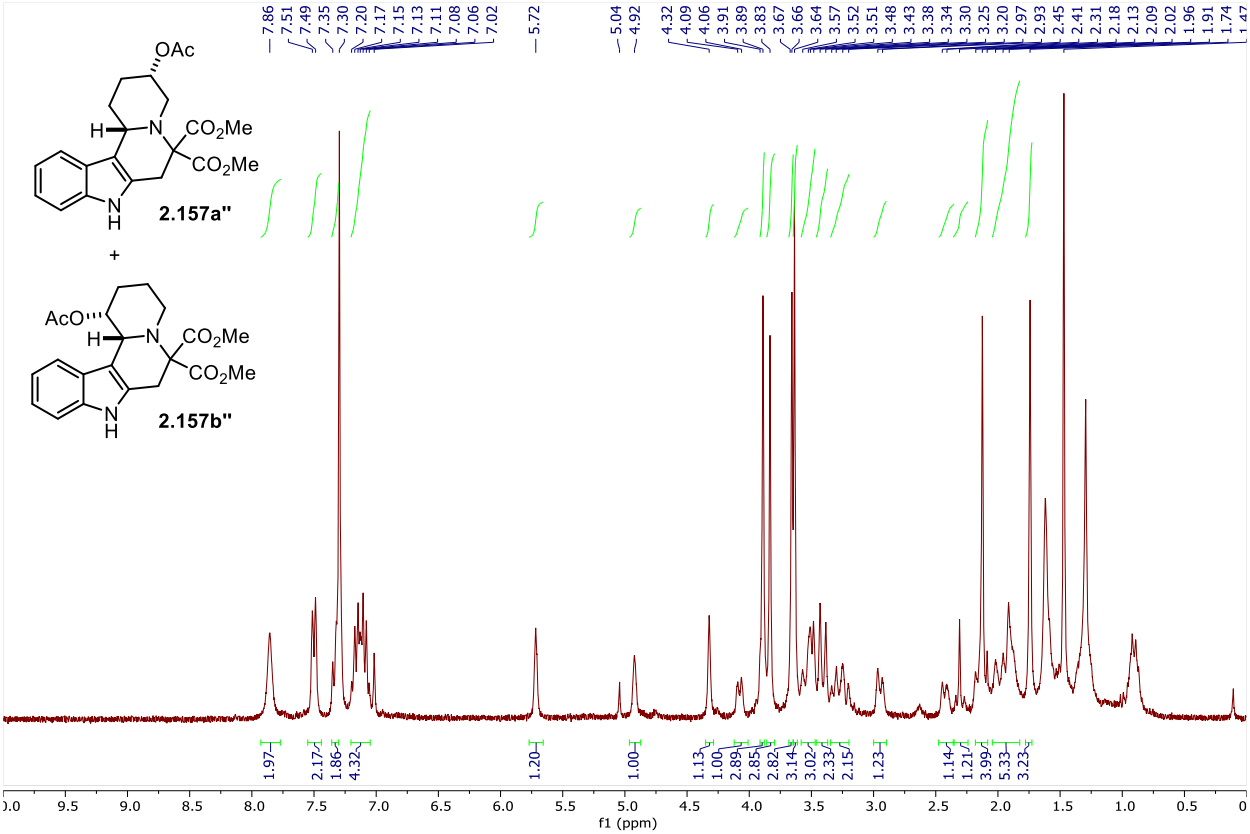

OAc
N
CO2Me
CO2Me
N3
2.131
f1 (ppm)

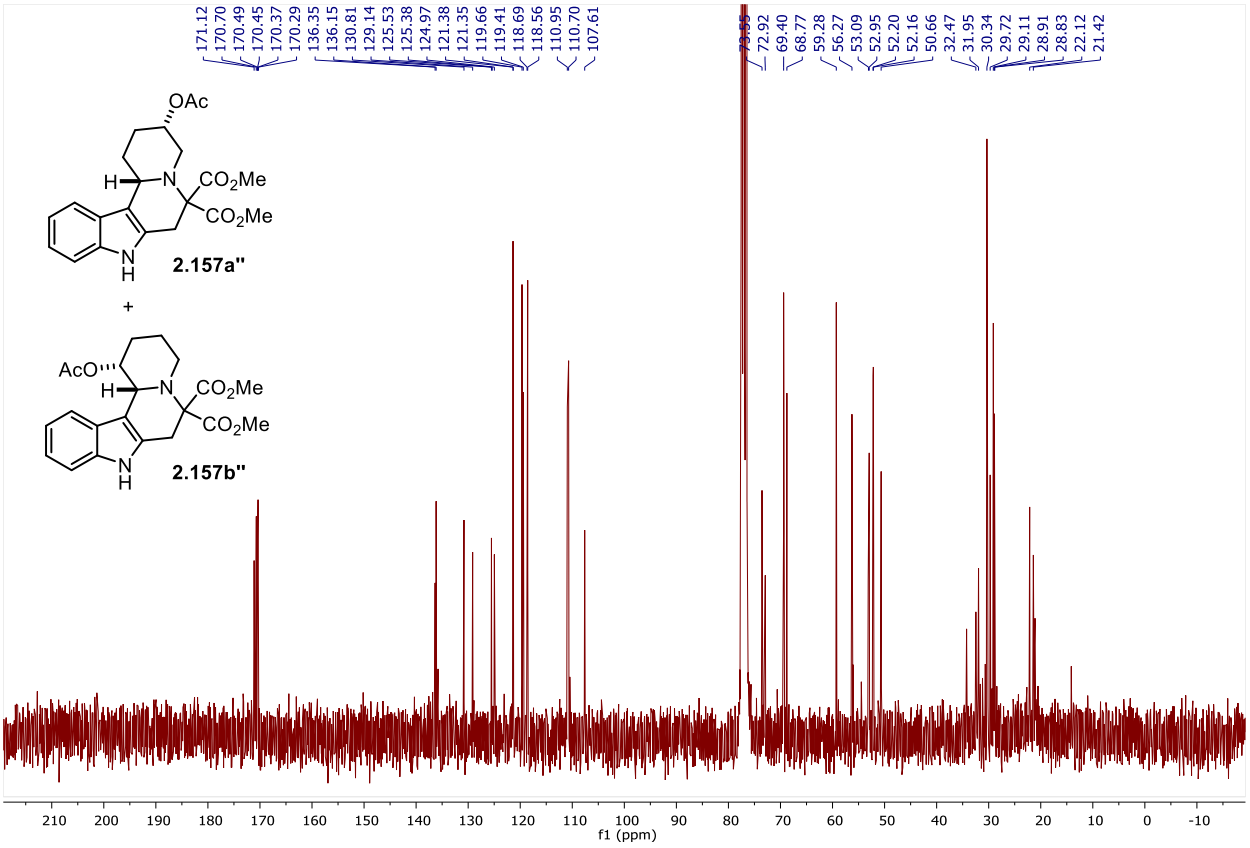

OAc
H
N
CO2Me
CO2Me
N
H
2.157a'
+
AcO
H
N
CO2Me
CO2Me
N
H
2.157b'
f1 (ppm)

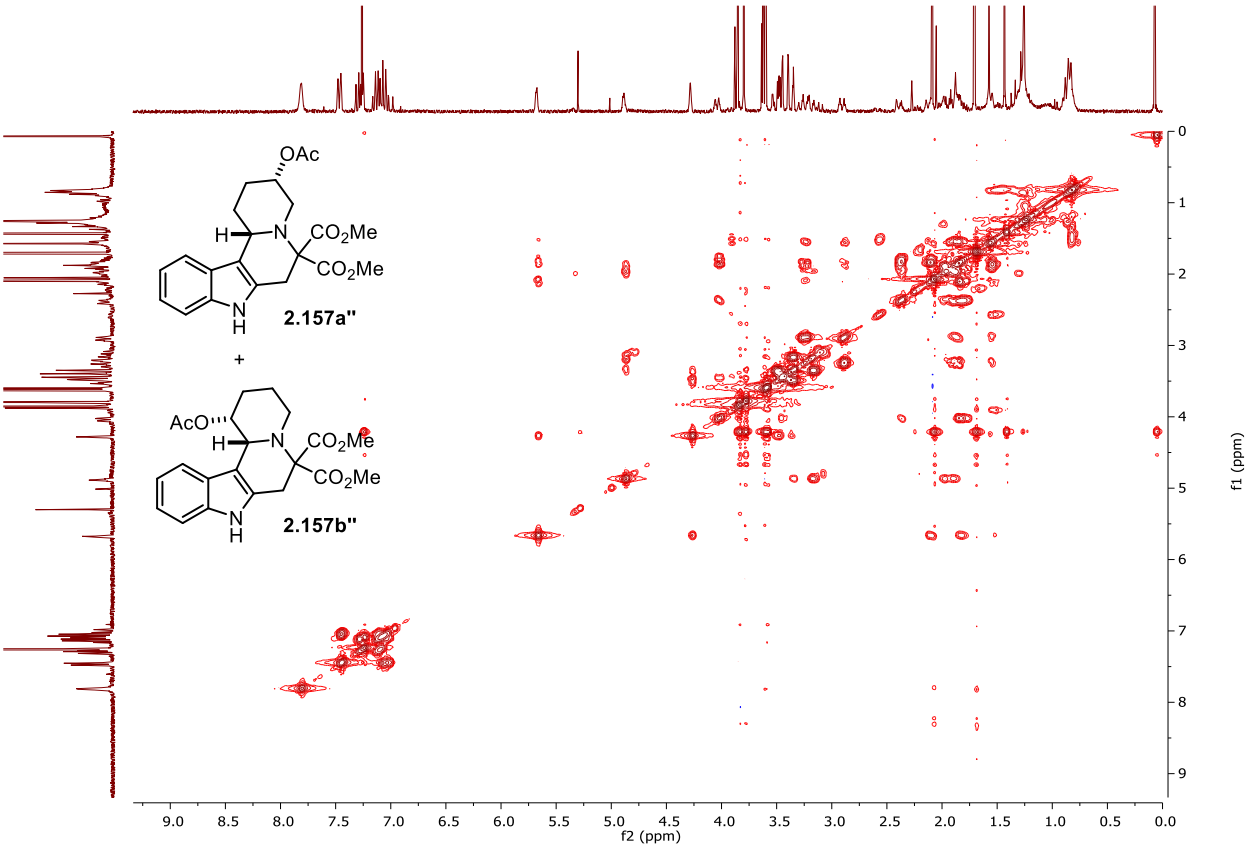

OAc
H
N
CO2Me
CO2Me
N
H
2.157a'
+
AcO
H
N
CO2Me
CO2Me
N
H
2.157b'
f1 (ppm)

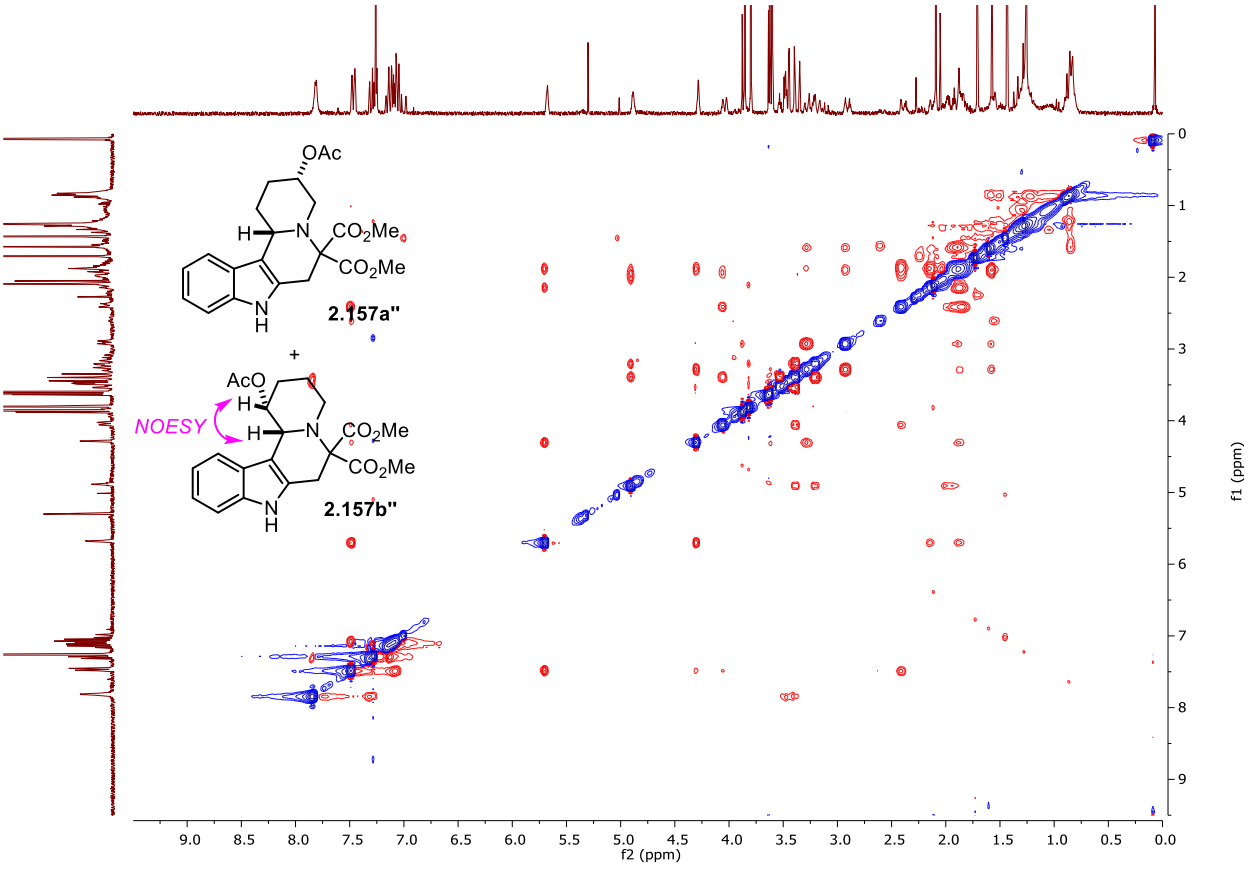

OAc
H
N
CO2Me
CO2Me
+
N
H
2.157a'
AcO
H
N
CO2Me
CO2Me
N
H
2.157b'
f1 (ppm)
f2 (ppm)

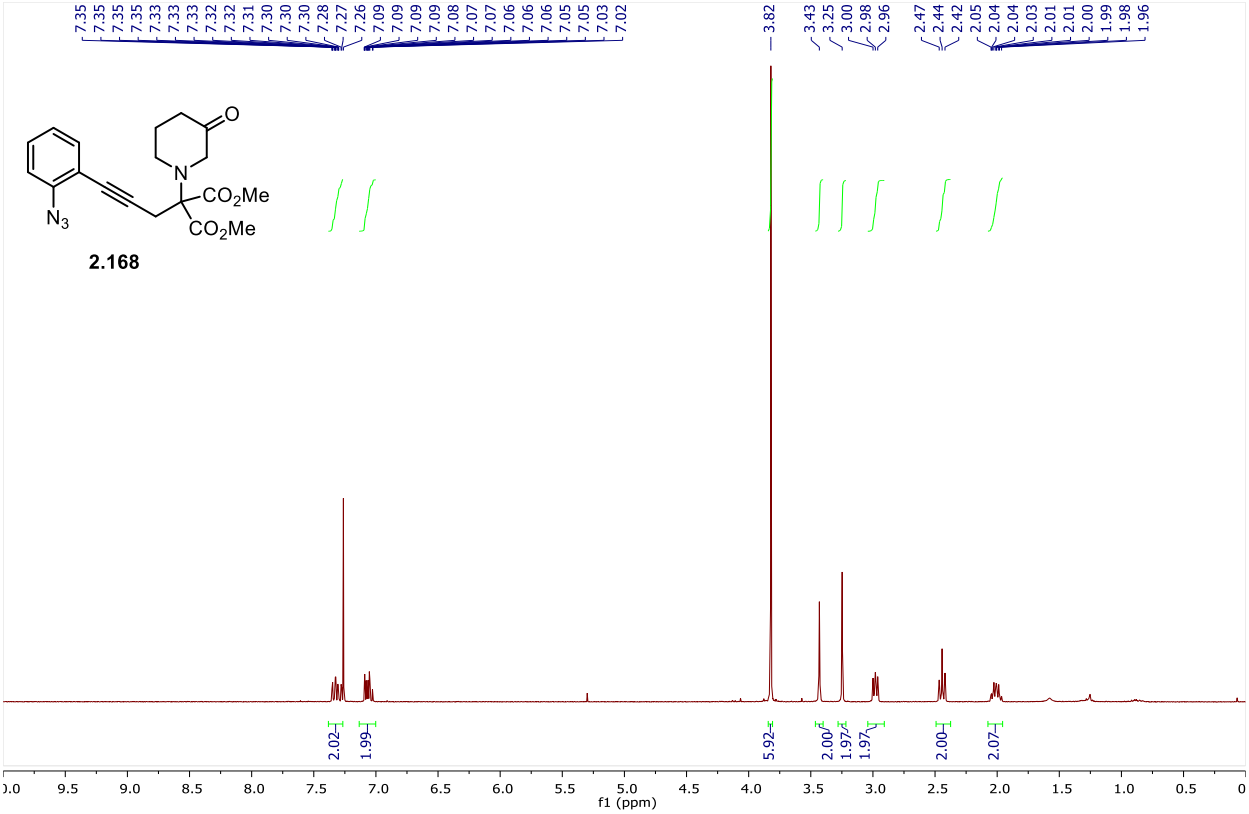

No
NOESY
H
OAc
H
N
CO2Me
CO2Me
+
N
H
2.157a'
AcO
H
N
CO2Me
CO2Me
N
H
2.157b'
f1 (ppm)
f2 (ppm)

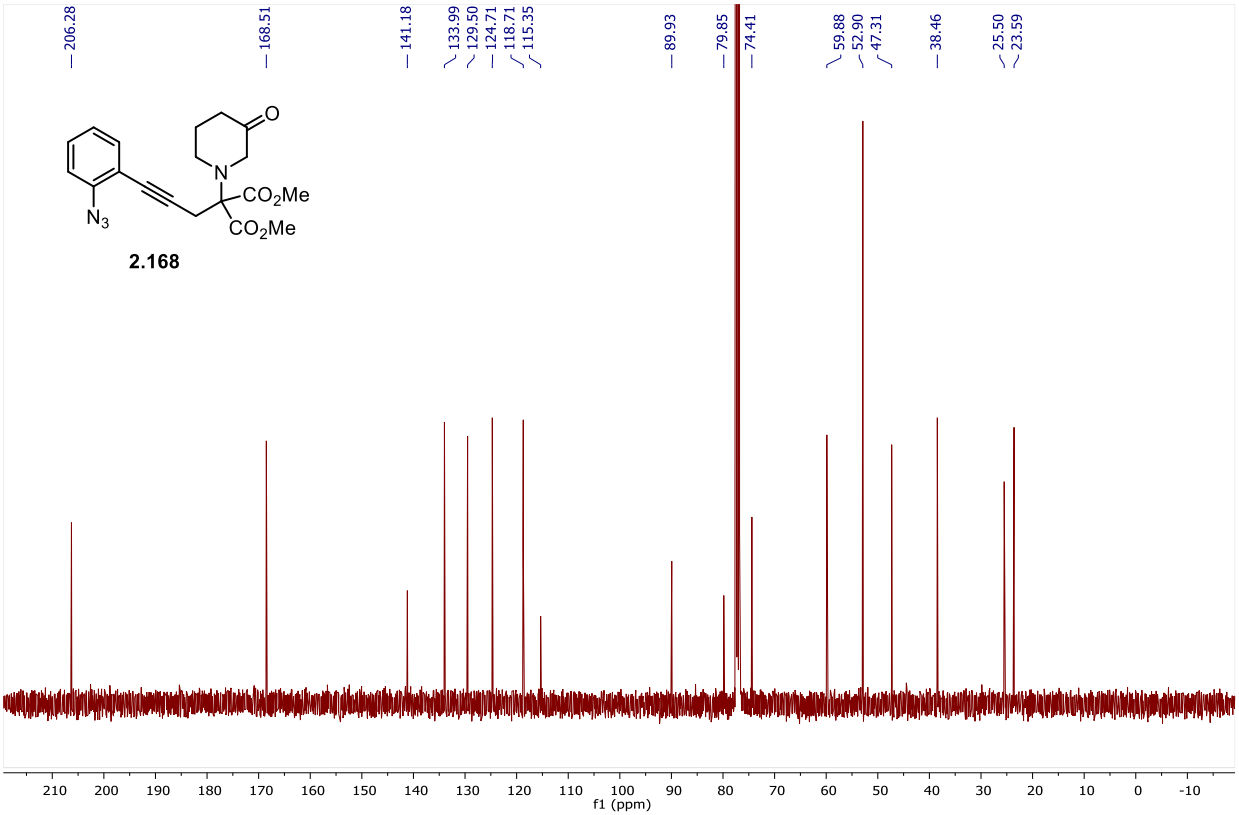

OAc
CO2Me
CO2Me
2.157a"
+
AcO
CO2Me
CO2Me
2.157b"
f1 (ppm)

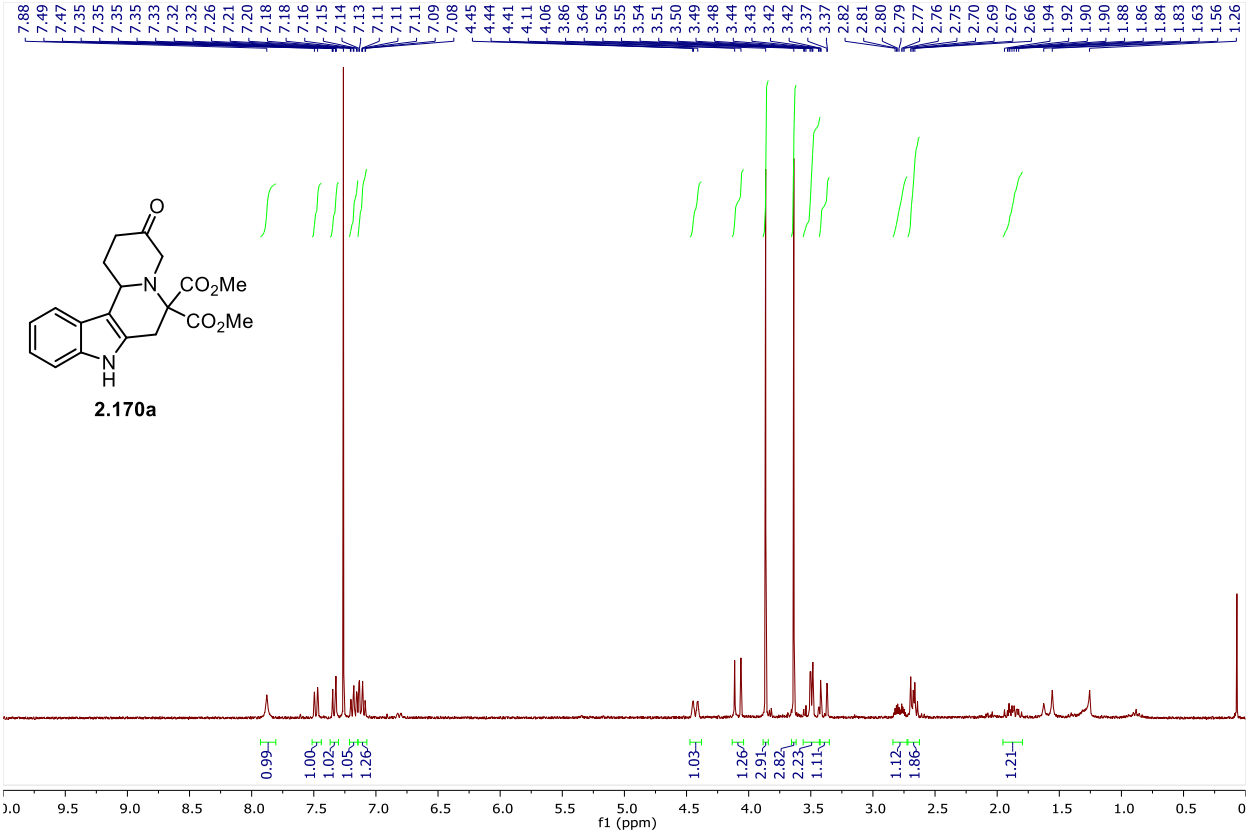

OAc
CO2Me
CO2Me
2.157a"
+
AcO
CO2Me
CO2Me
2.157b"
f1 (ppm)

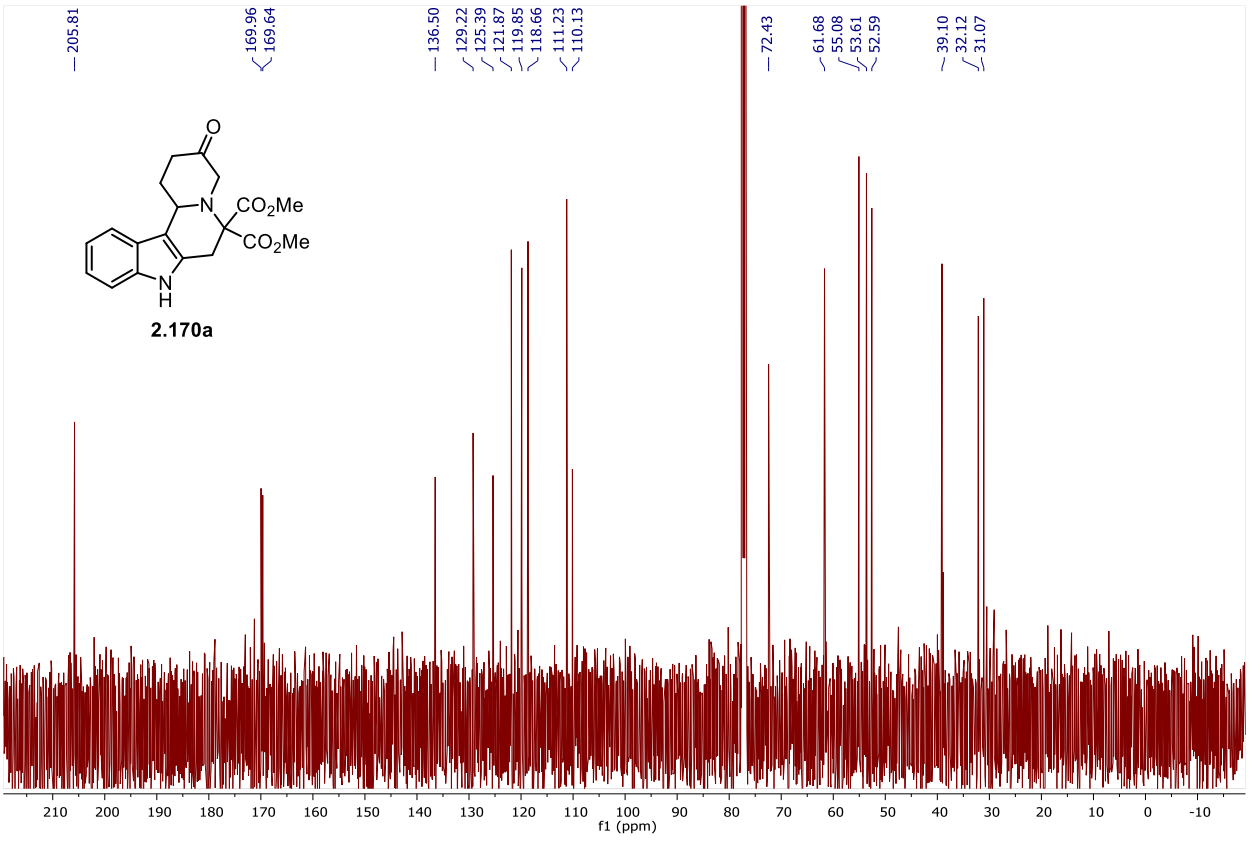

OAc
H
N
CO2Me
CO2Me
N
H
2.157a"
+
AcO
H
N
CO2Me
CO2Me
N
H
2.157b"
f2 (ppm)
f1 (ppm)

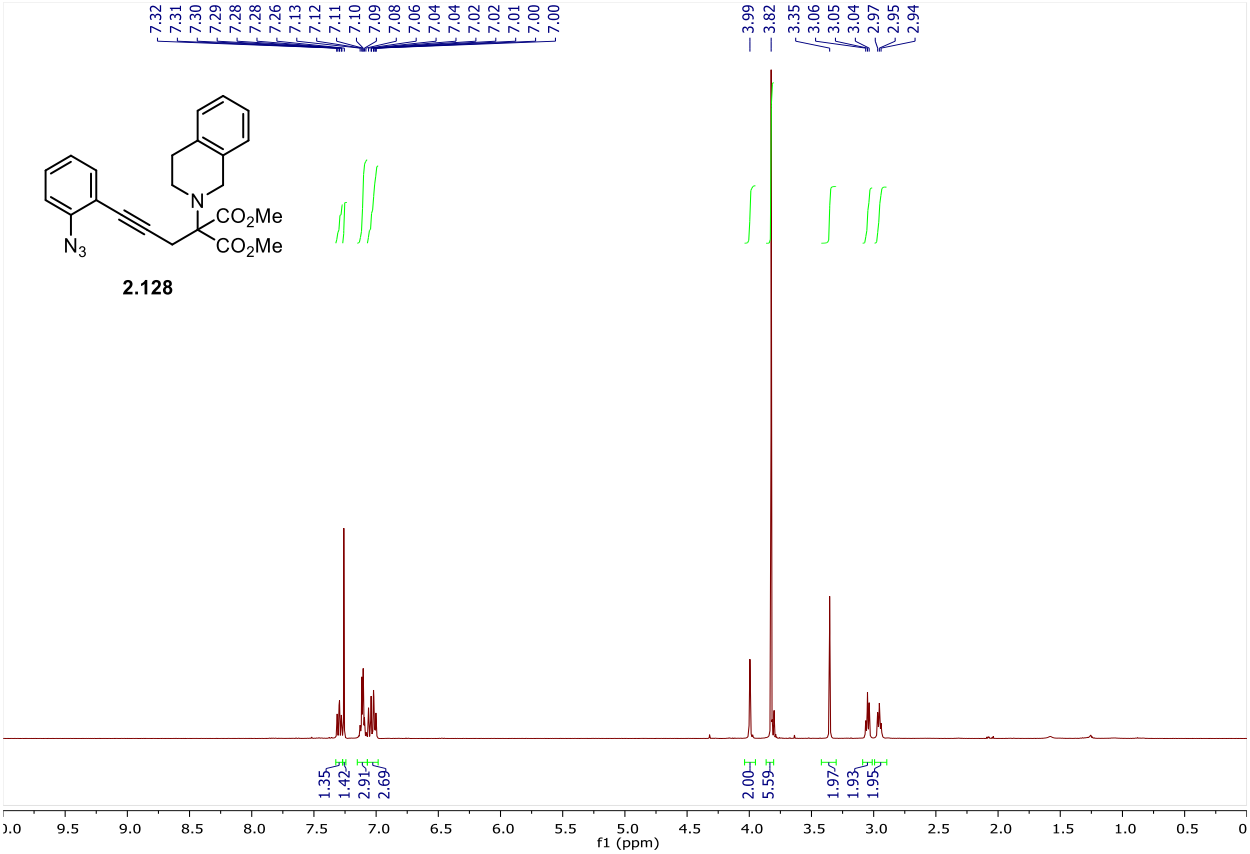

OAc
H
N
CO2Me
CO2Me
N
H
2.157a"
+
AcO
H
NOESY
H
N
CO2Me
CO2Me
N
H
2.157b"
f2 (ppm)
f1 (ppm)

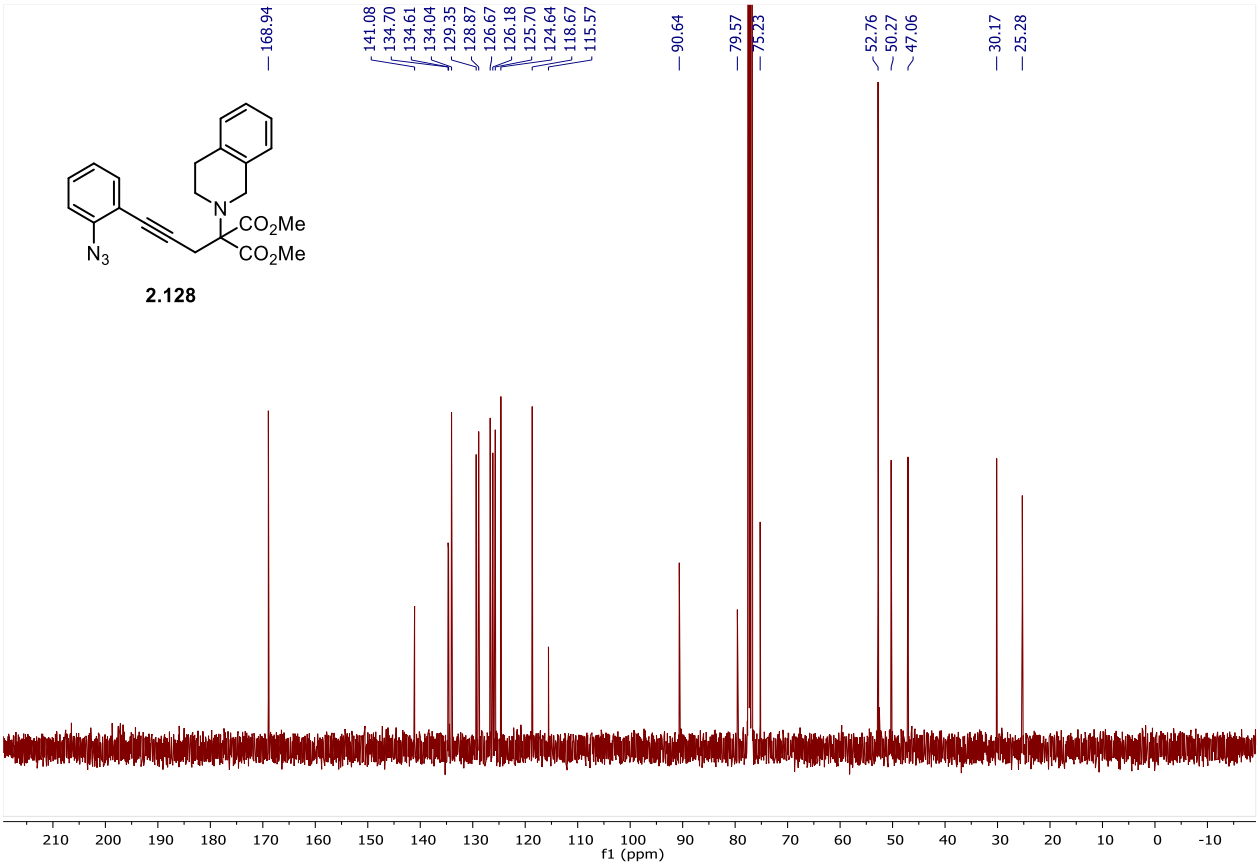

7.35 7.35 7.35 7.35 7.33 7.33 7.33 7.32 7.32 7.31 7.30 7.30 7.30 7.28 7.27 7.26 7.09 7.09 7.09 7.09 7.08 7.07 7.07 7.06 7.06 7.06 7.05 7.05 7.03 7.02
3.82 3.43 3.25 3.00 2.98 2.96 2.47 2.44 2.42 2.05 2.04 2.04 2.03 2.01 2.01 2.00 1.99 1.98 1.96
O
N
CO2Me
CO2Me
N3
2.168
2.02 1.99 5.92 2.00 1.97 1.97 2.00 2.07
f1 (ppm)

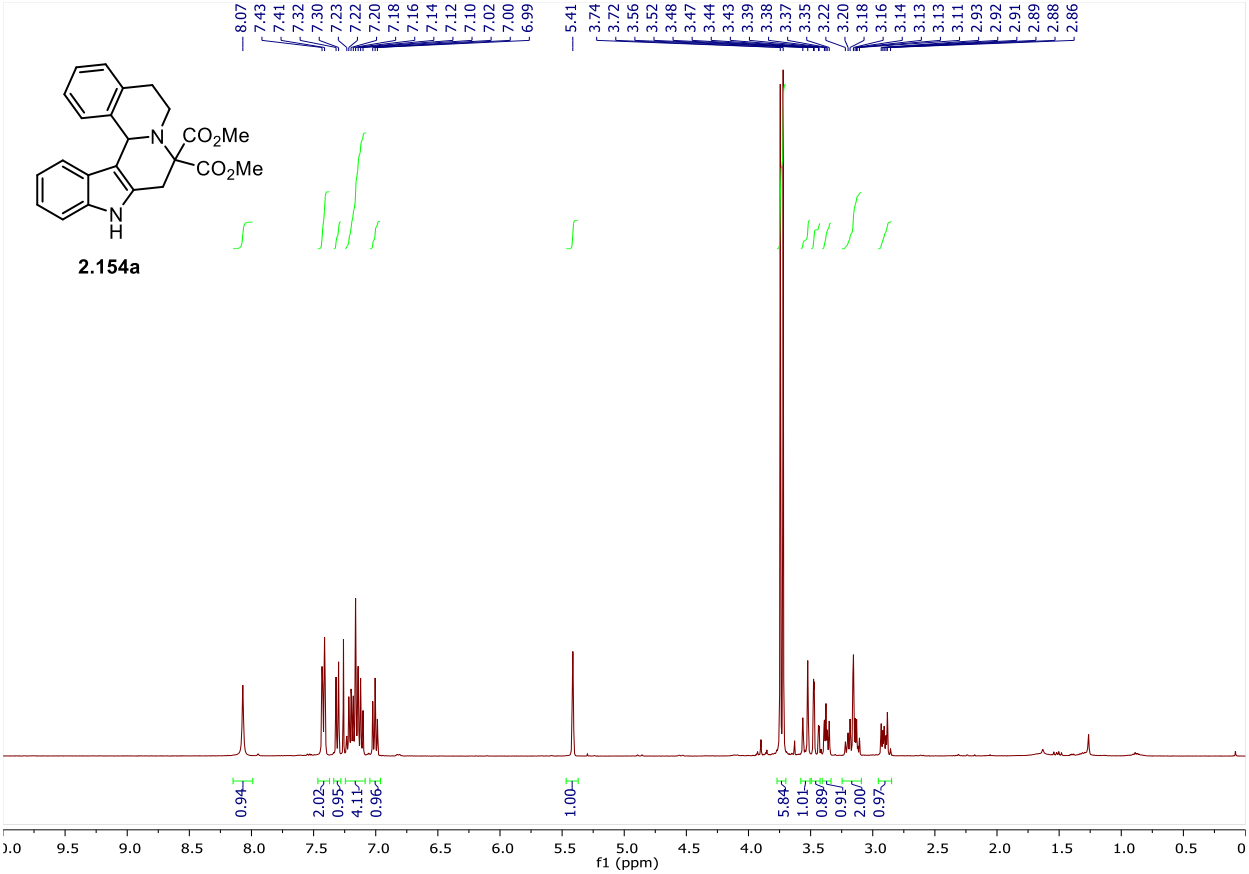

206.28 168.51 141.18 133.99 129.50 124.71 118.71 115.35 89.93 79.85 74.41 59.88 52.90 47.31 38.46 25.50 23.59
O
N
CO2Me
CO2Me
N3
2.168
f1 (ppm)

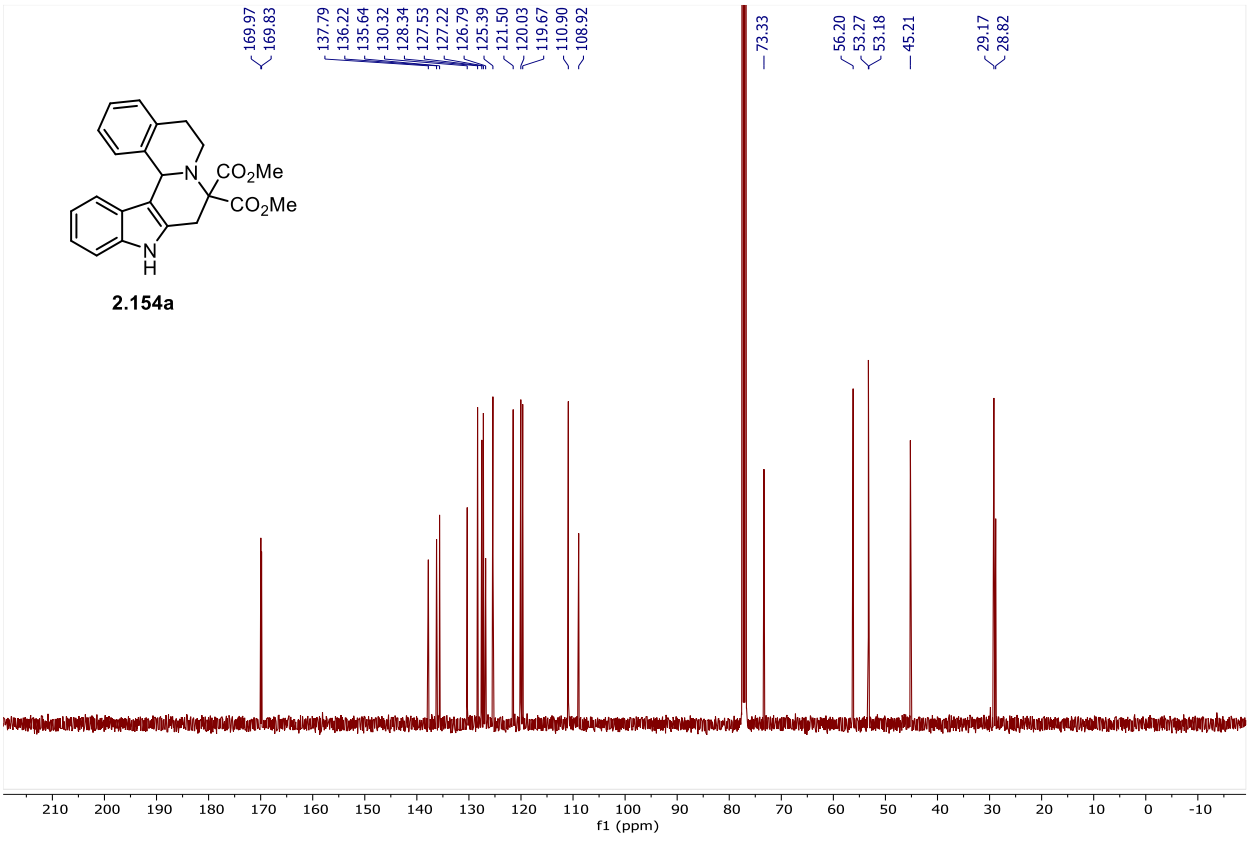

7.88 7.49 7.47 7.35 7.35 7.35 7.35 7.33 7.32 7.32 7.26 7.21 7.20 7.18 7.18 7.16 7.15 7.14 7.13 7.11 7.11 7.11 7.09 7.08
4.45 4.44 4.41 4.11 4.06 3.86 3.64 3.56 3.55 3.54 3.51 3.50 3.49 3.48 3.44 3.43 3.42 3.42 3.37 3.37
2.82 2.81 2.80 2.79 2.77 2.76 2.75 2.70 2.69 2.67 2.66 1.94 1.92 1.90 1.90 1.88 1.86 1.84 1.83 1.63 1.56 1.26
O
N
CO2Me
CO2Me
N
H
2.170a
0.99 1.00 1.02 1.05 1.26 1.03 1.26 2.91 2.82 2.23 1.11 1.12 1.86 1.21
f1 (ppm)

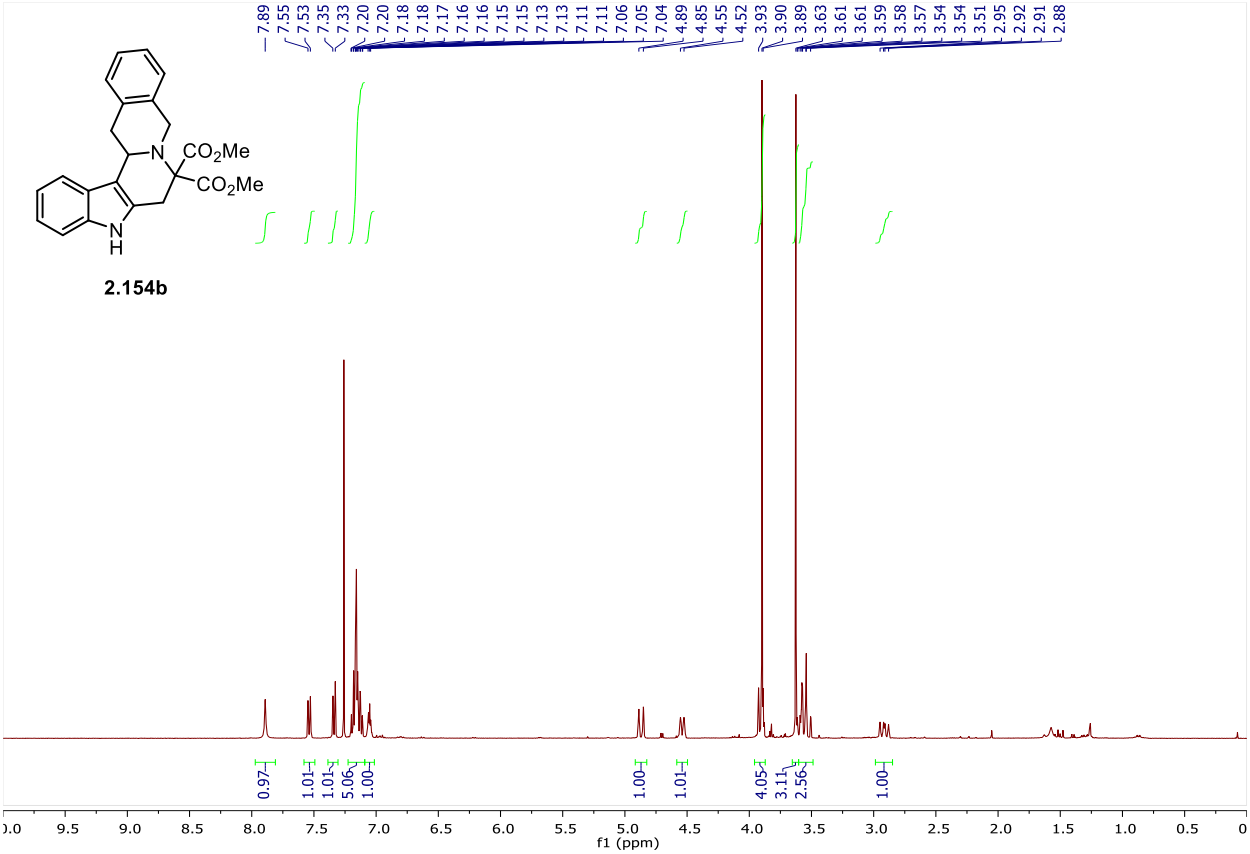

205.81
169.96 169.64
136.50 129.22 125.39 121.87 119.85 118.66 111.23 110.13
72.43
61.68 55.08 53.61 52.59
39.10 32.12 31.07
O
N
CO2Me
CO2Me
N
H
2.170a
f1 (ppm)

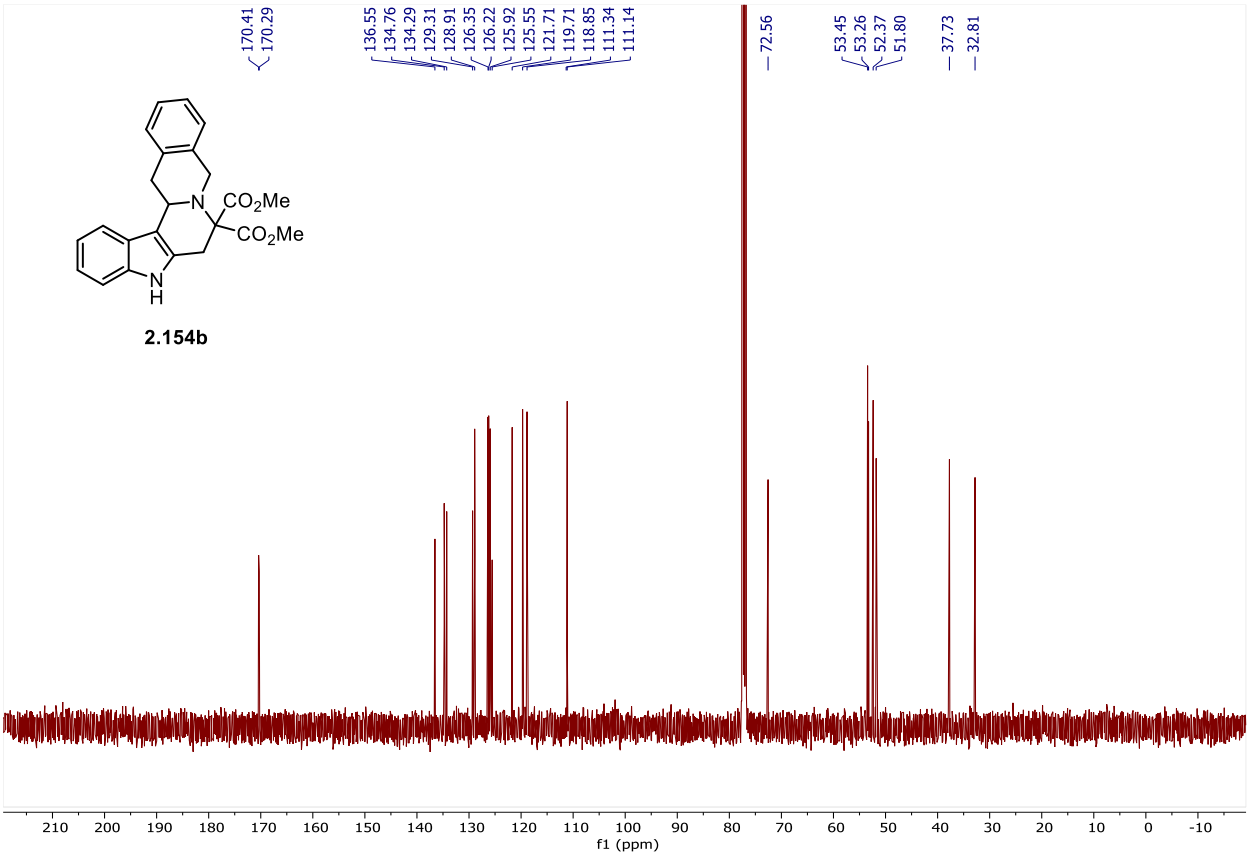

7.32
7.31
7.30
7.29
7.28
7.28
7.26
7.13
7.12
7.11
7.10
7.09
7.08
7.06
7.04
7.04
7.02
7.02
7.01
7.00
7.00
3.99
3.82
3.35
3.06
3.05
3.04
2.97
2.95
2.94
N
CO2Me
CO2Me
N3
2.128
1.35
1.42
2.91
2.69
2.00
5.59
1.97
1.93
1.95
f1 (ppm)

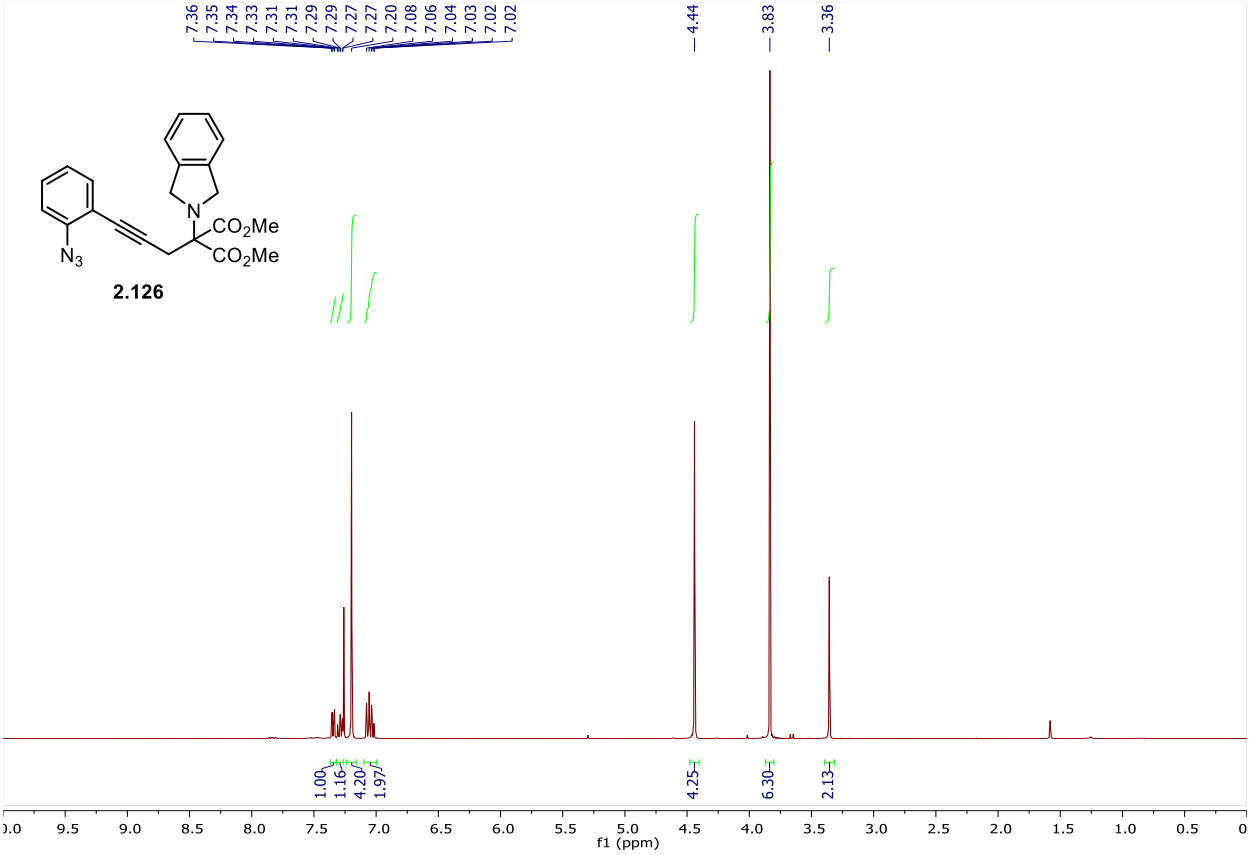

168.94
141.08
134.70
134.61
134.04
129.35
128.87
126.67
126.18
125.70
124.64
118.67
115.57
90.64
79.57
75.23
52.76
50.27
47.06
30.17
25.28
N
CO2Me
CO2Me
N3
2.128
f1 (ppm)

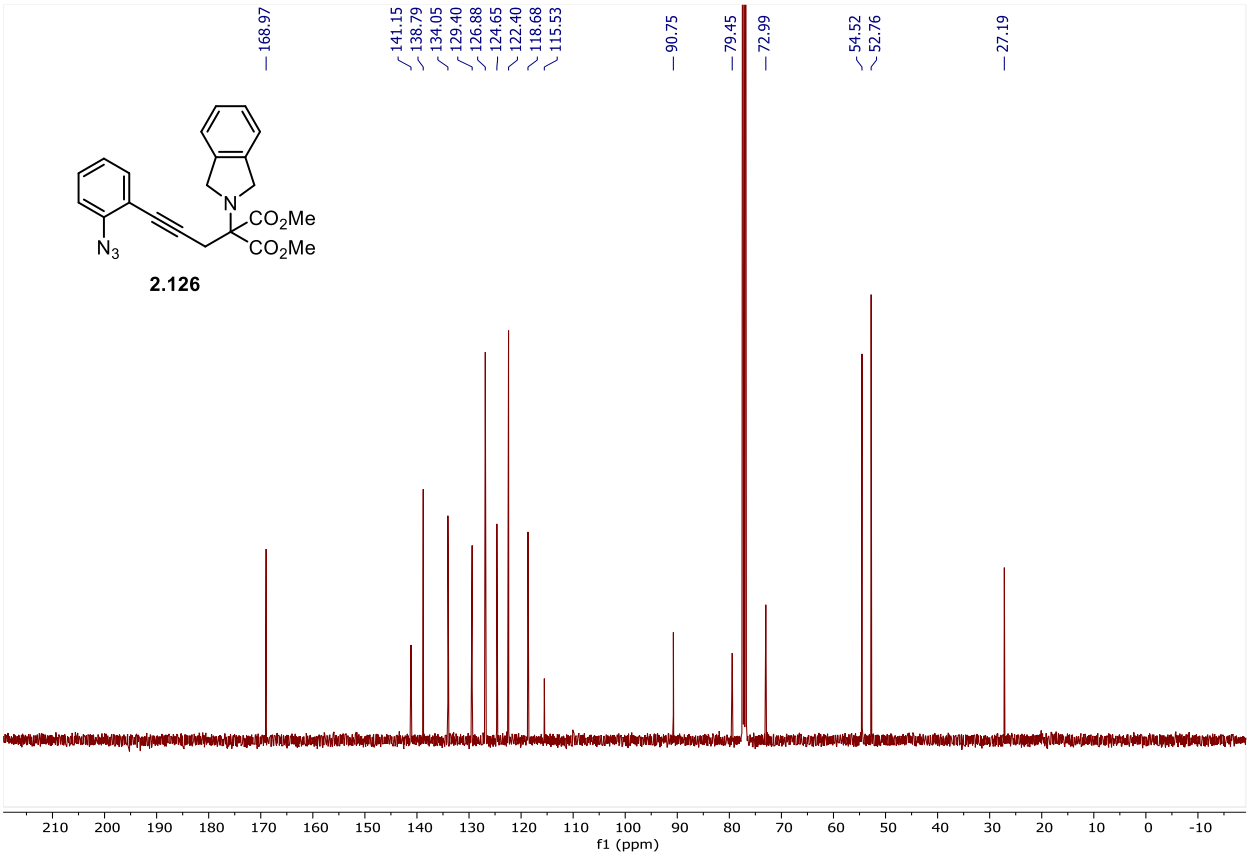

8.07
7.43
7.41
7.32
7.30
7.23
7.22
7.20
7.18
7.16
7.14
7.12
7.10
7.02
7.00
6.99
5.41
3.74
3.72
3.56
3.52
3.48
3.47
3.44
3.43
3.39
3.38
3.37
3.35
3.22
3.20
3.18
3.16
3.14
3.13
3.13
3.11
2.93
2.92
2.91
2.89
2.88
2.86
CO2Me
CO2Me
N
H
2.154a
0.94
2.02
0.95
4.11
0.96
1.00
5.84
1.01
0.89
0.91
2.00
0.97
f1 (ppm)

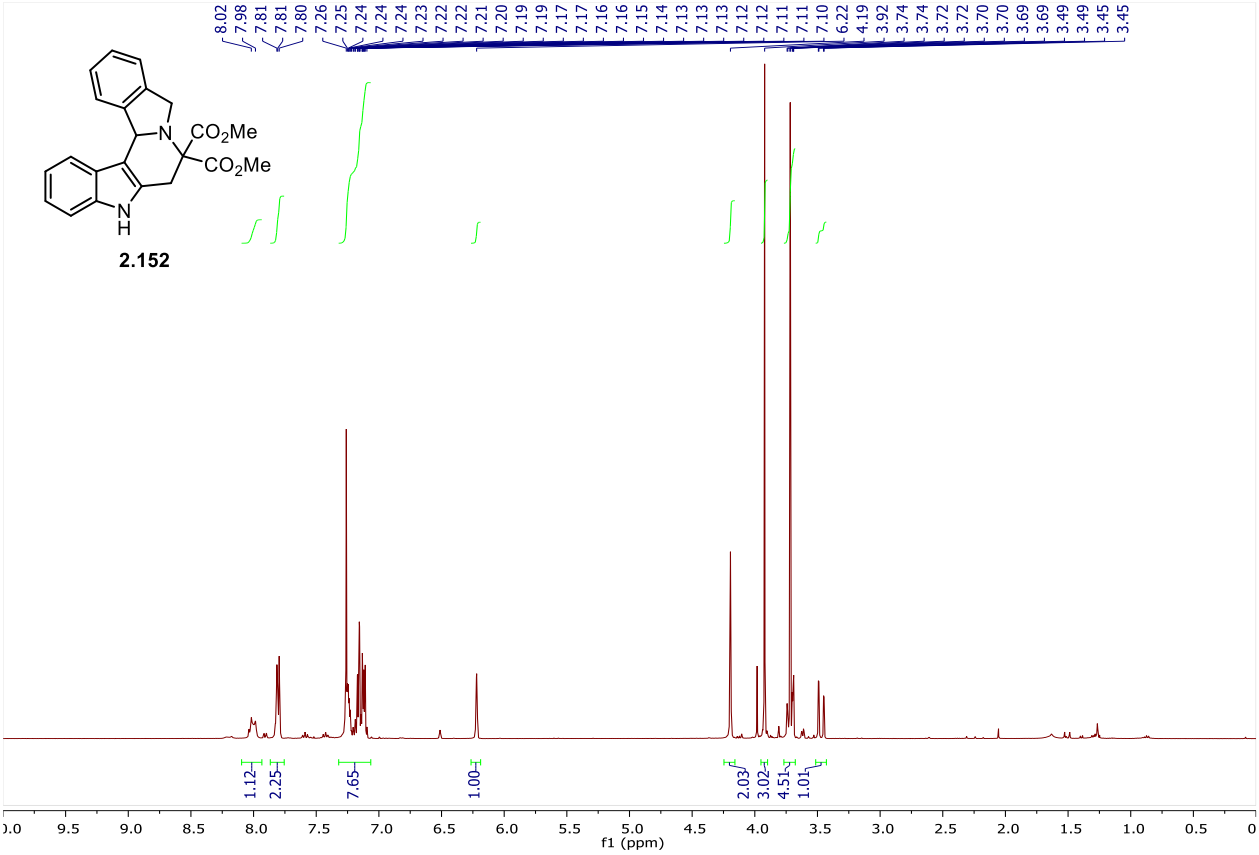

169.97
169.83
137.79
136.22
135.64
130.32
128.34
127.53
127.22
126.79
125.39
121.50
120.03
119.67
110.90
108.92
73.33
56.20
53.27
53.18
45.21
29.17
28.82
CO2Me
CO2Me
N
H
2.154a
f1 (ppm)

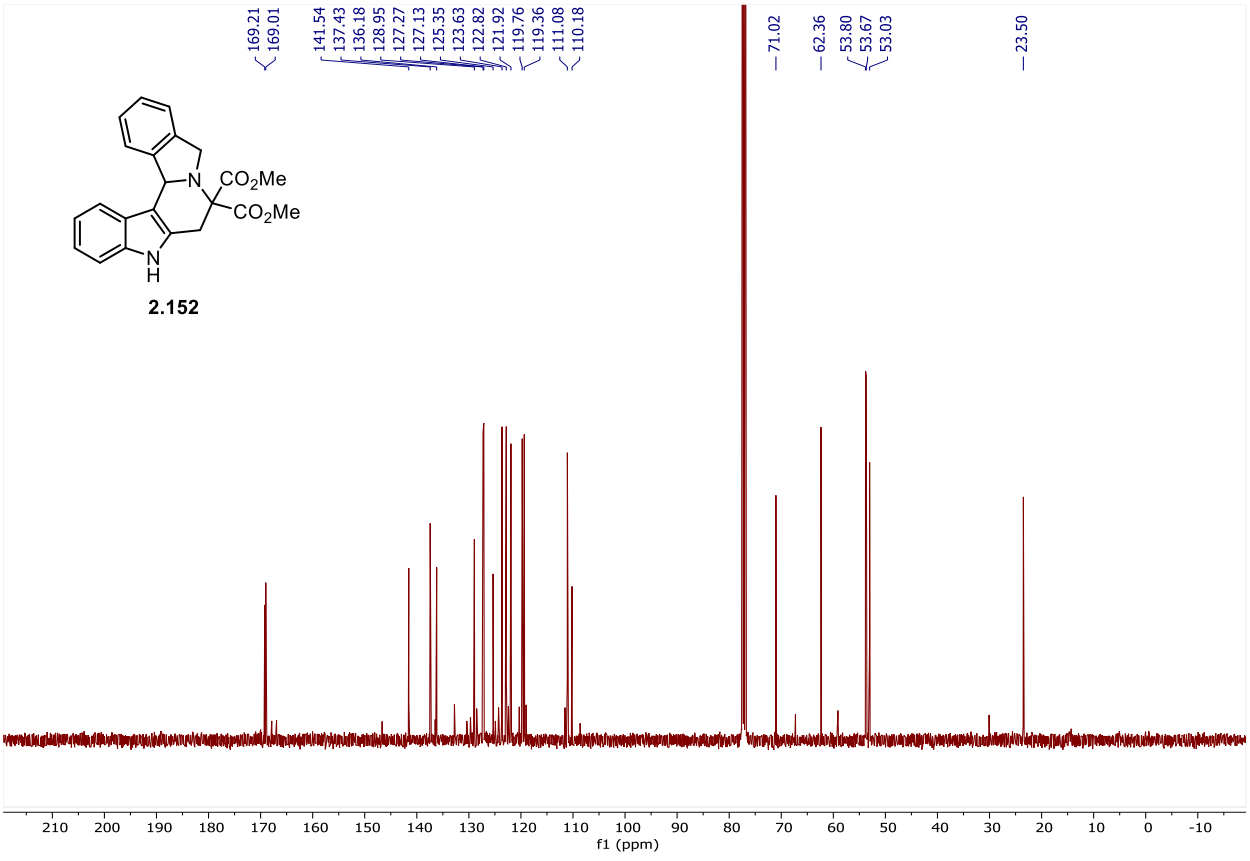

7.89
7.55
7.53
7.35
7.33
7.20
7.20
7.18
7.18
7.17
7.16
7.16
7.15
7.15
7.13
7.13
7.11
7.11
7.06
7.05
7.04
4.89
4.85
4.55
4.52
3.93
3.90
3.89
3.63
3.61
3.61
3.59
3.58
3.57
3.54
3.54
3.51
2.95
2.92
2.91
2.88
CO2Me
CO2Me
N
H
2.154b
0.97
1.01
1.01
5.06
1.00
1.00
1.01
4.05
3.11
2.56
1.00
f1 (ppm)

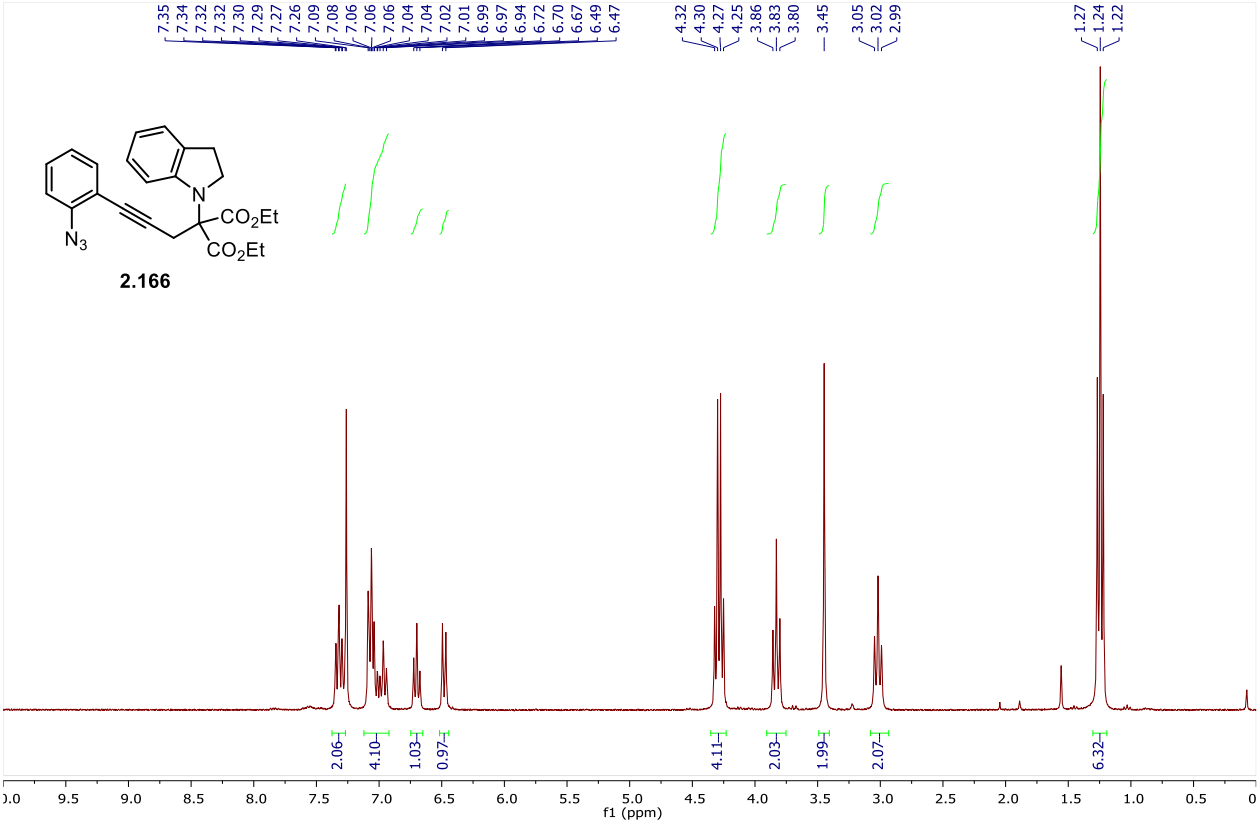

170.41
170.29
136.55
134.76
134.29
129.31
128.91
126.35
126.22
125.92
125.55
121.71
119.71
118.85
111.34
111.14
72.56
53.45
53.26
52.37
51.80
37.73
32.81
CO2Me
CO2Me
N
H
2.154b
f1 (ppm)

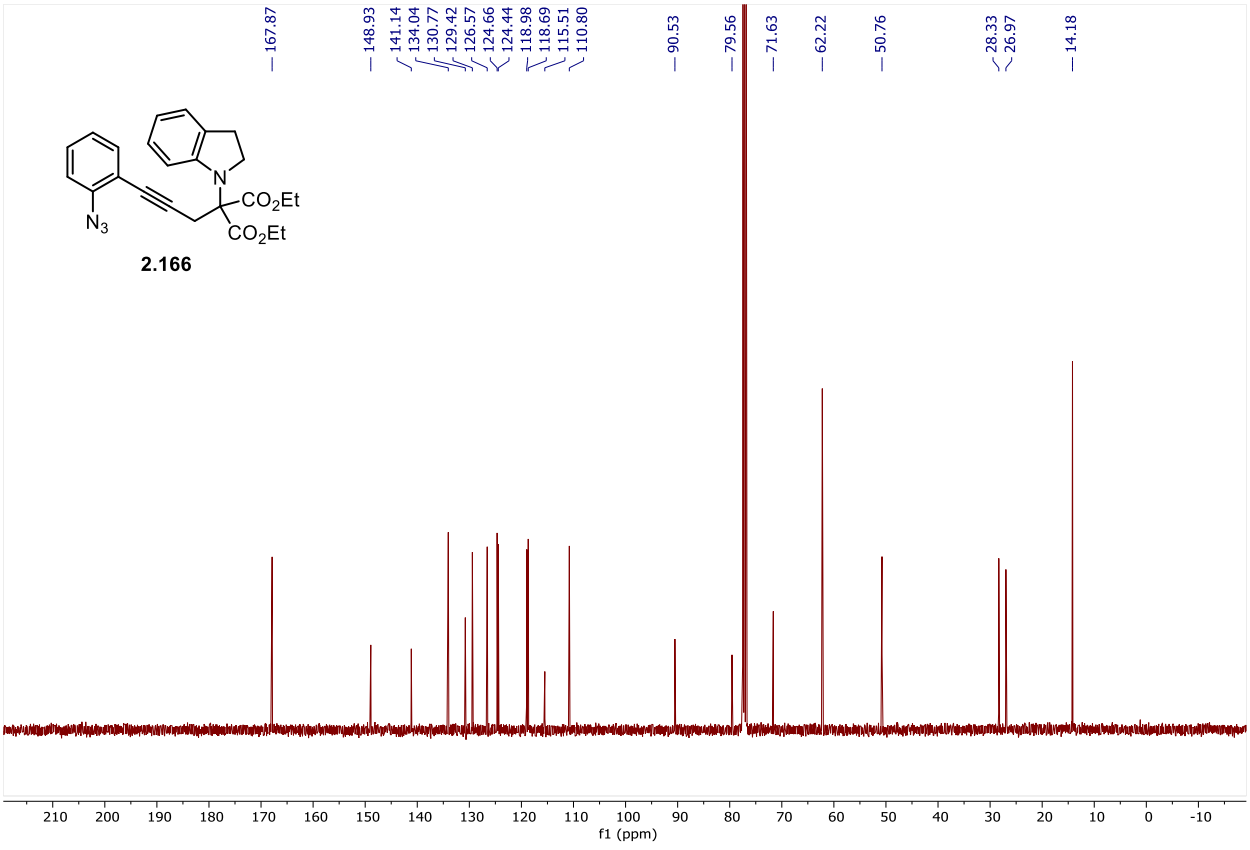

7.36
7.35
7.34
7.33
7.31
7.31
7.29
7.29
7.27
7.27
7.20
7.08
7.06
7.04
7.03
7.02
7.02
4.44
3.83
3.36
N
CO2Me
CO2Me
N3
2.126
1.00
1.16
4.20
1.97
4.25
6.30
2.13
f1 (ppm)

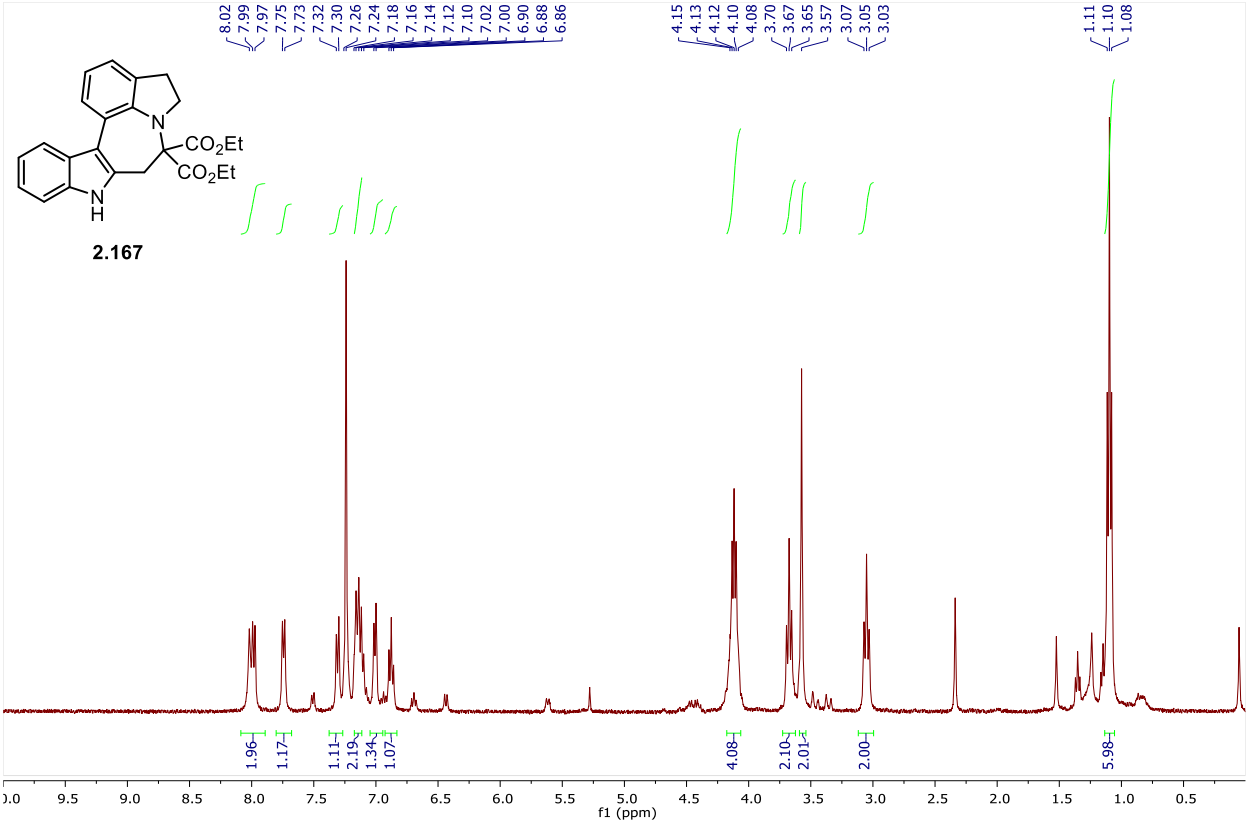

168.97
141.15
138.79
134.05
129.40
126.88
124.65
122.40
118.68
115.53
90.75
79.45
72.99
54.52
52.76
27.19
N
CO2Me
CO2Me
N3
2.126
f1 (ppm)

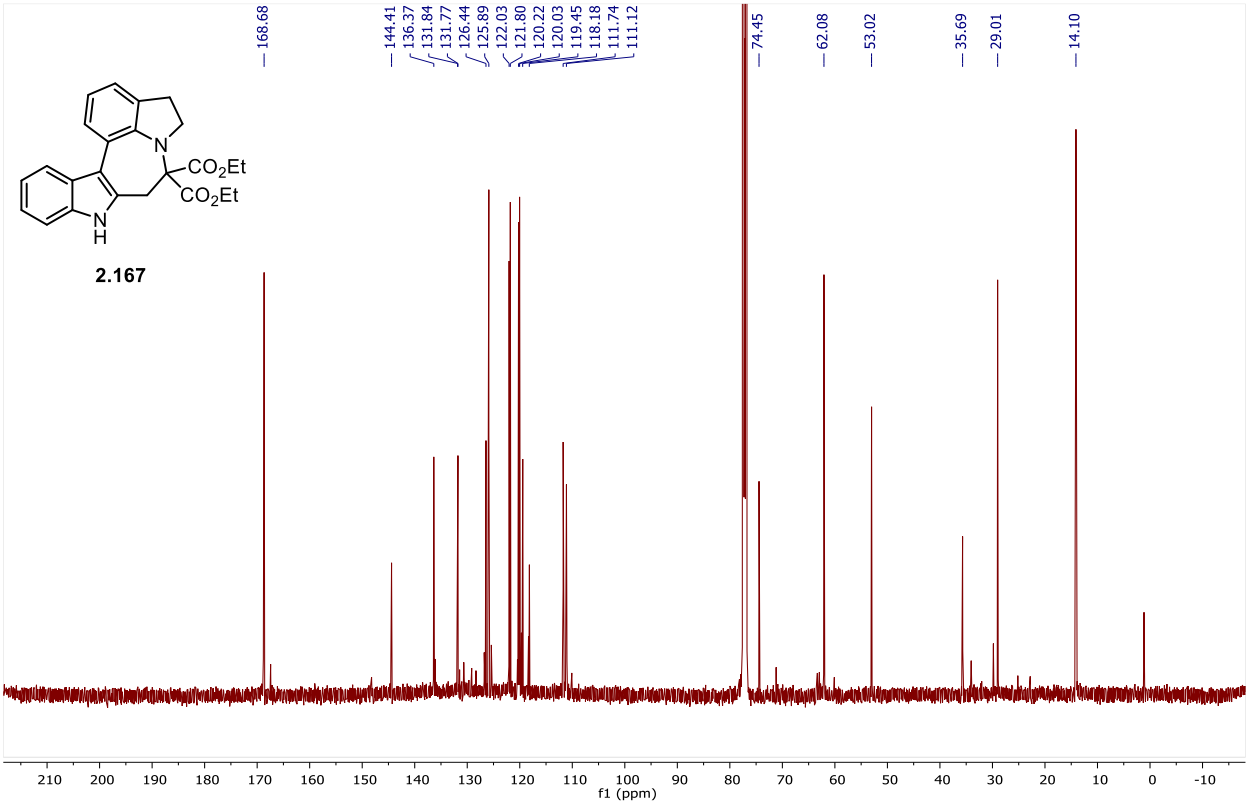

8.02 7.98 7.81 7.81 7.80 7.26 7.25 7.24 7.24 7.24 7.23 7.22 7.22 7.21 7.20 7.19 7.19 7.17 7.17 7.16 7.16 7.15 7.14 7.13 7.13 7.13 7.12 7.12 7.11 7.11 7.10 6.22 4.19 3.92 3.74 3.74 3.72 3.70 3.70 3.69 3.69 3.49 3.49 3.45 3.45
CO2Me
CO2Me
N
H
2.152
1.12 2.25 7.65 1.00 2.03 3.02 4.51 1.01
f1 (ppm)

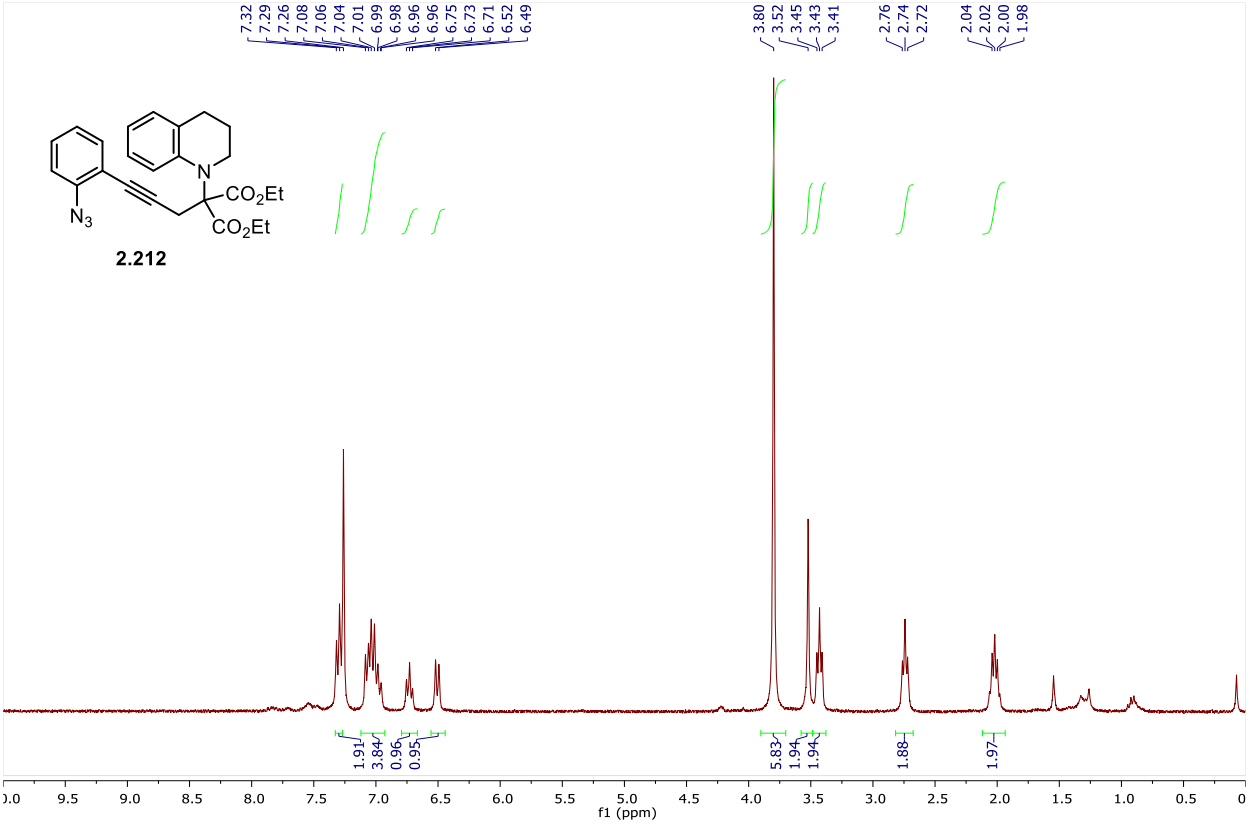

169.21 169.01 141.54 137.43 136.18 128.95 127.27 127.13 125.35 123.63 122.82 121.92 119.76 119.36 111.08 110.18 71.02 62.36 53.80 53.67 53.03 23.50
CO2Me
CO2Me
N
H
2.152
f1 (ppm)

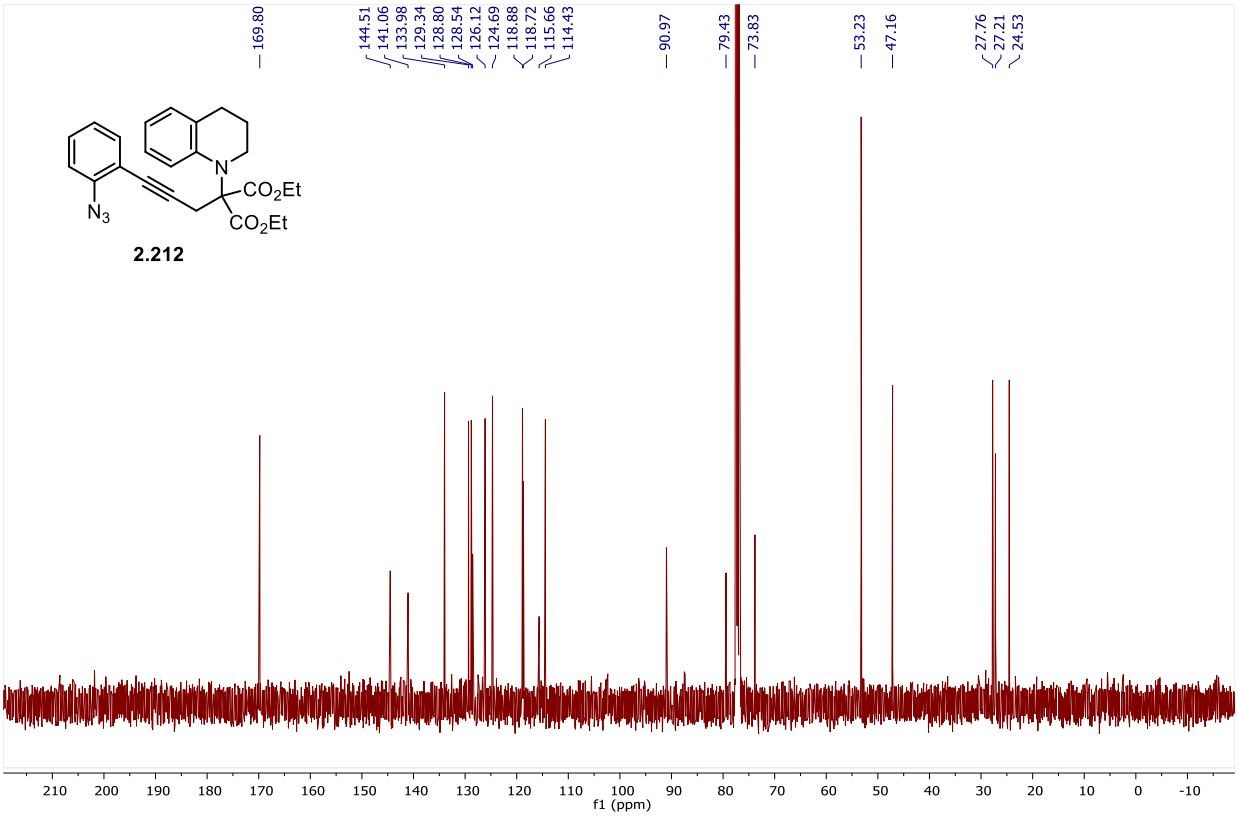

7.35
7.34
7.32
7.32
7.30
7.29
7.27
7.26
7.09
7.08
7.06
7.06
7.06
7.04
7.04
7.02
7.01
6.99
6.97
6.94
6.72
6.70
6.67
6.49
6.47
4.32
4.30
4.27
4.25
3.86
3.83
3.80
3.45
3.05
3.02
2.99
1.27
1.24
1.22
N
CO2Et
CO2Et
N3
2.166
2.06
4.10
1.03
0.97
4.11
2.03
1.99
2.07
6.32
f1 (ppm)

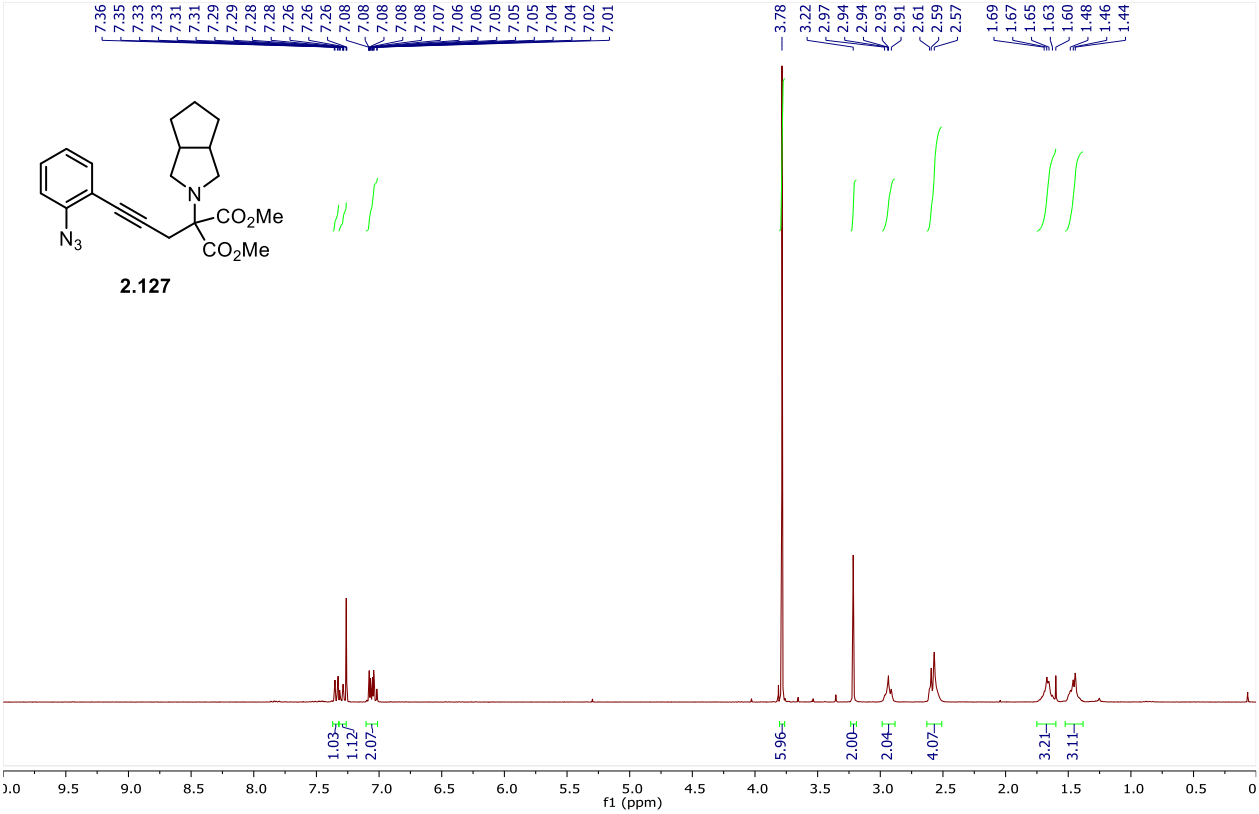

167.87
148.93
141.14
134.04
130.77
129.42
126.57
124.66
124.44
118.98
118.69
115.51
110.80
90.53
79.56
71.63
62.22
50.76
28.33
26.97
14.18
N
CO2Et
CO2Et
N3
2.166
f1 (ppm)

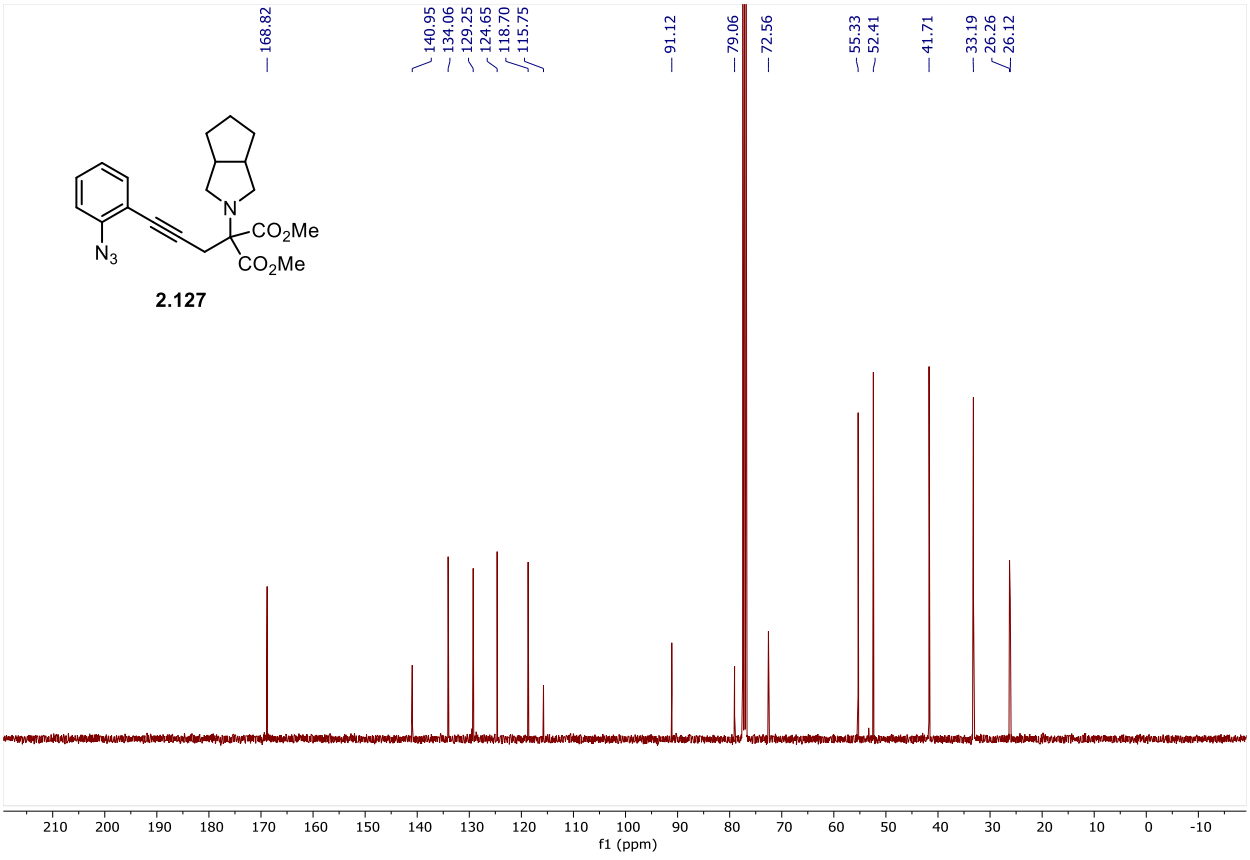

8.02
7.99
7.97
7.75
7.73
7.32
7.30
7.26
7.24
7.18
7.16
7.14
7.12
7.10
7.02
7.00
6.90
6.88
6.86
4.15
4.13
4.12
4.10
4.08
3.70
3.67
3.65
3.57
3.07
3.05
3.03
1.11
1.10
1.08
CO2Et
CO2Et
N
H
2.167
1.96
1.17
1.11
2.19
1.34
1.07
4.08
2.10
2.01
2.00
5.98
f1 (ppm)

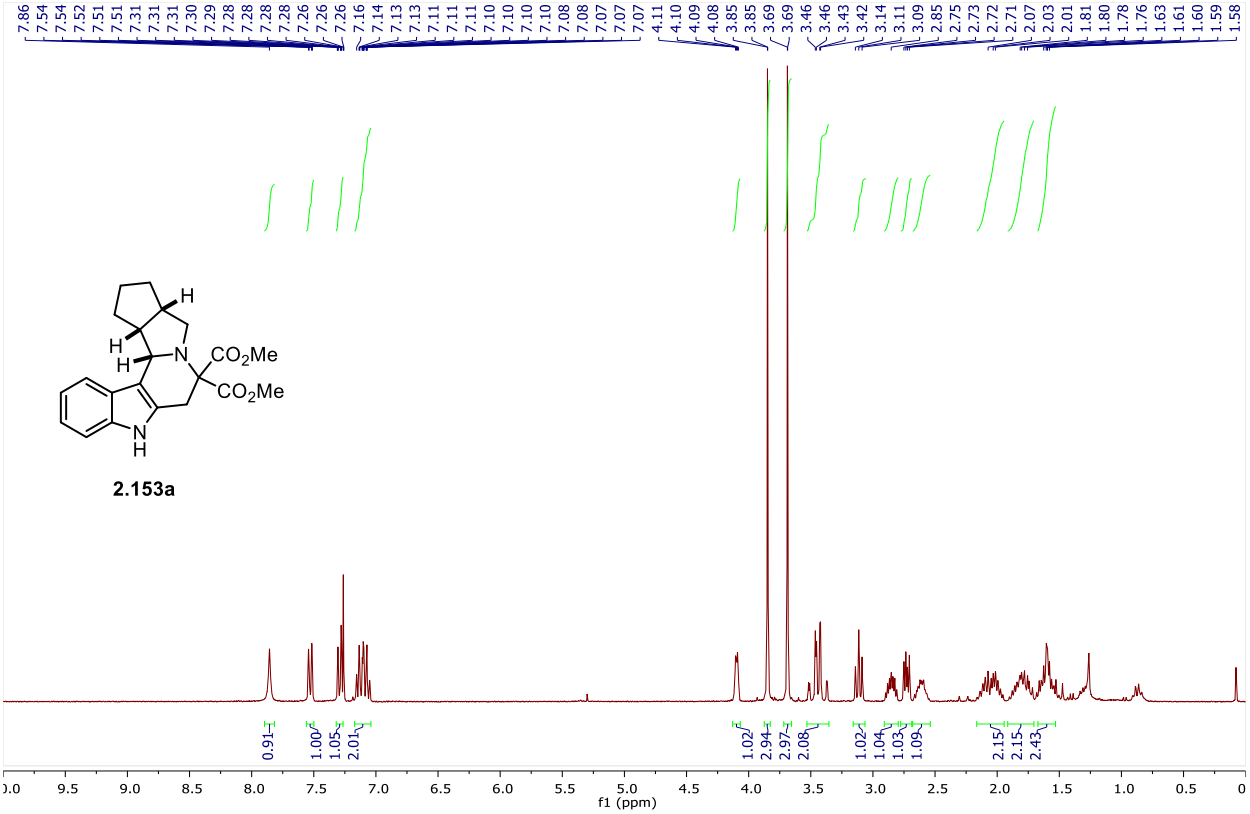

168.68
144.41
136.37
131.84
131.77
126.44
125.89
122.03
121.80
120.22
120.03
119.45
118.18
111.74
111.12
74.45
62.08
53.02
35.69
29.01
14.10
CO2Et
CO2Et
N
H
2.167
f1 (ppm)

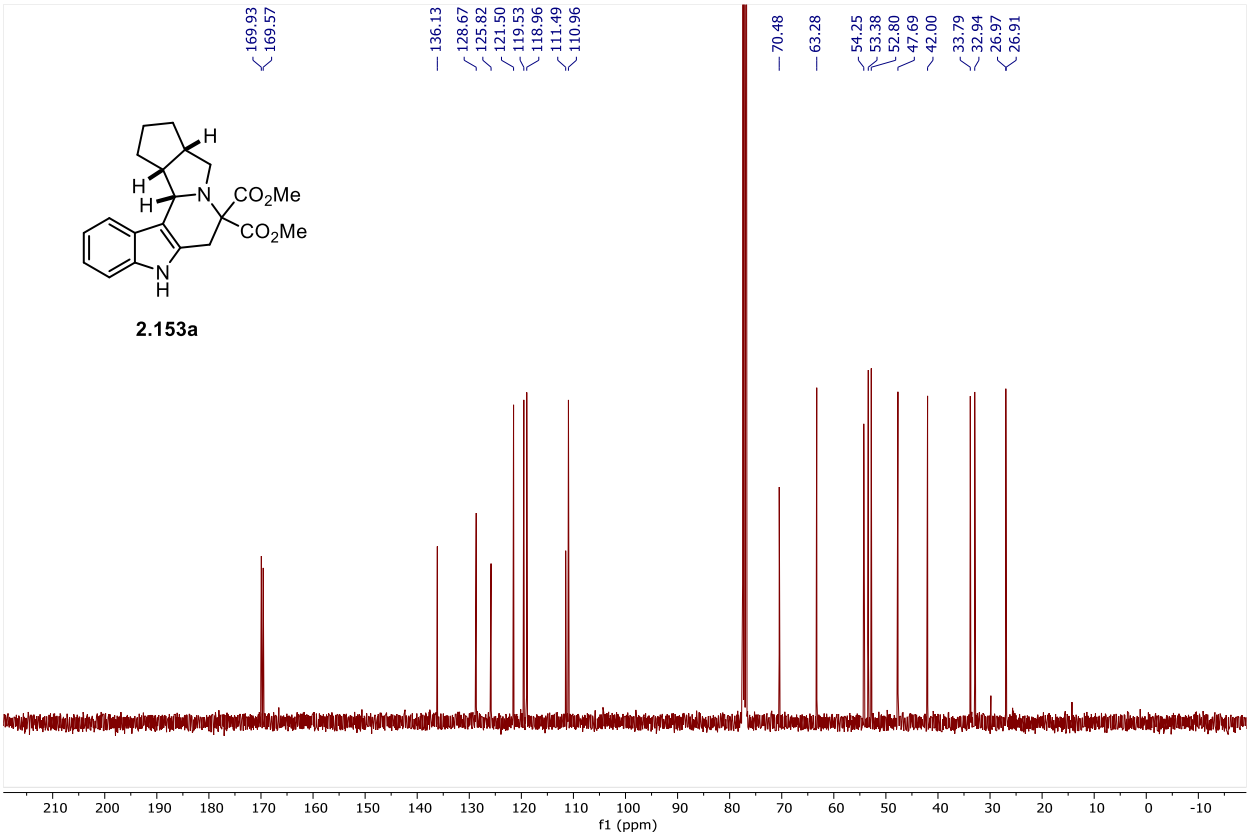

7.32
7.29
7.26
7.08
7.06
7.04
7.01
6.99
6.98
6.96
6.96
6.75
6.73
6.71
6.52
6.49
3.80
3.52
3.45
3.43
3.41
2.76
2.74
2.72
2.04
2.02
2.00
1.98
N
CO2Et
CO2Et
N3
2.212
1.91
3.84
0.96
0.95
5.83
1.94
1.94
1.88
1.97
f1 (ppm)

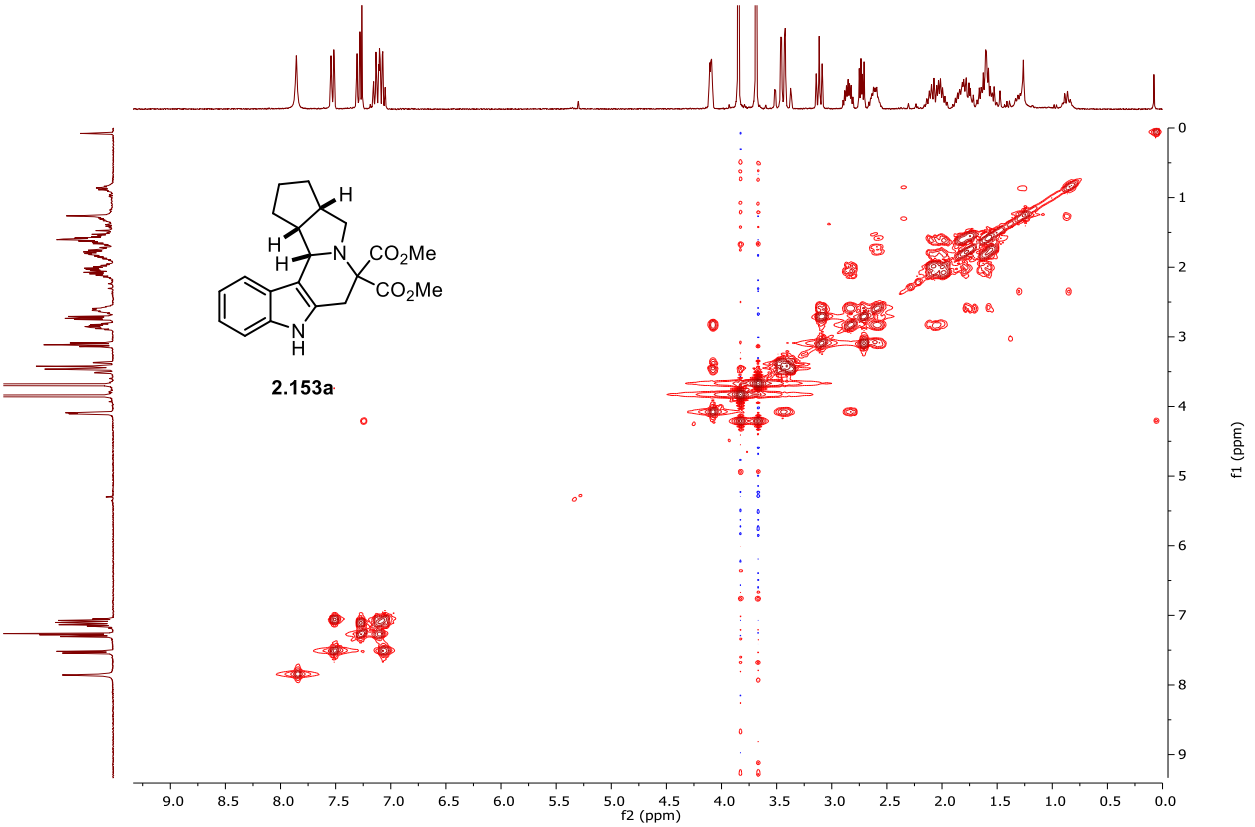

169.80
144.51
141.06
133.98
129.34
128.80
128.54
126.12
124.69
118.88
118.72
115.66
114.43
90.97
79.43
73.83
53.23
47.16
27.76
27.21
24.53
N
CO2Et
CO2Et
N3
2.212
f1 (ppm)

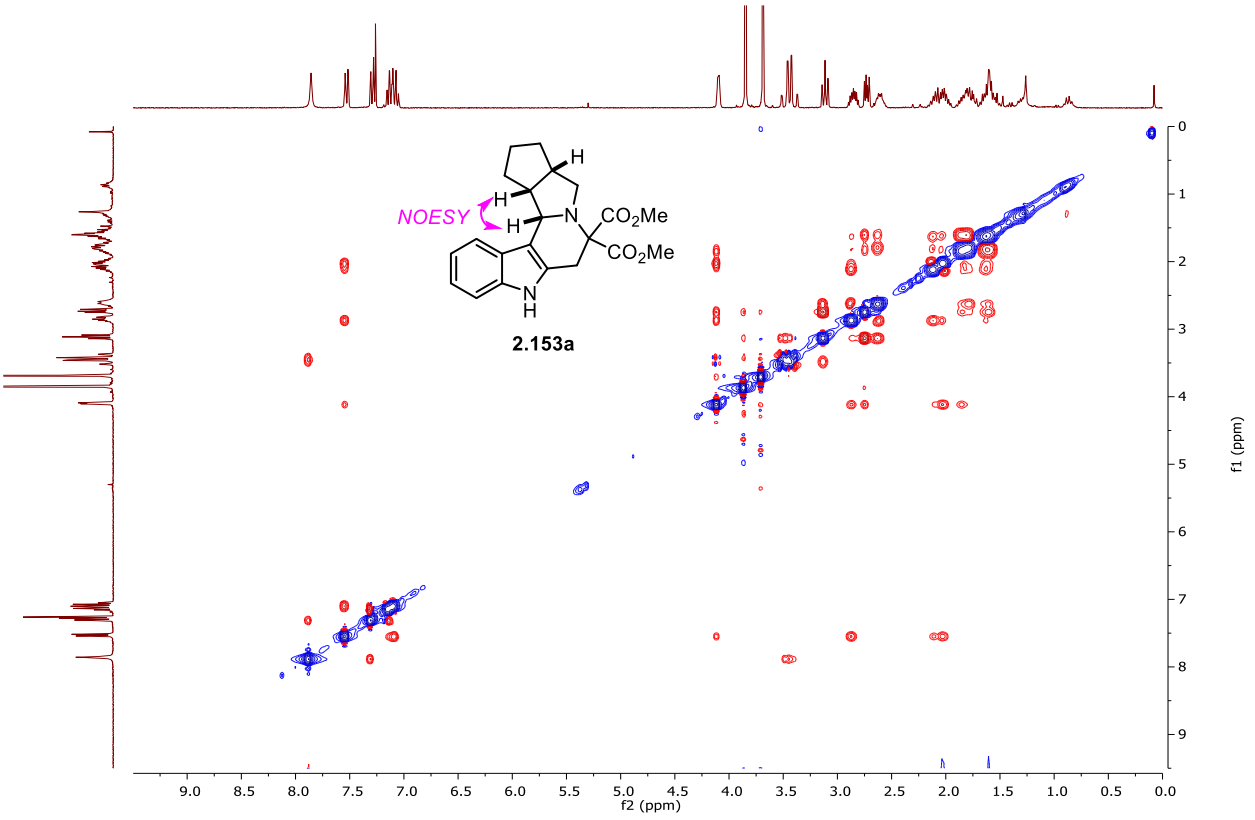

7.36 7.35 7.33 7.33 7.31 7.31 7.29 7.29 7.28 7.28 7.26 7.26 7.26 7.08 7.08 7.08 7.08 7.08 7.07 7.06 7.06 7.05 7.05 7.05 7.04 7.04 7.02 7.01
3.78 3.22 2.97 2.94 2.94 2.93 2.91 2.61 2.59 2.57 1.69 1.67 1.65 1.63 1.60 1.48 1.46 1.44
1.03 1.12 2.07 5.96 2.00 2.04 4.07 3.21 3.11
f1 (ppm)
2.127

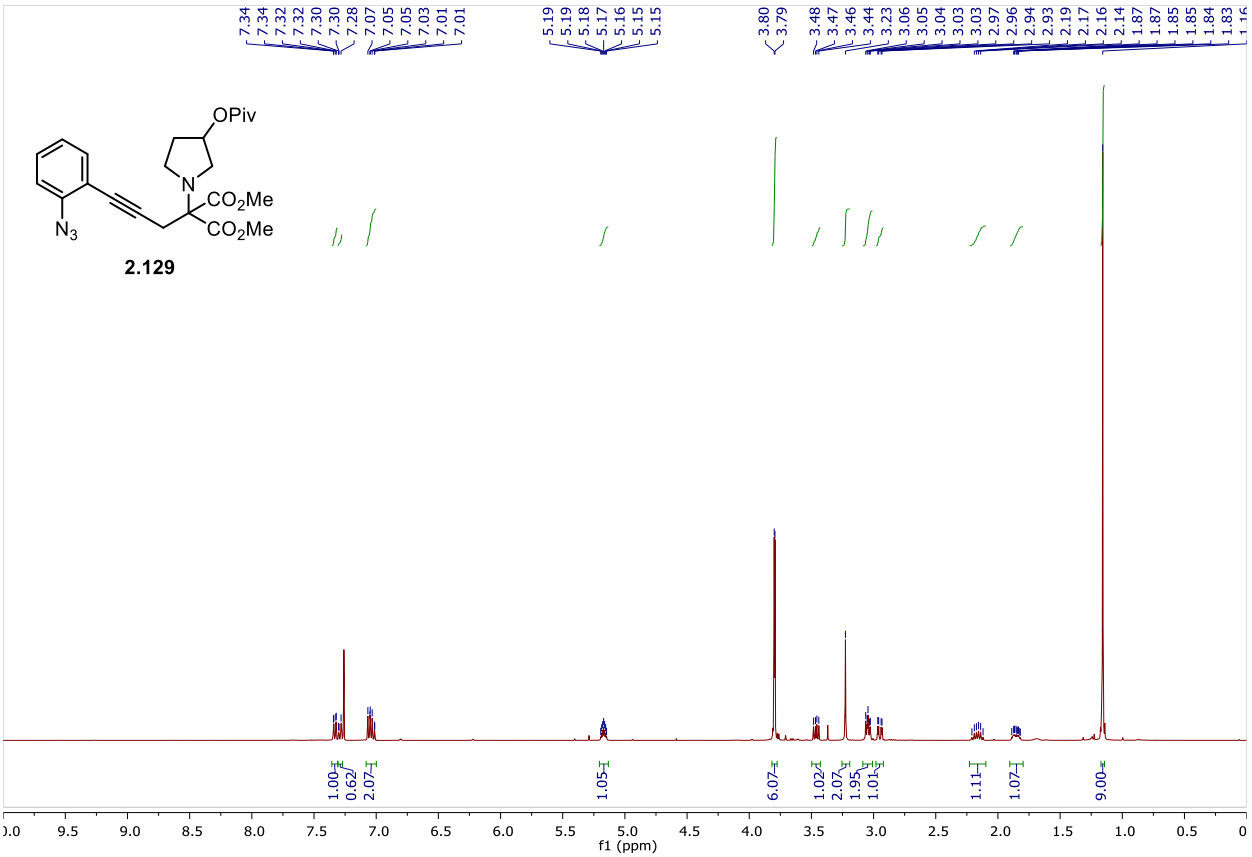

168.82 140.95 134.06 129.25 124.65 118.70 115.75 91.12 79.06 72.56 55.33 52.41 41.71 33.19 26.26 26.12
f1 (ppm)
2.127

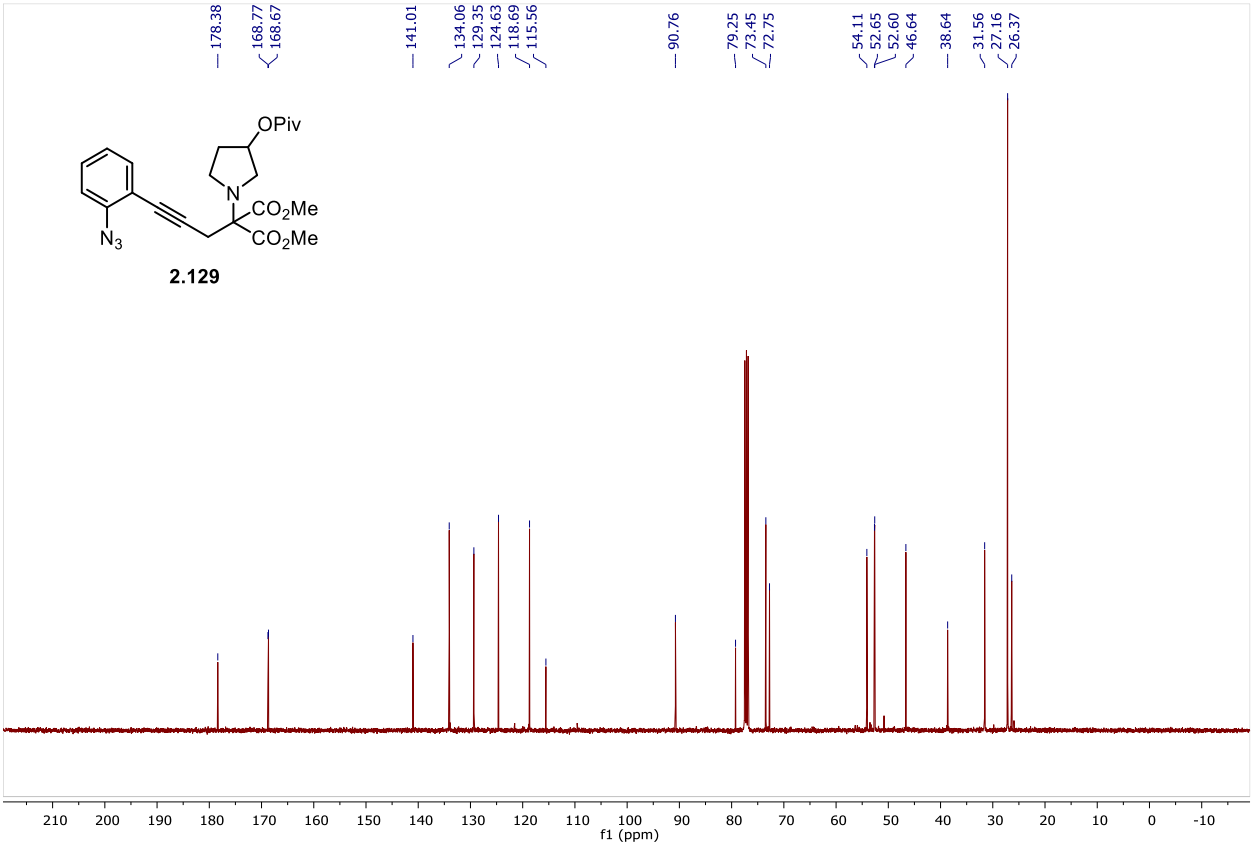

7.86 7.54 7.54 7.52 7.51 7.51 7.31 7.31 7.31 7.30 7.29 7.28 7.28 7.28 7.28 7.26 7.26 7.26 7.16 7.14 7.13 7.13 7.11 7.11 7.11 7.10 7.10 7.10 7.10 7.08 7.08 7.07 7.07 7.07 4.11 4.10 4.09 4.08 3.85 3.85 3.69 3.69 3.46 3.46 3.43 3.42 3.14 3.11 3.09 2.85 2.75 2.73 2.72 2.71 2.07 2.03 2.01 1.81 1.80 1.78 1.76 1.63 1.61 1.60 1.59 1.58
H
H
H
N
CO2Me
CO2Me
N
H
2.153a
0.91 1.00 1.05 2.01 1.02 2.94 2.97 2.08 1.02 1.04 1.03 1.09 2.15 2.15 2.43
9.5 9.0 8.5 8.0 7.5 7.0 6.5 6.0 5.5 5.0 4.5 4.0 3.5 3.0 2.5 2.0 1.5 1.0 0.5 0
f1 (ppm)

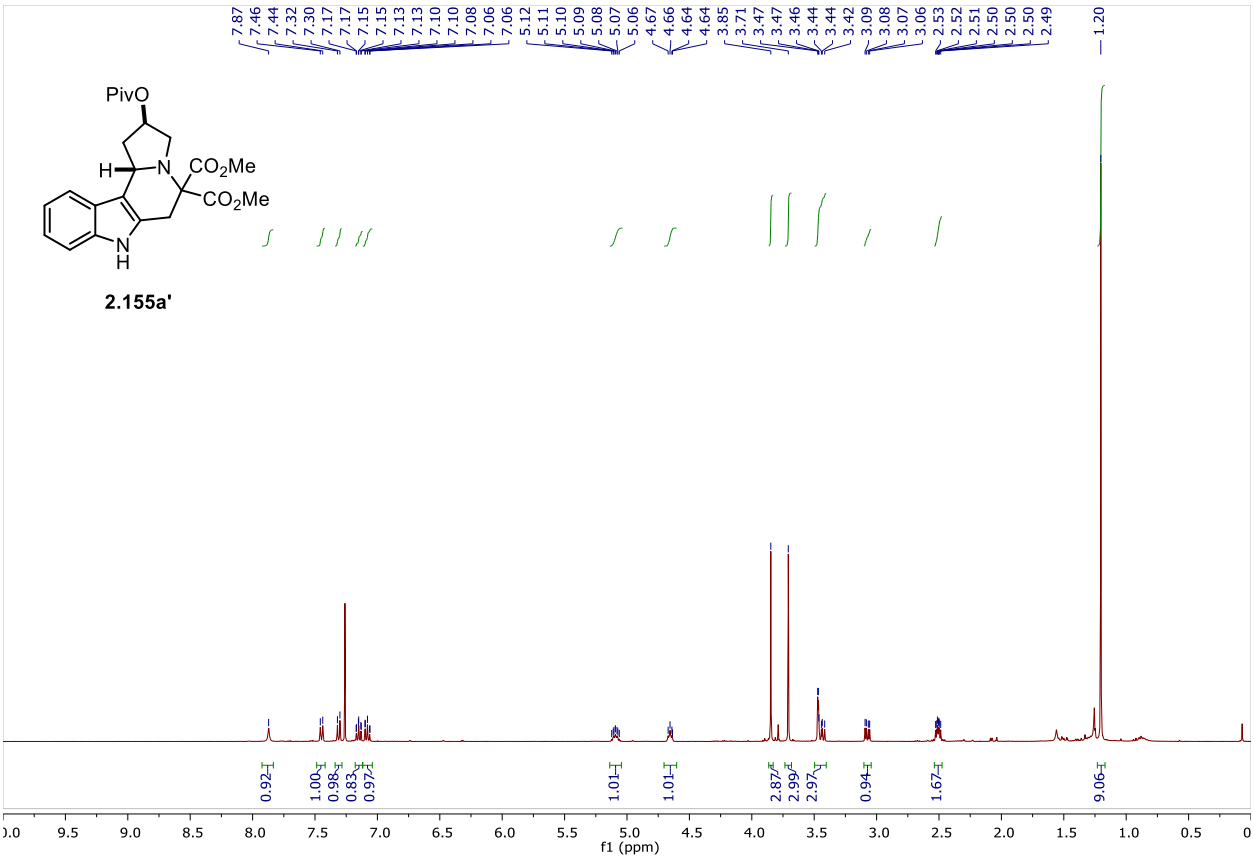

169.93 169.57 136.13 128.67 125.82 121.50 119.53 118.96 111.49 110.96 70.48 63.28 54.25 53.38 52.80 47.69 42.00 33.79 32.94 26.97 26.91
H
H
H
N
CO2Me
CO2Me
N
H
2.153a
210 200 190 180 170 160 150 140 130 120 110 100 90 80 70 60 50 40 30 20 10 0 -10
f1 (ppm)

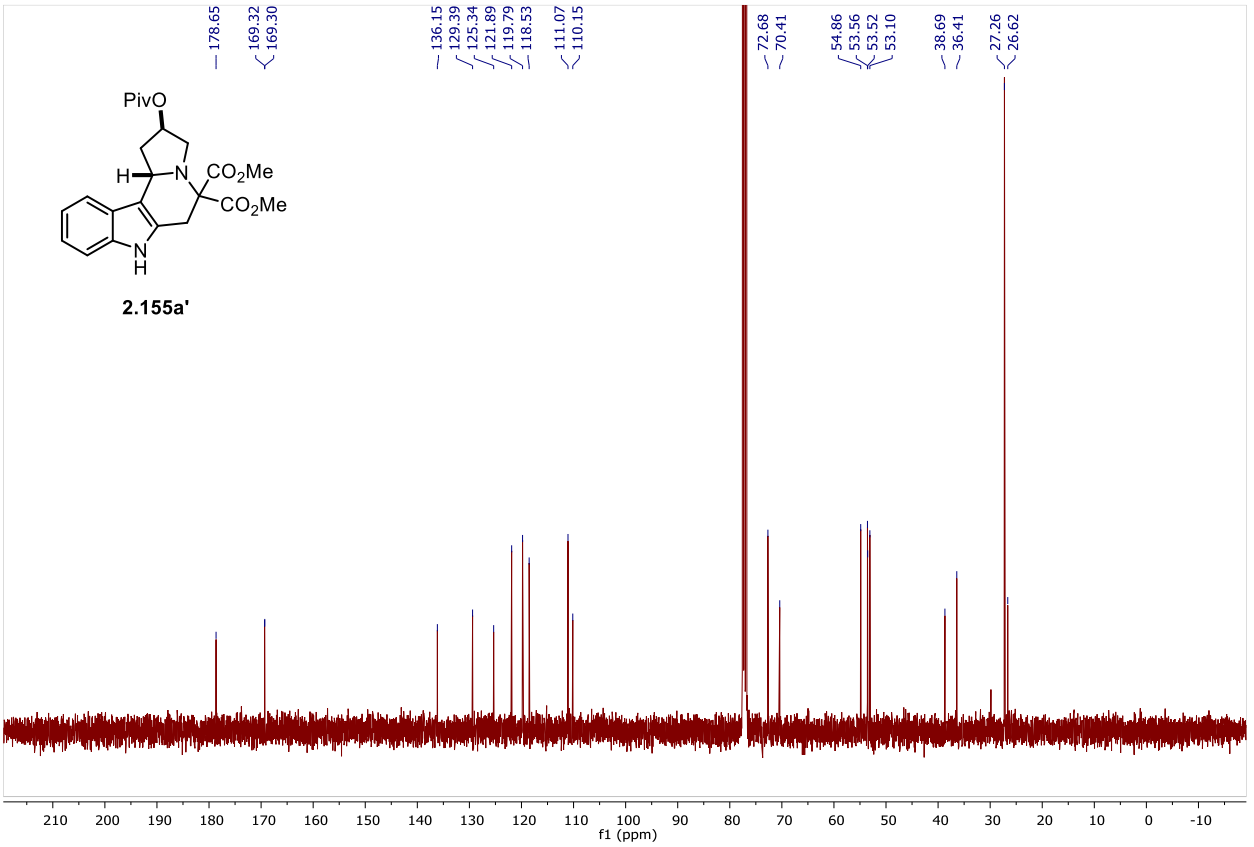

H
H
H
N
CO2Me
CO2Me
N
H
2.153a
f2 (ppm)
f1 (ppm)

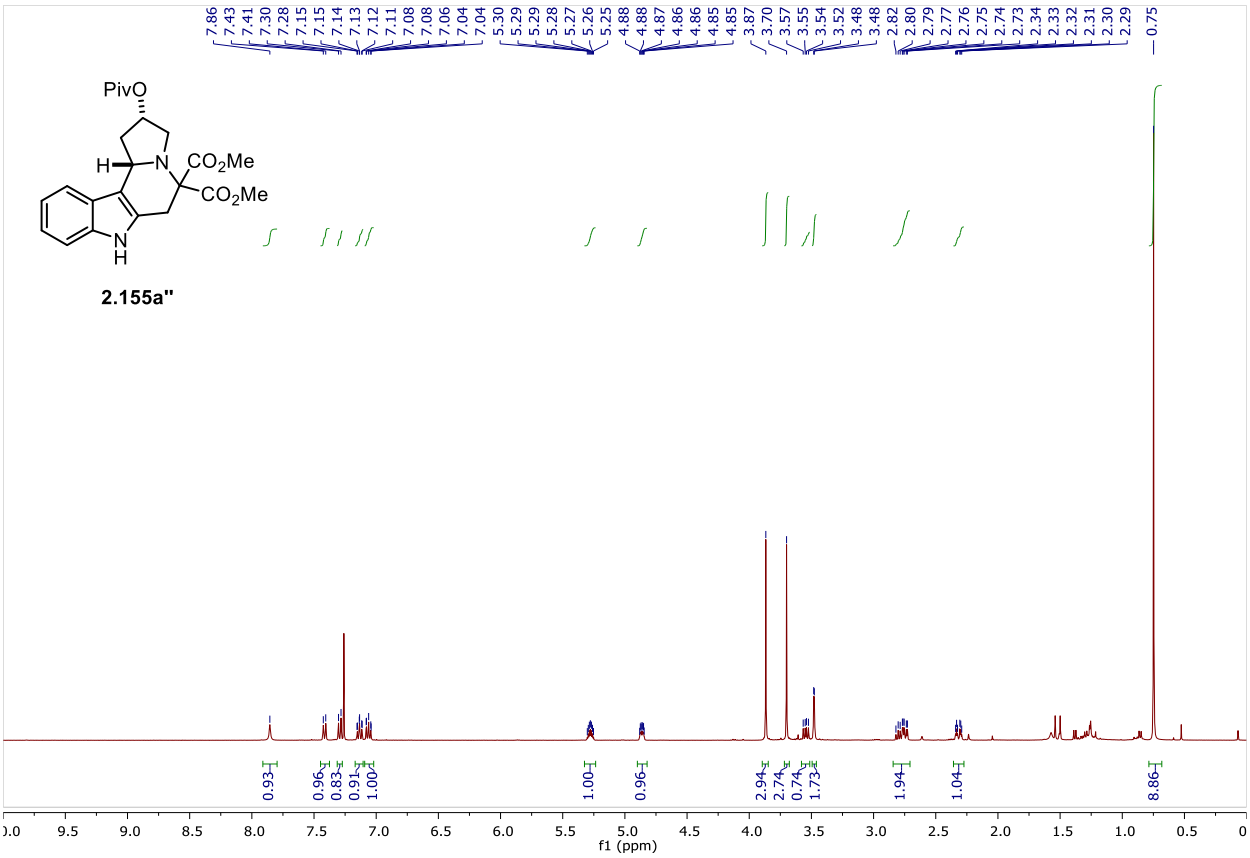

NOESY
H
H
H
N
CO2Me
CO2Me
N
H
2.153a
f2 (ppm)
f1 (ppm)

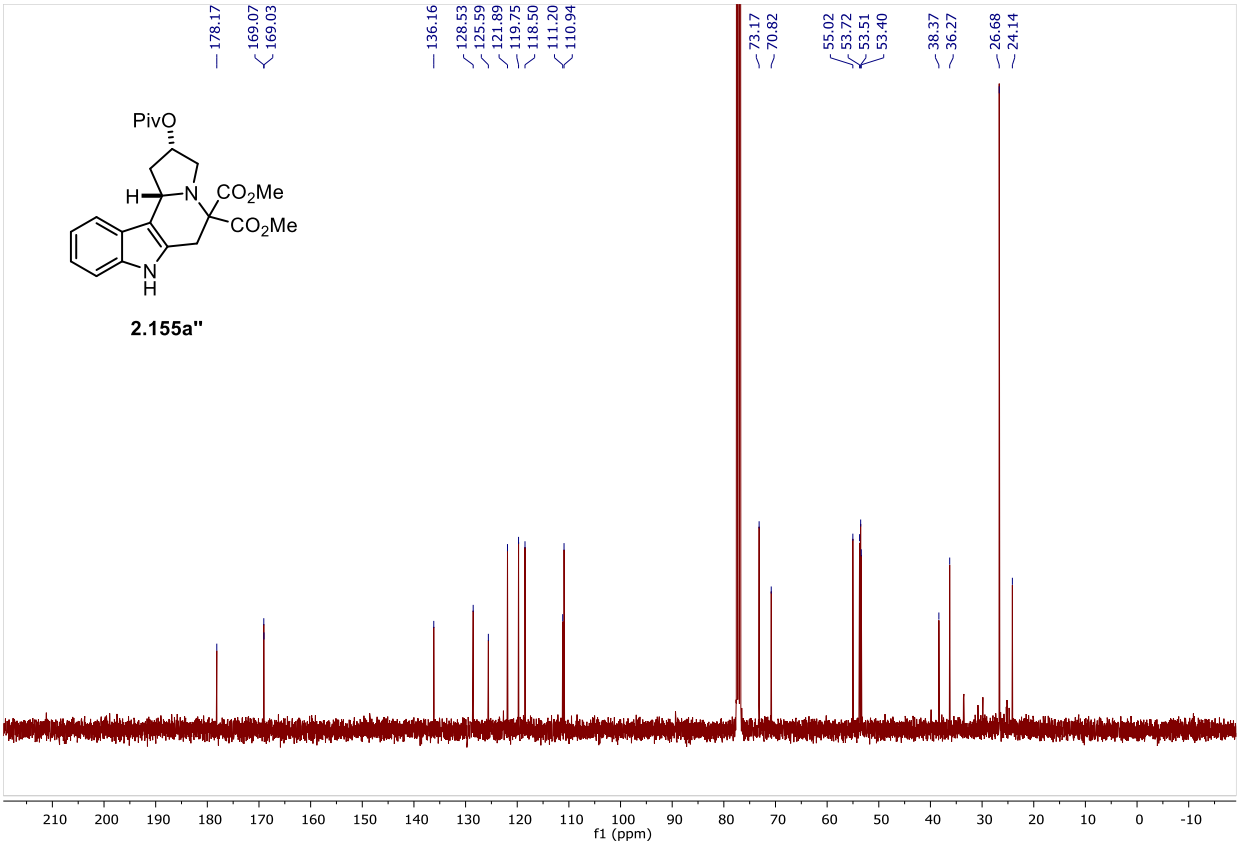

OPiv
N
CO2Me
CO2Me
N3
2.129
f1 (ppm)

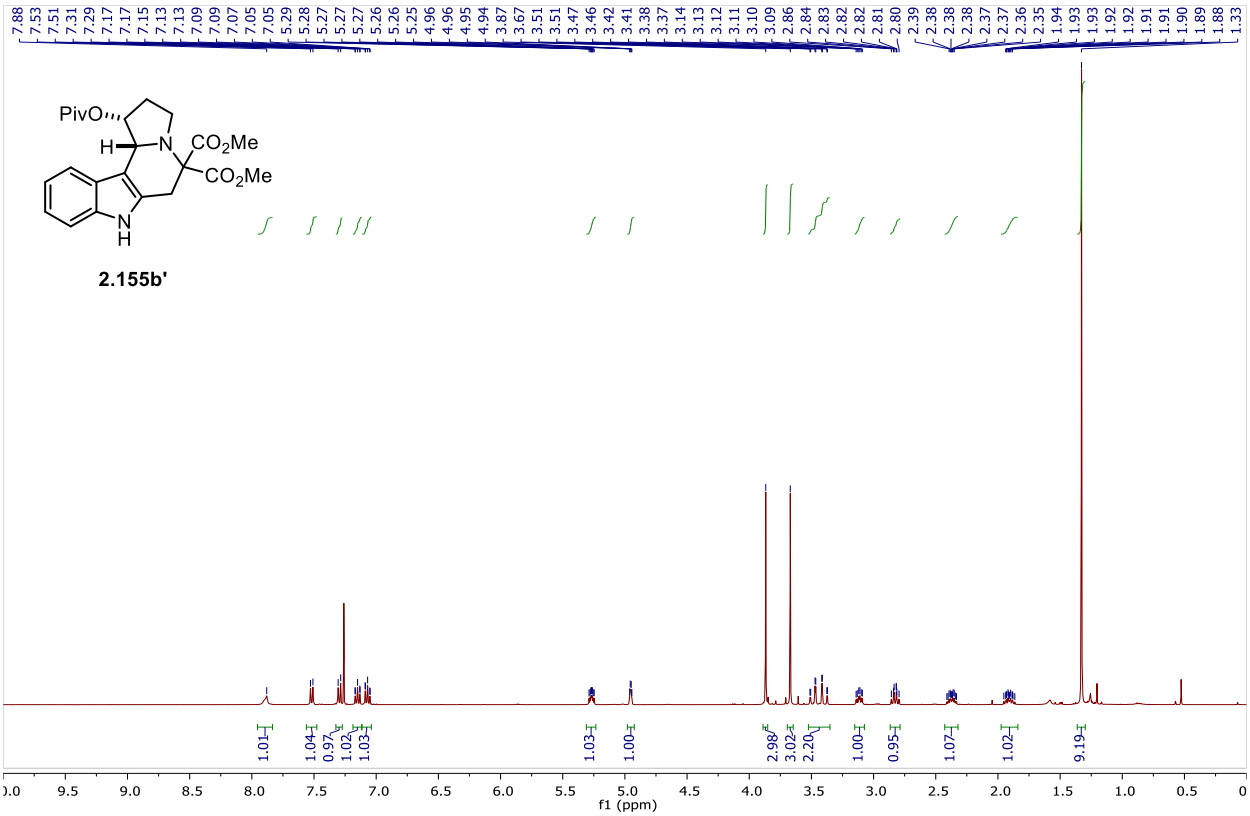

OPiv
N
CO2Me
CO2Me
N3
2.129
f1 (ppm)

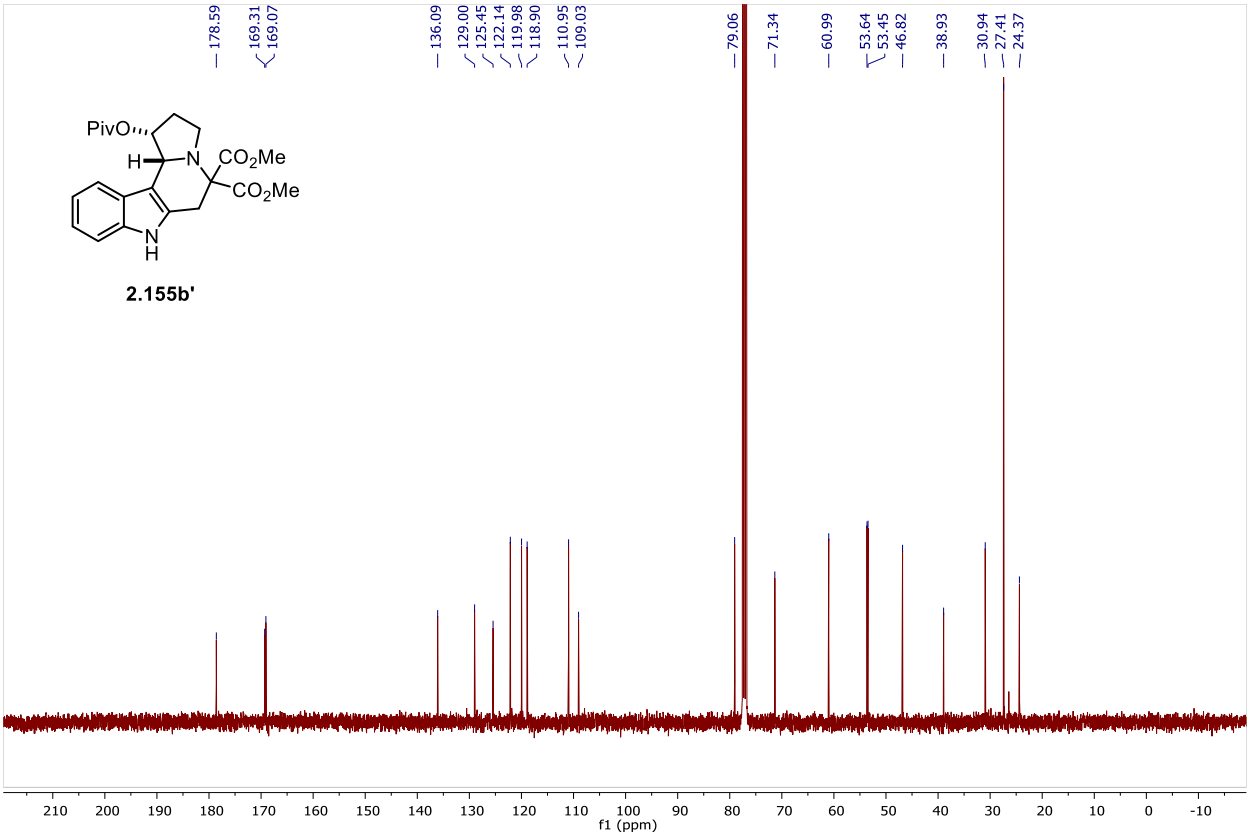

PivO
H
N
CO2Me
CO2Me
N
H
2.155a'
7.87 7.46 7.44 7.32 7.30 7.17 7.17 7.15 7.15 7.13 7.13 7.10 7.10 7.08 7.06 7.06
5.12 5.11 5.10 5.09 5.08 5.07 5.06
4.67 4.66 4.64 4.64
3.85 3.71 3.47 3.47 3.46 3.44 3.44 3.42
3.09 3.08 3.07 3.06
2.53 2.52 2.51 2.50 2.50 2.50 2.49
1.20
0.92 1.00 0.98 0.83 0.97 1.01 1.01 2.87 2.99 2.97 0.94 1.67 9.06
f1 (ppm)

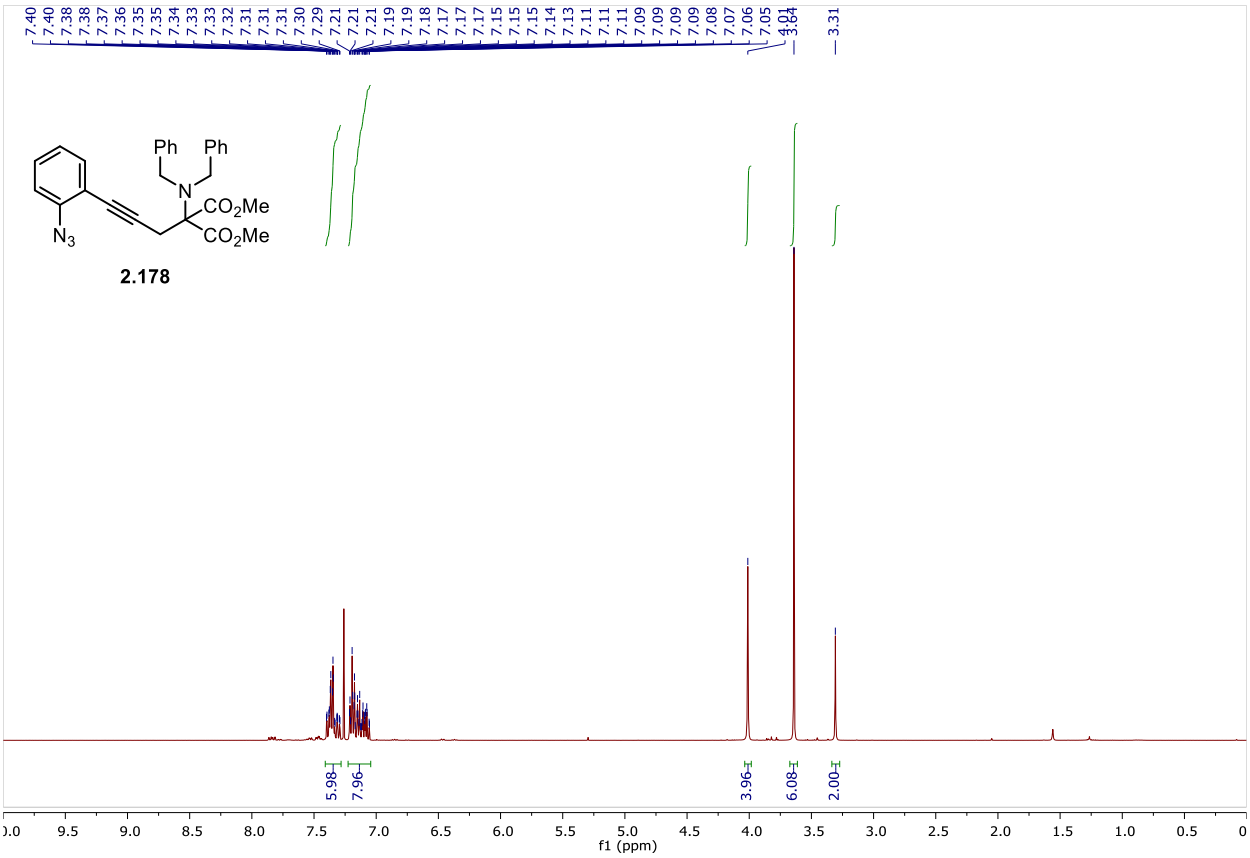

PivO
H
N
CO2Me
CO2Me
N
H
2.155a'
178.65
169.32 169.30
136.15 129.39 125.34 121.89 119.79 118.53
111.07 110.15
72.68 70.41
54.86 53.56 53.52 53.10
38.69 36.41
27.26 26.62
f1 (ppm)

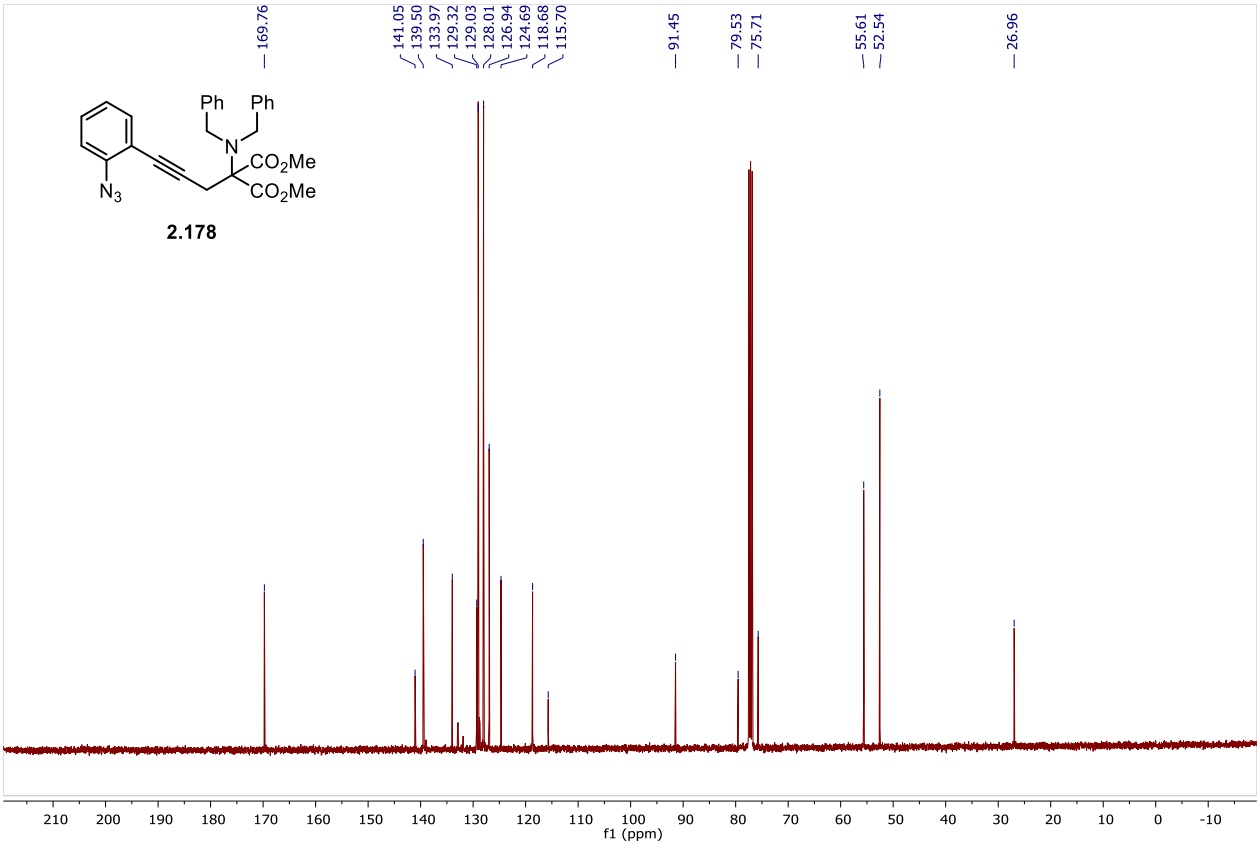

PivO
H
N
CO2Me
CO2Me
N
H
2.155a''
f1 (ppm)

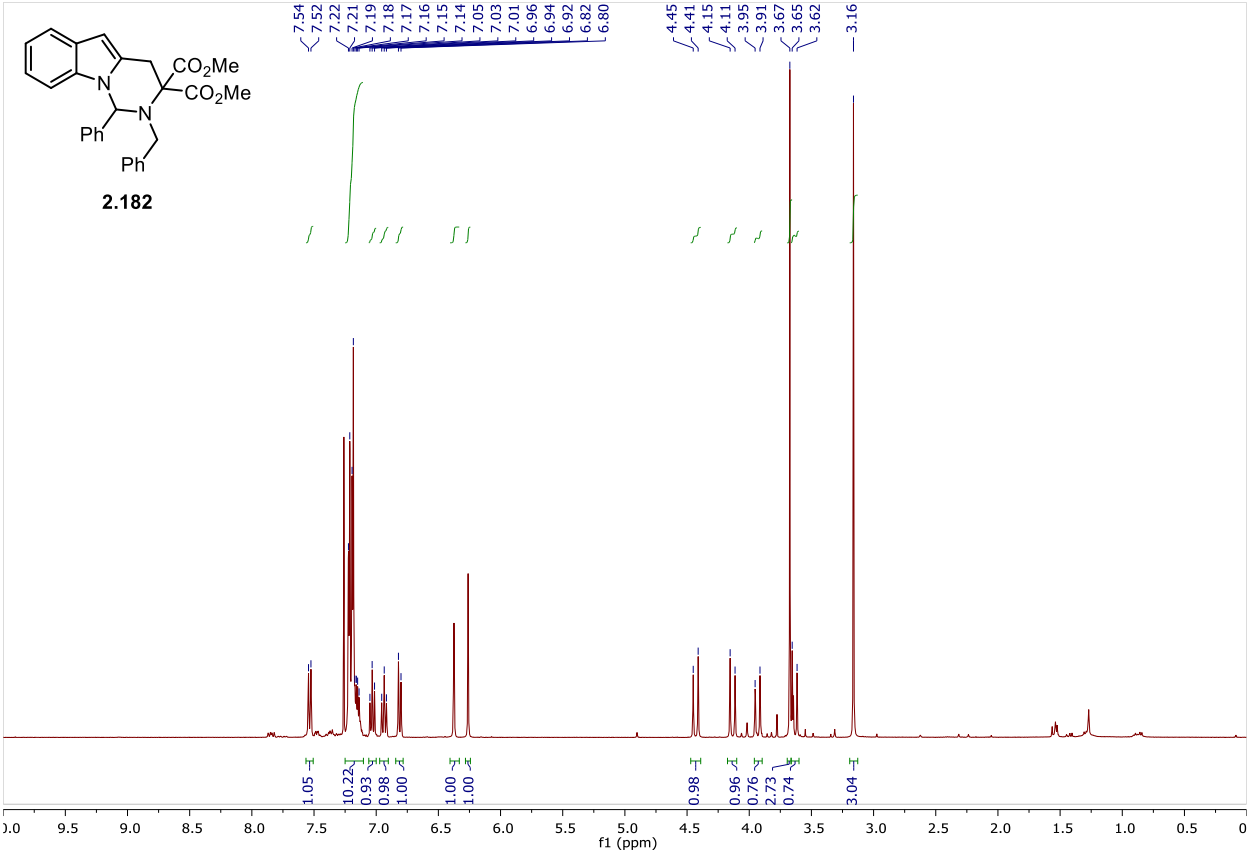

PivO
H
N
CO2Me
CO2Me
N
H
2.155a''
f1 (ppm)

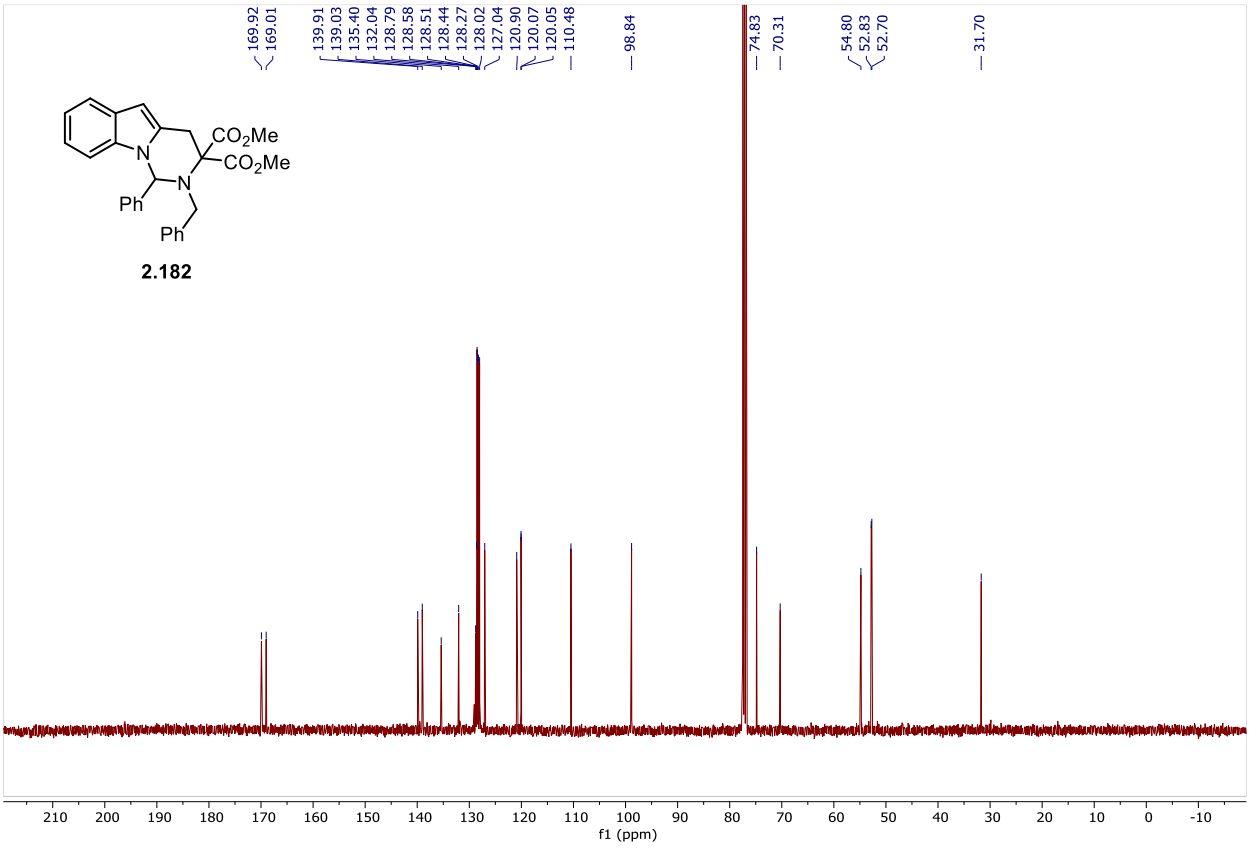

PivO
H
N
CO2Me
CO2Me
N
H
2.155b'
f1 (ppm)

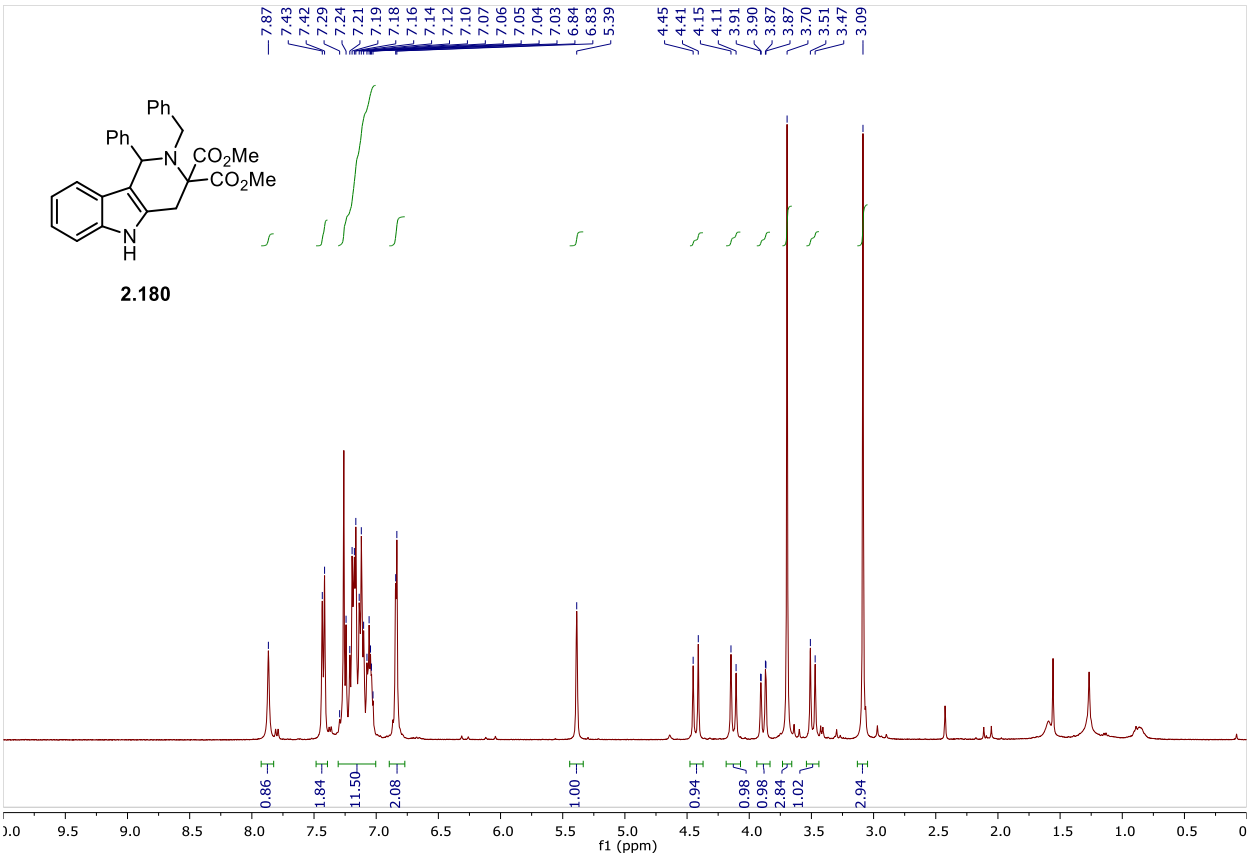

PivO
H
N
CO2Me
CO2Me
N
H
2.155b'
f1 (ppm)

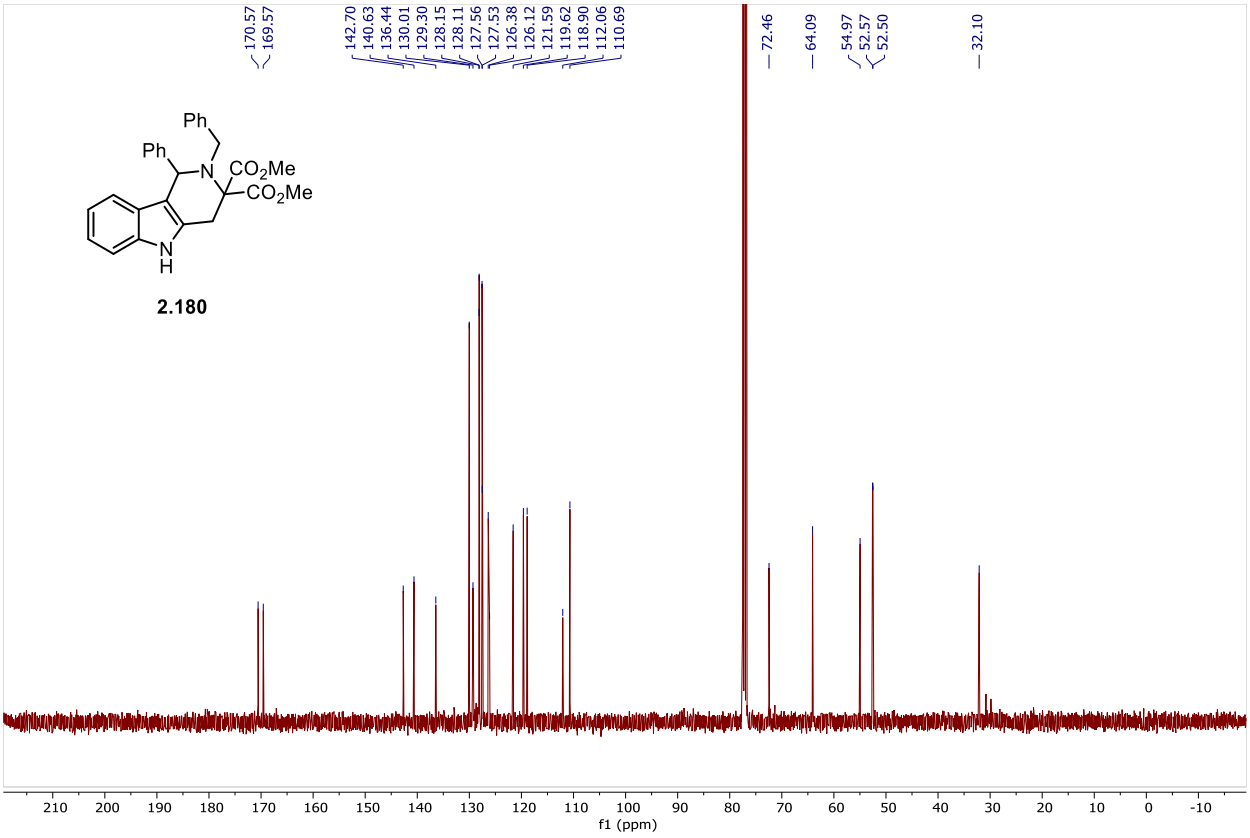

Ph
Ph
N
CO2Me
CO2Me
N3
2.178
f1 (ppm)

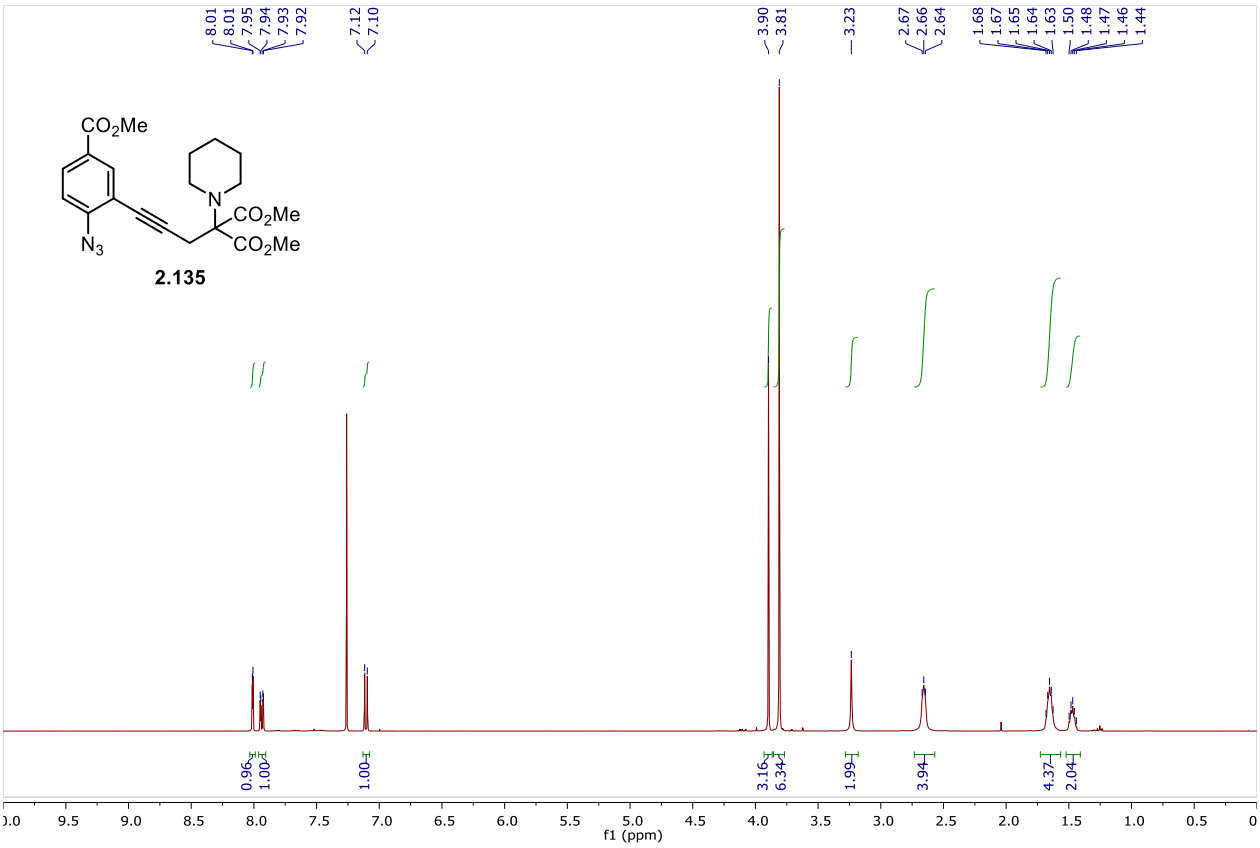

Ph
Ph
N
CO2Me
CO2Me
N3
2.178
f1 (ppm)

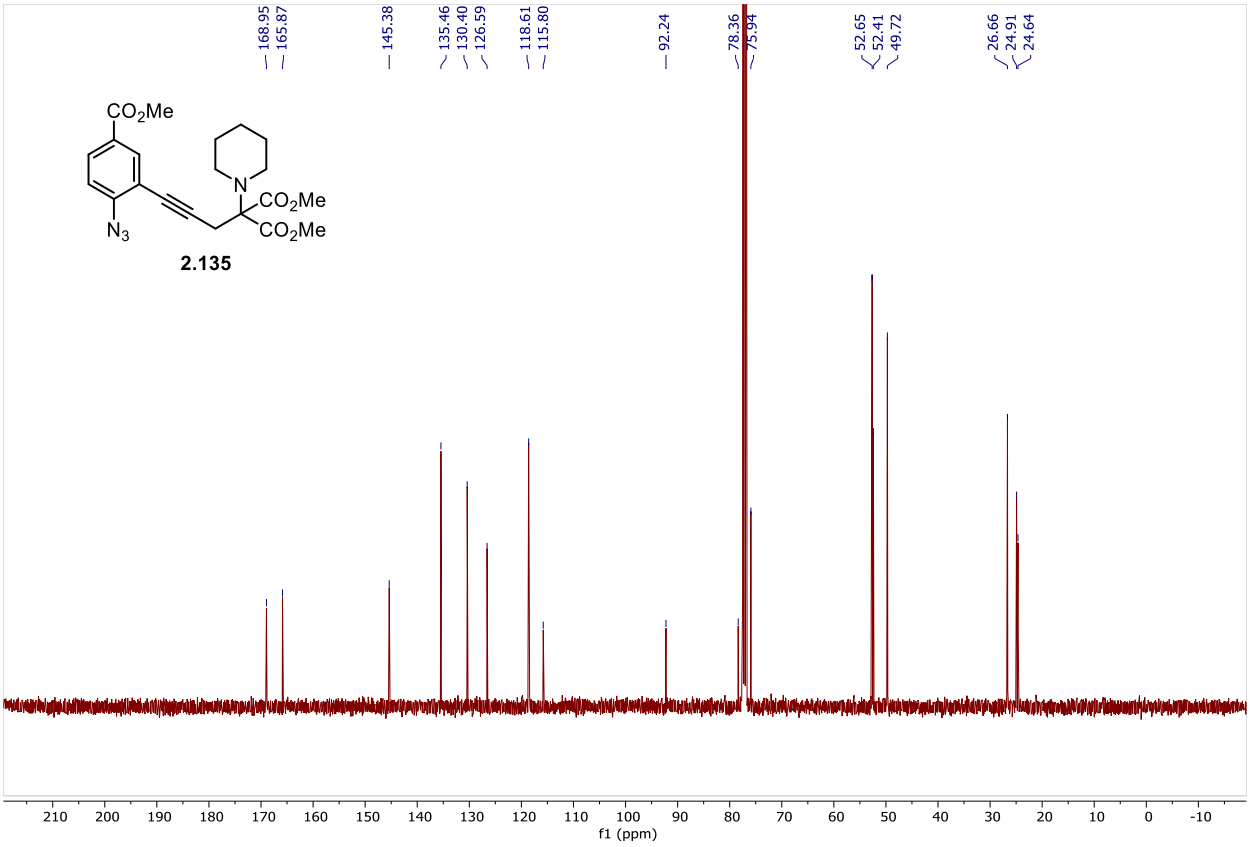

CO2Me
CO2Me
N
N
Ph
Ph
2.182
7.54
7.52
7.22
7.21
7.19
7.18
7.17
7.16
7.15
7.14
7.05
7.03
7.01
6.96
6.94
6.92
6.82
6.80
4.45
4.41
4.15
4.11
3.95
3.91
3.67
3.65
3.62
3.16
1.05
10.22
0.93
0.98
1.00
1.00
1.00
0.98
0.96
0.76
2.73
0.74
3.04
f1 (ppm)

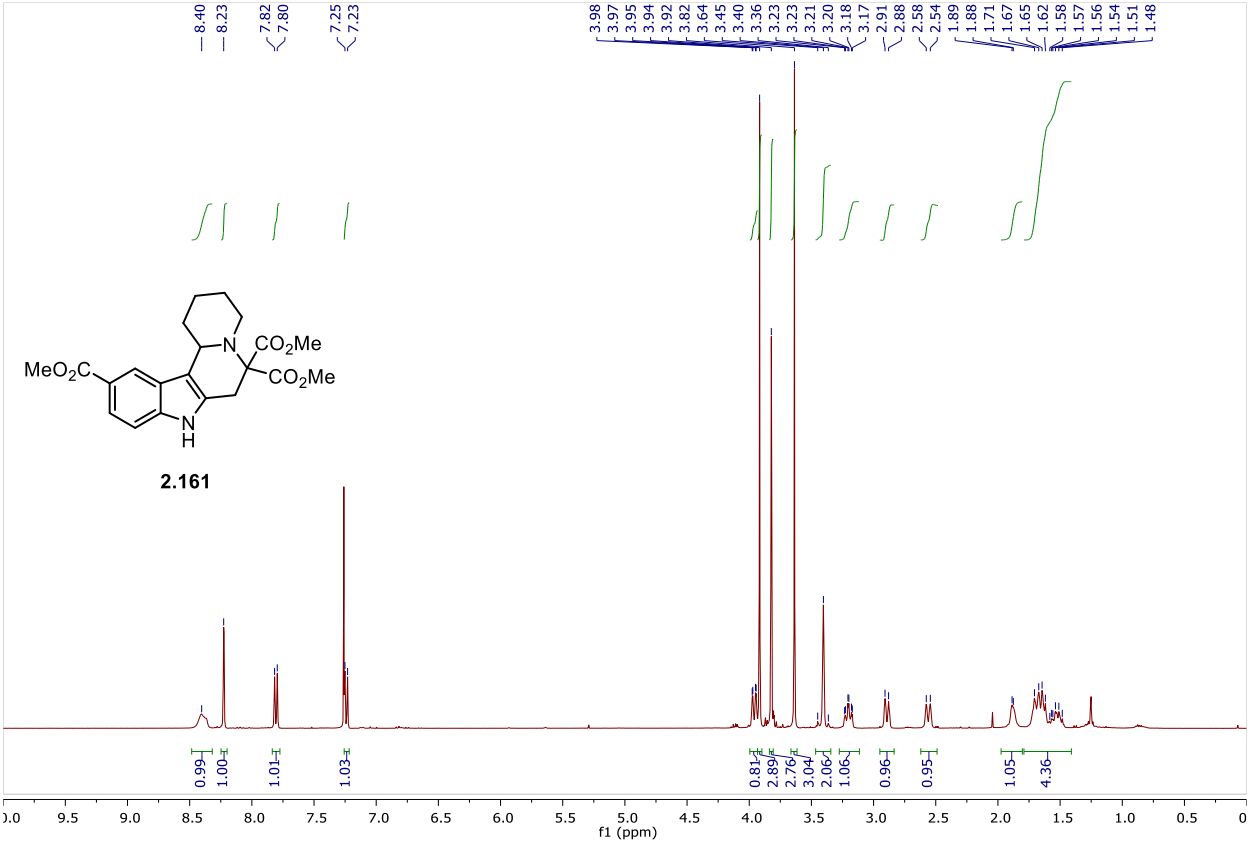

CO2Me
CO2Me
N
N
Ph
Ph
2.182
169.92
169.01
139.91
139.03
135.40
132.04
128.79
128.58
128.51
128.44
128.27
128.02
127.04
120.90
120.07
120.05
110.48
98.84
74.83
70.31
54.80
52.83
52.70
31.70
f1 (ppm)

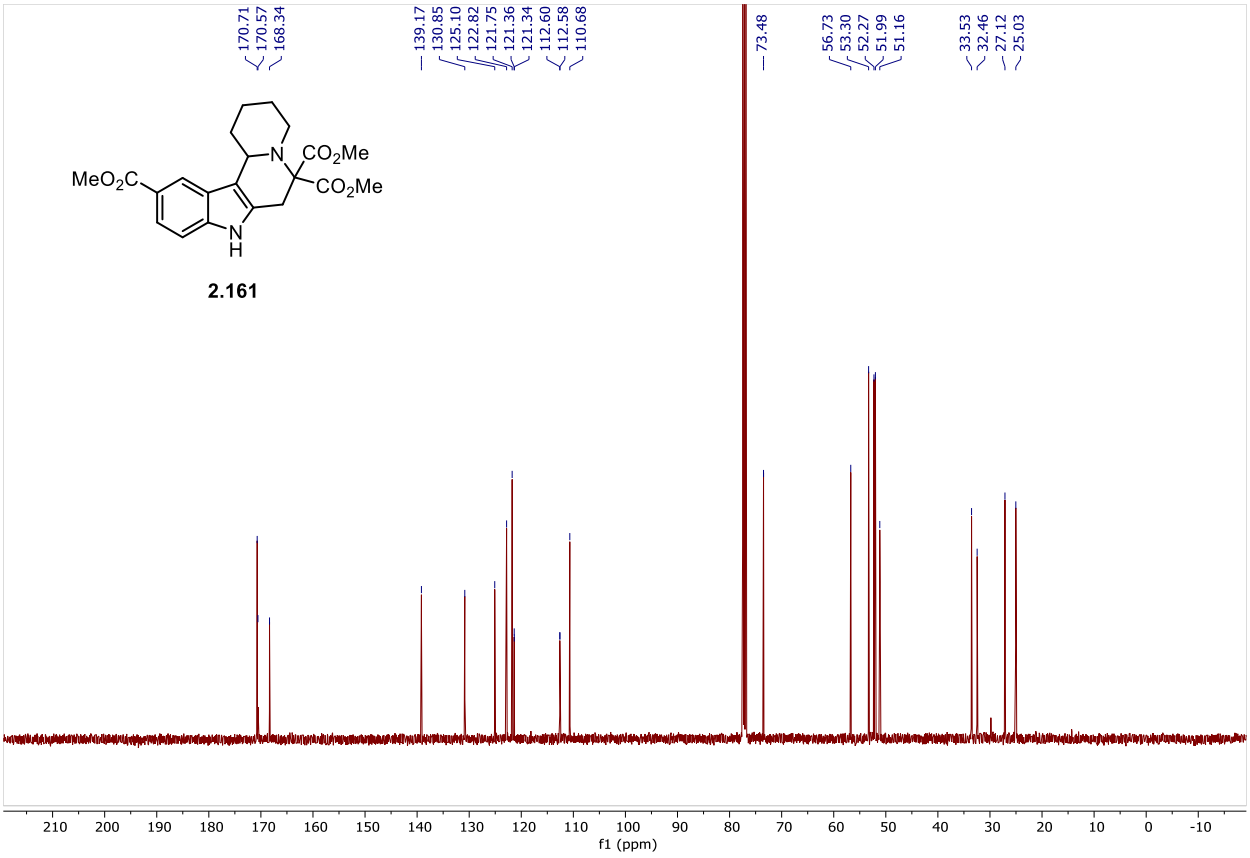

7.87
7.43
7.42
7.29
7.24
7.21
7.19
7.18
7.16
7.14
7.12
7.10
7.07
7.06
7.05
7.04
7.03
6.84
6.83
5.39
4.45
4.41
4.15
4.11
3.91
3.90
3.87
3.87
3.70
3.51
3.47
3.09
Ph
Ph
N
CO2Me
CO2Me
N
H
2.180
0.86
1.84
11.50
2.08
1.00
0.94
0.98
0.98
2.84
1.02
2.94
f1 (ppm)

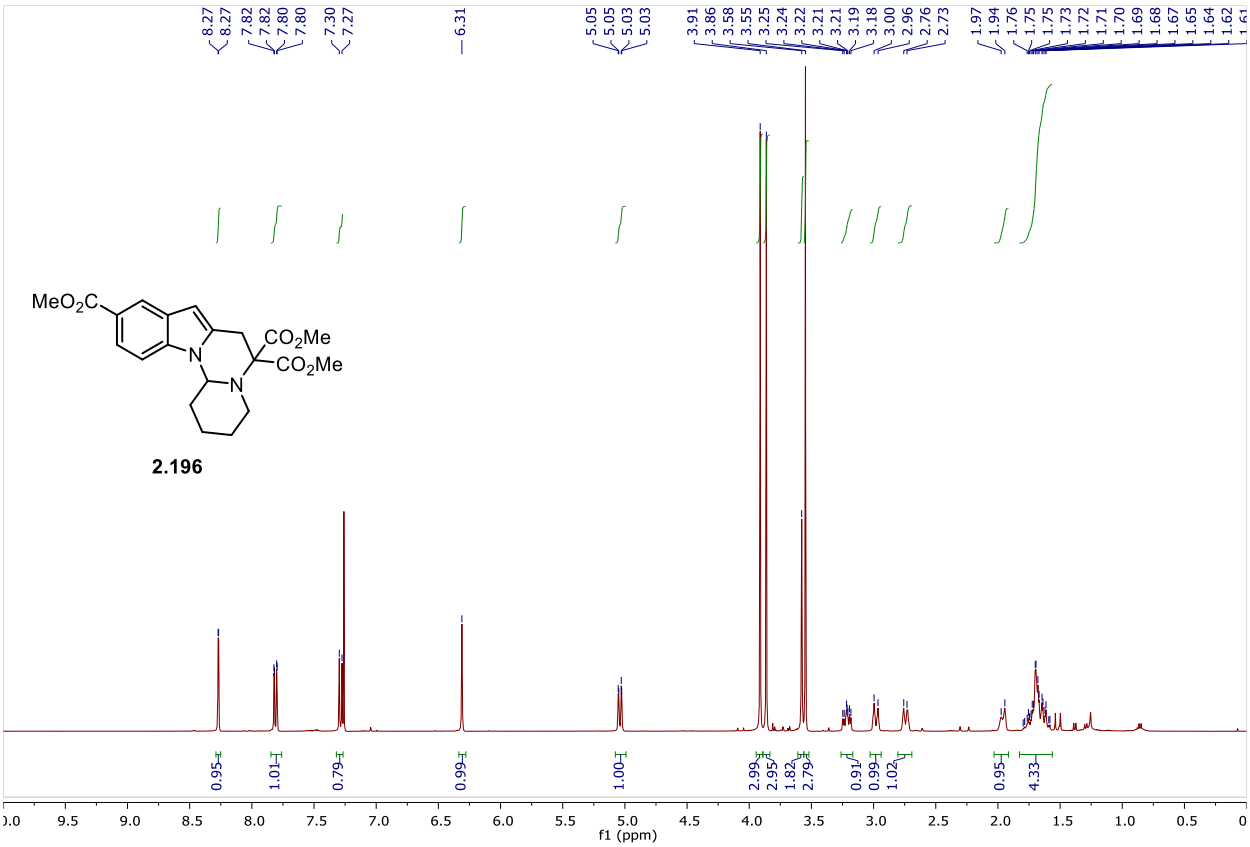

170.57
169.57
142.70
140.63
136.44
130.01
129.30
128.15
128.11
127.56
127.53
126.38
126.12
121.59
119.62
118.90
112.06
110.69
72.46
64.09
54.97
52.57
52.50
32.10
Ph
Ph
N
CO2Me
CO2Me
N
H
2.180
f1 (ppm)

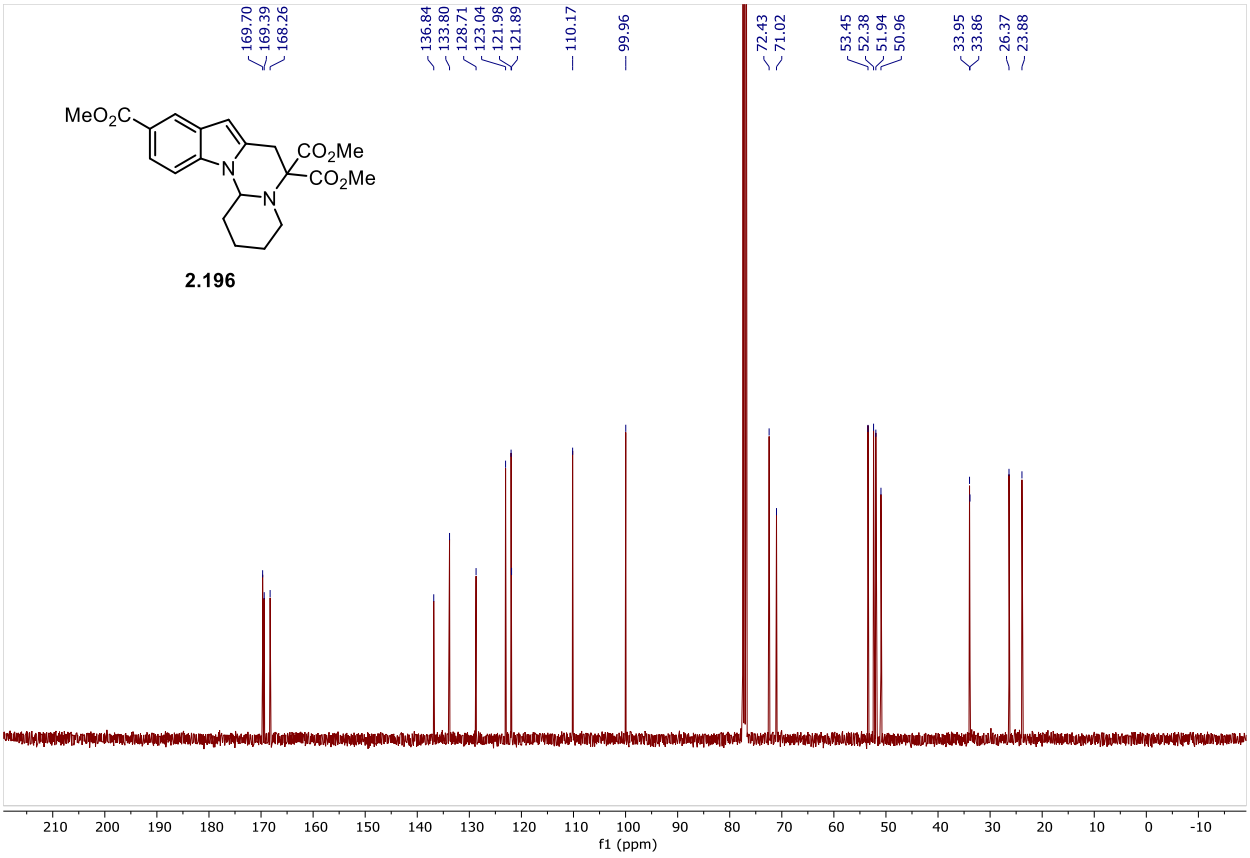

8.01
8.01
7.95
7.94
7.93
7.92
7.12
7.10
3.90
3.81
3.23
2.67
2.66
2.64
1.68
1.67
1.65
1.64
1.63
1.50
1.48
1.47
1.46
1.44
CO2Me
N
CO2Me
CO2Me
N3
2.135
0.96
1.00
1.00
3.16
6.34
1.99
3.94
4.37
2.04
f1 (ppm)

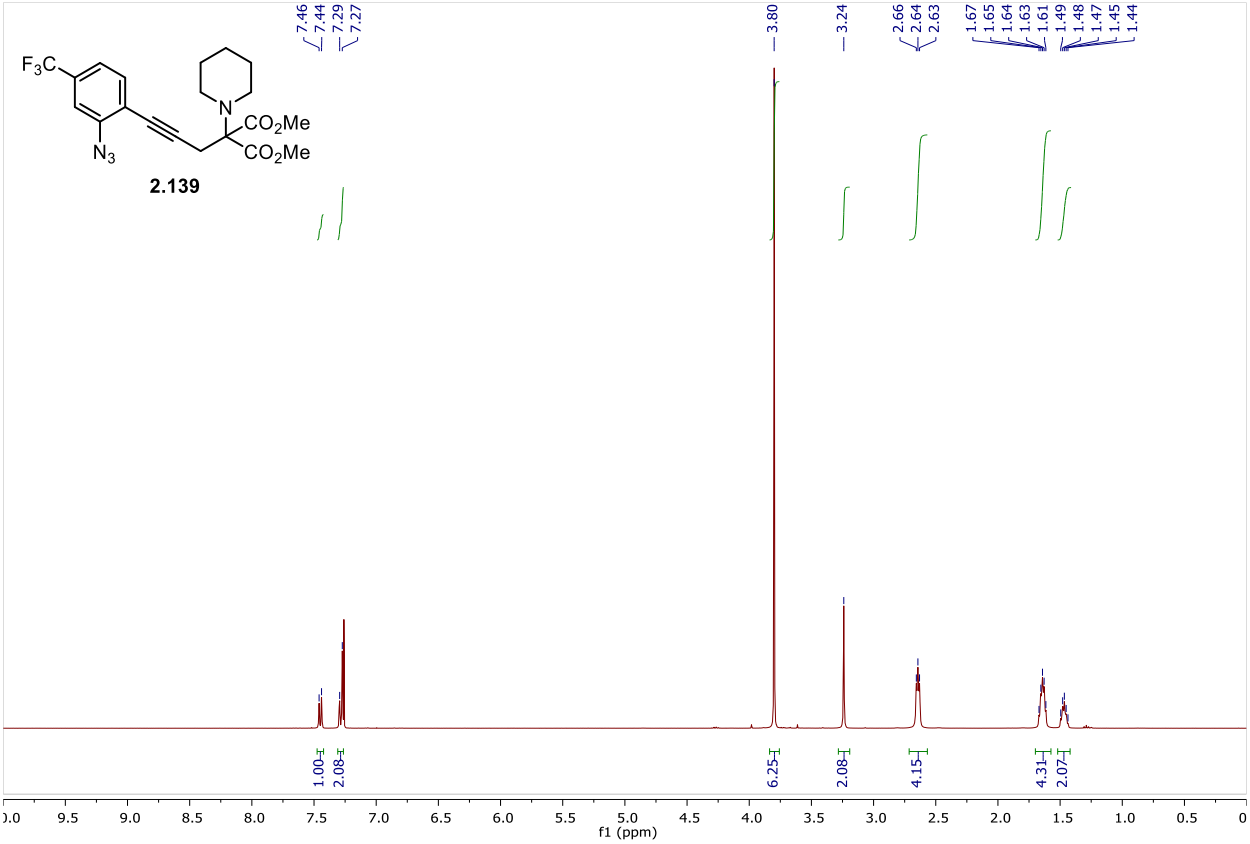

168.95
165.87
145.38
135.46
130.40
126.59
118.61
115.80
92.24
78.36
75.94
52.65
52.41
49.72
26.66
24.91
24.64
CO2Me
N
CO2Me
CO2Me
N3
2.135
f1 (ppm)

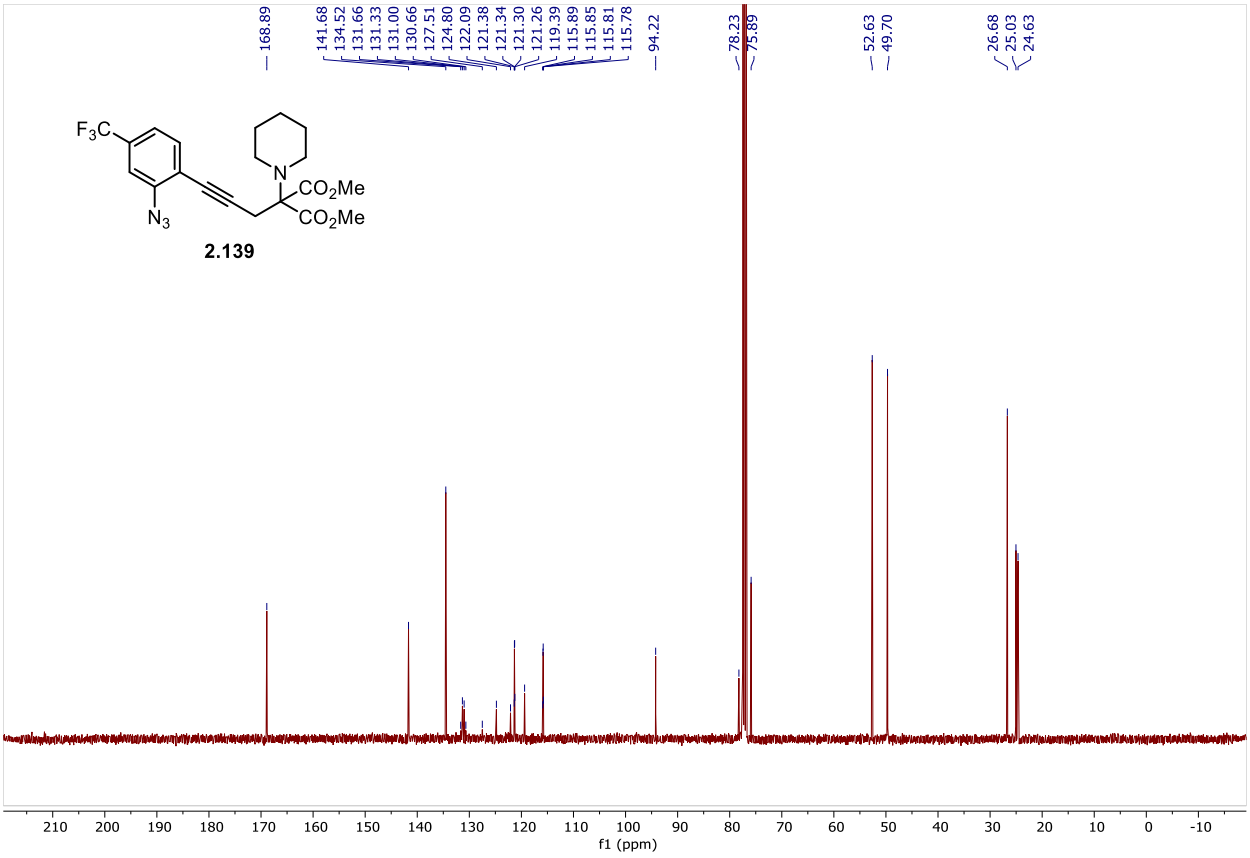

8.40
8.23
7.82
7.80
7.25
7.23
3.98
3.97
3.95
3.94
3.92
3.82
3.64
3.45
3.40
3.36
3.23
3.21
3.20
3.18
3.17
2.91
2.88
2.58
2.54
1.89
1.88
1.71
1.67
1.65
1.62
1.58
1.57
1.56
1.54
1.51
1.48
MeO2C
CO2Me
CO2Me
N
H
2.161
0.99
1.00
1.01
1.03
0.81
2.89
2.76
3.04
2.06
1.06
0.96
0.95
1.05
4.36
f1 (ppm)

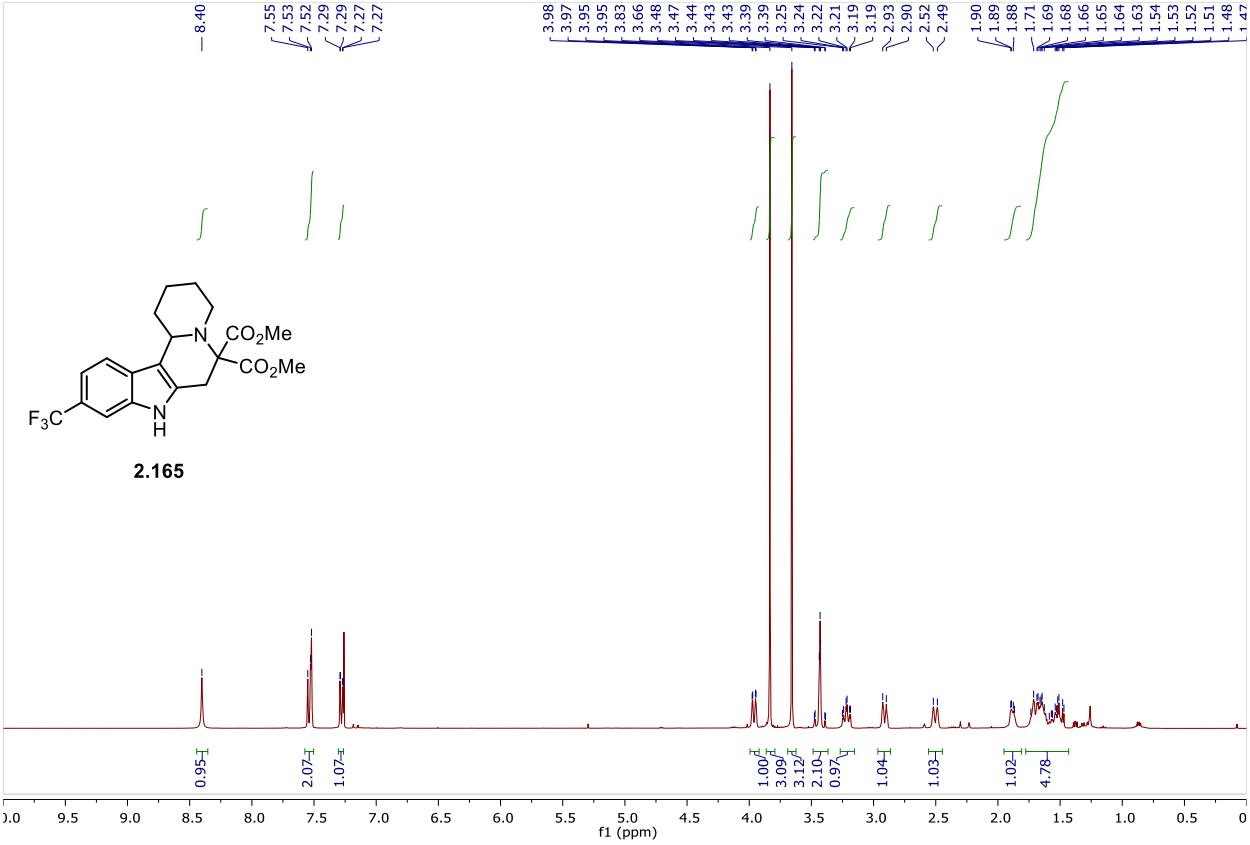

170.71
170.57
168.34
139.17
130.85
125.10
122.82
121.75
121.36
121.34
112.60
112.58
110.68
73.48
56.73
53.30
52.27
51.99
51.16
33.53
32.46
27.12
25.03
MeO2C
CO2Me
CO2Me
N
H
2.161
f1 (ppm)

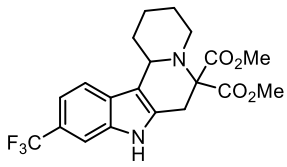

MeO2C
CO2Me
CO2Me
N
N
2.196
f1 (ppm)


MeO2C
CO2Me
CO2Me
N
N
2.196
f1 (ppm)


7.46
7.44
7.29
7.27
3.80
3.24
2.66
2.64
2.63
1.67
1.65
1.64
1.63
1.61
1.49
1.48
1.47
1.45
1.44
F3C
N3
N
CO2Me
CO2Me
2.139
1.00
2.08
6.25
2.08
4.15
4.31
2.07
f1 (ppm)


168.89
141.68
134.52
131.66
131.33
131.00
130.66
127.51
124.80
122.09
121.38
121.34
121.30
121.26
119.39
115.89
115.85
115.81
115.78
94.22
78.23
75.89
52.63
49.70
26.68
25.03
24.63
F3C
N3
N
CO2Me
CO2Me
2.139
f1 (ppm)


8.40
7.55
7.53
7.52
7.29
7.29
7.27
7.27
3.98
3.97
3.95
3.95
3.83
3.66
3.48
3.47
3.44
3.43
3.43
3.39
3.39
3.25
3.24
3.22
3.21
3.19
3.19
2.93
2.90
2.52
2.49
1.90
1.89
1.88
1.71
1.69
1.69
1.68
1.66
1.65
1.64
1.63
1.54
1.53
1.52
1.51
1.48
1.47
0.95
2.07
1.07
1.00
3.09
3.12
2.10
0.97
1.04
1.03
1.02
4.78
f1 (ppm)

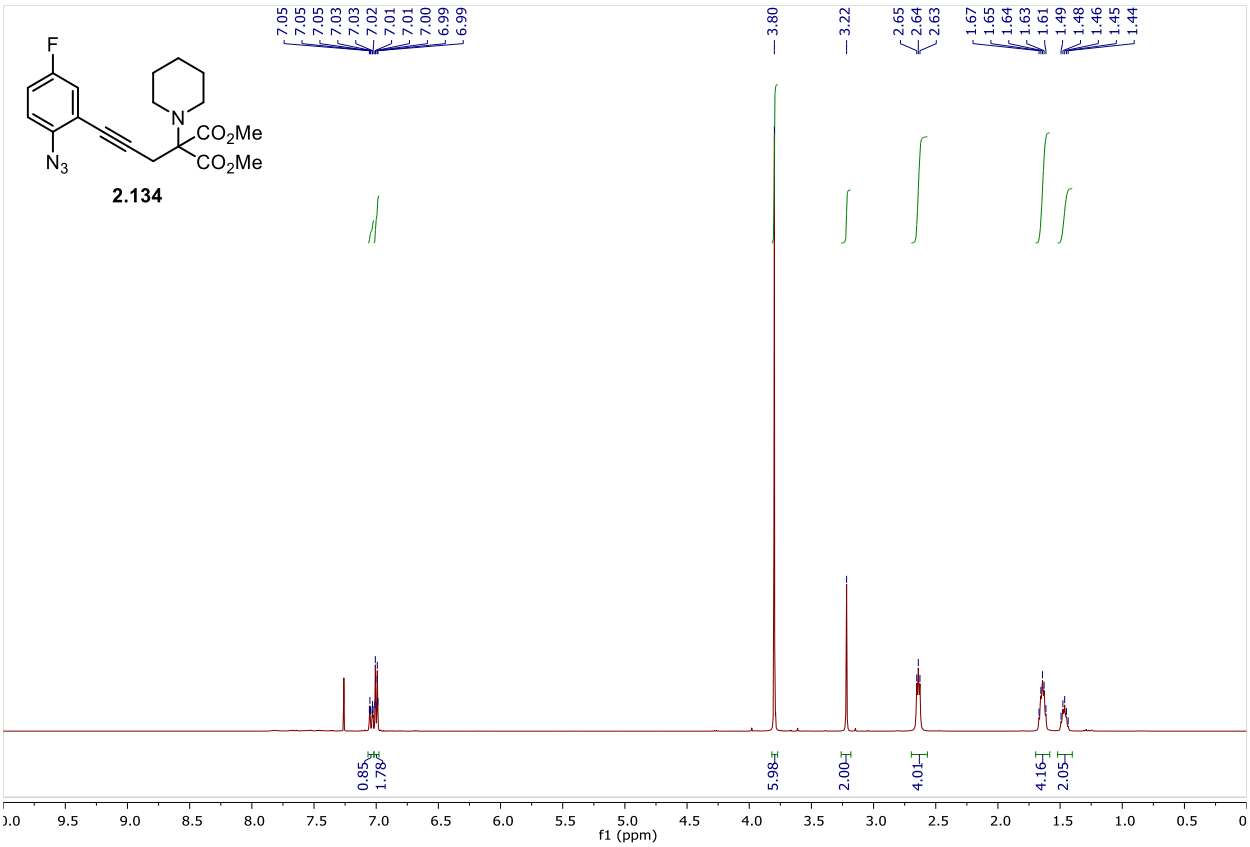

N
CO2Me
CO2Me
F3C
N
H

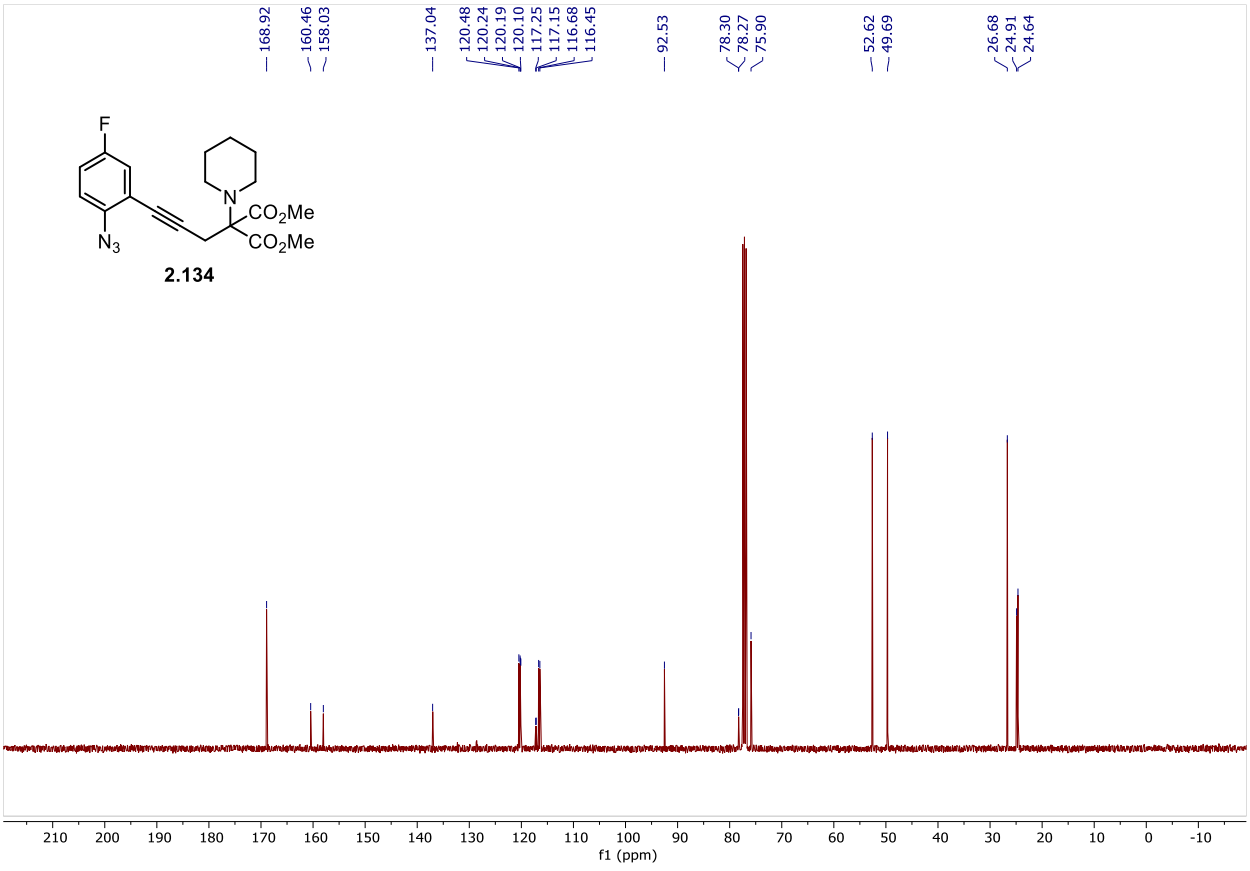
2.165

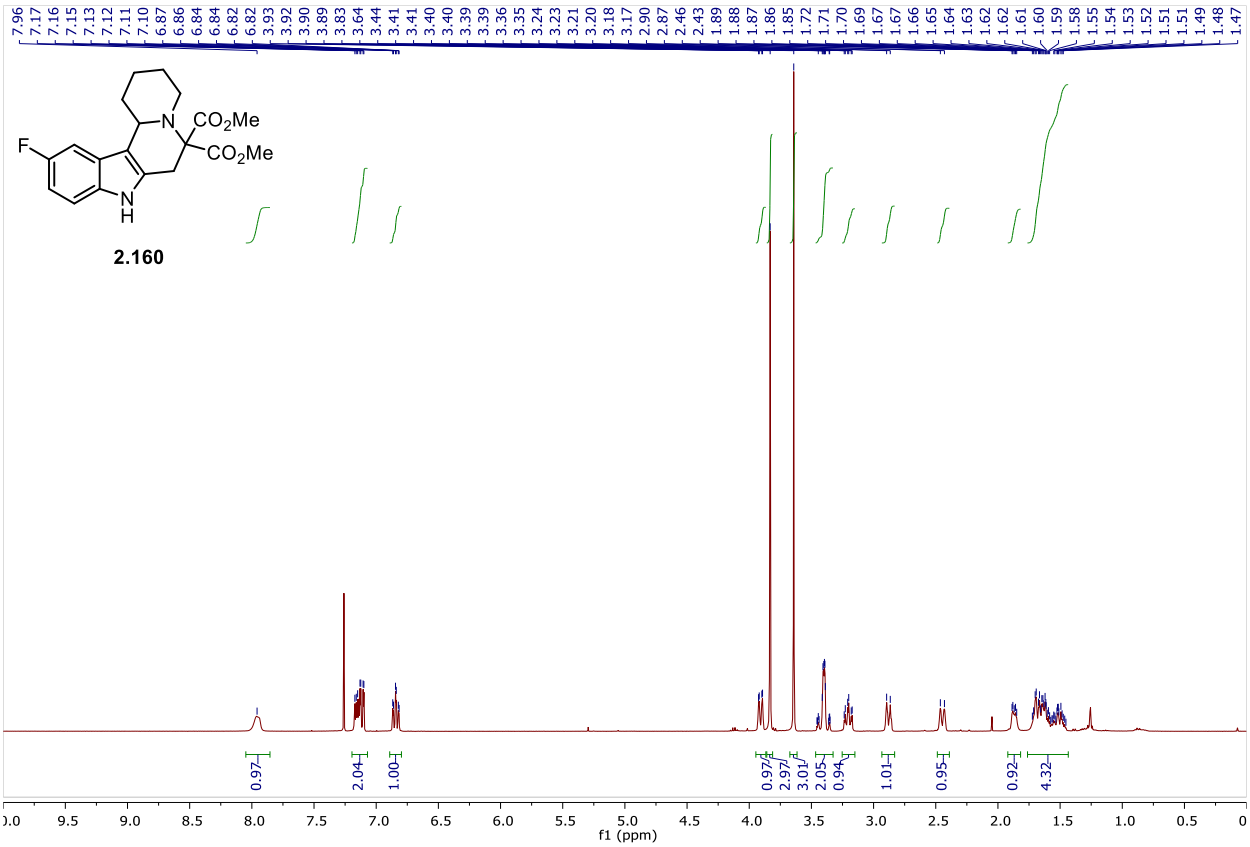
170.66
170.61
135.37
132.34
129.38
127.70
126.68
123.99
123.76
123.44
123.13
122.81
121.29
119.16
116.18
116.14
116.11
116.07
111.71
108.56
108.52
108.47
108.43
73.47
56.72
53.35
52.36
51.18
33.37
32.57
27.09
25.01
f1 (ppm)

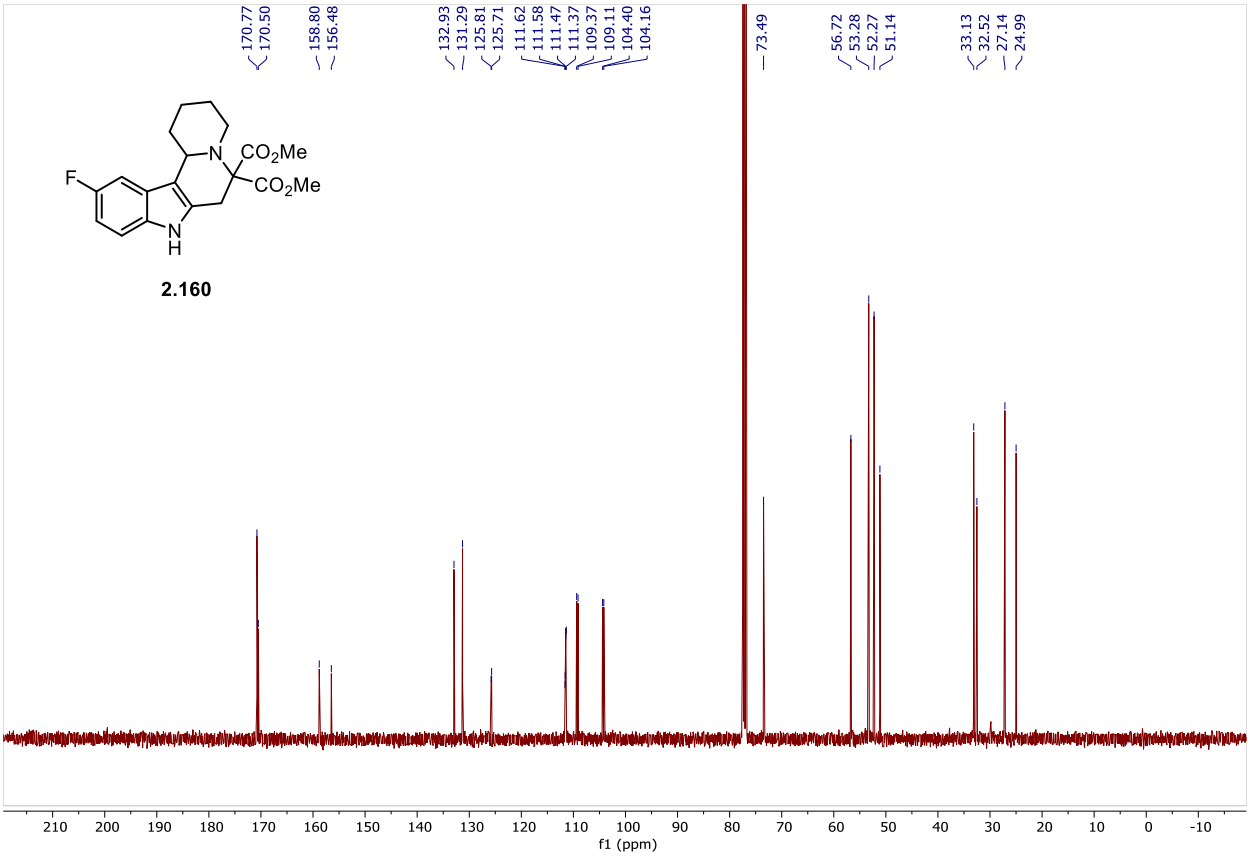
N
CO2Me
CO2Me
F3C
N
H

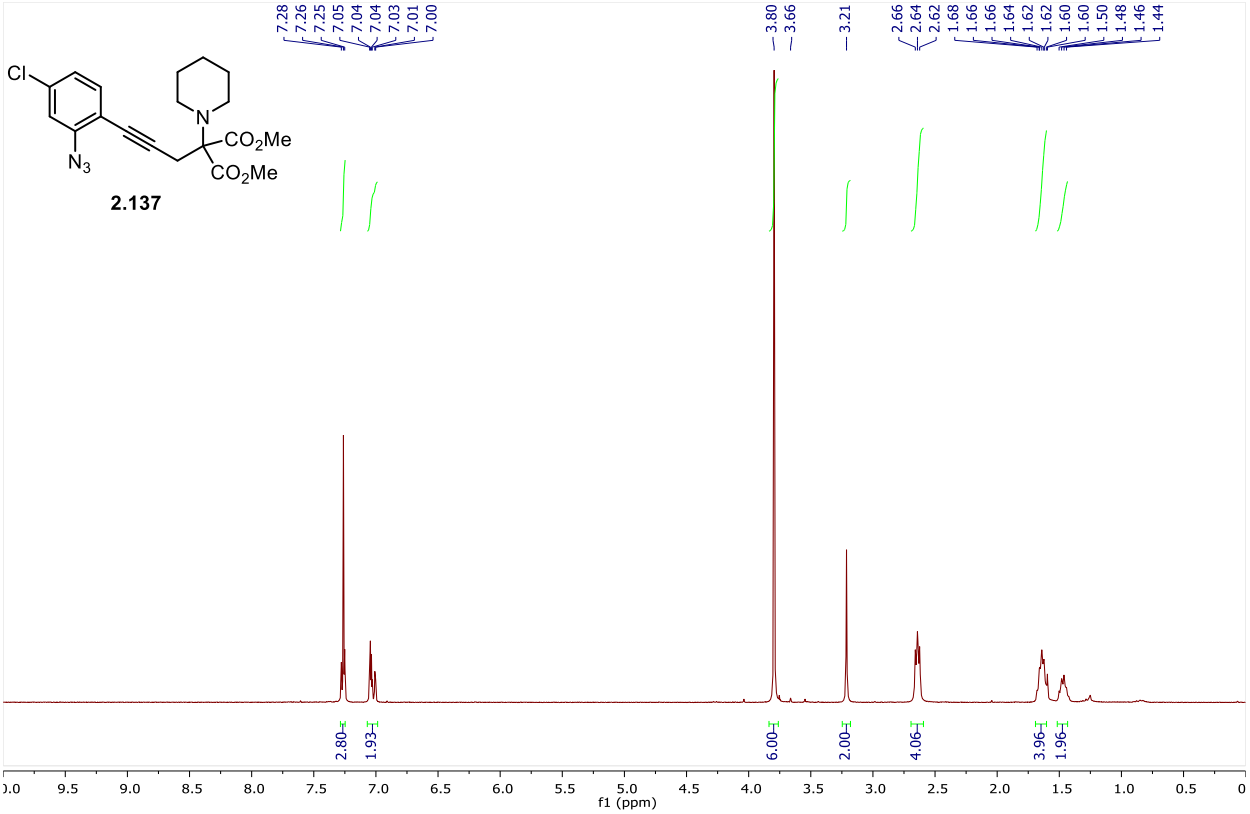
2.165

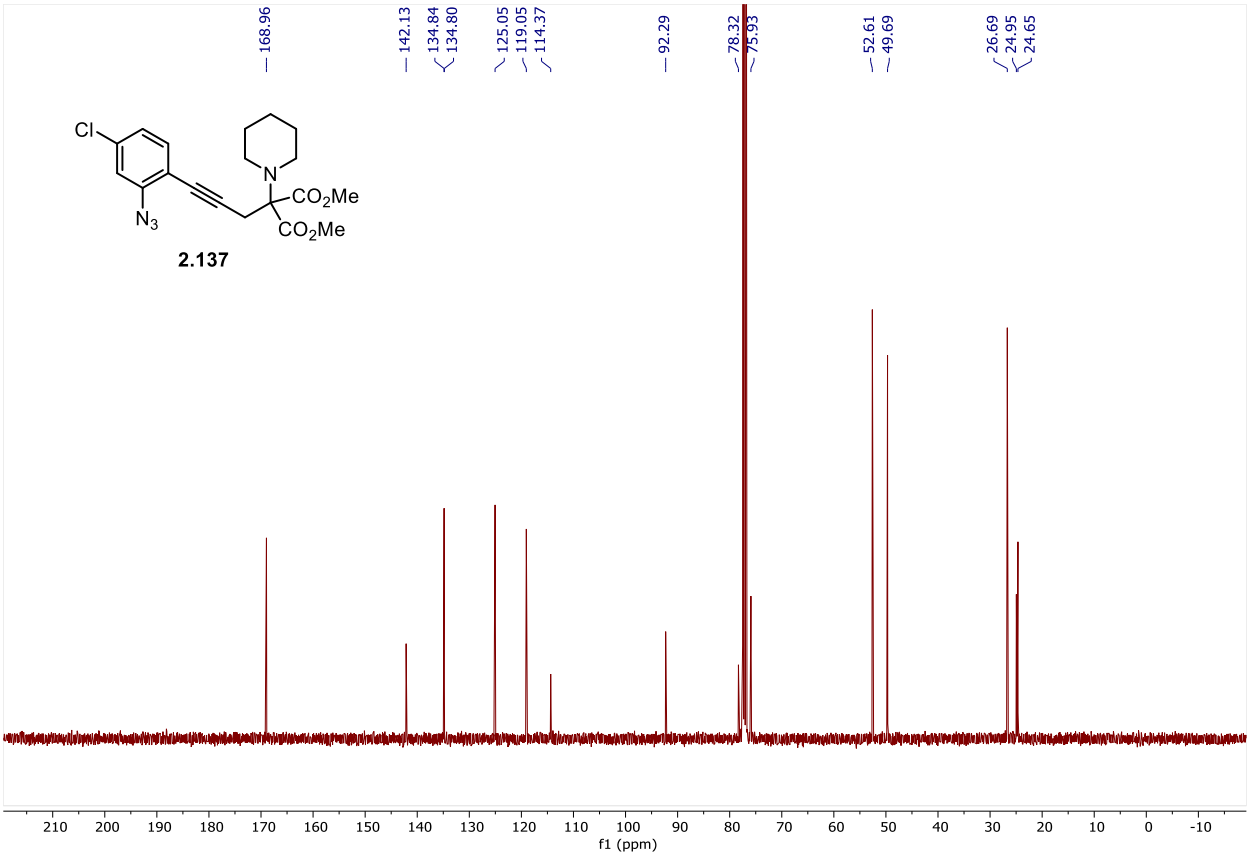

F
N
CO2Me
CO2Me
N3
2.134
7.05
7.05
7.05
7.03
7.03
7.02
7.01
7.01
7.00
6.99
6.99
3.80
3.22
2.65
2.64
2.63
1.67
1.65
1.64
1.63
1.61
1.49
1.48
1.46
1.45
1.44
0.85
1.78
5.98
2.00
4.01
4.16
2.05
f1 (ppm)

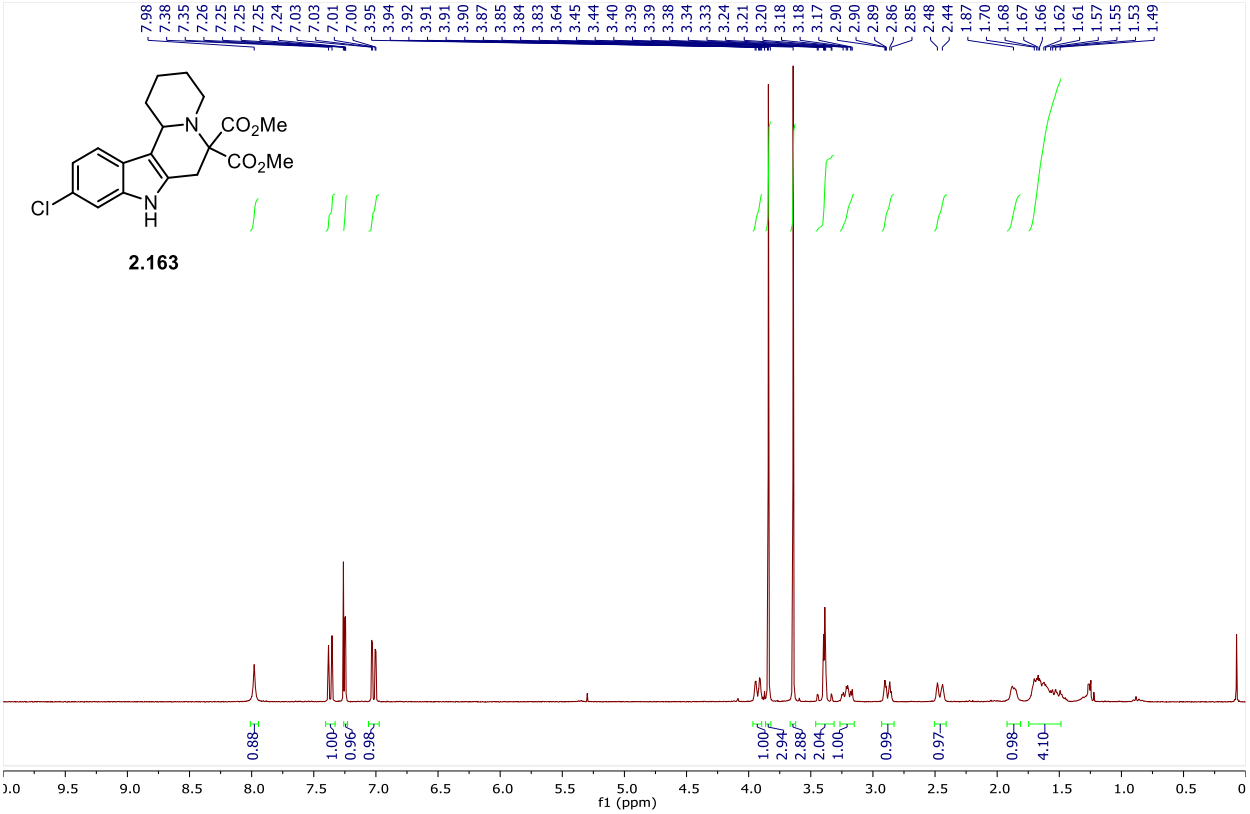

F
N
CO2Me
CO2Me
N3
2.134
168.92
160.46
158.03
137.04
120.48
120.24
120.19
120.10
117.25
117.15
116.68
116.45
92.53
78.30
78.27
75.90
52.62
49.69
26.68
24.91
24.64
f1 (ppm)

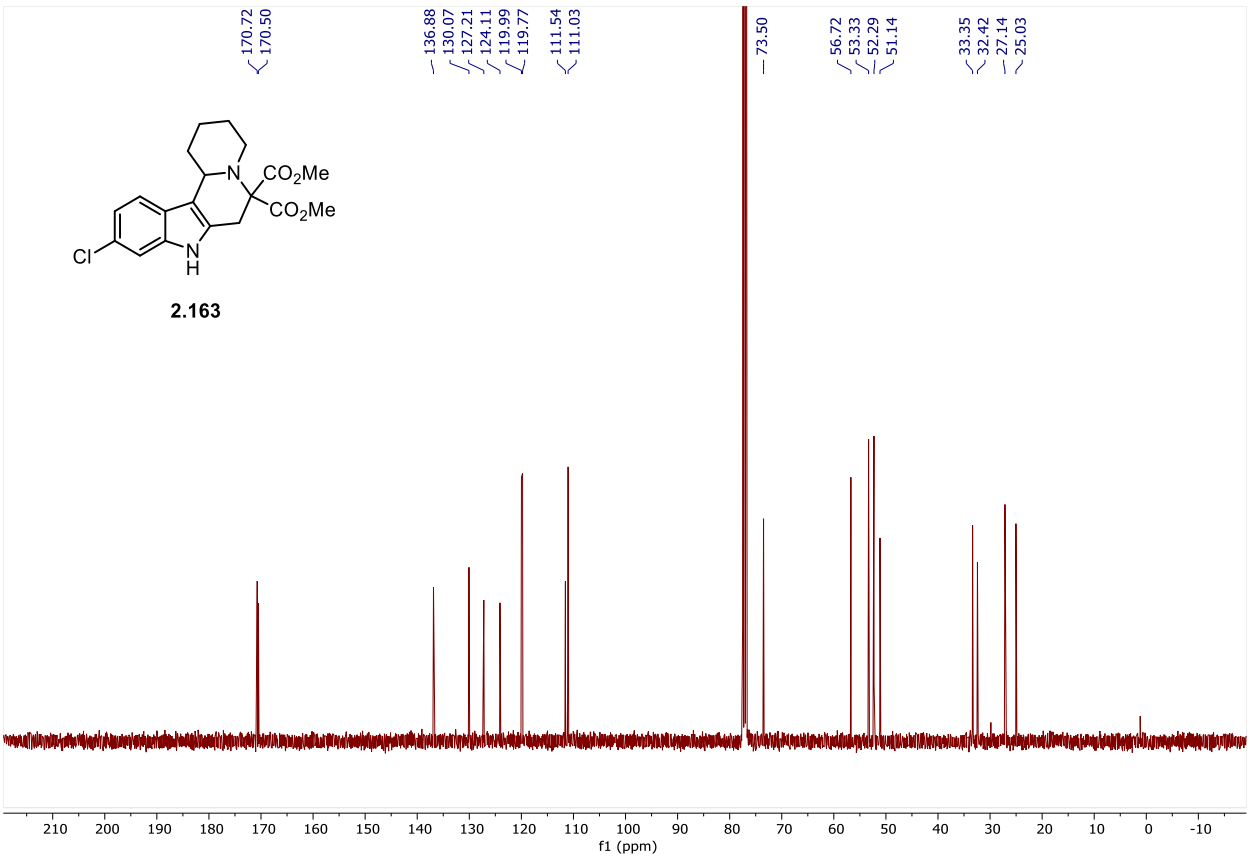

7.96 7.17 7.16 7.15 7.13 7.12 7.11 7.10 6.87 6.86 6.84 6.84 6.82 6.82 3.93 3.92 3.90 3.89 3.83 3.64 3.44 3.41 3.41 3.40 3.40 3.39 3.39 3.36 3.35 3.24 3.23 3.21 3.20 3.18 3.17 2.90 2.87 2.46 2.43 1.89 1.88 1.87 1.86 1.85 1.72 1.71 1.70 1.69 1.67 1.67 1.66 1.65 1.64 1.63 1.62 1.62 1.61 1.60 1.59 1.58 1.55 1.54 1.53 1.52 1.51 1.51 1.49 1.48 1.47
F
N
H
CO2Me
CO2Me
2.160
0.97
2.04
1.00
0.97
2.97
3.01
2.05
0.94
1.01
0.95
0.92
4.32
f1 (ppm)

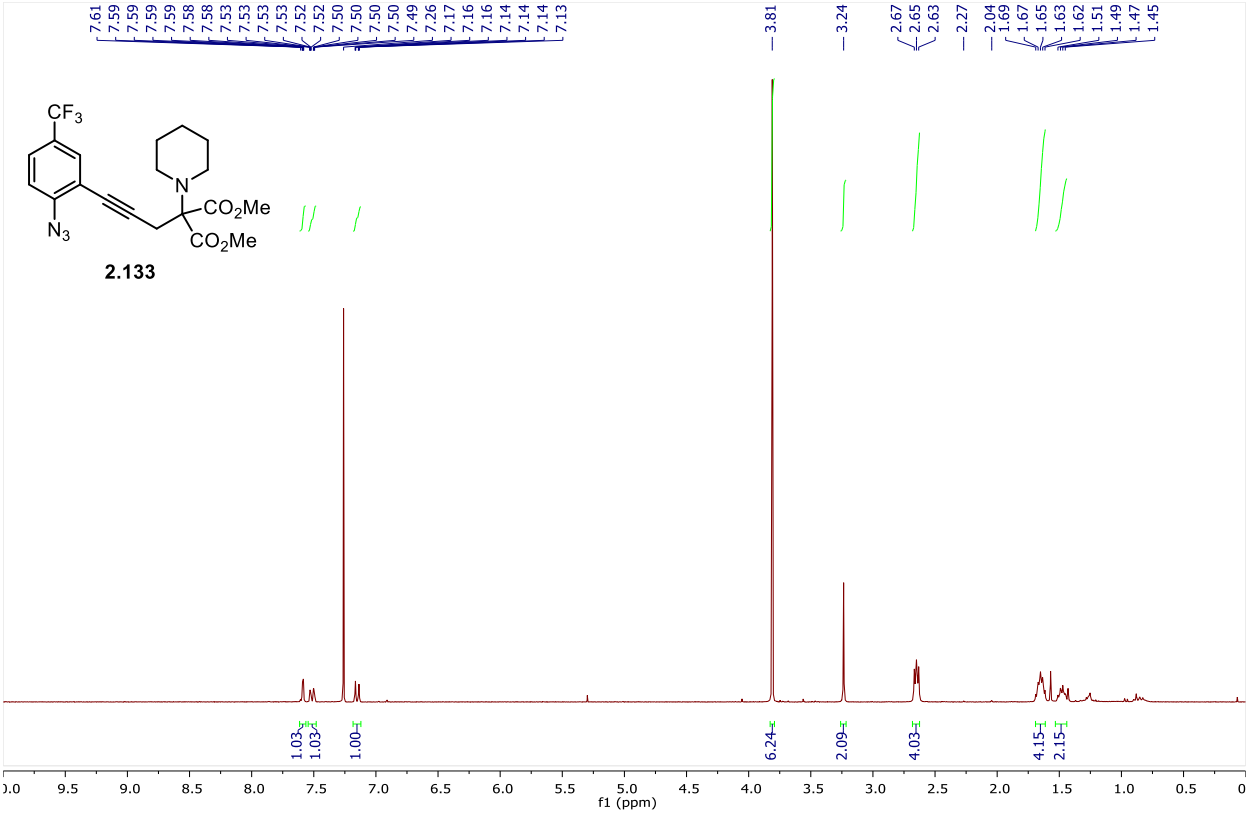

170.77 170.50 158.80 156.48 132.93 131.29 125.81 125.71 111.62 111.58 111.47 111.37 109.37 109.11 104.40 104.16 73.49 56.72 53.28 52.27 51.14 33.13 32.52 27.14 24.99
F
N
H
CO2Me
CO2Me
2.160
f1 (ppm)

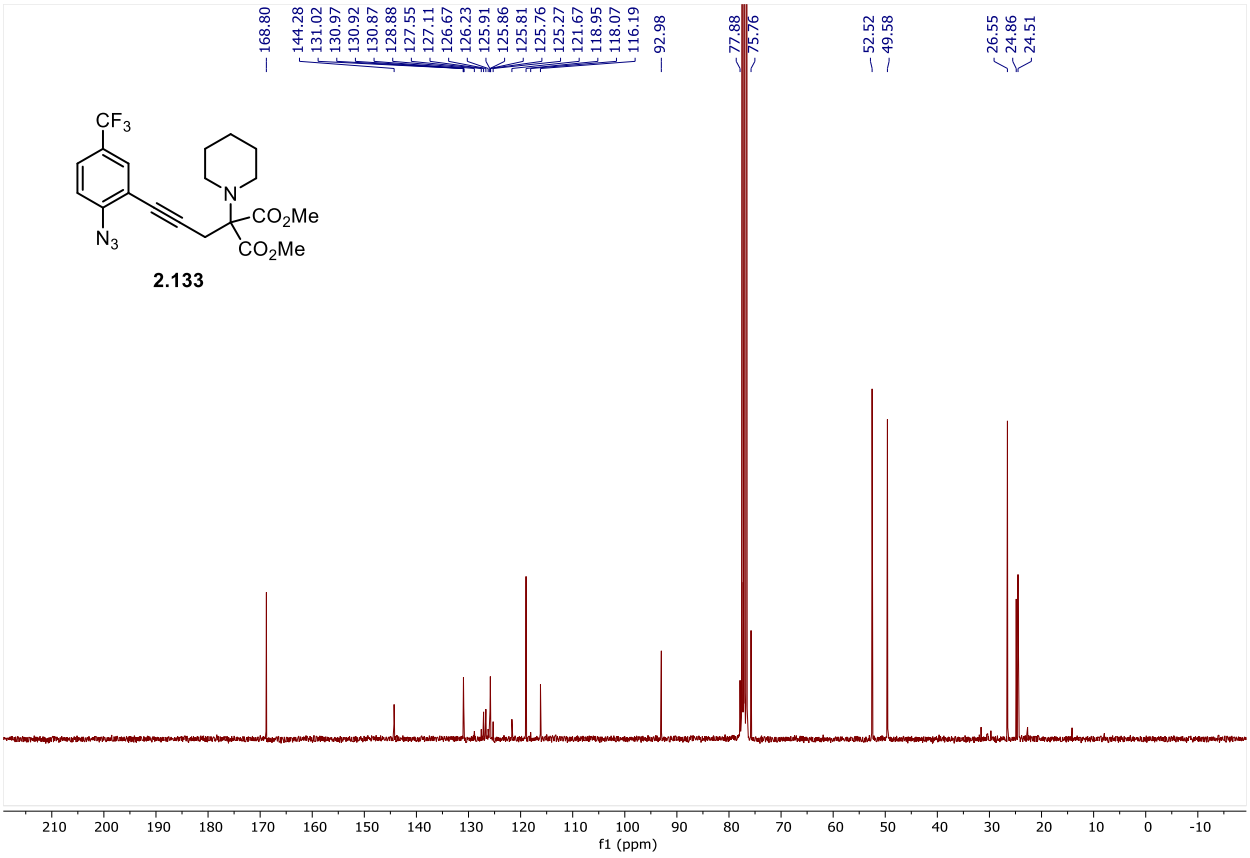

7.28
7.26
7.25
7.05
7.04
7.04
7.03
7.01
7.00
3.80
3.66
3.21
2.66
2.64
2.62
1.68
1.66
1.66
1.64
1.62
1.62
1.60
1.60
1.50
1.48
1.46
1.44
Cl
N
CO2Me
CO2Me
N3
2.137
2.80
1.93
6.00
2.00
4.06
3.96
1.96
f1 (ppm)

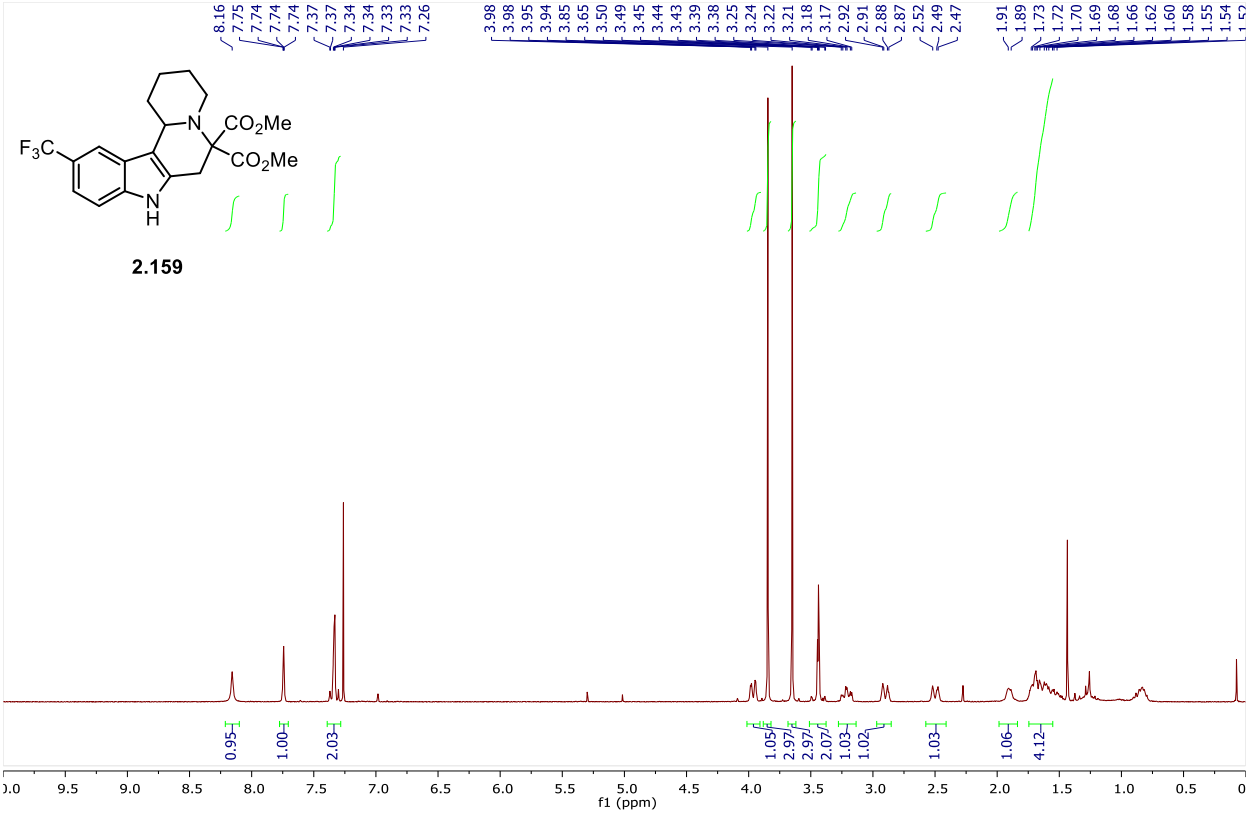

168.96
142.13
134.84
134.80
125.05
119.05
114.37
92.29
78.32
75.93
52.61
49.69
26.69
24.95
24.65
Cl
N
CO2Me
CO2Me
N3
2.137
f1 (ppm)

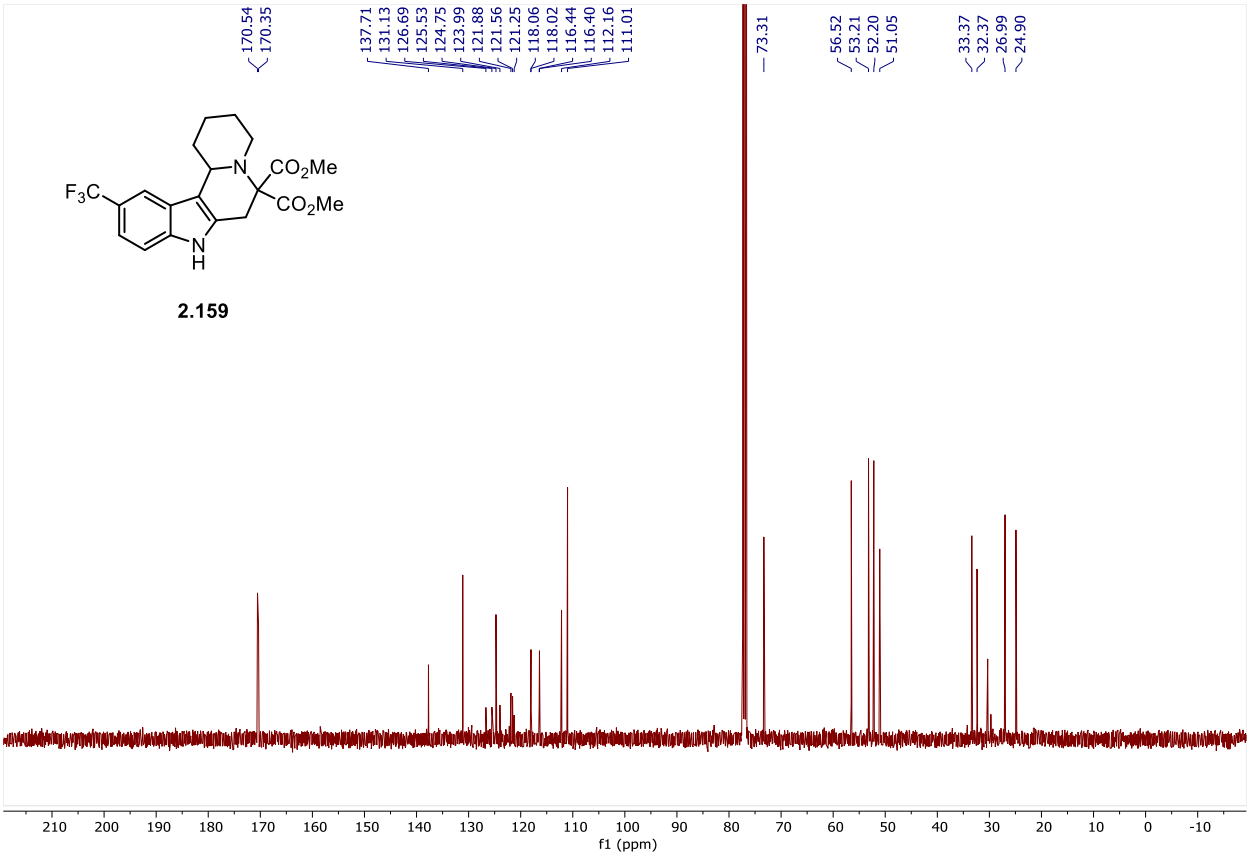

7.98 7.38 7.35 7.26 7.25 7.25 7.25 7.24 7.03 7.03 7.01 7.00 3.95 3.94 3.92 3.91 3.91 3.90 3.87 3.85 3.84 3.83 3.64 3.45 3.44 3.40 3.39 3.39 3.38 3.34 3.33 3.24 3.21 3.20 3.18 3.18 3.17 2.90 2.90 2.89 2.86 2.85 2.48 2.44 1.87 1.70 1.68 1.67 1.66 1.62 1.61 1.57 1.55 1.53 1.49
CO2Me
CO2Me
Cl
N
H
2.163
0.88 1.00 0.96 0.98 1.00 2.94 2.88 2.04 1.00 0.99 0.97 0.98 4.10
f1 (ppm)

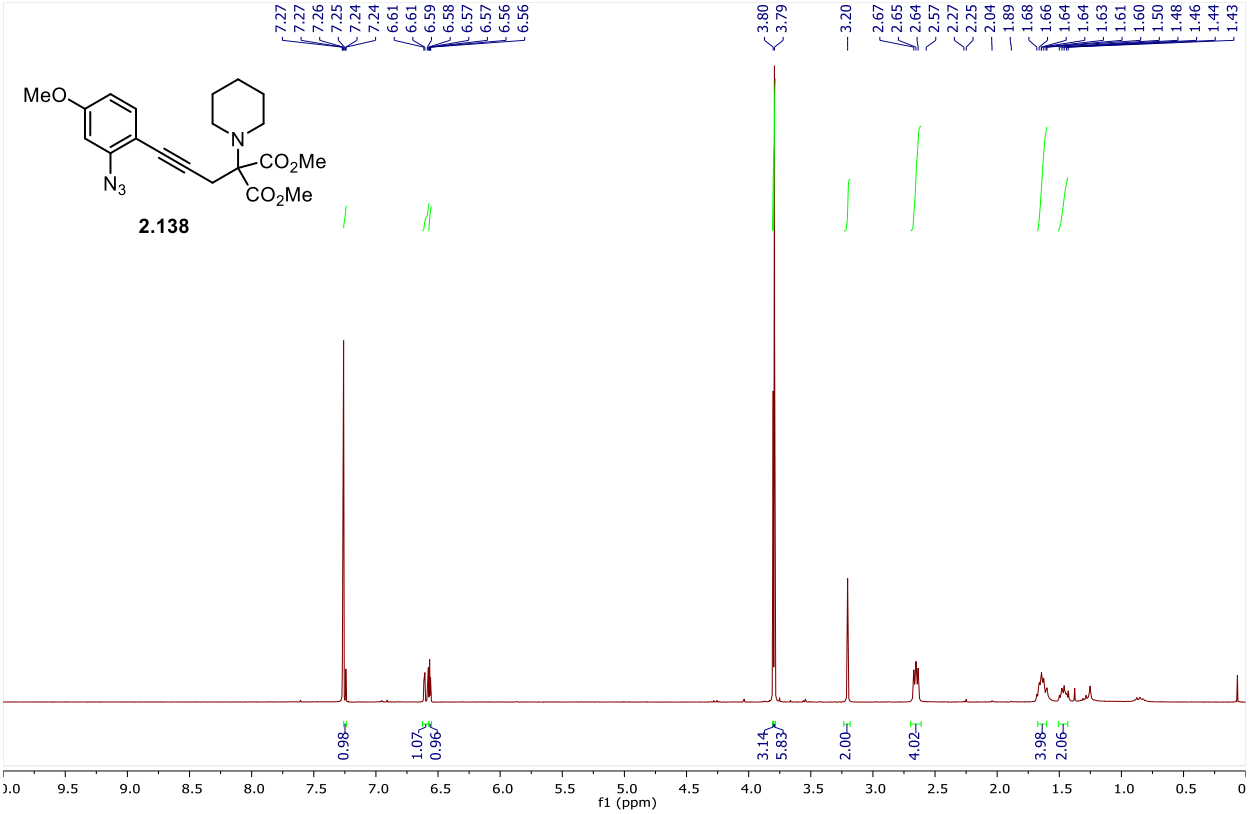

170.72 170.50 136.88 130.07 127.21 124.11 119.99 119.77 111.54 111.03 73.50 56.72 53.33 52.29 51.14 33.35 32.42 27.14 25.03
CO2Me
CO2Me
Cl
N
H
2.163
f1 (ppm)

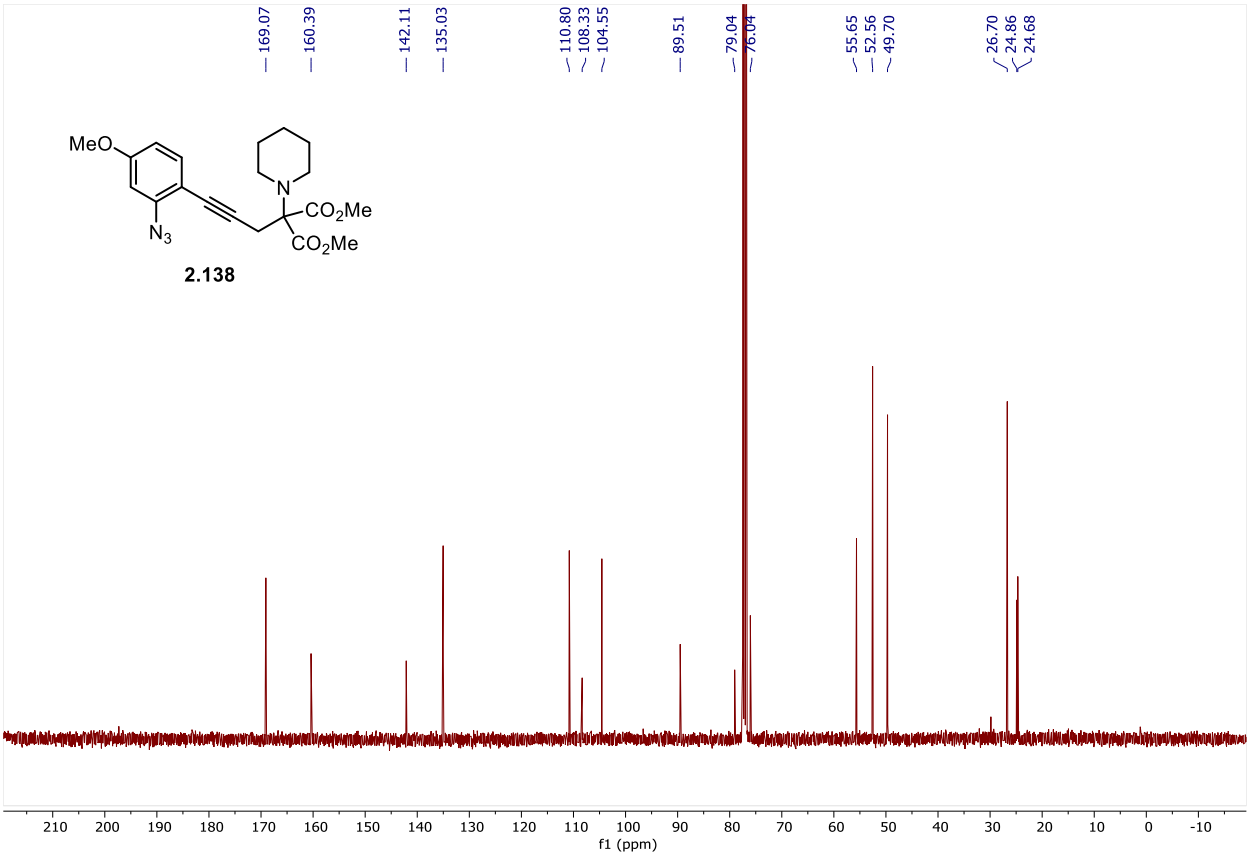

7.61 7.59 7.59 7.59 7.59 7.58 7.58 7.53 7.53 7.53 7.53 7.52 7.52 7.50 7.50 7.50 7.50 7.50 7.49 7.26 7.17 7.16 7.16 7.14 7.14 7.14 7.13
3.81
3.24
2.67 2.65 2.63
2.27
2.04 1.69 1.67 1.65 1.63 1.62 1.51 1.49 1.47 1.45
CF3
N3
N
CO2Me
CO2Me
2.133
1.03 1.03 1.00 6.24 2.09 4.03 4.15 2.15
f1 (ppm)

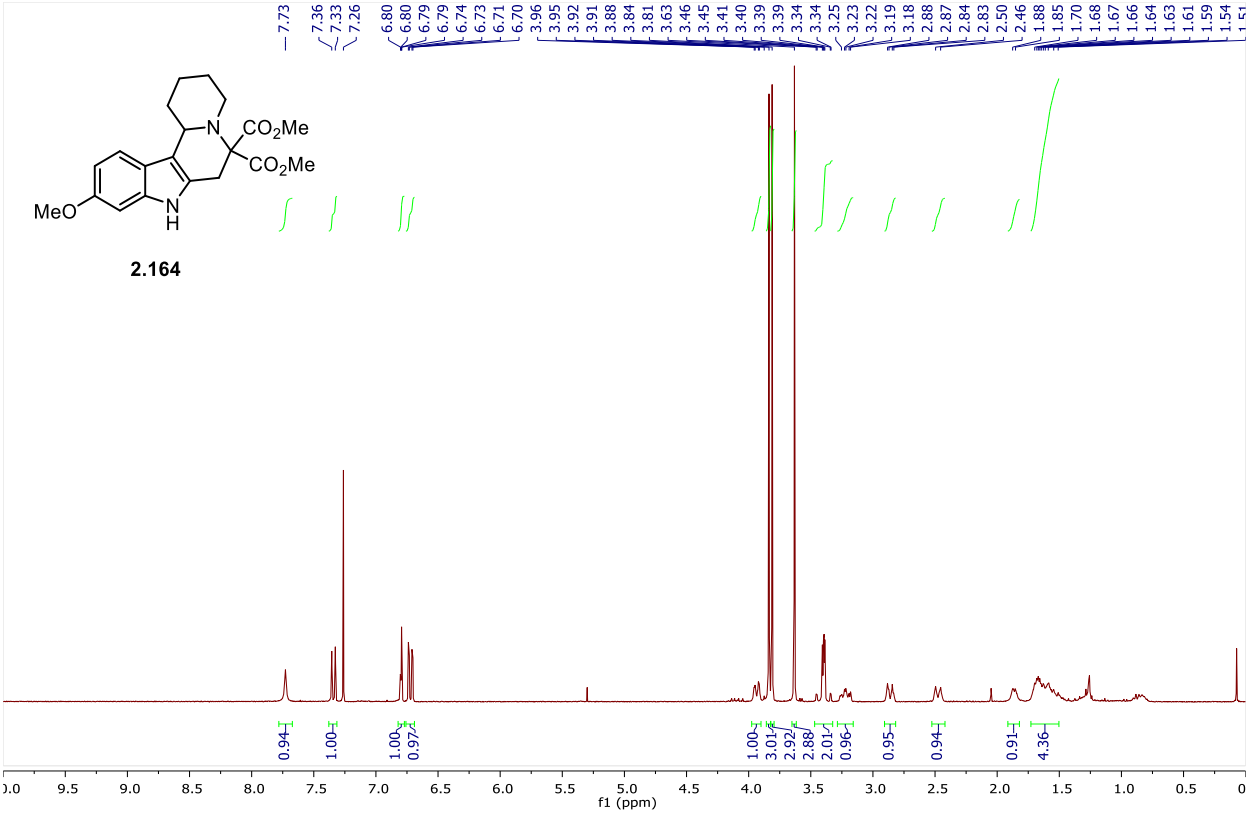

168.80
144.28 131.02 130.97 130.92 130.87 128.88 127.55 127.11 126.67 126.23 125.91 125.86 125.81 125.76 125.27 121.67 118.95 118.07 116.19
92.98
77.88 75.76
52.52 49.58
26.55 24.86 24.51
CF3
N3
N
CO2Me
CO2Me
2.133
f1 (ppm)

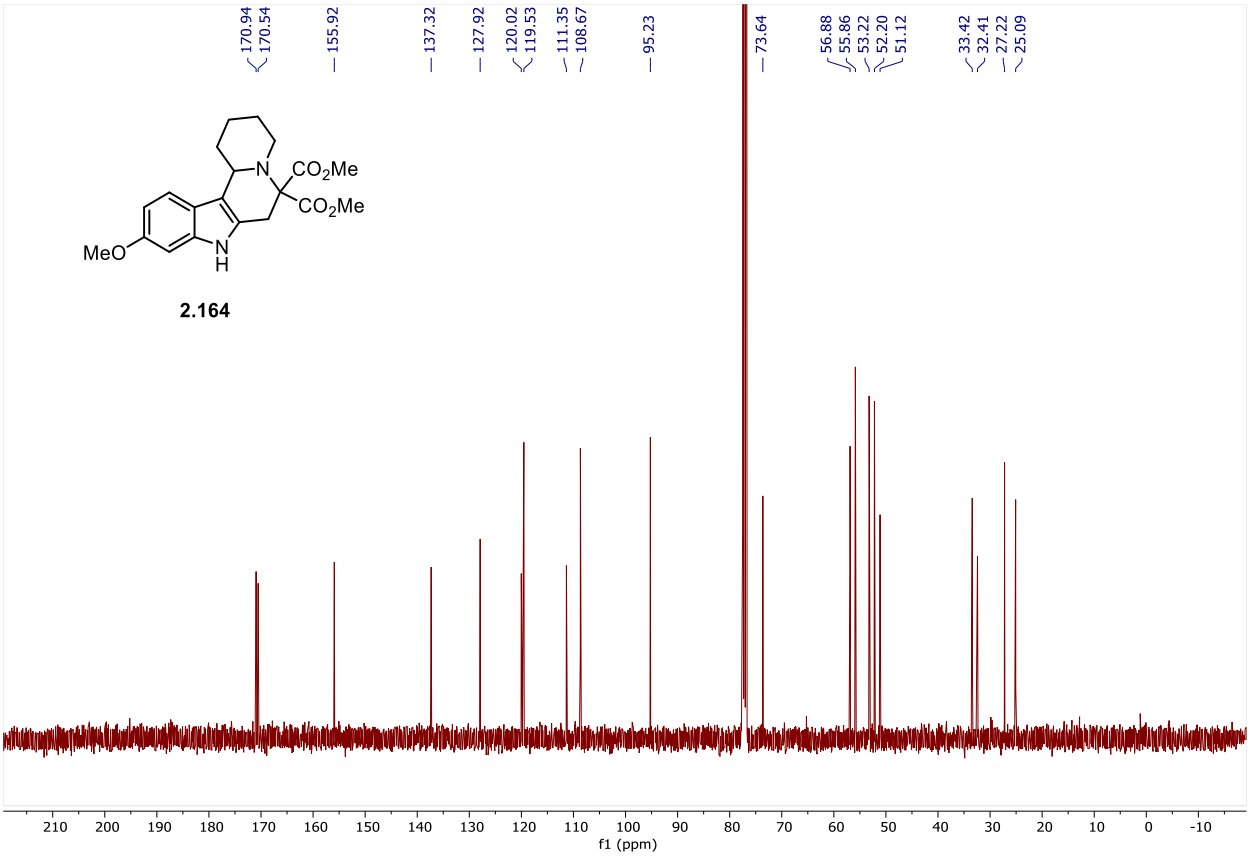

8.16
7.75
7.74
7.74
7.74
7.37
7.37
7.34
7.34
7.33
7.33
7.26
3.98
3.98
3.95
3.94
3.85
3.65
3.50
3.49
3.45
3.44
3.43
3.39
3.38
3.25
3.24
3.22
3.21
3.18
3.17
2.92
2.91
2.88
2.87
2.52
2.49
2.47
1.91
1.89
1.73
1.72
1.70
1.69
1.68
1.66
1.62
1.60
1.58
1.55
1.54
F3C
CO2Me
CO2Me
N
H
2.159
0.95
1.00
2.03
1.05
2.97
2.97
2.07
1.03
1.02
1.03
1.06
4.12
f1 (ppm)

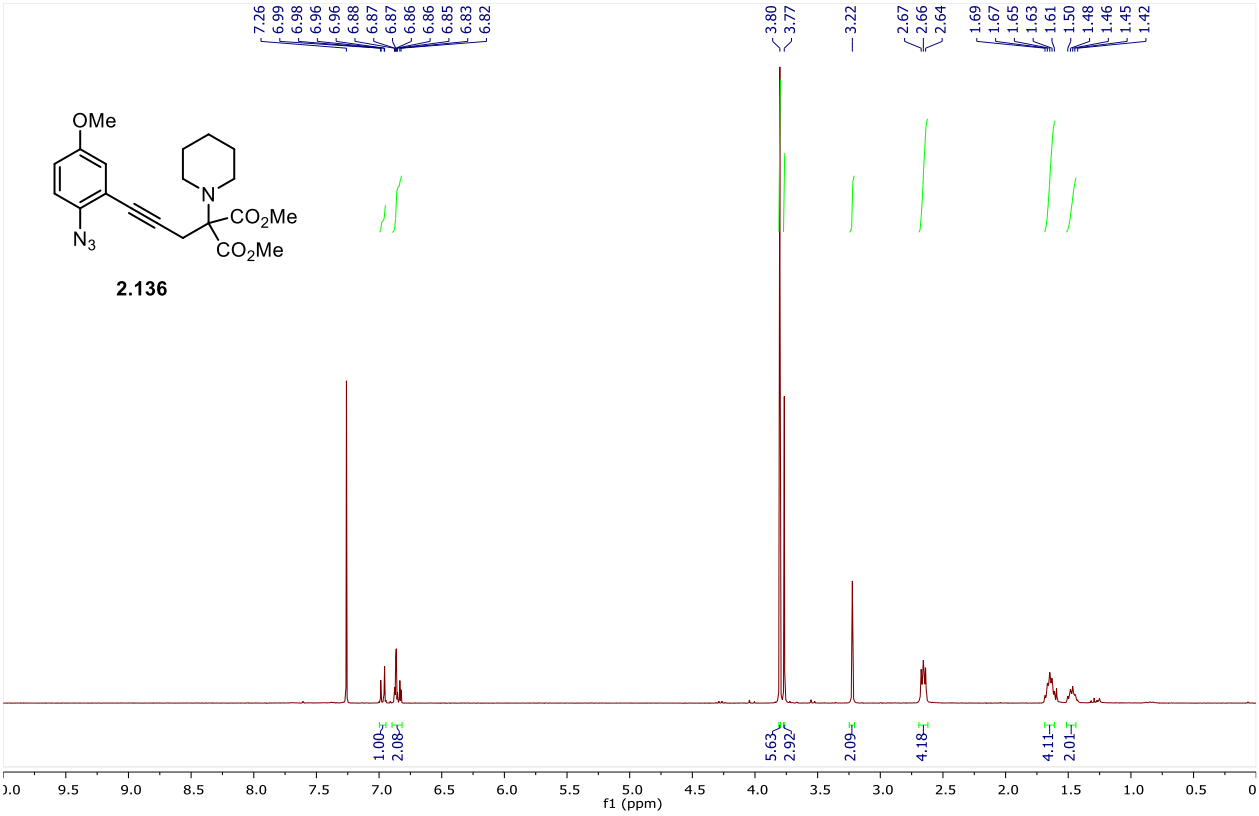

170.54
170.35
137.71
131.13
126.69
125.53
124.75
123.99
121.88
121.56
121.25
118.06
118.02
116.44
116.40
112.16
111.01
73.31
56.52
53.21
52.20
51.05
33.37
32.37
26.99
24.90
F3C
CO2Me
CO2Me
N
H
2.159
f1 (ppm)

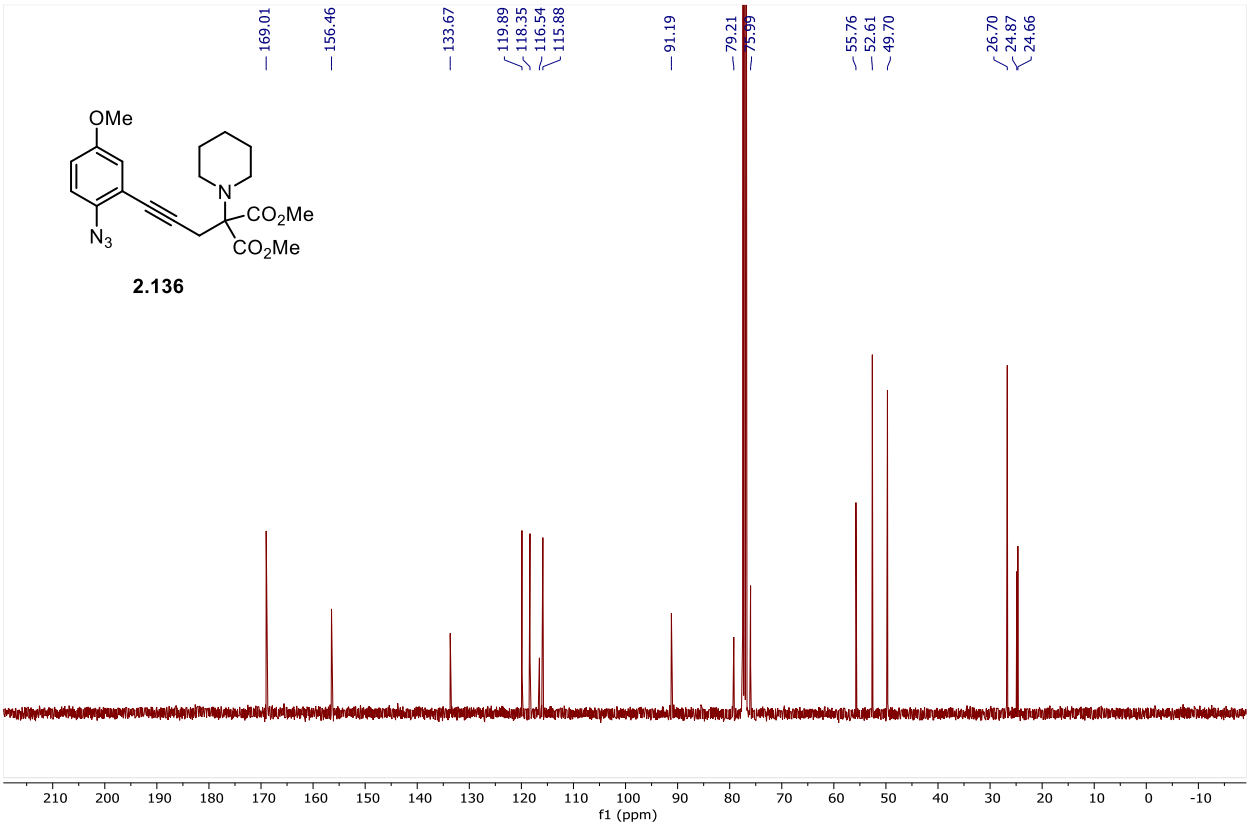

MeO
N
N3
CO2Me
CO2Me
2.138
7.27
7.27
7.26
7.25
7.24
7.24
6.61
6.61
6.59
6.58
6.57
6.57
6.56
6.56
3.80
3.79
3.20
2.67
2.65
2.64
2.57
2.27
2.25
2.04
1.89
1.68
1.66
1.64
1.64
1.63
1.61
1.60
1.50
1.48
1.46
1.44
1.43
0.98
1.07
0.96
3.14
5.83
2.00
4.02
3.98
2.06
f1 (ppm)

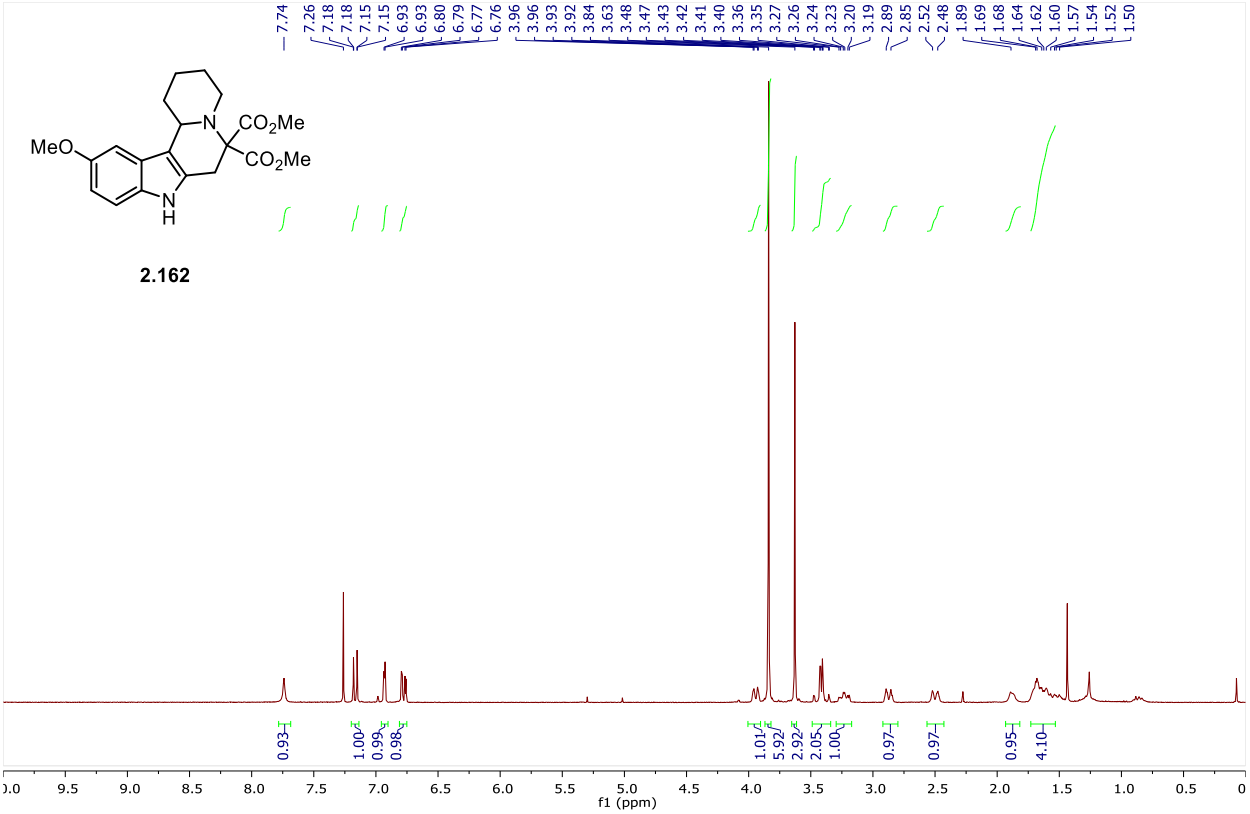

MeO
N
N3
CO2Me
CO2Me
2.138
169.07
160.39
142.11
135.03
110.80
108.33
104.55
89.51
79.04
76.04
55.65
52.56
49.70
26.70
24.86
24.68
f1 (ppm)

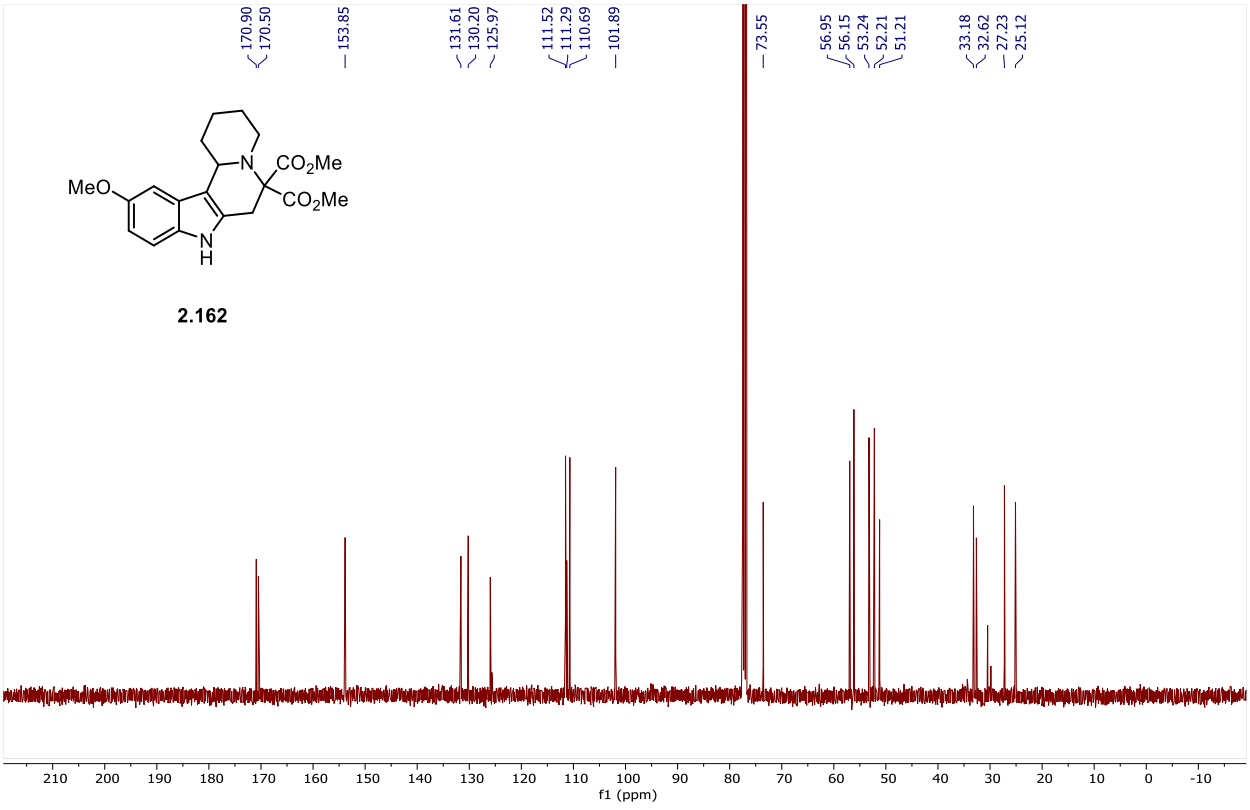

7.73
7.36
7.33
7.26
6.80
6.80
6.79
6.79
6.74
6.73
6.71
6.70
3.96
3.95
3.92
3.91
3.88
3.84
3.81
3.63
3.46
3.45
3.41
3.40
3.39
3.39
3.34
3.34
3.25
3.23
3.22
3.19
3.18
2.88
2.87
2.84
2.83
2.50
2.46
1.88
1.85
1.70
1.68
1.67
1.66
1.64
1.63
1.61
1.59
1.54
CO2Me
CO2Me
MeO
N
H
2.164
0.94
1.00
1.00
0.97
1.00
3.01
2.92
2.88
2.01
0.96
0.95
0.94
0.91
4.36
f1 (ppm)

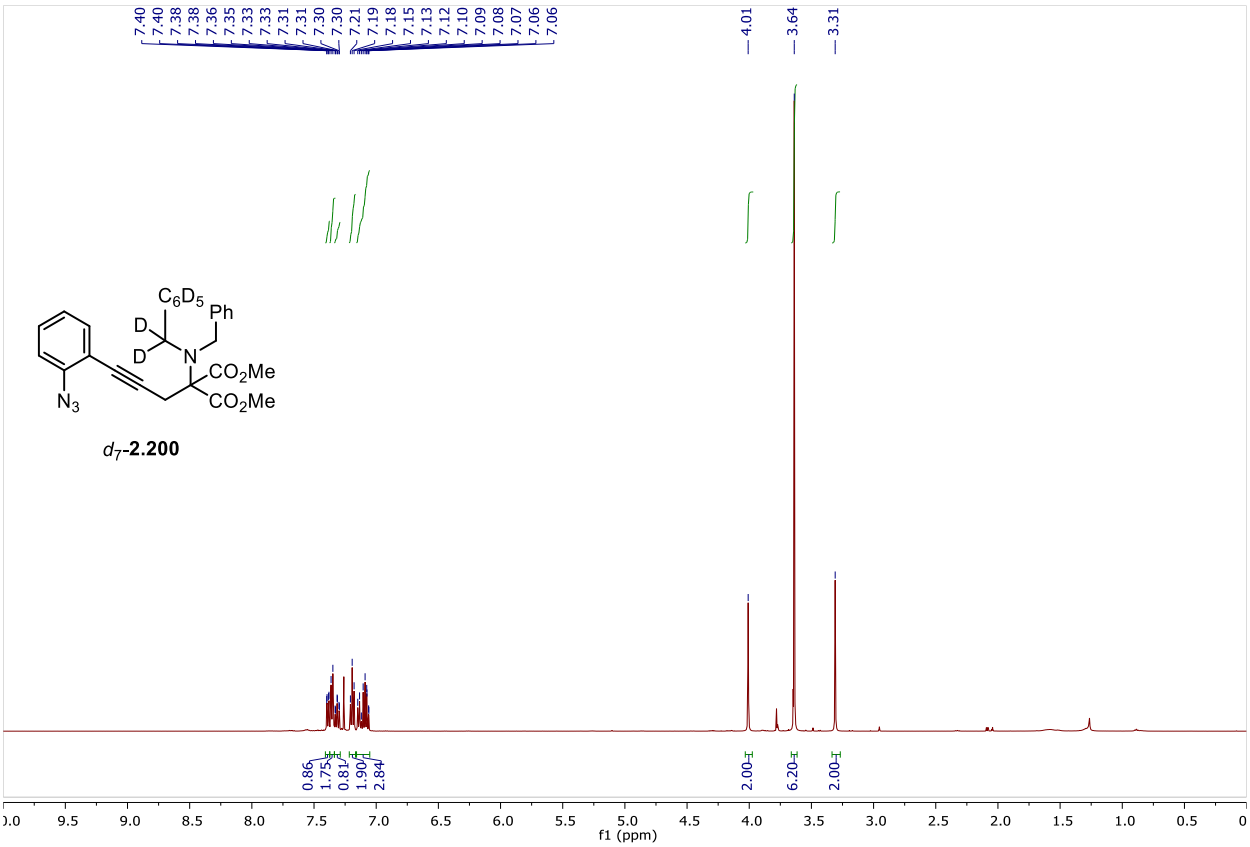

170.94
170.54
155.92
137.32
127.92
120.02
119.53
111.35
108.67
95.23
73.64
56.88
55.86
53.22
52.20
51.12
33.42
32.41
27.22
25.09
CO2Me
CO2Me
MeO
N
H
2.164
f1 (ppm)


7.26
6.99
6.98
6.96
6.96
6.88
6.87
6.87
6.86
6.86
6.85
6.83
6.82
3.80
3.77
3.22
2.67
2.66
2.64
1.69
1.67
1.65
1.63
1.61
1.50
1.48
1.46
1.45
1.42
OMe
N
CO2Me
CO2Me
N3
2.136
1.00
2.08
5.63
2.92
2.09
4.18
4.11
2.01
f1 (ppm)

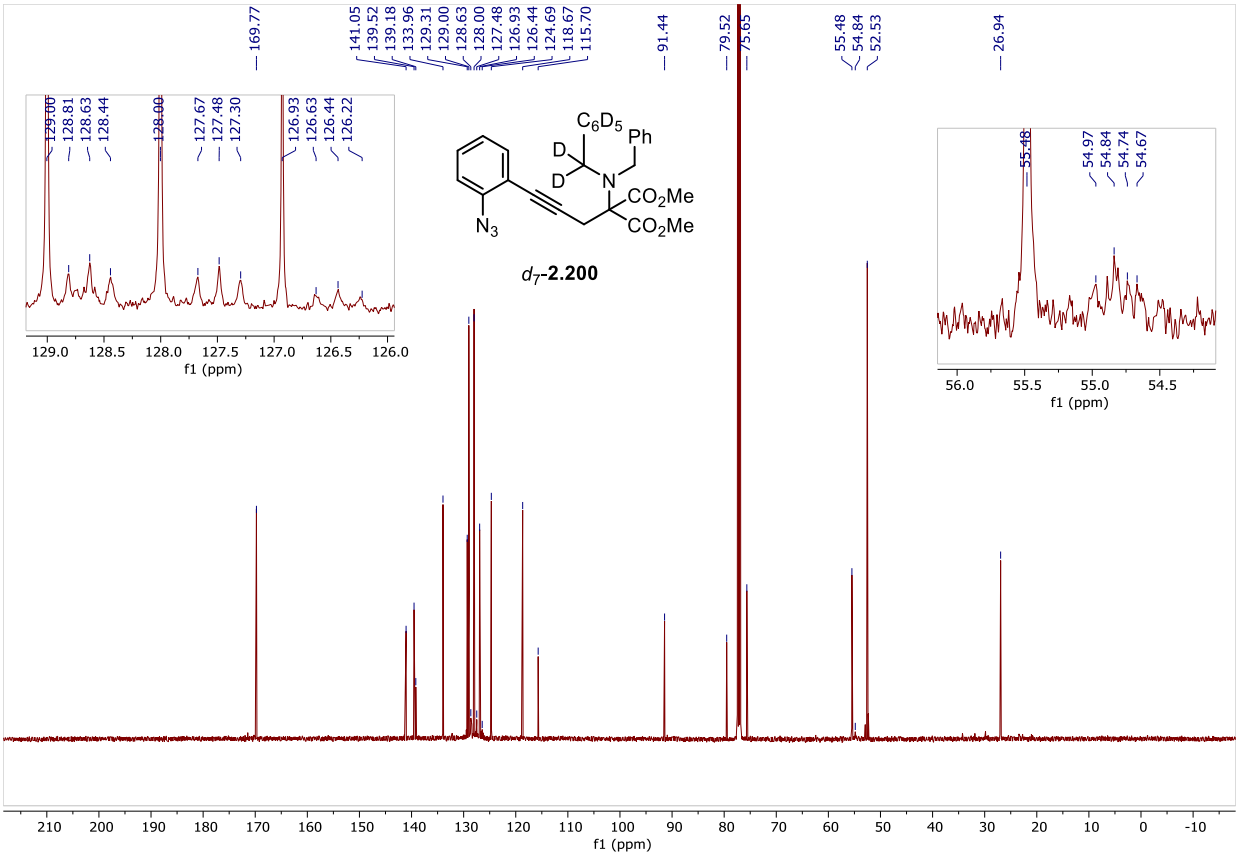

169.01
156.46
133.67
119.89
118.35
116.54
115.88
91.19
79.21
75.99
55.76
52.61
49.70
26.70
24.87
24.66
OMe
N
CO2Me
CO2Me
N3
2.136
f1 (ppm)


MeO
CO2Me
CO2Me
N
H
2.162
f1 (ppm)

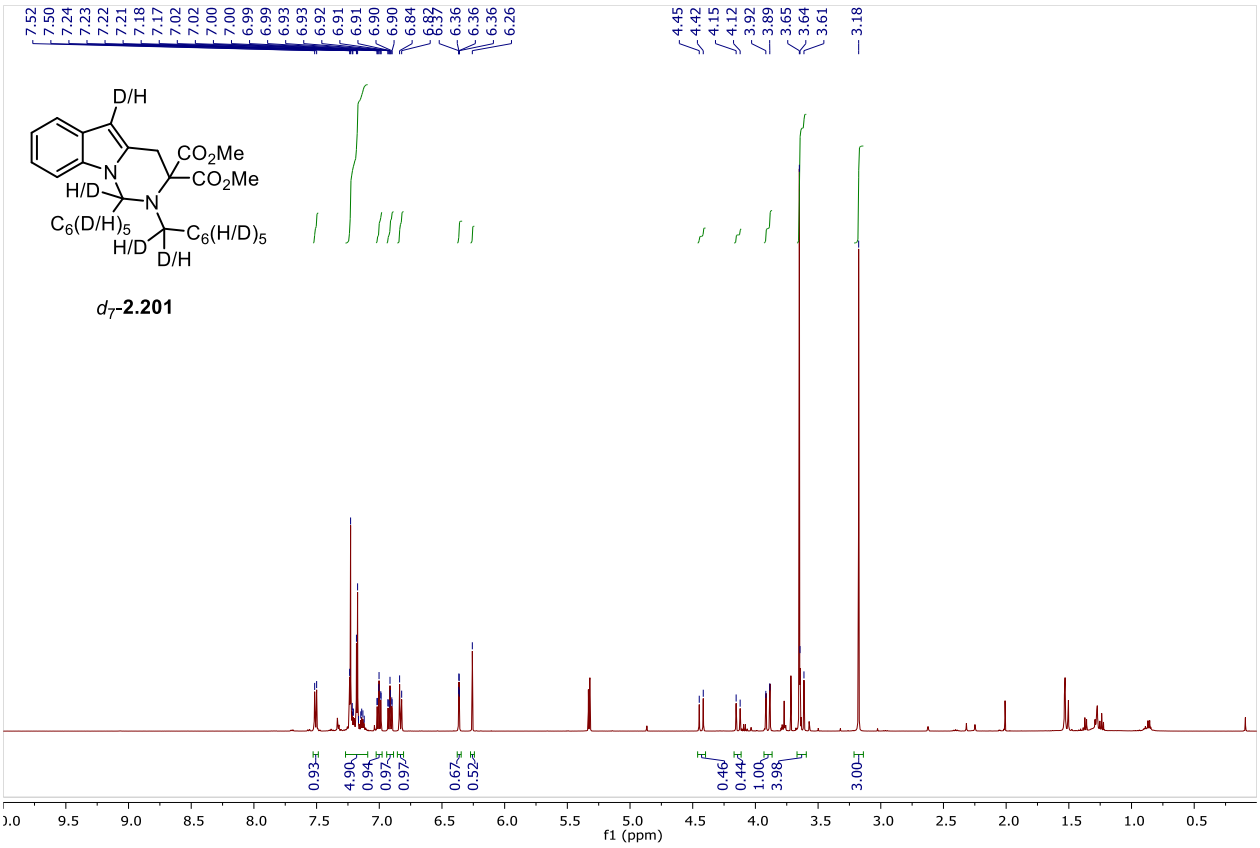

MeO
CO2Me
CO2Me
N
H
2.162
f1 (ppm)



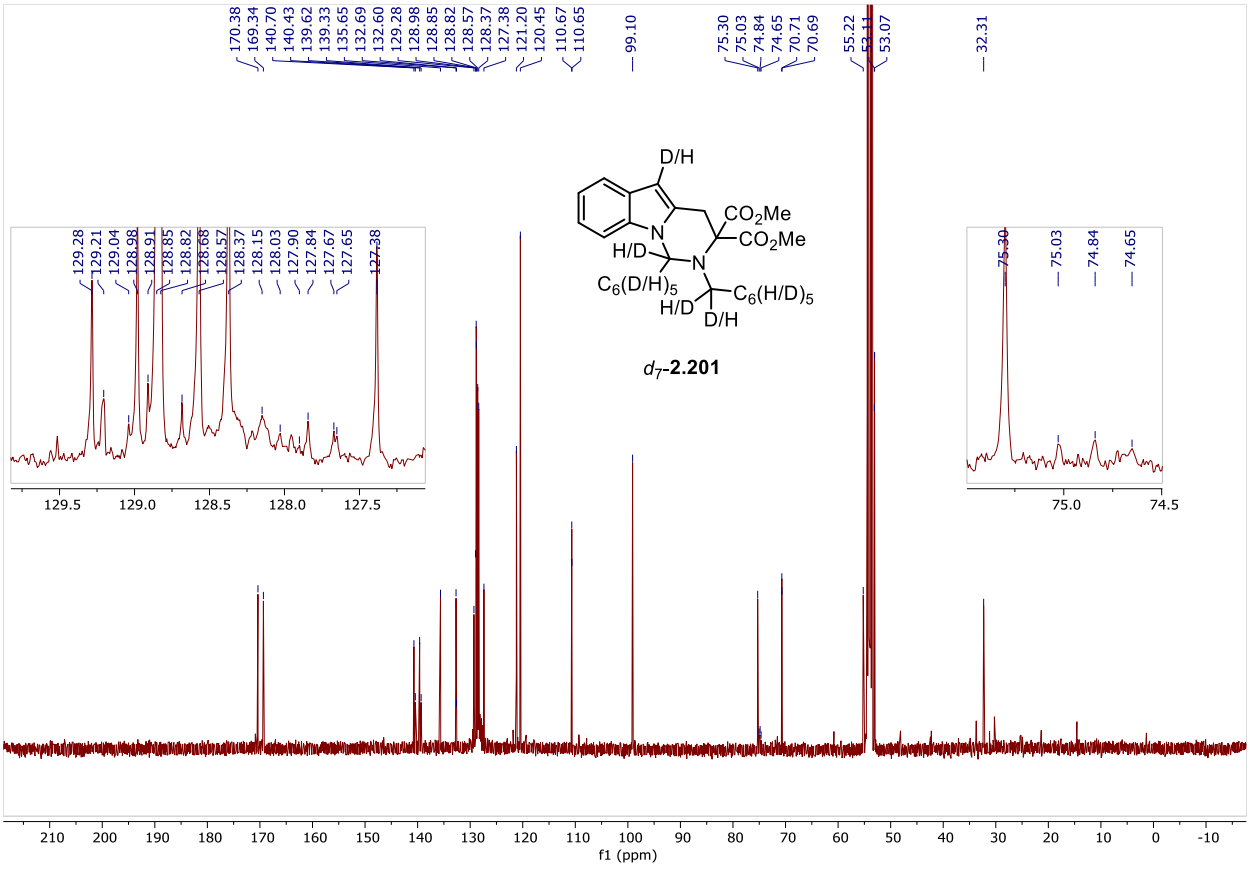
d_7-**2.200**



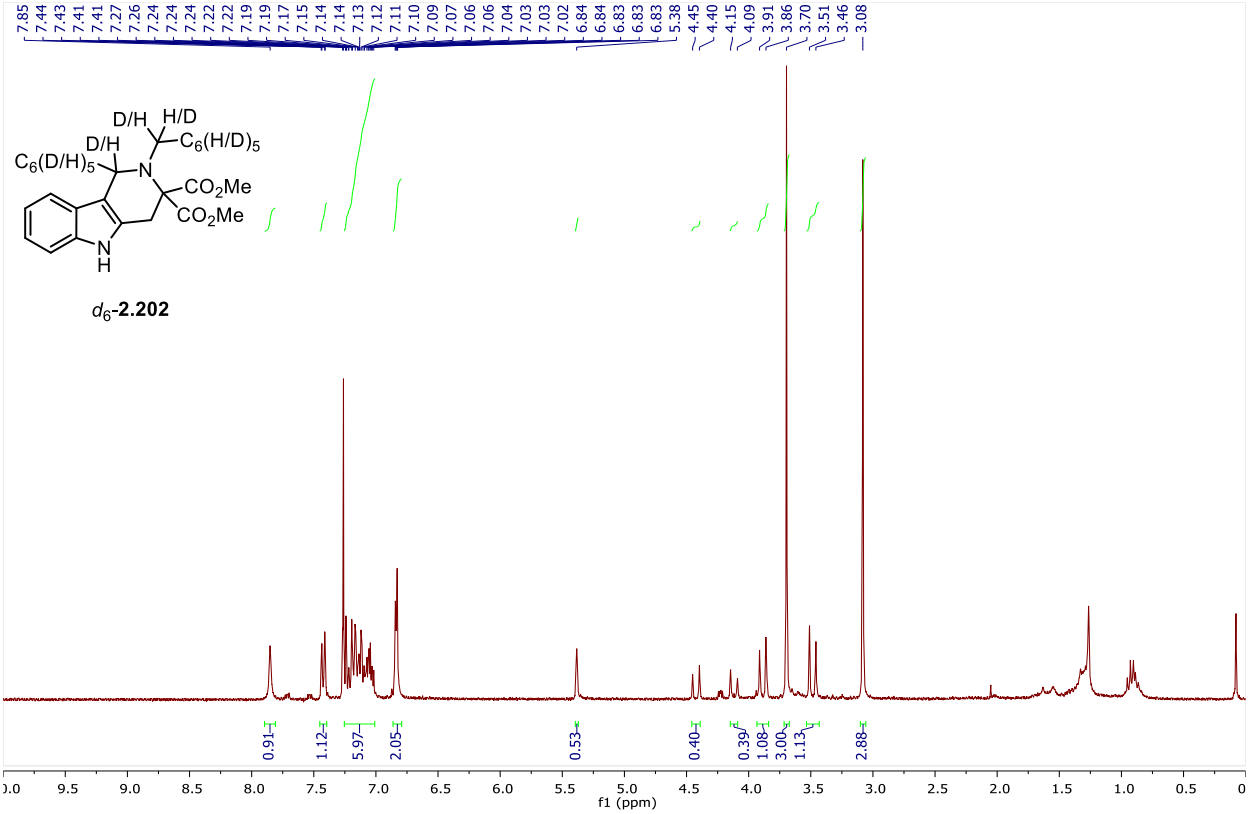
d_7-**2.200**

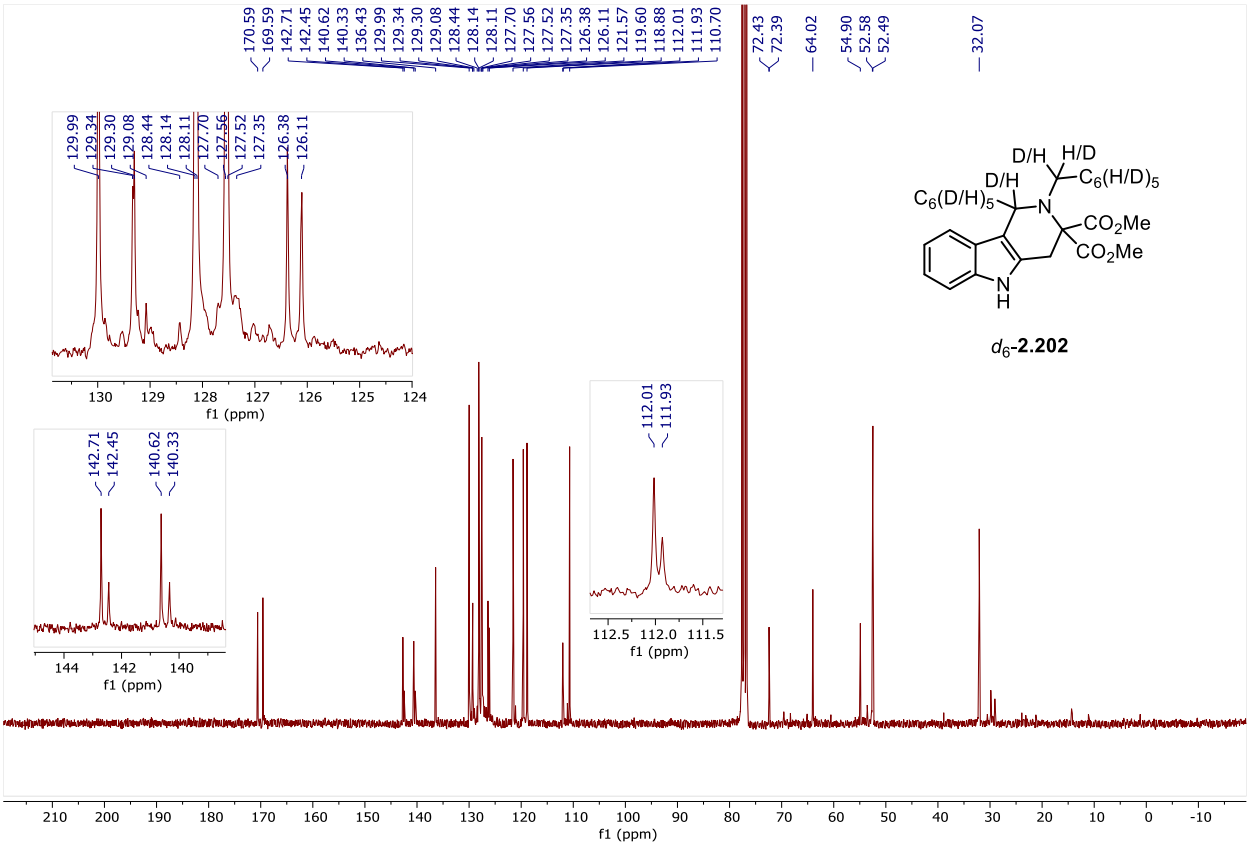


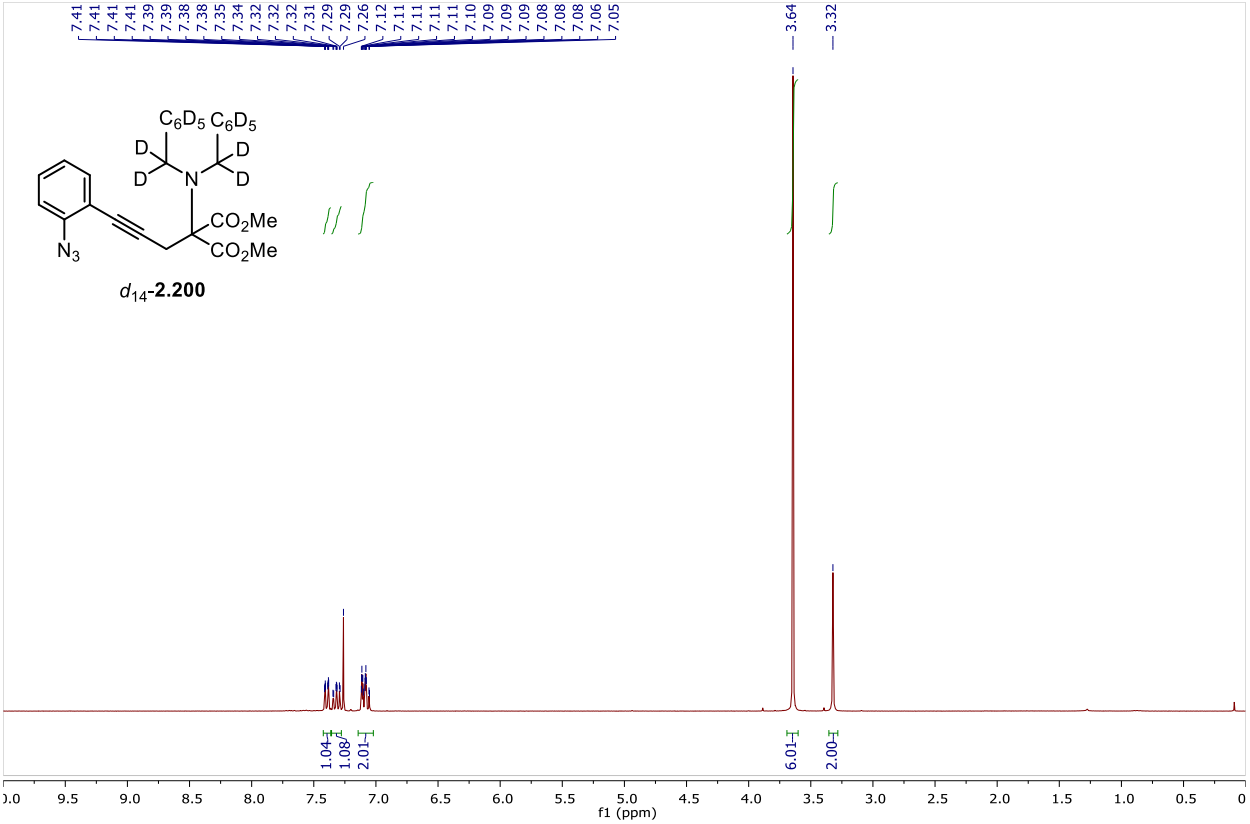
d$_7$-**2.201**

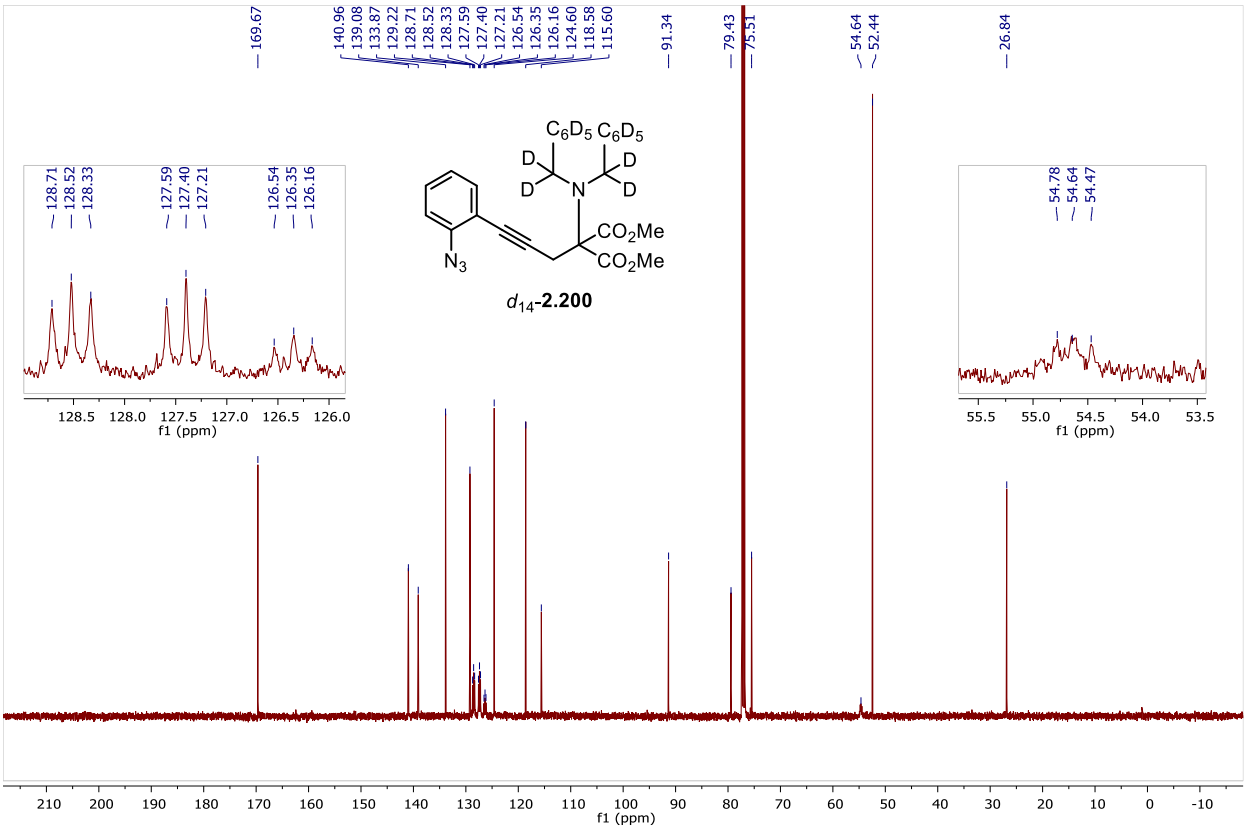


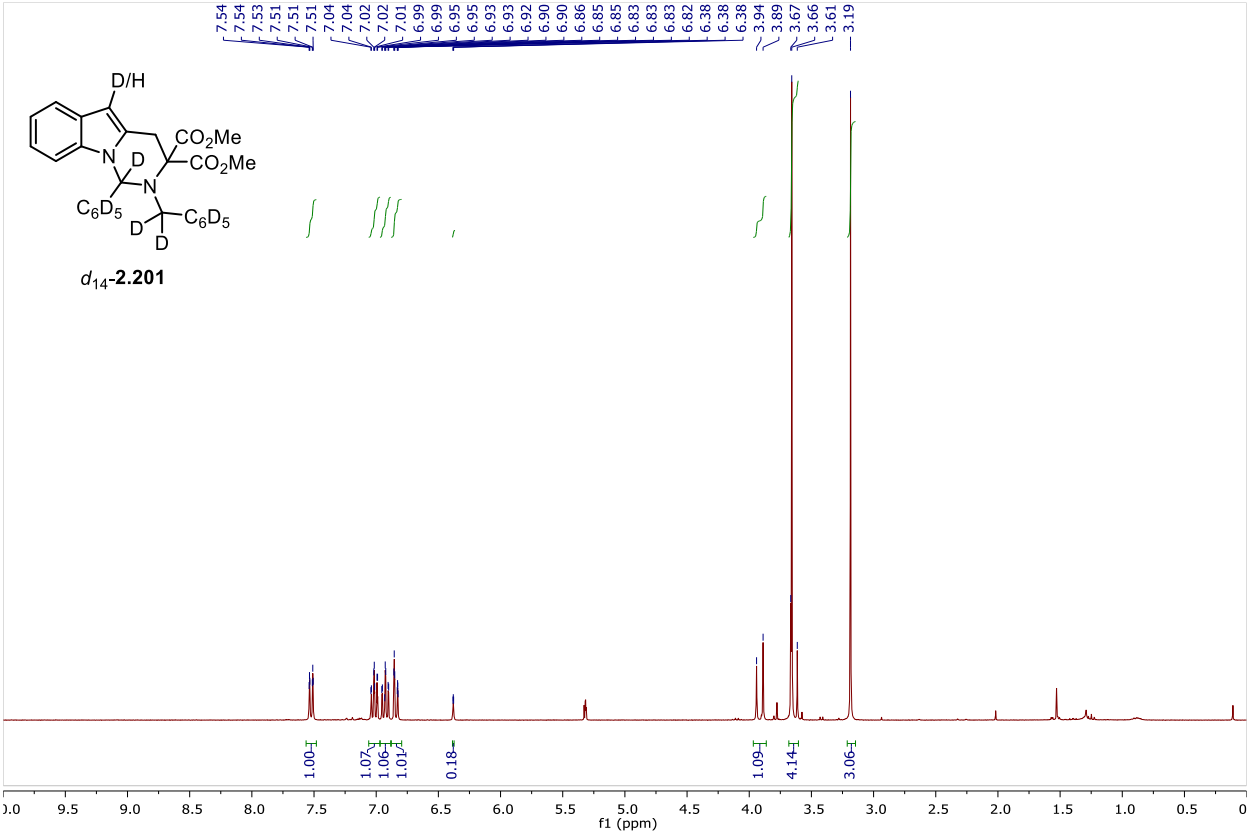
d$_7$-**2.201**

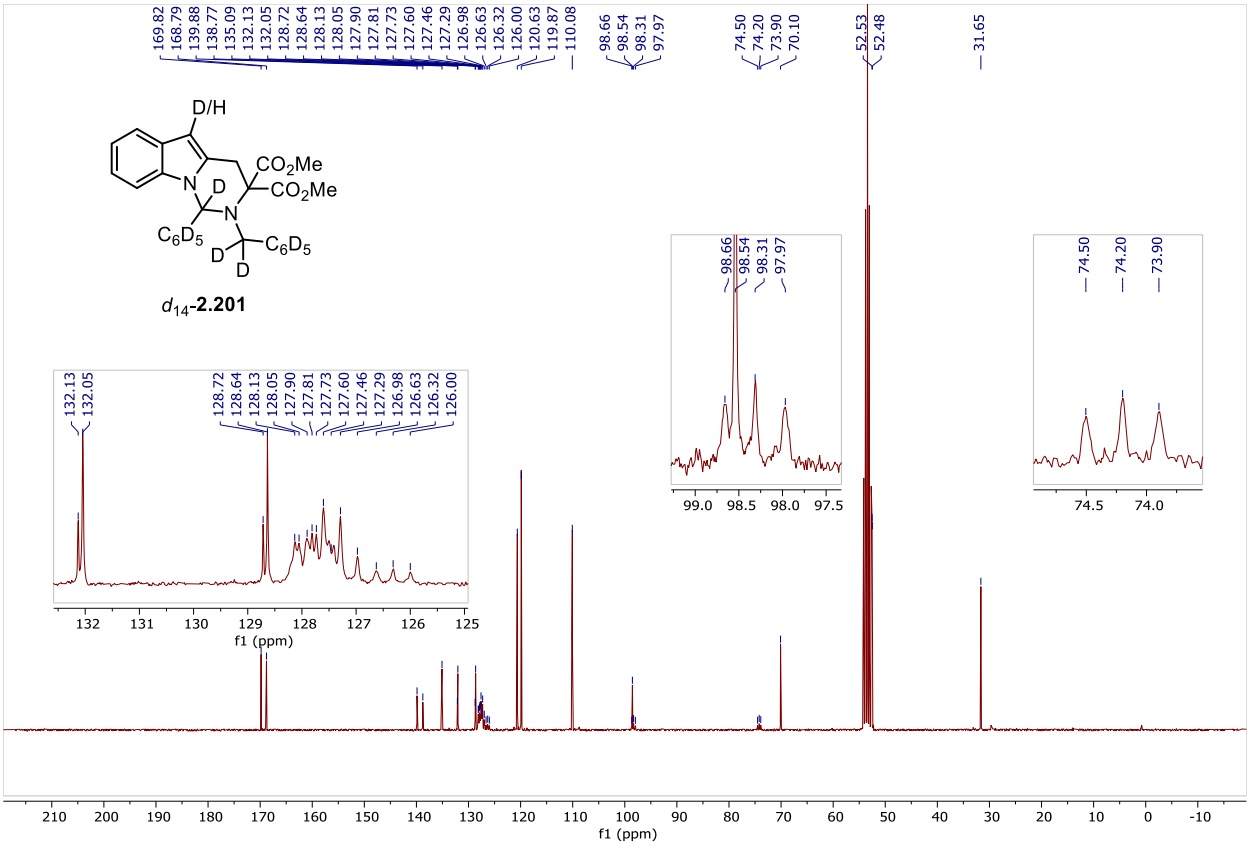

D/H
H/D
C6(H/D)5
D/H
C6(D/H)5
N
CO2Me
CO2Me
N
H
d6-2.202
f1 (ppm)

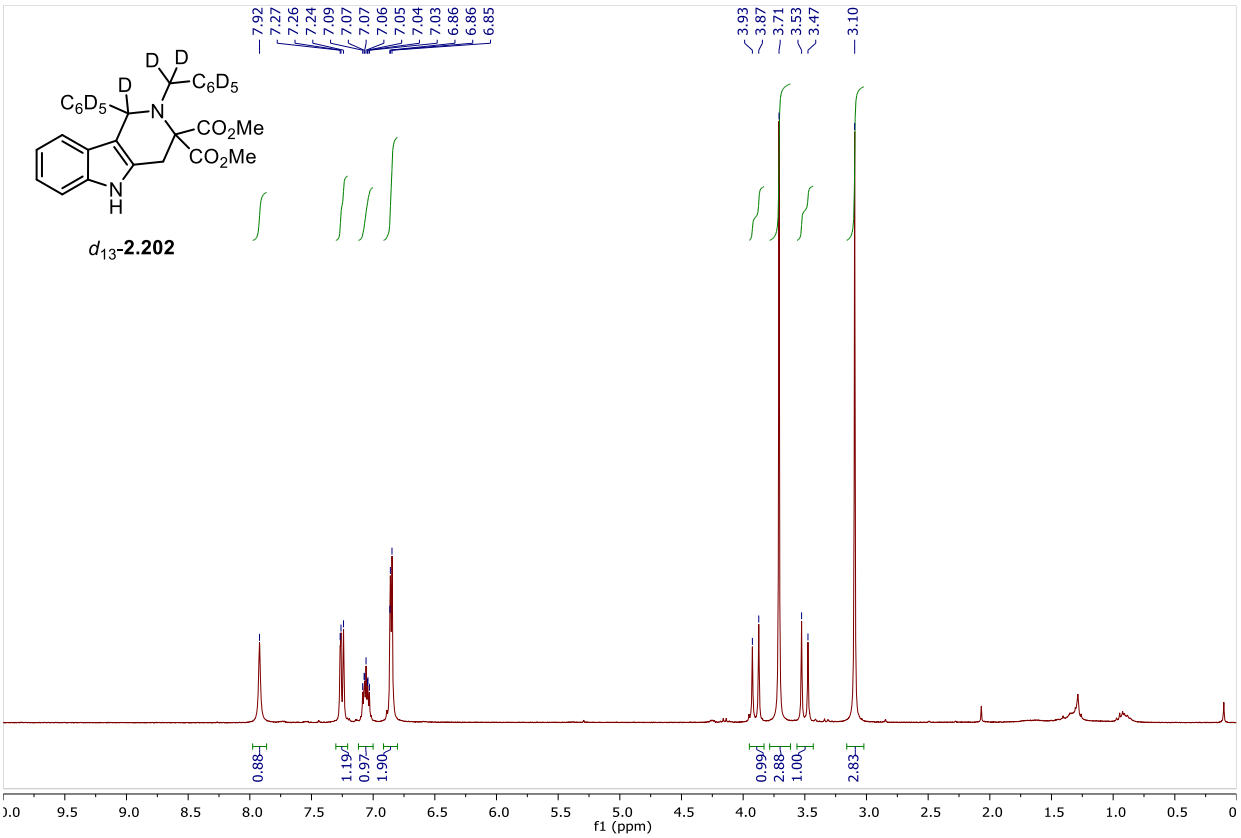

D/H
H/D
C6(H/D)5
D/H
C6(D/H)5
N
CO2Me
CO2Me
N
H
d6-2.202
f1 (ppm)

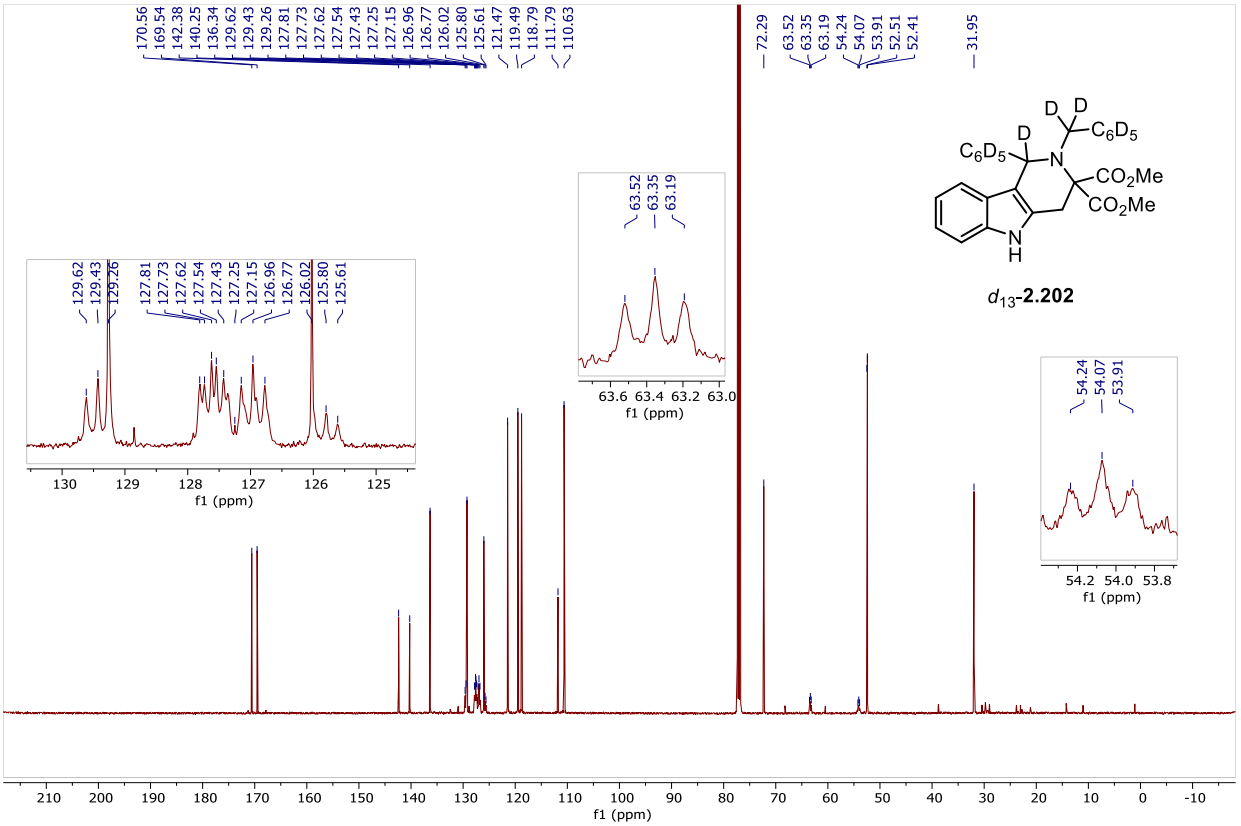

7.41
7.41
7.41
7.41
7.39
7.39
7.38
7.38
7.35
7.34
7.32
7.32
7.32
7.31
7.29
7.29
7.26
7.12
7.11
7.11
7.11
7.11
7.10
7.09
7.09
7.09
7.08
7.08
7.08
7.06
7.05
3.64
3.32
C6D5 C6D5
D
D
D
D
N
CO2Me
CO2Me
N3
d14-2.200
1.04
1.08
2.01
6.01
2.00
f1 (ppm)

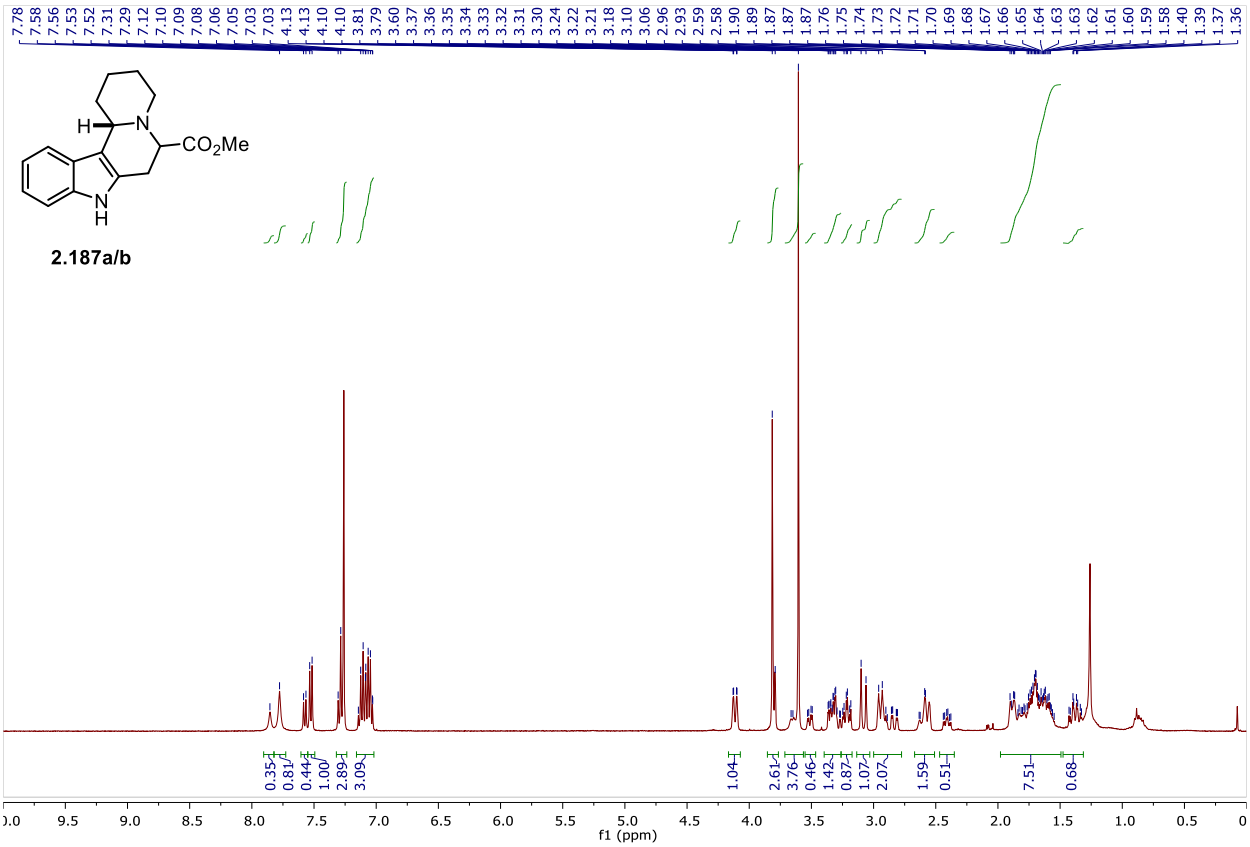

169.67
140.96
139.08
133.87
129.22
128.71
128.52
128.33
127.59
127.40
127.21
126.54
126.35
126.16
124.60
118.58
115.60
91.34
79.43
75.51
54.64
52.44
26.84
128.71
128.52
128.33
127.59
127.40
127.21
126.54
126.35
126.16
54.78
54.64
54.47
C6D5 C6D5
D
D
D
D
N
CO2Me
CO2Me
N3
d14-2.200
f1 (ppm)
f1 (ppm)
f1 (ppm)

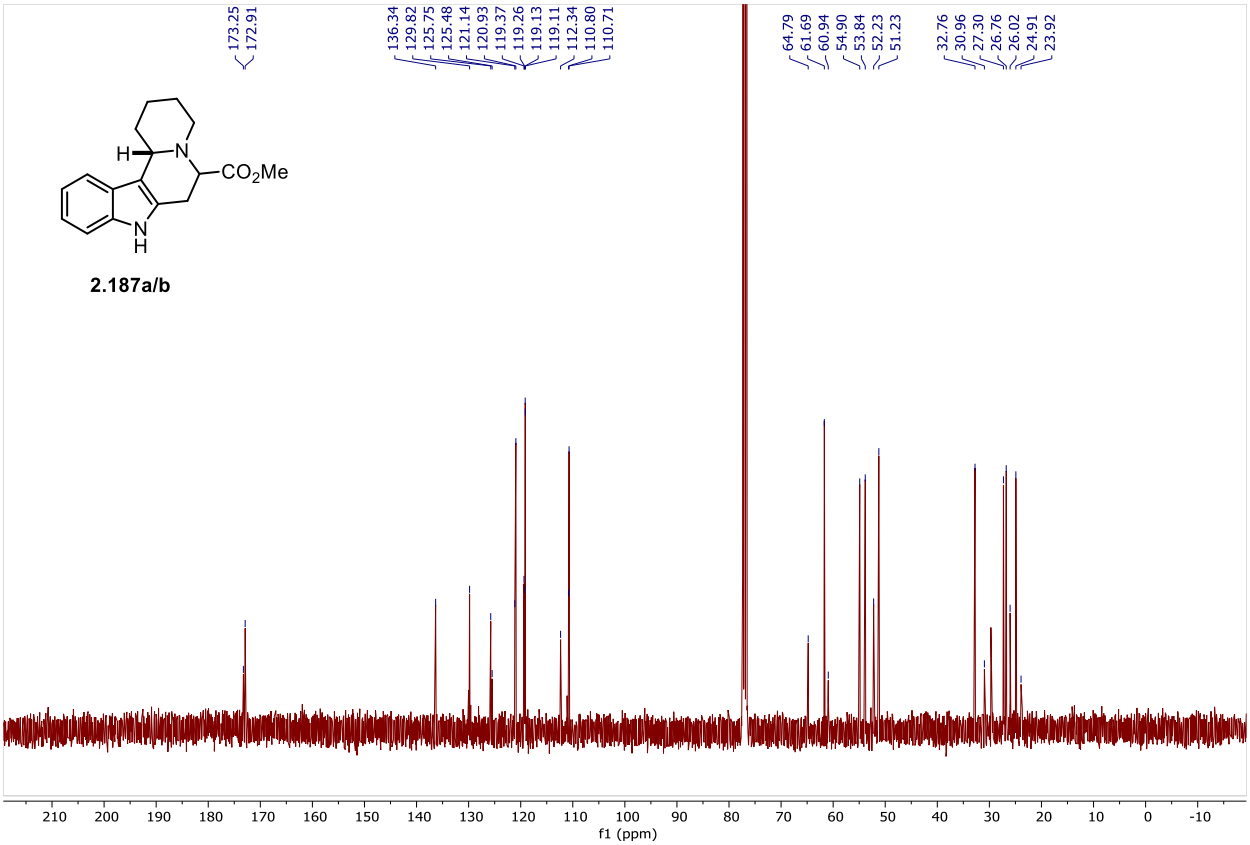

D/H
CO2Me
CO2Me
N
D
N
C6D5
D
C6D5
D
D
d14-2.201
f1 (ppm)

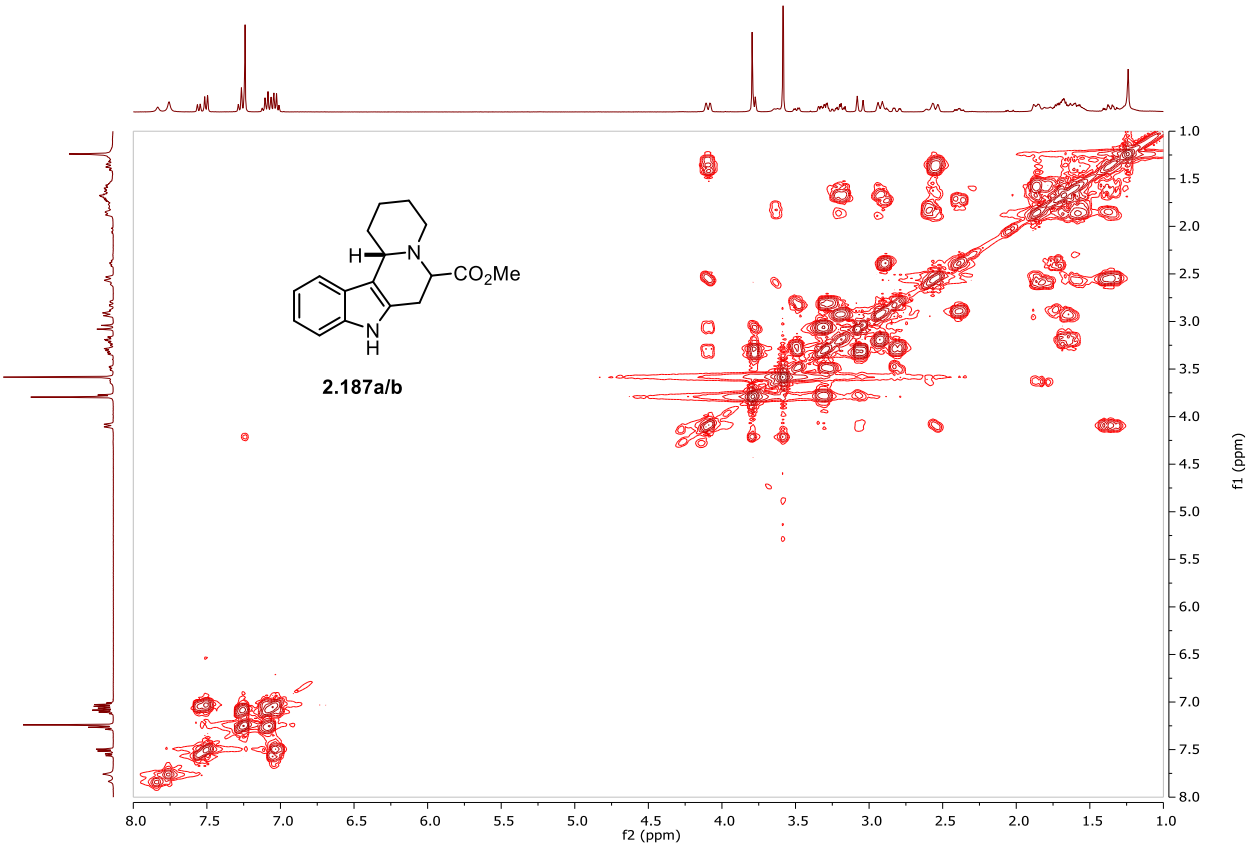

D/H
CO2Me
CO2Me
N
D
N
C6D5
D
C6D5
D
d14-2.201
f1 (ppm)

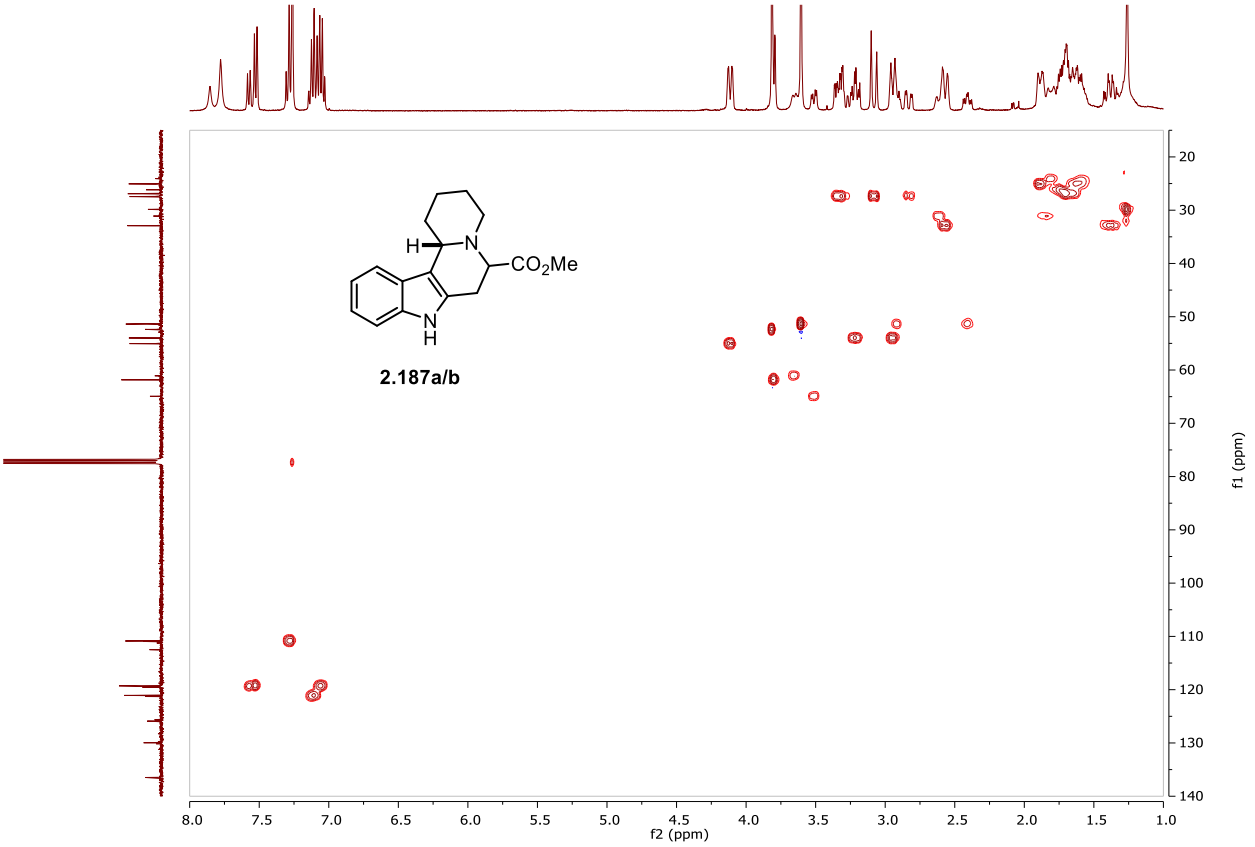

7.92
7.27
7.26
7.24
7.09
7.07
7.07
7.06
7.05
7.04
7.03
6.86
6.86
6.85
3.93
3.87
3.71
3.53
3.47
3.10
D
D
C6D5
D
C6D5
N
CO2Me
CO2Me
N
H
d13-2.202
0.88
1.19
0.97
1.90
0.99
2.88
1.00
2.83
f1 (ppm)

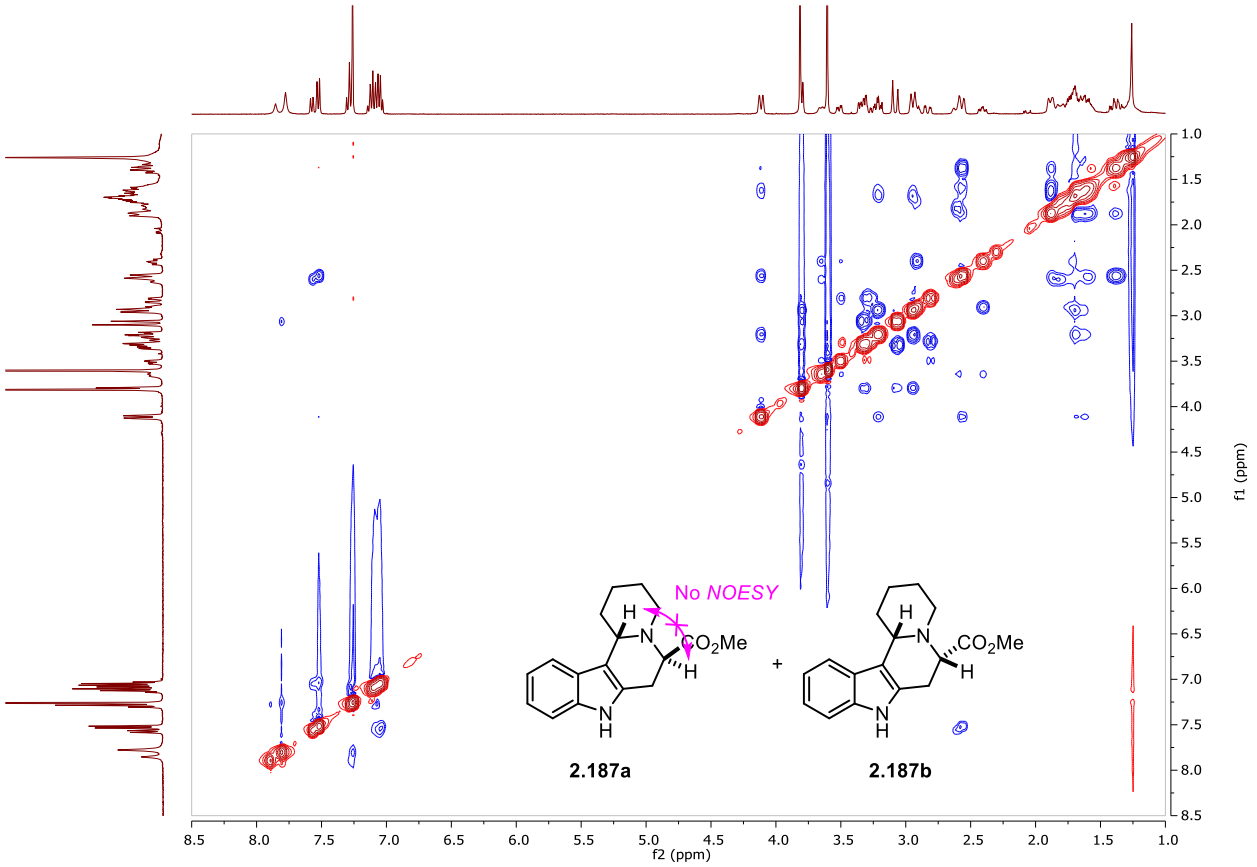

170.56
169.54
142.38
140.25
136.34
129.62
129.43
129.26
127.81
127.73
127.62
127.54
127.43
127.25
127.15
126.96
126.77
126.02
125.80
125.61
121.47
119.49
118.79
111.79
110.63
72.29
63.52
63.35
63.19
54.24
54.07
53.91
52.51
52.41
31.95
D
D
C6D5
D
C6D5
N
CO2Me
CO2Me
N
H
d13-2.202
f1 (ppm)

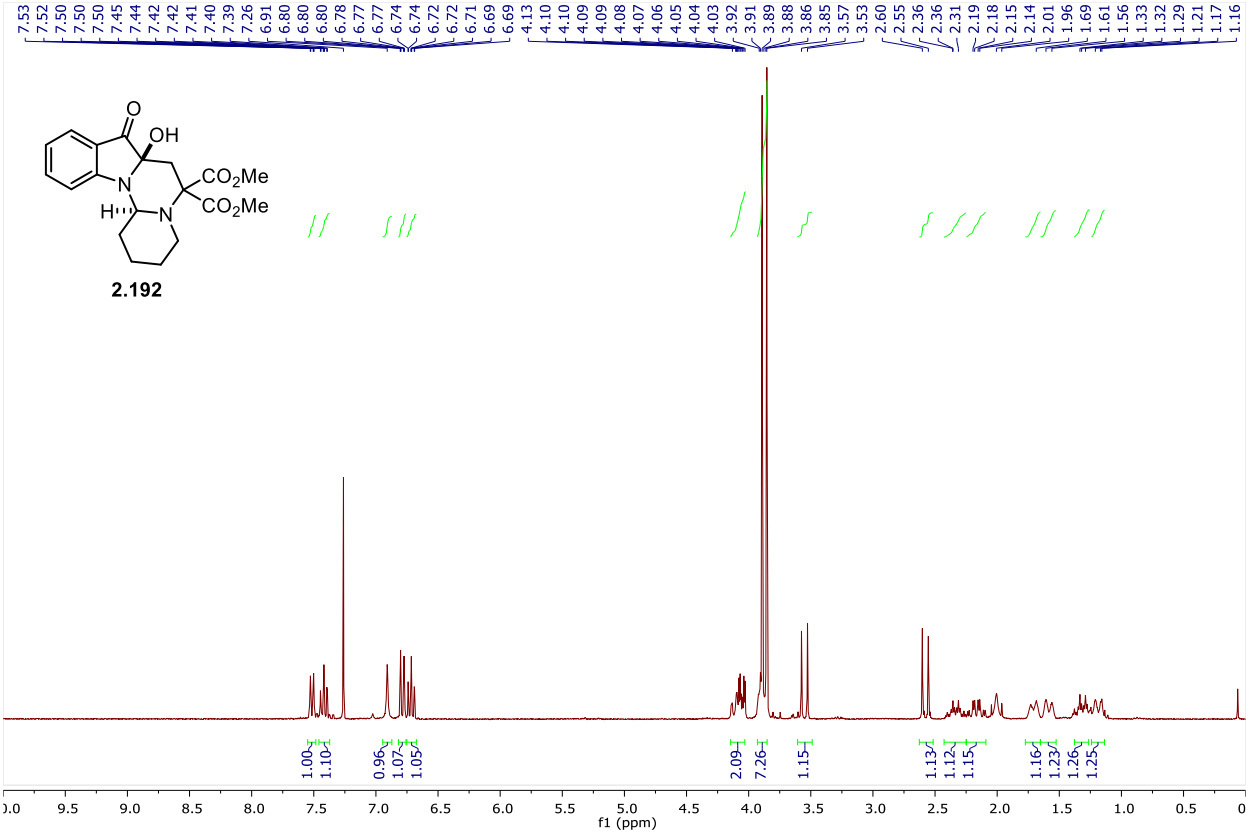

7.78 7.58 7.56 7.53 7.52 7.31 7.29 7.12 7.10 7.09 7.08 7.06 7.05 7.03 7.03 4.13 4.13 4.10 4.10 3.81 3.79 3.60 3.37 3.36 3.35 3.34 3.33 3.32 3.31 3.30 3.24 3.22 3.21 3.18 3.10 3.06 2.96 2.93 2.59 2.58 1.90 1.89 1.87 1.87 1.87 1.76 1.75 1.74 1.73 1.72 1.71 1.70 1.69 1.68 1.67 1.66 1.65 1.64 1.63 1.63 1.62 1.61 1.60 1.59 1.58 1.40 1.39 1.37 1.36
H
N
CO2Me
N
H
2.187a/b
0.35 0.81 0.44 1.00 2.89 3.09 1.04 2.61 3.76 0.46 1.42 0.87 1.07 2.07 1.59 0.51 7.51 0.68
9.5 9.0 8.5 8.0 7.5 7.0 6.5 6.0 5.5 5.0 4.5 4.0 3.5 3.0 2.5 2.0 1.5 1.0 0.5 0
f1 (ppm)

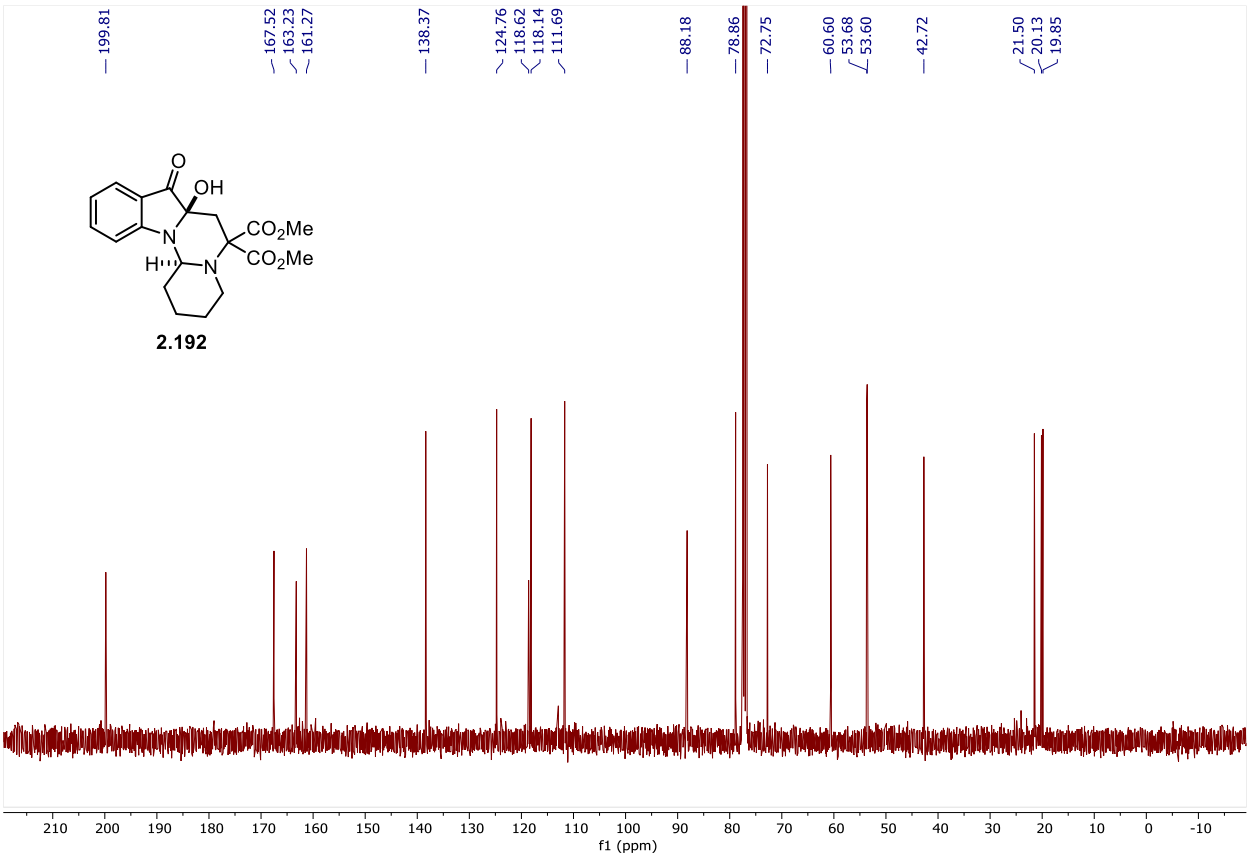

173.25 172.91 136.34 129.82 125.75 125.48 121.14 120.93 119.37 119.26 119.13 119.11 112.34 110.80 110.71 64.79 61.69 60.94 54.90 53.84 52.23 51.23 32.76 30.96 27.30 26.76 26.02 24.91 23.92
H
N
CO2Me
N
H
2.187a/b
210 200 190 180 170 160 150 140 130 120 110 100 90 80 70 60 50 40 30 20 10 0 -10
f1 (ppm)

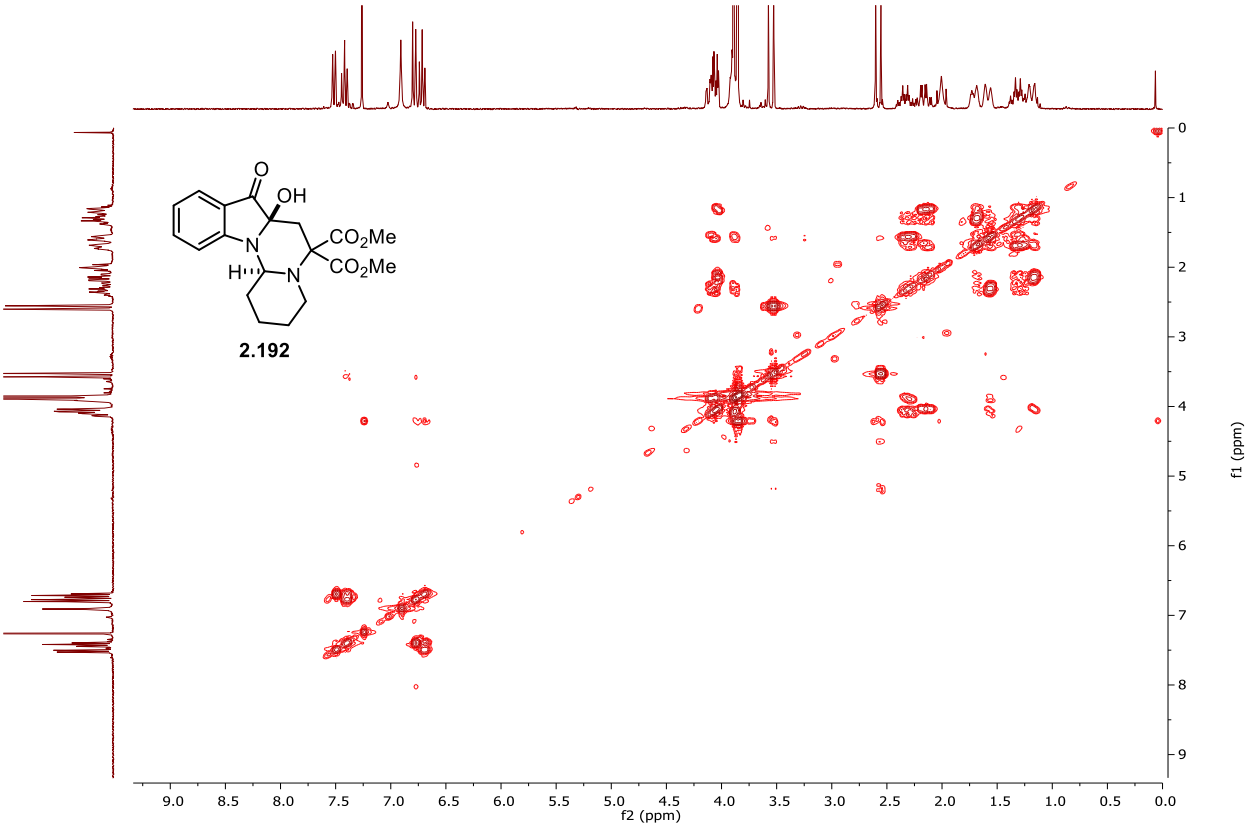

H
N
CO2Me
N
H
2.187a/b
f2 (ppm)
f1 (ppm)

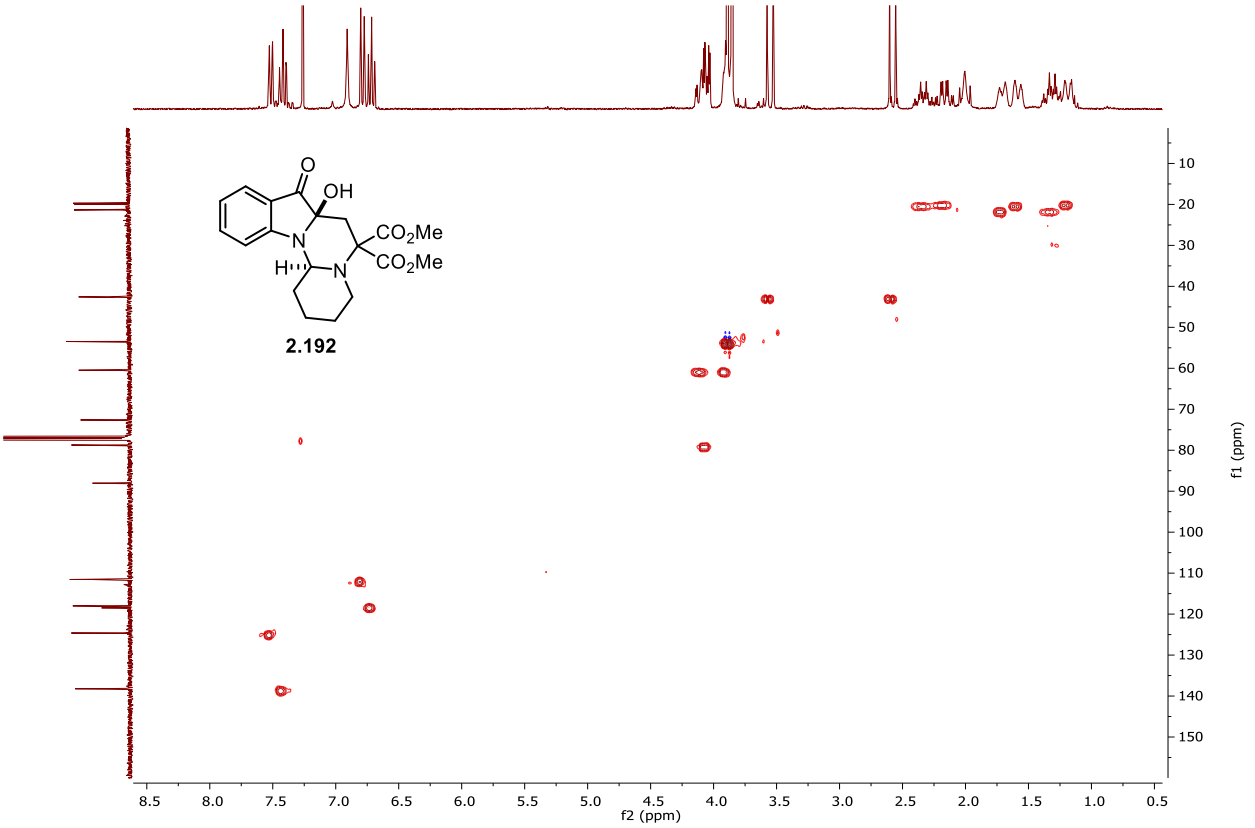

H
N
CO2Me
N
H
2.187a/b
f2 (ppm)
f1 (ppm)

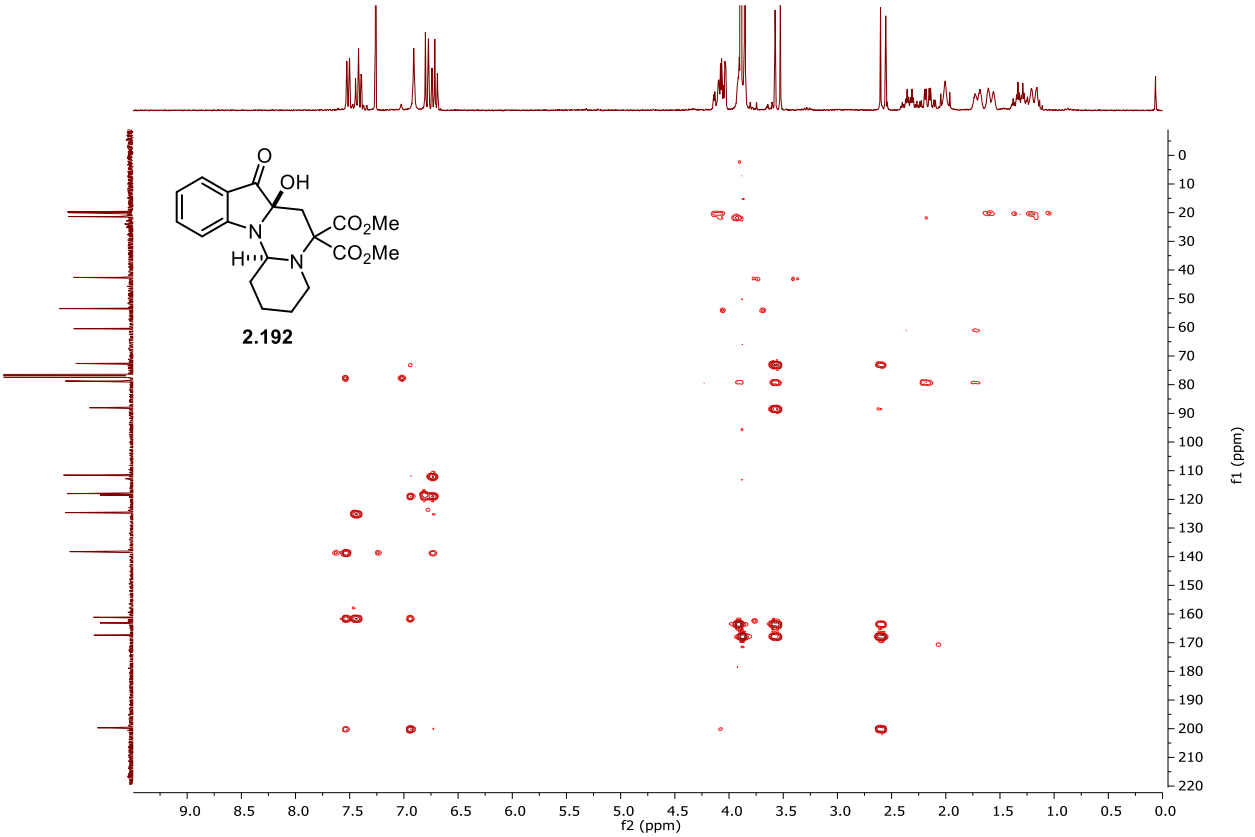

No NOESY
H
N
CO2Me
H
N
H
+
H
N
CO2Me
H
N
H
2.187a
2.187b
f2 (ppm)
f1 (ppm)

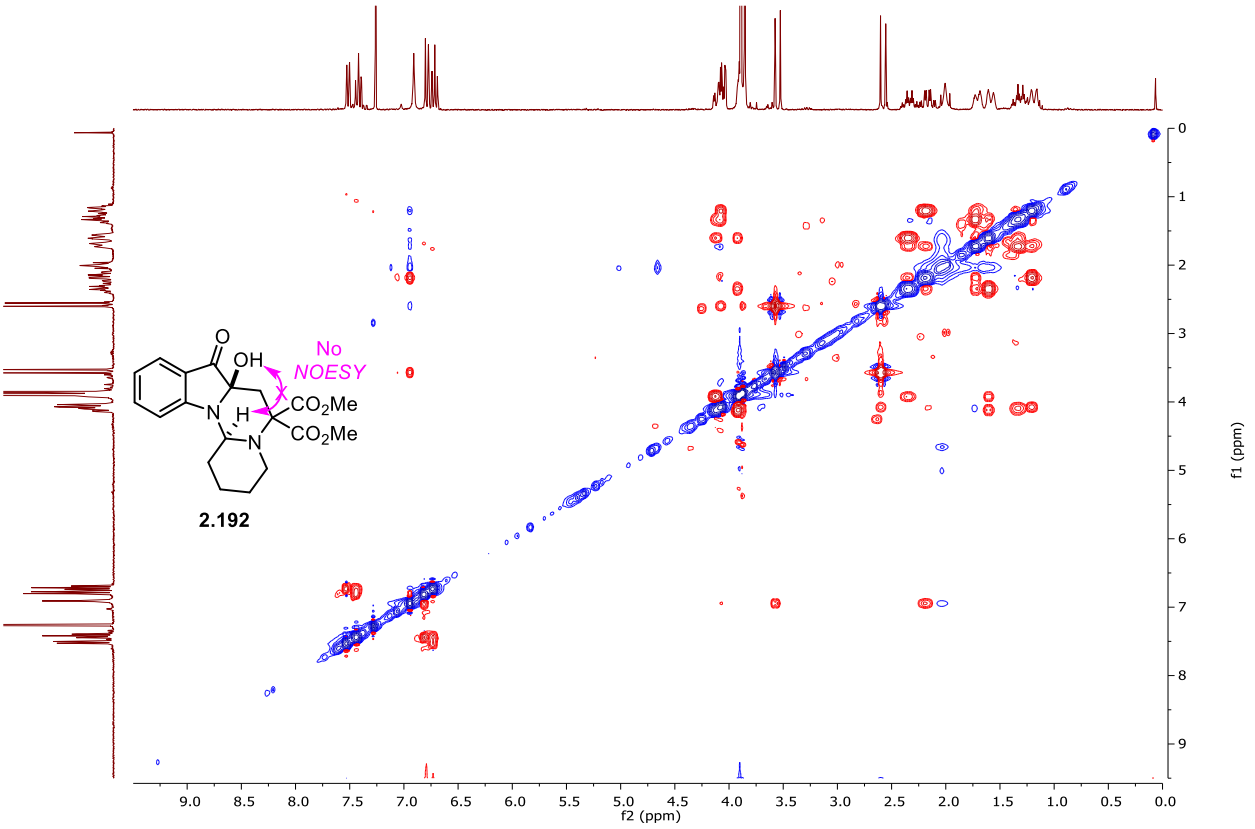

7.53 7.52 7.50 7.50 7.50 7.45 7.44 7.42 7.42 7.41 7.40 7.39 7.26 6.91 6.80 6.80 6.80 6.78 6.77 6.77 6.74 6.74 6.72 6.72 6.71 6.69 6.69
4.13 4.10 4.10 4.09 4.09 4.08 4.07 4.06 4.05 4.04 4.03 3.92 3.91 3.89 3.88 3.86 3.85 3.57 3.53
2.60 2.55 2.36 2.36 2.31 2.19 2.18 2.15 2.14 2.01 1.96 1.69 1.61 1.56 1.33 1.32 1.29 1.21 1.17 1.16
O
OH
N
H
N
CO2Me
CO2Me
2.192
1.00 1.10 0.96 1.07 1.05 2.09 7.26 1.15 1.13 1.12 1.15 1.16 1.23 1.26 1.25
f1 (ppm)

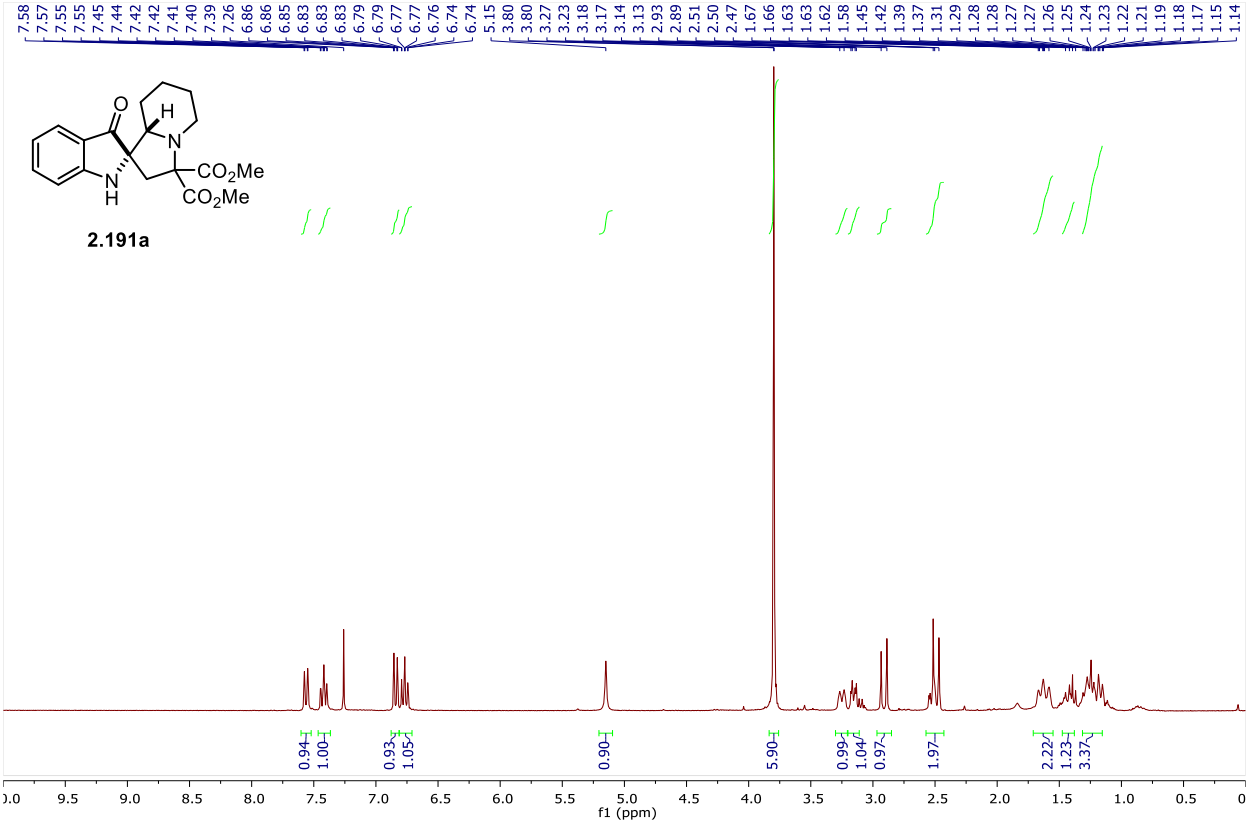

199.81
167.52 163.23 161.27
138.37
124.76 118.62 118.14 111.69
88.18
78.86
72.75
60.60 53.68 53.60
42.72
21.50 20.13 19.85
O
OH
N
H
N
CO2Me
CO2Me
2.192
f1 (ppm)

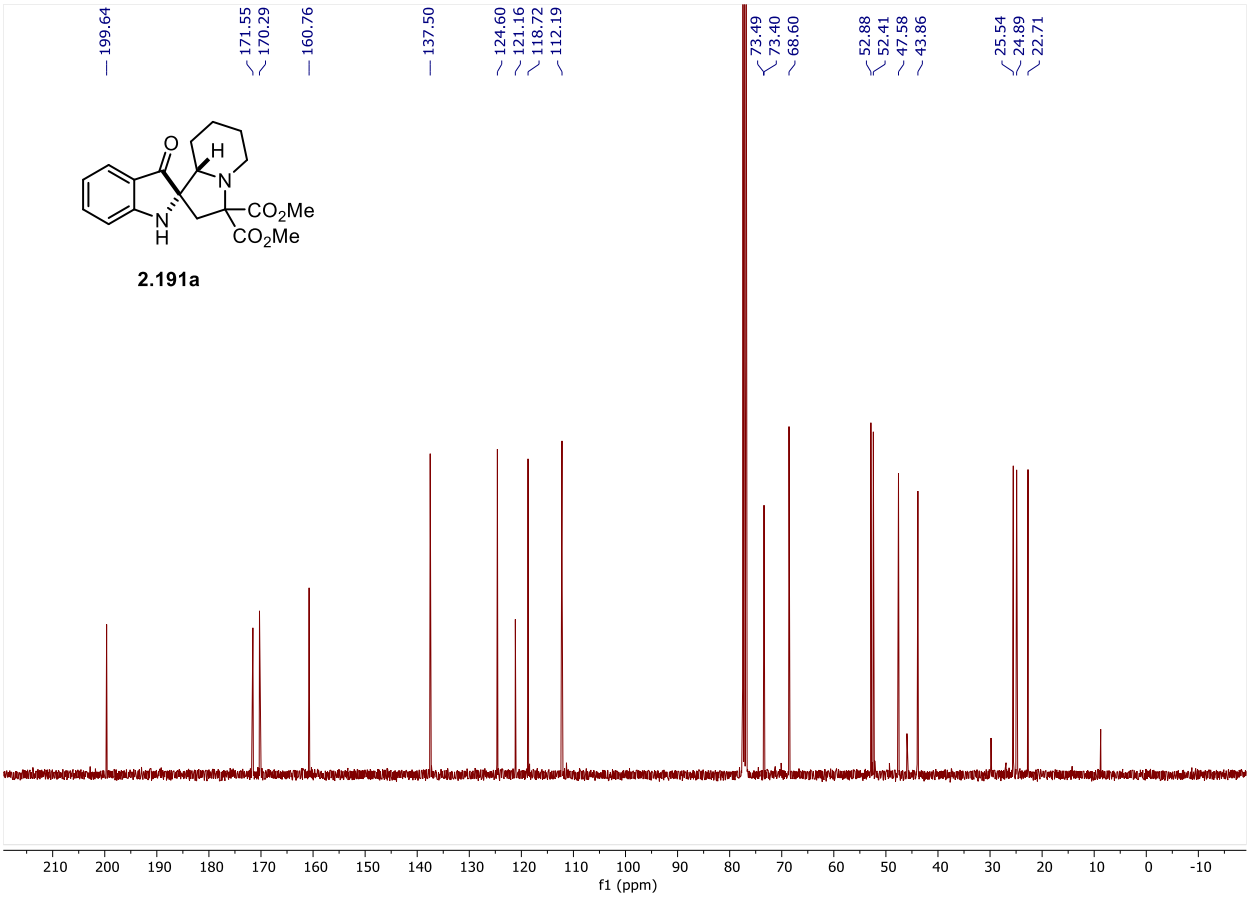

O
OH
N
H
N
CO2Me
CO2Me
2.192
f2 (ppm)
f1 (ppm)

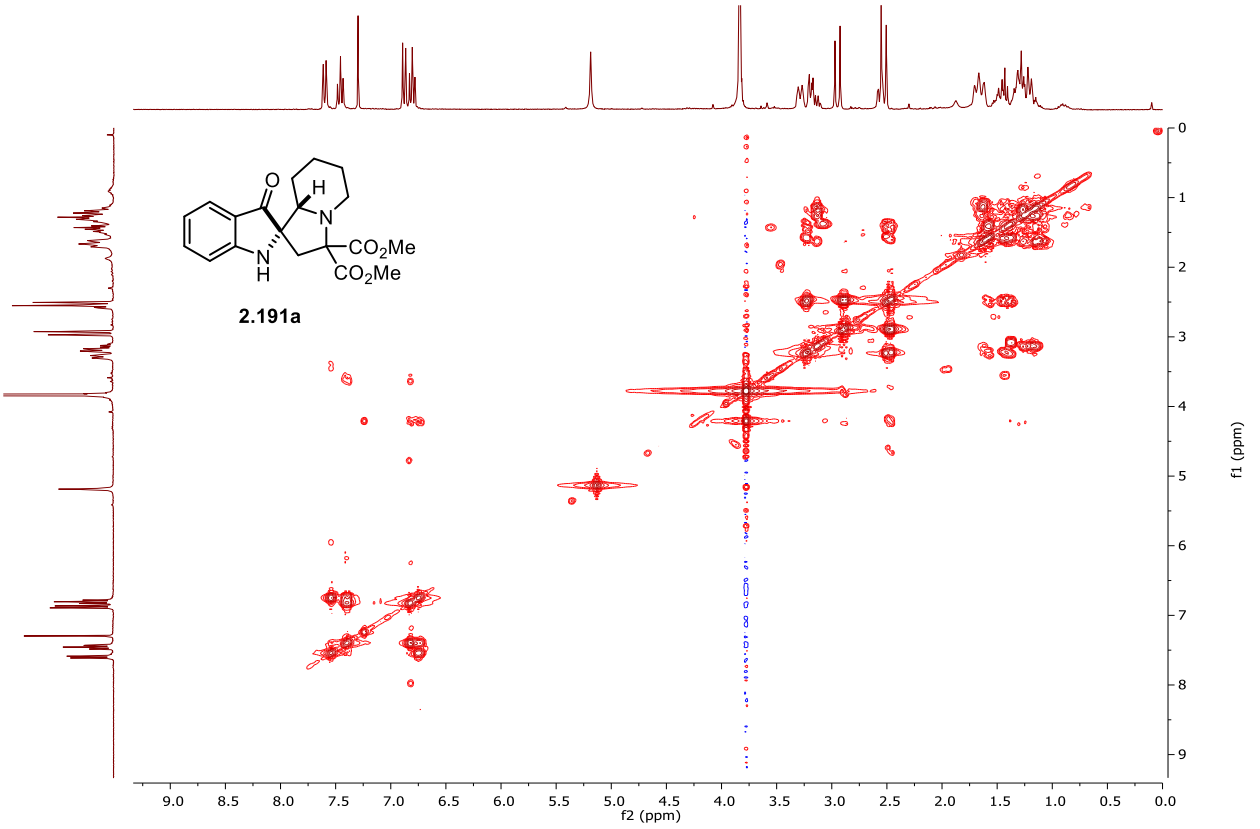

O
OH
N
H
N
CO2Me
CO2Me
2.192
f2 (ppm)
f1 (ppm)

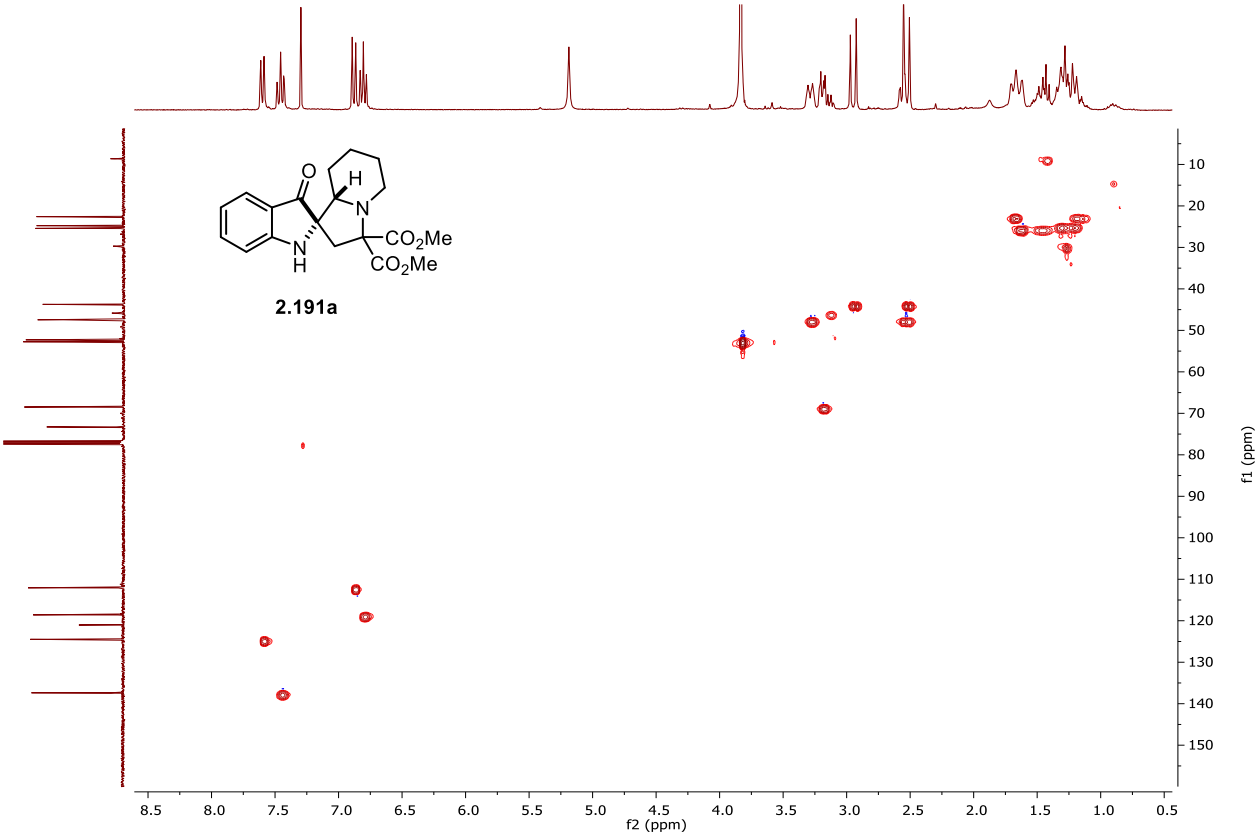

O
OH
N
H
N
CO2Me
CO2Me
2.192
f2 (ppm)
f1 (ppm)

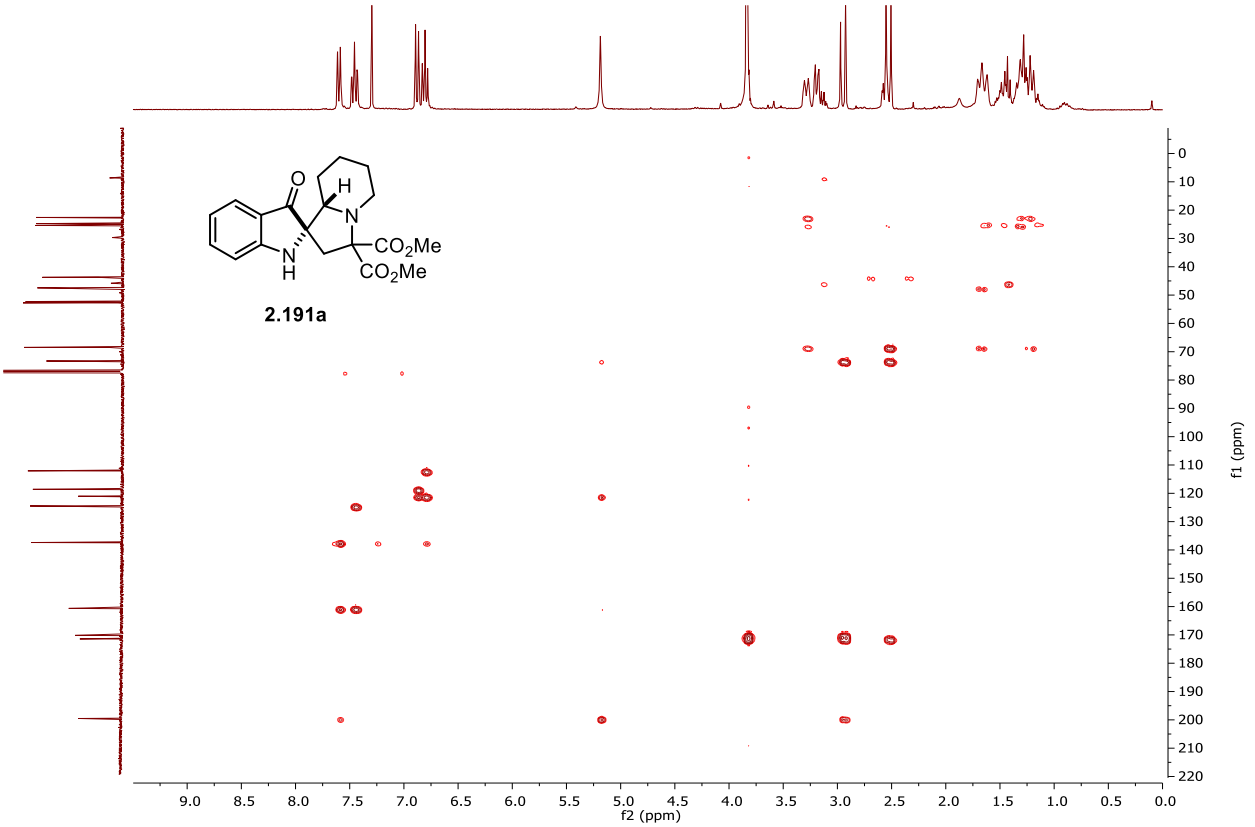

O
OH
N
H
N
CO2Me
CO2Me
No
NOESY
2.192
f2 (ppm)
f1 (ppm)

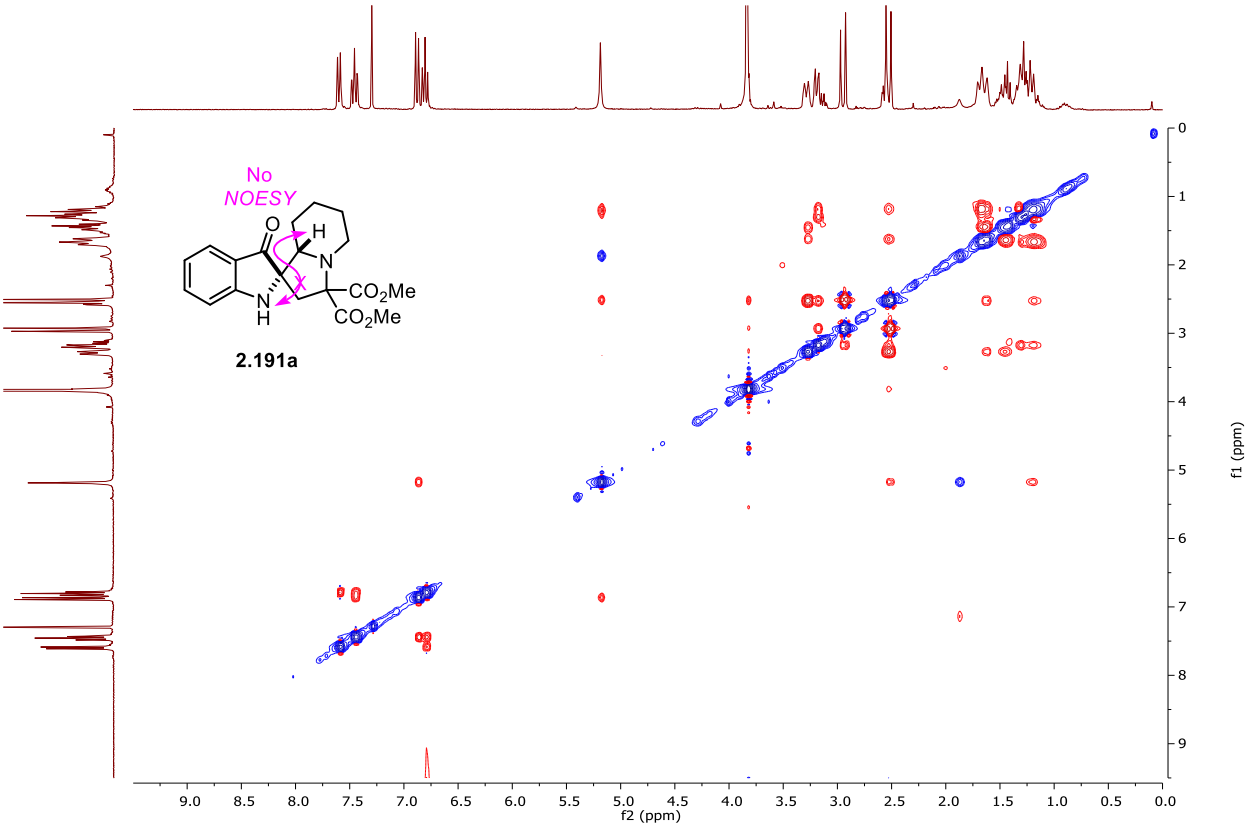

7.58 7.57 7.55 7.55 7.45 7.44 7.42 7.42 7.41 7.40 7.39 7.26 6.86 6.85 6.83 6.83 6.83 6.79 6.79 6.77 6.77 6.76 6.74 6.74 5.15 3.80 3.80 3.27 3.23 3.18 3.17 3.14 3.13 2.93 2.89 2.51 2.50 2.47 1.67 1.66 1.63 1.63 1.62 1.58 1.45 1.42 1.39 1.37 1.31 1.29 1.28 1.27 1.27 1.26 1.25 1.24 1.23 1.22 1.21 1.19 1.18 1.17 1.15 1.14
O
H
N
N
H
CO2Me
CO2Me
2.191a
0.94 1.00 0.93 1.05 0.90 5.90 0.99 1.04 0.97 1.97 2.22 1.23 3.37
f1 (ppm)

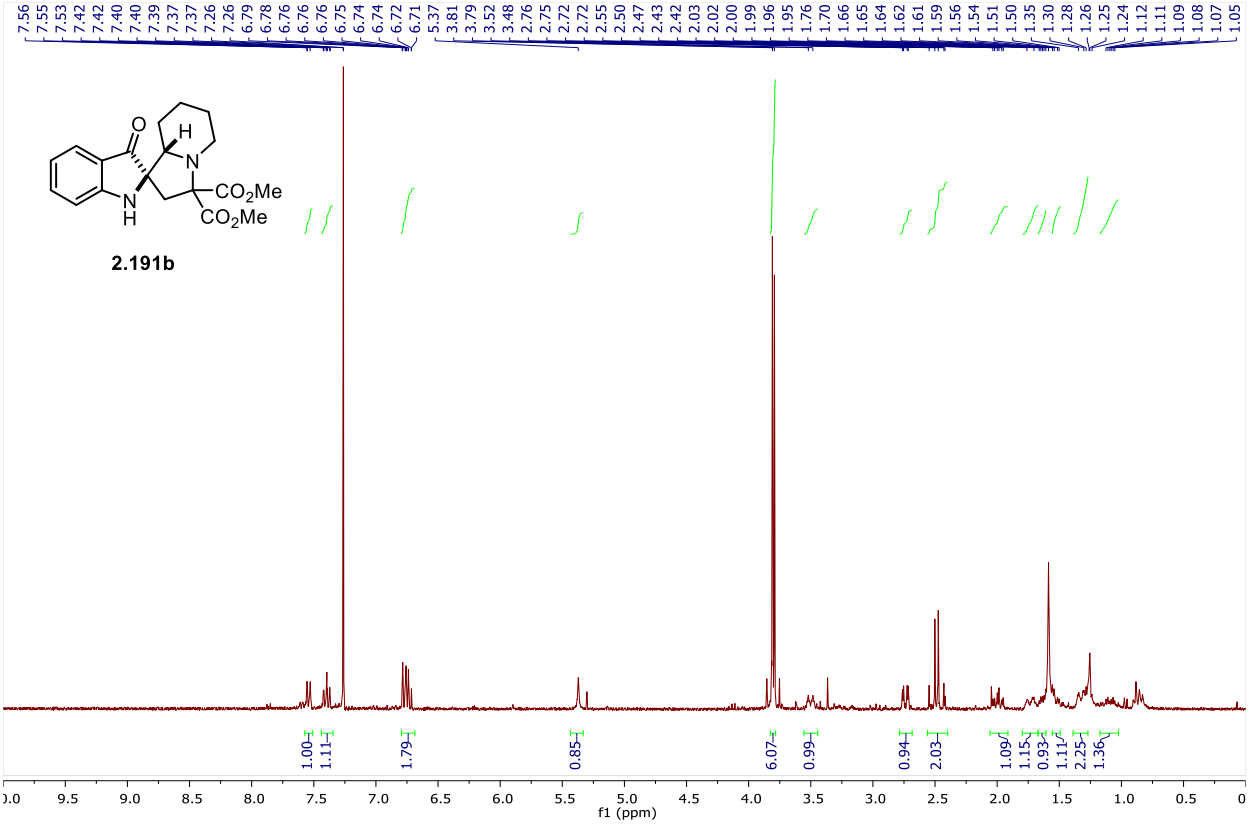

199.64
171.55
170.29
160.76
137.50
124.60
121.16
118.72
112.19
73.49
73.40
68.60
52.88
52.41
47.58
43.86
25.54
24.89
22.71
O
H
N
N
H
CO2Me
CO2Me
2.191a
f1 (ppm)

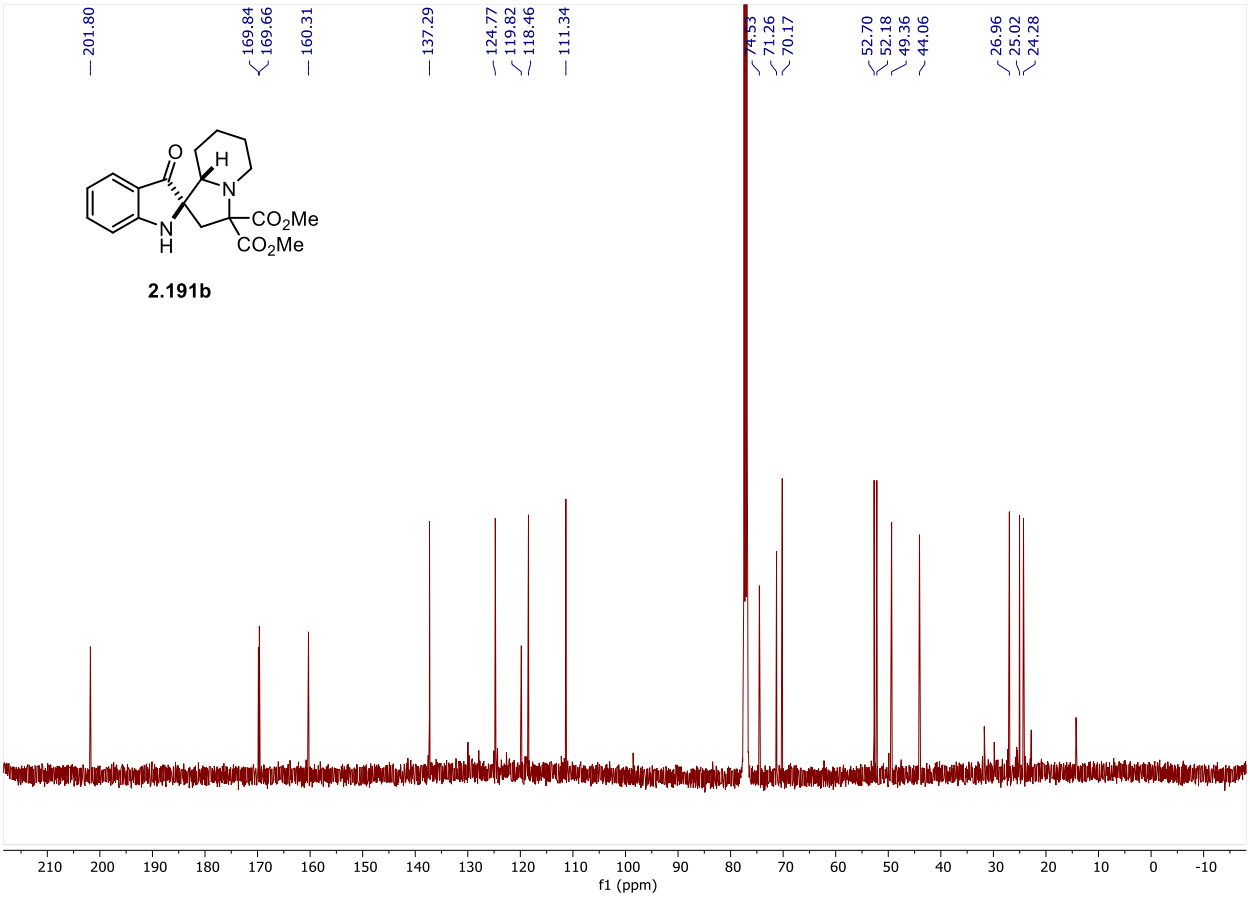

O
H
N
N
H
CO2Me
CO2Me
2.191a
f2 (ppm)
f1 (ppm)

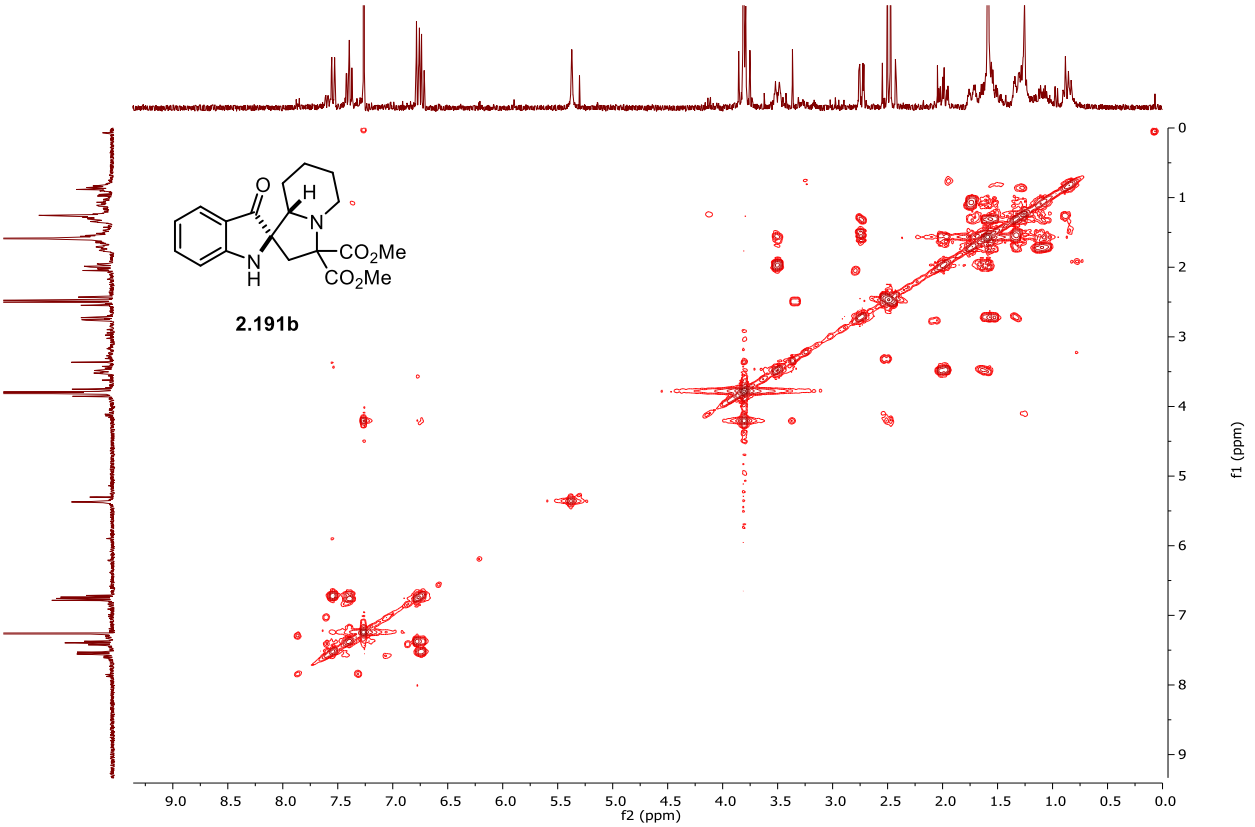

O
H
N
N
H
CO2Me
CO2Me
2.191a
f2 (ppm)
f1 (ppm)

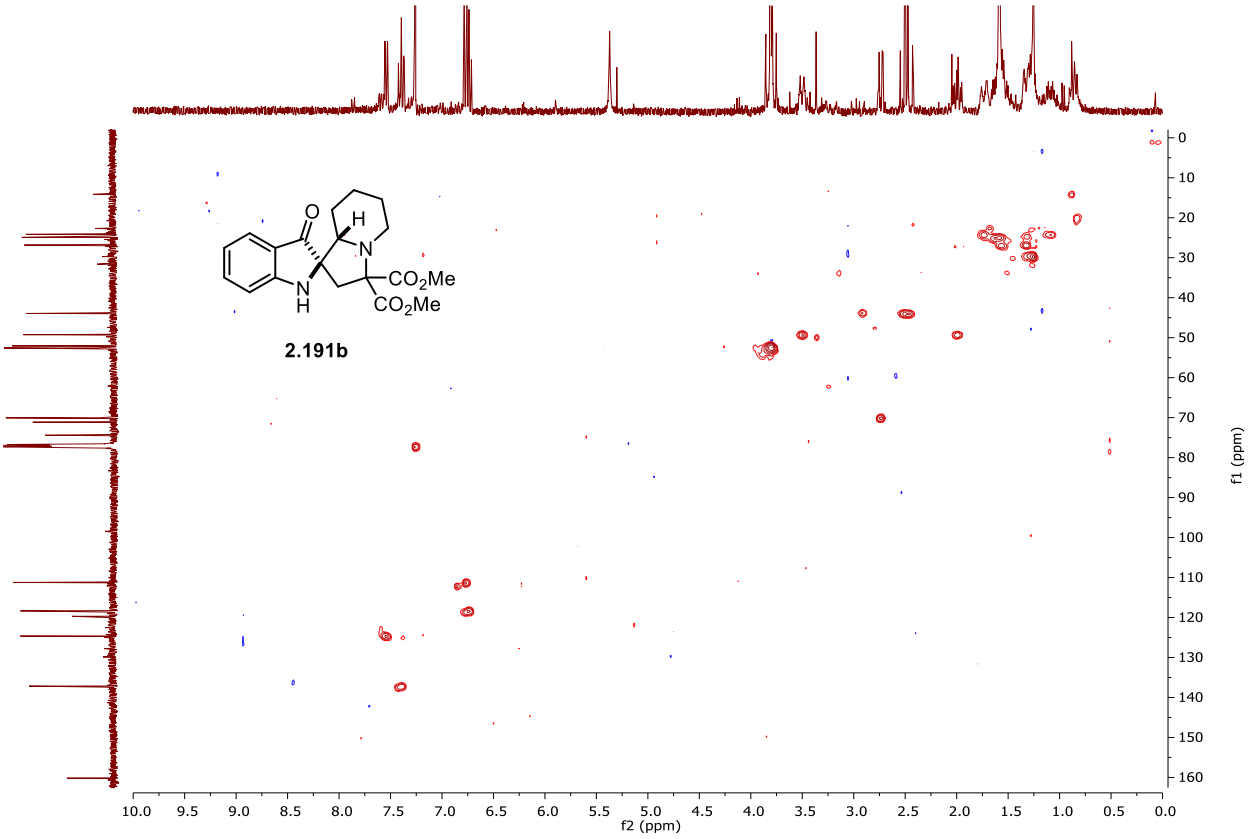

O
H
N
N
H
CO2Me
CO2Me
2.191a
f2 (ppm)
f1 (ppm)

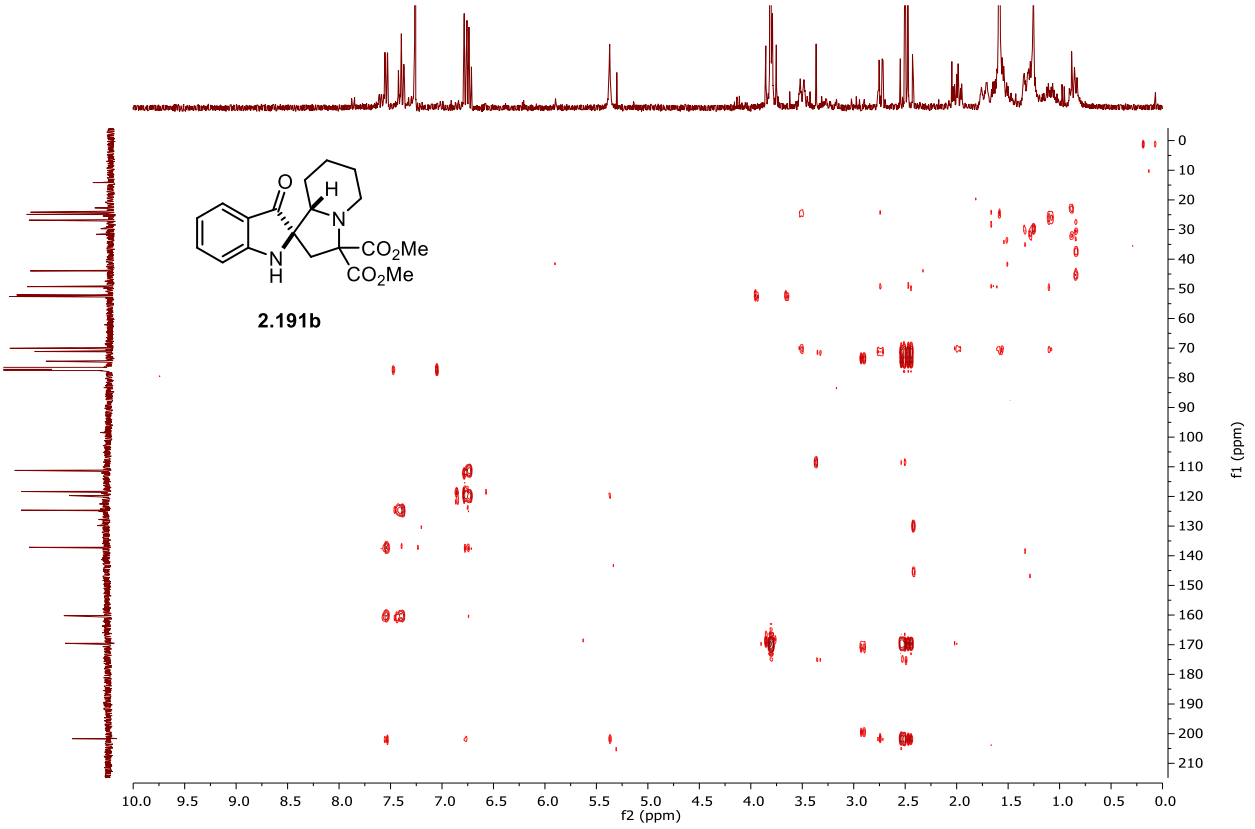

No
NOESY
O
H
N
N
H
CO2Me
CO2Me
2.191a
f2 (ppm)
f1 (ppm)

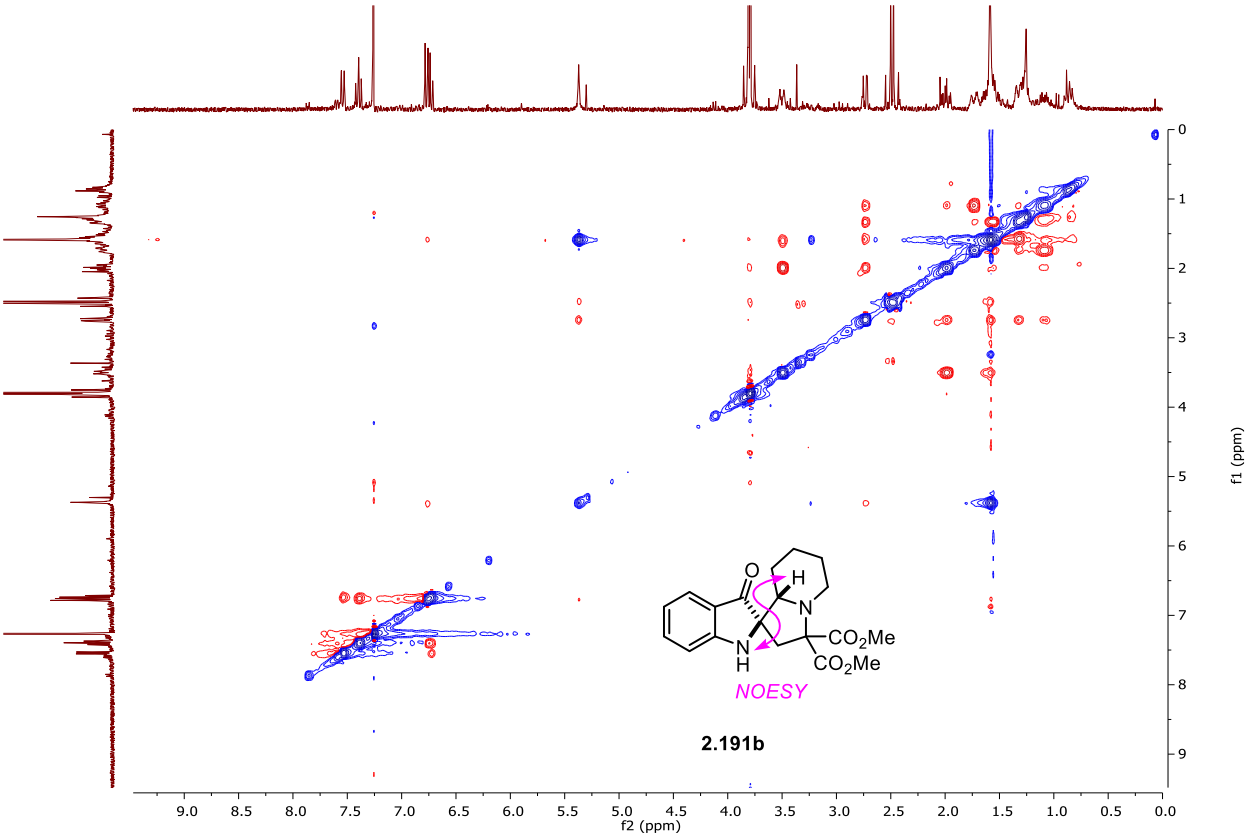

7.56 7.55 7.53 7.42 7.42 7.40 7.40 7.39 7.37 7.37 7.26 7.26 6.79 6.78 6.76 6.76 6.76 6.75 6.74 6.74 6.72 6.71 5.37 3.81 3.79 3.52 3.48 2.76 2.75 2.72 2.72 2.55 2.50 2.47 2.43 2.42 2.03 2.02 2.00 1.99 1.96 1.95 1.76 1.70 1.66 1.65 1.64 1.62 1.61 1.59 1.56 1.54 1.51 1.50 1.35 1.30 1.28 1.26 1.25 1.24 1.12 1.11 1.09 1.08 1.07 1.05
O
H
N
N
H
CO2Me
CO2Me
2.191b
1.00 1.11 1.79 0.85 6.07 0.99 0.94 2.03 1.09 1.15 0.93 1.11 2.25 1.36
f1 (ppm)

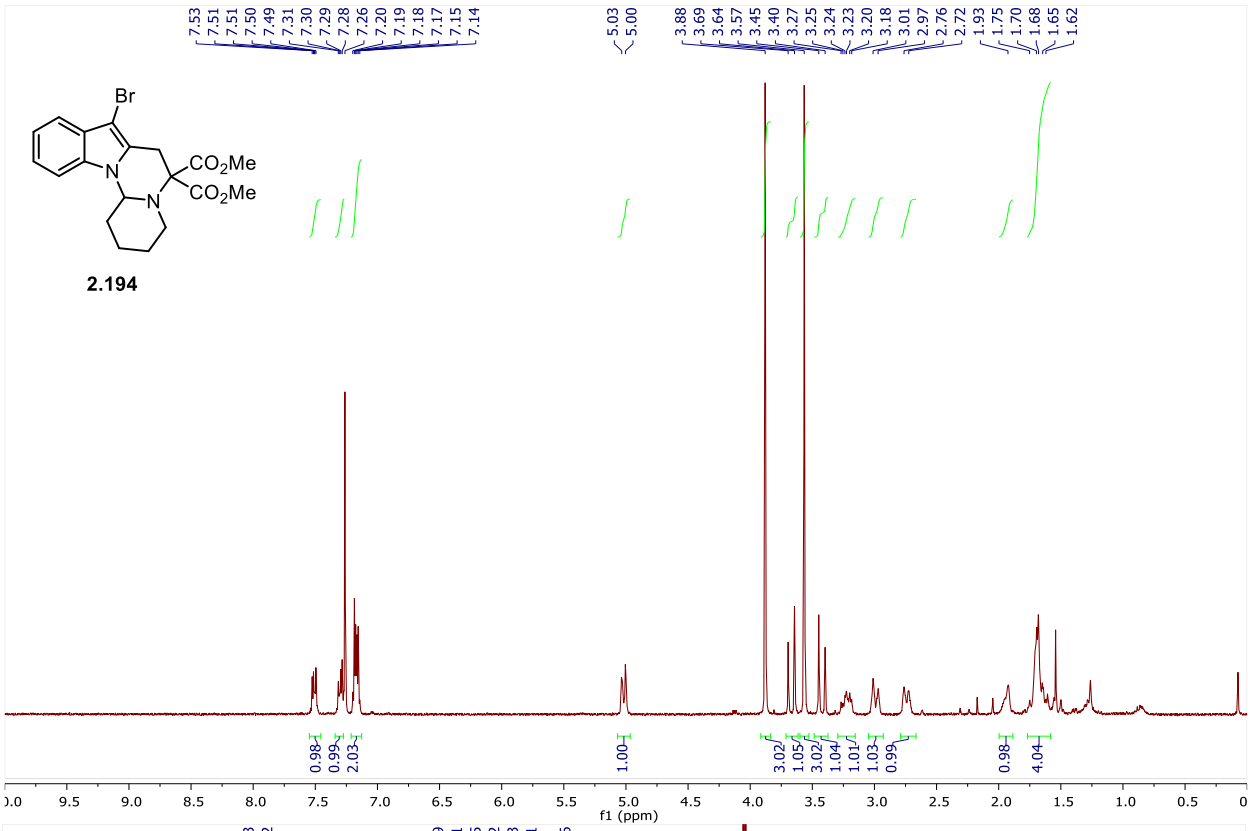

201.80
169.84
169.66
160.31
137.29
124.77
119.82
118.46
111.34
74.53
71.26
70.17
52.70
52.18
49.36
44.06
26.96
25.02
24.28
O
H
N
N
H
CO2Me
CO2Me
2.191b
f1 (ppm)

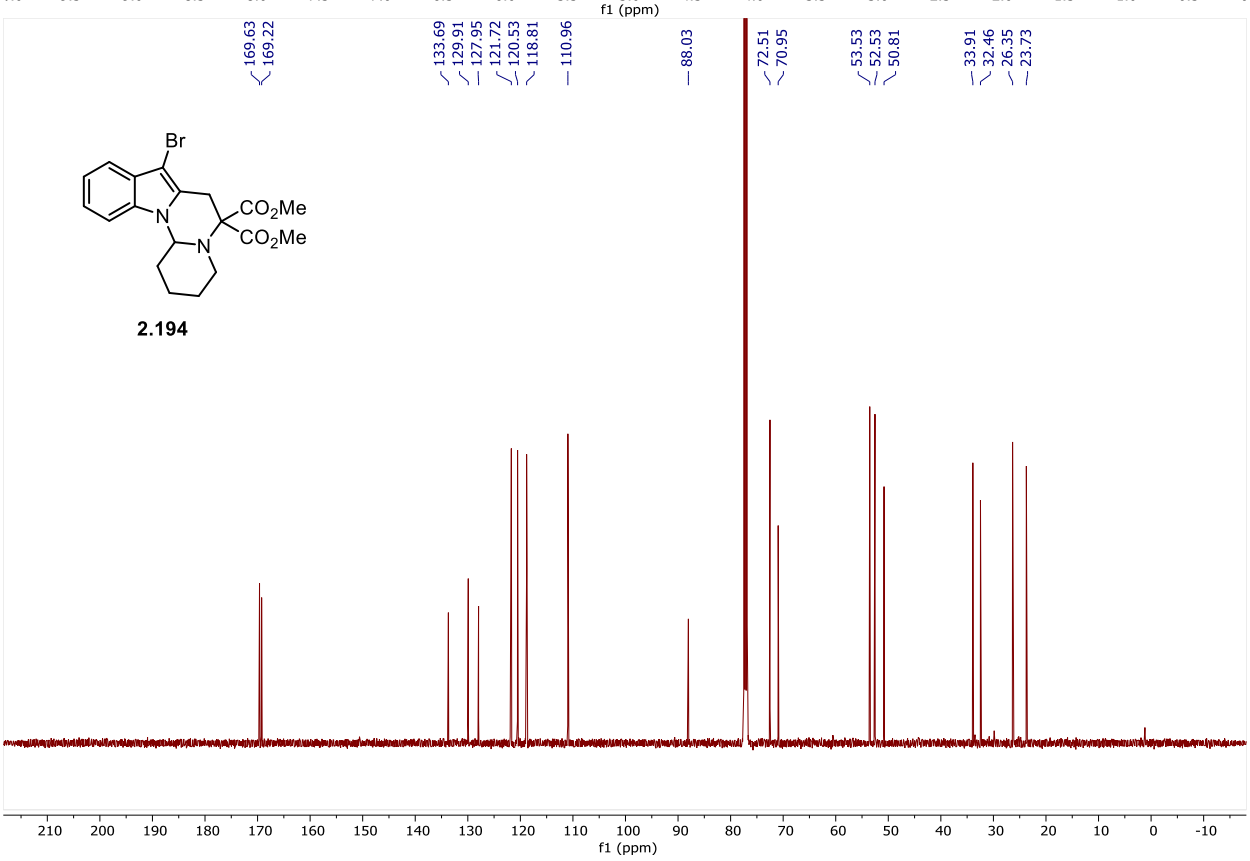

O
H
N
N
H
CO2Me
CO2Me
2.191b
f2 (ppm)
f1 (ppm)


O
H
N
N
H
CO2Me
CO2Me
2.191b
f2 (ppm)
f1 (ppm)


O
H
N
N
H
CO2Me
CO2Me
2.191b
f2 (ppm)
f1 (ppm)


O
H
N
N
H
CO2Me
CO2Me
NOESY
2.191b
f2 (ppm)
f1 (ppm)


Br
CO2Me
CO2Me
N
N
2.194
7.53 7.51 7.51 7.50 7.49 7.31 7.30 7.29 7.28 7.26 7.20 7.19 7.18 7.17 7.15 7.14
5.03 5.00
3.88 3.69 3.64 3.57 3.45 3.40 3.27 3.25 3.24 3.23 3.20 3.18 3.01 2.97 2.76 2.72
1.93 1.75 1.70 1.68 1.65 1.62
0.98 0.99 2.03 1.00 3.02 1.05 3.02 1.04 1.01 1.03 0.99 0.98 4.04
f1 (ppm)

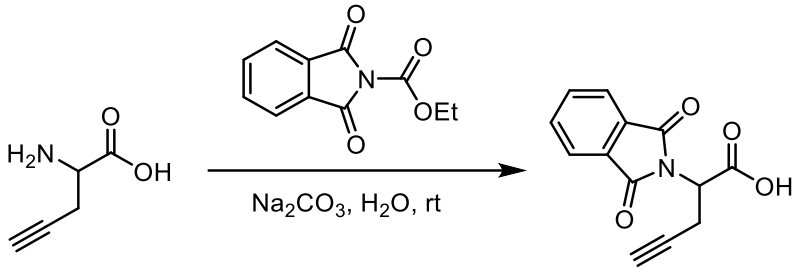

Br
CO2Me
CO2Me
N
N
2.194
169.63 169.22
133.69 129.91 127.95 121.72 120.53 118.81 110.96
88.03
72.51 70.95
53.53 52.53 50.81
33.91 32.46 26.35 23.73
f1 (ppm)

6.2.3 DFT studies and calculations

Potential energy surface data and the Cartesian coordinates for the reported minima/maxima are showcased in detail and have been published in the following report: David F. León Rayo, Ali Mansour, Wenbin Wu, Benjamin N. Bhawal and Fabien Gagosz*. *Angew. Chem. Int. Ed.* **2022**, e202212893.

6.3 Supporting information for Chapter 3

6.3.1 Experimental procedures



3.98 **3.94**

A round-bottom flask open to the surrounding atmosphere was charged with sodium carbonate (33.8 mg, 0.319 mmol, 1.05 equiv.) and dissolved in water (0.81 mL, 0.4 M) with vigorous stirring. Commercially available *DL*-propargylglycine **3.98** (34.4 mg, 0.304 mmol, 1.0 equiv.) was then added in one portion. Once fully dissolved, *N*-(carbethoxy)phthalimide (86.7 mg, 0.395 mmol, 1.3 equiv.) is added in one portion and the heterogeneous reaction mixture left to stir vigorously overnight (~12–16 hours). The next day, the reaction appeared homogeneous and TLC analysis indicated complete consumption of the starting material. A small volume of sat. $NaHCO_{3(aq)}$ was added to the reaction to result in a pH of ~8 and was poured into a separatory funnel. The basic aqueous phase was extracted with EtOAc (x2) to remove any organic impurities. The collected aqueous phase was then cooled to 0 °C in an ice-bath with magnetic stirring and slowly acidified to a pH of ~2–3 with 3 M $HCl_{(aq)}$. At this pH, the desired product precipitates out of solution and can be collected by vacuum filtration and washed several times with small volumes of cold water. Carboxylic acid **3.94** is obtained as a white solid (51 mg, 69% yield) with analytical data that matches that which is reported in the literature.

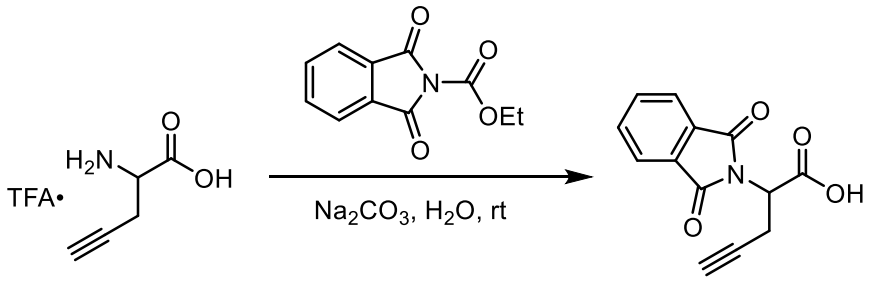
TLC: R_f 0.27 (2% AcOH:60% Et_2O:hexanes), UV (254 nm) and *p*-anisaldehyde

^{1}H-NMR (300 MHz, $CDCl_3$): δ 9.20 (br s, 1H), 7.93–7.85 (m, 2H), 7.79–7.71 (m, 2H), 5.14 (dd, J = 11.2, 4.9 Hz, 1H), 3.26 (ddd, J = 17.3, 11.2, 2.7 Hz, 1H), 3.09 (ddd, J = 17.3, 5.0, 2.7 Hz), 1.91 (t, J = 2.7 Hz, 1H).

^{13}C-NMR (101 MHz, CDCl3): δ 172.8, 167.3, 134.5, 131.8, 124.0, 78.9, 71.2, 50.5, 19.5.

HRMS (ESI): Calculated for $C_{13}H_9NNaO_4$ [M+Na]+: 266.0405; found: *m/z* 266.0429.

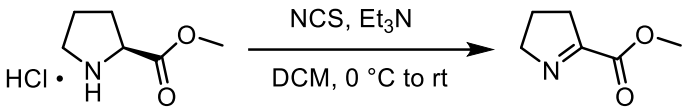
Carboxylic acid **3.94** from **3.98**•TFA:



3.98•TFA **3.94**

The reaction was performed on a larger scale (~2 g) using the TFA salt of propargylglycine (**3.98**•TFA) as the substrate. Experimental conditions are the exact same as those described above but using 2 equiv. of sodium carbonate. A round-bottom flask open to the surrounding atmosphere was charged with sodium carbonate (1.86 g, 17.30 mmol, 2.05 equiv.) and dissolved in water (21.5 mL, 0.4 M) with vigorous stirring. **3.98**•TFA (1.95 g, 8.58 mmol, 1.0 equiv.) was then added in one portion. Once fully dissolved, *N*-(carbethoxy)phthalimide (2.45 g, 11.16 mmol, 1.3 equiv.) is added in one portion and the heterogeneous reaction mixture left to stir vigorously overnight (~12–16 hours). The next day, the reaction appeared homogeneous and TLC analysis indicated complete consumption of the starting material. A small volume of sat. $NaHCO_{3(aq)}$ was added to the reaction to result in a pH of ~8 and was poured into a separatory funnel. The basic aqueous phase was extracted with EtOAc (x2) to remove any organic impurities. The collected aqueous phase was then cooled to 0 °C in an ice-bath with magnetic stirring and slowly acidified to a pH of ~2–3 with 3 M $HCl_{(aq)}$. At this pH, the desired product precipitates out of solution and can be collected by vacuum filtration and washed several times with small volumes of cold water. Carboxylic acid

3.94 is obtained as a white solid (1.71 g, 82% yield) with analytical data that matches that which is reported in the literature.



3.21

To a round-bottom flask charged with commercially available *L*-proline methyl ester hydrochloride (30.1 g, 182 mmol, 1.0 equiv.) is added anhydrous DCM (600 mL, 0.3 M) and cooled to 0 °C using a water/ice bath. Et_3N (58.0 mL, 418 mmol, 2.3 equiv.) is added dropwise which results in the formation of a white precipitate. At this point, NCS (26.7 g, 200 mmol, 1.1 equiv.) is added slowly and in portions (if NCS is added too quickly, the yield of imine **3.21** tends to drop). Once all the NCS has been added, the reaction is brought to room temperature and stirred for 3 hours at which point TLC indicated complete consumption of the starting material. The reaction mixture was diluted with Et_2O and poured into a separatory funnel containing a 1:1 mixture of water and sat. $NH_4Cl_{(aq)}$. The aqueous phase was extracted with DCM (x3) and the combined organics washed again with sat. $NaHCO_{3(aq)}$. The organic phase was dried over anhydrous $MgSO_4$, filtered, and then concentrated under reduced pressure to afford a yellow oil. Purification by vacuum distillation using a short-path distillation apparatus gave imine **3.21** (bp: 85–90 °C at 10 mbar) as a clear liquid (18.3 g, 88% yield) with analytical data that matches that which is reported in the literature.

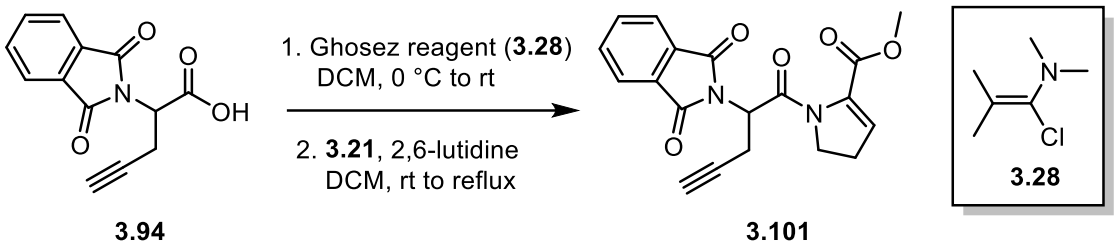
Note: Imine **3.21** can be stored in the fridge for several weeks but tends to colour (first to pale-yellow and then to orange). At the pale-yellow stage, the imine can be used without any noticeable loss of reactivity in the subsequent enamide synthesis, but it is recommended to freshly distill it before use if it happens to reach the orange stage.

TLC: R_f 0.31 (50% EtOAc:hexanes), *p*-anisaldehyde

^{1}H-NMR (300 MHz, $CDCl_3$): δ 4.14–4.04 (m, 2H), 3.85 (s, 3H), 2.86–2.76 (m, 2H), 1.97 (p, *J* = 7.9 Hz, 2H).

^{13}C-NMR (101 MHz, $CDCl_3$): δ 168.4, 163.3, 62.7, 52.7, 35.4, 22.2.

HRMS (ESI): Calculated for $C_6H_{10}NO_2$ $[M+H]^+$: 128.0723; found: *m*/*z* 128.0720.



3.94 **3.101**

To a round-bottom pressure vessel containing carboxylic acid **3.94** (2.32 g, 9.54 mmol, 1.0 equiv.) is added anhydrous DCM (68.0 mL) and cooled to 0 °C in a water/ice bath. The Ghosez reagent **3.28** (1.66 g, 12.4 mmol, 1.3 equiv.) was then added dropwise and the heterogeneous reaction mixture is left stirring and allowed to warm to room temperature gradually (~1.5–2 hours) at which point the reaction will have become completely homogeneous. Once the reaction had reached room temperature, a solution of imine **3.21** (1.58 g, 12.4 mmol, 1.3 equiv.) and 2,6-lutidine (2.89 mL, 24.8 mmol, 2.6 equiv.) in anhydrous DCM (27.0 mL) is added to the pressure vessel slowly (total concentration of the reaction is now 0.1 M) and allowed to stir at room temperature for 2 hours. The rubber septum on the pressure vessel is replaced with a Teflon screwcap and tightly sealed before being submerged in a 60 °C oil bath and allowed to reflux for an additional 2–3 hours. The pressure vessel is removed from the oil bath and allowed to cool to room temperature before being opened and poured into a separatory funnel containing 1 M $HCl_{(aq)}$ and the aqueous phase extracted with DCM (x3). The combined organics are dried over anhydrous $MgSO_4$, filtered, and concentrated under reduced pressure to afford an orange-tinted semi-solid that is contaminated with *N*,*N*-dimethylisobutyramide. Tritruation with cold DCM gave enamide **3.101** as a fluffy white powder (3.21 g, 96% yield) with analytical data that matches that which is reported in the literature.

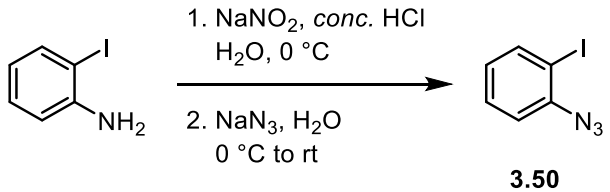
TLC: R_f 0.33 (50% EtOAc:hexanes), UV (254 nm) and *p*-anisaldehyde

^{1}H-NMR (500 MHz, $CDCl_3$): δ 7.90–7.85 (m, 2H), 7.78–7.73 (m, 2H), 6.02 (t, *J* = 3.0 Hz, 1H), 5.23 (dd, *J* = 10.3, 5.0 Hz, 1H), 4.18 (td, *J* = 10.5, 3.5 Hz, 1H), 3.80 (s, 3H), 3.80–3.72 (m, 1H), 3.20 (ddd, *J* = 17.5, 10.3, 2.7 Hz, 1H), 3.03 (ddd, *J* = 17.5, 5.0, 2.7 Hz, 1H), 2.74 (dtd, *J* = 17.6, 9.8, 2.6 Hz, 1H), 2.50 (ddt, *J* = 17.5, 10.4, 3.5 Hz, 1H), 1.87 (t, *J* = 2.7 Hz, 1H).

^{13}C-NMR (126 MHz, $CDCl_3$): δ 167.1, 166.3, 161.4, 136.5, 134.6, 131.5, 123.9, 79.7, 71.1, 52.5, 51.4, 50.2, 29.3, 20.0.[v]

HRMS (ESI): Calculated for $C_{19}H_{16}N_2NaO_5$ $[M+Na]^+$: 375.0938; found: *m*/*z* 375.0957.

[v]One carbon signal is missing due to overlap.



3.50

To a round-bottom flask open to the surrounding atmosphere is added 2-iodoaniline (6.37 g, 29.1 mmol, 1.0 equiv.) and water (97.0 mL, 0.3 M) and is cooled to 0 °C in a water/ice bath. At this point, concentrated HCl (~12 M, 24.3 mL, 10 equiv.) is added dropwise and the now pale white suspension stirred for 10 minutes. $NaNO_2$ (2.21 g, 32.0 mmol, 1.1 equiv.) is then added as a solution in water (10 mL) dropwise and allowed to stir at 0 °C for 1 hour at which point the reaction mixture will have become homogeneous and taken on a yellow color. After 1 hour, NaN_3 (2.27 g, 34.9 mmol, 1.2 equiv.) as a solution in water (10 mL) is added dropwise at which point gas evolution is observed. After all the NaN_3 is added, the reaction mixture is removed from the water/ice bath and allowed to stir at room temperature for 2 hours before being quenched with sat. $Na_2S_2O_{5(aq)}$ and extracted with EtOAc (x3). The organic extracts are combined and dried over anhydrous $MgSO_4$, filtered, and then concentrated under reduced pressure to afford a dark amber liquid. Purification by flash-column chromatography (5% EtOAc:hexanes) gave azide **3.50** as a dark yellow liquid (6.87 g, 98% yield) with analytical data that matches that which is reported in the literature.

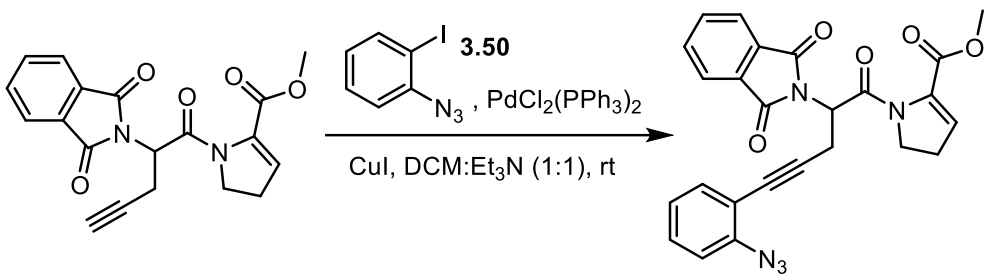
Note: This reaction generates highly reactive and potentially explosive diazonium intermediates. Caution should be taken to ensure the initial steps of the reaction are always done at 0 °C and that NaN_3 addition is done carefully and slowly. Always perform this reaction in a well-ventilated fume hood and if on very large scale – behind a blast shield.

TLC: R_f 0.73 (10% EtOAc:hexanes), UV (254 nm)

^{1}H-NMR (300 MHz, $CDCl_3$): δ 7.79 (dd, *J* = 7.9, 1.4 Hz, 1H), 7.43–7.34 (m, 1H), 7.14 (dd, *J* = 8.0, 1.4 Hz, 1H), 6.87 (dddd, *J* = 7.9, 7.3, 1.4, 0.4 Hz, 1H).

^{13}C-NMR (101 MHz, $CDCl_3$): δ 141.7, 140.1, 129.7, 126.4, 118.6, 87.9.

HRMS (EI): Calculated for $C_6H_4IN_3$ $[M]^+$: 244.9450; found: *m*/*z* 244.9410.



3.101 **3.103**

To a round-bottom flask charged with enamide **3.101** (1.54 g, 4.37 mmol, 1.0 equiv.) is added anhydrous DCM and Et_3N (1:1, 55.0 mL, 0.08 M) and the reaction mixture is degassed with a strong flow of nitrogen gas (~15 min). 1-azido-2-iodobenzene **3.50** (2.14 g, 8.74 mmol, 2.0 equiv.) is then added in one portion *via* syringe. At this point, $PdCl_2(PPh_3)_2$ (154 mg, 0.219 mmol, 5 mol%) and CuI (83.3 mg, 0.437 mmol, 10 mol%) are added simultaneously and the reaction is left to stir for 2 hours. Once TLC indicated complete consumption of the starting material, the reaction is quenched with the addition of water and poured into a separatory funnel. The aqueous phase is washed with DCM (x3) and the organic extracts are collected, dried over anhydrous $MgSO_4$, filtered, and concentrated under reduced pressure to afford a dark amber oil. Purification by flash-column chromatography (gradient of 45–60% EtOAc:hexanes) gave the arylazide **3.103** as a light-brown solid (1.36 g, 75% yield).

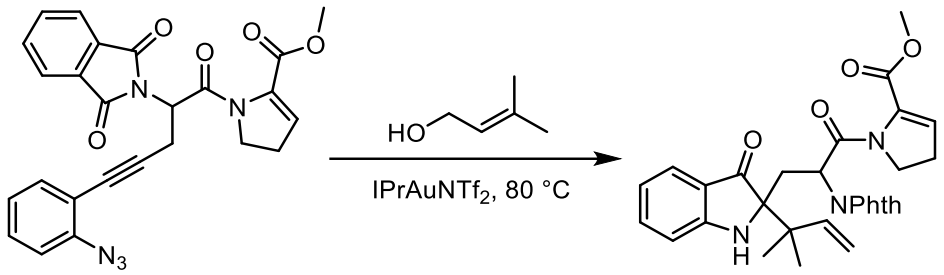
TLC: R_f 0.35 (50% EtOAc:hexanes), UV (254 nm) and $KMnO_4$

^{1}H-NMR (300 MHz, $CDCl_3$): δ 7.92–7.83 (m, 2H), 7.78–7.71 (m, 2H), 7.25–7.15 (m, 2H), 6.99–6.90 (m, 2H), 6.02 (t, *J* = 2.9 Hz, 1H), 5.31 (dd, *J* = 10.7, 4.9 Hz, 1H), 4.25–4.12 (m, 1H), 3.80 (s, 3H), 3.83–3.71 (m, 1H), 3.53 (dd, *J* = 17.7, 10.7 Hz, 1H), 3.25 (dd, *J* = 17.6, 4.9 Hz, 1H), 2.75 (dtd, *J* = 17.6, 9.8, 2.6 Hz, 1H), 2.50 (ddt, *J* = 17.5, 10.3, 3.5 Hz, 1H).

^{13}C-NMR (126 MHz, $CDCl_3$): δ 167.1, 166.4, 161.4, 140.9, 136.5, 134.5, 133.7, 131.7, 129.2, 124.6, 123.7, 118.4, 115.3, 91.3, 78.8, 52.5, 51.5, 50.2, 29.3, 21.2.[w]

HRMS (ESI): Calculated for $C_{25}H_{19}N_5NaO_5$ $[M+Na]^+$: 492.1262; found: *m*/*z* 492.1284.

[w]One carbon signal is missing due to overlap.



3.103 **3.35**

To an oven-dried round-bottom flask open to the surrounding atmosphere is added arylazide **3.103** (23.3 mg, 0.049 mmol, 1.0 equiv.) and $IPrAuNTf_2$ (4.3 mg, 0.0049 mmol, 10 mol%), followed by freshly distilled 3-methyl-2-buten-1-ol (prenyl alcohol) as solvent (0.33 mL, 0.15 M). The flask is then sealed and submerged in an 80 °C oil bath and allowed to stir at that temperature for 2 hours. After, the flask is removed from the oil bath and allowed to come to room temperature before the excess solvent is removed under reduced pressure. Purification by flash-column chromatography (80% Et_2O:hexanes) gave pseudoindoxyl **3.35** as a dark yellow foam and as a mixture of diastereoisomers which were inseparable (12.3 mg, *d.r.* ~1:1, 47% yield) with analytical data that matches that which is reported in the literature.

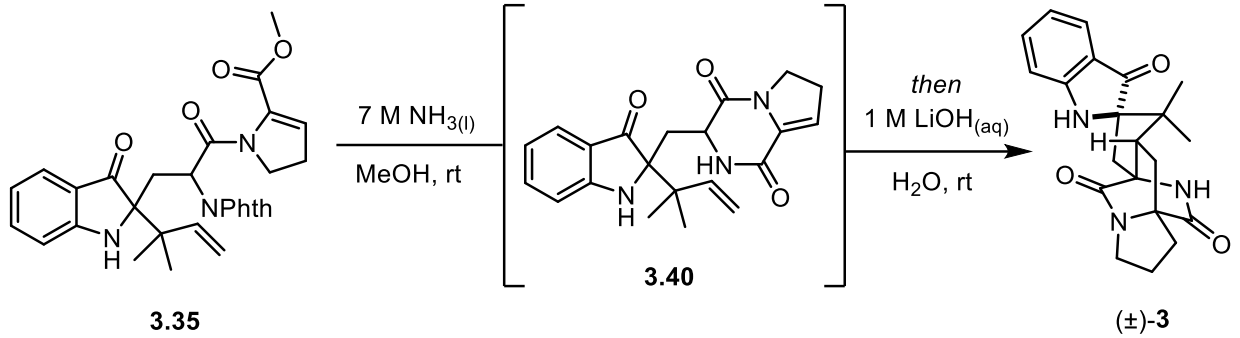
TLC: R_f 0.29 (100% Et_2O), UV (254 nm or 366 nm faint) and *p*-anisaldehyde

^{1}H-NMR (300 MHz, $CDCl_3$): δ 7.76–7.71 (m, 2H), 7.71–7.65 (m, 2H), 7.62 (s, 4H), 7.47–7.35 (m, 3H), 6.96 (ddd, *J* = 8.3, 7.0, 1.3 Hz, 1H), 6.84 (d, *J* = 8.2 Hz, 1H), 6.71 (t, *J* = 7.4 Hz, 1H), 6.62 (t, *J* = 7.4 Hz, 1H), 6.18–6.00 (m, 3H), 5.95 (br s, 2H), 5.23 (br s, 1H), 5.12 (qd, *J* = 6.3, 1.2 Hz, 3H), 5.05 (br s, 1H), 4.89 (dd, *J* = 11.6, 3.4 Hz, 1H), 4.71 (br s, 1H), 4.53 (dd, *J* = 8.8, 4.1 Hz, 1H), 4.05 (t, *J* = 9.2 Hz, 1H), 3.99–3.88 (m, 1H), 3.83–3.69 (m, 8H), 3.47–3.25 (m, 2H), 2.72 (td, *J* = 8.4, 2.9 Hz, 2H), 2.59 (dd, *J* = 14.9, 3.5 Hz, 1H), 2.44 (td, *J* = 8.7, 3.5 Hz, 3H), 1.15 (s, 3H), 1.14 (s, 3H), 1.00 (s, 3H), 0.99 (s, 3H).

^{13}C-NMR (126 MHz, $CDCl_3$): δ 203.3, 167.8, 167.2, 166.9, 162.0, 161.3, 160.9, 143.0, 142.9, 137.3, 136.9, 136.9, 136.6, 134.6, 134.3, 133.9, 131.7, 131.6, 124.4, 124.3, 123.6, 123.2, 122.1, 121.8, 118.7, 118.2, 114.7, 114.6, 111.7, 111.1, 72.0, 71.7, 52.5, 52.5, 50.3, 48.9, 48.6, 44.4, 43.8, 34.2, 29.8, 29.3, 29.2, 21.9, 21.7, 21.3, 21.2.[x]

HRMS (ESI): Calculated for $C_{30}H_{29}N_3NaO_6$ $[M+Na]^+$: 550.1948; found: *m*/*z* 550.1954.

[x]Several carbon signals are missing due to overlap.



To a round-bottom flask charged with pseudoindoxyl **3.35** (7.1 mg, 0.013 mmol, 1.0 equiv.) is added a methanolic solution of ammonia (7 M, 0.50 mL, 0.03 M). This mixture is stirred at room temperature for 1 hour at which point TLC analysis indicated complete consumption of the starting material. The solvent is removed under reduced pressure and replaced with a 1 M solution of aqueous LiOH (1.3 mL, 0.01 M). This mixture is stirred vigorously at room temperature for 2 hours before the addition of a sat. NH_4Cl solution and pouring the contents of the flask into a separatory funnel. The aqueous phase is then washed with DCM (x5) and the organic fractions collected, dried over anhydrous Na_2SO_4, filtered, and concentrated under reduced pressure to afford a dark yellow residue. Purification by flash-column chromatography (30% THF:$CHCl_3$) gave the natural product (±)-brevianamide A as a yellow solid (2.6 mg, 52% over 2 steps). The spectroscopic data of our synthetic sample of (±)-brevianamide A matched those which were reported by Lawrence and Smith (see Tables 5 and 5.1 below).

TLC: R_f 0.34 (30% THF:$CHCl_3$), UV (254 nm or 366 nm) and *p*-anisaldehyde

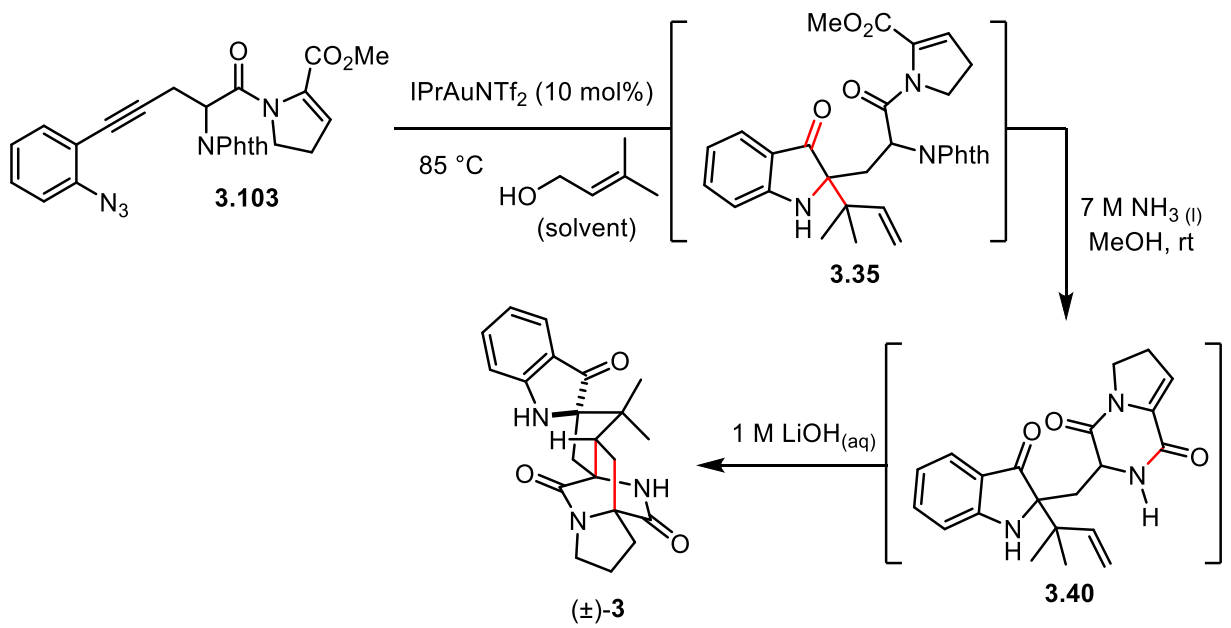
^{1}H-NMR (300 MHz, $CDCl_3$): δ 7.58 (d, *J* = 7.7 Hz, 1H), 7.45 (td, *J* = 7.6, 1.3 Hz, 1H), 6.85–6.77 (m, 2H), 6.64 (br s, 1H), 4.94 (br s, 1H), 3.46 (tt, *J* = 7.0, 3.4 Hz, 2H), 2.84–2.72 (m, 2H), 2.44–2.31 (m, 2H), 2.04 (p, *J* = 6.8 Hz, 2H), 1.97–1.78 (m, 3H), 1.12 (s, 3H), 0.93 (s, 3H).

^{13}C-NMR (126 MHz, $CDCl_3$): δ 202.2, 172.4, 169.8, 160.2, 137.8, 124.9, 121.2, 119.4, 112.1, 78.9, 69.5, 67.8, 55.7, 48.5, 44.1, 37.4, 29.2, 29.0, 25.1, 24.1, 20.0.

IR (neat): ῡ 3339, 3276, 2955, 2917, 2849, 1708, 1658, 1617, 1491, 1437, 1399 cm^{-1}.

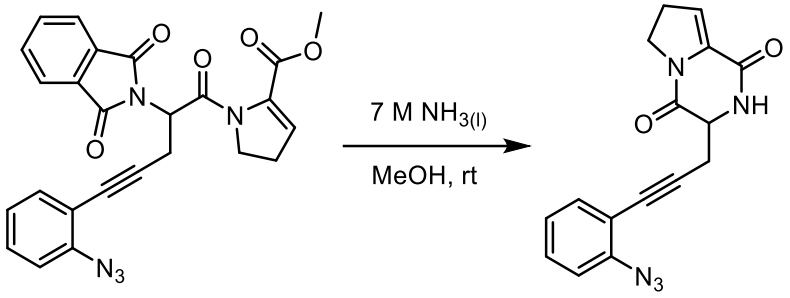
HRMS (ESI): Calculated for $C_{21}H_{23}N_3NaO_3$ $[M+Na]^+$: 388.1637; found: *m*/*z* 388.1614.

One-pot synthesis of (±)-brevianamide A (**3**) starting from arylazide **3.103**:



To an oven-dried round-bottom flask open to the surrounding atmosphere is added arylazide **3.103** (28.7 mg, 0.061 mmol, 1.0 equiv.) and $IPrAuNTf_2$ (5.3 mg, 0.0061 mmol, 10 mol%), followed by freshly distilled 3-methyl-2-buten-1-ol (prenyl alcohol) as solvent (0.40 mL, 0.15 M). The flask is then sealed and submerged in an 80 °C oil bath and allowed to stir at that temperature for 2 hours at which point the reaction had darkened and taken on a dark yellow hue. Once TLC analysis indicated complete consumption of the starting material, the flask was removed from the oil bath and allowed to cool to room temperature. Once cool, a methanolic solution of ammonia (7 M, 2.0 mL) is added and the reaction is left to stir at room temperature for 45 minutes. Analysis by TLC indicated complete conversion to the intermediate diketopiperazine **3.40** (highly fluorescent) and thus a 1 M solution of aqueous LiOH (6.1 mL) was added directly to affect the biomimetic [4+2] reaction. After addition of LiOH, the reaction mixture was left at room temperature for 1.5 hours with vigorous stirring. Once complete conversion to (±)-**3** had been observed by TLC, the reaction was diluted with a small amount of sat. NH_4Cl and then extracted with DCM (x6). All the organic fractions were collected, dried over anhydrous Na_2SO_4, filtered, and concentrated under reduced pressure to afford a dark yellow/amber residue. Purification by flash-column chromatography (45% acetone:hexanes) gave the natural product (±)-brevianamide A as a yellow solid (6 mg, 28%

over 3 steps). The spectroscopic data of this sample was in accordance with the sample produced by the stepwise protocol shown above.



3.103 **3.41**

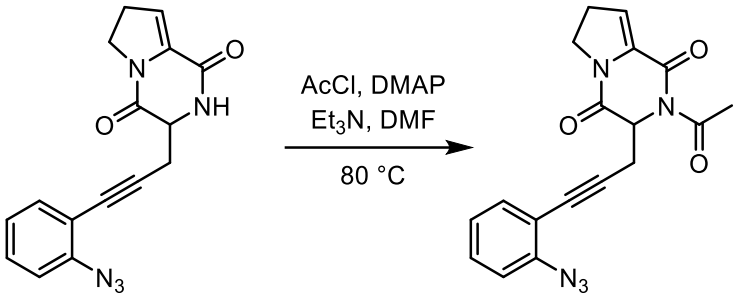
To a round-bottom flask charged with arylazide **3.103** (998 mg, 2.10 mmol, 1.0 equiv.) is added methanolic ammonia (7 M, 70.0 mL, 0.03 M). This heterogenous mixture is stirred vigorously at room temperature for 4 hours, at which point TLC indicated complete consumption of the starting material. The solvent is removed under reduced pressure to afford a crude off-yellow solid that is contaminated with phthalimide. Purification by flash-column chromatography (first 100% EtOAc, then solvent switch to 3% MeOH:1% Et_3N:DCM) gave diketopiperazine **3.41** as an off-white solid (568 mg, 88% yield).

TLC: R_f 0.13 (100% EtOAc), UV (254 nm) and $KMnO_4$

^{1}H-NMR (500 MHz, *d*$_6$-DMSO): δ 8.45 (d, *J* = 2.3 Hz, 1H), 7.41 (td, *J* = 7.9, 1.6 Hz, 1H), 7.29 (dd, *J* = 8.0, 1.3 Hz, 2H), 7.15 (td, *J* = 7.5, 1.2 Hz, 1H), 5.96 (t, *J* = 3.0 Hz, 1H), 4.36 (q, *J* = 3.9 Hz, 1H), 3.92 (ddt, *J* = 12.2, 7.6, 3.7 Hz, 2H), 3.03 (dd, *J* = 17.1, 3.2 Hz, 1H), 2.82 (dd, *J* = 17.1, 4.6 Hz, 1H), 2.75–2.56 (m, 2H).

^{13}C-NMR (101 MHz, *d*$_6$-DMSO): δ 161.3, 156.6, 140.5, 133.6, 133.0, 129.8, 125.0, 119.2, 116.9, 114.2, 91.0, 79.1, 55.5, 45.2, 27.3, 25.9.

HRMS (ESI): Calculated for $C_{16}H_{13}N_5NaO_2$ $[M+Na]^+$: 330.0967; found: *m*/*z* 330.0944.



3.41 **3.104**

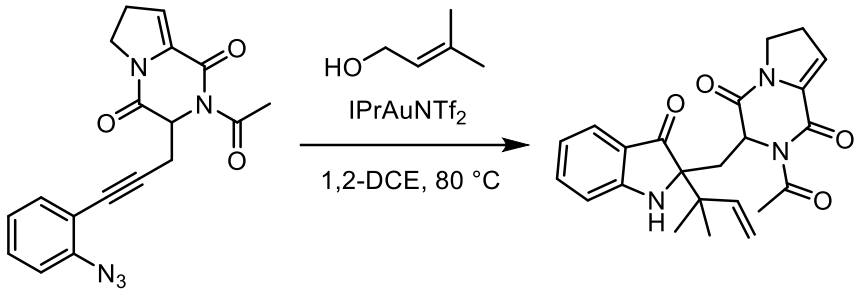
To a round-bottom flask charged with diketopiperazine **3.41** (56.4 mg, 0.184 mmol, 1.0 equiv.) is added anhydrous DMF (1.80 mL, 0.1 M), followed by DMAP (44.8 mg, 0.367 mmol, 2.0 equiv.) and submerged in an 80 °C oil bath until a homogeneous mixture is formed. Triethylamine (0.10 mL, 0.734 mmol, 4.0 equiv.) is added first, then acetyl chloride (0.13 mL, 1.83 mmol, 10 equiv.) is added dropwise resulting in a dark brown mixture with white fumes in the flask head space. The reaction is left stirring at the same temperature for 40 minutes, at which point TLC analysis will have indicated complete consumption of the starting material. The reaction is removed from the oil bath and allowed to cool to room temperature before being quenched with water and EtOAc (30 mL). The contents of the flask are poured into a separatory funnel and the organic phase washed with water (x3) to remove DMF. The organic phase is collected, dried over anhydrous $MgSO_4$, filtered, and concentrated under reduced pressure to afford a dark amber residue. Purification by flash-column chromatography (50% EtOAc:hexanes) gave acetylated diketopiperazine **3.104** as a pale orange viscous oil (59.7 mg, 93% yield).

TLC: R_f 0.62 (100% EtOAc), UV (254 nm) and $KMnO_4$

^{1}H-NMR (500 MHz, $CDCl_3$): δ 7.35 (td, *J* = 7.8, 1.6 Hz, 1H), 7.29 (dd, *J* = 7.8, 1.6 Hz, 1H), 7.14–7.06 (m, 2H), 6.27 (t, *J* = 3.2 Hz, 1H), 5.23 (t, *J* = 3.8 Hz, 1H), 4.23 (ddd, *J* = 12.3, 11.3, 6.3 Hz, 1H), 4.01 (td, *J* = 11.9, 7.9 Hz, 1H), 3.29–3.19 (m, 2H), 2.85–2.67 (m, 2H), 2.66 (s, 3H).

^{13}C-NMR (101 MHz, $CDCl_3$): δ 172.3, 161.9, 157.9, 141.3, 134.5, 133.4, 129.8, 124.8, 122.0, 118.7, 114.8, 89.9, 81.0, 57.6, 45.5, 28.6, 27.3, 25.6.

HRMS (ESI): Calculated for $C_{18}H_{15}N_5NaO_3$ $[M+Na]^+$: 372.1073; found: *m*/*z* 372.1085.



3.104 **3.105**

To an oven-dried round-bottom flask open to the surrounding atmosphere is added acetylated diketopiperazine **3.104** (29.4 mg, 0.0841 mmol, 1.0 equiv.), freshly distilled 3-methyl-2-buten-1-ol (85 μL, 0.841 mmol, 10 equiv.), and $IPrAuNTf_2$ (7.3 mg, 0.00841 mmol, 10 mol%), followed by anhydrous 1,2-DCE (0.81 mL, 0.15 M). The flask is then sealed and submerged in an 80 °C oil bath and allowed to stir at that temperature for 30 minutes. After, the flask is removed from the oil bath and allowed to come to room temperature before the excess solvent is removed under reduced pressure. Due to issues during purification, the yield of pseudoindoxyl **3.105** (38%, *d.r.* 5:1) was assessed by crude NMR using DMF as an external standard. For characterization purposes, a sample was purified by preparative TLC (50% EtOAc:hexanes run twice, then 32% acetone:hexanes) to give pseudoindoxyl **3.105** as a dark yellow foam and as a mixture of diastereoisomers (~2:1 after purification as seen by the relative integrations in the ^{1}H NMR) which were inseparable. For clarity, an * is used to denote the minor diastereoisomer in the ^{1}H-NMR spectrum for isolated or overlapping signals.

TLC: R_f 0.15 (60% EtOAc:hexanes), UV (254 nm or 366 nm) and *p*-anisaldehyde

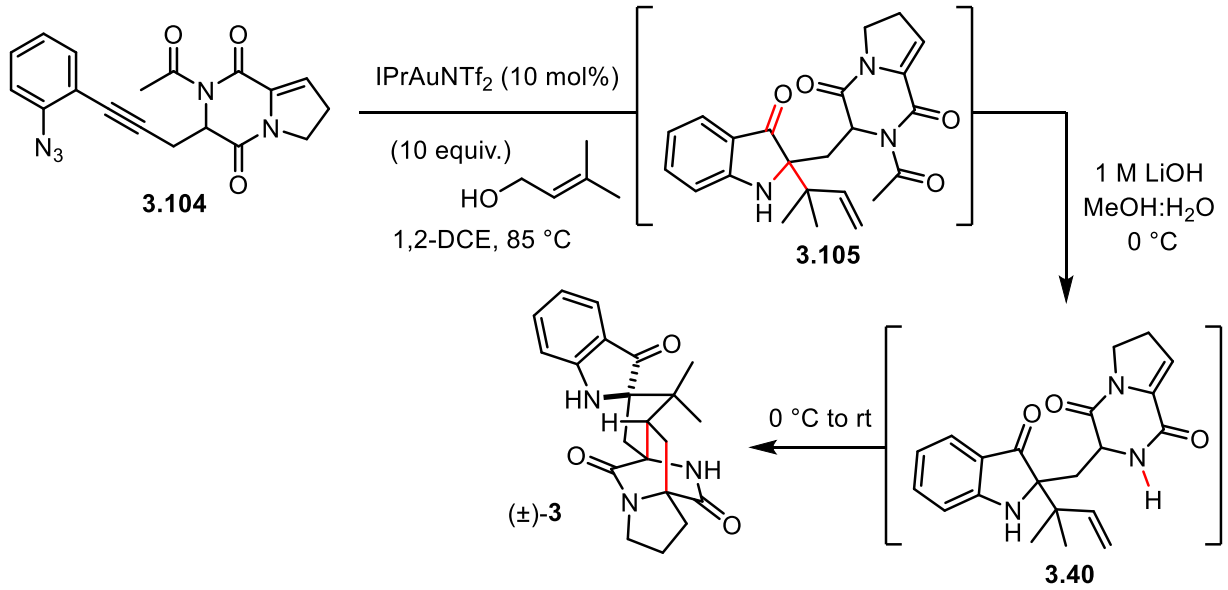
^{1}H-NMR (300 MHz, $CDCl_3$): δ 7.53 (d, *J* = 7.7 Hz, 1H*), 7.48 (d, *J* = 7.7 Hz, 1H), 7.39–7.32 (m, 1H*), 7.36–7.29 (m, 1H), 6.85–6.75 (m, 1H*), 6.71 (d, *J* = 8.2 Hz, 1H*), 6.67 (d, *J* = 8.2 Hz, 1H), 5.98 (dd, *J* = 17.3, 10.8 Hz, 1H), 5.79 (t, *J* = 3.2 Hz, 1H*), 5.72 (t, *J* = 3.2 Hz, 1H), 5.19–4.96 (m, 3H*), 4.68 (br s, 1H*), 4.65 (br s, 1H), 4.04–3.79 (m, 2H*), 2.95 (dd, *J* = 14.9, 5.3 Hz, 1H), 2.70 (dd, *J* = 14.9, 3.0 Hz, 1H), 2.64–2.53 (m, 2H*), 2.52 (s, 3H*), 2.49 (s, 3H), 1.11 (s, 3H*), 0.86 (s, 3H*).

^{13}C-NMR (126 MHz, $CDCl_3$): δ 202.8, 202.3, 172.9, 172.6, 163.4, 163.3, 160.9, 160.3, 156.7, 156.4, 142.6, 137.5, 137.3, 137.1, 133.3, 133.2, 125.5, 125.1, 122.1, 121.6, 121.1, 120.8, 119.4,

119.3, 116.6, 115.4, 111.6, 110.9, 71.1, 68.6, 56.8, 56.5, 45.5, 44.2, 37.9, 36.6, 34.6, 28.4, 28.3, 28.3, 28.1, 26.1, 21.4, 21.0, 18.2.[y]

HRMS (ESI): Calculated for $C_{23}H_{25}N_3NaO_4$ $[M+Na]^+$: 430.1743; found: *m/z* 430.1727.

One-pot synthesis of (±)-**3** starting from acetylated diketopiperazine **3.104**:



To an oven-dried round-bottom flask open to the surrounding atmosphere is added acetylated diketopiperazine **3.104** (20.4 mg, 0.0583 mmol, 1.0 equiv.), freshly distilled 3-methyl-2-buten-1-ol (60 µL, 0.583 mmol, 10 equiv.), and $IPrAuNTf_2$ (5.1 mg, 0.00583 mmol, 10 mol%) followed by anhydrous 1,2-DCE (0.38 mL, 0.15 M). The flask is then sealed and submerged in an 80 °C oil bath and allowed to stir at that temperature for 30 minutes at which point TLC analysis indicated complete consumption of the starting material, so the flask was removed from the oil bath and allowed to cool to room temperature, then cooled to 0 °C in a water/ice bath. Once cold, a 1 M solution of aqueous LiOH and methanol (1:1, 2.9 mL) was added dropwise which immediately resulted in darkening of the mixture. After 1.5 hours, none of the intermediate pseudoindoxyl **3.105** was visible by TLC and only a more polar highly fluorescent compound was observed. At this point, the reaction was removed from the water/ice bath and allowed to warm to room temperature to affect the biomimetic [4+2] reaction. After another 1.5 hours, complete conversion to (±)-

[y]One carbon signal is missing due to overlap.

brevianamide A had been observed by TLC, and the reaction was diluted with a small amount of sat. NH_4Cl and then extracted with DCM (x6). All the organic fractions were collected, dried over anhydrous Na_2SO_4, filtered, and concentrated under reduced pressure to afford a dark yellow/amber residue. Purification by flash-column chromatography (30% THF:$CHCl_3$) gave the natural product (±)-brevianamide A as a yellow solid (4.5 mg, 21% over 3 steps). The spectroscopic data of this sample was in accordance with the sample produced by the stepwise protocol shown above.

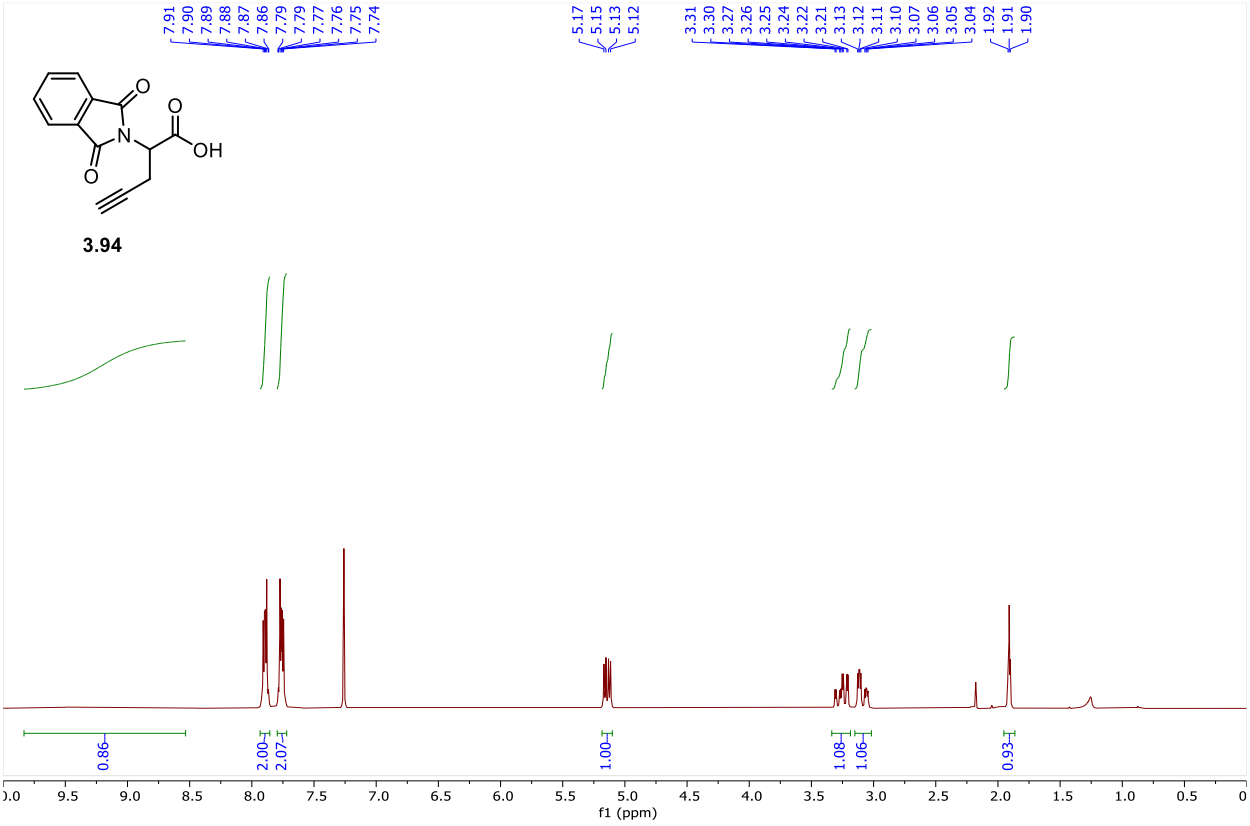
Table 6: Comparison of ^{1}H-NMR data of our synthetic sample of (±)-brevianamide A (**3**) to the sample prepared by the group of Lawrence

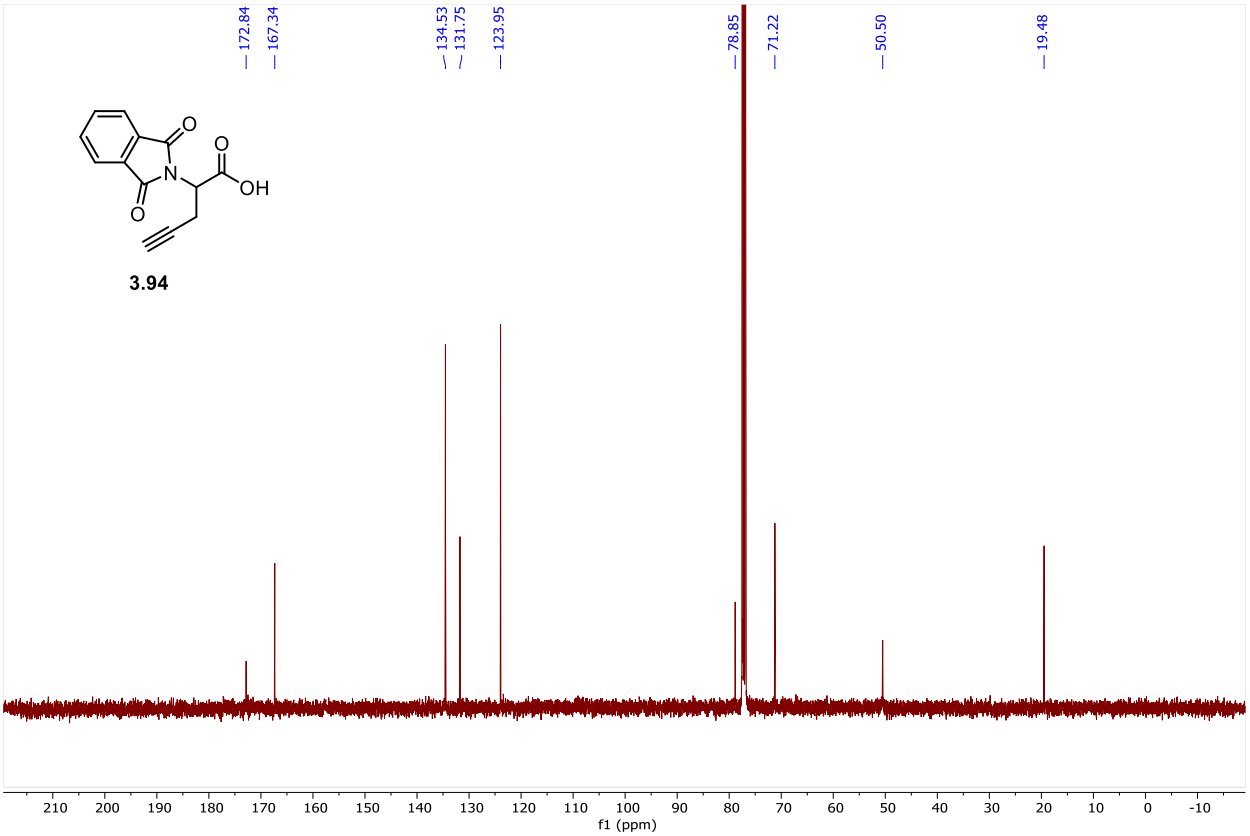
Lawrences sample (+)-brevianamide A (**3**), 500 MHz, $CDCl_3$	**Our work** (±)-brevianamide A (**3**), 300 MHz, $CDCl_3$
7.57 (dd, *J* = 7.7, 1.2 Hz, 1H)	7.58 (d, *J* = 7.7 Hz, 1H)
7.44 (ddd, *J* = 8.3, 7.1, 1.4 Hz, 1H)	7.45 (td, *J* = 7.6, 1.3 Hz, 1H)
6.84–6.78 (m, 2H)	6.85–6.77 (m, 2H)
6.62 (br s, 1H)	6.64 (br s, 1H)
4.98 (br s, 1H)	4.94 (br s, 1H)
3.52–3.41 (m, 2H)	3.46 (tt, *J* = 7.0, 3.4 Hz, 2H)
2.81–2.74 (m, 2H)	2.84–2.72 (m, 2H)
2.40 (ddd, *J* = 9.8, 7.3, 1.1 Hz, 1H), 2.35 (d, *J* = 15.6 Hz, 1H)	2.44–2.31 (m, 2H)
2.04 (app. pd, *J* = 6.8, 1.6 Hz, 2H)	2.04 (p, *J* = 6.8 Hz, 2H)
1.96–1.81 (m, 3H)	1.97–1.78 (m, 3H)
1.12 (s, 3H)	1.12 (s, 3H)
0.93 (s, 3H)	0.93 (s, 3H)

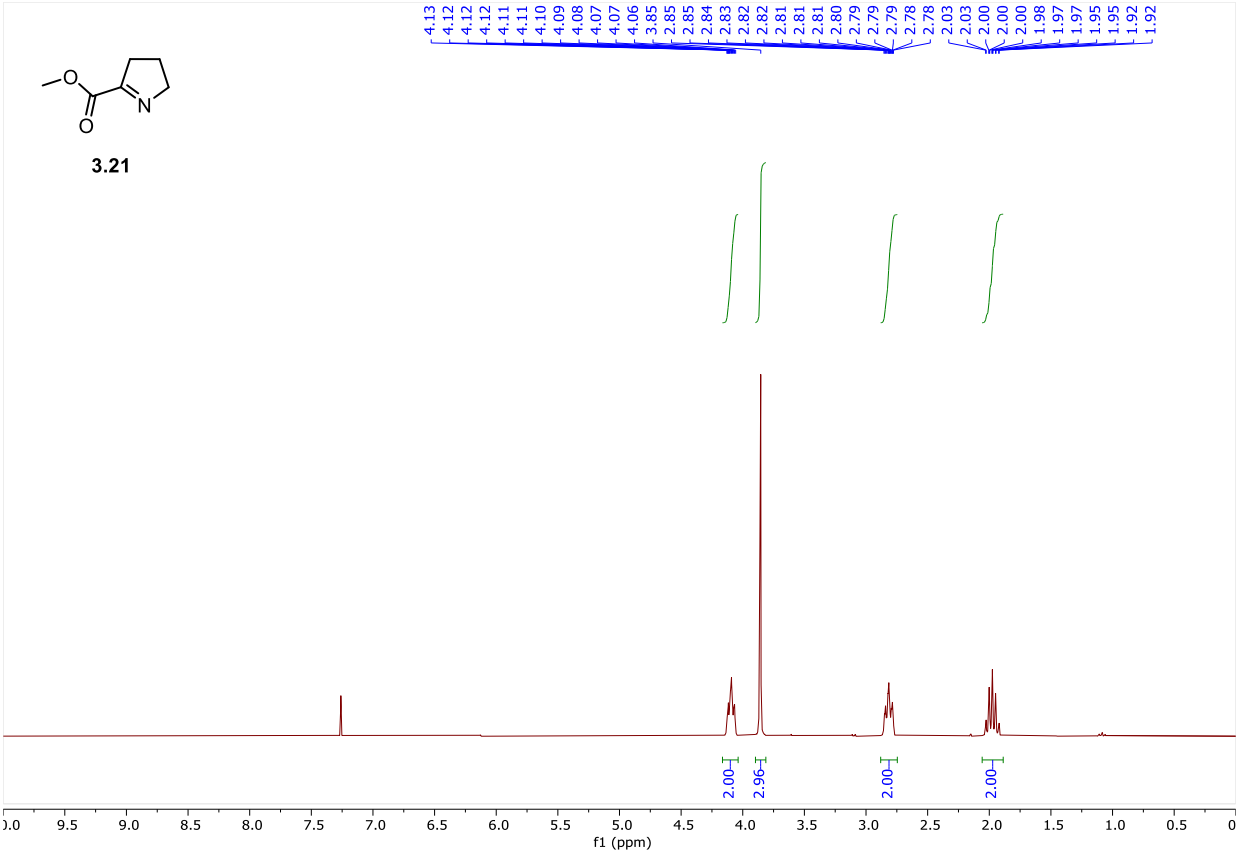
Table 6.1: Comparison of ^{13}C-NMR data of our synthetic sample of (±)-brevianamide A (**3**) to the sample prepared by the group of Lawrence

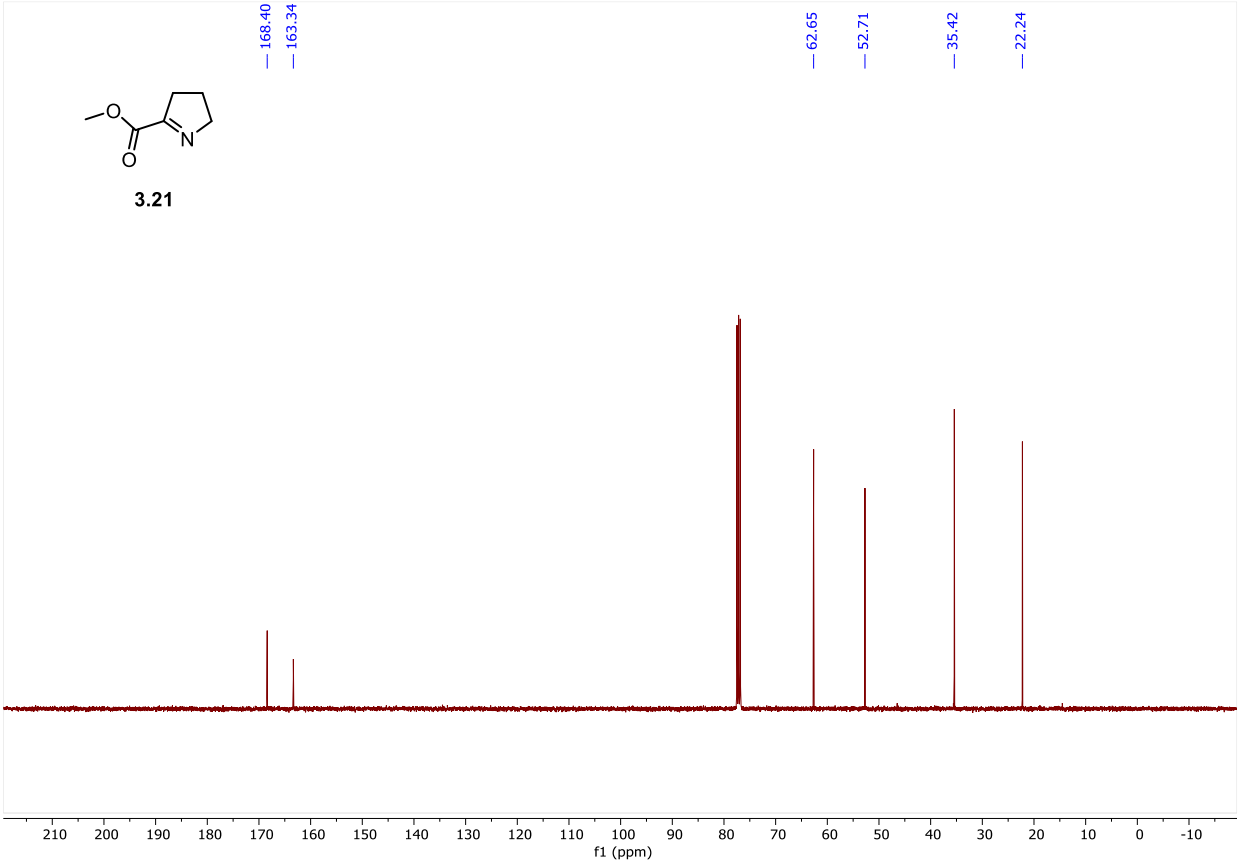
Lawrences sample (+)-brevianamide A (**3**), 126 MHz, $CDCl_3$	**Our work** (±)-brevianamide A (**3**), 126 MHz, $CDCl_3$
202.2	202.2
172.4	172.4
169.8	169.8
160.2	160.2
137.8	137.8
124.8	124.9
121.2	121.2
119.3	119.4
112.1	112.1
78.9	78.9
69.5	69.5
67.8	67.8
55.7	55.7
48.4	48.5
44.1	44.1
37.4	37.4
29.2	29.2
29.0	29.0
25.1	25.1
24.1	24.1
19.9	20.0

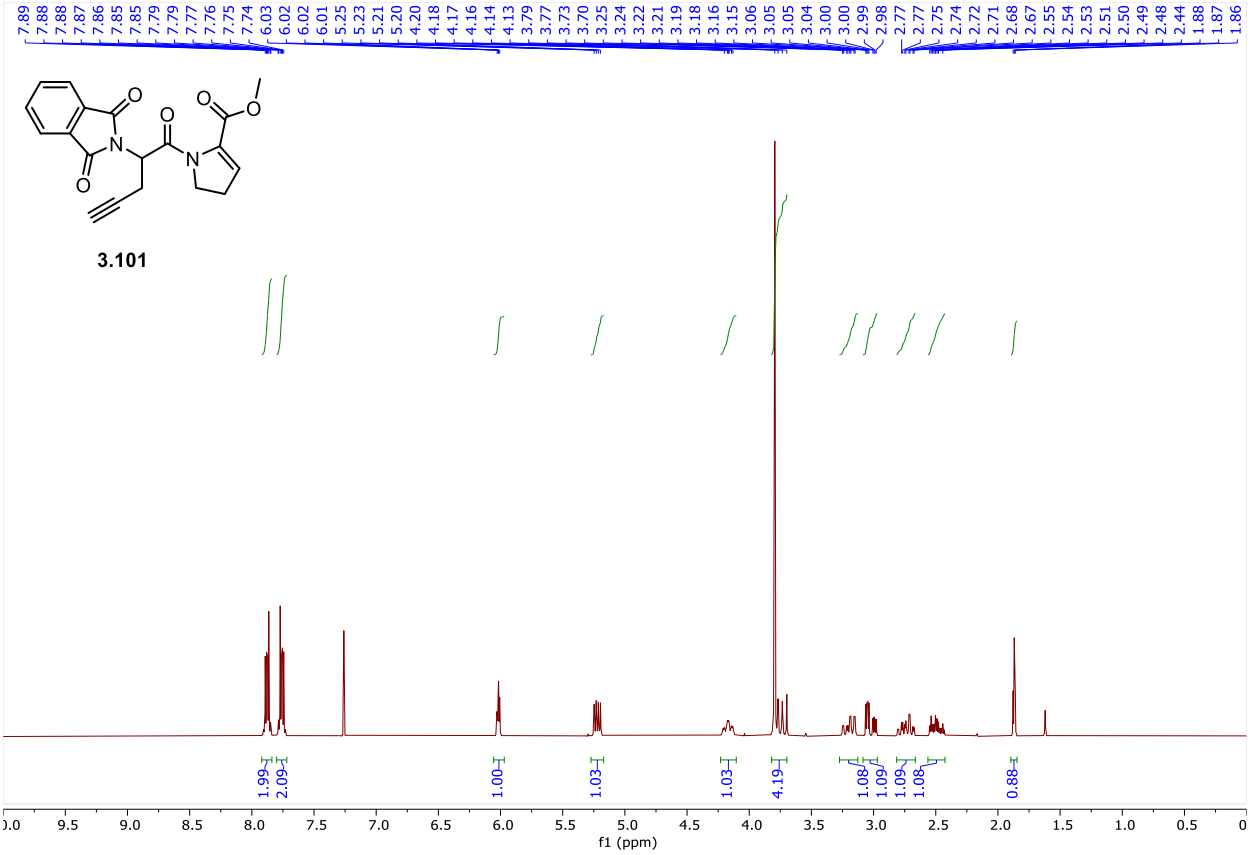
6.3.2 ^{1}H- and ^{13}C-NMR spectra

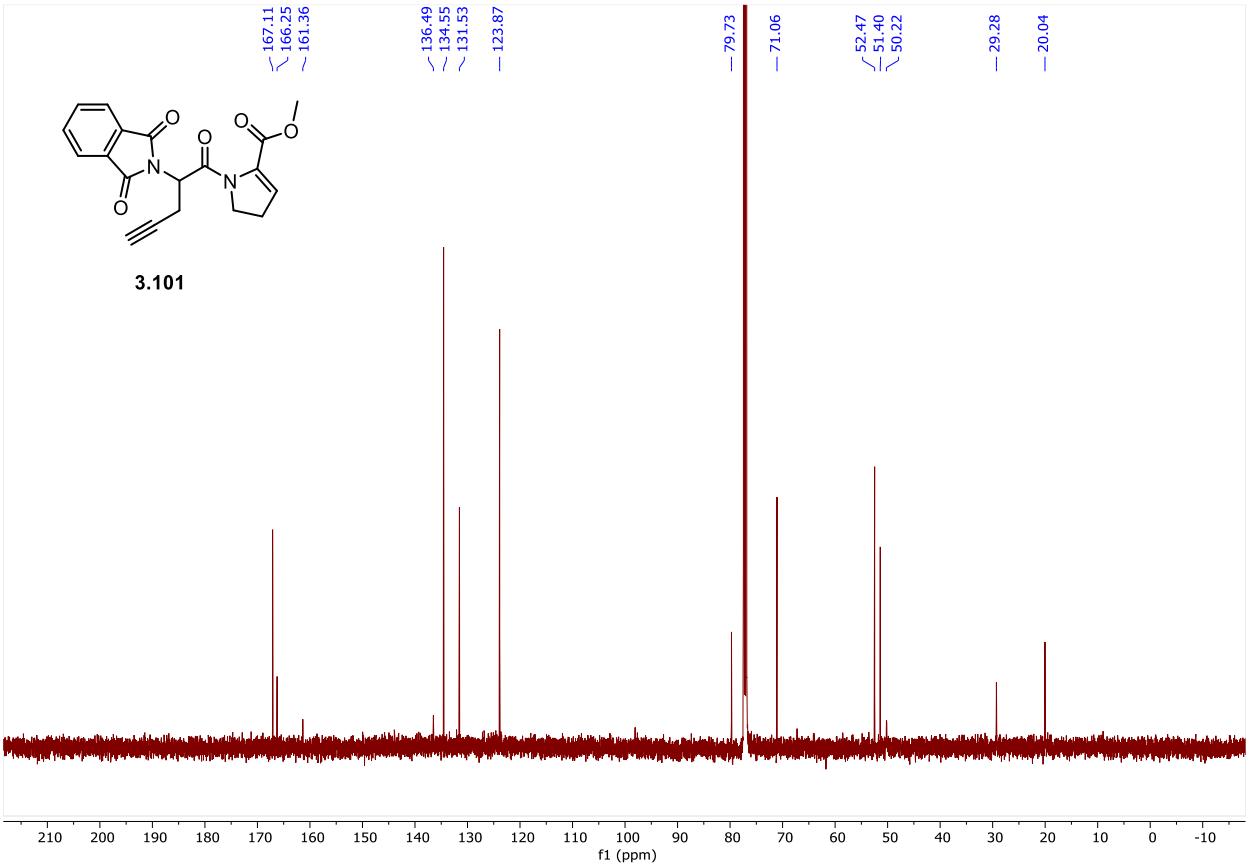


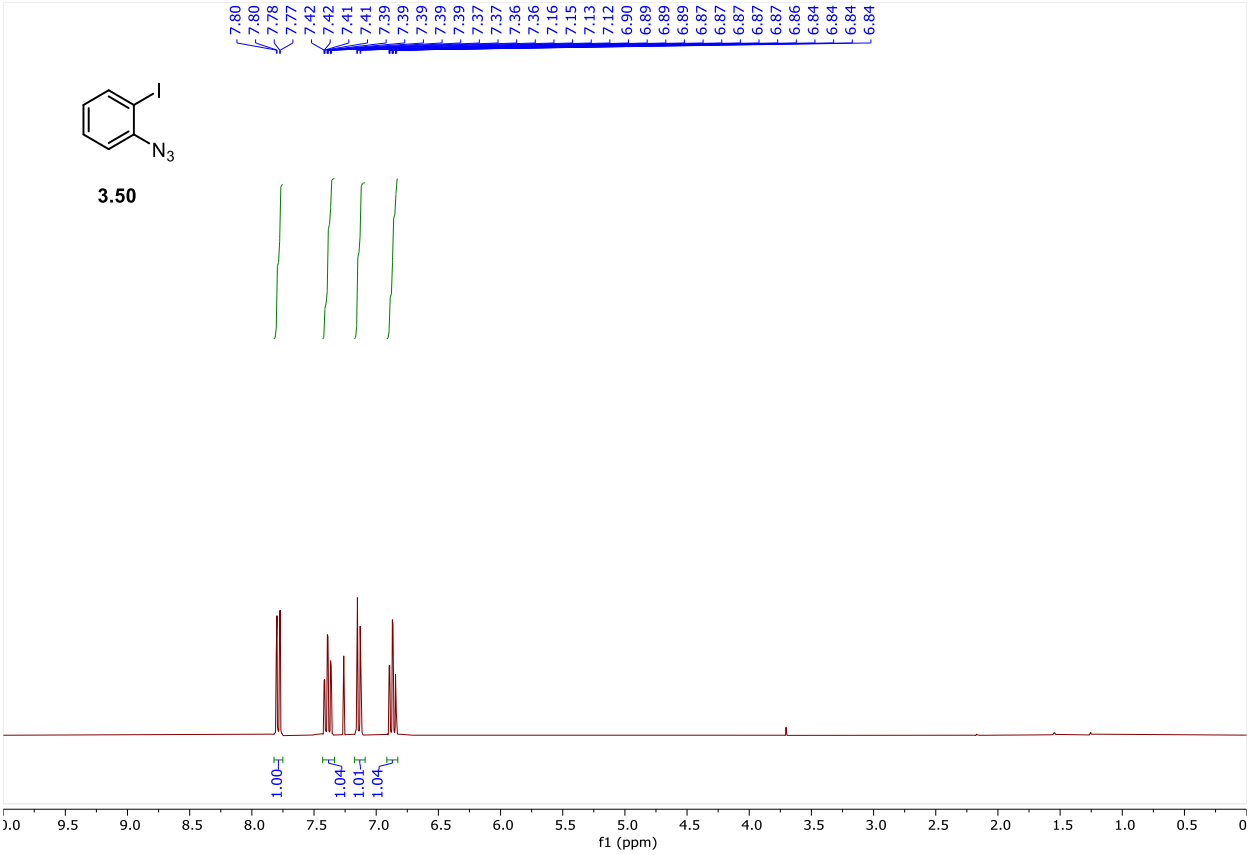


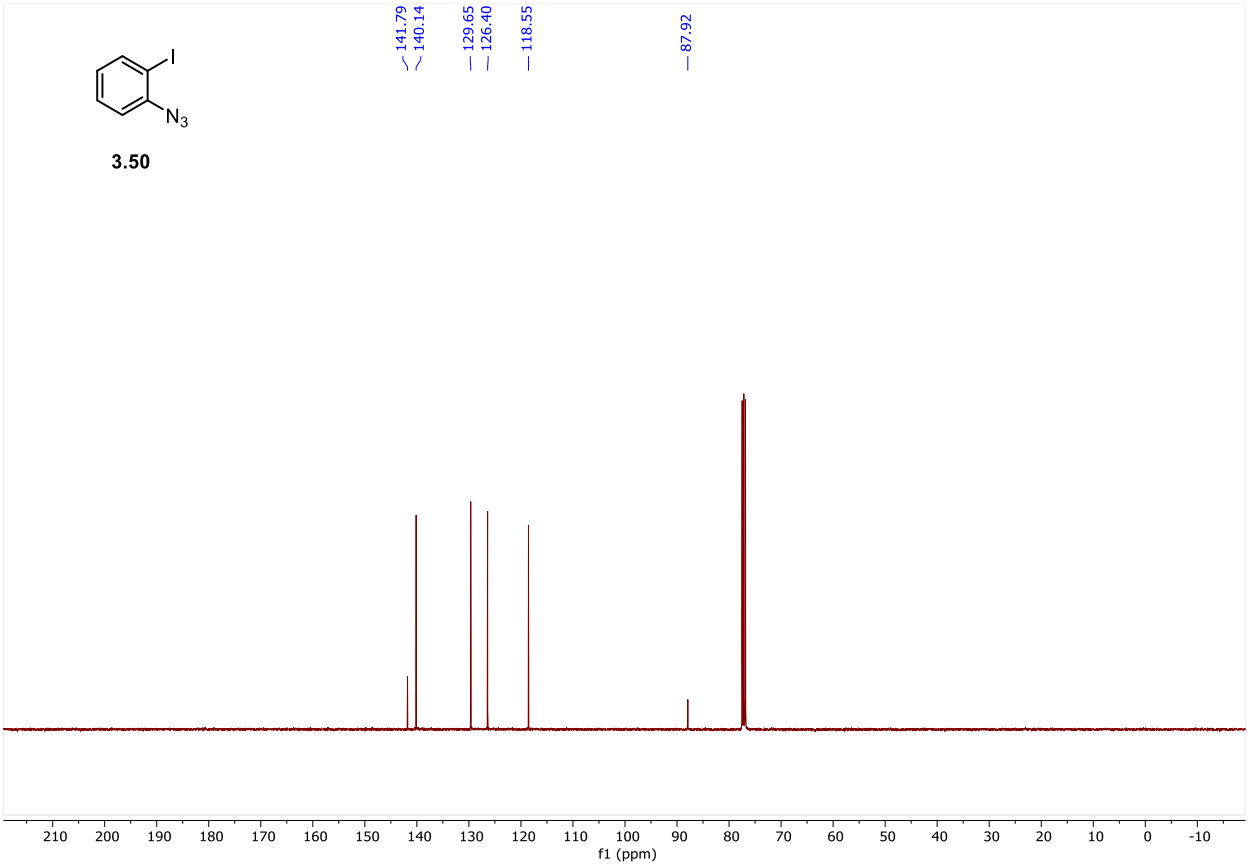

4.13 4.12 4.12 4.12 4.11 4.11 4.10 4.09 4.08 4.07 4.07 4.06 3.85 2.85 2.85 2.84 2.83 2.82 2.82 2.81 2.81 2.81 2.80 2.79 2.79 2.79 2.78 2.78 2.03 2.03 2.00 2.00 2.00 1.98 1.97 1.97 1.95 1.95 1.92 1.92
O
O
N
3.21
2.00 2.96 2.00 2.00
f1 (ppm)

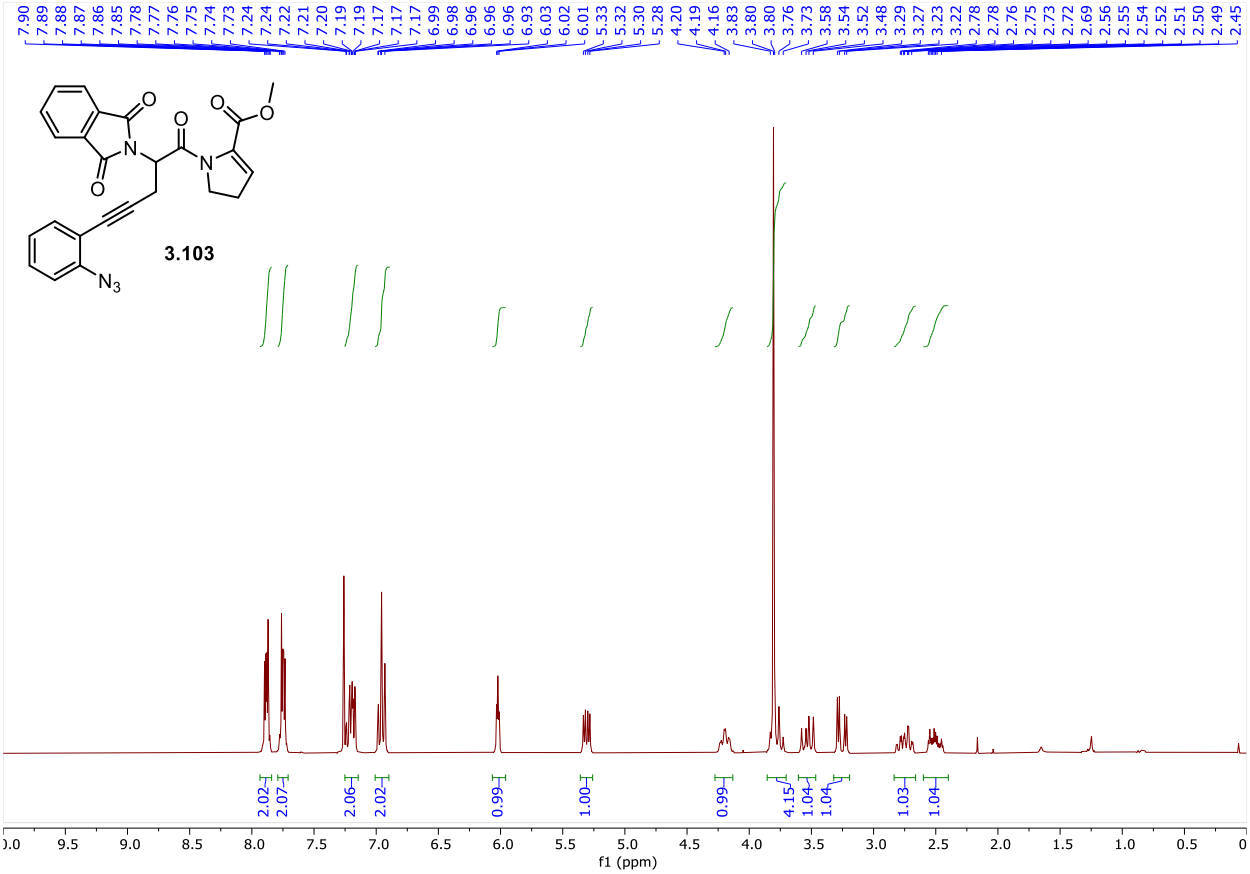

168.40 163.34 62.65 52.71 35.42 22.24
O
O
N
3.21
f1 (ppm)

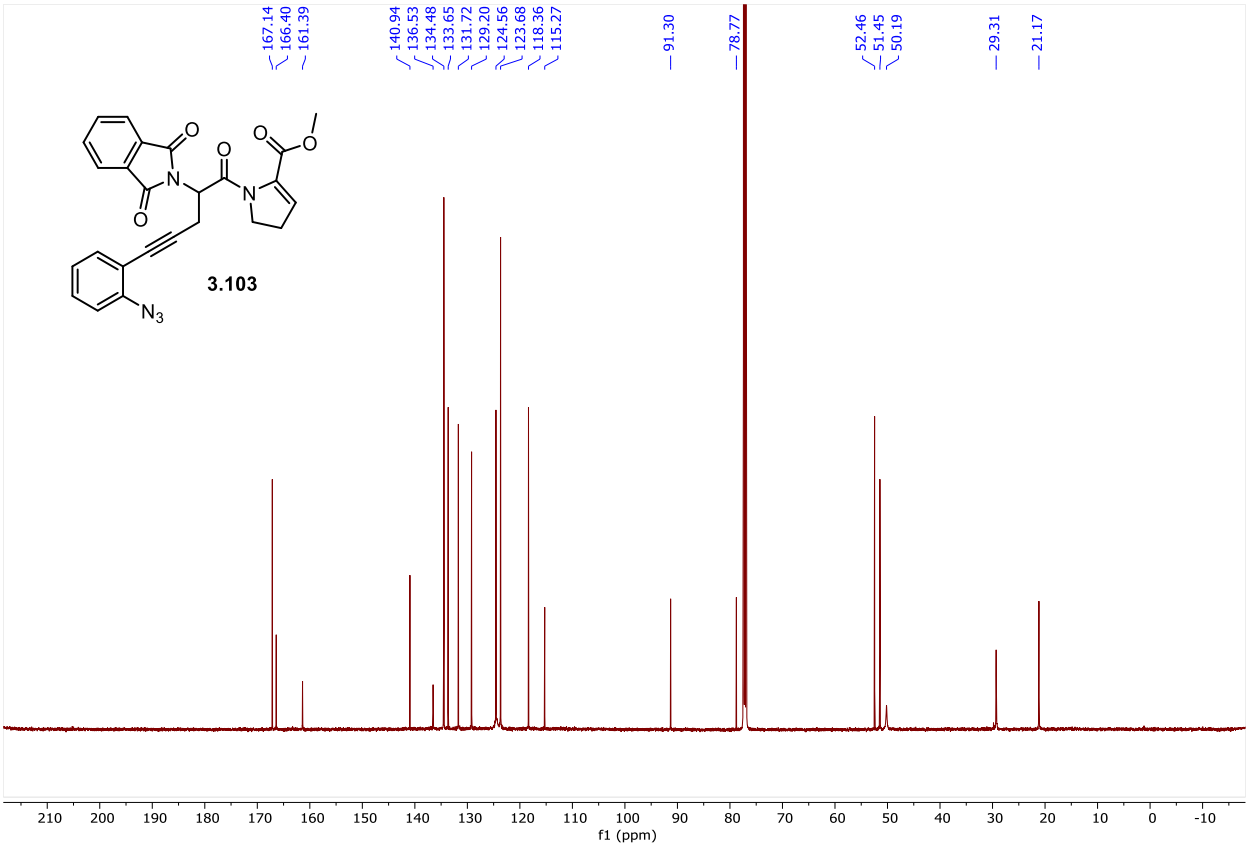

7.89 7.88 7.88 7.87 7.86 7.85 7.85 7.79 7.79 7.77 7.76 7.75 7.74 6.03 6.02 6.02 6.01 5.25 5.23 5.21 5.20 4.20 4.18 4.17 4.16 4.14 4.13 3.79 3.77 3.73 3.70 3.25 3.24 3.22 3.21 3.19 3.18 3.16 3.15 3.06 3.05 3.05 3.04 3.00 3.00 2.99 2.98 2.77 2.77 2.75 2.74 2.72 2.71 2.68 2.67 2.55 2.54 2.53 2.51 2.50 2.49 2.48 2.44 1.88 1.87 1.86
3.101
1.99 2.09 1.00 1.03 1.03 4.19 1.08 1.09 1.09 1.08 0.88
f1 (ppm)

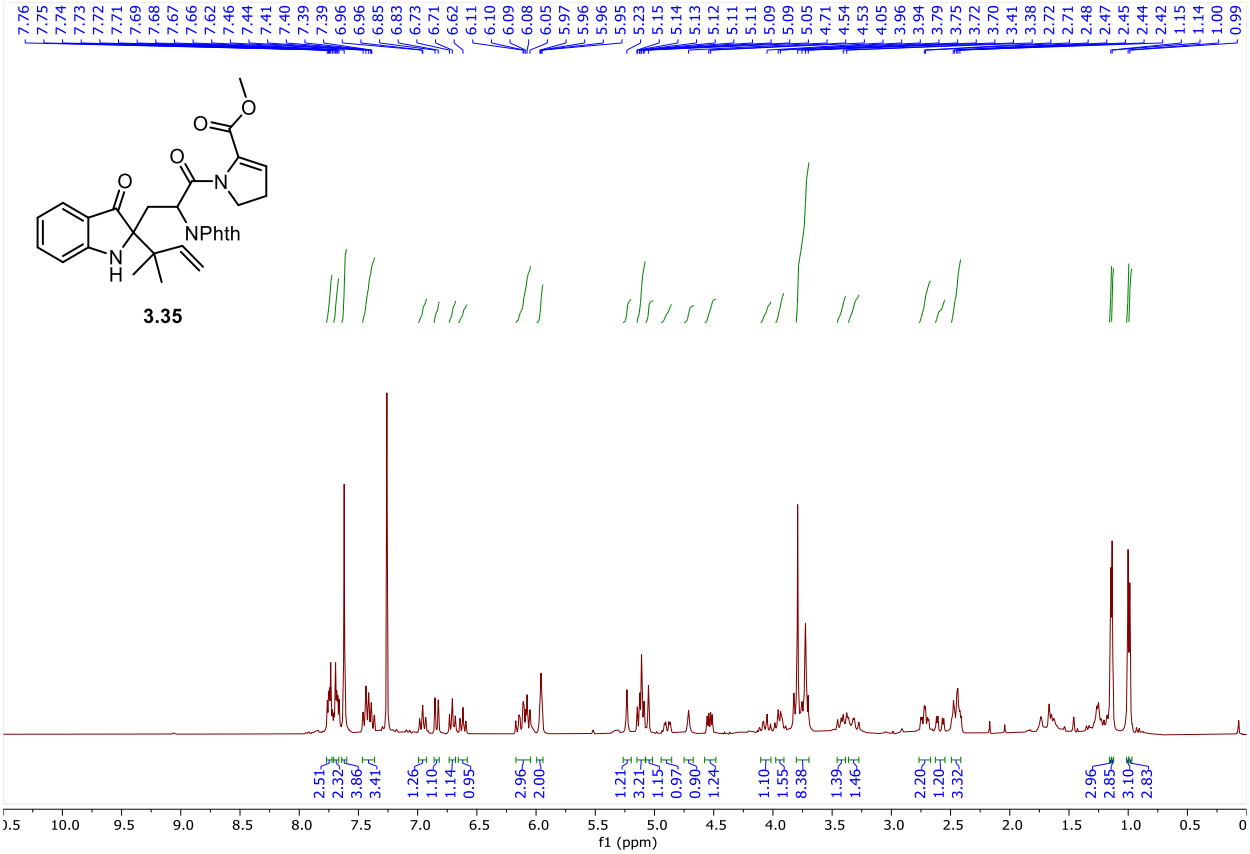

167.11 166.25 161.36 136.49 134.55 131.53 123.87 79.73 71.06 52.47 51.40 50.22 29.28 20.04
3.101
f1 (ppm)

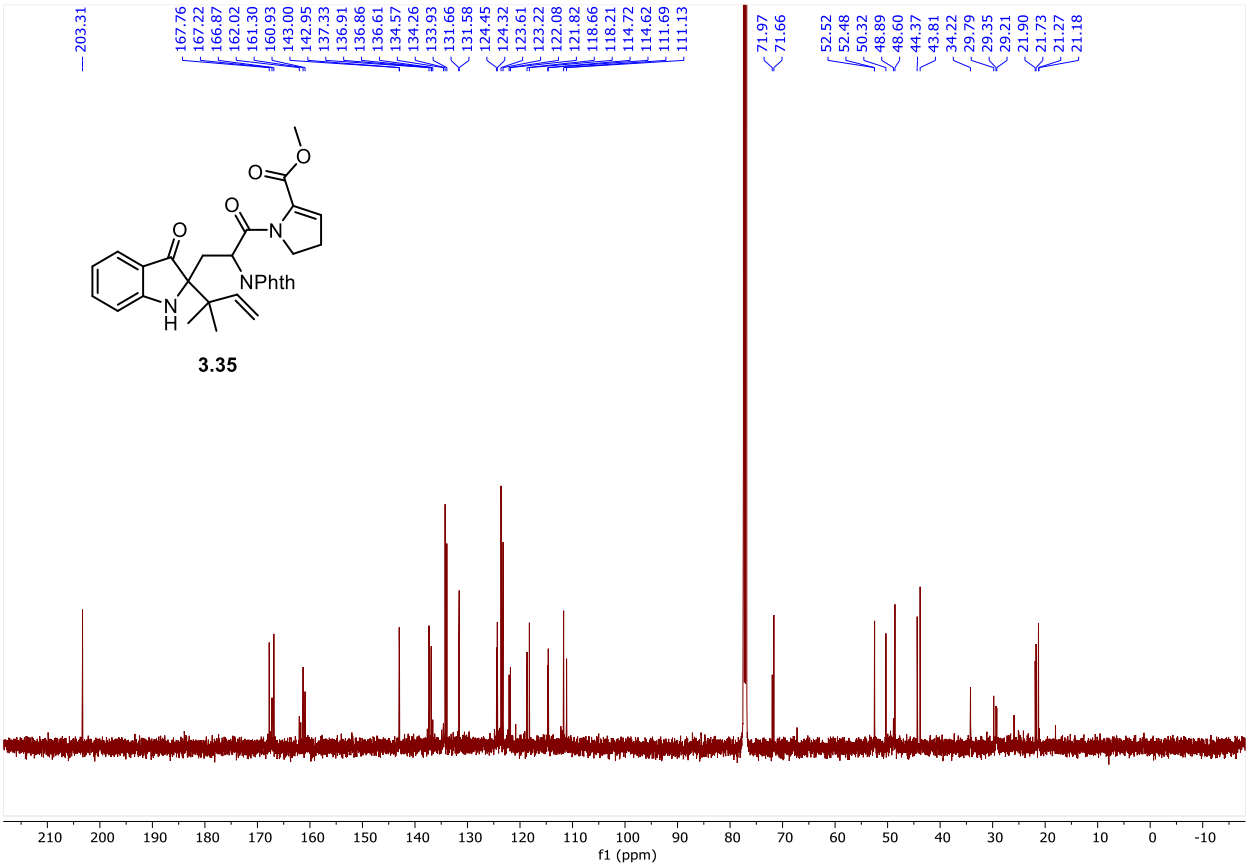

7.80
7.80
7.78
7.77
7.42
7.42
7.41
7.41
7.39
7.39
7.39
7.39
7.39
7.37
7.37
7.36
7.36
7.16
7.15
7.13
7.12
6.90
6.89
6.89
6.89
6.87
6.87
6.87
6.87
6.87
6.86
6.84
6.84
6.84
6.84
I
N3
3.50
1.00
1.04
1.01
1.04
f1 (ppm)

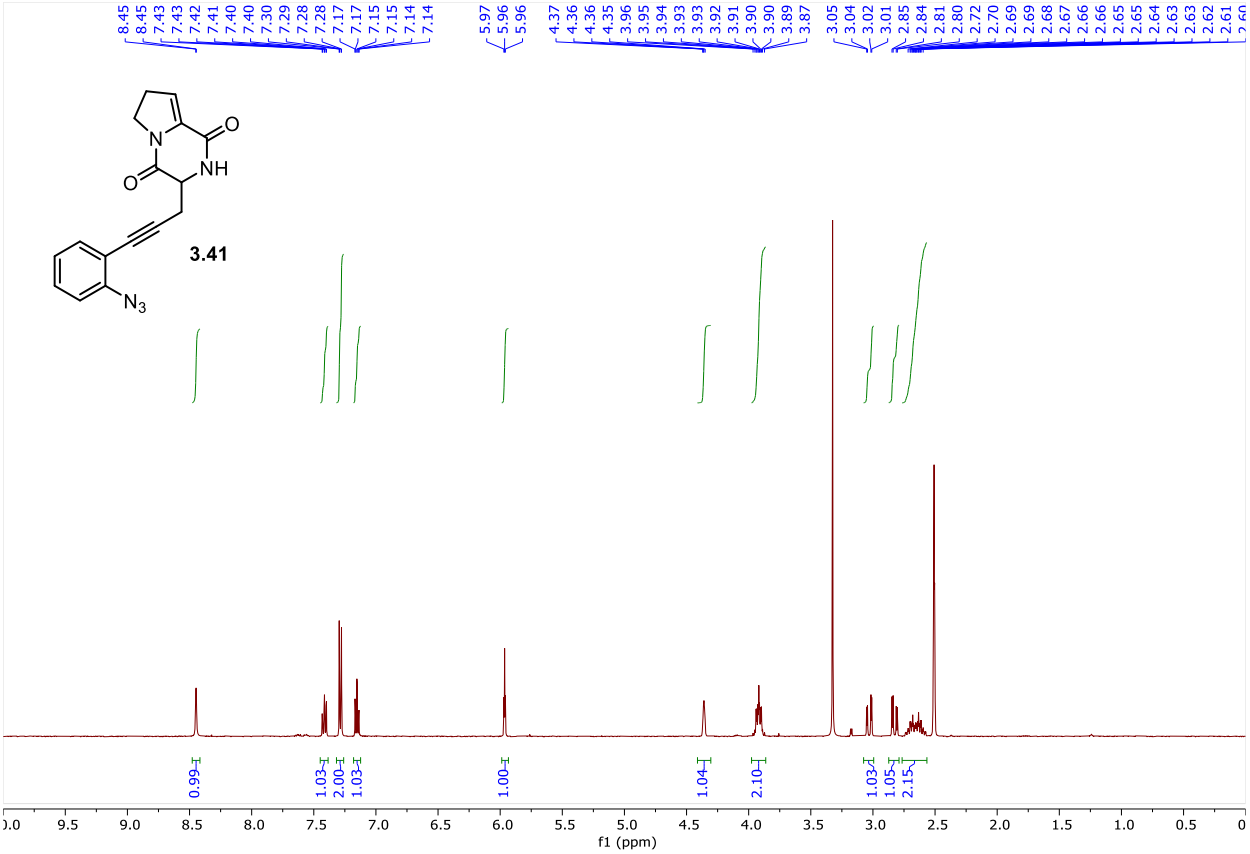

141.79
140.14
129.65
126.40
118.55
87.92
I
N3
3.50
f1 (ppm)

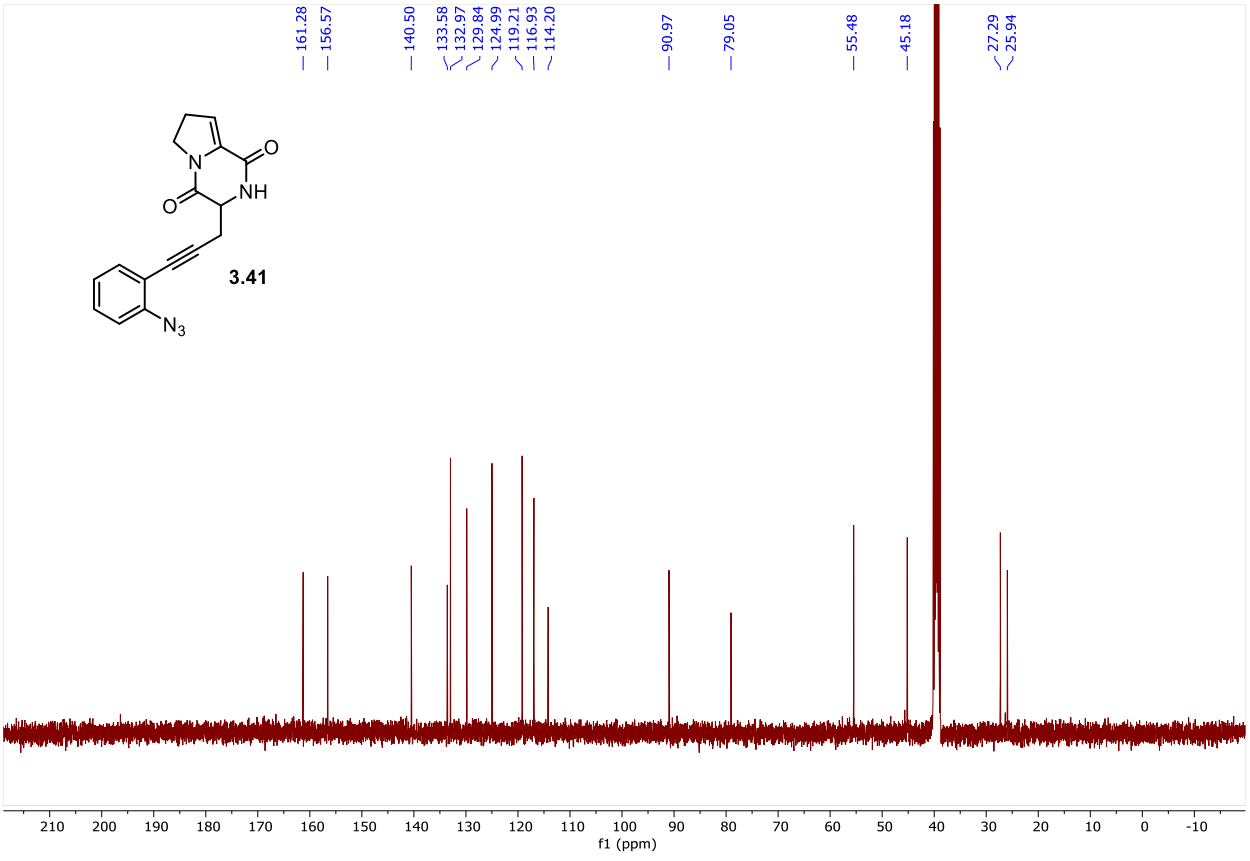

7.90 7.89 7.88 7.87 7.86 7.85 7.78 7.77 7.76 7.75 7.74 7.73 7.24 7.24 7.22 7.21 7.20 7.19 7.19 7.17 7.17 7.17 6.99 6.98 6.96 6.96 6.96 6.93 6.03 6.02 6.01 5.33 5.32 5.30 5.28 4.20 4.19 4.16 3.83 3.80 3.80 3.76 3.73 3.58 3.54 3.52 3.48 3.29 3.27 3.23 3.22 2.78 2.78 2.76 2.75 2.73 2.72 2.69 2.56 2.55 2.54 2.52 2.51 2.50 2.49 2.45
3.103
2.02 2.07 2.06 2.02 0.99 1.00 0.99 4.15 1.04 1.04 1.03 1.04
f1 (ppm)

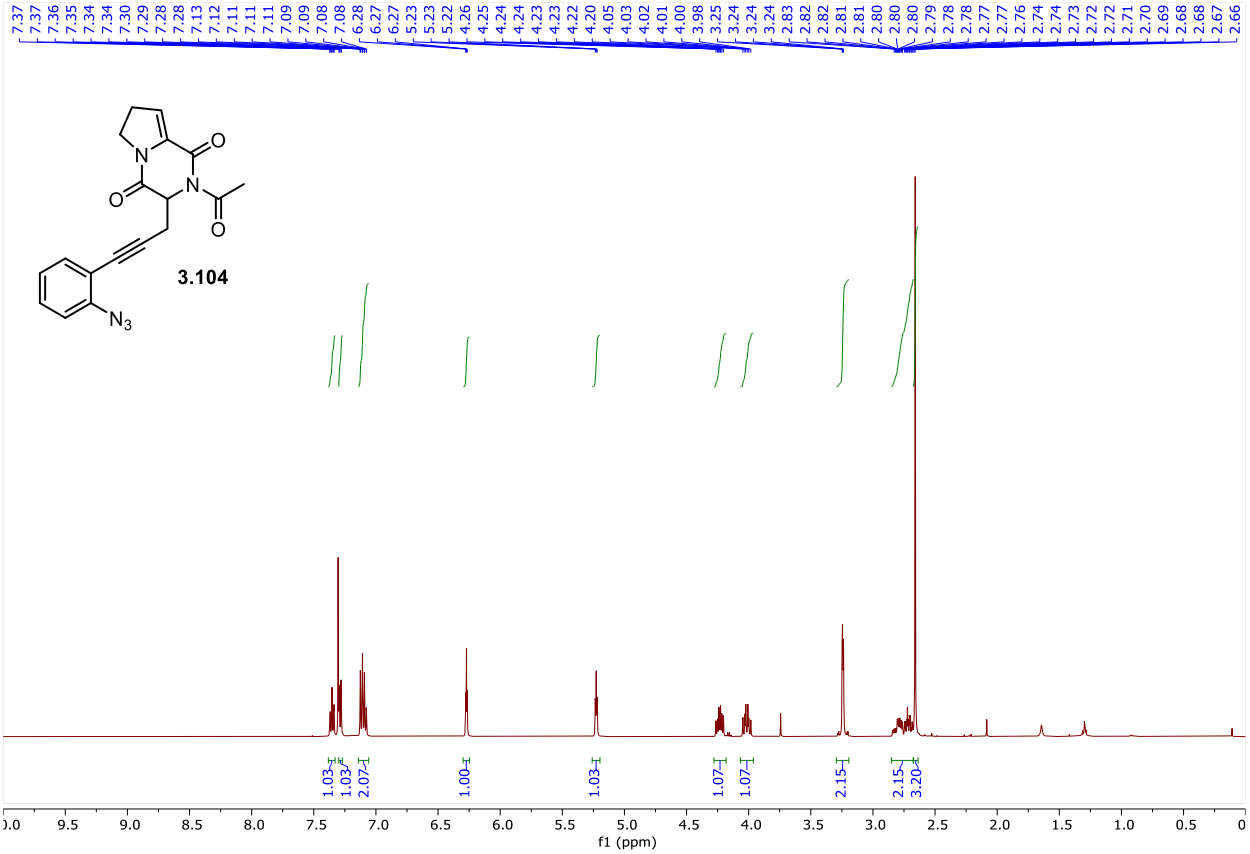

167.14 166.40 161.39 140.94 136.53 134.48 133.65 131.72 129.20 124.56 123.68 118.36 115.27 91.30 78.77 52.46 51.45 50.19 29.31 21.17
3.103
f1 (ppm)

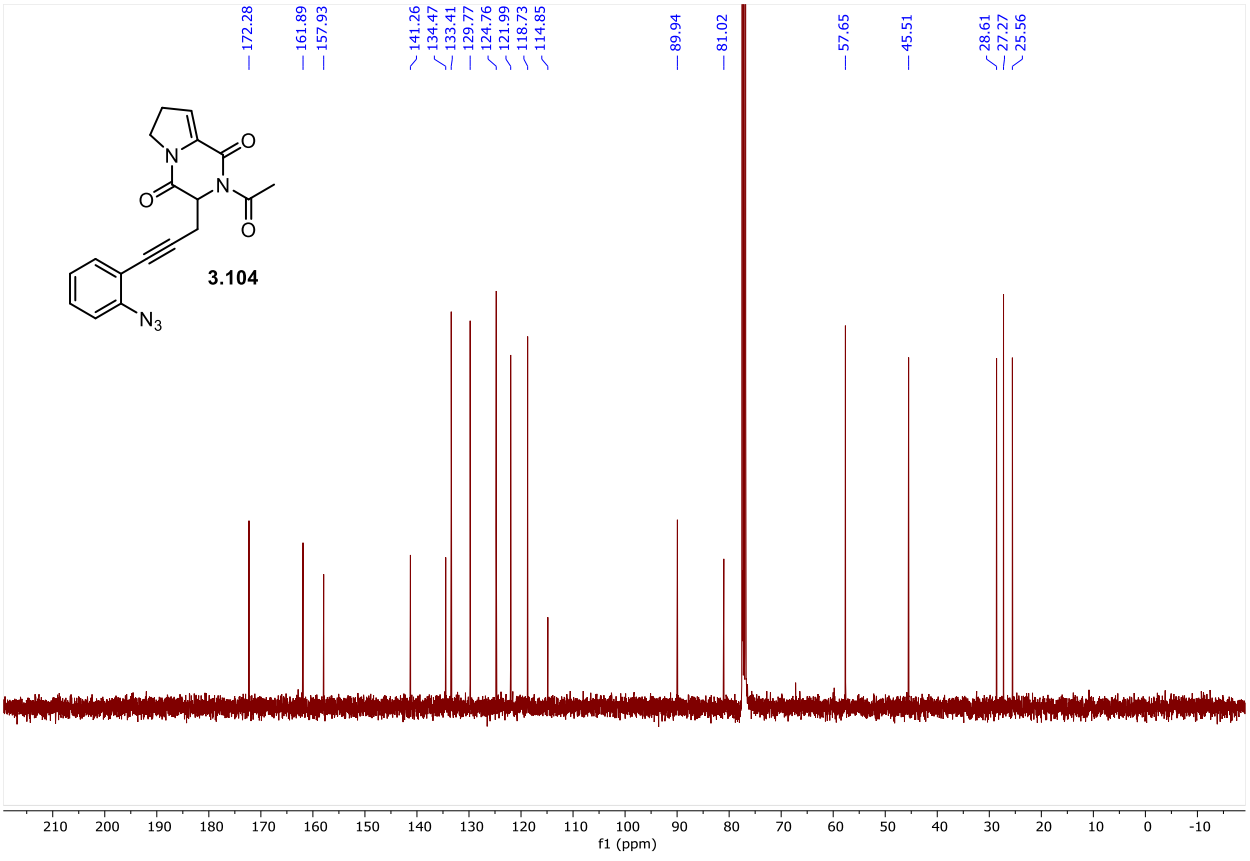

NPhth
3.35
f1 (ppm)

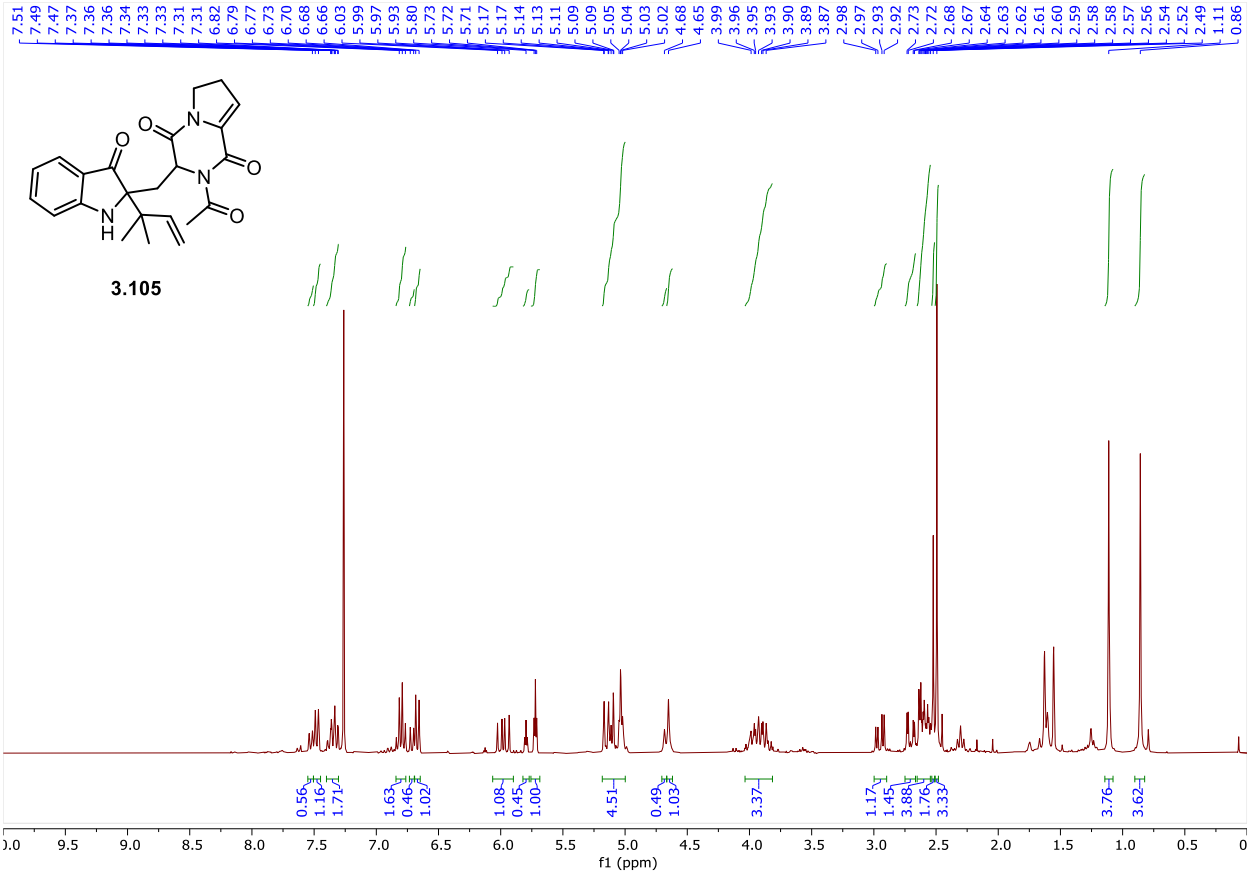

NPhth
3.35
f1 (ppm)

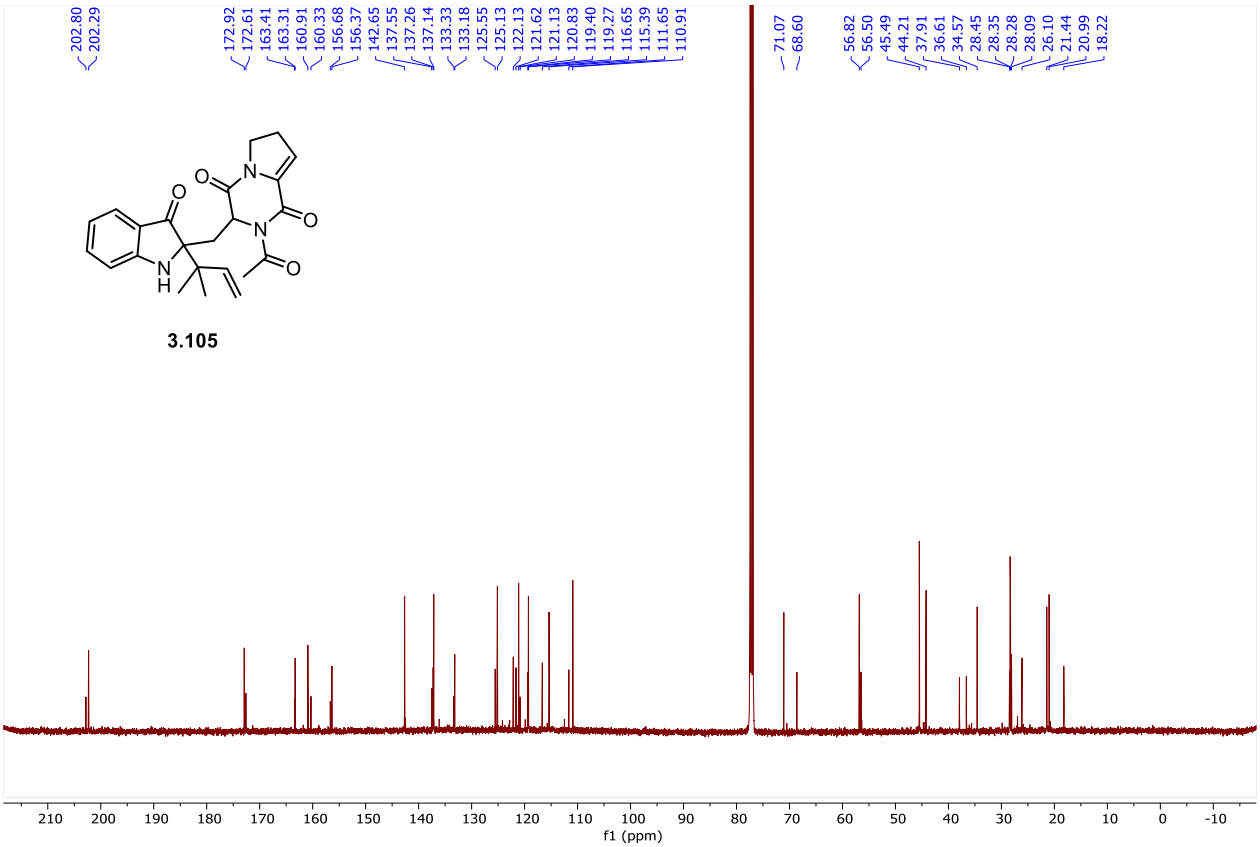

8.45
8.45
7.43
7.43
7.42
7.41
7.40
7.40
7.30
7.29
7.28
7.28
7.17
7.17
7.15
7.15
7.14
7.14
5.97
5.96
5.96
4.37
4.36
4.36
4.35
3.96
3.95
3.94
3.93
3.93
3.92
3.91
3.90
3.90
3.89
3.87
3.05
3.04
3.02
3.01
2.85
2.84
2.81
2.80
2.72
2.70
2.69
2.69
2.68
2.67
2.66
2.65
2.65
2.64
2.63
2.63
2.62
2.61
O
NH
O
N
3.41
N3
0.99
1.03
2.00
1.03
1.00
1.04
2.10
1.03
1.05
2.15
f1 (ppm)

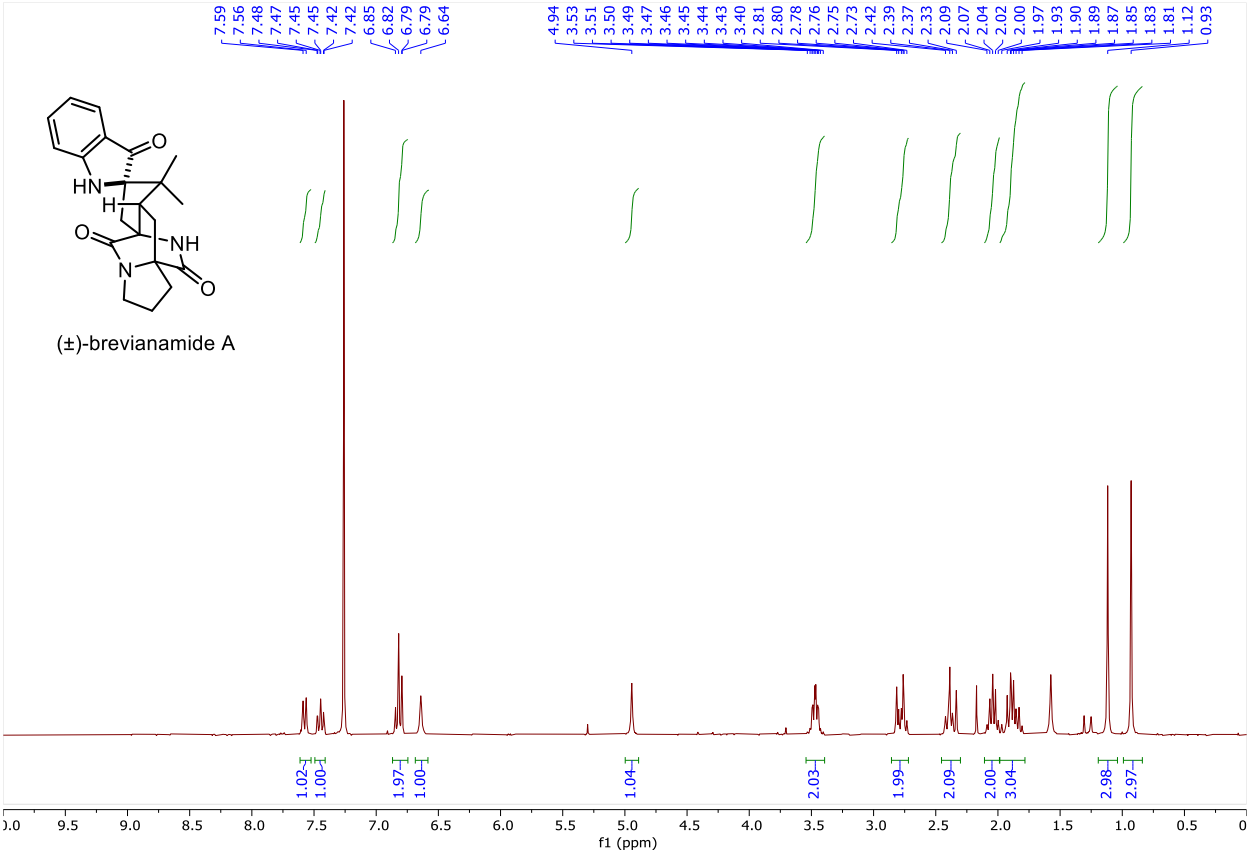

161.28
156.57
140.50
133.58
132.97
129.84
124.99
119.21
116.93
114.20
90.97
79.05
55.48
45.18
27.29
25.94
O
NH
O
N
3.41
N3
f1 (ppm)

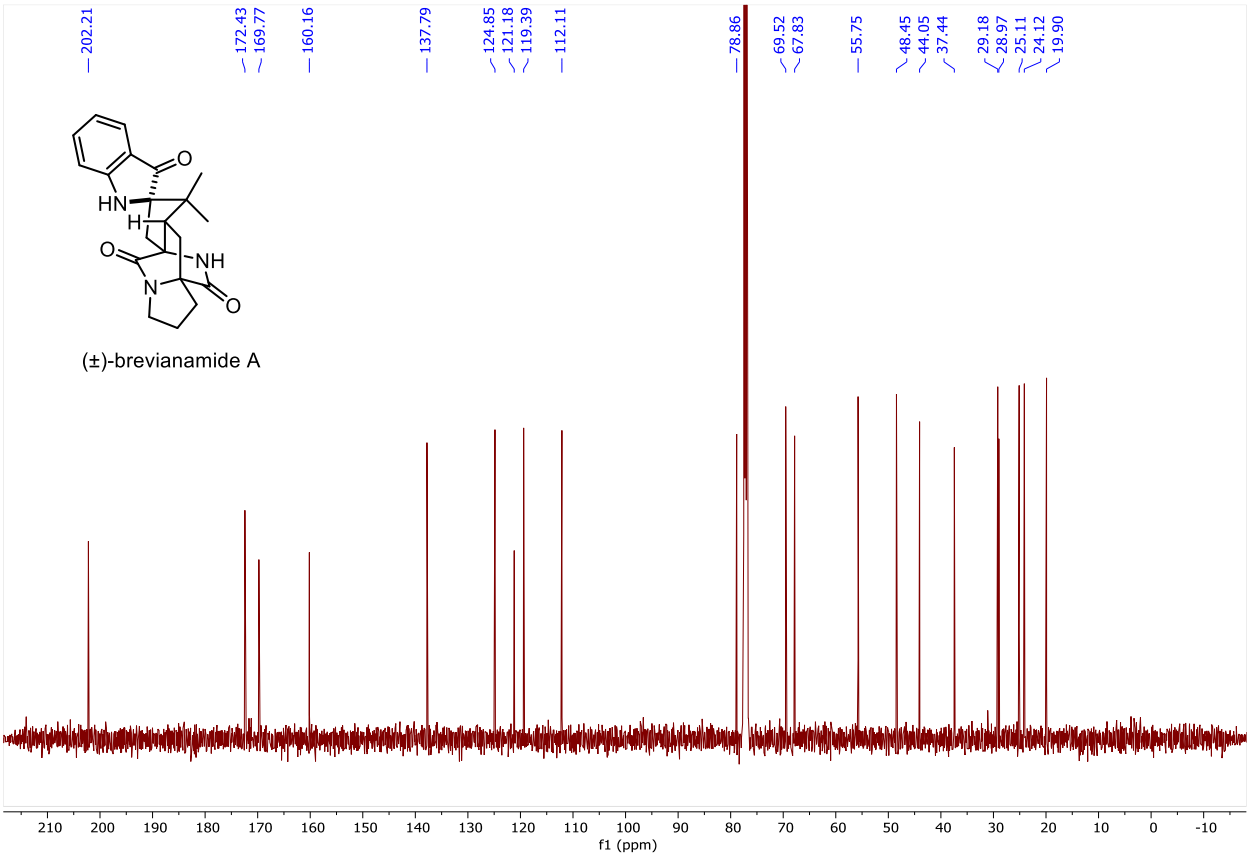

7.37 7.37 7.36 7.35 7.34 7.34 7.30 7.29 7.28 7.28 7.13 7.12 7.11 7.11 7.11 7.11 7.09 7.09 7.08 7.08 7.08 6.28 6.27 6.27 5.23 5.23 5.22 4.26 4.25 4.24 4.24 4.23 4.23 4.22 4.20 4.05 4.03 4.02 4.01 4.00 3.98 3.25 3.24 3.24 3.24 2.83 2.82 2.82 2.81 2.81 2.80 2.80 2.80 2.79 2.78 2.78 2.77 2.77 2.76 2.74 2.74 2.73 2.72 2.72 2.71 2.70 2.69 2.68 2.68 2.67 2.66
3.104
1.03 1.03 2.07 1.00 1.03 1.07 1.07 2.15 2.15 3.20
f1 (ppm)


172.28 161.89 157.93 141.26 134.47 133.41 129.77 124.76 121.99 118.73 114.85 89.94 81.02 57.65 45.51 28.61 27.27 25.56
3.104
f1 (ppm)


7.51 7.49 7.47 7.37 7.36 7.36 7.34 7.33 7.33 7.31 7.31 6.82 6.79 6.77 6.73 6.70 6.68 6.66 6.03 5.99 5.97 5.93 5.80 5.73 5.72 5.71 5.17 5.17 5.14 5.13 5.11 5.09 5.09 5.05 5.04 5.03 5.02 4.68 4.65 3.99 3.96 3.95 3.93 3.90 3.89 3.87 2.98 2.97 2.93 2.92 2.73 2.72 2.68 2.67 2.64 2.63 2.62 2.61 2.60 2.59 2.58 2.58 2.57 2.56 2.54 2.52 2.49 1.11 0.86
3.105
0.56 1.16 1.71 1.63 0.46 1.02 1.08 0.45 1.00 4.51 0.49 1.03 3.37 1.17 1.45 3.88 1.76 3.33 3.76 3.62
f1 (ppm)


202.80 202.29 172.92 172.61 163.41 163.31 160.91 160.33 156.68 156.37 142.65 137.55 137.26 137.14 133.33 133.18 125.55 125.13 122.13 121.62 121.13 120.83 119.40 119.27 116.65 115.39 111.65 110.91 71.07 68.60 56.82 56.50 45.49 44.21 37.91 36.61 34.57 28.45 28.35 28.28 28.09 26.10 21.44 20.99 18.22
3.105
f1 (ppm)

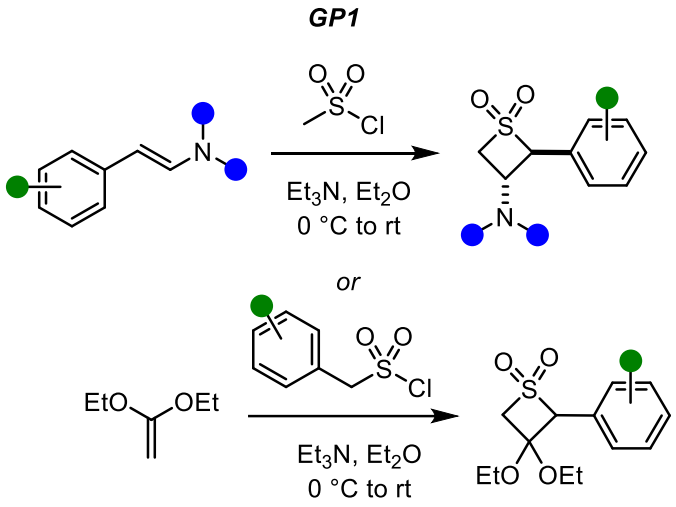

7.59 7.56 7.48 7.47 7.45 7.45 7.42 7.42 6.85 6.82 6.79 6.79 6.64
4.94 3.53 3.51 3.50 3.49 3.47 3.46 3.45 3.44 3.43 3.40 2.81 2.80 2.78 2.76 2.75 2.73 2.42 2.39 2.37 2.33 2.09 2.07 2.04 2.02 2.00 1.97 1.93 1.90 1.89 1.87 1.85 1.83 1.81 1.12 0.93
HN
H
O
NH
N
O
O
(±)-brevianamide A
1.02 1.00 1.97 1.00 1.04 2.03 1.99 2.09 2.00 3.04 2.98 2.97
f1 (ppm)


202.21
172.43 169.77 160.16 137.79 124.85 121.18 119.39 112.11
78.86
69.52 67.83 55.75 48.45 44.05 37.44 29.18 28.97 25.11 24.12 19.90
HN
H
O
NH
N
O
O
(±)-brevianamide A
f1 (ppm)

6.4 Supporting information for Chapter 4

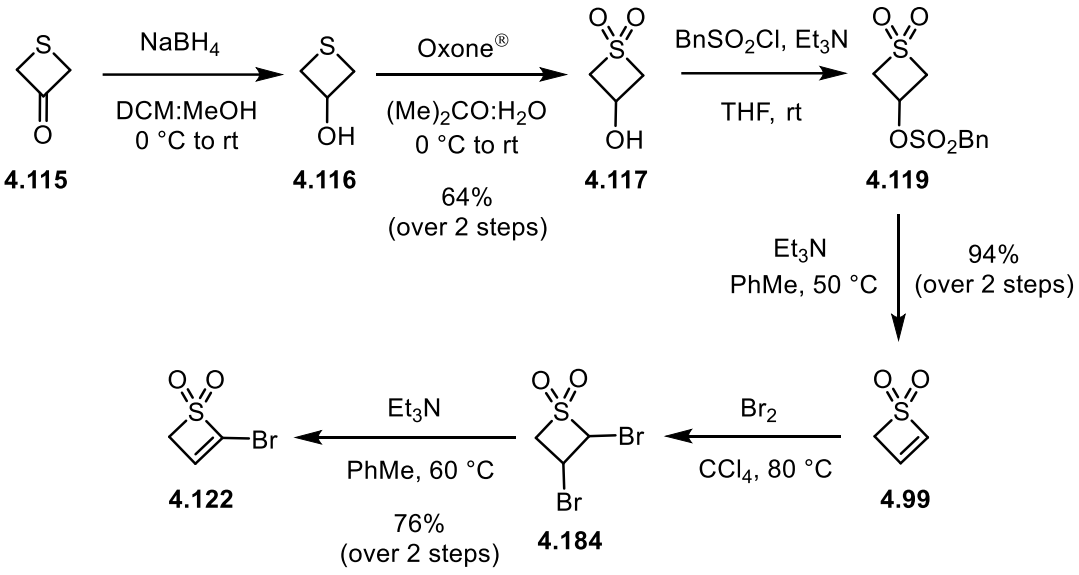
This section incorporates data from a currently on-going project and as such not all compound characterization has been included. As a preliminary support for identity of new compounds (in addition to pure ^{1}H- and ^{13}C-NMR spectra), low-resolution mass analysis (LRMS) has been provided with mention to any relevant fragmentation patterns. In anticipation for peer-reviewed publication, high-resolution mass analysis (HRMS) will be conducted in due course.

6.4.1 Experimental procedures

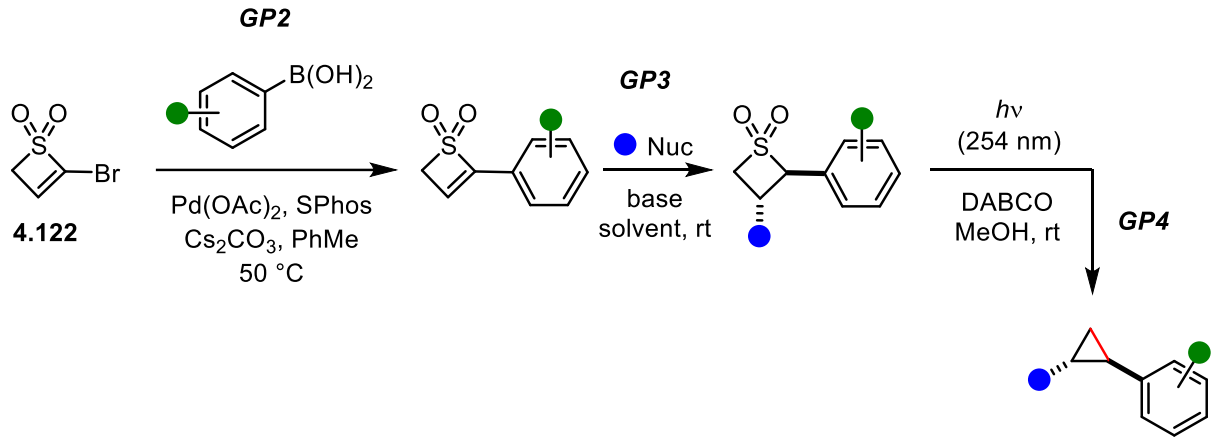


GP1:

Aryl enamines (1 equiv.) or ketene acetal (1 equiv.) and Et_3N (1.2 equiv.) were dissolved in anhydrous Et_2O (0.4 M) and cooled to 0 °C. MsCl (1.05 equiv.) or arylmethanesulfonyl chlorides (1.05 equiv.) were then added dropwise at 0 °C and the reaction was then brought to room temperature and aged overnight. At that point, TLC analysis indicated completion and the reaction was quenched with water and poured into a separatory funnel and extracted with EtOAc (3x). The organic layers were collected, dried over Na_2SO_4, filtered, and concentrated *in-vacuo*. The crude residue was then purified by flash-column chromatography.



Procedures for each step towards the synthesis of 2-bromothiete-1,1-dioxide **4.122** will be shown below.



GP2:

2-bromothiete-1,1-dioxide (1 equiv.) was added to a flame-dried flask followed by $Pd(OAc)_2$ (5 mol%), SPhos (10 mol%), arylboronic acid (1.5 equiv.), and Cs_2CO_3 (2 equiv.) in that order. Anhydrous and degassed PhMe (0.15 M) was then added, and the mixture brought to 50 °C where it was left to age overnight. Once TLC analysis indicated completion, the mixture was cooled to room temperature, diluted with EtOAc, and filtered over a short bed of silica gel (eluting with

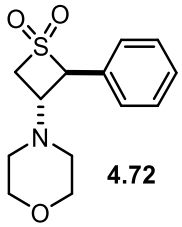
EtOAc) until the filtrate ran clear. The filtrate was then concentrated *in-vacuo* and purified by flash-column chromatography.

GP3:

2-arylated thiete-1,1-dioxides (1 equiv.) were dissolved in the indicated solvent (0.1 M) and then the corresponding base (if present) (1.1–1.5 equiv.) and nucleophiles (1.3–10 equiv.) were added at room temperature. The reaction was then left to age for 15 minutes to several hours. Once the reaction was deemed complete by TLC analysis, the reaction mixture was concentrated *in-vacuo* or poured into a separatory funnel for extraction. The crude material was then purified by flash-column chromatography.

GP4:

3-substituted 2-arylthietane-1,1-dioxides (1 equiv.) and DABCO (1 equiv.) were added to a screw-cap quartz vial and subsequently dissolved in MeOH (0.03 M). The mixture was then degassed using a strong stream of nitrogen gas that was bubbled through the solution (while stirring) for 2–3 minutes. Once the mixture had been sparged, the vial was sealed, and the vial placed in a Rayonet photoreactor and irradiated at 254 nm for 4–7 hours depending on the substrate. TLC analysis was used to check for consumption of the starting material in addition to TLC/MS analysis. Once complete, the contents of the vial were transferred to a flask and concentrated *in-vacuo*. Purification by flash-column chromatography afforded the cyclopropane products.



4.72

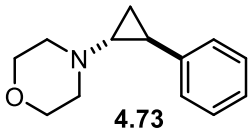
Prepared from (*E*)-*N*-(2-phenylethenyl)morpholine (504 mg, 2.66 mmol) and methanesulfonyl chloride (0.22 mL, 2.79 mmol) following GP1. Purification over silica (eluent: 55% EtOAc:hexanes). Thietane-1,1-dioxide **4.72** was obtained as a pale-yellow solid: 621 mg, 87% yield.

TLC: R_f 0.42 (70% EtOAc:hexanes), $KMnO_4$

^{1}H-NMR (300 MHz, $CDCl_3$): δ 7.44–7.39 (m, 5H), 5.29 (dt, *J* = 8.4, 0.9 Hz, 1H), 4.11 (ddd, *J* = 12.6, 8.4, 1.0 Hz, 1H), 3.99 (ddd, *J* = 12.7, 8.1, 0.7 Hz, 1H), 3.78–3.57 (m, 4H), 3.41 (q, *J* = 8.3 Hz, 1H), 2.44–2.25 (m, 4H).

^{13}C-NMR (101 MHz, $CDCl_3$): δ 130.3, 129.6, 129.2, 129.0, 84.8, 66.5, 64.8, 54.2, 52.0.

MS-APCI+: 117.1 ([M-C_4H_8NO-SO_2]$^+$, 85%), 126.1 (21%), 158.0 (12%), 176.0 (18%), 189.1 (13%), 202.0 ([M+H-SO_2]$^+$, 97%), 203.0 (50%), 204.1 (68%), 206.0 (68%), 268.0 ([M+H]$^+$, 74%), 269.0 (15%).



4.73

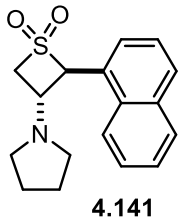
Prepared from thietane-1,1-dioxide **4.72** (25 mg, 0.094 mmol) following GP4. Reaction time: 4 hr. Purification over silica (eluent: 1% Et_3N:45% EtOAc:hexanes). Cyclopropane **4.73** was obtained as a pale oil: 8.5 mg, 49% yield.

TLC: R_f 0.48 (60% EtOAc:hexanes), ninhydrin

^{1}H-NMR (300 MHz, $CDCl_3$): δ 7.26 (m, 2H), 7.17 (m, 1H), 7.06 (m, 2H), 3.70 (dd, *J* = 5.6, 3.9 Hz, 4H), 2.66 (t, *J* = 4.7 Hz, 4H), 2.01 (td, *J* = 6.0, 2.9 Hz, 1H), 1.91 (ddd, *J* = 7.3, 4.3, 3.2 Hz, 1H), 1.13 (dt, *J* = 9.5, 4.7 Hz, 1H), 0.97 (dt, *J* = 6.9, 5.5 Hz, 1H).

^{13}C-NMR (76 MHz, $CDCl_3$): δ 141.9, 128.3, 126.1, 125.7, 66.9, 53.4, 49.0, 24.2, 16.1.

HRMS (ESI): Calculated for $C_{13}H_{17}NNaO$ [M+Na]$^+$: 204.1388; found: *m/z* 204.1400.



4.141

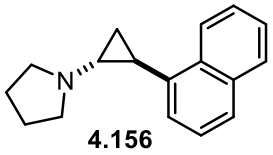
Prepared from (*E*)-*N*-(2-naphthalen-1-ylethenyl)pyrrolidine (191 mg, 0.854 mmol) and methanesulfonyl chloride (73 μL, 0.939 mmol) following GP1. Purification over silica (eluent: 60% EtOAc:hexanes). Thietane-1,1-dioxide **4.141** was obtained as a pale-yellow solid: 23 mg, 10% yield.

TLC: R_f 0.26 (60% EtOAc:hexanes), $KMnO_4$

^{1}H-NMR (500 MHz, $CDCl_3$): δ 8.20 (d, *J* = 8.5 Hz, 1H), 7.93–7.86 (m, 2H), 7.73 (d, *J* = 7.2 Hz, 1H), 7.63 (ddd, *J* = 8.4, 6.9, 1.4 Hz, 1H), 7.60–7.50 (m, 2H), 6.21 (d, *J* = 8.3 Hz, 1H), 4.26–4.12 (m, 2H), 3.85 (q, *J* = 8.2 Hz, 1H), 2.58–2.48 (m, 2H), 2.48–2.41 (m, 2H), 1.94–1.59 (m, 4H).

^{13}C-NMR (126 MHz, $CDCl_3$): δ 134.0, 131.8, 129.9, 129.1, 127.6, 126.5, 126.1, 126.1, 125.3, 122.9, 81.6, 65.39, 52.7, 51.3, 23.7.

HRMS (ESI): Calculated for $C_{17}H_{19}NNaO_2S$ $[M+Na]^+$: 324.1037; found: *m/z* 324.1043.



4.156

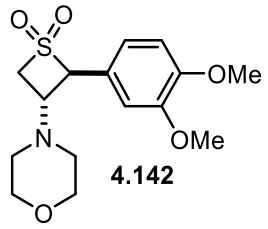
Prepared from thietane-1,1-dioxide **4.141** (20.3 mg, 0.0683 mmol) following GP4 and without DABCO. Reaction time: 2 hr. Purification over silica (eluent: 1% Et_3N:40% EtOAc:hexanes). Cyclopropane **4.156** was obtained as a pale oil: 6 mg, 40% yield.

TLC: R_f 0.14 (50% EtOAc:hexanes), ninhydrin

^{1}H-NMR (300 MHz, $CDCl_3$): δ 8.46–8.36 (m, 1H), 7.94–7.78 (m, 1H), 7.75–7.66 (m, 1H), 7.61–7.43 (m, 2H), 7.38 (dd, *J* = 8.2, 7.1 Hz, 1H), 7.21 (dt, *J* = 7.1, 1.2 Hz, 1H), 2.94–2.76 (m, 4H), 2.61–2.49 (m, 1H), 2.04 (dt, *J* = 7.3, 3.8 Hz, 1H), 1.96–1.77 (m, 4H), 1.35–1.23 (m, 1H), 1.05 (ddd, *J* = 7.1, 6.0, 4.9 Hz, 1H).

^{13}C-NMR (151 MHz, $CDCl_3$): δ 137.7, 133.7, 133.2, 128.7, 126.7, 125.9, 125.8, 125.5, 124.3, 123.5, 54.2, 44.8, 23.9, 21.9, 15.0.

HRMS (ESI): Calculated for $C_{17}H_{20}N$ $[M+H]^+$: 238.1564; found: *m/z* 238.1596.



4.142

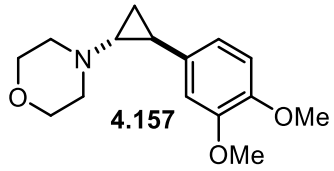
Prepared from (*E*)-*N*-(2-(3,4-dimethoxyphenyl)ethenyl)morpholine (203 mg, 0.816 mmol) and methanesulfonyl chloride (69 μL, 0.897 mmol) following GP1. Purification over silica (eluent: 100% EtOAc). Thietane-1,1-dioxide **4.142** was obtained as an off-white solid: 105 mg, 40% yield.

TLC: R_f 0.26 (100% EtOAc:hexanes), $KMnO_4$

^{1}H-NMR (300 MHz, $CDCl_3$): δ 6.98 (dd, *J* = 8.4, 2.0 Hz, 1H), 6.94–6.85 (m, 2H), 5.22 (d, *J* = 8.5 Hz, 1H), 4.07 (ddd, *J* = 12.6, 8.4, 1.0 Hz, 1H), 4.00–3.93 (m, 1H), 3.91 (s, 3H), 3.89 (s, 3H), 3.75–3.58 (m, 4H), 3.35 (q, *J* = 8.3 Hz, 1H), 2.35 (tt, *J* = 11.7, 6.6 Hz, 4H).

^{13}C-NMR (126 MHz, $CDCl_3$): δ 150.2, 149.4, 122.7, 121.7, 111.8, 111.5, 84.8, 66.5, 64.5, 56.2, 56.1, 54.6, 52.1.

MS-APCI+: 59.2 (14%), 177.0 ($[M-C_4H_8NO-SO_2]^+$, 32%), 264.0 ($[M+H-SO_2]^+$, 99%), 265.1 (19%), 328.0 ($[M+H]^+$, 41%).



4.157

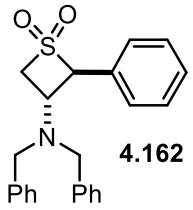
Prepared from thietane-1,1-dioxide **4.142** (32 mg, 0.097 mmol) following GP4 and without DABCO. Reaction time: 5 hr. Purification over silica (eluent: 85% EtOAc:hexanes). Cyclopropane **4.157** was obtained as a pale-yellow oil: 9.5 mg, 39% yield.

TLC: R_f 0.23 (100% EtOAc:hexanes), ninhydrin

^{1}H-NMR (300 MHz, $CDCl_3$): δ 6.81–6.72 (m, 1H), 6.65–6.55 (m, 2H), 3.87 (s, 3H), 3.84 (s, 3H), 3.74–3.60 (m, 4H), 2.66 (dd, *J* = 5.7, 3.8 Hz, 4H), 1.95 (ddd, *J* = 9.3, 5.8, 3.2 Hz, 1H), 1.85 (ddd, *J* = 7.3, 4.3, 3.2 Hz, 1H), 1.07 (ddd, *J* = 9.4, 5.1, 4.3 Hz, 1H), 0.90 (ddd, *J* = 6.9, 5.8, 5.1 Hz, 1H).

^{13}C-NMR (126 MHz, $CDCl_3$): δ 149.0, 147.4, 134.6, 118.1, 111.4, 110.1, 67.1, 56.1, 56.0, 53.6, 48.8, 24.0, 15.9.

MS-APCI+: 177.0 ($[M-C_4H_8NO]^+$, 37%), 264.0 ($[M+H]^+$, 97%), 265.0 (16%).



4.162

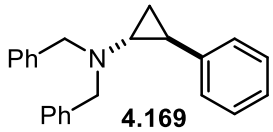
Prepared from (*E*)-*N*,*N*-dibenzyl-2-phenylethen-1-amine (326 mg, 1.08 mmol) and methanesulfonyl chloride (89 μL, 1.14 mmol) following GP1. Purification over silica (eluent: 18% EtOAc:hexanes). Thietane-1,1-dioxide **4.162** was obtained as a pale viscous oil: 157 mg, 40% yield.

TLC: R_f 0.25 (18% EtOAc:hexanes), $KMnO_4$

^{1}H-NMR (300 MHz, $CDCl_3$): δ 7.41–7.18 (m, 15H), 5.48–5.36 (m, 1H), 4.07–3.87 (m, 3H), 3.69 (d, *J* = 14.0 Hz, 2H), 3.55 (d, *J* = 14.0 Hz, 2H).

^{13}C-NMR (126 MHz, $CDCl_3$): δ 137.7, 130.4, 129.4, 129.1 (2C), 128.8, 128.7, 127.8, 83.9, 64.2, 56.1, 51.6.

HRMS (ESI): Calculated for $C_{23}H_{23}NNaO_2S$ $[M+Na]^+$: 400.1347; found: *m/z* 400.1347.



4.169

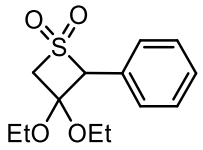
Prepared from thietane-1,1-dioxide **4.162** (38 mg, 0.101 mmol) following GP4 and without DABCO. Reaction time: 2 hr. Purification over silica (eluent: 10% EtOAc:hexanes). Cyclopropane **4.169** was obtained as a colourless solid: 3.3 mg, 10% yield.

TLC: R_f 0.79 (18% EtOAc:hexanes), ninhydrin

^{1}H-NMR (300 MHz, $CDCl_3$): δ 7.35–7.23 (m, 10H), 7.22–7.14 (m, 2H), 7.15–7.07 (m, 1H), 6.83–6.73 (m, 2H), 3.77 (d, *J* = 13.5 Hz, 2H), 3.66 (d, *J* = 13.5 Hz, 2H), 2.03 (ddd, *J* = 7.2, 4.4, 3.2 Hz, 1H), 1.81 (ddd, *J* = 9.2, 6.0, 3.2 Hz, 1H), 1.08–0.99 (m, 1H), 0.95 (q, *J* = 6.0 Hz, 1H).

^{13}C-NMR (126 MHz, $CDCl_3$): δ 142.2, 138.8, 129.5, 128.2, 128.1, 127.0, 125.9, 125.5, 58.6, 47.7, 26.6, 17.7.

MS-APCI+: 59.2 (22%), 117.0 ($[M-C_{14}H_{14}N]^+$, 10%), 124.0 (10%), 314.1 ($[M+H]^+$, 96%), 315.1 (25%).



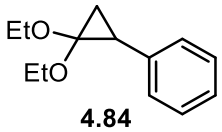
4.83

Prepared from diethyl ketene acetal (886 mg, 7.63 mmol) and phenylmethanesulfonyl chloride (1.45 g, 7.63 mmol) following GP1. Purification by trituration with cold Et_2O. Thietane-1,1-dioxide **4.83** was obtained as a white solid: 600 mg, 30% yield.

TLC: R_f 0.21 (20% EtOAc:hexanes), *p*-anisaldehyde

^{1}H-NMR (300 MHz, $CDCl_3$): δ 7.61–7.49 (m, 2H), 7.44–7.34 (m, 3H), 5.45 (d, *J* = 1.5 Hz, 1H), 4.33–4.18 (m, 2H), 3.54–3.39 (m, 3H), 3.30 (dq, *J* = 9.4, 7.0 Hz, 1H), 1.22 (t, *J* = 7.1 Hz, 3H), 1.14 (t, *J* = 7.0 Hz, 3H).

^{13}C-NMR (76 MHz, $CDCl_3$): δ 131.2, 130.7, 129.3, 129.0, 128.4, 128.0, 94.0, 88.8, 71.1, 59.8, 58.9, 15.0, 14.6.



4.84

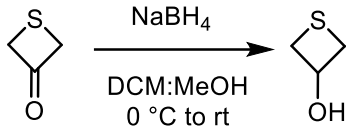
Prepared from thietane-1,1-dioxide **4.83** (31 mg, 0.112 mmol) following GP4. Reaction time: 5 hr. Purification over silica (eluent: 5% Et_2O:hexanes). Cyclopropane **4.84** was obtained as a pale-yellow oil: 9 mg, 42% yield.

TLC: R_f 0.6 (5% Et_2O:hexanes), *p*-anisaldehyde

^{1}H-NMR (300 MHz, $CDCl_3$): δ 7.31–7.15 (m, 5H), 3.84–3.69 (m, 2H), 3.63 (dq, *J* = 9.4, 7.4 Hz, 1H), 3.27 (dq, *J* = 9.5, 7.1 Hz, 1H), 2.40 (dd, *J* = 10.3, 7.1 Hz, 1H), 1.46 (dd, *J* = 10.3, 6.0 Hz, 1H), 1.33 (dd, *J* = 7.1, 6.0 Hz, 1H), 1.26 (t, *J* = 7.1 Hz, 3H), 1.02 (t, *J* = 7.1 Hz, 3H).

^{13}C-NMR (76 MHz, $CDCl_3$): δ 137.8, 128.1, 127.6, 125.9, 92.4, 62.3, 61.8, 30.8, 19.8, 15.5, 15.2.

MS-APCI+: 133.0 (97%), 159.0 (13%), 161.0 ($[M-C_2H_5O]^+$, 63%), 189.1 ($[M+H-H_2O]^+$, 15%), 205.0 (37%), 206.0 (20%), 275.0 (15%), 321.1 (25%), 367.1 (10%), 381.2 (10%).

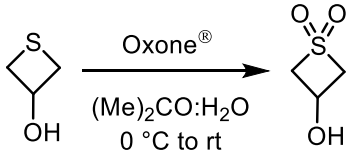


4.115 **4.116**

Thietan-3-one (**4.115**, 1 equiv.) was dissolved in a 4:1 mixture of DCM:MeOH (1 M) and cooled to 0 °C. $NaBH_4$ (3 equiv.) was then added in portions and the mixture was aged at room temperature for two hours. Once complete as indicated by TLC analysis, the reaction was brought back to 0 °C and quenched with aqueous HCl until effervescence ceased. At this point, the mixture was poured into a separatory funnel and extracted with EtOAc (DCM does not solubilize the product very well). The organic layers are combined, dried with Na_2SO_4, filtered, and concentrated *in-vacuo* with the water bath temperature set to 25 °C (the product is slightly volatile). A crude and turbid oil was obtained that contained the product thietan-3-ol **4.116** in addition to some minor impurities. **4.116** was used as is without further purification and with characterization data that agreed with the literature.

TLC: R_f 0.3 (22% EtOAc:hexanes), $KMnO_4$

^{1}H-NMR (300 MHz, $CDCl_3$): δ 4.88 (p, *J* = 7.8 Hz, 1H), 3.36 (td, *J* = 8.0, 1.9 Hz, 2H), 3.26 (td, *J* = 7.5, 1.9 Hz, 2H).



4.116 **4.117**

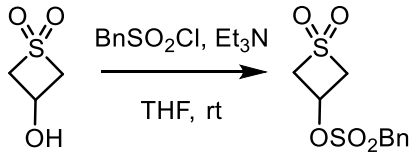
Crude thietan-3-ol (**4.116**, *ca*. 1 equiv.) was dissolved in acetone and cooled to 0 °C. Oxone® (2.5 equiv.) was dissolved in water and added dropwise to the solution of **4.116** (total concentration 0.1 M, 1:1 acetone:water). After the addition, the mixture was left to warm to room temperature and stirred overnight. Once TLC analysis indicated completion, the mixture was cooled back to 0 °C and quenched with a sat. $Na_2S_2O_{5(aq)}$ solution (~4 mL/mmol of **4.116**) and evaporated *in-vacuo* until a dry mass of off-white solid was obtained. The solids were broken up and suspended in a copious amount of acetone (~30 mL/mmol of **4.116**) and stirred vigorously to both dissolve the product and break up any large solids. After 20 minutes, $MgSO_4$ was added to the mixture and

vigorous stirring was continued for another 5 minutes. At that point, the entire mixture was filtered over a bed of celite/$MgSO_4$ and the acetone evaporated. The product 3-hydroxythietane-1,1-dioxide **4.117** was obtained as a white solid (64% yield over two steps) and was used as is without further purification and possessed characterization data that agreed with the literature.

TLC: R_f 0.4 (80% EtOAc:hexanes), $KMnO_4$

^{1}H-NMR (300 MHz, $(CD_3)_2CO$): δ 4.74 (tt, *J* = 7.3, 3.7 Hz, 1H), 4.50–4.33 (m, 2H), 4.04–3.90 (m, 2H).

^{13}C-NMR (151 MHz, $(CD_3)_2CO$): δ 74.1, 52.6.

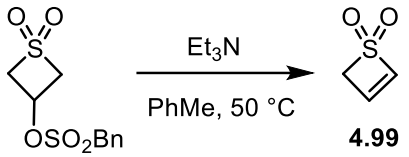


4.117 **4.119**

3-hydroxythietane-1,1-dioxide (**4.117**, 1 equiv.) and phenylmethanesulfonyl chloride (1.5 equiv.) were suspended in anhydrous THF (0.2 M), followed by the dropwise addition of Et_3N (1.4 equiv.) at room temperature. The mixture was then vigorously stirred for two hours and then checked for completion by TLC. If not yet complete, more phenylmethanesulfonyl chloride and Et_3N were added. Once complete, a thick white precipitate corresponding to triethylammonium hydrochloride as well as the product will have formed. To quench the reaction, water was added, and the mixture left to stir for 15 minutes. After 15 minutes, the mixture was filtered to collect the insoluble product **4.119** as a fluffy white powder and was dried. The filtrate is poured into a separatory funnel and extracted with EtOAc (3x) with the organic layers collected and dried over $MgSO_4$, filtered, and concentrated *in-vacuo*. The product **4.119** crashes out as a white powder that was combined with the solids obtained from the first filtration. Benzylsulfonate **4.119** was deemed pure enough for use without further purification and possessed characterization data that agreed with the literature.

TLC: R_f 0.8 (80% EtOAc:hexanes), $KMnO_4$

^{1}H-NMR (300 MHz, d_6-DMSO): δ 5.39 (tt, *J* = 7.4, 2.4 Hz, 1H), 4.86 (s, 2H), 4.83–4.69 (m, 2H), 4.37–4.25 (m, 2H).



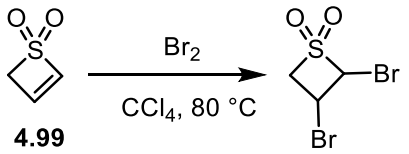
4.119 **4.99**

Benzylsulfonate (**4.119**, 1 equiv.) was suspended in anhydrous PhMe and brought to 50 °C. Once at 50 °C, Et_3N (8 equiv.) was added as a solution in anhydrous PhMe (total concentration of **4.119** is now 0.1 M) and the reaction left to age for two hours. At that point, ^{1}H-NMR analysis of an aliquot of the reaction indicated no starting material was remaining. The reaction mixture was then cooled down to room temperature and evaporated *in-vacuo* to a crude solid mass. Water and EtOAc were added to the mixture and then poured into a separatory funnel to extract with more EtOAc (3x). The organic layers were combined and dried with $MgSO_4$, filtered, and concentrated *in-vacuo* to afford thiete-1,1-dioxide **4.99** as a crude solid. Purification by flash-column chromatography (80% Et_2O:hexanes) gave the product as low melting white crystals (94% yield over two steps) and possessed characterization data that agreed with the literature.

TLC: R_f 0.22 (80% Et_2O:hexanes), $KMnO_4$

^{1}H-NMR (300 MHz, $CDCl_3$): δ 7.15 (dtd, *J* = 3.2, 1.7, 0.7 Hz, 1H), 6.78 (dt, *J* = 4.1, 0.5 Hz, 1H), 4.58 (dd, *J* = 1.6, 0.6 Hz, 2H).

^{13}C-NMR (101 MHz, $CDCl_3$): δ 148.6, 136.9, 72.3.



4.99 **4.184**

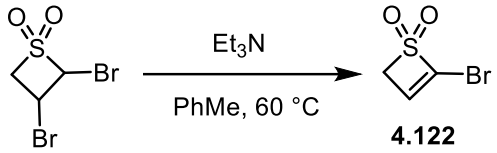
Thiete-1,1-dioxide (**4.99**, 1 equiv.) was dissolved in anhydrous CCl_4 (0.7 M) and then bromine (2.5 equiv.) was added dropwise. The mixture was brought to reflux (80 °C) and left to age for two hours at which point TLC analysis indicated completion. Once complete, the mixture was brought to room temperature and quenched with a sat. $Na_2S_2O_{5(aq)}$ solution and poured into a separatory funnel to be extracted with DCM (3x). The organic layers were combined, dried over $MgSO_4$, filtered, and concentrated *in-vacuo* to afford a crude oil. Purification by flash-column

chromatography (35% Et_2O:hexanes) gave pure 2,3-dibromothietane-1,1-dioxide **4.184** as an off-white solid and possessed characterization data that agreed with the literature.

TLC: R_f 0.84 (80% Et_2O:hexanes), $KMnO_4$

^{1}H-NMR (300 MHz, $CDCl_3$): δ 5.83 (dt, *J* = 6.6, 1.5 Hz, 1H), 4.73 (ddd, *J* = 13.6, 9.5, 1.2 Hz, 1H), 4.45 (ddd, *J* = 13.6, 7.4, 1.6 Hz, 1H), 4.33 (ddd, *J* = 9.4, 7.4, 6.6 Hz, 1H).

^{13}C-NMR (126 MHz, $CDCl_3$): δ 75.5, 72.6, 30.1.



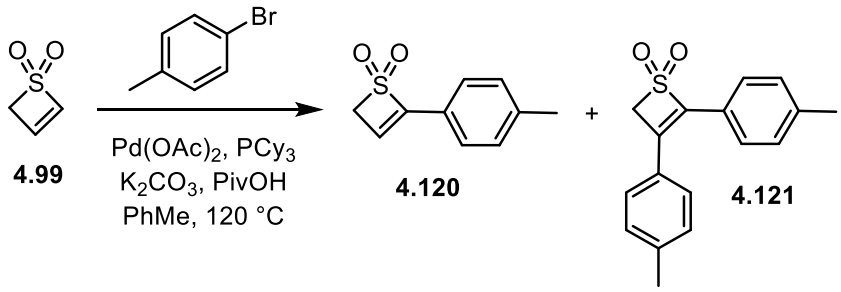
4.184 **4.122**

2,3-dibromothietane-1,1-dioxide (**4.184**, 1 equiv.) was dissolved in anhydrous PhMe (0.25 M) and Et_3N (1.2 equiv.) was added dropwise (rapid precipitate formation). The mixture was brought to 60 °C and left to age for one hour, at which point TLC analysis indicated complete consumption of the starting material. At that point, the reaction was quenched with water and poured into a separatory funnel to be extracted with EtOAc (3x). The organic layers were combined and dried with $MgSO_4$, filtered, and concentrated *in-vacuo* to afford a crude solid. Purification by flash-column chromatography (70% Et_2O:hexanes) gave pure 2-bromothiete-1,1-dioxide **4.122** as an off-white solid (76% yield over two steps) and possessed characterization data that agreed with the literature.

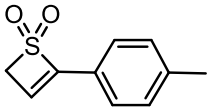
TLC: R_f 0.36 (70% Et_2O:hexanes), $KMnO_4$

^{1}H-NMR (300 MHz, $CDCl_3$): δ 7.16 (t, *J* = 1.7 Hz, 1H), 4.54 (d, *J* = 1.8 Hz, 2H).

^{13}C-NMR (76 MHz, $CDCl_3$): δ 134.7, 128.4, 70.7.



Thiete-1,1-dioxide **4.99** (16 mg, 0.156 mmol, 1 equiv.) was added to a flame-dried pressure vessel and dissolved in anhydrous and degassed PhMe (0.1 M, 1.6 mL). Next, K_2CO_3 (43 mg, 0.313 mmol, 2 equiv.) and $Pd(OAc)_2$ (1.4 mg, 0.0062 mmol, 4 mol%) were added followed by PCy_3 (3.5 mg, 0.012 mmol, 8 mol%) that was added as a solution in anhydrous and degassed PhMe (PCy_3 is air-sensitive and was weighed in a glove box and transferred to the reaction flask *via* syringe). After the addition of the ligand, 4-bromotoluene (40 mg, 0.234 mmol, 1.5 equiv.) and PivOH (4.8 mg, 0.046 mmol, 30 mol%) were added. The mixture was then sealed and transferred into a preheated oil bath, brought to reflux (120 °C), and left to age for three hours at which point TLC analysis indicated completion. The reaction was then quenched with water and poured into a separatory funnel and extracted with EtOAc (3x). The organic layers were collected, dried with Na_2SO_4, filtered, and concentrated *in-vacuo*. Purification by flash-column chromatography (55% Et_2O:hexanes) gave 2-arylated product **4.120** as a pale-yellow solid (13 mg, 50% yield) and 2,3-*bis*-arylated product **4.121** as a yellow solid (12 mg, 28% yield).



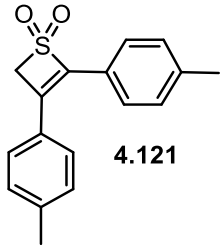
4.120

TLC: R_f 0.44 (84% Et_2O:hexanes), $KMnO_4$

^{1}H-NMR (300 MHz, $CDCl_3$): δ 7.42 (d, *J* = 8.1 Hz, 2H), 7.24 (d, *J* = 7.9 Hz, 2H), 6.92 (t, *J* = 1.8 Hz, 1H), 4.55 (d, *J* = 1.8 Hz, 2H), 2.39 (s, 3H).

^{13}C-NMR (76 MHz, $CDCl_3$): δ 160.2, 141.6, 130.1, 126.8, 123.6, 122.6, 69.8, 21.8.

MS-APCI+: 119.0 (66%), 147.0 (43%), 194.9 ($[M+H]^+$, 76%), 195.8 (11%), 411.1 (99%), 412.1 (31%), 443.1 (19%).

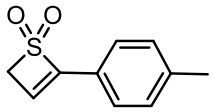


4.121

TLC: R_f 0.67 (84% Et_2O:hexanes), $KMnO_4$

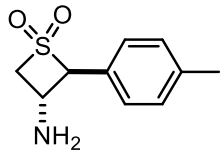
^{1}H-NMR (300 MHz, $CDCl_3$): δ 7.53 (d, *J* = 8.2 Hz, 2H), 7.40 (d, *J* = 8.2 Hz, 2H), 7.26–7.17 (m, 4H), 4.79 (s, 2H), 2.40 (s, 3H), 2.39 (s, 3H).

^{13}C-NMR (101 MHz, $CDCl_3$): δ 148.8, 142.2, 140.9, 137.4, 130.0, 129.9, 128.2, 127.8, 127.4, 124.5, 70.1, 21.8, 21.7.



4.120

Prepared from 2-bromothiete-1,1-dioxide **4.122** (189 mg, 1.03 mmol) following GP2 using 4-tolylboronic acid. Purification over silica (eluent: 70% DCM:hexanes). 2-tolylthiete-1,1-dioxide **4.120** was obtained as a pale-yellow solid: 172 mg, 87% yield. Characterization data matched that which was reported for the C-H activation strategy from above.



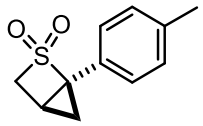
4.159

Prepared from 2-tolylthiete-1,1-dioxide **4.120** (25 mg, 0.130 mmol) following GP3 using 28 wt% $NH_4OH_{(aq)}$ as nucleophile/solvent and *t*-BuOH as co-solvent (1:1). Purification over silica (eluent: 2% MeOH: 1% Et_3N: 97% DCM). Thietane-1,1-dioxide **4.159** was obtained as a pale-yellow solid: 17 mg, 62% yield.

TLC: R_f 0.10 (60% EtOAc:hexanes), $KMnO_4$ and ninhydrin

^{1}H-NMR (300 MHz, $CDCl_3$): δ 7.29 (d, *J* = 8.1 Hz, 2H), 7.23 (d, *J* = 8.1 Hz, 2H), 5.06 (d, *J* = 7.9 Hz, 1H), 4.25 (dd, *J* = 12.6, 8.5 Hz, 1H), 4.04 (q, *J* = 7.9 Hz, 1H), 3.89 (dd, *J* = 12.5, 7.6 Hz, 1H), 2.37 (s, 3H), 1.68 (br s, 2H).

^{13}C-NMR (101 MHz, $CDCl_3$): δ 139.7, 129.9, 128.8, 126.8, 89.5, 69.3, 43.5, 21.4.



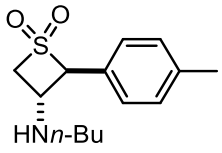
4.165

Prepared from 2-tolylthiete-1,1-dioxide **4.120** (27 mg, 0.137 mmol) following GP3 using Me_3SI as nucleophile, KO*t*-Bu as base, and DMSO as solvent. Cyclopropyl fused thietane-1,1-dioxide **4.165** was obtained as an orange oil: 10 mg, 35% yield.

TLC: R_f 0.4 (40% EtOAc:hexanes), *p*-anisaldehyde

^{1}H-NMR (300 MHz, $CDCl_3$): δ 7.39 (d, *J* = 8.1 Hz, 2H), 7.20 (d, *J* = 8.0 Hz, 2H), 4.13 (ddd, *J* = 12.0, 5.4, 2.0 Hz, 1H), 3.56 (d, *J* = 12.0 Hz, 1H), 2.39–2.31 (m, 4H), 2.08 (dd, *J* = 6.8, 3.3 Hz, 1H), 1.85 (td, *J* = 7.0, 2.0 Hz, 1H).

^{13}C-NMR (151 MHz, $CDCl_3$): δ 139.6, 130.3, 129.6, 126.2, 68.6, 64.9, 29.8, 21.4, 11.1.



4.160

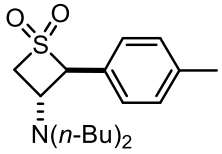
Prepared from 2-tolylthiete-1,1-dioxide **4.120** (26 mg, 0.132 mmol) following GP3 using butylamine as nucleophile and THF as solvent. Thietane-1,1-dioxide **4.160** was obtained as a white solid: 36 mg, quantitative yield.

TLC: R_f 0.6 (68% EtOAc:hexanes), $KMnO_4$

^{1}H-NMR (300 MHz, $CDCl_3$): δ 7.32–7.27 (m, 2H), 7.23 (d, *J* = 8.0 Hz, 2H), 5.16–5.07 (m, 1H), 4.32–4.11 (m, 1H), 3.94–3.76 (m, 2H), 2.50 (tt, *J* = 7.3, 3.8 Hz, 2H), 2.37 (s, 3H), 1.52–1.35 (m, 2H), 1.35–1.21 (m, 2H), 0.87 (t, *J* = 7.2 Hz, 3H).

^{13}C-NMR (151 MHz, $CDCl_3$): δ 139.5, 129.9, 128.8, 127.5, 87.5, 67.6, 48.5, 48.2, 32.1, 21.4, 20.4, 14.0.

MS-APCI+: 204.4 ($[M+H-SO_2]^+$, 28%), 268.1 ($[M+H]^+$, 96%), 269.0 (45%), 270.0 (20%), 535.1 (14%).



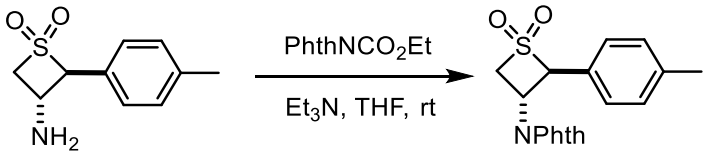
4.161

Prepared from 2-tolylthiete-1,1-dioxide **4.120** (22 mg, 0.114 mmol) following GP3 using dibutylamine as nucleophile and THF as solvent. Purification over silica (eluent: 15% EtOAc:hexanes). Thietane-1,1-dioxide **4.161** was obtained as a white solid: 18 mg, 48% yield.

TLC: R_f 0.6 (20% EtOAc:hexanes), $KMnO_4$

^{1}H-NMR (500 MHz, $CDCl_3$): δ 7.31 (d, *J* = 8.0 Hz, 2H), 7.21 (d, *J* = 7.9 Hz, 2H), 5.19 (d, *J* = 8.6 Hz, 1H), 4.03 (dd, *J* = 12.6, 8.6 Hz, 1H), 3.94 (dd, *J* = 12.6, 8.3 Hz, 1H), 3.81 (q, *J* = 8.5 Hz, 1H), 2.41 (ddt, *J* = 12.8, 7.3, 4.1 Hz, 4H), 2.36 (s, 3H), 1.37–1.22 (m, 4H), 1.15 (tt, *J* = 16.0, 7.1 Hz, 4H), 0.81 (t, *J* = 7.3 Hz, 6H).

^{13}C-NMR (126 MHz, $CDCl_3$): δ 139.4, 129.7, 129.0, 127.7, 84.4, 64.9, 51.9, 50.5, 28.2, 21.4, 20.4, 14.0.



4.159 **4.164**

3-amino-2-tolylthietane-1,1-dioxide **4.159** (20 mg, 0.093 mmol, 1 equiv.) was dissolved in THF (0.4 M, 0.23 mL) and *N*-carbethoxyphthalimide (27 mg, 0.121 mmol, 1.3 equiv.) was added all at once followed by Et_3N (17 μL, 0.121 mmol, 1.3 equiv.). The reaction was left to age at room temperature overnight and then quenched with water, diluted with EtOAc, and poured into a separatory funnel. Several extractions of the organic layer with water (13x) were then conducted to remove the ethyl carbamate by-product. The EtOAc layer was then dried over $MgSO_4$, filtered,

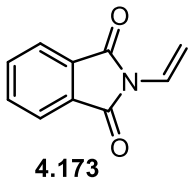
and concentrated *in-vacuo*. The residue was purified by flash-column chromatography (first 52% Et_2O:hexanes to remove $PhthNCO_2Et$, then 3% MeOH:DCM to flush the product). *N*-phthaloyl product **4.164** was obtained as a white solid (35 mg, 72% yield).

TLC: R_f 0.56 (40% EtOAc:hexanes), $KMnO_4$

^{1}H-NMR (300 MHz, $CDCl_3$): δ 7.92–7.81 (m, 2H), 7.82–7.69 (m, 2H), 7.36 (d, *J* = 8.2 Hz, 2H), 7.23 (d, *J* = 8.0 Hz, 2H), 6.37 (d, *J* = 9.8 Hz, 1H), 5.41 (q, *J* = 9.5 Hz, 1H), 4.99 (dd, *J* = 12.3, 9.6 Hz, 1H), 4.20 (ddd, *J* = 12.5, 9.4, 1.0 Hz, 1H), 2.35 (s, 3H).

^{13}C-NMR (126 MHz, $CDCl_3$): δ 167.4, 140.1, 134.9, 131.4, 130.0, 128.8, 125.4, 124.0, 82.3, 63.1, 38.8, 21.4.

MS-APCI+: 276.0 (85%), 277.0 ($[M-SO_2]^+$, 21%), 278.1 ($[M+H-SO_2]^+$, 96%), 279.0 (21%), 306.0 (60%), 307.1 (11%), 324.0 (15%), 342.0 ($[M+H]^+$, 44%).

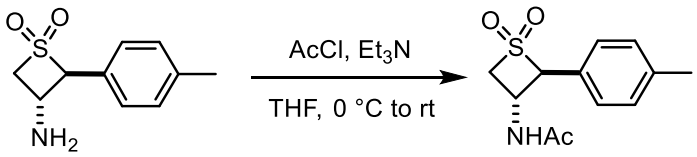


4.173

Prepared from *N*-phthaloyl product **4.164** (29 mg, 0.0849 mmol) following GP4, using a 2:1 mixture of DCM:MeOH as solvent. Reaction time: 7 hr. Purification over silica (eluent: 10% EtOAc:hexanes). *N*-vinylphthalimide **4.173** was obtained as a white solid: 5 mg, 35% yield. Characterization data agrees with the literature.

TLC: R_f 0.57 (40% EtOAc:hexanes), *p*-anisaldehyde

^{1}H-NMR (300 MHz, $CDCl_3$): δ 7.87 (td, *J* = 5.3, 2.1 Hz, 2H), 7.76 (td, *J* = 5.3, 2.1 Hz, 2H), 6.88 (dd, *J* = 16.4, 9.9 Hz, 1H), 6.09 (d, *J* = 16.4 Hz, 1H), 5.05 (d, *J* = 9.9 Hz, 1H).



4.159 **4.139**

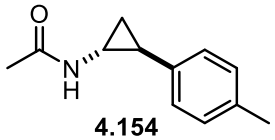
3-amino-2-tolylthietane-1,1-dioxide **4.159** (28 mg, 0.132 mmol, 1 equiv.) was dissolved in anhydrous THF (0.1 M, 0.3 mL) and cooled to 0 °C. Et_3N (24 μL, 0.172 mmol, 1.3 equiv.) was added and then followed by AcCl (12 μL, 0.172 mmol, 1.3 equiv.) and the reaction was warmed to room temperature and left to age for two hours. At that point, TLC analysis indicated completion and the reaction was quenched with water and poured into a separatory funnel to be extracted with EtOAc (3x). The organic layers were collected, dried with Na_2SO_4, filtered, and concentrated *in-vacuo*. The *N*-acetyl product **4.139** was isolated as an off-white solid (34 mg, quantitative yield) and as a mixture of rotamers that was used as is without further purification.

TLC: R_f 0.23 (100% EtOAc), $KMnO_4$

^{1}H-NMR (300 MHz, $CDCl_3$): δ 7.31–7.19 (m, 4H), 6.70–6.41 (m, 1H), 5.40 (d, *J* = 7.8 Hz, 1H), 4.85 (dt, *J* = 15.5, 7.4 Hz, 1H), 4.47–4.32 (m, 1H), 4.10 (ddd, *J* = 13.4, 7.3, 1.3 Hz, 1H), 2.36 (s, 3H), 1.94 (s, *J* = 5.1 Hz, 3H).

^{13}C-NMR (76 MHz, $CDCl_3$): δ 170.7, 170.6, 140.0, 130.0, 128.6, 128.6, 126.2, 126.2, 86.6, 86.5, 68.1, 68.0, 39.6, 39.6, 23.1, 23.1, 21.4.

MS-APCI+: 148.1 (100%), 190.0 ($[M+H-SO_2]^+$, 14%), 254.0 ($[M+H]^+$, 71%).



4.154

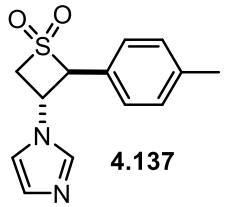
Prepared from *N*-acetyl product **4.139** (20 mg, 0.079 mmol) following GP4. Reaction time: 5 hr. Purification over silica (eluent: 1% Et_3N: 66% EtOAc:hexanes). Cyclopropane **4.154** was obtained as a pale oil: 5.2 mg, 35% yield as a mixture of rotamers.

TLC: R_f 0.35 (90% EtOAc:hexanes), $KMnO_4$

^{1}H-NMR (300 MHz, $CDCl_3$): δ 7.17–6.92 (m, 4H), 5.73 (br s, 1H), 3.13–2.82 (m, 1H), 2.38–2.27 (m, 3H), 2.14–1.95 (m, 4H), 1.31–1.07 (m, 2H).

^{13}C-NMR (126 MHz, $CDCl_3$): δ 175.1, 171.3, 137.4, 135.6, 129.4, 129.3, 129.2, 128.9, 126.6, 125.8, 34.4, 32.1, 28.5, 26.5, 24.4, 23.4, 21.1, 17.4, 16.4, 12.1.

MS-APCI+: 131.1 ($[M-C_2H_4NO]^+$, 32%), 148.0 (38%), 190.0 ($[M+H]^+$, 100%), 191.0 (19%), 248.2 (39%).



4.137

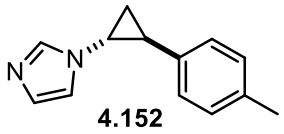
Prepared from 2-tolylthiete-1,1-dioxide **4.120** (27 mg, 0.138 mmol) following GP3 using imidazole as nucleophile, DIPEA as base, and DCM as solvent. Purification over silica (eluent: 100% EtOAc then 6% MeOH: 94% DCM). Thietane-1,1-dioxide **4.137** was obtained as a white solid: 31 mg, 85% yield.

TLC: R_f 0.09 (60% EtOAc:hexanes), $KMnO_4$

^{1}H-NMR (300 MHz, $CDCl_3$): δ 7.55 (t, *J* = 1.2 Hz, 1H), 7.36–7.26 (m, 4H), 7.16 (t, *J* = 1.2 Hz, 1H), 7.10 (t, *J* = 1.4 Hz, 1H), 5.61 (d, *J* = 8.3 Hz, 1H), 5.20–5.05 (m, 1H), 4.62 (ddd, *J* = 13.5, 9.3, 0.9 Hz, 1H), 4.48 (ddd, *J* = 13.5, 8.1, 1.2 Hz, 1H), 2.39 (s, 3H).

^{13}C-NMR (151 MHz, $CDCl_3$): δ 140.8, 136.4, 131.6, 130.3, 128.6, 125.5, 116.6, 88.3, 67.7, 46.1, 21.4.

MS-APCI+: 59.2 (19%), 263.0 ($[M+H]^+$, 99%), 263.9 (21%).



4.152

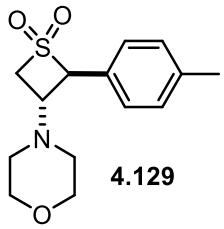
Prepared from thietane-1,1-dioxide **4.137** (24 mg, 0.0903 mmol) following GP4. Reaction time: 6 hr. Purification over silica (eluent: 90% EtOAc:hexanes). Cyclopropane **4.152** was obtained as a clear oil: 12.6 mg, 70% yield.

TLC: R_f 0.34 (6% MeOH:DCM), $KMnO_4$

^{1}H-NMR (300 MHz, $CDCl_3$): δ 7.62 (br s, 1H), 7.15 (d, *J* = 7.9 Hz, 2H), 7.08–7.00 (m, 4H), 3.49 (dt, *J* = 7.7, 3.9 Hz, 1H), 2.42 (ddd, *J* = 9.9, 6.4, 3.3 Hz, 1H), 2.35 (s, 3H), 1.61 (ddd, *J* = 10.2, 6.1, 4.4 Hz, 1H), 1.51–1.38 (m, 1H).

^{13}C-NMR (101 MHz, $CDCl_3$): δ 137.5, 136.6, 136.0, 129.5, 129.3, 126.3, 119.7, 36.5, 24.3, 21.1, 15.2.

MS-APCI+: 131.1 ([M-$C_3H_3N_2$]$^+$, 42%), 199.4 ([M+H]$^+$, 99%), 200.0 (42%).



4.129

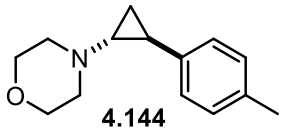
Prepared from 2-tolylthiete-1,1-dioxide **4.120** (25 mg, 0.127 mmol) following GP3 using morpholine as nucleophile and THF as solvent. Purification over silica (eluent: 64% EtOAc:hexanes). Thietane-1,1-dioxide **4.129** was obtained as a clear oil: 36 mg, quantitative yield.

TLC: R_f 0.39 (60% EtOAc:hexanes), $KMnO_4$

^{1}H-NMR (300 MHz, $CDCl_3$): δ 7.30 (d, *J* = 8.0 Hz, 2H), 7.22 (d, *J* = 8.0 Hz, 2H), 5.25 (d, *J* = 8.4 Hz, 1H), 4.08 (dd, *J* = 12.6, 8.4 Hz, 1H), 3.96 (dd, *J* = 12.5, 8.2 Hz, 1H), 3.71–3.57 (m, 4H), 3.37 (q, *J* = 8.2 Hz, 1H), 2.41–2.25 (m, 7H).

^{13}C-NMR (76 MHz, $CDCl_3$): δ 139.7, 129.9, 128.8, 127.3, 84.7, 66.4, 64.7, 54.2, 52.0, 21.4.

MS-APCI+: 131.1 ([M-C_4H_8NO]$^+$, 13%), 218.1 ([M+H-SO_2]$^+$, 38%), 282.4 ([M+H]$^+$, 96%), 283.0 (42%), 284.1 (15%).



4.144

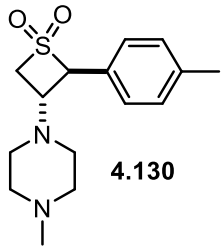
Prepared from thietane-1,1-dioxide **4.129** (25 mg, 0.0877 mmol) following GP4. Reaction time: 7 hr. Purification over silica (eluent: 1% Et_3N: 25% EtOAc:hexanes). Cyclopropane **4.144** was obtained as a clear oil: 10 mg, 53% yield.

TLC: R_f 0.55 (68% EtOAc:hexanes), ninhydrin

^{1}H-NMR (300 MHz, $CDCl_3$): δ 7.07 (d, *J* = 8.0 Hz, 2H), 6.96 (d, *J* = 8.1 Hz, 2H), 3.74–3.65 (m, 4H), 2.70–2.61 (m, 4H), 2.31 (s, 3H), 1.98 (ddd, *J* = 9.0, 5.6, 3.3 Hz, 1H), 1.87 (dt, *J* = 7.2, 3.8 Hz, 1H), 1.09 (dt, *J* = 9.2, 4.5 Hz, 1H), 0.99–0.87 (m, 1H).

^{13}C-NMR (101 MHz, $CDCl_3$): δ 138.9, 135.4, 129.1, 126.1, 67.1, 53.6, 49.1, 24.0, 21.2, 16.0.

MS-APCI+: 59.2 (12%), 131.1 ([M-C_4H_8NO]$^+$, 85%), 132.0 (10%), 218.1 ([M+H]$^+$, 96%), 219.1 (22%).



4.130

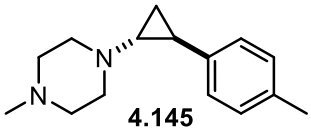
Prepared from 2-tolylthiete-1,1-dioxide **4.120** (23.5 mg, 0.121 mmol) following GP3 using *N*-methylpiperazine as nucleophile and THF as solvent. Purification over silica (eluent: 6% MeOH:DCM). Thietane-1,1-dioxide **4.130** was obtained as a white solid: 35 mg, 97% yield.

TLC: R_f 0.11 (62% EtOAc:hexanes), $KMnO_4$

^{1}H-NMR (500 MHz, $CDCl_3$): δ 7.29 (d, *J* = 8.0 Hz, 2H), 7.22 (d, *J* = 7.9 Hz, 2H), 5.24 (d, *J* = 8.4 Hz, 1H), 4.07 (dd, *J* = 12.6, 8.5 Hz, 1H), 3.96 (dd, *J* = 12.6, 8.2 Hz, 1H), 3.39 (q, *J* = 8.3 Hz, 1H), 2.48–2.29 (m, 11H), 2.24 (s, 3H).

^{13}C-NMR (126 MHz, $CDCl_3$): δ 139.6, 129.9, 128.8, 127.4, 84.7, 64.9, 54.5, 54.0, 51.5, 45.9, 21.3.

MS-APCI+: 131.1 ([M-$C_5H_{11}N_2$]$^+$, 96%), 132.1 (17%), 216.1 ([M-CH_2SO_2]$^+$, 13%), 229.1 (18%), 231.1 ([M+H-SO_2]$^+$, 73%), 232.0 (15%), 295.0 ([M+H]$^+$, 96%), 296.1 (25%).



4.145

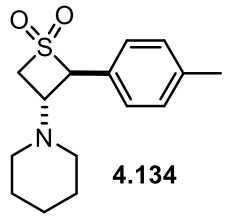
Prepared from thietane-1,1-dioxide **4.130** (25 mg, 0.0855 mmol) following GP4. Reaction time: 7 hr. Purification over silica (eluent: 8% MeOH:DCM). Cyclopropane **4.145** was obtained as an amber oil: 10 mg, 51% yield.

TLC: R_f 0.19 (7% MeOH:DCM), ninhydrin

^{1}H-NMR (300 MHz, $CDCl_3$): δ 7.06 (d, *J* = 7.9 Hz, 2H), 6.95 (d, *J* = 8.1 Hz, 2H), 2.81–2.25 (m, 14H), 1.95 (ddd, *J* = 9.3, 5.8, 3.0 Hz, 1H), 1.85 (dt, *J* = 7.2, 3.8 Hz, 1H), 1.07 (dt, *J* = 9.5, 4.7 Hz, 1H), 0.98–0.86 (m, 1H).

^{13}C-NMR (126 MHz, $CDCl_3$): δ 139.0, 135.3, 129.1, 126.1, 55.0, 52.8, 48.6, 46.0, 24.2, 21.1, 16.2.

MS-APCI+: 70.2 (15%), 91.1 (15%), 105.1 (13%), 113.1 (14%), 131.1 ($[M-C_5H_{11}N_2]^+$, 96%), 132.1 (15%), 231.3 ($[M+H]^+$, 96%), 232.1 (38%).



4.134

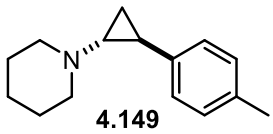
Prepared from 2-tolylthiete-1,1-dioxide **4.120** (26 mg, 0.1333 mmol) following GP3 using piperidine as nucleophile and THF as solvent. Purification over silica (eluent: 38% EtOAc:hexanes). Thietane-1,1-dioxide **4.134** was obtained as a clear oil: 36.5 mg, 98% yield.

TLC: R_f 0.63 (65% EtOAc:hexanes), $KMnO_4$

^{1}H-NMR (600 MHz, $CDCl_3$): δ 7.31 (d, *J* = 8.0 Hz, 2H), 7.22 (d, *J* = 7.9 Hz, 2H), 5.25 (d, *J* = 8.4 Hz, 1H), 4.06 (dd, *J* = 12.6, 8.4 Hz, 1H), 3.97 (dd, *J* = 12.6, 8.3 Hz, 1H), 3.33 (q, *J* = 8.4 Hz, 1H), 2.36 (s, 3H), 2.32–2.15 (m, 4H), 1.54 (qt, *J* = 11.5, 6.6 Hz, 4H), 1.43–1.35 (m, 2H).

^{13}C-NMR (151 MHz, $CDCl_3$): δ 139.4, 129.8, 128.9, 127.7, 84.8, 65.2, 54.5, 52.9, 25.5, 23.7, 21.4.

MS-APCI+: 216.1 ($[M+H-SO_2]^+$, 17%), 280.0 ($[M+H]^+$, 100%), 281.0 (23%).



4.149

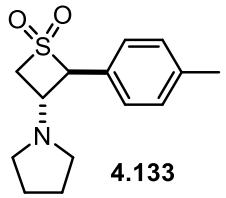
Prepared from thietane-1,1-dioxide **4.134** (25 mg, 0.091 mmol) following GP4. Reaction time: 8 hr. Purification over silica (eluent: 1% Et_3N: 20% Et_2O:hexanes). Cyclopropane **4.149** was obtained as a clear oil: 8.5 mg, 48% yield.

TLC: R_f 0.58 (40% EtOAc:hexanes), ninhydrin

^{1}H-NMR (300 MHz, $CDCl_3$): δ 7.06 (d, *J* = 8.0 Hz, 3H), 6.97 (d, *J* = 8.1 Hz, 3H), 2.65–2.53 (m, 4H), 2.31 (s, 3H), 1.97 (td, *J* = 5.7, 2.9 Hz, 1H), 1.77 (dt, *J* = 7.4, 3.8 Hz, 1H), 1.57 (p, *J* = 5.6 Hz, 4H), 1.49–1.41 (m, 2H), 1.09 (dt, *J* = 9.5, 4.8 Hz, 1H), 0.95–0.87 (m, 1H).

^{13}C-NMR (151 MHz, $CDCl_3$): δ 139.5, 135.1, 129.0, 126.1, 54.6, 49.8, 26.0, 24.5, 24.2, 21.1, 16.4.

MS-APCI+: 59.2 (21%), 135.1 (15%), 147.0 (15%), 216.1 ($[M+H]^+$, 96%), 217.1 (17%).



4.133

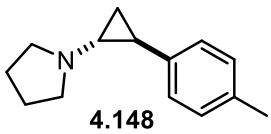
Prepared from 2-tolylthiete-1,1-dioxide **4.120** (25.5 mg, 0.1313 mmol) following GP3 using pyrrolidine as nucleophile and THF as solvent. Purification over silica (eluent: 60% EtOAc:hexanes). Thietane-1,1-dioxide **4.133** was obtained as a white solid: 34 mg, 97% yield.

TLC: R_f 0.37 (64% EtOAc:hexanes), $KMnO_4$

^{1}H-NMR (300 MHz, $CDCl_3$): δ 7.33 (d, *J* = 8.2 Hz, 2H), 7.22 (d, *J* = 7.9 Hz, 2H), 5.28 (d, *J* = 8.4 Hz, 1H), 4.16–3.96 (m, 2H), 3.42 (q, *J* = 8.3 Hz, 1H), 2.49–2.37 (m, 4H), 2.37 (s, 3H), 1.85–1.68 (m, 4H).

^{13}C-NMR (75 MHz, $CDCl_3$): δ 139.4, 129.6, 129.0, 127.2, 85.6, 65.5, 53.6, 52.8, 23.6, 21.2.

MS-APCI+: 202.1 (13%), 266.1 ($[M+H]^+$, 98%), 267.0 (92%), 268.0 (32%), 531.1 (12%).

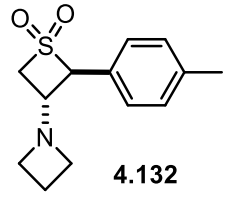


4.148

Prepared from thietane-1,1-dioxide **4.133** (23 mg, 0.087 mmol) following GP4. Reaction time: 7.5 hr. Purification over silica (eluent: 66% EtOAc:hexanes). Cyclopropane **4.148** was obtained as an amber oil: 7 mg, 43% yield.

TLC: R_f 0.22 (66% EtOAc:hexanes), ninhydrin

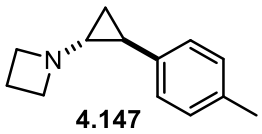
^{1}H-NMR (300 MHz, $CDCl_3$): δ 7.07 (d, *J* = 8.0 Hz, 2H), 6.97 (d, *J* = 8.0 Hz, 2H), 2.79–2.66 (m, 4H), 2.30 (s, 3H), 2.06–1.97 (m, 1H), 1.89–1.73 (m, 5H), 1.21–1.09 (m, 1H), 0.98–0.84 (m, 1H).
^{13}C-NMR (126 MHz, $CDCl_3$): δ 139.2, 135.2, 129.1, 126.2, 53.9, 46.4, 29.8, 23.7, 21.1, 16.2.
MS-APCI+: 131.1 ($[M-C_4H_8N]^+$, 96%), 132.1 (16%), 202.1 ($[M+H]^+$, 75%), 203.1 (15%).



4.132

Prepared from 2-tolylthiete-1,1-dioxide **4.120** (25 mg, 0.128 mmol) following GP3 using azetidine as nucleophile and THF as solvent. Purification over silica (eluent: 68% EtOAc:hexanes). Thietane-1,1-dioxide **4.132** was obtained as a white solid: 34 mg, quantitative yield.

TLC: R_f 0.20 (50% EtOAc:hexanes), $KMnO_4$
^{1}H-NMR (500 MHz, $CDCl_3$): δ 7.29 (d, *J* = 8.1 Hz, 2H), 7.22 (d, *J* = 8.0 Hz, 2H), 5.13 (d, *J* = 7.7 Hz, 1H), 4.02 (dd, *J* = 12.9, 8.5 Hz, 1H), 3.87 (dd, *J* = 12.9, 7.3 Hz, 1H), 3.54 (q, *J* = 7.6 Hz, 1H), 3.24–3.13 (m, 4H), 2.36 (s, 3H), 2.06 (p, *J* = 7.1 Hz, 2H).
^{13}C-NMR (126 MHz, $CDCl_3$): δ 139.5, 129.8, 128.9, 127.6, 85.0, 64.7, 55.1, 53.5, 21.4, 17.4.
MS-APCI+: 187.0 ($[M-SO_2]^+$, 17%), 188.1 ($[M+H-SO_2]^+$, 34%), 252.0 ($[M+H]^+$, 99%), 252.9 (21%).



4.147

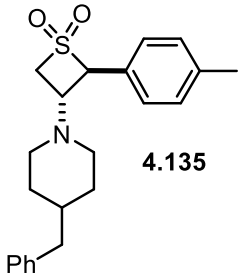
Prepared from thietane-1,1-dioxide **4.132** (22.7 mg, 0.0903 mmol) following GP4. Reaction time: 5 hr. Purification over silica (eluent: 1% Et_3N:EtOAc). Cyclopropane **4.147** was obtained as an amber oil: 7 mg, 42% yield.

TLC: R_f 0.22 (1% Et_3N: 95% EtOAc:hexanes), ninhydrin

^{1}H-NMR (300 MHz, $CDCl_3$): δ 7.06 (d, *J* = 8.0 Hz, 2H), 6.93 (d, *J* = 8.1 Hz, 2H), 3.35 (t, *J* = 6.9 Hz, 4H), 2.30 (s, 3H), 2.14–2.00 (m, 3H), 1.89 (ddd, *J* = 9.0, 5.8, 3.0 Hz, 1H), 1.00 (dt, *J* = 9.4, 4.7 Hz, 1H), 0.84 (dt, *J* = 7.0, 5.5 Hz, 1H).

^{13}C-NMR (126 MHz, $CDCl_3$): δ 139.1, 135.2, 129.0, 126.1, 54.7, 49.1, 23.1, 21.1, 17.6, 15.6.

MS-APCI+: 131.1 ([M-C_3H_6N]$^+$, 43%), 160.0 (11%), 188.1 ([M+H]$^+$, 98%), 189.1 (26%).



4.135

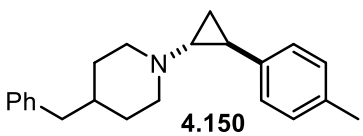
Prepared from 2-tolylthiete-1,1-dioxide **4.120** (27 mg, 0.140 mmol) following GP3 using 4-benzylpiperidine as nucleophile and THF as solvent. Purification over silica (eluent: 30% EtOAc:hexanes). Thietane-1,1-dioxide **4.135** was obtained as a clear oil: 52 mg, quantitative yield.

TLC: R_f 0.48 (35% EtOAc:hexanes), $KMnO_4$

^{1}H-NMR (300 MHz, $CDCl_3$): δ 7.29 (d, *J* = 8.2 Hz, 2H), 7.25–7.13 (m, 5H), 7.12–7.04 (m, 2H), 5.23 (d, *J* = 8.5 Hz, 1H), 4.06 (dd, *J* = 12.2, 8.9 Hz, 1H), 3.95 (dd, *J* = 12.5, 8.2 Hz, 1H), 3.32 (q, *J* = 8.4 Hz, 1H), 2.81–2.71 (m, 1H), 2.70–2.61 (m, 1H), 2.50 (d, *J* = 6.9 Hz, 2H), 2.35 (s, 3H), 2.00–1.85 (m, 1H), 1.78–1.59 (m, 2H), 1.58–1.37 (m, 2H), 1.36–1.12 (m, 2H).

^{13}C-NMR (126 MHz, $CDCl_3$): δ 140.3, 139.5, 129.8, 129.1, 128.9, 128.3, 127.7, 126.1, 84.9, 65.2, 54.4, 52.4, 52.4, 43.0, 37.3, 31.7, 31.7, 21.4.

MS-APCI+: 131.1 ([M-$C_5H_{11}N_2$-SO_2]$^+$, 45%), 174.0 (11%), 291.1 ([M-CH_2SO_2]$^+$, 12%), 304.1 (66%), 305.3 ([M-SO_2]$^+$, 33%), 306.1 ([M+H-SO_2]$^+$, 80%), 307.2 (24%), 308.2 (32%), 370.1 ([M+H]$^+$, 100%), 371.1 (28%), 372.0 (14%).



4.150

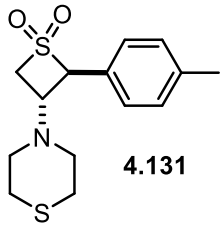
Prepared from thietane-1,1-dioxide **4.135** (33 mg, 0.0901 mmol) following GP4. Reaction time: 6.5 hr. Purification over silica (eluent: 1% Et_3N: 8% EtOAc:hexanes). Cyclopropane **4.150** was obtained as a pale-yellow oil: 12.5 mg, 45% yield.

TLC: R_f 0.67 (28% EtOAc:hexanes), ninhydrin

^{1}H-NMR (500 MHz, $CDCl_3$): δ 7.28 (t, *J* = 7.5 Hz, 2H), 7.23–7.15 (m, 1H), 7.14 (d, *J* = 7.1 Hz, 2H), 7.06 (d, *J* = 7.9 Hz, 2H), 6.96 (d, *J* = 8.0 Hz, 2H), 3.11–3.01 (m, 2H), 2.60–2.47 (m, 2H), 2.30 (s, 3H), 2.13 (q, *J* = 12.1 Hz, 2H), 2.00–1.92 (m, 1H), 1.81–1.73 (m, 1H), 1.64 (d, *J* = 13.0 Hz, 2H), 1.61–1.50 (m, 1H), 1.34–1.22 (m, 2H), 1.12–1.04 (m, 1H), 0.91 (q, *J* = 5.7 Hz, 1H).

^{13}C-NMR (126 MHz, $CDCl_3$): δ 140.8, 139.4, 135.2, 129.3, 129.0, 128.3, 126.1, 125.9, 54.3, 53.6, 49.3, 43.4, 38.1, 32.2, 32.1, 24.3, 21.1, 16.5.

MS-APCI+: 91.1 (11%), 131.1 ([M-$C_{12}H_{16}N$]$^+$, 100%), 132.1 (21%), 306.1 ([M+H]$^+$, 67%), 307.2 (17%).



4.131

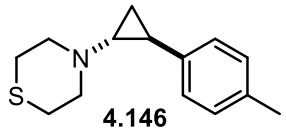
Prepared from 2-tolylthiete-1,1-dioxide **4.120** (26 mg, 0.133 mmol) following GP3 using thiomorpholine as nucleophile and THF as solvent. Purification over silica (eluent: 35% EtOAc:hexanes). Thietane-1,1-dioxide **4.131** was obtained as a pale-yellow oil: 37 mg, 94% yield.

TLC: R_f 0.62 (60% EtOAc:hexanes), $KMnO_4$

^{1}H-NMR (300 MHz, $CDCl_3$): δ 7.30 (d, *J* = 8.1 Hz, 2H), 7.23 (d, *J* = 8.2 Hz, 2H), 5.21 (d, *J* = 8.4 Hz, 1H), 4.09 (dd, *J* = 12.7, 8.4 Hz, 1H), 3.94 (dd, *J* = 12.6, 8.2 Hz, 1H), 3.46 (q, *J* = 8.3 Hz, 1H), 2.77–2.52 (m, 8H), 2.37 (s, 3H).

^{13}C-NMR (76 MHz, $CDCl_3$): δ 139.7, 130.0, 128.8, 127.4, 84.6, 64.9, 54.1, 53.3, 27.6, 21.4.

MS-APCI+: 234.0 ([M+H-SO_2]$^+$, 25%), 298.4 ([M+H]$^+$, 99%), 299.0 (42%), 300.0 (48%), 595.0 (13%).



4.146

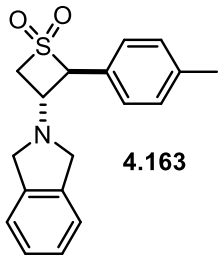
Prepared from thietane-1,1-dioxide **4.131** (27 mg, 0.0901 mmol) following GP4. Reaction time: 6 hr. Purification over silica (eluent: 1% Et_3N: 8% Et_2O:hexanes). Cyclopropane **4.146** was obtained as a pale-yellow oil: 9.7 mg, 46% yield.

TLC: R_f 0.64 (35% EtOAc:hexanes), ninhydrin

^{1}H-NMR (300 MHz, $CDCl_3$): δ 7.07 (d, *J* = 7.8 Hz, 2H), 6.95 (d, *J* = 8.1 Hz, 2H), 2.96–2.86 (m, 4H), 2.66 (dd, *J* = 6.3, 3.8 Hz, 4H), 2.31 (s, 3H), 2.03–1.86 (m, 2H), 1.06 (dt, *J* = 9.0, 5.0 Hz, 1H), 1.00–0.89 (m, 1H).

^{13}C-NMR (126 MHz, $CDCl_3$): δ 139.0, 135.4, 129.1, 126.1, 55.1, 49.5, 28.0, 24.7, 21.1, 16.7.

MS-APCI+: 131.1 ($[M-C_4H_8NS]^+$, 86%), 132.0 (10%), 234.0 ($[M+H]^+$, 100%), 235.1 (28%), 236.0 (12%).



4.163

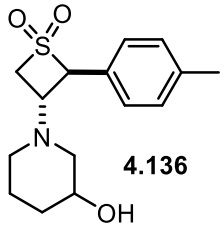
Prepared from 2-tolylthiete-1,1-dioxide **4.120** (26 mg, 0.133 mmol) following GP3 using isoindoline as nucleophile and THF as solvent. Purification over silica (eluent: 30% EtOAc:hexanes). Thietane-1,1-dioxide **4.163** was obtained as a pale-brown oil that darkens upon standing: 41.5 mg, 98% yield.

TLC: R_f 0.42 (35% EtOAc:hexanes), $KMnO_4$

^{1}H-NMR (300 MHz, $CDCl_3$): δ 7.38 (d, *J* = 8.1 Hz, 2H), 7.26 (d, *J* = 7.9 Hz, 2H), 7.23–7.11 (m, 4H), 5.40 (d, *J* = 8.1 Hz, 1H), 4.23–4.08 (m, 2H), 3.95–3.79 (m, 5H), 2.40 (s, 3H).

^{13}C-NMR (76 MHz, $CDCl_3$): δ 139.8, 138.8, 129.9, 129.2, 127.4, 127.1, 122.5, 85.6, 65.4, 57.7, 53.4, 21.4.

MS-APCI+: 59.2 (40%), 250.0 ($[M+H-SO_2]^+$, 42%), 314.2 ($[M+H]^+$, 94%), 315.2 (23%).



4.136

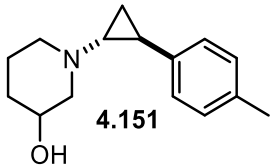
Prepared from 2-tolylthiete-1,1-dioxide **4.120** (16 mg, 0.082 mmol) following GP3 using 3-hydroxypiperidine as nucleophile and THF as solvent. Purification over silica (eluent: 100% EtOAc). Thietane-1,1-dioxide **4.136** was obtained as a pale-yellow solid: 23.5 mg, 97% yield and as an inseparable mixture of diastereoisomers (~1.5:1 *d.r.*).

TLC: R_f 0.26 (100% EtOAc), $KMnO_4$

^{1}H-NMR (400 MHz, $CDCl_3$): δ 7.30 (d, *J* = 8.0 Hz, 2H), 7.22 (d, *J* = 8.0 Hz, 2H), 5.29–5.18 (m, 1H), 4.09 (dddd, *J* = 12.8, 8.3, 6.2, 0.9 Hz, 1H), 3.96 (td, *J* = 13.0, 8.1 Hz, 1H), 3.85–3.69 (m, 1H), 3.41 (qd, *J* = 8.3, 4.3 Hz, 1H), 2.52–2.11 (m, 8H), 1.85–1.40 (m, 4H).

^{13}C-NMR (101 MHz, $CDCl_3$): δ 139.5, 129.8, 129.8, 128.8, 128.7, 127.3, 84.8, 84.6, 65.7, 65.1, 58.5, 53.9, 53.8, 52.0, 31.3, 21.3.

MS-APCI+: 232.3 ($[M+H-SO_2]^+$, 17%), 283.9 (32%), 296.0 ($[M+H]^+$, 98%), 297.1 (22%), 298.0 (11%).



4.151

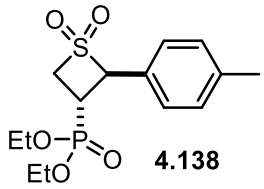
Prepared from thietane-1,1-dioxide **4.136** (19 mg, 0.0640 mmol) following GP4. Reaction time: 4.5 hr. Purification over silica (eluent: 1% Et_3N: 60% EtOAc:hexanes). Cyclopropane **4.151** was obtained as a pale-yellow oil: 6.4 mg, 43% yield and as an inseparable mixture of diastereoisomers (~1:1 *d.r.*).

TLC: R_f 0.22 (80% EtOAc:hexanes), ninhydrin

^{1}H-NMR (300 MHz, $CDCl_3$): δ 7.06 (d, *J* = 8.0 Hz, 2H), 7.00–6.87 (m, 4H), 3.89–3.77 (m, 1H), 2.80–2.61 (m, 3H), 2.53–2.40 (m, 1H), 2.30 (s, 3H), 2.01–1.70 (m, 3H), 1.68–1.46 (m, 3H), 1.12–0.98 (m, 1H), 0.97–0.81 (m, 2H).

^{13}C-NMR (126 MHz, $CDCl_3$): δ 139.1, 135.3, 129.1, 126.2, 126.1, 66.2, 60.6, 60.3, 53.8, 53.6, 48.9, 48.9, 31.9, 30.5, 29.9, 24.7, 24.7, 21.6, 21.1, 16.7, 16.7.

MS-APCI+: 131.1 ([M-$C_5H_{10}NO$]$^+$, 36%), 232.4 ([M+H]$^+$, 99%), 233.1 (47%).



4.138

Prepared from 2-tolylthiete-1,1-dioxide **4.120** (26 mg, 0.133 mmol) following GP3 using diethylphosphite as nucleophile, DBU as base, and THF as solvent. Purification over silica (eluent: 72% EtOAc:hexanes). Thietane-1,1-dioxide **4.138** was obtained as a white solid: 58 mg, quantitative yield.

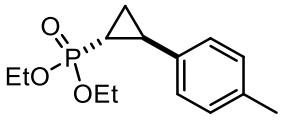
TLC: R_f 0.20 (66% EtOAc:hexanes), $KMnO_4$

^{1}H-NMR (300 MHz, $CDCl_3$): δ 7.31 (d, *J* = 8.2 Hz, 2H), 7.22 (d, *J* = 8.1 Hz, 2H), 5.55 (d, *J* = 11.1 Hz, 1H), 4.29 (dd, *J* = 12.7, 10.7 Hz, 1H), 4.16–3.84 (m, 5H), 3.00 (q, *J* = 10.8 Hz, 1H), 2.36 (s, 3H), 1.20 (td, *J* = 7.1, 4.6 Hz, 6H).

^{13}C-NMR (76 MHz, $CDCl_3$): δ 140.0, 129.8, 128.7, 126.3, 82.9, 63.3, 63.2, 63.1, 63.0, 62.7, 26.7, 24.7, 21.4, 16.4, 16.3.

^{31}P-NMR (122 MHz, $CDCl_3$) δ 23.5.

MS-APCI+: 59.2 (20%), 268.0 ([M-SO_2]$^+$, 100%), 269.0 ([M+H-SO_2]$^+$, 85%), 270.0 (13%), 315.0 (35%), 333.1 ([M+H]$^+$, 67%), 334.0 (20%).



4.153

Prepared from thietane-1,1-dioxide **4.138** (30 mg, 0.0896 mmol) following GP4. Reaction time: 5.5 hr. Purification over silica (eluent: 72% EtOAc:hexanes). Cyclopropane **4.153** was obtained as a clear oil: 23.7 mg, 98% yield and as an inseparable mixture of diastereoisomers (~5:1 *d.r.*).

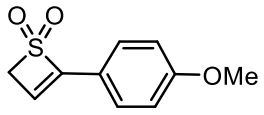
TLC: R_f 0.25 (75% EtOAc:hexanes), $KMnO_4$

^{1}H-NMR (300 MHz, $CDCl_3$): δ 7.26–6.96 (m, 4H), 4.22–3.59 (m, 4H), 2.56–2.22 (m, 4H), 1.66–1.05 (m, 9H).

^{13}C-NMR (126 MHz, $CDCl_3$): δ 137.2, 137.1, 136.3, 129.4, 129.3, 128.6, 126.2, 62.1, 62.0 (2C), 61.5, 61.3, 21.6, 21.2, 21.1, 21.0, 20.9, 16.6, 16.6, 16.4, 15.7, 14.2, 12.7 (2C), 9.2.

^{31}P-NMR (121 MHz, $CDCl_3$) δ 26.5, 26.3.

MS-APCI+: 195.0 (12%), 213.0 (100%), 241.0 (55%), 269.0 (67%).



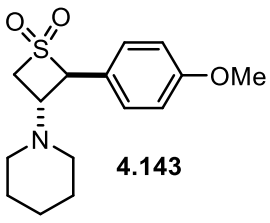
4.185

Prepared from 2-bromothiete-1,1-dioxide **4.122** (165.5 mg, 0.904 mmol) following GP2 using 4-methoxyphenylboronic acid. Purification over silica (eluent: 80% DCM:hexanes). 2-(4-methoxyphenyl)thiete-1,1-dioxide **4.185** was obtained as a pale-yellow solid: 117 mg, 62% yield.

TLC: R_f 0.24 (80% DCM:hexanes), $KMnO_4$

^{1}H-NMR (400 MHz, $CDCl_3$): δ 7.47 (d, *J* = 8.6 Hz, 2H), 6.94 (d, *J* = 8.7 Hz, 2H), 6.85–6.79 (m, 1H), 4.58–4.53 (m, 2H), 3.84 (s, 3H).

^{13}C-NMR (101 MHz, $CDCl_3$): δ 161.7, 159.8, 128.5, 120.9, 118.9, 114.9, 69.8, 55.6.



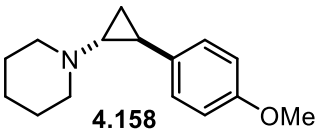
4.143

Prepared from 2-(4-methoxyphenyl)thiete-1,1-dioxide **4.185** (24 mg, 0.114 mmol) following GP3 using piperidine as nucleophile and THF as solvent. Purification over silica (eluent: 55% EtOAc:hexanes). Thietane-1,1-dioxide **4.143** was obtained as a yellow solid: 31 mg, 92% yield.

TLC: R_f 0.62 (60% EtOAc:hexanes), $KMnO_4$

^{1}H-NMR (400 MHz, $CDCl_3$): δ 7.34 (d, *J* = 8.7 Hz, 2H), 6.93 (d, *J* = 8.7 Hz, 2H), 5.22 (d, *J* = 8.5 Hz, 1H), 4.15–4.01 (m, 1H), 3.95 (dd, *J* = 12.6, 8.3 Hz, 1H), 3.81 (s, 3H), 3.29 (q, *J* = 8.4 Hz, 1H), 2.37–2.14 (m, 4H), 1.54 (dp, *J* = 10.5, 6.4 Hz, 4H), 1.39 (q, *J* = 5.5 Hz, 2H).

^{13}C-NMR (101 MHz, $CDCl_3$): δ 160.4, 130.3, 122.9, 114.5, 84.5, 65.0, 55.4, 55.0, 53.0, 25.5, 23.7.



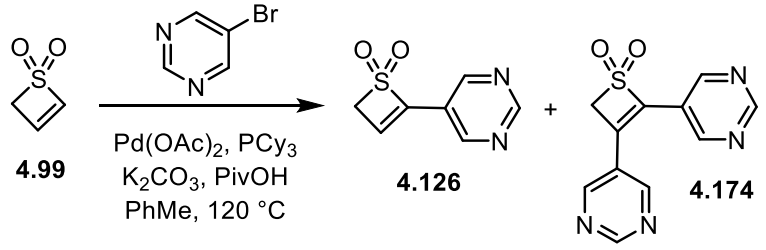
4.158

Prepared from thietane-1,1-dioxide **4.143** (33.5 mg, 0.1134 mmol) following GP4. Reaction time: 4.5 hr. Purification over silica (eluent: 1% Et_3N: 10% EtOAc:hexanes). Cyclopropane **4.158** was obtained as a yellow solid: 11.3 mg, 43% yield.

TLC: R_f 0.5 (60% EtOAc:hexanes), $KMnO_4$

^{1}H-NMR (400 MHz, $CDCl_3$): δ 7.04–6.96 (m, 2H), 6.84–6.76 (m, 2H), 3.78 (s, 3H), 2.67–2.51 (m, 4H), 1.99–1.90 (m, 1H), 1.76–1.69 (m, 1H), 1.63–1.51 (m, 4H), 1.50–1.39 (m, 2H), 1.10–1.02 (m, 1H), 0.87 (q, *J* = 5.7 Hz, 1H).

^{13}C-NMR (101 MHz, $CDCl_3$): δ 157.8, 134.5, 127.4, 113.8, 55.5, 54.6, 49.5, 26.0, 24.6, 23.8, 16.1.



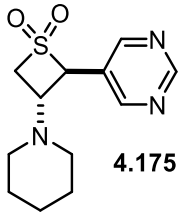
4.99 **4.126** **4.174**

Thiete-1,1-dioxide **4.99** (121 mg, 1.16 mmol, 1 equiv.) was added to a flame-dried pressure vessel and dissolved in anhydrous and degassed PhMe (0.1 M, 11.6 mL). Next, K_2CO_3 (320 mg, 2.31 mmol, 2 equiv.) and $Pd(OAc)_2$ (10.4 mg, 0.046 mmol, 4 mol%) were added followed by PCy_3 (26 mg, 0.092 mmol, 8 mol%) that was added as a solution in anhydrous and degassed PhMe (PCy_3 is air-sensitive and was weighed in a glove box and transferred to the reaction flask *via* syringe). After the addition of the ligand, 5-bromopyrimidine (276 mg, 1.74 mmol, 1.5 equiv.) and PivOH (35.5 mg, 0.348 mmol, 30 mol%) were added. The mixture was then sealed and transferred into a preheated oil bath, brought to reflux (120 °C), and left to age for two hours (longer reaction times resulted in more 2,3-*bis*-arylated product being formed). The reaction was then quenched with water and poured into a separatory funnel and extracted with EtOAc (3x). The organic layers were collected, dried with Na_2SO_4, filtered, and concentrated *in-vacuo*. Purification by flash-column chromatography (10% $(Me)_2CO$:DCM) gave product **4.126** as a yellow solid (44 mg, 21% yield). The by-product **4.174** was not isolated.

TLC: R_f 0.58 (35% $(Me)_2CO$:DCM), $KMnO_4$

^{1}H-NMR (300 MHz, $CDCl_3$): δ 9.29 (s, 1H), 8.91 (s, 2H), 7.30 (t, *J* = 1.9 Hz, 1H), 4.72 (d, *J* = 1.8 Hz, 2H).

^{13}C-NMR (151 MHz, $CDCl_3$): δ 159.9, 154.7, 128.8, 121.8, 71.4.



4.175

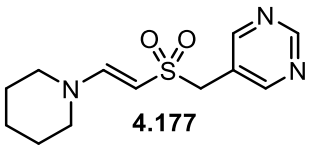
Prepared from 2-(pyrimidin-5-yl)thiete-1,1-dioxide **4.126** (32 mg, 0.177 mmol) following GP3 using piperidine as nucleophile and THF as solvent. Purification over silica (eluent: 1% Et_3N: 80% EtOAc:hexanes). Thietane-1,1-dioxide **4.175** was obtained as an off-white solid: 45 mg, 95% yield.

TLC: R_f 0.41 (1% Et_3N:EtOAc), $KMnO_4$

^{1}H-NMR (300 MHz, $CDCl_3$): δ 9.24 (s, 1H), 8.83 (s, 2H), 5.22 (d, *J* = 8.3 Hz, 1H), 4.20 (ddd, *J* = 12.8, 8.4, 0.9 Hz, 1H), 4.09 (dd, *J* = 12.9, 8.2 Hz, 1H), 3.34 (q, *J* = 8.3 Hz, 1H), 2.26 (t, *J* = 5.0 Hz, 4H), 1.63–1.50 (m, 4H), 1.41 (q, *J* = 5.6 Hz, 2H).

^{13}C-NMR (126 MHz, $CDCl_3$): δ 159.2, 157.1, 125.6, 79.5, 65.8, 54.6, 52.8, 25.5, 23.6.

MS-APCI+: 86.2 (19%), 204.0 (15%), 268.0 ($[M+H]^+$, 99%), 268.9 (20%), 297.1 (12%), 313.2 (22%).



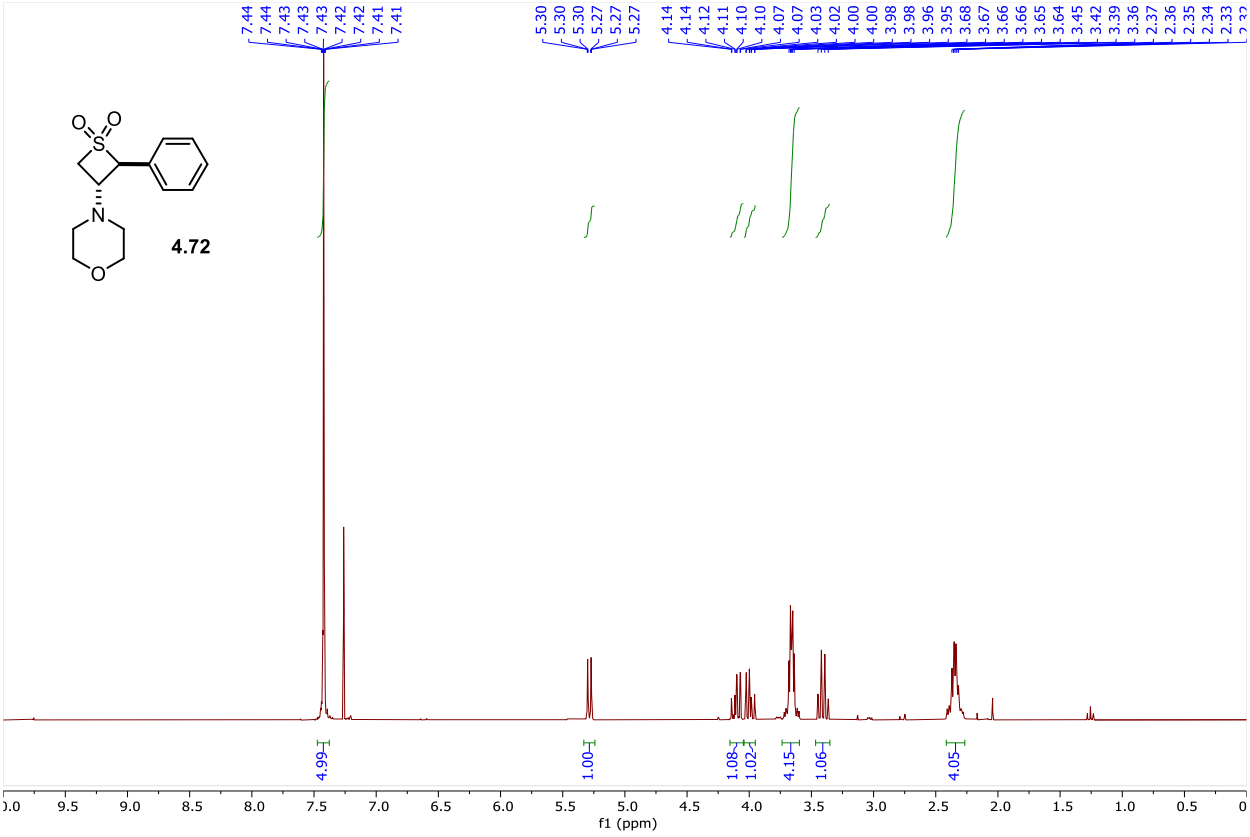
4.177

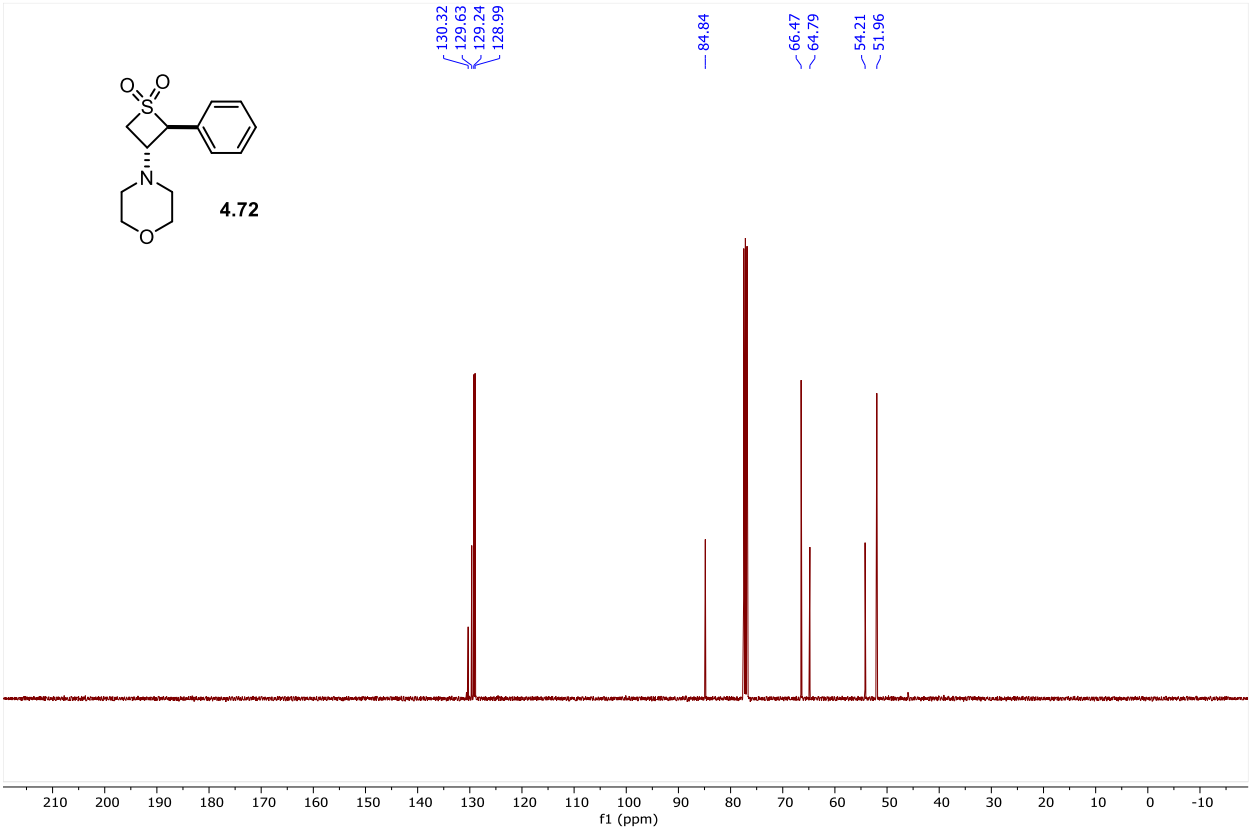
Prepared from thietane-1,1-dioxide **4.175** (24 mg, 0.0901 mmol) following GP4. Reaction time: 3 hr. Cyclopropane **4.176** was not obtained. Instead, crude ^{1}H-NMR data seems to support the ring opened product **4.177**.

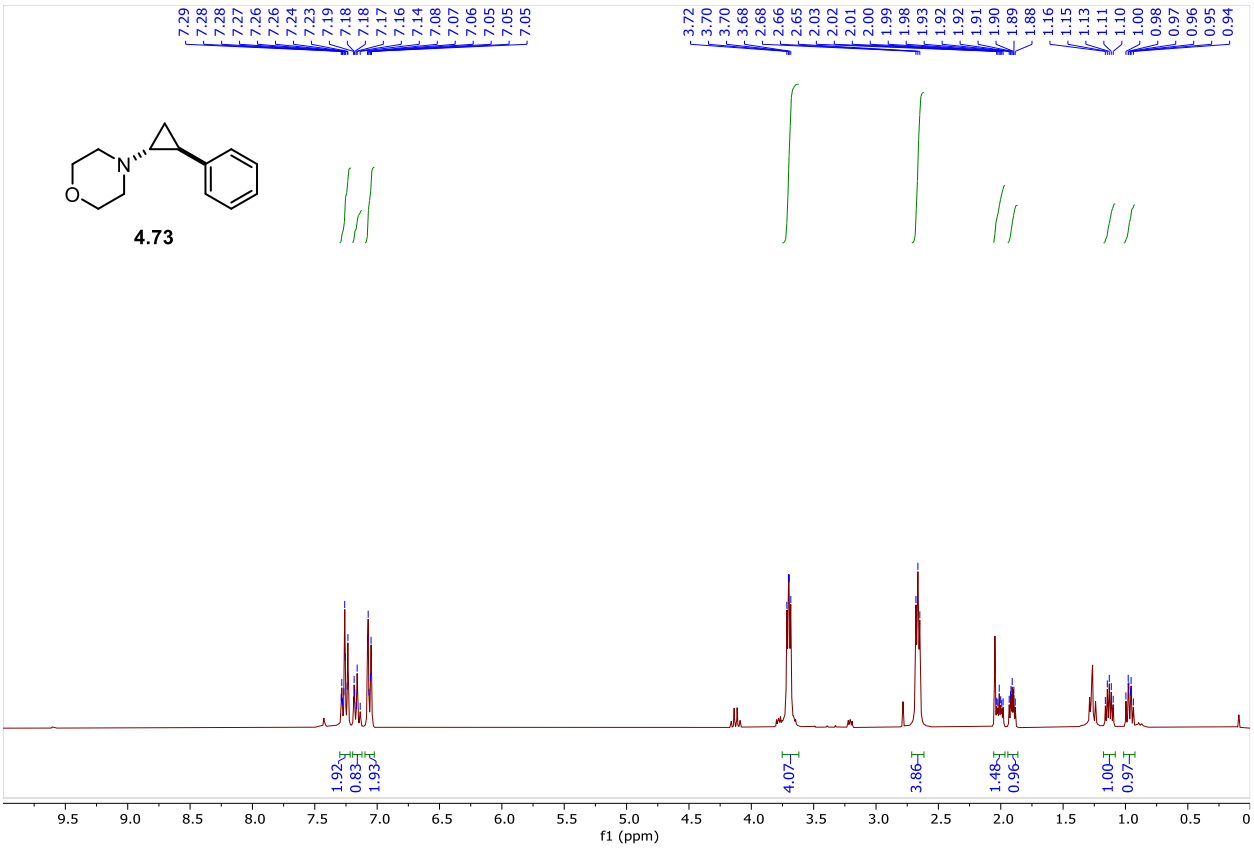
TLC: R_f 0.19 (1% Et_3N:EtOAc), $KMnO_4$

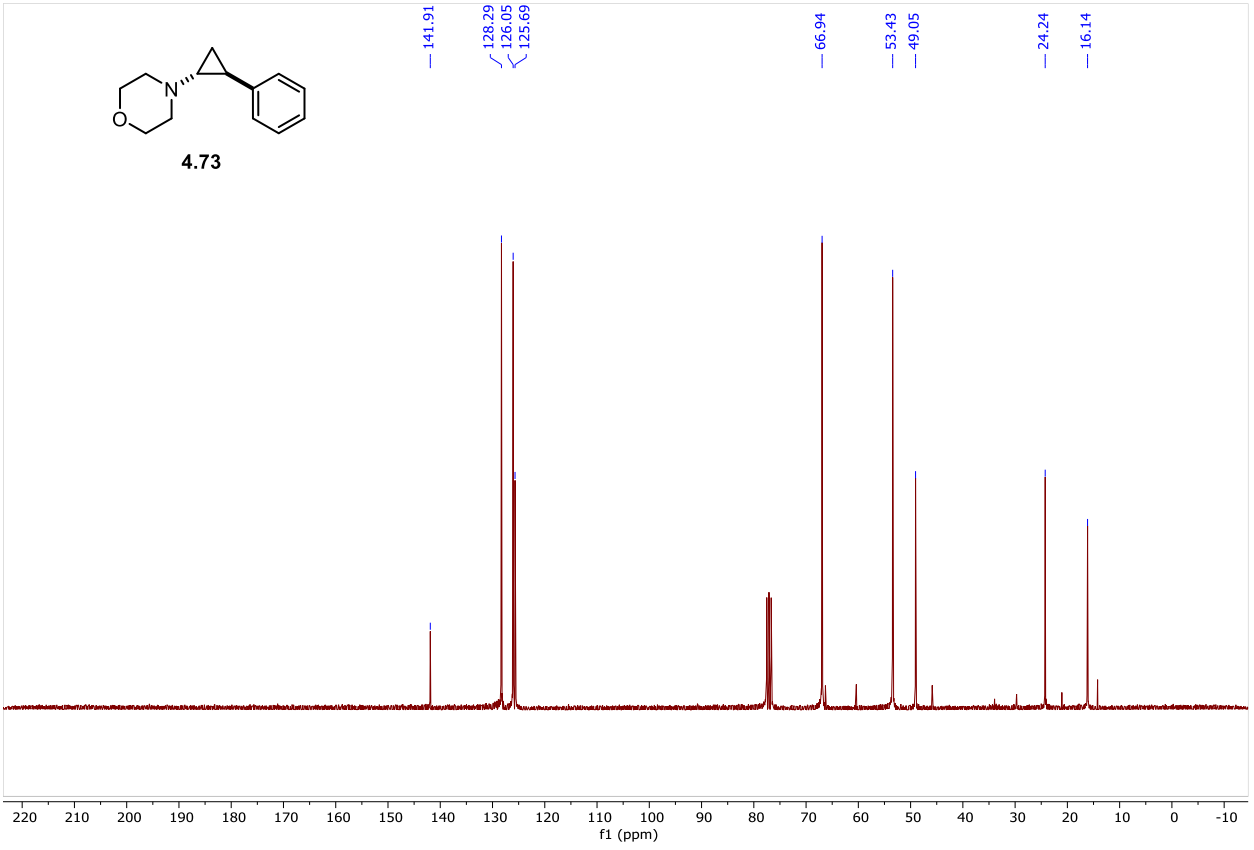
^{1}H-NMR (300 MHz, $CDCl_3$): δ 9.15 (s, 1H), 8.71 (s, 2H), 6.78 (d, *J* = 12.7 Hz, 1H), 4.69 (d, *J* = 12.6 Hz, 1H), 4.13 (s, 2H), 3.26–2.98 (m, 4H), 1.68–1.48 (m, 6H).

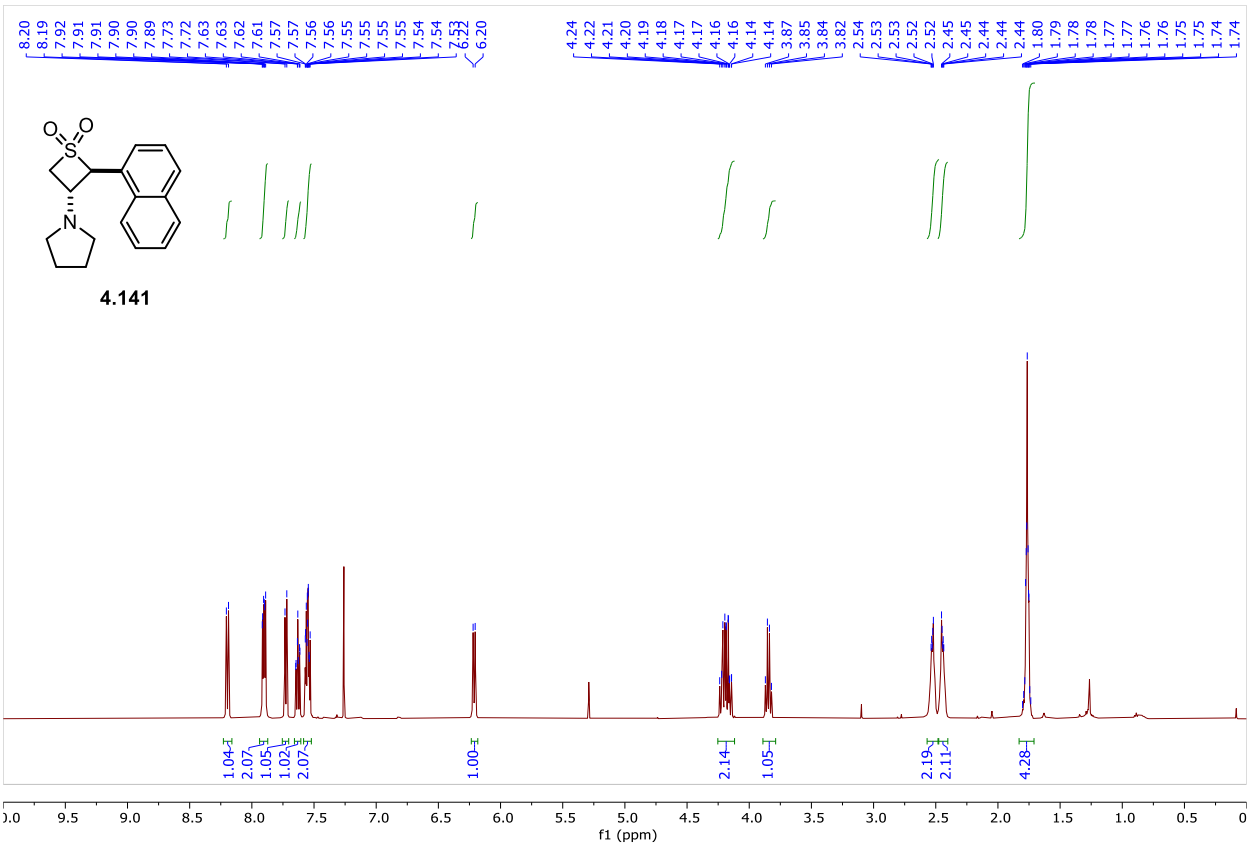
6.4.2 ^{1}H- and ^{13}C-NMR Spectra

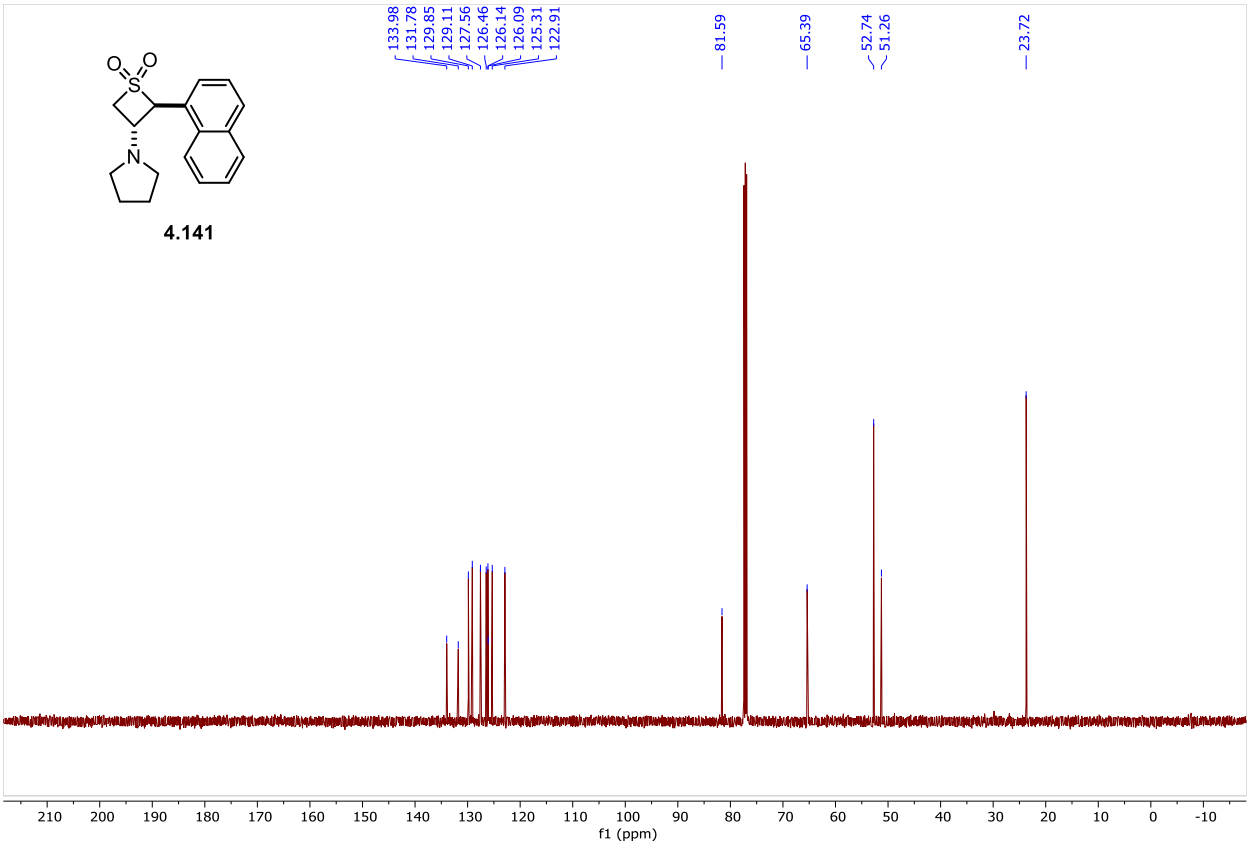


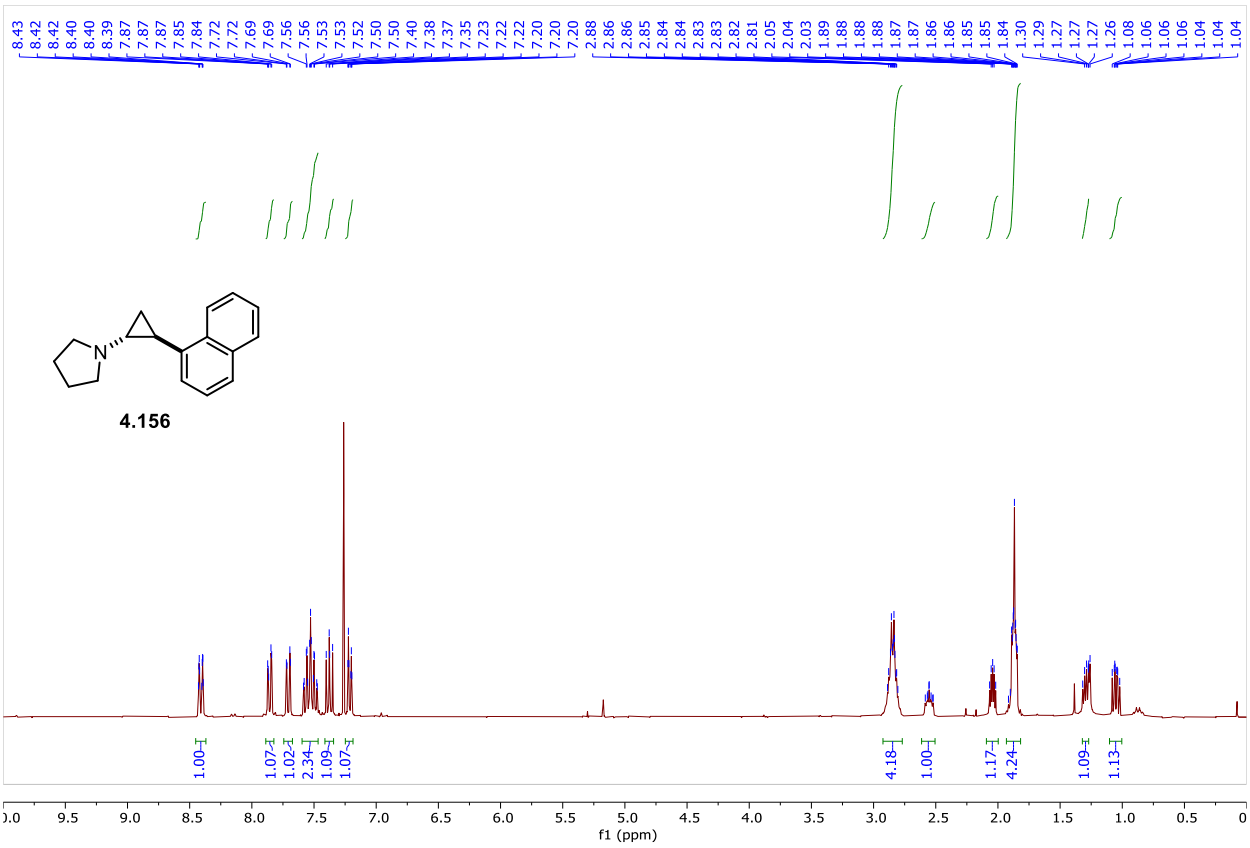


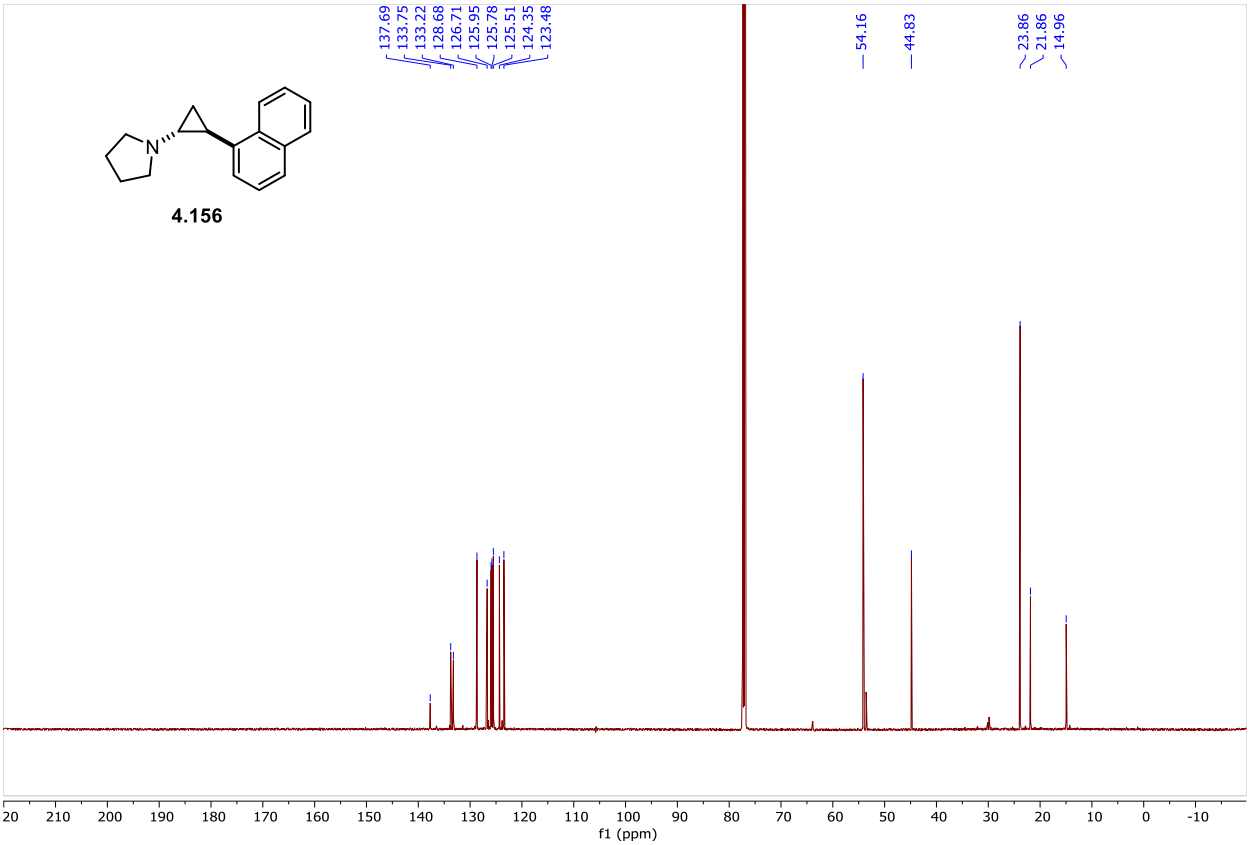

7.29 7.28 7.28 7.27 7.26 7.26 7.24 7.23 7.19 7.18 7.18 7.17 7.16 7.14 7.08 7.07 7.06 7.05 7.05 7.05
3.72 3.70 3.70 3.68 2.68 2.66 2.65 2.03 2.02 2.01 2.00 1.99 1.98 1.93 1.92 1.92 1.91 1.90 1.89 1.88 1.16 1.15 1.13 1.11 1.10 1.00 0.98 0.97 0.96 0.95 0.94
4.73
1.92 0.83 1.93 4.07 3.86 1.48 0.96 1.00 0.97
f1 (ppm)

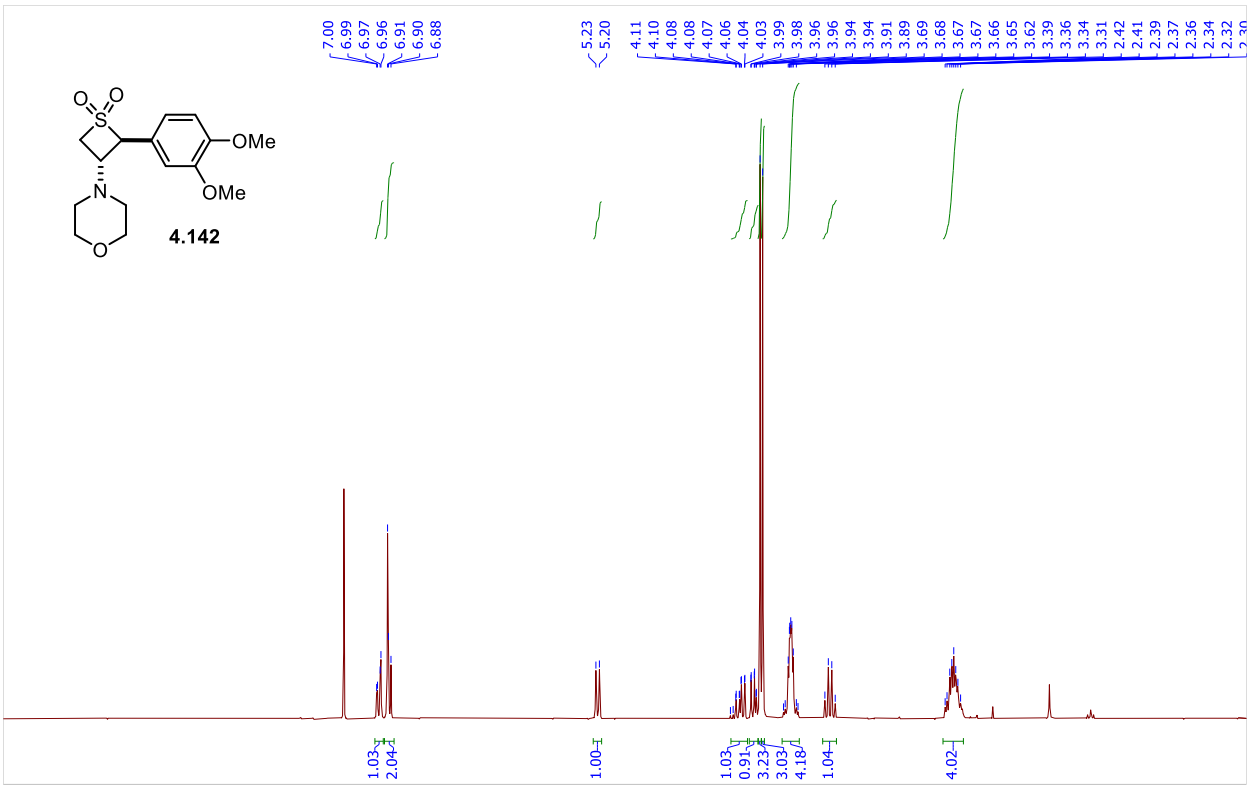

141.91 128.29 126.05 125.69 66.94 53.43 49.05 24.24 16.14
4.73
f1 (ppm)

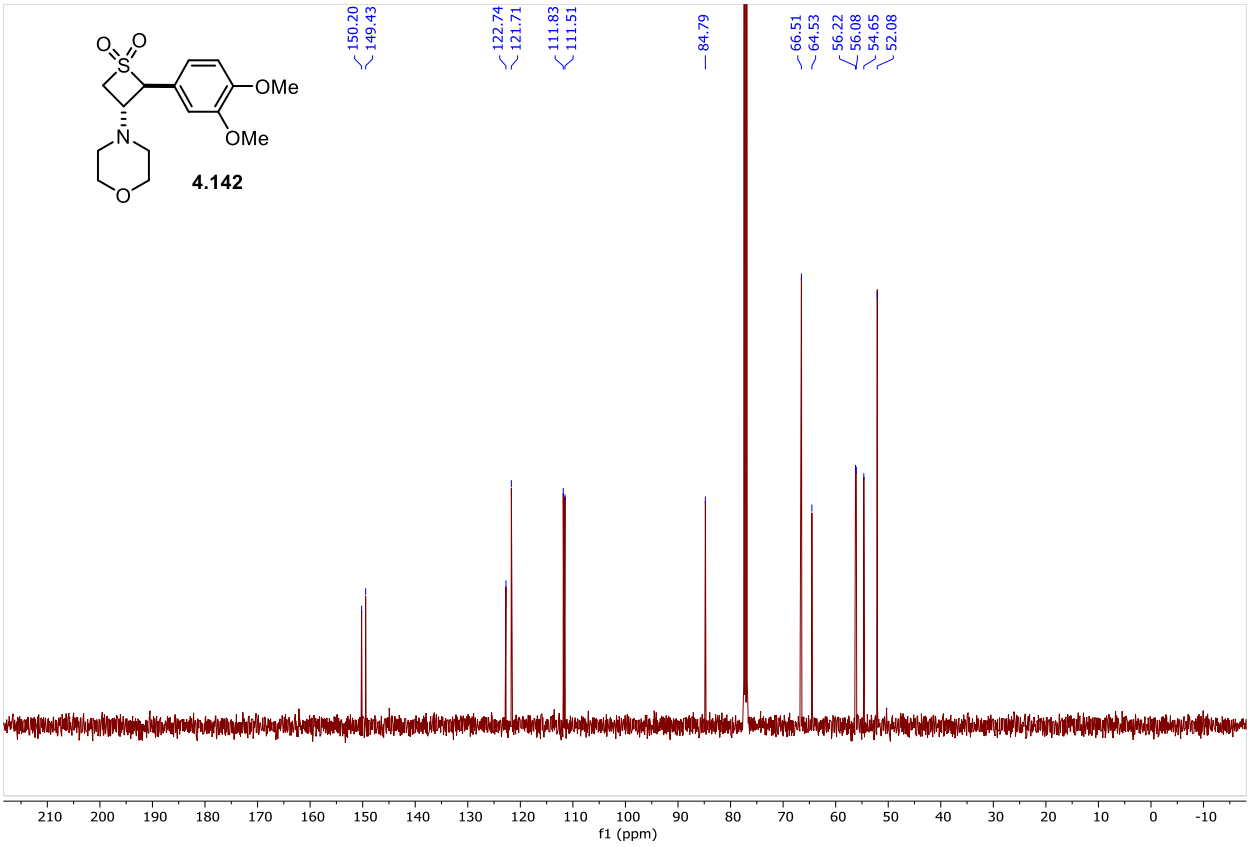

4.141
f1 (ppm)

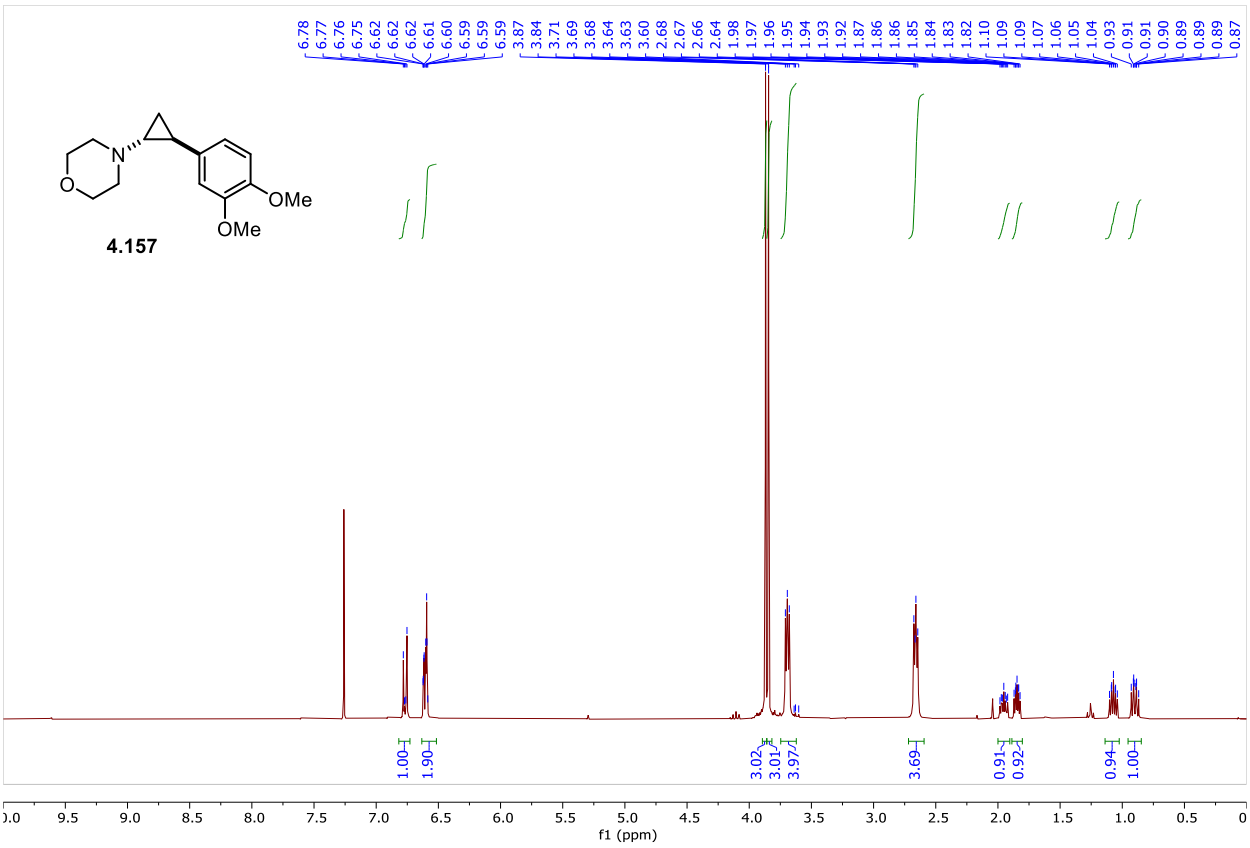

4.141
f1 (ppm)

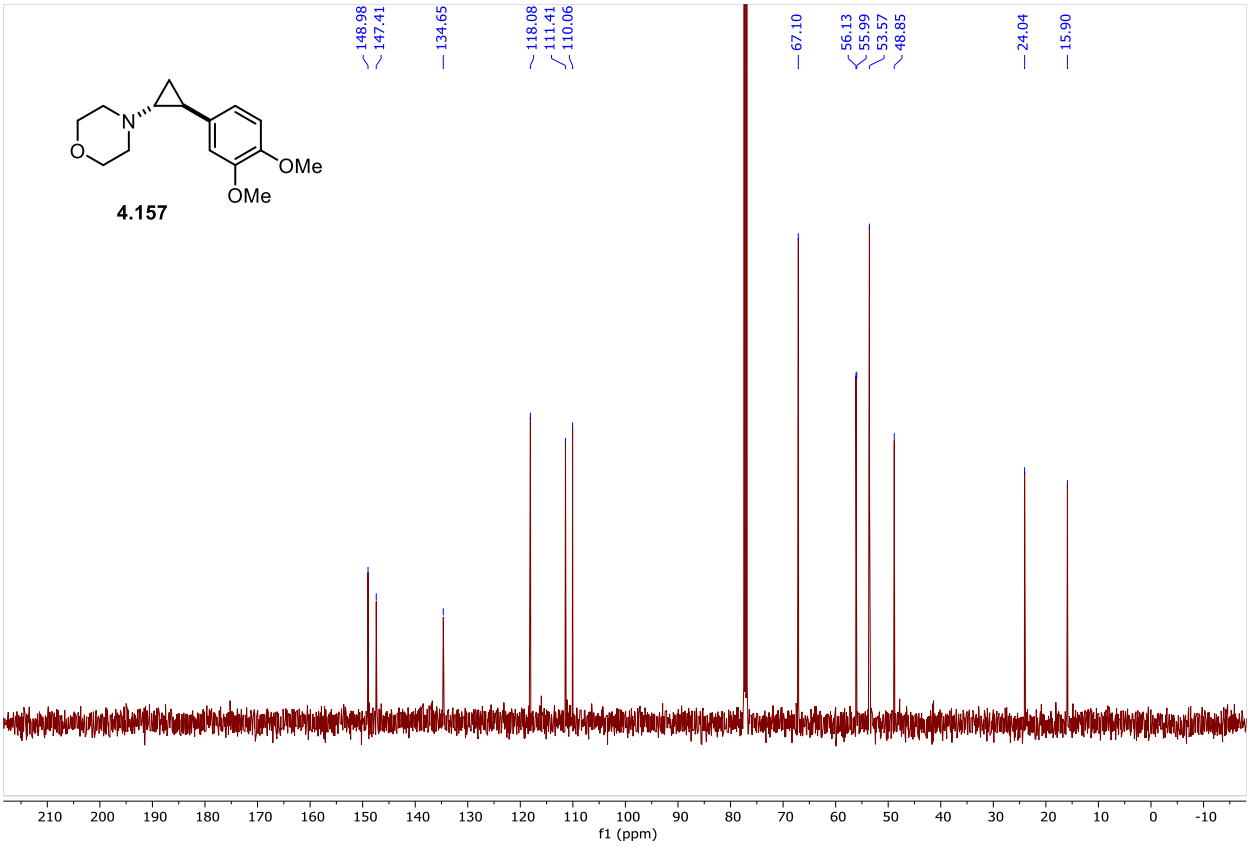

8.43 8.42 8.42 8.40 8.40 8.39 7.87 7.87 7.87 7.85 7.84 7.72 7.72 7.69 7.69 7.56 7.56 7.53 7.53 7.52 7.50 7.50 7.40 7.38 7.37 7.35 7.23 7.22 7.22 7.20 7.20 7.20 2.88 2.86 2.86 2.85 2.84 2.84 2.83 2.83 2.82 2.81 2.05 2.04 2.03 1.89 1.88 1.88 1.88 1.87 1.87 1.86 1.86 1.85 1.85 1.84 1.30 1.29 1.27 1.27 1.27 1.26 1.08 1.06 1.06 1.06 1.04 1.04 1.04
4.156
1.00 1.07 1.02 2.34 1.09 1.07 4.18 1.00 1.17 4.24 1.09 1.13
f1 (ppm)

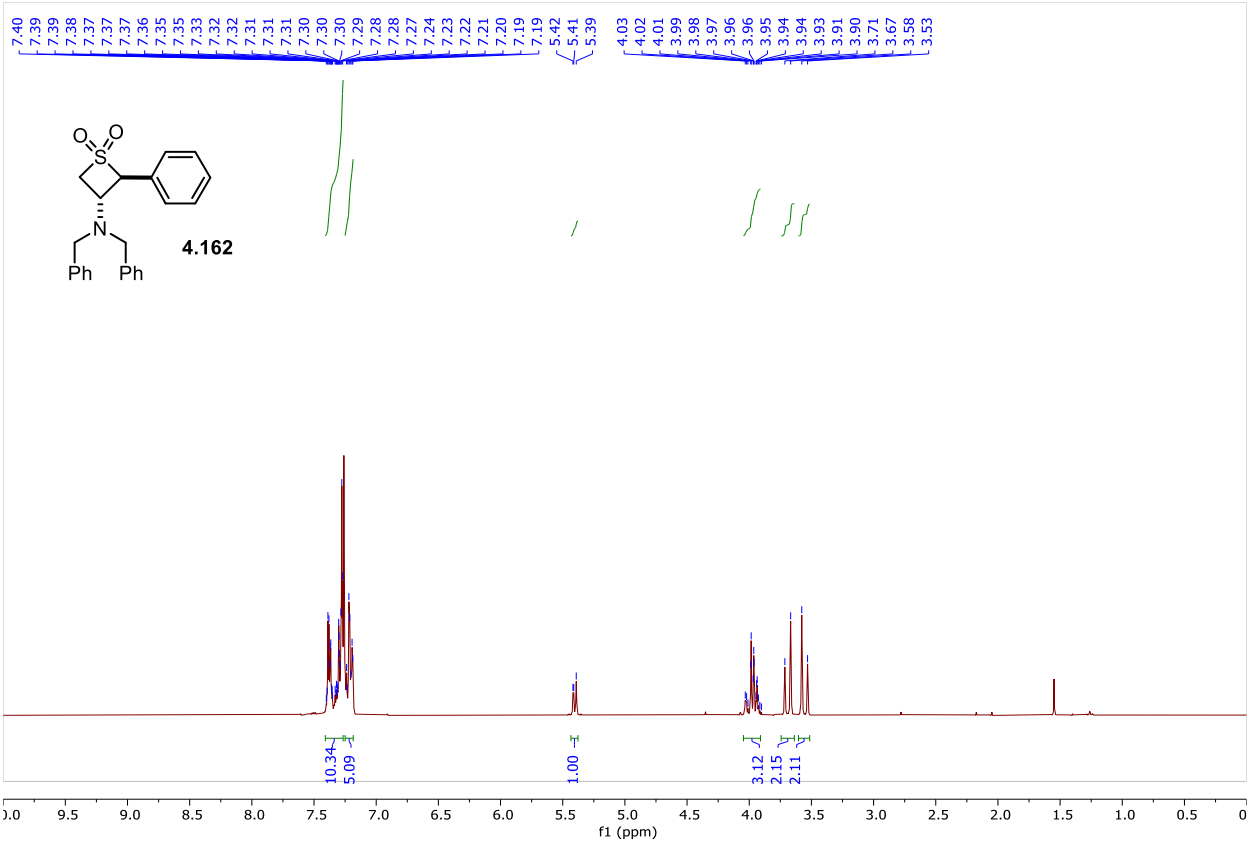

137.69 133.75 133.22 128.68 126.71 125.95 125.78 125.51 124.35 123.48 54.16 44.83 23.86 21.86 14.96
4.156
f1 (ppm)

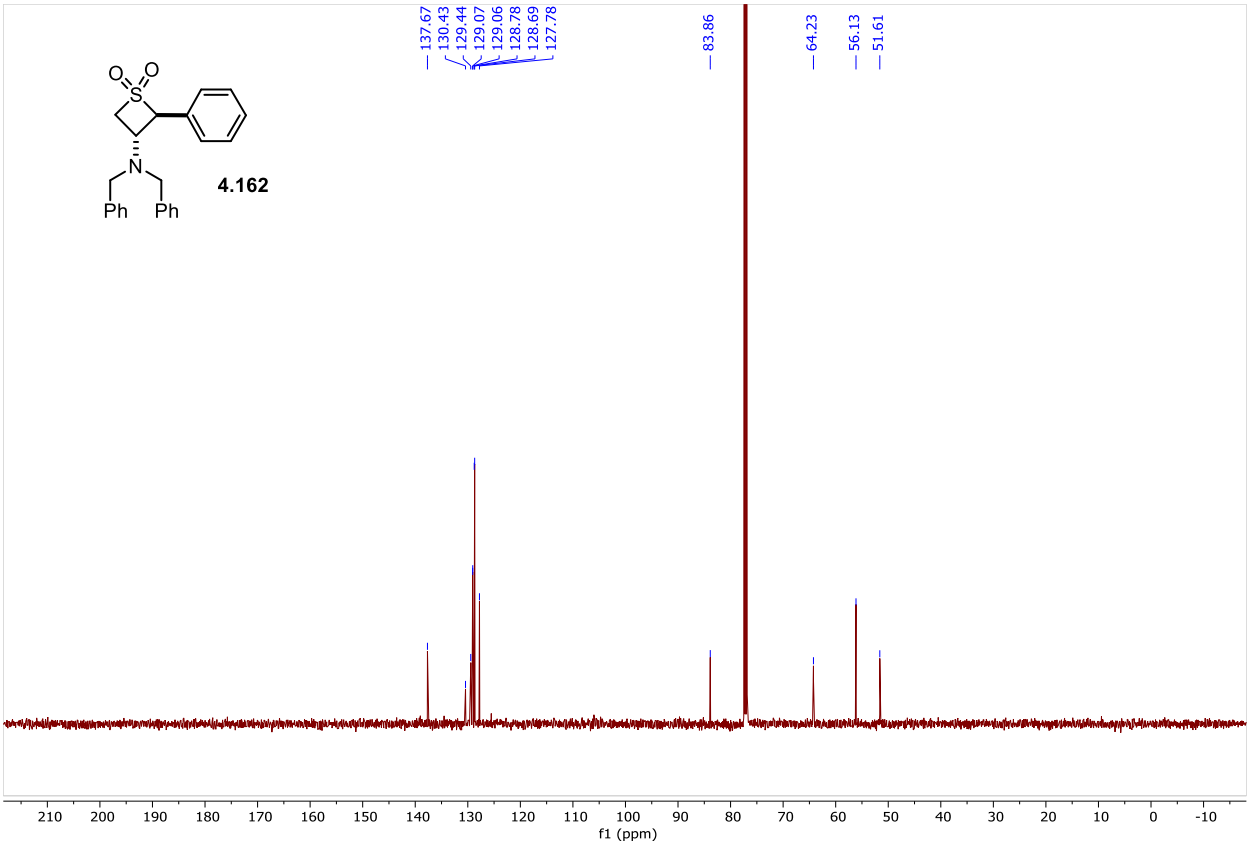

4.142
OMe
OMe
f1 (ppm)

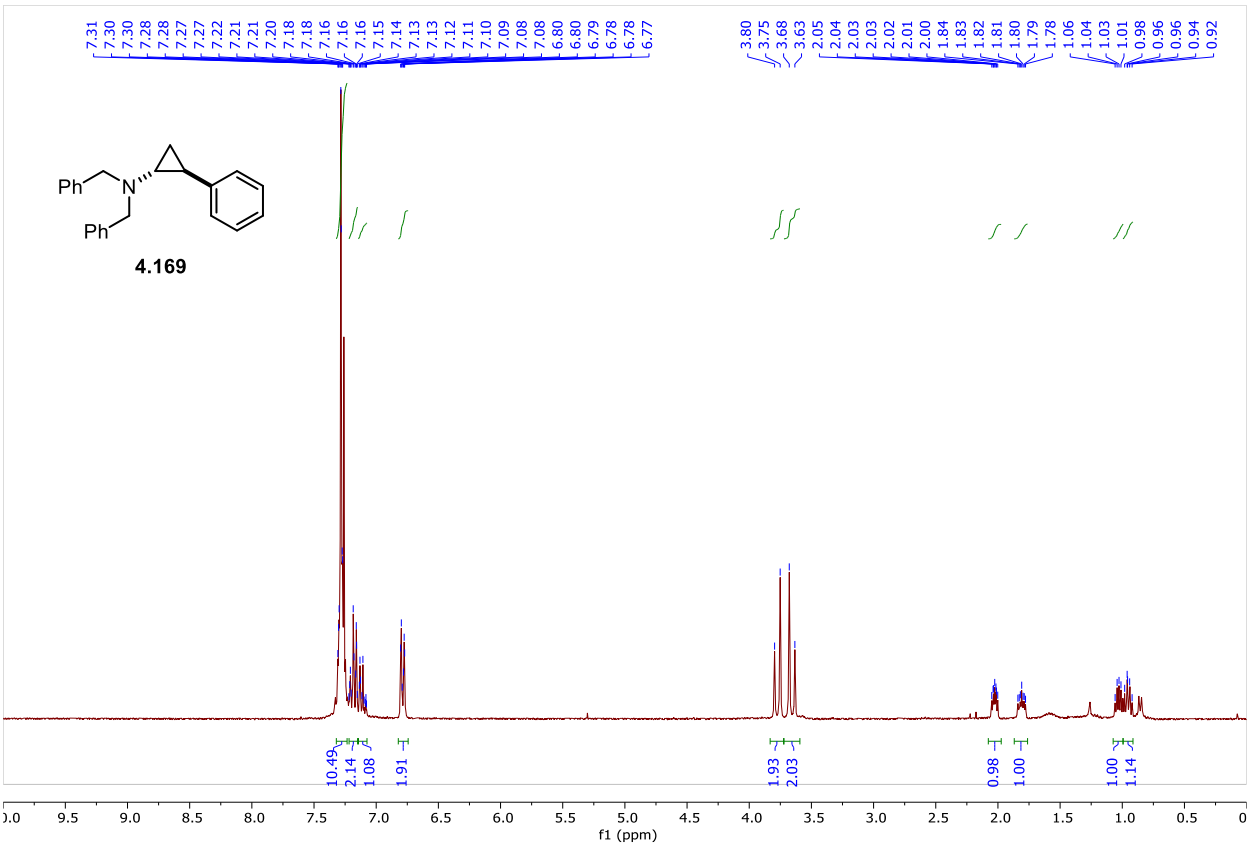

4.142
OMe
OMe
f1 (ppm)

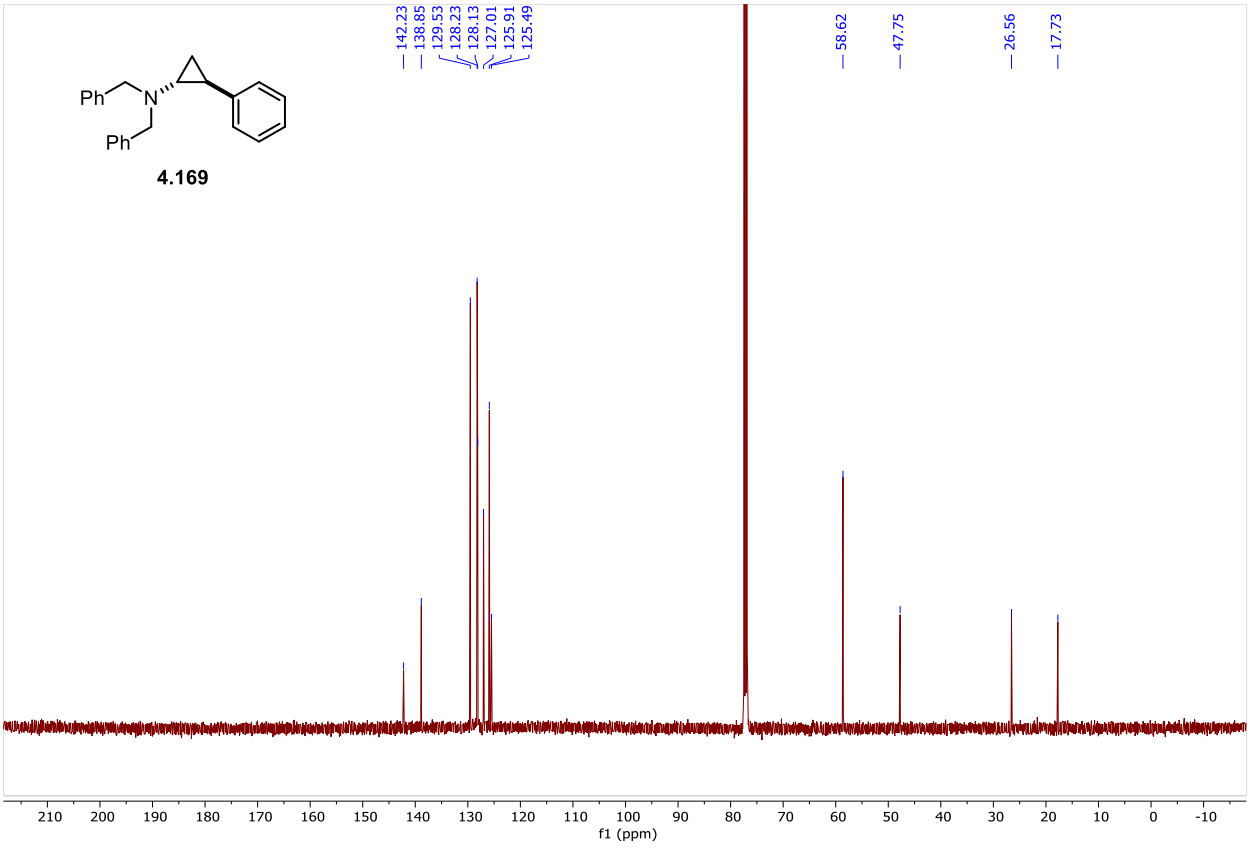

4.157
OMe
OMe
f1 (ppm)

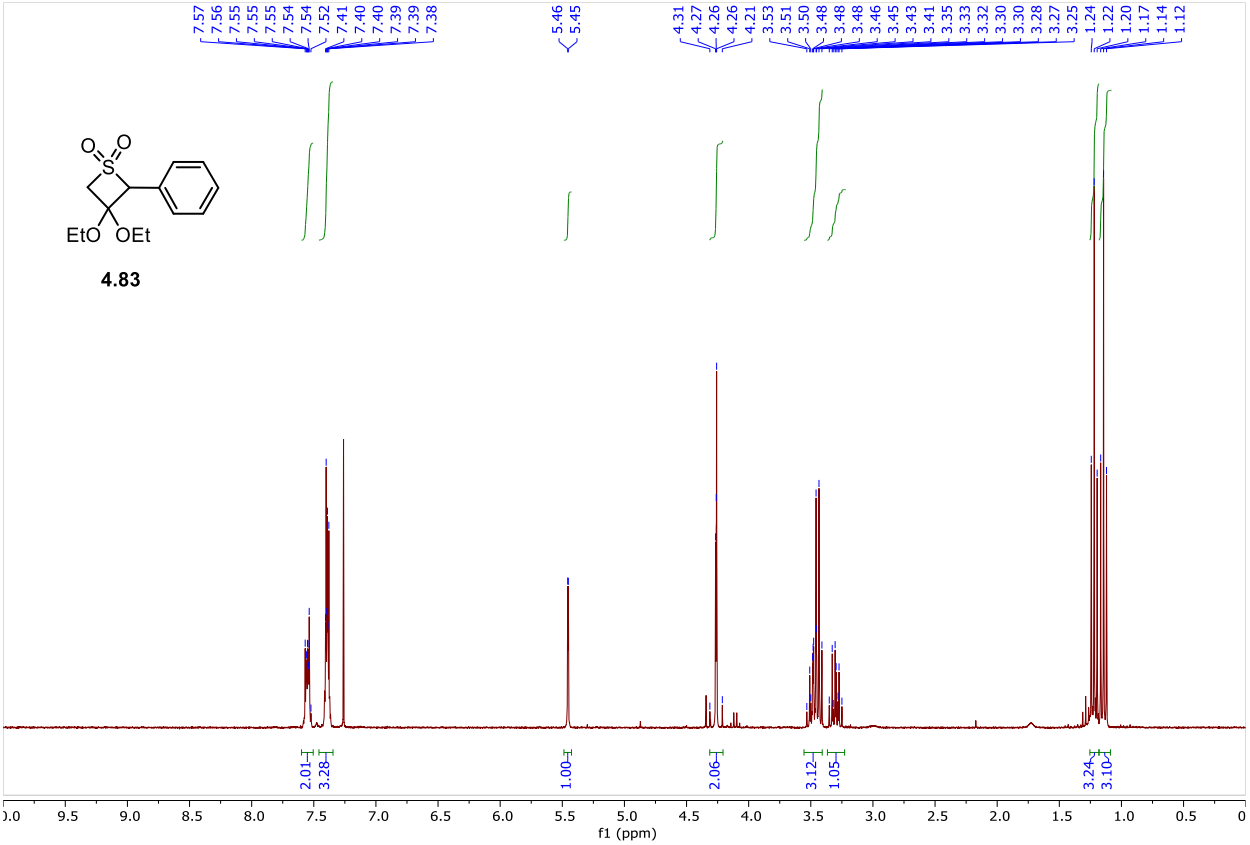

4.157
OMe
OMe
f1 (ppm)

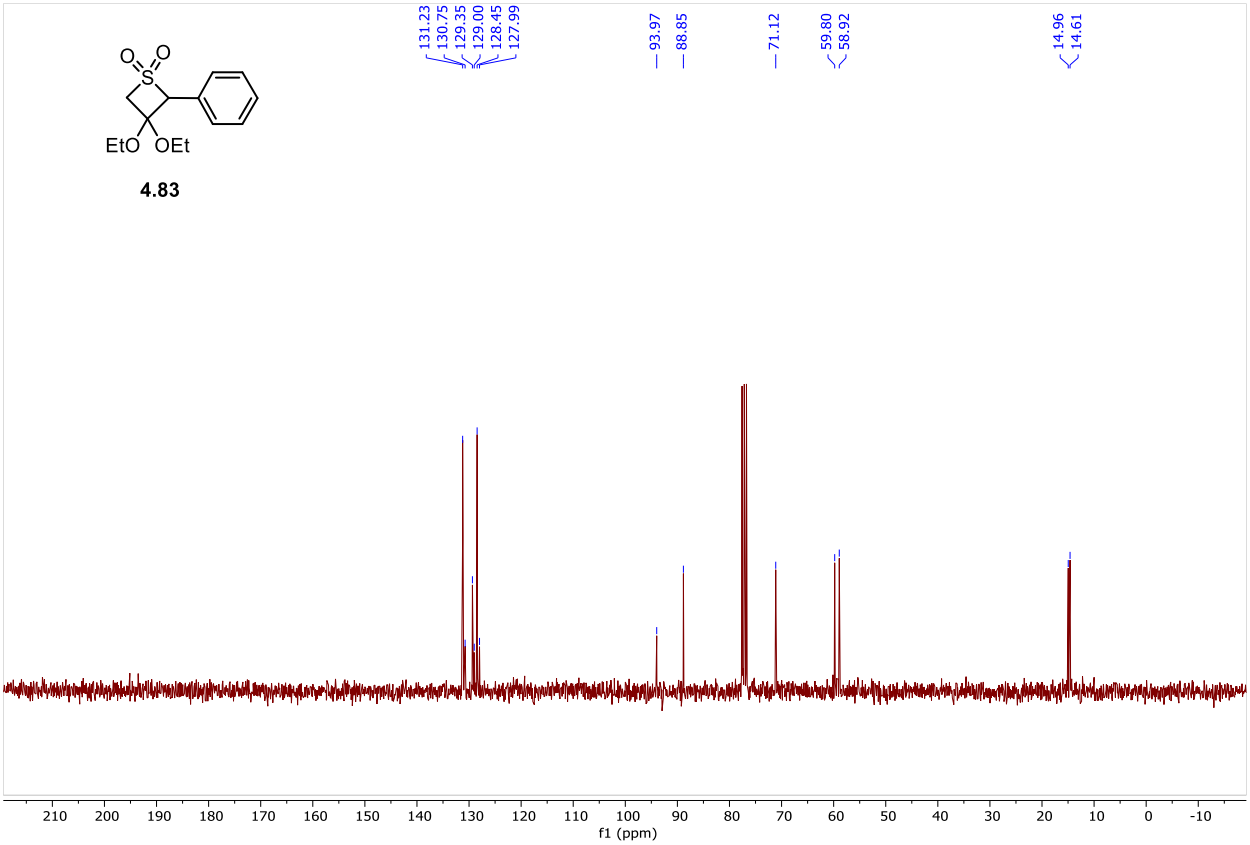

7.40 7.39 7.39 7.38 7.37 7.37 7.37 7.36 7.35 7.35 7.33 7.32 7.32 7.31 7.31 7.31 7.30 7.30 7.30 7.29 7.28 7.28 7.27 7.24 7.23 7.22 7.21 7.20 7.19 7.19 5.42 5.41 5.39 4.03 4.02 4.01 3.99 3.98 3.97 3.96 3.96 3.95 3.94 3.94 3.93 3.91 3.90 3.71 3.67 3.58 3.53
4.162
Ph Ph
10.34 5.09 1.00 3.12 2.15 2.11
f1 (ppm)

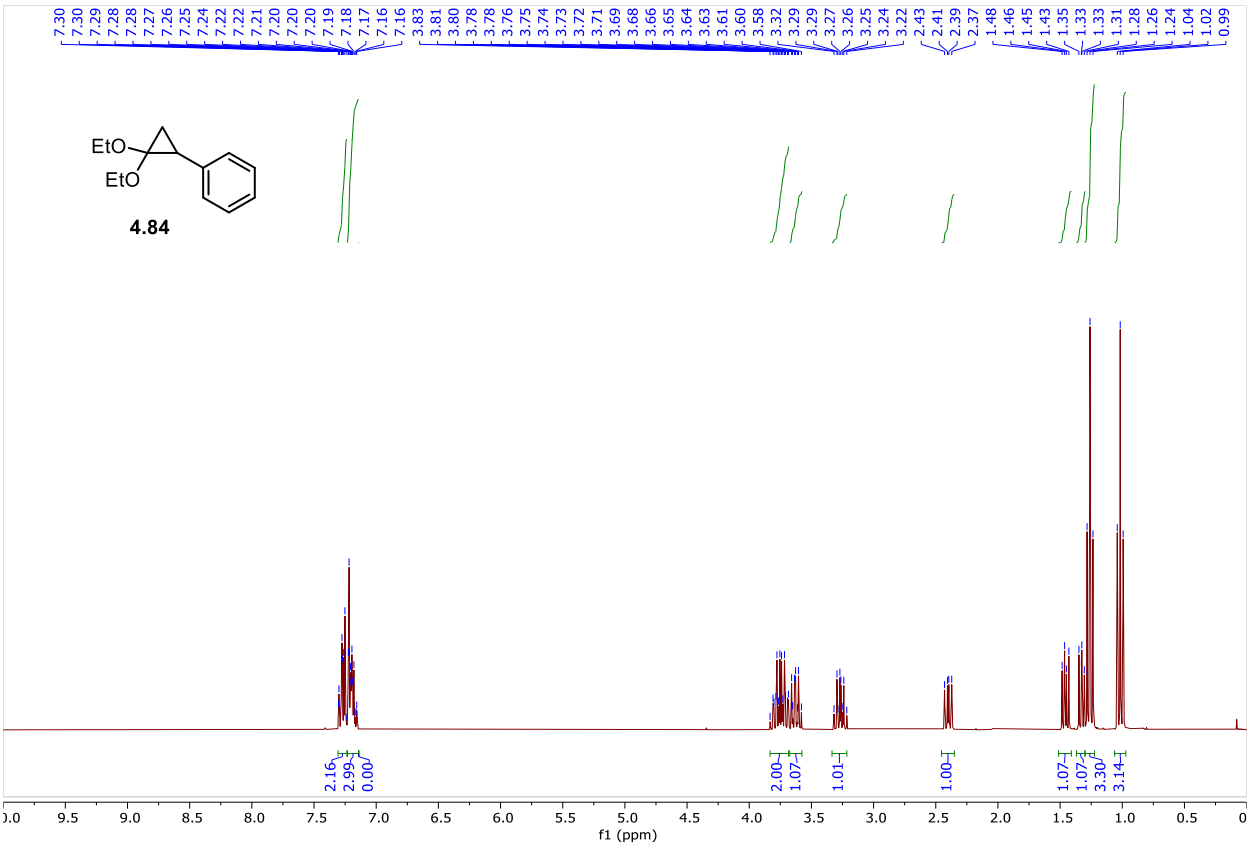

137.67 130.43 129.44 129.07 129.06 128.78 128.69 127.78 83.86 64.23 56.13 51.61
4.162
Ph Ph
f1 (ppm)

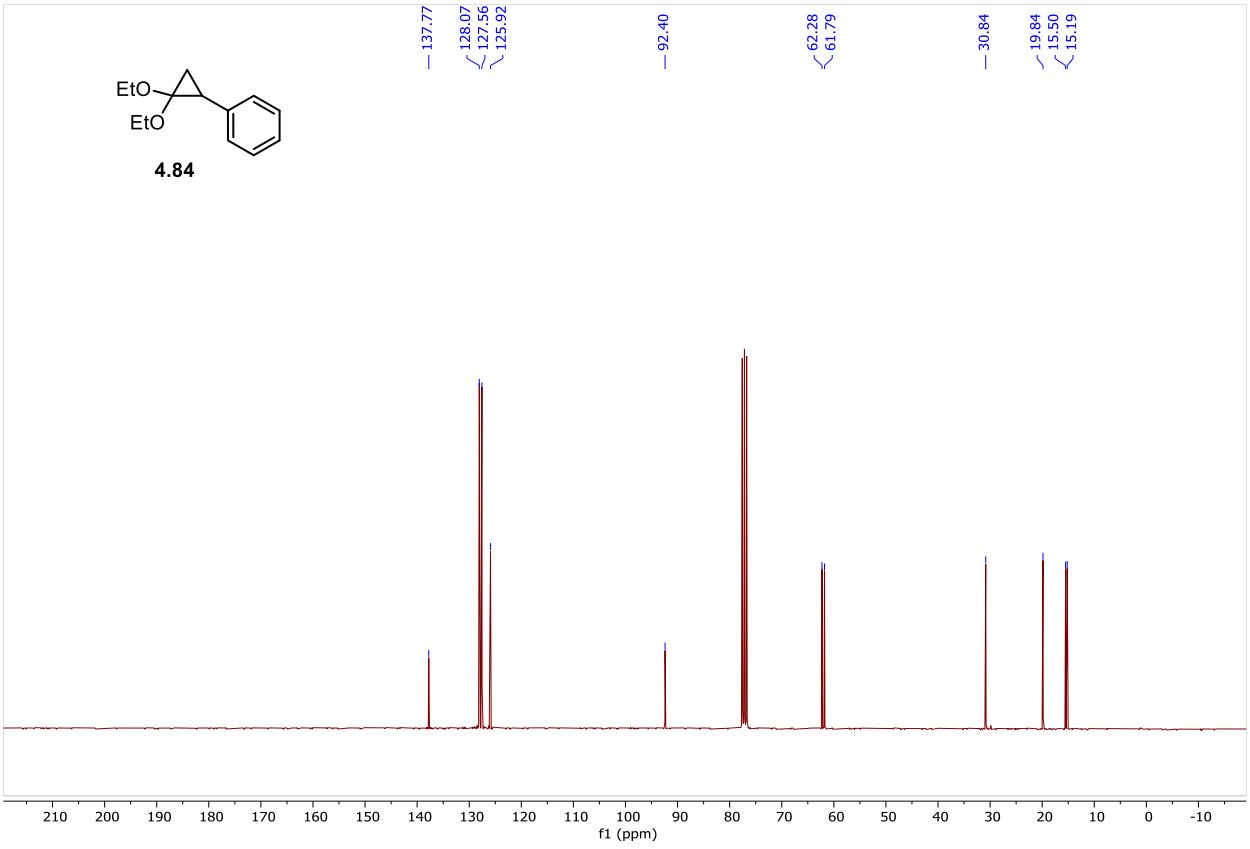

Ph
N
Ph
4.169
f1 (ppm)

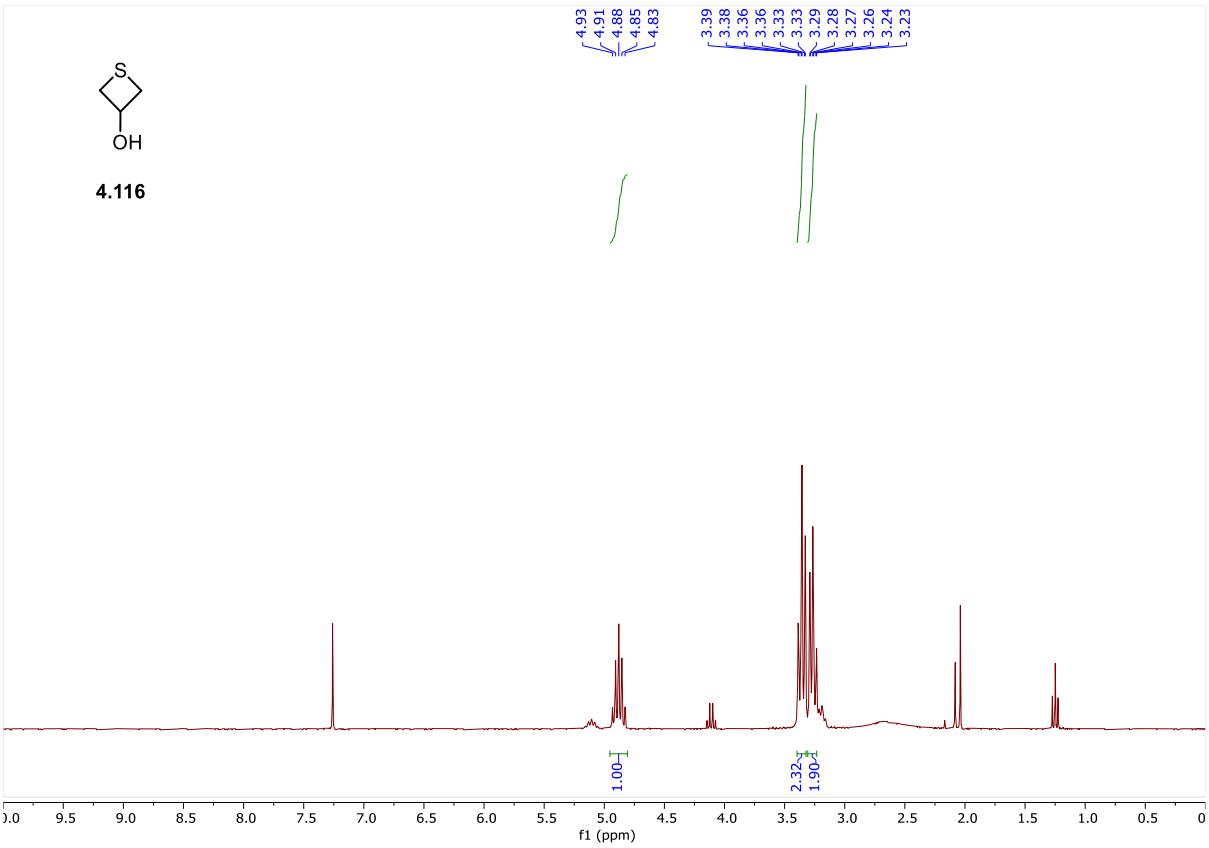

Ph
N
Ph
4.169
f1 (ppm)

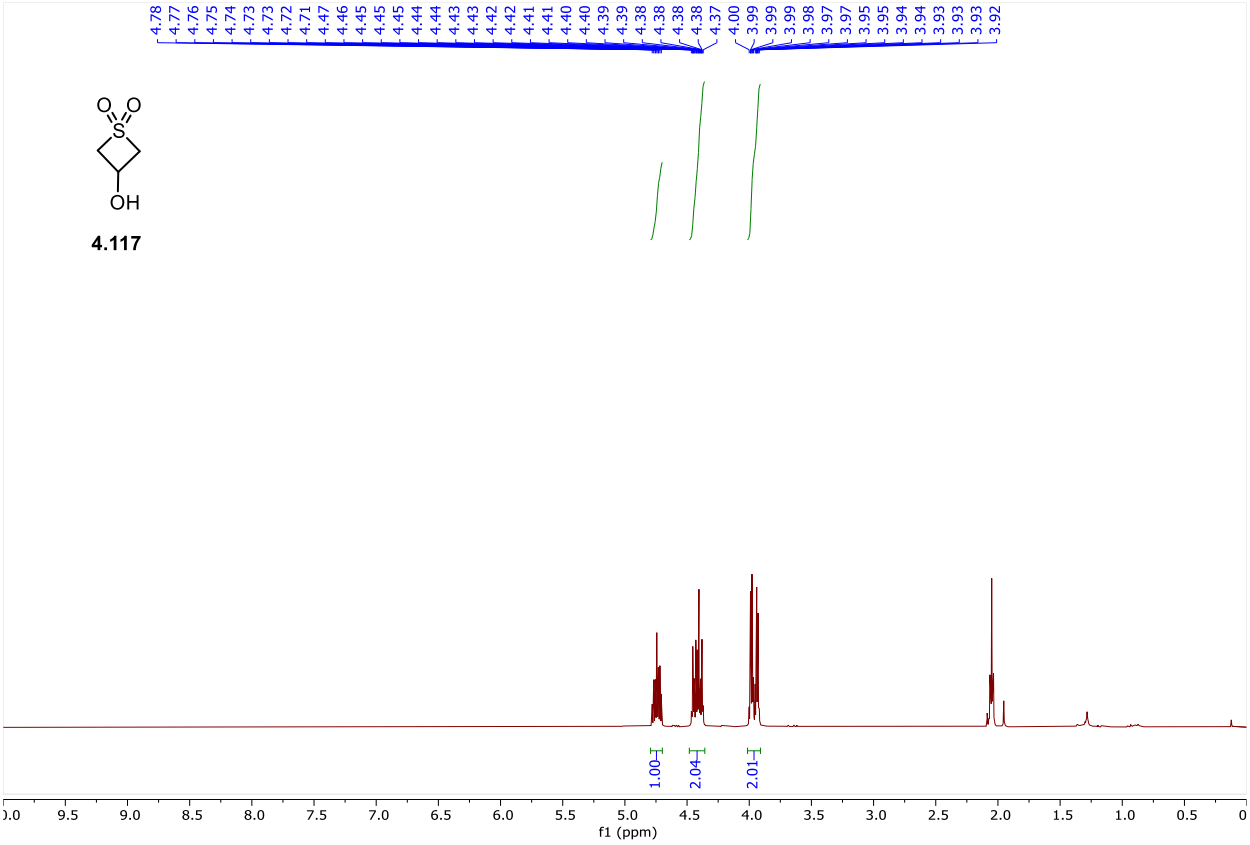

7.57 7.56 7.55 7.55 7.55 7.54 7.54 7.52 7.41 7.40 7.40 7.39 7.39 7.38
5.46 5.45
4.31 4.27 4.26 4.26 4.21
3.53 3.51 3.50 3.48 3.48 3.46 3.45 3.43 3.41 3.35 3.33 3.32 3.30 3.30 3.28 3.27 3.25
1.24 1.22 1.20 1.17 1.14 1.12
EtO OEt
4.83
2.01 3.28 1.00 2.06 3.12 1.05 3.24 3.10
f1 (ppm)

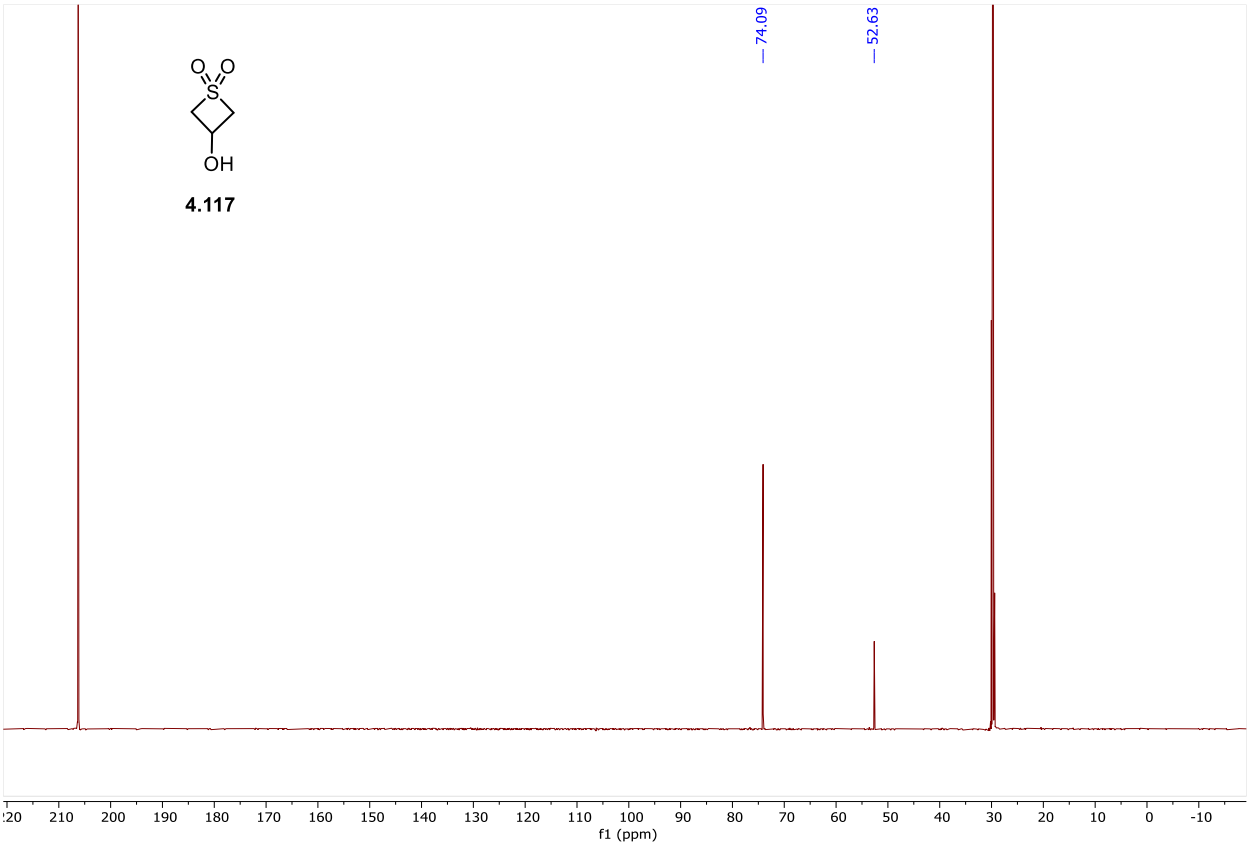

131.23 130.75 129.35 129.00 128.45 127.99
93.97 88.85 71.12 59.80 58.92 14.96 14.61
EtO OEt
4.83
f1 (ppm)

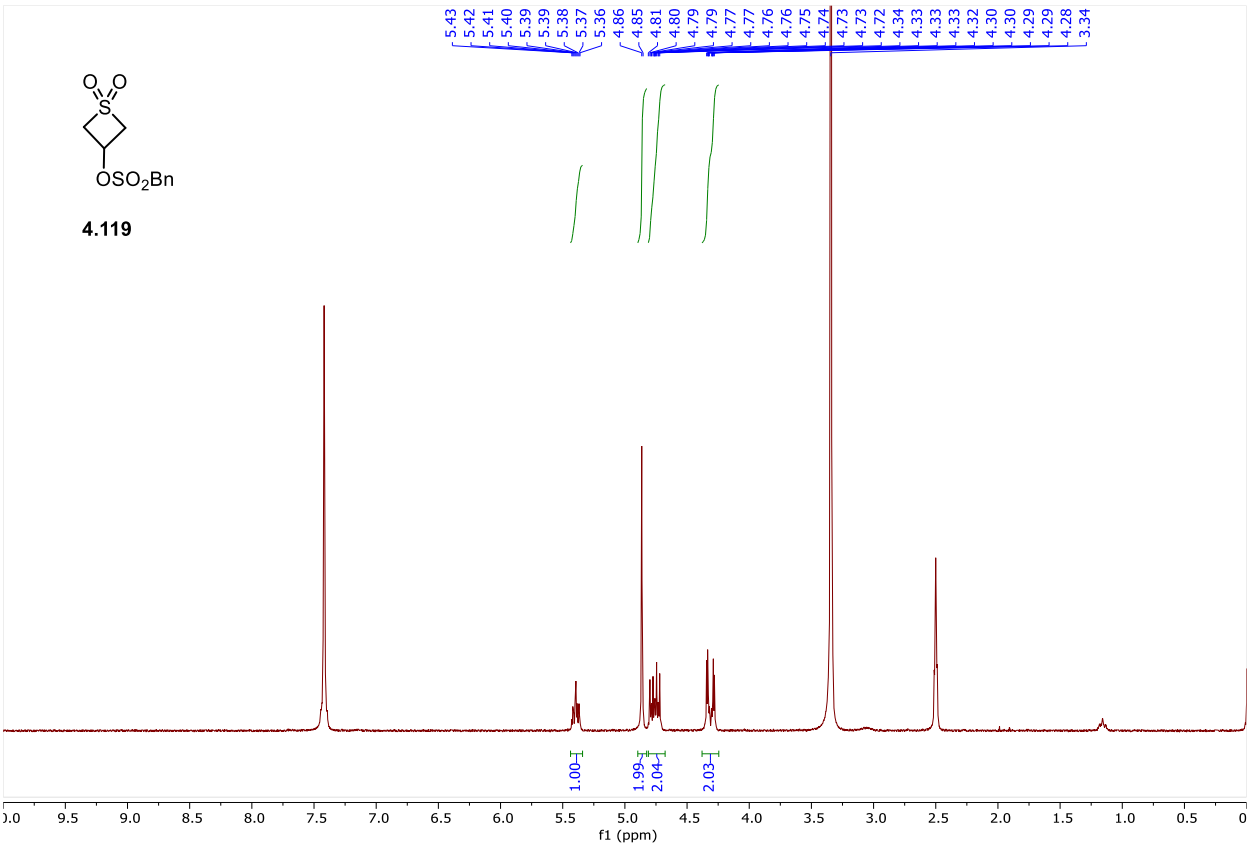

EtO
EtO
4.84
f1 (ppm)

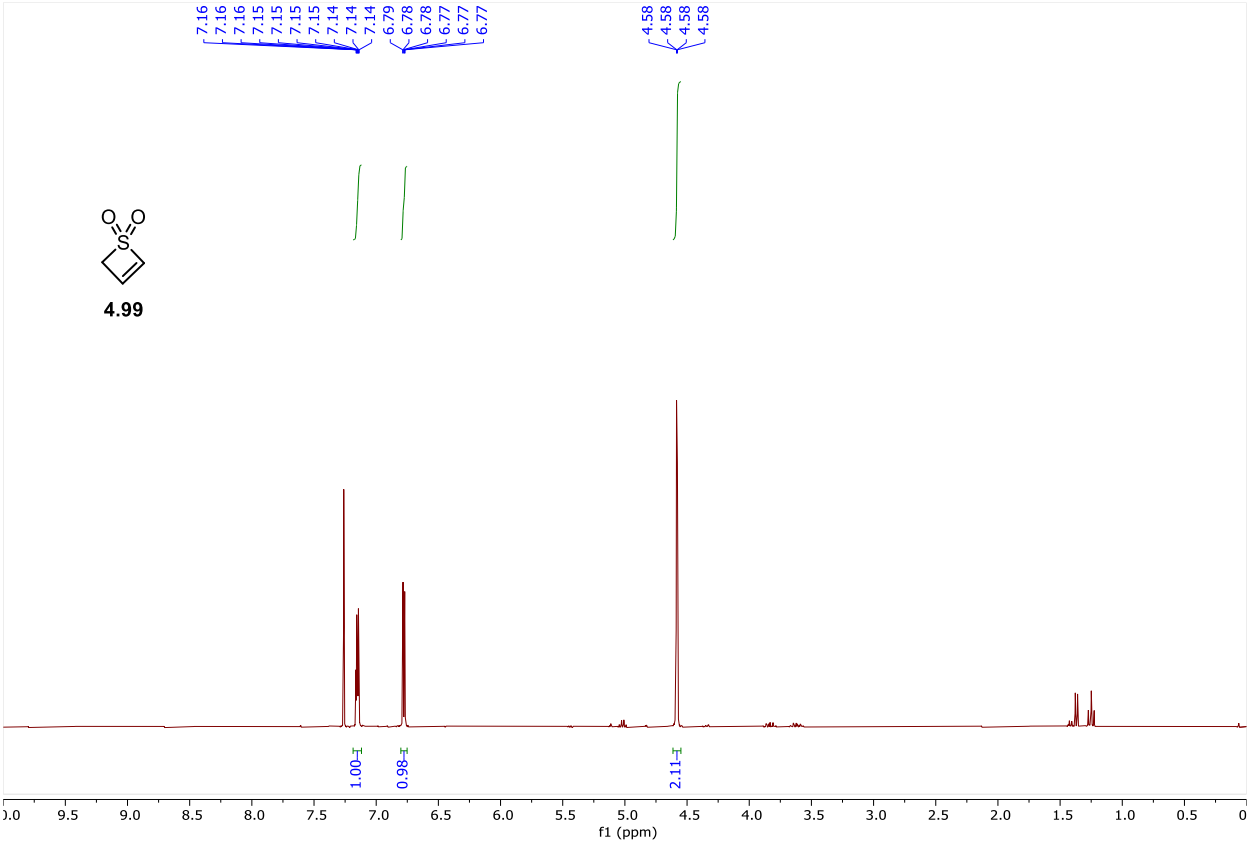

EtO
EtO
4.84
f1 (ppm)


S
OH
4.116
4.93
4.91
4.88
4.85
4.83
3.39
3.38
3.36
3.36
3.33
3.33
3.29
3.28
3.27
3.26
3.24
3.23
1.00
2.32
1.90
f1 (ppm)

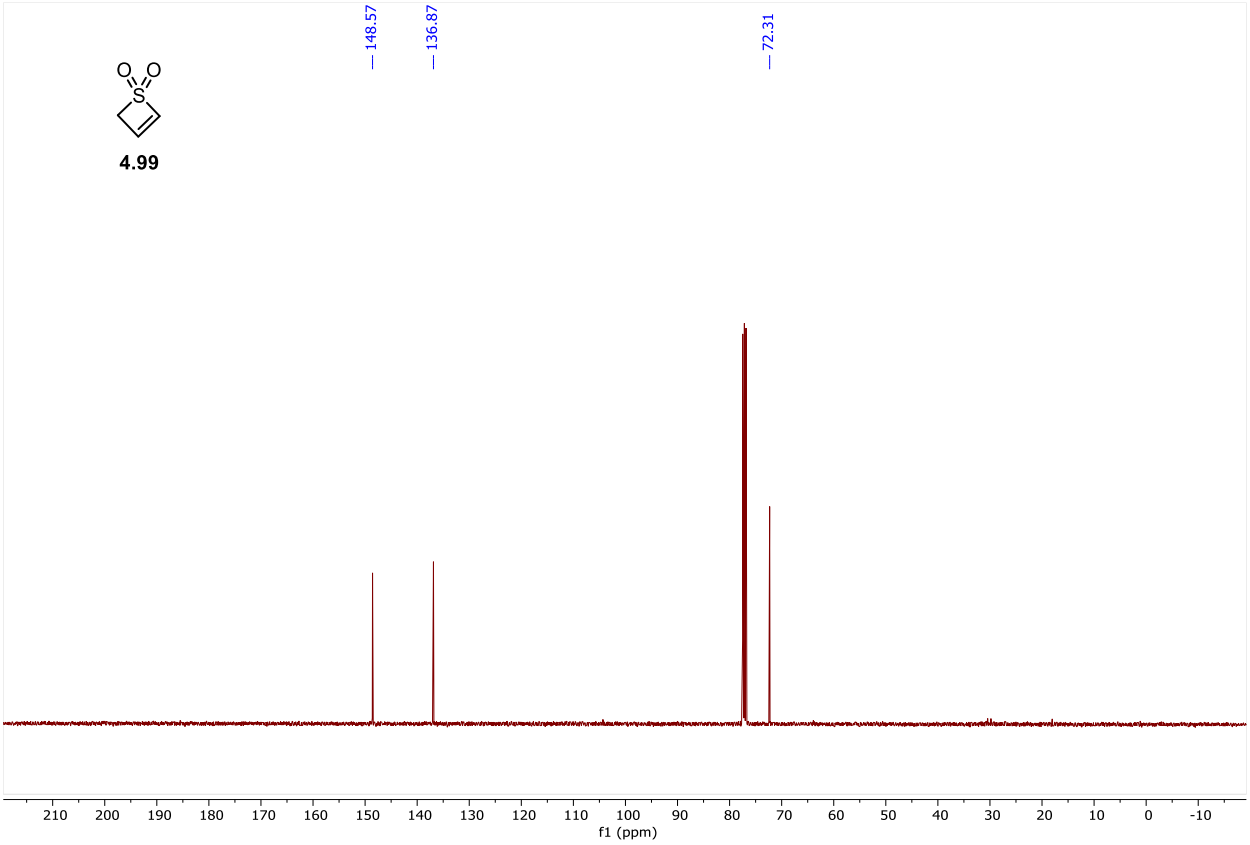

4.78 4.77 4.76 4.75 4.74 4.73 4.73 4.72 4.71 4.47 4.46 4.45 4.45 4.45 4.44 4.44 4.43 4.43 4.42 4.42 4.41 4.41 4.40 4.40 4.39 4.39 4.38 4.38 4.38 4.38 4.37 4.00 3.99 3.99 3.99 3.98 3.97 3.97 3.95 3.95 3.94 3.94 3.93 3.93 3.93 3.92
O
O
S
OH
4.117
1.00
2.04
2.01
f1 (ppm)


74.09
52.63
O
O
S
OH
4.117
f1 (ppm)

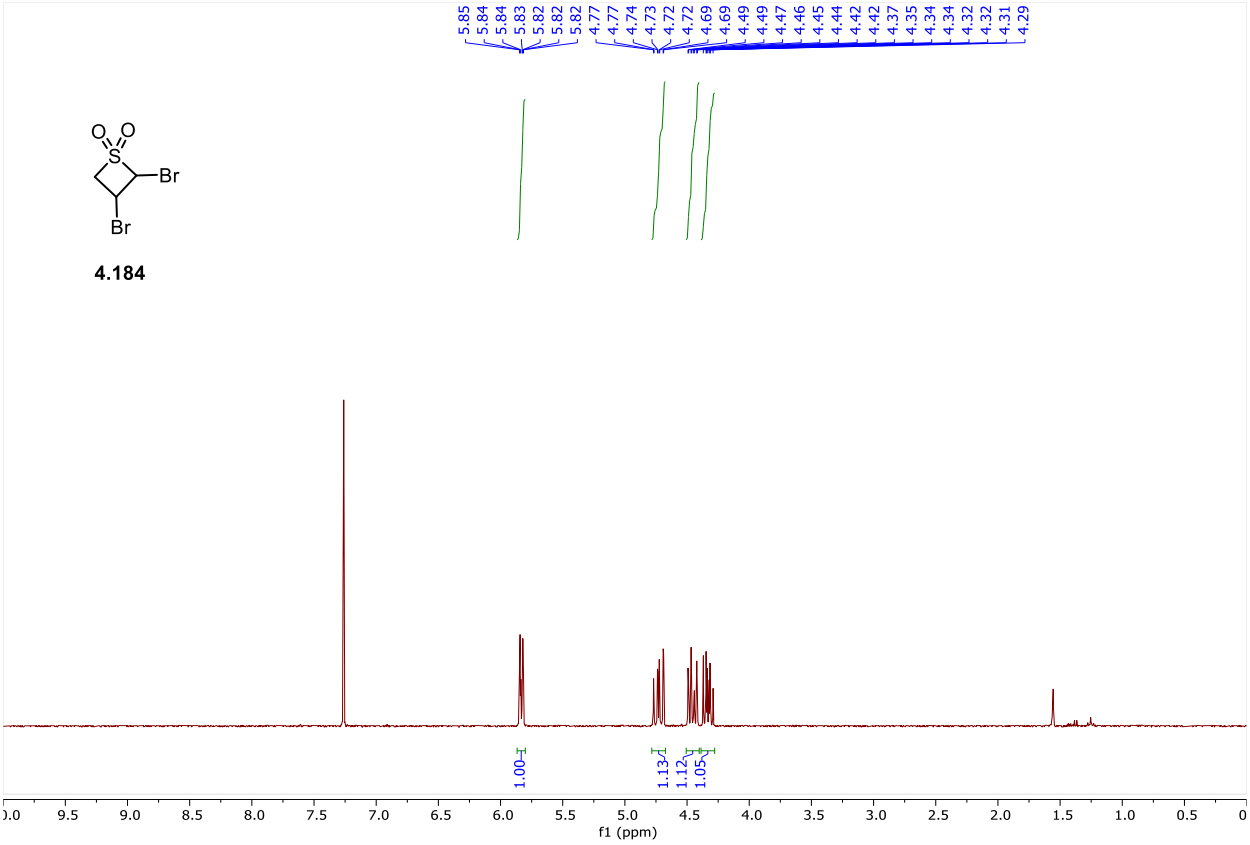

5.43
5.42
5.41
5.40
5.39
5.39
5.38
5.37
5.36
4.86
4.85
4.81
4.80
4.79
4.79
4.77
4.77
4.76
4.76
4.75
4.74
4.73
4.73
4.72
4.34
4.33
4.33
4.32
4.30
4.30
4.29
4.29
4.28
3.34
OSO2Bn
4.119
1.00
1.99
2.04
2.03
f1 (ppm)

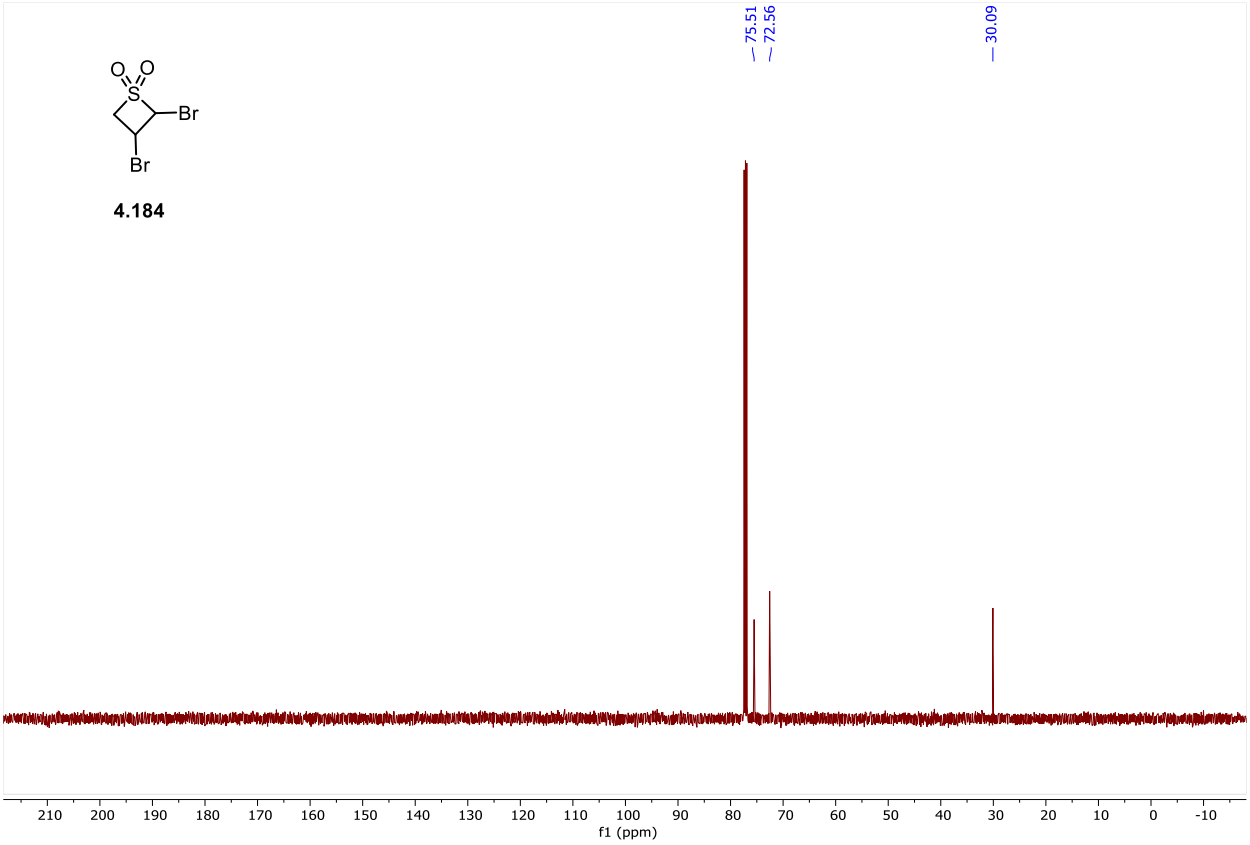

7.16
7.16
7.16
7.15
7.15
7.15
7.15
7.14
7.14
7.14
6.79
6.78
6.78
6.77
6.77
6.77
4.58
4.58
4.58
4.58
1.00
0.98
2.11
f1 (ppm)

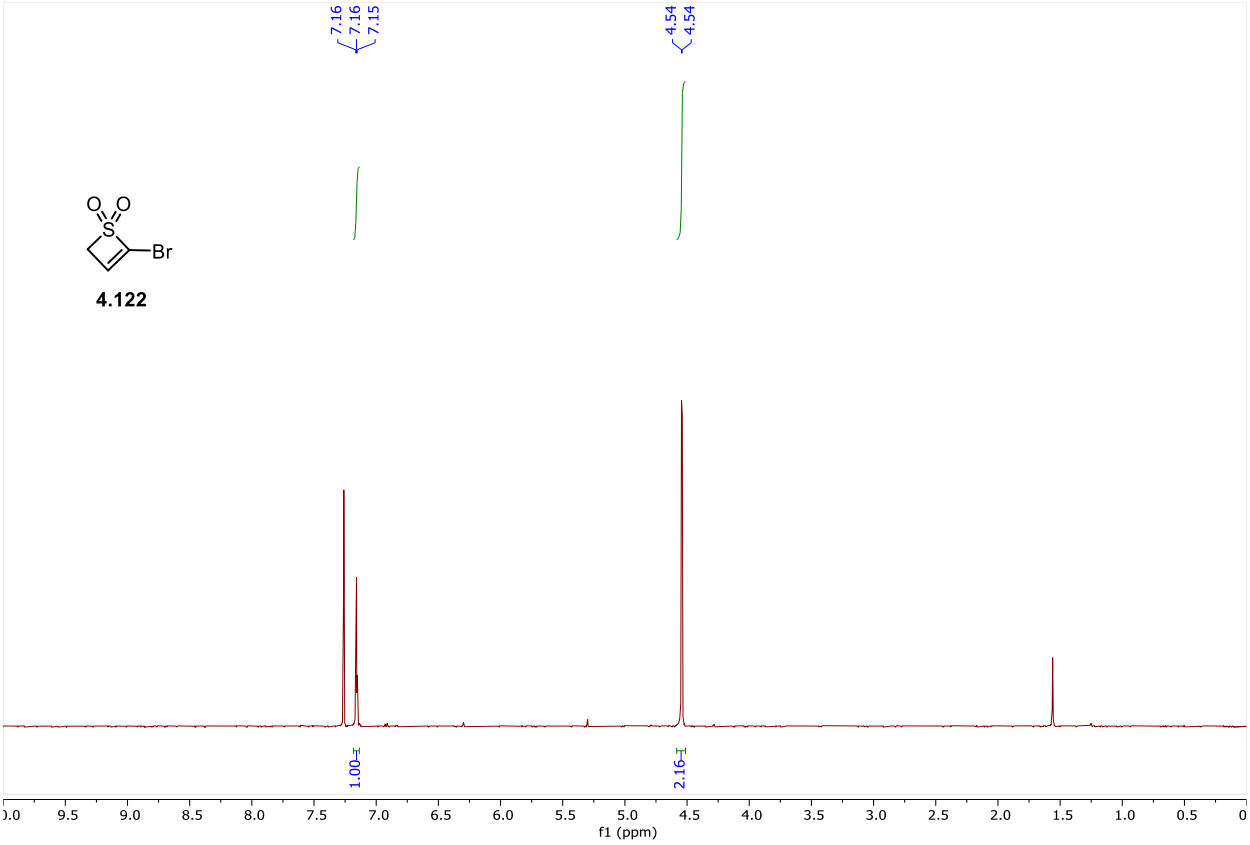
4.99

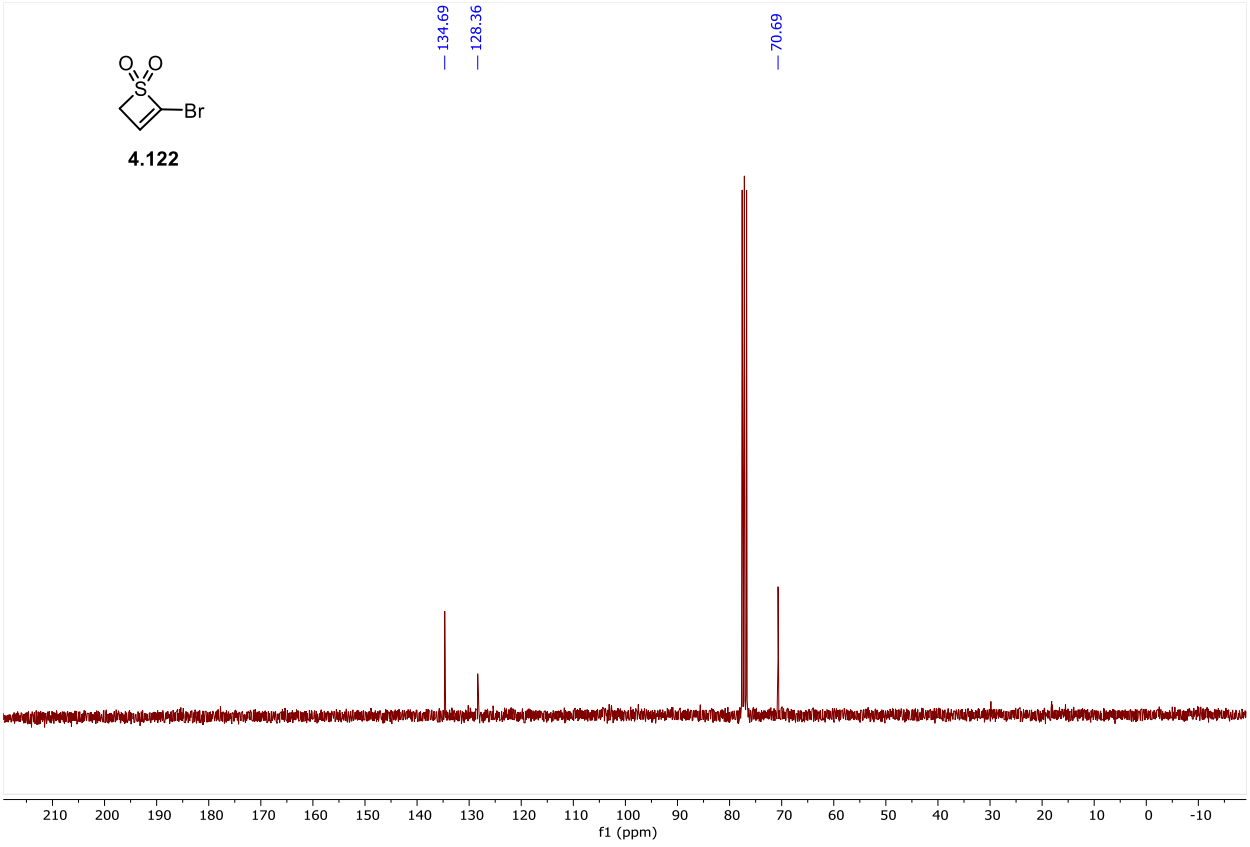

148.57
136.87
72.31
f1 (ppm)

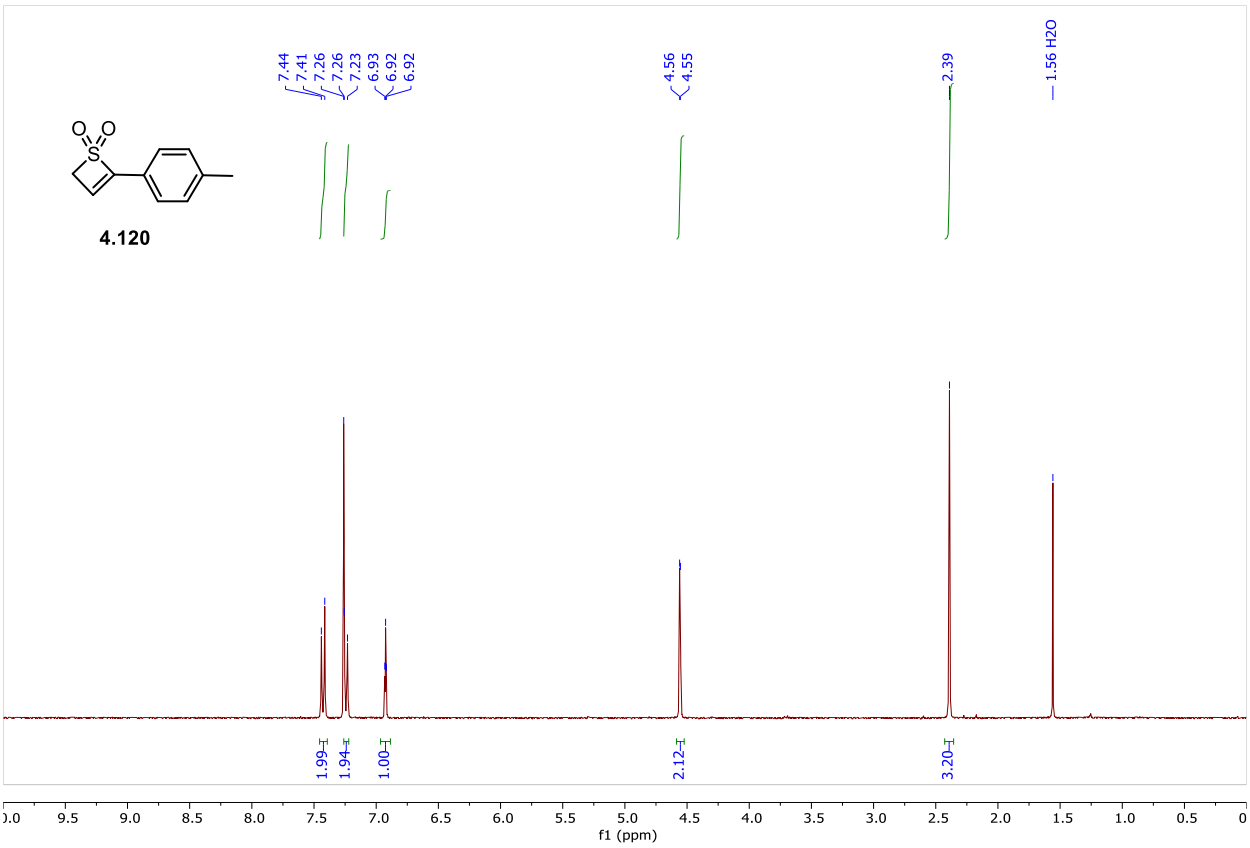
4.99

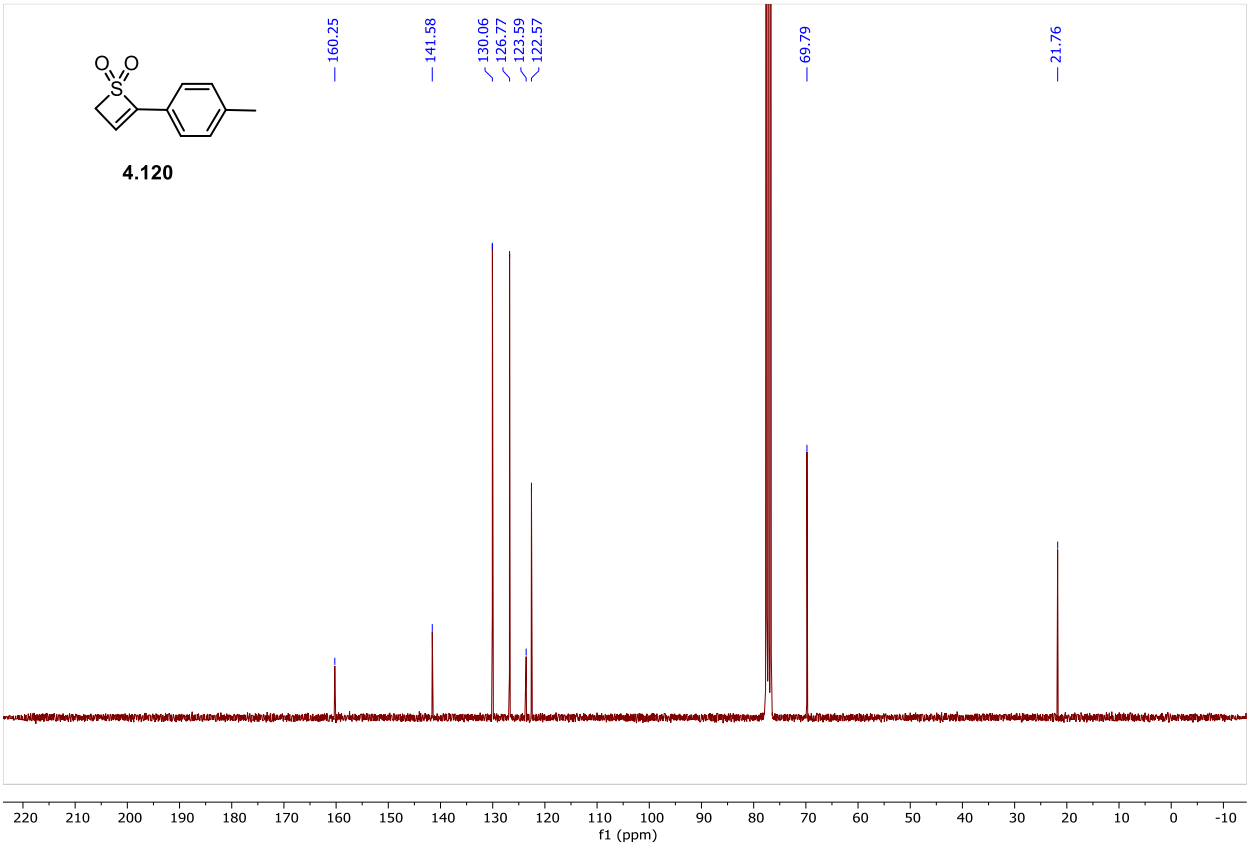

5.85
5.84
5.84
5.83
5.82
5.82
5.82
4.77
4.77
4.74
4.73
4.72
4.72
4.69
4.69
4.49
4.49
4.47
4.46
4.45
4.44
4.42
4.42
4.37
4.35
4.34
4.34
4.32
4.32
4.31
4.29
O
O
S
Br
Br
4.184
1.00
1.13
1.12
1.05
f1 (ppm)

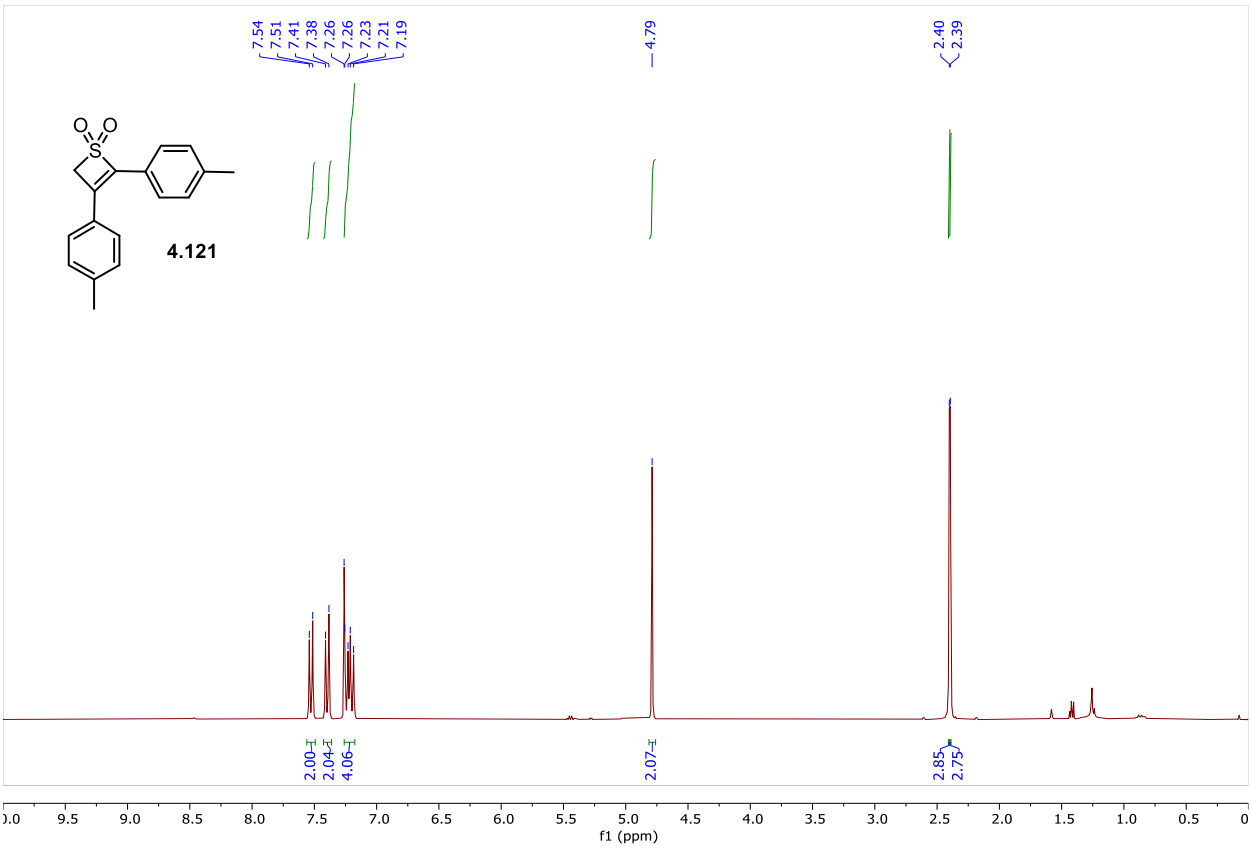

75.51
72.56
30.09
O
O
S
Br
Br
4.184
f1 (ppm)

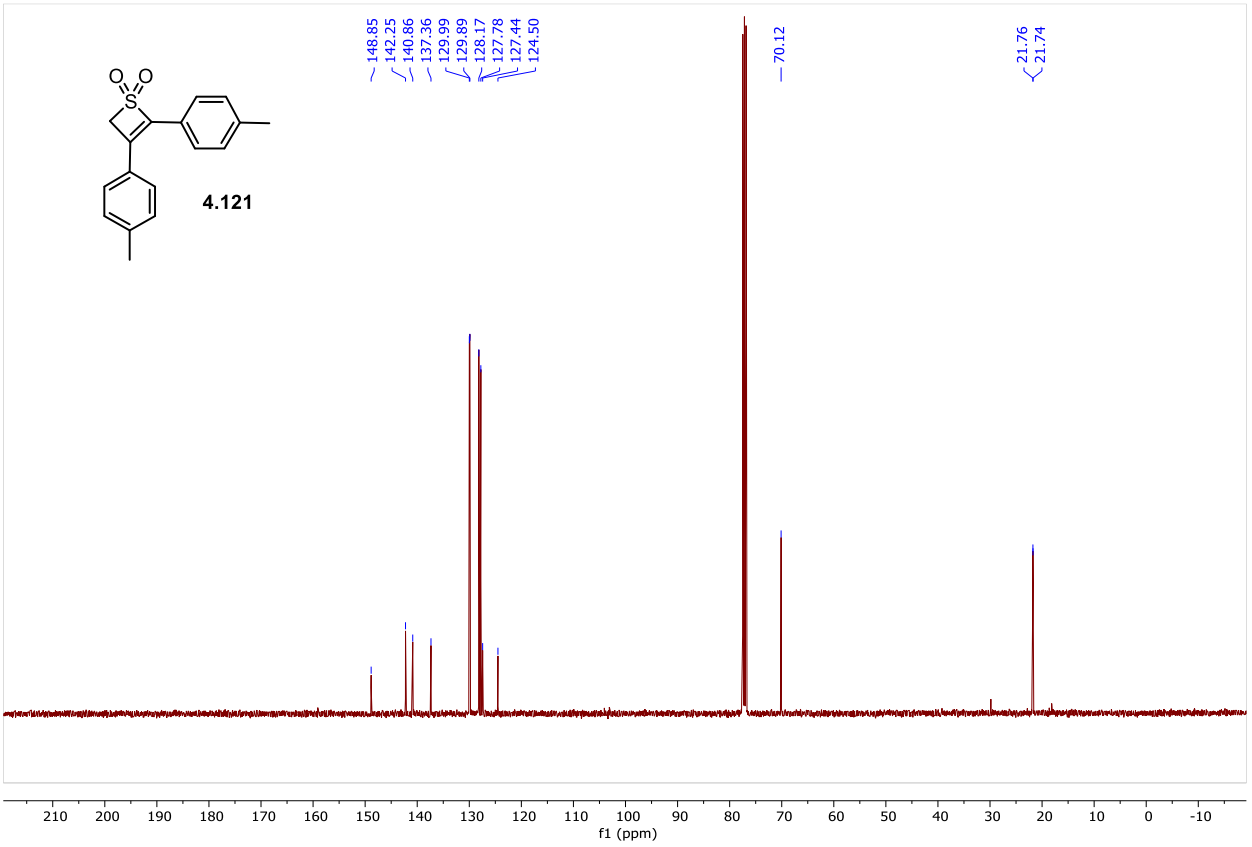

7.16
7.16
7.15
4.54
4.54
Br
4.122
1.00
2.16
f1 (ppm)

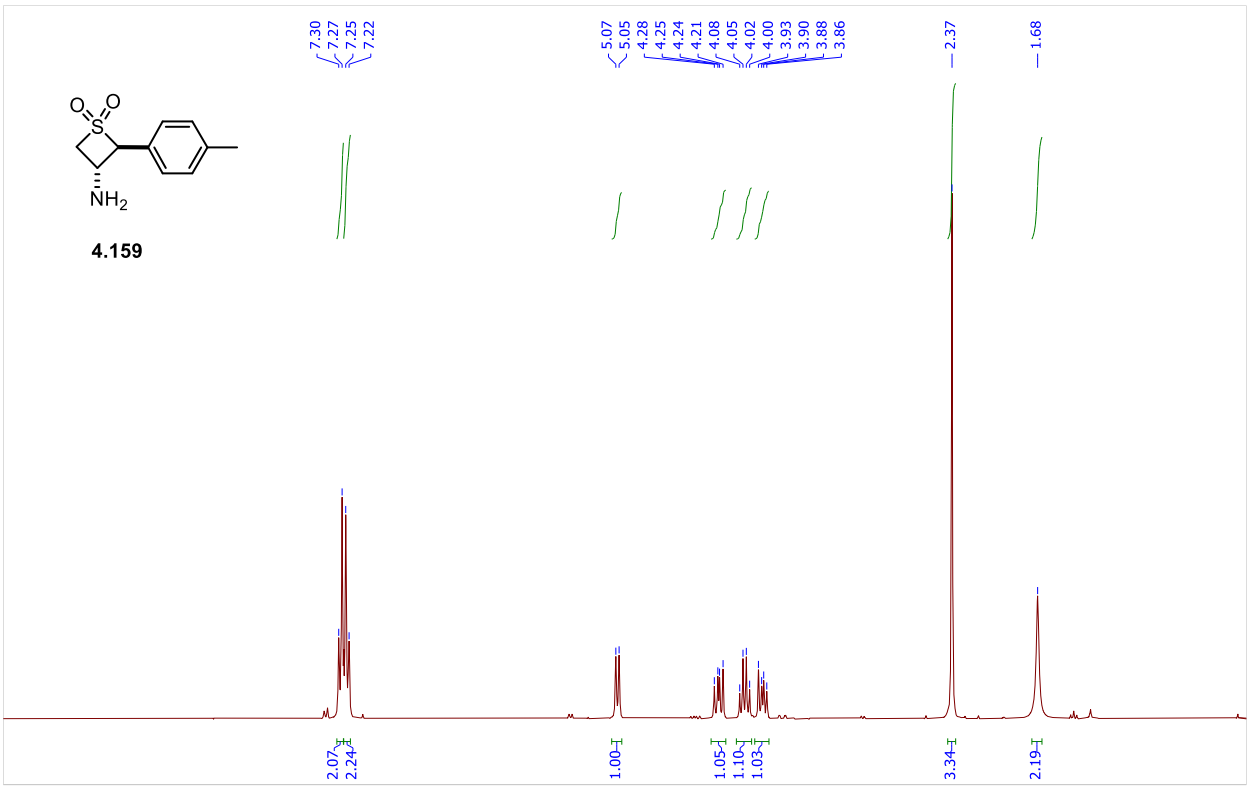

134.69
128.36
70.69
Br
4.122
f1 (ppm)

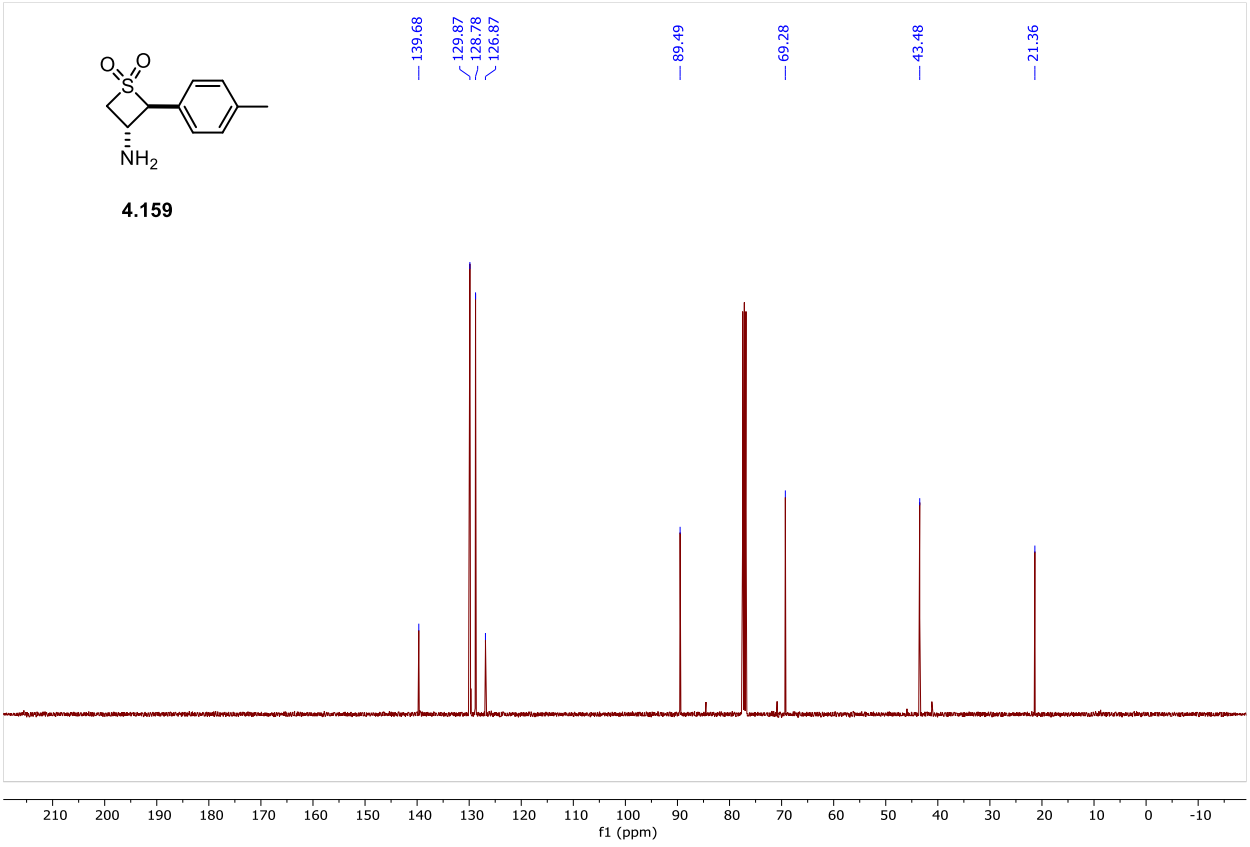

7.44
7.41
7.26
7.26
7.23
6.93
6.92
6.92
4.56
4.55
2.39
1.56 H2O
4.120
1.99
1.94
1.00
2.12
3.20
f1 (ppm)

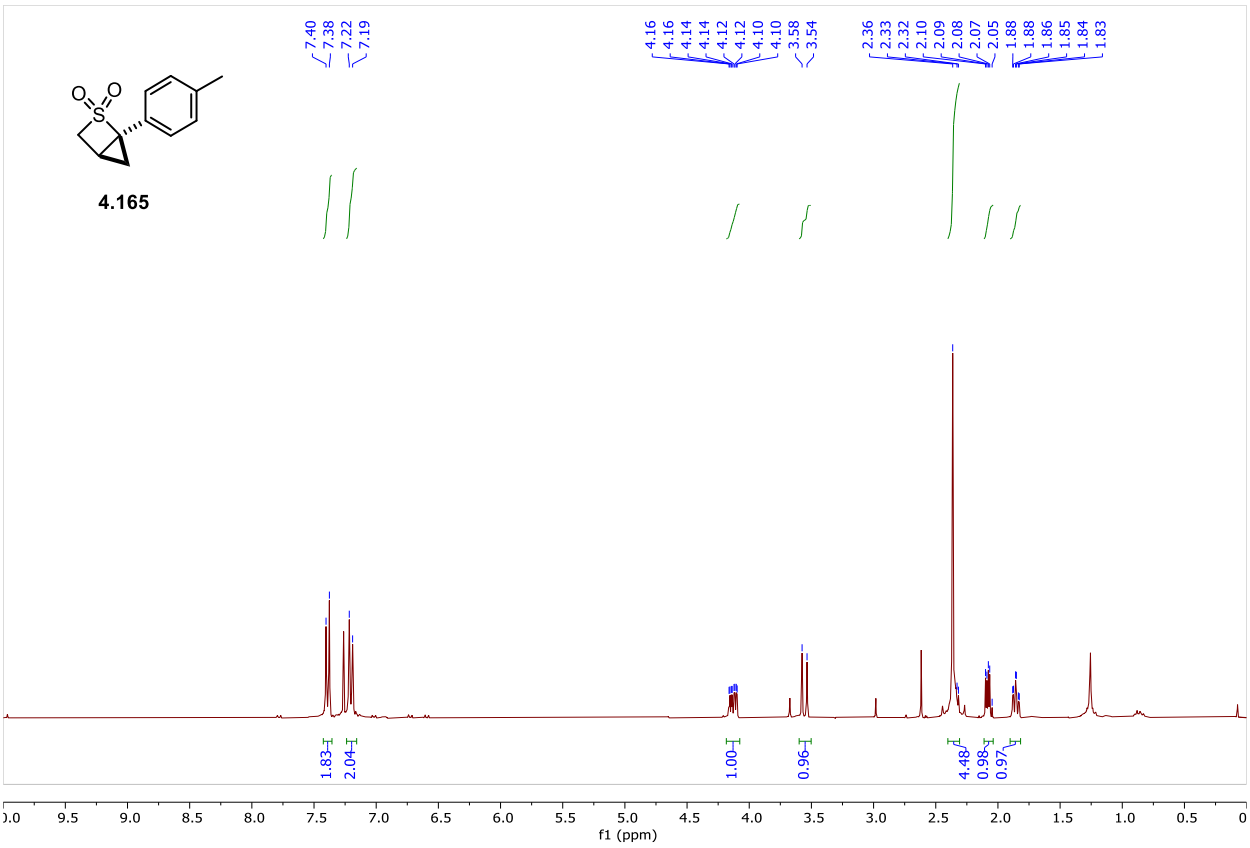

160.25
141.58
130.06
126.77
123.59
122.57
69.79
21.76
4.120
f1 (ppm)

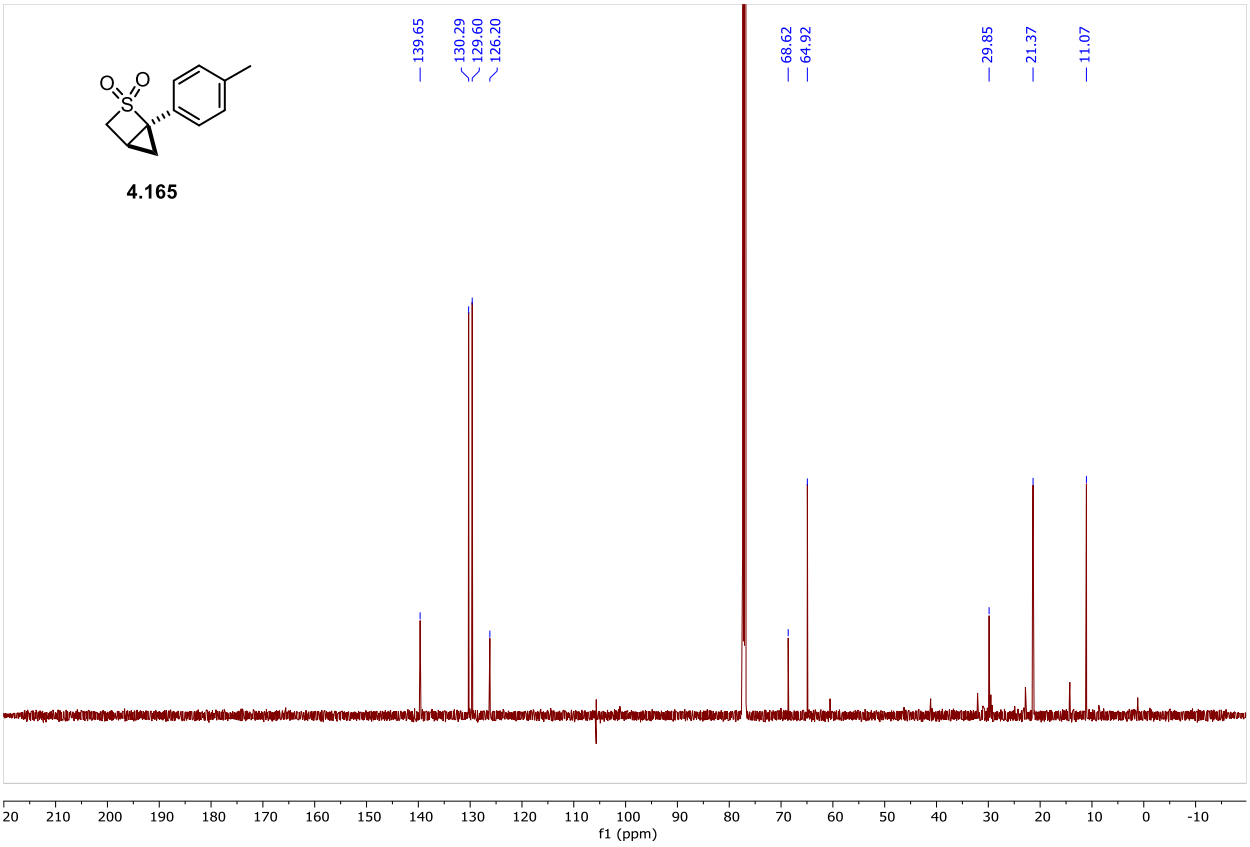

7.54
7.51
7.41
7.38
7.26
7.26
7.23
7.21
7.19
4.79
2.40
2.39
4.121
2.00
2.04
4.06
2.07
2.85
2.75
f1 (ppm)

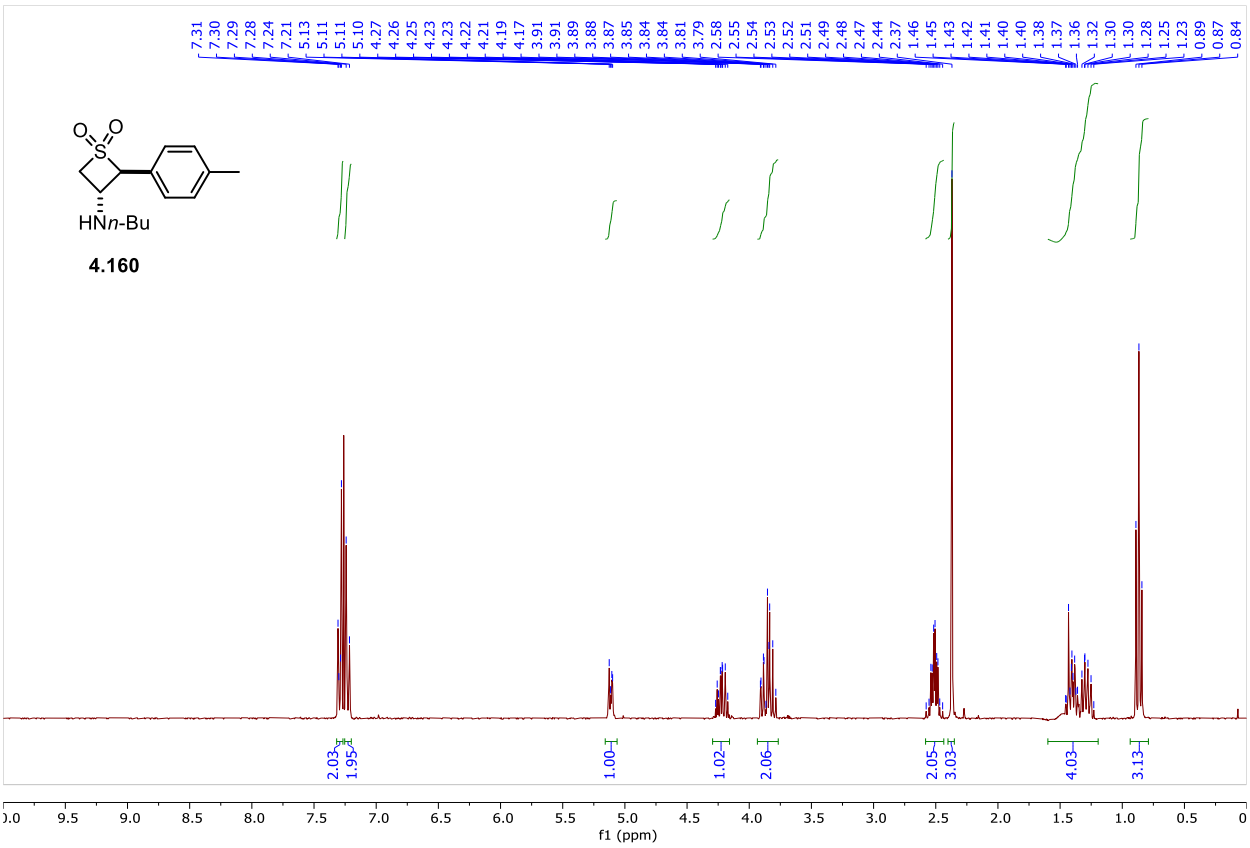

148.85
142.25
140.86
137.36
129.99
129.89
128.17
127.78
127.44
124.50
70.12
21.76
21.74
4.121
f1 (ppm)

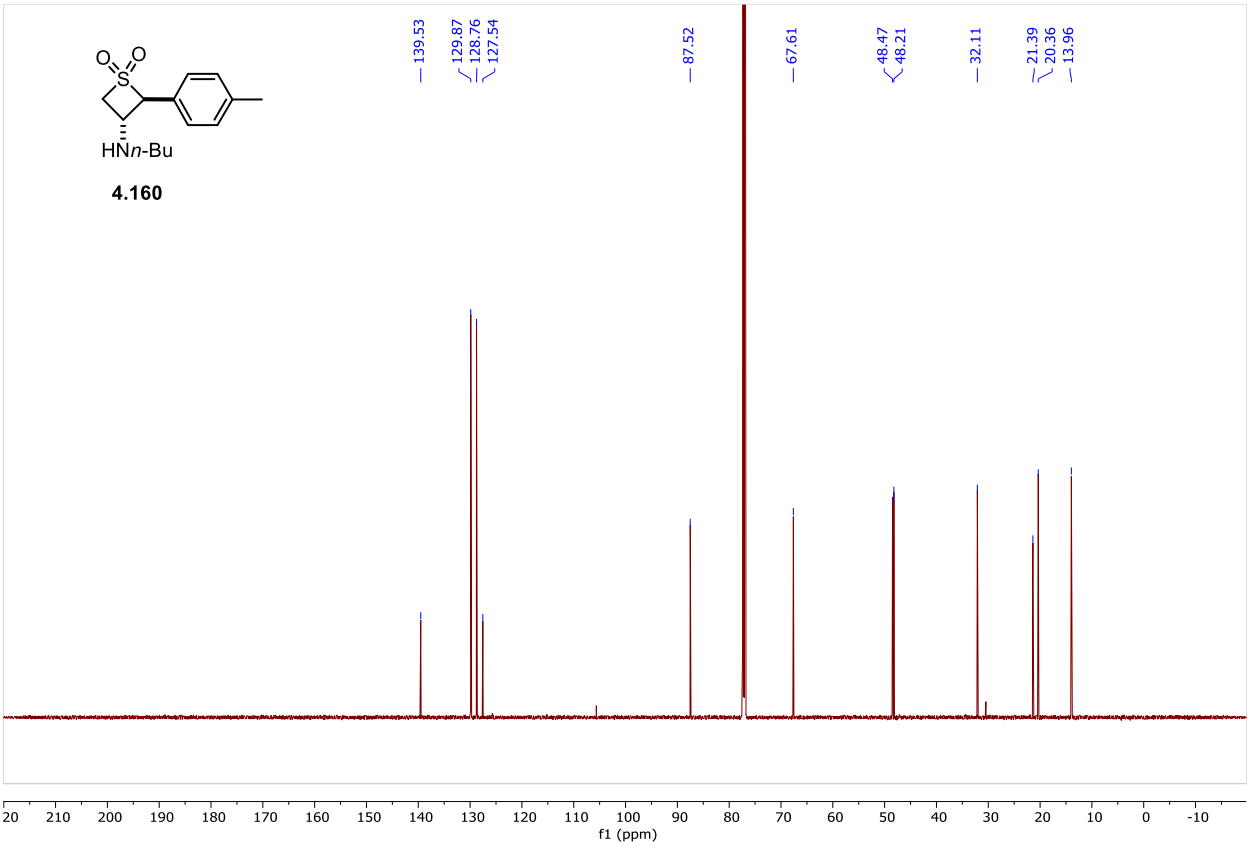

7.30
7.27
7.25
7.22
5.07
5.05
4.28
4.25
4.24
4.21
4.08
4.05
4.02
4.00
3.93
3.90
3.88
3.86
2.37
1.68
O
O
S
NH2
4.159
2.07
2.24
1.00
1.05
1.10
1.03
3.34
2.19
f1 (ppm)

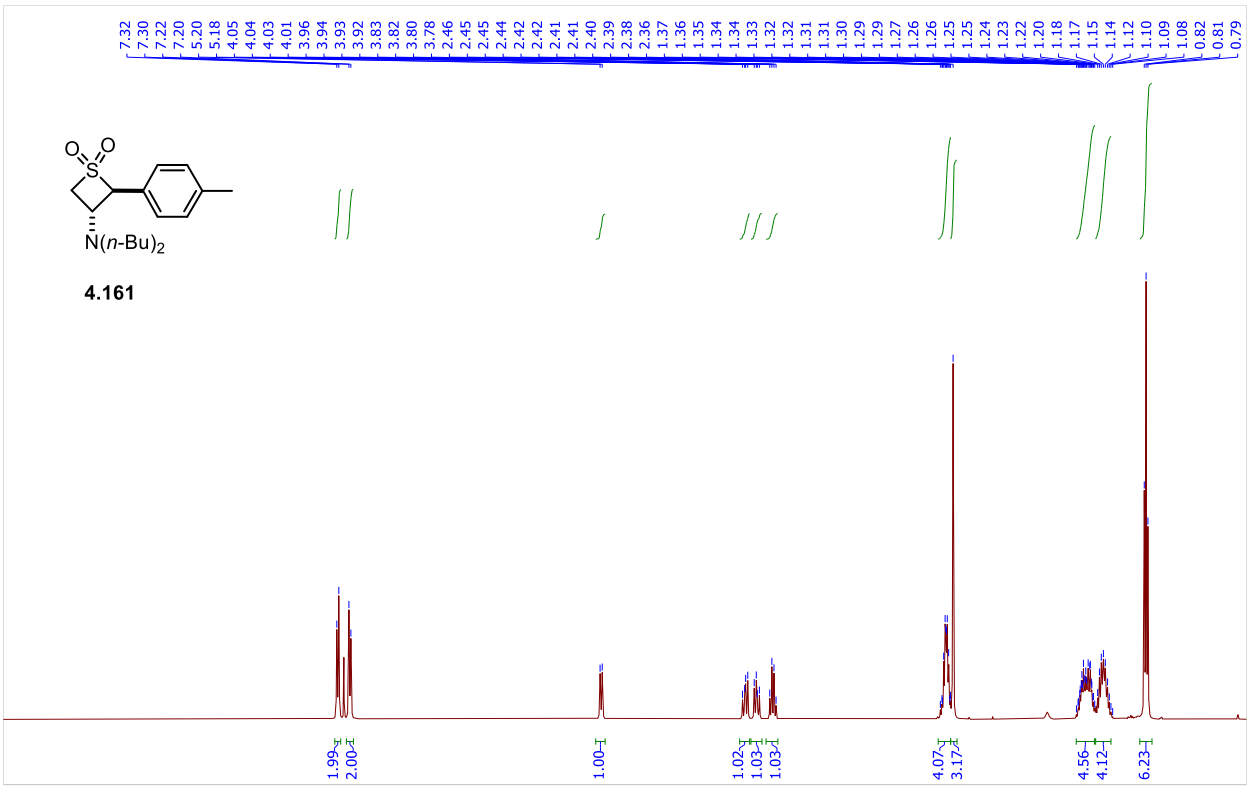

139.68
129.87
128.78
126.87
89.49
69.28
43.48
21.36
O
O
S
NH2
4.159
f1 (ppm)

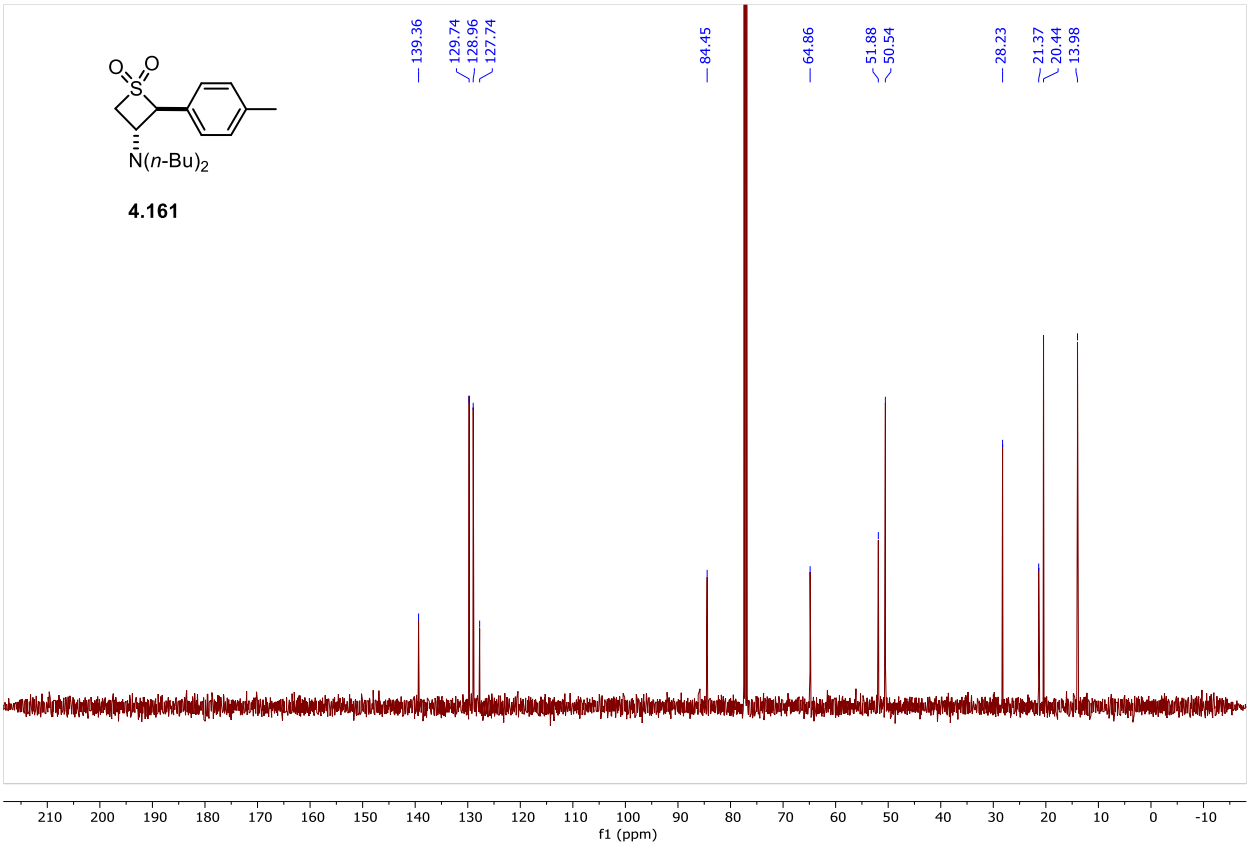

4.165
7.40
7.38
7.22
7.19
4.16
4.16
4.14
4.14
4.12
4.12
4.10
4.10
3.58
3.54
2.36
2.33
2.32
2.10
2.09
2.08
2.07
2.05
1.88
1.88
1.86
1.85
1.84
1.83
1.83
2.04
1.00
0.96
4.48
0.98
0.97
f1 (ppm)

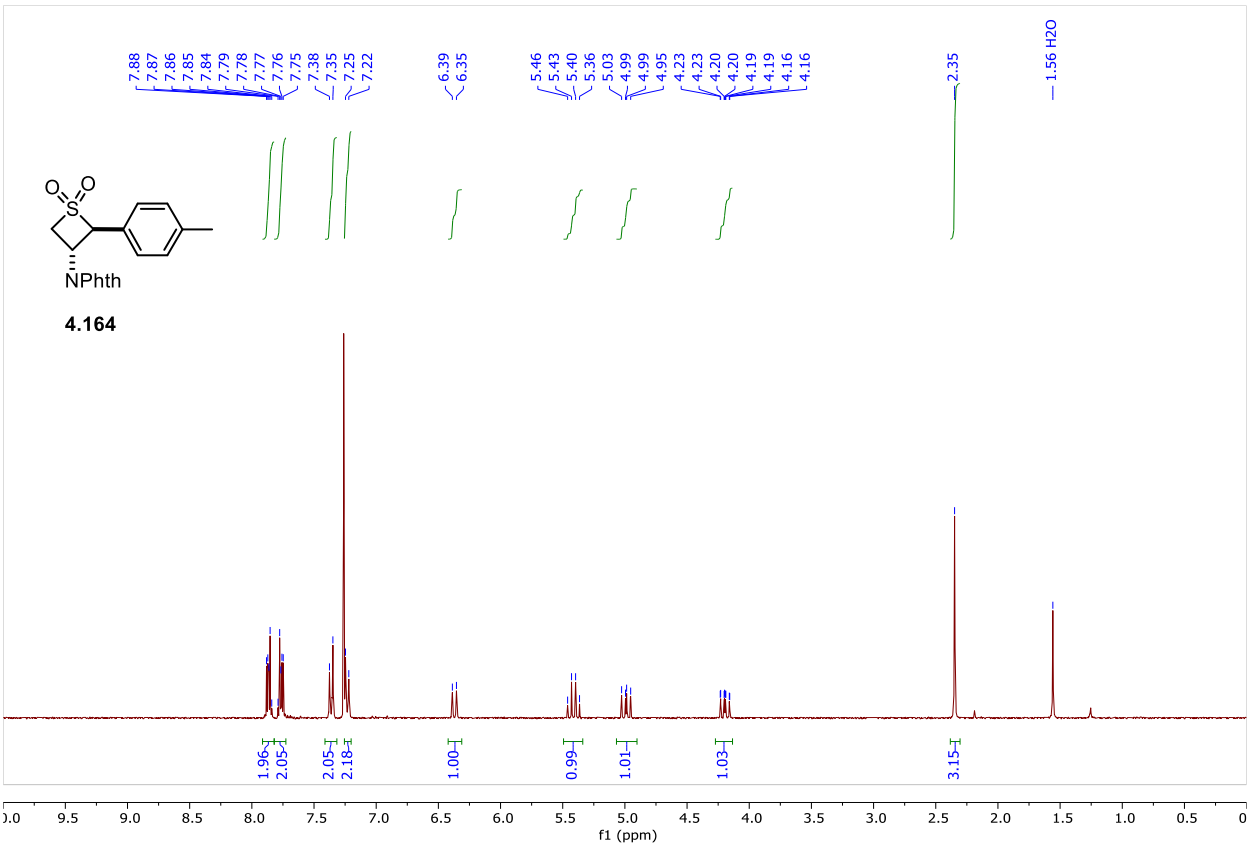

4.165
139.65
130.29
129.60
126.20
68.62
64.92
29.85
21.37
11.07
f1 (ppm)

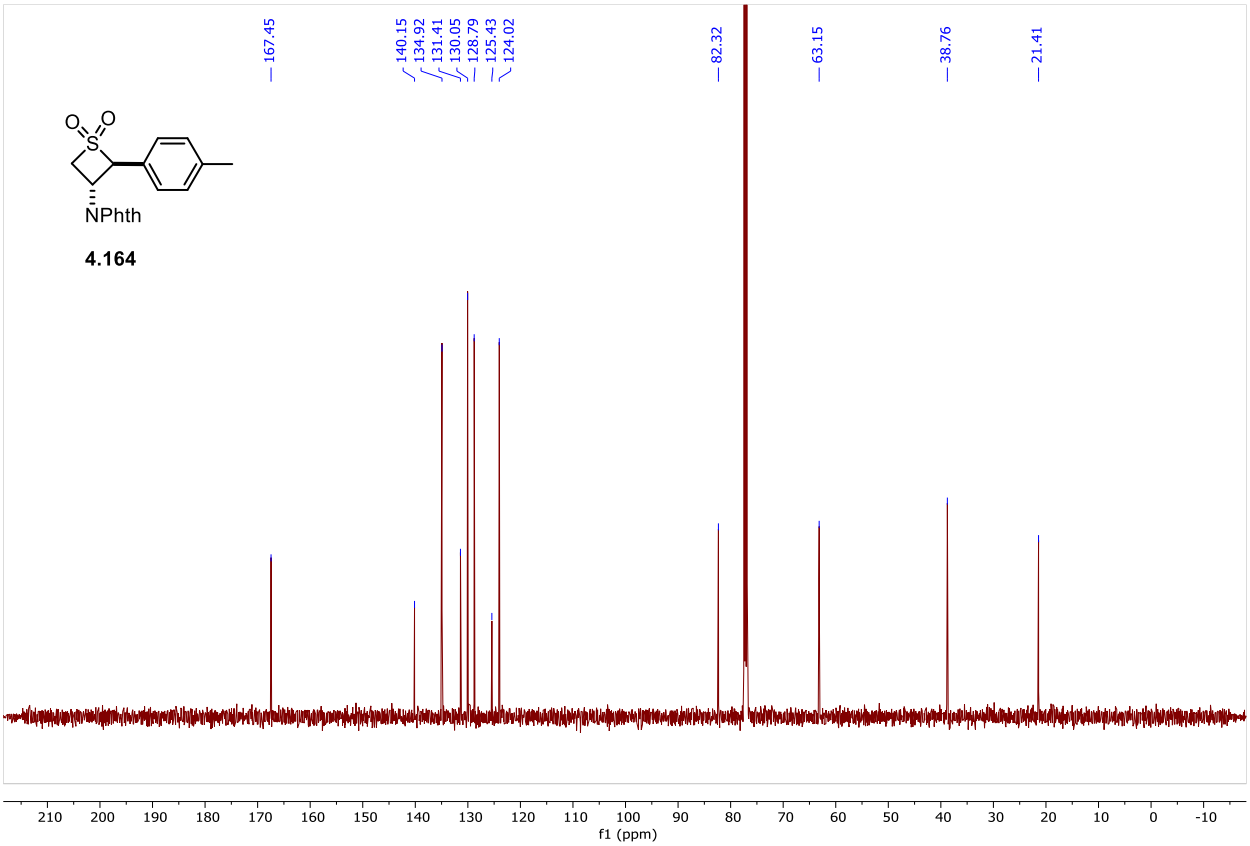

HNn-Bu
4.160
7.31 7.30 7.29 7.28 7.24 7.21 5.13 5.11 5.11 5.10 4.27 4.26 4.25 4.23 4.23 4.22 4.21 4.19 4.17 3.91 3.91 3.89 3.88 3.87 3.85 3.84 3.84 3.81 3.79 2.58 2.55 2.54 2.53 2.52 2.51 2.49 2.48 2.47 2.44 2.37 1.46 1.45 1.43 1.42 1.41 1.40 1.40 1.38 1.37 1.36 1.32 1.30 1.30 1.28 1.25 1.23 0.89 0.87 0.84
2.03 1.95 1.00 1.02 2.06 2.05 3.03 4.03 3.13
f1 (ppm)

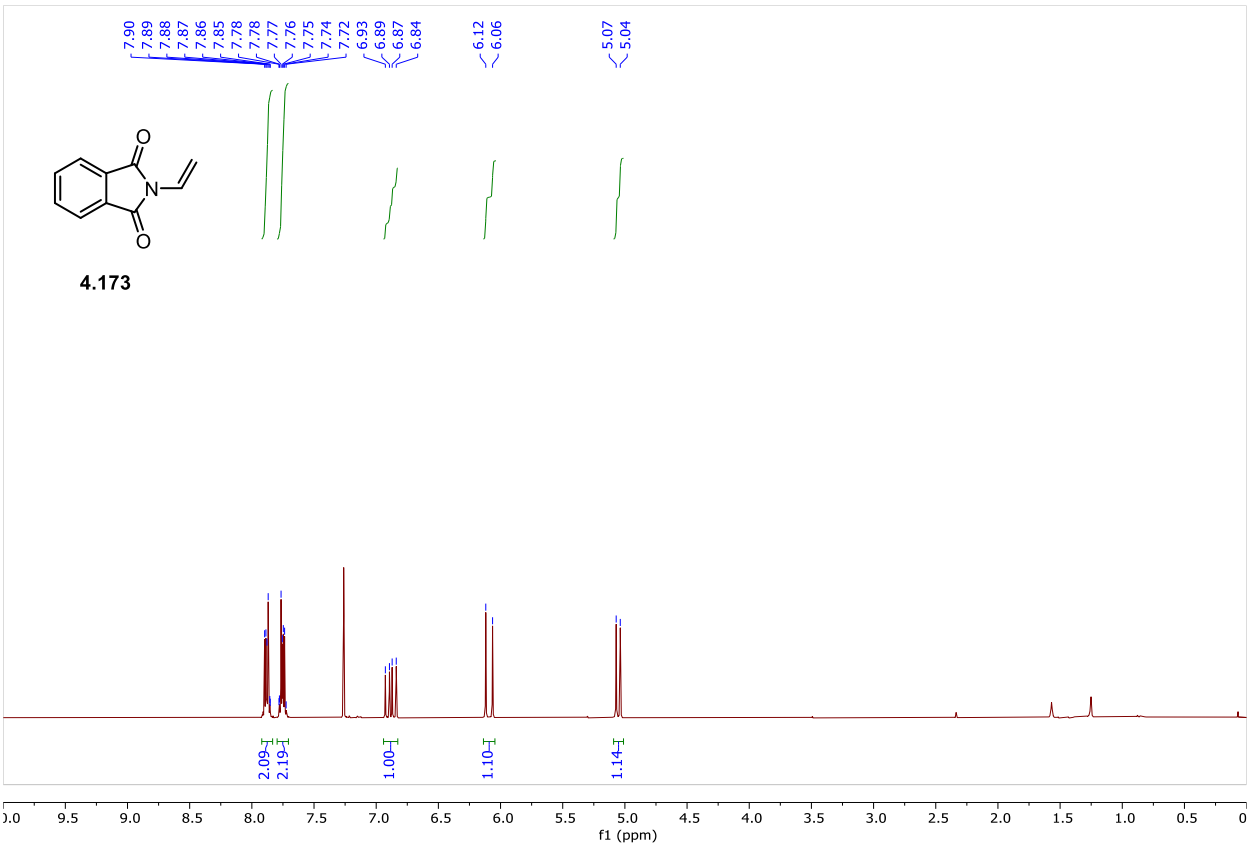

HNn-Bu
4.160
139.53 129.87 128.76 127.54 87.52 67.61 48.47 48.21 32.11 21.39 20.36 13.96
f1 (ppm)

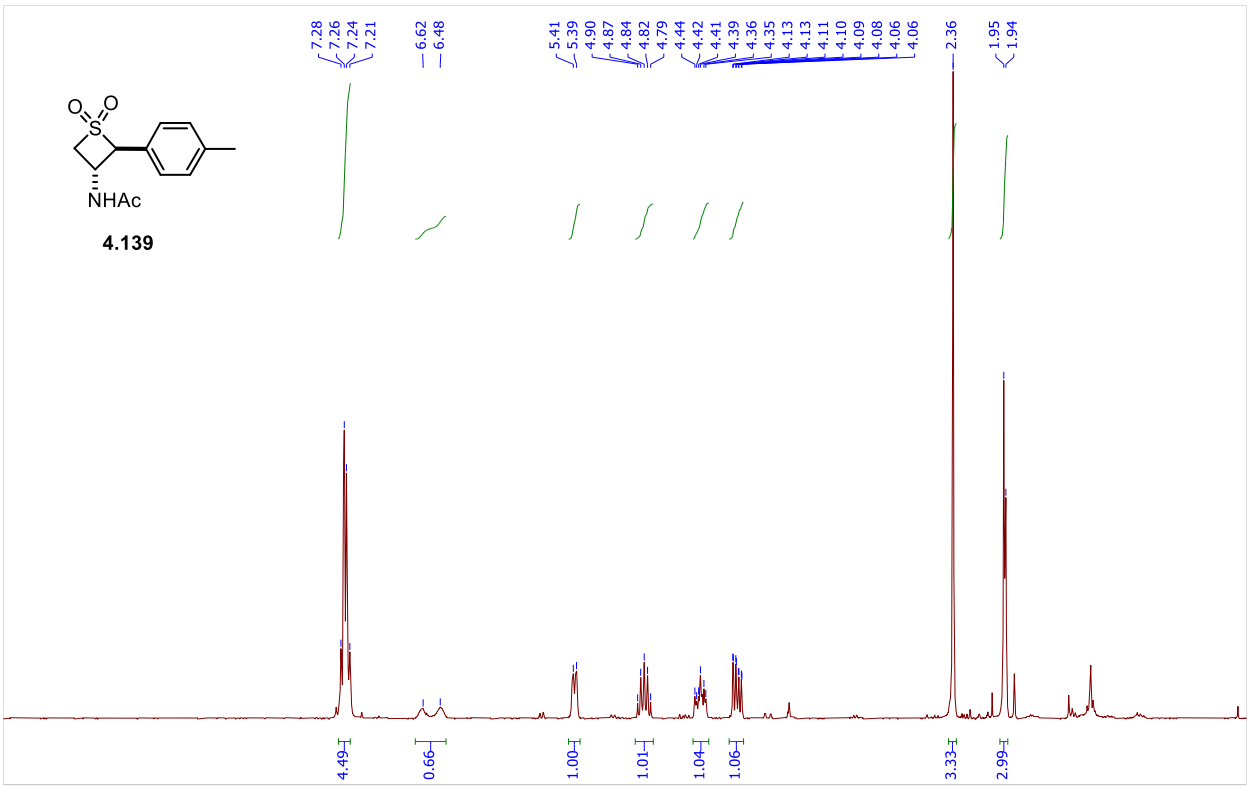

7.32 7.30 7.22 7.20 5.20 5.18 4.05 4.04 4.03 4.01 3.96 3.94 3.93 3.92 3.83 3.82 3.80 3.78 2.46 2.45 2.45 2.44 2.42 2.42 2.41 2.41 2.40 2.39 2.38 2.36 1.37 1.36 1.35 1.34 1.34 1.33 1.32 1.32 1.31 1.31 1.30 1.29 1.29 1.27 1.26 1.26 1.25 1.25 1.24 1.23 1.22 1.20 1.18 1.17 1.15 1.14 1.12 1.10 1.09 1.08 0.82 0.81 0.79
N(n-Bu)2
4.161
1.99 2.00 1.00 1.02 1.03 1.03 4.07 3.17 4.56 4.12 6.23
9.5 9.0 8.5 8.0 7.5 7.0 6.5 6.0 5.5 5.0 4.5 4.0 3.5 3.0 2.5 2.0 1.5 1.0 0.5 0
f1 (ppm)

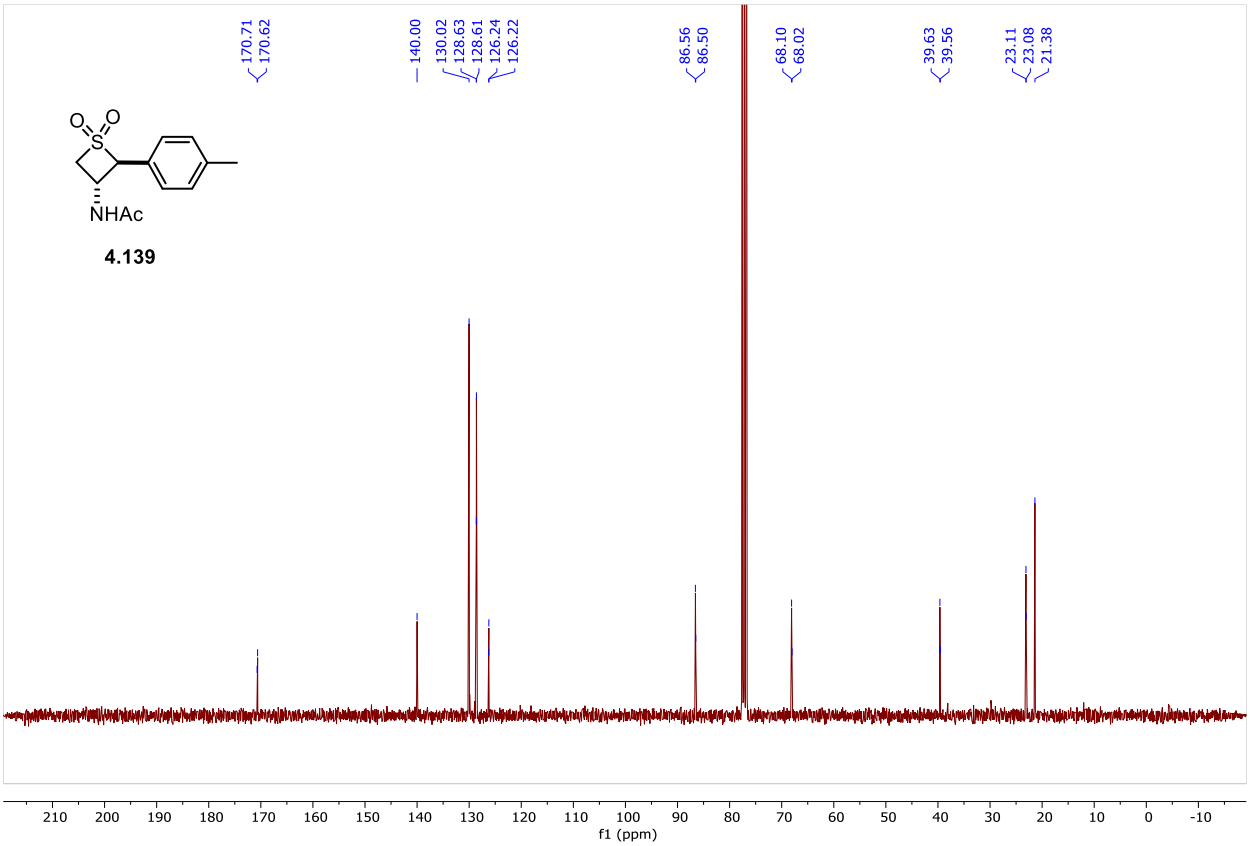

139.36 129.74 128.96 127.74 84.45 64.86 51.88 50.54 28.23 21.37 20.44 13.98
N(n-Bu)2
4.161
210 200 190 180 170 160 150 140 130 120 110 100 90 80 70 60 50 40 30 20 10 0 -10
f1 (ppm)

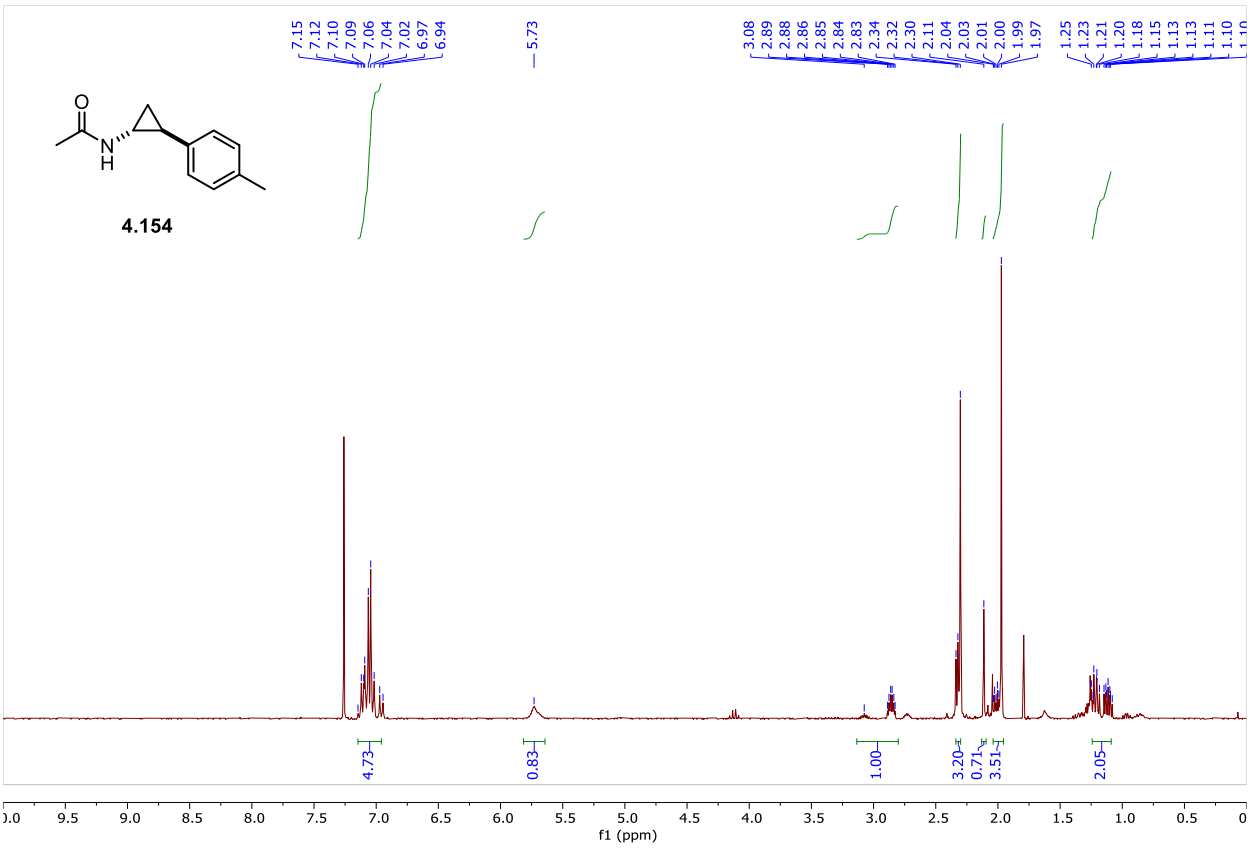

7.88
7.87
7.86
7.85
7.84
7.79
7.78
7.77
7.76
7.75
7.38
7.35
7.25
7.22
6.39
6.35
5.46
5.43
5.40
5.36
5.03
4.99
4.99
4.95
4.23
4.23
4.20
4.20
4.19
4.19
4.16
4.16
2.35
1.56 H2O
NPhth
4.164
1.96
2.05
2.05
2.18
1.00
0.99
1.01
1.03
3.15
f1 (ppm)

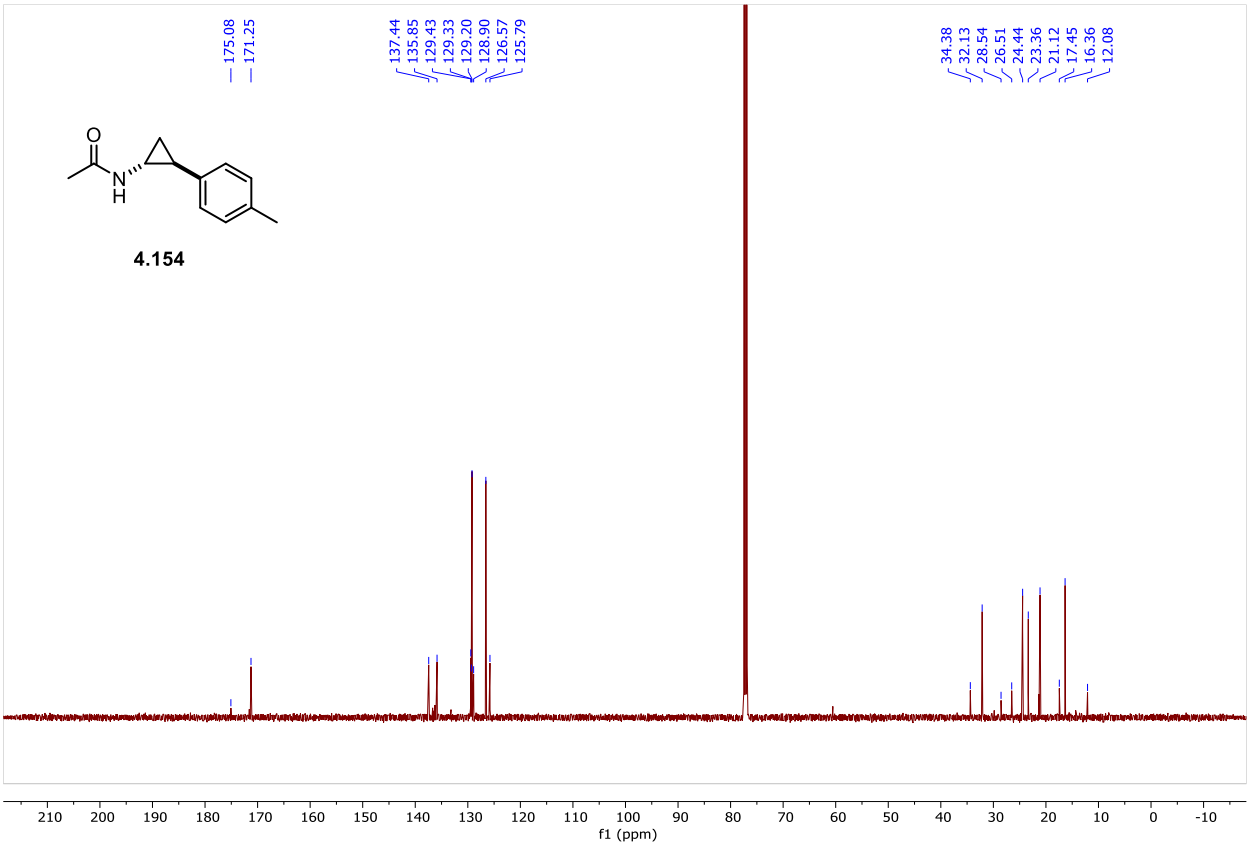

167.45
140.15
134.92
131.41
130.05
128.79
125.43
124.02
82.32
63.15
38.76
21.41
NPhth
4.164
f1 (ppm)

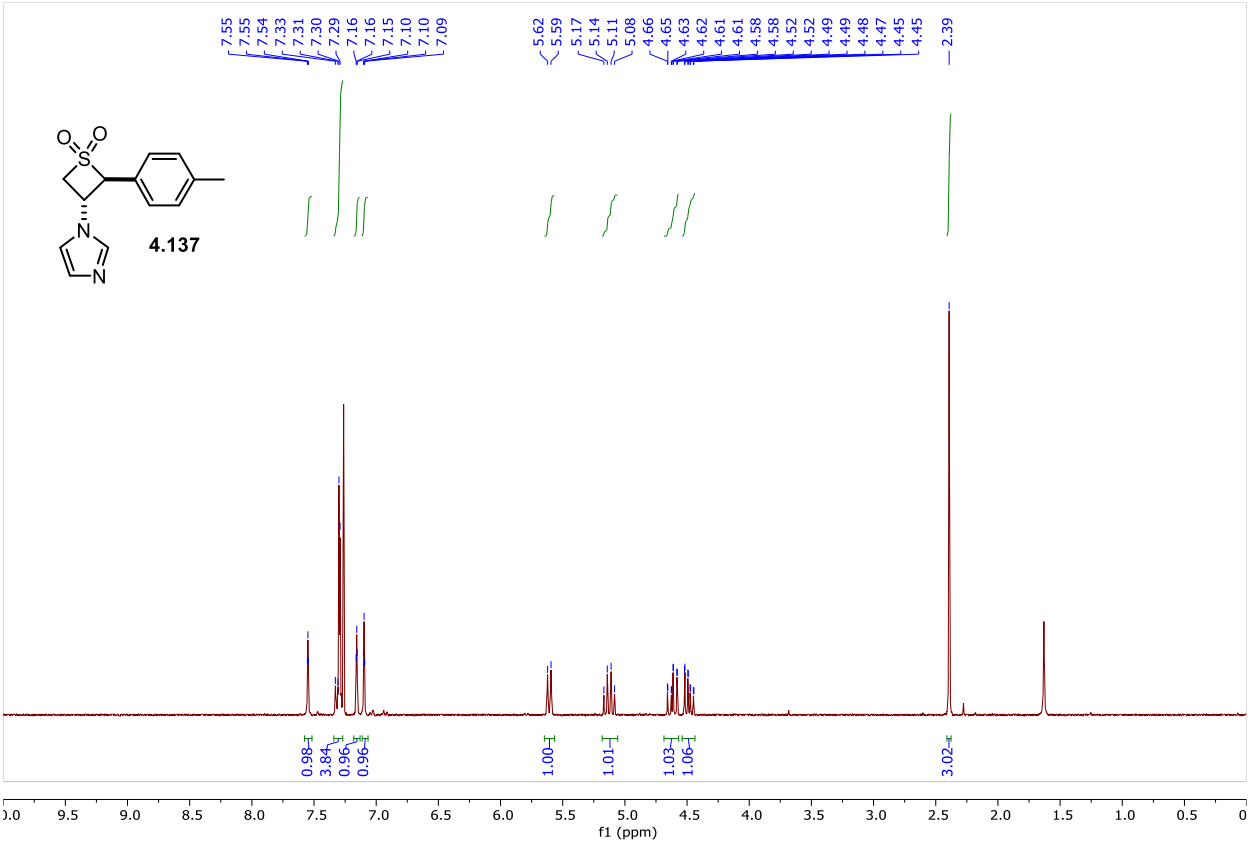

7.90
7.89
7.88
7.87
7.86
7.85
7.78
7.78
7.77
7.76
7.75
7.74
7.72
6.93
6.89
6.87
6.84
6.12
6.06
5.07
5.04
O
N
O
4.173
2.09
2.19
1.00
1.10
1.14
f1 (ppm)

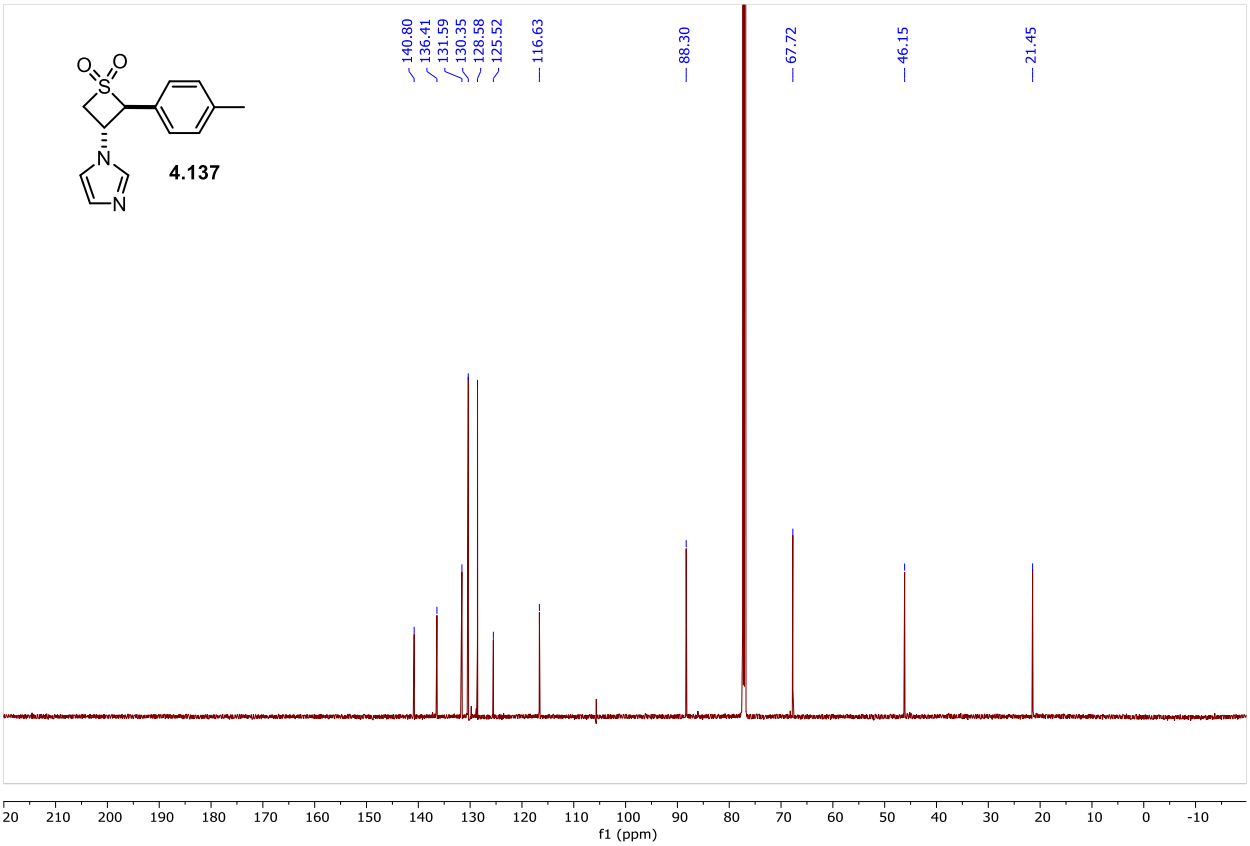

7.28
7.26
7.24
7.21
6.62
6.48
5.41
5.39
4.90
4.87
4.84
4.82
4.79
4.44
4.42
4.41
4.39
4.36
4.35
4.13
4.13
4.11
4.10
4.09
4.08
4.06
4.06
2.36
1.95
1.94
NHAc
4.139
4.49
0.66
1.00
1.01
1.04
1.06
3.33
2.99
f1 (ppm)

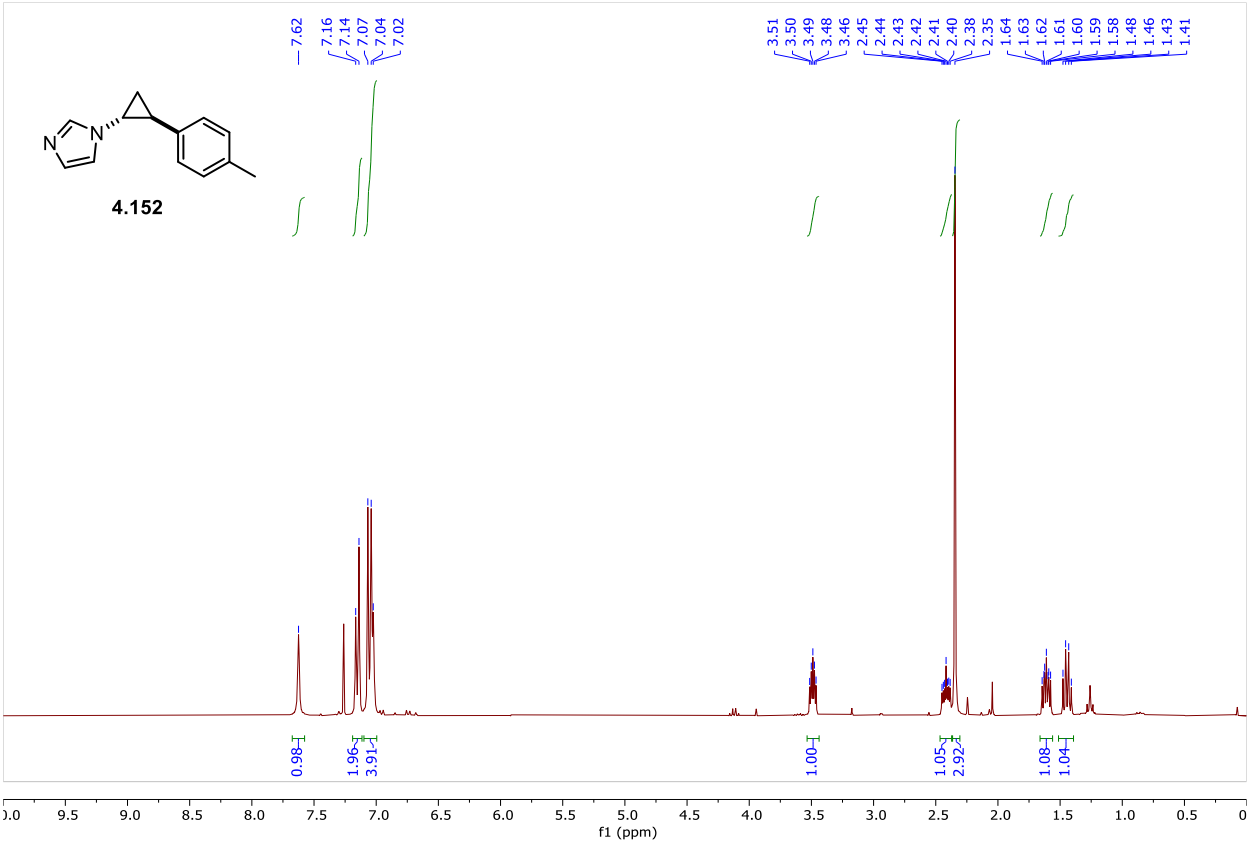

170.71
170.62
140.00
130.02
128.63
128.61
126.24
126.22
86.56
86.50
68.10
68.02
39.63
39.56
23.11
23.08
21.38
NHAc
4.139
f1 (ppm)

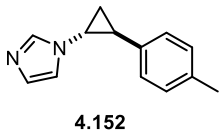

7.15
7.12
7.10
7.09
7.06
7.04
7.02
6.97
6.94
5.73
3.08
2.89
2.88
2.86
2.85
2.84
2.83
2.34
2.32
2.30
2.11
2.04
2.03
2.01
2.00
1.99
1.97
1.25
1.23
1.21
1.20
1.18
1.15
1.13
1.11
1.10
4.154
4.73
0.83
1.00
3.20
0.71
3.51
2.05
f1 (ppm)


175.08
171.25
137.44
135.85
129.43
129.33
129.20
128.90
126.57
125.79
34.38
32.13
28.54
26.51
24.44
23.36
21.12
17.45
16.36
12.08
4.154
f1 (ppm)


7.55
7.55
7.54
7.33
7.31
7.30
7.29
7.16
7.16
7.15
7.10
7.10
7.09
5.62
5.59
5.17
5.14
5.11
5.08
4.66
4.65
4.63
4.62
4.61
4.61
4.58
4.58
4.52
4.52
4.49
4.49
4.48
4.47
4.45
4.45
2.39
4.137
0.98
3.84
0.96
0.96
1.00
1.01
1.03
1.06
3.02
f1 (ppm)

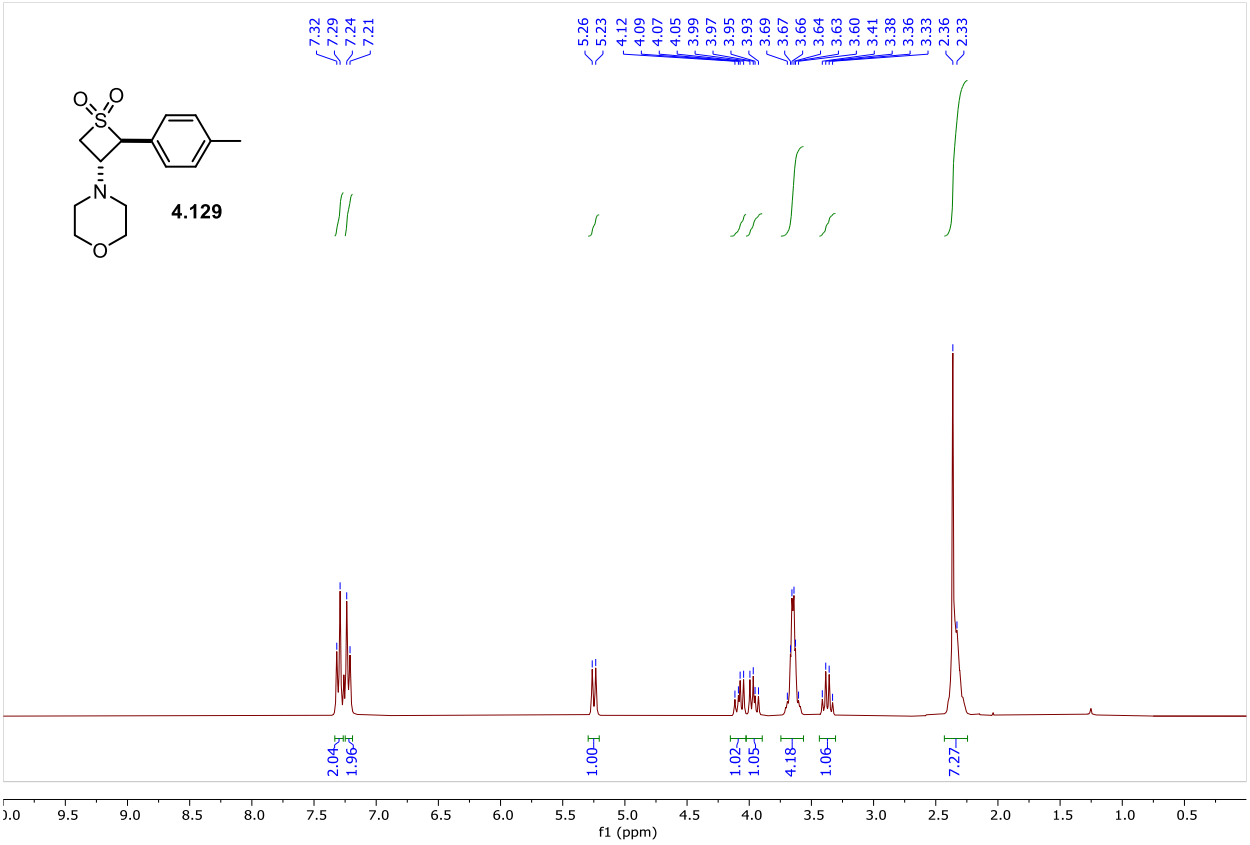

140.80
136.41
131.59
130.35
128.58
125.52
116.63
88.30
67.72
46.15
21.45
4.137
f1 (ppm)

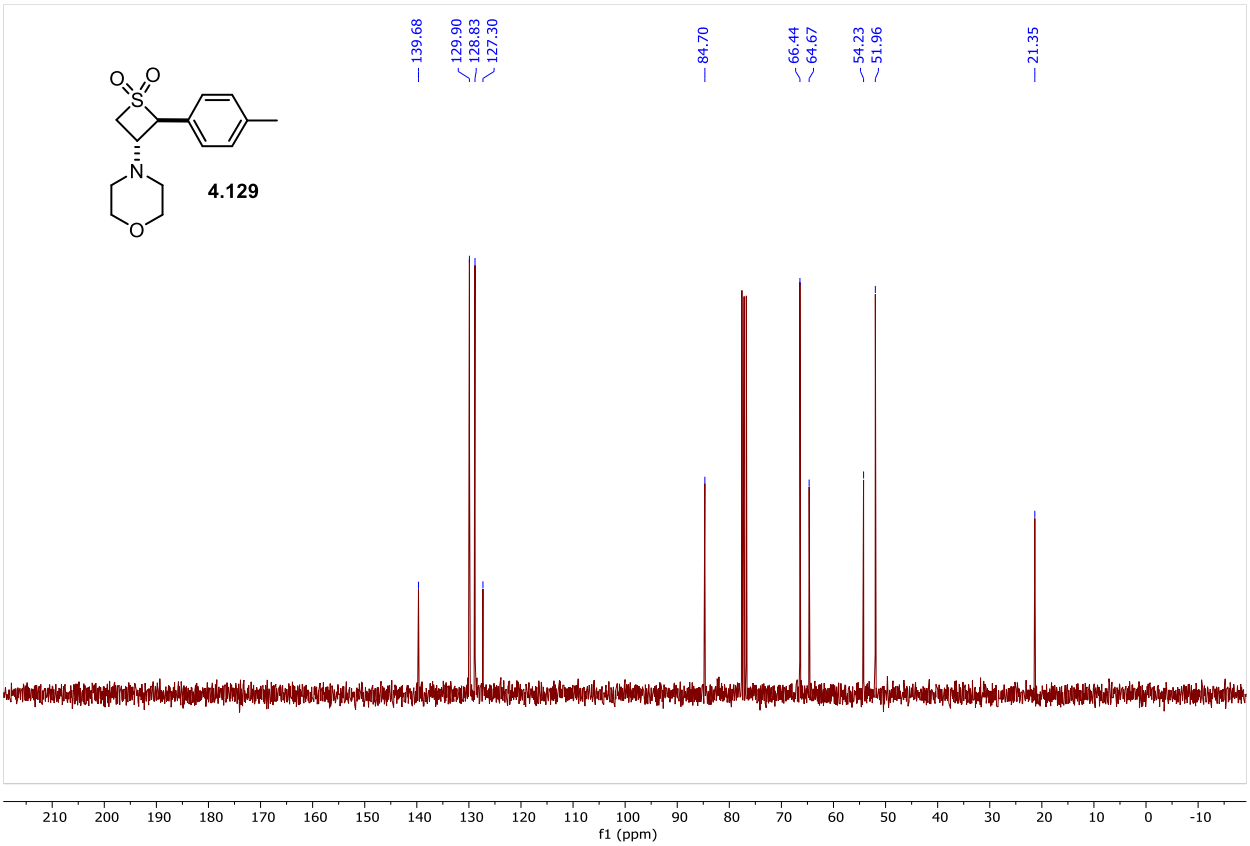

7.62
7.16
7.14
7.07
7.04
7.02
3.51
3.50
3.49
3.48
3.46
2.45
2.44
2.43
2.42
2.41
2.40
2.38
2.35
1.64
1.63
1.62
1.61
1.60
1.59
1.58
1.48
1.46
1.43
1.41
0.98
1.96
3.91
1.00
1.05
2.92
1.08
1.04
f1 (ppm)

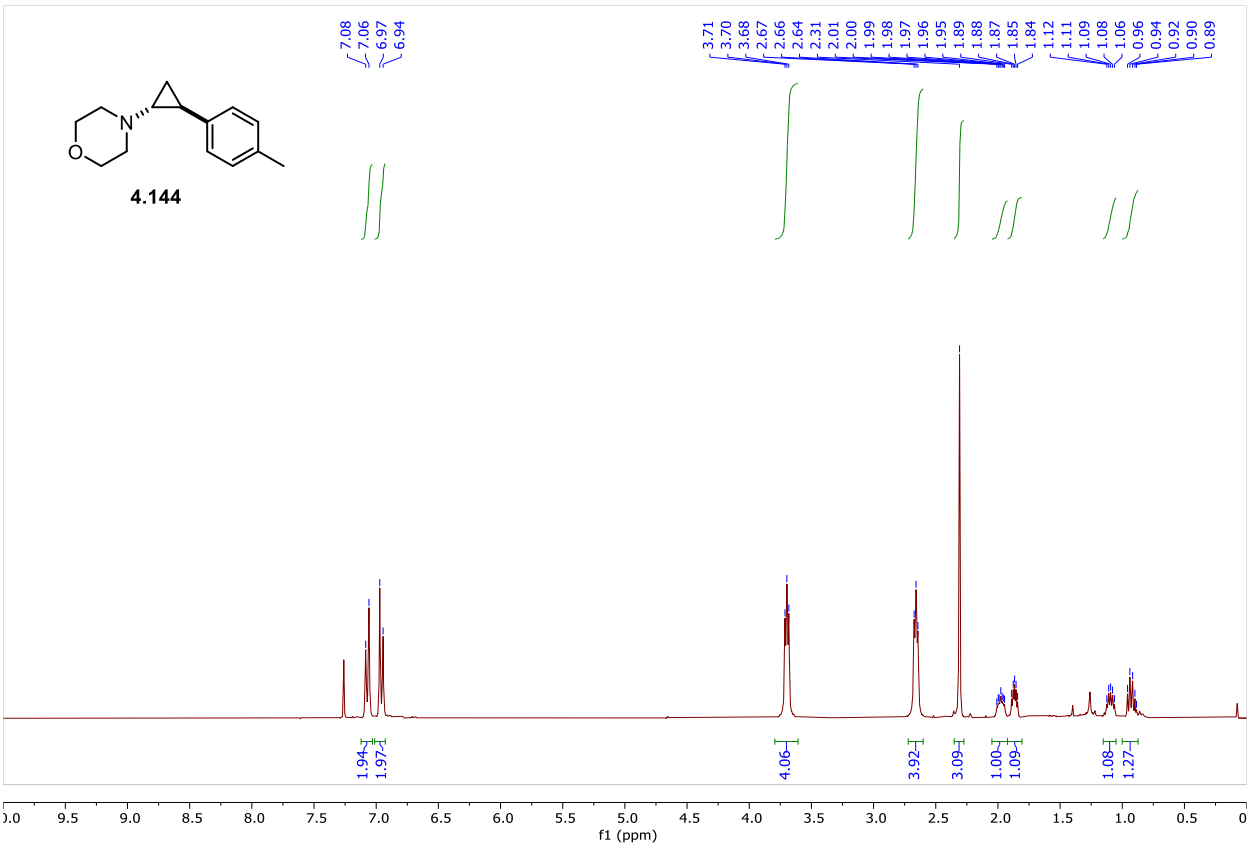


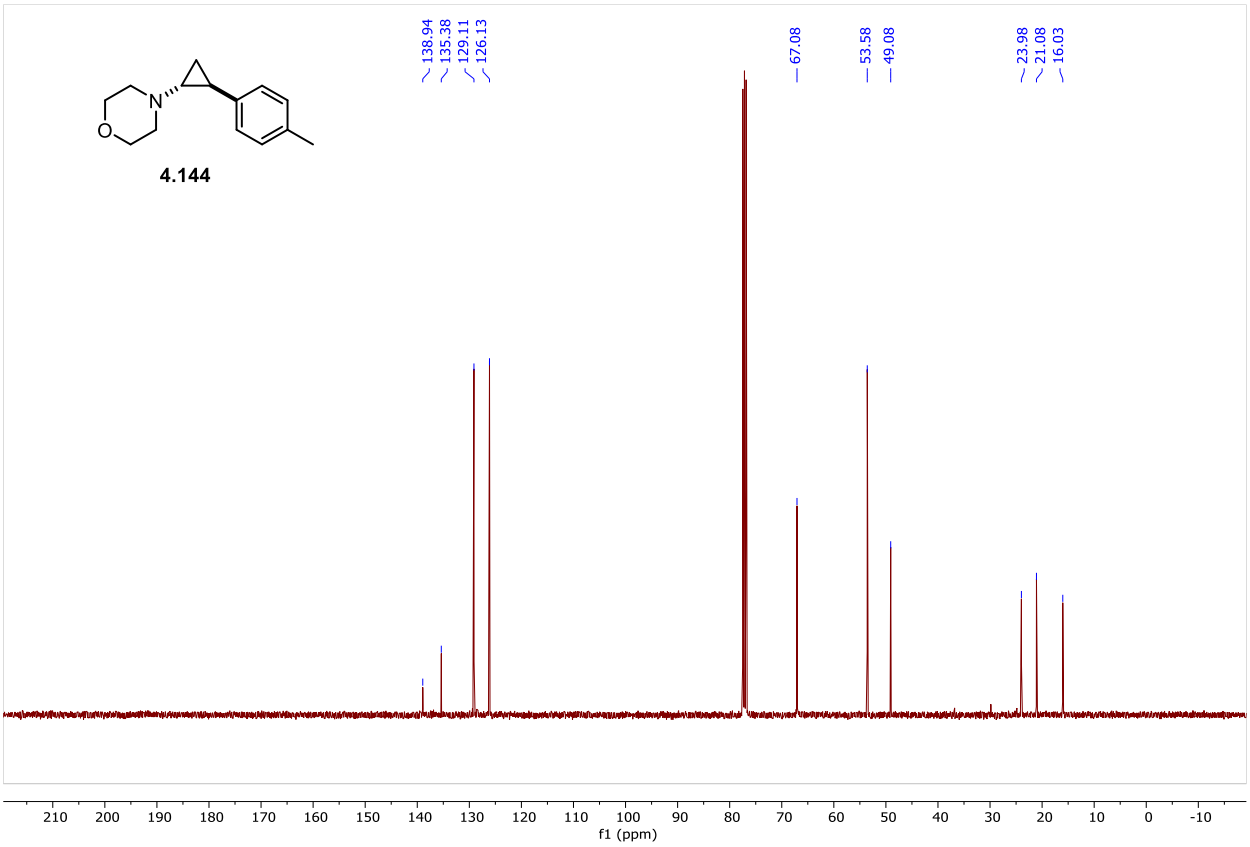
4.152

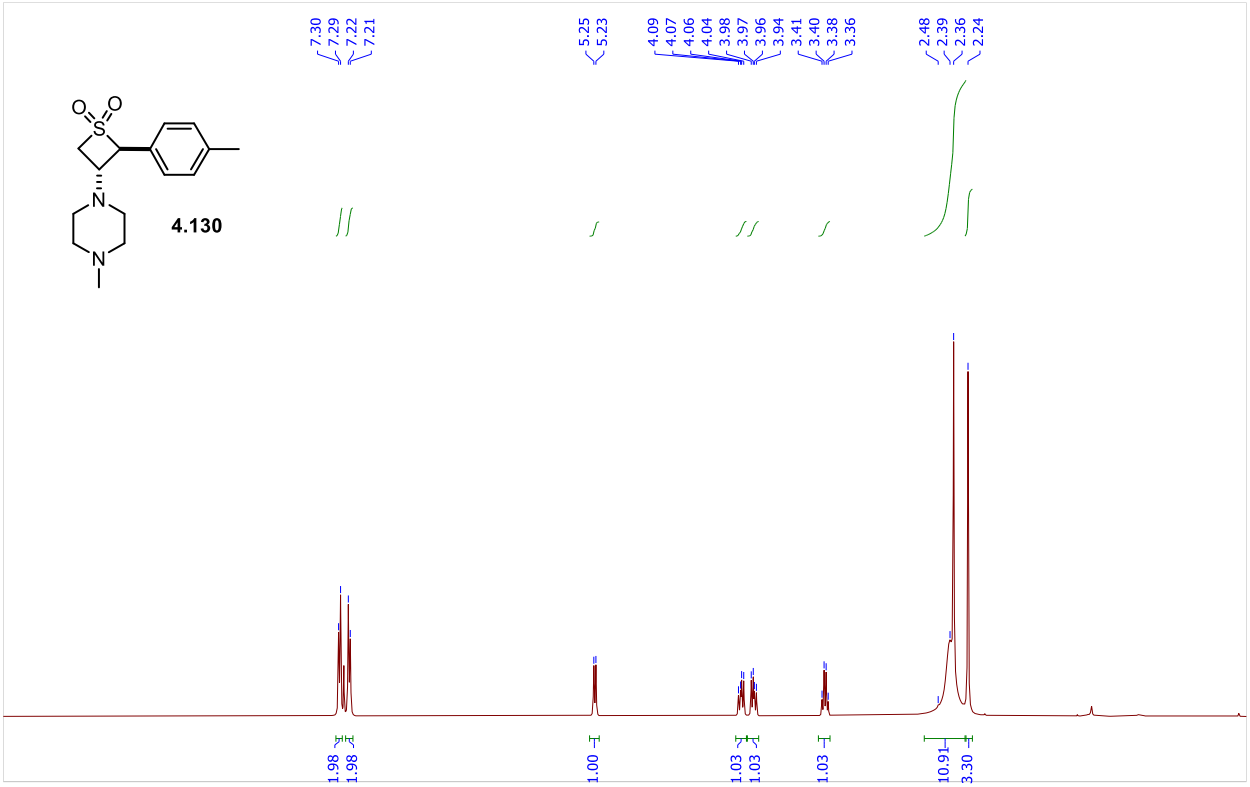
137.53
136.62
136.02
129.50
129.33
126.28
119.67
36.52
24.32
21.12
15.25
f1 (ppm)

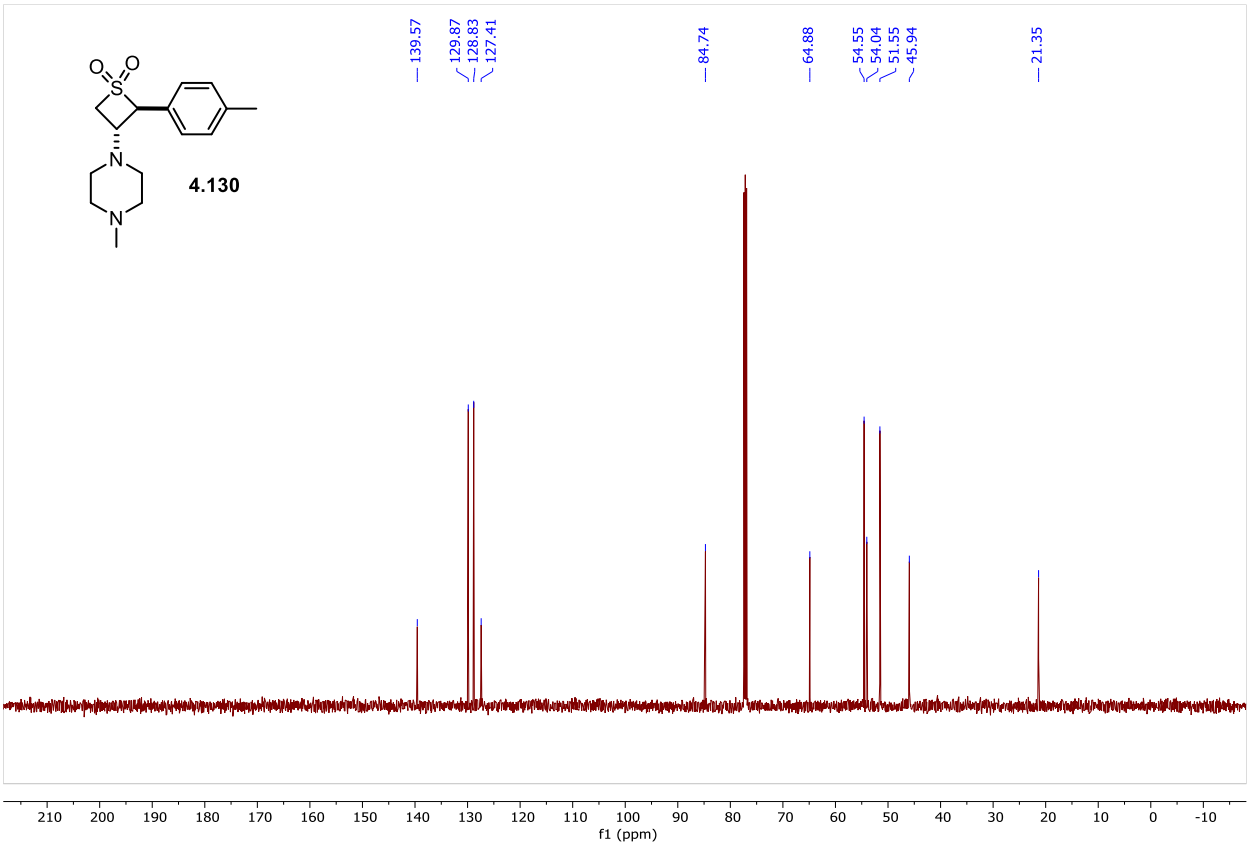

7.32
7.29
7.24
7.21
5.26
5.23
4.12
4.09
4.07
4.05
3.99
3.97
3.95
3.93
3.69
3.67
3.66
3.64
3.63
3.60
3.41
3.38
3.36
3.33
2.36
2.33
4.129
2.04
1.96
1.00
1.02
1.05
4.18
1.06
7.27
f1 (ppm)

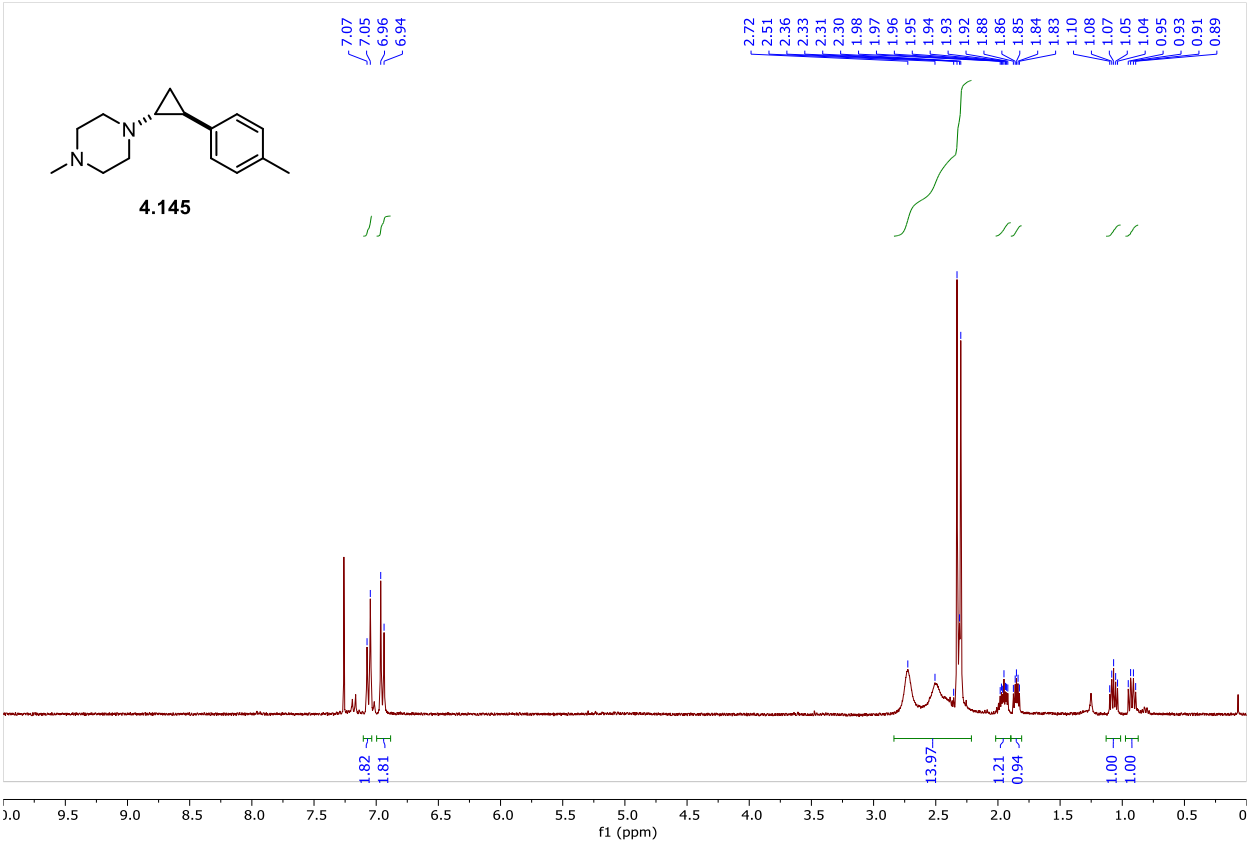

139.68
129.90
128.83
127.30
84.70
66.44
64.67
54.23
51.96
21.35
4.129
f1 (ppm)

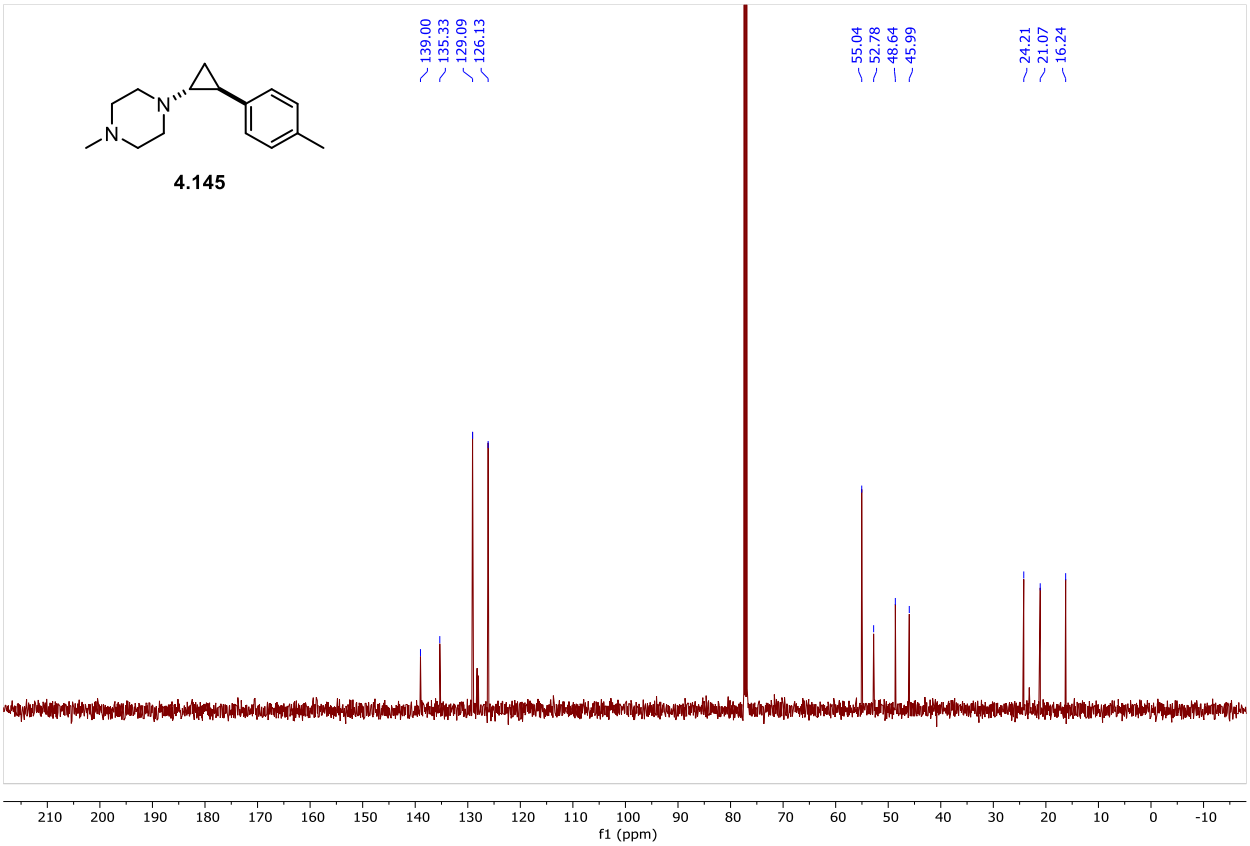

7.08
7.06
6.97
6.94
3.71
3.70
3.68
2.67
2.66
2.64
2.31
2.01
2.00
1.99
1.98
1.97
1.96
1.95
1.89
1.88
1.87
1.85
1.84
1.12
1.11
1.09
1.08
1.06
0.96
0.94
0.92
0.90
0.89
4.144
1.94
1.97
4.06
3.92
3.09
1.00
1.09
1.08
1.27
f1 (ppm)

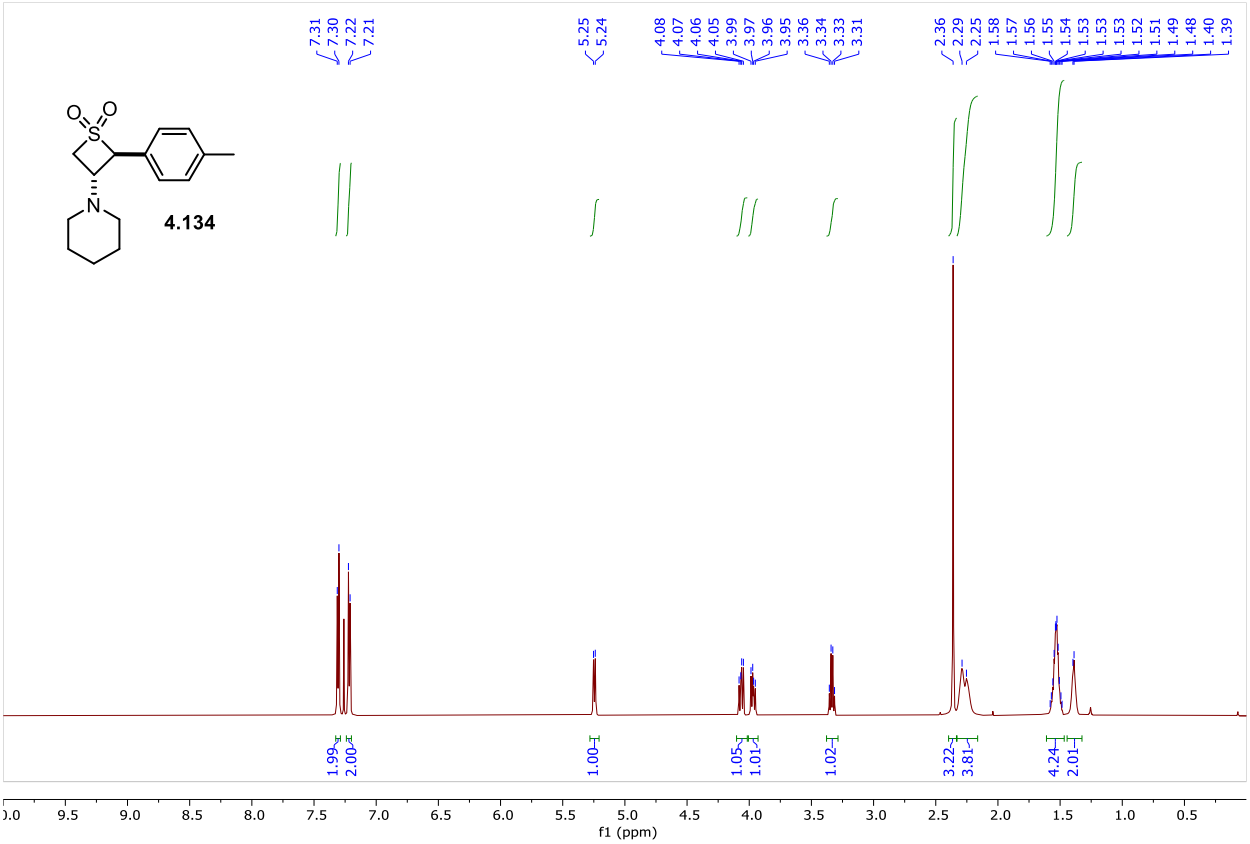

138.94
135.38
129.11
126.13
67.08
53.58
49.08
23.98
21.08
16.03
4.144
f1 (ppm)

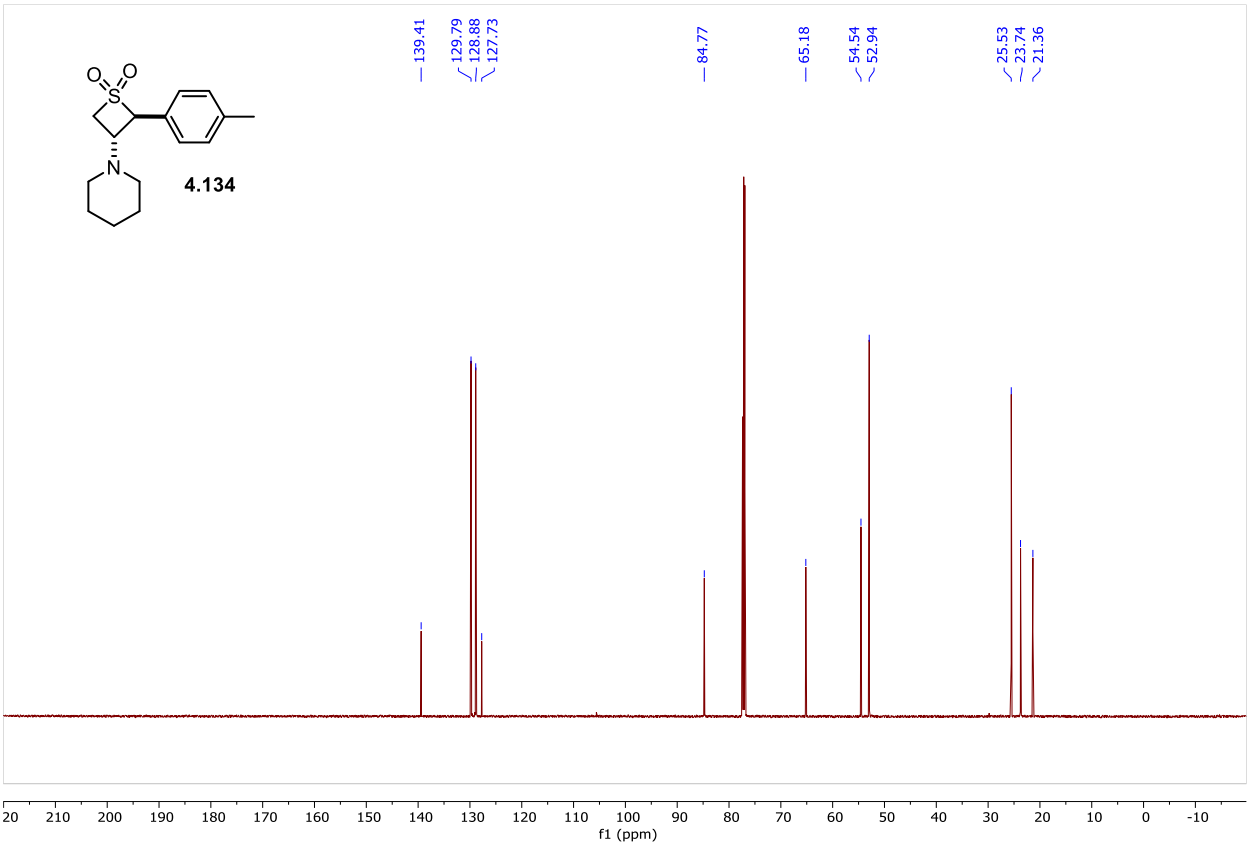

7.30
7.29
7.22
7.21
5.25
5.23
4.09
4.07
4.06
4.04
3.98
3.97
3.96
3.94
3.41
3.40
3.38
3.36
2.48
2.39
2.36
2.24
4.130
1.98
1.98
1.00
1.03
1.03
1.03
10.91
3.30
f1 (ppm)

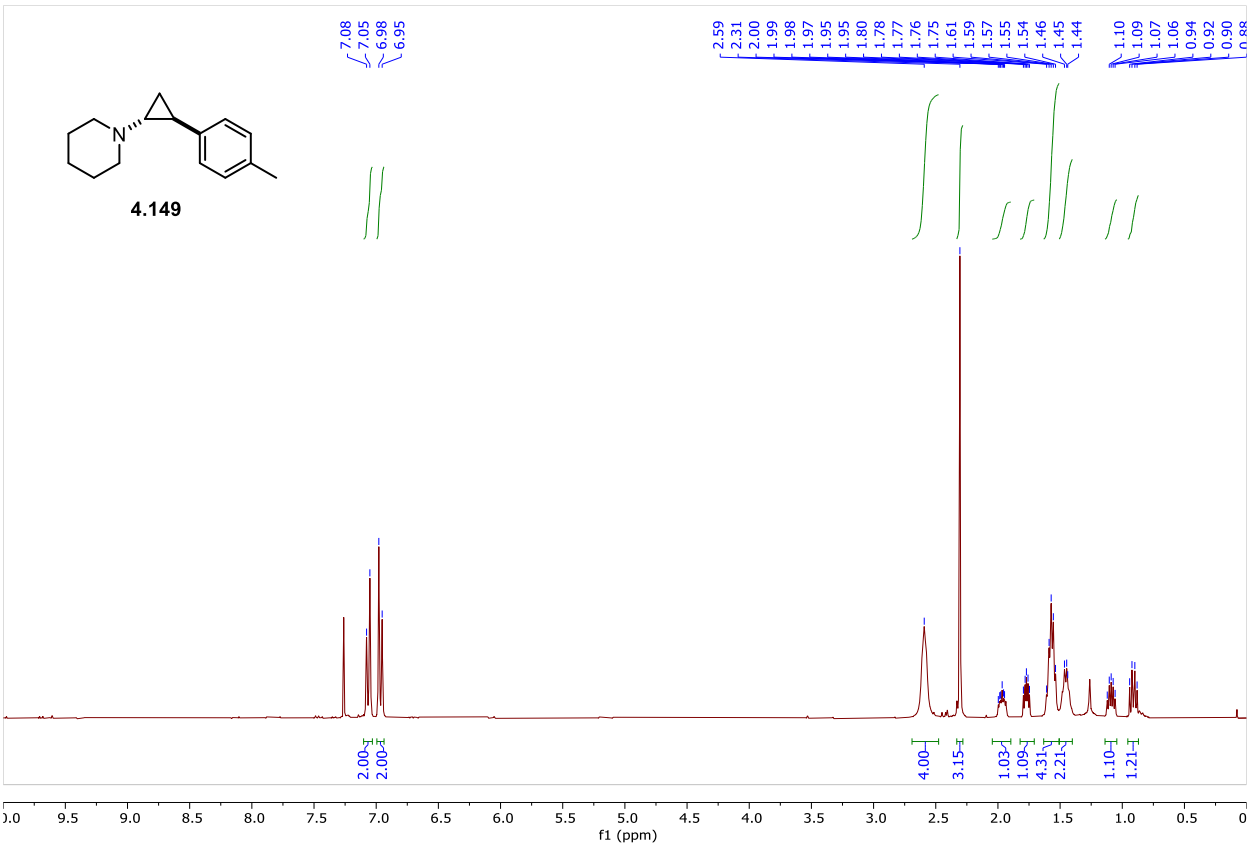

139.57
129.87
128.83
127.41
84.74
64.88
54.55
54.04
51.55
45.94
21.35
4.130
f1 (ppm)

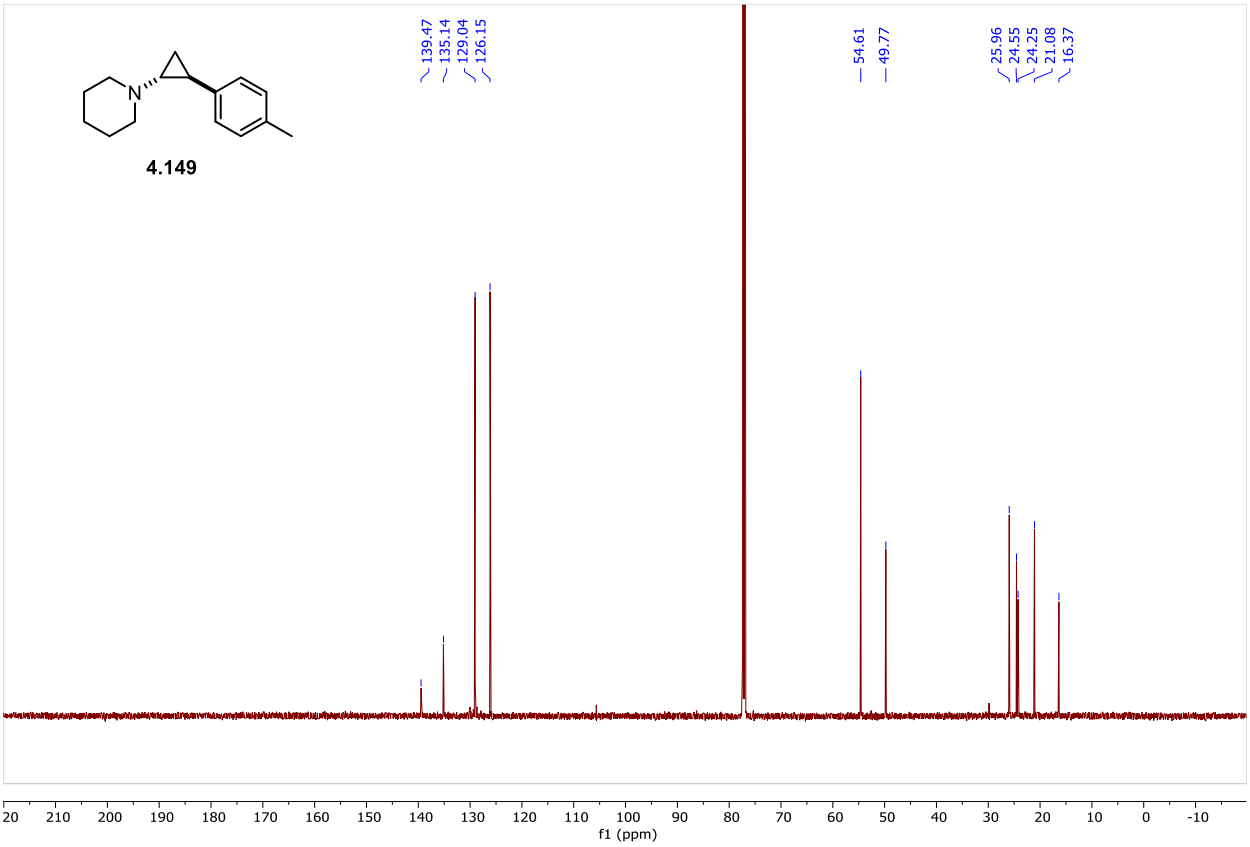

7.07
7.05
6.96
6.94
2.72
2.51
2.36
2.33
2.31
2.30
1.98
1.97
1.96
1.95
1.94
1.93
1.92
1.88
1.86
1.85
1.84
1.83
1.10
1.08
1.07
1.05
1.04
0.95
0.93
0.91
0.89
4.145
1.82
1.81
13.97
1.21
0.94
1.00
1.00
f1 (ppm)

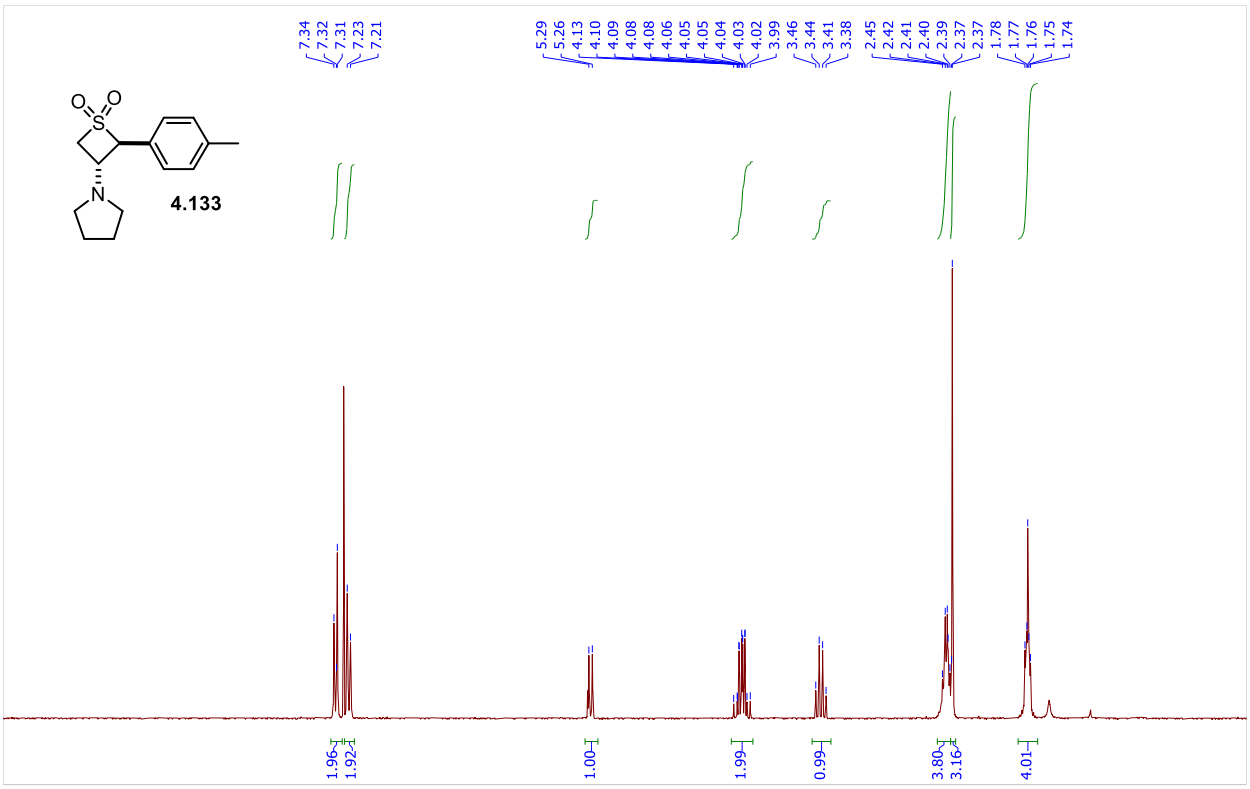

139.00
135.33
129.09
126.13
55.04
52.78
48.64
45.99
24.21
21.07
16.24
4.145
f1 (ppm)

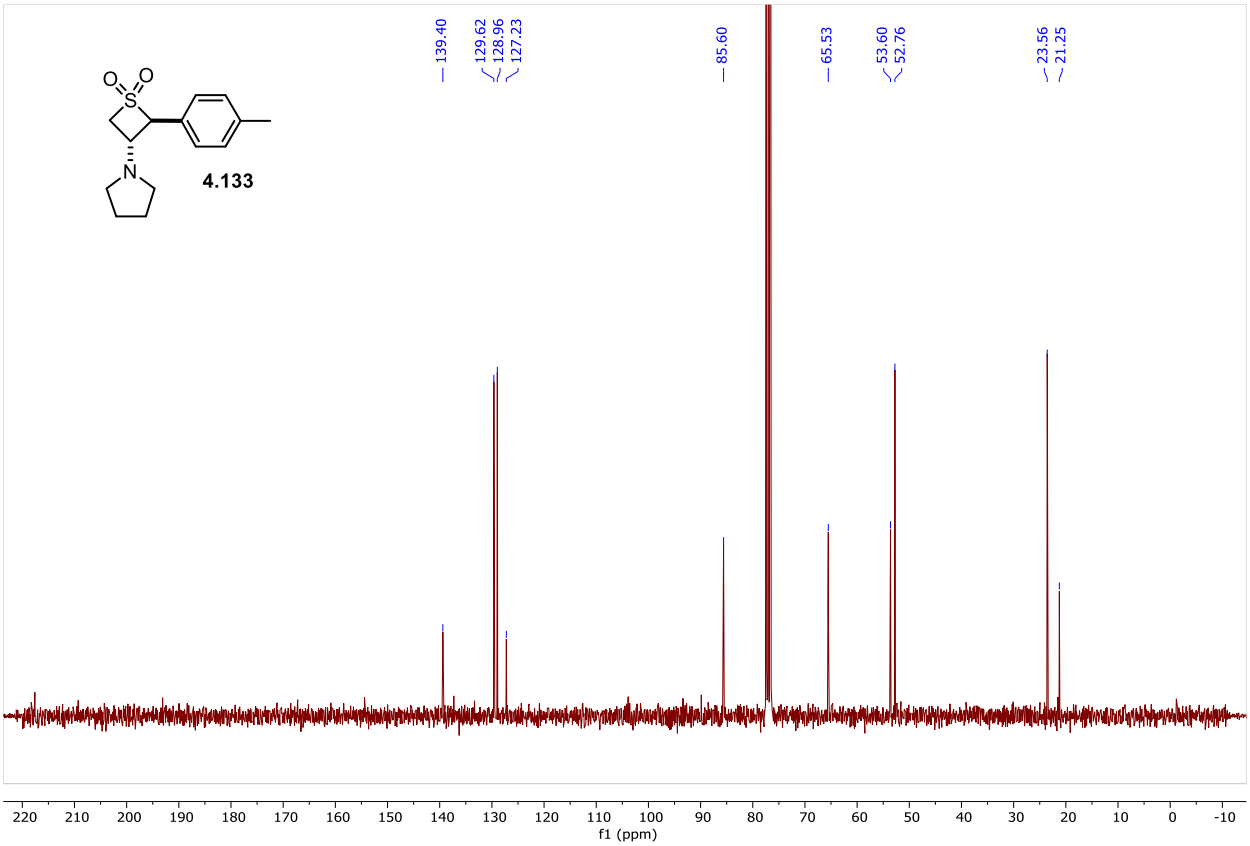

7.31
7.30
7.22
7.21
5.25
5.24
4.08
4.07
4.06
4.05
3.99
3.97
3.96
3.95
3.36
3.34
3.33
3.31
2.36
2.29
2.25
1.58
1.57
1.56
1.55
1.54
1.53
1.53
1.53
1.52
1.51
1.49
1.48
1.40
1.39
4.134
1.99
2.00
1.00
1.05
1.01
1.02
3.22
3.81
4.24
2.01
f1 (ppm)

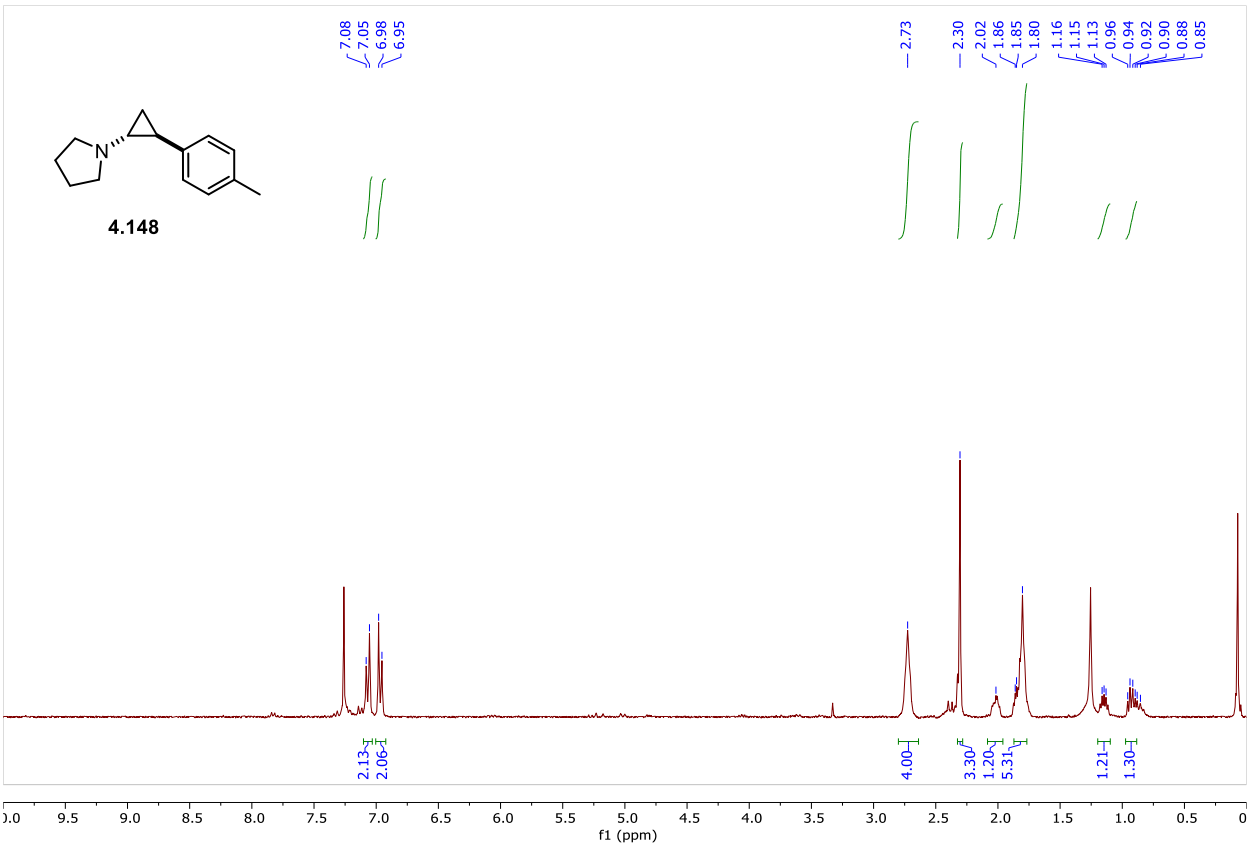

139.41
129.79
128.88
127.73
84.77
65.18
54.54
52.94
25.53
23.74
21.36
4.134
f1 (ppm)

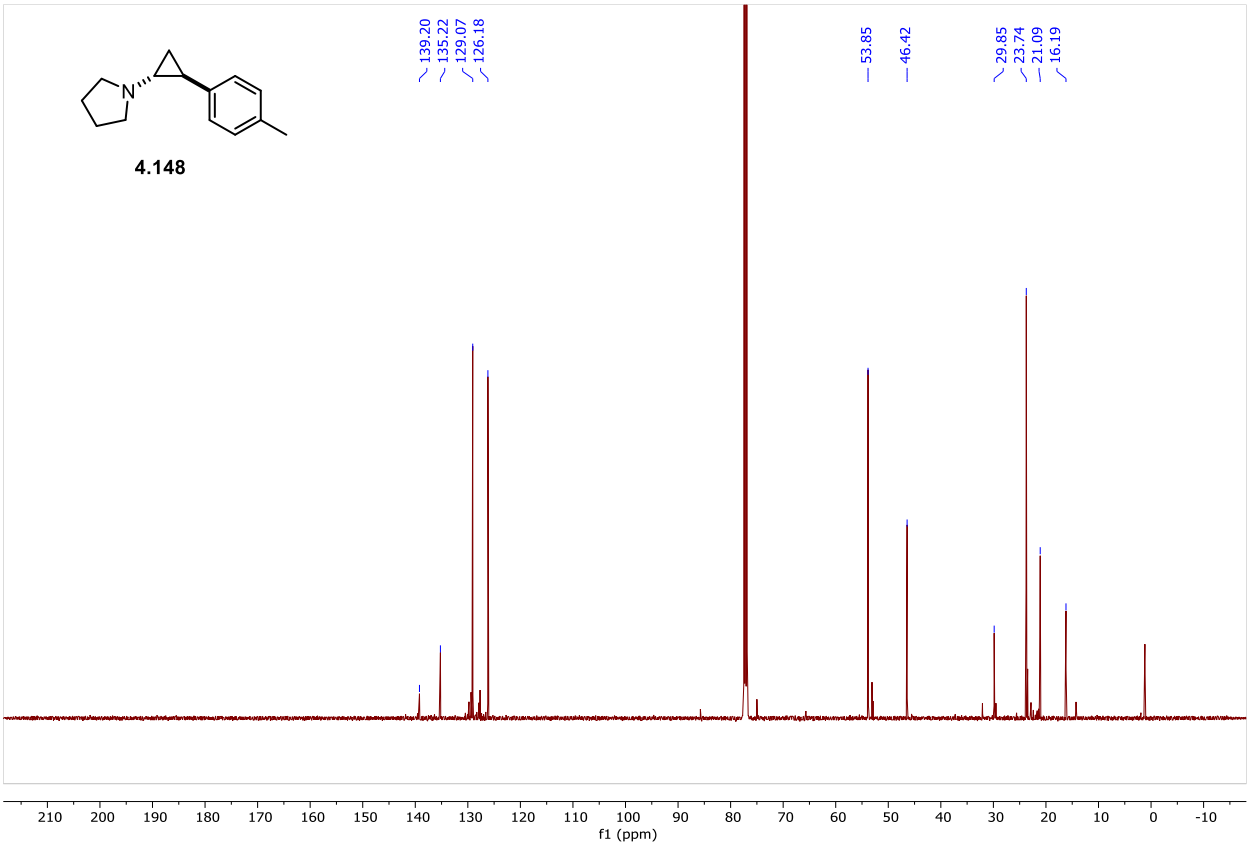

7.08
7.05
6.98
6.95
2.59
2.31
2.00
1.99
1.98
1.97
1.95
1.95
1.80
1.78
1.77
1.76
1.75
1.61
1.59
1.57
1.55
1.54
1.46
1.45
1.44
1.10
1.09
1.07
1.06
0.94
0.92
0.90
4.149
2.00
2.00
4.00
3.15
1.03
1.09
4.31
2.21
1.10
1.21
f1 (ppm)

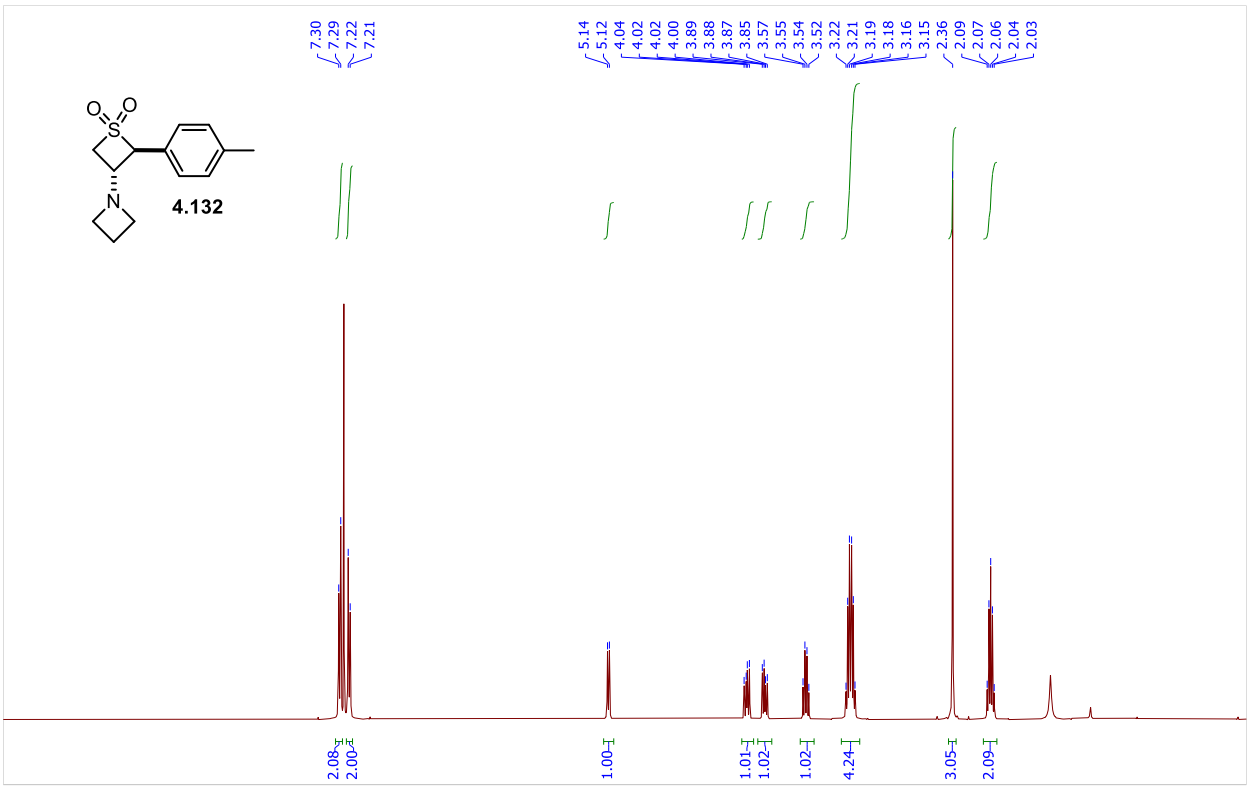

139.47
135.14
129.04
126.15
54.61
49.77
25.96
24.55
24.25
21.08
16.37
4.149
f1 (ppm)

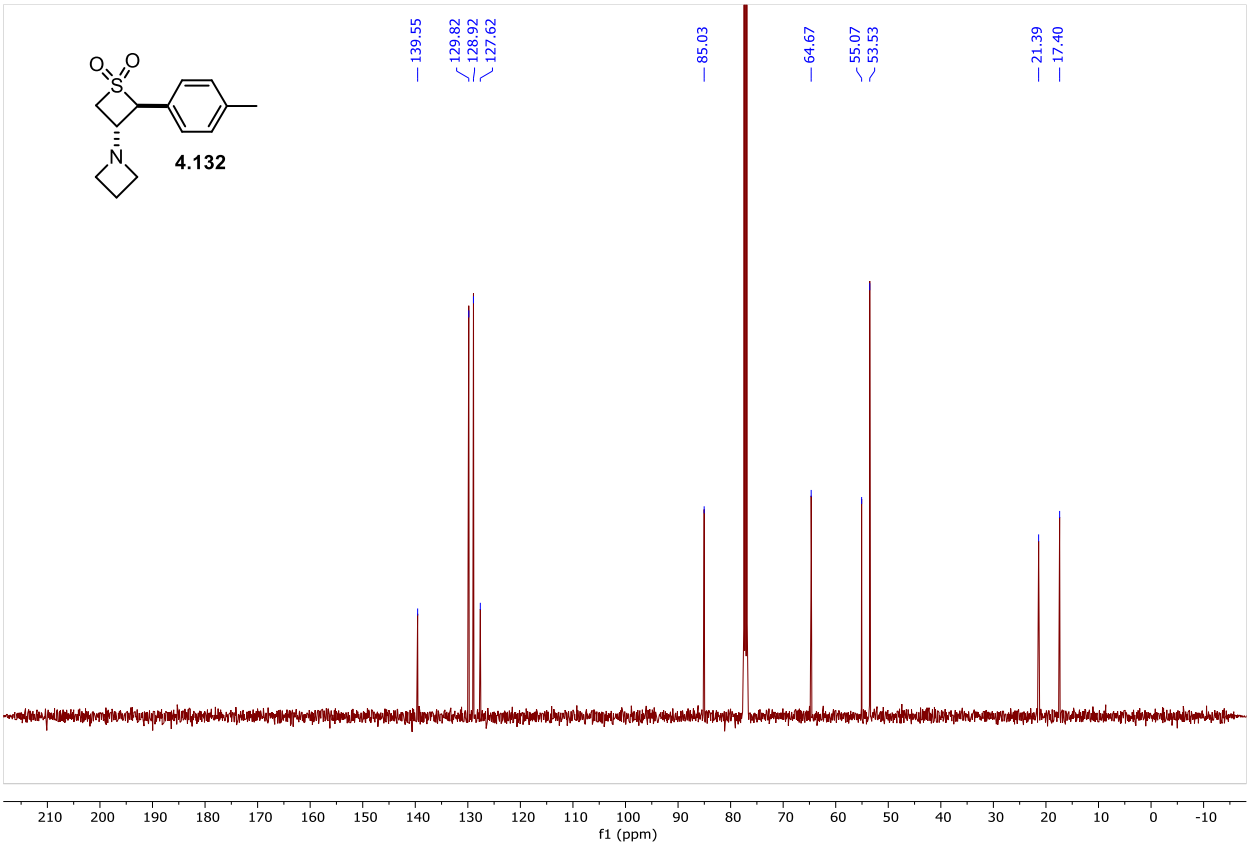

7.34
7.32
7.31
7.23
7.21
5.29
5.26
4.13
4.10
4.09
4.08
4.08
4.06
4.05
4.05
4.04
4.03
4.02
3.99
3.46
3.44
3.41
3.38
2.45
2.42
2.41
2.40
2.39
2.37
2.37
1.78
1.77
1.76
1.75
1.74
4.133
1.96
1.92
1.00
1.99
0.99
3.80
3.16
4.01
f1 (ppm)

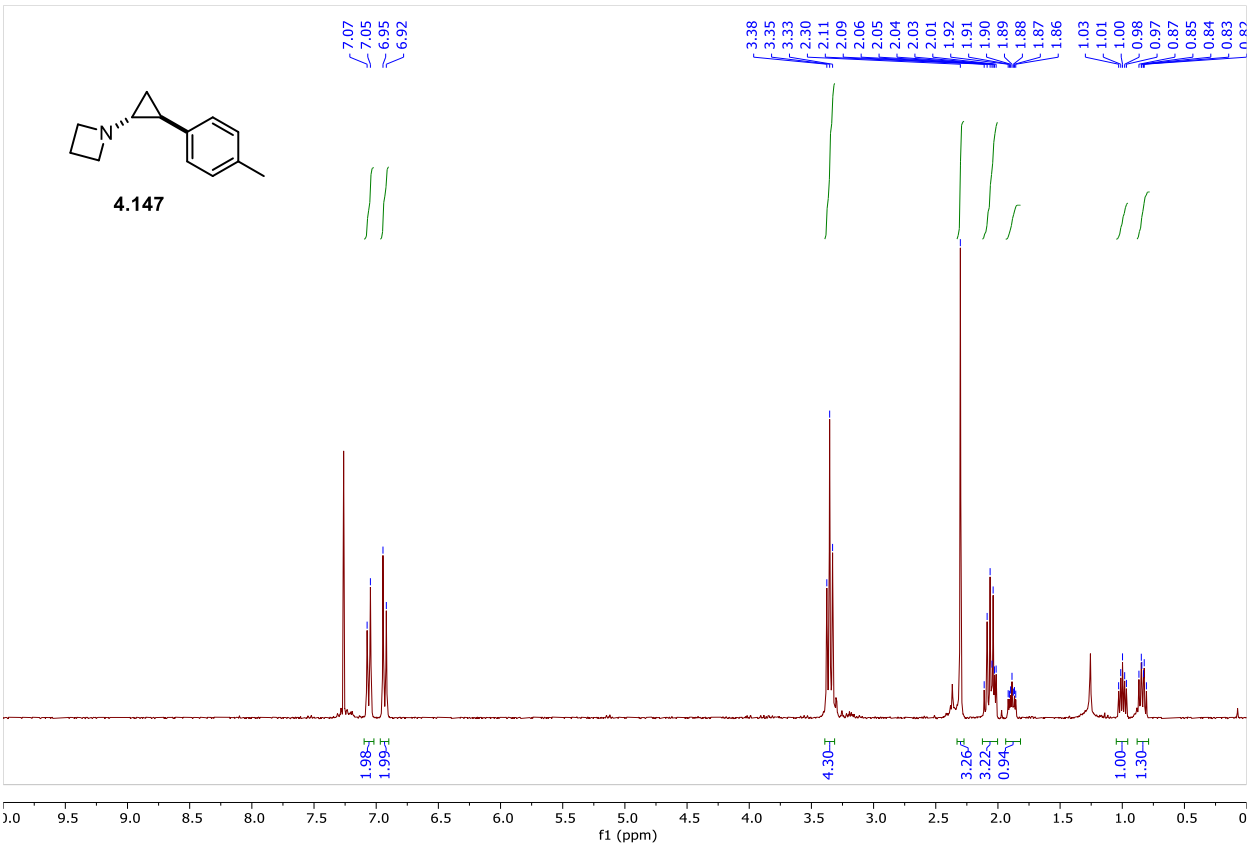

139.40
129.62
128.96
127.23
85.60
65.53
53.60
52.76
23.56
21.25
4.133
f1 (ppm)

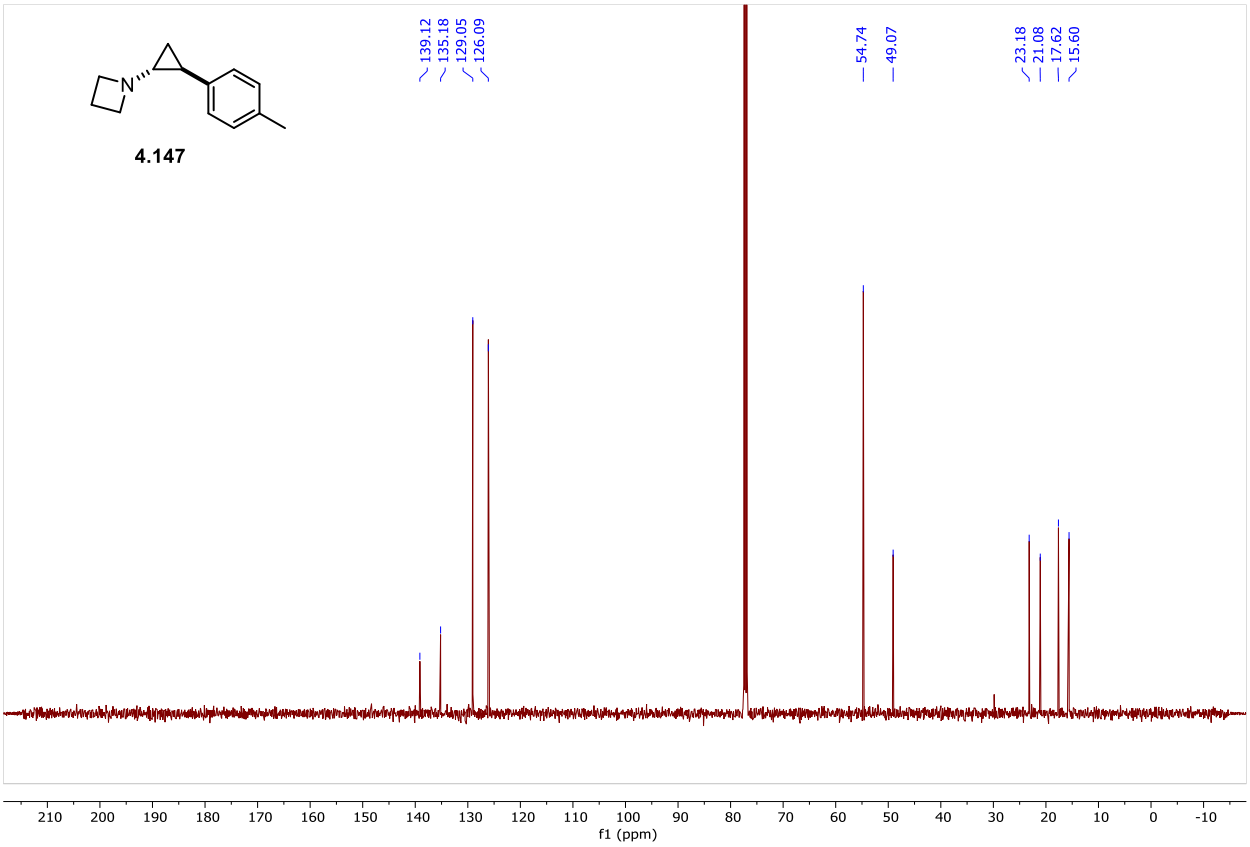

7.08
7.05
6.98
6.95
2.73
2.30
2.02
1.86
1.85
1.80
1.16
1.15
1.13
0.96
0.94
0.92
0.90
0.88
0.85
2.13
2.06
4.00
3.30
1.20
5.31
1.21
1.30
f1 (ppm)

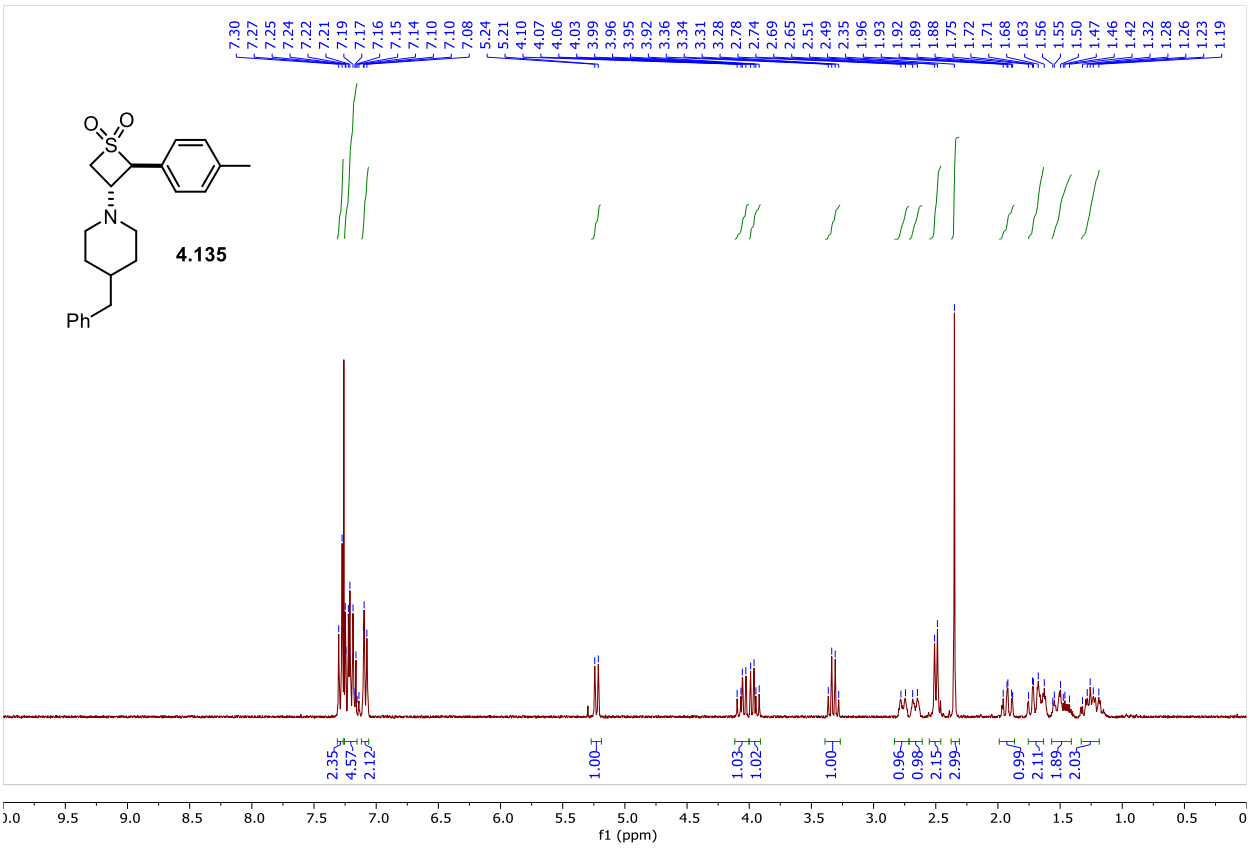

4.148
139.20
135.22
129.07
126.18
53.85
46.42
29.85
23.74
21.09
16.19
f1 (ppm)

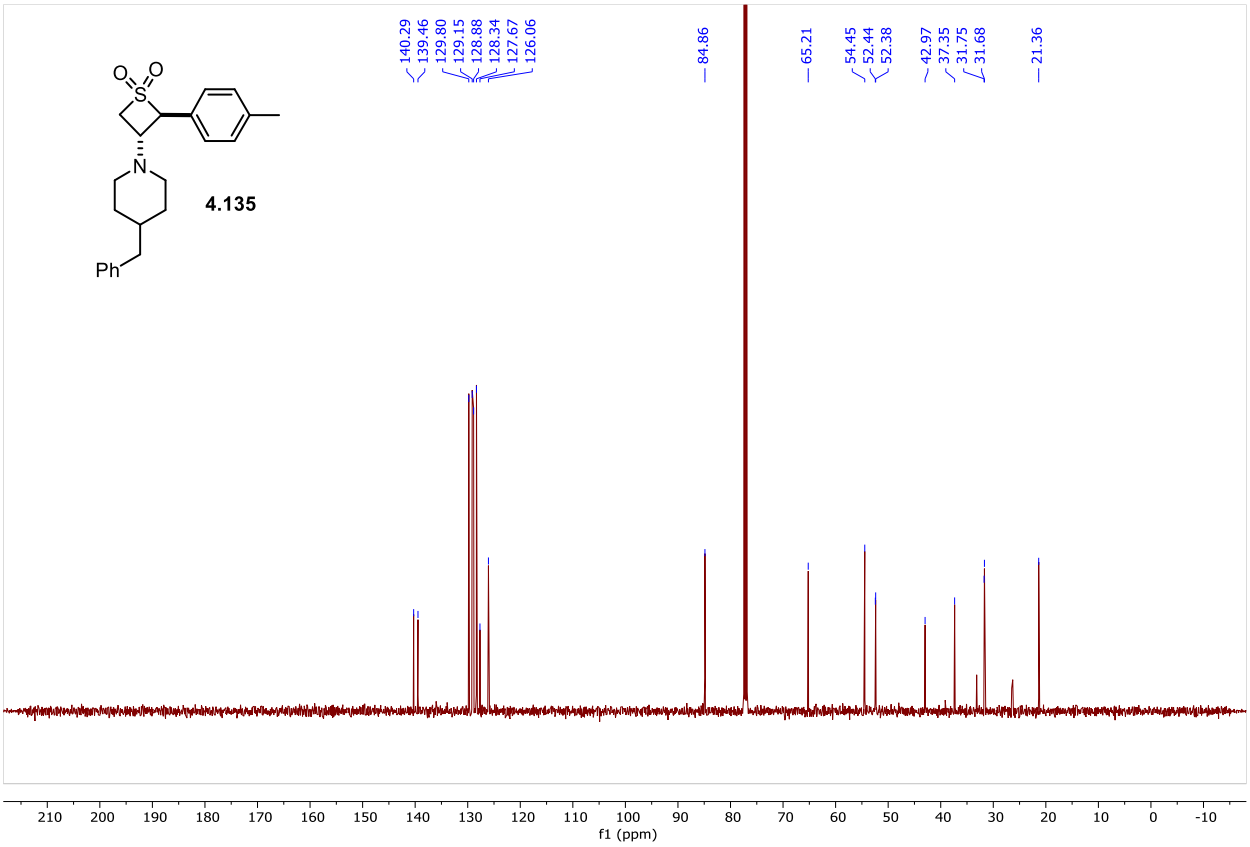

7.30
7.29
7.22
7.21
5.14
5.12
4.04
4.02
4.02
4.00
3.89
3.88
3.87
3.85
3.57
3.55
3.54
3.52
3.22
3.21
3.19
3.18
3.16
3.15
2.36
2.09
2.07
2.06
2.04
2.03
4.132
2.08
2.00
1.00
1.01
1.02
1.02
4.24
3.05
2.09
f1 (ppm)

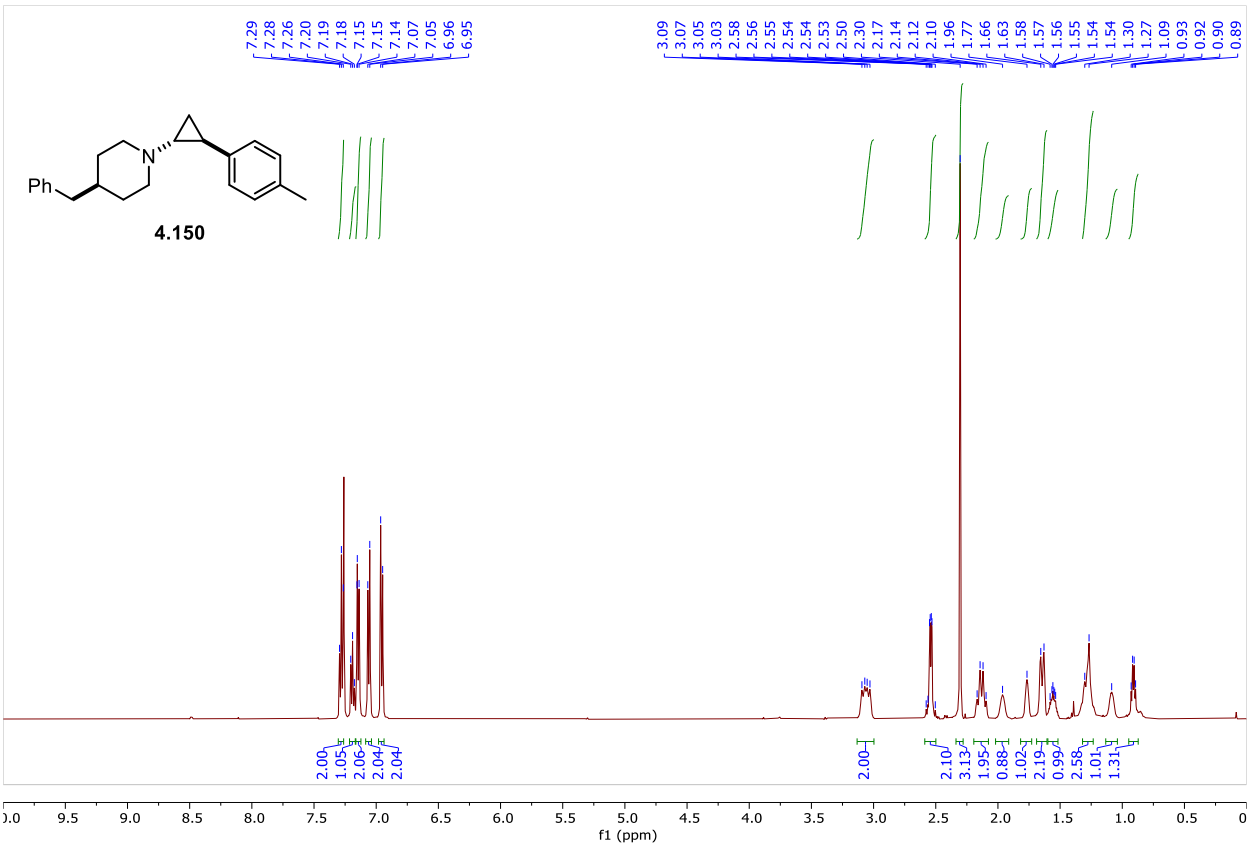

139.55
129.82
128.92
127.62
85.03
64.67
55.07
53.53
21.39
17.40
4.132
f1 (ppm)

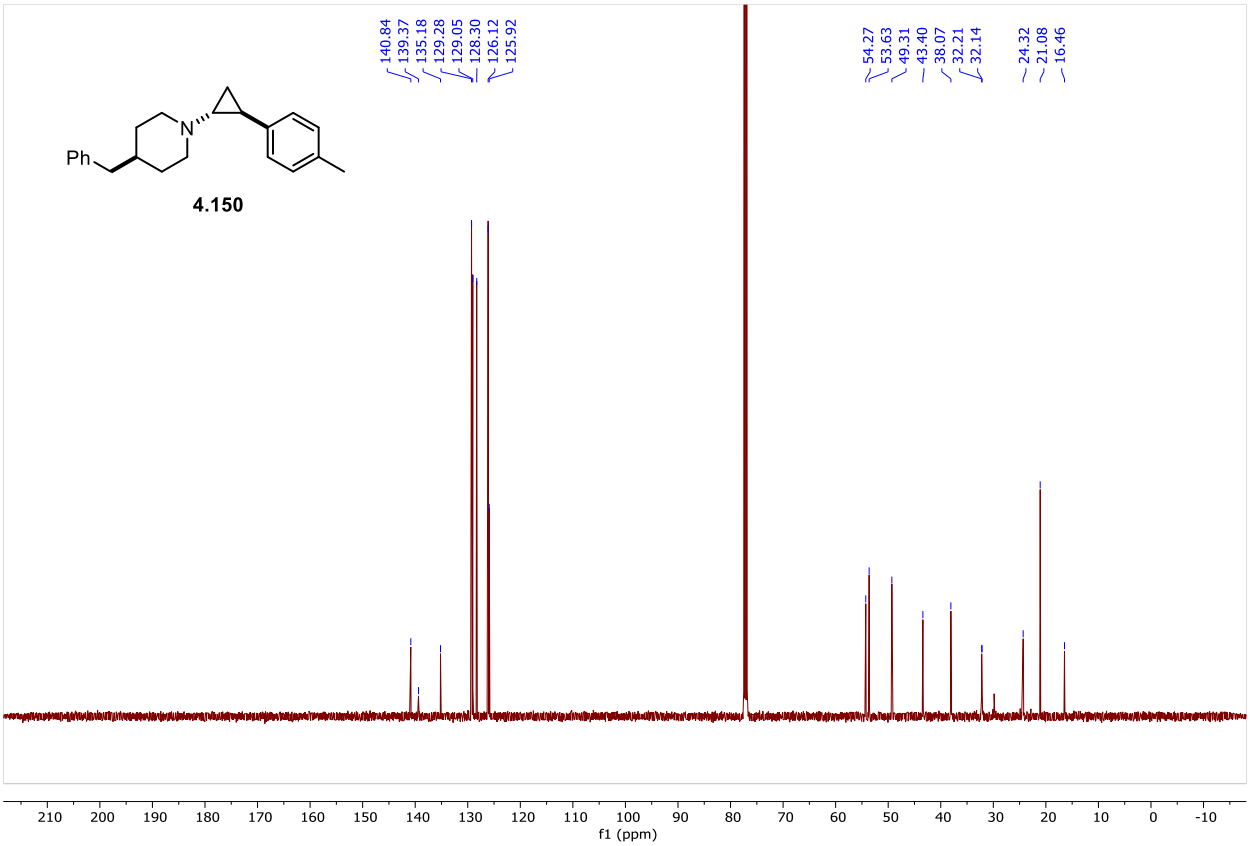

4.147
7.07
7.05
6.95
6.92
3.38
3.35
3.33
3.30
2.11
2.09
2.06
2.05
2.04
2.03
2.01
1.92
1.91
1.90
1.89
1.88
1.87
1.86
1.03
1.01
1.00
0.98
0.97
0.87
0.85
0.84
0.83
1.98
1.99
4.30
3.26
3.22
0.94
1.00
1.30
f1 (ppm)

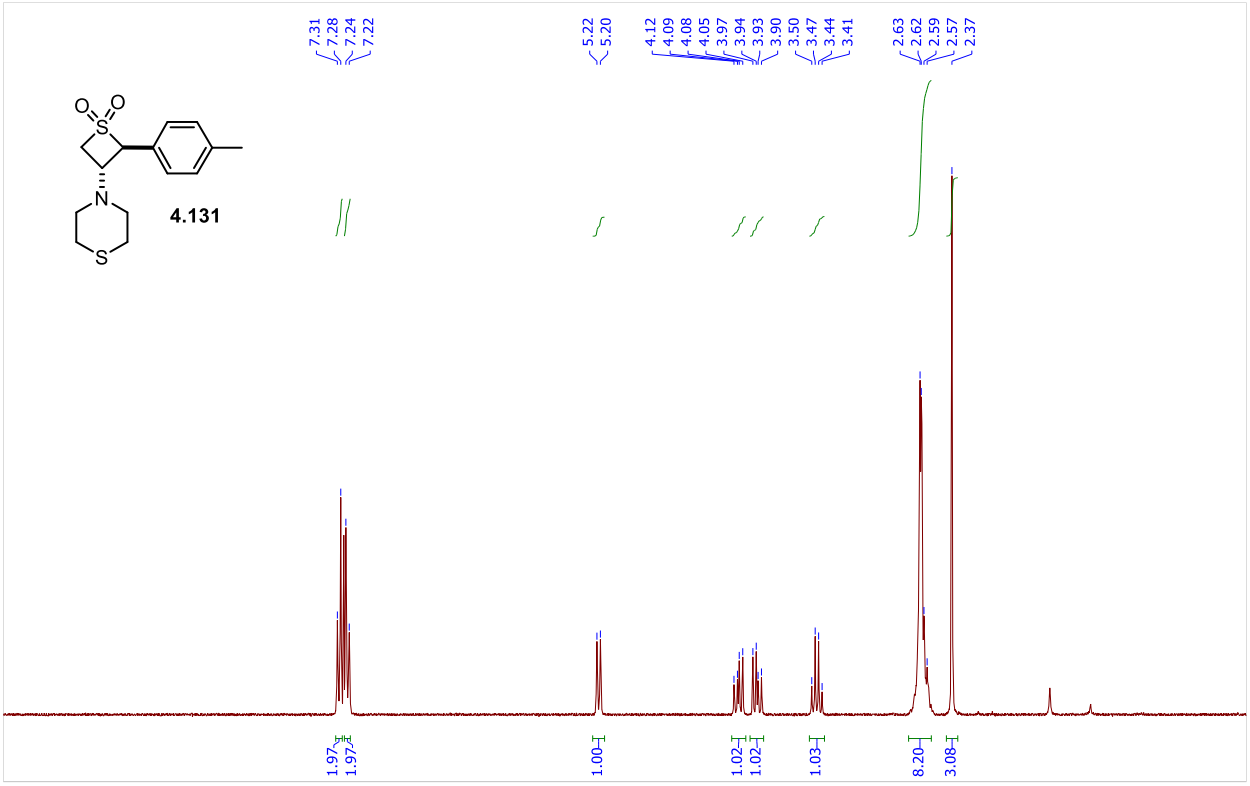

4.147
139.12
135.18
129.05
126.09
54.74
49.07
23.18
21.08
17.62
15.60
f1 (ppm)

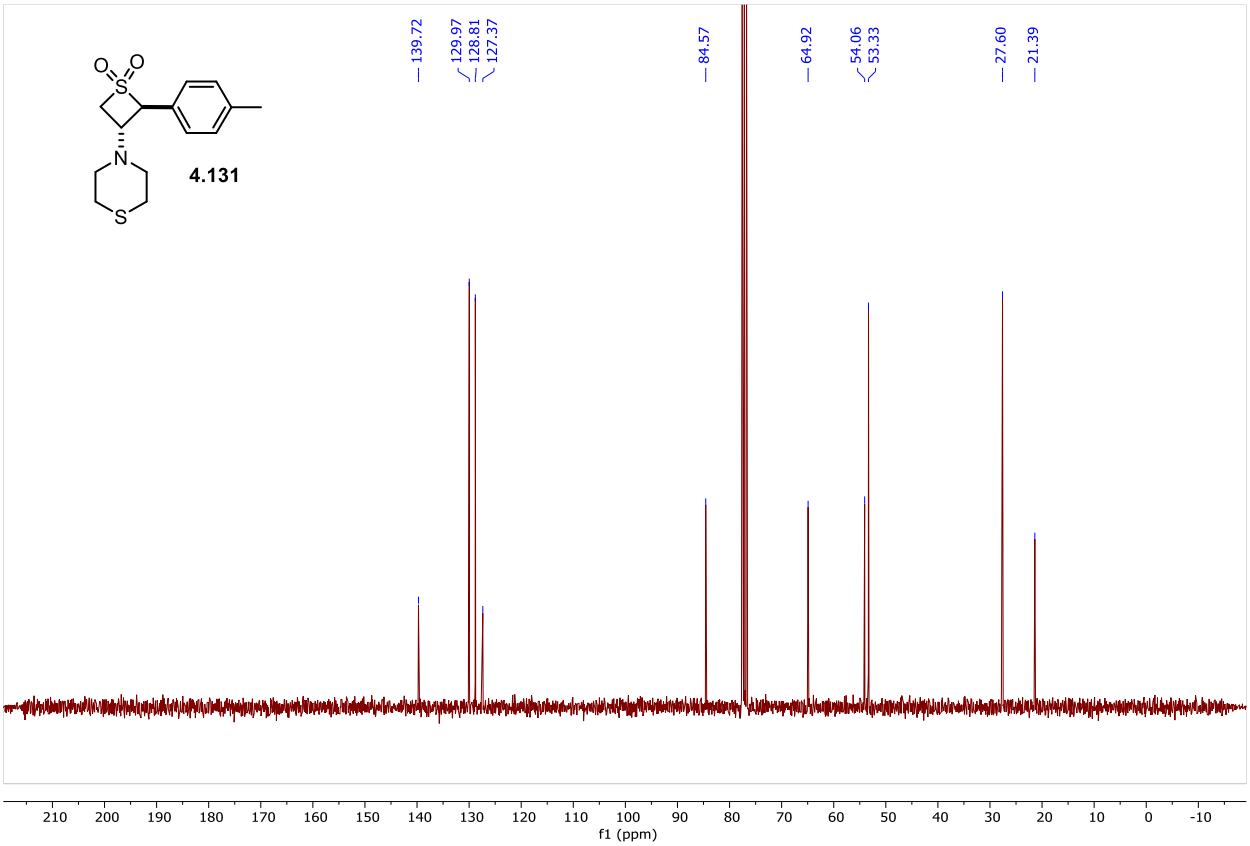

7.30 7.27 7.25 7.24 7.22 7.21 7.19 7.17 7.16 7.15 7.14 7.10 7.10 7.08
5.24 5.21 4.10 4.07 4.06 4.03 3.99 3.96 3.95 3.92 3.36 3.34 3.31 3.28 2.78 2.74 2.69 2.65 2.51 2.49 2.35 1.96 1.93 1.92 1.89 1.88 1.75 1.72 1.71 1.68 1.63 1.56 1.55 1.50 1.47 1.46 1.42 1.32 1.28 1.26 1.23 1.19
4.135
Ph
2.35 4.57 2.12 1.00 1.03 1.02 1.00 0.96 0.98 2.15 2.99 0.99 2.11 1.89 2.03
f1 (ppm)

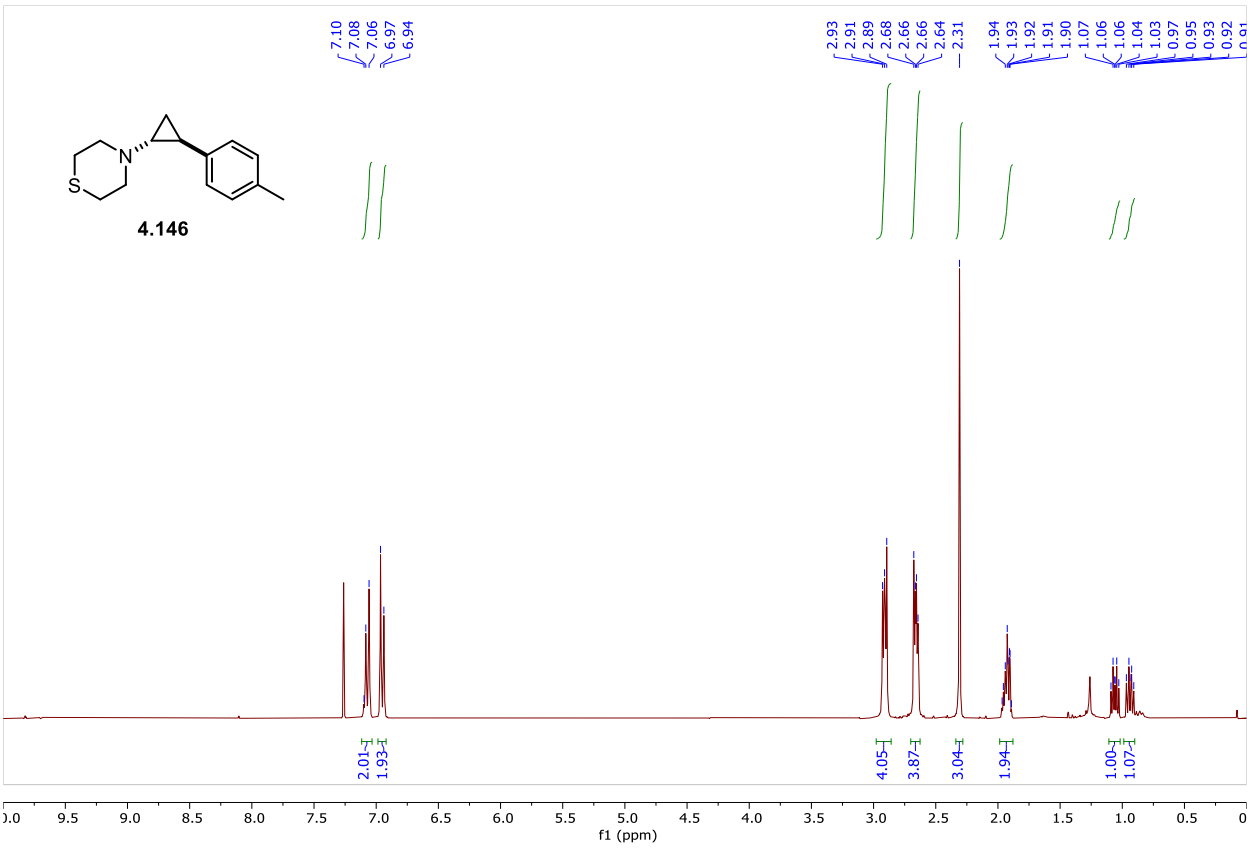

140.29 139.46 129.80 129.15 128.88 128.34 127.67 126.06
84.86
65.21
54.45 52.44 52.38
42.97 37.35 31.75 31.68
21.36
4.135
Ph
f1 (ppm)

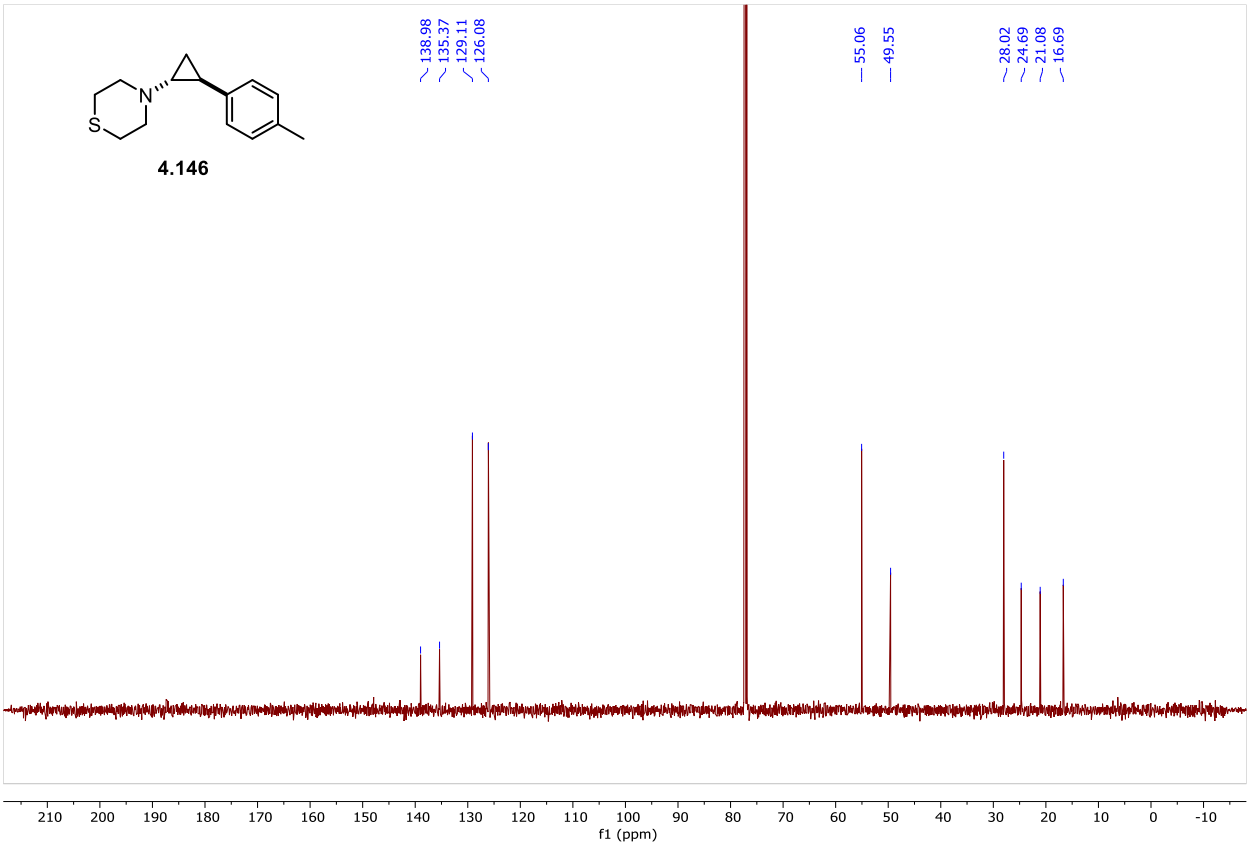

7.29
7.28
7.26
7.20
7.19
7.18
7.15
7.15
7.14
7.07
7.05
6.96
6.95
3.09
3.07
3.05
3.03
2.58
2.56
2.55
2.54
2.54
2.53
2.50
2.30
2.17
2.14
2.12
2.10
1.96
1.77
1.66
1.63
1.58
1.57
1.56
1.55
1.54
1.54
1.30
1.27
1.09
0.93
0.92
0.90
0.89
Ph
N
4.150
2.00
1.05
2.06
2.04
2.04
2.00
2.10
3.13
1.95
0.88
1.02
2.19
0.99
2.58
1.01
1.31
f1 (ppm)

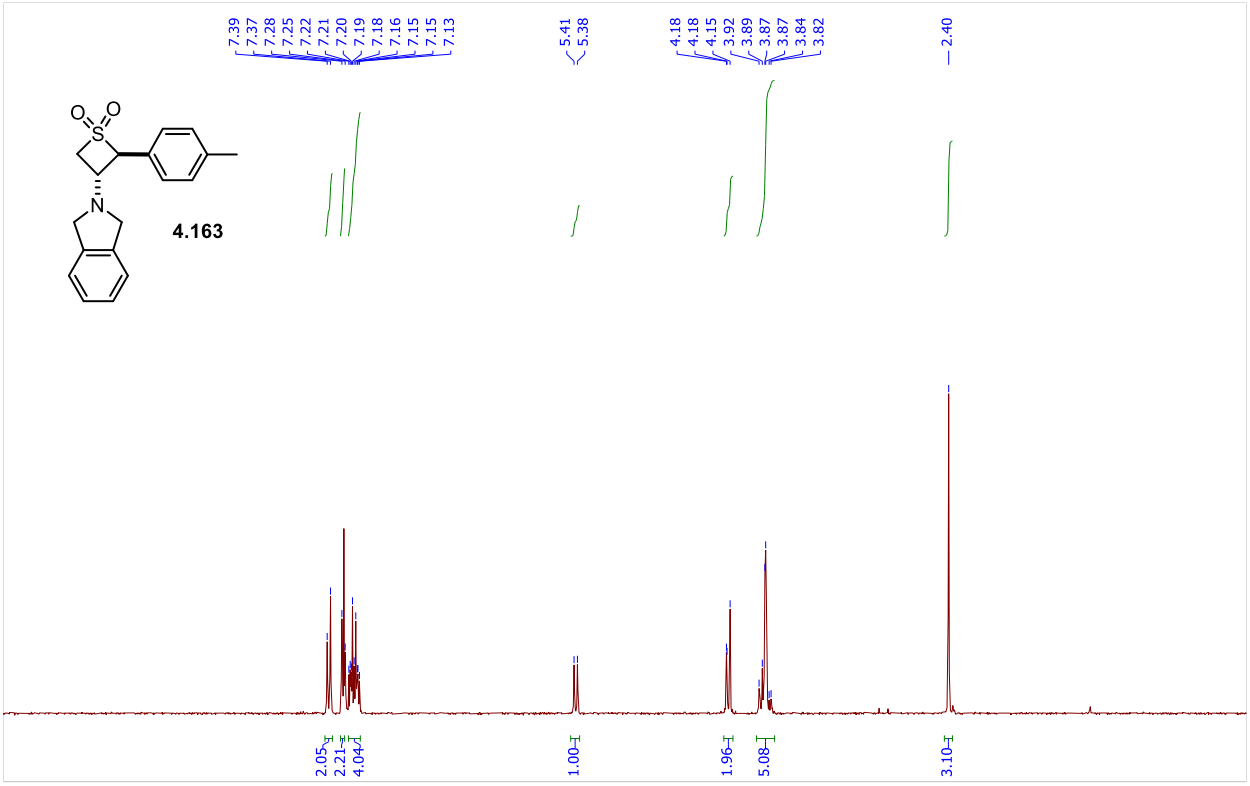

140.84
139.37
135.18
129.28
129.05
128.30
126.12
125.92
54.27
53.63
49.31
43.40
38.07
32.21
32.14
24.32
21.08
16.46
Ph
N
4.150
f1 (ppm)

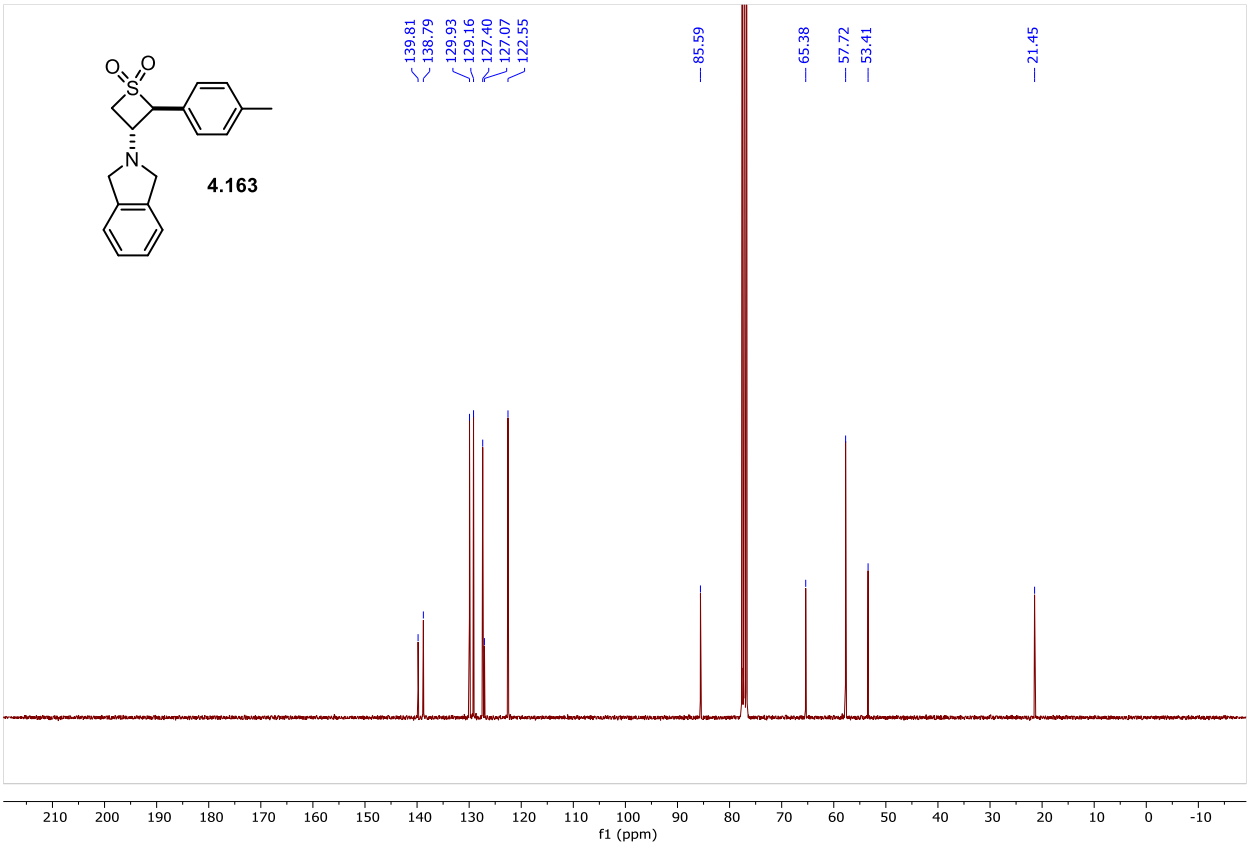

7.31
7.28
7.24
7.22
5.22
5.20
4.12
4.09
4.08
4.05
3.97
3.94
3.93
3.90
3.50
3.47
3.44
3.41
2.63
2.62
2.59
2.57
2.37
4.131
1.97
1.97
1.00
1.02
1.02
1.03
8.20
3.08
f1 (ppm)

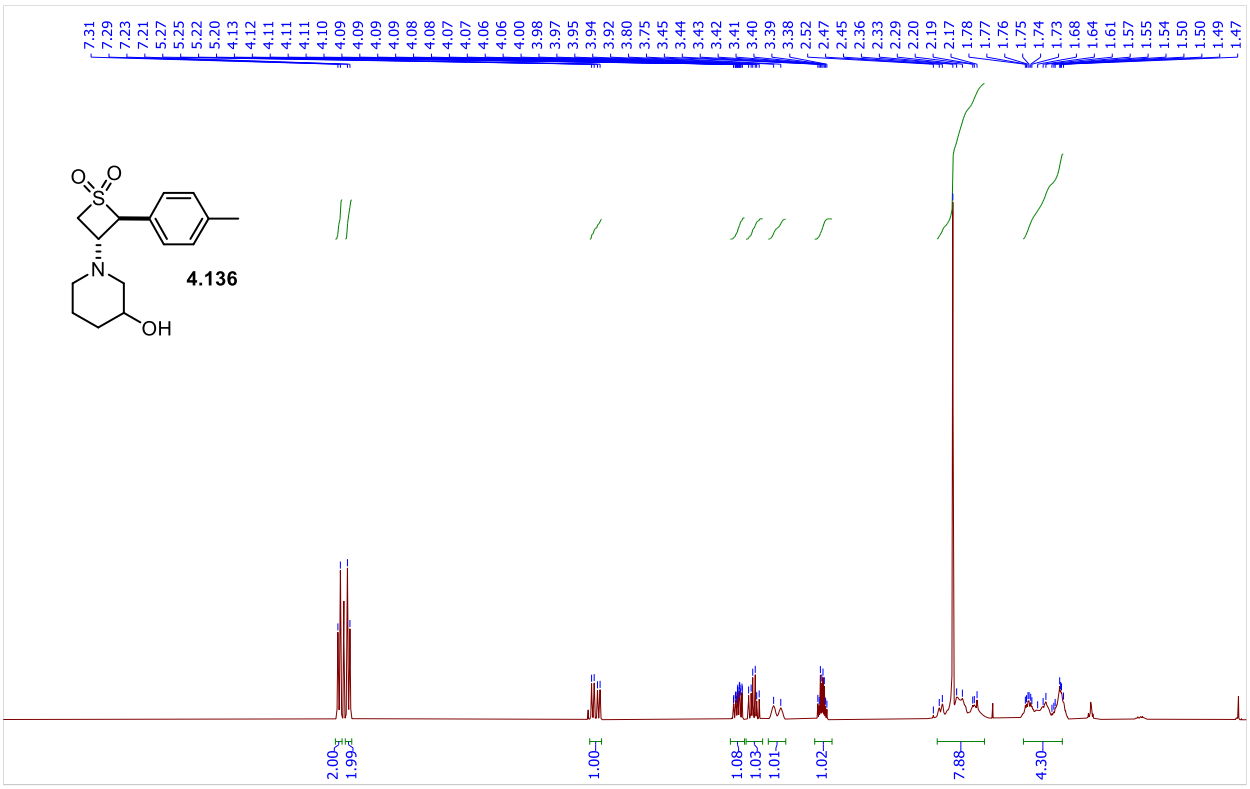

139.72
129.97
128.81
127.37
84.57
64.92
54.06
53.33
27.60
21.39
4.131
f1 (ppm)

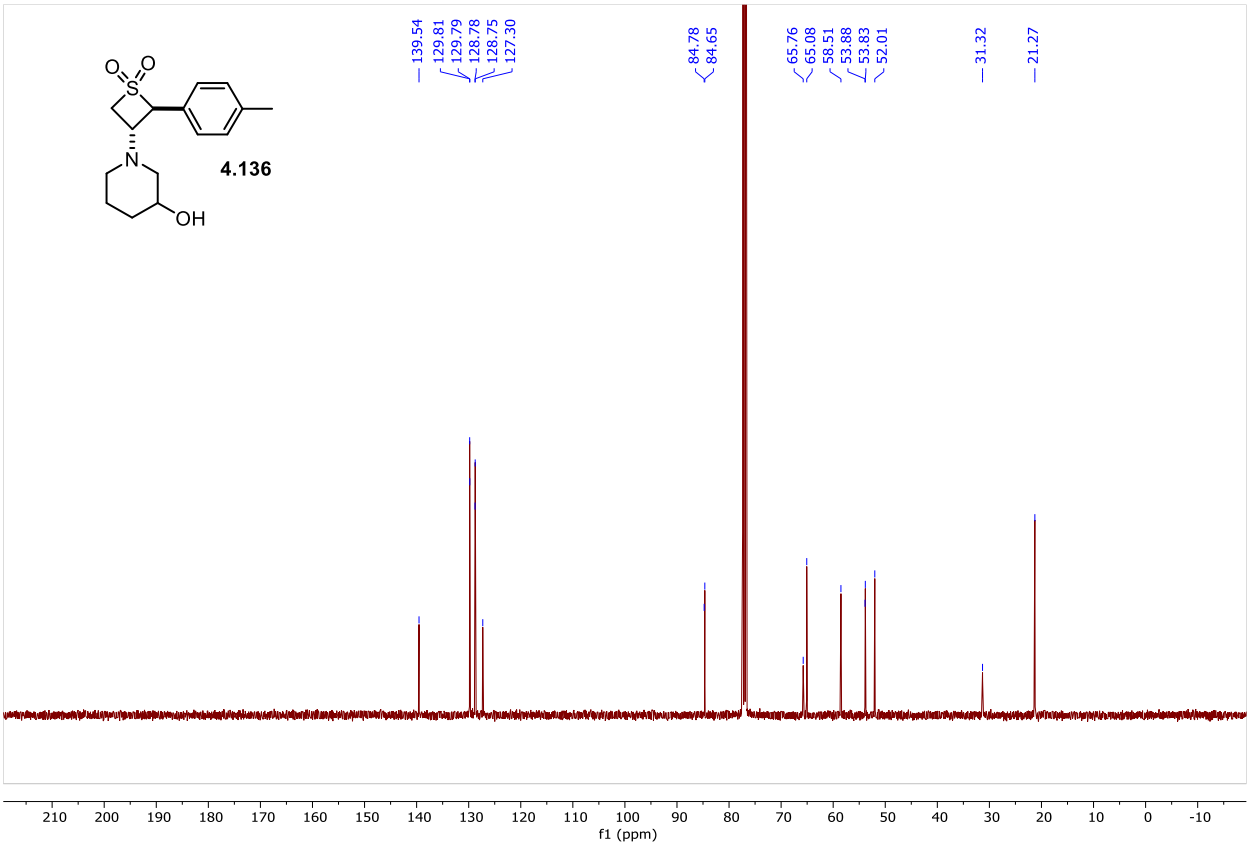

7.10
7.08
7.06
6.97
6.94
2.93
2.91
2.89
2.68
2.66
2.66
2.64
2.31
1.94
1.93
1.92
1.91
1.90
1.07
1.06
1.06
1.04
1.03
0.97
0.95
0.93
0.92
4.146
2.01
1.93
4.05
3.87
3.04
1.94
1.00
1.07
f1 (ppm)

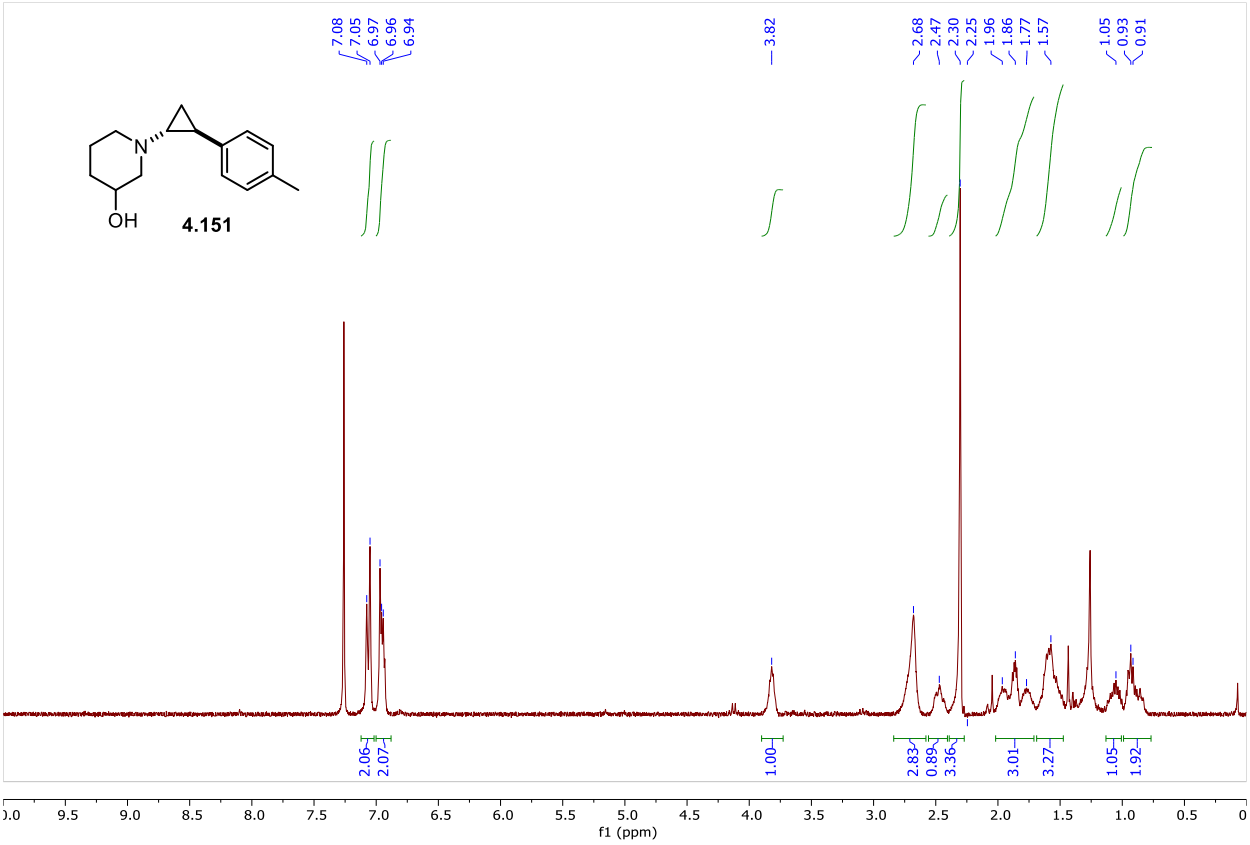

138.98
135.37
129.11
126.08
55.06
49.55
28.02
24.69
21.08
16.69
4.146
f1 (ppm)

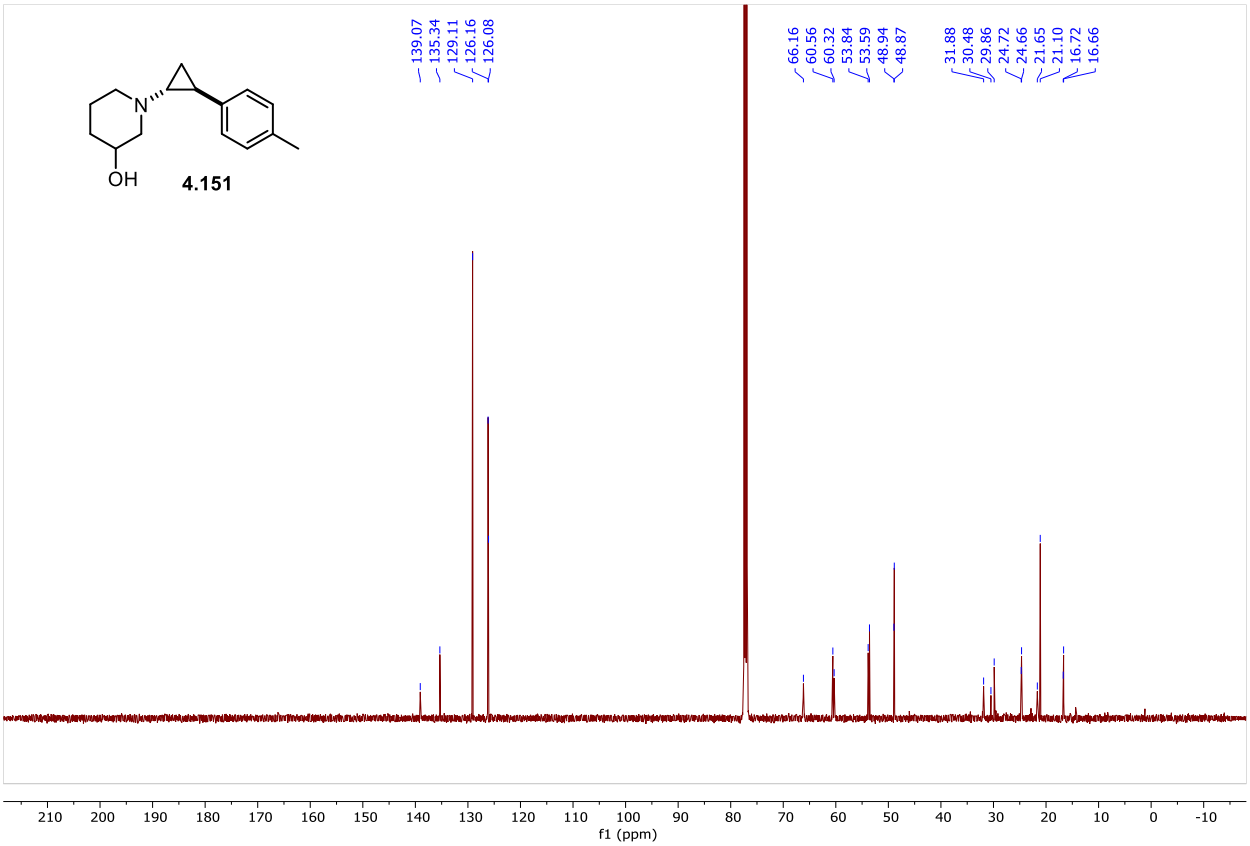

7.39
7.37
7.28
7.25
7.22
7.21
7.20
7.19
7.18
7.16
7.15
7.15
7.13
5.41
5.38
4.18
4.18
4.15
3.92
3.89
3.87
3.87
3.84
3.82
2.40
4.163
2.05
2.21
4.04
1.00
1.96
5.08
3.10
f1 (ppm)

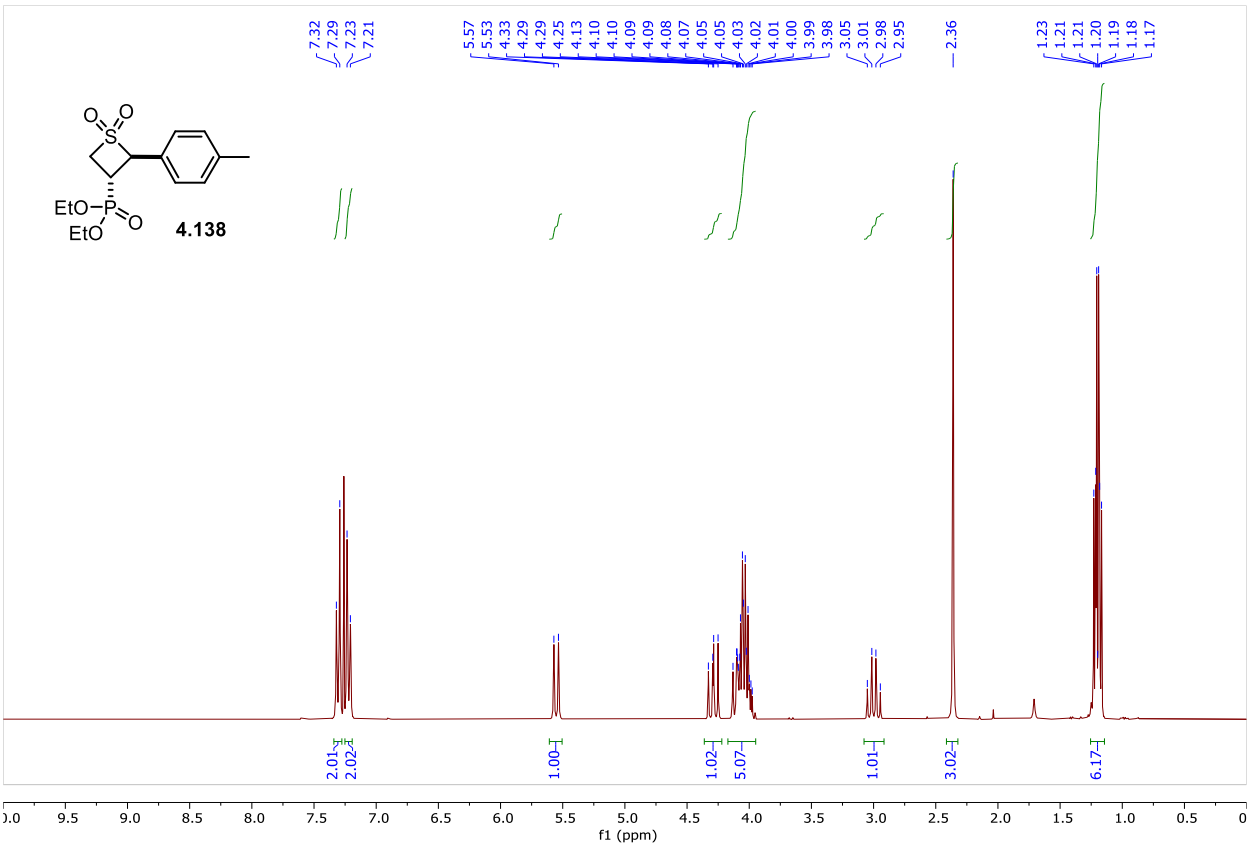

139.81
138.79
129.93
129.16
127.40
127.07
122.55
85.59
65.38
57.72
53.41
21.45
4.163
f1 (ppm)

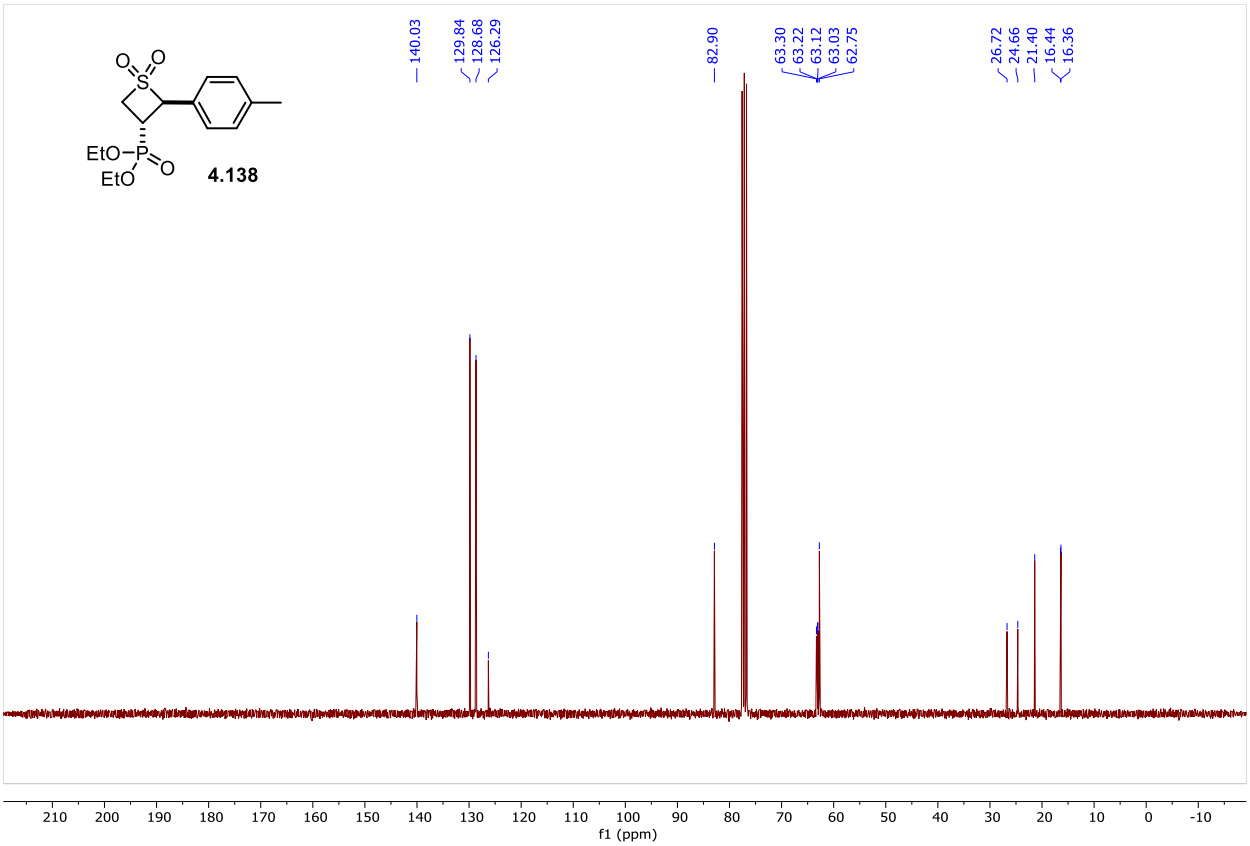

4.136
OH
f1 (ppm)

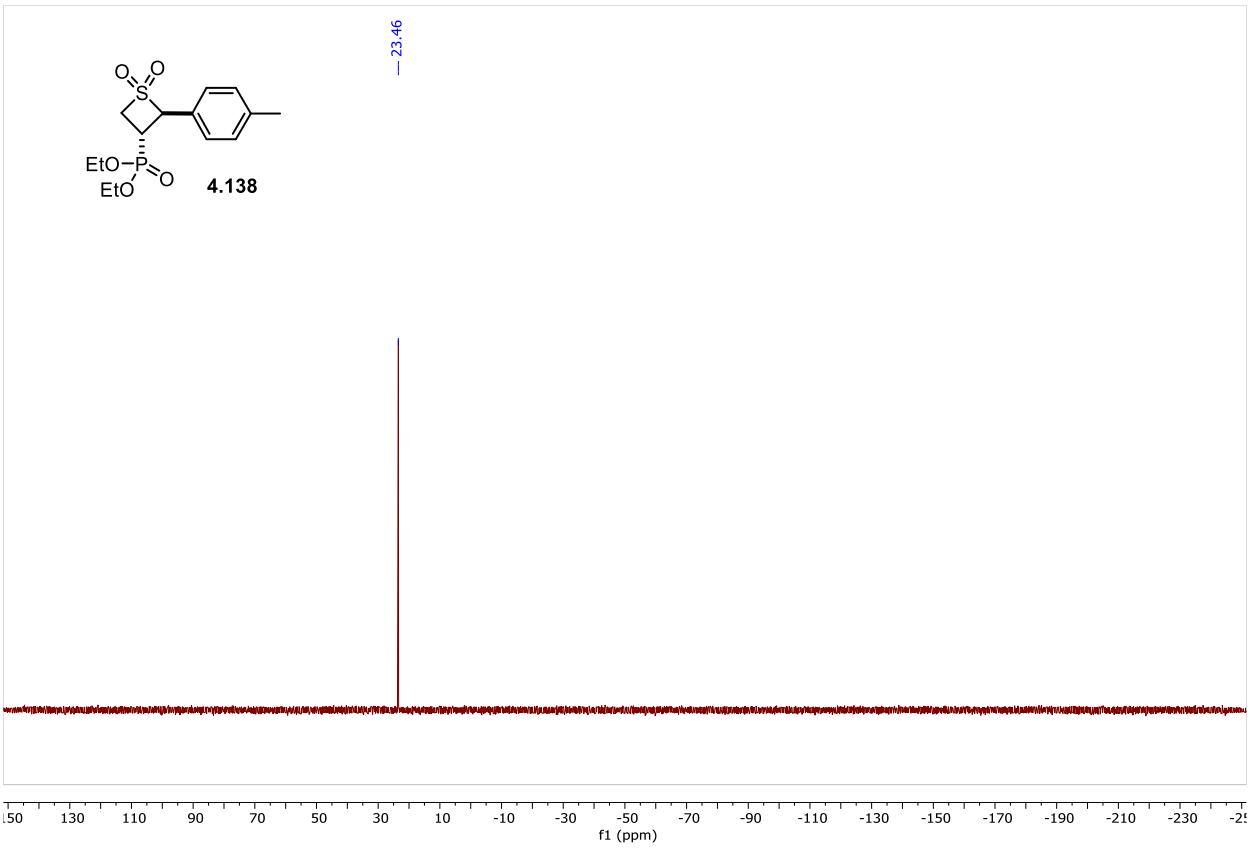

4.136
OH
f1 (ppm)

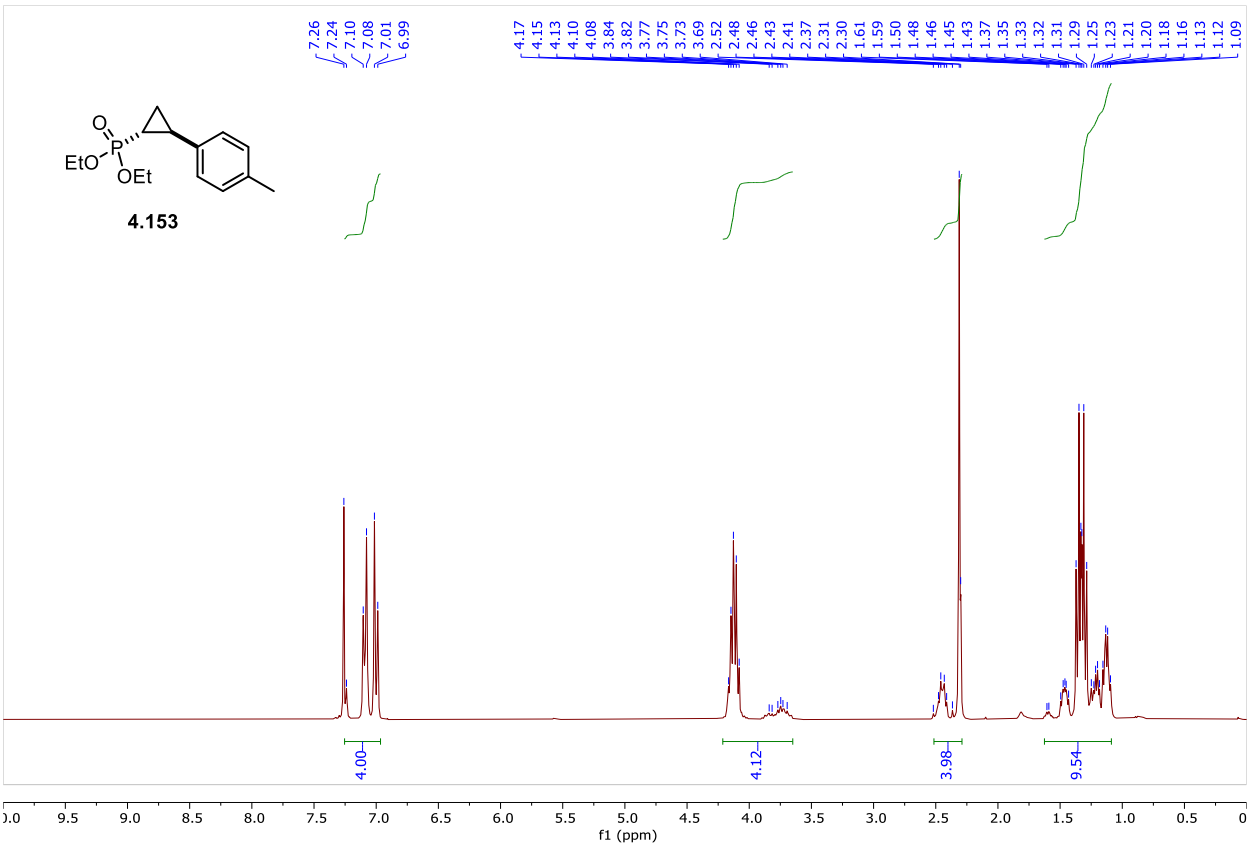

7.08
7.05
6.97
6.96
6.94
3.82
2.68
2.47
2.30
2.25
1.96
1.86
1.77
1.57
1.05
0.93
0.91
OH
4.151
2.06
2.07
1.00
2.83
0.89
3.36
3.01
3.27
1.05
1.92
f1 (ppm)

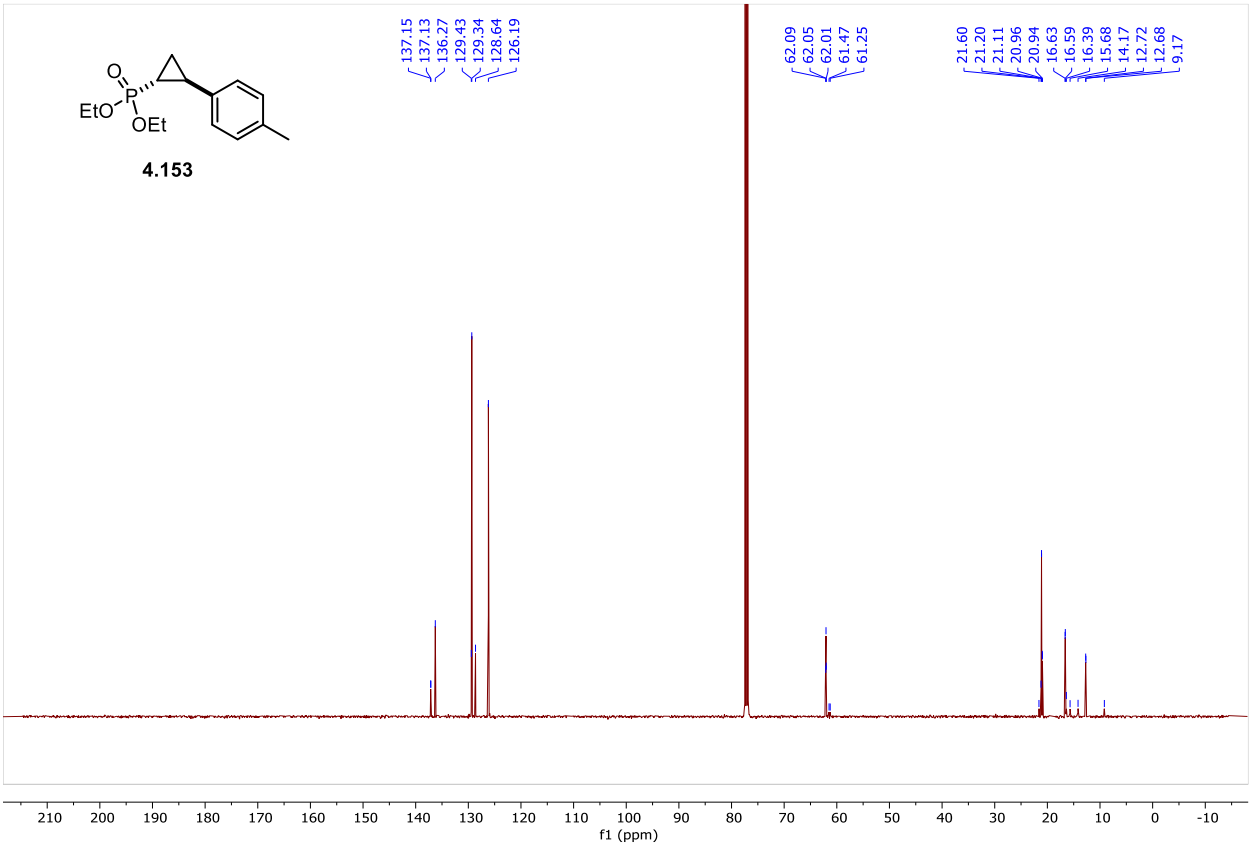

139.07
135.34
129.11
126.16
126.08
66.16
60.56
60.32
53.84
53.59
48.94
48.87
31.88
30.48
29.86
24.72
24.66
21.65
21.10
16.72
16.66
OH
4.151
f1 (ppm)

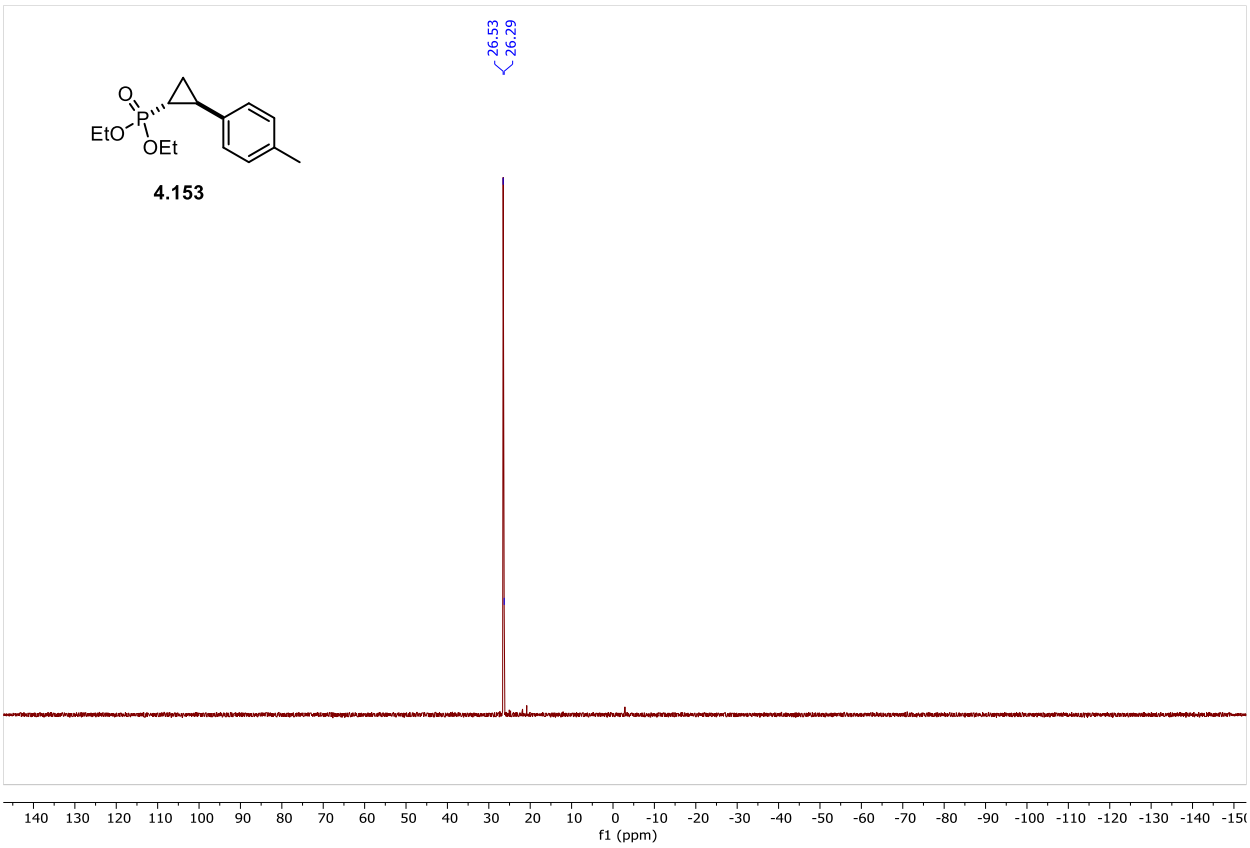

7.32
7.29
7.23
7.21
5.57
5.53
4.33
4.29
4.29
4.25
4.13
4.10
4.10
4.09
4.09
4.08
4.07
4.05
4.05
4.03
4.02
4.01
4.00
3.99
3.98
3.05
3.01
2.98
2.95
2.36
1.23
1.21
1.21
1.20
1.19
1.18
1.17
4.138
2.01
2.02
1.00
1.02
5.07
1.01
3.02
6.17
f1 (ppm)

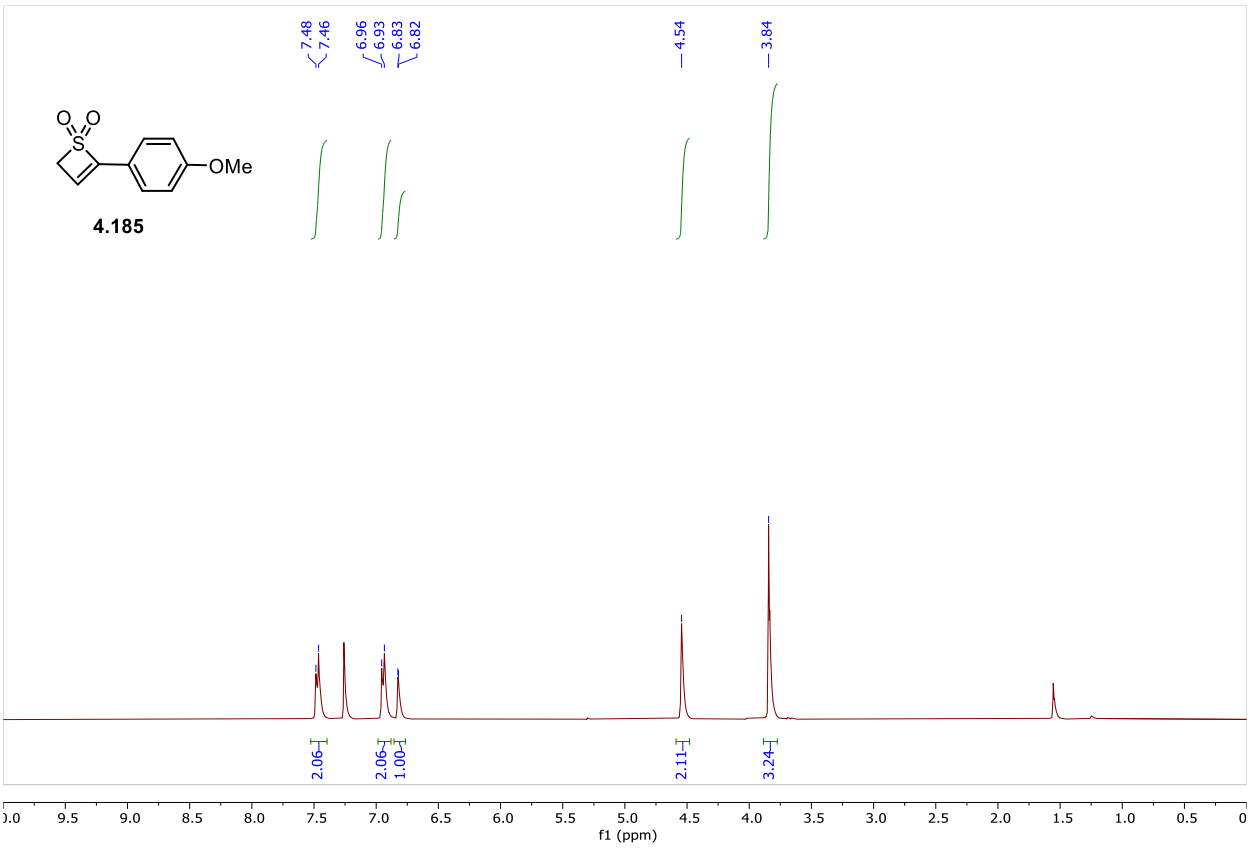

140.03
129.84
128.68
126.29
82.90
63.30
63.22
63.12
63.03
62.75
26.72
24.66
21.40
16.44
16.36
4.138
f1 (ppm)

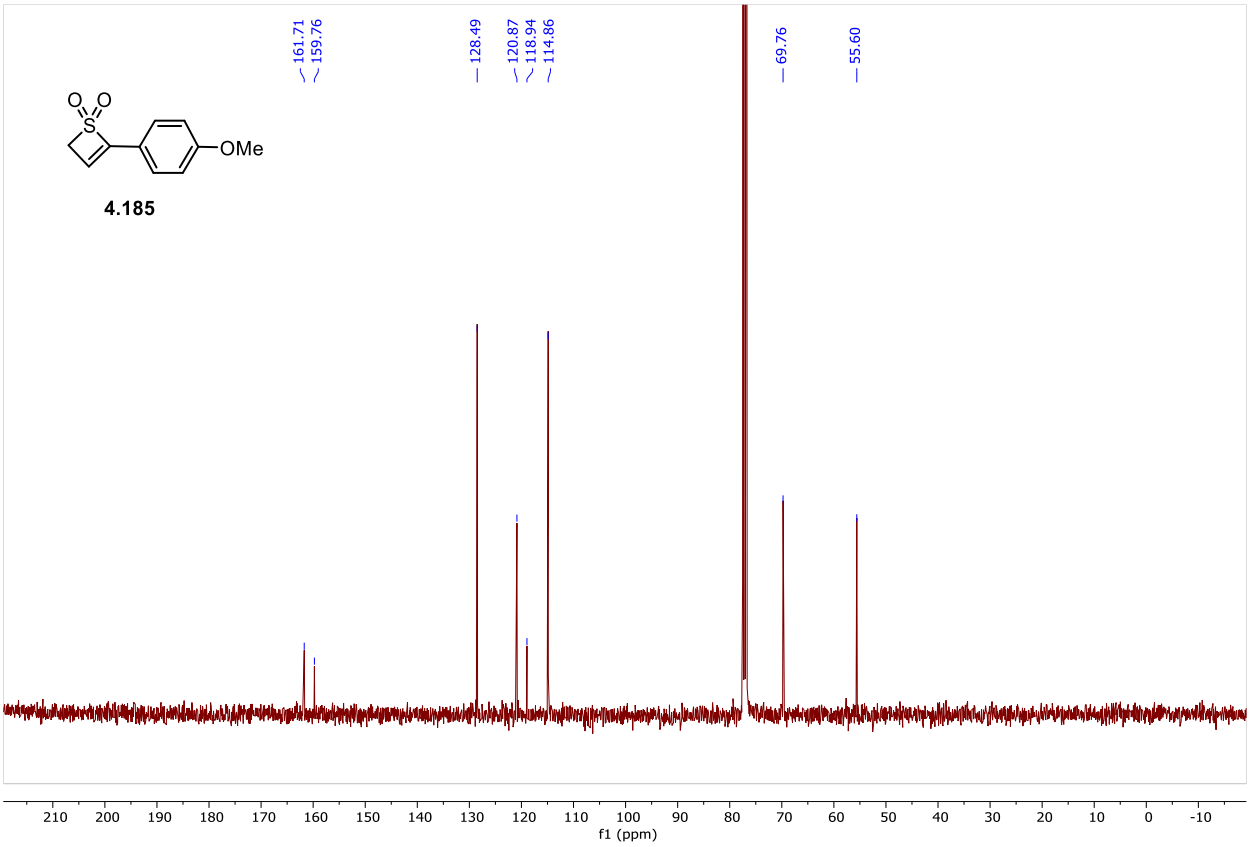

23.46
EtO
P
O
EtO
O
O
S
4.138
150
130
110
90
70
50
30
10
-10
-30
-50
-70
-90
-110
-130
-150
-170
-190
-210
-230
f1 (ppm)

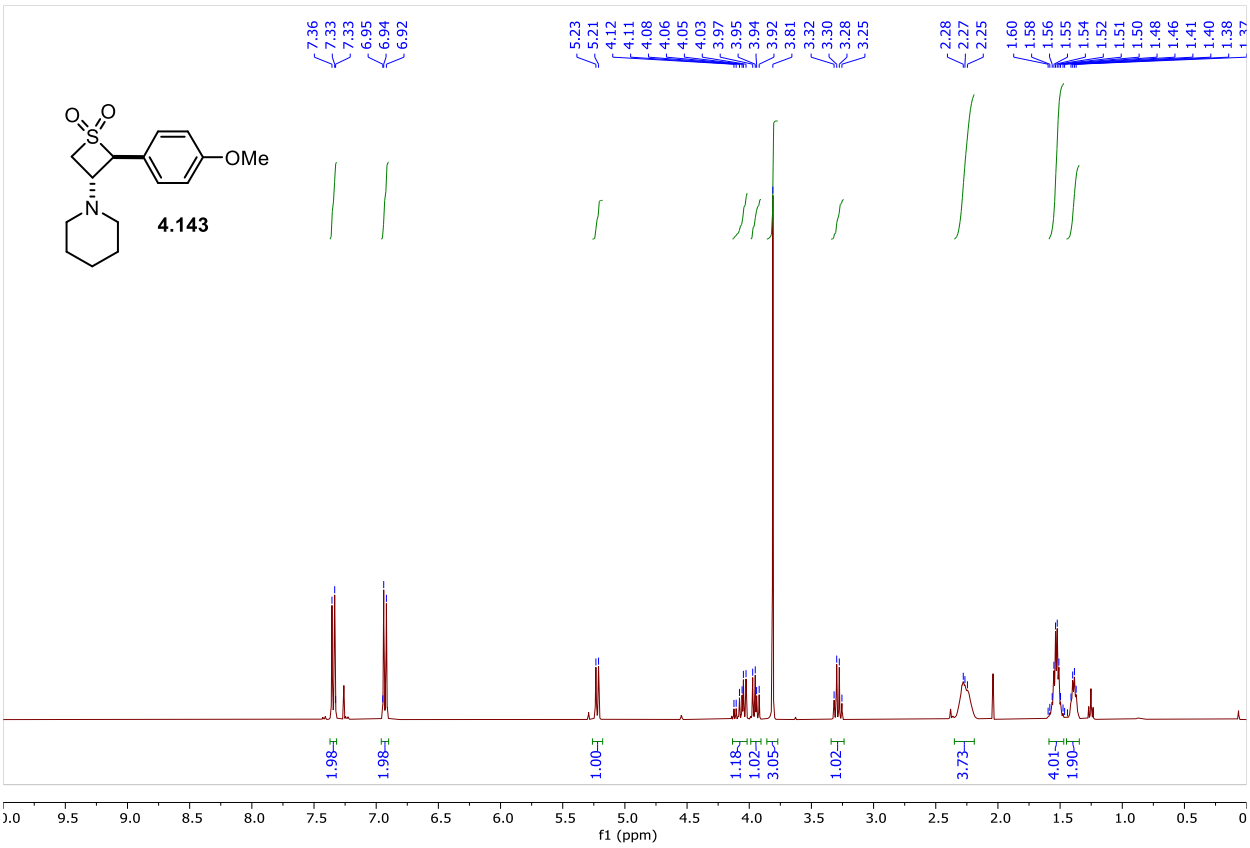

7.26
7.24
7.10
7.08
7.01
6.99
4.17
4.15
4.13
4.10
4.08
3.84
3.82
3.77
3.75
3.73
3.69
2.52
2.48
2.46
2.43
2.41
2.37
2.31
2.30
1.61
1.59
1.50
1.48
1.46
1.45
1.43
1.37
1.35
1.33
1.32
1.31
1.29
1.25
1.23
1.21
1.20
1.18
1.16
1.13
1.12
1.09
EtO
OEt
4.153
4.00
4.12
3.98
9.54
f1 (ppm)

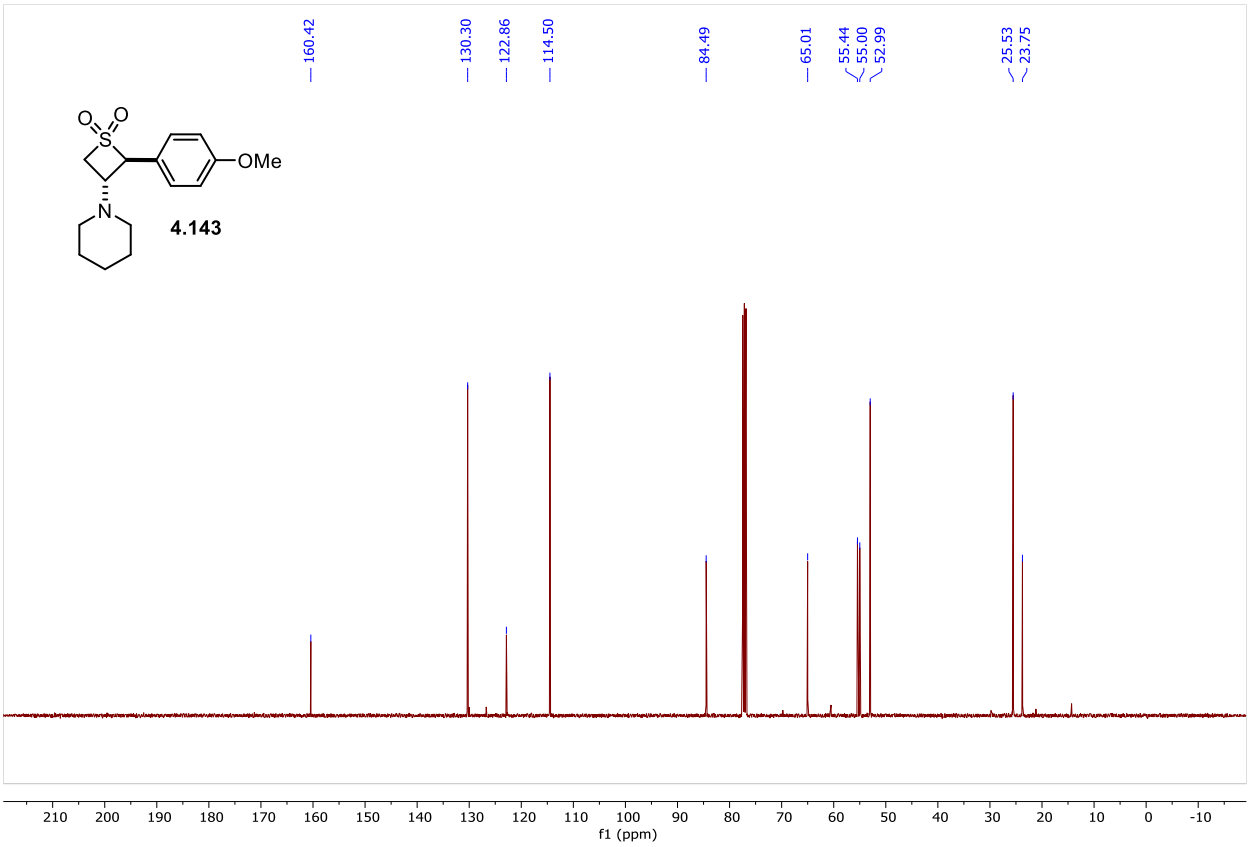

137.15
137.13
136.27
129.43
129.34
128.64
126.19
62.09
62.05
62.01
61.47
61.25
21.60
21.20
21.11
20.96
20.94
16.63
16.59
16.39
15.68
14.17
12.72
12.68
9.17
EtO
OEt
4.153
f1 (ppm)

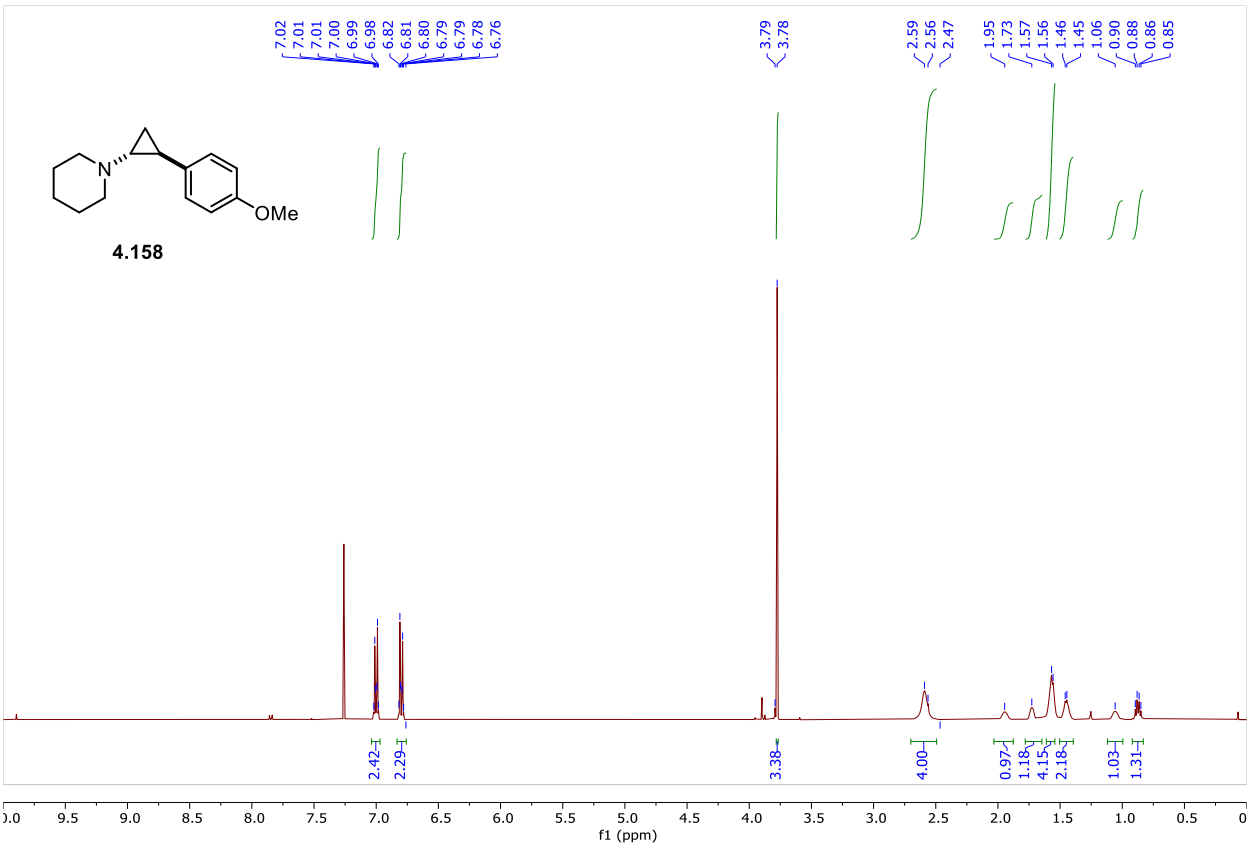

26.53
26.29
O
P
EtO
OEt
4.153
140 130 120 110 100 90 80 70 60 50 40 30 20 10 0 -10 -20 -30 -40 -50 -60 -70 -80 -90 -100 -110 -120 -130 -140
f1 (ppm)

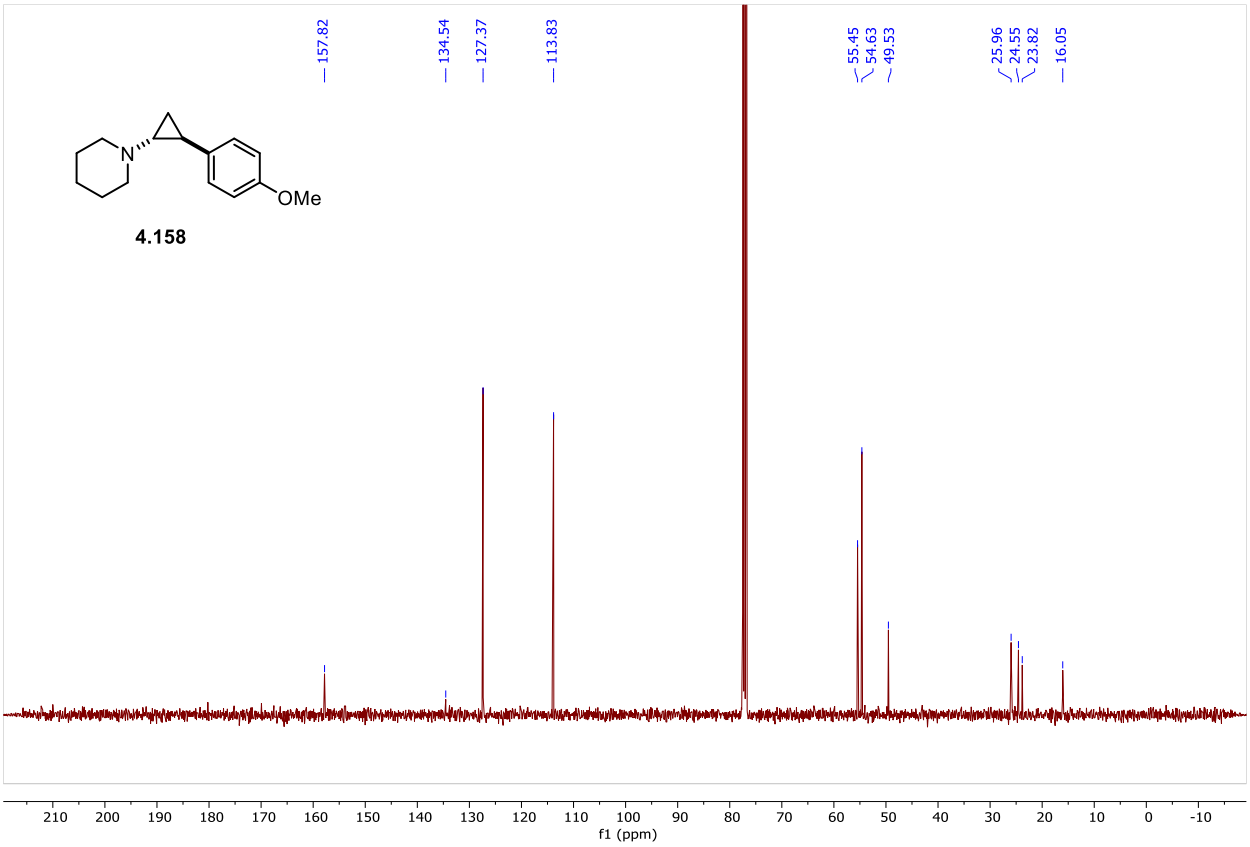

7.48
7.46
6.96
6.93
6.83
6.82
4.54
3.84
OMe
4.185
2.06
2.06
1.00
2.11
3.24
f1 (ppm)

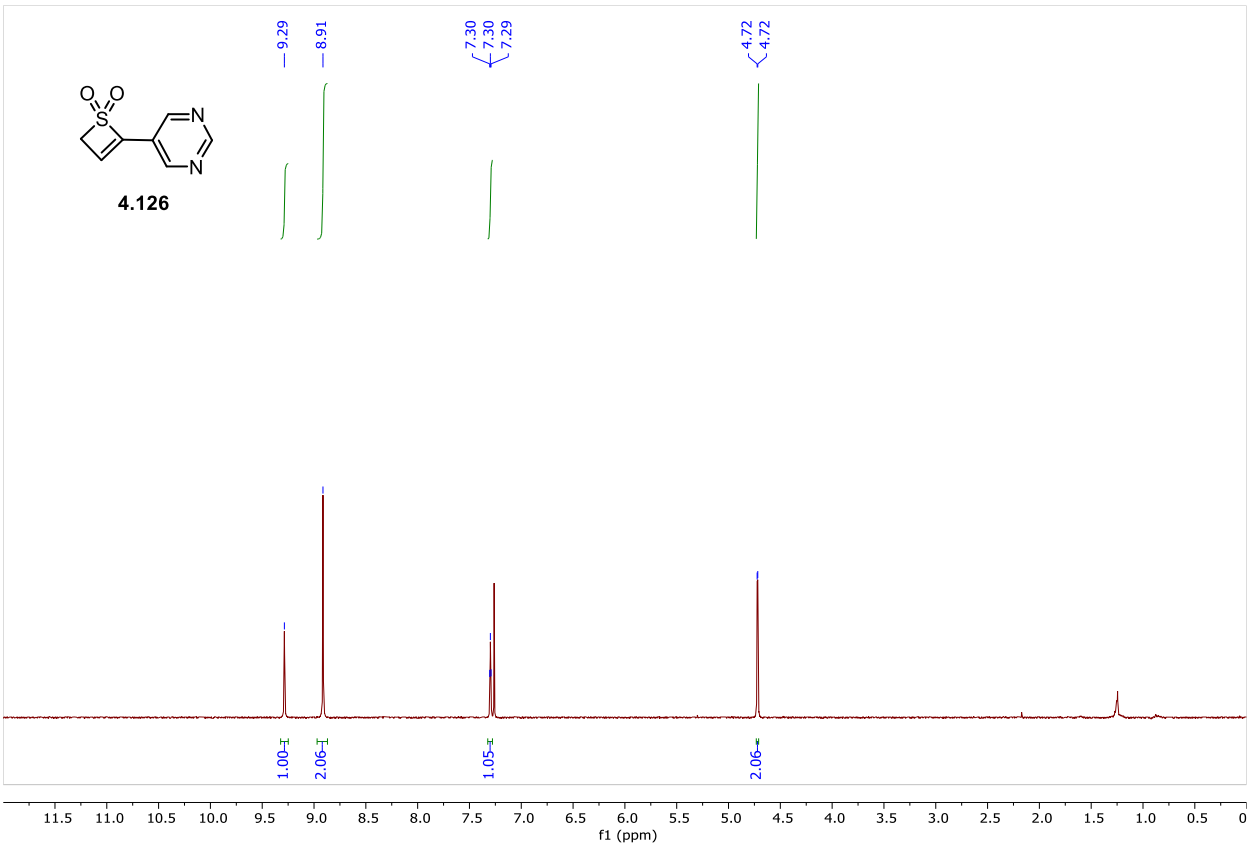

161.71
159.76
128.49
120.87
118.94
114.86
69.76
55.60
OMe
4.185
f1 (ppm)

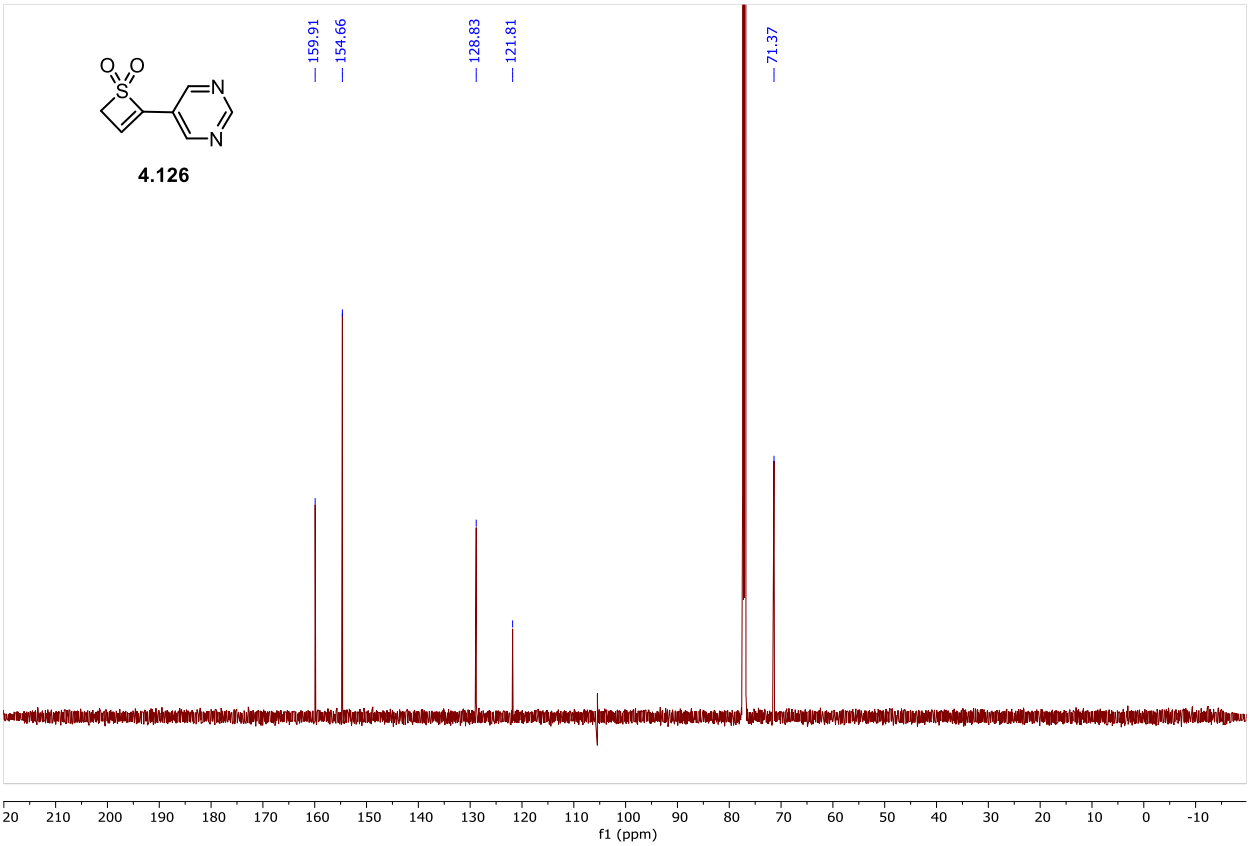

4.143
OMe
7.36
7.33
7.33
6.95
6.94
6.92
5.23
5.21
4.12
4.11
4.08
4.06
4.05
4.03
3.97
3.95
3.94
3.92
3.81
3.32
3.30
3.28
3.25
2.28
2.27
2.25
1.60
1.58
1.56
1.55
1.54
1.52
1.51
1.50
1.48
1.46
1.41
1.40
1.38
1.98
1.98
1.00
1.18
1.02
3.05
1.02
3.73
4.01
1.90
f1 (ppm)

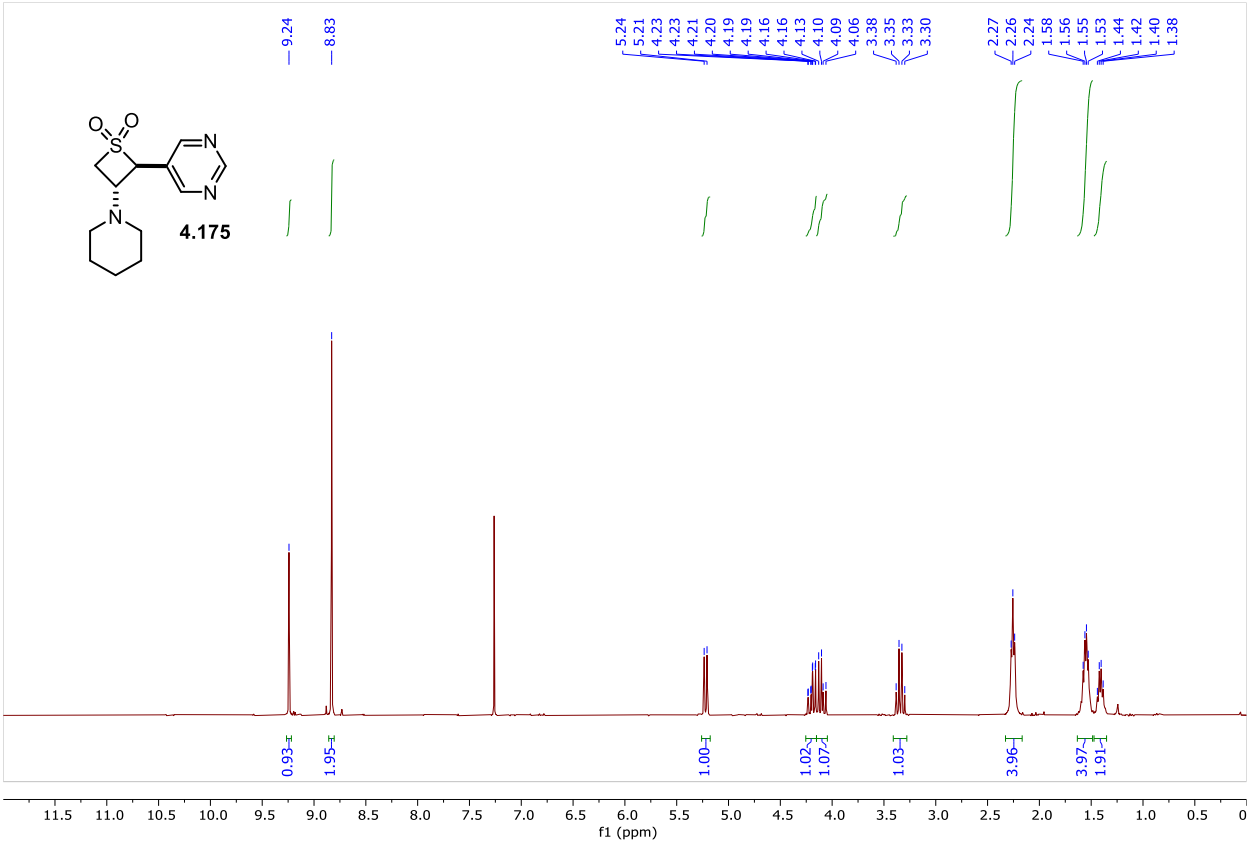

4.143
OMe
160.42
130.30
122.86
114.50
84.49
65.01
55.44
55.00
52.99
25.53
23.75
f1 (ppm)

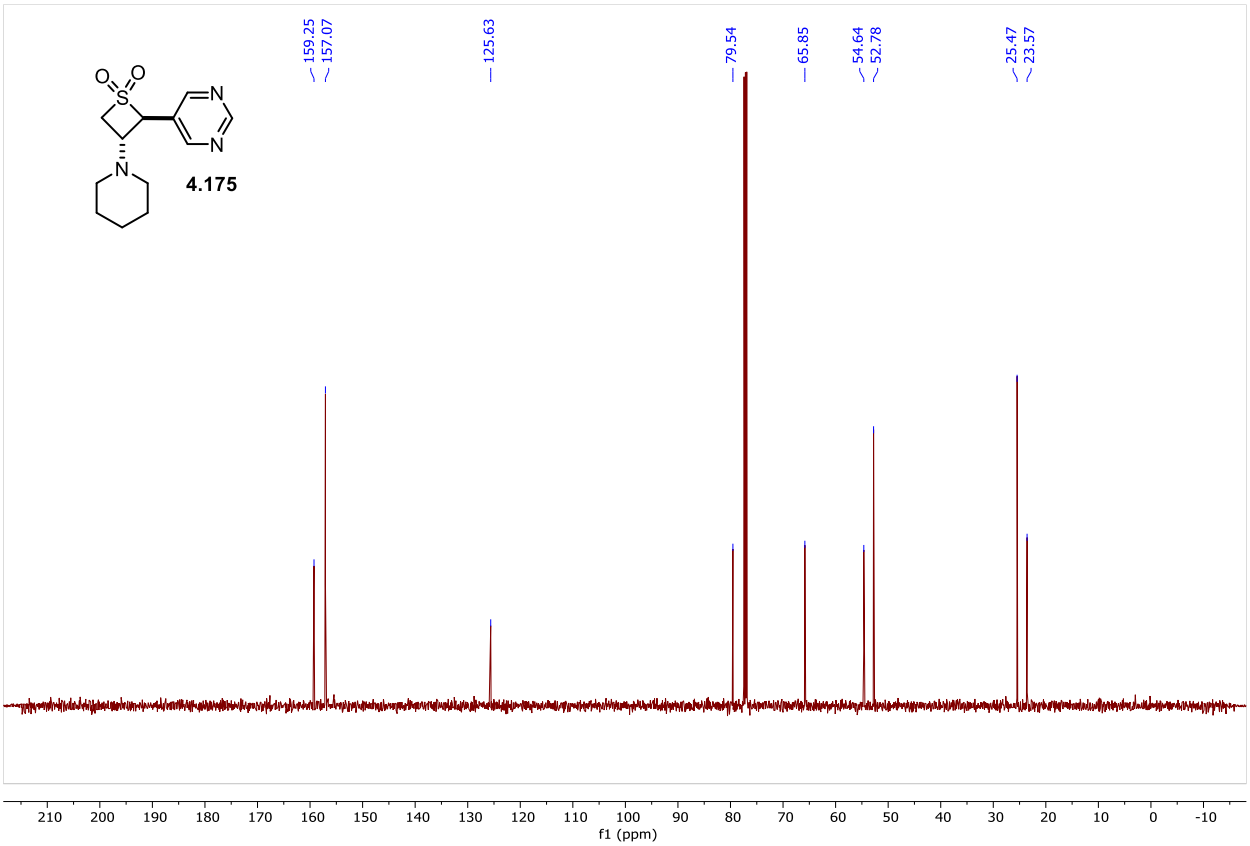

7.02
7.01
7.01
7.00
6.99
6.98
6.82
6.81
6.80
6.79
6.79
6.78
6.76
3.79
3.78
2.59
2.56
2.47
1.95
1.73
1.57
1.56
1.46
1.45
1.06
0.90
0.88
0.86
0.85
OMe
4.158
2.42
2.29
3.38
4.00
0.97
1.18
4.15
2.18
1.03
1.31
f1 (ppm)

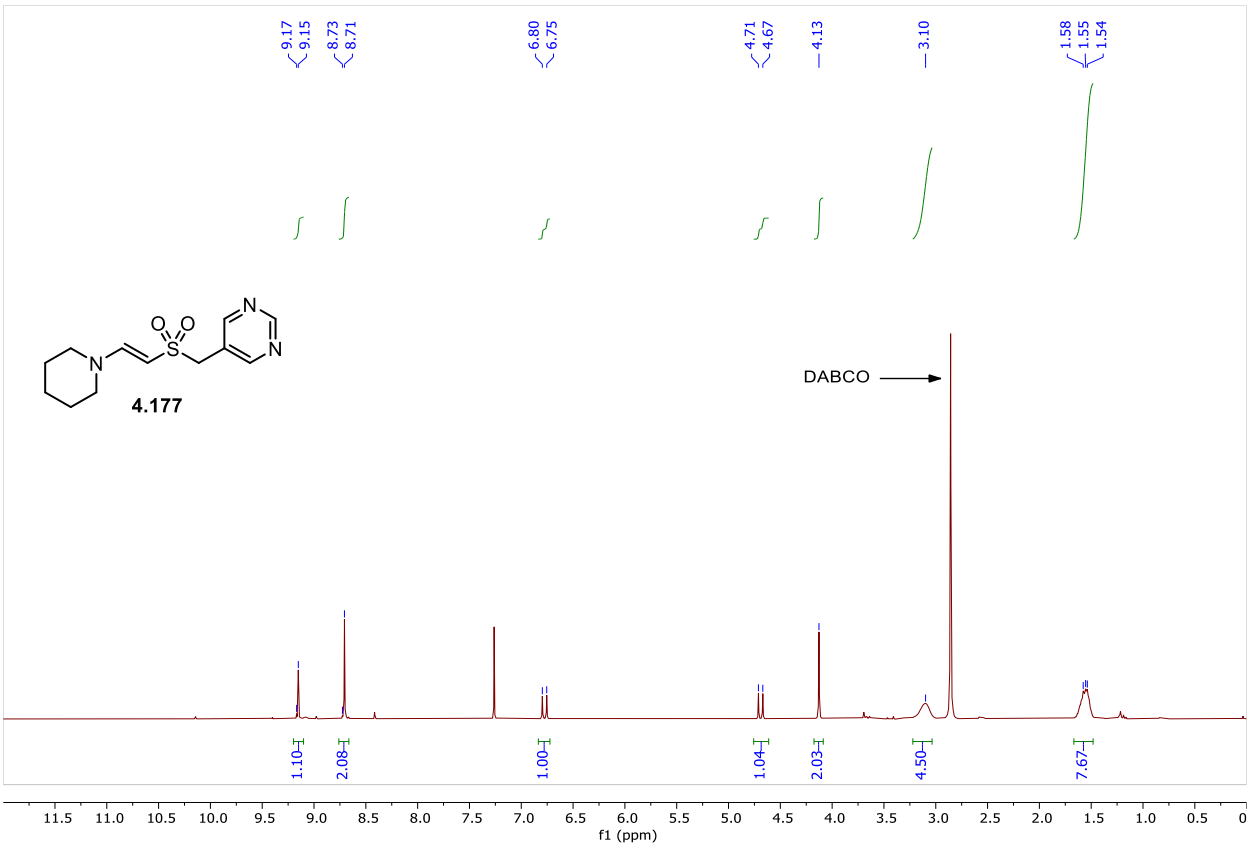

157.82
134.54
127.37
113.83
55.45
54.63
49.53
25.96
24.55
23.82
16.05
OMe
4.158
f1 (ppm)


9.29
8.91
7.30
7.30
7.29
4.72
4.72
4.126
1.00
2.06
1.05
2.06
11.5 11.0 10.5 10.0 9.5 9.0 8.5 8.0 7.5 7.0 6.5 6.0 5.5 5.0 4.5 4.0 3.5 3.0 2.5 2.0 1.5 1.0 0.5 0
f1 (ppm)


159.91
154.66
128.83
121.81
71.37
4.126
20 210 200 190 180 170 160 150 140 130 120 110 100 90 80 70 60 50 40 30 20 10 0 -10
f1 (ppm)


9.24
8.83
5.24
5.21
4.23
4.23
4.21
4.20
4.19
4.19
4.16
4.16
4.13
4.10
4.09
4.06
3.38
3.35
3.33
3.30
2.27
2.26
2.24
1.58
1.56
1.55
1.53
1.44
1.42
1.40
1.38
4.175
0.93
1.95
1.00
1.02
1.07
1.03
3.96
3.97
1.91
f1 (ppm)


159.25
157.07
125.63
79.54
65.85
54.64
52.78
25.47
23.57
4.175
f1 (ppm)


9.17
9.15
8.73
8.71
6.80
6.75
4.71
4.67
4.13
3.10
1.58
1.55
1.54
DABCO
4.177
1.10
2.08
1.00
1.04
2.03
4.50
7.67
11.5 11.0 10.5 10.0 9.5 9.0 8.5 8.0 7.5 7.0 6.5 6.0 5.5 5.0 4.5 4.0 3.5 3.0 2.5 2.0 1.5 1.0 0.5 0
f1 (ppm)

REFERENCES

1. Stylianakis, I.; Kolocouris, A. Comprehensive Overview of Homogeneous Gold-Catalyzed Transformations of π-Systems for Application Scientists. *Catalysts* **2023,** *13* (6), 921– 974.
2. Ito, Y.; Sawamura, M.; Hayashi, T. Catalytic asymmetric aldol reaction: reaction of aldehydes with isocyanoacetate catalyzed by a chiral ferrocenylphosphine-gold(I) complex. *J. Am. Chem. Soc.* **1986,** *108* (20), 6405–6406.
3. Li, Z.; Brouwer, C.; He, C. Gold-Catalyzed Organic Transformations. *Chem. Rev.* **2008,** *108* (8), 3239–3265.
4. Shahzad, S. A.; Sajid, M. A.; Khan, Z. A.; Canseco-Gonzalez, D. Gold catalysis in organic transformations: A review. *Synth. Commun.* **2017,** *47* (8), 735–755.
5. Dorel, R.; Echavarren, A. M. Gold(I)-Catalyzed Activation of Alkynes for the Construction of Molecular Complexity. *Chem. Rev.* **2015,** *115* (17), 9028–9072.
6. Gorin, D. J.; Toste, F. D. Relativistic effects in homogeneous gold catalysis. *Nature* **2007,** *446*, 395–403.
7. Fürstner, A.; Davies, P. W. Catalytic Carbophilic Activation: Catalysis by Platinum and Gold π Acids. *Angew. Chem. Int. Ed.* **2007,** *46* (19), 3410–3449.
8. Nakanishi, W.; Yamanaka, M.; Nakamura, E. Reactivity and Stability of Organocopper(I), Silver(I), and Gold(I) Ate Compounds and Their Trivalent Derivatives. *J. Am. Chem. Soc.* **2005,** *127* (5), 1446–1453.
9. Halliday, C. J. V.; Lynam, J. M. Gold–alkynyls in catalysis: alkyne activation, gold cumulenes and nuclearity. *Dalton Trans.* **2016,** *45* (32), 12611–12626.
10. Shapiro, N. D.; Toste, F. D. Synthesis and structural characterization of isolable phosphine coinage metal π-complexes. *PNAS* **2008,** *105* (8), 2779–2782.
11. Jia, M.; Bandini, M. Counterion Effects in Homogeneous Gold Catalysis. *ACS Catal.* **2015,** *5* (3), 1638–1652.
12. Homs, A.; Obradors, C.; Leboeuf, D.; Echavarren, A. M. Dissecting Anion Effects in Gold(I)-Catalyzed Intermolecular Cycloadditions. *Adv. Synth. Catal.* **2014,** *356* (1), 221–228.
13. Kumar, A.; Patil, N. T. Ligand-Enabled Sustainable Gold Catalysis. *ACS Sustainable Chem. Eng.* **2022,** *10* (21), 6900–6918.
14. Lu, Z.; Li, T.; Mudshinge, S. R.; Xu, B.; Hammond, G. B. Optimization of Catalysts and Conditions in Gold(I) Catalysis—Counterion and Additive Effects. *Chem. Rev.* **2021,** *121* (14), 8452–8477.
15. Collado, A.; Nelson, D. J.; Nolan, S. P. Optimizing Catalyst and Reaction Conditions in Gold(I) Catalysis–Ligand Development. *Chem. Rev.* **2021,** *121* (14), 8559–8612.
16. Wegener, M.; Huber, F.; Bolli, C.; Jenne, C.; Kirsch, S. F. Silver-Free Activation of Ligated Gold(I) Chlorides: The Use of $[Me_3NB_{12}Cl_{11}]^-$ as a Weakly Coordinating Anion in Homogeneous Gold Catalysis. *Chem. Eur. J.* **2015,** *21* (3), 1328–1336.
17. Mézailles, N.; Ricard, L.; Gagosz, F. Phosphine Gold(I) Bis-(trifluoromethanesulfonyl)imidate Complexes as New Highly Efficient and Air-Stable Catalysts for the Cycloisomerization of Enynes. *Org. Lett.* **2005,** *7* (19), 4133–4136.
18. Ricard, L.; Gagosz, F. Synthesis and Reactivity of Air-Stable *N*-Heterocyclic Carbene Gold(I) Bis(trifluoromethanesulfonyl)imidate Complexes. *Organometallics* **2007,** *26* (19), 4704–4707.

19. Nieto-Oberhuber, C.; López, S.; Muñoz, M. P.; Cárdenas, D. J.; Buñuel, E.; Nevado, C.; Echavarren, A. M. Divergent Mechanisms for the Skeletal Rearrangement and [2+2] Cycloaddition of Enynes Catalyzed by Gold. *Angew. Chem. Int. Ed.* **2005,** *44* (38), 6146–6148.
20. de Frémont, P.; Stevens, E. D.; Fructos, M. R.; Mar Díaz-Requejo, M.; Pérez, P. J.; Nolan, S. P. Synthesis, isolation and characterization of cationic gold(i) *N*-heterocyclic carbene (NHC) complexes. *Chem. Commun.* **2006,** *19*, 2045–2047.
21. Benitez, D.; Shapiro, N. D.; Tkatchouk, E.; Wang, Y.; Goddard, W. A.; Toste, F. D. A bonding model for gold(I) carbene complexes. *Nat. Chem.* **2009,** *1* (6), 482–486.
22. Wang, Y.; Muratore, M. E.; Echavarren, A. M. Gold Carbene or Carbenoid: Is There a Difference? *Chem. Eur. J.* **2015,** *21* (20), 7332–7339.
23. Campeau, D.; León Rayo, D. F.; Mansour, A.; Muratov, K.; Gagosz, F. Gold-Catalyzed Reactions of Specially Activated Alkynes, Allenes, and Alkenes. *Chem. Rev.* **2021,** *121* (14), 8756–8867.
24. Jiménez-Núñez, E.; Echavarren, A. M. Gold-Catalyzed Cycloisomerizations of Enynes: A Mechanistic Perspective. *Chem. Rev.* **2008,** *108* (8), 3326–3350.
25. Kumar, M.; Kaliya, K.; Maurya, S. K. Recent progress in the homogeneous gold-catalysed cycloisomerisation reactions. *Org. Biomol. Chem.* **2023,** *21* (16), 3276–3295.
26. Lee, Y.-C.; Kumar, K. Gold(I) Catalyzed Enyne Cycloisomerization – A Roadmap to Privileged Heterocyclic Scaffolds. *Isr. J. Chem.* **2018,** *58* (5), 531–556.
27. Marín-Luna, M.; Nieto Faza, O.; Silva López, C. Gold-Catalyzed Homogeneous (Cyclo)Isomerization Reactions. *Front. Chem.* **2019,** *7*, 1–22.
28. Obradors, C.; Echavarren, A. M. Gold-Catalyzed Rearrangements and Beyond. *Acc. Chem. Res.* **2014,** *47* (3), 902–912.
29. Simonneau, A.; Harrak, Y.; Jeanne-Julien, L.; Lemière, G.; Mouriès-Mansuy, V.; Goddard, J.-P.; Malacria, M.; Fensterbank, L. Ring Expansions Within the Gold-Catalyzed Cycloisomerization of O-Tethered 1,6-Enynes. Application to the Synthesis of Natural Product-like Macrocycles. *ChemCatChem* **2013,** *5* (5), 1096–1099.
30. Nieto-Oberhuber, C.; Muñoz, M. P.; Buñuel, E.; Nevado, C.; Cárdenas, D. J.; Echavarren, A. M. Cationic Gold(I) Complexes: Highly Alkynophilic Catalysts for the exo- and endo-Cyclization of Enynes. *Angew. Chem. Int. Ed.* **2004,** *43* (18), 2402–2406.
31. Amijs, C. H. M.; López-Carrillo, V.; Raducan, M.; Pérez-Galán, P.; Ferrer, C.; Echavarren, A. M. Gold(I)-Catalyzed Intermolecular Addition of Carbon Nucleophiles to 1,5- and 1,6-Enynes. *J. Org. Chem.* **2008,** *73* (19), 7721–7730.
32. Kennedy-Smith, J. J.; Staben, S. T.; Toste, F. D. Gold(I)-Catalyzed Conia-Ene Reaction of β-Ketoesters with Alkynes. *J. Am. Chem. Soc.* **2004,** *126* (14), 4526–4527.
33. Menon, R. S.; Findlay, A. D.; Bissember, A. C.; Banwell, M. G. The Au(I)-Catalyzed Intramolecular Hydroarylation of Terminal Alkynes Under Mild Conditions: Application to the Synthesis of 2H-Chromenes, Coumarins, Benzofurans, and Dihydroquinolines. *J. Org. Chem.* **2009,** *74* (22), 8901–8903.
34. Liu, Y.; Xu, W.; Wang, X. Gold(I)-Catalyzed Tandem Cyclization Approach to Tetracyclic Indolines. *Org. Lett.* **2010,** *12* (7), 1448–1451.
35. Huang, H.; Zhou, Y.; Liu, H. Recent advances in the gold-catalyzed additions to C–C multiple bonds. *Beilstein J. Org. Chem.* **2011,** *7*, 897–936.
36. Hashmi, A. S. K. Gold-Catalyzed Organic Reactions. *Chem. Rev.* **2007,** *107* (7), 3180–3211.

37. Budde, W. L.; Dessy, R. E. The Homogeneously Catalyzed Hydration of Acetylenes by Mercuric Perchlorate-Perchloric Acid: Evidence for a Bis-(acetylene)-Mercuric Ion Complex as an Intermediate. *J. Am. Chem. Soc.* **1963,** *85* (24), 3964–3970.
38. Muratov, K.; Gagosz, F. Confinement-Induced Selectivities in Gold(I) Catalysis—The Benefit of Using Bulky Tri-(ortho-biaryl)phosphine Ligands. *Angew. Chem. Int. Ed.* **2022,** *61* (28), e202203452.
39. Antoniotti, S.; Genin, E.; Michelet, V.; Genêt, J.-P. Highly Efficient Access to Strained Bicyclic Ketals via Gold-Catalyzed Cycloisomerization of Bis-homopropargylic Diols. *J. Am. Chem. Soc.* **2005,** *127* (28), 9976–9977.
40. Aponick, A.; Li, C.-Y.; Malinge, J.; Marques, E. F. An Extremely Facile Synthesis of Furans, Pyrroles, and Thiophenes by the Dehydrative Cyclization of Propargyl Alcohols. *Org. Lett.* **2009,** *11* (20), 4624–4627.
41. Hirano, K.; Inaba, Y.; Takahashi, N.; Shimano, M.; Oishi, S.; Fujii, N.; Ohno, H. Direct Synthesis of Fused Indoles by Gold-Catalyzed Cascade Cyclization of Diynes. *J. Org. Chem.* **2011,** *76* (5), 1212–1227.
42. Yu, Y.-F.; Shu, C.; Zhou, B.; Li, J.-Q.; Zhou, J.-M.; Ye, L.-W. Efficient and practical synthesis of enantioenriched 2,3-dihydropyrroles through gold-catalyzed anti-Markovnikov hydroamination of chiral homopropargyl sulfonamides. *Chem. Commun.* **2015,** *51* (11), 2126–2129.
43. Wu, H.-C.; Yang, C.-W.; Hwang, L.-C.; Wu, M.-J. Au(i)-catalyzed and iodine-mediated cyclization of enynylpyrazoles to provide pyrazolo[1,5-a]pyridines. *Org. Biomol. Chem.* **2012,** *10* (33), 6640–6648.
44. Mauleon, P.; Toste, F. D. Gold-Catalyzed Reactions of Propargyl Esters, Propargyl Alcohols, and Related Compounds. In *Modern Gold Catalyzed Synthesis*, **2012**; pp 75–134.
45. Soriano, E.; Marco-Contelles, J. Mechanistic Insights on the Cycloisomerization of Polyunsaturated Precursors Catalyzed by Platinum and Gold Complexes. *Acc. Chem. Res.* **2009,** *42* (8), 1026–1036.
46. Moreau, X.; Goddard, J.-P.; Bernard, M.; Lemière, G.; López-Romero, J. M.; Mainetti, E.; Marion, N.; Mouriès, V.; Thorimbert, S.; Fensterbank, L.; Malacria, M. Gold- vs. Platinum-Catalyzed Polycyclizations by O-Acyl Migration. Solvent-Free Reactions. *Adv. Synth. Catal.* **2008,** *350* (1), 43–48.
47. Boreux, A.; Lambion, A.; Campeau, D.; Sanita, M.; Coronel, R.; Riant, O.; Gagosz, F. Gold-catalyzed synthesis of β-trifluoromethylated α,β-unsaturated ketones from CF3-substituted propargylic carboxylates and their reactivity in Diels-Alder reactions. *Tetrahedron* **2018,** *74* (38), 5232–5239.
48. Zheng, Z.; Ma, X.; Cheng, X.; Zhao, K.; Gutman, K.; Li, T.; Zhang, L. Homogeneous Gold-Catalyzed Oxidation Reactions. *Chem. Rev.* **2021,** *121* (14), 8979–9038.
49. Ye, L.-W.; Zhu, X.-Q.; Sahani, R. L.; Xu, Y.; Qian, P.-C.; Liu, R.-S. Nitrene Transfer and Carbene Transfer in Gold Catalysis. *Chem. Rev.* **2021,** *121* (14), 9039–9112.
50. Ye, L.; He, W.; Zhang, L. Gold-Catalyzed One-Step Practical Synthesis of Oxetan-3-ones from Readily Available Propargylic Alcohols. *J. Am. Chem. Soc.* **2010,** *132* (25), 8550–8551.
51. He, W.; Li, C.; Zhang, L. An Efficient [2 + 2 + 1] Synthesis of 2,5-Disubstituted Oxazoles via Gold-Catalyzed Intermolecular Alkyne Oxidation. *J. Am. Chem. Soc.* **2011,** *133* (22), 8482–8485.

52. Gagosz, F. Gold Vinylidenes as Useful Intermediates in Synthetic Organic Chemistry. *Synthesis* **2019,** *51* (05), 1087–1099.
53. Harris, R. J.; Widenhoefer, R. A. Gold carbenes, gold-stabilized carbocations, and cationic intermediates relevant to gold-catalysed enyne cycloaddition. *Chem. Soc. Rev.* **2016,** *45* (16), 4533–4551.
54. Wang, T.; Hashmi, A. S. K. 1,2-Migrations onto Gold Carbene Centers. *Chem. Rev.* **2021,** *121* (14), 8948–8978.
55. Wieteck, M.; Tokimizu, Y.; Rudolph, M.; Rominger, F.; Ohno, H.; Fujii, N.; Hashmi, A. S. K. Dual Gold Catalysis: Synthesis of Polycyclic Compounds via C-H Insertion of Gold Vinylidenes. *Chem. Eur. J.* **2014,** *20* (49), 16331–16336.
56. Vachhani, D. D.; Galli, M.; Jacobs, J.; Van Meervelt, L.; Van der Eycken, E. V. Synthesis of (spiro)cyclopentapyridinones via Csp^3–H functionalization: a post-Ugi gold-catalyzed regioselective tandem cyclization. *Chem. Commun.* **2013,** *49* (64), 7171–7173.
57. Hashmi, A. S. K.; Lauterbach, T.; Nösel, P.; Vilhelmsen, M. H.; Rudolph, M.; Rominger, F. Dual Gold Catalysis: σ,π-Propyne Acetylide and Hydroxyl-Bridged Digold Complexes as Easy-To-Prepare and Easy-To-Handle Precatalysts. *Chem. Eur. J.* **2013,** *19* (3), 1058–1065.
58. Hashmi, A. S. K.; Wieteck, M.; Braun, I.; Nösel, P.; Jongbloed, L.; Rudolph, M.; Rominger, F. Gold-Catalyzed Synthesis of Dibenzopentalenes – Evidence for Gold Vinylidenes. *Adv. Synth. Catal.* **2012,** *354* (4), 555–562.
59. Hashmi, A. S. K.; Wieteck, M.; Braun, I.; Rudolph, M.; Rominger, F. Gold Vinylidene Complexes: Intermolecular C(sp^3)-H Insertions and Cyclopropanations Pathways. *Angew. Chem. Int. Ed.* **2012,** *51* (42), 10633–10637.
60. Pflästerer, D.; Hashmi, A. S. K. Gold catalysis in total synthesis – recent achievements. *Chem. Soc. Rev.* **2016,** *45* (5), 1331–1367.
61. Li, Y.; Dai, M. Total Syntheses of the Reported Structures of Curcusones I and J through Tandem Gold Catalysis. *Angew. Chem. Int. Ed.* **2017,** *56* (38), 11624–11627.
62. Sethofer, S. G.; Staben, S. T.; Hung, O. Y.; Toste, F. D. Au(I)-Catalyzed Ring Expanding Cycloisomerizations: Total Synthesis of Ventricosene. *Org. Lett.* **2008,** *10* (19), 4315–4318.
63. Sugimoto, K.; Toyoshima, K.; Nonaka, S.; Kotaki, K.; Ueda, H.; Tokuyama, H. Protecting-Group-Free Total Synthesis of (−)-Rhazinilam and (−)-Rhazinicine using a Gold-Catalyzed Cascade Cyclization. *Angew. Chem. Int. Ed.* **2013,** *52* (28), 7168–7171.
64. He, J.; Wasa, M.; Chan, K. S. L.; Shao, Q.; Yu, J.-Q. Palladium-Catalyzed Transformations of Alkyl C–H Bonds. *Chem. Rev.* **2017,** *117* (13), 8754–8786.
65. Kancherla, S.; Jørgensen, K. B.; Fernández-Ibáñez, M. Á. Recent Developments in Palladium-Catalysed Non-Directed C–H Bond Activation in Arenes. *Synthesis* **2019,** *51* (03), 643–663.
66. Gandeepan, P.; Müller, T.; Zell, D.; Cera, G.; Warratz, S.; Ackermann, L. 3d Transition Metals for C–H Activation. *Chem. Rev.* **2019,** *119* (4), 2192–2452.
67. Colby, D. A.; Tsai, A. S.; Bergman, R. G.; Ellman, J. A. Rhodium Catalyzed Chelation-Assisted C–H Bond Functionalization Reactions. *Acc. Chem. Res.* **2012,** *45* (6), 814–825.
68. Boorman, T. C.; Larrosa, I. Gold-mediated C–H bond functionalisation. *Chem. Soc. Rev.* **2011,** *40* (4), 1910–1925.
69. Dick, A. R.; Sanford, M. S. Transition metal catalyzed oxidative functionalization of carbon–hydrogen bonds. *Tetrahedron* **2006,** *62* (11), 2439–2463.

70. Haibach, M. C.; Seidel, D. C-H Bond Functionalization through Intramolecular Hydride Transfer. *Angew. Chem. Int. Ed.* **2014,** *53* (20), 5010–5036.
71. Peng, B.; Maulide, N. The Redox-Neutral Approach to C-H Functionalization. *Chem. Eur. J.* **2013,** *19* (40), 13274–13287.
72. Xie, J.; Pan, C.; Abdukader, A.; Zhu, C. Gold-catalyzed C(sp^3)–H bond functionalization. *Chem. Soc. Rev.* **2014,** *43* (15), 5245–5256.
73. Wang, L.; Xiao, J. Advancement in Cascade [1,n]-Hydrogen Transfer/Cyclization: A Method for Direct Functionalization of Inactive C(sp^3)-H Bonds. *Adv. Synth. Catal.* **2014,** *356* (6), 1137–1171.
74. Jurberg, I. D.; Odabachian, Y.; Gagosz, F. Hydroalkylation of Alkynyl Ethers via a Gold(I)-Catalyzed 1,5-Hydride Shift/Cyclization Sequence. *J. Am. Chem. Soc.* **2010,** *132* (10), 3543–3552.
75. Zhao, Q.; Gagosz, F. Synthesis of Allenamides and Structurally Related Compounds by a Gold-Catalyzed Hydride Shift Process. *Adv. Synth. Catal.* **2017,** *359* (18), 3108–3113.
76. Boreux, A.; Lonca, G. H.; Riant, O.; Gagosz, F. Synthesis of Trifluoromethyl-allenes by Gold-Catalyzed Rearrangement of Propargyl Benzyl Ethers. *Org. Lett.* **2016,** *18* (19), 5162–5165.
77. Bolte, B.; Odabachian, Y.; Gagosz, F. Gold(I)-Catalyzed Rearrangement of Propargyl Benzyl Ethers: A Practical Method for the Generation and in Situ Transformation of Substituted Allenes. *J. Amer. Chem. Soc.* **2010,** *132* (21), 7294–7296.
78. Lu, X.-L.; Lyu, M.-Y.; Peng, X.-S.; Wong, H. N. C. Gold(I)-Catalyzed Tandem Cycloisomerization of 1,5-Enyne Ethers by Hydride Transfer. *Angew. Chem. Int. Ed.* **2018,** *57* (35), 11365–11368.
79. Sutro, J. L.; Fürstner, A. Total Synthesis of the Allenic Macrolide (+)-Archangiumide. *J. Am. Chem. Soc.* **2024,** *146* (4), 2345–2350.
80. Lo, V. K.-Y.; Wong, M.-K.; Che, C.-M. Gold-Catalyzed Highly Enantioselective Synthesis of Axially Chiral Allenes. *Org. Lett.* **2008,** *10* (3), 517–519.
81. Cui, L.; Peng, Y.; Zhang, L. A Two-Step, Formal [4 + 2] Approach toward Piperidin-4-ones via Au Catalysis. *J. Am. Chem. Soc.* **2009,** *131* (24), 8394–8395.
82. Noey, E. L.; Luo, Y.; Zhang, L.; Houk, K. N. Mechanism of Gold(I)-Catalyzed Rearrangements of Acetylenic Amine-N-Oxides: Computational Investigations Lead to a New Mechanism Confirmed by Experiment. *J. Am. Chem. Soc.* **2012,** *134* (2), 1078–1084.
83. Wu, X.; Chen, S.-S.; Hu, Y.; Gong, L.-Z. Gold-Catalyzed [1,5]-Hydride Shift onto Unactivated Alkynes To Trigger an Intermolecular Diels–Alder Reaction. *Org. Lett.* **2014,** *16* (14), 3820–3823.
84. Zhou, G.; Zhang, J. Product-selectivity control by the nature of the catalyst: Lewis acid-catalyzed selective formation of ring-fused tetrahydroquinolines and tetrahydroazepines via intramolecular redox reaction. *Chem. Commun.* **2010,** *46* (35), 6593–6595.
85. Zhou, G.; Liu, F.; Zhang, J. Enantioselective Gold-Catalyzed Functionalization of Unreactive sp^3 C-H Bonds through a Redox–Neutral Domino Reaction. *Chem. Eur. J.* **2011,** *17* (11), 3101–3104.
86. Tian, J.-J.; Sun, W.; Li, R.-R.; Tian, G.-X.; Wang, X.-C. Borane/Gold(I)-Catalyzed C−H Functionalization Reactions and Cycloaddition Reactions of Amines and α-Alkynylenones. *Angew. Chem. Int. Ed.* **2022,** *61* (35), e202208427.

87. He, Y.-P.; Wu, H.; Chen, D.-F.; Yu, J.; Gong, L.-Z. Cascade Hydroamination/Redox Reaction for the Synthesis of Cyclic Aminals Catalyzed by a Combined Gold Complex and Brønsted Acid. *Chem. Eur. J.* **2013,** *19* (17), 5232–5237.
88. Davies, H. M. L.; Manning, J. R. Catalytic C–H functionalization by metal carbenoid and nitrenoid insertion. *Nature* **2008,** *451* (7177), 417–424.
89. Luo, Y.; Zhang, X.; Xia, Y., Recent advances in transition-metal catalyzed nitrene transfer reactions with carbamates. *Chin. Chem. Lett.* **2024,** *35* (3), 108778–108788.
90. Roizen, J. L.; Harvey, M. E.; Du Bois, J. Metal-Catalyzed Nitrogen-Atom Transfer Methods for the Oxidation of Aliphatic C–H Bonds. *Acc. Chem. Res.* **2012,** *45* (6), 911–922.
91. Sahani, R. L.; Ye, L.-W.; Liu, R.-S. Chapter Three - Synthesis of nitrogen-containing molecules via transition metal-catalyzed reactions on isoxazoles, anthranils and benzoisoxazoles. In *Advances in Organometallic Chemistry*, Pérez, P. J., Ed. Academic Press: **2020**; Vol. 73, pp 195–251.
92. Aguilar, E.; Santamaría, J. Gold-catalyzed heterocyclic syntheses through α-imino gold carbene complexes as intermediates. *Org. Chem. Front.* **2019,** *6* (9), 1513–1540.
93. Davies, P. W.; Garzón, M. Nucleophilic Nitrenoids Through π-Acid Catalysis: Providing a Common Basis for Rapid Access into Diverse Nitrogen Heterocycles. *Asian J. Org. Chem.* **2015,** *4* (8), 694–708.
94. Liao Yun, Z. L.; Yinghua Y.; Gui, C.; Xueliang, H. N-Heterocycle Synthesis via Gold-Catalyzed Intermolecular Nitrene Transfer Reactions of Alkynes. *Chin. J. Org. Chem.* **2017,** *37* (11), 2785–2799.
95. Li, L.; Tan, T.-D.; Zhang, Y.-Q.; Liu, X.; Ye, L.-W. Recent advances in transition-metal-catalyzed reactions of alkynes with isoxazoles. *Org. Biomol. Chem.* **2017,** *15* (40), 8483–8492.
96. Prechter, A.; Henrion, G.; Faudot dit Bel, P.; Gagosz, F. Gold-Catalyzed Synthesis of Functionalized Pyridines by Using 2H-Azirines as Synthetic Equivalents of Alkenyl Nitrenes. *Angew. Chem. Int. Ed.* **2014,** *53* (19), 4959–4963.
97. Jin, L.; Wu, Y.; Zhao, X. Theoretical Insight into the Mechanism of Gold(I)-Catalyzed Rearrangement of 2-Propargyl 2H-Azirines to Pyridines. *J. Org. Chem.* **2015,** *80* (7), 3547–3555.
98. Xiao, X. Y.; Zhou, A. H.; Shu, C.; Pan, F.; Li, T.; Ye, L. W. Atom-Economic Synthesis of Fully Substituted 2-Aminopyrroles via Gold-Catalyzed Formal [3+2] Cycloaddition between Ynamides and Isoxazoles. *Chem. Asian J.* **2015,** *10* (9), 1854–1858.
99. Jin, H.; Huang, L.; Xie, J.; Rudolph, M.; Rominger, F.; Hashmi, A. S. Gold-Catalyzed C-H Annulation of Anthranils with Alkynes: A Facile, Flexible, and Atom-Economical Synthesis of Unprotected 7-Acylindoles. *Angew. Chem. Int. Ed.* **2016,** *55* (2), 794–797.
100. Black, D. S.; Kumar, N.; Mitchell, P. S. R. Synthesis of Pyrroloquinolines as Indole Analogues of Flavonols. *J. Org. Chem.* **2002,** *67* (8), 2464–2473.
101. Chatzopoulou, E.; Davies, P. W. Highly regioselective synthesis of 2,4,5-(hetero)aryl substituted oxazoles by intermolecular [3+2]-cycloaddition of unsymmetrical internal alkynes. *Chem. Commun.* **2013,** *49* (77), 8617–8619.
102. Garzon, M.; Davies, P. W. A direct route into fused imidazo-diazines and imidazo-pyridines using nucleophilic nitrenoids in a gold-catalyzed formal [3 + 2]-dipolar cycloaddition. *Org. Lett.* **2014,** *16* (18), 4850–4853.

103. Tian, X.; Song, L.; Rudolph, M.; Rominger, F.; Oeser, T.; Hashmi, A. S. K. Sulfilimines as Versatile Nitrene Transfer Reagents: Facile Access to Diverse Aza-Heterocycles. *Angew. Chem. Int. Ed.* **2019,** *58* (11), 3589–3593.
104. Tian, X.; Song, L.; Han, C.; Zhang, C.; Wu, Y.; Rudolph, M.; Rominger, F.; Hashmi, A. S. K. Gold(III)-Catalyzed Formal [3 + 2] Annulations of N-Acyl Sulfilimines with Ynamides for the Synthesis of 4-Aminooxazoles. *Org. Lett.* **2019,** *21* (8), 2937–2940.
105. Tian, X.; Song, L.; Rudolph, M.; Rominger, F.; Hashmi, A. S. K. Synthesis of 2-Aminoindoles through Gold-Catalyzed C–H Annulations of Sulfilimines with N-Arylynamides. *Org. Lett.* **2019,** *21* (11), 4327–4330.
106. Tian, X.; Song, L.; Rudolph, M.; Wang, Q.; Song, X.; Rominger, F.; Hashmi, A. S. K. *N*-Pyridinyl Sulfilimines as a Source for α-Imino Gold Carbenes: Access to 2-Amino-Substituted *N*-Fused Imidazoles. *Org. Lett.* **2019,** *21* (6), 1598–1601.
107. Gorin, D. J.; Davis, N. R.; Toste, F. D. Gold(I)-Catalyzed Intramolecular Acetylenic Schmidt Reaction. *J. Am. Chem. Soc.* **2005,** *127* (32), 11260–11261.
108. Lonca, G. H.; Tejo, C.; Chan, H. L.; Chiba, S.; Gagosz, F. Gold(i)-catalyzed 6-endo-dig azide–yne cyclization: efficient access to 2H-1,3-oxazines. *Chem. Commun.* **2017,** *53* (4), 736–739.
109. Lu, B.; Luo, Y.; Liu, L.; Ye, L.; Wang, Y.; Zhang, L. Umpolung Reactivity of Indole through Gold Catalysis. *Angew. Chem. Int. Ed.* **2011,** *50* (36), 8358–8362.
110. Wetzel, A.; Gagosz, F. Gold-Catalyzed Transformation of 2-Alkynyl Arylazides: Efficient Access to the Valuable Pseudoindoxyl and Indolyl Frameworks. *Angew. Chem. Int. Ed.* **2011,** *50* (32), 7354–7358.
111. Xiao, Y.; Zhang, L. Synthesis of Bicyclic Imidazoles via [2 + 3] Cycloaddition between Nitriles and Regioselectively Generated α-Imino Gold Carbene Intermediates. *Org. Lett.* **2012,** *14* (17), 4662–4665.
112. Cai, J.; Wu, B.; Rong, G.; Zhang, C.; Qiu, L.; Xu, X. Gold-catalyzed Bicyclization of Diaryl Alkynes: Synthesis of Polycyclic Fused Indole and Spirooxindole Derivatives. *Org. Lett.* **2018,** *20* (9), 2733–2736.
113. Li, N.; Lian, X.-L.; Li, Y.-H.; Wang, T.-Y.; Han, Z.-Y.; Zhang, L.; Gong, L.-Z. Gold-Catalyzed Direct Assembly of Aryl-Annulated Carbazoles from 2-Alkynyl Arylazides and Alkynes. *Org. Lett.* **2016,** *18* (17), 4178–4181.
114. Yan, Z.-Y.; Xiao, Y.; Zhang, L. Gold Catalyzed One-Step Construction of 2,3-Dihydro-1H-Pyrrolizines with an Electron-Withdrawing group in the 5-position: A Formal Synthesis of 7-Methoxymitosene. *Angew. Chem. Int. Ed.* **2012,** *51* (34), 8624–8627.
115. Shu, C.; Wang, Y. H.; Shen, C. H.; Ruan, P. P.; Lu, X.; Ye, L. W. Gold-Catalyzed Intermolecular Ynamide Amination-Initiated Aza-Nazarov Cyclization: Access to Functionalized 2-Aminopyrroles. *Org. Lett.* **2016,** *18* (13), 3254–3257.
116. Greiner, L. C.; Matsuoka, J.; Inuki, S.; Ohno, H. Azido-Alkynes in Gold(I)-Catalyzed Indole Syntheses. *Chem. Rec.* **2021,** *21* (12), 3897–3910.
117. Wetzel, A.; Gagosz, F. Gold-Catalyzed Transformation of 2-Alkynyl Arylazides: Efficient Access to the Valuable Pseudoindoxyl and Indolyl Frameworks. *Angew. Chem. Int. Ed.* **2011,** *50* (32), 7354–7358.
118. Sapsford, K. E.; Algar, W. R.; Berti, L.; Gemmill, K. B.; Casey, B. J.; Oh, E.; Stewart, M. H.; Medintz, I. L. Functionalizing Nanoparticles with Biological Molecules: Developing Chemistries that Facilitate Nanotechnology. *Chem. Rev.* **2013,** *113* (3), 1904–2074.

119. Tokimizu, Y.; Oishi, S.; Fujii, N.; Ohno, H. Gold-catalyzed cascade cyclization of (azido)ynamides: an efficient strategy for the construction of indoloquinolines. *Org. Lett.* **2014,** *16* (11), 3138–3141.
120. Greiner, L. C.; Inuki, S.; Arichi, N.; Oishi, S.; Suzuki, R.; Iwai, T.; Sawamura, M.; Hashmi, A. S. K.; Ohno, H. Access to Indole-Fused Benzannulated Medium-Sized Rings through a Gold(I)-Catalyzed Cascade Cyclization of Azido-Alkynes. *Chem. Eur. J.* **2021,** *27* (51), 12992–12997.
121. Gronnier, C.; Odabachian, Y.; Gagosz, F. Gold(I)-catalyzed formation of dihydroquinolines and indoles from N-aminophenyl propargyl malonates. *Chem. Commun.* **2011,** *47* (1), 218–220.
122. Jurberg, I. D.; Ikeda, K.; Antwi-Omane, D.; Gagosz, F. Synthesis of Functionalized Chromenes and Benzofurans from Aryloxy Propargyl Malonates. *Isr. J. Chem.* **2013,** *53* (11–12), 915–922.
123. Jurberg, I. D.; Gagosz, F. Formation of cinnoline derivatives by a gold(I)-catalyzed hydroarylation of N-propargyl-N′-arylhydrazines. *J. Organomet. Chem.* **2011,** *696* (1), 37–41.
124. Paul Krapcho, A.; Lovey, A. J. Decarbalkoxylations of geminal diesters, β-keto esters and α-cyano esters effected by sodium chloride in dimethyl sulpoxide. *Tetrahedron Lett.* **1973,** *14* (12), 957–960.
125. Li, Y.; Ge, L.; Muhammad, M. T.; Bao, H. Recent Progress on Radical Decarboxylative Alkylation for Csp^3–C Bond Formation. *Synthesis* **2017,** *49* (24), 5263–5284.
126. Martin, D. B. C.; Vanderwal, C. D. A synthesis of strychnine by a longest linear sequence of six steps. *Chem. Sci.* **2011,** *2* (4), 649–651.
127. Norwood IV, V. M.; Huigens III, R. W. Harnessing the Chemistry of the Indole Heterocycle to Drive Discoveries in Biology and Medicine. *ChemBioChem* **2019,** *20* (18), 2273–2297.
128. Xu, J.; Liang, L.; Zheng, H.; Chi, Y. R.; Tong, R. Green oxidation of indoles using halide catalysis. *Nat. Commun.* **2019,** *10* (1), 4754–4755.
129. Nge, C.-E.; Gan, C.-Y.; Lim, K.-H.; Ting, K.-N.; Low, Y.-Y.; Kam, T.-S. Criofolinine and Vernavosine, New Pentacyclic Indole Alkaloids Incorporating Pyrroloazepine and Pyridopyrimidine Moieties Derived from a Common Yohimbine Precursor. *Org. Lett.* **2014,** *16* (24), 6330–6333.
130. Angyal, P.; Hegedüs, K.; Mészáros, B. B.; Daru, J.; Dudás, Á.; Galambos, A. R.; Essmat, N.; Al-Khrasani, M.; Varga, S.; Soós, T. Total Synthesis and Structural Plasticity of Kratom Pseudoindoxyl Metabolites. *Angew. Chem. Int. Ed.* **2023,** *62* (35), e202303700.
131. Finefield, J. M.; Frisvad, J. C.; Sherman, D. H.; Williams, R. M. Fungal Origins of the Bicyclo[2.2.2]diazaoctane Ring System of Prenylated Indole Alkaloids. *J. Nat. Prod.* **2012,** *75* (4), 812–833.
132. Bhattarai, K.; Bhattarai, K.; Kabir, M. E.; Bastola, R.; Baral, B. Chapter Six - Fungal natural products galaxy: Biochemistry and molecular genetics toward blockbuster drugs discovery. In *Advances in Genetics*, Kumar, D., Ed. Academic Press: **2021**; Vol. 107, pp 193–284.
133. Klas, K. R.; Kato, H.; Frisvad, J. C.; Yu, F.; Newmister, S. A.; Fraley, A. E.; Sherman, D. H.; Tsukamoto, S.; Williams, R. M. Structural and stereochemical diversity in prenylated indole alkaloids containing the bicyclo[2.2.2]diazaoctane ring system from marine and terrestrial fungi. *Nat. Prod. Rep.* **2018,** *35* (6), 532–558.

134. Miller, K. A.; Williams, R. M. Synthetic approaches to the bicyclo[2.2.2]diazaoctane ring system common to the paraherquamides, stephacidins and related prenylated indole alkaloids. *Chem. Soc. Rev.* **2009,** *38* (11), 3160–3174.
135. Godfrey, R. C.; Green, N. J.; Nichol, G. S.; Lawrence, A. L. Total synthesis of brevianamide A. *Nat. Chem.* **2020,** *12* (7), 615–619.
136. Yamazaki, M.; Okuyama, E.; Kobayashi, M.; Inoue, H. The structure of paraherquamide, a toxic metabolite from *Penicillium paraherquei*. *Tetrahedron Lett.* **1981,** *22* (2), 135–136.
137. Hayashi, H.; Nishimoto, Y.; Nozaki, H. Asperparaline A, a new paralytic alkaloid from *Aspergillus japonicus* JV-23. *Tetrahedron Lett.* **1997,** *38* (32), 5655–5658.
138. Figueroa, M.; González, M. D. C.; Mata, R. Malbrancheamide B, a novel compound from the fungus *Malbranchea aurantiaca l*. *Nat. Prod. Res.* **2008,** *22* (8), 709–714.
139. Martínez-Luis, S.; Rodríguez, R.; Acevedo, L.; González, M. C.; Lira-Rocha, A.; Mata, R. Malbrancheamide, a new calmodulin inhibitor from the fungus *Malbranchea aurantiaca*. *Tetrahedron* **2006,** *62* (8), 1817–1822.
140. Birch, A. J.; Wright, J. J. The brevianamides: a new class of fungal alkaloid. *J. Chem. Soc. D: Chem. Commun.* **1969,** *12*, 644–645.
141. Kato, H.; Yoshida, T.; Tokue, T.; Nojiri, Y.; Hirota, H.; Ohta, T.; Williams, R. M.; Tsukamoto, S. Notoamides A–D: Prenylated Indole Alkaloids Isolated from a Marine-Derived Fungus, *Aspergillus sp*. *Angew. Chem. Int. Ed.* **2007,** *46* (13), 2254–2256.
142. Qian-Cutrone, J.; Huang, S.; Shu, Y.-Z.; Vyas, D.; Fairchild, C.; Menendez, A.; Krampitz, K.; Dalterio, R.; Klohr, S. E.; Gao, Q. Stephacidin A and B: Two Structurally Novel, Selective Inhibitors of the Testosterone-Dependent Prostate LNCαP Cells. *J. Am. Chem. Soc.* **2002,** *124* (49), 14556–14557.
143. Kagiyama, I.; Kato, H.; Nehira, T.; Frisvad, J. C.; Sherman, D. H.; Williams, R. M.; Tsukamoto, S. Taichunamides: Prenylated Indole Alkaloids from *Aspergillus taichungensis* (IBT-19404). *Angew. Chem. Int. Ed.* **2016,** *55* (3), 1128–1132.
144. Robertson, A. P.; Clark, C. L.; Burns, T. A.; Thompson, D. P.; Geary, T. G.; Trailovic, S. M.; Martin, R. J. Paraherquamide and 2-Deoxy-paraherquamide Distinguish Cholinergic Receptor Subtypes in *Ascaris* Muscle. *J. Pharm. Exp. Ther.* **2002,** *302* (3), 853–860.
145. Lin, Z.; Wen, J.; Zhu, T.; Fang, Y.; Gu, Q.; Zhu, W. Chrysogenamide A from an Endophytic Fungus Associated with *Cistanche deserticola* and Its Neuroprotective Effect on SH-SY5Y Cells. *J. Antibiot.* **2008,** *61* (2), 81–85.
146. Little, P. R.; Hodge, A.; Maeder, S. J.; Wirtherle, N. C.; Nicholas, D. R.; Cox, G. G.; Conder, G. A. Efficacy of a combined oral formulation of derquantel–abamectin against the adult and larval stages of nematodes in sheep, including anthelmintic-resistant strains. *Vet. Paras.* **2011,** *181* (2), 180–193.
147. Williams, R. M. Total Synthesis and Biosynthesis of the Paraherquamides: An Intriguing Story of the Biological Diels-Alder Construction. *Chem. Pharm. Bull.* **2002,** *50* (6), 711–740.
148. Branco, P.; Lourenço, A. The Asymmetric Aza-Diels–Alder Reaction. In *Synthetic Approaches to Nonaromatic Nitrogen Heterocycles*, **2020**; pp 371–398.
149. Birch, A. J.; Russell, R. A. Studies in relation to biosynthesis—XLIV: Structural elucidations of brevianamides-B, -C, -D and -F. *Tetrahedron* **1972,** *28* (11), 2999–3008.
150. Coetzer, J. The structure and absolute configuration of 5-bromobrevianamide A. *Acta Crystallogr., Sect. B* **1974,** *30* (9), 2254–2256.

151. Bird, B. A.; Remaley, A. T.; Campbell, I. M. Brevianamides A and B Are Formed Only After Conidiation Has Begun in Solid Cultures of *Penicillium brevicompactum*. *Appl. Environ. Microbiol.* **1981,** *42* (3), 521–525.
152. Birch, A. J.; Wright, J. J. Studies in relation to biosynthesis—XLII: The structural elucidation and some aspects of the biosynthesis of the brevianamides-A and -E. *Tetrahedron* **1970,** *26* (10), 2329–2344.
153. Paterson, R. R. M.; Simmonds, M. J. S.; Kemmelmeier, C.; Blaney, W. M. Effects of brevianamide A, its photolysis product brevianamide D, and ochratoxin A from two Penicillium strains on the insect pests *Spodoptera frugiperda* and *Heliothis virescens*. *Mycol. Res.* **1990,** *94* (4), 538–542.
154. Baldas, J.; Birch, A. J.; Russell, R. A. Studies in relation to biosynthesis. Part XLVI. Incorporation of cyclo-L-tryptophyl-L-proline into brevianamide A. *J. Chem. Soc., Perkin Trans.* **1974,** *0*, 50–52.
155. Steyn, P. S. The structures of five diketopiperazines from *Aspergillus ustus*. *Tetrahedron* **1973,** *29* (1), 107–120.
156. Porter, A. E. A.; Sammes, P. G. A Diels–Alder reaction of possible biosynthetic importance. *J. Chem. Soc. D: Chem. Commun.* **1970,** *17*, 1103.
157. Birch, A. J. Terpenoid compounds of mixed biogenetic origins. *J. Agric. Food Chem.* **1971,** *19* (6), 1088–1092.
158. Williams, R. M.; Glinka, T.; Kwast, E. Facial selectivity of the intramolecular S_N2' cyclization: stereocontrolled total synthesis of brevianamide B. *J. Am. Chem. Soc.* **1988,** *110* (17), 5927–5929.
159. Williams, R. M.; Kwast, E.; Coffman, H.; Glinka, T. Remarkable enantio-divergent biogenesis of brevianamide A and B. *J. Am. Chem. Soc.* **1989,** *111* (8), 3064–3065.
160. Sanz-Cervera, J. F.; Glinka, T.; Williams, R. M. Biosynthesis of brevianamides A and B: in search of the biosynthetic diels-alder construction. *Tetrahedron* **1993,** *49* (38), 8471–8482.
161. Domingo, L. R.; Zaragozá, R. J.; Williams, R. M. Studies on the Biosynthesis of Paraherquamide A and VM99955. A Theoretical Study of Intramolecular Diels−Alder Cycloaddition. *J. Org. Chem.* **2003,** *68* (7), 2895–2902.
162. Williams, R. M.; Sanz-Cervera, J. F.; Sancenón, F.; Marco, J. A.; Halligan, K. M. Biomimetic diels–alder cyclizations for the construction of the brevianamide, paraherquamide, sclerotamide, asperparaline and VM55599 ring systems. *Bioorg. Med. Chem.* **1998,** *6* (8), 1233–1241.
163. Williams, R. M.; Cox, R. J. Paraherquamides, Brevianamides, and Asperparalines: Laboratory Synthesis and Biosynthesis. An Interim Report. *Acc. Chem. Res.* **2003,** *36* (2), 127–139.
164. Stocking, E. M.; Williams, R. M. Chemistry and Biology of Biosynthetic Diels–Alder Reactions. *Angew. Chem. Int. Ed.* **2003,** *42* (27), 3078–3115.
165. Ye, Y.; Du, L.; Zhang, X.; Newmister, S. A.; McCauley, M.; Alegre-Requena, J. V.; Zhang, W.; Mu, S.; Minami, A.; Fraley, A. E.; Adrover-Castellano, M. L.; Carney, N. A.; Shende, V. V.; Qi, F.; Oikawa, H.; Kato, H.; Tsukamoto, S.; Paton, R. S.; Williams, R. M.; Sherman, D. H.; Li, S. Fungal-derived brevianamide assembly by a stereoselective semipinacolase. *Nat. Catal.* **2020,** *3* (6), 497–506.

166. Domingo, L. R.; Sanz-Cervera, J. F.; Williams, R. M.; Picher, M. T.; Marco, J. A. Biosynthesis of the Brevianamides. An ab Initio Study of the Biosynthetic Intramolecular Diels−Alder Cycloaddition. *J. Org. Chem.* **1997,** *62* (6), 1662–1667.
167. Xu, F.; Smith, M. W. A general approach to 2,2-disubstituted indoxyls: total synthesis of brevianamide A and trigonoliimine C. *Chem. Sci.* **2021,** *12* (41), 13756–13763.
168. Greshock, T. J.; Williams, R. M. Improved Biomimetic Total Synthesis of d,l-Stephacidin A. *Org. Lett.* **2007,** *9* (21), 4255–4258.
169. Huy, P.; Neudörfl, J.-M.; Schmalz, H.-G. A Practical Synthesis of Trans-3-Substituted Proline Derivatives through 1,4-Addition. *Org. Lett.* **2011,** *13* (2), 216–219.
170. Hutchison, A. J.; Kishi, Y. Stereospecific total synthesis of dl-austamide. *J. Am. Chem. Soc.* **1979,** *101* (22), 6786–6788.
171. Baran, P. S.; Corey, E. J. A Short Synthetic Route to (+)-Austamide, (+)-Deoxyisoaustamide, and (+)-Hydratoaustamide from a Common Precursor by a Novel Palladium-Mediated Indole → Dihydroindoloazocine Cyclization. *J. Am. Chem. Soc.* **2002,** *124* (27), 7904–7905.
172. Amatov, T.; Pohl, R.; Cisařová, I.; Jahn, U. Sequential Oxidative and Reductive Radical Cyclization Approach toward Asperparaline C and Synthesis of Its 8-Oxo Analogue. *Org. Lett.* **2017,** *19* (5), 1152–1155.
173. Dokli, I.; Pohl, R.; Klepetářová, B.; Jahn, U. First total synthesis of ent-asperparaline C and assignment of the absolute configuration of asperparaline C. *Chem. Commun.* **2019,** *55* (27), 3931–3934.
174. Potter, G. T.; Jayson, G. C.; Miller, G. J.; Gardiner, J. M. An Updated Synthesis of the Diazo-Transfer Reagent Imidazole-1-sulfonyl Azide Hydrogen Sulfate. *J. Org. Chem.* **2016,** *81* (8), 3443–3446.
175. McArthur, C. R.; Worster, P. M.; Okon, A. U. Amino Group Blocking. Improved Method for N-Phthaloylation Using N-(Ethoxycarbonyl)phthalimide. *Synth. Commun.* **1983,** *13* (4), 311–318.
176. Casimir, J. R.; Guichard, G.; Briand, J.-P. Methyl 2-((Succinimidooxy)carbonyl)benzoate (MSB): A New, Efficient Reagent for N-Phthaloylation of Amino Acid and Peptide Derivatives. *J. Org. Chem.* **2002,** *67* (11), 3764–3768.
177. Li, Q.; Seiple, I. B. Modular, Scalable Synthesis of Group A Streptogramin Antibiotics. *J. Am. Chem. Soc.* **2017,** *139* (38), 13304–13307.
178. Ghosez, L.; Haveaux, B.; Viehe, H. G. Alkyl and Aryl α-Chloro Enamines. *Angew. Chem. Int. Ed.* **1969,** *8* (6), 454–455.
179. Fürstner, A.; Konetzki, I. Total Synthesis of Caloporoside. *J. Org. Chem.* **1998,** *63* (9), 3072–3080.
180. Ebner, C.; Carreira, E. M. Cyclopropanation Strategies in Recent Total Syntheses. *Chem. Rev.* **2017,** *117* (18), 11651–11679.
181. Wiberg, K. B. The Concept of Strain in Organic Chemistry. *Angew. Chem. Int. Ed.* **1986,** *25* (4), 312–322.
182. de Meijere, A. Bonding Properties of Cyclopropane and Their Chemical Consequences. *Angew. Chem. Int. Ed.* **1979,** *18* (11), 809–826.
183. Wiberg, K. B. Bent Bonds in Organic Compounds. *Acc. Chem. Res.* **1996,** *29* (5), 229–234.

184. Wiberg, K. B.; Bader, R. F. W.; Lau, C. D. H. Theoretical analysis of hydrocarbon properties. Additivity of group properties and the origin of strain energy. *J. Am. Chem. Soc.* **1987,** *109* (4), 1001–1012.
185. Cavitt, M. A.; Phun, L. H.; France, S. Intramolecular donor–acceptor cyclopropane ring-opening cyclizations. *Chem. Soc. Rev.* **2014,** *43* (3), 804–818.
186. Kantorowski, E. J.; Kurth, M. J. Expansion to Seven-Membered Rings. *Tetrahedron* **2000,** *56* (26), 4317–4353.
187. Talele, T. T. The "Cyclopropyl Fragment" is a Versatile Player that Frequently Appears in Preclinical/Clinical Drug Molecules. *J. Med. Chem.* **2016,** *59* (19), 8712–8756.
188. Donaldson, W. A. Synthesis of cyclopropane containing natural products. *Tetrahedron* **2001,** *57* (41), 8589–8627.
189. Schröder, F. Present and Future of Cyclopropanations in Fragrance Chemistry. *Chem. Biodivers.* **2014,** *11* (11), 1734–1751.
190. Brackmann, F.; de Meijere, A. Natural Occurrence, Syntheses, and Applications of Cyclopropyl-Group-Containing α-Amino Acids. 1-Aminocyclopropanecarboxylic Acid and Other 2,3-Methanoamino Acids. *Chem. Rev.* **2007,** *107* (11), 4493–4537.
191. Lamberth, C. Small ring chemistry in crop protection. *Tetrahedron* **2019,** *75* (33), 4365–4383.
192. McGrath, N. A.; Brichacek, M.; Njardarson, J. T. A Graphical Journey of Innovative Organic Architectures That Have Improved Our Lives. *J. Chem. Ed.* **2010,** *87* (12), 1348–1349.
193. Bartoli, G.; Bencivenni, G.; Dalpozzo, R. Asymmetric Cyclopropanation Reactions. *Synthesis* **2014,** *46* (08), 979–1029.
194. Lebel, H.; Marcoux, J.-F.; Molinaro, C.; Charette, A. B. Stereoselective Cyclopropanation Reactions. *Chem. Rev.* **2003,** *103* (4), 977–1050.
195. Wu, W.; Lin, Z.; Jiang, H. Recent advances in the synthesis of cyclopropanes. *Org. Biomol. Chem.* **2018,** *16* (40), 7315–7329.
196. Li, P.; Zhao, J.; Shi, L.; Wang, J.; Shi, X.; Li, F. Iodine-catalyzed diazo activation to access radical reactivity. *Nat. Commun.* **2018,** *9* (1), 1972–1980.
197. Kulinkovich, O. G.; de Meijere, A. 1,*n*-Dicarbanionic Titanium Intermediates from Monocarbanionic Organometallics and Their Application in Organic Synthesis. *Chem. Rev.* **2000,** *100* (8), 2789–2834.
198. Pasco, M.; Gilboa, N.; Mejuch, T.; Marek, I. The Renaissance of Zinc Carbenoid in Stereoselective Synthesis in Acyclic Systems. *Organometallics* **2013,** *32* (4), 942–950.
199. Charette, A. B.; Juteau, H. Design of Amphoteric Bifunctional Ligands: Application to the Enantioselective Simmons-Smith Cyclopropanation of Allylic Alcohols. *J. Am. Chem. Soc.* **1994,** *116* (6), 2651–2652.
200. Beaulieu, L.-P. B.; Zimmer, L. E.; Charette, A. B. Enantio- and Diastereoselective Iodocyclopropanation of Allylic Alcohols by Using a Substituted Zinc Carbenoid. *Chem. Eur. J.* **2009,** *15* (44), 11829–11832.
201. Aggarwal, V. K.; Fang, G. Y.; Meek, G. Highly Diastereoselective Simmons−Smith Cyclopropanation of Allylic Amines. *Org. Lett.* **2003,** *5* (23), 4417–4420.
202. Du, H.; Long, J.; Shi, Y. Catalytic Asymmetric Simmons−Smith Cyclopropanation of Silyl Enol Ethers. Efficient Synthesis of Optically Active Cyclopropanol Derivatives. *Org. Lett.* **2006,** *8* (13), 2827–2829.

203. Doyle, M. P. Catalytic methods for metal carbene transformations. *Chem. Rev.* **1986,** *86* (5), 919–939.
204. Rasmussen, T.; Jensen, J. F.; Østergaard, N.; Tanner, D.; Ziegler, T.; Norrby, P.-O. On the Mechanism of the Copper-Catalyzed Cyclopropanation Reaction. *Chem. Eur. J.* **2002,** *8* (1), 177–184.
205. Evans, D. A.; Woerpel, K. A.; Hinman, M. M.; Faul, M. M. Bis(oxazolines) as chiral ligands in metal-catalyzed asymmetric reactions. Catalytic, asymmetric cyclopropanation of olefins. *J. Am. Chem. Soc.* **1991,** *113* (2), 726–728.
206. David, E.; Milanole, G.; Ivashkin, P.; Couve-Bonnaire, S.; Jubault, P.; Pannecoucke, X. Syntheses and Applications of Monofluorinated Cyclopropanes. *Chem. Eur. J.* **2012,** *18* (47), 14904–14917.
207. Pons, A.; Ivashkin, P.; Poisson, T.; Charette, A. B.; Pannecoucke, X.; Jubault, P. Catalytic Enantioselective Synthesis of Halocyclopropanes. *Chem. Eur. J.* **2016,** *22* (18), 6239–6242.
208. Chen, Y.; Ruppel, J. V.; Zhang, X. P. Cobalt-Catalyzed Asymmetric Cyclopropanation of Electron-Deficient Olefins. *J. Am. Chem. Soc.* **2007,** *129* (40), 12074–12075.
209. Perkin , W. H. Ueber die Einwirkung von Aethylenbromid auf Malonsäureäther. *Ber. dtsch. Chem. Ges.* **1884,** *17* (1), 54–59.
210. Corey, E. J.; Chaykovsky, M. Dimethylsulfoxonium Methylide. *J. Am. Chem. Soc.* **1962,** *84* (5), 867–868.
211. Leiva de Faria, M.; de A. Magalhães, R.; Silva, F. C.; de O. Matias, L. G.; Ceschi, M. A.; Brocksom, U.; John Brocksom, T. Enantiodivergent syntheses of cycloheptenone intermediates for guaiane sesquiterpenes. *Tetrahedron: Asymmetry* **2000,** *11* (20), 4093–4103.
212. Miyamura, S.; Itami, K.; Yamaguchi, J. Syntheses of Biologically Active 2-Arylcyclopropylamines. *Synthesis* **2017,** *49* (6), 1131–1149.
213. Xuan, Y.-N.; Nie, S.-Z.; Dong, L.-T.; Zhang, J.-M.; Yan, M. Highly Enantioselective Synthesis of Nitrocyclopropanes via Organocatalytic Conjugate Addition of Bromomalonate to α,β-Unsaturated Nitroalkenes. *Org. Lett.* **2009,** *11* (7), 1583–1586.
214. Amputch, M. A.; Matamoros, R.; Little, R. D. Asymmetric induction in the Michael Initiated Ring Closure reaction. *Tetrahedron* **1994,** *50* (19), 5591–5614.
215. Engel, P. S. Mechanism of the thermal and photochemical decomposition of azoalkanes. *Chem. Rev.* **1980,** *80* (2), 99–150.
216. Wender, P. A.; Kee, J.-M.; Warrington, J. M. Practical Synthesis of Prostratin, DPP, and their Analogs, Adjuvant Leads Against Latent HIV. *Science* **2008,** *320* (5876), 649–652.
217. García Ruano, J. L.; Peromingo, M. T.; Martín, M. R.; Tito, A. A New Entry to Enantiopure Polysubstituted Cyclopropanes: Stereoselective Denitrogenation of Sulfinylpyrazolines under $Yb(OTf)_3$ Catalysis. *Org. Lett.* **2006,** *8* (15), 3295–3298.
218. Conia, J. M.; Salaun, J. R. Cyclobutane ring contractions not involving carbonium ions. *Acc. Chem. Res.* **1972,** *5* (1), 33–40.
219. Ross, A. G.; Townsend, S. D.; Danishefsky, S. J. Halocycloalkenones as Diels–Alder Dienophiles. Applications to Generating Useful Structural Patterns. *J. Org. Chem.* **2013,** *78* (1), 204–210.
220. Baumann, A. N.; Schüppel, F.; Eisold, M.; Kreppel, A.; de Vivie-Riedle, R.; Didier, D. Oxidative Ring Contraction of Cyclobutenes: General Approach to Cyclopropylketones including Mechanistic Insights. *J. Org. Chem.* **2018,** *83* (9), 4905–4921.

221. Jones, G.; Strugnell, S. A.; DeLuca, H. F. Current Understanding of the Molecular Actions of Vitamin D. *Physiol. Rev.* **1998,** *78* (4), 1193–1231.
222. Romero, N. A.; Nicewicz, D. A. Organic Photoredox Catalysis. *Chem. Rev.* **2016,** *116* (17), 10075–10166.
223. Dutta, S.; Erchinger, J. E.; Strieth-Kalthoff, F.; Kleinmans, R.; Glorius, F. Energy transfer photocatalysis: exciting modes of reactivity. *Chem. Soc. Rev.* **2024,** *53* (3), 1068–1089.
224. Großkopf, J.; Kratz, T.; Rigotti, T.; Bach, T. Enantioselective Photochemical Reactions Enabled by Triplet Energy Transfer. *Chem. Rev.* **2022,** *122* (2), 1626–1653.
225. Hoffmann, N. Photochemical Reactions as Key Steps in Organic Synthesis. *Chem. Rev.* **2008,** *108* (3), 1052–1103.
226. Narayanam, J. M. R.; Stephenson, C. R. J. Visible light photoredox catalysis: applications in organic synthesis. *Chem. Soc. Rev.* **2011,** *40* (1), 102–113.
227. Schultz, D. M.; Yoon, T. P. Solar Synthesis: Prospects in Visible Light Photocatalysis. *Science* **2014,** *343* (6174), 985–993.
228. Nájera, C.; Yus, M. Desulfonylation reactions: Recent developments. *Tetrahedron* **1999,** *55* (35), 10547–10658.
229. Chu, X.-Q.; Ge, D.; Cui, Y.-Y.; Shen, Z.-L.; Li, C.-J. Desulfonylation via Radical Process: Recent Developments in Organic Synthesis. *Chem. Rev.* **2021,** *121* (20), 12548–12680.
230. Chatgilialoglu, C. Sulfonyl Radicals. In *Sulphones and Sulphoxides*, **1988**; pp 1089–1113.
231. Kim, S.; Kim, S. Tin-Free Radical Carbon–Carbon Bond-Forming Reactions Based on α-Scission of Alkylsulfonyl Radicals. *Bull. Chem. Soc. Jpn.* **2007,** *80* (5), 809–822.
232. Kim, S.; Lim, C. J. Tin-Free Radical-Mediated C-C Bond Formations with Alkyl Allyl Sulfones as Radical Precursors. *Angew. Chem. Int. Ed.* **2002,** *41* (17), 3265–3267.
233. Schwarz, J.; König, B. Decarboxylative Alkynylation of Biomass-Derived Compounds by Metal-Free Visible Light Photocatalysis. *ChemPhotoChem* **2017,** *1* (5), 237–242.
234. Huang, H.-G.; Li, W.; Zhong, D.; Wang, H.-C.; Zhao, J.; Liu, W.-B. Trifluoromethanesulfonyl azide as a bifunctional reagent for metal-free azidotrifluoromethylation of unactivated alkenes. *Chem. Sci.* **2021,** *12* (9), 3210–3215.
235. Fagnoni, M.; Dondi, D.; Ravelli, D.; Albini, A. Photocatalysis for the Formation of the C−C Bond. *Chem. Rev.* **2007,** *107* (6), 2725–2756.
236. Lovering, F. Escape from Flatland: complexity and promiscuity. *MedChemComm* **2013,** *4* (3), 515–519.
237. Durst, T.; Huang, J. C.; Sharma, N. K.; Smith, D. J. H. Photochemical extrusion of sulfur dioxide from sultines. *Can. J. Chem.* **1978,** *56* (4), 512–516.
238. Finlay, J. D.; Smith, D. J. H.; Durst, T. The Photolysis of 2-Phenylthietan-1,1-dioxides; Preparation of Substituted Cyclopropanes. *Synthesis* **1978,** *8*, 579–580.
239. Dittmer, D. C.; Sedergran, T. C. Four-Membered Sulfur Heterocycles. In *Chemistry of Heterocyclic Compounds*, **1985**; pp 431–768.
240. Stork, G.; Borowitz, I. J. Four-Membered Sulfones From Enamines and Aliphatic Sulfonyl Halides. *J. Am. Chem. Soc.* **1962,** *84* (2), 313.
241. Wannagat, U.; Kuckertz, H. Silyl-Subsituted Sulfur Amides and Imides. *Angew. Chem. Int. Ed.* **1962,** *1* (2), 113.
242. Mansson, C. M. F.; Burns, N. Z. Aqueous Amine-Tolerant [2+2] Photocycloadditions of Unactivated Olefins. *J. Am. Chem. Soc.* **2022,** *144* (43), 19689–19694.

243. Kubas, G. J.; Larson, A. C.; Ryan, R. R. Reactions of quinuclidine *N*-oxide and other amine oxides with sulfur dioxide. Structure of quinuclidine sulfur trioxide. *J. Org. Chem.* **1979,** *44* (22), 3867–3871.
244. Seyed Hashtroudi, M.; Fathi Vavsari, V.; Balalaie, S., DABSO as a SO_2 gas surrogate in the synthesis of organic structures. *Org. Biomol. Chem.* **2022,** *20* (11), 2149–2163.
245. Truce, W. E.; Norell, J. R. Thietane Dioxide Derivatives via the Interaction of Sulfonyl Chlorides with Ketene Diethylacetal. *J. Am. Chem. Soc.* **1963,** *85* (20), 3231–3236.
246. Siryi, S. A.; Timoshenko, V. M.; Rudenko, T. V.; Markitanov, Y. M.; Rusanov, E. B.; Shermolovich, Y. G. Synthesis of Monosubstituted Trifluoromethylated Derivatives of 2H-thiete, Dihydrothiophenes, and 2H-thiopyrans. *Chem. Heterocycl. Compd.* **2022,** *58* (2), 106–115.
247. Baumann, A. N.; Reiners, F.; Siegle, A. F.; Mayer, P.; Trapp, O.; Didier, D. Thiete Dioxides as Templates Towards Twisted Scaffolds and Macrocyclic Structures. *Chem. Eur. J.* **2020,** *26* (27), 6029–6035.
248. Eisold, M.; Müller-Deku, A.; Reiners, F.; Didier, D. Parallel Approaches for the Functionalization of Thietes: α-Metalation versus C–H Activation. *Org. Lett.* **2018,** *20* (15), 4654–4658.
249. Akhlaghinia, B.; Rahimizadeh, M.; Eshghi, H.; Zhaleh, S.; Rezazadeh, S. Green synthesis of thiiranes from oxiranes under solvent- and catalyst-free conditions. *J. Sulfur Chem.* **2012,** *33* (3), 351–361.
250. Tomashevskii, A. A.; Sokolov, V. V.; Potekhin, A. A. Reaction of 4-(N,N-Dimethylaminophenyl)magnesium Bromide with Palladium Tetrakis(triphenylphosphine). *Russ. J. Org. Chem.* **2003,** *39* (2), 226–234.
251. King, J. F.; Mayo, P. d.; McIntosh, C. L.; Piers, K.; Smith, D. J. H. Thermolysis of thiete 1,1-dioxide and related species. *Can. J. Chem.* **1970,** *48* (23), 3704–3715.
252. Dittmer, D.; Christy, M., Notes-Thiete Sulfone. *J. Org. Chem.* **1961,** *26* (4), 1324–1326.
253. Kremsmair, A.; Sunagatullina, A. S.; Bole, L. J.; Mastropierro, P.; Graßl, S.; Wilke, H. R.; Godineau, E.; Hevia, E.; Knochel, P. Exploiting Coordination Effects for the Regioselective Zincation of Diazines Using TMPZnX·LiX (X=Cl, Br). *Angew. Chem. Int. Ed.* **2022,** *61* (40), e202210491.
254. Rehm, T. H. Flow Photochemistry as a Tool in Organic Synthesis. *Chem. Eur. J.* **2020,** *26* (71), 16952–16974.